EEG - fMRI

Physiological Basis, Technique, and Applications

Christoph Mulert
Louis Lemieux
Editors

Second Edition

OPEN ACCESS

Springer

EEG - fMRI

Christoph Mulert • Louis Lemieux
Editors

EEG - fMRI

Physiological Basis, Technique, and Applications

Second Edition

Springer

Editors
Christoph Mulert
Centre of Psychiatry, Justus Liebig University
Giessen, Germany

Louis Lemieux
UCL Queen Square Institute of Neurology, UCL
London, UK

ISBN 978-3-031-07120-1 ISBN 978-3-031-07121-8 (eBook)
https://doi.org/10.1007/978-3-031-07121-8

This Springer imprint is published by the registered company Springer Nature Switzerland AG
The registered company address is: Gewerbestrasse 11, 6330 Cham, Switzerland

Preface to the Second Edition

More than 10 years after the first edition of the textbook EEG-fMRI it was obviously necessary not only to revisit and update the existing contents but also to include coverage of important and innovative topics with new chapters. The new developments are very promising offering new concepts, new methodological challenges and solutions as well as first applications. For example, the new Chap. 14 "Non-invasive Brain Stimulation with Multimodal Acquisitions" by Alexander T. Sack, Teresa Schumann and Tom A. de Graaf, describing concepts, methods and findings based on the combination of TMS with fMRI and EEG-fMRI. In a similar way, the new Chap. 13 "Real-Time fMRI Neurofeedback with Simultaneous EEG" by Vadim Zotev, Ahmad Mayeli, Chung Ki Wong and Jerzy Bodurka introduces the promising concept of a potential therapeutic use of these methods, the technical details and first applications suggesting potential benefit for patients with major depression. The new Chap. 20 "Simultaneous EEG-fMRI in Psychiatry" by Gebhard Sammer and Christoph Mulert summarizes studies using EEG-fMRI in patients with anxiety disorders, attention deficit hyperactivity disorder, major depression or schizophrenia. The new Chap. 29 "Sparse and Data-Driven Methods for Concurrent EEG-fMRI" by Pamela K. Douglas, Farzad Vasheghani-Farahni, Ariana Anderson and Jerome Gilles gives a superb overview about sparse empirical techniques for sampling, cleaning and jointly analysing concurrently recorded EEG-fMRI data. Last but not least, the new Chap. 30 "Integrating EEG-fMRI Through Brain Simulation" by Michael Schirner and Petra Ritter offers insights into the fascinating world of the computational simulation of brain signals, using the rich data of simultaneous EEG-fMRI to learn about underlying neural activity and neural mechanisms.

Amongst the first edition chapters that have been substantially updated or even completely rewritten are Chap. 1 "Principles of Multimodal Functional Imaging and Data Integration" by Arno Villringer and ourselves, Chap. 8 "EEG Quality: The Pulse Artefact" by Rodolfo Abreu, Jose Jorge and Patricia Figueiredo, and Chap. 12 "Experimental Design and Data Analysis Strategies" by Jonathan Wirsich, Andrew P. Bagshaw, Maxime Guye, Louis Lemieux and Christian-G. Bénar with addition of the impact of EEG-fMRI in connectivity studies, and the combination of concurrent fMRI and intracerebral EEG recordings in epilepsy research.

Very sadly, our highly respected colleague and friend Fernando Lopes da Silva passed away before the publication of this edition (Michel et al. 2019). We are

extremely thankful to his family for allowing us to include the updated version of his supremely authoritative Chap. 2 “EEG: Origin and Measurement”.

Both the editors and the contributors learned a lot during the preparation of this second edition. For example, EEG-fMRI has become an established tool for many researchers to such a degree that EEG-fMRI no longer appears in the title of many articles. While this has made the task of preparing this edition more arduous, we interpret this as a sign that although many methodological, conceptual or technical advances have been made, in other respects EEG-fMRI has become just a normal part of our toolbox.

We would like to thank all of the contributors for their hard work and patience throughout the editing and the production process. We are particularly grateful to Barbara Zöhrer and Smitha Diveshan of Springer for all their support in preparing the second edition.

Reference

Michel CM, Baillet S, Benar C et al (2019) In memoriam: Fernando Lopes da Silva (1935–2019). Brain Topogr 32:519–522. https://doi.org/10.1007/s10548-019-00720-0

Giessen, Germany
London, UK

Christoph Mulert
Louis Lemieux

Contents

Part I

Background

Principles of Multimodal Functional Imaging and Data Integration

1

Arno Villringer, Christoph Mulert, and Louis Lemieux

1.1 Introduction

In a system as complex as the human brain, one cannot conceive of meaningful events involving a change in a single observable (physiological) parameter. Therefore, achieving the ultimate aim of a complete understanding of brain events and brain activity in general will require the integration of a variety of observations related to these events. Multimodal imaging, or more generally measurements whereby data from various types of instruments are brought together, has arisen from this realisation, partly because some events are best observed in one modality and the investigator is interested in another (e.g. a more recently developed modality) and to be honest sometimes as a response to the technical challenge of combining modalities for simultaneous observations. Fundamentally, multimodal imaging should allow the investigator to address the question: what happens to brain observable Z when observable X changes (or event Y occurs)?

A. Villringer (✉)
Department of Neurology, Max Planck Institute for Human Cognitive and Brain Sciences, Leipzig, Germany
e-mail: Villringer@cbs.mpg.de

C. Mulert
Centre of Psychiatry, Justus Liebig University, Giessen, Germany
e-mail: Christoph.mulert@psychiat.med.uni-giessen.de

L. Lemieux
UCL Queen Square Institute of Neurology, UCL, London, UK
e-mail: louis.lemieux@ucl.ac.uk

C. Mulert, L. Lemieux (eds.), *EEG - fMRI*,
https://doi.org/10.1007/978-3-031-07121-8_1

In the second half of the twentieth century, and particularly since the 1990s, a rapid development of noninvasive functional and structural brain imaging methods has occurred. While some of these developments have resulted from gradual improvements in some methods, other developments have led to completely new approaches for measuring brain activity, affording new types of information about the brain. In the former case, the older methods were eventually replaced [e.g. scintigraphic methods by positron emission tomography (PET) and SPECT or low-field MRI (magnetic resonance imaging) by higher-field MRI]. In the latter case, however, newer developments have not replaced older ones; rather, they have been added to an ever-larger orchestra of functional and structural neuroimaging methods consisting of techniques that offer complementary information about the brain. Table 1.1 gives an overview of currently available methods for noninvasive brain imaging and the principle that each exploits.

While in some instances combining multimodal measurements is a relatively straightforward task from a technical point of view [e.g. transcranial ultrasound/near-infrared optical spectroscopy (TCD/NIRS)], the combination of other methods poses major technical challenges (e.g. EEG–fMRI, PET–MRI) especially when moving to ultrahigh-field strengths at 7 T or 9.4 T. Table 1.2 summarises which imaging techniques have been combined successfully in order to perform simultaneous observations. While all the methods listed in Table 1.2 measure brain activity, another multimodal approach combines techniques which stimulate/modulate brain activity with methods which assess brain activity, e.g. the combination of transcranial magnetic stimulation (TMS) with PET or even triple combinations such as TMS with EEG–fMRI. While these approaches are not further addressed in this book, they are listed—for completeness of multimodal imaging—in Table 1.3.

While the physical principles underlying each method are crucial to the feasibility of multimodal integration (Tables 1.1, 1.2 and 1.3), subtler aspects of (or variations on) the basic principle (e.g. choice of pulse sequence in MRI, application of contrast agents in CT, MRI or ultrasound) determine the precise aspect of neurophysiology that can be captured in any given application (for an earlier review, see Villringer and Dirnagl 1995). From the standpoint of a neuroscientist, it seems more appropriate to categorise methods according to the neurophysiological processes that they reflect rather than according to the physical principle. Table 1.4 illustrates how different neuroimaging modalities can provide complementary

Table 1.1 Noninvasive brain imaging methods

Method	Physical principle
Computerised tomography (CT)	Absorption of X-rays
Positron emission tomography (PET)	Emission/detection of positrons
Magnetic resonance imaging (MRI)	Nuclear magnetic resonance (NMR)
Optical imaging	Light absorption, scattering, fluorescence
Electroencephalography (EEG)	Electrical potentials
Magnetoencephalography (MEG)	Magnetic fields
Electrical impedance tomography (EIT)	Changes in electrical impedance
Ultrasound	Doppler effect in ultrasound

Table 1.2 Multimodal neuroimaging: combining different neuroimaging methods

Combination	References	Comments
EEG–MRI	Ives et al. (1993), Busch et al. (1995), Bonmassar et al. (1999, 2001), Allen et al. (1998, 2000), Lemieux et al. (1997, 2001a, b), Goldman et al. (2000), Krakow et al. (2000), Vasios et al. (2006), Neuner et al. (2013)	Although the feasibility of this combination was shown a few years back, broad usage started with further developments in equipment, artefact elimination and analysis
NIRS–MRI	Kleinschmidt et al. (1996), Kida et al. (1996), Punwani et al. (1998), Toronov et al. (2001), Mehagnoul-Schipper et al. (2002), Strangman et al. (2002)	
TES–MRI	Brandt et al. (1996)	
MRI–MEG	Zotev et al. (2008)	
fTCD–MRI	Not found	Probably feasible, since combined ultrasound and MRI systems have been demonstrated (McDannold et al. 2003)
PET–NIRS	Villringer et al. (1997), Polinder-Bos et al. (2020)	
PET–fTCD	Sabri et al. (2003)	
PET–EEG	Buchsbaum et al. (1984), Sadato et al. (1998), Barrington et al. (1998), Gamma et al. (2004)	
PET–MEG	Not found	Feasible in principle, but no example of a successful combination was found
PET–CT		Mainly used in clinical oncology (Beyer et al. 2000)
PET–MRI	Catana et al. (2008), Judenhofer et al. (2008), Kim et al. (2020)	
EEG–MEG	Salustri and Chapman (1989), Buchner et al. (1994), Plummer et al. (2019)	
EEG–NIRS	Hoshi et al. (1994), Steinhoff et al. (1996), Kirkpatrick et al. (1998), Obrig et al. (2002), Shin et al. (2018)	
MEG–NIRS	Mackert et al. (2004), Seki et al. (2012)	
NIRS–TCD	Terborg et al. (2003)	

neurophysiological information that may allow neuroscientists to identify which combination is currently available and matches their interest. For example, in the assessment of brain activity for a certain cognitive task, it might be useful to combine the spatial resolution and relatively uniform spatial coverage of fMRI with evoked potentials measured using scalp electroencephalography (EEG) to a high temporal resolution (along with the large amount of knowledge on cognitive correlates accumulated over decades of research) in order to elucidate how the spatiotemporal haemodynamic and electrical patterns are correlated.

Table 1.3 Multimodal neuroimaging: combining stimulation methods with neuroimaging methods

Combination	References	Comments
TMS–PET	Paus et al. (1997)	
TES–MRI	Brandt et al. (1996)	First combination of transcranial stimulation with MRI
TMS–MRI	Bohning et al. (1998), Bestmann et al. (2003), Ruff et al. (2006)	
TDCS–MRI	Antal et al. (2011)	
FUS–MRI	Legon et al. (2018)	
TMS–EEG	Paus et al. (2001), Kähkönen et al. (2004)	
TDCS–EEG	Faria et al. (2012)	
TMS–NIRS	Mochizuki et al. (2006)	
TDCS–NIRS	Jindal et al. (2015)	The study by Jindal combined TDCS with NIRS and EEG
FUS–EEG	Legon et al. (2014)	
TMS–EEG–MRI	Peters et al. (2020)	Combination of three methods

FUS focused ultrasound stimulation, *DCS* transcranial direct current stimulation, *NIRS* near-infrared spectroscopy, *TMS* transcranial magnetic stimulation, *TES* transcranial electrical stimulation, *TMS* transcranial magnetic stimulation

Table 1.4 Physiological parameters and noninvasive brain imaging methods

Physiological parameters	Technique	Method
Vascular/metabolic parameters		
Cerebral blood flow	MRI	Arterial spin labelling (ASL)
		Bolus track MRI
	Positron emission tomography	H_2O PET
		Butanol–PET
	SPECT	ECD–SPECT
	Optical imaging Ultrasound	Bolus track near-infrared spectroscopy/imaging Functional ultrasound imaging (human studies so far only in neonates over open fontanelle and invasively)
Δ[deoxyhaemoglobin]	MRI	Blood-oxygen-level-dependent
	Optical imaging	Near-infrared spectroscopy
Plasma volume	MRI	Bolus track MRI
	Optical	Bolus track optical imaging
Corpuscular volume	PET	CO–PET
	MRI	VASO
Glucose consumption	PET	Deoxyglucose PET

Table 1.4 (continued)

Physiological parameters	Technique	Method
Oxygen consumption	PET	O_2 PET
	MRI	BOLD and CBF–MRI (calibrated with CO_2 challenge)
Electrophysiological markers of brain activity		
"Field potentials" (presumably reflecting synaptic activity)	EEG	Event-related evoked potentials
Action potentials (high-frequency bursts)	EEG–MEG	High-frequency oscillations
Evoked fields (presumably reflecting synaptic activity)	MEG	Event-related evoked magnetic fields
Assessment of background rhythms and evoked rhythms	EEG, MEG	Assessment of occipital alpha rhythms
Molecular markers		
Various markers of energy metabolism containing phosphorus: ATP, ADP, creatinine phosphate	MR	P31 magnetic resonance spectroscopy
Various molecules in millimolar concentration range: lactate, *N*-acetyl-aspartate, glutamate, GABA, etc.	MR	H1 magnetic resonance spectroscopy
Other molecular markers at smaller concentrations	PET	PET of various positron-emitting tracers
	Optical	Fluorescence detection of various fluorescent/phosphorescent tracers
Brain morphology/volumetry		
Volumes of brain areas	MRI	Voxel-based morphometry (VBM)
Orientation of nerve fibres	MRI	Diffusion tensor imaging
Others		
Cell volume	MRI	Diffusion imaging
	Optical	Scattering

1.2 Modes of Data Integration

The integration of different measurement modalities can be achieved in a variety of ways, reflecting both the level of synchrony between the data acquired for each modality and the ways in which the data from each modality are used to analyse or interpret the findings. We refer to these as modes of integration.

It goes almost without saying that the study of a given phenomenon using multiple modalities requires that all signals relate to the same phenomenon. However, the ways in which the data can be usefully acquired depend on what type of phenomenon and which aspect of the phenomenon one is interested in. For example, in experimental studies involving controlled tasks or stimuli, serial single-modality acquisitions may be adequate, and it is less clear why it may be advantageous to combine methods in order to acquire the multimodal data simultaneously.

Similarly, a range of analytical strategies for multimodal datasets are available that are suited to different modes of acquisition and reflect varying degrees of sophistication of the underlying (integrative) model. For example, spatial coregistration of independently analysed unimodal data represents one of the simplest forms of integration—comparison, while the estimation of biophysical models of brain activity based on multimodal data must be one of the end-points of the multimodal integration project.

1.3 Multimodal Data Acquisition Strategies: Degree of Synchrony

In an ideal world, a single instrument would combine all imaging modalities, and all brain imaging datasets would be multimodal. However, human brain imaging instruments are generally single modality, except for magnetoencephalography (MEG) systems, which often comprise an EEG recording system. Therefore, investigators interested in obtaining multimodal measurements must carefully consider the practical difficulties associated with simultaneous measurements in relation to the expected benefits for the data. These difficulties include (a) higher costs (e.g. adaptation of instruments to the new environment, such as nonmagnetic materials for MR compatibility), (b) interactions between instruments that can lead to data quality degradation (e.g. EEG artefacts during MRI data acquisition) or increased health risks for subjects (higher risk of introducing magnetic material into the MR environment). These issues are discussed in greater detail in chapters 7 "EEG Instrumentation and Safety in the MRI Environment", 8 "EEG Quality: The Pulse Artifact", 9 "EEG Quality: The Image Acquisition Artefact", 10 "Image Quality Issues", and 11 "EEG-fMRI at Ultrahigh Magnetic Fields: B.0 >= 3 Tesla".

Given satisfactory technical solutions to the above problems, there are clear theoretical benefits in performing simultaneous multimodal acquisitions, although their value will depend on the specific scientific questions being asked. The main consideration is whether one is confident that *the same thing* (brain activity) will happen if the experiment is repeated across modalities. Given that the human brain cannot be entirely controlled, a degree of interevent signal variability is inevitable (above and beyond any measurement uncertainty due to the instruments), and the issue boils down to whether one can guarantee that the parameters of interest would behave identically across sessions. This means that multimodal studies based on the parameterisation of individual events must be performed in a single session with simultaneous measurements from all modalities. According to the same reasoning, multimodal studies of unpredictable events (interevent timing variability) also require simultaneous data acquisitions.

For studies of effects averaged over multiple events (such as traditional evoked response studies), intersession bias due to differences in the environment or possible learning effects, for example, must be avoided, and so the need for simultaneous acquisitions in a single session must be carefully considered. In all other circumstances, non-simultaneous multimodal acquisitions may be adequate.

Note that while inferences made based on non-simultaneously acquired multimodal datasets can also be made based on simultaneously acquired datasets, the reverse is not true, given the loss of information on interevent variability in the former type of acquisition.

An interesting special case is noninvasive brain–computer interface and neurofeedback: Here the purpose of neuroimaging is not primarily the understanding of neural processes, but to provide a fast and decodable neural signal. For example, the combination of fNIRS and EEG has shown promise for enhanced BCI performance (Fazli et al. 2012) and the combination of EEG and fMRI for neurofeedback (Zotev et al. 2014).

1.4 Multimodal Data Integration Strategies

Data from multiple modalities, and inferences made from them, can be brought together in various ways that can be characterised by the degree to which the relationship between the signals is incorporated into a model. At one end of the scale, modalities are simply compared in time or space and may be subjected to correlation analyses, for example. At the other end of the scale, we have methodologies that aim to model the multimodal signals from more fundamental building blocks, such as neuronal activity and biophysical forward models.

1.4.1 Spatial Coregistration

Cross-validation of measurements is one of the most common motivations for multimodal imaging. In this approach, information on the distribution of brain activity involved in a given process obtained independently from a number of modalities is compared, usually with the aim of assessing the value of a new localising technique. For example, the localising information provided by EEG-correlated fMRI regarding the generators of interictal spikes or event-related potentials has been compared to EEG source reconstruction, thus potentially validating the results from the former technique; however, there are many reasons for a possible lack of perfect spatial concordance, and the very notion of a gold standard is debatable in this specific context (Lemieux et al. 2001a, b; Benar et al. 2003; Mulert et al. 2004) (see Table 1.5 for other examples).

The comparison of two independent measures of brain activity at a given location can increase our understanding of the mechanisms that give rise to the signals. For example, the mechanisms that lead to T2*-weighted fMRI during functional activation (Kwong et al. 1992; Ogawa et al. 1992; Frahm et al. 1992; Bandettini et al. 1992) were studied by comparing fMRI and NIRS, which rely on the differential light absorption of deoxy-Hb. It had been previously shown that the T2*-weighted MRI signal can change with haemoglobin oxygenation [the blood-oxygen-level-dependent (BOLD) effect; Ogawa et al. 1990; Turner et al. 1991]; however, there are many other determinants of the T2* signal. Studies

Table 1.5 Examples of cross-validation of EEG–MEG source estimation using tomographic functional brain imaging

Source estimation approach	Imaging validation method	References
MEG dipole source analysis	fMRI, PET, SPECT	Walter et al. (1992), Stefan et al. (1992)
EEG dipole source analysis	fMRI, PET	Menon et al. (1997), Grimm et al. (1998)
MEG linear source estimates		Not yet done
EEG linear source estimates	fMRI, PET	Gamma et al. (2004), Mulert et al. (2004)

Table 1.6 Examples of neurophysiological parameters studied using multimodal comparisons

Parameters measured for validation	Simultaneous combination of methods	References
Deoxy-Hb	fMRI and NIRS	Kleinschmidt et al. (1996), Kida et al. (1996), Punwani et al. (1998), Toronov et al. (2001), Mehagnoul-Schipper et al. (2002), Strangman et al. (2002)
Cerebral blood flow	[15O]–PET and ASL–MRI	Fan et al. (2017)
Cerebral oxygen extraction fraction (OEF)	[15O]–PET and quantitative susceptibility mapping plus quantitative BOLD (QSM + qBOLD)	Cho et al. (2021)
Cerebral blood flow	Bolus track MRI and bolus track optical imaging	Feasible in principle, not yet done
Cerebral blood flow	Bolus track optical imaging (NIRS) and transcranial Doppler sonography (TCD)	Klaessens et al. (2005)
Corpuscular blood volume (total haemoglobin)	CO–PET and NIRS	Not yet done, although feasible in principle

comparing the results of the two methods confirmed that T2*-weighted fMRI signal increases during functional activation correlate with local drops in [deoxy-Hb] (Kleinschmidt et al. 1996; Kida et al. 1996; Punwani et al. 1998; Toronov et al. 2001; Mehagnoul-Schipper et al. 2002; Strangman et al. 2002). Other examples of multimodal comparisons are given in Table 1.6.

1.4.2 Asymmetric Integration

A more advanced form of multimodal data integration than spatial comparison for validation or interpretation purposes is the use of data from one modality in the analysis of data from other modalities. This can be either spatially or temporally

based. In the spatial domain, activated brain regions identified using PET or fMRI have been used as constraints or priors for the solution of the EEG–MEG inverse problem (Heinze et al. 1994; Liu et al. 1998; Daunizeau et al. 2006; Stancak et al. 2005; Babiloni et al. 2003).

Asymmetric integration in the temporal domain is commonly performed for the analysis of haemodynamic correlates of brain activity captured on EEG and in particular in simultaneous acquisitions. For example, new insights into the relationship between neuronal activity and BOLD have been obtained by building models of BOLD change incorporating specific aspects of evoked responses measured at the single-trial level in simultaneous EEG and fMRI acquisitions (Debener et al. 2005; Eichele et al. 2005; Mulert et al. 2008). A further variant is the assessment of evoked brain activity at different baseline states of the brain [e.g. sleep states (Portas et al. 2000), vigilance, attention, etc.], with the latter being identified by one method (often EEG) and the former either by the other method (e.g. fMRI) or again by a combination of the two (EEG–fMRI).

EEG usually provides the time or state marker in imaging studies of spontaneous brain activity: this is the EEG-derived hypothesis-driven approach to fMRI analysis. The paradigmatic example for the latter is the study of the haemodynamic correlates of epileptic spikes recorded noninvasively (Warach et al. 1996; Lemieux et al. 2001a, b; Krakow et al. 2001a, b) or with intracranial EEG (Sharma et al. 2019). Again, one dataset (EEG) is used as a predictor of vascular changes in fMRI, PET or NIRS data. A similar situation is the assessment of vascular correlates of spontaneous changes in EEG rhythms (Goldman et al. 2002; Laufs et al. 2003; Moosmann et al. 2003) or of certain EEG features (e.g. slow waves during light sleep) of sleep (Betta et al. 2021). Examples are given in Table 1.7.

Table 1.7 Examples of multimodal imaging that follows the principles of "adding complementary information" and "identifying and measuring"

Neurophysiological event	Measurement parameters	Combination of methods	References
Event-related brain activity under peripheral stimulation	Evoked potential (EEG), BOLD (fMRI)	EEG, MRI	Bonmassar et al. (1999, 2001), Allen et al. (2000), Goldman et al. (2000), Mulert et al. (2004, 2008), Becker et al. (2005)
	Evoked potential (EEG), BOLD	EEG, NIRS	Obrig et al. (2002), Horovitz and Gore (2004)
Variations in event-related brain activity under peripheral stimulation	Evoked potential (EEG), BOLD (fMRI)	EEG, MRI	Debener et al. (2005), Eichele et al. (2005), Benar et al. (2007), Mulert et al. (2008)

(continued)

Table 1.7 (continued)

Neurophysiological event	Measurement parameters	Combination of methods	References
Alpha rhythms (background)	Occipital alpha rhythm (EEG), BOLD (fMRI)	EEG, MRI	Goldman et al. (2002), Moosmann et al. (2003), Laufs et al. (2003)
	Occipital alpha rhythm (EEG), deoxy-Hb concentration changes (NIRS)	EEG, NIRS	Moosmann et al. (2003)
	Occipital alpha rhythm (EEG), cerebral blood flow (FDG–PET)	EEG, PET	Sheridan et al. (1988)
	Occipital alpha rhythm (EEG), cerebral blood flow (H_2O–PET)	EEG, PET	Sadato et al. (1998)
Epileptic brain activity	Epileptic spikes (EEG), BOLD (fMRI)	EEG, MRI	Warach et al. (1996), Lemieux et al. (2001a, b), Krakow et al. (2001a, b)
	Epileptic spikes (EEG), cerebral blood flow changes (flow-sensitive MRI)	EEG, MRI	Warach et al. (1994), Hamandi et al. (2008), Carmichael et al. (2008)
	Epileptic spikes (EEG), cerebral blood flow changes (flow-sensitive MRI), BOLD (fMRI)	EEG, MRI	Hamandi et al. (2008), Carmichael et al. (2008)
	Generalised spike-wave discharges (GSWD), BOLD (fMRI)	EEG, fMRI	Pugnaghi et al. (2014)
	Epileptic spikes (EEG), haemoglobin oxygenation changes (NIRS)	NIRS, EEG	Buchheim et al. (2004)
	Epileptic spikes (EEG), glucose metabolism (FDG–PET)	EEG, PET	Barrington et al. (1998)
	Epileptic spikes (intracranial EEG), BOLD (fMRI)	icEEG, fMRI	Sharma et al. (2019)
Sharp waves	Epileptic spikes (intracranial EEG), BOLD (fMRI)	icEEG, MRI	Murta et al. (2016)
Evoked brain activity dependent on sleep state	Sleep stage (EEG), evoked potential (EEG), BOLD (fMRI)	EEG, MRI	Portas et al. (2000)
Pericentral alpha and beta rhythms	Pericentral rhythms (EEG), BOLD (fMRI)	EEG, fMRI	Ritter et al. (2009)

Table 1.7 (continued)

Neurophysiological event	Measurement parameters	Combination of methods	References
Gamma band oscillation	40 Hz oscillation (EEG), BOLD (fMRI)	EEG, fMRI	Foucher et al. (2003)
Sleep-related EEG patterns	Sleep spindles and K-complexes, BOLD (fMRI) 0.5–2 Hz slow waves during NREM sleep, BOLD (fMRI) CMRO2 at transition from wakefulness to sleep EEG synchronisation phases of sleep instability, BOLD (fMRI)	EEG, fMRI	Caporro et al. (2012) Betta et al. (2021) Caporale et al. (2021) Kokkinos et al. (2019)
Bursts of action potentials (spike bursts)	High-frequency oscillations (600 Hz) in EEG, BOLD (fMRI)	High-frequency EEG and fMRI	Ritter et al. (2008)
Evoked potentials (EEG) and evoked magnetic fields (MEG) (orthogonal to each other), both reflecting synaptic activity		MEG and EEG	Siedenberg et al. (1996)
Spreading depression	Cell swelling assessed by DWI and DC–EEG Cell swelling assessed by DC–EEG and changes in light scattering and haemoglobin oxygenation assessed by NIRS	MRI, EEG MRI, NIRS	Busch et al. (1995) Kohl et al. (1998)
Slow neuronal events and vascular response Phase-amplitude coupling	Slow neuronal depolarisation changes assessed by DC–MEG; changes in haemoglobin oxygenation assessed by NIRS Motor task-related electrophysiological rhythmic activities (intracranial EEG) and BOLD (fMRI)	NIRS, MEG icEEG, MRI	Mackert et al. (2004, 2008) Murta et al. (2017)

1.4.3 Symmetrical Data Fusion

The bias intrinsic to asymmetric data analysis strategies may reflect a preference on the part of the investigator, due to greater familiarity with, or better characterisation of (e.g. due to historical precedence), one of the signals of interest. As the

relationship between signals from different modalities and the underlying generative mechanisms becomes better understood, this form of bias may diminish, and more symmetric data integration strategies can emerge. For example, heuristic models of the relationship between EEG and BOLD can be integrated into joint source estimation schemes (Daunizeau et al. 2007; Brookings et al. 2009; Tan et al. 2015).

Some investigators have proposed a more fundamental approach to data integration aimed at creating biophysical models that relate the data from each modality within a unified framework in order to overcome current limitations in the interpretation of multimodal data and ultimately relate observations to the fundamental brain mechanisms. For example, while overlaying PET or NIRS activation maps with structural MRI can give an impression of a precise relationship between brain activity and structure, our understanding is ultimately limited by the lack of a proper model relating the two. This is also the case for the superposition of EP time courses at the millisecond time scale over fMRI activation sites that spatially coincide with electrical or magnetic source estimates. The spatial integration of EEG and fMRI is a much more complex issue than simply one offering another (independent) dimension to the other.

Data fusion at this neurophysiological level will require new computational models that link neuronal activity to haemodynamic, electrical, magnetic and other observables. This fundamental development represents the next frontier in neuroimaging and will be discussed in Chaps. 25, 28 and 29.

1.5 Summary

Multimodal brain imaging is a key tool for gaining a comprehensive understanding of brain activity, since any single imaging method is limited to observing a limited aspect of brain function. We have noted that the validation of one imaging method using another has been a common reason for employing multimodal approaches over the last few years and that various combinations of imaging methods may be useful, depending on the specific research questions that are being asked. However, the combination of information about the electrical activity of the brain with data on the corresponding haemodynamic changes, which offers superior spatial information, represents one of the most powerful examples of a multimodal imaging technique and is one that is capable of providing new insights into brain function. While data acquired in separate sessions can be appropriate for some research questions, only simultaneous EEG–fMRI offers the opportunity to relate both modalities to actual brain events, an issue that is relevant to not only epilepsy but also numerous research questions in basic and cognitive neuroscience. In these cases, we believe that the extra effort required to deal with the specific practical problems of such a combination is easily outweighed by the potential new insights into human brain function that it offers. We hope to demonstrate this in the rest of this book.

References

Allen PJ, Josephs O, Turner R (2000) A method for removing imaging artifact from continuous EEG recorded during functional MRI. NeuroImage 12(2):230–239

Allen PJ, Polizzi G, Krakow K, Fish DR, Lemieux L (1998) Identification of EEG events in the MR scanner: the problem of pulse artifact and a method for its subtraction. NeuroImage 8(3):229–239

Antal A, Polania R, Schmidt-Samoa C, Dechent P, Paulus W (2011) Transcranial direct current stimulation over the primary motor cortex during fMRI. NeuroImage 55(2):590–596

Babiloni F, Babiloni C, Carducci F, Romani GL, Rossini PM, Angelone LM, Cincotti F (2003) Multimodal integration of high-resolution EEG and functional magnetic resonance imaging data: a simulation study. NeuroImage 19(1):1–15

Bandettini PA, Wong EC, Hinks RS, Tikofsky RS, Hyde JS (1992) Time course EPI of human brain function during task activation. Magn Reson Med 25(2):390–397

Barrington SF, Koutroumanidis M, Agathonikou A, Marsden PK, Binnie CD, Polkey CE, Maisey MN, Panayiotopoulos CP (1998) Clinical value of "ictal" FDG-positron emission tomography and the routine use of simultaneous scalp EEG studies in patients with intractable partial epilepsies. Epilepsia 39(7):753–766

Becker R, Ritter P, Moosmann M, Villringer A (2005) Visual evoked potentials recovered from fMRI scan periods. Hum Brain Mapp 26:221–230

Benar C, Aghakhani Y, Wang Y, Izenberg A, Al Asmi A, Dubeau F, Gotman J (2003) Quality of EEG in simultaneous EEG-fMRI for epilepsy. Clin Neurophysiol 114:569–580

Benar CG, Schon D, Grimault S, Nazarian B, Burle B, Roth M, Badier JM, Marquis P, Liegeois-Chauvel C, Anton JL (2007) Single-trial analysis of oddball event-related potentials in simultaneous EEG-fMRI. Hum Brain Mapp 28:602–613

Bestmann S, Baudewig J, Frahm J (2003) On the synchronization of transcranial magnetic stimulation and functional echo-planar imaging. J Magn Reson Imaging 17(3):309–316

Betta M, Handjaras G, Leo A, Federici A, Farinelli V, Ricciardi E, Siclari F, Meletti S, Ballotta D, Benuzzi F, Bernardi G (2021) Cortical and subcortical hemodynamic changes during sleep slow waves in human light sleep. NeuroImage 236:118117

Beyer T, Townsend DW, Brun T, Kinahan PE, Charron M, Roddy R, Jerin J, Young J, Byars L, Nutt R (2000) A combined PET/CT scanner for clinical oncology. J Nucl Med 41(8):1369–79

Bohning DE, Shastri A, Nahas Z, Lorberbaum JP, Andersen SW, Dannels WR, Haxthausen EU, Vincent DJ, George MS (1998) Echoplanar BOLD fMRI of brain activation induced by concurrent transcranial magnetic stimulation. Investig Radiol 33(6):336–340

Bonmassar G, Anami K, Ives J, Belliveau JW (1999) Visual evoked potential (VEP) measured by simultaneous 64-channel EEG and 3T fMRI. Neuroreport 10(9):1893–1897

Bonmassar G, Schwartz DP, Liu AK, Kwong KK, Dale AM, Belliveau JW (2001) Spatiotemporal brain imaging of visual-evoked activity using interleaved EEG and fMRI recordings. NeuroImage 13(6 Pt 1):1035–1043

Brandt SA, Davis TL, Obrig H, Meyer BU, Belliveau JW, Rosen BR, Villringer A (1996) Functional magnetic resonance imaging shows localized brain activation during serial transcranial stimulation in man. Neuroreport 7:734–736

Brookings T, Ortigue S, Grafton S, Carlson J (2009) Using ICA and realistic BOLD models to obtain joint EEG/fMRI solutions to the problem of source localization. NeuroImage 44:411–420

Buchheim K, Obrig H, v Pannwitz W, Müller A, Heekeren H, Villringer A, Meierkord H (2004) Decrease in haemoglobin oxygenation during absence seizures in adult humans. Neurosci Lett 354(2):119–122

Buchner H, Fuchs M, Wischmann HA, Dössel O, Ludwig I, Knepper A, Berg P (1994) Source analysis of median nerve and finger stimulated somatosensory evoked potentials: multichannel simultaneous recording of electric and magnetic fields combined with 3D-MR tomography. Brain Topogr 6(4):299–310

Buchsbaum MS, Kessler R, King A, Johnson J, Cappelletti J (1984) Simultaneous cerebral glucography with positron emission tomography and topographic electroencephalography. Prog Brain Res 62:263–9. https://doi.org/10.1016/S0079-6123(08)62182-2. PMID: 6335920

Busch E, Hoehn-Berlage M, Eis M, Gyngell ML, Hossmann KA (1995) Simultaneous recording of EEG, DC potential and diffusion-weighted NMR imaging during potassium induced cortical spreading depression in rats. NMR Biomed 8(2):59–64

Caporale A, Lee H, Lei H, Rao H, Langham MC, Detre JA, Wu PH, Wehrli FW (2021) Cerebral metabolic rate of oxygen during transition from wakefulness to sleep measured with high temporal resolution OxFlow MRI with concurrent EEG. J Cereb Blood Flow Metab 41(4):780–792

Caporro M, Haneef Z, Yeh HJ, Lenartowicz A, Buttinelli C, Parvizi J, Stern JM (2012) Functional MRI of sleep spindles and K-complexes. Clin Neurophysiol 123(2):303–309

Carmichael DW, Hamandi K, Laufs H, Duncan JS, Thomas DL, Lemieux L (2008) An investigation of the relationship between BOLD and perfusion signal changes during epileptic generalised spike wave activity. Magn Reson Imaging 26:870–873

Catana C, Procissi D, Wu Y, Judenhofer MS, Qi J, Pichler BJ, Jacobs RE, Cherry SR (2008) Simultaneous in vivo positron emission tomography and magnetic resonance imaging. Proc Natl Acad Sci U S A 105(10):3705–3710

Cho J, Lee J, An H, Goyal MS, Su Y, Wang Y (2021) Cerebral oxygen extraction fraction (OEF): comparison of challenge-free gradient echo QSM+qBOLD (QQ) with (15)O PET in healthy adults. J Cereb Blood Flow Metab 41(7):1658–1668

Daunizeau J, Mattout J, Clonda D, Goulard B, Benali H, Lina JM (2006) Bayesian spatio-temporal approach for EEG source reconstruction: conciliating ECD and distributed models. IEEE Trans Biomed Eng 53(3):503–16. https://doi.org/10.1109/TBME.2005.869791

Daunizeau J, Grova C, Marrelec G, Mattout J, Jbabdi S, Pelegrini-Issac M, Lina JM, Benali H (2007) Symmetrical event-related EEG/fMRI information fusion in a variational Bayesian framework. NeuroImage 36:69–87

Debener S, Ullsperger M, Siegel M, Fiehler K, von Cramon DY, Engel AK (2005) Trial-by-trial coupling of concurrent electroencephalogram and functional magnetic resonance imaging identifies the dynamics of performance monitoring. J Neurosci 25(50):11730–11737

Eichele T, Specht K, Moosmann M, Jongsma ML, Quiroga RQ, Nordby H, Hugdahl K (2005) Assessing the spatiotemporal evolution of neuronal activation with single-trial event-related potentials and functional MRI. Proc Natl Acad Sci U S A 102:17798–17803

Fan AP, Guo J, Khalighi MM, Gulaka PK, Shen B, Park JH, Gandhi H, Holley D, Rutledge O, Singh P, Haywood T, Steinberg GK, Chin FT, Zaharchuk G (2017) Long-delay arterial spin labeling provides more accurate cerebral blood flow measurements in Moyamoya patients: a simultaneous positron emission tomography/MRI study. Stroke 48(9):2441–2449

Faria P, Fregni F, Sebastião F, Dias AI, Leal A (2012) Feasibility of focal transcranial DC polarization with simultaneous EEG recording: preliminary assessment in healthy subjects and human epilepsy. Epilepsy Behav 25(3):417–425

Fazli S, Mehnert J, Steinbrink J, Curio G, Villringer A, Müller KR, Blankertz B (2012) Enhanced performance by a hybrid NIRS-EEG brain computer interface. NeuroImage 59(1):519–529

Foucher JR, Otzenberger H, Gounot D (2003) The BOLD response and the gamma oscillations respond differently than evoked potentials: an interleaved EEG-fMRI study. BMC Neurosci 4:22

Frahm J, Bruhn H, Merboldt KD, Hänicke W (1992) Dynamic MR imaging of human brain oxygenation during rest and photic stimulation. J Magn Reson Imaging 2(5):501–505

Gamma A, Lehmann D, Frei E, Iwata K, Pascual-Marqui RD, Vollenweider FX (2004) Comparison of simultaneously recorded [$H_2{}^{15}O$]-PET and LORETA during cognitive and pharmacological activation. Hum Brain Mapp 22(2):83–96

Goldman RI, Stern JM, Engel J Jr, Cohen MS (2000) Acquiring simultaneous EEG and functional MRI. Clin Neurophysiol 111(11):1974–1980

Goldman RI, Stern JM, Engel J Jr, Cohen MS (2002) Simultaneous EEG and fMRI of the alpha rhythm. Neuroreport 13(18):2487–2492

Grimm C, Schreiber A, Kristeva-Feige R, Mergner T, Hennig J, Lucking CH (1998) A comparison between electric source localisation and fMRI during somatosensory stimulation. Electroencephalogr Clin Neurophysiol 106:22–29

Hamandi K, Laufs H, Noth U, Carmichael DW, Duncan JS, Lemieux L (2008) BOLD and perfusion changes during epileptic generalised spike wave activity. NeuroImage 39:608–618

Heinze HJ, Mangun GR, Burchert W, Hinrichs H, Scholz M, Munte TF, Gos A, Scherg M, Johannes S, Hundeshagen H (1994) Combined spatial and temporal imaging of brain activity during visual selective attention in humans. Nature 372:543–546

Horovitz SG, Gore JC (2004) Simultaneous event-related potential and near-infrared spectroscopic studies of semantic processing. Hum Brain Mapp 22(2):110–115

Hoshi Y, Mizukami S, Tamura M (1994) Dynamic features of hemodynamic and metabolic changes in the human brain during all-night sleep as revealed by near-infrared spectroscopy. Brain Res 652(2):257–262

Ives JR, Warach S, Schmitt F, Edelman RR, Schomer DL (1993) Monitoring the patient's EEG during echo planar MRI. Electroencephalogr Clin Neurophysiol 87:417–420

Jindal U, Sood M, Dutta A, Chowdhury SR (2015) Development of point of care testing device for neurovascular coupling from simultaneous recording of EEG and NIRS during anodal transcranial direct current stimulation. IEEE J Transl Eng Health Med 3:2000112

Judenhofer MS, Wehrl HF, Newport DF, Catana C, Siegel SB, Becker M, Thielscher A, Kneilling M, Lichy MP, Eichner M, Klingel K, Reischl G, Widmaier S, Röcken M, Nutt RE, Machulla HJ, Uludag K, Cherry SR, Claussen CD, Pichler BJ (2008) Simultaneous PET-MRI: a new approach for functional and morphological imaging. Nat Med 14(4):459–465

Kähkönen S, Wilenius J, Komssi S, Ilmoniemi RJ (2004) Distinct differences in cortical reactivity of motor and prefrontal cortices to magnetic stimulation. Clin Neurophysiol 115(3):583–588

Kida I, Yamamoto T, Tamura M (1996) Interpretation of BOLD MRI signals in rat brain using simultaneously measured near-infrared spectrophotometric information. NMR Biomed 9(8):333–338

Kim H, Hua Y, Chen HT, Tsai HM, Chen CT, Karczmar G, Fan X, Xi D, Xie Q, Chou CY, Kao CM (2020) Design, evaluation and initial imaging results of a PET insert based on strip-line readout for simultaneous PET/MRI. Nucl Instrum Methods Phys Res A 959:163575

Kirkpatrick PJ, Lam J, Al-Rawi P, Smielewski P, Czosnyka M (1998) Defining thresholds for critical ischemia by using near-infrared spectroscopy in the adult brain. J Neurosurg 89(3):389–394

Klaessens JH, Hopman JC, van Wijk MC, Djien Liem K, Thijssen JM (2005) Assessment of local changes of cerebral perfusion and blood concentration by near infrared spectroscopy and ultrasound contrast densitometry. Brain and Development 27(6):406–414

Kleinschmidt A, Obrig H, Requardt M, Merboldt KD, Dirnagl U, Villringer A, Frahm J (1996) Simultaneous recording of cerebral blood oxygenation changes during human brain activation by magnetic resonance imaging and near-infrared spectroscopy. J Cereb Blood Flow Metab 16(5):817–826

Kohl M, Lindauer U, Dirnagl U, Villringer A (1998) Separation of changes in light scattering and chromophore concentrations during cortical spreading depression in rats. Opt Lett 23(7):555–557

Kokkinos V, Vulliémoz S, Koupparis AM, Koutroumanidis M, Kostopoulos GK, Lemieux L, Garganis K (2019) A hemodynamic network involving the insula, the cingulate, and the basal forebrain correlates with EEG synchronization phases of sleep instability. Sleep 42(4):zsy259

Krakow K, Allen PJ, Symms MR, Lemieux L, Josephs O, Fish DR (2000) EEG recording during fMRI experiments: image quality. Hum Brain Mapp 10(1):10–15

Krakow K, Lemieux L, Messina D, Scott CA, Symms MR, Duncan JS, Fish DR (2001a) Spatio-temporal imaging of focal interictal epileptiform activity using EEG-triggered functional MRI. Epileptic Disord 3(2):67–74

Krakow K, Messina D, Lemieux L, Duncan JS, Fish DR (2001b) Functional MRI activation of individual interictal epileptiform spikes. NeuroImage 13(3):502–505

Kwong KK, Belliveau JW, Chesler DA, Goldberg IE, Weisskoff RM, Poncelet BP, Kennedy DN, Hoppel BE, Cohen MS, Turner R, Brady TJ, Rosen BR (1992) Dynamic magnetic resonance imaging of human brain activity during primary sensory stimulation. Proc Natl Acad Sci U S A 89(12):5675–5679

Laufs H, Kleinschmidt A, Beyerle A, Eger E, Salek-Haddadi A, Preibisch C, Krakow K (2003) EEG-correlated fMRI of human alpha activity. NeuroImage 19:1463–1476

Legon W, Ai L, Bansal P, Mueller JK (2018) Neuromodulation with single-element transcranial focused ultrasound in human thalamus. Hum Brain Mapp 39(5):1995–2006

Legon W, Sato TF, Opitz A, Mueller J, Barbour A, Williams A, Tyler WJ (2014) Transcranial focused ultrasound modulates the activity of primary somatosensory cortex in humans. Nat Neurosci 17(2):322–329

Lemieux L, Allen PJ, Franconi F, Symms MR, Fish DR (1997) Recording of EEG during fMRI experiments: patient safety. Magn Reson Med 38(6):943–952

Lemieux L, Krakow K, Fish DR (2001a) Comparison of spike-triggered functional MRI BOLD activation and EEG dipole model localization. NeuroImage 14(5):1097–1104

Lemieux L, Salek-Haddadi A, Josephs O, Allen P, Toms N, Scott C, Krakow K, Turner R, Fish DR (2001b) Event-related fMRI with simultaneous and continuous EEG: description of the method and initial case report. NeuroImage 14(3):780–787

Liu AK, Belliveau JW, Dale AM (1998) Spatiotemporal imaging of human brain activity using functional MRI constrained magnetoencephalography data: Monte Carlo simulations. Proc Natl Acad Sci U S A 95:8945–8950

Mackert BM, Leistner S, Sander T, Liebert A, Wabnitz H, Burghoff M, Trahms L, Macdonald R, Curio G (2008) Dynamics of cortical neurovascular coupling analyzed by simultaneous DC-magnetoencephalography and time-resolved near-infrared spectroscopy. NeuroImage 39(3):979–986

Mackert BM, Wübbeler G, Leistner S, Uludag K, Obrig H, Villringer A, Trahms L, Curio G (2004) Neurovascular coupling analyzed non-invasively in the human brain. Neuroreport 15(1):63–66

McDannold N, Moss M, Killiany R, Rosene DL, King RL, Jolesz FA, Hynynen K (2003) MRI-guided focused ultrasound surgery in the brain: tests in a primate model. Magn Reson Med 49(6):1188–1191

Mehagnoul-Schipper DJ, van der Kallen BF, Colier WN, van der Sluijs MC, van Erning LJ, Thijssen HO, Oeseburg B, Hoefnagels WH, Jansen RW (2002) Simultaneous measurements of cerebral oxygenation changes during brain activation by near-infrared spectroscopy and functional magnetic resonance imaging in healthy young and elderly subjects. Hum Brain Mapp 16(1):14–23

Menon V, Ford JM, Lim KO, Glover GH, Pfefferbaum A (1997) Combined event-related fMRI and EEG evidence for temporal-parietal cortex activation during target detection. Neuroreport 8:3029–3037

Mochizuki H, Ugawa Y, Terao Y, Sakai KL (2006) Cortical hemoglobin-concentration changes under the coil induced by single-pulse TMS in humans: a simultaneous recording with near-infrared spectroscopy. Exp Brain Res 169(3):302–310

Moosmann M, Ritter P, Krastel I, Brink A, Thees S, Blankenburg F, Taskin B, Obrig H, Villringer A (2003) Correlates of alpha rhythm in functional magnetic resonance imaging and near infrared spectroscopy. NeuroImage 20:145–158

Mulert C, Jäger L, Schmitt R, Bussfeld P, Pogarell O, Möller HJ, Juckel G, Hegerl U (2004) Integration of fMRI and simultaneous EEG: towards a comprehensive understanding of localization and time-course of brain activity in target detection. NeuroImage 22(1):83–94

Mulert C, Seifert C, Leicht G, Kirsch V, Ertl M, Karch S, Moosmann M, Lutz J, Möller HJ, Hegerl U, Pogarell O, Jäger L (2008) Single-trial coupling of EEG and fMRI reveals the involvement of early anterior cingulate cortex activation in effortful decision making. NeuroImage 42(1):158–168

Murta T, Chaudhary UJ, Tierney TM, Dias A, Leite M, Carmichael DW, Figueiredo P, Lemieux L (2017) Phase-amplitude coupling and the BOLD signal: a simultaneous intracranial EEG (icEEG)—fMRI study in humans performing a finger-tapping task. NeuroImage 146:438–451

Murta T, Hu L, Tierney TM, Chaudhary UJ, Walker MC, Carmichael DW, Figueiredo P, Lemieux L (2016) A study of the electro-haemodynamic coupling using simultaneously acquired intracranial EEG and fMRI data in humans. NeuroImage 142:371–380

Neuner I, Warbrick T, Arrubla J, Felder J, Celik A, Reske M, Boers F, Shah NJ (2013) EEG acquisition in ultra-high static magnetic fields up to 9.4 T. NeuroImage 68:214–220

Obrig H, Israel H, Kohl-Bareis M, Uludag K, Wenzel R, Müller B, Arnold G, Villringer A (2002) Habituation of the visually evoked potential and its vascular response: implications for neurovascular coupling in the healthy adult. NeuroImage 17(1):1–18

Ogawa S, Lee TM, Kay AR, Tank DW (1990) Brain magnetic resonance imaging with contrast dependent on blood oxygenation. Proc Natl Acad Sci U S A 87(24):9868–9872

Ogawa S, Tank DW, Menon R, Ellermann JM, Kim SG, Merkle H, Ugurbil K (1992) Intrinsic signal changes accompanying sensory stimulation: functional brain mapping with magnetic resonance imaging. Proc Natl Acad Sci U S A 89(13):5951–5955

Paus T, Jech R, Thompson CJ, Comeau R, Peters T, Evans AC (1997) Transcranial magnetic stimulation during positron emission tomography: a new method for studying connectivity of the human cerebral cortex. J Neurosci 17(9):3178–3184

Paus T, Sipila PK, Strafella AP (2001) Synchronization of neuronal activity in the human primary motor cortex by transcranial magnetic stimulation: an EEG study. J Neurophysiol 86(4):1983–1990

Peters JC, Reithler J, Graaf TA, Schuhmann T, Goebel R, Sack AT (2020) Concurrent human TMS-EEG-fMRI enables monitoring of oscillatory brain state-dependent gating of cortico-subcortical network activity. Commun Biol 3(1):40

Plummer C, Vogrin SJ, Woods WP, Murphy MA, Cook MJ, Liley DTJ (2019) Interictal and ictal source localization for epilepsy surgery using high-density EEG with MEG: a prospective long-term study. Brain 142(4):932–951

Polinder-Bos HA, Elting JWJ, Aries MJ, García DV, Willemsen AT, van Laar PJ, Kuipers J, Krijnen WP, Slart RH, Luurtsema G, Westerhuis R, Gansevoort RT, Gaillard CA, Franssen CF (2020) Changes in cerebral oxygenation and cerebral blood flow during hemodialysis—a simultaneous near-infrared spectroscopy and positron emission tomography study. J Cereb Blood Flow Metab 40(2):328–340

Portas CM, Krakow K, Allen P, Josephs O, Armony JL, Frith CD (2000) Auditory processing across the sleep-wake cycle: simultaneous EEG and fMRI monitoring in humans. Neuron 28(3):991–999

Pugnaghi M, Carmichael DW, Vaudano AE, Chaudhary UJ, Benuzzi F, Di Bonaventura C, Giallonardo AT, Rodionov R, Walker MC, Duncan JS, Meletti S, Lemieux L (2014) Generalized spike and waves: effect of discharge duration on brain networks as revealed by BOLD fMRI. Brain Topogr 27(1):123–137

Punwani S, Ordidge RJ, Cooper CE, Amess P, Clemence M (1998) MRI measurements of cerebral deoxyhaemoglobin concentration [dHb]—correlation with near infrared spectroscopy (NIRS). NMR Biomed 11(6):281–289

Ritter P, Freyer F, Curio G, Villringer A (2008) High-frequency (600 Hz) population spikes in human EEG delineate thalamic and cortical fMRI activation sites. Neuroimage 42(2):483–90. https://doi.org/10.1016/j.neuroimage.2008.05.026

Ritter P, Moosmann M, Villringer A (2009) Rolandic alpha and beta EEG rhythms' strengths are inversely related to fMRI-BOLD signal in primary somatosensory and motor cortex1. Hum Brain Mapp 30:1168–1187

Ruff CC, Blankenburg F, Bjoertomt O, Bestmann S, Freeman E, Haynes JD, Rees G, Josephs O, Deichmann R, Driver J (2006) Curr Biol 16(15):1479–1488

Sabri O, Owega A, Schreckenberger M, Sturz L, Fimm B, Kunert P, Meyer PT, Sander D, Klingelhöfer J (2003) A truly simultaneous combination of functional transcranial Doppler sonography and $H_2{}^{15}O$ PET adds fundamental new information on differences in cognitive activation between schizophrenics and healthy control subjects. J Nucl Med 44(5):671–681

Sadato N, Nakamura S, Oohashi T, Nishina E, Fuwamoto Y, Waki A, Yonekura Y (1998) Neural networks for generation and suppression of alpha rhythm: a PET study. Neuroreport 9(5):893–897

Salustri C, Chapman RM (1989) A simple method for 3-dimensional localization of epileptic activity recorded by simultaneous EEG and MEG. Electroencephalogr Clin Neurophysiol 73(6):473–478

Seki Y, Miyashita T, Kandori A, Maki A, Koizumi H (2012) Simultaneous measurement of neuronal activity and cortical hemodynamics by unshielded magnetoencephalography and near-infrared spectroscopy. J Biomed Opt 17(10):107001

Sharma NK, Pedreira C, Chaudhary UJ, Centeno M, Carmichael DW, Yadee T, Murta T, Diehl B, Lemieux L (2019) BOLD mapping of human epileptic spikes recorded during simultaneous intracranial EEG-fMRI: the impact of automated spike classification. NeuroImage 184:981–992

Sheridan PH, Sato S, Foster N, Bruno G, Cox C, Fedio P, Chase TN (1988) Relation of EEG alpha background to parietal lobe function in Alzheimer's disease as measured by positron emission tomography and psychometry. Neurology 38(5):747–750

Shin J, von Lühmann A, Kim DW, Mehnert J, Hwang HJ, Müller KR (2018) Simultaneous acquisition of EEG and NIRS during cognitive tasks for an open access dataset. Sci Data 5:180003

Siedenberg R, Goodin DS, Aminoff MJ, Rowley HA, Roberts TP (1996) Abstract comparison of late components in simultaneously recorded event-related electrical potentials and event-related magnetic fields. Electroencephalogr Clin Neurophysiol 99(2):191–194

Stancak A, Polacek H, Vrana J, Rachmanova R, Hoechstetter K, Tintra J, Scherg M (2005) EEG source analysis and fMRI reveal two electrical sources in the fronto-parietal operculum during subepidermal finger stimulation. NeuroImage 25:8–20

Stefan H, Schneider S, Feistel H, Pawlik G, Schuler P, Abraham Fuchs K, Schlegel T, Neubauer U, Huk WJ (1992) Ictal and interictal activity in partial epilepsy recorded with multichannel magnetoelectroencephalography: correlation of electroencephalography/electrocorticography, magnetic resonance imaging, single photon emission computed tomography, and positron emission tomography findings. Epilepsia 33:874–887

Steinhoff BJ, Herrendorf G, Kurth C (1996) Ictal near infrared spectroscopy in temporal lobe epilepsy: a pilot study. Seizure 5(2):97–101

Strangman G, Culver JP, Thompson JH, Boas DA (2002) A quantitative comparison of simultaneous BOLD fMRI and NIRS recordings during functional brain activation. NeuroImage 17(2):719–731

Tan A, Fu Z, Tu Y, Hung YS, Zhang Z (2015) Joint source separation of simultaneous EEG-fMRI recording in two experimental conditions using common spatial patterns. Annu Int Conf IEEE Eng Med Biol Soc 2015(2015):2633–2636

Terborg C, Birkner T, Schack B, Weiller C, Röther J (2003) Noninvasive monitoring of cerebral oxygenation during vasomotor reactivity tests by a new near-infrared spectroscopy device. Cerebrovasc Dis 16(1):36–41

Toronov V, Webb A, Choi JH, Wolf M, Michalos A, Gratton E, Hueber D (2001) Investigation of human brain hemodynamics by simultaneous near-infrared spectroscopy and functional magnetic resonance imaging. Med Phys 28(4):521–527

Turner R, Le Bihan D, Moonen CT, Despres D, Frank J (1991) Echo-planar time course MRI of cat brain oxygenation changes. Magn Reson Med 22(1):159–166

Vasios CE, Angelone LM, Purdon PL, Ahveninen J, Belliveau JW, Bonmassar G (2006) EEG/(f) MRI measurements at 7 Tesla using a new EEG cap ("InkCap"). NeuroImage 33(4):1082–1092

Villringer A, Dirnagl U (1995) Coupling of brain activity and cerebral blood flow: basis of functional neuroimaging. Cerebrovasc Brain Metab Rev 7(3):240–276

Villringer K, Minoshima S, Hock C, Obrig H, Ziegler S, Dirnagl U, Schwaiger M, Villringer A (1997) Comparison of near infrared spectroscopy and positron emission tomography in the assessment of frontal brain activation in humans. Adv Exp Med Biol 413:149–153

Walter H, Kristeva R, Knorr U, Schlaug G, Huang Y, Steinmetz H, Nebeling B, Herzog H, Seitz RJ (1992) Individual somatotopy of primary sensorimotor cortex revealed by intermodal matching of MEG, PET, and MRI. Brain Topogr 5:183–187

Warach S, Ives JR, Schlaug G, Patel MR, Darby DG, Thangaraj V, Edelman RR, Schomer DL (1996) EEG-triggered echo-planar functional MRI in epilepsy. Neurology 47(1):89–93

Warach S, Levin JM, Schomer DL, Holman BL, Edelman RR (1994) Hyperperfusion of ictal seizure focus demonstrated by MR perfusion imaging. AJNR Am J Neuroradiol 15(5):965–968

Zotev VS, Matlashov AN, Volegov PL, Savukov IM, Espy MA, Mosher JC, Gomez JJ, Kraus RH Jr (2008) Microtesla MRI of the human brain combined with MEG. J Magn Reson 194:115–120

Zotev V, Phillips R, Yuan H, Misaki M, Bodurka J (2014) Self-regulation of human brain activity using simultaneous real-time fMRI and EEG neurofeedback. NeuroImage 85(Pt 3):985–995

EEG: Origin and Measurement

2

Fernando Lopes da Silva

2.1 Introduction to the Electrophysiology of the Brain

The existence of the electrical activity of the brain (i.e. the electroencephalogram or EEG) was discovered more than a century ago by Caton (1875). After the demonstration that the EEG could be recorded from the human scalp by Berger in the 1920s (Berger 1929), it made a slow start before it became accepted as a method of analysis of brain functions in health and disease. It is interesting to note that this acceptance came only after the demonstration by Adrian and Mathews (1934) that the EEG, namely, the alpha rhythm, was likely generated in the occipital lobes in man and was not artefactual. However, the neuronal sources of the alpha rhythm remained undefined until the 1970s, when we demonstrated, in dog, that the alpha rhythm is generated by a dipole layer centred in layers IV and V of the visual cortex (Lopes da Silva and Storm van Leeuwen 1977). It may be not surprising that the mechanisms of generation and the functional significance of the EEG remained controversial for a relatively long time considering the complexity of the underlying systems of neuronal generators on the one hand and the rather involved transfer of signals from the cortical surface to the scalp due to the topological and electrical properties of the volume conductor (brain, cerebrospinal fluid, skull, scalp) on the other.

Fernando Lopes da Silva passed away before publication of this work was completed (Michel 2019).

F. L. da Silva (✉)
Centre of NeuroSciences, Swammerdam Institute for Life Sciences, University of Amsterdam, Amsterdam, The Netherlands

Department of Bioengineering, Instituto Superior Técnico, Universidade de Lisboa, Lisbon, Portugal
e-mail: louis.lemieux@ucl.ac.uk

C. Mulert, L. Lemieux (eds.), *EEG - fMRI*,
https://doi.org/10.1007/978-3-031-07121-8_2

The EEG consists of the summed electrical activities of populations of neurons, with a modest contribution from glial cells. The neurons are excitable cells with characteristic intrinsic electrical properties, and their activity produces electrical and magnetic fields. These fields may be recorded by means of electrodes at a short distance from the sources (the local EEG or local field potentials, LFPs) or from the cortical surface (the electrocorticogram or ECoG), or at longer distances, even from the scalp (i.e. the EEG, in the most common sense). The associated MEG is usually recorded via sensors, which are placed at short distances around the scalp and are highly sensitive to changes of the very weak neuronal magnetic fields.

2.2 Origin of EEG and MEG: Cellular Sources

Neurons generate time-varying electrical currents when activated. These are ionic currents generated at the level of cellular membranes; in other words, they consist of transmembrane currents. We can distinguish two main forms of neuronal activation (Lopes da Silva and van Rotterdam 2005; Lopes da Silva 2002; Nunez 1995): the fast depolarisation of the neuronal membranes, which results in the action potential mediated by sodium and potassium voltage-dependent ionic conductances gNa and gK (DR), and the slower changes in membrane potential due to synaptic activation, mediated by several neurotransmitter systems. The action potential consists of a rapid change in membrane potential such that the intracellular potential suddenly jumps from negative to positive and quickly (in 1 or 2 ms) returns to the resting intracellular negativity. In this way, an impulse is generated that has the remarkable property of propagating along axons and dendrites without loss of amplitude. Regarding the slower postsynaptic potentials, two main kinds have to be distinguished, the excitatory (EPSPs) and the inhibitory (IPSPs) potentials, which depend on the kind of neurotransmitter and corresponding receptor and their interactions with specific ionic channels and/or intracellular second messengers.

Generally speaking, at the level of a synapse in the case of the EPSP, the transmembrane current is carried by positive ions inwards (e.g. Na^+). In the case of the IPSP, it is carried by negative ions inwards (e.g. Cl^-) or positive ions (e.g. K^+) outwards. Thus, the positive electric current is directed to the extracellular medium in the case of an EPSP and is directed from the inside of the neuron to the outside in the case of an IPSP (Fig. 2.1).

As a consequence of these currents, an active sink is generated in the extracellular medium at the level of an excitatory synapse, whereas in the case of an inhibitory synapse, an active source occurs. The flows of these compensating extracellularly currents depend on the electrical properties of the local tissue. Glial cells occupy an important part of the space between neurons and are coupled to one another by gap junctions. The conductivity of the latter is very sensitive to changes in pH and extracellular K^+ and Ca^{2+} and can therefore be modulated under various physiological and pathological conditions (Huang et al. 2005). Furthermore, the volume of the extracellular space may change under various physiological and pathological conditions, which will also be reflected in changes in tissue conductivity.

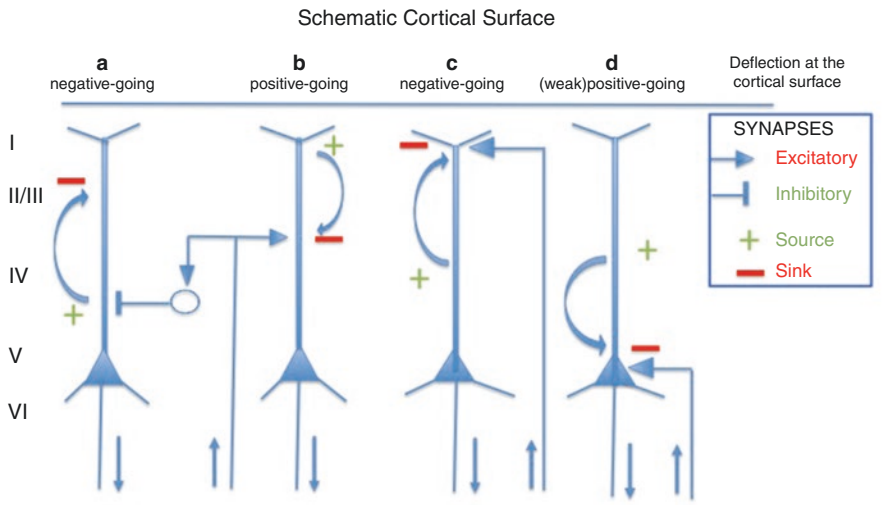

Fig. 2.1 Schematic representation of four typical cases of cortical generators of LFPs, elicited in one case by inhibitory (**a**) and in the other three (**b**, **c**, **d**) by excitatory synaptic activity, at different sites along the soma-dendritic membrane of a pyramidal cell with soma in layer V. The symbols representing excitatory and inhibitory synapses and sinks (−) and sources (+) are indicated in the inset on the right-hand side. The direction of extracellular currents is indicated by the curved arrows. (**a**) Inhibitory synaptic activity (note the extracellular current pointing away from the synapse) causing an active source at the level of layers IV/V and a more superficial sink in layers II/III. At the cortical surface, this would result in a negative-going deflection. Note that the interneuron (circle) represents a stellate cell that would generate an approximately closed field and would not generate a field potential measurable far from its source. (**b**) Excitatory synaptic activity on the apical dendrite of a pyramidal cell at the level of layers III/IV causing an extracellular active sink in the middle of the cortex and a passive source in superficial layers. This configuration would lead to a positive-going deflection at the cortical surface. (**c**) Excitatory synaptic activity at the level of the distal apical dendrite causing an active sink in superficial layers and a deeper-lying passive source; this would result in a negative-going deflection at the cortical surface. (**d**) Excitatory synaptic activation near the soma causes a local sink and a source in the middle cortical layers; this configuration would lead to a positive-going potential, but it would be relatively weak (smaller) due to the distance from the source to the cortical surface [*Own scheme, Adapted with permission from* Amzica and Lopes da Silva (2018). *In: Schomer DL, Lopes da Silva FH, eds. Niedermeyer's Electroencephalography: Basic Principles, Clinical Applications and Related Fields. 7th ed. Oxford University Press 2018: pp 20–62*]

Since there is no accumulation of charge anywhere in the medium, the transmembrane currents that flow in or out of the neuron at the active synaptic sites are compensated by currents that flow in the opposite direction elsewhere along the neuronal membrane. Consequently, in the case of an EPSP, besides the active sink at the level of the synapse, there are distributed passive sources along the soma-dendritic membrane. The opposite occurs in the case of an IPSP: besides the active source at the level of the synapse, distributed passive sinks are formed along the soma-dendritic membrane; this is illustrated in a very simplified form in Fig. 2.1.

Therefore, we can state that synaptic activity at a given site of the soma-dendritic membrane of a neuron causes a sink–source configuration in the extracellular

medium around the neurons. In the context of the present discussion, we have to take into consideration the geometry of the neuronal sources of electrical activity. Indeed, the neurons that mainly contribute to the MEG or the EEG are those that form "open fields" according to the classic description of Lorente de Nó (1947), i.e. the pyramidal neurons of the cortex, since the latter are arranged in palisades with the apical dendrites aligned perpendicularly to the cortical surface. Pyramidal neurons, when activated with a certain degree of synchrony, generate coherent electric/magnetic fields. In this way, these neurons are akin to "current dipoles", the activity of which can be detected by electrodes placed at relatively small distances. This description summarises the classic view, but more recent detailed studies by Riera et al. (2012) showed that extracellular potentials recorded in the rat barrel cortex do not sum to zero over the volume of a neocortical column, as one would expect according to the general description presented above. This implies that besides ohmic or resistive currents, currents due to ion diffusion should also be taken into account; in this way also cortical current source monopoles may transiently coexist along with dipolar sources at the microscopic scale. Monopoles, however, do not generate magnetic fields and are thus not seen in the MEG, contrary to the case of the EEG. This property should be considered when comparing simultaneously recorded EEG and MEG, particularly of evoked field potentials. These observations have been substantiated by modelling studies by Halnes et al. (2015) and Cabo and Riera (2014).

In quantitative terms, our current level of knowledge about the neuronal sources of EEG/MEG signals has benefited a great deal from recent model studies combining in vitro recordings and computational simulations, such as those proposed by the group of Yoshio Okada. These authors adapted the detailed compartmental models of Traub et al. (1994) and Traub and Miles (1991) and applied them to hippocampal slices kept in vitro and also to the neocortex. Measured electric and magnetic activities were compared with the theoretical results of a computer model. The study of Murakami and Okada (2006) in the neocortex is particularly relevant to the present discussion because it has yielded some results that may help interpret EEG and MEG recordings from the scalp. These authors made a computer model, based on that proposed by Mainen and Sejnowski (1996), of the four main types of cortical neurons, taking into account their realistic shapes. Each neuron is described as a 3D compartmental model, where each compartment has its typical geometric dimensions, passive electrical properties (membrane capacitance and resistance, intracellular resistance) and five voltage-dependent ionic conductances; the quantitative values of these variables were taken from the literature. For example, the maximal sodium conductance gNa was assumed to be 40 pS/μm^2 based on the measurements of Stuart and Sakman (1994), but several values were used in a trial-and-error way to reproduce experimental results. Neuronal activity was obtained by stimulating each neuron with an intracellular current injected at the soma. The intracellular current is represented by a vector quantity Q.

According to this model, the overall magnitude of Q for the activity of one pyramidal neuron of layers V and II/III is on the order of 0.29–0.90 pA, a value that is of the same order of magnitude as that estimated for hippocampal pyramidal

neurons (Okada et al. 1997). Murakami and Okada (2006) point out that, assuming a Q of 0.2 pA per cortical pyramidal neuron, a population of 50,000 synchronously active cells would generate a field with a magnitude of 10 nA, which corresponds precisely to the value measurable from the human cortex using the MEG according to Hämäläinen et al. (1993). According to the latter, the average value of the volume current density of the cerebral cortex is 175 nA/mm^2 (=nA mm/mm^3) for normal background activity. Assuming a cortical thickness of 3 mm, the average value of the corresponding surface current density is 525 nA/mm, and the average value of the dipole moment $m_i(t)$ associated with a neuronal population i of surface s_i is $M = s_i \times 525$ (nA mm).

Note that the quantitative description discussed above is valid assuming that the active cells are *synchronously active*. In many circumstances, however, the degree of synchrony, or correlation between different units, within a neuronal population can vary considerably. This implies that the degree of correlation in the population has a major influence on the size of LFPs measured at a distance. The contribution of elementary PSPS to LFPs recorded at a distance from the sources is, on average, more substantial than that of action potentials or spikes, since the former tend to be much more strongly correlated. Interestingly, modelling studies by Reimann et al. (2013) revealed that active currents (i.e. associated with spikes), not synaptic ones, can dominate the generation of LFPs, in the high-frequency range. This effect is stronger if the degree of correlation between the spikes within a neuronal population is large, namely, if it is mediated by "gap junctions" (also termed electrical synapses). Thus a local field may gather contributions both of low-frequency activities comprising postsynaptic LFPs and passive currents (dominant up to ±80 Hz) and higher-frequency activities that include, among other high-frequency oscillations (HFOs), as ripple (80–250 Hz) and fast-ripple (>250 Hz) oscillations.

We will return to these concepts when discussing volume conduction and source estimation.

2.3 Main Types of Rhythmical EEG/MEG Activities: Phenomenology and Functional Significance

We do not consider all different types of rhythmical activities that can be recorded from the brain here, only some prominent activities that are frequently the object of neurocognitive studies, namely, sleep rhythms, activities in the theta and alpha frequency range and beta/gamma rhythms. A comprehensive, erudite and thoughtful analysis of these and other brain rhythms can be found in Buzsáki's (2006) monography *Rhythms of the Brain*.

2.3.1 Sleep EEG Phenomena

In the neurophysiology of sleep, two classic EEG phenomena have been established: the *spindles* or waves between 7 and 14 Hz, also called sleep or *sigma*

spindles, which appear at sleep onset, and the *delta waves* (1–4 Hz), which are paradigmatic of deeper stages of sleep. Steriade and his group in Quebec described another *very slow oscillation* (0.6–1 Hz) in animals that is able to modulate the occurrence of different typical EEG sleep events, such as delta waves, sleep spindles and even short, high-frequency bursts (Amzica and Steriade 1998).

The very slow oscillation is generated within the cortex. All major classes of neurons in the cerebral cortex display this very slow oscillation. In the EEG one can distinguish a depth-positive wave (surface-negative) followed by a sharper depth-negative wave (surface-positive); during the depth-positive EEG wave, cortical neurons are hyperpolarised (corresponding to the deep sources shown in Fig. 2.1a), whereas during the sharp depth-negative EEG deflection, cortical neurons are depolarised (corresponding to the deep sinks shown in Fig. 2.1b). The synchronous activity between all types of cortical neurons and EEG relies on the integrity of intracortical synaptic connections. Blocking axonal transmission between two cortical sites through local micro-injections of lidocaine, the very slow oscillation survives at both locations and conserves some degree of synchronisation; this suggests that, besides direct intracortical connections, other connections, in particular cortico-thalamo-cortical pathways, as well as networks of gap junctions, might contribute to synchronise very slow oscillations across the cortex. For a more detailed account of the cellular and membrane processes underlying the very slow oscillation, see Amzica and Lopes da Silva (2018).

This very slow oscillation has now also been demonstrated in the human EEG and in the MEG, as indicated above. One of the functional correlates of the very slow cortical oscillation is the fact that, at the EEG level, each sequence of depolarising–hyperpolarising episodes within an oscillatory cycle corresponds to a waveform called K-complex.

The sleep spindles are generated in thalamo-cortical circuits and result from the interplay between intrinsic membrane properties of the thalamo-cortical relay (TCR) neurons and of the GABAergic neurons of the reticular nucleus and the properties of the circuits to which these neurons belong. It is clear that the spindles are a collective property of the neuronal populations. Experimental evidence has demonstrated that sleep spindle oscillations are generated in the thalamus since they can be recorded in this brain area after decortication and high brain stem transection. However, the very slow rhythm (0.6–1 Hz) is generated intracortically, since it survives thalamic lesions, but it is disrupted by intracortical lesions. Interestingly, we may note that the rhythmicity of the very slow oscillation appears to be reflected in that of the typical K-complexes of human EEG during non-REM sleep (Amzica and Steriade 1997).

One question is: how are these oscillations controlled by modulating systems? It is known that sleep spindles are under brain stem control. It is a well-known neurophysiological phenomenon that electrical stimulation of the brain stem can block thalamo-cortical oscillations, causing “EEG desynchronisation”, as shown in classic studies by Moruzzi and Magoun (1949). This desynchronisation is caused mainly by the activation of cholinergic inputs arising from the mesopontine cholinergic nuclei, namely, the pedunculopontine tegmental (PPT) and the laterodorsal

tegmental (LTD) areas. Indeed, both the reticular nucleus and the TCR neurons receive cholinergic synapses. The extensive physiological analysis by Sun et al. (2013) of the influence of cholinergic inputs on the neurons of the reticular nucleus showed that cholinergic activation of these neurons elicits a biphasic excitatory–inhibitory response mediated by activation of postsynaptic nicotinic (nAChRs) and muscarinic (mAChRs) receptors, respectively. In this way brief trains of cholinergic inputs to these neurons can cause a transient depolarisation followed by a long-lasting hyperpolarisation; in contrast, cholinergic activation causes depolarisation of TCR neurons due to the suppression of various potassium currents (Curró Dossi et al. 1991); these distinct effects of brain stem cholinergic inputs on thalamic neurons are noteworthy. Therefore the result in vivo of the activation of cholinergic inputs to the thalamus is complex. Nonetheless Curró Dossi et al. (1991) state that a general effect of mesopontine cholinergic activation is EEG desynchronisation. In addition, the reticular nucleus receives also inputs from the basal forebrain that may be GABAergic and can also exert a strong inhibition on the reticular neurons, leading to the subsequent suppression of spindle oscillations. In addition, monoaminergic inputs from the brain stem, namely, those arising at the mesopontine junction (i.e. from the noradrenergic neurons of the locus coeruleus and the serotoninergic neurons of the dorsal raphe nuclei), also modulate the rhythmic activities of the forebrain. These neuronal systems have only a weak thalamic projection, but they have a diffuse projection to the cortex. Metabotropic glutamate receptors also appear to exert a modulating influence on the activation of thalamic circuits by descending cortico-thalamic systems.

Because this point is often misunderstood, we should emphasise that slow-wave sleep, characterised by typical EEG delta activity, does not correspond to a state where cortical neurons are inactive. On the contrary, in this sleep state, cortical neurons can display mean rates of firing similar to those that they show during wakefulness and/or REM sleep. Regarding the neuronal firing patterns, the main difference between delta sleep on the one hand and wakefulness and REM sleep on the other is that, in the former, the neurons tend to display rather long bursts of spikes with relatively prolonged interburst periods of silence, whereas in the latter, the firing pattern is more continuous. The functional meaning of these peculiar firing patterns of delta sleep has not yet been unravelled.

In general terms we can state that EEG signals co-vary strongly with different levels of arousal and consciousness. The changes in EEG with increasing levels of anaesthesia are typical examples of this property.

2.3.2 Theta Rhythms

Theta activity (frequency range 4–7.5 Hz) is most conspicuous in limbic brain areas in animals (Buzsáki 2006). The presence of theta rhythms in humans has been a matter of controversy, but this activity has been clearly recorded in the hippocampus of epileptic patients with indwelling electrodes (Arnolds et al. 1980; Kahana et al. 1999; Ekstrom et al. 2005), or by way of mesio-temporal corticography with

foramen ovale electrodes (Bódizs et al. 2001), and also using magnetoencephalography (MEG) in normal subjects (Tesche and Karhu 2000). In all these studies, human hippocampal theta rhythm was studied under specific behavioural conditions.

In this context the findings of Cornwell et al. (2008) who reported hippocampal and parahippocampal theta oscillations during a spatial navigation task (virtual reality Morris water maze), particularly during goal-directed navigation relative to aimless movements, using a whole-head 275-channel MEG system in normal subjects, are noteworthy. With respect to the neuronal sources of theta rhythmic activities in limbic structures, mainly in the hippocampus and for a general discussion of cellular processes underlying theta oscillations, see Amzica and Lopes da Silva (2018).

The normal theta activity should not be confused with pathological theta waves, described as a slowing down of alpha activity in human EEG. The presence of theta frequency activity in posterior cortical areas in waking EEG of adults is abnormal and is indicative of various pathological conditions. Nonetheless EEG activity within the theta frequency range may be clearly seen in the EEG of normal infants and children and in adults during drowsiness (Krishnan et al. 2018).

In addition, a midline theta rhythm (4–7 Hz) has been described with maximum at Cz in scalp EEG recordings, associated with cognitive tasks, although the cortical sources of this rhythmic activity have not yet been clearly demonstrated. A specially interesting aspect is that theta activity often does not appear in isolation; indeed theta oscillations can modulate gamma oscillations by a process of cross-frequency phase coupling (Lopes da Silva 2013). This has been specially put in evidence by Jensen and Colgin (2007) who proposed that oscillatory coding manifest as gamma-band activity (30–150 Hz) coupled to theta oscillations (5–8 Hz) likely plays a role in neuronal information processing, particularly in the case of memory tasks.

2.3.3 Alpha Rhythms of Neocortex and Thalamus

Alpha rhythms recorded from the occipital areas occur in relaxed awake animals and show a typical reactivity to closure of the eyes. Background illumination can result in decreased alpha rhythm amplitude (Paskewitz and Orne 1973; Cram et al. 1977), while investigations of the suspected relationship between heart rate and alpha have not led to any firm conclusions (Surwillo 1965).

Although the frequency range of alpha rhythms overlaps that of sleep spindles, these two types of phenomena differ in a number of aspects. Namely, the behavioural states at which these types of oscillations occur are quite different, and their distributions over the thalamus and cortex also differ considerably.

The basic mechanisms responsible for alpha oscillations at the cellular level have not been described in detail. The reason for this is the inherent difficulty of studying a phenomenon that—by definition—occurs in the state of relaxed wakefulness, under conditions where measurement of the underlying membrane currents is not a simple task, since this cannot be done under anaesthesia. To overcome this difficulty, some researchers have assumed that spindles occurring under barbiturate anaesthesia would be analogous to alpha rhythms (Andersen and Anderson 1968).

This analogy, however, was challenged on experimental grounds because a comparative investigation of alpha rhythms obtained during restful wakefulness upon closure of the eyes, and spindles induced by barbiturates, recorded from the same sites over the visual cortex and lateral geniculate nuclei in dog, presented differences in frequency, spindle duration, topographic distribution and amount of coherence among different cortical and thalamic sites (Lopes da Silva et al. 1973). Investigations combining multiple electrode arrays placed on the cortical surface, intracortical depth profiles and intrathalamic recordings from several thalamic nuclei unravelled a number of elementary properties of alpha rhythms (Lopes da Silva 1991):

- In the visual cortex, alpha waves are generated by a current dipole layer centred at the level of the somata and basal dendrites of the pyramidal neurons of layers IV and V.
- The coherence between alpha waves recorded from neighbouring cortical sites is greater than any thalamo-cortical coherence.
- The influence of alpha signals recorded from the pulvinar nucleus of the thalamus on cortical rhythms can be conspicuously large, depending on the cortical area, but intracortical factors play also a significant role in establishing cortical domains of alpha activity.

These experimental findings led to the conclusion that, in addition to the influence of some thalamic nuclei (mainly the pulvinar) on the generation of alpha rhythms in the visual cortex, there are systems of surface-parallel intracortical connections that are responsible for the propagation of alpha rhythms over the cortex. These oscillations appear to be generated in small patches of the cortex that behave as epicentres, from which they propagate at relatively slow velocities, about 0.3 cm/s. This type of spatial propagation has been confirmed, in general terms, by experimental and model studies. A comprehensive study of alpha rhythms in the visual cortex of the cat (Rougeul-Buser and Buser 1997; Buser and Rougeul-Buser 2005) showed characteristics corresponding closely to those of alpha rhythms in man and in dog. It was found that this rhythmic activity was localised to a limited part of the primary visual cortex area 18 and the border between 17 and 18.

These early findings obtained in dog and cat were further extended by experimental studies in awake monkey by Bollimunta et al. (2008, 2011) who using fine microelectrode arrays implanted across the visual cortical areas V2 and V4 and the inferior temporal cortex combining current source density analysis (CSD) and multiunit activity (MUA), identified intracortical alpha current generators, with the infragranular neurons (layer V) acting as primary local generator. The analysis of the coherence between CSD sinks, and local MUA in infragranular and granular layers showed that these cells are depolarised and tend to generate action potentials during the local current sinks; however, at the supragranular layer, the coherence between CSD sinks and MUA was poor, suggesting that the cells of this layer are inhibited, possibly due to inhibitory inputs from layer V interneurons that innervate superficial pyramidal cells.

These properties were reanalysed also in the visual cortex of awake monkeys during spontaneous activity by van Kerkoerle et al. (2014), who reported that alpha waves are indeed initiated in infragranular layer V but also in supragranular layers I and II; alpha activity both from layer V and from layers I and II showed phase advance with respect to activity in layer IV. A subsequent study by Haegens et al. (2015), also using CSD and MUA in awake monkey, described alpha current generators in the supragranular, granular and infragranular layers. These authors found that the strongest alpha LFP power, however, was encountered in deep layers.

In this context, more insights into the sources of alpha rhythms in humans were obtained using EEG and MEG recordings integrated with anatomical information obtained from magnetic resonance images (MRI), as shown in Fig. 2.2.

Different sources of alpha rhythms were found to be mainly concentrated in the region around the calcarine fissure, with most sources occurring within 2 cm from the midline. In addition to the alpha rhythms of the visual cortex, rhythmic activities with about the same frequency range (in man, 8–13 Hz; in cat, 12–15 Hz) have been shown to occur in other cortical areas, namely, in the somatosensory cortex (SI areas 1, 2 and 3). These activities are known as "rolandic *mu rhythms*" or "wicket rhythms" (named after the appearance of the EEG records on the scalp in man) and have a typical reactivity, since they appear when the subject is at rest and are blocked by movement. The mu rhythm is particularly pronounced in the hand area of the somatosensory cortex, and it reacts typically to the movement of closing the fists. In the cat, there is no significant coherence between the mu rhythm of the SI cortex and the alpha rhythm of the visual cortex, which supports the general idea that these two types of rhythms are independent. Furthermore, mu rhythms of the SI area also differ from the alpha rhythms of the visual cortex recorded in the same animal, in that the former have systematically higher frequencies than the latter, the difference being about 2 Hz. Mu rhythms were also recorded in thalamic nuclei, namely, in the ventroposterior lateral nucleus. The mu rhythm has also been identified in MEG recordings over the rolandic sulcus, particularly over the somatomotor hand area. In addition, another spontaneous MEG activity, the so-called tau rhythm, was detected over the auditory cortex. This rhythmic activity was reduced by sound stimuli. This MEG tau rhythm, which was first described by the group of Hari (Hari et al. 1997; Lehtelä et al. 1997), is apparently similar to an EEG rhythm that was found using epidural electrodes over the midtemporal region by Niedermeyer (2005), who called it "third rhythm" or "independent temporal alphoid rhythm".

The presence of dominant activity within the alpha frequency range has been interpreted, since Adrian and Mathews (1934), as indicating an "idling state" of the brain, although paradoxical findings with alpha enhancement by attention tasks were reported (Ray and Cole 1985). These observations are now well understood since a number of findings, both of visual alpha and sensorimotor mu rhythms, have shown that enhancement and attenuation of these rhythmic activities can be recorded simultaneously at different sites and successively depending on a given task. This can be explained taking into consideration the interaction between different thalamocortical modules, as put in evidence in computer models of the thalamo-cortico-thalamic system (Suffczynski et al. 2001).

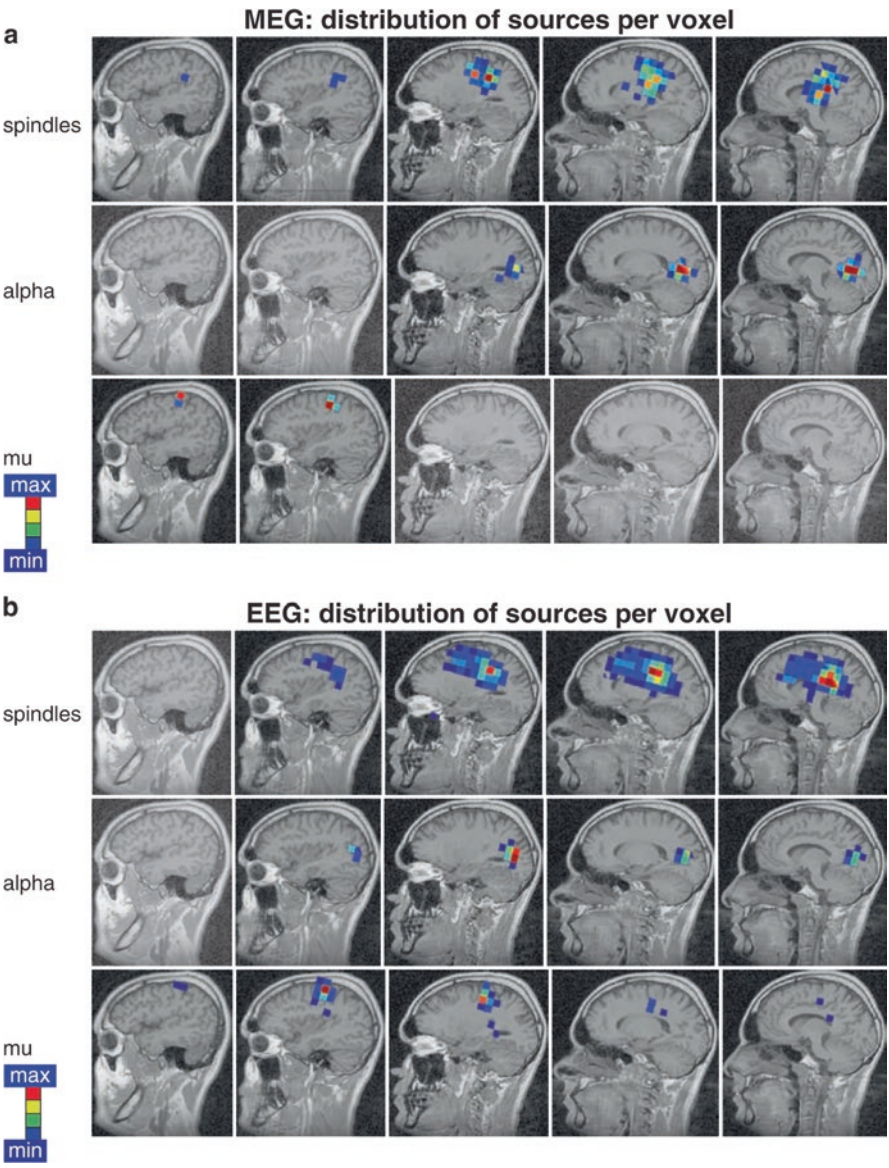

Fig. 2.2 (**a**, **b**) Dipole density plots of the MEG and EEG sleep spindles, alpha and mu rhythms of one subject. Voxels containing a relative high amount of dipoles are shown in *red*. *Blue* voxels contain relatively few dipoles. Voxels comprising less than 10% of the maximal amount of dipoles present in the red voxels are omitted for clarity. (**a**) MEG data: the "hot spots" for the MEG spindles are located in the centroposterior areas. (**b**) EEG data: the plots demonstrate that there is no overlap of the alpha and mu clusters. Furthermore, the "hot spot" of the alpha rhythm is located more superficially than those of the spindles, whereas the spindle cluster is more widespread than that of the alpha rhythm. The EEG sleep spindle dipoles spread to more frontal areas than the MEG data (*Adapted from* Manshanden et al. 2002)

In this respect, the experimental findings by Rihs et al. (2007, 2009) showing enhancement of occipital alpha associated with active suppression of unattended positions during a visual spatial orienting task provide further evidence for the facilitating role of alpha-power decreases (event-related alpha desynchronisation [ERD]) versus the inhibitory role of alpha-power enhancement (event-related alpha synchronisation [ERS]) of attentional processes (Pfurtscheller and Lopes da Silva 1999). Indeed alpha desynchronisation in a specific area occurs as attention is focussed on information processing related to that particular brain system. This is also the core of Klimesch's inhibition-timing hypothesis formulated to account for the role of alpha oscillations (Klimesch et al. 2007). Accordingly, alpha ERS plays an active role in the inhibitory control and timing of cortical processing, whereas ERD reflects the gradual release of inhibition associated with the emergence of complex spreading activation processes, mainly in the form of spectral activity in the beta frequency range, as described below in more detail.

The cellular mechanisms responsible for the generation of alpha rhythms have recently been unveiled using in vitro preparations of thalamic nuclei. Hughes et al. (2004) showed that in the lateral geniculate nucleus, oscillations in the alpha frequency range can be generated by the pharmacological activation of the metabotropic glutamate receptor (mGluR) mGluR1a. These oscillations display similarities with thalamic alpha rhythms recorded in the intact animal. Hughes and Crunelli (2005) discovered that the occurrence of these oscillations depends on the activity of a subset of thalamo-cortical (TC) neurons termed high-threshold (HT) bursting cells, which are interconnected via gap junctions. These in vitro thalamic alpha rhythms can slow down until the theta frequency range when the TC neuron population is less depolarised.

2.3.4 Beta and Gamma Activity of the Neocortex

The identification and characterisation of high-frequency rhythms in the neocortex have concentrated mainly on two neocortical areas, the visual cortex and the somatomotor cortex. Here we examine some of the properties of *beta/gamma* rhythmic activities of these two areas, although beta/gamma rhythmic activities have also been recorded in other brain areas, in particular in olfactory cortex (Freeman 2005).

Commonly, the EEG of the *visual cortex* is associated with the alpha rhythm, with its typical reactivity upon closing and opening the eyes, as described above. However, different types of rhythmic activities can be recorded from the same cortical areas. In the dog, we showed that the EEG spectral density was characterised by peaks within the beta/gamma frequency range while the animal was looking attentively at a visual stimulus (Lopes da Silva et al. 1970). Similarly, Freeman and van Dijk (1987) found in the visual cortex of a rhesus monkey that fast EEG rhythms (spectral peak of 30 ± 3.7 Hz) occurred during a conditioned task in response to a visual stimulus. A related finding is the discovery by the group of Charles Gray and Wolf Singer (Gray et al. 1989) and by Eckhorn et al. (1988) of

oscillations within the beta/gamma frequency range (most commonly between 30 and 60 Hz) in the firing of individual neurons of the visual cortex in response to moving light bars. It was demonstrated using auto- and cross-correlation analyses that neurons tended to fire in synchrony, in an oscillatory mode, within cortical patches that could extend up to distances of about 7 mm. The oscillations in neuronal firing rate were correlated with those of the LFPs. The cortical oscillations are modulated by the activation of the mesencephalic reticular formation (MRF), but the stimulation of the MRF alone does not change the pattern of firing of the cortical neurons (Munk et al. 1996). However, MRF stimulation increases the amplitude and coherence of both the LFP and multiunit responses when applied jointly with a visual stimulus.

In the *somatomotor cortex*, beta/gamma oscillations of both neuronal firing and LFPs were also described in the awake cat by the group of Buser and Rougeul-Buser (2005) and Bouyer et al. (1987), particularly when the animal was in a state of enhanced vigilance while watching an unreachable mouse. Also, fast oscillations were found in the somatomotor cortex in monkey during a state of enhanced attention (Rougeul et al. 1979). Oscillations of 25–35 Hz occurred in the sensorimotor cortex of awake, behaving monkeys in both LFPs and single−/multiunit recordings. They were particularly apparent during the performance of motor tasks that required fine finger movements and focussed attention. These oscillations were coherent over cortical patches extending up to at least 14 mm that included the cortical representation of the arm. Synchronous oscillations straddling the central sulcus were also found, so they may reflect the integration of sensory and motor processes. The LFP reversed polarity at about 800 μm under the cortical surface indicates that the source of the LFP is in the superficial cortical layers. It is noteworthy that at least some of the cortical beta/gamma rhythmic activities appear to depend on projecting dopaminergic fibres arising in the ventral tegmental area, but the extent to which the beta rhythms of the somatomotor cortex are related to thalamic or other subcortical activities is not yet clear.

Currently there is a considerable interest in better defining the cortical domains of beta/gamma oscillations, and their modulation by imagination in the human EEG/ECoG, with the objective of using those signals in *brain–computer interfaces* (*BCI*). Within a BCI perspective, Branco et al. (2017) studied how hand movements are encoded in the ECoG of the sensorimotor cortex and found clear broadband (50–130 Hz) increases in primary somatosensory and primary motor cortex prior to movement onset, combined with decreases of alpha/beta frequency band (10–30 Hz). These results are being explored in practical BCI applications. A most notable case of this kind of approach was published by Vansteensel et al. (2016) who realised a BCI consisting of subdural electrodes placed over the motor cortex in a locked-in amyotrophic lateral sclerosis (ALS) patient, who, nonetheless, was able to control a computer typing program at a rate of two letters per minute, weeks long, by imagining moving the hand contralateral to the side of the implanted electrodes.

With respect to the origin of beta/gamma rhythmic activity, several experimental facts have led to the interpretation that these rhythmic activities are primarily

generated in the cortex itself. These include the fact that oscillations in the beta/gamma frequency range were easily recorded from different cortical sites but not from simultaneously obtained recordings from thalamic electrodes and the observation that in the visual cortex there are neurons that show oscillatory firing rates with a phase difference of about a quarter cycle, which indicates that a local recurrent feedback circuit may be responsible for the oscillations. Nevertheless, it is possible that thalamic neuronal networks also contribute to the cortical beta/gamma rhythmic activity, since oscillatory activity (about 40 Hz) has been observed (Steriade et al. 1996) in neurons of the intralaminar centrolateral nucleus, which project widely to the cerebral cortex. The question cannot be phrased as a simple alternative between a cortical and a thalamic rhythmic process, both considered as exclusive mechanisms. As we have discussed in relation to other rhythmic activities of the mammalian brain, *both network- and membrane-intrinsic properties cooperate* in shaping the behaviour of the population, including its rhythmic properties and its ability to synchronise the neuronal elements. Recently, new observations made in vitro have shed light on the sources of these fast cortical rhythms. In an in vitro model of the cortex, the group of Whittington and Traub (Roopun et al. 2006) showed concurrent but independently generated gamma (30–70 Hz) rhythms in layer II/III and beta2 (20–30 Hz) rhythms in layer V somatosensory cortex. The beta2 rhythm occurred robustly in layer V intrinsically bursting (IB) neurons in the form of bursts admixed with spikelets and single action potentials. It was blocked by reducing gap junction conductance with carbenoxolone and was unaffected by the blockade of synaptic transmission sufficient to ablate the layer II/III gamma rhythm. It could also be seen in the absence of synaptic transmission with axonal excitability enhanced with 4-aminopyridine, suggesting a nonsynaptic rhythm mediated by axonal excitation. A network model based on the hypothesis of electrical coupling via axons is consistent with this hypothesis. The frequency of this network beta2 rhythm appears to depend on the magnitude of the M current, a non-inactivating potassium current found in many neuronal cell types that can be modulated by a large array of receptor types, including muscarinic cholinergic receptors, in IB interneurons. These findings suggest the possibility that a normally occurring cortical network oscillation involved in motor control could be generated largely or entirely by nonsynaptic mechanisms. According to these authors, higher beta2 frequency oscillations occur mainly during the anticipatory period leading up to a movement in response to a sensory cue. Indeed, it was found that layer V pyramidal neurons and motor cortex LFPs displayed coherence at beta2 frequencies with hand and forearm EMG in monkeys performing a precision grip task (Baker et al. 1999). This group showed that the generation of beta2 in layer V stands in contrast to that of gamma rhythms in layers II/III; the latter may underlie mainly corticocortical synchronisation. There are probably a variety of rhythmic activities in the beta/gamma range with different behavioural correlates, as discussed below with respect to event-related (de)synchronisation of EEG/MEG phenomena.

The findings, in the monkey visual cortex, of van Kerkoerle et al. (2014) already mentioned above are very relevant to better understand the interaction between

alpha and gamma activities in the processing of visual information in the cortex. Indeed it appears that alpha and gamma oscillations characterise different directions of information flow in the visual cortex. Simultaneous recordings in visual area V1 and V4 demonstrated that alpha and gamma oscillations can coexist during a single task but occur in opposite directions. Estimations of time delays from the slope of frequency spectra showed that V1 leads to V4 by 3 ms for the gamma rhythm but lags V4 by 9 ms for alpha. These authors suggest that this difference between time-lags may be accounted for by a difference in synaptic time constants, since NMDA channels which play a role in the feedback effects mediated by alpha activity have a longer time constant than that of AMPA channels which are important for the feedforward propagation of gamma activity to higher visual areas. This propagation of alpha oscillations is in agreement with reports of ECoG recordings in humans, where Bahramisharif et al. (2013) showed that bursts of gamma activity propagate over neocortex and are locked to the phase of traveling alpha waves. Accordingly, these authors note that alpha oscillations serve to coordinate gamma activity both in time and in space.

In this context it is interesting to consider changes in EEG/MEG phenomena, particularly in the beta and gamma frequency ranges, that are event-related and reflect a decrease or an increase in the synchrony of the underlying neuronal populations. The former is called event-related desynchronisation (ERD), and the latter event-related synchronisation (ERS) (Pfurtscheller and Lopes da Silva 1999). In relation to a hand movement, both the 10–12 Hz mu rhythm and the beta (around 20 Hz) display ERD but with a different distribution over the scalp, although both activities are localised around the central sulcus. The mu rhythm ERD exhibits its maximum magnitude more posteriorly than the beta activity, indicating that it is generated mainly in the post-rolandic somatosensory cortex, whereas the low beta activity is preferentially generated in the pre-rolandic motor area. In addition, after a voluntary movement, the central region exhibits a localised beta ERS that becomes evident in the first second after cessation of the movement, at a time where the rolandic mu rhythm still presents a desynchronised pattern. The exact frequency of this rebound beta ERS can vary considerably with the subject and type of movement. This beta ERS is observed not only after a real movement but also after an imagined movement. Furthermore, ERS in the gamma frequency band (around 36–40 Hz) can also be found over the central regions, preceding the execution of a movement, in contrast with the beta ERS, which has its maximum after the termination of the movement (Fig. 2.3).

Our understanding of the significance of ERS of the *beta* frequency range, which typically occurs after a movement, has been greatly enhanced by the observation that when this form of ERS occurs, the excitability of the corticospinal pathways decreases, as revealed by means of transcranial magnetic stimulation. This supports the hypothesis that the postmovement beta ERS corresponds to a deactivated state of the motor cortex (Pfurtscheller et al. 1996). In contrast, the ERS in the *gamma* frequency band appears to reflect a state of active information processing.

From this perspective, it is important to note the likely connection between gamma oscillations and synaptic plasticity. As Buzsáki (2006) colourfully writes,

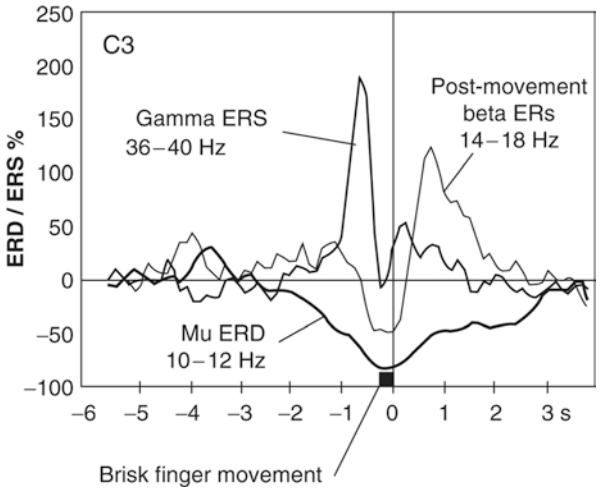

Fig. 2.3 Event-related desynchronization (ERD) and event-related synchronization (ERS) from one normal subject during self-paced voluntary movement. EEG recorded from C3. The results for three frequency bands are shown: alpha band (mu) 10–12 Hz ERD, beta 14–18 Hz ERD–ERS and gamma 36–40 Hz ERS. The data analysis is triggered with respect to movement offset (vertical line at 0 s). Note that the ERDs or ERSs of different frequency bands have different dynamics: about 2 s before the movement of the mu ERD appears, followed by a pre-movement beta ERD that changes to a postmovement ERS, a burst of gamma ERS appears just before the movement [*Adapted from Pfurtscheller G, Lopes da Silva FH. (2018) EEG event-related Desynchronization and event-related Synchronization. In: Schomer DL, Lopes da Silva FH, eds. Niedermeyer's Electroencephalography: Basic Principles, Clinical Applications and Related Fields. 7th ed. Oxford University Press 2018: p1020 (Fig. 40.10)*]

the gamma oscillation may be considered the "buzz" that provides the central timing mechanism that is essential for modulating synaptic strength, and in this way, it may stabilise the formation of neuronal assemblies in the cortex.

2.3.5 DC and Ultraslow Potentials

Is it possible to record DC on MEG or EEG? And if so, what is its physiological meaning? There are a lot of physical limitations (electrode impedances, electrode polarisation, skin/electrolyte junction) that do not allow EEG signals to be recorded down to 0 Hz, which would correspond to real DC or "direct current". Also, environmental low-frequency noise imposes limitations on MEG with similar consequences. The point, however, is not to record down to the real DC level but to extend the effective frequency band to very low frequencies on the order of 0.1 Hz. (For a discussion of misconceptions of the meaning of "DC" in electroencephalography, see Niedermeyer's footnote in Speckmann and Elger 2005.) The recording of ultraslow MEG/EEG signals can be achieved using appropriate techniques, as discussed, for example, for the EEG by Vanhatalo et al. (2005) and for the MEG by Burghoff

et al. (2004). Phenomena such as the contingent negative variation (CNV) and the Bereitschaftspotential (readiness potential) are typical cases of very slow shifts of electric potential or magnetic fields that can be typically recorded using appropriate recording and analysis techniques.

In addition, EEG activities in the spectral range below 0.1 Hz (also called ultra- or infra-slow potentials or in short "DC" potentials) have been proposed as being generated at the interface between cerebrospinal fluid and blood as a function of the partial pressure of CO_2 (pCO_2). Such "DC" potentials were suggested to originate across the blood–brain barrier (Amzica and Lopes da Silva 2018). In this respect the model of Voipio et al. (2003) has been especially useful to understand how large DC shifts that can be recorded on the scalp in response to hypo- or hypercapnia are not generated by networks of neurons and/or glial cells. Indeed Nita et al. (2004) demonstrated that such ventilation-induced DC shifts occurred in the absence of any change in the neuronal or glial membrane potential and are not caused by cortical current dipolar sources. Likely, other parenchymal elements (blood–brain barrier, blood flow, capillary epithelial cells) can participate in the genesis of such "DC" potentials that translate into EEG signals at the very low spectral band.

During slow-wave sleep, ultraslow-frequency components (around 0.5 Hz) have been recorded in the human EEG (Achermann and Borbély 1997; Amzica and Steriade 1997) and in MEG (Simon et al. 2000), which correspond to the ultraslow oscillations that can be recorded intracellularly from cortical neurons through layers II to VI, and consist of prolonged depolarising and hyperpolarising components, as have been analysed in detail by Steriade (2006).

2.4 Origin of the EEG/MEG II: Generators, Volume Conduction and Source Estimation

In order to take the next step towards an understanding of how EEG/MEG signals recorded outside the skull are generated, we have to take the folding of the cortex into consideration. The fact that the cortex is folded, forming gyri and sulci, implies that some populations of neurons have apical dendrites that are perpendicular to the overlying skull (i.e. those that are at the top of a gyrus), whereas others are parallel to the skull (i.e. those that are on the wall of a sulcus). The orientation of the neurons with respect to the skull is an important factor in the appearance of the EEG and MEG signals recorded outside the skull. This is particularly the case for MEG, since the latter "sees" only those magnetic fields that are perpendicular to the skull due to the physical properties of magnetic fields, the way MEG is measured and the approximately spherical shape of the head. In effect, the observed magnetic fields are generated by neuronal currents that are oriented tangentially to the skull. In contrast, those that are oriented radially to the skull do not generate a magnetic field outside the head but contribute to the EEG.

The area of cortex within which the neuronal population must be synchronously active to produce a measurable EEG/MEG signal at the scalp is an important consideration when interpreting these signals. To address this problem, we must first

point out some classical concepts about cortical organisation. The cortex is organised according to the columnar principle, as proposed in the 1970s by Mountcastle (see review from 1997), which means that the basic unit of the mature neocortex is the *minicolumn*, "a narrow chain of neurons extending vertically across the cellular layers II/VI, perpendicular to the pial surface", with a cross-section of diameter ~40–50 μm. A primate minicolumn contains about 80–100 neurons, although this number may vary between areas; in the striate cortex, the cell density appears to be 2.5 times larger. Many minicolumns are bound together by short-range horizontal connections and thus form what have been denominated *cortical columns* or cortical modules (Mountcastle 1997). One *column* in the somatic sensory cortex contains about 80 minicolumns and is roughly hexagonal with a width of about 300–400 μm (Favorov and Diamond 1990). These estimates can be used to give a rough answer to the question formulated above. Assuming that a minicolumn with a diameter of 40 μm contains 100 cells, the cortical surface corresponding to 50,000 cells should form a patch with a cross-sectional area of about 0.63 mm^2. If this cortical patch took a circular form, then its diameter would be about 0.88 mm. Buxhoeveden and Casanova (2002) noted that, from a functional perspective, cortical columns may exist in different dynamic states, and they coined the term "physiological macrocolumn" to indicate a set of cortical columns that cooperate to realise a given functional state or neural process. These physiological macrocolumns must be considered dynamic ensembles such that the number of columns contributing to a macrocolumn may vary as a function of time. It is important to note that neurons in separate columns can present synchronous oscillatory activities, as mediated by tangential and recurrent connections between different columns (Gray et al. 1989; Freiwald et al. 1995).

Above we have already stressed the relevance of the degree of correlation, or synchrony, between neuronal activities in cortical columns, with respect to the strength of the resulting LFPs.

A general problem in EEG/MEG is how to estimate the neuronal sources that are responsible for a certain distribution of electrical potentials or of magnetic fields recorded at the scalp. This is called the *inverse problem* of EEG/MEG; this an ill-posed problem in the sense that it has no unique solution: there are an infinite number of possible source configurations that give rise to a given set of measured scalp potentials or magnetic fields (von Helmholtz 2004). Therefore, the estimation of EEG and MEG sources requires assumptions about the nature of the sources. The simplest source model is a *current dipole*, as indicated in the previous section. However, such a model does not imply that somewhere in the brain there is a point current dipole. Rather, it suggests that the EEG/MEG scalp distribution is best represented by an *equivalent* dipolar current source. This choice has been shown to be useful and accurate for certain types of activity, such as the event-related potentials (ERPs) and focal epileptic spikes. In such circumstances, the solution of the EEG/MEG inverse problem that is obtained based on the equivalent current dipole can be thought of as the centroid of the dipole layers that are active at a certain moment, in the statistical sense. An increase in the number of dipoles can easily lead to rather complex and ambiguous interpretations. Nevertheless, methods have been

developed in order to obtain estimates of multiple dipoles using only the a priori criterion that they must be located at the surface of the cortex. An example of an algorithm that performs such an analysis is MUSIC (multiple signal classification). An alternative approach is to use linear estimation methods that apply the minimum norm constraint to estimate the sources within a given surface or volume of the brain.

A main feature of any estimation of EEG/MEG sources is the volume conduction problem, which allows the calculation of the field values given a postulated generator configuration (the so-called *forward* part of the *inverse* problem). A commonly used forward model is that of the three concentric conducting spheres, for which a convenient analytical expression for the surface potentials (or magnetic field) due to a dipole is available. However, realistically shaped volume conductor models derived from the individual subject's MRI images have been shown to improve the accuracy of the localisation of the sources, particularly in nonspherical parts of the head (Fuchs et al. 2007). Individual boundary element method (BEM) models derived from the subject's MRI represent the "gold standard" and have clear advantages over simplified spherical shell models. The core of the solution of the inverse problem is of course the reconstruction of brain (cortical) sources from scalp-recorded EEG/MEG signals. As indicated above the classic solution is to calculate dipolar sources, but currently this approach has been extended using distributed source imaging approaches, including constraints in order to estimate well-posed inverse solutions; relevant technical aspects are described by Michel and He (2018).

Anisotropic volume conduction properties of the bone layer or the white matter fibres can be modelled by the finite element methods (FEM), but the latter require considerable computational power and are thus not used in daily applications. The development of diffusion tensor magnetic resonance imaging (DT-MRI) provides a means to estimate the anisotropic conductivity of the cerebral white matter, which may further improve the accuracy of the EEG forward solution (Wolters et al. 2006). To reduce the computational effort, head models derived from an averaged MRI dataset have been proposed (Fuchs et al. 2007). New approaches are currently being explored that combine fMRI and EEG/MEG data in order to create more specific spatial constraints in order to reduce the solution space for the estimation of the underlying neuronal sources (Liu and He 2008). This aspect of EEG and fMRI data fusion is addressed in more detail in Chap. 27.

In general, the problems posed by the complexity of the volume conductor, including the scalp, skull, cerebrospinal fluid layer and brain, are easier to solve in the case of the MEG than of the EEG, since these different media have different conductivities, which affects the EEG much more than the MEG. Therefore, a major advantage of MEG over EEG is the relative simplicity of the forward modelling and its consequences for source localisation. This means that when a dipole source algorithm is used on the basis of MEG recordings, a single homogeneous sphere model of the volume conductor can lead to a satisfactory solution.

The conductivity values that should be used for the different shells surrounding the sources, brain, cerebrospinal fluid, skull and scalp have been estimated in a number of studies, using both in vitro and in vivo measurements. In general, we can assume that the brain and scalp have the same conductivity. Using electrical

impedance tomography, a wide variation in the ratio of resistivities r_{skull}/r_{brain} was encountered among subjects, most frequently in the range of 20–50 (Gonçalves et al. 2003). These results indicate that in order to obtain an estimate of the sources of a given potential distribution over the scalp as precisely as possible, conductivities measured in the same subject should preferentially be used.

2.5 Localisation Methods Applied to Spontaneous Oscillatory Activities: Alpha, Mu and Sleep Spindles

A basic question in EEG/MEG studies is whether the main rhythmic activities—alpha and mu rhythms on the one hand and sleep spindles on the other—are generated in distinct or overlapping cortical areas. In order to solve this question, advanced spatiotemporal analysis methods are necessary. We should note that the estimation of equivalent dipole models is only meaningful if the scalp field has focal character and the number of possible active areas can be anticipated with reasonable accuracy. The recent development of a new algorithm (Manshanden et al. 2002) aimed at estimating sources of large datasets, as is the case for this kind of spontaneous EEG oscillation, allowed estimating whether generators of spontaneous MEG/EEG alpha and mu rhythms and sleep spindles are distributed over distinct or over-overlapping cortical areas to be addressed. The basic approach consisted of finding well-fitting dipoles using a dipole model applied to successive time samples of a burst of an oscillation. The equivalent dipoles encountered were plotted on the corresponding MRI slice of the brain, as shown in Fig. 2.2 (a for the EEG and b for the MEG).

It is important to consider what equivalent dipolar sources of spontaneous brain activity may represent. Sleep spindles, alpha rhythms and mu rhythms are spontaneously occurring brain rhythms that can be recorded from the scalp. This suggests that extended cortical areas are involved in the generation of these signals. The use of equivalent dipoles as source models for these distributed brain activities yields an oversimplified solution to the problem of determining the underlying sources of these signals. The equivalent dipoles should be viewed simply as descriptors of the "centre of gravity" that best describe, in a statistical sense, the spatial distribution of the corresponding active cortical area at a given time. The positions of the dipoles with respect to the cortical surface depend on the extent and geometry of the activated cortical area: superficially positioned dipoles (i.e. near to the cortical surface), such as those of the mu rhythm, correspond to more localised cortical activity, while deeplying dipoles, like those of sleep spindles, instead represent the activity of extended cortical surfaces. Thus, dipole locations provide only an approximation of the localisation of the active brain area and the extension of the area. When comparing the results of the alpha rhythms and of the sleep spindles (Fig. 2.2), we should emphasise that there is no overlap of the centres of gravity of these two kinds of rhythms. This indicates that different regions of the cortex are involved in the generation of these brain rhythms. The same applies to the mu rhythm, which appeared to be generated in a different brain region compared to the alpha rhythm and sleep spindles. The superficial location of the mu rhythm dipoles (especially in MEG, Fig. 2.2b) suggests that

the mu rhythm is generated in a relatively well-localised cortical area. Thus, the equivalent dipole model appears to be an adequate model for the estimation of mu sources. A comparison of the results obtained in the same subject based on EEG (Fig. 2.2a) or on MEG (Fig. 2.2b) data shows that the dipoles estimated using the latter occupy a more circumscribed number of voxels than those based on the former; this is particularly clear for the spatial distribution of the dipolar sources of sleep spindles and the mu rhythm. The close spatial relationship of the MEG mu rhythm dipoles to the dipoles of the N20 component of the medial nerve somatosensory-evoked fields demonstrates that the mu rhythm arises from the cortex around the central sulcus.

The advent of simultaneous EEG–fMRI acquisitions (Lemieux et al. 1997; Goldman et al. 2002; Krakow et al. 2000) has allowed the study of the haemodynamic correlates of spontaneous variations of alpha rhythm (Laufs et al. 2003; Moosmann et al. 2003), focussing on group results. In this kind of work, it is important to study individual subjects, since there is a considerable variability with respect to these phenomena among normal subjects. Gonçalves et al. (2006) and de Munck et al. (2007) found a negative correlation between the BOLD signal and the average power time series within the alpha band (8–12 Hz) in extensive areas of the occipital, parietal and frontal lobes. In small thalamic areas, the BOLD signal was positively correlated with the alpha-power. Results suggest that the resting state varies among subjects and sometimes even within one subject. As the resting state plays an important role in many fMRI experiments, the simultaneous recording of fMRI and EEG is advisable; see the chapters "Brain Rhythms" (Chap. 15), "Sleep" (Chap. 16), "EEG–fMRI in Adults with Focal Epilepsy" (Chap. 17), "EEG–fMRI in Idiopathic Generalised Epilepsy (Adults)" (Chap. 18) and "EEG–fMRI in Children with Epilepsy" (Chap. 19) for further discussions of this issue in the healthy and pathological brain. In general, BOLD signals reflect most often the intensity of neuronal activity, as both synaptic activity and action potentials contribute to the metabolic activity measured by BOLD. The relationship between BOLD and neuronal activity is most often linear (Shmuel and Maier 2015).

2.6 Conclusions

Knowledge of the electrical and magnetic fields generated by local neuronal networks is of interest to the neuroscientist because these signals can yield relevant information about the modes of activity of neuronal populations. This is particularly relevant when attempting to understand higher-order brain functions such as perception, action programming and memory trace formation. It is becoming increasingly clear that these functions are mediated by dynamical assemblies of neurons. In this respect, knowledge of the properties of the individual neurons is not sufficient. It is necessary to understand how populations of neurons interact and undergo self-organisation processes to form dynamical assemblies. The latter constitute the functional substrate of complex brain functions. These neuronal assemblies generate patterns of dendritic currents and action potentials of course, but these patterns are usually difficult to evaluate experimentally due to the multitude of parameters and the

complexity of the structures. Nevertheless, the concerted action of these assemblies can also be revealed in the LFPs that can be recorded at distance from the generators as EEG or MEG signals. However, extracting information from EEG or MEG signals about the functional state of a local neuronal network poses a number of nontrivial problems that must be solved by combining anatomical/physiological with biophysical/mathematical concepts and tools (Wadman and Lopes da Silva 2018). Indeed, given a certain EEG or MEG signal, it is not possible to precisely reconstruct the behaviour of the underlying neuronal elements, since this inverse problem does not have a unique solution. Therefore, it is necessary to assume specific models of the neuronal elements and their interactions in dynamical assemblies in order to make sense of the LFPs. This implies that it is necessary to construct models that incorporate knowledge about cellular/membrane properties with those for the local circuits, their spatial organisation and organisation patterns. Furthermore, intracranial EEG studies (such as those in patients with epilepsy being evaluated for surgery) demonstrate that a significant amount of brain activity does not appear in the EEG or MEG. This consideration, along with the fundamental limitations of the EEG/MEG inverse problem and the difficulty involved in estimating large or complex networks of generators, suggests that functional imaging combined with EEG can play a significant role in improving our understanding of brain activity.

References

Achermann P, Borbély AA (1997) Low-frequency (<1 Hz) oscillations in the human sleep electroencephalogram. Neuroscience 81(1):213–222

Adrian ED, Mathews BHC (1934) The interpretation of potential waves in the cortex. J Physiol 81:440–471

Amzica F, Lopes da Silva FH (2018) Cellular substrates of brain rhythms. In: Schomer DL, Lopes da Silva FH (eds) Niedermeyer's electroencephalography: basic principles, clinical applications and related fields, 7th edn. Oxford University Press, Oxford, pp 20–62

Amzica F, Steriade M (1998) Electrophysiological correlates of sleep delta waves. Electroencephalography and Clinical Neurophysiology 107(2):69–83, ISSN 0013-4694, https://doi.org/10.1016/S0013-4694(98)00051-0.

Amzica F, Steriade M (1997) The K-complex: its slow (<1-Hz) rhythmicity and relation to delta waves. Neurology 49(4):952–959

Andersen P, Anderson SA (1968) Physiological basis of the alpha rhythm. Appleton-Century-Croft, New York. 235 pp.

Arnolds DE, Lopes da Silva FH, Aitink JW, Kamp A, Boeijinga P (1980) The spectral properties of hippocampal EEG related to behaviour in man. Electroencephalogr Clin Neurophysiol 50:324–328

Bahramisharif A, van Gerven MAJ, Aarnoutse EJ, Mercier MR, Schwartz TH, Foxe JJ, Ramsey NF, Jensen O (2013) Propagating neocortical gamma bursts are coordinated by traveling alpha waves. J Neurosci 33(48):18849–18854

Baker SN, Kilner JM, Pinches EM, Lemon RN (1999) The role of synchrony and oscillations in the motor output. Exp Brain Res 128:109–117

Berger H (1929) Über des Elekrenkephalogramm des Menschen. Arch Psychiat Nervenkr 87:527–570

Bódizs R, Kántor S, Szabó G, Szucs A, Eross L, Hálasz P (2001) Rhythmic hippocampal slow oscillation characterizes REM sleep in humans. Hippocampus 11:747–753

Bollimunta A, Chen Y, Schroeder CE, Ding M (2008) Neuronal mechanisms of cortical alpha oscillations in awake-behaving macaques. J Neurosci 28:9976–9988
Bollimunta A, Mo J, Schroeder CE, Ding M (2011) Neuronal mechanisms and attentional modulation of corticothalamic alpha oscillations. J Neurosci 31(13):4935–4943
Bouyer JJ, Montaron MF, Vahnée JM, Albert MP, Rougeul A (1987) Anatomical localization of cortical beta rhythms in cat. Neuroscience 22(3):863–869
Branco MP, Freudenberg ZV, Aarnoutse EJ, Bleichner MG, Vansteensel MJ, Ramsey NF (2017) Decoding hand gesture from primary somatosensory cortex using high-density ECoG. NeuroImage 147:130–142
Burghoff M, Sander TH, Schnabel A, Drung D, Trahms L, Curio G, Mackert BM (2004) DC-magnetoencephalography: direct measurements in a magnetically extremely-well-shielded room. Appl Phys Lett 85:6278–6280
Buser P, Rougeul-Buser A (2005) Visual attention in behaving cats: attention shifts and sustained attention episodes are accompanied by distinct electrocortical activities. Behav Brain Res 164(1):42–51
Buxhoeveden DP, Casanova MF (2002) The minicolumn hypothesis in neuroscience. Brain 125:935–951
Buzsáki G (2006) Rhythms of the brain. Oxford University Press, Oxford
Cabo A, Riera J (2014) How the active and diffusional nature of brain tissues can generate monopole signals at micrometer sized measures. arXiv:1410.0274 [physics.bio-ph]
Caton R (1875) The electric currents of the brain. Br Med J 2:278
Cornwell BR, Johnson LL, Holroyd T, Carver FW, Grillon C (2008) Human hippocampal and parahippocampal theta during goal-directed spatial navigation predicts performance on a virtual Morris water maze. J Neurosci 28:5983–5990
Cram JR, Kohlenberg RJ, Singer M (1977) Operant control of alpha EEG and the effects of illumination and eye closure. Psychosom Med 39(1):11–18
Curró Dossi R, Paré D, Steriade M (1991) Short-lasting nicotinic and long-lasting muscarinic depolarizing responses of thalamocortical neurons to stimulation of mesopontine cholinergic nuclei. J Neurophysiol 65(3):393–406
de Munck JC, Gonçalves SI, Huijboom L, Kuijer JP, Pouwels PJ, Heethaar RM, Lopes da Silva FH (2007) The hemodynamic response of the alpha rhythm: an EEG/fMRI study. NeuroImage 35(3):1142–1151
Eckhorn R, Bauer R, Jordan W, Brosch M, Kruse W, Munk M, Reitboeck HJ (1988) Coherent oscillations: a mechanism of feature linking in the visual cortex? Multiple electrode and correlation analyses in the cat. Biol Cybern 60(2):121–130
Ekstrom AD, Caplan JB, Ho E, Shattuck K, Fried I, Kahana MJ (2005) Human hippocampal theta activity during virtual navigation. Hippocampus 15:881–889
Favorov OV, Diamond ME (1990) Demonstration of discrete place-defined columns—segregates—in the cat SI. J Comp Neurol 298(1):97–112
Freeman WJ (2005) Origin, structure, and role of background EEG activity. Part 3. Neural frame classification. Clin Neurophysiol 116(5):1118–1129
Freeman WJ, van Dijk BW (1987) Spatial patterns of visual cortical fast EEG during conditioned reflex in a rhesus monkey. Brain Res 422(2):267–276
Freiwald WA, Kreiter AK, Singer W (1995) Stimulus dependent inter-columnar synchronization of single unit responses in cat area 17. Neuroreport 6:2348–2352
Fuchs M, Wagner M, Kastner J (2007) Development of volume conductor and source models to localize epileptic foci. J Clin Neurophysiol 24(2):101–119
Goldman RI, Stern JM, Engel J Jr, Cohen M (2002) Simultaneous EEG and fMRI of the alpha rhythm. Neuroreport 13(18):2487–2492
Gonçalves SI, de Munck JC, Pouwels PJ, Schoonhoven R, Kuijer JP, Maurits NM, Hoogduin JM, Van Someren EJ, Heethaar RM, Lopes da Silva FH (2006) Correlating the alpha rhythm to BOLD using simultaneous EEG/fMRI: inter-subject variability. NeuroImage 30(1):203–213
Gonçalves SI, de Munck JC, Verbunt JP, Bijma F, Heethaar RM, Lopes da Silva F (2003) In vivo measurement of the brain and skull resistivities using an EIT-based method and realistic models for the head. IEEE Trans Biomed Eng 50(6):754–767

Gray CM, König P, Engel AK, Singer W (1989) Oscillatory responses in cat visual cortex exhibit inter-columnar synchronization which reflects global stimulus properties. Nature 338(6213):334–337

Haegens S, Barczak A, Musacchia G, Lipton ML, Mehta AD, Lakatos P, Schroeder CE (2015) Laminar profile and physiology of the alpha rhythm in primary visual, auditory, and somatosensory regions of neocortex. J Neurosci 35(42):14341–14352

Halnes G, Mäki-Marttunen T, Keller D, Pettersen KH, Einevoll GT (2015) The effect of ionic diffusion on extracellular potentials in neural tissue. ArXiv: 1505.06033v2 [physics.bio-ph]

Hämäläinen MS, Hari R, Ilmoniemi R, Knuutila J, Lounasmaa O (1993) Magnetoencephalography. Theory, instrumentation and applications to the noninvasive study of human brain function. Rev Mod Phys 65:413–497

Hari R, Salmelin R, Mäkelä JP, Salenius S, Helle M (1997) Magnetoencephalographic cortical rhythms. Int J Psychophysiol 26(1–3):51–62

Huang TY, Cherkas PS, Rosenthal DW, Hanani M (2005) Dye coupling among satellite glial cells in mammalian dorsal root ganglia. Brain Res 1036(1–2):42–49

Hughes SW, Crunelli V (2005) Thalamic mechanisms of EEG alpha rhythms and their pathological implications. Neuroscientist 11(4):357–372

Hughes SW, Lörincz M, Cope DW, Blethyn KL, Kékesi KA, Parri HR, Juhasz G, Crunelli V (2004) Synchronized oscillations at alpha and theta frequencies in the lateral geniculate nucleus. Neuron 42:253–268

Jensen O, Colgin LL (2007) Cross-frequency coupling between neuronal oscillations. Trends Cogn Sci 11(7):267–269

Kahana MJ, Sekuler R, Caplan JB, Kirschen M, Madsen JR (1999) Human theta oscillations exhibit task dependence during virtual maze navigation. Nature 399:781–784

Klimesch W, Sauseng P, Hanslmayr S (2007) EEG alpha oscillations: the inhibition-timing hypothesis. Brain Res Rev 53:63–88

Krakow K, Allen PJ, Symms MR, Lemieux L, Josephs O, Fish DR (2000) EEG recording during fMRI experiments: image quality. Hum Brain Mapp 10:10–15

Krishnan V, Chang BS, Schomer DL (2018) Normal EEG in wakefulness and sleep: adults and elderly. In: Schomer DL, Lopes da Silva FH (eds) Niedermeyer's electroencephalography: basic principles, clinical applications and related fields, 7th edn. Oxford University Press, pp 202–228

Laufs H, Kleinschmidt A, Beyerle A, Eger E, Salek-Haddadi A, Preibisch C, Krakow K (2003) EEG-correlated fMRI of human alpha activity. NeuroImage 19:1463–1476

Lehtelä L, Salmelin R, Hari R (1997) Evidence for reactive magnetic 10-Hz rhythm in the human auditory cortex. Neurosci Lett 222(2):111–114

Lemieux L, Allen PJ, Franconi F, Symms MR, Fish DR (1997) Recording of EEG during fMRI experiments: patient safety. Magn Reson Med 38:943–952

Liu Z, He B (2008) FMRI-EEG integrated cortical source imaging by use of time-variant spatial constraints. NeuroImage 39(3):1198–1121

Lopes da Silva F (1991) Neural mechanisms underlying brain waves: from neural membranes to networks. Electroencephalogr Clin Neurophysiol 79(2):81–93

Lopes da Silva FH (2002) Electrical potentials. In: Ramachandran VS (ed) Encyclopedia of the human brain. Elsevier, New York, pp 147–167

Lopes da Silva FH (2013) EEG and MEG: relevance to neuroscience. Neuron 80(2013):1112–1128

Lopes da Silva FH, Storm van Leeuwen W (1977) The cortical source of the alpha rhythm. Neurosci Lett 6:237–241

Lopes da Silva FH, van Lierop T, Schrijver CF, Storm van Leeuwen W (1973) Essential differences between alpha rhythms and barbiturate spindles: spectra and thalamo-cortical coherences. Electroencephalogr Clin Neurophysiol 35(6):641–645

Lopes da Silva FH, van Rotterdam A (2005) Biophysical aspects of EEG and magnetoencephalographic generation. In: Niedermeyer E, Lopes da Silva F (eds) Electroencephalography: basic principles, clinical applications and related fields, 5th edn. Lippincott, Williams & Wilkins, New York

Lopes da Silva FH, van Rotterdam A, Storm van Leeuwen W, Tielen AM (1970) Dynamic characteristics of visual evoked potentials in the dog. II. Beta frequency selectivity in evoked potentials and background activity. Electroencephalogr Clin Neurophysiol 29(3):260–268
Lorente de Nó R (1947) Action potential of the motoneurons of the hypoglossus nucleus. J Cell Comp Physiol 29:207–287
Mainen ZF, Sejnowski TJ (1996) Influence of dendritic structure on firing patterns in model neocortical neurons. Nature 382:363–366
Manshanden I, De Munck JC, Simon NR, Lopes da Silva FH (2002) Source localization of MEG sleep spindles and the relation to sources of alpha band rhythms. Clin Neurophysiol 113(12):1937–1947
Michel CM, Baillet S, Benar C, Bertrand O, Gotman J, He B, Huiskamp G-J, Lemieux L, Makeig S, Pascual-Leone A, Salmelin R, Seri S, Valdes-Sosa P, Wendling F (2019) In Memoriam: Fernando Lopes da Silva (1935–2019). Brain Topography 32(4):519–522. s10548-019-00720-0. https://doi.org/10.1007/s10548-019-00720-0
Michel CM, He B (2018) EEG mapping and source imaging. In: Schomer DL, Lopes da Silva FH (eds) Niedermeyer's electroencephalography: basic principles, clinical applications and related fields, 7th edn. Oxford University Press, Oxford, pp 1135–1156
Moosmann M, Ritter P, Krastel I, Brink A, Thees S, Blankenburg F, Taskin B, Obrig H, Villringer A (2003) Correlates of alpha rhythm in functional magnetic resonance imaging and near infrared spectroscopy. NeuroImage 20:145–158
Moruzzi G, Magoun HW (1949) Brain stem reticular formation and activation of the EEG. Electroencephalogr Clin Neurophysiol 1(4):455–473
Mountcastle VB (1997) The columnar organization of the neocortex. Brain 120:701–722
Munk MH, Roelfsema PR, König P, Engel AK, Singer W (1996) Role of reticular activation in the modulation of intracortical synchronization. Science 272(5259):271–274
Murakami S, Okada Y (2006) Contributions of principal neocortical neurons to magnetoencephalography and electroencephalography signals. J Physiol 575(3):925–936
Niedermeyer E (2005) The normal EEG in the waking adult. In: Niedermeyer E, Lopes da Silva FH (eds) Electroencephalography: basic principles, clinical applications and related fields, 5th edn. Lippincott, Williams & Wilkins, New York
Nita DA, Vanhatalo S, Lafortune FD, Voipio J, Kaila K, Amzica F (2004) Nonneuronal origin of CO_2-related DC EEG shifts: an in vivo study in the cat. J Neurophysiol 92:1011–1022
Nunez PL (1995) Neocortical dynamics and human EEG rhythms. Oxford University Press, New York
Okada YC, Wu J, Kyuhou S (1997) Genesis of MEG signals in a mammalian CNS structure. Electroencephalogr Clin Neurophysiol 103:474–485
Paskewitz DA, Orne MT (1973) Visual effects on alpha feedback training. Science 181(97):360–363
Pfurtscheller G, Lopes da Silva FH (1999) Event-related EEG/MEG synchronization and desynchronization: basic principles. Clin Neurophysiol 110(11):1842–1857
Pfurtscheller G, Stancak A Jr, Neuper C (1996) Post-movement beta synchronization. A correlate of an idling motor area? Electroencephalogr Clin Neurophysiol 98:281–293
Ray WJ, Cole HW (1985) EEG alpha activity reflects attentional demands, and beta activity reflects emotional and cognitive processes. Science 228:750–752
Reimann MW, Anastassiou CA, Perin R, Hill SL, Markram H, Koch C (2013) A biophysically detailed model of neocortical local field potentials predicts the critical role of active membrane currents. Neuron 79:375–390
Riera JJ, Ogawa T, Goto T, Sumiyoshi A, Nonaka H, Evans A, Miyakawa H, Kawashima R (2012) Pitfalls in the dipolar model for the neocortical EEG sources. J Neurophysiol 108:956–975
Rihs TA, Michel CM, Thut G (2007) Mechanisms of selective inhibition in visual spatial attention are indexed by alpha-band EEG synchronization. Eur J Neurosci 25:603–610
Rihs TA, Michel CM, Thut G (2009) A bias for posterior alpha-band power suppression versus enhancement during shifting versus maintenance of spatial attention. NeuroImage 44:190–199
Roopun AK, Middleton SJ, Cunningham MO, LeBeau FE, Bibbig A, Whittington MA, Traub RD (2006) A beta2-frequency (20–30 Hz) oscillation in nonsynaptic networks of somatosensory cortex. Proc Natl Acad Sci U S A 103(42):15646–15650

Rougeul A, Bouyer JJ, Dedet L, Debray O (1979) Fast somato-parietal rhythms during combined focal attention and immobility in baboon and squirrel monkey. Electroencephalogr Clin Neurophysiol 46(3):310–319

Rougeul-Buser A, Buser P (1997) Rhythms in the alpha band in cats and their behavioural correlates. Int J Psychophysiol 26(1–3):191–203

Shmuel A, Maier A (2015) Neurophysiological basis of functional MRI. In: Ugurbil K, Uludag K, Berliner LJ (eds) fMRI: from nuclear spins to brain function, Biological magnetic resonance, vol 30. Springer Science and Business Media, New York

Simon NR, Manshanden I, Lopes da Silva FH (2000) A MEG study of sleep. Brain Res 860(1–2):64–76

Speckmann E-J, Elger CE (2005) Introduction to the neurophysiological basis of EEG and DC potentials. In: Niedermeyer E, Lopes da Silva FH (eds) Electroencephalography: basic principles, clinical applications and related fields, 5th edn. Lippincott, Williams & Wilkins, New York, pp 17–29

Steriade M (2006) Grouping of brain rhythms in corticothalamic systems. Neuroscience 137(4):1087–1106

Steriade M, Contreras D, Amzica F, Timofeev I (1996) Synchronization of fast (30–40 Hz) spontaneous oscillations in intrathalamic and thalamocortical networks. J Neurosci 16(8):2788–2808

Stuart GJ, Sakman B (1994) Active propagation of somatic action potentials into neocortical pyramidal cell dendrites. Nature 367:68–72

Suffczynski P, Kalitzin S, Pfurtscheller G, Lopes da Silva FH (2001) Computational model of thalamo-cortical networks: dynamical control of alpha rhythms in relation to focal attention. Int J Psychophysiol 43:25–40

Sun Y-G, Pita-Almenar JD, Wu C-S, Renger JJ, Uebele VN, Lu H-C, Beierlein M (2013) Biphasic cholinergic synaptic transmission controls action potential activity in thalamic reticular nucleus neurons. J Neurosci 33(5):2048–2059

Surwillo WW (1965) The relation of amplitude of alpha rhythm to heart rate. Psychophysiology 1(3):247–252

Tesche CD, Karhu J (2000) Theta oscillations index human hippocampal activation during a working memory task. Proc Natl Acad Sci U S A 97:919–924

Traub RD, Jefferys JGR, Miles R, Whittington MA, Tóth K (1994) A branching dendritic model of a rodent CA3 pyramidal neurone. J Physiol 481:79–95

Traub RD, Miles R (1991) Neuronal networks of the hippocampus. Cambridge University Press, New York

van Kerkoerle T, Self MW, Dagnino B et al (2014) Alpha and gamma oscillations characterize feedback and feedforward processing in monkey visual cortex. Proc Natl Acad Sci U S A 111:14332–14341

Vanhatalo S, Voipio J, Kaila K (2005) Full-band EEG (FbEEG): an emerging standard in electroencephalography. Clin Neurophysiol 116(1):1–8

Vansteensel MJ, Pels EGM, Bleichner MG, Branco MP, Denison T, Freudenberg ZV, Gosselaar P, Leinders S, Ottens TH, van den Boom MA, van Rijen PC, Aarnoutse EJ, Ramsey NF (2016) Fully implanted brain-computer interface in a locked-in patient with ALS. N Engl J Med 375:2060–2066

Voipio J, Tallgren P, Heinonen E, Vanhatalo S, Kaila K (2003) Millivolt-scale DC shifts in the human scalp EEG: evidence for a nonneuronal generator. J Neurophysiol 89:2208–2214

Von Helmholtz HLF (2004) Some laws concerning the distribution of electric currents in volume conductors with applications to experiments on animal electricity. Proc IEEE 92(5):868–870

Wadman WJ, Lopes da Silva FH (2018) Biophysical aspects of EEG and MEG generation. In: Schomer DL, Lopes da Silva FH (eds) Niedermeyer's electroencephalography: basic principles, clinical applications and related fields, vol 2018, 7th edn. Oxford University Press, Oxford, pp 89–103

Wolters CH, Anwander A, Tricoche X, Weinstein D, Koch MA, MacLeod RS (2006) Influence of tissue conductivity anisotropy on EEG/MEG field and return current computation in a realistic head model: a simulation and visualization study using high-resolution finite element modeling. NeuroImage 30(3):813–826

The Basics of Functional Magnetic Resonance Imaging

3

Ralf Deichmann, Ulrike Nöth, Alberto Merola, and Nikolaus Weiskopf

3.1 The Basics of MR Imaging

3.1.1 Spins in an External Magnetic Field

In magnetic resonance imaging (MRI), the signal that is measured usually arises from the nuclei of the tissue's hydrogen atoms (i.e. *protons*). A proton possesses a physical property, its *spin*, which behaves roughly speaking like a compass needle: each spin has a small magnetic dipole moment and aligns in an external magnetic field. If the tissue is brought into the strong magnetic field inside the magnetic resonance (MR) scanner bore, spins will align either antiparallel or parallel to the magnetic field B. At the field strengths relevant here, a tiny majority of the spins assume the latter alignment, and their magnetic moments add up, giving rise to a net macroscopic magnetisation M which is parallel to B, representing a state of equilibrium (Fig. 3.1, left). Thus, the existence of this magnetisation inside the magnetic field is an indicator of the presence of protons, and the measurement of M with a certain spatial resolution can be used to construct a proton image.

R. Deichmann (✉) · U. Nöth
Brain Imaging Center, Goethe University, Frankfurt am Main, Germany
e-mail: deichmann@med.uni-frankfurt.de; noeth@med.uni-frankfurt.de

A. Merola · N. Weiskopf
Department of Neurophysics, Max Planck Institute for Human Cognitive and Brain Sciences, Leipzig, Germany
e-mail: amerola@cbs.mpg.de; weiskopf@cbs.mpg.de

C. Mulert, L. Lemieux (eds.), *EEG - fMRI*,
https://doi.org/10.1007/978-3-031-07121-8_3

3.1.2 The Magnetic Resonance Effect

The measurement of M is possible due to the following physical effect: if the protons inside the magnetic field B are exposed to an electromagnetic wave with a specific frequency, the so-called *Larmor frequency*, the magnetisation M, is tilted in proportion to the exposure duration (Fig. 3.1, right). The tilted magnetisation then rotates around the magnetic field vector (Fig. 3.2). This movement, called *precession*, is similar to the behaviour of an ordinary spinning top. During precession, the protons send out an electromagnetic wave that has the Larmor frequency (Fig. 3.2). The important point is that the Larmor frequency is proportional to the magnetic field B, with a value of 42.6 MHz per Tesla, where Tesla (T) is the unit of the magnetic field strength. Thus, for clinical MR scanners which usually have a field strength of 1.5 or 3 T, the Larmor frequency amounts to about 64 or 128 MHz, respectively, which encompasses the range of frequencies used for FM broadcasting. It should be noted that the tilted magnetisation gradually returns to its original state or equilibrium. This effect, called *relaxation*, will be discussed below.

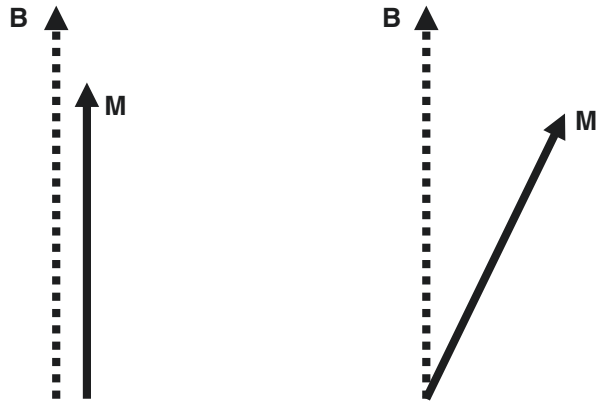

Fig. 3.1 Spins align in an external magnetic field B, giving rise to a macroscopic *magnetisation* M which is parallel to B (*left*). If the protons inside the magnetic field B are exposed to an electromagnetic wave with the *Larmor frequency*, the magnetisation M is tilted (*right*)

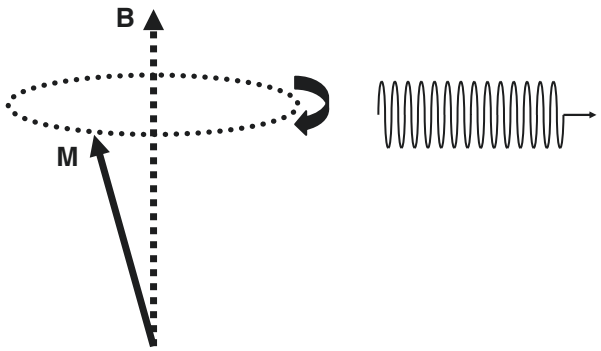

Fig. 3.2 The tilted magnetisation rotates around the magnetic field vector, sending out an electromagnetic wave with the Larmor frequency

In summary, *M* (and thus the presence of protons) is detected in the following way: the sample is placed inside the MR scanner and thus exposed to a strong static magnetic field *B*. As a consequence, a macroscopic magnetisation *M* parallel to *B* builds up. An electromagnetic wave with the Larmor frequency and duration of a few milliseconds is transmitted using equipment similar to a small FM radio broadcasting station. This gives rise to a tilt and a subsequent precession of the magnetisation vector. After sending the initial electromagnetic pulse, a detector similar to an FM radio tuned to the Larmor frequency is switched on. If a signal is detected, there must be protons inside the sample under investigation. It is important to note that the initial step of tilting the magnetisation only works if the frequency of the transmitted electromagnetic signal is exactly the protons' Larmor frequency. Thus, we are dealing with a typical resonance effect, giving rise to the expression MRI. The MR effect was first described in 1946 (Bloch et al. 1946; Purcell et al. 1946).

3.1.3 Spatial Encoding in MR Imaging

As described so far, the MR effect only allows the detection of the presence of protons. The question of how spatial resolution of the protons throughout the sample can be achieved to produce an image now arises. This will be discussed step by step for three orthogonal directions that are defined relative to the brain as follows: *x* (left/right), *y* (anterior/posterior) and *z* (superior/inferior).

3.1.3.1 Frequency Encoding

Figure 3.3 (left) shows a so-called *pulse diagram*, a schematic description of an MR experiment. On the *RF (radiofrequency) axis*, there is the initial electromagnetic pulse that tilts the magnetisation and the signal acquired subsequently. Below, there is the *gradient axis*, showing that during signal acquisition a *gradient* G_x is switched on. This means that during acquisition the magnetic field is modified in a way that it increases linearly in the *x*-direction. Thus, during acquisition, the protons' Larmor frequency depends on their position inside the brain, i.e. on their *x*-coordinate. Figure 3.3 (right) shows two small brain regions and the signal that protons inside these regions send out while the gradient is switched on: the protons in the region on the left-hand side are exposed to a slightly reduced magnetic field, so they send out an electromagnetic wave with a slightly lower frequency. The signal sent out by the protons in the region on the right-hand side has a higher frequency. The "FM radio" detects the sum signal from all protons. This signal undergoes a *frequency analysis* (mathematically, this process is called a *Fourier transform*), resulting in the signal's frequency spectrum. The exact positions of the protons (or at least their *x*-coordinates) can then be deduced from the signal's frequency spectrum. Thus, this process is called *frequency encoding*. The gradient that is switched on during signal acquisition (or signal "readout") is called the *read gradient*. It should be noted that this gradient is on during acquisition only, not during the initial RF pulse. Otherwise, the spins would have different, position-dependent Larmor frequencies while the electromagnetic wave is being sent, so the magnetisation would be tilted for only some of the spins. The use of magnetic field gradients to achieve spatial resolution was first proposed by Lauterbur (1973).

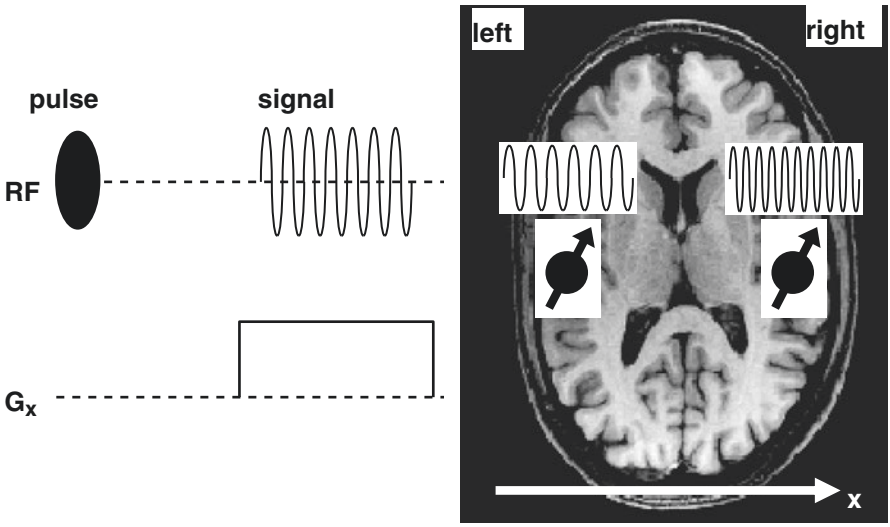

Fig. 3.3 The concept of frequency encoding: due to the *read gradient* (x-direction), the magnetic field increases linearly in the x-direction. Consequently, during acquisition, the protons' Larmor frequencies depend on their positions inside the brain. The exact positions of the protons (or at least their x-coordinates) can then be deduced from the frequency spectrum

3.1.3.2 Phase Encoding

The experiment described above allows for spatial resolution in one direction only. A 2D experiment is depicted in Fig. 3.4. This time, the pulse diagram comprises an RF axis and two gradient axes for gradients in the x- and y-directions. Parts of this experiment correspond to the one described above: the initial RF pulse tilts the magnetisation, and a signal is acquired while the read gradient G_x is switched on, so the protons' x-coordinates can be deduced from their signal frequencies. In addition, a gradient in the direction perpendicular to the read gradient, G_y, is switched on between the initial RF pulse and the acquisition process. The effect of this gradient is explained in Fig. 3.4 (right) for two brain regions with the same x-coordinates but different y-coordinates: while the gradient G_y is switched on, the protons in the anterior region have a higher Larmor frequency than the protons in the posterior one. The effect on the Larmor frequency only lasts as long as G_y is switched on. Once G_y is switched off and G_x is switched on, the signals from both regions have the same Larmor frequencies because they have the same x-coordinate. However, the starting points of the signals from the anterior and posterior regions are different: for the example shown in Fig. 3.4, the signal from the anterior region has a maximum value when acquisition starts, whereas the signal from the posterior region has a minimum value. Thus, the signals appear shifted in time—they have different *phases*. In summary, the x-coordinate can be deduced from the signal frequency and the y-coordinate from the signal phase. The gradient G_y is called the *phase encoding (PE) gradient*, and the process of switching an imaging gradient between spin excitation and signal acquisition is referred to as PE. It should be noted that an exact determination of the

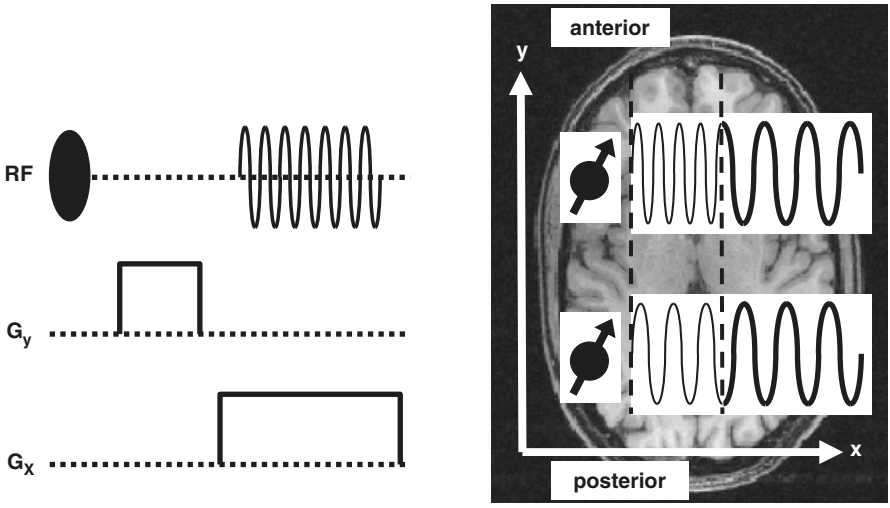

Fig. 3.4 The concept of phase encoding (PE): while the *phase gradient* (*y*-direction) is switched on, protons with different *y*-coordinates precess with different frequencies, leading to different starting points (*phases*) when the acquisition begins. Thus, the *y*-coordinate can be deduced from the phase and the *x*-coordinate from the frequency

y-coordinate requires the repetition of the experiment depicted in Fig. 3.4 using different PE gradients. Thus, in Fig. 3.8, which shows a complete imaging experiment, the PE gradient (i.e. the gradient in the *y*-direction) is depicted as a "ladder" with an arrow, reflecting the different PE gradient amplitudes.

3.1.3.3 Slice Selection

Figure 3.5 shows an experiment with spatial resolution in three directions. Basically, this experiment corresponds to the one discussed above, comprising a phase gradient and a read gradient. However, this time a gradient G_z is switched on at the beginning of the experiment and remains on during the transmission of the RF pulse. Due to this gradient, the magnetic field strength and thus the protons' Larmor frequencies increase in this direction. Let us assume that within a certain axial slice the Larmor frequency has a value of f_0 (Fig. 3.5, *right*). If an RF pulse with this frequency is sent, it will tilt the magnetisation within this slice only. It cannot influence protons in the upper or lower parts of the brain, because their Larmor frequencies are higher or lower than f_0, so there is no resonance (in a certain way, this resembles a swing that can only be pushed effectively when using the correct rhythm/frequency). Thus, only protons inside the selected slice are tilted (or "excited") and can contribute to the signal. In summary, the combination of an RF pulse and a gradient causes a slice-selective excitation. The gradient G_z is also referred to as the *slice gradient* or *slice-selective gradient*. The spatial encoding within the excited slice is then achieved with the help of the read gradient G_x and the phase gradient G_y, as described above. This process is repeated for different excitation frequencies in order to acquire multislice image datasets.

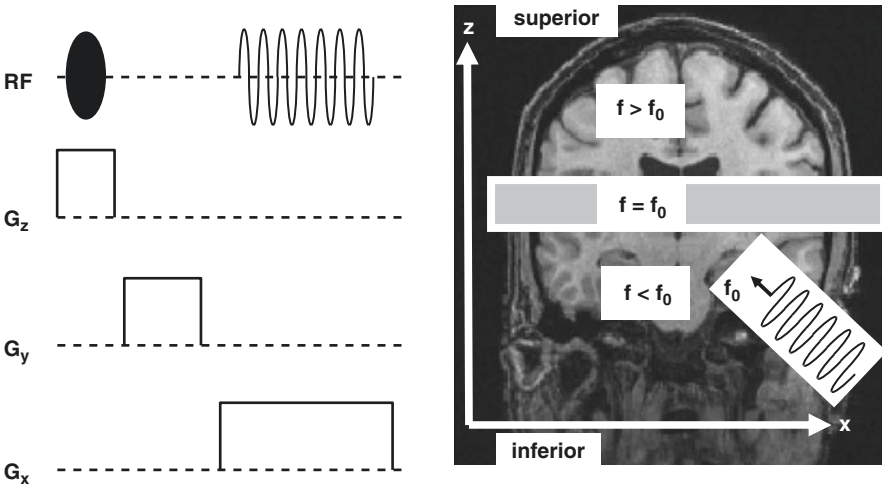

Fig. 3.5 The concept of slice selection: due to the *slice gradient* (z-direction), protons with different z-coordinates have different Larmor frequencies. Thus, an RF pulse with a specific frequency can only excite protons within a certain slice

3.1.4 Relaxation Times T1 and T2

After an RF pulse has tilted the magnetisation vector, precession takes place, as shown in Fig. 3.2. However, as noted previously, precession has a limited duration: after a while, the magnetisation is once again parallel to the static magnetic field, i.e. at equilibrium. This process is called *relaxation*. Relaxation consists of two simultaneous processes, as follows.

The *longitudinal* component of the tilted magnetisation (i.e. the component parallel to the magnetic field) approaches a maximum value (the so-called *equilibrium value*) with the time constant T1, the *longitudinal relaxation time*. This process is also called *spin-lattice relaxation* because free water spins transfer energy to the surrounding environment, the *lattice*.

The *transverse* component of the tilted magnetisation (i.e. the component perpendicular to the magnetic field) vanishes with the time constant T2, the *transverse relaxation time*. This process is also called *spin-spin relaxation* because it arises from free water spins exchanging small amounts of energy.

In the human brain, there are a wide variety of T1 values: at 3 T, approximate T1 values are 850 ms (white matter); 1300 ms (grey matter); and 4500 ms (CSF) (Wansapura et al. 1999). Thus, MRI acquisition sequences that exploit T1 contrast are commonly used to visualise and quantify brain morphology. Examples for T1-weighted techniques are T1-weighted spin echo sequences, T1-weighted fast gradient echo sequences like FLASH (Haase 1990) and magnetisation-prepared sequences such as MP-RAGE (Mugler and Brookeman 1990) and MDEFT (Ugurbil et al. 1993). It should be noted that T1 values are field-dependent. As an example,

T1 values in white/grey matter are approximately 650/1100 ms at 1.5 T but 1200/2000 ms at 7 T (Rooney et al. 2007).

For T2, there is less contrast between white matter and grey matter, with values at 3 T amounting to about 60 ms in brain tissue and 45 ms in iron-rich regions such as the globus pallidus (Nöth et al. 2017). However, CSF has a very long T2 value (about 2000 ms), providing a means of distinguishing between brain tissue and fluid compartments like oedema. Thus, T2-weighted acquisition techniques such as T2-weighted spin echo sequences are often used to detect lesions.

3.1.5 The Relaxation Time T2* and Gradient Echoes

Figure 3.6 shows a series of MR images acquired on a phantom (in this case, a simple glass sphere filled with water). A tiny piece of metal was firmly attached to the outside of the phantom (red arrow). The metal has the effect of distorting the static magnetic field in its immediate environment (circled area). The images were acquired with increasing values of the *echo time* (TE) which is the time difference between the initial RF pulse and signal acquisition (see Fig. 3.8, left). The first effect to be noted is that the phantom signal decreases with increasing TE. This is to be expected as the transverse magnetisation, which gives rise to the signal, decays due to transverse relaxation effects, as described in the previous section. The second effect is that the signal decay is much faster in the area where the magnetic field is distorted. This can be explained as follows: due to the field inhomogeneity, spins at different positions in space will be exposed to different field strengths, so they will have different Larmor frequencies. Consequently, the spins *dephase*—i.e. their magnetisation vectors rotate at different speeds, thus pointing in different directions, so their contributions to the net magnetisation cancel each other, causing a fast signal decay. In general, it can be said that any inhomogeneity of the static magnetic field will have a similar effect, resulting in accelerated signal decay. Thus, the signal decays with the

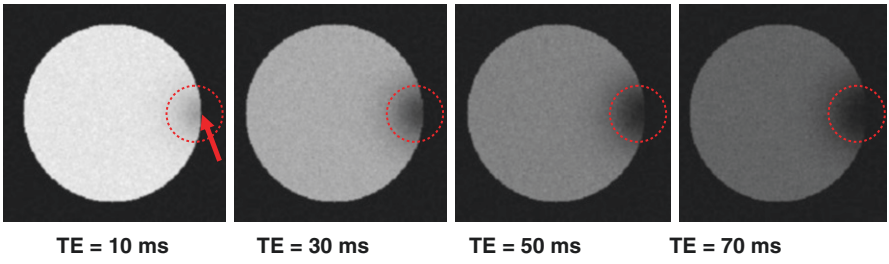

Fig. 3.6 A series of images acquired on a water phantom with different *echo times* (TE). Due to transverse relaxation effects, the signal decreases with increasing TE. A small piece of metal was attached to the phantom (position marked with red arrow). This causes a distortion of the static magnetic field inside the circled area where the signal decays more rapidly. In summary, the signal decays with the *effective transverse relaxation time T2**, which is shortened by magnetic field inhomogeneities

effective (apparent) transverse relaxation time T2*, which depends on the degree of field inhomogeneity and can be considerably shorter than T2.

This poses a specific problem for the MRI methods discussed so far. As explained above (see Fig. 3.3), frequency encoding is achieved by switching a gradient in a certain spatial direction. Since gradients are artificial magnetic field inhomogeneities, this causes an accelerated signal decay, as shown in Fig. 3.7 (left). In particular, the maximum signal occurs at the beginning of the gradient. However, this part of the signal may provide erroneous spatial information because gradients require a certain switching time to achieve a stable value. The problem can be avoided by using the *gradient echo* concept shown in Fig. 3.7 (right): before the acquisition, a negative gradient is deliberately switched on and causes spin *dephasing*. Since the subsequent positive read gradient is just an inversion of the previous gradient, the dephasing effect is inverted, so the spins *rephase* and a strong signal called *gradient echo* occurs. Importantly, the maximum of the gradient echo is located at a time point where the read gradient has achieved a stable value. Gradient echo methods are widely used, in particular for functional imaging.

Figure 3.8 (left) shows a typical gradient echo imaging sequence. Before the acquisition, a negative gradient in the *x*-direction causes spin dephasing. When the positive read gradient is switched on, the spins rephase and a gradient echo occurs. In addition, a negative gradient is switched on after the slice gradient to compensate for dephasing effects due to this gradient that would otherwise reduce the signal strength. It should be noted that in gradient echo techniques, spin dephasing compensation only occurs for the gradients that are inverted. All other field inhomogeneities cause additional spin dephasing and thus reduce the T2* value. Consequently, gradient echo images are T2* weighted, displaying lower image intensities in areas of reduced T2* due to local inhomogeneities of the static magnetic field.

The choice of the echo time (TE) determines the T2* contrast: if TE is too short, the spins do not have sufficient time to dephase, so T2* weighting is poor. If on the

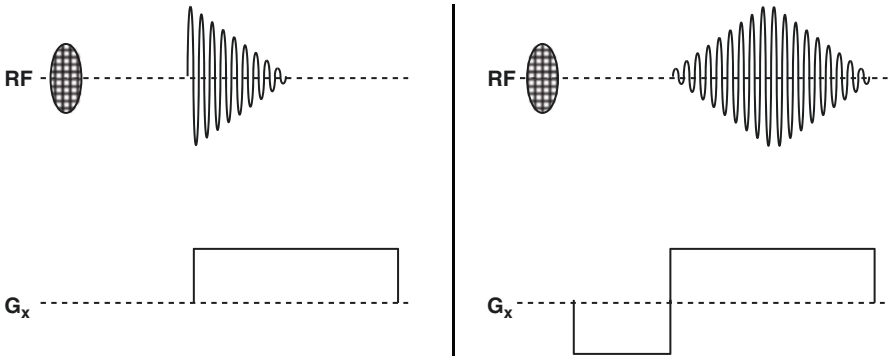

Fig. 3.7 (*Left*) In the presence of a gradient, the signal decays rapidly since a gradient constitutes a magnetic field inhomogeneity. (*Right*) The gradient echo concept: an initial negative gradient causes *dephasing* of the spins. After inversion of the gradient, this process is reversed (*rephasing*), and the signal returns (*gradient echo*)

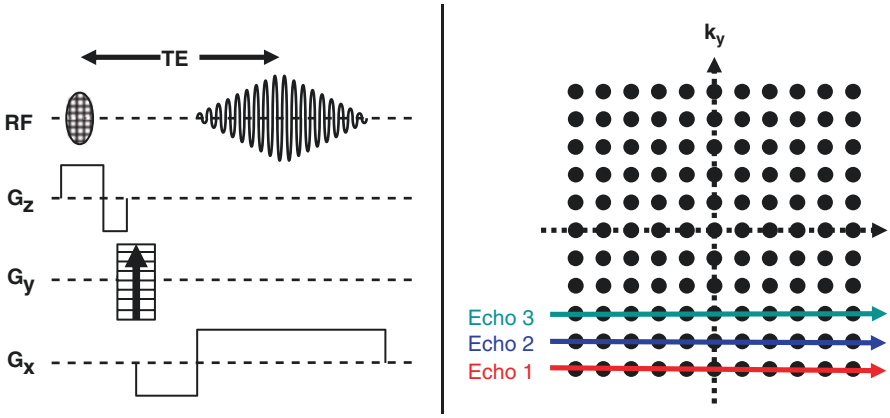

Fig. 3.8 (*Left*) A complete gradient echo imaging experiment. The *echo time (TE)* is defined as the time difference between the RF excitation and the centre of the gradient echo. *(Right*) Schematic description of *k*-space coverage for this gradient echo experiment, filling *horizontal lines* successively from the *left* to the *right*

other hand TE is considerably longer than T2*, the signal will have decayed by the time the acquisition starts, so the signal-to-noise ratio (SNR) of the image will be poor. The best T2* weighting is achieved if TE is approximately T2*.

Gradient echo techniques are of major importance for functional imaging studies because neuronal activations lead to small changes of T2* in the surrounding brain tissue and thus to intensity variations in T2*-weighted gradient echo images. This effect, which is called the blood oxygenation level-dependent (BOLD) effect, will be discussed in a later section.

3.1.6 *k*-Space

k-Space is a mathematical concept that is extremely useful for describing MR acquisition sequences, in particular the echo planar imaging sequence, which is the mainstay of functional magnetic resonance imaging (fMRI). This section will give a quick non-mathematical introduction to *k*-space.

Let us assume that a single data point is acquired, for example, one of the data points forming a gradient echo. Between the acquisition of this data point and the preceding RF excitation pulse, a gradient G_x (in the read direction) and a gradient G_y (in the phase direction) are switched on for a certain duration. The data point's *k-values* k_x and k_y are then defined as the areas under the respective gradients (i.e. the product of gradient strength and gradient duration). For example, in Fig. 3.4 the k_y value of any data point constituting the signal is the area under the preceding PE gradient G_y, and the k_x value is the area under the read gradient G_x up to the time when the data point is acquired. This means that the data points constituting the signal in Fig. 3.4 have the same k_y value but different, increasing k_x values. Based on

this definition, we can now analyse the k values of the data points in the various gradient echoes that are acquired according to Fig. 3.8 (left). Please keep in mind that the experiment depicted in Fig. 3.8 is repeated several times using different values for the PE gradient G_y, i.e. several gradient echoes with different degrees of PE are acquired. Let us start with the k_x values: the first data point of each gradient echo is preceded by the negative gradient on the G_x axis only, so it has a negative k_x value. The other data points are preceded by the initial negative gradient plus the positive read gradient of increasing duration, so they have increasing k_x values. However, all data points belonging to the same echo are preceded by the same gradient G_y, so they have the same k_y value, which is negative for the first echo because G_y starts with a negative value. The different k values of the data points belonging to the gradient echo can be depicted in a 2D k-space diagram, as shown in Fig. 3.8 (right): obviously, the data points cover the bottom-most horizontal line in k-space. For the next echo, the PE gradient G_y has a higher value, so k_y is increased and the data points constituting this echo cover the next highest horizontal line in k-space (Fig. 3.8, right). In summary, one can say that for any particular MR imaging experiment, several data points with different combinations of k_x and k_y must be acquired, covering the complete 2D k-space, as shown in Fig. 3.8 (right). For the experiment described in Fig. 3.8 (left), k-space is covered in horizontal lines, filling each line successively from the left to the right.

3.1.7 Echo Planar Imaging (EPI)

The gradient echo sequence depicted in Fig. 3.8 (left) is relatively time-consuming, mainly because each repetition with a new PE gradient requires its own slice-selective excitation pulse. Special gradient echo techniques such as single-shot EPI have been developed to circumvent this limitation (Mansfield 1977). EPI is schematically described in Fig. 3.9 (left). After slice-selective excitation, a series of gradient echoes are acquired by successive inversions of the read gradient. A short gradient pulse in the y-direction, the so-called blip, is switched on between successive acquisitions. Thus, the degree of PE for a specific echo is given by the initial negative gradient in the y-direction and the sum of the blips up to the echo acquisition time. In summary, this satisfies the conditions posed above for imaging (performance of a series of acquisitions while a read gradient in the x-direction is turned on, with each acquisition being preceded by phase gradients in the y-direction with different degrees of PE), so a full image can be constructed from the acquired data. There is only one excitation pulse, so the technique is very fast, with typical acquisition times of less than 100 ms per slice. Gradient echo EPI images are heavily T2* weighted, displaying reduced image intensity in areas affected by local magnetic field inhomogeneities, as explained above. As we will see below, T2* weighting and speed of acquisition make this technique ideally suited for functional MRI.

The k-space analysis is relatively simple: for the first echo, the data points have increasing k_x values, ranging from a negative to a positive value but the same negative k_y value due to the preceding PE gradient G_y. Thus, this echo covers the

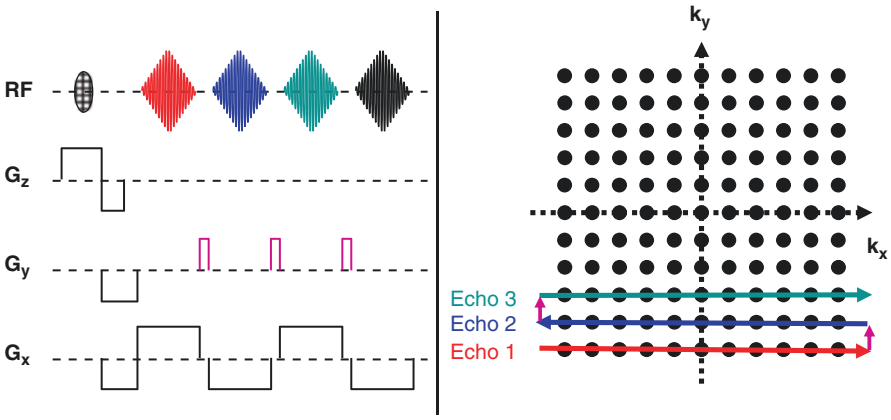

Fig. 3.9 (*Left*) Schematic description of single-shot echo planar imaging (EPI): a series of gradient echoes is acquired by successive inversions of the read gradient. Due to short intermediate *y*-gradient pulses (*blips*), the echoes have different degrees of PE. (*Right*) Schematic description of *k*-space coverage for EPI, filling *odd horizontal lines* successively from the *left* to the *right* and *even horizontal lines* successively from the *right* to the *left*

bottom-most horizontal line in *k*-space, as shown in Fig. 3.9 (right). For the second echo, k_y is increased due to the intermediate blip. The k_x values of this echo range from a positive to a negative value, so this echo covers the next horizontal line in *k*-space but *in reverse order*. In summary, it can be said that *k*-space is covered in horizontal lines in EPI, with odd lines filled successively from the left to the right, and even lines from the right to the left. This *k*-space line-filling order reversal, which allows for fast data acquisition, can also give rise to artefacts (see Chap. 10).

3.1.8 Spin Echoes

For the sake of completeness, the occurrence of spin echoes will be briefly described in this section. The basic experiment is described in Fig. 3.10 (top). A 90° pulse tilts the magnetisation vector, and a strong signal can be observed directly after the excitation (time point 1). This signal decays with the time constant T2*. After a short while, a 180° pulse is applied (between time points 2 and 3). As a consequence, the signal builds up again (time point 4). This effect is known as *spin echo* (Hahn 1950) and can be explained as follows (bottom part of Fig. 3.10). Directly after the excitation (time point 1), all of the spins are aligned, forming a strong signal. However, they start to rotate (black arrow), usually with different Larmor frequencies due to field inhomogeneities, as described above. For simplicity, let us assume there are three spin ensembles: a "fast" one (red), an "average" one (blue) and a "slow" one (green). After a while (time point 2), the "fast" spins are relatively advanced, whereas the "slow" spins are lagging behind. Consequently, the spins are dephased and the signal has decayed. The 180° pulse rotates the spins around the axis of

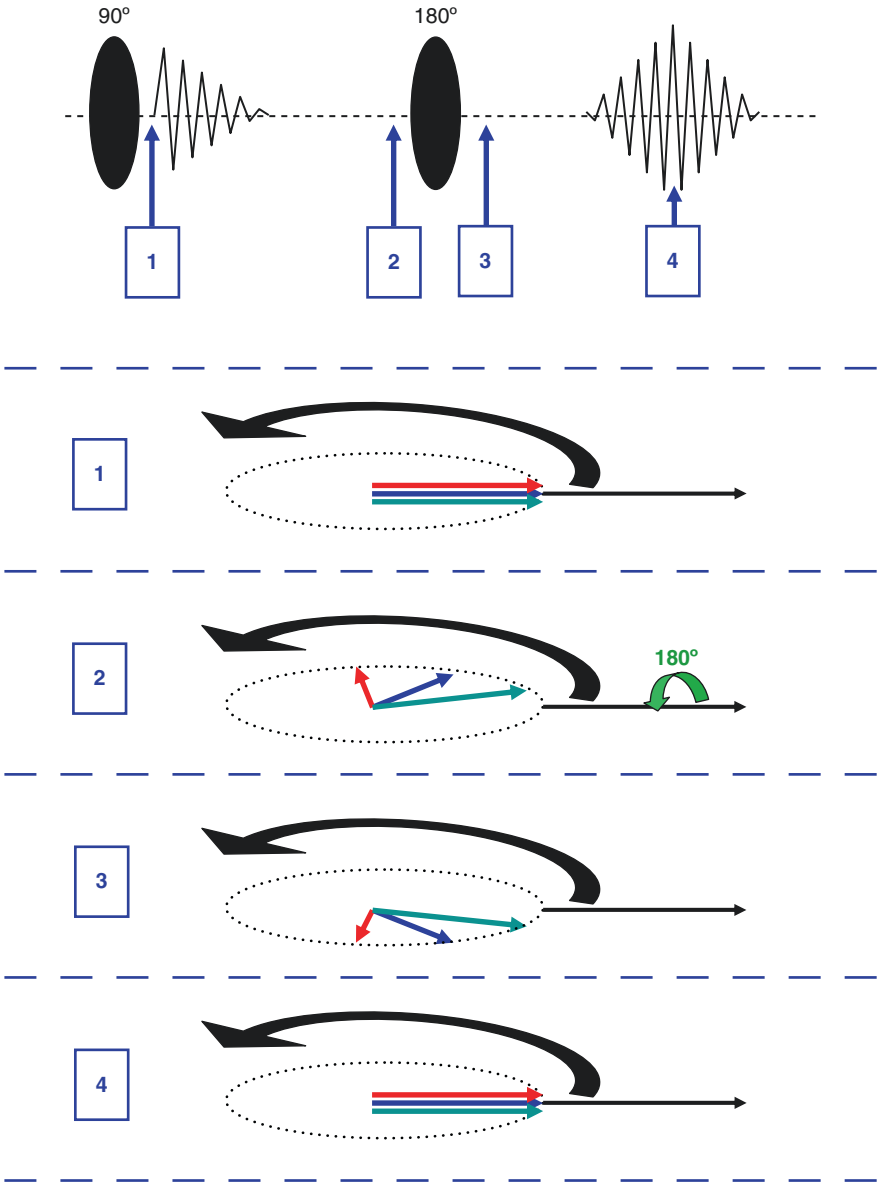

Fig. 3.10 Schematic description of the spin echo effect, indicating the magnetisation vectors of three spin ensembles with high (*red*), medium (*blue*) and low (*green*) Larmor frequencies. At time point 2, the signal is dephased because the *red* vector is advanced, while the *green* one is lagging behind. After application of the 180° pulse, this constellation is inverted. As a consequence, the *red* vector "catches up", and at time point 4, the vectors are realigned, resulting in the spin echo signal

initial alignment (green arrow). This leads to a fundamental change in constellation (time point 3): the "fast" spins are now lagging behind, while the "slow" ones are well advanced. However, the direction of precession remains unchanged (black arrow), so the "fast" spins catch up, and after a while (time point 4), the spins are realigned, once again forming a strong signal, the spin echo. This procedure compensates for the effects of *all* field inhomogeneities, so spin echoes are T2-weighted (in contrast to gradient echoes, which are T2*-weighted).

As described above, T2-weighted spin echo sequences are widely used in clinical practice for the detection of lesions. To shorten the experiment duration, a fast spin echo sequence dubbed RARE (Hennig et al. 1986) is frequently used (also known as the *turbo spin echo* sequence or *fast spin echo* sequence). This sequence is basically similar to the EPI technique described above; however, to achieve T2 weighting, a series of spin echoes (rather than gradient echoes) are acquired by applying 180° pulses between subsequent echoes.

3.1.9 The Specific Absorption Rate (SAR)

When RF pulses are applied in MRI experiments, energy is transferred to the spin system. The problem is that RF pulses also induce electrical currents in the tissue, which lead to tissue heating. As a consequence, only a fraction of the transmitted RF energy is used for spin excitation, and the remaining part causes unwanted heating effects. The SAR is the RF power absorbed by the tissue, measured in watts per kilogram of body weight. For safety reasons, the SAR must not exceed certain limits. As an example, the maximum allowed SAR averaged over the head is 3.2 W/kg. The SAR depends strongly on the MRI technique in use. For example, EPI is a low-SAR technique because only a single RF pulse is required per imaging slice. In contrast, fast spin echo techniques like RARE (turbo spin echo) are high-SAR techniques because a series of 180° pulses is required to create a train of spin echoes. It should be noted that SAR values increase with the scanner's magnetic field strength. Due to the higher Larmor frequency and the fact that tissue conductivity increases with the frequency, a larger proportion of the energy is converted into heat. As a consequence, it may be difficult to run high-SAR sequences on high-field scanners.

The insertion of conductive material (such as EEG electrodes and leads) inside the scanner bore is problematic because induced currents can heat up the hardware, resulting in a risk of causing local RF burns where the hardware is in contact with the skin. Thus, high-SAR sequences should not be used in concurrent EEG–fMRI acquisitions. Additionally, in studies of this kind, the standard RF setup (whole-body coil for RF transmission and head coil for signal reception) should be avoided; a head transmit/receive coil should be used instead, to reduce the exposure of equipment to RF fields. The dependence of electrode heating on the RF coil type and the SAR has been tested experimentally (Nöth et al. 2012). The issue of safety in relation to EEG–fMRI is discussed in detail in Chap. 7.

3.2 The Cerebral Blood Flow (CBF)

3.2.1 Definition, Order of Magnitude and Measurement

Brain perfusion or CBF is a measure of the delivery of arterial blood, and thus of oxygen, to the brain tissue. An increase in CBF is caused, for example, by brain activation due to a higher demand of oxygen during neuronal activity; this CBF increase results in a higher oxyhaemoglobin concentration at the site of activity, leading to the "BOLD effect" described in Sect. 3.4 of this chapter. Therefore, the site of brain activation can be determined by measuring CBF changes (Luh et al. 2000). On the other hand, a decrease in CBF will lead to low levels of oxygen (hypoxia), to which the brain is very vulnerable, which can cause brain damage in severe cases, such as in cases of ischaemic stroke. In general, CBF is a crucial parameter for diagnosing, treating and understanding the mechanisms underlying various pathological conditions (Grade et al. 2015; Haller et al. 2016), in particular stroke (Wang et al. 2013), epilepsy (Storti et al. 2014), cancer (White et al. 2014) and dementia (Le Heron et al. 2014). Combined EEG–CBF measurements have been successfully performed in the field of epilepsy (Stefanovic et al. 2005; Hamandi et al. 2008; Carmichael et al. 2008); see Chaps. 17, 18, and 19.

CBF can be quantified in terms of the rate of delivery of arterial blood $\Delta V_B/\Delta t$ (measured in mL per min) to the capillaries of a particular volume V or mass m of the brain tissue (measured in units of 100 mL or 100 g, respectively; see also Fig. 3.11):

$$\mathrm{CBF} = \frac{1}{V} \cdot \frac{\Delta V_B}{\Delta t}.$$

Approximate values for global CBF in healthy adults are 60 mL/100 g/min in grey matter and 20 mL/100 g/min in white matter (Biagi et al. 2007), although the range of values found in the literature is large.

It should be noted that only blood in the capillaries contributes to CBF, while blood passing through the tissue in arteries (or arterioles) and veins (or venules) does not.

There are two major MR methods for measuring CBF, *arterial spin labelling (ASL)* and *dynamic susceptibility contrast (DSC) MRI*.

DSC MRI uses a paramagnetic gadolinium-based contrast agent, which is injected intravenously as a tracer, so this method is invasive. The contrast agent locally reduces the relaxation times T1, T2 and T2*. The passage of the contrast agent bolus through the tissue of interest is usually monitored by acquiring a time series of T2- or T2*-weighted images (e.g. using the EPI sequence), because the respective imaging sequences have a higher temporal resolution than T1-weighted sequences. By analysing the signal time course of the bolus passage, which has a duration of typically a few seconds, information on the CBF, the cerebral blood volume (CBV) and the mean transit time (MTT) can be derived (Buxton 2002, pp. 310–350). Since changes of the transverse relaxation

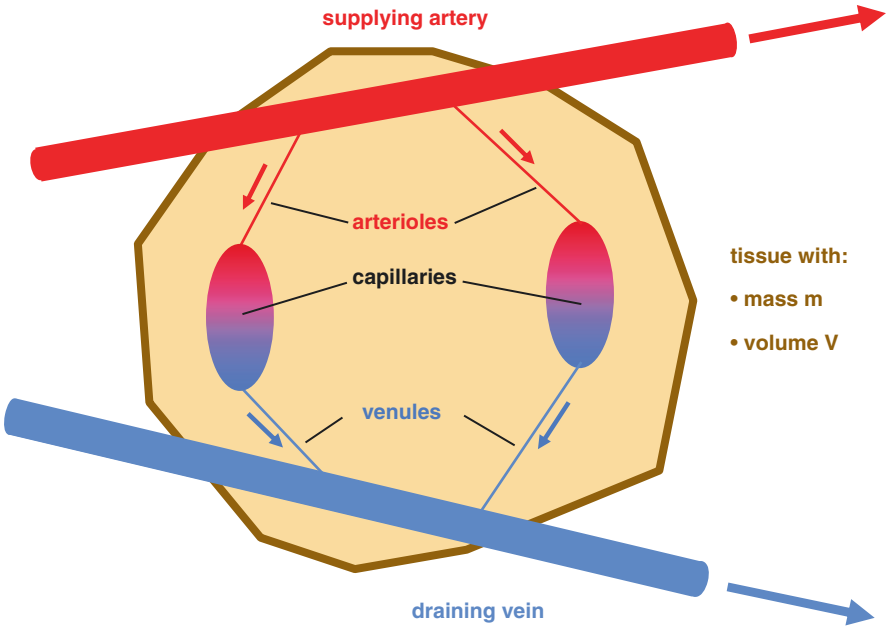

Fig. 3.11 The cerebral blood flow (CBF) is the rate of delivery of arterial blood to the capillaries of a particular volume *V* or mass *m* of the brain tissue. Only blood in the capillaries contributes to the CBF. Blood passing through the tissue in arteries (or arterioles) and veins (or venules) does not contribute

rates 1/T2* and 1/T2 can be assumed to be proportional to the contrast agent concentration, the latter can be obtained from changes in signal intensity, from which concentration-time curves can be derived. The advantage of this method is a high SNR. However, absolute CBF quantification is complicated as the proportionality constants in the various relationships are not accurately known (Willats and Calamante 2013). In addition, DSC MRI does not allow for repeated CBF measurements before complete washout of the contrast agent. *Dynamic contrast-enhanced (DCE)* MRI is based on T1-weighted imaging after intravenous injection of the paramagnetic contrast agent; however, due to the lower temporal resolution, it is less frequently used for brain perfusion measurements.

In contrast to the DSC method, ASL uses inverted blood spins as a tracer and is completely noninvasive. With a time resolution of approximately 4 min (for quantitative high-resolution multislice or 3D CBF maps), it allows for serial determination of CBF. The disadvantage is the low SNR and the short lifetime of the tracer (which decays with T1). Therefore, ASL does profit from measurements at high magnetic field strengths that intrinsically provide increased SNR and longer T1 values. In the following paragraphs, only the noninvasive ASL method will be discussed because of its widespread use in human studies.

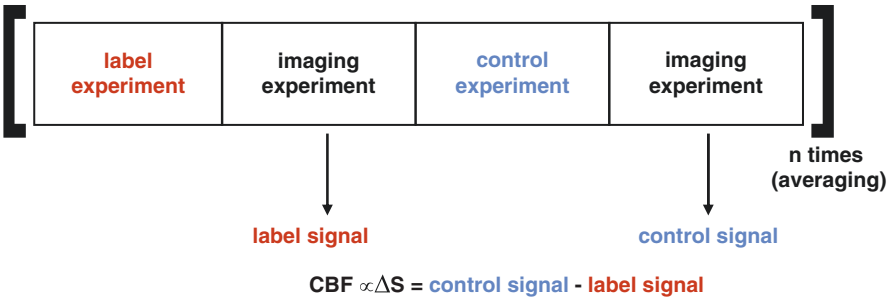

Fig. 3.12 Schematic description of the arterial spin labelling (ASL) method for CBF quantification: two types of images are acquired, through either a label experiment or a control experiment. The CBF is proportional to the difference image. To increase the signal-to-noise ratio, the acquisition is usually averaged several times

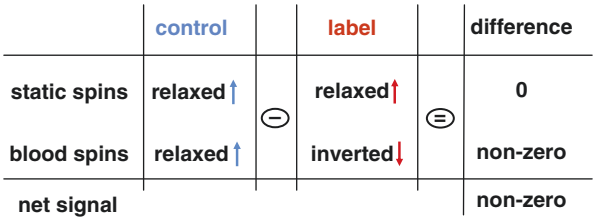

Fig. 3.13 Schematic description of the ASL method for CBF quantification: static spins are fully relaxed for both the control and the label experiment. In contrast, blood spins are inverted for the label experiment. Thus, the difference image shows the signal for blood spins only

3.2.2 Arterial Spin Labelling Measurements

An ASL measurement consists of a label experiment, where a magnetisation preparation (inversion) of inflowing blood is performed before its entry into the imaging slice(s), and a control experiment, where no preparation of the inflowing blood is performed. Images are acquired after each experiment, giving the label and control signals (Fig. 3.12). The CBF is proportional to the difference in signal:

$$\mathrm{CBF} \propto \Delta S = S_{\mathrm{control}} - S_{\mathrm{label}}$$

The fact that the signal difference only shows perfused areas can be explained as follows. The signal in the imaging slice arises from the static tissue spins and the moving blood spins. The static spins provide the same signal in the label and control scans, so they do not contribute to the difference image. The inflowing blood spins, however, are relaxed in the control scan and inverted in the label scan, which results in a positive signal in the difference image (Fig. 3.13).

It should be noted that ΔS is generally on the order of 1% of the average signal strength in the label and control images, so a small measurement error in S_{control} or S_{label} will result in a large error for CBF.

3.2.3 Labelling Methods

The basic ASL labelling methods are continuous (CASL), pseudo-continuous (pCASL) and pulsed (PASL) arterial spin labelling. CASL uses special long-duration low-amplitude RF pulses in combination with a strong gradient in flow direction to continuously invert blood spins passing through a thin slice before entering the imaging area. This results in a bolus of inverted blood of a well-defined length and a relatively high SNR. However, high RF power consumption, leading to high SAR values, eddy current effects due to strong gradients as well as magnetization transfer (MT) effects due to long RF pulses can be a problem. A separate labelling coil is advantageous but technically more challenging because it requires an additional transmit channel. In pCASL, an RF pulse train with varying gradients (Dai et al. 2008) achieves the same labelling as in CASL with reduced SAR and MT effects. PASL uses a short RF pulse in combination with a weak gradient to invert spins inside a broad slab, resulting in a reduction of the SAR, eddy currents and MT effects. However, the bolus of inverted blood spins has a spatial and temporal extent which is usually not well defined, leading to a reduced SNR, as blood spins located in the bolus region distal to the imaging slice will experience a longer period of T1 relaxation before entering the imaging area. More recent and specialised forms of ASL are velocity-selective (VS-ASL) and acceleration-selective ASL (AccASL), where the labelling of blood is based on its flow velocity and acceleration, respectively, rather than on spatial location, thus minimizing the transit delay and related errors (Wong 2013; Schmid et al. 2017). Territorial ASL (T-ASL) labels blood in selected feeding vessel(s) which perfuse specific brain regions (Hartkamp et al. 2013).

3.2.4 Quantification Problems in ASL

There are several sources of systematic error in CBF quantification (Wong 2005) that are related to problems affecting static and blood spins. Static spins can be erroneously influenced by subject motion and by the label experiment via the magnetisation transfer effect (increasing with the duration of inversion pulses), eddy currents (increasing with decreasing inversion slice thickness) and imperfect slice profiles (increasing with slice thickness). Blood spins can lead to errors due to inflow from areas that are not affected by the label experiment (causing underestimation of the CBF), intravascular signal from labelled blood designed to perfuse capillaries in more distal slices (causing overestimation of the CBF) and a low labelling efficiency.

The following parameters influence the difference signal ΔS and need to be taken into account in CBF quantification: the transit delay (the time labelled blood needs to travel from the labelling site to the imaging slice), the natural time width τ of the bolus (depends on the thickness of the labelling slice and the velocity distribution of the spins inside), the T1 decay of labelled blood (leads to reduced SNR in the difference signal) and the exchange of water between labelled blood and the brain tissue which have a different T1.

Quantification for PASL can be improved by using saturation pulses on the labelling slice that cut off the tail of the bolus, leading to a well-defined bolus length. This makes the method independent of (1) the natural time width of the bolus, as the bolus length is now defined by the time between the labelling pulse and saturation pulse, and (2) under certain conditions of the transit delay, too. The respective sequences are QUIPSS II (Wong et al. 1998), where a single broad saturation pulse is applied to the whole of the labelling slice (some quantification errors still remain due to imperfect slice profiles), and Q2TIPS (Luh et al. 1999), where a train of thin-slice saturation pulses (with a much better slice profile) is applied at the end of the labelling slice proximal to the imaging region (instead of one broad saturation pulse to the whole of the labelling slice), thus further improving quantification. Saturation of the imaging slice before the labelling/control experiment reduces errors for the static spins due to the imperfect slice profile of the broad labelling slice and has the additional advantage that adding the label and control images yields an image showing the BOLD effect (Wong et al. 1997; Luh et al. 2000), as discussed later. A detailed review of the issues discussed in this section can be found in Wong (2005).

Concise advice on acquisition and control of the ASL signal and on quantification and processing of ASL data is given in the book chapter "ASL: Blood Perfusion Measurement Using Arterial Spin Labelling" by van der Kleij and Petersen (Cergignani et al. 2018, pp. 288–294).

3.3 The Cerebral Blood Volume (CBV)

3.3.1 Definition, Order of Magnitude and Measurement

The blood volume per tissue mass or volume (mL/100 g or mL/100 mL) is expressed as the CBV. In the human brain, typical values are approximately 5 mL/(100 mL) in grey matter and 2.5 mL/(100 mL) in white matter (Kuppusamy et al. 1996; Leenders et al. 1990). The CBV is an important parameter in normal brain physiology and pathophysiology. It is used as a measure of brain activity in fMRI (Belliveau et al. 1991; Lu et al. 2003; Vanduffel et al. 2001; Huber et al. 2017). In particular, direct measurements of CBV help elucidate the complex interplay between CBF, CBV and blood oxygenation underlying the BOLD effect used in the majority of current fMRI studies, and are important for the quantitative mapping of the cerebral metabolic rate of oxygen consumption ($CMRO_2$; Kida et al. 2007). CBV is also used as a marker of disease, for example, in the assessment of brain vasculature diseases (Kader and Young 1996).

Various MR methods were developed to measure the CBV, and these fall into two main categories: methods using contrast agents (Belliveau et al. 1991; Ostergaard et al. 1998; Schwarzbauer et al. 1993; Vanduffel et al. 2001; Shen et al. 1993) and a more recently developed contrast agent-free method (vascular space occupancy; VASO) (Lu et al. 2003).

3.3.2 Contrast Agent-Based Methods

There are two main contrast agent-based methods: dynamic and steady-state imaging. In each case, a paramagnetic contrast agent is injected, reducing the intravascular relaxation times. In dynamic imaging, the passage of a bolus of contrast agent after intravenous injection is traced. The signal time curve allows for a CBV estimation which is typically based on a model of tracer kinetics (Tofts 2003, pp. 365–390). In steady-state imaging, images acquired before and after injection are compared. A sufficient waiting time is employed to ensure that the contrast agent concentration in the blood has reached a steady state.

3.3.2.1 Dynamic Imaging

Dynamic imaging methods vary mainly depending on the contrast agent used, the MRI contrast acquired and the time resolution.

Two methods in use are DSC and DCE MRI, previously introduced for their application in the measurement of CBF (see Sect. 3.2.1).

In DSC imaging, after the injection of the paramagnetic contrast agent (normally a gadolinium chelate, such as Gd-DTPA), the signal time course is monitored with a T2- or T2*-weighted MR sequence. The area under the signal time curve is proportional to the CBV (Rosen et al. 1990). Since the proportionality constant is not generally known, the relative CBV (rCBV) can be calculated, where a value of 100% corresponds to pure blood. The rCBV can be obtained from the ratio of the signal in the region of interest to the signal from voxels that contain blood only (e.g. inside the superior sagittal sinus). Since DSC imaging requires a high temporal resolution of about a second to sample the signal time course adequately, the spatial resolution is limited. Thus, partial volume effects complicate the assessment of CBV, and large vessels cannot be excluded (Lin et al. 1999). Moreover, the signal intensity may be too low in blood-only voxels during the bolus passage. Recirculation of the contrast agent after the first pass and an unknown arterial input function further complicate the assessment (Tofts 2003, pp. 365–390). Therefore, often only quotients of CBV values are reported, for example, comparing two homologous brain areas in the left and right hemispheres or tissues of interest.

Similarly, in DCE imaging the signal time course following the injection of a bolus of paramagnetic contrast agent is monitored, but with a T1-weighted MR sequence (Dean et al. 1992). The time dynamics are in this case slower, requiring a lower temporal resolution but an acquisition period of about twice as much as for DSC (typically 2–3 min). While DCE is found to be less sensitive to sources of nuisance affecting DSC, it is characterized by lower contrast to noise that might hinder the precision of CBV estimates, especially for weakly vascularized regions (Sourbron and Buckley 2013).

A third group of dynamic imaging methods exploits iron-based contrast agents to estimate relative CBV or the dynamic changes in CBV. These contrast agents are composites of iron-oxide nanoparticles that, thanks to their small size, are not rapidly cleared from the plasma pool, providing a T2* contrast that is dependent on CBV dynamics, but much stronger than that naturally occurring, for instance, due to

the presence of deoxyhaemoglobin exploited in fMRI BOLD imaging. Originally applied to animal models, iron-based methods have gained more popularity also for human brain applications, mainly for clinical protocols (Mandeville 2012; Qiu et al. 2012) but also for applications with healthy subjects (Baumgartner et al. 2016). Note that these methods and contrast agents are known by several names, such as MION (Shen et al. 1993), IRON (Mandeville 2012), ferumoxytol (Christen et al. 2012) and USPIO (Kim et al. 2013).

3.3.2.2 Steady-State Imaging

The CBV can also be estimated from steady-state imaging (Kuppusamy et al. 1996; Moseley et al. 1992; Schwarzbauer et al. 1993). For this method, it is assumed that two separate compartments contribute to the signal: an extravascular (brain parenchyma) and an intravascular (blood vessels) compartment. When a paramagnetic contrast agent is injected, it will selectively lower T1 in the intravascular compartment, leading to a signal increase in T1-weighted images. The increase in signal permits the size of the intravascular compartment, i.e. the CBV, to be calculated. Two acquisitions are performed, one before and one after the injection of the contrast agent, allowing for sufficient time to reach a steady-state distribution of the contrast agent. Since the data are acquired in the steady state, the imaging sequence does not need to be fast, allowing for higher spatial resolution and high SNR. Therefore, 3D gradient echo sequences are usually used for imaging.

In the original implementation, a quantitative T1 map was acquired before and after contrast agent injection (Schwarzbauer et al. 1993), using a spoiled, fast, low-angle shot (FLASH) technique (Haase 1990). The longitudinal relaxation rate R1 = 1/T1 is obtained for a voxel containing the tissue of interest and a control voxel containing blood only. The CBV can be computed as (Schwarzbauer et al. 1993)

$$\mathrm{CBV} = \frac{\mathrm{R1}_{post}\left(\mathrm{tissue}\right) - \mathrm{R1}_{pre}\left(\mathrm{tissue}\right)}{\mathrm{R1}_{post}\left(\mathrm{blood}\right) - \mathrm{R1}_{pre}\left(\mathrm{blood}\right)}.$$

Since in spoiled FLASH the signal change $S_{\mathrm{post}} - S_{\mathrm{pre}}$ is roughly proportional to the underlying change in relaxation rate $\mathrm{R1}_{\mathrm{post}} - \mathrm{R1}_{\mathrm{pre}}$, the CBV can be directly estimated from the signals for the two voxels, bypassing T1/R1 quantification (Kuppusamy et al. 1996):

$$\mathrm{CBV} = \frac{S_{post}\left(\mathrm{tissue}\right) - S_{pre}\left(\mathrm{tissue}\right)}{S_{post}\left(\mathrm{blood}\right) - S_{pre}\left(\mathrm{blood}\right)}.$$

The steady-state approach was further modified to include an inversion of the longitudinal magnetisation prior to FLASH acquisition (Perles-Barbacaru and Lahrech 2007). The inversion time (TI) and the repetition time (TR) are chosen in a way that the signal from compartments with long T1 values is nulled, leading to complete suppression of the extravascular signal. In contrast, intravascular blood yields the maximum signal since the blood T1 is strongly reduced due to the contrast agent. Thus, the total signal S_{post} arises from intravascular blood only. A second measurement without T1 weighting is performed, choosing long TR and TI values,

which yields a signal S_0 arising from all compartments. As a consequence, the CBV can be obtained from the quotient S_{post}/S_0. To exclude residual signal contributions, another T1-weighted measurement before contrast agent administration is performed, and the CBV is obtained from

$$\mathrm{CBV} = \frac{S_{post} - S_{pre}}{S_0}.$$

The steady-state methods assume that the intra- and extravascular compartments are separate. This assumption can be violated when, for example, the blood–brain barrier is damaged or if diffusion of water across the capillary walls is significant (Perles-Barbacaru and Lahrech 2007), thus resulting in a misestimation of the CBV.

3.3.3 Contrast Agent-Free Method: Vascular Space Occupancy Measurement

The VASO imaging technique measures CBV without an exogenous contrast agent. VASO imaging is primarily used qualitatively for fMRI, but quantitative CBV measurements are possible in combination with a contrast agent (Lu et al. 2005; Uh et al. 2009). Usually, a gradient echo EPI acquisition is preceded by a global inversion that nulls the blood signal. Thus, an increase in CBV results in a reduction of signal intensity. The original version of VASO-fMRI allowed for the acquisition of a single slice only (Lu et al. 2003) but was later extended to multislice (Lu et al. 2004) and then 3D acquisitions (Poser and Norris 2009).

Compared to contrast agent-based techniques, VASO-fMRI offers the advantage that it is noninvasive and can be repeated as often as necessary. Further, it is not sensitive to extravascular signal changes, since it uses the intravascular blood as an endogenous contrast agent. Finally, due to vasodilation taking place in proximity to the site of neuronal activation, VASO-fMRI is found to show higher spatial specificity compared, for instance, to BOLD fMRI (Huber et al. 2017; Poser and Norris 2009).

However, VASO-fMRI can systematically misestimate the changes in CBV due to brain activation (Donahue et al. 2006; Scouten and Constable 2007), which has been attributed to different factors. In particular, inflow effects, BOLD signal weighting, contributions of cerebrospinal fluid signal and partial volume effects of white and grey matter affect the results and complicate their interpretation (Donahue et al. 2006; Scouten and Constable 2007).

3.4 The BOLD Effect and Functional MRI

Most functional MR imaging studies exploit the intrinsic BOLD contrast mechanism (Ogawa et al. 1990; Kwong et al. 1992). In the following discussion, we use the classic stimulus-induced activation model to explain the BOLD effect. However, it is important to keep in mind that numerous investigations such as EEG-correlated fMRI studies concern the resting state, in which one often seeks to reveal patterns

of signal change that may not correspond to stimulus or task-driven effects, such as spontaneous fluctuations in brain activity: epilepsy, sleep, brain rhythms, etc. In general, it has been observed that in brain images based on gradient echo techniques with a suitable echo time (TE), signal amplitudes are temporarily enhanced in regions of neuronal activation (increase in neuronal activity). This effect can be explained roughly as follows. During the resting state, local oxygen concentrations are relatively low, so blood contains a high concentration of *deoxyhaemoglobin*, which is *paramagnetic* (i.e. it locally increases the static magnetic field), whereas the brain tissue is *diamagnetic* (i.e. it tends to slightly decrease the static magnetic field). This means that at the interfaces of vessels and brain tissue there are magnetic field inhomogeneities that shorten T2* and give rise to a signal reduction in T2*-weighted gradient echo images, as explained above. After neuronal activation, more oxygen is transported to the site of activation via an increased CBF, leading to a washout of deoxyhaemoglobin and an increased concentration of *oxyhaemoglobin*, which is diamagnetic. Thus, the magnetic properties of blood and brain tissue become more similar, field inhomogeneities are reduced and the local image intensity increases.

In reality, matters are more complicated. Figure 3.14 shows a typical signal time course following neuronal activation associated with an external stimulus (task) or spontaneous brain activity, the so-called *haemodynamic response*. Initially, there is a slight signal *decrease*. This *initial dip* is not always observed and has been reported for high field strengths (Buxton 2001). Afterwards, there is a *positive BOLD response* that persists for about 5–10 s. For the remaining time, up to 30 s after the onset of the stimulus, there is a signal *undershoot* (van Zijl et al. 2012). The physiology behind these effects is only partially understood. In particular, it is not clear how the coupling between neuronal activity and blood flow is mediated (Attwell and Iadecola 2002; Filosa et al. 2016) and which aspect or aspects of neuronal activity it best reflects. This is one of the questions that studies combining electrophysiology/EEG with fMRI may help elucidate (Logothetis et al. 2001; Shmuel et al. 2006; Laufs et al. 2003; Moosmann et al. 2003; Siero et al. 2014). Here, we focus on the vascular response itself, for which a thorough discussion of the various theories can be found in the literature (Buxton et al. 2004; Chen and Pike 2009). In this section, one of the most commonly cited models will be presented: the so-called *balloon model* (Buxton et al. 1998, 2004; Buxton 2012). Extensions to this model have also been proposed, with a more detailed modelling of the role of the neural activation (Havlicek et al. 2015). The important physiological parameters that influence the BOLD effect are the cerebral metabolic rate of oxygen consumption ($CMRO_2$), the CBF and the CBV. The typical time courses of these parameters after activation are schematically sketched in Fig. 3.14.

According to this model, directly after the onset of neuronal activation, the $CMRO_2$ is increased. The consumption of oxygen leads to a higher concentration of deoxyhaemoglobin, which reduces the signal, resulting in the initial dip. However, after a very short while, the CBF and the CBV go up, with opposing effects: due to the increased CBF, oxygen is transported to the site of activation,

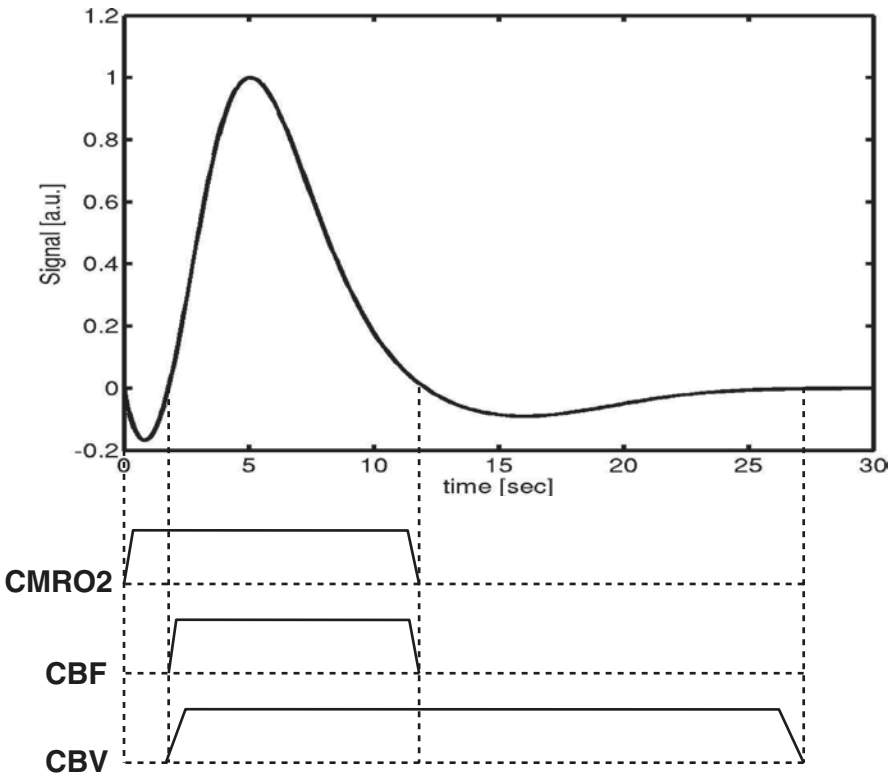

Fig. 3.14 A typical haemodynamic response function following a stimulus, showing a negative *initial dip*, a strong *positive BOLD response* and a subsequent negative *undershoot*. These phenomena can be explained with the different time constants of the underlying physiological parameters: the cerebral metabolic rate of oxygen consumption ($CMRO_2$), the cerebral blood flow (CBF) and the cerebral blood volume (CBV)

giving rise to a decreased concentration of deoxyhaemoglobin and thus to a higher signal, as explained above. The increase in CBV is concomitant with a higher concentration of deoxyhaemoglobin, lowering the signal. However, the effect of the CBF increase outpaces the signal reduction caused by the higher $CMRO_2$ and CBV values, resulting in a positive BOLD response. After about 10 s, $CMRO_2$ and CBF return to their baseline levels. The relaxation of CBV is slower, so for a certain time there is an increased concentration of deoxyhaemoglobin due to the higher blood volume, which reduces the signal, resulting in the undershoot.

So far, we have focussed on the positive BOLD response for simplicity. However, it is important to note that the BOLD response curve may be inverted; in other words the large BOLD change that occurs after 5–10 s may be negative, as observed in various fMRI (Shmuel et al. 2006; Stefanovic et al. 2004) and EEG–fMRI studies (Hamandi et al. 2008; Laufs et al. 2003; Moosmann et al. 2003). Though the

underlying mechanism is not completely understood, one important element is a decrease in blood flow consistent with a decrease in neuronal activity in the cortex compared to the baseline (Hamandi et al. 2008; Carmichael et al. 2008; Havlicek et al. 2015). For example, it was shown that a decrease in global neuronal activity in primate visual cortex is accompanied by a negative BOLD response (Shmuel et al. 2006). Increased local field potential (LFP) activity, on the other hand, was shown to correlate well with the positive BOLD response (Logothetis et al. 2001). Although the majority of the studies exploited the main BOLD response after 5–10 s, some studies also targeted the initial dip and the undershoot for high-resolution fMRI (see in the review by Goense et al. 2016). Moreover, both negative transients in the BOLD response were also studied in the context of models of the BOLD effect (see the review by Buxton et al. (2004) and Buxton (2012) and more recent studies from Havlicek et al. (2017) and Sten et al. (2017)).

From an imaging perspective, the T2* contrast and the contrast of the BOLD response are in the first instance determined by the choice of the echo time (TE), as previously discussed (see Sect. 3.1.5). The practical question arises which echo time (TE) should be chosen to achieve maximum BOLD contrast. Figure 3.15 shows the theoretical BOLD signal depending on TE for a T2* value of 45 ms (which is the approximate T2* of brain tissue at a field strength of 3 T). The result corresponds to the discussion above (see Sect. 3.1.5). For short TE, the spins do not have sufficient time to dephase, so the effect is small. For very long TE, there are signal losses due to relaxation effects. Optimum results can be obtained at 45 ms at 3 T, i.e. when TE equals T2*. However, as described above, gradient echo sequences are susceptible to *all* field inhomogeneities, so there are signal losses in brain areas where the static magnetic field is typically distorted due to the vicinity of air-filled cavities (e.g. in the orbitofrontal and temporal areas). Thus, the TE chosen should be as short as possible to avoid signal losses but as long as necessary to achieve an adequate BOLD contrast. According to Fig. 3.15, there is still a strong BOLD signal for a TE of 30 ms, which is the recommended value for fMRI studies carried out on 3 T scanners. At 1.5 T, a TE of 50 ms should be chosen due to the prolonged T2* values at lower field strengths.

At higher field strengths, as, e.g. 7 T, even sub-millimetre resolutions can be achieved and were exploited for studies of the mesoscopic structures ($\leq$1 mm) of the human neocortex, such as the layers or columnar structures (see reviews from Cheng (2018) and Schluppeck et al. (2018)). The use of fMRI for characterizing such subtle structures poses exceptional demands on the contrast-to-noise ratio and effective spatial resolution. Particularly, the draining of deoxygenated blood through the venules causes a dispersion effect in higher cortical layers, leading to a poor effective point spread function (Turner 2002; Shmuel et al. 2007; Polimeni et al. 2010). Thus, the correction and reduction of this effect has become an active area of research, leading to new spatial modelling approaches (Markuerkiaga et al. 2016). This type of high-resolution imaging is a promising technique for investigating mesoscopic functional neuroanatomical structures that mediate important brain functions (e.g. ocular dominance columns; Yacoub et al. 2008).

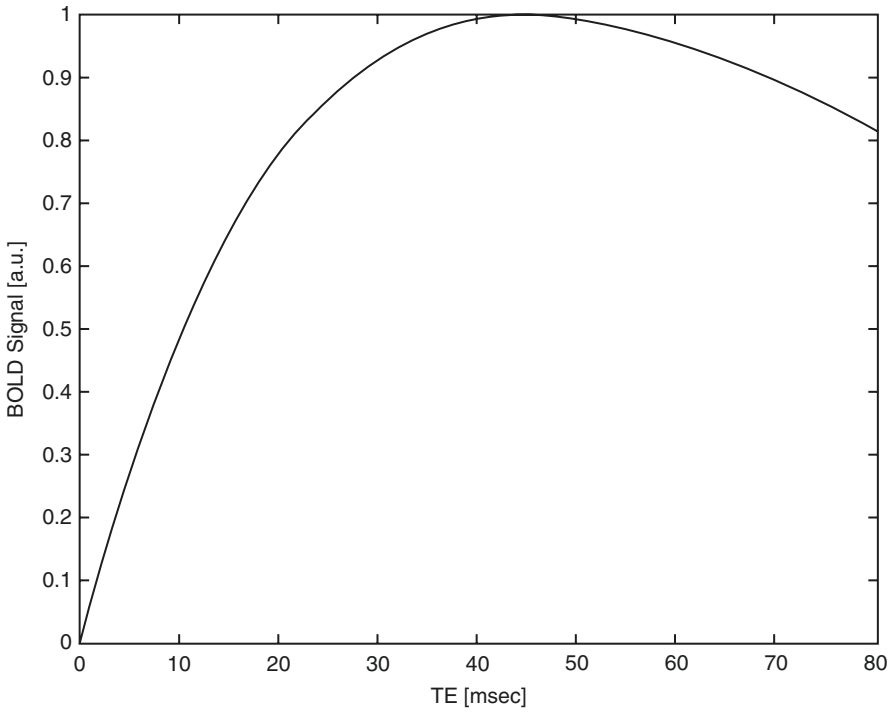

Fig. 3.15 Dependence of the theoretical BOLD sensitivity on the chosen echo time (TE) at 3 T

References

Attwell D, Iadecola C (2002) The neural basis of functional brain imaging signals. Trends Neurosci 25:621–625

Baumgartner R, Cho W, Coimbra A, Chen C, Wang Z, Struyk A, Venketasubramanian N, Low M, Gargano C, Zhao F, Williams D, Reese T, Seah S, Feng D, Apreleva S, Petersen E, Evelhoch JL (2016) Evaluation of an fMRI USPIO-based assay in healthy human volunteers. J Magn Reson Imaging 46:124–133

Belliveau JW, Kennedy DN Jr, McKinstry RC, Buchbinder BR, Weisskoff RM, Cohen MS, Vevea JM, Brady TJ, Rosen BR (1991) Functional mapping of the human visual cortex by magnetic resonance imaging. Science 254:716–719

Biagi L, Abbruzzese A, Bianchi MC, Alsop DC, Del Guerra A, Tosetti M (2007) Age dependence of cerebral perfusion assessed by magnetic resonance continuous arterial spin labeling. J Magn Reson Imaging 25:696–702

Bloch F, Hansen WW, Packard M (1946) Nuclear induction. Phys Rev 69:127

Buxton RB (2001) The elusive initial dip. Neuroimage 13:953–958

Buxton RB (2002) Introduction to functional magnetic resonance imaging: principles and techniques. Cambridge University Press, Cambridge

Buxton RB (2012) Dynamic models of BOLD contrast. Neuroimage 62:953–961

Buxton RB, Wong EC, Frank LR (1998) Dynamics of blood flow and oxygenation changes during brain activation: the balloon model. Magn Reson Med 39:855–864

Buxton RB, Uludag K, Dubowitz DJ, Liu TT (2004) Modeling the hemodynamic response to brain activation. Neuroimage 23:S220–S233

Carmichael DW, Hamandi K, Laufs H, Duncan JS, Thomas DL, Lemieux L (2008) An investigation of the relationship between BOLD and perfusion signal changes during epileptic generalised spike wave activity. Magn Reson Imaging 26(7):870–873
Cergignani M, Dowell NG, Tofts P (eds) (2018) Quantitative MRI of the brain: principles of physical measurement. CRC Press, Boca Raton
Chen JJ, Pike GB (2009) Origins of the BOLD post-stimulus undershoot. Neuroimage 46:559–568
Cheng K (2018) Exploration of human visual cortex using high spatial resolution functional magnetic resonance imaging. Neuroimaging 164:4–9
Christen T, Ni W, Qiu D, Schmiedeskamp H, Bammer R, Moseley M, Zaharchuk G (2012) High-resolution cerebral blood volume imaging in humans using the blood pool contrast agent ferumoxytol. Magn Reson Med 70:705–710
Dai W, Garcia D, de Bazelaire C, Alsop DC (2008) Continuous flow-driven inversion for arterial spin labeling using pulsed radio frequency and gradient fields. Magn Reson Med 60:1488–1497
Dean BL, Lee C, Kirsch JE, Runge VM, Dempsey RM, Pettigrew LC (1992) Cerebral hemodynamics and cerebral blood volume: MR assessment using gadolinium contrast agents and Tl-weighted turbo-FLASH imaging. Am J Neurorad 13:39–48
Donahue MJ, Lu H, Jones CK, Edden RA, Pekar JJ, van Zijl PC (2006) Theoretical and experimental investigation of the VASO contrast mechanism. Magn Reson Med 56:1261–1273
Filosa JA, Morrison HW, Iddings JA, Du W, Kim KJ (2016) Beyond neurovascular coupling, role of astrocytes in the regulation of vascular tone. Neuroscience 323:96–109
Goense J, Bohraus Y, Logothetis NK (2016) fMRI at high spatial resolution: implications for BOLD-models. Front Comput Neurosci 10:66. https://doi.org/10.3389/fncom.2016.00066
Grade M, Hernandez Tamames JA, Pizzini FB, Achten E, Golay X, Smits M (2015) A neuroradiologist's guide to arterial spin labeling MRI in clinical practice. Neuroradiology 57:1181–1202
Haase A (1990) Snapshot FLASH MRI: applications to T1, T2, and chemical-shift imaging. Magn Reson Med 13:77–89
Hahn EL (1950) Spin echoes. Phys Rev 80:580–594
Haller S, Zaharchuk G, Thomas DL, Lovblad K-O, Barkhof F, Golay X (2016) Arterial spin labeling perfusion of the brain: emerging clinical applications. Radiology 281:337–356
Hamandi K, Laufs H, Nöth U, Carmichael DW, Duncan JS, Lemieux L (2008) BOLD and perfusion changes during epileptic generalised spike wave activity. Neuroimage 39:608–618
Hartkamp NS, Petersen ET, De Vis JB, Bokkers RPH, Hendrikse J (2013) Mapping of cerebral perfusion territories using territorial arterial spin labeling: techniques and clinical application. NMR Biomed 26:901–912
Havlicek M, Roebroeck A, Friston KJ, Gardumi A, Ivanov D, Uludag K (2015) Physiologically informed dynamic causal modeling of fMRI data. Neuroimage 122:355–372
Havlicek M, Ivanov D, Roebroeck A, Uludag K (2017) Determining excitatory and inhibitory neuronal activity from multimodal fMRI data using a generative hemodynamic model. Front Neurosci 11:616. https://doi.org/10.3389/fnins.2017.00616
Hennig J, Nauerth A, Friedburg H (1986) RARE imaging: a fast imaging method for clinical MR. Magn Reson Med 3:823–833
Huber L, Handwerker DA, Jangraw DC, Chen G, Hall A, Stüber C, Gonzalez-Castillo J, Ivanov D, Marrett S, Guidi M, Goense J, Poser BA, Bandettini PA (2017) High-resolution CBV-fMRI allows mapping of laminar activity and connectivity of cortical input and output in human M1. Neuron 96:1253–1263.e7
Kader A, Young WL (1996) The effects of intracranial arteriovenous malformations on cerebral hemodynamics. Neurosurg Clin N Am 7:767–781
Kida I, Rothman DL, Hyder F (2007) Dynamics of changes in blood flow, volume, and oxygenation: implications for dynamic functional magnetic resonance imaging calibration. J Cereb Blood Flow Metab 27:690–696
Kim SG, Harel N, Jin T, Kim T, Lee P, Zhao F (2013) Cerebral blood volume MRI with intravascular superparamagnetic iron oxide nanoparticles. NMR Biomed 26:949–962

Kuppusamy K, Lin W, Cizek GR, Haacke EM (1996) In vivo regional cerebral blood volume: quantitative assessment with 3D T1-weighted pre- and postcontrast MR imaging. Radiology 201:106–112

Kwong KK, Belliveau JW, Chesler DA, Goldberg IE, Weisskoff RM, Poncelet BP, Kennedy DN, Hoppel BE, Cohen MS, Turner R, Cheng HM, Brady TJ, Rosen BR (1992) Dynamic magnetic resonance imaging of human brain activity during primary sensory stimulation. Proc Natl Acad Sci U S A 89:5675–5679

Laufs H, Kleinschmidt A, Beyerle A, Eger E, Salek-Haddadi A, Preibisch C, Krakow K (2003) EEG-correlated fMRI of human alpha activity. Neuroimage 19:1463–1476

Lauterbur PC (1973) Image formation by induced local interactions: examples employing nuclear magnetic resonance. Nature 242:190–191

Le Heron CJ, Wright SL, Melzer TR, Myall DJ, MacAskill MR, Livingston L, Keenan RJ, Watts R, Dalrymple-Alford JC, Anderson TJ (2014) Comparing cerebral perfusion in Alzheimer's disease and Parkinson's disease dementia: an ASL-MRI study. J Cereb Blood Flow Metab 34:964–970

Leenders KL, Perani D, Lammertsma AA, Heather JD, Buckingham P, Healy MJ, Gibbs JM, Wise RJ, Hatazawa J, Herold S, Beany RP, Brooks DJ, Spinks T, Rhodes C, Frackowiak RSJ, Jones T (1990) Cerebral blood flow, blood volume and oxygen utilization. Normal values and effect of age. Brain 113(1):27–47

Lin W, Celik A, Paczynski RP (1999) Regional cerebral blood volume: a comparison of the dynamic imaging and the steady state methods. J Magn Reson Imaging 9(1):44–52

Logothetis NK, Pauls J, Augath M, Trinath T, Oeltermann A (2001) Neurophysiological investigation of the basis of the fMRI signal. Nature 412:150–157

Lu H, Golay X, Pekar JJ, van Zijl PC (2003) Functional magnetic resonance imaging based on changes in vascular space occupancy. Magn Reson Med 50:263–274

Lu H, van Zijl PC, Hendrikse J, Golay X (2004) Multiple acquisitions with global inversion cycling (MAGIC): a multislice technique for vascular-space-occupancy dependent fMRI. Magn Reson Med 51:9–15

Lu H, Law M, Johnson G, Ge Y, van Zijl PC, Helpern JA (2005) Novel approach to the measurement of absolute cerebral blood volume using vascular-space-occupancy magnetic resonance imaging. Magn Reson Med 54:1403–1411

Luh WM, Wong EC, Bandettini PA, Hyde JS (1999) QUIPSS II with thin-slice TI1 periodic saturation: a method for improving accuracy of quantitative perfusion imaging using pulsed arterial spin labeling. Magn Reson Med 41:1246–1254

Luh WM, Wong EC, Bandettini PA, Ward BD, Hyde JS (2000) Comparison of simultaneously measured perfusion and BOLD signal increases during brain activation with T_1-based tissue identification. Magn Reson Med 44:137–143

Mandeville JB (2012) IRON fMRI measurements of CBV and implications for BOLD signal. Neuroimage 62(2):1000–1008

Mansfield P (1977) Multiplanar image formation using NMR spin echoes. J Phys C Solid State Phys 10:L55–L58

Markuerkiaga I, Barth M, Norris DG (2016) A cortical vascular model for examining the specificity of the laminar BOLD signal. Neuroimage 132:491–498

Moosmann M, Ritter P, Krastel I, Brink A, Thees S, Blankenburg F, Taskin B, Obrig H, Villringer A (2003) Correlates of alpha rhythm in functional magnetic resonance imaging and near infrared spectroscopy. Neuroimage 20:145–158

Moseley ME, Chew WM, White DL, Kucharczyk J, Litt L, Derugin N, Dupon J, Brasch RC, Norman D (1992) Hypercarbia-induced changes in cerebral blood volume in the cat: a 1H MRI and intravascular contrast agent study. Magn Reson Med 23:21–30

Mugler JP III, Brookeman JR (1990) Three-dimensional magnetization-prepared rapid gradient-echo imaging (3D MP RAGE). Magn Reson Med 15:152–157

Nöth U, Laufs H, Störmer R, Deichmann R (2012) Simultaneous electroencephalography-functional MRI at 3 T: an analysis of safety risks imposed by performing anatomical reference scans with the EEG equipment in place. J Magn Reson Imaging 35:561–571

Nöth U, Shrestha M, Schüre JR, Deichmann R (2017) Quantitative in vivo T2 mapping using fast spin echo techniques—a linear correction procedure. Neuroimage 157:476–485
Ogawa S, Lee TM, Nayak AS, Glynn P (1990) Oxygenation-sensitive contrast in magnetic resonance image of rodent brain at high magnetic fields. Magn Reson Med 14:68–78
Ostergaard L, Smith DF, Vestergaard-Poulsen P, Hansen SB, Gee AD, Gjedde A, Gyldensted C (1998) Absolute cerebral blood flow and blood volume measured by magnetic resonance imaging bolus tracking: comparison with positron emission tomography values. J Cereb Blood Flow Metab 18:425–432
Perles-Barbacaru AT, Lahrech H (2007) A new magnetic resonance imaging method for mapping the cerebral blood volume fraction: the rapid steady-state T1 method. J Cereb Blood Flow Metab 27:618–631
Polimeni JR, Fischl B, Greve DN, Wald LL (2010) Laminar analysis of 7 T BOLD using an imposed spatial activation pattern in human V1. Neuroimage 52:1334–1346
Poser BA, Norris DG (2009) 3D single-shot VASO using a Maxwell gradient compensated GRASE sequence. Magn Reson Med 62:255–262
Purcell EM, Torrey HC, Pound RV (1946) Resonance absorption by nuclear magnetic moments in a solid. Phys Rev 69:37–38
Qiu D, Zaharchuk G, Christen T, Ni WW, Moseley ME (2012) Contrast-enhanced functional blood volume imaging (CE-fBVI): enhanced sensitivity for brain activation in humans using the ultrasmall superparamagnetic iron oxide agent ferumoxytol. Neuroimage 62:1726–1731
Rooney WD, Johnson G, Li X, Cohen ER, Kim S-G, Ugurbil K, Springer CS (2007) Magnetic field and tissue dependencies of human brain longitudinal 1H2O relaxation in vivo. Magn Reson Med 57:308–318
Rosen BR, Belliveau JW, Vevea JM, Brady TJ (1990) Perfusion imaging with NMR contrast agents. Magn Reson Med 14:249–265
Schluppeck D, Panchuelo RM, Francis ST (2018) Exploring structure and function of sensory cortex with 7T MRI. Neuroimage 164:10–17
Schmid S, Petersen ET, Van Osch MJP (2017) Insight into the labeling mechanism of acceleration selective arterial spin labeling. Magn Reson Mater Phys 30:165–174
Schwarzbauer C, Syha J, Haase A (1993) Quantification of regional blood volumes by rapid T1 mapping. Magn Reson Med 29:709–712
Scouten A, Constable RT (2007) Applications and limitations of whole-brain MAGIC VASO functional imaging. Magn Reson Med 58:306–315
Shen T, Weissleder R, Papisov M, Bogdanov A, Brady TJ (1993) Monocrystalline iron oxide nanocompounds (MION): physicochemical properties. Magn Reson Med 9:599–604
Shmuel A, Augath M, Oeltermann A, Logothetis NK (2006) Negative functional MRI response correlates with decreases in neuronal activity in monkey visual area V1. Nat Neurosci 9:569–577
Shmuel A, Yacoub E, Chaimow D, Logothetis NK, Ugurbil K (2007) Spatio-temporal point-spread function of fMRI signal in human gray matter at 7 Tesla. Neuroimage 35:539–552
Siero JCW, Hermes D, Hoogduin H, Luijten PR, Ramsey NF, Petridou N (2014) BOLD matches neuronal activity at the mm scale: a combined 7 T fMRI and ECoG study in human sensorimotor cortex. Neuroimage 101:177–184
Sourbron SP, Buckley DL (2013) Classic models for dynamic contrast-enhanced MRI. NMR Biomed 26:1004–1027
Stefanovic B, Warnking JM, Pike GB (2004) Hemodynamic and metabolic responses to neuronal inhibition. Neuroimage 22:771–778
Stefanovic B, Warnking JM, Kobayashi E, Bagshaw AP, Hawco C, Dubeau F, Gotman J, Pike GB (2005) Hemodynamic and metabolic responses to activation, deactivation and epileptic discharges. Neuroimage 28:205–215
Sten S, Witt ST, Cedersund G, Elinder F (2017) Neural inhibition can explain negative BOLD responses: a mechanistic modelling and fMRI study. Neuroimage 158:219–231
Storti SF, Boscolo Galazzo I, Del Felice A, Pizzini FB, Arcaro C, Formaggio E, Mai R, Manganotti P (2014) Combining ESI, ASL and PET for quantitative assessment of drug-resistant focal epilepsy. Neuroimage 102:49–59

Tofts P (2003) Quantitative MRI of the brain: measuring changes caused by disease. Wiley, Chichester

Turner R (2002) How much cortex can a vein drain? Downstream dilution of activation-related cerebral blood oxygenation changes. Neuroimage 16:1062–1067

Ugurbil K, Garwood M, Ellermann J, Hendrich K, Hinke R, Hu X, Kim SG, Menon R, Merkle H, Ogawa S, Salmi R (1993) Imaging at high magnetic fields: initial experiences at 4 T. Magn Reson Q 9:259–277

Uh J, Lewis-Amezcua K, Varghese R, Lu H (2009) On the measurement of absolute cerebral blood volume (CBV) using vascular-space-occupancy (VASO) MRI. Magn Reson Med 61:659–667

van Zijl PC, Hua J, Lu H (2012) The BOLD post-stimulus undershoot, one of the most debated issues in fMRI. Neuroimage 62:1092–1102

Vanduffel W, Fize D, Mandeville JB, Nelissen K, Van Hecke P, Rosen BR, Tootell RB, Orban GA (2001) Visual motion processing investigated using contrast agent-enhanced fMRI in awake behaving monkeys. Neuron 32:565–577

Wang DJJ, Alger JR, Qiao JX, Gunther M, Pope WB, Saver JL, Salamon N, Liebeskind DS for the UCLA Stroke Investigators (2013) Multi-delay multi-parametric arterial spin-labeled perfusion MRI in acute ischemic stroke—comparison with dynamic susceptibility contrast enhanced perfusion imaging. Neuroimage Clin 3:1–7

Wansapura JP, Holland SK, Dunn RS, Ball WS (1999) NMR relaxation times in the human brain at 3.0 Tesla. J Magn Reson Imaging 9:531–538

White CM, Pope WB, Zaw T, Qiao J, Naeini KM, Lai A, Nghiemphu PL, Wang JJ, Cloughesy TF, Ellingson BM (2014) Regional and voxel-wise comparisons of blood flow measurements between dynamic susceptibility contrast magnetic resonance imaging (DSC-MRI) and arterial spin labeling (ASL) in brain tumors. J Neuroimaging 24:23–30

Willats L, Calamante F (2013) The 39 steps: evading error and deciphering the secrets for accurate dynamic susceptibility contrast MRI. NMR Biomed 26:913–931

Wong EC (2005) Quantifying CBF with pulsed ASL: technical and pulse sequence factors. J Magn Reson Imaging 22:727–731

Wong EC (2013) New developments in arterial spin labeling pulse sequences. NMR Biomed 26:887–891

Wong EC, Buxton RB, Frank LR (1997) Implementation of quantitative perfusion imaging techniques for functional brain mapping using pulsed arterial spin labeling. NMR Biomed 10:237–249

Wong EC, Buxton RB, Frank LR (1998) Quantitative imaging of perfusion using a single subtraction (QUIPPS and QUIPSS II). Magn Reson Med 39:702–708

Yacoub E, Harel N, Ugurbil K (2008) High-field fMRI unveils orientation columns in humans. Proc Natl Acad Sci U S A 105(30):10607–10612

Locally Measured Neuronal Correlates of Functional MRI Signals

4

Amir Shmuel and Alexander Maier

4.1 Blood Oxygenation Level-Dependent (BOLD) Signals

The majority of functional brain imaging studies in humans rely on functional magnetic resonance imaging (fMRI) (Bandettini et al. 1992; Kwong et al. 1992; Ogawa et al. 1992). The most commonly used fMRI contrast is the BOLD signal (Ogawa et al. 1990). The BOLD signal is inversely proportional to the local content of deoxyhemoglobin (deoxyHb). When neuronal activity increases, local arterial cerebral blood flow (CBF) increases to a larger extent than the metabolic increase in oxygen consumption (Fox and Raichle 1986; Hoge et al. 1999). In other words, following increased neuronal activity, CBF overcompensates for the increased need for oxygenated blood. As a result, deoxyHb content drops within local capillaries, venules, and draining veins. This process can be monitored via MRI by tracking the changing magnitude of the BOLD signal over time (Buxton et al. 2004). fMRI signals are only indirect measures of neuronal activity, which rely on intermediary processes such as neurovascular coupling and MR contrast. Therefore, the interpretation of fMRI data relies heavily on inferences about how this hemodynamic response relates to local changes in neural activity. In order to fully utilize fMRI as an effective method to study brain function, it is vital to understand how metabolic and hemodynamic responses relate to the underlying neural activity.

A. Shmuel (✉)
McConnell Brain Imaging Centre, Montreal Neurological Institute, McGill University, Montreal, QC, Canada
e-mail: amir.shmuel@mcgill.ca

A. Maier
Department of Psychology, Vanderbilt University, Nashville, TN, USA
e-mail: alex.maier@vanderbilt.edu

C. Mulert, L. Lemieux (eds.), *EEG - fMRI*,
https://doi.org/10.1007/978-3-031-07121-8_4

4.2 Extracellular Neurophysiological Signals

Neurons receive inputs via synapses that are located at their soma and their dendrites. These inputs take the form of two post-synaptic potentials, excitatory and inhibitory post-synaptic potentials (EPSPs and IPSPs), respectively. These post-synaptic potentials can be measured directly using intracellular or patch-clamp techniques. However, there are significant technical challenges associated with these measurements such as the requirement for complete immobilization of the sampled tissue. Thus, most in vivo studies resort to measuring electric activity in the extracellular space. Post-synaptic *input* potentials propagate along the neuron's dendrites toward its soma. Depending on the ratio of concurrent excitatory to inhibitory synaptic inputs, as well as on the synchronization between excitatory inputs, action potentials (spikes) may get initiated at the soma's axon hillock. Action potentials propagate along the axon toward the cell's pre-synaptic axonal terminals, where they release the all-or-none *output* of the neuron to its recipients. This signaling is done through chemical neurotransmitters or neuromodulators that diffuse from vesicles into the synaptic cleft.

The vast majority of intracortical neurophysiological measurements (recordings) are based on extracellular voltages. Extracellular recordings measure electric signals within the extracellular medium, which reflect both synaptic and spiking activities. However, extracellular recordings cannot resolve the membrane potentials of isolated neurons. When inactive, the majority of neurons harbor a voltage gradient of about 60–70 mV across their lipid membranes. Neurons maintain this voltage gradient by actively moving certain anions from the extracellular medium into their cell bodies via specialized ion pump membrane proteins. The resulting potential difference between a neuron's intracellular space and the extracellular medium is called the "resting potential." Put differently, the inside of an inactive neuron contains more negative charge than the extracellular medium. When there is a membrane potential difference between two distinct regions of the neuron, current will start to flow between them. This current flow within neurons causes a canceling return current in the extracellular space to flow in the opposite direction. Importantly, each of these currents remains isolated within its respective compartment.

In contrast, neuronal activity (both the synaptic input and the axonal output in the form of action potentials) takes the form of ionic current flow *between* the extracellular fluid and intracellular compartments. The net negative (anionic) influx into an inactive neuron hyperpolarizes that cell. The result of such currents is that the neuron's inside is even more negative than before, which makes its activation less likely. Hyperpolarizing inputs thus act as inhibitory currents. Physiologically, these kinds of anionic currents take the form of inhibitory post-synaptic potentials (IPSPs).

Cationic influx into neurons, on the other hand, depolarizes neurons until they reach a threshold of activation. Once this threshold is reached, the neuron will initiate an action potential. Physiologically, excitatory currents occur at synaptic sites in the form of excitatory post-synaptic potentials or (EPSPs).

By convention, a site through which currents either enter or leave a given system is termed a current source or a current sink, respectively. Note that the sign (i.e.,

direction) of the current is dependent on the perspective of the observer. Consequently, the definition of what constitutes a current sink or source is also relative. When neuronal activity is concerned, however, it has become customary to refer to excitatory (depolarizing) currents as a current sink. Thus, neuronal current sinks are typically indicative of a site of synaptic excitation. To close the current loop, other regions of the same neuron will undergo net effluxes of positive ions. This current source thus leads to passive return currents (Nicholson 1973). The electrical dipole that results from the spatial separation between the current sink and source forms the basis of the time-varying voltage difference that can be measured with nearby microelectrodes. In other words, the microscopic ionic fluxes across the nerve cell membrane that arise from neuronal activation sum to extracellular voltage fluctuations that can be recorded as the extracellular broad-band signal.

Local field potentials (LFPs) refer to the bulk of extracellular voltage changes established by activity in a large number of neurons nearby a microelectrode placed within the extracellular space in vivo (Fig. 4.1). The highest magnitude of the

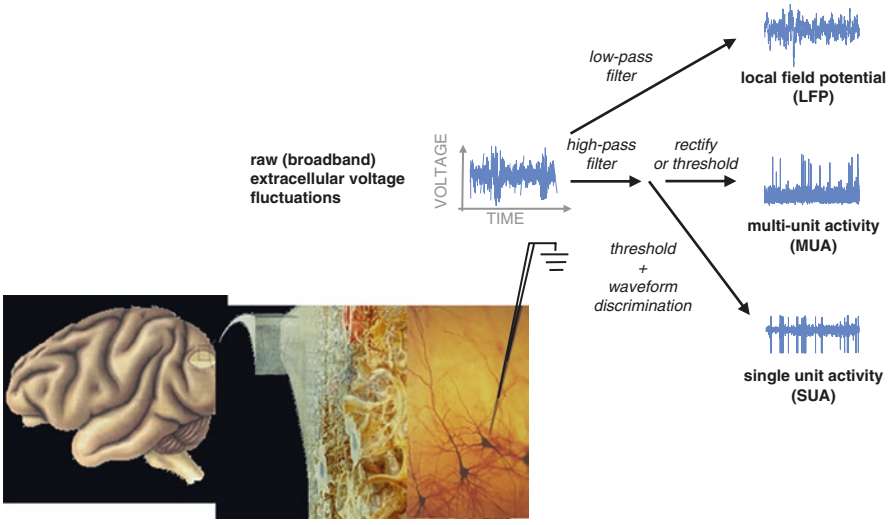

Fig. 4.1 Types of extracellular neurophysiological signals. Neurophysiologists commonly discriminate three major classes of signals that can be measured with microelectrodes placed inside the neuropil. (1) Depending on the material, geometry, and exact position of the probe, it is possible to isolate action potentials (spikes) of one or more isolated neurons. This single-unit activity (SUA) is quantified in a three-stage process. First, using band-limiting filters, the raw extracellular voltage gets narrowed down to a frequency band that matches the bandwidth of action potentials (~1 kHz). Next, the occurrence of individual impulses gets marked by determining the time points at which the signal exceeded a certain threshold. In the final step, waveform analysis gets applied to discriminate individual neurons. (2) The activity of larger populations of neurons (multi-unit activity, MUA) can be assessed by band-limiting the raw data to the frequency range of spiking activity, followed by either indiscriminate thresholding or by simple full-wave rectification in order to obtain the time-varying envelope of the band-limited signal. (3) Band-limiting the raw data into frequencies below the spectral range of spiking activity results in a signal called the local field potential or LFP

time-varying variance of extracellular voltage fluctuations occurs in the lowest frequency range. LFP magnitude decreases exponentially for increased LFP frequency. Given this predominance of low-frequency power in their spectral composition, LFPs are usually analyzed in reference to the frequency domain (i.e., in time-frequency analysis or in frequency bands also used in classical EEG: delta, theta, alpha, beta, and gamma; Fig. 4.2). Importantly, LFPs consist of a continuous spectrum rather than a few discrete frequencies. Under some conditions, LFPs exhibit repeating patterns for limited periods of time, thus resembling actual oscillations at set frequencies. However, such oscillatory LFPs are the exception rather than the norm. Most frequently, cortical LFPs exhibit no sustained periodicity and therefore are better characterized as irregular fluctuations.

LFPs have proven to be a useful measure of local neural activity as they can provide an indication of (mostly) synaptic processes without the need for

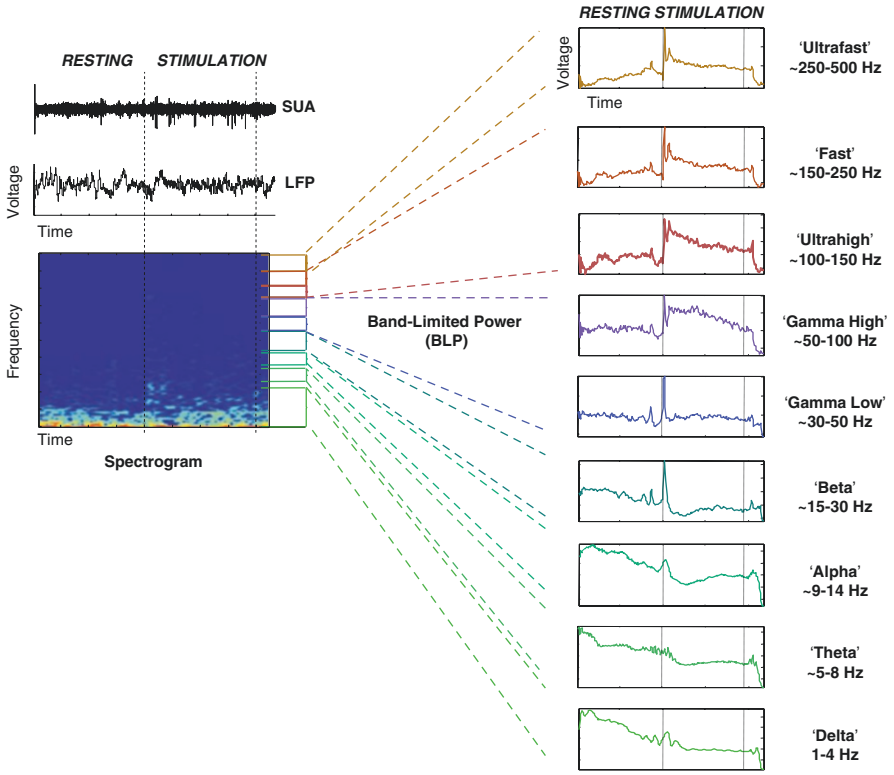

Fig. 4.2 Decomposition of LFP into frequency bands. The LFP represents a complex signal that is dominated by slow-varying, large-amplitude fluctuations. Averaging raw LFP, although informative, thus tends to over-represent its low-frequency content. A common way to circumvent this bias is to break up the signal into its frequency components and study their evolution over time. This can be done either (1) by band-bass filtering the LFP into discrete frequency bands and estimating the band-limited power (BLP) or by (2) directly transforming the signal into the frequency domain using the Fourier transform or related mathematical techniques. *SUA*, single-unit activity

intracellular recordings. Nonetheless, LFPs are not perfect indicators of neuronal activity since LFPs arise from a multitude of neural events that cannot be easily disentangled. Specifically, LFPs' amplitudes depend on multiple factors, such as the magnitude and spatial distribution of the underlying current sources and sinks, as well as on their temporal synchrony. The functional anatomy, relative position, and orientation of activated cells further influence the measured LFPs. For instance, stimulation of Purkinje cells in the cerebellum gives rise to large, coherent LFPs. The same can be found for pyramidal cells in the cerebral cortex because their dendrites are predominantly oriented parallel to each other, which supports linear spatial summation of voltages. Some interneurons, on the other hand, do not contribute to LFPs in the same way, as their dendrites are distributed in a radial, star-shaped pattern (Lauritzen 2005). Moreover, according to the relative timing of the neurons' activation and their relative geometrical arrangement, field potentials generated by two or more neurons may add up or cancel each other across the extracellular space (for reviews on field potentials, see Freeman (1975) and Logothetis (2002)).

With most microelectrodes of suitable geometry placed in the close vicinity of neurons, the slow-varying LFPs will be recorded simultaneously with the action potentials of nearby neurons. Analytically, LFPs can be dissociated from spiking activity by temporal filtering of the raw broad-band signal into two bands of frequencies above ~300 Hz and below ~150 Hz to separate the spiking activity of neurons (multi-unit activity, MUA) and LFPs, respectively (Figs. 4.1 and 4.2).

Separating LFPs and spiking-related activity by their frequency content, as described above, can be justified theoretically (Logothetis 2002). Both EPSPs and IPSPs are relatively slow events (10–100 ms long). In contrast, action potentials happen rather fast (0.4–2 ms long). As a direct consequence, the power spectra for synaptic events are predominated by much lower frequencies than that of spikes. Specifically, the average frequency spectrum of action potentials exhibits a peak around 1 kHz, while the frequency spectra of simulated EPSPs peak below 150 Hz. The same split across frequencies is found when comparing the frequency spectrum of a series of scattered synaptic events to the spectrum of spiking events.

Combined intra- and extracellular measurements further support the notion that LFPs have a synaptic-dendritic origin (e.g., Pedemonte et al. 1998). Moreover, current source density (CSD) analysis, a neurophysiological measurement technique that allows for the quantification of current flow within the neuropil, indicates that LFPs correspond to a weighted average of synchronized dendro-somatic activity from neurons within 0.5–3 mm of the electrode tip (Mitzdorf 1987; Juergens et al. 1999).

To summarize, there is converging theoretical and empirical evidence to support the concept that LFPs mainly reflect synaptic events, including synchronized synaptic input from afferent fibers as well as synaptic activity originating from local neurons. Specifically, LFPs seem to represent the summed synaptic activity of neurons that are located within ~2 mm of the recording electrode tip. In contrast, MUA seems to correspond to a weighted sum of action potentials within a ~200 μm radius from the electrode tip. The MUA is deemed to be dominated by the action potentials of pyramidal cells. However, action potentials from axons of passage, dendrites, and local interneurons likely also play a role.

It is important to note that neocortical neurons are not spread out randomly. Instead, cortical neurons are grouped within a well-ordered layered layout that largely repeats itself across the cortical mantle. This cortical lamination can be made visible using a variety of histological staining techniques. The exact number of layers that can be discerned depends on the type of histological stain and varies between cortical areas and individual species (DeFelipe et al. 2002). This variability in cortical layer count has prompted neuroanatomists to propose a variety of slightly different labeling schemes (Billings-Gagliardi et al. 1974; Marín-Padilla 1998). However, the current consensus follows neuroanatomist Korbinian Brodmann's (1868–1918) original plan of dividing the neocortex into six major laminae. These six basic cortical layers are often grouped further into three major laminar domains. In particular, layer 4 and its various sublayers are commonly referred to as the "granular layers" due to the predominance of small neurons that give rise to a fine-grained appearance in some histological stains. Accordingly, superficial layers 1–3 have been termed the "supragranular" layers, while deeper layers 5 and 6 are referred to as "infragranular" layers. Some neocortical areas seem to harbor no or little layer 4 and are thus referred to as "agranular cortex." Cortical areas with less than four layers (such as the olfactory cortex and the hippocampus) are thought to be distinct from the neocortex and distinguished as "allocortex," accordingly.

The reasoning for the above labeling scheme is that the connection patterns between these three main laminar compartments, as well as their interconnections with other cortical and subcortical sites, share a common scheme across the mammalian neocortex (but see Haug 1987; Horton and Adams 2005; Nelson 2002). This observation has given rise to the hypothesis that there is a "canonical" blueprint to the cortical laminar circuitry that is constant across the cortical sheet (Hubel and Wiesel 1974; Rockel et al. 1980). The signal flow across this stereotypical microcircuit has been mapped using a combination of anatomical and physiological techniques (e.g., Bode-Greuel et al. 1987; Nowak et al. 1995). A consensus model derived from these studies (Douglas et al. 1989; Douglas and Martin 2004; Bannister 2005; Lübke and Feldmeyer 2007; Felleman and Van Essen 1991; Sotero et al. 2010) suggests that the bulk of the ascending signals arrives in the granular compartment. Granular neurons then pass these signals onto neurons in the supragranular layers, where the ascending signals are integrated with other cortico-cortical and subcortical inputs. The supragranular neurons then project these integrated signals to other cortical areas as well as to neurons in the infragranular layers. Infragranular neurons back-project to the granular and supragranular layers, thus forming a reverberating loop between the superficial and deep cortical layers. Infragranular neurons additionally project to thalamic nuclei and other subcortical structures (Thomson and Bannister 2003).

While this stereotypical template of excitatory cortical laminar circuitry is still an idealized concept (Silberberg et al. 2002; Herculano-Houzel et al. 2008; Rakic 2008), it has been a popular concept for macroscopic models of cortical connectivity. Following the logic outlined above, any inter-cortical projections that originate outside granular layer 4 and terminate in layer 4 of another area are defined as ascending or "feedforward." Projections that innervate another area by sparing

granular layer 4 are characterized as descending or "feedback" (Rockland and Drash 1996). Using this framework, one can derive a rough wiring diagram of the functional "circuitry" between cortical areas based on their laminar interconnections. The popular "distributed but hierarchical" schematic that is commonly applied to cortical sensory areas such as the visual system is mainly based on this organizational principle (Felleman and Van Essen 1991).

The anatomical distinction of cortical layers outlined above is of great importance for the interpretation of fMRI signals. For one, fMRI has followed a steady trend toward resolving activity within and between cortical layers (e.g., Self et al. 2019; Lawrence et al. 2017; Trampel et al. 2019; Stephan et al. 2019; Huber et al. 2017), as its spatial resolution continues to improve (e.g., Mittmann et al. 2011; Polimeni et al. 2010; Goense et al. 2016; Chaimow et al. 2018). However, the laminar differences of cortical organization outlined above are also relevant for fMRI data that—in the majority of studies—lack the spatial precision to differentiate between these laminae. In line with the anatomical separation of neurons across cortical layers, functional activation differs along the same microscopic scales (Schroeder et al. 1998; Snodderly and Gur 1995; Bollimunta et al. 2008; Hansen and Dragoi 2011; Ninomiya et al. 2015; Sotero et al. 2015; Engel et al. 2016; Klein et al. 2016; Dougherty et al. 2017; van Kerkoerle et al. 2017; Hembrook-Short et al. 2017; Nandy et al. 2017; Cox et al. 2019; Sajad et al. 2019). For example, recent work has shown that the LFPs within the upper cortical layers (1–4) of the monkey visual cortex share little commonality with LFPs in the lower two cortical layers. This functional separation holds for both ongoing activity and sensory stimulation (Maier et al. 2010, 2011; Buffalo et al. 2011; Bastos et al. 2018). Likewise, the LFPs within cortical layers 1–5 of the rat somatosensory show different synchronization patterns relative to the LFPs in layer 6 (Sotero et al. 2015). These results suggest that the heterogeneity of neuronal activity along the cortical thickness needs to be taken into account when comparing neuronal signals to fMRI measurements (Maier et al. 2014).

4.3 Relationship Between Neuronal Activity and fMRI Signals

In the temporal domain, the BOLD response appears as a sluggish, low-pass filtered version of the neurophysiological response. A straightforward explanation for this observation is that changes in blood flow occur on a much slower time scale than changes in neuronal activity: BOLD responses to brief, discrete stimulation transpire within hundreds of milliseconds to seconds, while neurophysiological responses typically take place within milliseconds or tens of milliseconds. The neuronal response to a visual stimulus in the primary visual cortex (V1), for example, occurs within 20–50 ms and peaks within 30–70 ms following the onset of stimulation (Maunsell and Gibson 1992). The onset of the associated vascular response lags 1.5–2.5 s behind this neuronal response. The measured onset of the corresponding BOLD response depends on the specific experimental paradigm, the signal-to-noise

ratio (SNR), the response magnitude, and analysis parameters. Characteristically, peak blood flow and maximal BOLD response are measured 5–6 s following exposure to a short stimulus. Hence, a vascular response to a synaptic input may still be developing by the time a second or more stimuli excite the active cortical region. Whenever such a temporal overlap between responses occurs, the vascular response to a stimulus may be influenced by preceding stimuli (Lauritzen 2005).

When it comes to space, the resolution of fMRI signals is influenced by both the choice of fMRI contrast and the strength of the magnetic field. It also depends on which aspect of the brain's vasculature is probed (e.g., capillaries, venules, or veins). The point-spread function (i.e., "blur") of the T2* BOLD response in human visual area V1 has been estimated as ~3.5 mm at 1.5 T (Engel et al. 1997) and less than 2 mm at 7 T (Shmuel et al. 2007). The point-spread function of T2 and T2* BOLD responses at 7 T relative to metabolic activity has been estimated as ~0.8 and ~1.0 mm, respectively (c.

4.4 Correlations Between Neurophysiological Signals and fMRI Responses

The vast majority of studies analyzing the link between neuronal, metabolic, and hemodynamic responses found a monotonic (or even linear) increase in metabolic and hemodynamic activity following increases in neural activity. For example, relative changes in the level of blood oxygenation in the cat primary visual cortex (area 18) are proportional to increases in neuronal activity during the first phase (the so-called initial dip) of the associated metabolic and hemodynamic response (Shmuel and Grinvald 1996; Fig. 4.3a). In the same vein, in rat somatosensory cortex, the rate of oxygen consumption is proportional to increases in neuronal activity during the late phase of the hemodynamic response (Smith et al. 2002; Fig. 4.3b). It has also been shown that the CBF response to stimulation of climbing fibers in the rat cerebellum is proportional to the integrated neuronal responses induced by that stimulation (Mathiesen et al. 1998).

The amplitudes of sensory (forepaw)-evoked potentials were found to linearly correlate with the BOLD responses in rat somatosensory cortex across several stimulus frequencies (Brinker et al. 1999). An analogous conclusion was reached for humans after observing the hemodynamic response to stimulation of the median nerve using different stimulus intensities (Arthurs and Boniface 2003). Likewise, in monkeys, visual stimuli with varying luminance contrasts elicited BOLD responses that were proportional to the corresponding increases in neuronal activity (Logothetis et al. 2001).

In addition to the linear relationship between neurophysiological and BOLD responses observed in the studies outlined above, other studies found evidence for nonlinear relationships between these two measures. The CBF response to stimulation of parallel fibers within the cerebellum has shown a sigmoidal relation to the summated increases in neuronal activity (Mathiesen et al. 1998; Fig. 4.4).

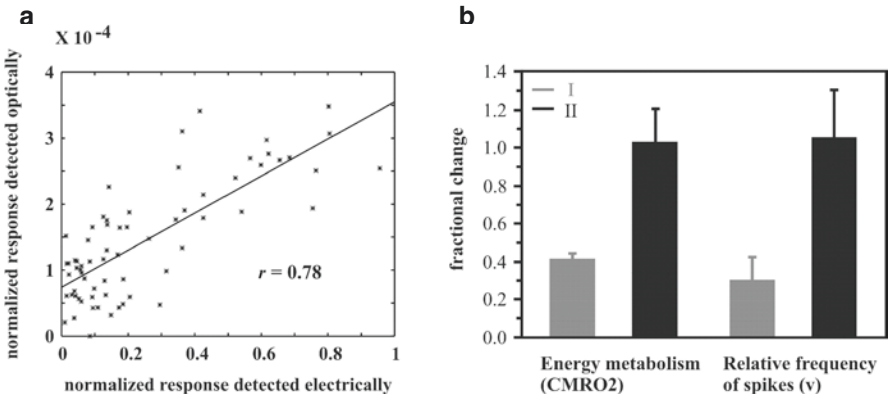

Fig. 4.3 Association between oxygen consumption and spiking activity. (**a**) Correlation between changes in blood oxygenation measured optically and the underlying action potential activity. These data were taken during the initial phase ("initial dip") of the response. Linear regression was used to generate the best linear fit to the data, which shows a high degree of linearity. (Modified from Fig. 7 of Shmuel and Grinvald (1996) with permission). (**b**) Stimulation of the rat forepaw led to comparative changes in oxygen consumption and spiking activity. Responses obtained from baseline conditions I and II are shown in *grey* and *black*, respectively. The baseline condition II was lowered by ~30% from baseline condition I due to a higher dosage of α-chloralose; however, the incremental response from condition II was larger. In both modalities, oxygen metabolism and spiking activity, the same levels of activation were approximately reached upon stimulation from the two different starting baseline levels. CMRO2, cerebral metabolic rate of oxygen. (Modified from Fig. 3 of Smith et al. (2002) with permission)

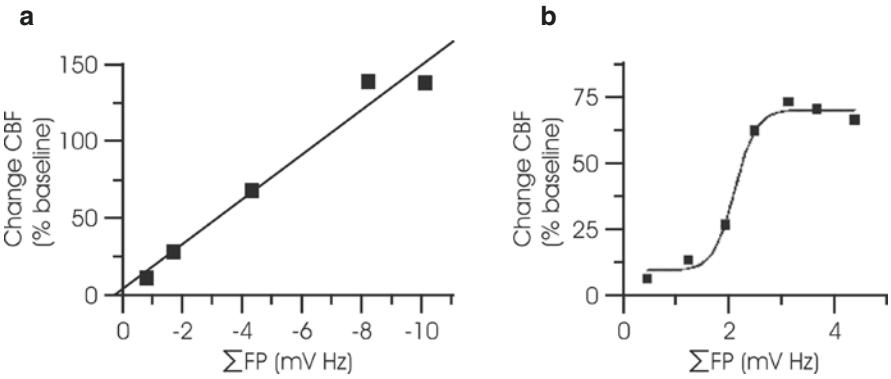

Fig. 4.4 Relationship between neuronal and hemodynamic responses in the rat cerebellum. (**a**) Frequency-dependent CBF increases in response to climbing fiber stimulation are correlated with the sum of active and passive post-synaptic activity. The figure presents the scatter plot of increases in CBF vs. summed field potentials (i.e., the product of field potential amplitudes and stimulation frequency). The line demonstrates the results of linear regression ($r = -0.985$, $P = 0.0022$). (**b**) Stimulation of parallel fibers at increasing frequencies leads to increases in summed field potentials and increases in CBF responses. The figure presents increases in CBF (ordinate) vs. summed field potentials (abscissa) from one rat, illustrating a sigmoidal relationship between the two variables. Both panels were modified from Mathiesen et al. (1998) (Figs. 4d and 5d) with permission

Devor et al. (2003) demonstrated a nonlinear relationship between neuronal and hemodynamic responses by combining optical measurements of hemodynamic signals with simultaneous recordings of neural activity. Specifically, in an event-related paradigm, the hemodynamic response continued to increase with stimulus intensity beyond the point of saturation of the electrical activity. Jones et al. (2004) and Sheth et al. (2004) reported similar observations. In the latter study, nonlinear models provided a better fit than linear models for the observed neurovascular coupling in the rat somatosensory cortex. Hoffmeyer et al. (2007) examined neurovascular coupling in rat sensory cortices in response to direct stimulation of transcallosal pathways. They showed that there is an exponential relationship between CBF responses and the summed amplitudes of neuronal activity. Nielsen and Lauritzen (2001) observed yet another type of nonlinearity, suggesting that a certain threshold of coordinated synaptic activity must be reached in order to trigger a hemodynamic response. Hence, synaptic activity needs to surpass a minimum threshold in order to cause an increase in CBF.

Overall, it appears that within a limited dynamic range of stimulus conditions, hemodynamic signals couple linearly to neuronal activity. In some parts of the brain or under certain stimulus conditions, however, this relationship takes on a nonlinear shape. Therefore, simply subtracting fMRI signal amplitudes obtained during two experimental conditions might not properly indicate the relative difference in underlying neuronal activity between these two states (Lauritzen 2005).

Interpreting fMRI data is complicated not only by the partially nonlinear relation between hemodynamics and neural activity but also by differences in the respective signal-to-noise ratio (SNR) of the two signals. The SNR of the neurophysiological signal associated with induced neuronal activity is about two orders of magnitude greater than that of the BOLD signal (Logothetis et al. 2001). Such a difference can, among other things, lead to statistical rejection ("false negatives") of valid activity during fMRI experiments, despite the fact that the underlying neural response is significant. These considerations are consistent with the finding that extensive averaging of fMRI data (which increases SNR) allows for more brain regions to be correctly classified as activated regions (Saad et al. 2003).

4.5 What Is the Neural Origin of fMRI Responses?

As indicated above, several studies have found a nearly linear relationship between metabolic and hemodynamic brain responses and local spiking activity. Specifically, Shmuel and Grinvald (1996) compared the optically measured reduction in blood oxygenation (the "initial dip") in the cat visual cortex to the concurrently elicited spiking response to visual stimuli of drifting gratings. They observed an approximately linear relationship between these two measures, indicating a correspondence between spiking responses and activity-dependent oxygen consumption during the initial, negative-going phase of the BOLD response, before the increase in CBF. Smith et al. (2002) recorded changes in cortical spiking activity during forepaw stimulation of anesthetized rats and found a similar connection between

oxygen consumption and spiking activity for the subsequent phase of the positive BOLD response when CBF is increased. They also measured the localized changes in oxygen consumption under the same conditions. The stimulus-induced changes in oxygen consumption were reported to be roughly proportional to the associated changes in spiking activity.

Rees et al. (2000) compared fMRI responses to visual motion stimuli in the motion-sensitive human area cortical MT+ to spiking responses obtained in monkey MT using matching stimuli. Responses in human MT+ showed a linear dependence on the coherence of motion signals, which mirrored similar changes in the rate of action potentials obtained in the animals using the same stimuli. Similar results were obtained by comparing BOLD responses in human V1 and action potential responses in monkey V1 to stimuli of varying brightness contrast (Heeger et al. 2000). These observations support the notion that fMRI responses of a cortical area are directly proportional to the average firing rate of its local cell population.

However, it is worth noting that synaptic activity is highly interrelated with the firing rates of pre-synaptic and post-synaptic neurons. This suggests that synaptic activity is also correlated with metabolic and hemodynamic responses. This assumption is particularly valid for the cerebral cortex, where the majority of synapses (both excitatory and inhibitory) originate locally, leaving only a minority of inputs from more remote cortical and subcortical structures (Braitenberg and Schuz 1991; Peters and Payne 1993; Peters and Sethares 1991). It thus seems reasonable to expect that an increase in local firing rates correlates with a comparative rise in local synaptic activity, which in turn leads to an increase in both the metabolic demand and vascular response.

Given the reasoning outlined above, it may not be surprising that in many cases, the BOLD signal has been found to correlate equally well with LFPs and spiking activity. For example, Mukamel et al. (2005) contrasted both single-unit activity and LFPs in the auditory cortex of two neurosurgical patients with the fMRI signals of healthy subjects during the presentation of an identical stimulus set. Their findings revealed a linear relationship between spiking activity, high-frequency LFPs, and the fMRI BOLD signal measured in the human auditory cortex. However, since the spiking activity was highly correlated with the high-frequency LFP, these results cannot answer the question regarding which of the two signals (LFP or spikes) has more predictive power for estimating the local BOLD response.

To summarize, the fMRI BOLD response can be taken as a dependable estimate of the average firing rate of the underlying neuronal population under a wide variety of stimulation conditions. Yet, correlation does not equal causation. The mere observation of close coupling between these signals does not imply that spiking activity drives (directly causes) the BOLD signal. One problem, in particular, is that the magnitude of local synaptic activity (and thus the resulting LFP) tends to be closely coupled with simultaneous changes in spike rate. In other words, it is difficult to attribute the relative roles of synaptic inputs versus the spiking output for hemodynamic changes given that both these processes tend to co-vary that closely. However, several studies managed to separate LFP and spiking responses in order to investigate their relative effects on the BOLD response.

Schwartz et al. (1979) measured localized brain-glucose metabolism in rats using 2-deoxyglucose autoradiography (Sokoloff et al. 1977). They subjected rats to an osmotic load that stimulated neuronal cell bodies in the supraoptic and paraventricular nuclei of the hypothalamus. The axon terminals of these neurons reside in the posterior pituitary gland, which is separated by a considerable distance from the stimulated cell bodies. The authors compared the metabolic activity in both locations and found that brain metabolism increased significantly in the area harboring the axon terminals (the posterior pituitary gland). In contrast, there were no measurable metabolism changes in the cell bodies residing in the hypothalamus. This finding is consistent with the known relationship between the metabolic cost of sustaining ionic gradients and the surface-area-to-volume ratio of neurons (Cohen and De Weer 1977; Ritchie 1967; Raichle and Mintum 2006). In general, their data support the notion that synaptic input, and not the spiking output, is the driving mechanism of localized changes in the brain metabolism (see Lauritzen (2005) for additional evidence).

Mathiesen et al. (1998) employed laser Doppler flow and extracellular neurophysiological recordings to differentiate between synaptic and spiking activities in order to investigate their relative impact on CBF in the rat cerebellum. Stimulation of the monosynaptic climbing fiber system triggered LFPs and complex spikes of Purkinje cells with concurrent increases in CBF. However, when spiking activity was inhibited, CBF increased despite the decrease in spiking activity (Fig. 4.5a). This discovery verified that activity-dependent CBF increases in the cerebellum depend on synaptic excitation and that the net spiking activity of Purkinje cells is insignificant for the vascular response.

Thomsen et al. (2004) examined the consequences of enhanced spiking activity on CBF in the rat cerebellum under conditions of disinhibition, which was achieved by blocking GABA (A) receptors with either bicuculline or picrotoxin. Disinhibition increased Purkinje cell spiking rates to 200–300% of control activity. However, there was no increase in basal CBF. This finding illustrates that increased spike activity alone is insufficient to affect CBF. In contrast, the neurovascular coupling between excitatory synaptic activity evoked by climbing fiber stimulation and CBF responses was maintained during disinhibition. Thus, increasing the spiking activity of principal neurons is neither sufficient nor necessary to elicit CBF responses. Instead, activation-dependent vascular signals seem to mainly reflect excitatory synaptic activity.

Logothetis et al. (2001) examined the relationship of the BOLD signal with LFPs and spiking activity in the monkey visual cortex. The largest increases in LFP power in response to visual stimulation were observed within the gamma frequency range (>30 Hz) of the LFPs. LFPs were found to reflect the time course of the BOLD response more accurately since both LFP power and BOLD tended to remain elevated for the duration of the visual stimulus, while spiking activity did not (Fig. 4.5b). Linear systems analysis revealed that LFPs yield a better approximation of the BOLD response than the spiking responses. A follow-up study in alert monkeys verified that LFPs are more accurate and more reliable predictors of the BOLD response, despite the fact that both LFPs and MUA correlate with the BOLD signal

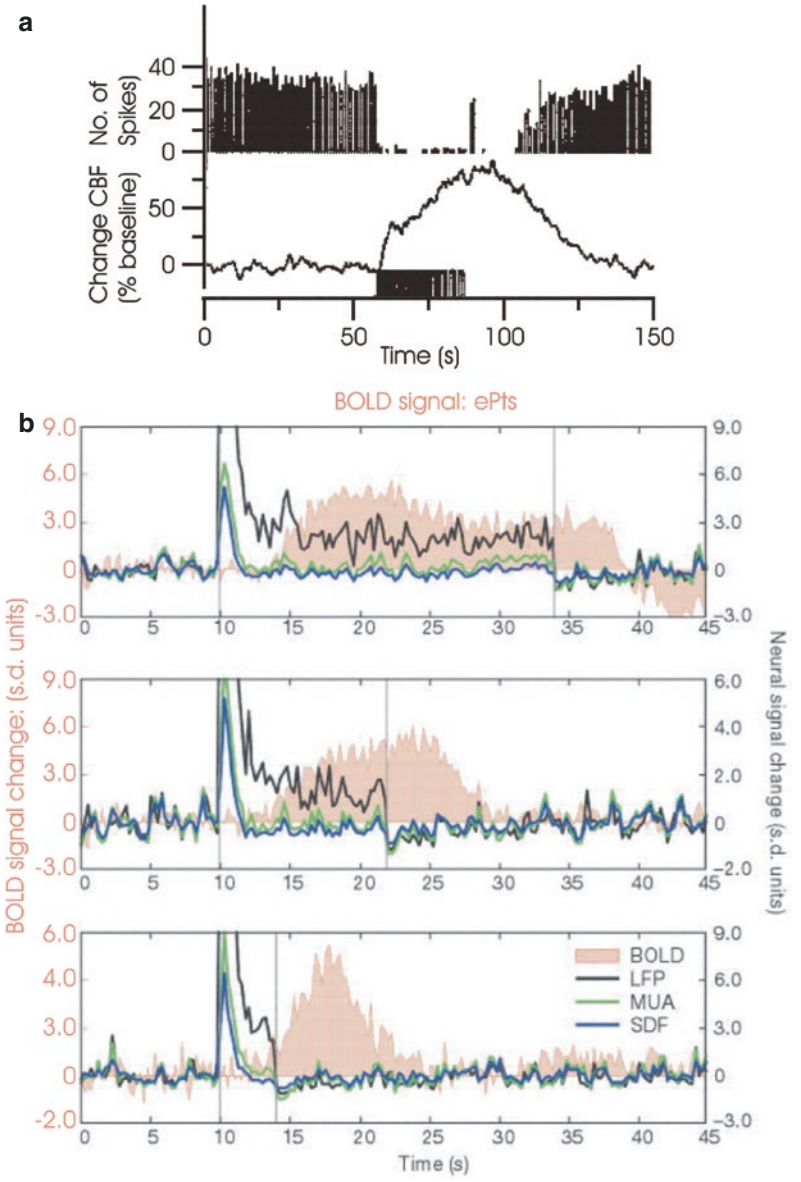

Fig. 4.5 CBF and BOLD responses correlate with LFPs. (**a**) Activity-dependent CBF increases and spike activity in response to parallel fiber stimulation in the cerebellum. Purkinje cell spiking activity diminished after 1–3 s of stimulation, and spontaneous firing did not return to baseline until 19–25 s after the end of stimulation (*upper plot*). CBF increased during stimulation and persisted for 5–10 s after the end of stimulation before returning to baseline after a lag of 40–50 s (*lower plot*). (Modified from Fig. 3a of Mathiesen et al. (1998) with permission). (**b**) Simultaneous neural and BOLD recordings from a cortical site showing a transient MUA response. Responses to a pulse stimulus of 4, 12, and 24 s are shown in the bottom, middle, and top plots, respectively. LFP is the sole signal showing time course matched in response to duration with that of the BOLD response. Both the spike density function (SDF) and the multi-unit activity (MUA) adapt back to baseline a couple of seconds after stimulus onset. The BOLD time series is from an ROI around the electrode. *CBF* cerebral blood flow, *ROI* region of interest. (Modified from Fig. 3 of Logothetis et al. (2001) with permission)

(Goense and Logothetis 2008). More recent work expanded this result by demonstrating that similar differences can be found in the rodent cortex, independently of whether local neural stimulation was achieved via sensory stimulation or optogenetic excitation (Iordanova et al. 2015). In either case, LFPs were well correlated with local cerebral blood flow, moderately with cerebral blood volume, and less correlated with blood oxygenation, while pre-synaptic firing rates had little impact on the vascular response.

Similar results were reported by Niessing et al. (2005), who recorded neurophysiological signals and optically measured hemodynamic responses in the cat visual cortex. Increasing visual stimulus strength resulted in enhanced spiking activity, high-frequency LFP power, and hemodynamic responses. However, hemodynamic responses were found to fluctuate when stimuli of constant intensity were presented to the animal. These fluctuations were only weakly related to the rate of action potentials. In contrast, they were tightly correlated with LFP power in the gamma range. When sorting the data according to the amplitude of the hemodynamic response, clear differences were detected with respect to the frequency distribution of the respective LFPs. Specifically, LFP power increases in the delta (~1–4 Hz), theta (~4–8 Hz), and alpha (~8–12 Hz) frequency bands were most prevalent for stimulus presentations that evoked the weakest hemodynamic responses. With the increasing hemodynamic response, the peak of LFP power shifted from the theta and alpha bands to the beta (~12–30 Hz) and lower gamma frequency bands. The strongest hemodynamic responses were linked to high power in the lower and upper gamma frequency bands. Quantifying the relationship between the strength of the hemodynamic response and LFP power in different frequency bands revealed that low-frequency activity in the delta band was negatively correlated with hemodynamic signal strength. Theta, alpha, and beta power levels were not significantly correlated with the vascular response. A weak and strong positive correspondence existed for LFP power in the lower and upper gamma bands, respectively. LFP power in the high-frequency range in particular is thought to increase with the local synaptic events, signifying a close association between hemodynamic responses and neuronal synchronization.

Viswanathan and Freeman (2007) demonstrated yet another dissociation between synaptic and spiking activities in the cat primary visual cortex. They presented visual stimuli composed of gratings that were drifting at different temporal frequencies. Simultaneously, they recorded neural responses and local tissue oxygenation that can serve as a proxy for the BOLD signal. Spiking activity decreased while LFP power in the lower gamma band became more prevalent when the temporal frequency of the gratings increased. Compared to their maximal responses, which were obtained at a stimulus frequency of 4 Hz, spiking activity and low-gamma LFPs dropped to approximately 15% and 85%, respectively, during visual stimulation at 20 Hz. LFP responses in the delta, theta, alpha, beta, and high-gamma bands plunged to approximately 40% of their maximal response at 4 Hz, while tissue oxygen fell to 60%. These results indicate the existence of close coupling between tissue oxygenation and LFP power, but not with spiking activity.

Interestingly, Bentley et al. (2016) found that oxygen responses were correlated with LFP power in different cortical areas of macaque monkeys, while the apparent hemodynamic coupling between the oxygen level and electrophysiology differed across areas. Specifically, they paired oxygen polarography, an electrode-based oxygen measurement technique, with standard electrophysiological recording to assess the relationship of oxygen and neural activity in two cortical areas: the task-negative posterior cingulate cortex (PCC) and the visually responsive task-positive area V3. Their finding suggests that cortical oxygen responses reflect concurrent changes in LFP power and that either the coupling of neural activity to blood flow and metabolism differs between areas or that computing a linear transformation from a single LFP band to the oxygen level does not capture the true physiological process.

Rauch et al. (2008) used an experimental dissociation between spiking and LFPs by injecting a neuromodulator that primarily acts on efferent neuronal membranes into the primary visual cortex of anesthetized monkeys. The neuromodulator reduced population spiking responses without significantly affecting either LFPs or BOLD activity, implying that the efferent neurons within the visual cortex pose a relatively small metabolic burden compared to the overall pre-synaptic and post-synaptic processing of incoming afferents. In other words, BOLD seems to predominantly reflect pre-synaptic and post-synaptic processing of incoming afferents to a particular cortical region.

So far, we have described both cases of coupling and of dissociation between spiking activity and the BOLD signal. Yet, the question remains: what determines whether the BOLD signal is associated with or dissociated from the spiking output of neurons in any specific paradigm? Using multiple electrodes in the human auditory cortex, Nir et al. (2007) measured spiking activity and LFPs and observed a wide range of coupling levels between the activity of individual neurons and gamma-range LFPs. The gamma LFPs were well correlated with BOLD signals measured across different individuals (r = 0.62). In contrast, the coupling of single-neuron spiking to BOLD responses was highly variable. However, the BOLD response was tightly related to interneuronal firing-rate correlations (r = 0.70). These results suggest that the BOLD signal could closely reflect spiking activity, depending on whether an experimental paradigm evokes a high degree of interneuronal correlation.

4.6 Neuronal Correlates of Negative BOLD Responses

Sustained negative responses are an interesting, pervasive phenomenon in functional brain imaging. Some hypotheses regarding the origin of these negative responses suggest a purely vascular basis for this phenomenon (such as "vascular blood steal"), concluding that the negative BOLD response (NBR) bears little relation to underlying neuronal activity (Harel et al. 2002; Kannurpatti and Biswal 2004). Shmuel et al. (2002) demonstrated a robust, sustained NBR in the human occipital cortex triggered by stimulating part of the visual field. This NBR was linked to decreases in CBF and consequently reductions in oxygen consumption. These results suggest that the NBR is associated with reductions in local neuronal activity. Similar links of NBRs to decreases in local CBF and oxygen consumption have been reported in the visual

(Uludağ et al. 2004; Pasley et al. 2007) and motor cortices (Stefanovic et al. 2004, 2005). In addition, Shmuel et al. (2006) employed a similar stimulation paradigm to the one they used in humans in the monkey primary visual cortex and obtained a similar NBR outside the stimulated brain regions. Using simultaneous fMRI and neurophysiological recordings, they then showed that the negative BOLD response was associated with local decreases in the neuronal activity below the baseline level of spontaneous activity. Trial-by-trial comparisons showed a tight coupling between the NBR and reduced neuronal activity. The NBR was linked to comparable decreases in LFPs and MUA. These findings indicate that a large component of the NBR stems from decreases in neuronal activity (Fig. 4.6).

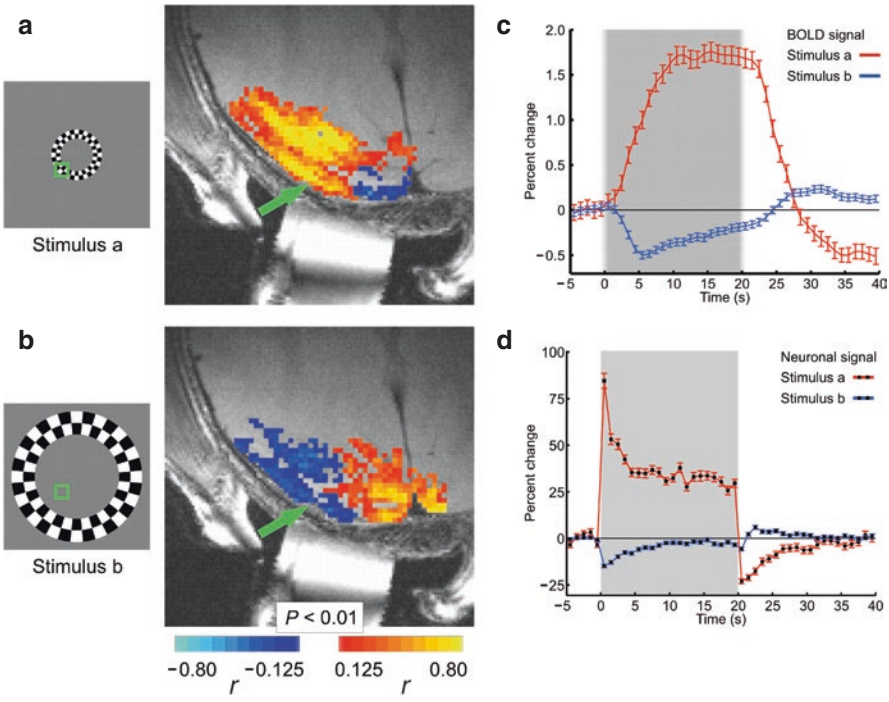

Fig. 4.6 Neuronal correlates of a negative BOLD response (NBR). (**a**, **b**) Patterns of response to a central and a peripheral visual field stimulus, respectively. The fMRI response from a single axial-oblique slice is superimposed on the corresponding anatomical image. *Green arrows* indicate the position of the recording electrode within visual area V1. *Green squares* represent the collective receptive field of the neurons in the vicinity of the electrode. The stimulus in (**a**) overlapped with the receptive field, invoking a positive BOLD response in the area directly surrounding the electrode. The stimulus in (**b**) did not overlap with the receptive field and induced an NBR in that same vicinity. (**c**) Time course (mean ± SEM) of the BOLD response sampled from the ROI around the electrode. (**d**) Neuronal responses to the stimuli presented in (**a**, **b**). Time courses (mean ± SEM) present the fractional change in power of the broad-band neuronal signal in response to stimuli that overlapped (*red*) or did not overlap (*blue*) with the receptive field. The data in (**c**, **d**) were averaged over all trials from 15 sessions. (All panels were modified from Shmuel et al. (2006) (Figs. 1a, b, and d and 2a) with permission)

The neuronal and vascular mechanisms underlying NBRs in rat primary somatosensory cortex were also studied by Devor et al. (2007) using optical imaging techniques. Stimulation of rat forepaws resulted in a central region of net depolarization surrounded by net hyperpolarization. Hemodynamic measurements revealed correspondence between the depolarized regions with an increase in local blood oxygenation, as well as an association between hyperpolarized cortical regions and decreased blood oxygenation. On the microscopic level of single arterioles, the vascular response was found to be composed of a combination of dilatory and constrictive phases. The relative amplitude of vasoconstriction co-varied with the strength of neuronal hyperpolarization and the corresponding decrease in oxygenation. These findings imply that neuronal inhibition and concomitant arteriolar vasoconstriction relate to decreased blood oxygenation, which would be consistent with a negative BOLD fMRI response.

Additional evidence linking negative BOLD responses to inhibited neuronal activity was demonstrated by Boorman et al. (2010). These authors employed electrical whisker-pad stimulation while imaging the rat somatosensory cortex. They demonstrated negative BOLD responses in deeper cortical layers. Separate two-dimensional optical imaging spectroscopy and laser Doppler flowmetry revealed that the NBR was the result of decreased blood volume and flow and increased levels of deoxyhemoglobin. Neural activity in the NBR region, measured with multichannel electrodes, varied considerably as a function of cortical depth. There was a decrease in neuronal activity in the deep cortical laminae. After cessation of whisker stimulation, there was a large increase in neural activity above baseline. Both the decrease in neuronal activity and the increase above baseline correlated well with the simultaneously measured blood flow, suggesting that the NBR is related to decreases in neural activity within the deep cortical layers.

4.7 Neuronal Correlates of Spontaneous Fluctuations in fMRI Signals

Early fMRI studies deemed the large cortical signal fluctuations that can be observed when a subject is resting without explicit stimulation or task instructions are just random, meaningless “noise.” However, more recent work has demonstrated that the spatio-temporal structure of these spontaneously occurring signal changes is not random at all. Instead, spontaneous fluctuations in BOLD are highly organized, and this spatial organization is consistent between subjects (Biswal et al. 1995; Fox and Raichle 2007). As a consequence, the relationship between BOLD and the underlying neural events in the resting state is of particular interest. These spontaneous fluctuations in fMRI signals are reminiscent of previously demonstrated spontaneous fluctuations in cortical neuronal signals observed in cats (Arieli et al. 1996) and monkeys (Leopold et al. 2003). Importantly, these resting-state fluctuations are correlated across large parts of the brain (Biswal et al. 1995), a phenomenon termed functional connectivity.

Several studies identified contributions of non-neuronal origins to spontaneous fluctuations in fMRI signals. These contributions include vascular vaso-motion (Mayhew et al. 1996) and respiration (Birn et al. 2006; Wise et al. 2004). However, there is also evidence for neural events giving rise to resting-state functional connectivity. Shmuel and Leopold (2008) obtained simultaneous fMRI and intracortical neurophysiological recordings in anesthetized, paralyzed monkeys that were either exposed to a uniform grey field or to complete darkness. They found an association between slow fluctuations in the spontaneous BOLD signals and concurrent fluctuations in the underlying local neuronal activity. This correlation varied with the BOLD signal time-lag relative to neuronal activity, resembling a traditional hemodynamic response function with peaks at a 6-s lag of the BOLD signal (Fig. 4.7a–j). These associations were consistently identified when the neuronal signal consisted of either relative power variations in the LFPs gamma band, MUA, or the spiking rate of a small group of neurons. Further examination of the relationship between the fMRI time series of different parts of the cortex and the neuronal activity measured within one cortical site revealed that widespread areas of the visual cortex in both hemispheres were significantly correlated with neuronal activity from a single recording site in area V1 (Fig. 4.7k). Assuming that Shmuel and Leopold's (2008) results from area V1 can be generalized to other cortical areas, fMRI-based functional connectivity between remote regions in the resting state can be linked to the synchronization of slow fluctuations in the underlying neuronal signals.

Schölvinck et al. (2010) replicated and expanded on these results using alert monkeys. Their results demonstrate widespread, positive correlations of fMRI signals over nearly the entire cerebral cortex with the spontaneous fluctuations in the LFPs measured at a single cortical site (Fig. 4.7). The spontaneous neural activity reported in that study accounted for 10% of the observed BOLD signal variance, which is a considerable fraction of the 50% explained variance during visual stimulation. Similar to the findings by Shmuel and Leopold (2008), the observed correlation was especially consistent for upper gamma-range frequencies (40–80 Hz; Fig. 4.7m). A strong, positive correlation was also detected in a band of lower frequencies (2–15 Hz), albeit with a lag closer to zero. Overall, these findings specify that the global constituent of fMRI fluctuations measured during the resting state is closely linked to neural activity.

Hutchison et al. (2015) uncovered similar results for the monkey prefrontal cortex. They measured both fMRI BOLD responses and LFPs in anesthetized animals that were not exposed to any explicit sensory stimulation. They also found that high-frequency LFPs were correlated with BOLD activity at the recording site, while low-frequency LFPs were not. They further showed that high-frequency (i.e., beta to low gamma) and low-frequency (i.e., delta to theta) LFP power were anti-correlated in the absence of any explicit stimuli. This finding corroborates the notion that complementary changes in low- and high-frequency bands are an intrinsic property of LFPs and explains why low- and high-frequency LFPs yield different correlations with the fMRI BOLD response.

Using an electrophysiology system that can record the full band of LFPs, Pan et al. (2013) demonstrated that in addition to correlation with the power of

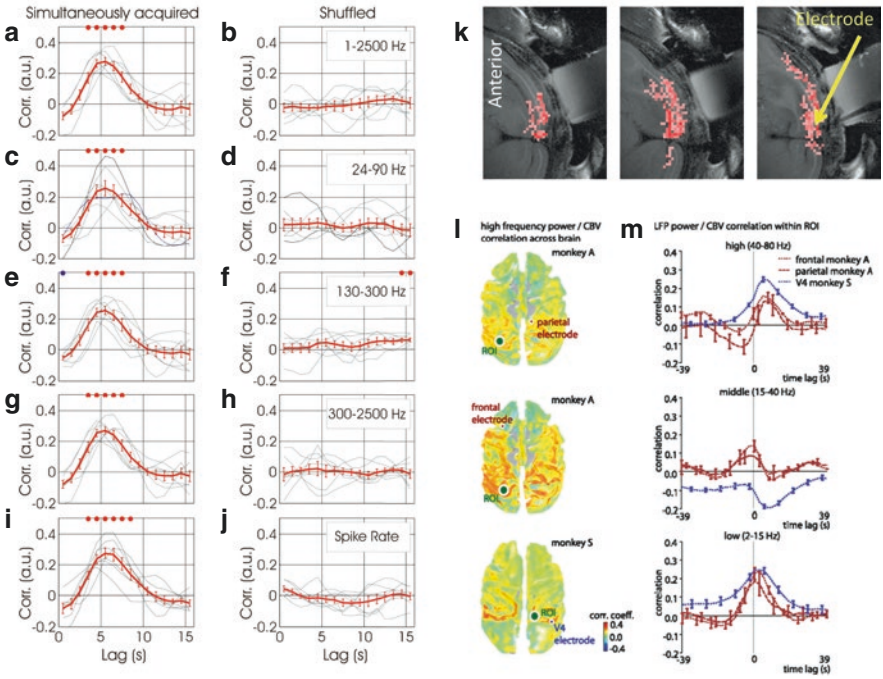

Fig. 4.7 Spontaneous fluctuations in BOLD signal correlate with the underlying neurophysiological activity. (**a**–**i**) Co-variation between spontaneous fluctuations in fMRI and neuronal signals as a function of temporal lag. (**a**) The grey curves show the correlation as a function of lag from each experiment. The red curve presents the correlation function averaged over seven experiments in five different monkeys (mean ± SEM). The vertical axis represents Spearman's correlation coefficient between BOLD and the fluctuations in relative (fractional change) power averaged over frequencies of the denoised broad-band neurophysiological signal acquired simultaneously with fMRI. The horizontal axis represents the lag between the two correlated signals, with positive lags standing for BOLD lagging behind the neuronal activity. (**b**) Correlation between the same signals as presented in (**a**), computed after breaking the simultaneity condition by shuffling the segments of BOLD and neuronal activity obtained within each experiment. (**c**–**h**) present correlation functions in the format used for (**a**) and (**b**), for the LFP, mid-range, and MUA bands, respectively. (**i**, **j**) present similar correlation functions for fluctuations in spiking activity, estimated by counting identified action potentials over 1 s epochs rather than using frequency-based analysis. (Modified from Shmuel and Leopold (2008), with permission). (**k**) Spatial extent of the correlation between the slow relative fluctuations in power averaged over frequencies of the broad-band neuronal signal recorded at the tip of the electrode (yellow arrow) and the fluctuations in BOLD measured voxel by voxel. Pink-colored voxels showed a statistically significant positive correlation between the neurophysiological activity recorded in one site in V1 and BOLD signals for a 5 s time-lag (*t*-test, averaging over the correlation obtained time-segment by time-segment, $p < 0.01$). (Modified from Shmuel and Leopold (2008), with permission). (**l**, **m**) Spatial extent of the fMRI correlation with high-frequency LFP in frontal area 6d, parietal area 7a, and occipital area V4. (**l**) In all cases, spatial correlations are bilateral and spread over large swathes of the cerebral cortex. (**m**) Cross-correlation functions between the fMRI and LFP power time courses for three electrodes outside V1 and for the three LFP frequency ranges: low (2–15 Hz), middle (15–40 Hz), and high (40–80 Hz). (Modified from Schölvinck et al. (2010), with permission). *CBV* cerebral blood volume, *LFP* local field potential

high-frequency LFPs, spontaneous fluctuations in BOLD signals also correlate with infra-slow, 0.05–0.25 Hz components of the neural signals.

4.8 Dissociations Between BOLD Responses and Neurophysiological Activity

The previous sections focused on cases where metabolic and hemodynamic responses largely corresponded to changes in neurophysiological activity. A few studies reported cases where these signals dissociated. Maier et al. (2008) investigated brain responses to a visual illusion in which a part of an image can become subjectively invisible. Perceptual disappearance of the visual stimulus elicited a robust drop in V1 fMRI signal in humans. In contrast, monkey single-neuron recordings failed to demonstrate such perception-related changes in V1 spiking. To investigate the basis of this discrepancy, they next measured both the BOLD response and electrophysiological signals. They found that all signals were in good agreement during conventional stimulus presentation, showing strong modulation to the presentation and removal of a visual stimulus. During perceptual suppression, however, only the BOLD response and low-frequency (5–30 Hz) LFP power showed decreases, whereas both spiking and high-frequency LFP power remained unaffected. These results demonstrate that the coupling between BOLD and electrophysiological signals in V1 is context-dependent, with a marked dissociation occurring during a state of perceptual suppression.

While Maier et al. (2008) observed changes in lower LFP frequency bands that corresponded to the BOLD signal, Sirotin and Das (2009) found evidence of a complete divergence of hemodynamic and neurophysiological signals. Using a dual-wavelength optical imaging technique that independently measured cerebral blood volume and oxygenation, they found two distinct components of the hemodynamic signal in V1 of alert animals. One component was reliably predictable from neuronal responses to visual stimulation. The other component, of almost comparable strength, was reported as an unknown signal that entrained to task structure of rhythmic stimulus presentations independently of visual input or of standard neural predictors of hemodynamics. The resulting data exhibited robust modulations of the hemodynamic signal at the stimulus presentation frequency, even though the animals were in complete darkness. This latter component showed predictive timing, with increases in cerebral blood volume in anticipation of future stimulus onsets. Sirotin and Das (2009) suggested the existence of a preparatory mechanism that brings additional arterial blood to the cortex in anticipation of expected tasks. This mechanism could be implemented via distal neuromodulatory control of cerebral arteries. This interpretation was challenged by several authors (e.g., Logothetis (2010) and Handwerker and Bandettini (2011)), indicating that the data presented by Sirotin and Das (2009) did show modulation of neuronal activity in V1, likely reducing spontaneous activity during fixation. The increased inhibition, visible in their spectrograms, may trigger CBV changes and yield anticipatory responses. It was hypothesized that the responses are due to site-specific effects of neuromodulatory input on the cortical

excitation-inhibition balance, mediated by norepinephrine released from the locus coeruleus. Others (e.g., Tan 2009) supported the findings and interpretation of Sirotin and Das (2009) and suggested that the task-related properties of these responses point to a possible link between regional cerebral microcirculation and dopaminergic signaling. It was hypothesized that dopamine plays a role in the task-dependent, "on-demand" allocation of metabolic resources.

It should be noted that both Maier et al. (2008) and Sirotin and Das (2009) pursued their measurements in alert animals, while the majority of other studies of neurovascular coupling used anesthetized animals. Neurovascular coupling depends on the state of the animal—alert or anesthetized (Paasonen et al. 2018)—and on the anesthesia regime (Franceschini et al. 2010; Paasonen et al. 2018; Bortel et al. 2020). The findings by Maier et al. (2008) and Sirotin and Das (2009) indicate that neurovascular coupling may be modified in the alert state, possibly via the action of neuromodulators that depend on behavioral state. This adds to the complexity of the interplay between neurophysiological signals and hemodynamic responses, which remains to be addressed in future studies.

References

Arieli A, Sterkin A, Grinvald A, Aertsen A (1996) Dynamics of ongoing activity: explanation of the large variability in evoked cortical responses. Science 273:1868–1871

Arthurs OJ, Boniface SJ (2003) What aspect of the fMRI BOLD signal best reflects the underlying electrophysiology in human somatosensory cortex? Clin Neurophysiol 114:1203–1209

Bandettini PA, Wong EC, Hinks RS, Tikofsky RS, Hyde JS (1992) Time course EPI of human brain function during task activation. Magn Reson Med 25:390–397

Bannister AP (2005) Inter- and intra-laminar connections of pyramidal cells in the neocortex. Neurosci Res 53:95–103

Bastos AM, Loonis R, Kornblith S, Lundqvist M, Miller EK (2018) Laminar recordings in frontal cortex suggest distinct layers for maintenance and control of working memory. Proc Natl Acad Sci U S A 115(5):1117–1122

Bentley WJ, Li JM, Snyder AZ, Raichle ME, Snyder LH (2016) Oxygen level and LFP in task-positive and task-negative areas: bridging BOLD fMRI and electrophysiology. Cereb Cortex 26(1):346–357

Billings-Gagliardi S, Chan-Palay V, Palay SL (1974) A review of lamination in area 17 of the visual cortex Macaca mulatta. J Neurocytol 3:619–629

Birn RM, Diamond JB, Smith MA, Bandettini PA (2006) Separating respiratory-variation-related fluctuations from neuronal-activity-related fluctuations in fMRI. Neuroimage 31:1536–1548

Biswal B, Yetkin FZ, Haughton VM, Hyde JS (1995) Functional connectivity in the motor cortex of resting human brain using echo-planar MRI. Magn Reson Med 34:537–541

Bode-Greuel KM, Singer W, Aldenhoff JB (1987) A current source density analysis of field potentials evoked in slices of visual cortex. Exp Brain Res 69:213–219

Bollimunta A, Chen Y, Schroeder CE, Ding M (2008) Neuronal mechanisms of cortical alpha oscillations in awake-behaving macaques. J Neurosci. 28:9976–9988

Boorman L, Kennerley AJ, Johnston D, Jones M, Zheng Y, Redgrave P, Berwick J (2010) Negative blood oxygen level dependence in the rat: a model for investigating the role of suppression in neurovascular coupling. J Neurosci 30:4285–4294

Bortel A, Pilgram R, Yao Z-S, Shmuel A (2020) Dexmedetomitine—commonly used in functional imaging studies—increases susceptibility to seizures in rats but not in wild type mice. Front Neurosci 14:832. https://doi.org/10.3389/fnins.2020.00832

Braitenberg V, Schuz A (1991) Anatomy of the cortex. Springer, Berlin
Brinker G, Bock C, Busch E, Krep H, Hossmann KA, Hoehn-Berlage M (1999) Simultaneous recording of evoked potentials and T2*-weighted MR images during somatosensory stimulation of rat. Magn Reson Med 41:469–473
Buffalo EA, Fries P, Landman R, Buschman TJ, Desimone R (2011) Laminar differences in gamma and alpha coherence in the ventral stream. Proc Natl Acad Sci U S A 108:11262–11267
Buxton RB, Uludag K, Dubowitz DJ, Liu TT (2004) Modeling the hemodynamic response to brain activation. Neuroimage 23:S220–S233
Chaimow D, Yacoub E, Uğurbil K, Shmuel A (2018) Spatial specificity of the functional MRI blood oxygenation response relative to neuronal activity. Neuroimage 164:32–47
Cohen LB, De Weer P (1977) Structural and metabolic processes directly related to action potential propagation. In: Brookhart JM, Mountcastle VB (eds) Handbook of physiology: the nervous system. American Physiological Society, Bethesda, pp 137–159
Cox MA, Dougherty K, Adams GK, Reavis EA, Westerberg JA, Moore BS, Leopold DA, Maier A (2019) Spiking suppression precedes cued attentional enhancement of neural responses in primary visual cortex. Cereb Cortex 29(1):77–90
DeFelipe J, Alonso-Nanclares L, Arellano JI (2002) Microstructure of the neocortex: comparative aspects. J Neurocytol 31:299–316
Devor A, Dunn AK, Andermann ML, Ulbert I, Boas DA, Dale AM (2003) Coupling of total hemoglobin concentration, oxygenation, and neural activity in rat somatosensory cortex. Neuron 39:353–359
Devor A, Tian P, Nishimura N, Teng IC, Hillman EMC, Narayanan SN, Ulbert I, Boas DA, Kleinfeld D, Dale AM (2007) Suppressed neuronal activity and concurrent arteriolar vasoconstriction may explain negative blood oxygenation level-dependent signal. J Neurosci 27:4452–4459
Dougherty K, Cox MA, Ninomiya T, Leopold DA, Maier A (2017) Ongoing alpha activity in V1 regulates visually driven spiking responses. Cereb Cortex 27(2):1113–1124
Douglas RJ, Martin KAC (2004) Neuronal circuits of the neocortex. Annu Rev Neurosci 27:419–451
Douglas RJ, Martin KAC, Whitteridge D (1989) A canonical microcircuit for neocortex. Neural Comput 1:480–488
Engel SA, Glover GH, Wandell BA (1997) Retinotopic organization in human visual cortex and the spatial precision of functional MRI. Cereb Cortex 7:181–192
Engel TA, Steinmetz NA, Gieselmann MA, Thiele A, Moore T, Boahen K (2016) Selective modulation of cortical state during spatial attention. Science 354(6316):1140–1144
Felleman DJ, Van Essen DC (1991) Distributed hierarchical processing in the primate cerebral cortex. Cereb Cortex 1:1–47
Fox PT, Raichle ME (1986) Focal physiological uncoupling of cerebral blood-flow and oxidative-metabolism during somatosensory stimulation in human-subjects. Proc Natl Acad Sci U S A 83:1140–1144
Fox MD, Raichle ME (2007) Spontaneous fluctuations in brain activity observed with functional magnetic resonance imaging. Nat Rev Neurosci 8(9):700–711
Franceschini MA, Radhakrishnan H, Thakur K, Wu W, Ruvinskaya S, Carp S, Boas DA (2010) The effect of different anesthetics on neurovascular coupling. Neuroimage 51:1367–1377
Freeman WJ (1975) Mass action in the nervous system. Academic, New York
Goense JBM, Logothetis NK (2008) Neurophysiology of the BOLD fMRI signal in awake monkeys. Curr Biol 18:631–640
Goense J, Bohraus Y, Logothetis NK (2016) fMRI at high spatial resolution: implications for BOLD-models. Front Comput Neurosci 10:66
Handwerker DA, Bandettini PA (2011) Hemodynamic signals not predicted? Not so: a comment on Sirotin and Das (2009). Neuroimage 55(4):1409–1412
Hansen BJ, Dragoi V (2011) Adaptation-induced synchronization in laminar cortical circuits. Proc Natl Acad Sci U S A 108:10720–10725

Harel N, Lee SP, Nagaoka T, Kim DS, Kim SG (2002) Origin of negative blood oxygenation level-dependent fMRI signals. J Cereb Blood Flow Metab 22:908–917

Haug H (1987) Brain sizes, surfaces, and neuronal sizes of the cortex cerebri: a stereological investigation of man and his variability and a comparison with some mammals (primates, whales, marsupials, insectivores, and one elephant). Am J Anat 180:126–142

Heeger DJ, Huk AC, Geisler WS, Albrecht DG (2000) Spikes versus BOLD: what does neuroimaging tell us about neuronal activity? Nat Neurosci 3:631–633

Hembrook-Short JR, Mock VL, Briggs F (2017) Attentional modulation of neuronal activity depends on neuronal feature selectivity. Curr Biol 27(13):1878–1887.e5

Herculano-Houzel S, Collins CE, Wong P, Kaas JH, Lent R (2008) The basic nonuniformity of the cerebral cortex. Proc Natl Acad Sci U S A 105:12593–12598

Hoffmeyer HW, Enager P, Thomsen KJ, Lauritzen MJ (2007) Nonlinear neurovascular coupling in rat sensory cortex by activation of transcallosal fibers. J Cereb Blood Flow Metab 27:575–585

Hoge RD, Atkinson J, Gill B, Crelier GR, Marrett S, Pike GB (1999) Linear coupling between cerebral blood flow and oxygen consumption in activated human cortex. Proc Natl Acad Sci U S A 96:9403–9408

Horton JC, Adams DL (2005) The cortical column: a structure without a function. Philos Trans R Soc Lond B Biol Sci 360:837–862

Hubel DH, Wiesel TN (1974) Uniformity of monkey striate cortex: a parallel relationship between field size, scatter, and magnification factor. J Comp Neurol 158:295–305

Huber L, Handwerker DA, Jangraw DC, Chen G, Hall A, Stüber C, Gonzalez-Castillo J, Ivanov D, Marrett S, Guidi M, Goense J, Poser BA, Bandettini PA (2017) High-resolution CBV-fMRI allows mapping of laminar activity and connectivity of cortical input and output in human M1. Neuron 96:1253–1263

Hutchison RM, Hashemi N, Gati JS, Menon RS, Everling S (2015) Electrophysiological signatures of spontaneous BOLD fluctuations in macaque prefrontal cortex. Neuroimage. 113:257–267

Iordanova B, Vazquez AL, Poplawsky AJ, Fukuda M, Kim SG (2015) Neural and hemodynamic responses to optogenetic and sensory stimulation in the rat somatosensory cortex. J Cereb Blood Flow Metab 6:922–932

Jones M, Hewson-Stoate N, Martindale J, Redgrave P, Mayhew J (2004) Nonlinear coupling of neural activity and CBF in rodent barrel cortex. Neuroimage 22:956–965

Juergens E, Guettler A, Eckhorn R (1999) Visual stimulation elicits locked and induced gamma oscillations in monkey intracortical- and EEG-potentials, but not in human EEG. Exp Brain Res 129:247–259

Kannurpatti SS, Biswal BB (2004) Negative functional response to sensory stimulation and its origins. J Cereb Blood Flow Metab 24:703–712

Klein C, Evrard HC, Shapcott KA, Haverkamp S, Logothetis NK, Schmid MC (2016) Cell-targeted optogenetics and electrical microstimulation reveal the primate koniocellular projection to supra-granular visual cortex. Neuron 90(1):143–151

Kwong KK, Belliveau JW, Chesler DA, Goldberg IE, Weisskoff RM, Poncelet BP, Kennedy DN, Hoppel BE, Cohen MS, Turner R, Cheng HM, Brady TJ, Rosen BR (1992) Dynamic magnetic resonance imaging of human brain activity during primary sensory stimulation. Proc Natl Acad Sci U S A 89:5675–5679

Lauritzen M (2005) Reading vascular changes in brain imaging: is dendritic calcium the key? Nat Rev Neurosci 6:77–85

Lawrence SJD, Formisano E, Muckli L, de Lange FP (2017) Laminar fMRI: applications for cognitive neuroscience. Neuroimage 197:785–791. S1053-8119(17)30572-4

Leopold DA, Murayama Y, Logothetis NK (2003) Very slow activity fluctuations in monkey visual cortex: implications for functional brain imaging. Cereb Cortex 13:423–433

Logothetis NK (2002) The neural basis of the blood-oxygen-level-dependent functional magnetic resonance imaging signal. Philos Trans R Soc Lond B 357:1003–1037

Logothetis NK (2010) Neurovascular uncoupling: much ado about nothing. Front Neuroenergetics 2:2

Logothetis NK, Pauls J, Augath M, Trinath T, Oeltermann A (2001) Neurophysiological investigation of the basis of the fMRI signal. Nature 412:150–157
Lübke J, Feldmeyer D (2007) Excitatory signal flow and connectivity in a cortical column: focus on barrel cortex. Brain Struct Funct 212:3–17
Maier A, Wilke M, Aura C, Zhu C, Ye FQ, Leopold DA (2008) Divergence of fMRI and neural signals in V1 during perceptual suppression in the awake monkey. Nat Neurosci 11(10):1193–1200
Maier A, Adams GK, Aura C, Leopold DA (2010) Distinct superficial and deep laminar domains of activity in the visual cortex during rest and stimulation. Front Syst Neurosci 4:31. https://doi.org/10.3389/fnsys.2010.00031
Maier A, Aura CJ, Leopold DA (2011) Infragranular sources of sustained local field potential responses in macaque primary visual cortex. J Neurosci 31:1971–1980
Maier A, Cox MA, Dougherty K, Moore B, Leopold D (2014) Anisotropy of ongoing neural activity in the primate visual cortex. Eye Brain 6(Suppl 1):113–120
Marín-Padilla M (1998) Cajal-Retzius cells and the development of the neocortex. Trends Neurosci 21:64–71
Mathiesen C, Caesar K, Akgoren N, Lauritzen M (1998) Modification of activity dependent increases of cerebral blood flow by excitatory synaptic activity and spikes in rat cerebellar cortex. J Physiol (Lond) 512:555–566
Maunsell JH, Gibson JR (1992) Visual response latencies in striate cortex of the macaque monkey. J Neurophysiol 68:1332–1344
Mayhew JE, Askew S, Zheng Y, Porrill J, Westby GW, Redgrave P, Rector DM, Harper RM (1996) Cerebral vasomotion: a 0.1-Hz oscillation in reflected light imaging of neural activity. Neuroimage 4:183–193
Mittmann W, Wallace DJ, Czubayko U, Herb JT, Schaefer AT, Looger LL, Denk W, Kerr JND (2011) Two-photon calcium imaging of evoked activity from L5 somatosensory neurons in vivo. Nat Neurosci 14:1089–1093
Mitzdorf U (1987) Properties of the evoked potential generators: current source-density analysis of visually evoked potentials in the cat cortex. Int J Neurosci 33:33–59
Mukamel R, Gelbard H, Arieli A, Hasson U, Fried I, Malach R (2005) Coupling between neuronal firing, field potentials, and fMR1 in human auditory cortex. Science 309:951–954
Nandy AS, Nassi JJ, Reynolds JH (2017) Laminar organization of attentional modulation in macaque visual area V4. Neuron 93(1):235–246
Nelson S (2002) Cortical microcircuits: diverse or canonical? Neuron 36:19–27
Nicholson C (1973) Theoretical analysis of field potentials in anisotropic ensembles of neuronal elements. IEEE Trans Biomed Eng 20:278–288
Nielsen A, Lauritzen M (2001) Coupling and uncoupling of activity-dependent increases of neuronal activity and blood flow in rat somatosensory cortex. J Physiol (Lond) 533:773–785
Niessing J, Ebisch B, Schmidt KE, Niessing M, Singer W, Galuske RA (2005) Hemodynamic signals correlate tightly with synchronized gamma oscillations. Science 309:948–951
Ninomiya T, Dougherty K, Godlove DC, Schall JD, Maier A (2015) Microcircuitry of agranular frontal cortex: contrasting laminar connectivity between occipital and frontal areas. J Neurophysiol 113(9):3242–3255
Nir Y, Fisch L, Mukamel R, Gelbard-Sagiv H, Arieli A, Fried I, Malach R (2007) Coupling between neuronal firing rate, gamma LFP, and BOLD fMRI is related to interneuronal correlations. Curr Biol 17:1275–1285
Nowak LG, Munk MH, Girard P, Bullier J (1995) Visual latencies in areas V1 and V2 of the macaque monkey. Vis Neurosci 12:371–384
Ogawa S, Lee TM, Kay AR, Tank DW (1990) Brain magnetic resonance imaging with contrast dependent on blood oxygenation. Proc Natl Acad Sci U S A 87:9868–9872
Ogawa S, Tank DW, Menon R, Ellermann JM, Kim SG, Merkle H, Ugurbil K (1992) Intrinsic signal changes accompanying sensory stimulation: functional brain mapping with magnetic-resonance-imaging. Proc Natl Acad Sci U S A 89:5951–5955
Paasonen J, Stenroos P, Salo RA, Kiviniemi V, Grohn O (2018) Functional connectivity under six anesthesia protocols and the awake condition in rat brain. Neuroimage 172:9–20

Pan W-J, Thompson GJ, Magnuson ME, Jaeger D, Keilholz S (2013) Infraslow LFP correlates to resting-state fMRI BOLD signals. Neuroimage 74:288–297
Pasley BN, Inglis BA, Freeman RD (2007) Analysis of oxygen metabolism implies a neural origin for the negative BOLD response in human visual cortex. Neuroimage 36:269–276
Pedemonte M, Barrenechea C, Nunez A, Gambini JP, Garcia-Austt E (1998) Membrane and circuit properties of lateral septum neurons: relationships with hippocampal rhythms. Brain Res 800:145–153
Peters A, Payne BR (1993) Numerical relationships between geniculocortical afferents and pyramidal cell modules in cat primary visual cortex. Cereb Cortex 3:69–78
Peters A, Sethares CJ (1991) Organization of pyramidal neurons in area 17 of monkey visual cortex. J Comp Neurol 306:1–23
Polimeni JR, Fischl B, Greve DN, Wald LL (2010) Laminar analysis of 7T BOLD using an imposed spatial activation pattern in human V1. Neuroimage 52:1334–1346
Raichle ME, Mintum MA (2006) Brain work and brain imaging. Annu Rev Neurosci 29:449–476
Rakic P (2008) Confusing cortical columns. Proc Natl Acad Sci U S A 105:12099–12100
Rauch A, Rainer G, Logothetis NK (2008) The effect of a serotonin-induced dissociation between spiking and perisynaptic activity on BOLD functional MRI. Proc Natl Acad Sci U S A 105:6759–6764
Rees G, Friston K, Koch C (2000) A direct quantitative relationship between the functional properties of human and macaque V5. Nat Neurosci 3:716–723
Ritchie JM (1967) The oxygen consumption of mammalian non-myelinated nerve fibers at rest and during activity. J Physiol (Lond) 188:309–329
Rockel AJ, Hiorns RW, Powell TP (1980) The basic uniformity in structure of the neocortex. Brain 103:221–244
Rockland KS, Drash GW (1996) Collateralized divergent feedback connections that target multiple cortical areas. J Comp Neurol 373:529–548
Saad ZS, Ropella KM, DeYoe EA, Bandettini PA (2003) The spatial extent of the BOLD response. Neuroimage 19:132–144
Sajad A, Godlove DC, Schall JD (2019) Cortical microcircuitry of performance monitoring. Nat Neurosci 2:265–274
Schölvinck M, Maier A, Ye F, Duyn J, Leopold DA (2010) Neural basis of global resting-state fMRI activity. Proc Natl Acad Sci U S A 107(22):10238–10243
Schroeder CE, Mehta AD, Givre SJ (1998) A spatiotemporal profile of visual system activation revealed by current source density analysis in the awake macaque. Cereb Cortex 8:575–592
Schwartz WJ, Smith CB, Davidsen L, Savaki H, Sokoloff L et al. (1979) Metabolic mapping of functional activity in the hypothalamo-neurohypophysial system of the rat. Science 205:723–725
Self MW, van Kerkoerle T, Goebel R, Roelfsema PR (2019) Benchmarking laminar fMRI: neuronal spiking and synaptic activity during top-down and bottom-up processing in the different layers of cortex. Neuroimage 197:806–817. S1053-8119(17)30517-7
Sheth SA, Nemoto M, Guiou M, Walker M, Pouratian N, Toga AW (2004) Linear and nonlinear relationships between neuronal activity, oxygen metabolism, and hemodynamic responses. Neuron 42:347–355
Shmuel A, Grinvald A (1996) Functional organization for direction of motion and its relationship to orientation maps in cat area 18. J Neurosci 16:6945–6964. and cover illustration
Shmuel A, Leopold DA (2008) Neuronal correlates of spontaneous fluctuations in fMRI signals in monkey visual cortex: implications for functional connectivity at rest. Hum Brain Mapp 29:751–761
Shmuel A, Yacoub E, Pfeuffer J, Van de Moortele PF, Adriany G, Hu XP, Ugurbil K (2002) Sustained negative BOLD, blood flow and oxygen consumption response and its coupling to the positive response in the human brain. Neuron 36:1195–1210
Shmuel A, Augath M, Oeltermann A, Logothetis NK (2006) Negative functional MRI response correlates with decreases in neuronal activity in monkey visual area V1. Nat Neurosci 9:569–577

Shmuel A, Yacoub E, Chaimow D, Logothetis NK, Ugurbil K (2007) Spatio-temporal point-spread function of fMRI signal in human gray matter at 7 Tesla. Neuroimage 35:539–552

Silberberg G, Gupta A, Markram H (2002) Stereotypy in neocortical microcircuits. Trends Neurosci 25:227–230

Sirotin YB, Das A (2009) Anticipatory haemodynamic signals in sensory cortex not predicted by local neuronal activity. Nature 457(7228):475–479

Smith AJ, Blumenfeld H, Behar KL, Rothman DL, Shulman RG, Hyder F (2002) Cerebral energetics and spiking frequency: the neurophysiological basis of fMRI. Proc Natl Acad Sci U S A 99:10765–10770

Snodderly DM, Gur M (1995) Organization of striate cortex of alert, trained monkeys (Macaca fascicularis): ongoing activity, stimulus selectivity, and widths of receptive field activating regions. J Neurophys 74:2100–2125

Sokoloff L, Reivich M, Kennedy C, Des Rosiers MH, Patlak CS, Pettigrew KD, Sakurada O, Shinohara M (1977) The [14C] deoxyglucose method for the measurement of local glucose utilization: theory, procedure and normal values in the conscious and anesthetized albino rat. J Neurochem 28:897–916

Sotero RC, Bortel A, Martínez-Cancino R, Neupane S, O'Connor P, Carbonell F, Shmuel A (2010) Anatomically-constrained effective connectivity among layers in a cortical column modeled and estimated from local field potentials. J Integr Neurosci 9:355–379

Sotero RC, Bortel A, Naaman S, Mocanu VM, Kropf P, Villeneuve MY, Shmuel A (2015) Laminar distribution of phase-amplitude coupling of spontaneous current sources and sinks. Front Neurosci 9:454

Stefanovic B, Warnking JM, Pike GB (2004) Hemodynamic and metabolic responses to neuronal inhibition. Neuroimage 22:771–778

Stefanovic B, Warnking JM, Kobayashi E, Bagshaw AP, Hawco C, Dubeau F, Gotman J, Pike GB (2005) Hemodynamic and metabolic responses to activation, deactivation and epileptic discharges. Neuroimage 28:205–215

Stephan KE, Petzschner FH, Kasper L, Bayer J, Wellstein KV, Stefanics G, Pruessmann KP, Heinzle J (2019) Laminar fMRI and computational theories of brain function. Neuroimage 197:699–706. S1053-8119(17)30908-4

Tan CA (2009) Anticipatory changes in regional cerebral hemodynamics: a new role for dopamine? J Neurophysiol 101:2738–2740

Thomsen K, Offenhauser N, Lauritzen M (2004) Principle neuron spiking: neither necessary nor sufficient for cerebral blood flow at rest or during activation in rat cerebellum. J Physiol (Lond) 560:181–189

Thomson AM, Bannister AP (2003) Interlaminar connections in the neocortex. Cereb Cortex 13:5–14

Trampel R, Bazin PL, Pine K, Weiskopf N (2019) In-vivo magnetic resonance imaging (MRI) of laminae in the human cortex. Neuroimage 197:707–715. S1053-8119(17)30785-1

Uludağ K, Dubowitz DJ, Yoder EJ, Restom K, Liu TT, Buxton RB (2004) Coupling of cerebral blood flow and oxygen consumption during physiological activation and deactivation measured with fMRI. Neuroimage 23:148–155

van Kerkoerle T, Self MW, Roelfsema PR (2017) Layer-specificity in the effects of attention and working memory on activity in primary visual cortex. Nat Commun. 8:13804

Viswanathan A, Freeman RD (2007) Neurometabolic coupling in cerebral cortex reflects synaptic more than spiking activity. Nat Neurosci 10:1308–1312

Wise RJS, Ide K, Poulin MJ, Tracey I (2004) Resting state fluctuations in arterial carbon dioxide induce significant low frequency variations in BOLD signal. Neuroimage 21:1652–1664

What Can fMRI Add to the ERP Story?

5

Christoph Mulert

5.1 Introduction

ERPs are unique measurements of brain activity offering information about the activity of the brain with a high temporal resolution. ERPs can be used to investigate cognition, somatosensory processing and pain, auditory and visual processing, to mention but a few of the most important applications. A high degree of specialization has emerged, so, for example, researchers interested in language processing can use the N400 potential (Kutas and Hillyard 1980; Friederici et al. 1993; Kiang et al. 2008), scientists looking at auditory attention can use the N1 potential (Hillyard et al. 1973; Naatanen and Picton 1987; Mulert et al. 2001), and groups interested in face processing may focus on the N170 (Sagiv and Bentin 2001; Taylor et al. 2004; Itier et al. 2006). While it is almost impossible to identify a single starting point of the ERP story since the early steps in evoked potential research started in the 1930s (Davis 1939), the discovery of the P300 in 1965 was an important milestone (Sutton et al. 1965). Researchers then started "to consider that we are involved in a breakthrough—evoked potentials are not just another physiological measure like the galvanic skin response, or pupillography, or heart rate, but something much more exciting—a direct reflection of time-locked activity of the brain associated with specific conscious processes in awake human subjects" (Sutton 1969). Even at that time, the authors described the influence of stimulus probability on the amplitude of the P300 potential (see Fig. 5.1).

This study provided evidence that it is not only the character of the stimulus that influences the evoked potential, but that there is also an endogenous influence of the reaction or attitude to the potential waveform. For a current review concerning the late positive potential and the P300, please see Hajcak and Foti (2020).

C. Mulert (✉)
Centre of Psychiatry, Justus-Liebig University, Giessen, Germany
e-mail: christoph.mulert@psychiat.med.uni-giessen.de

C. Mulert, L. Lemieux (eds.), *EEG - fMRI*,
https://doi.org/10.1007/978-3-031-07121-8_5

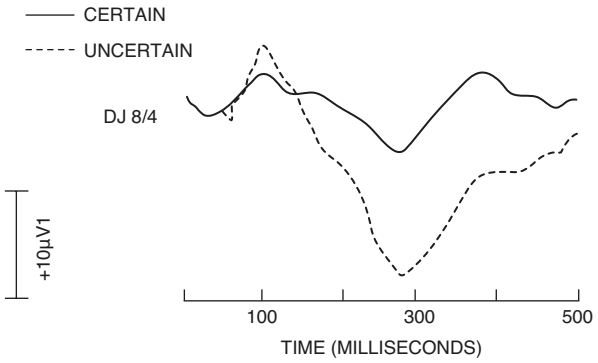

Fig. 5.1 This is part of the original figure from the first publication describing the P300 potential (Sutton et al. 1965; Fig. 1, p. 1187). The P300 was evoked with a stimulus uncertainty paradigm using paired stimuli (cue and test stimuli, $P = 0.33$ occurrence of uncertain test stimuli) and not with the "odd ball paradigm," which is commonly used today. (Reprinted with the permission of AAAS)

Similar milestones were, for instance, the identification of the contingent negative variation (CNV) (Walter et al. 1964) and the detection of an influence of selective attention on the N1 potential (Hillyard et al. 1973).

ERPs have been used extensively in investigations of patients with neuropsychiatric diseases (for a review, see Pogarell et al. 2007). For example, reduced P300 amplitudes are a common finding in patients with schizophrenia (Salisbury et al. 1998; Mathalon et al. 2000; Jeon and Polich 2003). This reduction seems to be especially pronounced in patients with poor premorbid adjustment, early and insidious onset, a chronic and deteriorating course of disease, negative symptoms, and a tendency to develop tardive dyskinesia (Hegerl et al. 1995). A small P300 has been found to predict nonresponse to neuroleptics concerning positive symptoms (Ford et al. 1994). In addition, patients with a "cycloid psychosis" (according to the classification by Leonhard), which is characterized by a favorable therapeutic response and long-term prognosis, do not show any reduction in P300 amplitude, or even an increase in amplitude in comparison to healthy controls (Strik et al. 1993a, b, 1997). Some lines of research with ERPs in neuropsychiatric patients gained intensified interest in the last few years. For example, the mismatch negativity MMN (Naatanen et al. 2007) is of great interest in predicting the outcome of subjects with increased clinical risk for psychosis (Atkinson et al. 2012; Bodatsch et al. 2015; Naatanen et al. 2016; Kim et al. 2018).

Interest in ERP research has also emerged due to the fact that ERPs often show a high heritability, in the range from 0.6 to 0.8 (Katsanis et al. 1997; Wright et al. 2001). Several ERP components (e.g. P300, P50) are now seen as intermediate phenotypes or endophenotypes and meet the criteria suggested by Gottesman (Gottesman and Gould 2003). ERPs have been introduced in the drug development process for psychiatric disorders such as schizophrenia. Since they can be modeled in preclinical studies, they offer opportunities for use as translational biomarkers (Javitt et al. 2008; Haaf et al. 2018).

Interestingly, current experimental designs allow to answer new research questions. For example, interesting new lines of research emerge around the interaction of bottom-up and top-down-processes with reward, looking at (novel) contralateral components of the N2Pc such as the target negativity or the distractor positivity (Hickey et al. 2009; Lockhofen et al. 2021).

Apart from the enormous and ongoing success of ERPs in several different research areas, the localization aspect of ERPs remains an area of investigation. In particular, it is obvious that all ERP analyses suffer more or less from the difficulty in determining precisely which parts of the brain are involved in the generation of a specific event-related potential. As described in Chap. 2 this difficulty is fundamental: it is called the "inverse problem" and was described more than 150 years ago (Helmholtz 1853). It means that different combinations of intracerebral sources can result in the same potential distribution on the scalp, and therefore that the inverse problem has no unique solution. Thus, attempts at EEG-based localizations are merely reasonable estimates. A starting assumption is that the combination of fMRI and ERPs may help in resolving this problem.

5.2 ERP Generator Localization

One traditional approach to learning about the localization of brain function as well as the generation of ERP has been to look at subjects with brain lesions. For example, an investigation of patients with bilateral damage to the hippocampus complex but undisturbed scalp P300 potentials suggested that the hippocampus does not contribute to the scalp P300 (Polich and Squire 1993), although the hippocampus is typically found to be responsive to targets but not to irrelevant stimuli using intracranial recordings (McCarthy et al. 1989). Intracranial recordings are another very interesting source of knowledge concerning the localization of ERP generators (Halgren et al. 1994, 1995a, b; Brazdil et al. 2005; Rosburg et al. 2005, 2007); see Fig. 5.2.

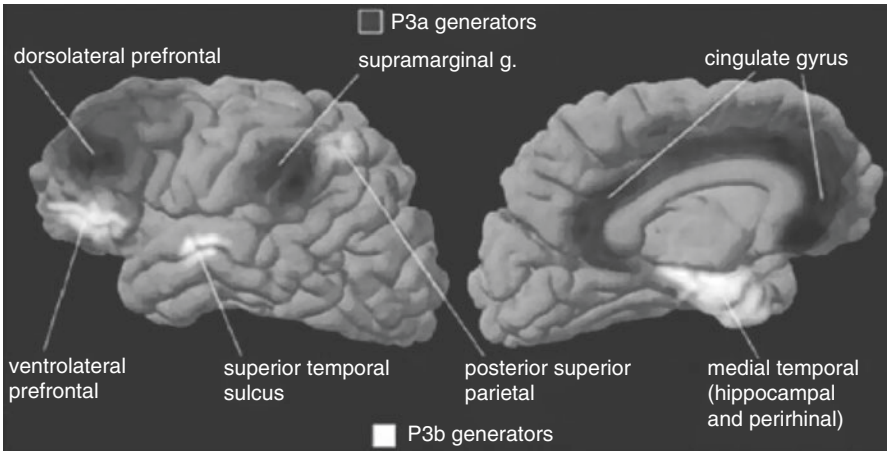

Fig. 5.2 Summary of intracranial findings concerning the generation of different aspects of the P300 potential (P3a and P3b). (Reprinted from Halgren et al. 1998 with the permission of Elsevier)

However, both approaches (lesion studies, intracranial recordings) are limited, although they may offer general information about ERP generation. Since both lesions and intracranial recordings can only be investigated in specifically selected groups, these strategies are not directly applicable for research questions concerning healthy controls or even the vast majority of neuropsychiatric patients.

5.3 The Inverse Problem of EEG

In the authoritative textbook entitled *Electroencephalography*, Fernando Lopesda Silva writes: "The ultimate aim of electroencephalography is to find the intracranial sources of the potentials recorded at the scalp" (Lopes da Silva 1993). However, this is a difficult task because of the Non-Unicity of the solution to the inverse problem of EEG. Focusing on this issue, several suggestions have been made during the last few decades for specific assumptions that may enable us to obtain plausible estimates of the underlying neural generators.

Apart from specific assumptions concerning the method of solving the inverse problem, additional assumptions have to be made concerning the (physical, geometric, anatomical) properties of the generator, conductive media, and recording electrodes. Early head models were simple spheres (typically four concentric spheres representing the brain tissue, the cerebrospinal fluid, the skull, and the scalp), but in the last few years more realistic head models using MRI information have been developed (Schneider 1974; Sencaj and Aunon 1982; Meijs et al. 1988; Hamalainen and Sarvas 1989).

Concerning the choice of generator model, one option to solve the inverse problem is the strategy of calculating a (equivalent) dipole (Schneider 1972; Henderson et al. 1975; Cuffin 1985; Scherg and von Cramon 1985, 1986; Scherg and Berg 1991). Such a dipole is a mathematical abstraction that is assumed to generate a potential on the scalp. By changing the parameters of the dipole (position, orientation), "forward solutions" can be calculated in order to get a possible scalp potential distribution. If the difference between a forward solution and the original scalp potential is small, the solution is generally sound. However, this does not mean that the solution is correct in terms of the real generators of brain activity—it only means that the solution is basically possible. This kind of solution is generally nonlinear. Since the correct estimation of the number of dipoles used in a model is an essential issue when attempting to find a valid localization, dipole source analyses have been used successfully in situations with a small number of active sources, such as localization of epileptic spikes (Scherg et al. 1999) or simple evoked potentials with activity mainly in the early sensory areas (Hegerl et al. 1994). In general, this strategy has some advantages if the number of active brain regions is small and additional information about the possible positions of the sources is available.

Another strategy for solving the inverse problem can be used with minimal prior information about the nature of the generators apart from anatomical constraints, which usually limit the solution space to the gray matter. The latter may be obtained from subject-specific or generic MRI scans. This kind of strategy has been introduced as minimum-norm estimation (MNE) by Hämäläinen and Ilmoniemi (Hamalainen and Ilmoniemi 1984, 1994; Wang et al. 1992; Ilmoniemi 1993). This

method has developed further over the last few years, including "weighted" minimum-norm solutions (WMN). For example, using MNE, separate time behaviors of the temporal and frontal mismatch negativity sources were found (Rinne et al. 2000).

The next important development was LORETA, which incorporates the "smoothness assumption" (Pascual-Marqui et al. 1994, 1999). Based on neurophysiological findings in a number of animal studies that neighboring neurons are most likely to be active synchronously and simultaneously (Llinas 1988; Gray et al. 1989), Pascual-Marqui proposed to assume that grid points in a current source model are more likely to be synchronized than grid points that are far from each other. This method has become quite popular during the last few years because comparisons of localization results with imaging methods such as fMRI or PET have often revealed a considerable overlap (see Fig. 5.3) (Pizzagalli et al. 2003; Mulert et al. 2004, 2005).

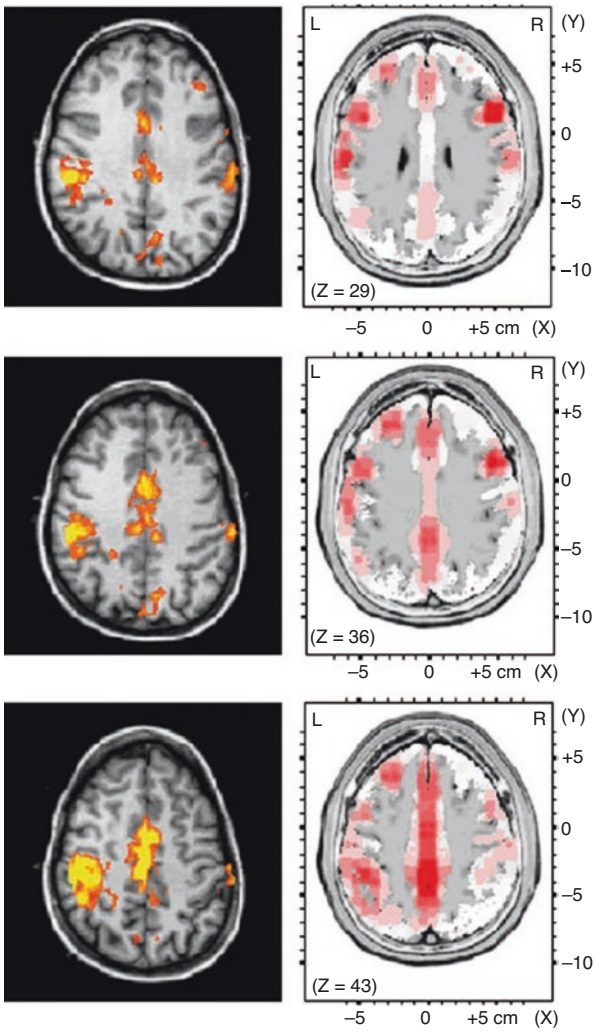

Fig. 5.3 Localization of brain activation evoked by an odd ball paradigm: activations in the fMRI analysis (*left*), and simultaneously acquired ERP activity localized independently with LORETA (*right*). (Reprinted from Mulert et al. 2004 with the permission of Elsevier)

Developments such as sLORETA (Pascual-Marqui 2002) and eLORETA have demonstrated even better localization accuracy (Wagner et al. 2004). Linear methods like LORETA seem to be advantageous if there is likely to be a large number of active sources, and if no information is available about the positions of the electrical generators. LORETA has been used in numerous studies, including investigations of ERP (Anderer et al. 2003; Molina et al. 2019), resting EEG activity (Gianotti et al. 2007; Ahmadi et al. 2020), sleep spindles (Ventouras et al. 2007), and patients with depression (Pizzagalli et al. 2001), schizophrenia (Mulert et al. 2001; Leicht et al. 2020), and epilepsy (Bela et al. 2007; Liu et al. 2021).

The development of methods for EEG-based localization is an active field with numerous propositions during the last few years, including hierarchical and empirical Bayesian approaches (Phillips et al. 2005; Friston et al. 2008; Trujillo-Barreto et al. 2008).

Obviously, the ongoing process of developing solutions for the inverse problem proves two points. Firstly, there is enormous interest in obtaining information about the neural generators of ERPs. Secondly, there is currently no method that is able to solve all of the complex "real-world" questions concerning ERP localization. However, today, we do have strategies to solve the inverse EEG problem with reasonable localization accuracy that can be used reliably for a number of experimental questions.

5.4 Does fMRI Help to Solve the Inverse Problem?

There are practical issues with combining ERP and fMRI information that are discussed in more detail in other chapters of this book, as well as theoretical aspects that are concerned with understanding the workings of the brain. Generally, different methods are sensitive to different aspects of brain function; while EEG/ERP emphasizes the aspect of the synchronization of neural ensembles, fMRI tends to point to regional specialization. Therefore, theoretically, a combination of EEG and fMRI is likely to significantly enhance our understanding of brain function.

From an ERP research point of view, the ability to correctly localize brain activity within millimeters, as offered by fMRI, is very attractive in terms of the additional information afforded to almost every aspect of ERP research. This perspective was apparently the starting point for studies that used a typical ERP paradigm for a fMRI study to identify the neural generators of the ERP components. Examples of this kind of study are provided by Menon et al. (1997), McCarthy et al. (1997), Linden et al. (1999). In these studies, the "oddball" paradigm was used, where frequent and infrequent stimuli are presented and attention must be paid to the infrequent stimulus (controlled by button pressing or counting). This paradigm is a classical ERP one that evokes the P300 component after a rare and relevant event.

The authors have described activity in the supramarginal gyrus and other inferior parietal regions and frontal midline areas. Since these regions were already found using intracranial recordings, lesion studies, or ERP-based inverse solutions, the idea of combining ERP with fMRI to get spatial information was supported (McCarthy et al. 1997; Menon et al. 1997; Linden et al. 1999).

At this point, it should be mentioned that there are, of course, several constellations in which a one-to-one relationship between scalp EEG/ERP information and BOLD signal changes cannot be expected. For example, neural activity may be related to BOLD signal changes but not to scalp EEG changes if—due to the spatial orientations of the electrical generators (e.g. self-cancelling sources in sulci or neuronal assemblies without a strictly parallel orientation)—the electrical signals are not measurable on the scalp. In addition, nonpyramidal neuron activity will not lead to measurable electrical activity on the scalp (Nunez and Silberstein 2000).

Conversely, the highly synchronous activities of a small number of neurons or phase shifts/changes in phase synchrony could result in a detectable EEG signal, but the associated hemodynamic changes may be small and not sufficiently above baseline values to survive statistical testing.

This issue of limited overlap between EEG measures and fMRI results has been addressed using different strategies. Obviously, it is especially relevant for any fMRI-constrained source analysis. Generally, when using fMRI activations as "seeding points" for dipoles, a close relationship between fMRI activation and electrical activity is assumed. However, if dipoles are seeded in a BOLD cluster that does not contribute to scalp potential, the whole dipole model and all resulting information (e.g. about the time courses of dipoles) could be inaccurate. Several validation strategies to deal with this problem have been suggested, such as scanning the whole brain with "probe sources" that suggest additional electrical generators not seen in the fMRI analysis (Bledowski et al. 2007).

Today the gold standard approach with respect to the relationship of EEG and fMRI is to use EEG-informed fMRI analysis based on single-trial variations of the EEG as regressors for an fMRI analysis (Nagai et al. 2004; Hinterberger et al. 2005; Debener et al. 2005; Eichele et al. 2005; Mulert et al. 2008). The full potential of this approach has been shown in a study by Eichele and colleagues, who separated different aspects of the BOLD signal with regard to their relationships with single EEG single-trial variations of different ERP components. One example of EEG–fMRI single-trial coupling is demonstrated in Fig. 5.4 (own data). Here, single-trial variations of the P300 potential were used to estimate the corresponding BOLD signal.

Single-trial coupling of EEG and fMRI is necessary if the focus of interest is the hemodynamic correlation of a specific ERP component. However, the results provided by this technique could also include brain regions that are not the actual electrical generators of the respective ERP component. This kind of strategy could also include BOLD activations of regions that are functionally very closely connected to the electrical generators of the respective ERP components, but are not the actual electrical generators themselves. Keeping this in mind, this kind of EEG-informed fMRI analysis is even more interesting considering the possibility of providing the functional neural networks engaged in a task.

At this point, it can be stated that fMRI has the potential to push forward our knowledge regarding the electrical generators of ERPs, but also that oversimplifications must be avoided since no general one-to-one relationship between EEG/ERP signal and fMRI signal can be premised.

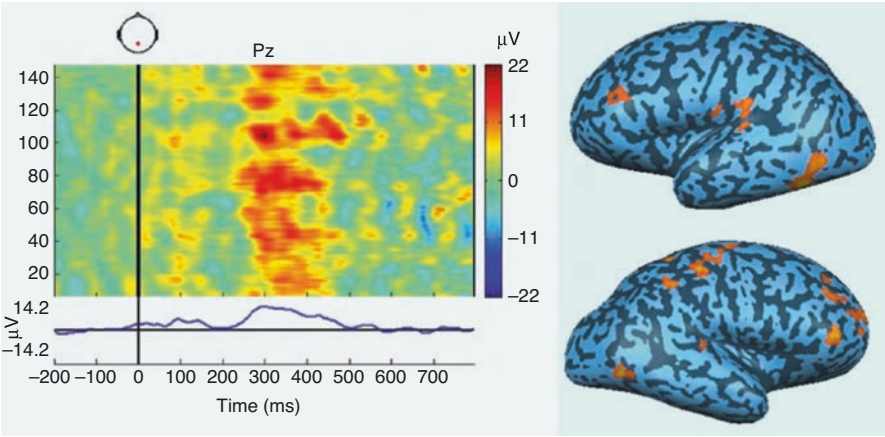

Fig. 5.4 *Left side*: single-trial variations of the P300 potential at Pz. *Right side*: specific P300-related fMRI activations based on single-trial coupling of the P300 amplitude variation and the corresponding BOLD signal (own data)

5.5 Further Aspects

While most chapters of this book deal with the direct combination of EEG and fMRI, it may also be worth posing the question of whether there could be an indirect influence of the fast-growing use of fMRI for many different research questions that have traditionally been investigated with ERPs. While such an assessment tends to be fragmentary and speculative, there may be at least two interesting aspects of it.

5.6 Serial Processing vs. Parallel and Reciprocal Network Activity

ERPs are usually defined in the time domain. Therefore, ERP components are obtained and described in sequence. For example, in auditory processing, early (brainstem) potentials can be numbered and distinguished from mid-latency potentials and late potentials. Accordingly, a sequence of information processing can be assumed. This assumption of serial information processing has influenced strategies to describe "mental chronometry" (Posner 2005), for instance, the separation of evoked responses in stimulus valuation processes and response-selection processes with separately measurable latencies (Falkenstein et al. 1994), or even four sequential steps (stimulus registration, stimulus selection, stimulus identification, stimulus categorization) (Dien et al. 2004). Since fMRI does not offer comparable time resolution, fMRI-based mental chronometry analyses are rare (Formisano et al. 2002; Formisano and Goebel 2003). However, functional connectivity analyses, widely used for fMRI data, have stressed the issue of reciprocal relationships between brain regions in a common neural network—an aspect that can easily be missed using

traditional EEG/ERP analysis techniques (Garrido et al. 2007; Mulert et al. 2007) but is adequately addressed today using EEG-based effective connectivity analyses in the source space (e.g. Steinmann et al. 2018).

5.7 Subcortical Processing

While subcortical structures such as the thalamus play an important role in the generation of brain rhythms and brain potentials (Lopes da Silva 1991; Steriade 1994; Hughes and Crunelli 2005), they cannot be directly assessed by scalp measurements of cortical activity. Accordingly, there are a "blind spot" and (for example) "attentional search light processes" (Crick 1984) that are probably mediated by thalamic structures (McAlonan et al. 2006), which in turn may have an enormous impact on cortical (electrical) processing and cannot be assessed with scalp EEG/ERP alone. Since fMRI can be used to gather information about thalamic activity, EEG/ERP research may also be stimulated here. For example, ERP components such as the feedback related negativity (FRN) and beta-oscillations in response to positive feedback (reward) can be recorded on the scalp (Leicht et al. 2013). Using trial-by-trial coupling of EEG and fMRI it is possible to detect involved subcortical brain regions such as the nucleus accumbens/ventral striatum (Andreou et al. 2017).

5.8 Conclusions

ERP research has been performed successfully for decades and will continue to be a major tool for brain research due to its unique properties (e.g. concerning temporal resolution). However, localization has always been a problematic but key issue in ERP research. Obviously, fMRI, with its ability to correctly localize to within millimeters, is capable of providing valuable information in relation to almost every research question that has already been addressed with just ERPs. While, in general, it cannot be expected that there is a one-to-one relationship between ERPs and the fMRI signal, it is still interesting that both signals are related directly or indirectly to synaptic activity. Combining EEG and fMRI can be very helpful in obtaining a deeper understanding of brain activity. For many practical issues (e.g. artifact correction) established solutions exist but some basic questions (e.g. the precise relationship between EEG and fMRI signals) remain the source of debate and investigations. Nevertheless, many studies have already shown the enormous impact of combination strategies and EEG-fMRI is now a helpful tool for many research questions.

References

Ahmadi M, Kazemi K, Kuc K, Cybulska-Klosowicz A, Zakrzewska M, Racicka-Pawlukiewicz E, Helfroush MS, Aarabi A (2020) Cortical source analysis of resting state EEG data in children with attention deficit hyperactivity disorder. Clin Neurophysiol 131:2115–2130

Anderer P, Saletu B et al (2003) Non-invasive localization of P300 sources in normal aging and age-associated memory impairment. Neurobiol Aging 24(3):463–479
Andreou C, Frielinghaus H, Rauh J, Mussmann M, Vauth S, Braun P, Leicht G, Mulert C (2017) Theta and high-beta networks for feedback processing: a simultaneous EEG-fMRI study in healthy male subjects. Transl Psychiatry 7:e1016
Atkinson RJ, Michie PT, Schall U (2012) Duration mismatch negativity and P3a in first-episode psychosis and individuals at ultra-high risk of psychosis. Biol Psychiatry 71:98–104
Bela C, Monika B et al (2007) Valproate selectively reduces EEG activity in anterior parts of the cortex in patients with idiopathic generalized epilepsy. A low resolution electromagnetic tomography (LORETA) study. Epilepsy Res 75(2&3):186–191
Bledowski C, Linden DE et al (2007) Combining electro physiology and functional imaging—different methods for different questions. Trends Cogn Sci 11(12):500–502
Bodatsch M, Brockhaus-Dumke A, Klosterkotter J, Ruhrmann S (2015) Forecasting psychosis by event-related potentials-systematic review and specific meta-analysis. Biol Psychiatry 77:951–958
Brazdil M, Dobsik M et al (2005) Combined event-related fMRI and intra cerebral ERP study of an auditory odd ball task. Neuroimage 26(1):285–293
Crick F (1984) Function of the thalamic reticular complex: the search light hypothesis. Proc Natl Acad Sci U S A 81(14):4586–4590
Cuffin BN (1985) A comparison of moving dipole inverse solutions using EEG's and MEG's. IEEE Trans Biomed Eng 32(11):905–910
Davis PA (1939) Effects of acoustic stimuli on the waking human brain. J Neurophysiol 2:494–499
Debener S, Ullsperger M et al (2005) Trial-by-trial coupling of concurrent electro encephalogram and functional magnetic resonance imaging identifies the dynamics of performance monitoring. J Neurosci 25(50):11730–11737
Dien J, Spencer KM et al (2004) Parsing the late positive complex: mental chronometry and the ERP components that inhabit the neighborhood of the P300. Psychophysiology 41(5):665–678
Eichele T, Specht K et al (2005) Assessing the spatio temporal evolution of neuronal activation with single-trial event-related potentials and functional MRI. Proc Natl Acad Sci U S A 102(49):17798–17803
Falkenstein M, Hohnsbein J et al (1994) Effects of choice complexity on different subcomponents of the late positive complex of the event-related potential. Electroencephalogr Clin Neurophysiol 92(2):148–160
Ford JM, White P et al (1994) Schizophrenic shave fewer and smaller P300s: a single-trial analysis. Biol Psychiatry 35(2):96–103
Formisano E, Goebel R (2003) Tracking cognitive processes with functional MRI mental chronometry. Curr Opin Neurobiol 13(2):174–181
Formisano E, Linden DE et al (2002) Tracking the mind's image in the brain I: time-resolved fMRI during visuospatial mental imagery. Neuron 35(1):185–194
Friederici AD, Pfeifer E et al (1993) Event-related brain potentials during natural speech processing: effects of semantic, morphological and syntactic violations. Brain Res Cogn Brain Res 1(3):183–192
Friston K, Harrison L et al (2008) Multiples parse priors for the M/EEG inverse problem. Neuroimage 39(3):1104–1120
Garrido MI, Kilner JM et al (2007) Evoked brain responses are generated by feedback loops. Proc Natl Acad Sci U S A 104(52):20961–20966
Gianotti LR, Kunig G et al (2007) Correlation between disease severity and brain electric LORETA tomography in Alzheimer's disease. Clin Neurophysiol 118(1):186–196
Gottesman II, Gould TD (2003) The endophenotype concept in psychiatry: etymology and strategic intentions. Am J Psychiatry 160(4):636–645
Gray CM, Konig P et al (1989) Oscillatory responses in cat visual cortex exhibit inter-columnar synchronization which reflects global stimulus properties. Nature 338(6213):334–337

Haaf M, Leicht G, Curic S, Mulert C (2018) Glutamatergic deficits in schizophrenia—biomarkers and pharmacological interventions within the ketamine model. Curr Pharm Biotechnol 19:293–307

Hajcak G, Foti D (2020) Significance?... Significance! Empirical, methodological, and theoretical connections between the late positive potential and P300 as neural responses to stimulus significance: an integrative review. Psychophysiology 57:e13570

Halgren E, Baudena P et al (1994) Spatio-temporal stages in face and word processing. 2. Depth-recorded potentials in the human frontal and Rolandic cortices [published erratum appears in J Physiol Paris 1994; 88(2): following 151]. J Physiol Paris 88(1):51–80

Halgren E, Baudena P et al (1995a) Intra cerebral potentials to rare target and distractor auditory and visual stimuli. I Superior temporal plane and parietal lobe. Electroencephalogr Clin Neurophysiol 94(3):191–220

Halgren E, Baudena P et al (1995b) Intra cerebral potentials to rare target and distractor auditory and visual stimuli. II. Medial, lateral and posterior temporal lobe. Electroencephalogr Clin Neurophysiol l94(4):229–250

Halgren E, Marinkovic K, Chauvel P (1998) Generators of the late cognitive potentials in auditory and visual odd ball tasks. Electroencephalogr Clin Neurophysiol 106:159–164

Hamalainen M, Ilmoniemi RJ (1984) Interpreting measured magnetic fields of the brain: estimates of current distributions (technical report TKK-F-A559). Helsinki University of Technology, Espoo

Hamalainen MS, Ilmoniemi RJ (1994) Interpreting magnetic fields of the brain: minimum norm estimates. Med Biol Eng Comput 32(1):35–42

Hamalainen MS, Sarvas J (1989) Realistic conductivity geometry model of the human head for interpretation of neuromagnetic data. IEEE Trans Biomed Eng 36(2):165–171

Hegerl U, Gallinat J et al (1994) Intensity dependence of auditory evoked dipole source activity. Int J Psychophysiol 17(1):1–13

Hegerl U, Juckel G et al (1995) Schizophrenics with small P300: a subgroup with an euro developmental disturbance and a high risk for tardive dyskinesia? Acta Psychiatr Scand 91(2):120–125

Helmholtz H (1853) Übereinige Gesetzeder Vertheilungelektrischer Strömeinkörperlichen Leiternmitder Anwendungaufdiethierisch-elektrischen Versuche. Annalender Physikund Chemie 89(211–233):353–377

Henderson CJ, Butler SR et al (1975) The localization of equivalent dipoles of EEG sources by the application of electrical field theory. Electroencephalogr Clin Neurophysiol 39(2):117–130

Hickey C, Di Lollo V, McDonald JJ (2009) Electrophysiological indices of target and distractor processing in visual search. J Cogn Neurosci 21:760–775

Hillyard SA, Hink RF et al (1973) Electrical signs of selective attention in the human brain. Science 182(108):177–180

Hinterberger T, Veit R et al (2005) Neuronal mechanisms underlying control of a brain-computer interface. Eur J Neurosci 21(11):3169–3181

Hughes SW, Crunelli V (2005) Thalamic mechanisms of EEG alpha rhythms and their pathological implications. Neuroscientist 11(4):357–372

Ilmoniemi RJ (1993) Models of source currents in the brain. Brain Topogr 5(4):331–336

Itier RJ, Latinus M et al (2006) Face, eye and object early processing: what is the face specificity? Neuroimage 29(2):667–676

Javitt DC, Spencer KM et al (2008) Neurophysiological biomarkers for drug development in schizophrenia. Nat Rev Drug Discov 7(1):68–83

Jeon YW, Polich J (2003) Meta-analysis of P300 and schizophrenia: patients, paradigms, and practical implications. Psychophysiology 40(5):684–701

Katsanis J, Iacono WG et al (1997) P300 event-related potential heritability in monozygotic and dizygotic twins. Psychophysiology 34(1):47–58

Kiang M, Kutas M et al (2008) An event-related brain potential study of direct and indirect semantic priming in schizophrenia. Am J Psychiatry 165(1):74–81

Kim M, Lee TH, Yoon YB, Lee TY, Kwon JS (2018) Predicting remission in subjects at clinical high risk for psychosis using mismatch negativity. Schizophr Bull 44:575–583
Kutas M, Hillyard SA (1980) Event-related brain potentials to semantically in appropriate and surprisingly large words. Biol Psychol 11(2):99–116
Leicht G, Troschutz S, Andreou C, Karamatskos E, Ertl M, Naber D, Mulert C (2013) Relationship between oscillatory neuronal activity during reward processing and trait impulsivity and sensation seeking. PLoS One 8:e83414
Leicht G, Andreou C, Nafe T, Nagele F, Rauh J, Curic S, Schauer P, Schottle D, Steinmann S, Mulert C (2020) Alterations of oscillatory neuronal activity during reward processing in schizophrenia. J Psychiatr Res 129:80–87
Linden DE, Prvulovic D et al (1999) The functional neuro anatomy of target detection: an fMRI study of visual and auditory odd ball tasks. Cereb Cortex 9(8):815–823
Liu H, Tang H, Wei W, Wang G, Du Y, Ruan J (2021) Altered peri-seizure EEG microstate dynamics in patients with absence epilepsy. Seizure 88:15–21
Llinas RR (1988) The intrinsic electrophysiological properties of mammalian neurons: insights into central nervous system function. Science 242(4886):1654–1664
Lockhofen DEL, Hubner N, Hemdan F, Sammer G, Henare D, Schubo A, Mulert C (2021) Differing time courses of reward-related attentional processing: an EEG source-space analysis. Brain Topogr 34:283–296
Lopes da Silva F (1991) Neural mechanisms underlying brain waves: from neural membranes to networks. Electroencephalogr Clin Neurophysiol 79(2):81–93
Lopes da Silva F (1993) EEG analysis: theory and practice. In: Niedermeyer E, Lopes DS (eds) Electroencephalography. Williams and Wilkins, Baltimore, p 1117
Mathalon DH, Ford JM et al (2000) Trait and state aspects of p300 amplitude reduction in schizophrenia: a retrospective longitudinal study. Biol Psychiatry 47(5):434–449
McAlonan K, Cavanaugh J et al (2006) Attentional modulation of thalamic reticular neurons. J Neurosci 26(16):4444–4450
McCarthy G, Wood CC et al (1989) Task-dependent field potentials in human hippocampal formation. J Neurosci 9(12):4253–4268
McCarthy G, Luby M et al (1997) Infrequent events transiently activate human prefrontal and parietal cortex as measured by functional MRI. J Neurophysiol 77(3):1630–1634
Meijs JW, Peters MJ et al (1988) Relative influence of model assumptions and measurement procedures in the analysis of the MEG. Med Biol Eng Comput 26(2):136–142
Menon V, Ford JM et al (1997) Combined event-related fMRI and EEG evidence for temporal-parietal cortex activation during target detection. Neuroreport 8(14):3029–3037
Molina V, Bachiller A, de Luis R, Lubeiro A, Poza J, Hornero R, Alonso JF, Mananas MA, Marques P, Romero S (2019) Topography of activation deficits in schizophrenia during P300 task related to cognition and structural connectivity. Eur Arch Psychiatry Clin Neurosci 269:419–428
Mulert C, Gallinat J et al (2001) Reduced event-related current density in the anterior cingulated cortex in schizophrenia. Neuroimage 13(4):589–600
Mulert C, Jager L et al (2004) Integration of fMRI and simultaneous EEG: towards a comprehensive understanding of localization and time-course of brain activity in target detection. Neuroimage 22(1):83–94
Mulert C, Jager L et al (2005) Sound level dependence of the primary auditory cortex: simultaneous measurement with 61-channel EEG and fMRI. Neuroimage 28(1):49–58
Mulert C, Leicht G et al (2007) Auditory cortex and anterior cingulated cortex sources of the early evoked gamma-band response: relationship to task difficulty and mental effort. Neuropsychologia 45(10):2294–2306
Mulert C, Seifert C et al (2008) Single-trial coupling of EEG and fMRI reveals the involvement of anterior cingulated cortex activation in effortful decision making. Neuroimage 42(1):158–168
Naatanen R, Picton T (1987) The N1 wave of the human electric and magnetic response to sound: are view and an analysis of the component structure. Psychophysiology 24(4):375–425

Naatanen R, Paavilainen P, Rinne T, Alho K (2007) The mismatch negativity (MMN) in basic research of central auditory processing: a review. Clin Neurophysiol 118:2544–2590
Naatanen R, Todd J, Schall U (2016) Mismatch negativity (MMN) as biomarker predicting psychosis in clinically at-risk individuals. Biol Psychol 116:36–40
Nagai Y, Critchley HD et al (2004) Brain activity relating to the contingent negative variation: an fMRI investigation. Neuroimage 21(4):1232–1241
Nunez PL, Silberstein RB (2000) On the relationship of synaptic activity to macroscopic measurements: does co-registration of EEG with fMRI make sense? Brain Topogr 13(2):79–96
Pascual-Marqui RD (2002) Standardized low-resolution brain electromagnetic tomography (sLORETA): technical details. Methods Find Exp Clin Pharmacol 24(Suppl D):5–12
Pascual-Marqui RD, Michel CM et al (1994) Low resolution electromagnetic tomography: a new method for localizing electrical activity in the brain. Int J Psychophysiol 18(1):49–65
Pascual-Marqui RD, Lehmann D et al (1999) Low resolution brain electromagnetic tomography (LORETA) functional imaging in acute, neuroleptic-naive, first-episode, productive schizophrenia. Psychiatry Res 90(3):169–179
Phillips C, Mattout J et al (2005) An empirical Bayesian solution to the source reconstruction problem in EEG. Neuroimage 24(4):997–1011
Pizzagalli D, Pascual-Marqui RD et al (2001) Anterior cingulated activity as a predictor of degree of treatment response in major depression: evidence from brain electrical tomography analysis. Am J Psychiatry 158(3):405–415
Pizzagalli DA, Oakes TR et al (2003) Coupling of theta activity and glucose metabolism in the human rostral anterior cingulated cortex: an EEG/PET study of normal and depressed subjects. Psychophysiology 40(6):939–949
Pogarell O, Mulert C et al (2007) Event-related potentials in psychiatry. Clin EEG Neurosci 38(1):25–34
Polich J, Squire LR (1993) P300 from amnesic patients with bilateral hippocampal lesions. Electroencephalogr Clin Neurophysiol 86(6):408–417
Posner MI (2005) Timing the brain: mental chronometry as a tool in neuroscience. PLoS Biol 3(2):e51
Rinne T, Alho K et al (2000) Separate time behaviors of the temporal and frontal mismatch negativity sources. Neuroimage 12(1):14–19
Rosburg T, Trautner P et al (2005) Subdural recordings of the mismatch negativity (MMN) in patients with focal epilepsy. Brain 128(Pt 4):819–828
Rosburg T, Trautner P et al (2007) Hippocampal event-related potentials to tone duration deviance in a passive odd ball paradigm in humans. Neuroimage 37(1):274–281
Sagiv N, Bentin S (2001) Structural encoding of human and schematic faces: holistic and part-based processes. J Cogn Neurosci 13(7):937–951
Salisbury DF, Shenton ME et al (1998) First-episode schizophrenic psychosis differs from first-episode affective psychosis and controls in P300 amplitude over left temporal lobe [published erratum appears in Arch Gen Psychiatry 1998;55(5):413]. Arch Gen Psychiatry 55(2):173–180
Scherg M, Berg P (1991) Use of prior knowledge in brain electromagnetic source analysis. Brain Topogr 4(2):143–150
Scherg M, von Cramon D (1985) Two bilateral sources of the late AEP as identified by a spatio-temporal dipole model. Electroencephalogr Clin Neurophysiol 62(1):32–44
Scherg M, von Cramon D (1986) Evoked dipole source potentials of the human auditory cortex. Electroencephalogr Clin Neurophysiol 65(5):344–360
Scherg M, Bast T et al (1999) Multiple source analysis of interictal spikes: goals, requirements, and clinical value. J Clin Neurophysiol 16(3):214–224
Schneider MR (1972) A multi stage process for computing virtual dipolar sources of EEG discharges from surface information. IEEE Trans Biomed Eng 19(1):1–12
Schneider M (1974) Effect of in homogeneities on surface signals coming from a cerebral current-dipole source. IEEE Trans Biomed Eng 2(1):52–54

Sencaj RW, Aunon JI (1982) Dipole localization of average and single visual evoked potentials. IEEE Trans Biomed Eng 29(1):26–33
Steinmann S, Meier J, Nolte G, Engel AK, Leicht G, Mulert C (2018) The Callosal relay model of interhemispheric communication: new evidence from effective connectivity analysis. Brain Topogr 31:218–226
Steriade M (1994) Sleep oscillations and their blockage by activating systems. J Psychiatry Neurosci 19(5):354–358
Strik WK, Dierks T et al (1993a) Differences in P300 amplitudes and topography between cycloid psychosis and schizophrenia in Leonhard's classification. Acta Psychiatr Scand 87(3):179–183
Strik WK, Dierks T et al (1993b) Amplitudes of auditory P300 in remitted and residual schizophrenics: correlations with clinical features. Neuropsychobiology 27(1):54–60
Strik WK, Fallgatter AJ et al (1997) Specific P300 features in patients with cycloid psychosis. Acta Psychiatr Scand 95(1):67–72
Sutton S (1969) The specification of psychological variables in an average evoked potential experiment. In: Donchin E, Lindsley DB (eds) Average evoked potentials. Methods, results and evaluations (NASASP-191). Columbia University Press, NewYork, pp 237–262
Sutton S, Braren M et al (1965) Evoked-potential correlates of stimulus uncertainty. Science 150(700):1187–1188
Taylor MJ, Batty M et al (2004) The faces of development: are view of early face processing over childhood. J Cogn Neurosci 16(8):1426–1442
Trujillo-Barreto NJ, Aubert-Vazquez E et al (2008) Bayesian M/EEG source reconstruction with spatio-temporal priors. Neuroimage 39(1):318–335
Ventouras EM, Alevizos I et al (2007) Independent components of sleep spindles. Conf Proc IEEE Eng Med Biol Soc 1:4002–4005
Wagner M, Fuchs M et al (2004) Evaluation of sLORETA in the presence of noise and multiple sources. Brain Topogr 16(4):277–280
Walter WG, Cooper R et al (1964) Contingent negative variation: an electric sign of sensorimotor association and expectancy in the human brain. Nature 203:380–384
Wang JZ, Williamson SJ et al (1992) Magnetic source images determined by a lead-field analysis: the unique minimum-norm least-squares estimation. IEEE Trans Biomed Eng 39(7):665–675
Wright MJ, Hansell NK et al (2001) Genetic influence on the variance in P3 amplitude and latency. Behav Genet 31(6):555–565

The Added Value of EEG-fMRI in Imaging Neuroscience

6

Rainer Goebel and Fabrizio Esposito

6.1 Introduction

The main objective of functional neuroimaging is to deepen our understanding of the neural substrate of cognitive functions by detecting and characterizing in space and time relevant changes of brain states and their relation to neuronal activity. Functional MRI (fMRI), electro-encephalography (EEG), and magneto-encephalography (MEG) are the most widespread non-invasive techniques available to experimental and clinical neuroscientists to achieve this objective starting from in vivo measures of brain electrical activity. Both fMRI and EEG assume that a given brain state can be decoded from the precise anatomical localization and the detailed temporal evolution of neuro-electrical brain activation signals, respectively. Starting from these common assumptions, fMRI neuroscientists have developed many different approaches to map brain states at a spatial resolution of a few millimeters and test many different neurophysiological and neuropathological hypotheses in normal and clinical populations, despite the limited temporal resolution of the available signals (see previous chapters). On the other hand, EEG neuroscientists have posed analogous questions and addressed similar problems by developing different approaches for the detailed temporal analysis of EEG recordings, despite the limited spatial detail of their findings.

R. Goebel
Department of Cognitive Neuroscience, Faculty of Psychology and Neuroscience, Maastricht University, Maastricht, The Netherlands
e-mail: r.goebel@maastrichtuniversity.nl

F. Esposito (✉)
Department of Advanced Medical and Surgical Sciences, School of Medicine and Surgery, University of Campania "Luigi Vanvitelli", Naples, Italy
e-mail: fabrizio.esposito@unicampania.it

C. Mulert, L. Lemieux (eds.), *EEG - fMRI*,
https://doi.org/10.1007/978-3-031-07121-8_6

The previous chapter has illustrated how fMRI can be used by the EEG neuroscientists to improve the quality of the EEG results and aid the problem of source localization.

The purpose of this chapter is to illustrate how the fMRI neuroscientist can integrate detailed temporal information by incorporating simultaneously recorded EEG signals into standard as well as sophisticated fMRI spatio-temporal modeling. We discuss how this can be achieved in such a way that new effects become detectable in the fMRI domain even when the original event or state change causing possible fMRI effects can only be characterized at very rapid temporal scales (e.g., millisecond) or frequency bands (above 1 Hz). Our description focuses on a conceptual level, and we refer the reader to other chapters in Part II for more details on problems such as EEG preprocessing.

We start from the problem of optimizing a common source space for fMRI and EEG signal projection through the use of anatomical and functional MRI models and EEG distributed inverse models. Then we explore different frameworks for the integrated analysis of simultaneously acquired EEG-fMRI data sets in the same space.

The basic limitation of both fMRI and EEG is represented by the indirect nature of measured brain signals, which always implies substantial interpretational efforts and caution to neuroscientists before drawing any general conclusions about the location and the electrical nature of the neural sources related to the investigated phenomena. Nonetheless, this general limitation can be elegantly counterbalanced by multi-modal simultaneous acquisition and comparative analysis approaches, which emphasize the diversity of the physical origin of fMRI and EEG signals with respect to the same neural generators. Nowadays, one of the most important goals of fMRI and EEG developers is to provide analysis tools, which optimally orient the neuroscientist toward the real-time comparative evaluation and interpretation of fMRI and EEG data. Indeed, widely used fMRI software packages have evolved from pure MRI/fMRI analysis programs to multi-modal neuroimaging packages, embedding suitable computational tools to address the combination of fMRI and EEG (simultaneous) measurements (see, e. g., Goebel 2012).

Historically, fMRI and EEG methodologies have followed asynchronous and independent paths of research and development with rather limited interaction until the end of the twentieth century, mostly due to technological reasons. Starting from the beginning of the twenty-first century, however, the advent of new systems equipped for the simultaneous acquisition of EEG and fMRI data from the same subject has boosted the research for integrated data modeling and analysis.

The combination of EEG and fMRI data sets into one unique data model is still a focus of intensive research and requires enormous efforts to integrate independent fields of knowledge such as physics, computer science and neuroscience. In fact, besides the classical problems of head modeling in EEG and hemodynamic modeling in fMRI, an additional difficulty is given by the need of understanding and modeling the ongoing correlations of EEG and fMRI data. Some crucial advancements toward the understanding of empirical EEG-fMRI correlations have been also achieved by further extending the model-based data integration schemes for

extra-cranial EEG data to similarly handle intra-cranial EEG data in the fMRI image space (see, e.g., Esposito et al. 2013).

In this chapter, we discuss different strategies available to the neuroimaging researcher for combining and integrating EEG data into the standard framework of fMRI image analysis. Specifically, we discuss how the fMRI analyst can fruitfully incorporate the rich content of temporal information in simultaneously acquired EEG time-series into a standard fMRI analysis. We emphasize the potentials and the importance of anatomically and functionally informing distributed EEG solutions in the context of the classical EEG inverse problem when attempting to link the spatial information extracted from fMRI data to the temporal information from EEG data in a common shared anatomical space.

6.2 The EEG-fMRI Integrated Source Space

Functional MRI data sets are normally acquired over the whole brain with voxel sizes in the range from 2 to 4 mm, albeit ultra-high-field scanners (i.e., with a static magnetic field higher than 3 T) are pushing this spatial resolution below 1 mm (e.g., Kemper et al. 2018). Since simultaneous sub-millimeter EEG-fMRI studies are not currently performed, starting from high-resolution co-registered T1-weighted MRI scans with 1 mm isotropic resolution provides sufficient anatomical detail for standard fMRI signals with 2–3 mm spatial resolution that can be interpolated and co-registered to 1 mm anatomical voxels. Moreover, the precise segmentation of the white matter volumes from the T1-weighted 1 mm MRI images allows identifying the white matter/gray matter boundary. From this inner cortical boundary, dense cortex meshes can be reconstructed with vertices located along the modeled surface. In many cognitive studies, voxel-based functional MRI time-series and spatial patterns can be projected on the cortical meshes by sampling activity within grey matter along the normal vector of each vertex. This results in mesh time-series for typically 100–200,000 vertices per hemisphere. Conversely, EEG signals are acquired from a number of scalp channels ranging from 20 to 300. Thereby, to aid the creation of a common source space for fMRI and EEG signal projection, cortex meshes obtained from MRI data are usually simplified by geometry-preserving mesh decimation algorithms resulting in meshes with a few thousand vertices (Fig. 6.1). As alternative, regular 3D rectangular grids made up of 3–10 mm voxels can be defined directly in the MRI volume space and used for fMRI resampling and EEG projection. In order to constrain the analysis on the cortical voxels, these grids are usually applied segmentation-derived cortical masks.

BOLD-fMRI temporal resolution is in the range of a few hundreds of milliseconds and is physically limited by the sluggishness of the hemodynamic response, which imposes time constants in the order of seconds (Boynton et al. 1996). EEG temporal resolution is in the order of 1 ms or less, but, even in high-density channel configurations, the effective spatial resolution of any detectable neural effects is physically limited by the distance of the neural sources from the electrodes and the inhomogeneous volume conductivity of the head which influences the propagation

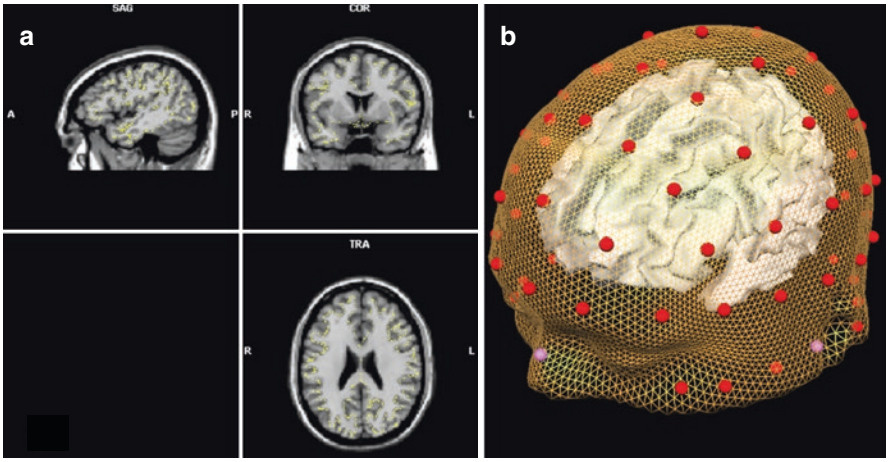

Fig. 6.1 Example of definition of the EEG-fMRI source space for the MNI template brain and the standard MNI 81-electrode EEG configuration. Source points are visible in the volume space (**a**) and correspond to the vertices of the cortical mesh (**b**) automatically registered to the EEG configuration. In the right panel (**b**), red spheres represent electrode positions, pink spheres represent fiducials and yellow and white meshes represent reconstructed head and cortex surfaces, respectively

of electric currents from the source to the electrodes through the different compartments of the cranium. In order to be detectable at distant electrodes, sufficiently large neuronal populations must be synchronously active, and the dendritic compartments of participating neurons must be oriented in parallel.

In the last few decades, important fMRI and EEG/MEG studies have been reported supporting the notion that the preparation of anatomically informed source spaces for time-series projection and neural activity representation significantly enhances the spatio-temporal patterns yielded by fMRI and EEG/MEG measurements with respect to neural source localization and dynamic brain state analysis (see, e.g., Kiebel et al. 2000; Dale & Sereno 1993; Dale et al. 1999, 2000).

In EEG-fMRI studies, voxel-level fMRI time-series are simultaneously acquired with EEG channel time-series. EEG configurations are normally digitized on the head of the subject prior to the MRI scanning session in such a way that automatic 2D–3D MRI image registration and surface-based reconstruction of the head and brain allow to spatially refer EEG and fMRI signals to the same 3D coordinate system. With these co-registration prerequisites, various approaches have been suggested to model EEG source signals including placing current dipoles in fMRI hot spots (Scherg 1990) and distributed source modeling (Hamalainen and Ilmoniemi 1984), which will be described in more detail below.

As described above, fMRI voxel-level BOLD time-courses can be projected from the voxel space to the cortex source space by sampling along the normal of a vertex from the inner (white matter/grey matter) to the outer (grey matter/CSF) boundary, and the corresponding time-courses are averaged to yield one unique

time-course at that vertex. As a result, fMRI data modeling and analysis can be performed directly in the cortex source space.

EEG channel time-series can be projected from the channel space to the cortex source space by placing a single current dipole in each vertex of the mesh and estimating the distributed solution for the EEG inverse problem constrained to the vertex positions (Dale & Sereno 1993; Dale et al. 2000).

More in general, assuming a mesh of N vertices and a linear (discrete) equivalent current dipole (ECD) model as a data model (see, e.g., Mosher and Leahy 1998; Mosher et al. 1999; Baillet et al. 2001), M channel time-series can be expressed as linear combinations of N dipolar source time-series:

$$\mathbf{y}(t) = \begin{pmatrix} y_1(t) \\ \dots \\ y_M(t) \end{pmatrix} = \mathbf{A} \cdot \begin{pmatrix} \mathbf{s}_1(t) \\ \dots \\ \mathbf{s}_N(t) \end{pmatrix} + \mathbf{n}(t) = \mathbf{A} \cdot \mathbf{s}(t) + \mathbf{n}(t) \tag{6.1}$$

In Eq. (6.1) the columns of matrix $\mathbf{A}$ ($M \times 3 * N$) contain the lead fields of the dipolar sources for the given M channel EEG configuration, while $\mathbf{s}_i(t) = [s_x(t), s_y(t), s_z(t)]^t$ represents the source activity time-series of the dipole placed on the ith vertex of the mesh, and $\mathbf{n}(t)$ represents the channel noise.

The lead fields for the EEG configurations are normally extracted from a precomputed volume conductor model applied to the head of the subject (Sarvas 1985; Berg and Scherg 1994; Mosher et al. 1999). Optionally, the dimensionality of the linear problem (6.1) is reduced by a factor of 3 by constraining not only the number and the location of the dipoles but also their orientations, e.g., using the normal unit vectors of the reconstructed cortical surface mesh (see, e.g., Dale et al. 2000; Lin et al. 2004, 2006).

All linear ECD-based inverse solutions can be expressed as a collection of spatial filters (one per source dipole component) which can be directly applied to channel data for generating the estimated source time-series in all vertices of the mesh:

$$\mathbf{x}(t) = \mathbf{W} \cdot \mathbf{y}(t) \tag{6.2}$$

Matrix $\mathbf{W}$ ($3 * N \times M$) contains the spatial filter weights (one collection per source dipole component), and $\mathbf{x}(t)$ is the estimated source time-series for all components and locations. Once the filter weights have been estimated (see below), Eq. (6.2) can be used for generating a "point" source time-series at each vertex of the mesh (virtual electrode; see, e.g., Brookes et al. 2005), or, in alternative, subsets of adjacent vertices in one or more pre-specified regions (regional sources) can be jointly summarized in their orientation and temporal (or spectro-temporal) variance via, e.g., principal component analysis (PCA) (Kayser and Tenke 2003). The solution (6.2) for one or more sources can be visualized in the channel space in the form of 2D or 3D EEG channel topographies. For regional sources and free-orientation EEG solutions, a possible way to reduce Eq. (6.2) to a single set of channel weights is to first average $\mathbf{W}$ matrix coefficients across all regional vertices separately for each orientation (X, Y, and Z) and then project the weights along the orientation

explaining the maximum variance of the projected data by means of a singular value decomposition (SVD). For orientation-constrained solutions, the maximum variance projection is not necessary.

The estimation of the inverse solution **W** can proceed by either filling one, two ,or three rows of **W** at each source location ("scanning" approach) or by attempting a total inversion of the distributed ECD model across the entire source space ("imaging" approach) (see, e.g., Darvas et al. 2004). For instance, dipole fitting methods (Scherg 1990), linearly constrained minimum variance (LCMV) beamformers (van Veen et al. 1997), and multiple signal classification (MUSIC; Mosher and Leahy 1998) are commonly used "scanning" approaches. Imaging approaches always require some form of regularization due to the ill-posed nature of the problem of inverting the linear model in Eq. (6.1) for $N > M$. A commonly adopted "imaging" approach is the weighted minimum norm (WMN) solution (Hamalainen and Ilmoniemi 1984; Hamalainen et al. 1993; Leahy et al. 1996) expressed by the formula:

$$\mathbf{W} = \mathbf{R}\mathbf{A}^{t}\left(\mathbf{A}\mathbf{R}\mathbf{A}^{t} + \lambda^{2}\mathbf{C}_{N}\right)^{-1} \tag{6.3}$$

where matrix **R** represents the "a priori" source covariance and is used to "inform" the source activities, $\mathbf{C}_N$ is the covariance matrix of the channel noise, and λ is a regularization parameter (Tikhonov and Arsenin 1977). A typical weighting scheme called "depth-weighting" (Lawson and Hanson 1974; Jeffs et al. 1987) specifies **R** as a diagonal matrix with non-zero entries inversely proportional to the γth power of lead field norms (γ being the depth-weighting parameter; see also Lin et al. 2004, 2006).

Other common imaging approaches, such as Laplacian-weighted minimum norm (LORETA, Pascual-Marqui et al. 1994) and local autoregressive average (LAURA, Grave de Peralta et al. 2004) (see also previous chapter and Michel et al. (2004) for review), are analogous to WMN but allow for additional constrains on the source covariance in a non-diagonal matrix **R**. Finally, some form of normalization (e.g., dynamic-SPM, Dale et al. 2000) or standardization (s-LORETA, Pascual-Marqui 2002) with respect to the source noise and signals can be applied to the filter weights in matrix **W** before the application to channel time-series. Finally, the WMN scheme has been also used for fMRI-constrained distributed inverse modeling by "modulating" the diagonal entries with local fMRI activity, e.g., via BOLD percent signal change estimates, and the off-diagonal entries with some functional connectivity measure such as inter-regional BOLD signal correlations (see, e.g., Liu et al. 1998; Dale et al. 2000; Babiloni et al. 2003).

6.3 Data Integration Strategies for EEG-fMRI Studies

The major motivation for the development of EEG-fMRI systems stems from the need of linking the precise and detailed spatial characterization of neural phenomena achievable with modern high-field fMRI to the precise and detailed temporal

characterization of neuronal phenomena achievable with modern high-density EEG. Despite the relevant problem of dealing with the presence of fMRI-specific artifacts in the collected EEG traces, the simultaneous acquisition of EEG and fMRI signals provides a strong neurophysiological and neuropsychological basis for establishing this link, by making sure that the same brain at the same time is studied while performing a cognitive task. Nonetheless both physical and physiological new issues have arisen about the intrinsic nature and the validity of EEG-fMRI signal correlations. The former refers to lack of knowledge about the real extent of temporal and spatial effect coupling between the two modalities. The latter refers to the different perspectives and expectations by neuroscientists from the fMRI and EEG fields. Based on these observations, we propose to consider two different symmetric approaches to the comparative analysis of simultaneously acquired EEG-fMRI data.

In one approach, EEG data are first analyzed in the channel or source space, and one or more sources are characterized in the (time or frequency) temporal domain. Thereby a temporal model for fMRI responses, e.g., a general linear model (GLM, Friston et al. 1995), is derived by extracting the trial-by-trial variation (modulation) or the spectro-temporal evolution of one or more pre-detected EEG sources (integration of fMRI and EEG in the temporal domain, Fig. 6.2). The effective integration of EEG data into the fMRI temporal model requires the application of a correction for fMRI hemodynamics, e.g., via linear convolution with a model hemodynamic response function (Boynton et al. 1996) and, with the sole exception of resting-state fMRI studies (Laufs et al. 2003), the orthogonalization of the EEG measures to the standard fMRI response (Feige et al. 2005; Eichele et al. 2005). The GLM results will then reveal brain regions related to an EEG-derived temporal reference.

In a second approach (integration of fMRI and EEG in the spatial domain, Fig. 6.3), fMRI spatial patterns are first extracted in the cortex source space and then used in combination with forward and inverse solutions for generating fMRI-derived channel topographies (inverse filters) in the context of EEG spatial modeling.

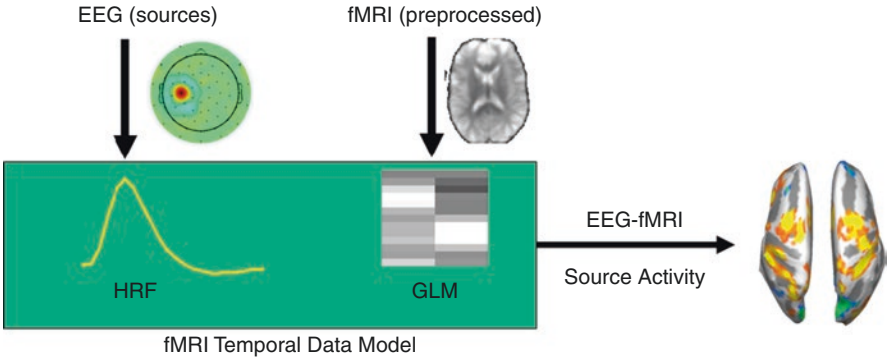

Fig. 6.2 Integration of fMRI and EEG data in the temporal domain

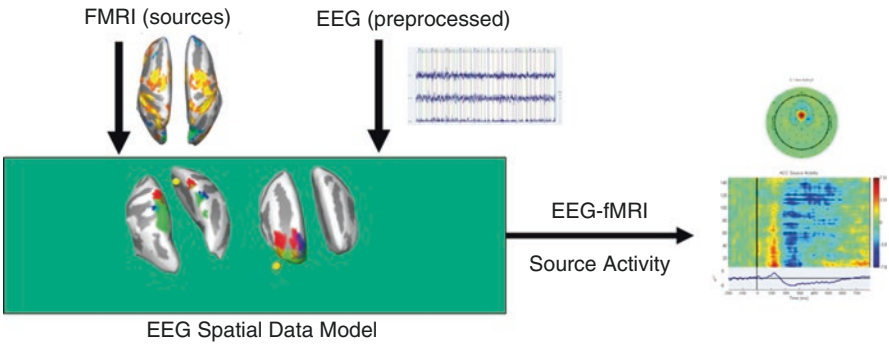

Fig. 6.3 Integration of fMRI and EEG data in the spatial domain

Thereby a detailed time or time-frequency characterization becomes associated with the fMRI spatial pattern. The fMRI spatial information can be either incorporated into the estimation of the distributed inverse solution (see, e.g., Liu et al. 1998; Babiloni et al. 2003) or simply used to select the regions of activity in the cortex source space to create the corresponding channel topography (regional source).

6.4 Illustration of the Integration of fMRI and EEG in the Temporal Domain

EEG-relevant neural processes can be characterized in the time or frequency domain. Short-lasting (few milliseconds) and broadband EEG processes are usually evaluated in the time domain and detected as amplitude peaks of the response at a specific latency, with positive or negative polarity (see previous chapter). Long-lasting and narrow-band EEG processes are usually evaluated in the frequency domain in terms of their spectral power and phase distribution in certain frequency ranges (Engel et al., 2001). Although it is possible to observe these processes in single or multiple channels, many studies have shown the importance of projecting EEG time-series from the channel space to a different space where specific sub-components are well separated and better studied. Two widely used approaches for EEG-fMRI integration in the temporal domain are based on independent component analysis (ICA) and canonical correlation analysis (CCA) (Rosa et al. 2010; Lei et al. 2012). For instance, temporal ICA (Hyvarinen et al. 2001) is a statistical technique which decomposes channel time-series into independent components by removing statistical redundancy between channel observations and has been proposed as a powerful tool for separating and rejecting EEG artifacts and for generating new hypotheses about the underlying source dynamics and origins (Makeig et al. 2002).

As an alternative to purely data-driven spaces, and especially when the principal aim of the study is to produce a local validation of the EEG source and a local interpretation of EEG-fMRI effect coupling, the preprocessed EEG channel time-series can be

first projected to an anatomically informed source space (e.g., a cortex source space) and then analyzed for the main or differential effects of a specific temporal feature.

Examples of this integration strategy are depicted in Figs. 6.4, 6.5, and 6.6. Figure 6.4 shows the results of a cortically constrained distributed source analysis performed on a 5000-vertex source space after estimation and application of a

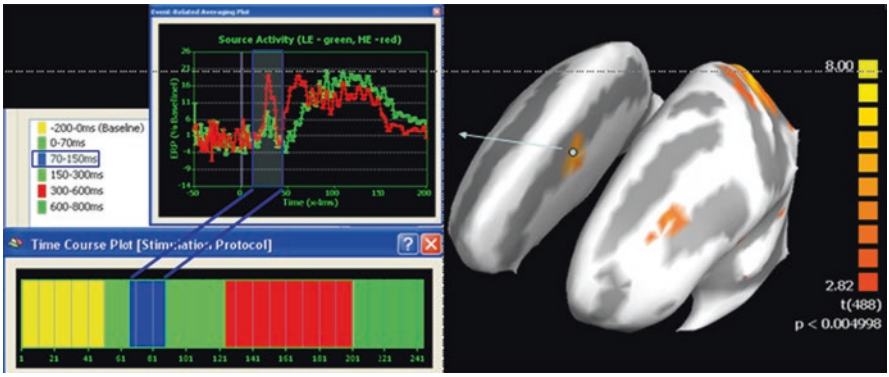

Fig. 6.4 Results of the EEG distributed source analysis in the cortical space

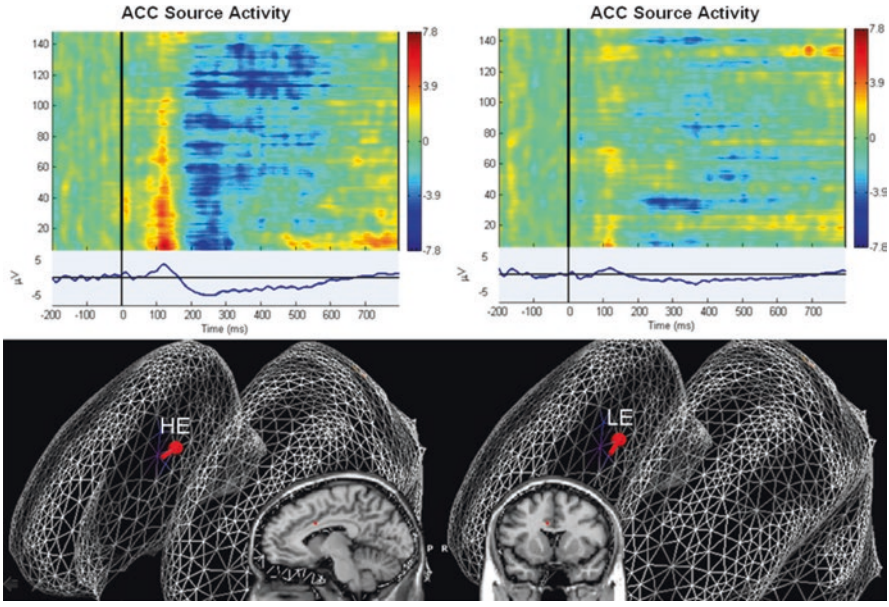

Fig. 6.5 Results of the EEG distributed source analysis in the cortical space and projection in the volume. Upper panels: source ERP images (single-trial and trial-averaged responses) for the HE (left) and LE (right) conditions. Lower panels: equivalent current dipole sources for the HE (left) and LE (right) conditions. The source location is displayed in the volume space (left, sagittal view; right, coronal view) as red points

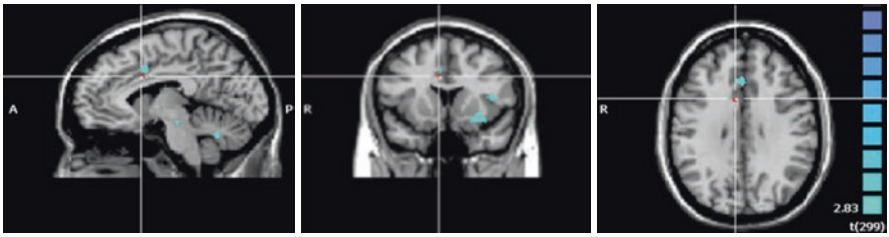

Fig. 6.6 FMRI (volume) GLM map obtained from the incorporation of the trial-by-trial amplitude modulation of the ERP source in the anterior cingulate cortex (ACC) during the HE session (triplanar view centered in the EEG source location)

WMN filter to the preprocessed EEG time-series from a single-subject EEG-fMRI experiment with a simple auditory-guided choice task performed under two levels of decision efforts (LE, low effort; HE, high effort) (for the detailed description of the experimental paradigm, see Mulert et al. 2005). Figure 6.5 shows the source ERP images for the two conditions (upper panels) and the equivalent dipoles estimated in the local peak of the ERPs (lower panels). Figure 6.6 shows the FMRI (volume) map obtained from the incorporation of the trial-by-trial amplitude modulation of the ERP source in the anterior cingulate cortex (ACC) during the HE session.

6.5 Illustration of the Integration of fMRI and EEG in the Spatial Domain

In the example of the previous paragraph, the high temporal resolution of simultaneously acquired EEG data has been used to augment the fMRI temporal model and to study neural events whose actual occurrence or effective characterization would be otherwise not possible at the fMRI temporal scale.

The alternative perspective is to assume that standard fMRI temporal models are sufficient to map the BOLD effects of the stimulus-evoked brain activity, thus producing a detailed spatial picture of the temporally evolving cognitive states as a stand-alone modality. In such cases, it might become extremely interesting for the fMRI cognitive scientist to enrich the meaning and the interpretation of fMRI spatio-temporal patterns with spatially selective EEG features using the available simultaneous EEG data.

Using the cortex source space as a common space for both fMRI and EEG data projection, it is possible to establish a spatial link between the ongoing fMRI activity in one or more (functionally connected) regions and the temporal or spectro-temporal variance of simultaneously acquired EEG data. Figures 6.7, 6.8, and 6.9 refer to the application of such an integration strategy (schematically illustrated in Fig. 6.3) to an EEG-fMRI block-design experiment (own data) based on a typical working-memory task, the *N*-back task (see, e.g., Esposito et al. 2006). According to this strategy, an fMRI spatial pattern is first obtained from

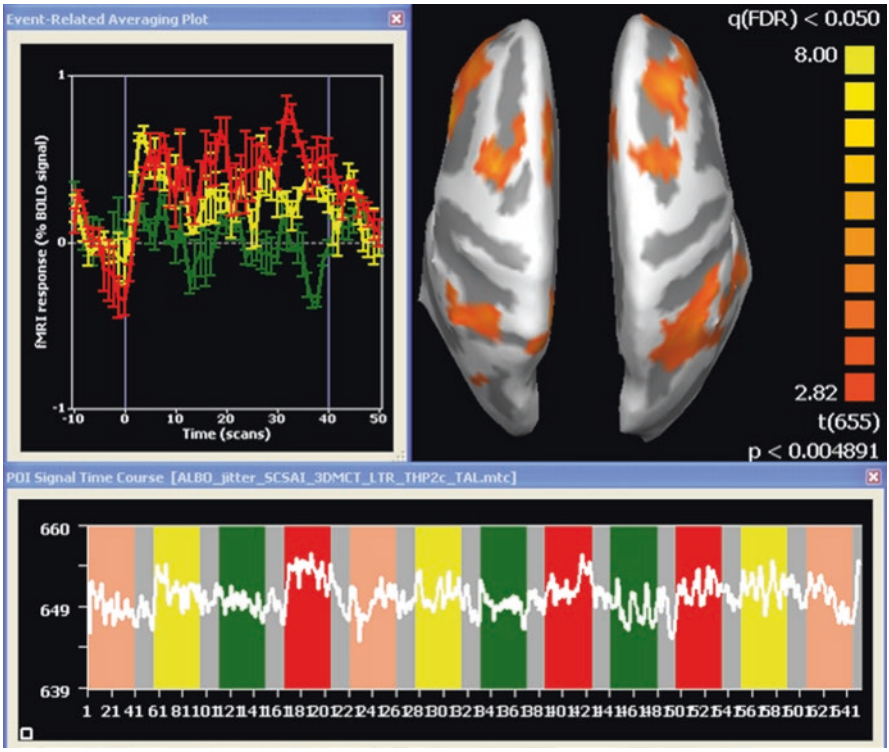

Fig. 6.7 FMRI spatial pattern of BOLD activity during the *N*-back working-memory task. Statistically significant (conjunction test, $P < 0.05$, FDR corrected) parametric BOLD responses are projected onto the cortex source space

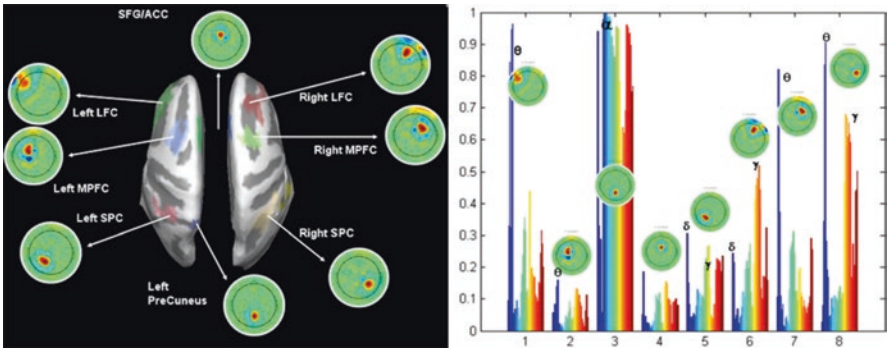

Fig. 6.8 FMRI regions of activity are converted to EEG topographies via the application of a WMN filter in the cortex source space (left). FMRI-derived regional sources are jointly analyzed in the temporal evolution of their frequency spectral distribution in the range between 0 and 50 Hz during the entire fMRI run (right). In this plot the normalized spectro-temporal variance contribution in different bands from each source is emphasized via color coding from the lowest (blue-cyan) to the highest (yellow-red) frequencies. Peaks of temporal variance in the delta, theta, alpha, beta, and gamma bands are marked on the plot

mesh time-series by performing standard GLM mapping of the linear differential contrasts among memory conditions in the cortex source space (Fig. 6.7 shows the conjunction map of the contrasts "2-back vs. 1-back" and "1-back vs. 0-back"). Then, the set of regions exhibiting statistically significant BOLD responses is used to generate a corresponding set of EEG regional sources (Fig. 6.8) using a cortically constrained distributed inverse solution (WMN) estimated on the same source space (Fig. 6.8). The WMN channel weightings of each regional source are visualized in the channel space as EEG topographies. Thereby the active fMRI network "selects" a network of EEG regional sources which can be jointly analyzed for their spectro-temporal features using, e.g., PCA. For instance, the normalized distribution of the source power spectral density across all sources in different frequency bands can be analyzed, and the variance of fundamental EEG rhythms during the fMRI experiment can be visualized (Fig. 6.9). According to this strategy, the fMRI network parametrically activated during the *N*-back task of Fig. 6.7 exhibited prevalent peaks in the theta band (mainly in the lateral-frontal and superior-lateral parietal sources) and, in more composite spectra, in the alpha and gamma band (anterior and posterior midline sources). The time-frequency plots, the theta power traces, and the temporal correlations of the theta power traces with the experimental conditions are shown in Fig. 6.8. A positive parametric trend of the EEG theta signals with the cognitive loads of the working-memory conditions is evident.

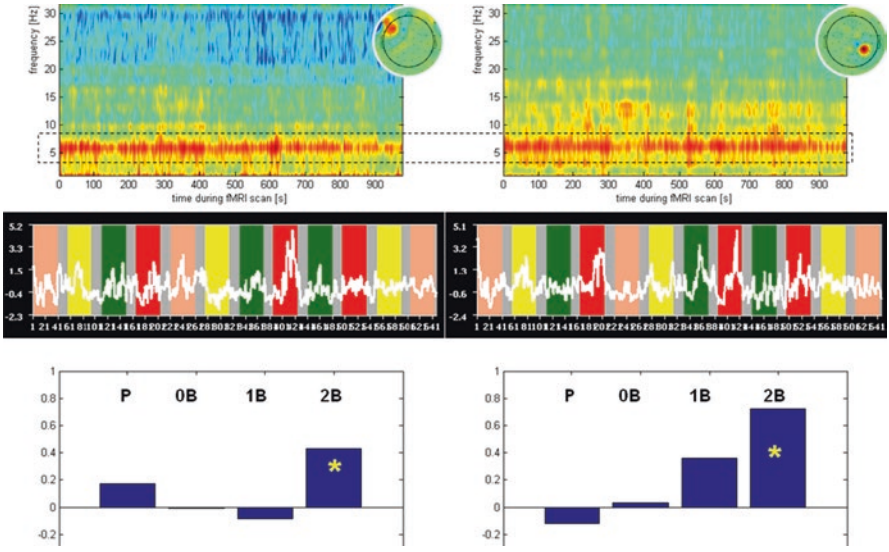

Fig. 6.9 Time-frequency plots (upper panels), theta power traces (central panels), and temporal correlations of the theta traces with the experimental conditions (lower panels) for the "principal" theta sources, associated with the left lateral frontal cortex (left panels) and right superior parietal cortex (right panels)

6.6 Direct Integration of fMRI and Intra-cranial EEG in the Spatial Domain

When projecting scalp EEG measurements to the cortex source space, the spatial link between the ongoing fMRI (temporal) activity and the ongoing EEG (temporal or spectro-temporal) activity depends on the accuracy of the forward and inverse solutions. However, due to the finite number of electrodes and all theoretical and physical issues related to electromagnetic field propagation and volume conduction (Acar et al. 2008; Mosher et al. 1999), scalp EEG will never achieve the same spatial resolution of fMRI.

An attractive solution to empirically address the spatial coupling between EEG and fMRI activities is therefore represented by the possibility to directly integrate fMRI recordings with intra-cranial EEG (iEEG) recordings when these would be available from the same subject (performing the same experiment). In fact, iEEG data are collected from electrodes placed directly on the cortical surface of surgically implanted patients, allowing for a comparable spatial resolution between the two modalities. In such cases, the ECD model in Eq. (6.2) could be replaced by a "direct" current dipole model with the same mathematical formulation in which parameters essentially model the "spread" of the iEEG activity around each electrode over contiguous mesh vertices as a function of the electrode-vertex distance (Esposito et al. 2013):

$$x_v(t,f) = \sum_{i=1}^{M} w_{iv} \cdot y_i(t,f)$$
$$w_{iv} = \begin{cases} \left(1 - \dfrac{d_{iv}}{d_{\max}}\right)^k & d_{iv} \le d_{\max} \\ 0 & d_{iv} \le d_{\max} \end{cases} \tag{6.4}$$

where $x_v(t,f)$ is the iEEG activity at mesh vertex v (time bin t, frequency bin f), $y_i(t,f)$ is the iEEG activity at electrode (time bin t, frequency bin f), and w_{iv} is the "weighting" function of the distance of electrode i from vertex v (d_{iv}).

This mathematical formulation allows flexibly increasing the weighting of the surface vertices that are closer to the electrode positions while ensuring both a "compact" support (i.e., the weight is exactly zero at a distance equal or higher than $d_{\max}$) and a spatial continuity at the boundary (i.e., the weight approaches zero when the distance approaches $d_{\max}$) of the spread area. More specifically, the parameters $d_{\max}$ and k in Eq. (6.4) allow to, respectively, control the radius and the attenuation of the activity spread around each electrode. As an example, Fig. 6.10 illustrates the application of this spatial model ($k = 2$, $d_{\max} = 1$ cm) to integrate the iEEG spectro-temporal activity with the fMRI BOLD activity, both elicited in the same subject by the passive viewing of a 10-s movie clip (single-subject data set from a cohort presented by Esposito et al. 2013).

Unfortunately, while scalp EEG can be safely, routinely, and simultaneously measured with fMRI in healthy individuals, iEEG electrodes can only be implanted

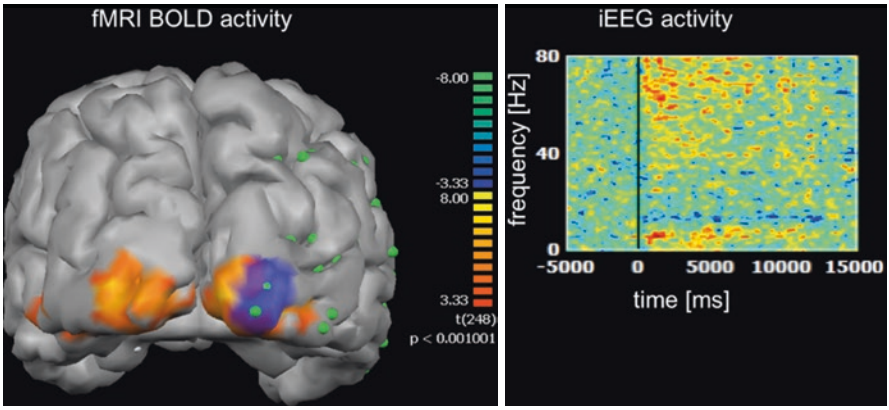

Fig. 6.10 Left panel: fMRI BOLD activation map (passive movie viewing vs. baseline, t statistics, $p < 0.001$) with superimposed spread model (transparent blue) of the iEEG activity over the cortical surface for "activated" electrodes. Green spheres are placed in the surface-registered positions of iEEG electrodes. Right panel: time-frequency iEEG plot (yellow-red, event-related synchronization; green-blue, event-related desynchronization). In this type of integration, fMRI BOLD activity changes serve as "localizer" for possible theta and gamma power changes in the common brain (cortex) space

in the brain of some exceptional patients (typically with drug-resistant epilepsy), and the actual position of the electrode sites are solely determined by purely clinical considerations. Thereby, these investigations rarely allow the coverage of the whole cortex.

6.7 Discussion

In this chapter, we have presented two alternative strategies available to the fMRI researcher for combining simultaneously acquired EEG and fMRI data sets into one integrated conceptual framework. We briefly illustrated the two approaches on two real-world single-subject EEG-fMRI data sets. Although these illustrations made use of specific data models and statistical techniques, the described frameworks are to be considered general with respect to the implementation of other fMRI or EEG data models. The proposed analysis pathways of Figs. 6.2 and 6.3 conceptually represent the general motivations and expectations of imaging neuroscientists with regard to EEG-fMRI practical applications from two opposite but symmetric views. The illustrated pathways have been also developed or suggested in the context of real-time EEG-fMRI brain-computer interfaces (see, e.g., Frolov et al. 2017) and for clinical intra-cranial EEG-fMRI studies on implanted patients (see, e.g., Hawsawi et al. 2017).

When integrating fMRI and EEG in the temporal domain (Fig. 6.2), the high temporal resolution of simultaneously acquired EEG data is used to augment the fMRI temporal model and study neural events whose actual occurrence or effective characterization would be otherwise not possible at the fMRI temporal scale. As a

result, we gain the capability of mapping the fMRI correlates of new events whose characterization cannot come from the sole experimental design. From the fMRI modeling and analysis viewpoint, this approach turns out to be very equivalent to the integration of online external or behavioral measures, such as reaction times, ratings, etc., which is a common practice in fMRI research. Nonetheless, there are two critical aspects implicit to this approach. First, it is required that not only an EEG source exists with a given observed feature (e.g., an ERP component within a given interval of latencies) but also that substantial trial-by-trial modulation exists during the entire experiment to produce a relatively noise-free fMRI predictor for a statistically powerful GLM. Normally the variance of EEG-derived predictors after orthogonalization to the standard stimulus-coding predictors can be very low, therefore impairing the single-subject and group-level random-effects GLM statistics. Orthogonalization is necessary to partial out the variance already explained by the stimulus function and isolates the real added value of embedding EEG features into the GLM. The use of large cohorts may suffer the additional variability caused by the different EEG reactivity of the subjects (Meltzer et al. 2007a, b). Second, significant effects are mapped for the EEG-fMRI correlations on a purely temporal basis. Therefore, additional difficulties can arise in the interpretation of fMRI activation clusters which are not well co-localized to the EEG source or even far away from it. In fact, while the full understanding of local EEG-fMRI correlations ultimately requires more sophisticated physical and empirical models for the effect coupling, both types of findings require interpretation with extreme caution. The coupling of electrophysiological and BOLD activity is complex also because the directionality of the EEG-BOLD correlations can be a function of both space and of frequency (see, e.g., Scheeringa et al. 2011; Maggioni et al. 2016); thereby, simultaneous EEG-fMRI studies employing a temporal integration scheme have sometimes left aside the sign of the correlations in the fMRI modeling (see, e.g., Walz et al. 2014).

The use of EEG source analysis has been shown to improve the fMRI modeling. However, the known limitations of EEG inverse models may sometimes produce "ghost" sources (see, e.g., Michel et al. 2004), thereby making the source projection itself of limited validity or even biasing the integration of EEG features in the fMRI temporal model. With respect to this point, the use of an intermediate non-anatomically informed source projection, such as ICA, might provide better results due to the temporal decorrelation of the signals. Although the co-localization of EEG and fMRI sources is sometimes presented and invoked as a source cross-validation scheme (see, e.g., Wibral et al. 2008), it might also well be that some of the EEG generators are spatially masked by volume conductor effects but pops out nicely anyway due to the fMRI functional connectivity. This is especially true for subcortical and thalamic effects which have been shown to be visible with EEG-fMRI (Feige et al. 2005) but which are also very difficult to isolate via EEG spatial modeling alone (Nunez and Srinivasan 2006). In such cases, the added value of the simultaneous EEG measure cannot be restricted to a pure cross-validation tool.

A number of multivariate EEG measures have been actually derived with the specific purpose of reflecting functional connectivity across the brain (Abreu et al. 2018a).

These include the so-called partial directed coherence (Biazoli et al. 2013) and the phase synchronization index (Mizuhara et al. 2005) within a given frequency band of interest. Particularly, a study by Abreu et al. (2018b) has shown how the latter measure is able to best predict BOLD signal changes associated with epileptic activity.

When integrating fMRI and EEG in the spatial domain (Fig. 6.3), the high spatial resolution and the local physical origin of fMRI signals are used to inform an EEG spatial model and characterize brain activity and cognitive states at typical EEG time and frequency scales. As a result, it becomes possible to enrich detailed pictures of fMRI-derived spatio-temporal patterns with high temporal resolution EEG-derived information.

The use of EEG distributed inverse models and a typical "imaging" approach (such as WMN) on a common anatomically informed (cortex) source space has been highlighted in this chapter. Besides the importance of this approach in the context of EEG studies (see, e.g., Riecke et al. 2009, 2012), this solution presents a number of attractive properties in the context of EEG-fMRI experiments where no single or a few isolated regions are selected, but rather distributed networks are involved in controlling the information flow and processing and execution of complex cognitive functions. In fact, although theoretically and technically possible, the use of ECD dipole fitting procedures would require placing at least one single dipole in each region of activity, whereas scanning approaches, such as beamforming, implicitly pose theoretical constraints about remote source correlations (van Veen et al. 1997). One more attractive property of imaging solutions for EEG-fMRI studies is the possibility to add distributed fMRI constraints directly in the WMN estimation (see, e.g., Liu et al. 1998; Dale et al. 2000; Babiloni et al. 2003). Nonetheless, for the purpose of the case illustrated here, we intended not to bias the contribution of the EEG sources with condition-specific fMRI effects.

We have shown how it is possible in practice to spatially select from fMRI patterns a set of regional EEG sources and jointly analyze their spectro-temporal contribution to the measured EEG variance in a simultaneous EEG-fMRI experiment. This is basically the first step before correlating any EEG spectro-temporal feature (e.g., band-specific power traces) to the experimental conditions of the EEG-fMRI experiments.

A different procedure to obtain a voxel-wise correspondence of the reconstructed EEG and fMRI signals has been introduced by Ostwald et al. (2011). In this case, EEG inverse modeling is combined with a set of information theoretic quantities that can be estimated from simultaneously acquired EEG-fMRI data, allowing the identification of either spatio-temporal or spatio-spectral relationships between EEG and fMRI in terms of information content of all available EEG data (not, e.g., from single electrodes).

There are, however, several caveats for this approach as well, which also requires interpretational cautions. First, according to this scheme, significant effects are mapped assuming EEG-fMRI correlations on a purely spatial basis. As for the combination in the temporal domain, combination in the spatial domain also expects more sophisticated physical and empirical models for EEG-fMRI effect coupling to be developed. Second, the known limitations of EEG inverse models do not allow concluding about the presence of one or more single EEG generators in each fMRI

region (Liu et al. 2006). It might well be that global effects or strong local effects from "close" regions substantially contribute to the spectral and temporal features of a given regional source. In this sense, the joint principal component analysis of multiple remote regional sources can be a more robust approach for identifying the presence of global effects (i.e., common to all regional sources) and differentially evaluate the relative contribution of each single region within the network.

Due to volume conduction effects, scalp recordings are known to be biased toward global activity (Nunez and Srinivasan 2006), and the purpose of the inverse spatial filters estimated via EEG spatial modeling is to remove as much as possible this bias and to enhance local activity. It must be also stated, however, that the presence of global activity throughout the selected EEG sources is not necessarily an artifact, whereas the excessive dominance of one source against all the others, especially if this happens on an extended time-frequency range, can be likely due to residual artifacts in the EEG data.

Several conjectures about fMRI and EEG brain dynamics have agreed that "high values of complexity necessarily correspond to an optimal synthesis of functional specialization and functional integration within a system" (Edelman and Tononi 2000; Nunez and Srinivasan 2006). Following up this conceptual framework, the technical search for the optimal integration of EEG and fMRI data will likely evolve toward a search for the optimal balance between global and local effect coupling.

An important contribution to the understanding (as well as to the practical interpretation and application) of the spatial coupling of fMRI and EEG brain dynamics has been provided by the combined modeling of intra-cranial EEG and fMRI data from the same subject (Esposito et al. 2013), as conceptually illustrated in previous paragraph. In fact, the comparison of intra-cranial EEG and fMRI offers the unique opportunity to map the relationship between hemodynamic and electrophysiological signals during cognitive processes that cannot be replicated in animal models (Kadipasaoglu et al. 2014). Particularly, it has been now fully established that intra-cranial EEG not only captures local oscillatory signals in the (high) gamma frequency band reflecting asynchronous summation of population firing but also that this kind of activity directly correlates with local BOLD activity, justifying the fundamental assumption of a direct source model that neural sources are geometrically distributed around each intra-cranial electrode. The use of such a direct source spatial integration model has provided a powerful tool to examine the local oscillatory EEG signals (both in the low- and high-frequency bands) in a wider spatial context by assessing the mapping of responsive intra-cranial channels at the group level (Singer et al. 2014), whereas further developments of this spatial integration model have mainly dealt with improving the accuracy of the registration of intra-cranial EEG data to individual cortical topology (see, e.g., Kadipasaoglu et al. 2014).

In summary, fMRI researchers can enrich topographically accurate fMRI data with precise timing information when performing simultaneous EEG-fMRI experiments. The outlined approaches may lead to new insights about the neuronal basis of cognitive processes but require sophisticated combined data analysis, preferentially in a common cortex space, as well as careful interpretation of obtained spatio-temporal results.

References

Abreu R, Leal A, Figueiredo P (2018a) EEG-informed fMRI: a review of data analysis methods. Front Hum Neurosci 12:29

Abreu R, Leal A, Lopes da Silva F, Figueiredo P (2018b) EEG synchronization measures predict epilepsy-related BOLD-fMRI fluctuations better than commonly used univariate metrics. Clin Neurophysiol 129(3):618–635

Acar ZA, Makeig S, Worrell G (2008) Head modeling and cortical source localizationin epilepsy. Conf Proc IEEE Eng Med Biol Soc 2008:3763–3766

Babiloni F, Babiloni C, Carducci F, Romani GL, Rossini PM, Angelone LM, Cincotti F (2003) Multimodal integration of high-resolution EEG and functional magnetic resonance imaging data: a simulation study. Neuroimage 19(1):1–15

Baillet S, Mosher JC, Leahy RM (2001) Electromagnetic brain mapping. IEEE Signal Process Mag 18(6):14–30

Berg P, Scherg M (1994) A fast method for forward computation of multiple-shell spherical head models. Electroencephalogr Clin Neurophysiol 90:58–64

Biazoli CE Jr, Sturzbecher M, White TP, Dos Santos Onias HH, Andrade KC, deAraujo DB, Sato JR (2013) Application of partial directed coherence to the analysis of resting-state EEG-fMRI data. Brain Connect 3(6):563–568

Boynton GM, Engel SA, Glover GH, Heeger DJ (1996) Linear systems analysis of functional magnetic resonance imaging in human V1. J Neurosci 16(13):4207–4221

Brookes MJ, Gibson AM, Hall SD, Furlong PL, Barnes GR, Hillebrand A, Singh KD, Holliday IE, Francis ST, Morris PG (2005) GLM-beamformer method demonstrates stationary field, alpha ERD and gamma ERS co-localisation with fMRI BOLD response in visual cortex. Neuroimage 26:302–308

Dale AM, Sereno MI (1993) Improved localization of cortical activity by combining EEG and MEG with MRI cortical surface reconstruction: a linear approach. J Cogn Neurosci 5:162–176

Dale AM, Fischl B, Sereno MI (1999) Cortical surface-based analysis: I. Segmentation and surface reconstruction. Neuroimage 9:179–194

Dale AM, Liu AK, Fischl BR, Buckner RL, Belliveau JW, Lewine JD, Halgren E (2000) Dynamic statistical parametric mapping: combining fMRI and MEG for high-resolution imaging of cortical activity. Neuron 26:55–67

Darvas F, Pantazis D, Kucukaltun-Yildirim E, Leahy RM (2004) Mapping human brain function with MEG and EEG: methods and validation. Neuroimage 23:S289–S299

Edelman GM, Tononi G (2000) A universe of consciounsness. Basic Books, New York

Eichele T, Specht K, Moosmann M, Jongsma ML, Quiroga RQ, Nordby H, Hugdahl K (2005) Assessing the spatiotemporal evolution of neuronal activation with single-trial event-related potentials and functional MRI. Proc Natl Acad Sci U S A 102(49):17798–17803

Engel AK, Fries P, Singer W (2001) Dynamic predictions: oscillations and synchrony in top-down processing. Nat Rev Neurosci 2(10):704–716

Esposito F, Bertolino A, Scarabino T, Latorre V, Blasi G, Popolizio T, Tedeschi G, Cirillo S, Goebel R, Di Salle F (2006) Independent component model of the default-mode brain function: assessing the impact of active thinking. Brain Res Bull 70(4–6):263–269

Esposito F, Singer N, Podlipsky I, Fried I, Hendler T, Goebel R (2013) Cortex-based inter-subject analysis of iEEG and fMRI data sets: application to sustained task-related BOLD and gamma responses. Neuroimage 66:457–468

Feige B, Scheffler K, Esposito F, Di Salle F, Hennig J, Seifritz E (2005) Cortical and subcortical correlates of electroencephalographic alpha rhythm modulation. J Neurophysiol 93(5):2864–2872

Friston KJ, Holmes AP, Poline JB, Grasby PJ, Williams SC, Frackowiak RS, Turner R (1995) Analysis of fMRI time-series revisited. Neuroimage 2(1):45–53

Frolov AA, Mokienko O, Lyukmanov R, Biryukova E, Kotov S, Turbina L, Nadareyshvily G, Bushkova Y (2017) Post-stroke rehabilitation training with a motor-imagery-based brain-computer interface (BCI)-controlled hand exoskeleton: a randomized controlled multicenter trial. Front Neurosci 11:400

Goebel R (2012) BrainVoyager—past, present, future. Neuroimage 62(2):748–756
Grave de Peralta R, Murray MM, Michel CM, Martuzzi R, Gonzalez Andino S (2004) Electrical neuroimaging based on biophysical constraints. Neuroimage 21:527–539
Hamalainen M, Ilmoniemi RJ (1984) Interpreting measured magnetic fields of the brain: estimates of current distributions. Technical report TKK-F-A559. Helsinki University of Technology
Hamalainen M, Hari R, Ilmoniemi R, Knuutila J, Lounasmaa O (1993) Magnetoencephalography—theory, instrumentation, and application to non-invasive studies of the working human brain. Rev Mod Phys 65:413–497
Hawsawi HB, Carmichael DW, Louis L (2017) Safety of simultaneous scalp or intracranial EEG during MRI: a review. Front Phys 5:42
Hyvarinen A, Karhunen J, Oya E (2001) Independent component analysis. John Wiley & Sons, New York
Jeffs B, Leahy R, Singh M (1987) An evaluation of methods for neuromagnetic image reconstruction. IEEE Trans Biomed Eng 34:713–723
Kadipasaoglu CM, Baboyan VG, Conner CR, Chen G, Saad ZS, Tandon N (2014) Surface-based mixed effects multilevel analysis of grouped human electrocorticography. Neuroimage 101:215–224
Kayser J, Tenke CE (2003) Optimizing PCA methodology for ERP component identification and measurement: theoretical rationale and empirical evaluation. Clin Neurophysiol 114(12):2307–2325
Kemper VG, De Martino F, Emmerling TC, Yacoub E, Goebel R (2018) High resolution data analysis strategies for mesoscale human functional MRI at 7 and 9.4T. Neuroimage 164:48–58
Kiebel SJ, Goebel R, Friston KJ (2000) Anatomically informed basis functions. Neuroimage 11(6):656–667
Laufs H, Krakow K, Sterzer P, Eger E, Beyerle A, Salek-Haddadi A, Kleinschmidt A (2003) Electroencephalographic signatures of attentional and cognitive default modes in spontaneous brain activity fluctuations at rest. Proc Natl Acad Sci U S A 100(19):11053–11058
Lawson CL, Hanson RJ (1974) Solving least squares problems. Prentice Hall, Englewood Cliffs
Leahy RM, Mosher JC, Philips JW (1996) A comparative study of minimum norm inverse methods for MEG imaging. In: Proceedings of the 10th international conference of biomagnetism
Lei X, Valdes-Sosa PA, Yao D (2012) EEG/fMRI fusion based on independent component analysis: integration of data-driven and model-driven methods. J Integr Neurosci 11:313–337
Lin FH, Witzel T, Hämäläinen MS, Dale AM, Belliveau JW, Stufflebeam SM (2004) Spectral spatiotemporal imaging of cortical oscillations and interactions in the human brain. Neuroimage 23:582–595
Lin FH, Witzel T, Ahlfors SP, Stufflebeam SM, Belliveau JW, Hämäläinen MS (2006) Assessing and improving the spatial accuracy in MEG source localization by depth-weighted minimum-norm estimates. Neuroimage 31:160–171
Liu AK, Belliveau JW, Dale AM (1998) Spatiotemporal imaging of human brain activity using functional MRI constrained magnetoencephalography data: Monte Carlo simulations. Proc Natl Acad Sci U S A 95(15):8945–8950
Liu Z, Kecman F, He B (2006) Effects of fMRI-EEG mismatches in cortical current density estimation integrating fMRI and EEG: a simulation study. Clin Neurophysiol 117(7):1610–1622
Maggioni E, Zucca C, Reni G, Cerutti S, Triulzi FM, Bianchi AM, Arrigoni F (2016) Investigation of the electrophysiological correlates of negative BOLD response during intermittent photic stimulation: an EEG-fMRI study. Hum Brain Mapp 37(6):2247–2262
Makeig S, Westerfield M, Jung TP, Enghoff S, Townsend J, Courchesne E, Sejnowski TJ (2002) Dynamic brain sources of visual evoked responses. Science 295(5555):690–694
Meltzer JA, Negishi M, Mayes LC, Constable RT (2007a) Individual differences in EEG theta and alpha dynamics during working memory correlate with fMRI responses across subjects. Clin Neurophysiol 118(11):2419–2436
Meltzer JA, Zaveri HP, Goncharova II, Distasio MM, Papademetris X, Spencer SS, Spencer DD, Constable RT (2007b) Effects of working memory load on oscillatory power in human intracranial EEG. Cereb Cortex 18(8):1843–1855

Michel CM, Murray MM, Lantz G, Gonzalez S, Spinelli L, Grave de Peralta R (2004) EEG source imaging. Clin Neurophysiol 115(10):2195–2222

Mizuhara H, Wang LQ, Kobayashi K, Yamaguchi Y (2005) Long-range EEG phase synchronization during an arithmetic task indexes a coherent cortical network simultaneously measured by fMRI. Neuroimage 27(3):553–563

Mosher JC, Leahy RM (1998) Recursive MUSIC: a framework for EEG and MEG source localization. IEEE Trans Biomed Eng 45(11):1342–1355

Mosher JC, Leahy R, Lewis P (1999) EEG and MEG: forward solutions for inverse methods. IEEE Trans Biomed Eng 46(3):245–259

Mulert C, Menzinger E, Leicht G, Pogarell O, Hegerl U (2005) Evidence for a close relationship between conscious effort and anterior cingulate cortex activity. Int J Psychophysiol 56:65–80

Nunez PL, Srinivasan R (2006) Electric fields of the brain. The neurophysics of EEG, 2nd edn. Oxford University Press, Oxford

Ostwald D, Porcaro C, Bagshaw AP (2011) Voxel-wise information theoretic EEG-fMRI feature integration. Neuroimage 55(3):1270–1286

Pascual-Marqui R (2002) Standardized low resolution brain electromagnetic tomography (sLORETA): technical details. Methods Find Exp Clin Pharmacol 24D:5–12

Pascual-Marqui R, Michel C, Lehman D (1994) Low resolution electromagnetic tomography: a new method for localizing electrical activity in the brain. Int J Psychophysiol 18:49–65

Riecke L, Esposito F, Bonte M, Formisano E (2009) Hearing illusory sounds in noise: the timing of sensory-perceptual transformations in auditory cortex. Neuron 64(4):550–561

Riecke L, Vanbussel M, Hausfeld L, Başkent D, Formisano E, Esposito F (2012) Hearing an illusory vowel in noise: suppression of auditory cortical activity. J Neurosci 32(23):8024–8034

Rosa MJ, Daunizeau J, Friston KJ (2010) EEG-fMRI integration: a critical review of biophysical modeling and data analysis approaches. J Integr Neurosci 9:453–476

Sarvas J (1985) Basic mathematical and electromagnetic concepts of the biomagnetic inverse problem. Phys Med Biol 32:11–22

Scheeringa R, Fries P, Petersson KM, Oostenveld R, Grothe I, Norris DG, Hagoort P, Bastiaansen MC (2011) Neuronal dynamics underlying high- and low-frequency EEG oscillations contribute independently to the human BOLD signal. Neuron 69(3):572–583

Scherg M (1990) Fundamentals of dipole source potential analysis. Adv Audiol 6:40–69

Singer N, Podlipsky I, Esposito F, Okon-Singer H, Andelman F, Kipervasser S, Neufeld MY, Goebel R, Fried I, Hendler T (2014) Distinct iEEG activity patterns in temporal-limbic and prefrontal sites induced by emotional intentionality. Cortex 60:121–138

Tikhonov A, Arsenin V (1977) Solutions to ill-posed problems. Wiley, New York

van Veen B, van Drongelen W, Yuchtman M, Suzuki A (1997) Localization of brain electrical activity via linearly constrained minimum variance spatial filtering. IEEE Trans Biomed Eng 44(9):867–880

Walz JM, Goldman RI, Carapezza M, Muraskin J, Brown TR, Sajda P (2014) Simultaneous EEG-fMRI reveals a temporal cascade of task-related and default-mode activations during a simple target detection task. Neuroimage 102:229–239

Wibral M, Turi G, Linden DE, Kaiser J, Bledowski C (2008) Decomposition of working memory-related scalp ERPs: crossvalidation of fMRI-constrained source analysis and ICA. Int J Psychophysiol 67(3):200–211

Part II

Technical and Methodological Aspects of Combined EEG-fMRI Experiments

EEG Instrumentation and Safety in the MRI Environment

7

Hassan B. Hawsawi, Philip J. Allen, Tracy Warbrick, Robert Störmer, Giannarita Iannotti, Frederic Grouiller, Serge Vulliemoz, and Louis Lemieux

Abbreviations

AC	Alternating current
DC	Direct current
ECG	Electrocardiogram
EEG	Electroencephalography

H. B. Hawsawi
UCL Queen Square Institute of Neurology, UCL, London, UK

MRI Unit, Epilepsy Society, Buckinghamshire, UK

Administration of Medical Physics, King Abdullah Medical City (KAMC), Makkah, Saudi Arabia
e-mail: hassan.hawsawi.15@ucl.ac.uk

P. J. Allen
Department of Clinical Neurophysiology, The National Hospital for Neurology and Neurosurgery, Queen Square, London, UK
e-mail: philip.allen@imperial.ac.uk

T. Warbrick · R. Störmer
Brain Products, GmbH, Gilching, Germany
e-mail: Tracy.Warbrick@brainproducts.com; Robert.Stoermer@brainproducts.com

G. Iannotti · F. Grouiller · S. Vulliemoz
EEG and Epilepsy Unit, Neurology, University Hospitals of Geneva, Geneva, Switzerland
e-mail: Giannina.Iannotti@unige.ch; Frederic.Grouiller@hcuge.ch; Serge.Vulliemoz@hcuge.ch

L. Lemieux (✉)
UCL Queen Square Institute of Neurology, UCL, London, UK

MRI Unit, Epilepsy Society, Buckinghamshire, UK
e-mail: louis.lemieux@ucl.ac.uk

C. Mulert, L. Lemieux (eds.), *EEG - fMRI*,
https://doi.org/10.1007/978-3-031-07121-8_7

emf	Electromotive force
EMG	Electromyography
EPI	Echo planar imaging
fMRI	Functional magnetic resonance imaging
MR	Magnetic resonance
MRI	Magnetic resonance imaging
RF	Radiofrequency
rms	Root mean square
SAR	Specific absorption rate

7.1 Introduction

The successful combination of electroencephalography (EEG) and fMRI demands careful consideration of three important issues: patient safety, EEG quality and image quality. In this chapter we first consider the implications these factors have for the design of EEG instrumentation, with emphasis on safety and EEG quality considerations, and then examine the precautions that must be taken to perform EEG recordings in the MR environment with acceptable additional risk for the subjects.

7.2 EEG Instrumentation

EEG instrumentation comprises electrodes and an acquisition system to amplify and digitise the EEG signals and reviews facilities for the display and analysis of the recorded waveforms. The design of EEG instrumentation appropriate for use in the magnetic resonance (MR) scanner must take into account a number of factors that are not applicable to conventional EEG equipment: the obvious requirement to avoid the introduction of ferrous materials into the scanner environment, the need to limit radiofrequency (RF) emissions to preserve image quality and most importantly the presence of static and time-varying magnetic fields and their associated EEG artefacts. These considerations dictate that EEG monitoring equipment used for diagnostic recordings in a clinical setting are not suitable for EEG–fMRI monitoring. In this section, we examine the influence exerted by the above factors on the design of EEG instrumentation. We start at the beginning of the EEG signal chain with a consideration of the electrodes and finish with the amplification and digitisation hardware. EEG artefact post-processing correction methods are discussed in detail in Chaps. 8 and 9. While it is mentioned briefly in this chapter, particularly in relation to its implications on EEG equipment design, the issue of MR image quality in the presence of EEG recording equipment is covered in Chap. 10.

7.2.1 Electrodes

The term EEG electrode is used here to describe the combination of the electrode head and connecting lead. In addition to the EEG quality issues discussed in this section, EEG electrodes also raise safety issues when used in the MR scanner; these will be discussed in Sect. 7.3 of this chapter. See Mullinger et al. 2008a for an overview of the image quality issues linked specifically to the presence of EEG electrodes in the MR scanner.

7.2.1.1 Electrode Materials

EEG electrodes are made in different types depending on the location of recording: (1) scalp EEG electrodes, which are placed in the external parts of the scalp, are made of gold, Ag/AgCl, stainless steel or plastic, with wires made of copper. Other newly developed materials were used for experimental testing such as water salt net that covers Ag/AgCl electrodes and Ink-Net (Poulsen et al. 2016). (2) Invasive intracranial EEG electrodes that are placed or implanted inside the brain are made of platinum–iridium, steel or platinum attached with nichrome wires.

7.2.1.2 Electrode Lead Arrangement

The electromotive force (emf) induced in a conductive loop is proportional to the rate of change of magnetic flux cutting the loop and the loop area:

$$V_{\text{induced}} = A \times \frac{\mathrm{d}B}{\mathrm{d}t}, \tag{7.1}$$

where

V_{induced} = emf induced in the loop.

A = loop area perpendicular to the field.

$\frac{\mathrm{d}B}{\mathrm{d}t}$ = rate of change of magnetic flux cutting the loop.

Hence, it is important to minimise the area of any loop formed by the electrode leads in order to reduce signal artefacts induced by the changing magnetic fields. A number of methods to achieve this have been reported (Goldman et al. 2000; Anami et al. 2003; Hoffmann et al. 2000; Negishi et al. 2004; Vasios et al. 2006); in essence, these involve bunching electrode leads together at a single point on the head and then further minimising the loop area, typically by twisting the wires together as far as possible along their entire path from the subject's head to the amplifier inputs. This not only keeps the leads in close proximity to each other but also results in the cancellation of the induced emfs in adjacent twists. Nevertheless, EEG is recorded between separate points on the head, and hence some loop area is inevitable. Goldman et al. proposed minimising this by

Fig. 7.1 Example of commercial EEG–fMRI instrumentation showing (**a**) electrode cap, (**b**) connector box containing current-limiting resistors, (**c**) battery power pack and (**d**) 32-channel EEG amplifier/digitiser. This instrumentation is sited adjacent to the scanner bore and transmits data to a receiver outside the Faraday shield via fibre optic links

recording from a chain of linked bipolar pairs connected to individual differential amplifiers (Goldman et al. 2000). Although this can present a smaller loop than encountered in common reference recordings, it is more restrictive in terms of electrode placement, particularly when the number of channels is large. More common is the use of electrode caps, which combine the advantage of multichannel referential recordings with relatively low loop areas (Baumann and Noll 1999; Bonmassar et al. 1999; Srivastava et al. 2005; Laufs et al. 2003; Iannetti et al. 2002) (Fig. 7.1). Chowdhury et al. studied the two types of electrode cables (ribbon and twisted) and determined that gradient artefact can be larger when using the ribbon cables (Chowdhury et al. 2015).

Although some groups have advocated shielding of the electrode leads (Hoffmann et al. 2000) and electrodes (Anami et al. 2003), presumably to reduce artefacts caused by electrostatic coupling to electric field sources in the scanner, a quantitative assessment of the benefit of this technique has not yet been reported. In addition, reducing the length of the EEG cable to 12 cm long can minimise the environmental artefacts to 84% at 7 T MRI scanners (Jorge et al. 2015). Minimisation of loop area is also important to ensure patient safety; this will be addressed in Sect. 7.3 of this chapter.

7.2.1.3 Electrode Lead Movement

EEG artefacts are induced not only by changing magnetic fields cutting a static loop but also by variation in loop area in the static field. Such variation can result from

the movement of the electrode leads caused by cardiac pulsation (Debener et al. 2007; Allen et al. 1998), small head movements (Hill et al. 1995) and scanner vibration (Garreffa et al. 2004). A variety of methods have been used to minimise these artefacts, such as weighing down the electrode leads where they pass out of the scanner using sand bags (Benar et al. 2003), placing padding under the leads and amplifier (Hoffmann et al. 2000), placing a tight bandage over the patient's head to secure individual electrode leads (Benar et al. 2003) or the use of an electrode cap (Kruggel et al. 2000). There is a general agreement that such fixation methods can reduce artefacts significantly.

Another important factor in reducing electrode lead movements (although not strictly part of the EEG instrumentation) is the reduction of patient head movement. Such immobilisation has been achieved using a vacuum cushion filled with polystyrene spheres (Benar et al. 2003; Anami et al. 2003). This method has been reported to be effective and well tolerated, the latter being an important factor in prolonged EEG–fMRI experiments, since any patient discomfort is likely to provoke gross movement, with its associated artefacts in both the EEG and magnetic resonance imaging (MRI) data.

In a comparison of three different methods for reducing lead and head movement (weighing down the leads, electrodes secured by a tight bandage, head fixed by vacuum cushion), Benar et al. found that the former was the most important and the vacuum cushion the least (Benar et al. 2003). It is interesting to note, however, that whereas artefacts in the range 30–50 μV were observed for the subjects in this study, Kruggel et al. observed artefact of up to 500 μV using a broadly comparable arrangement (stretchable cap, twisted leads weighed down with rice bags, head restrained by cushions) (Kruggel et al. 2000). This tenfold difference (which cannot be attributed entirely to the different scanner fields in these studies, of 1.5 and 3 T, respectively) suggests that these artefact minimisation techniques are very sensitive, and hence local experimentation may be necessary to find the optimal arrangement.

Another method to reduce EEG artefacts in MR-compatible EEG caps 256-EGI with the wires attached in the front of the MR scanner is to place the electrode wires under the spine of the patient. Indeed, even though previous studies did not report the effectiveness of this EEG artefact reduction method, at least one manufacturer of MR-compatible EEG caps (Electrical Geodesics, Inc., Oregon, USA) recommends the use of this procedure.

7.2.2 EEG Recording System

The EEG recorded in the MR scanner is contaminated by two different sources of interference that do not afflict EEG recordings. The first is often referred to as pulse artefact (or ballistocardiogram, BCG, although it may not be entirely of ballistic origin) which is caused by multiple factors associated with the cardiac cycle, such as pulse-related movement of the electrodes or blood flow in the static field. It is typically 10–100 μV in amplitude and overlaps the EEG frequency range (Allen

et al. 1998). A variety of techniques have been developed to reduce these artefacts (Allen et al. 1998; Goldman et al. 2000; Bonmassar et al. 2002; Benar et al. 2003); these make no additional demands on the EEG instrumentation above those required for conventional clinical EEG. Other studies make use of electrocardiogram (ECG) signals (Allen et al. 1998; Niazy et al. 2005; Iannotti et al. 2015) and the motion of the head that partially contains the pulse artefact to reduce these pulse artefacts (Jorge et al. 2015).

The second source of interference is often referred to as imaging (or sometimes gradient) artefact and represents the emfs induced in the electrode lead loops by the changing magnetic fields applied during imaging. It has two distinct components, attributable to the gradient and RF fields, respectively. The former range in frequency from the slice repetition interval (typically 10–20 Hz) up to the kHz range. The RF fields have a fundamental component at the Larmor frequency of the scanner, ranging from 63 MHz for 1.5 T up to 300 MHz for 7 T, but also lower-frequency components reflecting the rate at which the RF is pulsed (Hoffmann et al. 2000) and the pulse shape. In contrast to pulse artefact, imaging artefact is normally significantly larger in amplitude than the EEG, often obscuring the waveforms completely (Allen et al. 2000). In the early days of this technique, the EEG and fMRI acquisitions were interleaved in time. In studies of epilepsy, this was typically achieved by triggering fMRI acquisition immediately after observing an epileptiform spike in the EEG (Warach et al. 1996; Seeck et al. 1998). It was accepted that the EEG recording during the image acquisition would be obscured. Subsequent developments in artefact subtraction methods have now made truly simultaneous EEG and fMRI recording routine. Although this makes greater demands on the EEG instrumentation, particularly with regard to filtering, sampling rate and dynamic range, it offers much greater freedom in experimental design and is now accepted as an essential requirement.

7.2.2.1 Filters

As RF artefacts occur at a frequency of many orders of magnitude higher than those of EEG, they can be reduced to an acceptable level by low-pass filtering with a −3 dB cut-off point that is substantially higher than the EEG bandwidth. For example, Anami et al. demonstrated that a 3000 Hz cut-off low-pass filter reduced the RF artefact to below 100 μV, substantially less than that of the gradient artefact (Anami et al. 2003) (Fig. 7.2). This filtering should, however, be implemented at the front end of the instrumentation to avoid possible demodulation of the RF into the EEG frequency range due to nonlinearities in subsequent active amplifier stages. Gradient artefacts, in contrast, overlap the EEG spectrum and hence cannot be removed by low-pass filtering alone. Nevertheless, analogue low-pass filtering prior to the main gain stage in the EEG amplifier is normally essential to prevent saturation by the high-amplitude gradient artefact. In order to maximise the attenuation of these artefacts, the cut-off frequency of this filter should be set as low as possible consistent with the recommended EEG bandwidth, typically 70 Hz (Deuschl and Eisen 1999). Attenuation of gradient artefact

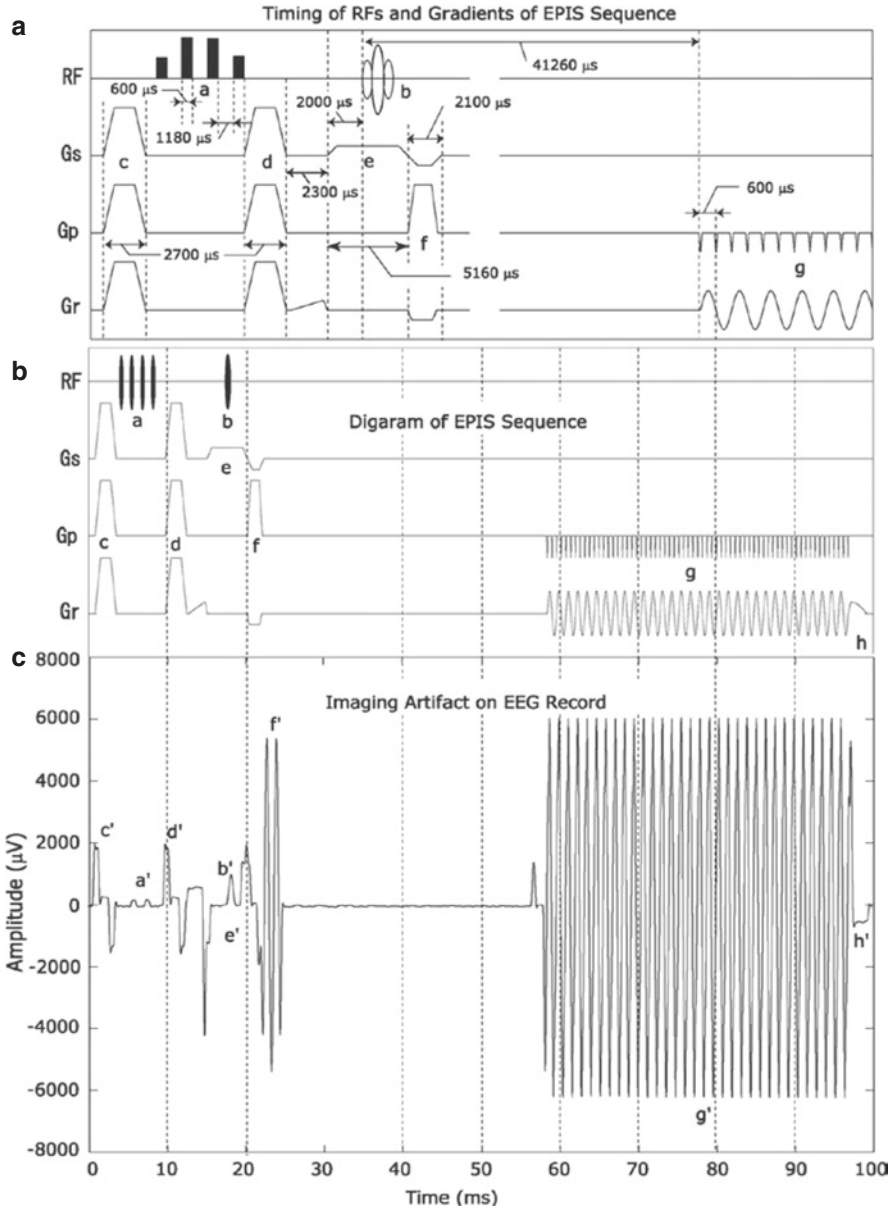

Fig. 7.2 (**a**) Timings of RF emission and gradient pulses in an fMRI sequence (EPIS, Siemens: ep2d_fid_60b2080_62_64.ekc). *RF* radiofrequency wave, *Gs* slice selection gradient, *Gp* phase encoding gradient, *Gr* readout gradient. *a*, fat suppression pulses (1–3–3–1 pulses); *b*, slice selection RF; *c*, *d*, *h*, spoilers; *e*, slice selection gradient; *f*, dephasing and rephrasing gradient; *g*, readout gradient. (**b**) Schematic diagram of whole EPIS sequence. (**c**) Imaging artefact waveform for one slice scan on a dummy EEG record with a phantom using the EPIS sequence. The artefact corresponding to each gradient component described above in (**a**) can be identified and is denoted by the same alphabet as that denoting the original gradient but with a prime. From Anami et al. (2003)

can be improved by using a higher-order (three or greater) analogue low-pass filter with a steeper roll-off. However, this comes at the expense of poorer phase-frequency linearity, which may result in distortion of EEG transients (Janssen et al. 1986) and hence should be avoided.

7.2.2.2 Sampling Rate

Given that low-pass filtering alone cannot remove all of the imaging artefacts, a variety of post-processing artefact subtraction methods have been developed. The artefact removal method most commonly used to date is based on the subtraction of an artefact template derived from averaging the artefact over a number of scan repetitions (Allen et al. 2000). Successful artefact subtraction by this method (and many of its subsequent enhancements; see, for example, Negishi et al. 2004; Benar et al. 2003) is dependent on accurate calculation of the artefact template. As the imaging artefact contains rapidly changing components, a fast sampling rate (typically 5 kHz) is required in order to capture these signals adequately (Allen et al. 2000). This is ten times higher than the rate used in conventional EEG equipment. Even at this high sampling rate, temporal jitter in the EEG sampling can lead to inaccuracies in the artefact template estimation that limit the effectiveness of this method (Cohen et al. 2001). Although technically feasible, increasing the sampling rate further results in very large datasets, especially for prolonged recordings using a large number of channels. Hence, an alternative approach has been proposed whereby the EEG sampling is synchronised to the MR scanner clock (Cohen et al. 2001). Mandelkow et al. demonstrated that this method can reduce the residual artefact, particularly the higher-frequency EEG components, and achieves good artefact reduction even when using a conventional EEG sampling rate of 500 Hz (Mandelkow et al. 2006). It is worth noting, however, that the EEG in this study was originally sampled at 5 kHz and then down-sampled to 500 Hz after the application of a seventh-order digital filter, an important step for preventing aliasing. As the authors comment, the application of such a high-order filter implemented in hardware prior to digitising at 500 Hz would inevitably distort the EEG due to its non-linear phase response. Nevertheless, the method holds a great promise for improving artefact suppression, particularly when there is a requirement to analyse higher-frequency EEG components such as the gamma bands. It therefore follows that the facility to synchronise the EEG sampling rate precisely to an external clock is a useful addition to the EEG instrumentation specification. This synchronisation also requires hardware to reduce the scanner clock to the EEG sampling rate (10 MHz to 5 kHz in the report by Mandelkow and up to 8 kHz for the EGI system (Electrical Geodesics 2010)), but this can be achieved independently of the EEG instrumentation, for example, by phase-locked loop circuitry (Mandelkow et al. 2006) or a clock divider.

7.2.2.3 Signal Range

The amplitude of gradient imaging artefact in the EEG is proportional to the loop area and the rate of change of magnetic flux cutting the loop, as described in Eq. (7.1). Allen et al. calculated that for a relatively high slew rate of 125 T m^{-1} s^{-1} and

a worst-case EEG lead loop area of 100 cm^2 located 0.2 m from the scanner isocentre, the induced artefact due to gradient fields is ±250 mV (Allen et al. 2000), more than two orders of magnitude greater than the recommended range (±1 mV) for conventional EEG equipment (Nuwer et al. 1999). In practice, careful alignment of electrode leads can help reduce the artefact amplitude substantially. Anami et al. recorded imaging artefact from electrodes on a phantom in a 1.5 T scanner using a typical blipped echo planar imaging (EPI) sequence (see Chap. 8), wide bandwidth [direct current (DC) to 3000 Hz] and 20 kHz sampling (Anami et al. 2003). This revealed a substantially lower maximum gradient artefact of 40 mV (Fig. 7.2). However, the use of faster slew rates or the acquisition of different physiological parameters such as electrocardiogram (ECG) and electromyography (EMG), which may necessarily involve larger loop areas, would result in proportionally larger artefact. It is therefore still important that the EEG instrumentation has sufficient range throughout the entire signal path to record these signals without saturating—if the artefact saturates, then the underlying physiological signal will be lost. It is important to note that saturation is not always obvious by inspection of the recorded EEG signal, due to the effect on the waveform of subsequent circuit stages such as alternating current (AC) coupling and additional high- and low-pass filters. The following factors need consideration when assessing whether EEG instrumentation has sufficient range: the amplitude and spectral distribution of the imaging artefact, the frequency response and location in the overall system of the analogue low-pass filters and the signal range at each stage of the EEG instrumentation. For example, Allen et al. described an EEG amplifier with an overall dynamic range in the passband of 33.3 mV, which, through the judicious use of gain and filter stages, could handle artefact of ±250 mV pk–pk at source without saturating (Allen et al. 2000).

7.2.2.4 Signal Resolution

In addition to providing sufficient signal range, the EEG instrumentation must also have adequate resolution. The minimum recommended resolution for conventional EEG equipment is 0.5 μV (Nuwer et al. 1999). Given the need for a large signal range of the order 20–30 mV as described above, this resolution would require 16 bits, which in practice requires a digitiser with more than 16 bits. However, given that the residual artefact from current pulse- and imaging-artefact subtraction methods is at least 5 μV (Allen et al. 2000) and that this error occurs independent of digitisation errors, 16-bit digitisation yields 14–15 effective bits, and hence a resolution of 1–2 μV is adequate. As artefact subtraction methods improve, greater bit depth may be justified, especially when recording lower-amplitude EEG activity such as event-related potentials (ERPs). The dynamic range can, however, be increased for these by averaging, albeit at the expense of longer recording time.

7.2.3 RF Emissions

The MRI scanner contains an extremely sensitive RF detector. Any RF emissions from the EEG instrumentation may lead to artefacts in the MR images if they fall in

the frequency range detected by the scanner. Potential sources of these emissions are active circuitry in EEG instrumentation located in the scanner room or the ingress of RF signals via conductors that breach the scanner's Faraday shield. For the former, careful design is required to minimise RF emissions, as even relatively low-frequency digital circuitry can generate signals in the RF range due to the presence of harmonics. These may pass into the head coil by conduction along the electrode leads or by radiation through space. A number of techniques can be used to minimise this interference: RF signals should be minimised at source by using low-power digital components, thereby minimising switching currents; all active circuitry should be enclosed in a conductive enclosure (Allen et al. 2000; Gualniera et al. 2004; Garreffa et al. 2004); and all conductive signal paths (e.g. connections to EEG electrodes and external battery packs) breaching this enclosure should do so via in-line RF filters (Fig. 7.3). Where active EEG instrumentation is located in the scanner room, EEG data is normally transmitted to a receiver in the console room via fibre optic cables, thereby eliminating the ingress of RF from outside the scanner (Figs. 7.1 and 7.2). This approach has been implemented in a number of commercial products.

Alternatively, the EEG instrumentation can be sited in the console room, with connection to the subject made via long electrode leads which pass through the Faraday shield (Huang-Hellinger et al. 1995; Anami et al. 2003). If the impedance of these leads is low, RF filtering must be applied at the point where the electrode leads breach the Faraday shield (Huang-Hellinger et al. 1995). Careful consideration must also be given to the safety implications of using such long cable runs with direct electrical connection to the patient, especially with regard to the accidental application of external voltage sources to these cables.

As stated previously, RF emissions will only cause image artefacts if they fall in the frequency range detected by the scanner receive coil and within the receiver

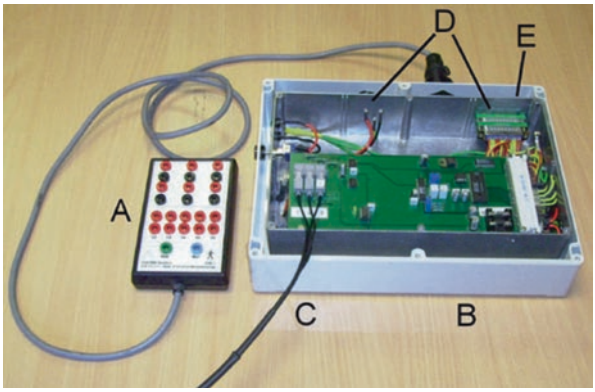

Fig. 7.3 Example of early in-house MRI-compatible EEG instrumentation developed in 2000 by the Queen Square group (Allen et al. 2000). (**a**), nonferrous electrode connector box suitable for mounting in the bore of the magnet; (**b**), EEG amplifier and digitiser; (**c**), fibre optic cables transmitting digitised EEG data to a receiver unit outside the scanner room; (**d**), in-line RF filters fitted to all signal lines breaching the shielded enclosure; (**e**), shielded enclosure limiting RF emissions

bandwidth used for the imaging experiment, which occupies a narrow range either side of the Larmor frequency. Hence, it is perfectly possible that EEG instrumentation that does not generate image artefact when used with one scanner may cause interference in another (Jorge et al. 2015). Hence, an empirical test of image artefact should be undertaken prior to introducing new EEG instrumentation.

7.2.4 Miscellaneous Factors

In addition to the essential characteristics described above for high-quality EEG recording in the MR scanner, EEG equipment should broadly meet the requirements for conventional EEG. The key parameters are as follows: maximum noise at input of 1.5 μV pk–pk, bandwidth 0.16–70 Hz, input impedance ≥100 MΩ and common mode rejection ≥110 dB (Nuwer et al. 1999). A DC input range of ±300 mV is sufficient to handle the likely range of electrode potentials (Kamp and Lopes Da Silva 1998). Built-in electrode impedance checking and a 50/60 Hz notch filter are desirable. Furthermore, for some additional noise that are caused by other equipment inside the MR environment, it is recommended to handle this issue offline rather than recording the EEG with a notch filter. Finally, the EEG review facilities should not be overlooked. Although the conventional requirements such as re-montaging flexible sensitivity and time base must obviously be provided, one specific additional requirement for EEG–fMRI instrumentation is the facility to correlate (e.g. mark and export) specific EEG events the corresponding fMRI data simply and accurately.

7.2.5 Summary

The first reported recording of EEG during fMRI (Ives et al. 1993) has led to the commercial development of EEG instrumentation designed specifically to meet many of the technical requirements described above, further extending the availability of the technique. Although further improvements in artefact minimisation would be desirable to record lower-amplitude activity such as ERPs or fast gamma activity, an EEG quality appropriate for studies of epilepsy and basic EEG rhythms can readily be achieved. However, it remains essential to pay careful attention to the entire recording setup comprising the subject, electrodes and EEG recording system in order to achieve optimal EEG signal quality. This will become even more important as higher-field scanners and studies of subtler EEG activity become increasingly common.

7.3 Safety

Recording EEG in the MR scanner raises important safety issues. First, there is the hazard associated with the introduction of ferromagnetic materials into the scanner environment. Secondly, currents induced in the electrodes and attached wires by the changing fields applied during imaging can present a hazard due to the following

mechanisms: eddy current heating of the electrode heads, currents induced in loops formed between the electrode leads and currents induced along electrode leads. The safety implications of induced currents are determined by the scanner's operating frequency, and therefore static field strength, with different biological mechanisms for damage for the gradient- and RF-related fields. We begin by considering the relevant safety limits before moving on to a more detailed examination of each specific hazard.

7.3.1 Safety Limits

In the absence of a safety standard specifically addressing combined EEG–fMRI, the onus has been on users of this technique to demonstrate compliance with the standards applicable individually to MR and EEG equipment. Hence, the following safety limits derived from these standards apply: (1) maximum permissible cerebral temperature of 38 °C, implying a maximum temperature increase due to scanner-induced heating of 1 °C (IEC 2016); (2) maximum permissible temperature of an applied part in skin contact (such as an electrode) of 43 °C (IEC 2016); (3) maximum permissible head average SAR of 3.2 W/Kg for 6 min scan duration (IEC 2016) or 3 W/kg for 5 min (Shellock 2004); (4) maximum permissible local SAR for the head of 10 W/kg averaged over 10 g of tissues (IEC 2016) or 8 W/kg averaged over 1 g of tissues (Shellock 2004); and (5) maximum permissible tissue contact currents ranging from 0.5 mA rms ($\approx$1 kHz) to 10 mA rms > 100 kHz (IEC 2016).

In addition, EEG instrumentation must meet the safety requirements for general medical electrical equipment (IEC 2016) and the particular standard for EEG equipment (IEC 2016).

7.3.2 Static Field

The principal safety issue associated with the static field is the force it exerts on ferromagnetic material. Fortunately, this is not a significant limitation since there are a range of nonferromagnetic materials that meet the requirements for high-quality EEG. These include combinations of silver, silver chloride, gold, carbon and conductive plastic for scalp recordings and iridium–platinum for intracerebral recordings. However, care should be taken to exclude the presence of ferromagnetic material in ancillary items, such as securing springs in electrode caps or amplifier connectors. Stainless steel sphenoidal electrodes are clearly unacceptable.

Any new instrumentation or device introduced into the scanner must also be tested for displacement force and torque that can cause hazards due to the "projectile effect" (Baumann and Noll 1999; Woods 2007; Nyenhuis 2003; Nyenhuis et al. 2005; Carmichael et al. 2010; Dal Molin and Hecker 2013), including for devices placed inside patients (implants; ISO 2012). In addition, it should be noted that any electronic components dependent on ferromagnetic behaviour (such as some switching DC–DC converters, ferrites) may not function when placed in close proximity

to the static field. Furthermore, electrical device safety must be considered inside and outside the MRI environment.

One further potential hazard is the current induced in an electrode lead loop moved through the nonuniform region of the static field, for example, when the patient is introduced into the scanner. This current will flow between electrodes and hence through the patient. Lemieux et al. investigated this at 1.5 T and identified that the effect was very small and hence no additional safety measures were required (Lemieux et al. 1997), which was also investigated in two 3 T MRI scanners (Carmichael et al. 2010).

7.3.3 Gradient Fields

The emf induced in an electrode lead loop by the gradient fields is proportional to the rate of change of magnetic flux cutting the loop and the loop area, as defined in Eq. (7.1). As the frequency of these fields typically does not extend much higher than 1 kHz, the dominant physiological effect is neuromuscular stimulation (Cohen et al. 1990; Schaefer et al. 2000; Georgi et al. 2004; Rezai et al. 2005; Bencsik et al. 2007). Lemieux et al. calculated that for a relatively high slew rate of 120 T m^{-1} s^{-1} and a worst case loop area of 400 cm^2, loop resistance must be at least 3.3 kΩ in order to meet the safe limit of 0.5 mA rms under a single fault condition, namely, the electrode leads accidentally shorting together (Lemieux et al. 1997). As a much higher value of current-limiting resistor is normally required to limit heating due to RF-induced currents, this does not present an additional constraint. Indeed, the inevitable tissue contact impedance presented at each electrode (of the order of 1 kΩ), combined with careful electrode lead arrangement to reduce the loop area below the pessimistic 400 cm^2, means that the current limit requirements can feasibly be met even if a current-limiting resistor is omitted. However, this would need further consideration if substantially higher slew rates were used or loop area was increased, for example, by recording from very widely spaced possibly noncephalic electrodes.

It is important to mention that heating can be caused by the switching gradient field (this can be calculated using Faraday's law) depending on the geometry of the object and the type of the metallic implant that interact with the gradient field (Graf et al. 2007; Lemieux et al. 1997). However, in case of EEG electrodes, the effect of the gradient fields on heating increases is small (Lemieux et al. 1997; Carmichael et al. 2010; Hawsawi et al. 2017).

7.3.4 Eddy Currents

The RF fields applied during scanning induce eddy currents in the electrodes (Lemieux et al. 1997). These currents are much greater than those induced in human tissue, due to the relatively higher electrical conductivity of the electrode material, and may result in Joule heating of the electrode (Roth et al. 1992). Previous studies

showed the effects of large electrical currents that cause skin burns in the application of diathermy (Aigner et al. 1997; Dempsey et al. 2001; Litvak et al. 2002; Hay 2005; Hawsawi et al. 2017). Lemieux et al. investigated eddy current heating of a silver/silver chloride electrode in a 1.5 T scanner [averaged specific absorption rate (SAR) 0.06 W/kg] and found a maximum temperature increase of <1 °C, comfortably within the permitted limit (Lemieux et al. 1997). Similar results have been found at higher field strengths: Mirsattari et al. found no temperature rise in a gold-plated pure silver electrode in a 1.5 T scanner (averaged SAR up to 1.6 W/kg) (Mirsattari et al. 2004); Stevens et al. found no significant heat increase in the same electrode or in a silver/silver chloride in carbon embedded plastic electrode at 4 T with a high-power pulse sequence (8 W average per TR) (Stevens et al. 2007).

There is, however, evidence that eddy current heating may prove more significant at 7 T: Vasios et al. recorded a 2.2 °C rise in a full-ring electrode following 22 min of high-power turbo spin echo (TSE) with a maximum local SAR of 11 W/kg (Vasios et al. 2006), a power level just above the maximum SAR limit (IEC 2016). Although this heating may not be due entirely to eddy currents (the temperature increase was recorded from a 32-electrode configuration and hence would include heating effects from currents induced in the associated conducting loops and elongated conductors), these clearly made a significant contribution since the temperature rise for the same configuration was reduced to 0.8 °C when the full-ring electrodes were replaced with half rings designed specifically to reduce eddy currents.

In summary, these experimental investigations indicate that at field strengths of 4 T or less, electrode heating due to eddy currents does not appear to pose a risk to patients. Above 4 T, more specialised electrode design and/or SAR limits may be required. See Chap. 11 for further discussion.

7.3.5 RF Fields

The dominant physiological effect of induced high-frequency currents (>100 kHz) is tissue heating. The interaction between the scanner's RF (B_1) field and electrode leads can result in heating via two related mechanisms. Firstly, the magnetic component of the B_1 field will induce an emf in any conductive loop formed by the electrode leads. This emf is proportional to the loop area cut by the field and the rate of change of the field (7.1). If tissue forms part of the loop, the induced emf will drive a current through this, causing heating. It is worth noting that in contrast to gradient field-induced currents, the capacitance between bundled electrode leads presents relatively low-impedance conductive loops at RF frequencies, even if the leads are not accidentally shorted together, i.e. the non-fault condition (Lemieux et al. 1997). Secondly, the electric component of the B_1 field can induce a current along the extended conductor formed by an electrode lead (the antenna effect). The magnitude of this current is influenced by a wide range of factors, including the proximity of the wires to the source of electric field in the MR transmitter coil (Hofman et al. 1996) and the resonant length of the electrode leads in relation to the

RF wavelength, with a theoretical maximum induced current for multiples of half wavelength (Pictet et al. 2000). As a broad guide, the resonant length of a straight wire in air is 2.35 m at 1.5 T and 1.17 m at 3 T (Dempsey et al. 2001), but this varies significantly according to the wire diameter, shape, insulation thickness and permittivity and tissue conductivity and permittivity (Yeung et al. 2002). Although it is known that the maximum temperature increase associated with these currents occurs in the tissue adjacent to the tip of a conductor, where the electric field is maximum (Yeung et al. 2002), accurate prediction of the associated temperature rise for a given scenario remains problematic and usually requires specific experimental testing. Both mechanisms for interaction of the electrodes and leads with the scanner RF fields are exacerbated by resonant conditions where the induction of much larger currents occurs (Dempsey et al. 2001); it is thus necessary to avoid these conditions.

In the first systematic study of safety due to RF heating of EEG electrodes in the MR scanner, Lemieux et al. investigated induced currents due to the electric and magnetic fields separately and concluded that the latter dominated and that a current-limiting resistor (12 kΩ) was required in the scalp electrode leads in order to limit contact currents to acceptable levels for a worst-case electrode lead loop (400 cm^2) and high SAR for a 1.5 T scanner (Lemieux et al. 1997). This additional resistance is small relative to the typical input impedance of an EEG amplifier (at least 10 MΩ) and hence does not degrade EEG signal quality significantly. This study was undertaken using a head RF transmit coil—the safety of EEG–fMRI for body RF coils has been investigated in several works that showed higher temperature levels and using body RF transmit coils should be avoided (Carmichael et al. 2008, 2010; Ciumas et al. 2013). These findings were in disagreement with Boucousis et al. (2012). The authors stressed the importance of performing a local risk assessment of the specific electrode and scanner setup using the methodology presented (Mirsattari et al. 2004; Hawsawi et al. 2017). Data supplied by the manufacturer on the relationship between B_1 and SAR for the quadrature transmit and receive head coil used in the GE Signa Excite 3 T scanner demonstrates that the RMS value of B_1 for a given SAR value (and body weight) is less than 50% of the value at 1.5 T, and therefore so will be the current induced in the EEG system–patient circuit, suggesting that the proposed safety measure is also adequate for this instrument, even taking into account the effect of the higher RF frequency.[1]

Our group has performed over 600 EEG–fMRI recordings at both 1.5 and 3 T using electrodes with current-limiting resistors without incident. Current-limiting resistors are included in a number of commercial electrodes and electrode caps designed for EEG–fMRI. Such studies have been performed at multiple centres worldwide over the last 19 years; as far as the author is aware, there have been no reports of adverse incidents resulting from these recording. However, a report showed skin burns around ECG electrode during the application of EEG–fMRI

[1] This corresponds to the fact that more heating is induced per unit B_1 at 3 T than at 1.5 T. The lower expected induced currents reflect the fact that the regulatory SAR limits are independent of field strength.

(Abdel-Rehim et al. 2014; Hawsawi et al. 2017). It has been proposed, on the basis of in vivo temperature measurements in a small number of subjects for a particular experimental setup, that additional resistors are not in fact necessary (Lazeyras et al. 2001) and the presence of these resistors may not be necessary at high fields such as 7 T (Angelone et al. 2006; see Hawsawi et al. 2017 for a review). However, their use does provide reassurance that even under worst-case conditions (including a single fault), the subject will not be harmed, with only a minimal associated increase in EEG noise.

An alternative approach to establishing the safety of RF/EEG electrode interactions is the measurement of temperature changes during the scanning of electrodes attached to a head phantom. This method has been used extensively in the safety assessment of implants in the MR scanner (Nyenhuis et al. 1999; Shellcok 2001; Carmichael et al. 2007a, 2008, 2010, 2012; Baker et al. 2004; Yeung et al. 2002; Gray et al. 2005; Boucousis et al. 2012; Ciumas et al. 2013; Hefft et al. 2013; Ahmadi et al. 2016; Darcey et al. 2016; Bhattacharyya et al. 2017; Shew et al. 2018) and more recently for EEG electrodes (Vasios et al. 2006; Angelone et al. 2006; Vanhatalo et al. 2014; Poulsen et al. 2016; Balasubramanian et al. 2017; Foged et al. 2017). The reliability of the temperature changes recorded using this approach is of course strongly influenced by the accuracy of the physical model and also the position and orientation of the temperature recording probe relative to the electrode or implant (Park et al. 2003; Mattei et al. 2006). In particular, the head phantom must have realistic geometric, thermal and electrical properties (Angelone et al. 2006; Rezai et al. 2002; Park et al. 2003). Although the absence of thermoregulation, which naturally operates in the living body through the blood flow (Athey 1989; Gokul et al. 2013; Acharya et al. 2014a, b), from the head models used to date is clearly an inaccuracy, this merely leads to a conservative estimate of the temperature increases expected in human studies (Akca et al. 2007). The electrode lead length is also important: Yeung et al. observed substantial differences in heating at the tip of a length of wire in response to small changes in its length (of the order of a few centimetres) (Yeung et al. 2002). Similarly, the proximity of conducting leads to the transmit coil (where the electric component of the RF field is maximal) can affect heating significantly (Dempsey et al. 2001; Georgi et al. 2004). It is also important to use electrode gel in order to accurately replicate the electrical contact between the phantom and electrode (Vasios et al. 2006). The precise location of a temperature probe in the electrode gel can also introduce significant measurement variability (Angelone et al. 2006). In summary, careful experimental technique combined with a knowledge of the wide range of factors that influence MR-induced heating is an essential prerequisite for a reliable safety assessment based on this methodology (Shellock 2007). Finally, it is important to note once again that measurements performed on one scanner are not transferable to other scanners and hence a local assessment combined with strict adherence to an experimental protocol is essential (Kainz 2007; Carmichael et al. 2007a).

One limitation of this empirical approach is the restricted spatial sampling that can be achieved with current MR-compatible thermometry (typically four sites).

This requires assumptions to be made regarding the location of the greatest temperature rise, which may be difficult to predict with certainty for a particular arrangement of electrode and leads in the scanner. One potential solution is to calculate temperature changes from a computational simulation of the electric field distribution resulting from the application of RF fields to a realistic head/electrode model. This approach allows the direct visualisation of the local SAR (and hence by application of the heat equation, the associated temperature changes; Collins et al. 2004) throughout the entire head volume, rather than just at selected sites (Angelone et al. 2004; Yeung et al. 2007; Jorge et al. 2015; Angelone et al. 2010a, b; Serano et al. 2015; Golestanirad et al. 2016a, b, 2017, 2019; Córcoles et al. 2017; Bhusal et al. 2018).

Angelone et al. have used this method to investigate RF heating of EEG electrodes at 7 T (Angelone et al. 2006). Electric field and SAR values were calculated using the finite difference time domain method applied to numerical models of the electrodes, leads, RF coil and anatomically accurate homogeneous head model. The simulated temperature changes were validated by comparison with those measured for an equivalent electrode/phantom head arrangement in the scanner, the two methods showing broad agreement in spatiotemporal distribution of temperature change. A maximum temperature rise inside the head of 3.4 °C (i.e. above the 1 °C safe limit) was identified for a high-power TSE sequence, indicating the need to limit SAR below the normal maximum permissible level (IEC 2016). Interestingly, the authors found minimal difference between the simulated SAR distributions for electrodes with and without a modelled current-limiting resistor. It is possible that at such high frequencies (300 MHz for 7 T), parasitic capacitance in the resistor reduces its impedance, thereby limiting its current-limiting capability. This suggests that discrete current-reducing resistors may not provide effective protection against SAR increases inside the head at 7 T, although their effect on contact currents, which might be expected to be maximal immediately adjacent to the electrodes (i.e. on the surface of the phantom), was less clear. Lower-temperature increases were recorded when using carbon leads, suggesting that distributed resistance in the electrode leads may be advantageous as assessed in 3 T (Kuusela et al. 2015) and 7 T MRI scanners (Mullinger et al. 2008b; Jorge et al. 2015). See Chap. 11 for further discussion of the specific issues related to high-field EEG–fMRI.

Carbon leads may also reduce magnetic susceptibility artefacts in the images (Van Genderingen et al. 1989; Van Audekerke et al. 2000). Although promising, the use of computational simulation to assess the safety of RF/EEG electrode interactions is relatively new: further validation is required before this technique can be used on its own to establish patient safety. Combining this computational method with temperature measurement in a comparable physical model may prove advantageous, with the former being used to identify the site of maximum heating and the latter to verify the temperature changes at the equivalent position in the physical model (Angelone et al. 2004, 2010a, b; Yeung et al. 2007; Jorge et al. 2015; Serano et al. 2015; Golestanirad et al. 2016a, b, 2017, 2019; Córcoles et al. 2017; Bhusal et al. 2018) following one of experimental standards such as ASTMF 2182-02a (2007).

Although many studies have recommended the use of SAR limits to ensure the safety of EEG–fMRI experiments (Angelone et al. 2004; Lemieux et al. 1997), such limits are both scanner- and RF coil-specific. Indeed, Baker et al. have demonstrated that the relationship between scanner-reported SAR and the associated heating of an implanted electrode can be highly variable, even between scanners of identical field strength from the same manufacturer (Baker et al. 2004; Carmichael et al. 2008, 2010). The differences in SAR calculations across MRI scanners were attributed to the different, manufacturer-specific, SAR estimation models that are not designed to account for the foreign objects that are introduced in the MRI environment (Carmichael et al. 2008). It is likely that this is also the case for scalp EEG electrodes, and hence it is important to recognise that a universal SAR limit calculated for a specific electrode set, although attractive in its simplicity, may not be reliable.

7.3.6 Implanted Electrodes

The above discussion of safety issues has only addressed scalp electrodes. Imaging for postsurgical localisation of intracranial electrodes (Carmichael et al. 2008; Davis et al. 1999; Erhardt et al. 2018) and the localisation of epileptic brain discharges and their networks are currently performed in a number of centres (Vulliemoz et al. 2011). In addition, deep brain stimulation (DBS) implants that are similar to intracranial implants in terms of geometry and manufacture have been utilised in patients for decades (Hawsawi et al. 2017). Retrospective examination of patients with implanted electrodes who underwent MR imaging indicates that the risks are generally low (Zhang et al. 1993; Davis et al. 1999; Brooks et al. 1992). More recently, a histopathology and heat-shock immunohistochemistry analysis of brain tissue obtained from patients who had undergone either structural MRI only with implanted electrodes, or structural MRI followed by fMRI with EEG recorded concurrently with implanted electrodes, showed no evidence of additional tissue damage in the vicinity of the electrodes related to exposure to MRI/fMRI (Liu et al.

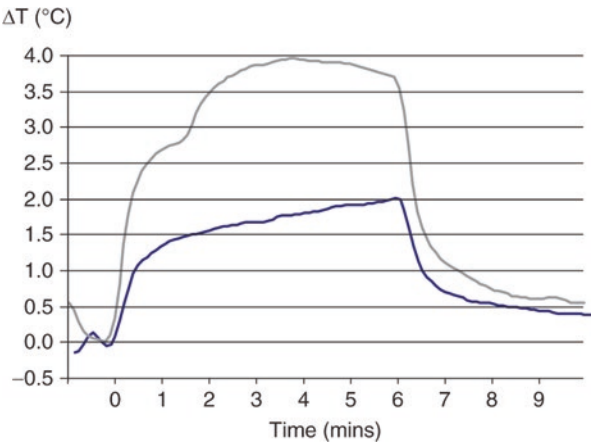

Fig. 7.4 Temperature increase with time for a subdural grid electrode contact, high SAR (2.4–2.5 W/kg). The *grey line* shows the temperature rise when all the electrode tails were in electrical contact, and the *blue line* when they were all separated

2022) In addition, a small number of studies have investigated the safety of imaging implanted electrodes and found no evidence of displacement force and RF heating beyond safe limits (Boucousis et al. 2005; Kanal et al. 1999). However, these studies only investigated single electrodes, whereas in practice these recordings involve multiple electrodes; no displacement or deflection issues were observed (Shellock 2001; Boucousis et al. 2012). More recently, Carmichael et al. measured RF heating for a combination of subdural strips and depth electrodes at 1.5 and 3 T (Carmichael et al. 2007b). This showed that, for high SAR (≈2.5 W/kg), the worst-case temperature increase only exceeded the 1 °C limit at 1.5 T when the electrode tails were shorted together (contrary to the manufacturer's recommendations); at 3 T the limit was exceeded even when the tails were isolated (Fig. 7.4). In addition, numerous studies were involved in the safety of DBS inside the MRI at 0.35 T (Gleason et al. 1992), at 1.5 T (Georgi et al. 2004; Rezai et al. 2002; Kainz et al. 2002; Finelli et al. 2002; Baker et al. 2004, 2005; Bhidayasiri et al. 2005; Carmichael et al. 2007a, b; Gorny et al. 2013; Kahan et al. 2015; Franceschi et al. 2016; Cabot et al. 2013), at 3 T and higher (Georgi et al. 2004; Rezai et al. 2002; Baker et al. 2005; Carmichael et al. 2007a, b; Gorny et al. 2013; Kahan et al. 2015; Shrivastava et al. 2010, 2012; Eryaman et al. 2011, 2013, 2019; Sammartino et al. 2016). Furthermore, implanted microelectrodes, which are utilised for single event or cellular EEG recording, were tested for the safety inside the MRI and showed temperature increases within the safety limit (Papadaki et al. 2016) despite the difficulty in estimating the focal temperature increases around these electrodes due to their small size. Clearly, a local investigation of temperature increases for a given specific electrode and lead length and arrangement, SAR, type of coil, type of scanner and pulse sequence, Scanner's field strength is essential in order to identify the safe SAR limit (Hawsawi et al. 2017).

The electrode's effective length (e.g. connected or disconnected from the amplification circuit, orientation and position relative to the RF coil and body have a strong influence on the amount of heating in surrounding tissues (Yeung et al. 2007; Assecondi et al. 2016).

7.3.7 Summary

RF-induced heating of electrodes or brain tissue is the principal safety issue in EEG–fMRI. The degree of heating is dependent on a wide range of factors, including the number of electrodes and their shape; lead arrangement, length and proximity to the scanner transmit coil; and scanner hardware, software and scanning sequence (Hawsawi et al. 2017). EEG–fMRI recordings using scalp electrodes with current-limiting resistors and minimised electrode lead loops have been shown to be safe at 1.5 T. Such studies have been performed at multiple centres with scanners up to 7 T for many years with no adverse incidents reported to our knowledge. However, limiting the SAR values and avoiding body transmit coils (Carmichael et al. 2008, 2010; Ciumas et al. 2013) are significant in minimising the hazards of RF-induced heating. In particular, the effectiveness of current-limiting resistors at higher RF frequencies is unclear. In view of the range and

sensitivity of the factors influencing RF heating, a local risk assessment and adherence to a strict experimental protocol is essential after following the manufacturers' guidelines (Hawsawi et al. 2017; Carmichael et al. 2012).

Acknowledgements We are grateful to Dr. David W. Carmichael for his helpful comments.

References

Abdel-Rehim S, Bagirathan S, Al-Benna S, O'Boyle C (2014). Burns from ECG leads in an MRI scanner: Case series and discussion of mechanisms. Ann Burns Fire Disasters. 27(4):215–8. PMID: 26336370; PMCID: PMC4544433

Acharya S, Gurung DB, Saxena VP (2014a) Transient temperature distribution in human males and females body due to variation in perfusion effect. Int J Appl Math 29:1263–1270

Acharya S, Gurung DB, Saxena VP (2014b) Human males and females body thermoregulation: perfusion effect analysis. J Ther Biol 45:30–36. https://doi.org/10.1016/j.jtherbio.2014.07.006

Ahmadi E, Katnani HA, Daftari Besheli L et al (2016) An electrocorticography grid with conductive nanoparticles in a polymer thick film on an organic substrate improves CT and MR imaging. Radiology 280:595–601. https://doi.org/10.1148/radiol.2016142529

Aigner N, Fialka C, Fritz A, Wruhs O, Zöch G (1997). Complications in the use of diathermy. Burns 23(3):256–64. https://doi.org/10.1016/s0305-4179(96)00113-1. PMID: 9232288

Akca IB, Oner Ferhanoglu MS, Yeung CJ et al (2007) Measuring local RF heating in MRI: simulating perfusion in a perfusionless phantom. J Magn Reson Imaging 26:1228–1235

Allen PJ, Polizzi G, Krakow K et al (1998) Identification of EEG events in the MR scanner: the problem of pulse artefact and a method for its subtraction. NeuroImage 8:229–239

Allen PJ, Josephs O, Turner R (2000) A method for removing imaging artefact from continuous EEG recorded during functional MRI. NeuroImage 12:230–239

Anami K, Mori T, Tanaka F et al (2003) Stepping stone sampling for retrieving artefact-free electroencephalogram during functional magnetic resonance imaging. NeuroImage 19:281–295

Angelone LM, Potthast A, Segonne F et al (2004) Metallic electrodes and leads in simultaneous EEG-MRI: specific absorption rate (SAR) simulation studies. Bioelectromagnetics 25:285–295

Angelone LM, Vasios CE, Wiggins G et al (2006) On the effect of resistive EEG electrodes and leads during 7T MRI: simulation and temperature measurement studies. NeuroImage 24:801–812

Angelone LM, Ahveninen J, Belliveau JW et al (2010a) Analysis of the role of lead resistivity in specific absorption rate for deep brain stimulator leads at 3T MRI. IEEE Trans Med Imaging 29:1029–1038. https://doi.org/10.1109/TMI.2010.2040624

Angelone LM, Bit-Babik G, Chou CK (2010b) Computational electromagnetic analysis in a human head model with EEG electrodes and leads exposed to RF-field sources at 915 MHz and 1748 MHz. Radiat Res 174:91–100. https://doi.org/10.1667/RR1933.1

Assecondi S, Lavallee C, Ferrari P et al (2016) Length matters: improved high field EEG–fMRI recordings using shorter EEG cables. J Neurosci Methods 269:74–87. https://doi.org/10.1016/j.jneumeth.2016.05.014

ASTMF 2182-02a (2007) Standard test method for measurement of radio frequency induced heating near passive implants during magnetic resonance imaging. In: ASTM committee F04 on medical and surgical materials and devices, subcommittee F04.15 on material test methods. ASTM International, West Conshohocken, PA

Athey T (1989) A model of the temperature rise in the head due to magnetic resonance imaging procedures. Magn Reson Med 9:177–184. https://doi.org/10.1002/mrm.1910090204

Baker KB, Tkach JA, Nyenhuis JA et al (2004) Evaluation of specific absorption rate as a dosimeter of MRI-related implant heating. J Magn Reson Imaging 20:315–320

Baker KB, Tkach J, Hall JD et al (2005) Reduction of magnetic resonance imaging-related heating in deep brain stimulation leads using a lead management device. Neurosurgery 57:392–397. https://doi.org/10.1227/01.NEU.0000176877.26994.0C

Balasubramanian M, Wells WM, Ives JR et al (2017) RF heating of gold cup and conductive plastic electrodes during simultaneous EEG and MRI. Neurodiagn J 57:69–83. https://doi.org/10.1080/21646821.2017.1256722

Baumann SB, Noll DC (1999) A modified electrode cap for EEG recordings in MRI scanners. Clin Neurophysiol 110:2189–2193

Benar CG, Aghakhani Y, Wang et al (2003) Quality of EEG in simultaneous EEG–fMRI for epilepsy. Clin Neurophysiol 114:569–580

Bencsik M, Bowtell R, Bowley R (2007) Electric fields induced in the human body by time-varying magnetic field gradients in MRI: numerical calculations and correlation analysis. Phys Med Biol 52:2337. https://doi.org/10.1088/0031-9155/52/9/001

Bhattacharyya PK, Mullin J, Lee BS et al (2017) Safety of externally stimulated intracranial electrodes during functional MRI at 1.5 T. Magn Reson Imaging 38:182–188

Bhidayasiri R, Bronstein JM, Sinha S et al (2005) Bilateral neurostimulation systems used for deep brain stimulation: in vitro study of MRI-related heating at 1.5 T and implications for clinical imaging of the brain. Magn Reson Imaging 23:549–555. https://doi.org/10.1016/j.mri.2005.02.007

Bhusal B, Bhattacharyya P, Baig T et al (2018) Measurements and simulation of RF heating of implanted stereo-electroencephalography electrodes during MR scans. Magn Reson Med 80(4):1676–1685

Bonmassar G, Anami K, Ives J et al (1999) Visual evoked potential (VEP) measured by simultaneous 64-channel EEG and 3T fMRI. Neuroreport 10:1893–1897

Bonmassar G, Purdon PL, Jaaslelainen IP et al (2002) Motion and ballistocardiogram artefact removal for interleaved recording of EEG and EPs during MRI. NeuroImage 16:1127–1141

Boucousis S, Edwards J, Goodyear BG et al (2005) Safety and feasibility of intracranial EEG–fMRI at 3 tesla. Epilepsia 46(S8):37. (abstract 1.071)

Boucousis SM, Beers CA, Cunningham CJ et al (2012) Feasibility of an intracranial EEG–fMRI protocol at 3T: risk assessment and image quality. NeuroImage 63:1237–1248. https://doi.org/10.1016/j.neuroimage.2012.08.008

Brooks ML, O'Connor MJ, Sperling MR et al (1992) Magnetic resonance imaging in localization of EEG depth electrodes for seizure monitoring. Epilepsia 33:888–891

Cabot E, Lloyd T, Christ A et al (2013) Evaluation of the RF heating of a generic deep brain stimulator exposed in 1.5 T magnetic resonance scanners. Bioelectromagnetics 34:104–113. https://doi.org/10.1002/bem.21745

Carmichael DW, Pinto S, Limousin-Dowsey P et al (2007a) Functional MRI with active, fully implanted, deep brain stimulation systems: safety and experimental confounds. NeuroImage 37:508–517

Carmichael DW, Thornton JS, Allen PJ et al (2007b) Safety of localizing intracranial EEG electrodes using MRI. Proc Int Soc Magn Reson Med 15:1073

Carmichael DW, Thornton JS, Rodionov R et al (2008) Safety of localizing epilepsy monitoring intracranial electroencephalograph electrodes using MRI: radiofrequency-induced heating. J Magn Reson Imaging 28:1233–1244. https://doi.org/10.1002/jmri.21583

Carmichael DW, Thornton JS, Rodionov R et al (2010) Feasibility of simultaneous intracranial EEG fMRI in humans: a safety study. NeuroImage 49:379–390. https://doi.org/10.1016/j.neuroimage.2009.07.062

Carmichael DW, Vulliemoz S, Rodionov R et al (2012) Simultaneous intracranial EEG–fMRI in humans: protocol considerations and data quality. NeuroImage 63:301–309. https://doi.org/10.1016/j.neuroimage.2012.05.056

Chowdhury ME, Mullinger KJ, Bowtell R (2015). Simultaneous EEG-fMRI: evaluating the effect of the cabling configuration on the gradient artefact. Phys Med Biol 60(12):N241–50. https://doi.org/10.1088/0031-9155/60/12/N241. Epub 2015 Jun 4. PMID: 26041140.

Ciumas C, Schaefers G, Bouvard S et al (2013) A phantom and animal study of temperature changes during fMRI with intracerebral depth electrodes. Epilepsy Res 108:57–65. https://doi.org/10.1016/j.eplepsyres.2013.10.016

Cohen MS, Weisskoff RM, Rzedzian RR et al (1990) Sensory stimulation by time-varying magnetic fields. Magn Reson Med 14:409–414. https://doi.org/10.1002/mrm.1910140226

Cohen MS, Goldman RI, Jerome E Jr (2001) Simultaneous EEG and fMRI made easy. In: Proc Annual Meeting of the Organization for Human Brain Mapping, Brighton, 10–14 June, 2001, p 6

Collins CM, Liu W, Wang J et al (2004) Temperature and SAR calculations for a human head within volume and surface coils at 64 and 300 MHz. J Magn Reson Imaging 19:650–656

Córcoles J, Zastrow E, Kuster N (2017) On the estimation of the worst-case implant-induced RF-heating in multi-channel MRI. Phys Med Biol 62(12):4711

Dal Molin R, Hecker B (2013) Implantable medical devices MRI safe. In: Blobel B, Pharow P, Parv L (eds) PHealth 2013: Proceedings of the 10th International Conference on wearable micro and nano technologies for personalized health, vol 189. IOS Press, Amsterdam, p 96

Darcey TM, Kobylarz EJ, Pearl MA et al (2016) Safe use of subdermal needles for intraoperative monitoring with MRI. Neurosurg Focus 40(3):E19

Davis LM, Spencer DD, Spencer SS et al (1999) MR imaging of implanted depth and subdural electrodes: is it safe? Epilepsy Res 35:95–98

Debener S, Mullinger KJ, Niazy RK et al (2007) Properties of the ballistocardiogram artefact as revealed by EEG recordings at 1.5, 3 and 7 T static magnetic field strength. Int J Pyschophysiol 67:188–199. https://doi.org/10.1016/j.ijpsycho.2007.05.015

Dempsey MF, Condon B, Hadley DM (2001) Investigation of the factors responsible for burns during MRI. J Magn Reson Imaging 13(4):627–631

Deuschl G, Eisen A (1999) Recommendations for the practice of clinical neurophysiology: guidelines of the International Federation of Clinical Neurophysiology, 2nd edn. Elsevier, Amsterdam

Electrical Geodesics (2010) EGI Operator's Manual. Electrical Geodesics

Erhardt JB, Fuhrer E, Gruschke OG et al (2018) Should patients with brain implants undergo MRI? J Neural Eng 15(4):041002

Eryaman Y, Akin B, Atalar E (2011) Reduction of implant RF heating through modification of transmit coil electric field. Magn Reson Med 65:1305–1313. https://doi.org/10.1002/mrm.22724

Eryaman Y, Turk EA, Oto C et al (2013) Reduction of the radiofrequency heating of metallic devices using a dual-drive birdcage coil. Magn Reson Med 69:845–852. https://doi.org/10.1002/mrm.24316

Eryaman Y, Kobayashi N, Moen S et al (2019) A simple geometric analysis method for measuring and mitigating RF induced currents on deep brain stimulation leads by multichannel transmission/reception. NeuroImage 184:658–668

Finelli DA, Rezai AR, Ruggieri PM et al (2002) MR imaging-related heating of deep brain stimulation electrodes: in vitro study. Am J Neuroradiol 23:1795–1802

Foged MT, Lindberg U, Vakamudi K et al (2017) Safety and EEG data quality of concurrent high-density EEG and high-speed fMRI at 3 tesla. PLoS One 12(5):e0178409

Franceschi AM, Wiggins GC, Mogilner AY et al (2016) Optimized, minimal specific absorption rate MRI for high-resolution imaging in patients with implanted deep brain stimulation electrodes. Am J Neuroradiol 37:1996–2000. https://doi.org/10.3174/ajnr.A4865

Garreffa G, Bianciardi M, Hagberg GE et al (2004) Simultaneous EEG–fMRI acquisition: how far is it from being a standardized technique? Magn Reson Imaging 22:1445–1455

Georgi JC, Lawrence AD, Mehta MA et al (2004) Active deep brain stimulation during MRI: a feasibility study. Magn Reson Med 51:380–388

Gleason CA, Kaula NF, Hricak H et al (1992) The effect of magnetic resonance imagers on implanted neurostimulators. Pacing Clin Electrophysiol 15:81–94. https://doi.org/10.1111/j.1540-8159.1992.tb02904.x

Gokul KC, Gurung DB, Adhikary PR (2013) Effect of blood perfusion and metabolism in temperature distribution in human eye. Adv Appl Math Biosci 4:13–23

Goldman RI, Stern JM, Engel J Jr et al (2000) Acquiring simultaneous EEG and functional MRI. Clin Neurophysiol 111:1974–1980

Golestanirad L, Angelone LM, Iacono MI et al (2016a) Local SAR near deep brain stimulation (DBS) electrodes at 64 and 127 MHz: a simulation study of the effect of extracranial loops. Magn Reson Med 78:1558–1565. https://doi.org/10.1002/mrm.26535

Golestanirad L, Keil B, Angelone LM et al (2016b) Feasibility of using linearly polarized rotating birdcage transmitters and close-fitting receive arrays in MRI to reduce SAR in the vicinity of deep brain simulation implants. Magn Reson Med 77:1701–1712. https://doi.org/10.1002/mrm.26220

Golestanirad L, Iacono MI, Keil B et al (2017) Construction and modeling of a reconfigurable MRI coil for lowering SAR in patients with deep brain stimulation implants. NeuroImage 147:577–588. https://doi.org/10.1016/j.neuroimage.2016.12.056

Golestanirad L, Kirsch J, Bonmassar G et al (2019) RF-induced heating in tissue near bilateral DBS implants during MRI at 1.5 T and 3T: the role of surgical lead management. NeuroImage 184:566–576

Gorny KR, Presti MF, Goerss SJ et al (2013) Measurements of RF heating during 3.0-T MRI of a pig implanted with deep brain stimulator. Magn Reson Imaging 31:783–788. https://doi.org/10.1016/j.mri.2012.11.005

Graf H, Steidle G, Schick F (2007) Heating of metallic implants and instruments induced by gradient switching in a 1.5-tesla whole-body unit. J Magn. Reson Imaging 26:1328–1333. https://doi.org/10.1002/jmri.21157

Gray RW, Bibens WT, Shellock FG (2005) Simple design changes to wires to substantially reduce MRI-induced heating at 1.5T: implications for implanted leads. Magn Reson Imaging 23:887–891

Gualniera G, Garreffa G, Morasso P et al (2004) A method for real-time artefact filtering during simultaneous EEG–fMRI acquisition: preliminary results. Neurocomputing 58–60:1171–1179

Hawsawi HB, Carmichael DW, Lemieux L (2017) Safety of simultaneous scalp or intracranial EEG during MRI: a review. Front Phys 5(42):52–76

Hay DJ (2005) Electrosurgery. Surgery 23:73–5. https://doi.org/10.1383/surg.23.2.73.60349

Hefft S, Brandt A, Zwick S, von Elverfeldt D, Mader I, Cordeiro J, Trippel M, Blumberg J, Schulze-Bonhage A (2013) Safety of hybrid electrodes for single-neuron recordings in humans. Neurosurgery 73(1):78–85

Hill RA, Chiappa KH, Huang-Hellinger F et al (1995) EEG during MR imaging: differentiation of movement artefact from paroxysmal cortical activity. Neurology 45:1942–1943

Hoffmann A, Jager L, Werhahn KJ et al (2000) Electroencephalography during functional echoplanar imaging: detection of epileptic spikes using post-processing methods. Magn Reson Med 44:791–798

Hofman MBM, De Cock CC, van der Linden JC et al (1996) Transesophageal cardiac pacing during magnetic resonance imaging: feasibility and safety considerations. Magn Reson Med 35:413–422

Huang-Hellinger FR, Breiter HC, McCormak G et al (1995) Simultaneous functional magnetic resonance imaging and electrophysiological recording. Hum Brain Mapp 3:13–23

Iannetti GD, Bonaventura CD, Pantano P et al (2002) fMRI/EEG in paroxysmal activity elicited by elimination of central vision and fixation. Neurology 58:976–979

Iannotti GR, Pittau F, Michel CM, Vulliemoz S, Grouiller F (2015) Pulse artifact detection in simultaneous EEG–fMRI recording based on EEG map topography. Brain Topogr 28(1):21–32

IEC (2016) Medical electrical equipment–Part 2–33: Particular requirements for the basic safety and essential performance of magnetic resonance equipment for medical diagnosis. International Electrotechnical Commission 60601–2-33:2010+A12:2016, Geneva

ISO (2012) Assessment of the safety of magnetic resonance imaging for patients with an active implantable medical device. International Organization for Standardization. International Organization of Standardization ISO TS 10974, Geneva

Ives JR, Warach S, Schmitt F et al (1993) Monitoring the patient's EEG during echo planar MRI. Electroencephalogr Clin Neurophysiol 87:417–420

Janssen R, Benignus VA, Grimes LM et al (1986) Unrecognized errors due to analog filtering of the brain-stem auditory evoked response. Electroencephalogr Clin Neurophysiol 65:203–211

Jorge J, Grouiller F, Ipek Ö et al (2015) Simultaneous EEG–fMRI at ultra-high field: artefact prevention and safety assessment. NeuroImage 105:132–144. https://doi.org/10.1016/j.neuroimage.2014.10.055

Kahan J, Papadaki A, White M et al (2015) The safety of using body-transmit MRI in patients with implanted deep brain stimulation devices. PLoS One 10:e0129077. https://doi.org/10.1371/journal.pone.0129077

Kainz W (2007) MR heating tests of MR critical implants. J Magn Reson Imaging 26:450–451

Kainz W, Neubauer G, Überbacher R (2002) Temperature measurement on neurological pulse generators during MR scans. Biomed Eng Online 1:2. https://doi.org/10.1186/1475-925X-1-2

Kamp A, Lopes Da Silva F (1998) Technological aspects of EEG recording. In: Niedermeyer E, Lopes Da Silva F (eds) Electroencephalography. Basic principles, clinical applications and related fields, 4th edn. Williams and Wilkins, Baltimore

Kanal E, Cida Meltzer C, Adelson PD et al (1999) Platinum subdural grid: MR imaging compatibility testing. Radiology 211:886–888

Kruggel F, Wiggins CJ, Herrmann CS et al (2000) Recording of the event related potentials during functional MRI at 3.0 tesla field strength. Magn Reson Med 44:277–282

Kuusela L, Turunen S, Valanne L et al (2015) Safety in simultaneous EEG-fMRI at 3 T: temperature measurements. Acta Radiol 56:739–745. https://doi.org/10.1177/0284185114536385

Laufs H, Kleinschmidt A, Beyerle A et al (2003) EEG-correlated fMRI of human activity. NeuroImage 19:1463–1476

Lazeyras F, Zimine I, Blanke O et al (2001) Functional MRI with simultaneous EEG recording: feasibility and application to motor and visual activation. J Magn Reson Imaging 13:943–948

Lemieux L, Allen PJ, Franconi F et al (1997) Recording of EEG during fMRI experiments: patient safety. Magn Reson Med 38:943–952

Liu JY, Hawsawi HB, Sharma N, Carmichael DW, Diehl B, Thom M and Lemieux L, (2022) Safety of intracranial electroencephalography during functional electromagnetic resonance imaging in humans at 1.5 tesla using a head transmit RF coil: Histopathological and heat-shock immunohistochemistry observations. NeuroImage 254: 119129. https://doi.org/10.1016/j.neuroimage.2022.119129

Litvak E, Foster KR, Repacholi MH (2002) Health and safety implications of exposure to electromagnetic fields in the frequency range 300 Hz to 10 MHz. Bioelectromagnetics. 23(1):68–82. https://doi.org/10.1002/bem.99. PMID: 11793407

Mandelkow H, Halder P, Boesiger P et al (2006) Synchronisation facilitates removal of MRI artefacts from concurrent EEG recordings and increases usable bandwidth. NeuroImage 32:1120–1126

Mattei E, Calcagnini G, Triventi M et al (2006) MRI induced heating of pacemaker leads: effect of temperature probe positioning and pacemaker placement on lead tip heating and local SAR. In: Engineering in medicine and biology society, 2006. EMBS'06. 28th Annual International Conference of the IEEE. IEEE, New York, pp 1889–1892

Mirsattari SM, Lee DH, Jones D et al (2004) MRI compatible EEG electrode system for routine use in the epilepsy monitoring unit and intensive care unit. Clin Neurophysiol 115:2175–2180

Mullinger K, Debener S, Coxon R, Bowtell R (2008a) Effects of simultaneous EEG recording on MRI data quality at 1.5, 3 and 7 tesla. Int J Psychophysiol 67:178–188. https://doi.org/10.1016/j.ijpsycho.2007.06.008

Mullinger K, Brookes M, Stevenson C, Morgan P, Bowtell R (2008b) Exploring the feasibility of simultaneous electroencephalography/functional magnetic resonance imaging at 7 T. Magn Reson Imaging 26:968–977. https://doi.org/10.1016/j.mri.2008.02.014

Negishi M, Abildgaard M, Nixon T et al (2004) Removal of time varying gradient artefacts from EEG data acquired during continuous fMRI. Clin Neurophysiol 115:2181–2192

Niazy RK, Beckmann CF, Iannetti GD, Brady JM, Smith SM (2005) Removal of FMRI environment artifacts from EEG data using optimal basis sets. NeuroImage 28(3):720–737

Nuwer MR, Comi G, Emerson R et al (1999) IFCN standards for digital recording of clinical EEG. In: Deuschl G, Eisen A (eds) Recommendations for the practice of clinical neurophysiology: guidelines of the International Federation of Clinical Neurophysiology, 2nd edn. Elsevier, Amsterdam

Nyenhuis JA (2003) Interactions of medical implants with the magnetic fields in MRI. In: Engineering in Medicine and Biology Society, 2003. Proceedings of the 25th Annual International Conference of the IEEE. MXp, Cancun, pp 3767–3770

Nyenhuis JA, Kildishev AV, Bourland JD et al (1999) Heating near implanted medical devices by the MRI RF-magnetic field. IEEE Trans Magn 35:4133–4135. https://doi.org/10.1109/20.800779

Nyenhuis JA, Park SM, Kamondetdacha R et al (2005) MRI and implanted medical devices: basic interactions with an emphasis on heating. IEEE Trans Device Mater Reliab 5:467–480. https://doi.org/10.1109/TDMR.2005.859033

Papadaki A, Carmichael D, McEvoy A, Miserocchi A, Yousry T, Diehl B, Lemieux L, Thornton JS (2016) Assessment of RF induced heating of intracranial micro-depth electrodes during MRI. In: Proceedings of the International Society for magnetic resonance in medicine, Singapore, p 2230

Park SM, Nyenhuis JA, Smith CD et al (2003) Gelled versus nongelled phantom material for measurement of MRI-induced temperature increases with bioimplants. IEEE Trans Magn 39:3367–3371

Pictet J, Meuli R, Wicky S et al (2000) Radiofrequency heating effects around resonant lengths of wire in MRI. Phys Med Biol 47:2973–2985

Poulsen C, Wakeman DG, Atefi SR et al (2016) Polymer thick film technology for improved simultaneous dEEG/MRI recording: safety and MRI data quality. Magn Reson Med 77:895–903. https://doi.org/10.1002/mrm.26116

Rezai AR, Finelli D, Nyenhuis JA et al (2002) Neurostimulation systems for deep brain stimulation: in vitro evaluation of magnetic resonance imaging-related heating at 1.5T. J Magn Reson Imaging 15:241–250

Rezai AR, Baker KB, Tkach JA et al (2005) Is magnetic resonance imaging safe for patients with neurostimulation systems used for deep brain stimulation? Neurosurgery 57:1056–1062. https://doi.org/10.1227/01.NEU.0000186935.87971.2a

Roth BJ, Pascual-Leone A, Cohen LG et al (1992) The heating of metal electrodes during rapid-rate magnetic stimulation: a possible safety hazard. Electroencephalogr Clin Neurophysiol 85:116–123

Sammartino F, Krishna V, Sankar T et al (2016) 3-tesla MRI in patients with fully implanted deep brain stimulation devices: a preliminary study in 10 patients. J Neurosurg 127(4):892–898. https://doi.org/10.3171/2016.9.JNS16908

Schaefer DJ, Bourland JD, Nyenhuis JA (2000) Review of patient safety in time-varying gradient fields. J Magn Reson Imaging 12:20–29. https://doi.org/10.1002/1522-2586(200007)12:1<20::AID-JMRI3>3.0.CO;2-Y

Seeck M, Lazeyras F, Michel CM et al (1998) Non-invasive epileptic focus localization using EEG-triggered functional MRI and electromagnetic tomography. Electroencephalogr Clin Neurophysiol 106:508–512

Serano P, Angelone LM, Katnani H et al (2015) A novel brain stimulation technology provides compatibility with MRI. Sci Rep 5:9805. https://doi.org/10.1038/srep09805

Shellock FG (2001) Metallic neurosurgical implants: evaluation of magnetic field interactions, heating, and artifacts at 1.5-tesla. J Magn Reson Imaging 14:295–299. https://doi.org/10.1002/jmri.1185

Shellock FG (2004) Reference manual for magnetic resonance safety, implants, and devices. Biomedical Reference Publishing Group, Los Angeles, p 378

Shellock FG (2007) Comments on MR heating tests for critical implants. J Magn Reson Imaging 26:1182–1185
Shew M, Wichova H, Lin J et al (2018) Magnetic resonance imaging with cochlear implants and auditory brainstem implants: are we truly practicing MRI safety? Laryngoscope 129(2):482–489
Shrivastava D, Abosch A, Hanson T et al (2010) Effect of the extracranial deep brain stimulation lead on radiofrequency heating at 9.4 tesla (400.2 MHz). J Magn Reson Imaging 32:600–607. https://doi.org/10.1002/jmri.22292
Shrivastava D, Abosch A, Hughes J et al (2012) Heating induced near deep brain stimulation lead electrodes during magnetic resonance imaging with a 3 T transceive volume head coil. Phys Med Biol 57:5651. https://doi.org/10.1088/0031-9155/57/17/5651
Srivastava G, Crottaz-Herbette S, Lau KM et al (2005) ICA-based procedures for removing ballistocardiogram artefacts from EEG data acquired in the MRI scanner. NeuroImage 24:50–60
Stevens TK, Ives JR, Martyn Klassen L et al (2007) MR compatibility of EEG electrodes at 4 tesla. J Magn Reson Imaging 25:872–877
Van Audekerke J, Peeters R, Verhoye M et al (2000) Special designed RF-antenna with integrated non-invasive carbon electrodes for simultaneous magnetic resonance imaging and electroencephalography acquisition at 7T. Magn Reson Imaging 18:887–891
Van Genderingen HR, Sprenger M, de Ridder JW et al (1989) Carbon-fiber electrodes and leads for electrocardiography during MR imaging. Radiology 171:872
Vanhatalo S, Alnajjar A, Nguyen VT et al (2014) Safety of EEG–fMRI recordings in newborn infants at 3T: a study using a baby-size phantom. Clin Neurophysiol 125(5):941–946
Vasios CE, Angelone LM, Purdon PL et al (2006) EEG/(f)MRI measurements at 7 tesla using a new EEG cap ("Inkcap"). NeuroImage 33:1082–1092
Vulliemoz S, Carmichael DW, Rosenkranz K et al (2011) Simultaneous intracranial EEG and fMRI of interictal epileptic discharges in humans. NeuroImage 54:182–190. https://doi.org/10.1016/j.neuroimage.2010.08.004
Warach S, Ives JR, Schlaug G et al (1996) EEG-triggered echo-planar functional MRI in epilepsy. Neurology 47:89–93
Woods TO (2007) Standards for medical devices in MRI: present and future. J Magn Reson Imaging 26:1186–1189
Yeung CJ, Susil RC, Atalar E (2002) RF safety index of wires in interventional MRI: using a safety index. Magn Reson Med 47:187–193
Yeung CJ, Karmarkar P, McVeigh ER (2007) Minimizing RF heating of conducting wires in MRI. Magn Reson Med 58:1028–1034. https://doi.org/10.1002/mrm.21410
Zhang J, Wilson CL, Levesque MF et al (1993) Temperature changes in nickel-chromium intracranial depth electrodes during MR scanning. Am J Neuroradiol 14:497–500

EEG Quality: The Pulse Artifact

8

R. Abreu, J. Jorge, and P. Figueiredo

8.1 Introduction

The acquisition of the electroencephalogram (EEG) inside magnetic resonance imaging (MRI) scanners has been pursued for over two decades, with the aim of obtaining both EEG and functional MRI (fMRI) measurements of brain activity simultaneously. The safety and feasibility of such simultaneous EEG-fMRI studies, and the insights about brain function that they can provide, are well documented (see Chap. 7 and Jorge et al. 2014; Laufs 2012; Murta et al. 2015; Hawsawi et al. 2017). However, the severe artifacts that contaminate the EEG signal acquired in the MRI environment remain a limiting aspect of EEG-fMRI research and are currently the focus of a substantial amount of work (e.g., see the review by Abreu et al. 2018). Besides the overwhelming artifact generated by the magnetic field gradients associated with the fMRI acquisition, which is the topic of another chapter in this book, the second most important artifact affecting the EEG recordings in the MRI

R. Abreu
Institute for Systems and Robotics—Lisboa, Lisbon, Portugal

Department of Bioengineering, Instituto Superior Técnico, Universidade de Lisboa, Lisbon, Portugal

Coimbra Institute for Biomedical Imaging and Translational Research, Institute for Nuclear Sciences Applied to Health, University of Coimbra, Coimbra, Portugal
e-mail: rodolfo.abreu@tecnico.ulisboa.pt

J. Jorge
CSEM - Swiss Center for Electronics and Microtechnology, Bern, Switzerland
e-mail: joao.jorge@csem.ch

P. Figueiredo (✉)
Institute for Systems and Robotics—Lisboa, Lisbon, Portugal

Department of Bioengineering, Instituto Superior Técnico, Universidade de Lisboa, Lisbon, Portugal
e-mail: patricia.figueiredo@tecnico.ulisboa.pt

C. Mulert, L. Lemieux (eds.), *EEG - fMRI*,
https://doi.org/10.1007/978-3-031-07121-8_8

scanner arises as a consequence of the ongoing function of the heart. It has been often referred to as the ballistocardiogram (BCG) artifact and as pulse artifact (PA)—we opt here for the latter terminology.

An illustrative example of the PA is presented in Fig. 8.1, which is taken from EEG data recorded simultaneously with fMRI on a human volunteer using a typical setup, at 3 Tesla. The amplitude of the EEG signal in representative channels is shown, together with the electrocardiographic (ECG) signal, over several cardiac cycles. The PA can be detected on the EEG channels as a waveform occurring at a certain delay relative to the R-peak on the ECG and exhibiting multiple polarity inversions, hence peaks, within each cardiac cycle. Consistently, the corresponding frequency spectra exhibit clear peaks at the heart rate and its harmonics, with a width that is related to heart rate variability. In Fig. 8.1, the average PA across multiple cardiac cycles is shown together with the average QRS complex obtained from the ECG. Despite some variability over multiple cardiac cycles, a pattern is observed consistently for all channels (as can be appreciated by the global field power (GFP) depicted in Fig. 8.1, which is defined as the standard deviation of the EEG signal across channels). A characteristic spatial distribution is also found for the PA, which nevertheless varies significantly over the cardiac cycle, evidencing its nonstationarity.

Although the PA exhibits considerably lower amplitude compared with the so-called gradient or imaging artifact, it has been proven substantially more difficult to correct for, and it is in fact widely recognized as the most challenging EEG artifact to handle in simultaneous EEG-fMRI studies. One limiting factor is the complexity of the mechanisms giving rise to the PA, which are not yet fully understood. On the other hand, the variability of the PA over multiple heartbeats limits the effectiveness of commonly employed artifact reduction strategies based on averaging multiple artifact occurrences. Additionally, the characteristics of the PA make it particularly prone to confounding the EEG signals of interest. Not only its amplitude but also its spectral profile (with frequencies related with the heart rate, around 1 Hz, and its harmonics) considerably overlap with EEG signals of neuronal origin, particularly in the delta and theta frequency bands but also possibly extending into the alpha band. As a consequence, the reduction of the PA can have a substantial impact on EEG data quality and the accurate analysis and quantification of the brain activity of interest.

In this chapter, the current knowledge regarding the biophysical mechanisms underlying the PA is first overviewed, by describing the theoretical principles of the hypothesized artifact sources and the existing experimental evidence. A number of considerations are then made regarding specific requirements and recommendations in the acquisition of simultaneous EEG-fMRI data. Subsequently, the various methods that can be used for reducing the PA in post-processing are presented, according to the type of approach employed, and their assessment is then discussed. Finally, a summary is provided with some final remarks regarding future directions.

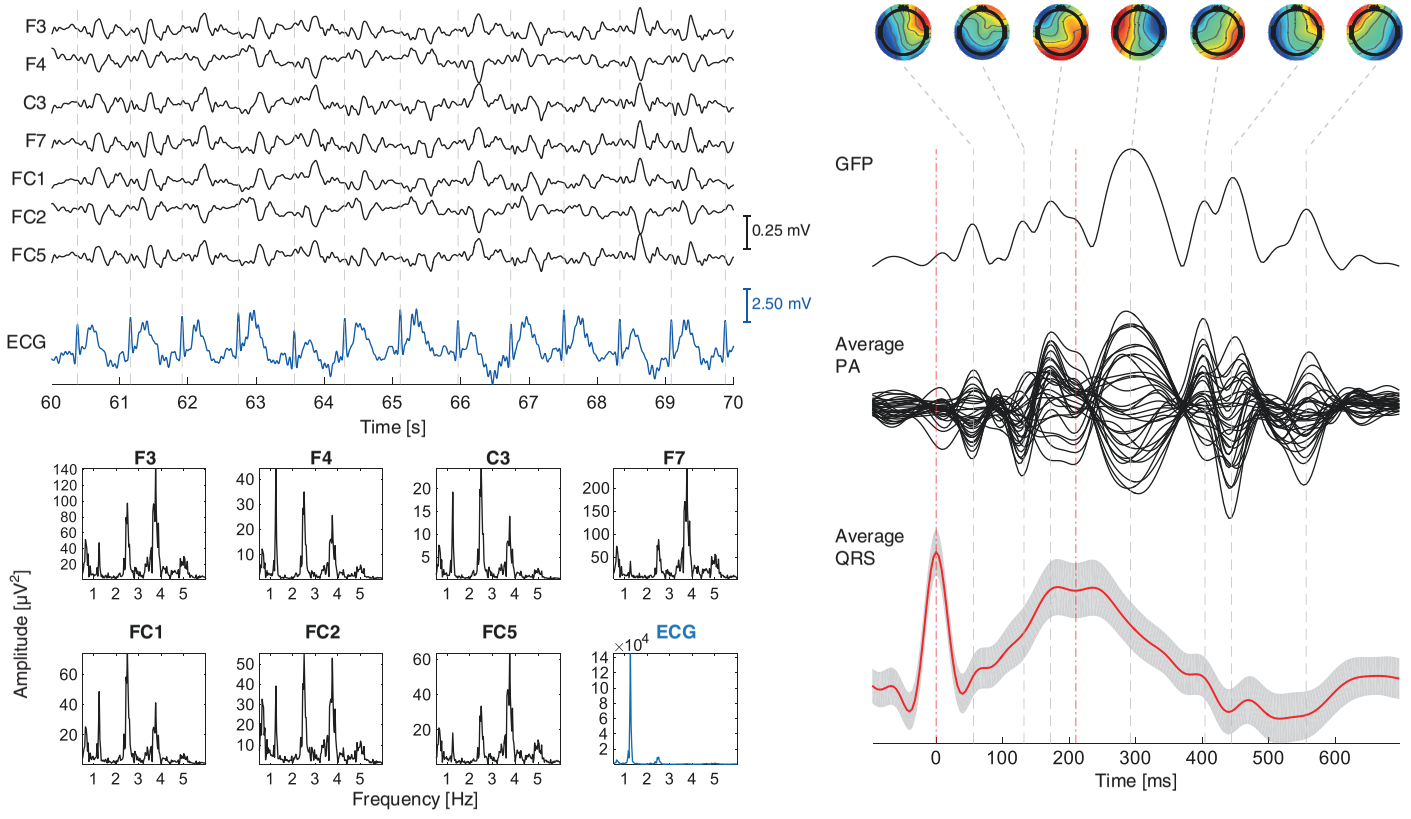

Fig. 8.1 Illustration and characteristics of the pulse artifact. (Left) Traces of 10 s from seven representative EEG channels (black lines) and the ECG signal (blue line) are shown (top), together with their associated power spectra (bottom). PA waveforms approximately time-locked with, but delayed from, the R-peaks of the ECG signal (dashed gray vertical lines) are clearly visible on the EEG. On the frequency domain, peaks at cardiac-related frequencies (fundamental frequency and harmonics) are also present. (Right) The average QRS complex of the ECG signal and the average PA across occurrences on the EEG are illustrated, together with the GFP of the average PA. The spatial distribution of the electrical potentials at the most prominent GFP peaks is also shown; the quite diverse spatial patterns evidence the nonstationarity of the PA

8.2 Biophysical Mechanisms

The PA is a consequence of the ongoing function of the heart and the concomitant pulsatile flow of blood to the head, when subjects are placed in the strong static magnetic field of MRI scanners. Understanding the biophysical mechanisms by which the PA is generated is essential to guide the development of effective correction strategies, as well as the choice of experimental designs and analysis techniques that are most robust against the potential confounds introduced by PA residuals. A number of studies have been dedicated to the assessment, characterization, and modeling of PA mechanisms, yielding important insights: the hypothesized sources and the experimental evidence supporting them will now be presented.

8.2.1 Hypothesized Sources

The current body of evidence suggests the existence of three biophysical mechanisms that may contribute to measurable PAs: (1) bulk head motion induced by the arrival of blood to the head, (2) pulsatile scalp dilation, and (3) Hall effects in the moving blood.

Bulk head motion follows each cardiac systole of the left ventricle, as blood is ejected to the systemic circulation. Once the ejected blood reaches the head and gets shunted into successively narrower arteries, it slows down and transfers momentum to the head, causing motion. Besides such bulk head motion, the scalp is also found to expand and contract throughout the cardiac cycle. Although the skull is a rigid structure, numerous arteries located between the skull and the scalp pulsate with blood flow, causing this pulsatile scalp dilation. During EEG recordings performed in the MRI scanner, both cardiac-related bulk head motion and pulsatile scalp dilation can cause motion of the EEG electrodes and wires and thereby contribute to the PA through a phenomenon termed electromagnetic induction. This interaction is described below.

Scalp EEG measures differences in electric potential between pairs of electrodes positioned on specific points of the scalp, such that each electrode pair effectively forms a conductive loop that includes the EEG amplifier, the EEG electrodes and wires, and the subject's head. A useful approximation to this system is that of a well-defined closed conductive loop, enclosing a surface Σ, and having no current flow (due to the very high impedance of the EEG amplifiers). In the MRI scanner, this loop is exposed to the static magnetic field, $\vec{B}_0$ (Fig. 8.2a). According to Faraday's law of induction, any change over time of the flux of $\vec{B}_0$ through the EEG loop will lead to an electromotive component $V(t)$, which depends on changes in the surface Σ, as follows:

$$V(t) = -\frac{d}{dt} \int_{\vec{r} \in \Sigma} \vec{B}_0(\vec{r}) \cdot \vec{N}(\vec{r},t)\, d\Sigma \tag{8.1}$$

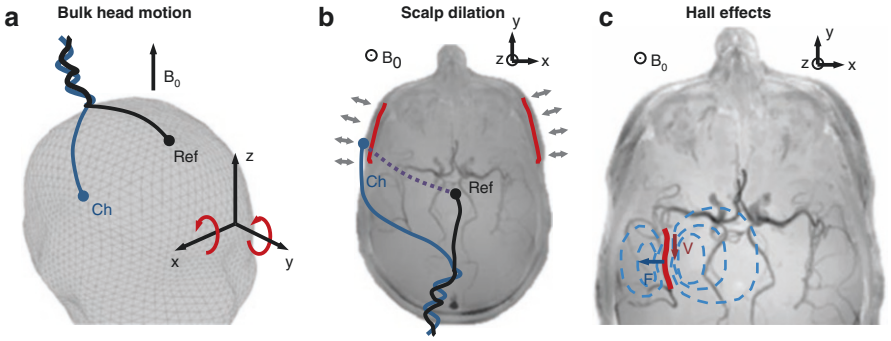

Fig. 8.2 Hypothesized mechanisms by which the pulse artifact is generated. (**a**) Bulk head motion: for a given channel Ch, the EEG signal measured relative to a reference electrode Ref may be added of an artifactual component if the surface Σ moves in $\vec{B}_0$, following Faraday's law. Σ will move together with the head every time ejected blood arrives, coming from the heart's left ventricle. Assuming $\vec{B}_0$ to be spatially homogeneous and oriented along the *z*-axis (feet-head), only rotations of the head along the *x*-axis (left-right) and *y*-axis (posterior-anterior) will effectively produce artifacts (represented by red arrows). In reality, Σ is not well defined as the loop includes head tissues; however, the closed-loop model (represented by a traced line) is a useful and informative approximation. (**b**) Scalp dilation: arteries running outside the skull, such as the temporal arteries (marked in red), can lead to scalp expansions and contractions when they pulsate, following the cardiac cycle; this will lead to changes in the geometry of the loop-enclosed surface Σ, generating artifacts as predicted by Faraday's law. (**c**) Hall effects in large arteries: when blood moves in $\vec{B}_0$ with a given velocity $\vec{v}$, in a large artery (example marked in red), its positively charged ions will experience a force $\vec{F}$ (marked in dark blue) perpendicular to $\vec{v}$ and $\vec{B}_0$, while negatively charged ions will experience the same force in the opposite direction; the resulting charge separation creates an artifactual electric potential distribution (depicted by white traced lines) that may be measurable by electrodes at the scalp. This head image corresponds to a maximum-intensity axial projection of a time-of-flight MRI acquisition, to illustrate a real arterial architecture

where $\vec{N}(\vec{r},t)$ denotes the normal to the surface at position $\vec{r}$ and instant *t* and the scalar product $\vec{B}_0(\vec{r})\cdot\vec{N}(\vec{r},t)$ can be seen as the projection of $\vec{N}$ along $\vec{B}_0$. As the EEG electrodes are attached to the scalp, both bulk head motion and scalp dilation can lead to changes in the EEG loop surface and/or in $\vec{N}(\vec{r},t)$. The temporal derivative of the integral term in Eq. (8.1) will therefore become nonzero, creating an artifactual component *V*(*t*) that is added to the measured EEG signal in each channel.

Equation 8.1 offers a number of valuable insights into the properties of the two induction-based PA contributions: (1) they scale linearly with the amplitude of $\vec{B}_0$ and will therefore be stronger at higher-field MRI systems; and (2) they increase with the area of the loop-enclosed surface Σ. Moreover, if we assume a spatially homogeneous static field oriented along a direction *z*, $\vec{B}_0(\vec{r}) = b_0\vec{e}_z$, Eq. 8.1 becomes

$$V(t) = -b_0\frac{d}{dt}\int_{\vec{r}\in\Sigma} n_z(\vec{r},t)\,d\Sigma \tag{8.2}$$

where n_z is the projection of $\vec{N}$ along z (Jorge et al. 2015a). Under this condition, and particularly in relation to bulk head motion contributions, it becomes clear that translations of the system as a rigid body, and rotations along z, will not affect $n_z\left(\vec{r},t\right)$ and thus will not contribute to induction-based artifacts.

This observation, however, does not apply to scalp dilation, because it can induce changes in the actual geometry of the enclosed surface, Σ, leading to nonrigid body motion (Fig. 8.2b), and it is therefore in general more complex to model. Moreover, for both rigid and nonrigid contributions alike, it is important to note that the model presented here is an approximation, which assumes a closed loop. In reality, the presence of the subject's head as a conductive volume prevents the determination of a well-defined area Σ, and the system needs to be described in terms of the scalar electric potential distribution, which depends on the head geometry and tissue conductivities. Nevertheless, the insights discussed above have been found to remain valid even in these more realistic conditions as well (Yan et al. 2010). Another important aspect to consider is the occurrence of (nonrigid) motion in the EEG wires, namely at the segments that transmit between the cap surface and the amplifier. In fact, cardiac-induced head motion and scalp dilation are likely to propagate from the head to these wire segments, and any exposed loop areas will contribute to the artifact as well (Jorge et al. 2015b). Also, in this case, both head translations and rotations may play important roles, which are difficult to model.

The third hypothesized source of the PA is the presence of Hall effects in the moving blood, which may generate electric potentials measurable by the EEG system. Blood is an electrically conductive fluid due to the presence of various ions such as Na^+, K^+, Ca^{2-}, and Cl^-. When flowing in the strong magnetic field $\vec{B}_0$, with a given velocity $\vec{v}$, these charged particles will experience a force $\vec{F}$ equal to

$$\vec{F} = q\vec{v} \times \vec{B}_0 \tag{8.3}$$

where q is the electric charge, and × denotes the vector product (Tenforde et al. 1983). Particles with opposite charges will thus experience forces in opposite directions. Their movement will generate an electric field inside the vessel, and in the surrounding tissues, which may be picked up at the scalp by the EEG electrodes as a difference in electric potential (Fig. 8.2c). Yan et al. (2010) studied the properties of this scalp potential by modeling a cylindrical vessel of length L and radius b embedded in an infinite conductive medium. The generated scalp potential could then be seen as that created by a simple current dipole (as often employed to model neuronal activity), oriented perpendicularly to the flow, $\vec{v}$, and the magnetic field, $\vec{B}_0$, with strength given by

$$\vec{Q} = \sigma\pi b^2 L\left(\vec{v} \times \vec{B}_0\right) \tag{8.4}$$

where σ is the conductivity of the surrounding medium (Yan et al. 2010).

Equations (8.3) and (8.4) provide important insights into the properties of Hall effect contributions, as follows:

1. They are expected to be most prominent in vessel segments that are least aligned with $\vec{B}_0$, i.e., where the flow velocity has a relevant component perpendicular to the field.
2. They are stronger for larger caliber vessels (larger b) and with stronger temporal variations in $\vec{v}$ across the cardiac cycle (necessary to generate fluctuations in the scalp potential and thereby signal artifacts)—suggesting that arteries, and not capillaries or draining veins, may generate the largest artifact contributions, given their caliber and pulsatility.
3. They decay with the square of the distance from the vessel to the scalp, due to the dipole-like behavior of the generated potentials (Nunez and Srinivasan 2006)—thereby downplaying the importance of deeper vessels.
4. They scale linearly with the field strength, $\vec{B}_0$.

Considering the three hypothesized generative mechanisms, it is straightforward to expect that PAs will vary in amplitude over the time window of a cardiac cycle and across EEG channels as well. Variations in anatomy and cardiovascular physiology across individuals are also likely to introduce differences in the generated PAs. Finally, variations in an individual's PA across heartbeats may also prove substantial, given that drifts in head orientation are fairly common during recording sessions and also considering the influence of other physiological processes such as the breathing cycle, for example. In the latter case, it is known, for instance that, even at rest, systolic blood pressure exhibits a cyclic variation that is coupled with the breathing cycle, with inspiratory periods being associated with a lower pressure compared to expiratory periods – a phenomenon known as "respiratory waves in arterial pressure" (Hall and Guyton 2015). Such pressure variations, affecting the blood ejected by the heart, could likely have an impact on all three hypothesized PA sources, inducing variability across heartbeats.

8.2.2 Experimental Evidence

In the past two decades, considerable work has been devoted to the investigation of the various hypothesized sources of the PA and to determining their relative importance. Although it is extremely challenging to isolate and characterize the different sources individually in practice, several studies have succeeded in providing important evidence affording some insight into these mechanisms.

Experimental measurements of the PA amplitude at various field strengths have generally shown that the artifact scales approximately linearly with $\vec{B}_0$ strength (Debener et al. 2008; Neuner et al. 2013), in agreement with theoretical

expectations for all the hypothesized PA sources. Optical measurements of head motion during MRI scans have shown that cardiac function can induce bulk head displacements in the order of 100 μm, particularly in the head-to-feet direction, and angular displacements in the order of 0.01°, particularly in pitch, i.e., "nodding" motion, over short time periods of less than 0.5 ms (Maclaren et al. 2012). In EEG-fMRI recordings, the use of tight head-fixation systems such as vacuum pillows and/or bite bars has been found to reduce PA peak amplitudes substantially, by more than 80% in some participants (Anami et al. 2002; Mullinger et al. 2013b). These effects suggest that cardiac-induced bulk head motion is a major source of the observed PAs. Results from computational modeling have shown agreement with this observation and further suggested that Hall effect contributions are relatively much smaller—approximately 20 times (Yan et al. 2010). However, experimental work recording EEG with the electrodes insulated from the scalp (suppressing Hall effects but not head motion contributions) also found important reductions in PA amplitude, of over 40% (Mullinger et al. 2013b), thereby challenging this notion.

The presence of scalp dilation contributions has proved the most challenging to investigate. Experimental work combining both head restraining and electrode insulation showed that PA residuals still persist (approximately 20%), although these could be at least partly due to imperfect suppression of the rigid body motion contributions (Mullinger et al. 2013b). Studies simulating scalp dilation experimentally in phantoms, using small inflatable air pillows underneath the EEG cap, produced artifact topographies that do not accurately match the main PA peak topographies typically observed in human data but which could underlie some of its subtler spatial features (Debener et al. 2008). In the temporal domain, early PA oscillations that have been found to occur before bulk head motion can play a dominant influence, showing mirrored polarity between the leftmost and rightmost lateral electrodes, which would be consistent with effects linked to scalp expansion (Debener et al. 2008). Altogether, the current body of evidence suggests that all three hypothesized PA sources likely contribute with measurable artifacts, albeit with bulk head motion probably playing the most important role (Maclaren et al. 2012).

Concerning PA variability, experimental evidence confirms that the artifact assumes complex spatiotemporal profiles, with multiple signal oscillations across the cardiac cycle, varying considerably across channels (Allen et al. 1998; Debener et al. 2008; Mullinger et al. 2013b). Substantial variations across individuals are also typically observed, both in amplitude and spatiotemporal morphology. Regarding the variability of the PA across heartbeats, the importance of changes in head position over the recording time has often been recognized and taken into consideration (Allen et al. 1998; Bonmassar et al. 2002). Recent experimental results have objectively confirmed the importance of this mechanism in PA variability (Jorge et al. 2019). Additionally, and in fact to a larger extent than head motion, the respiratory cycle and fluctuations in heart rate itself have also been found linked to significant variations in PA shape and amplitude across cycles, over relatively short timescales of only a few heartbeats (Jorge

et al. 2019). Aside from the PA waveform itself, others have also found important variability in the PA timing, i.e., the time difference between each cardiac depolarization (ECG) and the resulting PA occurrence (Marino et al. 2018a). Altogether, these findings of multiple sources of variability demonstrate the complexity of PAs, and of their underlying mechanisms and interactions, and highlight the considerable challenges involved in adequate PA triggering, modeling, and reduction.

8.3 Data Acquisition Considerations

Despite the increasing effectiveness of PA reduction methods, this remains a challenging post-processing correction. It is therefore crucial to take appropriate steps on the acquisition side to minimize a priori the appearance of the PA on the EEG data as much as possible. The configuration of the EEG-fMRI setup can be optimized in order to minimize MR-related artifacts on the EEG, in general. This may include the use of shorter and bundled EEG leads when feasible (Assecondi et al. 2016; Jorge et al. 2015b) and their careful placement along the magnet bore in order to isolate them from any scanner vibrations as well as possible (Mullinger et al. 2013a).

Additionally, artifacts associated with head motion, including not only the PA but also voluntary head motion, can also be minimized by restraining head motion. In the study by Anami et al. (2002), a head-fixation system was proposed, whereby a pillow is inserted to fill the gap between the subjects' head and the head coils which is subsequently deflated until small head movements are suppressed. The use of bite bars has also been found to effectively reduce the amplitude of the PA by more than 80% in some participants (Mullinger et al. 2013b). In the case of ERP studies, the experimental design can be adjusted in order to minimize the PA specifically. For example, Ertl et al. (2010) proposed to display the stimuli time-locked with the cardiac pulse. Because the PA is known to appear on the EEG approximately 150–500 ms after the QRS complex, the ERPs of interest are less prone to be affected by the artifact.

Most of the pulse artifact reduction methods rely on triggering events based on the R-peak extracted from cardiac traces recorded concurrently with the EEG (and the fMRI). Care must be taken when using the ECG for this purpose, because it becomes severely distorted in the MR environment (Niendorf et al. 2012), and is further degraded by the gradient artifact during the fMRI acquisitions (or by its residuals after gradient artifact correction), which may compromise the ability to detect R-peaks. According to a well-accepted recommendation (Mullinger et al. 2013a), a sufficiently good quality (clean and undistorted) ECG signal can in principle be recorded from a single electrode placed at the base of the back of the subject, with the respective lead stretched along the paravertebral line. This allows for maximization of the signal-to-noise ratio of the R-peak, by minimizing motion artifacts associated with breathing (compared to placements on the chest) while also providing subject comfort. The requirements on the resistance of the ECG

electrodes are not as large as those on the EEG electrodes, given the typically larger amplitude of the cardiac signals. Nevertheless, the impedance of ECG electrodes should be kept below 50 kΩ in order to ensure sufficient data quality for R-peak detection (Mullinger et al. 2013a).

Although potentially more prone to motion artifacts, other electrode placement configurations have also been used, namely, the triangularly shaped distribution of two electrodes over the chest with the reference on the scalp (Iannotti et al. 2015; Mullinger et al. 2013b). Alternatively, the vectorcardiogram (VCG) has been considered as a potential substitute of the ECG in this context (Mullinger et al. 2008). It uses a 3D orthogonal lead system capable of temporally and spatially resolving the electromotive forces generated by cardiac depolarization, and it has been shown to be less affected by the gradient artifact (Mullinger et al. 2008, 2013a). Because ECG is still the most commonly used technique, here we refer to the cardiac traces as ECG signals, for the sake of simplicity.

8.4 Artifact Reduction Methods

In this section, we review the most relevant methods for PA reduction (Table 8.1). In general, these can be subdivided into three main types. First, the most commonly used type consists of the time-domain subtraction of PA temporal waveform templates extracted from the EEG data. These can be obtained by averaging across neighboring artifact occurrences, for instance, or by explicitly estimating the pulse waveform. Second, methods exploring the spatiotemporal distribution of the PA have been used and are mostly based on blind source separation techniques, particularly independent component analysis (ICA). Their purpose is to separate EEG artifact sources from neuronal sources and then remove (or correct) artifact sources when back-reconstructing the EEG data to its original space. Third, some approaches rely on dedicated sensors to measure the artifact waveforms independently from the EEG, followed by their modeling and subtraction from the PA-contaminated EEG signal. After surveying the several PA reduction methods falling into each of these three main approaches, the most common criteria used for evaluating PA reduction are presented, and some considerations on how to prevent/minimize the PA are then provided.

8.4.1 Temporal Waveform-Based Methods

The seminal paper by Allen et al. (1998) introduced what is still the most commonly used method for PA reduction: the average artifact subtraction (AAS) algorithm (illustrated in Fig. 8.3). AAS operates in the time domain of the EEG sensor space on a channel-by-channel basis and computes a temporal template to be subtracted from each PA occurrence by averaging across a number of artifact occurrences neighboring it. For this purpose, it is necessary to first detect the instances at which the PA occurs. Assuming that the artifact is approximately

Table 8.1 List of PA reduction methods

Type of approach	Subtype	Brief description	Reference
Temporal waveform-based		AAS	Allen et al. (2000)
		OBS	Marino et al. (2018b) and Niazy et al. (2005)
		PA estimation from EEG signal	Iannotti et al. (2015), Javed et al. (2014), Krishnaswamy et al. (2016), and Wong et al. (2018)
Spatiotemporal pattern-based	*ICA with PA-related IC selection and removal (based on)*	Correlation with ECG or PA templates	Mantini et al. (2007) and Srivastava et al. (2005)
		Autocorrelation function	Deburchgraeve et al. (2008)
		Spectral content	Vanderperren et al. (2007)
		Peak-to-peak values	Vanderperren et al. (2010)
		Variance explained	Debener et al. (2008)
		Constrained ICA (automatic IC selection)	Leclercq et al. (2009)
	Combination of ICA with AAS/OBS	OBS + IC removal	Debener et al. (2005, 2007)
		IC removal + OBS on remaining ICs	Liu et al. (2012)
		AAS/OBS on selected ICs	Abreu et al. (2016b)
Sensor-based		Piezoelectric motion sensors	Bonmassar et al. (2002) and Hill et al. (1995)
		Loops of carbon fiber wire	Masterton et al. (2007)
		Reference layers	Chowdhury et al. (2014), Luo et al. (2014), and Steyrl et al. (2017)
		Subset of insulated electrodes to capture artifacts	Jorge et al. (2015a) and Xia et al. (2014a, b)
		Prospective motion correction (PMC) using camera tracker	LeVan et al. (2013)

time-locked with the heartbeat, a reference point is identified in each cardiac cycle, typically by recording the ECG simultaneously with the EEG and then finding its R-peaks. Because the appearance of the PA on the EEG is delayed in relation to the R-peaks on the ECG, a time delay must be considered. In its original implementation, the AAS defines a fixed delay of 210 ms based on empirical observations from the data. Based on the above description, it is clear that AAS relies on three main assumptions: (1) the PA and the EEG signal of interest are uncorrelated; (2) the PA remains stable across a limited number of successive heartbeats; and (3) the time delay between the R-peaks and the PA occurrences is

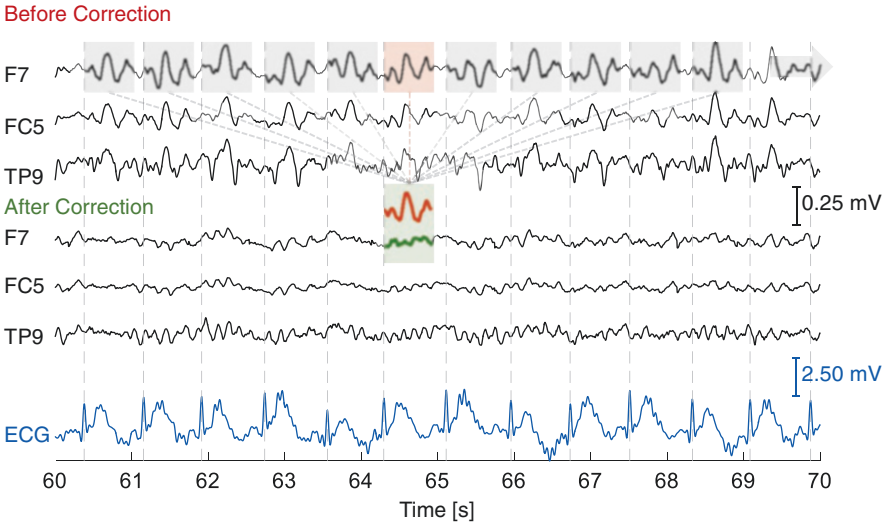

Fig. 8.3 Illustration of an AAS-based method for reduction of the pulse artifact: A 10 s segment of the time courses of three representative EEG channels is shown, before (top) and after (middle) correction, together with the corresponding ECG time course (bottom). An example artifact occurrence is highlighted by the red box; the corresponding average artifact waveform (red trace) was computed by averaging across 11 artifact windows around (and including) the artifact occurrence to be reduced (gray boxes and red box); this was then subtracted from the artifact occurrence, yielding the artifact-corrected EEG segment (green trace)

stable across the entire recording. Moreover, the number of PA occurrences used to build the template critically determines the performance of AAS. In fact, using a large number of PA occurrences leads to an accurate PA template but reduces its sensitivity to temporal fluctuations in PA, and thus it may yield poor artifact reduction. In contrast, templates based on the averaging of few PA occurrences strongly attenuate the artifact but may also reduce EEG signal of interest that was not sufficiently averaged out.

Because of its strong assumptions and known limitations, several modifications of the AAS have been proposed in order to circumvent them. The most influential work was presented in 2005 by Niazy et al., where the assumption of PA stability is addressed. For that purpose, principal component analysis (PCA) is applied to all PA occurrences in order to build an optimal basis set (OBS), comprising a given number of principal components (PCs) that explain the PA variance to some extent (Niazy et al. 2005). Artifact reduction is then achieved by fitting the basis set to each PA occurrence, followed by a subtraction of the fit. The performance of OBS is determined by the number of PCs comprising the basis set, with a larger number of PCs yielding stronger PA reduction; as in AAS, this may also result in the attenuation of EEG signal of interest. Quite recently, Marino et al. (2018b) modified the original OBS to account for variable delays between the R-peaks and PA occurrences, by estimating them on a beat-to-beat basis, and showed that a more accurate

PA reduction can be achieved which compromises the EEG signal of interest to a lesser extent.

Alternatively, a less common approach consists in estimating the PA waveform from the entire EEG recording and directly subtracting it from the data (for each channel separately). One proposed method estimates the PA waveform as a linear combination of several cardiac-related harmonics (Krishnaswamy et al. 2016), while another one combines the empirical mode decomposition (EMD) of the EEG data with PCA (Javed et al. 2014). Regarding the latter, it is assumed that the PA is roughly periodic, and thus EMD is first applied to retrieve the oscillatory modes present in the data, while PCA is used to extract the PCs associated with the PA. In a more recent work, a multiple-scale peak detection algorithm is proposed for the automatic determination of the BCG cycle directly from the EEG data (Wong et al. 2018). In a different approach, based on the observed topographical distribution of the PA, an artifact template was simply estimated from the difference signal between the right and left electrodes most affected by the artifact (facial and temporal) and was then used in subsequent AAS correction (Iannotti et al. 2015).

8.4.2 Spatiotemporal Pattern-Based Methods

In order to account for not only the temporal waveform but also the spatial distribution of the artifact, blind source separation techniques have been widely used for the identification of PA sources and subsequent artifact reduction. Temporal ICA is by far the most common technique, whereby an $N \times M$ EEG dataset, with N channels and M time points, is decomposed into a linear combination of L independent components (ICs) with $N \times L$ weights (Bell and Sejnowski 1995; Lee et al. 1999). It is typically assumed that the number of sources in the brain is equal to the number of EEG channels and, in that case, the equation describing the relationship between the EEG signal, $\mathbf{E}$, and the independent components, $\mathbf{I}$, is given by

$$\mathbf{I}_{[N\times M]} = \mathbf{W}_{[N\times N]} \cdot \mathbf{E}_{[N\times M]} \tag{8.5}$$

where $\mathbf{W}$ represents the unmixing matrix which carries the coefficients of the linear combination between the EEG data and the ICs (Bell and Sejnowski 1995; Lee et al. 1999). Artifact reduction can then be obtained by removing the contribution of the PA sources from the reconstruction of the EEG (illustrated in Fig. 8.4):

$$\mathbf{E}_{\text{cor}} = \mathbf{X} \cdot \mathbf{Z} \cdot \mathbf{I} \tag{8.6}$$

where $\mathbf{E}_{\text{cor}}$ is the corrected EEG signal, and $\mathbf{Z}$ is a $N \times N$ diagonal matrix in which the z_{ii} element is equal to 0 if the i-th source is associated with the PA and 1 otherwise; $\mathbf{X}$ denotes the mixing matrix, that is, the inverse of $\mathbf{W}$, representing the spatial patterns, or topographies, associated with each source.

Naturally, this type of PA reduction methods relies on two major assumptions: (1) ICA is capable of separating the PA sources from other EEG sources contributing to the measured signal; and (2) PA sources can be accurately classified among

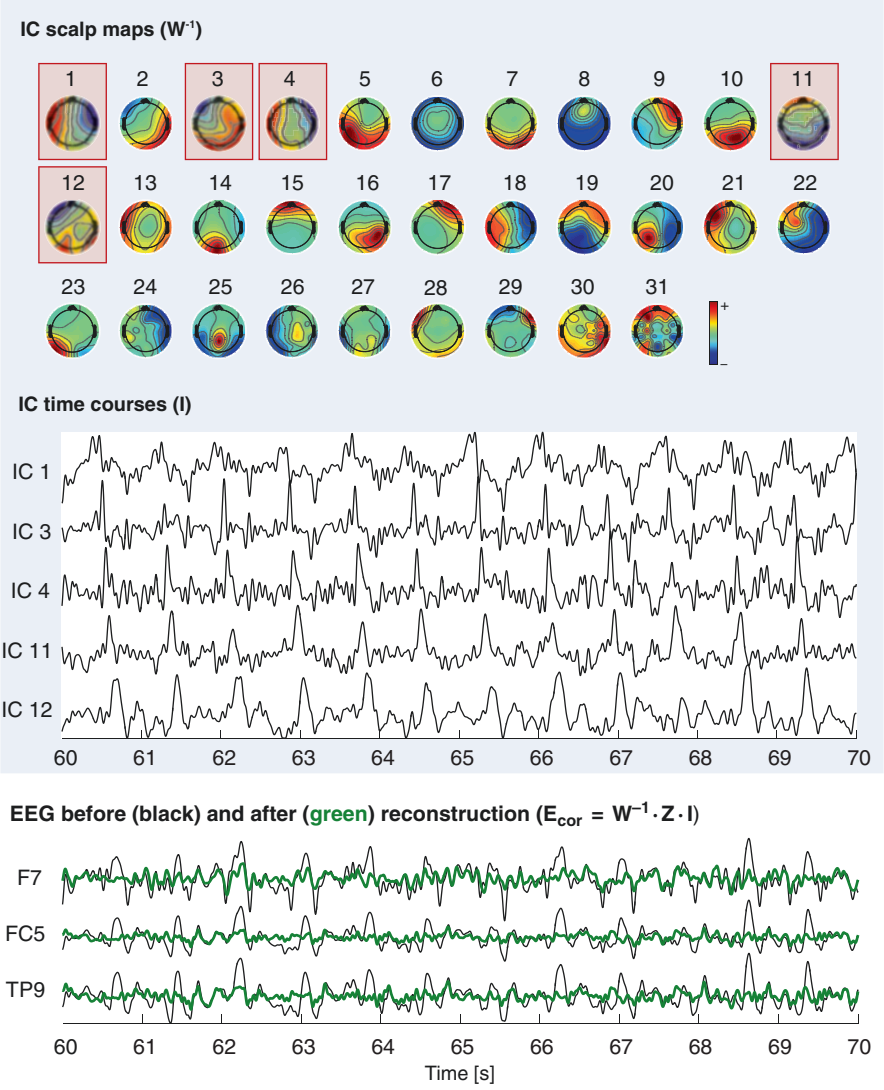

Fig. 8.4 Illustration of an ICA-based method for reduction of the pulse artifact: The scalp maps of the 31 ICs obtained by temporal ICA of the EEG data are shown (top); ICs 1, 3, 4, 11, and 12 (highlighted with the red box) were classified as PA-related using the PROJIC algorithm (Abreu et al. 2016a). A 10 s segment of their time courses is shown (middle). The corresponding 10 s segment of the time courses of three representative EEG channels is also shown (bottom), before (black) and after (green) correction, by removing all the selected ICs from the reconstruction of the EEG data

all estimated sources. Most of the work in this field has been dedicated to selecting the best criterion (or combination of criteria) for accurately classifying the PA sources. The first studies assumed a direct relationship between the PA sources and cardiac signals. This can be evaluated in the time domain, by identifying the EEG sources exhibiting the highest correlation (Mantini et al. 2007; Srivastava et al. 2005) or mutual information (Liu et al. 2012) with the ECG signal. In the frequency domain, the PA sources can be determined as those exhibiting peaks at their autocorrelation functions and/or power spectra associated with the cardiac signal (Deburchgraeve et al. 2008; Vanderperren et al. 2007). In a more indirect fashion, one can select the PA sources as those explaining the largest amount of variance of the PA (Debener et al. 2008). Following this rationale, we have proposed the PROJIC (*PROJection onto Independent Components*) algorithm, whereby the average PA occurrence of each channel is first projected onto the source space by means of the corresponding unmixing matrix **W**. The power of each projection, computed as the squared sum for each time instant, is then clustered by *k*-means; sources assigned to high-powered clusters are deemed PA-related (Abreu et al. 2016a, b).

Despite its reported success, the plausibility of using ICA for PA reduction can be questioned. In fact, one of the strongest assumptions of ICA is the spatial stationarity of the sources to be estimated. The recognized, but frequently overlooked, nonstationarity of the PA sources may then hamper the ability of ICA to separate them from the remaining sources. One of the first attempts to tackle this was through the development of the so-called constrained ICA technique, where constraining conditions reflecting known PA characteristics are introduced during the decomposition procedure, leading to the automatic identification of PA sources (Leclercq et al. 2009). Nonetheless, the most popular approaches for circumventing the limitations of ICA and AAS (or OBS) rely on the combination of PA reduction methods based on temporal waveforms and spatiotemporal patterns. The first study using such rationale assumed that after the employment of OBS, residual PA was still present, which could be further attenuated by decomposing the OBS-corrected EEG signal with ICA and eliminating the contribution of the PA sources (Debener et al. 2005, 2007). In order to specifically tackle the nonstationarity issue of the PA sources, Liu et al. (2012) applied ICA to the EEG signal and assumed that the PA contributed to all sources in varying degrees. The PA reduction procedure was then performed in two steps: the PA sources were first identified as those exhibiting the highest mutual information with the ECG and their contribution eliminated, followed by the application of a modified version of OBS to the remaining sources. We have recently proposed the application of AAS or OBS also in the source space, but only to PA sources, which are subsequently kept in the EEG signal reconstruction together with the original non-PA sources (Abreu et al. 2016a). In contrast with Liu et al. (2012), this approach aims to preserve the physiological signal as much as possible without compromising artifact removal effectiveness.

8.4.3 Sensor-Based Methods

Additional sensors can be used to independently monitor pulse-driven and voluntary head movements during concurrent EEG-fMRI recordings; this information can then be used to de-noise the EEG signals. Various sensor-based approaches have been proposed to date, differing essentially in two aspects: (1) the type of sensors used and (2) the method applied for artifact correction using the sensor information.

Early attempts employed a piezoelectric transducer attached to the subjects' head to measure head motion and used its signal to estimate motion-related artifacts in general and the PA, in particular, on the EEG (Bonmassar et al. 2002; Hill et al. 1995). In a similar approach, LeVan et al. (2013) recently used an optical tracking system designed to monitor head motion inside the scanner (Maclaren et al. 2012). In order to correct the PA contribution on the EEG data, the measured motion parameters were first converted into velocities, and the PA was then modeled as a linear combination of the low-pass filtered velocities, followed by its subtraction from the EEG.

Besides the use of piezoelectric and optical sensors to measure head motion, a few studies have used sensors directly measuring the electric currents induced by the PA and head motion in general, in the MR environment. First, carbon-wire loops attached to the EEG cap were employed, and the artifacts at each EEG electrode were estimated as linear combinations of the sensor signal time courses (Bonmassar et al. 2002; Masterton et al. 2007). For weight estimation, the authors employed time adaptive techniques to account for the nonstationarity of the PA, including adaptive noise reduction based on Kalman filtering (Bonmassar et al. 2002) or recursive least squares estimation (Masterton et al. 2007), for example.

In order to more specifically measure the artifacts induced at each EEG electrode, the concept of reference layers emerged. These are based on attaching an additional electrode net on top of the main EEG net, separated by an insulating layer (Chowdhury et al. 2014; Luo et al. 2014). With this setup, the original EEG electrodes capture a mixture of neuronal signals and artifacts, while those above the insulating layer are only sensitive to the artifacts, as they are physically attached to, but electrically isolated from, the subjects' head. A direct subtraction between the original and insulated electrodes can then be applied to reduce the artifacts (Chowdhury et al. 2014; Luo et al. 2014).

Considering the already typically intricate EEG-fMRI setups, the use of additional sensors may be questioned in terms of feasibility or even prohibitive in some clinical sites. A more practical approach that avoids the need for additional recording hardware was proposed by Xia et al. (2014a), which consists of defining a set of insulated electrodes spatially surrounding each uninsulated electrode on the EEG cap in order to build an estimate of the local PA. Following this rationale, methods to determine the optimal minimum number of electrodes to be insulated have been developed based on the spatial redundancy of the PA measured from neighboring electrodes (Xia et al. 2014a). More recently, an even simpler approach was proposed by Jorge et al. (2015a), which introduces only small changes to a standard EEG cap. In this case, a limited number of the existing EEG electrodes are used as motion sensors by insulating them from the scalp and directly connecting them to the reference electrode. Different methods can then be used to estimate

the artifact at each EEG electrode position, similarly to the separate loop approaches.

In general, the use of sensor-based reference artifact information has been found quite valuable, with various advantages relative to EEG data-based methods, because such information (1) is independent from EEG activity of neuronal origin, (2) is sensitive to variability in the PA across heartbeats, (3) does not require accurate PA triggering, and (4) allows relatively straightforward implementations of real-time artifact correction (Masterton et al. 2007; Steyrl et al. 2018). Nevertheless, some potential limitations do exist. From a practical standpoint, the need for additional recording hardware increases the complexity of experimental setups and subject preparation and must be properly validated to ensure safety. From a conceptual standpoint, most of the proposed approaches employ considerably less sensor channels than EEG channels and therefore need to assume that the PA in each EEG channel can be accurately modeled by a combination of the available sensors. Moreover, not all hypothesized sources of the PA are captured by external sensors—bulk head motion, and possibly scalp dilation, can be measured, but Hall effect contributions are more challenging and have not been probed so far. The latter may introduce PA variability that is not adequately accounted for and could be one cause for the observation that even the most comprehensive methods, such as reference layer-based de-noising, are still most effective when used in combination with EEG data-based methods such as AAS (Chowdhury et al. 2014; Murray et al. 2008; Steyrl et al. 2017, 2018), as well as amplitude-fitting approaches (Steyrl et al. 2017). Altogether, sensor-based methods are currently a topic of active research and development (Hermans et al. 2016).

8.4.4 Artifact Reduction Evaluation

One of the most accurate and simplest ways of assessing the performance of PA reduction methods is to quantify changes in event-related potentials (ERPs) measured during simultaneous EEG-fMRI studies of event-related activity. It is then possible to assess not only the amount of PA reduction but also its effects on the EEG signal of interest. Several metrics have been proposed in the literature to quantify the effects of PA reduction on ERPs, namely, their intertrial variability (Vanderperren et al. 2010) and signal-to-noise ratio (Debener et al. 2007), both known to be affected by the PA. It is also possible to quantify differences between the ERPs extracted from EEG data acquired outside the MR scanner, which are free of PA, and those measured simultaneously with fMRI. When the frequency content of an ERP is known, the power within that frequency band can also be compared before and after PA reduction (Xia et al. 2014a).

In resting-state EEG-fMRI studies, the task of assessing the performance of PA reduction methods is more challenging, particularly in what concerns the preservation of the EEG signal of interest. Thus, only PA reduction is quantified, typically by computing the root-mean-square value (Vanderperren et al. 2010) or the peak-to-peak value (Chowdhury et al. 2014) of the EEG signal at the PA occurrences before and after correction. Because of its roughly periodic nature, PA reduction has also been quantified in the frequency domain by the average spectral power across

windows around the cardiac fundamental frequency and its first harmonics (Liu et al. 2012). In a recent study, we proposed an evaluation pipeline that aims to assess not only PA reduction but also preservation of EEG signal of interest, in resting-state data (Abreu et al. 2016a). This is achieved by computing the spectral power over both PA and non-PA frequency bands before and after correction and then linearly combining their ratios using a weighting factor reflecting the importance given to the preservation of EEG signal of interest relative to PA reduction.

A few systematic comparisons between different PA reduction methods have been reported in the literature. In one report, Grouiller et al. (2007) found that AAS was the method of choice if highly accurate R-peak detection was achieved. Additionally, and as discussed in Vanderperren et al. (2010), OBS- and ICA-based approaches only yielded comparable results if the ICA parameters were fine-tuned. In fact, optimizing the algorithms' parameters has been shown to critically affect the effectiveness and reliability of the subsequent analyses (Abreu et al. 2016a; Vanderperren et al. 2010), particularly at high magnetic field strengths (Debener et al. 2008). In our report (Abreu et al. 2016a), AAS was the method exhibiting the second best results in terms of accurately reducing the PA while preserving the EEG signal of interest. In contrast, purely ICA-based methods either resulted in substantial residual artifacts or a significantly distorted EEG signal. The best results were obtained by combining ICA to separate the PA sources, with AAS to correct the PA occurrences in the source space. We believe that this may be a relatively straightforward and effective solution for PA correction, which does not require additional hardware.

8.5 Conclusion

The artifact induced on the EEG recorded inside the MRI scanner due to the function of the heart remains as one of the most challenging aspects of simultaneous EEG-fMRI studies. Various artifact reduction techniques have been proposed and tested over the last few decades. While combinations of ICA- with AAS-based methods have been found to be the most effective in typical EEG-fMRI experimental setups, a few studies have shown promising results when separately measuring head motion with appropriate sensors. Although such sensor-based approaches require modifications of the experimental setup, they have the advantage of taking the temporal variability of the artifact into account in a direct, empirical way. In parallel, considerable progress has been made over the past decade in the understanding of the artifact's underlying biophysical mechanisms, which may be incorporated to further improve current artifact reduction techniques. Perhaps even more importantly, knowledge of the multiple artifact sources and their relative contributions should be used to leverage efforts to minimize the occurrence of the PA in the first place. In the future, we believe that EEG-fMRI setups should be carefully optimized with the aim of minimizing the induction of EEG artifacts in general and the PA in particular, while complementary artifact reduction methods should be further improved by better accounting for the artifact's properties.

Acknowledgments We acknowledge the financial support by the Portuguese Science Foundation (FCT) through grants LARSyS (UIDB/50009/2020), MIG_N2Treat (PTDC/EMDEMD/29675/2017) and NeurAugVR (PTDC/CCICOM/31485/2017), by the Swiss National Science Foundation (SNSF) through grant 185909, and by the CIBM Centre for Biomedical Imaging.

References

Abreu R, Leite M, Jorge J, Grouiller F, van der Zwaag W, Leal A, Figueiredo P (2016a) Ballistocardiogram artifact correction taking into account physiological signal preservation in simultaneous EEG-fMRI. NeuroImage 135:45–63. https://doi.org/10.1016/j.neuroimage.2016.03.034

Abreu R, Leite M, Leal A, Figueiredo P (2016b) Objective selection of epilepsy-related independent components from EEG data. J Neurosci Methods 258:67–78. https://doi.org/10.1016/j.jneumeth.2015.10.003

Abreu R, Leal A, Figueiredo P (2018) EEG-informed fMRI: a review of data analysis methods. Front Hum Neurosci 12:29. https://doi.org/10.3389/fnhum.2018.00029

Allen PJ, Polizzi G, Krakow K, Fish DR, Lemieux L (1998) Identification of EEG events in the MR scanner: the problem of pulse artifact and a method for its subtraction. NeuroImage 8:229–239. https://doi.org/10.1006/nimg.1998.0361

Allen PJ, Josephs O, Turner R (2000) A method for removing imaging artifact from continuous EEG recorded during functional MRI. NeuroImage 12:230–239. https://doi.org/10.1006/nimg.2000.0599

Anami K, Saitoh O, Yumoto M, Tanaka F, Kawagoe Y, Ohnishi T, Matsuda H (2002) Reduction of ballistocardiogram with a vacuum head-fixating system during simultaneous fMRI and multichannel monopolar EEG recording. Int Congr Ser 1232:427–431. https://doi.org/10.1016/S0531-5131(01)00624-0

Assecondi S, Lavallee C, Ferrari P, Jovicich J (2016) Length matters: improved high field EEG-fMRI recordings using shorter EEG cables. J Neurosci Methods 269:74–87. https://doi.org/10.1016/j.jneumeth.2016.05.014

Bell AJ, Sejnowski TJ (1995) An information-maximization approach to blind separation and blind deconvolution. Neural Comput 7:1129–1159. https://doi.org/10.1162/neco.1995.7.6.1129

Bonmassar G, Purdon PL, Jääskeläinen IP, Chiappa K, Solo V, Brown EN, Belliveau JW (2002) Motion and ballistocardiogram artifact removal for interleaved recording of EEG and EPs during MRI. NeuroImage 16:1127–1141. https://doi.org/10.1006/nimg.2002.1125

Chowdhury MEH, Mullinger KJ, Glover P, Bowtell R (2014) Reference layer artefact subtraction (RLAS): a novel method of minimizing EEG artefacts during simultaneous fMRI. NeuroImage 84:307–319. https://doi.org/10.1016/j.neuroimage.2013.08.039

Debener S, Ullsperger M, Siegel M, Fiehler K, von Cramon DY, Engel AK (2005) Trial-by-trial coupling of concurrent electroencephalogram and functional magnetic resonance imaging identifies the dynamics of performance monitoring. J Neurosci 25:11730–11737. https://doi.org/10.1523/JNEUROSCI.3286-05.2005

Debener S, Strobel A, Sorger B, Peters J, Kranczioch C, Engel AK, Goebel R (2007) Improved quality of auditory event-related potentials recorded simultaneously with 3-T fMRI: removal of the ballistocardiogram artefact. NeuroImage 34:587–597. https://doi.org/10.1016/j.neuroimage.2006.09.031

Debener S, Mullinger KJ, Niazy RK, Bowtell RW (2008) Properties of the ballistocardiogram artefact as revealed by EEG recordings at 1.5, 3 and 7 T static magnetic field strength. Int J Psychophysiol 67:189–199. https://doi.org/10.1016/j.ijpsycho.2007.05.015

Deburchgraeve W, Cherian PJ, De Vos M, Swarte RM, Blok JH, Visser GH, Govaert P, Van Huffel S (2008) Automated neonatal seizure detection mimicking a human observer reading EEG. Clin Neurophysiol 119:2447–2454. https://doi.org/10.1016/j.clinph.2008.07.281

Ertl M, Kirsch V, Leicht G, Karch S, Olbrich S, Reiser M, Hegerl U, Pogarell O, Mulert C (2010) Avoiding the ballistocardiogram (BCG) artifact of EEG data acquired simultaneously with fMRI by pulse-triggered presentation of stimuli. J Neurosci Methods 186:231–241. https://doi.org/10.1016/J.JNEUMETH.2009.11.009

Grouiller F, Vercueil L, Krainik A, Segebarth C, Kahane P, David O (2007) A comparative study of different artefact removal algorithms for EEG signals acquired during functional MRI. NeuroImage 38:124–137. https://doi.org/10.1016/j.neuroimage.2007.07.025

Hall JE, Guyton AC (2015) Textbook of medical physiology, 11th edn. Elsevier Health Sciences, Philadelphia, PA

Hawsawi H, Carmichael DW, Lemieux L (2017) Safety of simultaneous scalp or intracranial EEG during MRI: a review. Front Phys 5:42. https://doi.org/10.3389/fphy.2017.00042

Hermans K, de Munck JC, Verdaasdonk R, Boon P, Krausz G, Prueckl R, Ossenblok P (2016) Effectiveness of reference signal-based methods for removal of EEG artifacts due to subtle movements during fMRI scanning. IEEE Trans Biomed Eng 63:2638–2646. https://doi.org/10.1109/TBME.2016.2602038

Hill RA, Chiappa KH, Huang-Hellinger F, Jenkins BG (1995) EEG during MR imaging: differentiation of movement artifact from paroxysmal cortical activity. Neurology 45:1942–1943. https://doi.org/10.1212/WNL.45.10.1942-A

Iannotti GR, Pittau F, Michel CM, Vulliemoz S, Grouiller F (2015) Pulse artifact detection in simultaneous EEG-fMRI recording based on EEG map topography. Brain Topogr 28:21–32. https://doi.org/10.1007/s10548-014-0409-z

Javed E, Faye I, Malik AS, Abdullah JM (2014) Reference-free reduction of ballistocardiogram artifact from EEG data using EMD-PCA. 2014. In: 5th International Conference Intelligent Advanced System Technological Convergence Sustainable Future ICIAS 2014—Proc, pp 14–19. https://doi.org/10.1109/ICIAS.2014.6869512

Jorge J, Van der Zwaag W, Figueiredo P (2014) EEG-fMRI integration for the study of human brain function. NeuroImage 102:24–34. https://doi.org/10.1016/j.neuroimage.2013.05.114

Jorge J, Grouiller F, Gruetter R, van der Zwaag W, Figueiredo P (2015a) Towards high-quality simultaneous EEG-fMRI at 7T: detection and reduction of EEG artifacts due to head motion. NeuroImage 120:143–153. https://doi.org/10.1016/j.neuroimage.2015.07.020

Jorge J, Grouiller F, Ipek Ö, Stoermer R, Michel CM, Figueiredo P, van der Zwaag W, Gruetter R (2015b) Simultaneous EEG-fMRI at ultra-high field: artifact prevention and safety assessment. NeuroImage 105:132–144. https://doi.org/10.1016/j.neuroimage.2014.10.055

Jorge J, Bouloc C, Bréchet L, Michel CM, Gruetter R (2019) Investigating the variability of cardiac pulse artifacts across heartbeats in simultaneous EEG-fMRI recordings: a 7T study. NeuroImage 191:21–35. https://doi.org/10.1016/J.NEUROIMAGE.2019.02.021

Krishnaswamy P, Bonmassar G, Poulsen C, Pierce ET, Purdon PL, Brown EN (2016) Reference-free removal of EEG-fMRI ballistocardiogram artifacts with harmonic regression. NeuroImage 128:398–412. https://doi.org/10.1016/j.neuroimage.2015.06.088

Laufs H (2012) A personalized history of EEG-fMRI integration. NeuroImage 62:1056–1067. https://doi.org/10.1016/j.neuroimage.2012.01.039

Leclercq Y, Balteau E, Dang-Vu T, Schabus M, Luxen A, Maquet P, Phillips C (2009) Rejection of pulse related artefact (PRA) from continuous electroencephalographic (EEG) time series recorded during functional magnetic resonance imaging (fMRI) using constraint independent component analysis (cICA). NeuroImage 44:679–691. https://doi.org/10.1016/j.neuroimage.2008.10.017

Lee T-W, Girolami M, Sejnowski TJ (1999) Independent component analysis using an extended Infomax algorithm for mixed Subgaussian and supergaussian sources. Neural Comput 11:417–441. https://doi.org/10.1162/089976699300016719

LeVan P, Maclaren J, Herbst M, Sostheim R, Zaitsev M, Hennig J (2013) Ballistocardiographic artifact removal from simultaneous EEG-fMRI using an optical motion-tracking system. NeuroImage 75:1–11. https://doi.org/10.1016/j.neuroimage.2013.02.039

Liu Z, de Zwart JA, van Gelderen P, Kuo LW, Duyn JH (2012) Statistical feature extraction for artifact removal from concurrent fMRI-EEG recordings. NeuroImage 59:2073–2087. https://doi.org/10.1016/j.neuroimage.2011.10.042

Luo Q, Huang X, Glover GH (2014) Ballistocardiogram artifact removal with a reference layer and standard EEG cap. J Neurosci Methods 233:137–149. https://doi.org/10.1016/J.JNEUMETH.2014.06.021

Maclaren J, Armstrong BSR, Barrows RT, Danishad KA, Ernst T (2012) Measurement and correction of microscopic head motion during magnetic resonance imaging of the brain. PLoS One 7:48088. https://doi.org/10.1371/journal.pone.0048088

Mantini D, Perrucci MG, Cugini S, Ferretti A, Romani GL, Del Gratta C (2007) Complete artifact removal for EEG recorded during continuous fMRI using independent component analysis. NeuroImage 34:598–607. https://doi.org/10.1016/j.neuroimage.2006.09.037

Marino M, Liu Q, Del Castello M, Corsi C, Wenderoth N, Mantini D (2018a) Heart–brain interactions in the MR environment: characterization of the ballistocardiogram in EEG signals collected during simultaneous fMRI. Brain Topogr 31:337–345. https://doi.org/10.1007/s10548-018-0631-1

Marino M, Liu Q, Koudelka V, Porcaro C, Hlinka J, Wenderoth N, Mantini D (2018b) Adaptive optimal basis set for BCG artifact removal in simultaneous EEG-fMRI. Sci Rep 8:8902. https://doi.org/10.1038/s41598-018-27187-6

Masterton RAJ, Abbott DF, Fleming SW, Jackson GD (2007) Measurement and reduction of motion and ballistocardiogram artefacts from simultaneous EEG and fMRI recordings. NeuroImage 37:202–211. https://doi.org/10.1016/j.neuroimage.2007.02.060

Mullinger KJ, Morgan PS, Bowtell RW (2008) Improved artifact correction for combined electroencephalography/functional MRI by means of synchronization and use of vectorcardiogram recordings. J Magn Reson Imaging 27:607–616. https://doi.org/10.1002/jmri.21277

Mullinger, Castellone P, Bowtell R (2013a) Best current practice for obtaining high quality EEG data during simultaneous FMRI. J Vis Exp 76:50283. https://doi.org/10.3791/50283

Mullinger, Havenhand J, Bowtell R (2013b) Identifying the sources of the pulse artefact in EEG recordings made inside an MR scanner. NeuroImage 71:75–83. https://doi.org/10.1016/j.neuroimage.2012.12.070

Murray MM, Brunet D, Michel CM (2008) Topographic ERP analyses: a step-by-step tutorial review. Brain Topogr 20:249–264. https://doi.org/10.1007/s10548-008-0054-5

Murta T, Leite M, Carmichael DW, Figueiredo P, Lemieux L (2015) Electrophysiological correlates of the BOLD signal for EEG-informed fMRI. Hum Brain Mapp 36:391–414. https://doi.org/10.1002/hbm.22623

Neuner I, Warbrick T, Arrubla J, Felder J, Celik A, Reske M, Boers F, Shah NJ (2013) EEG acquisition in ultra-high static magnetic fields up to 9.4T. NeuroImage 68:214–220. https://doi.org/10.1016/j.neuroimage.2012.11.064

Niazy RK, Beckmann CF, Iannetti GD, Brady JM, Smith SM (2005) Removal of FMRI environment artifacts from EEG data using optimal basis sets. NeuroImage 28:720–737. https://doi.org/10.1016/j.neuroimage.2005.06.067

Niendorf T, Winter L, Frauenrath T (2012) Electrocardiogram in an MRI environment: clinical needs, practical considerations, safety implications, technical solutions and future directions. In: Advances in electrocardiograms-methods and analysis. InTech, London. https://doi.org/10.5772/24340

Nunez PL, Srinivasan R (2006) Electric fields of the brain the Neurophysics of EEG, 2nd edn. Oxford University Press, Oxford

Srivastava G, Crottaz-Herbette S, Lau KM, Glover GH, Menon V (2005) ICA-based procedures for removing ballistocardiogram artifacts from EEG data acquired in the MRI scanner. NeuroImage 24:50–60. https://doi.org/10.1016/j.neuroimage.2004.09.041

Steyrl D, Krausz G, Koschutnig K, Edlinger G, Müller-Putz GR (2017) Reference layer adaptive filtering (RLAF) for EEG artifact reduction in simultaneous EEG-fMRI. J Neural Eng 14:026003. https://doi.org/10.1088/1741-2552/14/2/026003

Steyrl D, Krausz G, Koschutnig K, Edlinger G, Müller-Putz GR (2018) Online reduction of artifacts in EEG of simultaneous EEG-fMRI using reference layer adaptive filtering (RLAF). Brain Topogr 31:129–149. https://doi.org/10.1007/s10548-017-0606-7

Tenforde TS, Gaffey CT, Moyer BR, Budlnger TF (1983) Cardiovascular alterations in Macaca monkeys exposed to stationary magnetic fields: experimental observations and theoretical analysis. Bioelectromagnetics 4:1–9. https://doi.org/10.1002/bem.2250040102

Vanderperren K, Ramautar J, Novitski N, De Vos M (2007) Ballistocardiogram artifacts in simultaneous EEG- fMRI acquisitions. Int J Bioelectromagn 9:146–150

Vanderperren K, De Vos M, Ramautar JR, Novitskiy N, Mennes M, Assecondi S, Vanrumste B, Stiers P, Van den Bergh BRH, Wagemans J, Lagae L, Sunaert S, Van Huffel S (2010) Removal of BCG artifacts from EEG recordings inside the MR scanner: a comparison of methodological and validation-related aspects. NeuroImage 50:920–934. https://doi.org/10.1016/j.neuroimage.2010.01.010

Wong CK, Luo Q, Zotev V, Phillips R, Chan KWC, Bodurka J (2018) Automatic cardiac cycle determination directly from EEG-fMRI data by multi-scale peak detection method. J Neurosci Methods 304:168–184. https://doi.org/10.1016/j.jneumeth.2018.03.017

Xia H, Ruan D, Cohen MS (2014a) Removing ballistocardiogram (BCG) artifact from full-scalp EEG acquired inside the MR scanner with orthogonal matching pursuit (OMP). Front Neurosci 8:1–12. https://doi.org/10.3389/fnins.2014.00218

Xia H, Ruan D, Cohen MS (2014b) Separation and reconstruction of BCG and EEG signals during continuous EEG and fMRI recordings. Front Neurosci 8:1–12. https://doi.org/10.3389/fnins.2014.00163

Yan WX, Mullinger KJ, Geirsdottir GB, Bowtell R (2010) Physical modeling of pulse artefact sources in simultaneous EEG/fMRI. Hum Brain Mapp 31:604–620. https://doi.org/10.1002/hbm.20891

EEG Quality: The Image Acquisition Artefact

9

Petra Ritter, Sven Rothlübbers, Robert Becker, Frank Freyer, and Arno Villringer

Abbreviations

AAS	Average artefact subtraction
ANC	Adaptive noise cancellation
FASTR	fMRI artefact slice template removal
FT	Fourier transform
IAR	Imaging artefact reduction
ICA	Independent component analysis
ITAS	Interpolation–template–alignment–subtraction
LPF	Low-pass filter
PCA	Principal component analysis
RF	Radiofrequency

P. Ritter (✉)
Berlin Institute of Health, Charité Universitätsmedizin Berlin, Berlin, Germany

Department of Neurology, Berlin NeuroImaging Center, Charité Universitaetsmedizin, Berlin, Germany
e-mail: petra.ritter@bih-charite.de

S. Rothlübbers
Fraunhofer Institute for Digital Medicine MEVIS, Bremen, Germany
e-mail: sven.rothluebbers@mevis.fraunhofer.de

R. Becker
University of Zurich, Zurich, Switzerland
e-mail: email@robertbecker.info

F. Freyer
Department of Neurology, Berlin NeuroImaging Center, Charité Universitaetsmedizin, Berlin, Germany

A. Villringer
Department of Neurology, Max Planck Institute for Human Cognitive and Brain Sciences, Leipzig, Germany
e-mail: villringer@cbs.mpg.de

C. Mulert, L. Lemieux (eds.), *EEG - fMRI*,
https://doi.org/10.1007/978-3-031-07121-8_9

SNR Signal-to-noise ratio
TDC Template drift compensation
TDD Template drift detection

9.1 Origin of the Image Acquisition Artefact

In this chapter, we focus on the artefacts that arise in the EEG during the fMRI acquisition process. Functional MRI using echo planar imaging (EPI) sequences involves the application of rapidly varying magnetic field gradients for spatial encoding of the MR signal and radiofrequency (RF) pulses for spin excitation (see Chap. 3). Early in the implementation of EEG–fMRI, it was observed that the acquisition of an MR image results in complete obscuration of the physiological EEG (Ives et al. 1993; Allen et al. 2000). Electromagnetic induction in the circuit formed by the electrodes, leads, patient and amplifier exposed to a time-varying magnetic field causes an electromotive force. Artefacts induced in the EEG by the scanning process itself have a strong deterministic component, due to the preprogrammed nature of the RF and gradient switching sequence, and therefore artefact correction is generally considered a lesser problem than pulse-related artefacts (see Chap. 8). Another artefact originating from the vibration of a scanner's active cooling system may show a slightly less deterministic nature but also a lower amplitude than the scanning artefact itself. According to Faraday's law of induction, the induced electromotive force is proportional to the time derivative of the magnetic flux (summation of the magnetic field perpendicular to the circuit plane over the area circuit), $d\Phi/dt$, and can therefore reflect changes in the field (gradient switching, RF) or in the circuit geometry or position relative to the field due to body motion (Lemieux et al. 1997). Therefore, the combination of body motion with image acquisition artefacts can lead to random variations that represent a real challenge for artefact correction.

9.2 Characteristics of the Image Acquisition Artefact

In a typical EPI BOLD acquisition, the amplitude of the image acquisition artefact can be more than two orders of magnitude higher than the physiological EEG signal (Allen et al. 2000; Felblinger et al. 1999). The largest rate of change of the magnetic field occurs during the application of the RF pulses (about 30,000 T/s) (Huang-Hellinger et al. 1995). However, the frequency of the RF pulses (e.g. 64 MHz at 1.5 T) lies well outside the frequency range of conventional EEG amplifiers resulting in greatly attenuated artefacts (Anami et al. 2003). For example, fMRI in a 1.5 T Siemens Magnetom Vision Scanner (Siemens Erlangen, Germany) produced image acquisition artefacts with amplitudes of up to 12 mV (Figs. 9.1

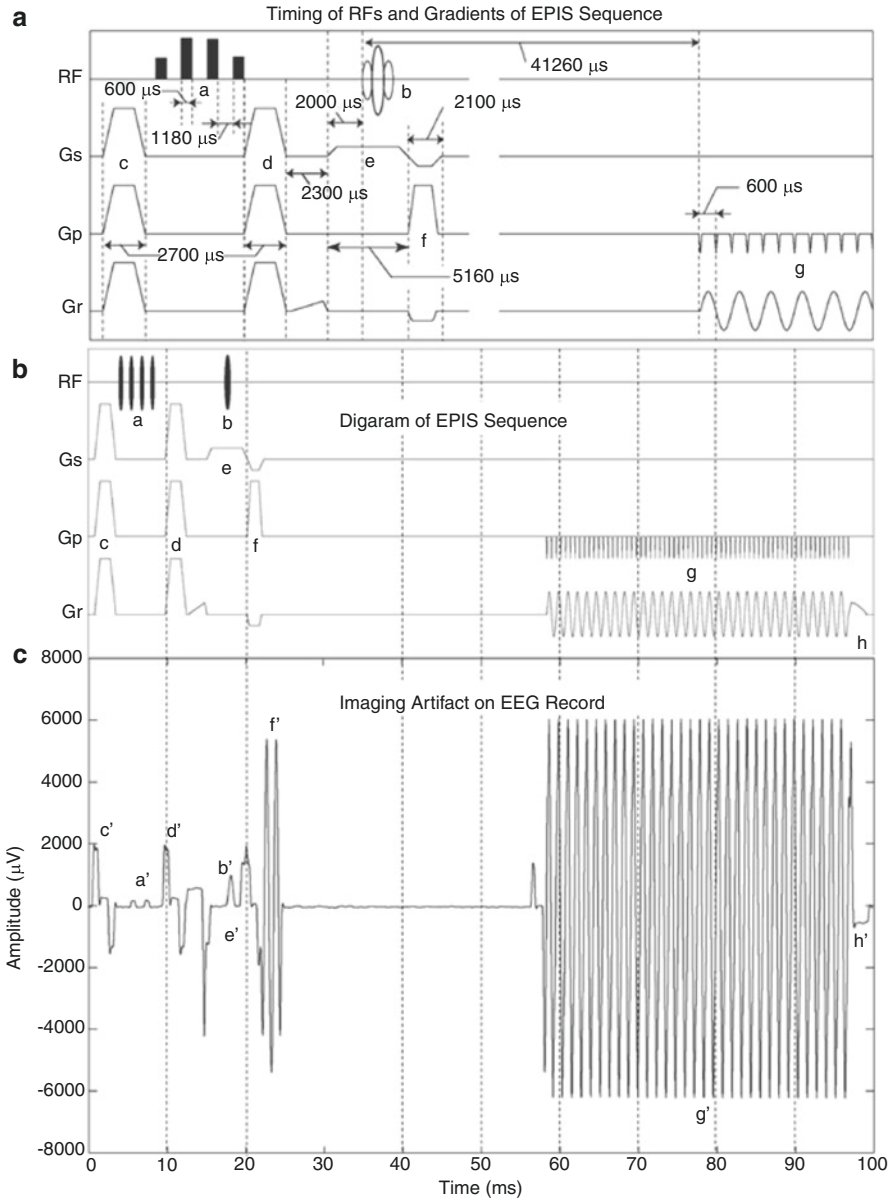

Fig. 9.1 (**a**–**c**) The waveform of the image acquisition artefact can be accurately measured using a sufficiently high digitisation rate and a band-pass filter—here 20 kHz/3 kHz. This is a representative artefact waveform from a EPI BOLD fMRI (EPI) sequence. (**a**) Timings of RF and gradients in an fMRI sequence (EPIS, Siemens: ep2d_fid_60b2080_62_64.ekc). *RF* radiofrequency wave, *Gs* slice selection gradient, *Gp* phase encoding gradient, *Gr* readout gradient. *a* fat suppression pulses (1-3-3-1 pulses), *b* slice selection RF, *c*, *d*, *h*, spoilers, *e* slice selection gradient, *f* dephasing and rephasing gradient, *g* readout gradient. (**b**) Schematic diagram of whole EPIS sequence. (**c**) Image acquisition artefact waveform for one slice scan on a dummy EEG record with a phantom using the EPIS sequence. The artefact corresponding to each gradient component described above in (**a**) can be identified and is denoted by the same alphabet as that denoting the original gradient but with a prime (Anami et al. 2003)

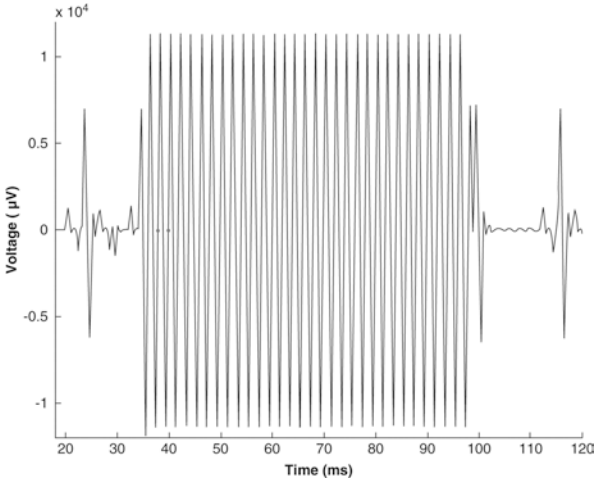

Fig. 9.2 The waveform of an image acquisition artefact during a single-slice acquisition (stepping-stone sequence) using a 1.5 T scanner (Siemens Vision). The artefact was recorded at a sampling rate of 5 kHz and using a 1 kHz hardware low-pass filter. Here the readout gradient has a frequency of 500 Hz (the *two red dots* indicate one gradient period of length 2 ms)

and 9.2). At 1.5 and 3 T, artefacts induced by gradient switching (10^3–10^4 μV) are generally much larger than those arising from RF pulses (up to 10^2 μV) (Anami et al. 2003).

The recorded artefact from one gradient pulse has the approximate differential waveform of the corresponding gradient pulse (Anami et al. 2003). The relative polarity and amplitude of the artefact varies across channels, but the timing of the rising and falling edges is the same across all channels. The frequency range of the image acquisition artefact exceeds that of standard clinical EEG equipment. The frequency of the readout gradient typically lies in the range of 500–900 Hz. Figures 9.1 and 9.2 illustrate typical time courses of the slice acquisition artefact. During periodic EPI BOLD scanning, the EEG is dominated by harmonics of the slice repetition frequency, typically in the range of 10–25 Hz (Fig. 9.3), convolved with harmonics of the volume repetition frequency of about 0.2–2 Hz (Mandelkow et al. 2006; Ritter et al. 2008a). The power spectrum of the image acquisition artefact thus overlaps that of the EEG.

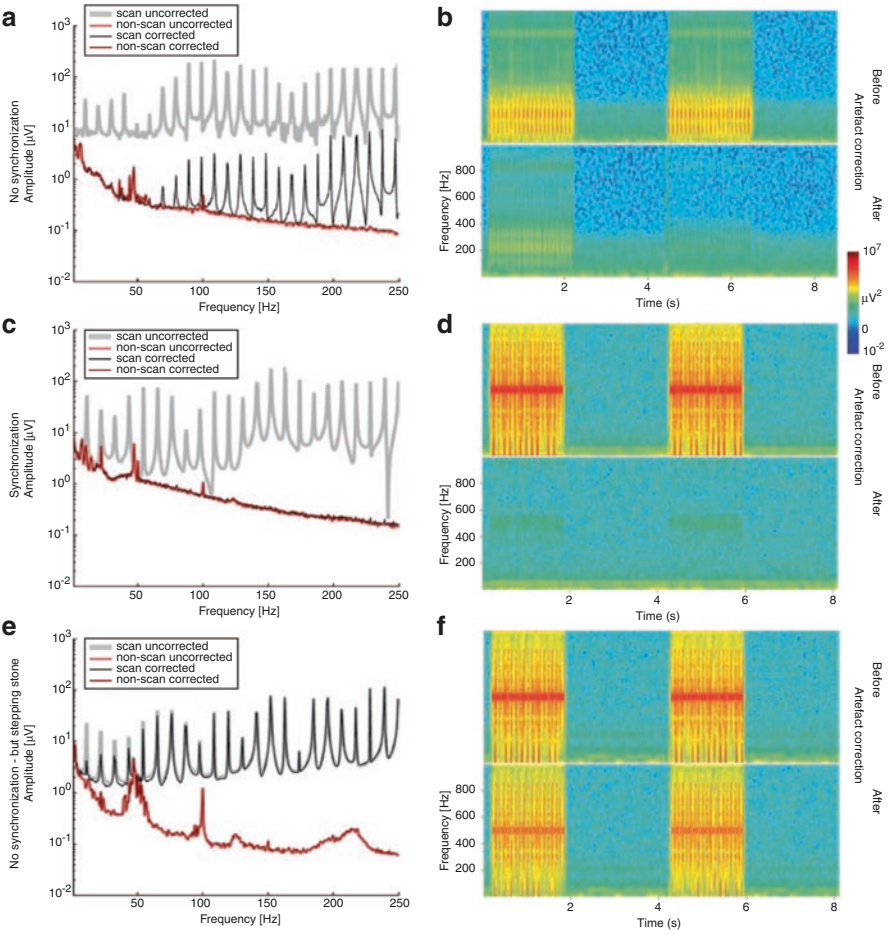

Fig. 9.3 (**a**–**f**) Fourier spectrum and time–frequency plots of EEG data from synchronised and unsynchronised EEG and fMRI data acquisitions before and after image acquisition artefact correction using a slightly modified interpolation–template–alignment–subtraction (ITAS) algorithm (Ritter et al. 2007). Fourier spectra were calculated for scan periods and for non-scan periods. The Fourier spectrum of the imaging artefact afflicted EEG is dominated by harmonics of the slice repetition frequency (10 Hz in this study). (**a**) Unsynchronised EEG–fMRI (1.5 T Siemens Sonata) with an unstable MR sequence. The application of a correction algorithm comprising interpolation, timing error correction and artefact template subtraction (using a slightly modified ITAS algorithm as described in Ritter et al. (2007)) yields good results in the frequency spectrum below 70 Hz. In (**b**), for the same EEG data, time–frequency plots *before* and *after* image artefact correction are depicted. (**c**) Synchronised EEG–fMRI (1.5 T Siemens Vision) with a temporally stable *stepping-stone* MR sequence; simple artefact template subtraction can yield good results across the entire frequency spectrum. (**d**) Here the time–frequency plot of the imaging artefact corrected EEG data shows only mild residual artefacts in the 500 Hz range, reflecting the switching rate of the readout gradient. (**e**) Interestingly, the same algorithm used in (**a**) and (**b**) is much less efficient when applied to an EEG obtained from an unsynchronised EEG–fMRI setup with a stepping-stone sequence. Strong image acquisition artefacts are visible after imaging artefact correction, even in the lower-frequency bands. This failure of the algorithm can be attributed to the oscillatory amplitude fluctuations of the image acquisition artefacts. (**f**) Here, the time–frequency plot of the imaging artefact corrected EEG is severely contaminated with residual artefacts

9.2.1 Characterisation of the Cooling Pump Artefact

The high magnetic field strengths (usually ≥1.5 T) for MR imaging are produced by a superconducting coil that operates at low temperatures and requires constant cooling via a helium-based cooling system. When a cold head cools the helium down to the required temperature, it induces mechanical vibration into the system. The vibrations of the cooling system can be audible outside the scanner and are transmitted into the scanner itself, the body of the scanned subject and the EEG equipment stationed inside the bore. This leads to an artefact that shows as an unwanted voltage induced into the measurement equipment and superimposed to the wanted physiological signal.

The artefact signal shows the signature of the pump vibration and can be directly attributed to the cooling process. It appears while the pump is running, not only during imaging. Different hypotheses exist as to how exactly the vibration leads to the EEG artefact, but no in-depth studies have been published in this regard. It might directly emerge as the conductive loops of the EEG are moved in the strong static magnetic field. This causes the magnetic flux of B_0 through them to change and result in induction. But indirect effects may likewise serve as explanation: As metallic parts of the scanner itself begin to vibrate inside the static field, eddy currents start to occur inside them. These create varying local electromagnetic fields that again cause induction in the EEG loops. After all, both effects may contribute to the artefact and their contributions may vary between setups.

The vibration caused by the cooling pump differs for different scanner types and may have different base frequencies in the order of 20 Hz–50 Hz, 75 Hz up to 150 Hz (Nierhaus et al. 2013; Neuner et al. 2014; Jorge et al. 2015a; Kim 2015; Rothlübbers 2015; Chen et al. 2020), interfering predominantly, but not exclusively, with measurements of the gamma frequency band. During the repetitive cycle of the mechanical motion inside the cold head, the amplitude of the base vibration is modulated. The cycle repetition time may, for instance, lie around 1 s (Rothlübbers 2015); see Fig. 9.4, left. In this case, the vibration is perceived as repetitive (e.g. 1 Hz) humming noise (~50 Hz) which shows as multiple sharp peaks in the frequency spectrum (Fig. 9.4, right). The repetition is however often neither exactly stable nor synchronous to the MR scanner's clock, as happened with the gradient artefact. It is also not possible to identify a trigger based on an external recording as the ECG for the pulse artefact. Hence, unlike gradient or pulse artefacts, the helium pump artefact does not exhibit an onset trigger signal. The artefact magnitude differs in the individual EEG channels but follows a common pattern. In its creation, the overall strength of the artefact depends on the mounting position and mounting strength of the cold head with respect to the scanner, and for some systems, it has even been reported negligible (Neuner et al. 2014). In acquisition, the recording equipment (Jorge et al. 2015a) and patient as well as their positioning are major factors that determine the artefact magnitude.

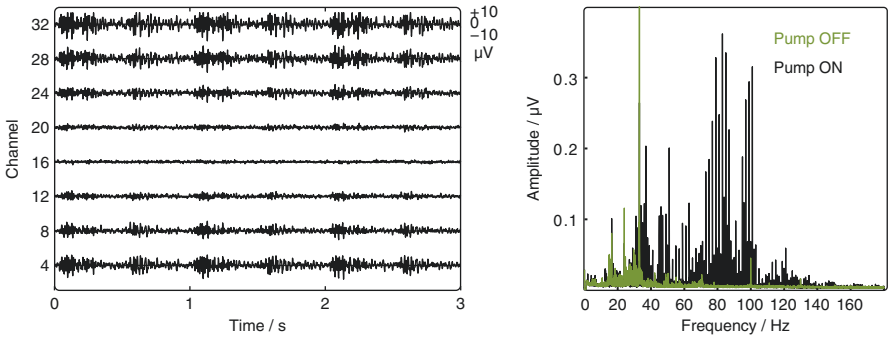

Fig. 9.4 Channel-by-channel noise of the cooling pump artefact showing the repetitive increases of magnitude (twice per ~1 s cycle) of a higher-frequency base signal (left) and respective frequency spectrum compared to baseline with pump switched off (right). Data acquired at a Siemens 7 T MRI system with the Brain Products 64-channel BrainAmpMR, as part of the work of Jorge et al. (2015a). The channels depicted on the left belong to a flat 32-channel acquisition cable, in the order of their physical layout. With the reference lead being in the centre (between channels 15 and 16), the loop area for each channel increases to the sides of the cable and with it so does the strength of the artefact

9.2.1.1 Cooling Pump Artefact Prevention

A common default mode of operation for the cooling system in clinics is "always on" in order to prevent loss of the main magnetic field strength and associated costs (helium boil-off, maintenance) and hazards. However, in general, it is possible to safely switch off the cooling system for a limited time. Some systems can do this automatically during imaging (Mullinger et al. 2008). Several studies report or recommend switching off the cooling system during experiments to improve EEG quality (Ritter and Villringer 2006; Ertl 2010; Nierhaus et al. 2013; Mullinger et al. 2013; Neuner et al. 2014). Nevertheless, some sites do not allow for such measures.

Additionally, it is possible to at least reduce the effect of the artefact by optimising the EEG acquisition setup to minimise induction artefacts. A study on a 7 T scanner (Jorge et al. 2015a) indicates a clear relation between cable configuration and sensitivity to the artefact: In general, shorter and more closely bundled cables should be considered.

9.2.1.2 Cooling Pump Artefact Removal

If the pump artefact cannot be avoided, the analysis of the EEG signal needs to account for it. Options are a discussion as to why the artefact does not affect the signal of interest significantly (Steyrl and Müller-Putz 2019) or an estimate that is does not interfere with the signal of interest (e.g. "gamma band not of interest"). Ideally however, the artefact can be further suppressed in post-processing.

The regularity of the helium cooling pump artefact is located somewhere between the very precise scanner gradient switching and the uncontrollable pulse artefact. Commonly, the correction for helium pump artefacts is performed after prior

correction for gradient switching and pulse artefacts. In order to extract the artefact, methods used for gradient artefact correction such as AAS can be helpful but may not be applicable without adaptation. Likewise, plain blind source separation ICA has not been reported effective yet (Kim 2015). Few algorithms have been reported to address the cooling pump artefact. These aim to factor in the variability of the artefact signal and implement measures to circumvent false-positive removal of physiological signal.

A local template averaging approach (Rothlübbers et al. 2015) can be used to discern artefact from physiological signal. To identify the unstable repetition time and determine the onset of the next cycle, a local autocorrelation approach is applied. An artefact template is obtained from the EEG channel sum. In order to prevent false-positive removal and conserve as much of the physiological signal as possible, the subtracted template is filtered in the frequency domain. The filter reduces the artefact spectrum to the clearly prominent peaks standing out from the background signal. Only then it is subtracted from the input signals of the individual channels.

Similarly, principal component analysis has been demonstrated (Kim et al. 2015) to identify characteristic patterns of the artefact. For this, the signal of a single channel is split into equally sized (2 s) sliding windows over the entire recording. Signal eigenvectors are determined and used to reconstruct parts of the signal recursively. In this work, the condition to accept an eigenvector to represent artefact data is that its spectrum shows a single clear peak in a frequency range 20 Hz–50 Hz and the related time series is characterised as sub-Gaussian.

Rather than reconstructing the artefact from recorded EEG data, methods can be pursued to record the artefact itself. For pulse artefact correction, methods that acquire a reference of the artefact signal (Luo et al. 2014; Chowdhury et al. 2014; Jorge et al. 2015b; Steyrl et al. 2018) have been shown to reduce gradient, pulse and subject motion artefacts (see Chap. 8). These might also prove helpful in pump artefact correction. A work on carbon-wire loop-based artefact recording (van der Meer 2016) indeed reports successful suppression of the pump artefact in this manner. A limitation of these methods is their additional complexity of the hardware. However, even if deemed to overcomplicate the setup for regular use, they could still be valuable tools for recording reference signals in order to judge the performance of correction algorithms.

Future research might involve training recurrent artificial neural networks to identify an artefact in EEG time series data. First approaches to modelling the detection of pulse artefact from ECG by training from a reference signal have been reported (McIntosh et al. 2019). Using gated recurrent units (GRUs), the authors generate network instances that identify the pulse artefact signal without the need for an explicit QRS detection. Consequentially, they conclude that such an approach could also be applied to cooling pump artefact detection. However, since the approach is a form of supervised learning, it does require a known artefact signal for training.

9.3 Avoiding Image Acquisition Artefacts: Interleaved EEG–fMRI Protocols

Depending on the type of brain activity one is interested in studying, interruptions in scanning can reduce the impact of image acquisition artefacts. In EEG-triggered fMRI, short series of fMRI images are acquired following the (random) occurrence of predefined EEG events such as epileptic discharges (Baudewig et al. 2001; Krakow et al. 1999; Lemieux et al. 2001; Seeck et al. 1998; Symms et al. 1999; Warach et al. 1996). Assuming that the peak of the BOLD changes associated with the neural activity of interest occurs with the same time delay as those of normal stimuli (typically 3–8 s), the delayed onset of fMRI acquisition relative to the neural response does not pose a problem. However, this approach requires that the T1 saturation effects are modelled explicitly (Krakow et al. 2002), and fMRI signal changes that occur over long timescales cannot be easily accounted for, given the irregular sampling.

In the periodic interleaved approach, MR acquisition is suspended at regular intervals, resulting in periods free of image acquisition artefacts on the EEG (Goldman et al. 2000, 2002; Ives et al. 1993; Kruggel et al. 2000; Sommer et al. 2003; Ritter et al. 2008a). Although interleaved protocols are generally less flexible and experimentally efficient than continuous measurements, they are suitable for certain forms of brain activity such as slowly varying rhythms and evoked responses. With longer acquisition times, unintentional fluctuations in attention and vigilance gain more relevance.

In multimodal studies of average evoked potentials/BOLD responses, a simultaneous EEG–fMRI setup is not always necessary (Horovitz et al. 2002, 2004; Opitz et al. 1999). In such cases, separate EEG and fMRI measurements offer a reasonable alternative. There are, however, a number of questions that can only be addressed by truly simultaneous EEG–fMRI acquisition, such as studies on single trials and spontaneous non-task-related activity; see Chaps. 1 and 12.

9.4 Reduction of Image Acquisition Artefacts

9.4.1 Reduction at the Source

Minimising conductor loop area and avoiding conductor motion should help to reduce image acquisition artefacts in concurrent EEG–fMRI. Movement can be reduced by stabilising the subject's or patient's head with a vacuum cushion and fixing the EEG electronic devices and wires using sandbags, for example (Anami et al. 2003; Benar et al. 2003). Electrodes should be made of nonferromagnetic materials such as silver, silver/silver chloride, gold-coated silver and carbon (Van Audekerkea et al. 2000) in order to prevent motion relative to the scalp resulting from the strong static magnetic field. Artefact-reducing materials for the leads connecting electrode rings and amplifier are, for example, carbon fibres (Goldman et al. 2000) or very thin copper leads (Easy Cap, FMS, Munich). Twisted dual leads have

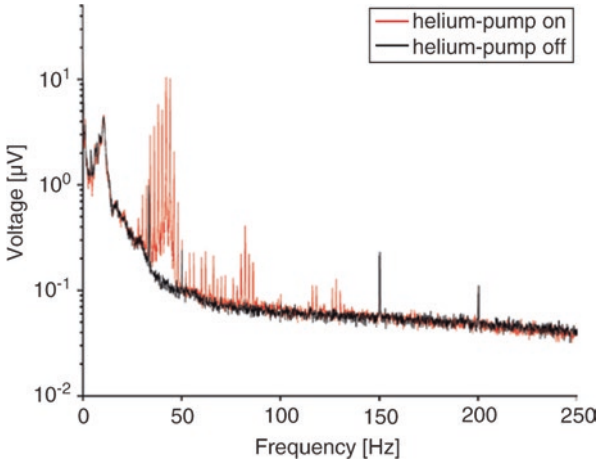

Fig. 9.5 Effects of the helium pump of the MR tomography on the frequency spectrum of the EEG. These data (of 5-min duration for each condition) were obtained in a 1.5 Tesla Siemens Sonata scanner during non-MR acquisition periods. Similar artefacts have been found in other MR systems, such as the 1.5 Tesla Siemens Vision and 3 T Siemens Trio scanners. Helium pump-associated artefacts are not related to MR image acquisition. They occur continuously, i.e. also in non-MR acquisition periods. These artefacts are caused by the piston of the helium cooling head, which strikes the aluminium tube that functions as a cold shield. This causes vibrations of the tube at its resonance frequency of typically around 40 Hz. Vibrations of the tube induce eddy currents that generate magnetic field changes leading to the observed artefacts. The spectral peak visible in the Fourier spectrum at 50 Hz and its higher harmonics can be assigned to line noise

the advantage that currents induced by motion and gradient switching cancel out since the currents induced in consecutive twists flow in opposing directions (Goldman et al. 2000). When possible, switching off the scanner's helium pump and patient monitoring devices can help to reduce vibration- and RF-related artefacts in the EEG (Fig. 9.5).

9.4.1.1 Stepping-Stone Sampling

Due to the short durations of image acquisition artefacts, a special MR sequence has been developed that allows EEG sampling at a digitisation rate of 1 kHz exclusively in the period in which the artefact resides around baseline level (Anami et al. 2003). This "stepping-stone" sampling of EEG data is only possible in combination with synchronisation of the EEG digitisation and scanner clock. Artefact amplitude is strongly attenuated (Fig. 9.6d), for example, to less than 5% in the study by Anami et al. (2003). Consequently, a greater dynamic range is available for the physiological EEG, allowing resolutions of 0.1 µV and below (Ritter et al. 2006; Freyer et al. 2009).

Non-MR signals such as EEG have been recorded using surplus RF receive bandwidth (Hanson et al. 2007). To this end, EEG signals amplified and

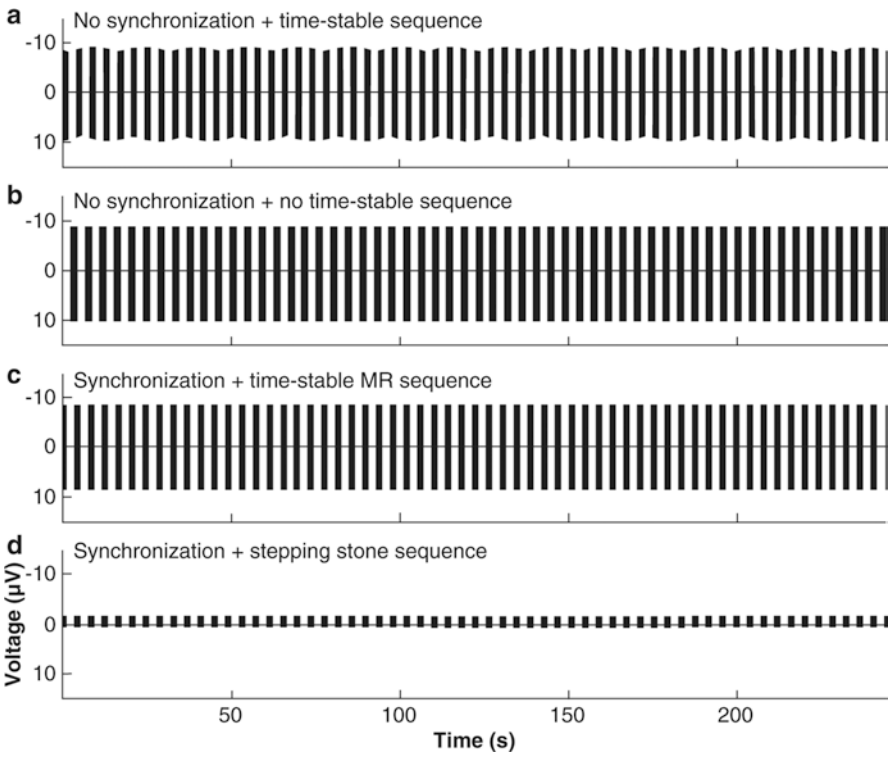

Fig. 9.6 (**a**–**d**) Comparison of imaging artefact waveforms obtained from three different interleaved EEG–fMRI acquisitions: 4 min of EEG data acquired simultaneously with fMRI. Sixty MR volumes were acquired in the 4-min recording time. Due to the high amplitudes of the artefacts, physiological EEG traces in between the image acquisition artefacts are only visible as a *flat line*. (**a**) Unsynchronised EEG and fMRI with a stable MR sequence and a TR that is an integer multiple of the EEG sampling rate yield EEG data containing image acquisition artefacts of high amplitudes and periodically varying shapes. (**b**) Unsynchronised EEG and fMRI with unstable MR sequence yield EEG data containing image acquisition artefacts of high amplitude and aperiodically varying shapes (see Fig. 9.7a for a zoomed-in depiction). (**c**) Synchronised EEG and fMRI in combination with a stable MR sequence yield image acquisition artefacts of high amplitude but constant shape (see Fig. 9.7b). (**d**) Application of the *stepping-stone* sequence and synchronised EEG–fMRI yields image acquisition artefacts of lower amplitudes with constant shapes

digitised within the scanner are transmitted as radio waves that are detectable by the MR system and subsequently reconstructed to fill the periphery of the MRI field of view. Gradient artefacts can be greatly reduced when sampled in periods free of gradient switching using a variant of the stepping-stone technique based on a gradient field detection and gating mechanism that does not require modification of the MR sequence, in contrast to the method by Anami et al. (2003).

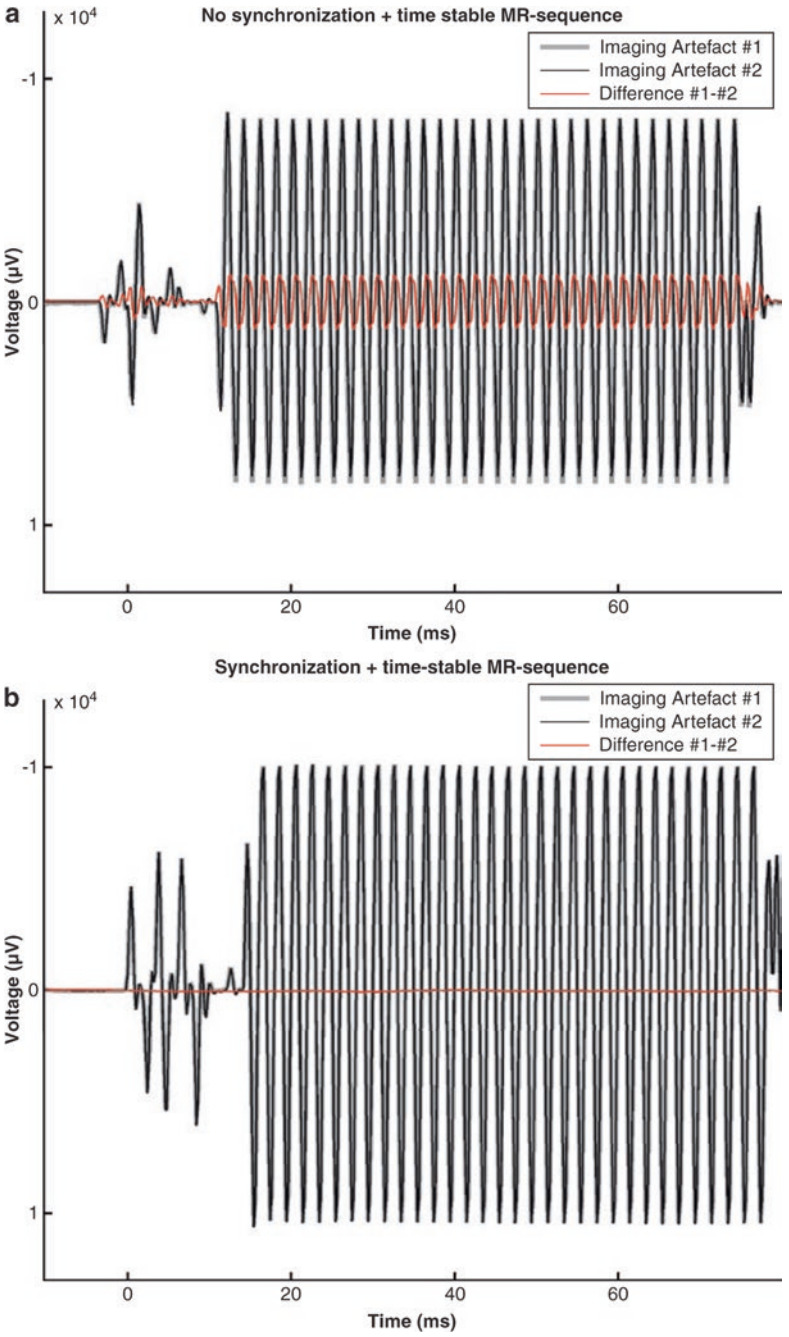

Fig. 9.7 (**a**, **b**) Stability of image acquisition artefacts: single-slice artefacts of two consecutive imaging volume artefacts are superimposed for comparison (black and grey line). Red indicates the difference wave for the two artefacts. (**a**) In the unsynchronised EEG–fMRI approach, consecutive image acquisition artefacts differ considerably, resulting in a distinct difference wave. (**b**) In the synchronised EEG–fMRI approach, consecutive image acquisition artefacts are identical, resulting in a difference wave that is almost zero and zero (i.e. only the physiological EEG signal is present)

9.4.2 Synchronisation of EEG and fMRI Data Acquisitions

The EEG and fMRI acquisition systems can run independently of each other or in synchrony, with important implications for data quality (see Chap. 7 for a discussion of EEG instrumentation). While simpler to implement than synchronised acquisitions, free-running independent EEG and fMRI data acquisitions can result in a great degree of variability in the shape of the artefact (Figs. 9.6a and 9.7a), which may be more difficult to remove using post-processing methods (discussed in the next section of this chapter). Synchronised acquisitions can be advantageous if the MR scan repetition time is chosen to be an integer multiple of the EEG sampling interval, resulting in stationary image acquisition artefacts (Figs. 9.6c, d and 9.7b), assuming that the artefact shape and amplitude do not change due to electrode movement and that the timing of the MR sequence is precise (Anami et al. 2003). In these circumstances, it is possible to reduce the EEG sampling rate down to 500 Hz with satisfactory results following post-processing artefact correction (Mandelkow et al. 2006).

It should be noted that for multislice EPI sequences, the type of slice acquisition must be considered, since it influences the precision of the TR (Mandelkow et al. 2006). When slice acquisitions are equidistant in time, the actual TR can deviate from the prescribed TR by the product of the scanner clock precision and the number of slices. A stationary image acquisition artefact will be obtained if the actual TR matches a common multiple of the EEG sample time (0.2 ms for 5 kHz) and of the product of scanner clock precision (0.1 μs for 10 MHz) and number of slices. For nonequidistant slice acquisitions with pauses between successive volume acquisitions, the TR is rounded to the full precision of the scanner clock, and stationary artefacts will be obtained if TR is a multiple of the EEG sample time. Such rounding differences have been reported for the Philips 3 T Achieva system running software release 1.2.2 (Mandelkow et al. 2006) and have been found by our group for the Siemens 1.5 T Sonata system running NUMARIS/4, version syngo MR 2004A.

In a phantom measurement, Mandelkow et al. (2006) demonstrated that residual artefact power dominates the post-processed EEG spectra above roughly 80 Hz for recordings without synchronisation. This is also visible in Fig. 9.3a, b, which show data from a healthy subject at 1.5 T. With synchronisation, however, spectral power up to 200 Hz remains largely within 10 dB of the spectrum obtained without simultaneous fMRI (Mandelkow et al. 2006). Figure 9.3c, d demonstrates the superior quality of the synchronised EEG of a subject at 1.5 T.

Synchronised EEG and fMRI digitisation has been used to study high-frequency (600 Hz) and very low amplitude (few 100 nV) components of the somatosensory evoked potential (Ritter et al. 2008a; Freyer et al. 2009) and spontaneous variations in the theta (3–6 Hz) and gamma (28–40 Hz) ranges (Giraud et al. 2007).

9.5 Correction of the Image Acquisition Artefact Using EEG Post-Processing

9.5.1 Artefact Template Subtraction

A widely applied processing method based on artefact template subtraction was demonstrated by Allen et al. (2000). This approach assumes that the shape of the gradient artefact does not change rapidly and that it is not correlated with the physiological signal (Hill et al. 1995). Channel-specific artefact templates are computed by averaging the EEG over a prespecified number of TR-related epochs and subtracted from the EEG traces in the current epoch, often referred to as average artefact subtraction (AAS). The epochs can be identified by recording a signal generated by the scanner that marks each image acquisition. The technique can be implemented in real time (Allen et al. 2000).

The averaging procedures implemented in different algorithms differ with respect to the number and selection of averaging epochs and their weighting. In the original implementation, the template consisted of a weighted sliding average of artefact epochs to account for possible changes of the artefact waveform over time and to account for a level of timing error and used adaptive noise cancellation (ANC) to further reduce residual image acquisition artefacts (Allen et al. 2000). A least mean square (LMS) algorithm could be used to adjust the weights of the ANC filter. This approach, however, needed a high sampling frequency, and some unsatisfactory results were obtained, even at sampling rates of 10 kHz (Niazy et al. 2005).

The Vision Analyzer algorithm (V.1.05.0002, BrainProducts, Munich, Germany) offers three different methods of template estimation: (1) all epochs, (2) a sliding average of a certain number of epochs and (3) a predefined number of initial scan epochs plus subsequent epochs exceeding a predefined cross-correlation with the initial template. Instead of a specific scanner-generated signal, epochs can be identified by searching for steep gradients or high amplitudes in the EEG exceeding a defined threshold. Recently, we have introduced a modified approach for dynamic template estimation where artefact epochs in the template are weighted according to a Fourier spectrum-based similarity measure. This approach allowed the recovery of ultrahigh-frequency EEG signatures with amplitudes in the nanovolt range even during image acquisition periods (Freyer et al. 2009).

Image acquisition artefact template subtraction has been successfully adopted for the reconstruction of spontaneous EEG signatures such as alpha rhythm (Goncalves et al. 2005; Laufs et al. 2003; Moosmann et al. 2003), Rolandic rhythms (Ritter et al. 2008b) and epileptic activity (Benar et al. 2003; Salek-Haddadi et al. 2002, 2003) and evoked potentials in the visual (Becker et al. 2005) and somatosensory system (Schubert et al. 2008).

As noted in the previous section (on synchronisation), the quality of artefact removal by template subtraction depends on the assumption of a stationary artefact, which is best satisfied when using synchronised systems (Fig. 9.3c) and when the exact TR of the MR sequence is a multiple of the sampling rate of the EEG. Jitter between EEG sampling and MR acquisition results in greater residual

artefacts following imaging artefact reduction (IAR), which are particularly prominent in the frequency spectrum approximately above 50 Hz (Figs. 9.3c, d and 9.6c). Low-pass filtering (cut-off around 50 and 80 Hz) can reduce residual artefacts. Although physiological signals above the cut-off frequency are removed by this procedure too, it can still be useful for the visual evaluation of the low-frequency EEG.

An alternative to the IAR method based on the frame-by-frame identification of the artefact uses an adaptive finite impulse response (FIR) filter (Wan et al. 2006). This method also assumes that the image acquisition artefacts are temporally stationary, except for a small frame-by-frame time shift. Using a Taylor expansion based on the average artefact waveform, the time-shifted image acquisition artefact of each frame was estimated using the average artefact waveform and its derivatives by LMS fitting. The algorithm outperformed simple average artefact template subtraction, which equals a zeroth-order FIR filter, but was not compared to artefact template subtraction combined with timing error correction.

An alternative to average artefact template subtraction, but one that is closely related to it, is based on online subtraction of a model of the image acquisition artefact that is estimated prior to EEG recording and subsequently fitted to the ongoing EEG for subtraction (Garreffa et al. 2003). A commercial software solution is also available for real-time imaging artefact correction based on gradient template subtraction and template drift compensation (TDC) (Vision RecView, MRI correction module, BrainProducts, Munich, Germany). In this case, synchronised EEG–fMRI is highly beneficial.

9.5.2 Computing and Correcting Timing Errors

Since image acquisition artefacts contain higher frequencies than the EEG sampling rate, timing errors can lead to considerable changes of the image acquisition artefact waveform in unsynchronised acquisitions. Therefore, timing errors must be considered in the calculation of the average artefact template and in subsequent template subtraction to achieve adequate artefact reduction.

One method is to divide data into epochs, each containing an MRI volume or scan acquisition period. The epochs are then interpolated (usually by a sinc function with a factor of 10–15) and subsequently aligned by maximising the cross-correlation to a reference period. After adjusting, epochs are downsampled to the original sampling frequency and subsequently averaged to calculate an artefact template (Allen et al. 2000; Negishi et al. 2004).

Another method relies on the calculation of multiple image acquisition artefact templates, each representing another waveform of the artefact (Benar et al. 2003). This algorithm is implemented in the Vision Analyzer (V.1.05.0004), providing so-called template drift detection (TDD) and subsequent TDC. Using the drift information provided by TDD, different average artefact templates are calculated. Each individual artefact is assigned to one template. Artefact correction is then obtained by subtracting the corresponding template from the respective artefact epoch.

Figure 9.6a, b shows two cases of unsynchronised EEG–fMRI acquisitions that require different strategies for optimal artefact correction. Figure 9.6a shows an EEG recorded during fMRI with a temporally stable sequence and with a TR that is an integer multiple of the EEG sampling time. In this case of periodically changing artefact waveforms, an efficient correction would be to bin the observed types of artefact waveforms and then perform selective template calculation and subtraction. Interpolation of artefact periods would not eliminate the systematic differences between successive periods. Figure 9.6b depicts unsynchronised EEG acquisition during an fMRI sequence that was neither temporally stable nor an integer multiple of the EEG sampling interval. This case would benefit from the interpolation of artefact epochs rather than from binning, due to the large inter-artefact waveform variability.

9.5.3 Temporal Principal Component Analysis

Violations of the stationarity assumption can occur independent of the degree of EEG and fMRI acquisition due to electrode movement in relation to the gradient coil and RF antenna, leading to a degradation in artefact template subtraction performance.

Negishi and colleagues proposed the application of temporal principal component analysis (PCA) to each EEG channel independently in order to remove residual artefacts (Negishi et al. 2004). Temporal PCA utilises the differential statistical characteristics of the variance of EEG epochs during and in-between scan acquisitions, yielding results similar to those obtained using IAR + ANC (Negishi et al. 2004).

The method called fMRI artefact slice template removal (FASTR) employs both artefact template subtraction and temporal PCA (Niazy et al. 2005). Again, slice-specific artefact templates are constructed as the local moving average plus a linear combination of basis functions describing the variation of residuals. The basis functions are derived by performing temporal PCA on the artefact residuals and selecting the dominant components to serve as a basis set. Finally, imaging artefact residuals are removed by an ANC filter (see below). This algorithm has been successfully applied in a continuous EEG–fMRI study of laser-evoked responses at 3 T (Iannetti et al. 2005). When the EEG signature of interest is of very high frequency, the beneficial outcome of a PCA-based post-processing can be further enhanced by employing a band-specific PCA in the high-frequency band in addition to the PCA on the broadband EEG. This cascaded PCA post-processing enables the recovery of ultrafast EEG signatures, which were otherwise obscured by imaging artefact residuals (Freyer et al. 2009).

9.5.4 Independent Component Analysis

Another approach to imaging artefact correction is independent component analysis (ICA) in addition to artefact template subtraction (Mantini et al. 2007). ICA is a

signal processing technique that recovers independent sources from a set of simultaneously recorded signals that result from a linear mixing of the source signals (Hyvarinen 1999; Mantini et al. 2007). Since EEG and image acquisition artefacts are generated by different independent processes and are therefore uncorrelated, ICA seems to be an appropriate approach. Mantini and colleagues categorised the ICA sources into two signal categories: brain signals and artefacts. This was done by visual inspection or in an automated approach by correlation to reference signals. Only sources classified as nonartificial were back-projected and used for further analysis. This approach proved to be capable of not only removing residual image acquisition artefacts but also ballistocardiogram and ocular artefacts.

Grouiller et al. (2007) compared an ICA-based imaging artefact removal approach to three other fundamental approaches to imaging artefact correction: IAR (Allen et al. 2000), FMRIB (Niazy et al. 2005) and Fourier transform (FT) filtering (Hoffmann et al. 2000). They used the implementation of the infomax ICA algorithm in the EEGLAB toolbox (Computational Neurobiology Laboratory, Salk Institute, La Jolla, CA, USA: http://www.sccn.ucsd.edu/eeglab/) (Bell and Sejnowski 1995). The authors selected the components that were correlated with the imaging artefact template. Selected components had a normalised cross-correlation coefficient higher than the average plus one standard deviation of that coefficient computed for all the components. The components representing image acquisition artefacts were excluded from the EEG reconstruction. Results for the performance of ICA, however, differed between simulations and real data (for details, see Sect. 9.6). Results obtained by Grouiller et al. (2007) indicate that ICA may not be applicable for efficiently estimating independent components in long time series of EEG data. A theoretical reason for this may be the spatial nonstationarity of the EEG and (especially) of the imaging artefact signal.

9.5.5 Filtering in the Frequency Domain

Image acquisition artefacts are periodic and distributed over a limited range of frequencies, suggesting that correction may be performed satisfactorily on the frequency domain. One such method is based on the comparison of the spectral content of EEG data acquired with and without simultaneous MR acquisition. The Fourier components of the signal corresponding to the MR-specific frequencies are set to zero for subsequent reprojection in signal space (Hoffmann et al. 2000). This algorithm was implemented in the FEMR programme provided by Schwarzer (Munich, Germany). The disadvantage of this method is that, due to a spectral overlap between the physiological EEG and image acquisition artefacts, some of the physiological EEG signal is removed as well. The method is characterised by ringing artefact (Benar et al. 2003), which results from discontinuities (e.g. gaps between scan acquisitions in interleaved EEG–fMRI) in the signals to be corrected. A similar approach relies on channel-wise subtraction of an average gradient artefact power spectrum—adapted by a scaling factor to the spectrum of the individual artefact—from the power spectrum of the artefact-distorted EEG (Sijbers et al. 1999). To filter

image acquisition artefacts in the frequency domain, one group (Grouiller et al. 2007) first calculated the FT of the imaging artefact template. Then, weights were applied to the spectral components of the FT of the EEG. For spectral components of the artefact afflicted EEG corresponding to strong spectral components in the artefact template, spectral filtering weights were set to the inverse. Thus, coefficients corresponding to the image acquisition artefact were attenuated. To obtain the corrected EEG, the inverse FT was applied. Grouiller et al. (2007) reported weighting coefficients to be inversely proportional to FT coefficients of the artefacts instead of zeroing them (Hoffmann et al. 2000), improved signal preservation and reduced ringing.

9.5.6 Between Prevention and Correction: Prospective Motion Correction and EEG Artefacts

Various prospective motion correction techniques are available to limit the impact of subject motion on MR image quality (Ordidge et al. 1994; Gallichan et al. 2016), with implications for EEG data quality, in particular due to variations in the image acquisition parameters which could undermine the assumptions of some correction methods such as those that rely on template artefact subtraction (Maziero et al. 2016). See Sect. 10.3 of Chap. 10 for further discussion of this issue.

9.6 Evaluation of Correction Methods

To date, artefact correction performance evaluation has not been performed consistently. In many EEG–fMRI studies, a single algorithm is chosen without proper justification, and often the quality of gradient artefact correction is assessed by visual inspection only. However, a more systematic approach to the choice of correction method may be advised for certain applications, such as the analysis of single events and nonaveraged EEG data, when residual artefacts do not cancel out, or those that rely on the quantitation of EEG power in certain spectral bands. The task of selecting a suitable correction algorithm would be greatly facilitated by standardising their evaluation and carefully considering the experimental requirements in terms of the EEG–fMRI protocol and features of the signal of interest (spectral signature, amplitude). In the following, we describe the main evaluation strategies employed to date.

Knowledge of the true signal is highly advantageous for the evaluation of signal filtering methods. This can be obtained in tests on phantoms and using signals generated by instruments offering the opportunity to assess both signal preservation and artefact reduction (Negishi et al. 2004; Schmid et al. 2006). Simulations have also been employed in which artificially generated signals (e.g. those extracted from recordings made under the control condition or simulated mathematically) are added to true artefacts (Allen et al. 2000; Grouiller et al. 2007). The main disadvantage of this approach is a lack of realism, in terms of the complexity of true

physiological signals, noise, subject movement and intersubject and inter-recording variability.

For tests based on real EEG, EEG recorded outside the MR environment should constitute the best gold standard. However, the specific evaluation of image acquisition artefact reduction methods can be performed adequately from signals recorded inside the scanner to compare signals captured without scanning (reference) and with scanning (and correction). For example, Allen et al. compared the signal's spectral content using this approach (Allen et al. 2000). In theory, a drawback of this approach is a lack of knowledge of the true EEG signal, in part due to the additional effects of the pulse artefact but also the sequential nature of the samples used for comparison. On the other hand, image acquisition artefact correction method performance evaluations based on signals recorded exclusively inside the scanner have the advantage that the pulse artefact is a common factor. Nonetheless, sequential measurements under the two experimental conditions may be particularly problematic for signals of interest with a high intrinsic variability, such as brain rhythms or epileptic discharges, but are possibly less so for evoked responses, where reproducible neuronal signals are more likely, although this bias can be reduced through adequate sampling.

Benar et al. (2003) compared Fourier filtering and template subtraction using EEGs obtained from patients with epilepsy, which were inspected by a trained observer after the application of both artefact correction methods. Visual subtraction was found to result in higher EEG quality than Fourier filtering.

Different gradient artefact correction algorithms based on the approach of template artefact subtraction were evaluated on data recorded with an unsynchronised EEG–fMRI setup using a visual stimulus presented to subjects at rest (Ritter et al. 2007). In this study, a combination of the following analyses was employed for performance estimation: (1) the degree of artefact reduction was evaluated by comparing the spectral content of the corrected data to that of gradient artefact-free EEG epochs for six predefined frequency bands ranging from theta to omega (1–250 Hz); (2) the preservation of non-gradient artefact components of the EEG after correction was evaluated twofold—by comparing the spectral content of non-acquisition EEG epochs before and after gradient artefact correction for the six predefined frequency bands and by exploring the impact of artefact correction on artificially generated signals added to the EEG. The study demonstrated that the amount of artefact reduction and the degree of physiological signal preservation are important complementary performance measures.

Another approach to the comparison of different artefact correction algorithms was based on the generation of artificial EEG and artificial image acquisition artefacts by a simple forward model (Grouiller et al. 2007). Modulations of the imaging artefact amplitude caused by subject motion and MRI and EEG clock asynchrony—which are typical of unsynchronised EEG-MRI setups—in combination with different EEG sampling rates were implemented in the model. The advantages of this approach include as follows: it allows the effects of different experimental or empirical parameters to be tested, knowledge of ground truth. The same group also evaluated artefact correction in real EEG data. To this end, after artefact correction, they

calculated correlation coefficients between the alpha power modulated by an eyes-open/eyes-closed paradigm and the task function and also correlation coefficients between interictal spikes acquired inside and outside the scanner. For the simulated data, the authors found that the ICA algorithm was the method that presented by far the best average results, although with a high-performance variability, indicating that this approach might be unstable. FASTR and IAR were approximately equivalent and FT performed significantly less well. For the real data, the IAR and FASTR algorithms obtained the best results. There was considerable discrepancy between the results obtained from simulations and from experimental data for the ICA approach, indicating a possible weakness of the modelling.

The authors assessed the effect of artefact correction on the fMRI results by comparing statistical parametric maps obtained from models based on alpha power with and without imaging artefact correction (Fig. 9.8). "…the discussed repertoire of available hardware and software solutions enables satisfying imaging-artefact correction. However, individual results can vary and therefore a continuous critical re-evaluation of results is necessary to ensure reasonable data quality".

We note that the advent of multiband fMRI (MB-fMRI) has not posed a substantial EEG data quality challenge using the template subtraction artefact correction method (Foged et al. 2017; Kyathanahally et al. 2017; Uji et al. 2018; Chen et al. 2020).

Recently, a MATLAB-based tool with a graphical user interface (GUI) has been published that allows for quantitative analyses of EEG and fMRI data features collected under different conditions, that is, separately or simultaneously and inside or outside the scanner (Schrooten et al. 2019). Such an approach may be useful for investigators interested in effects that do not absolutely necessitate simultaneous recordings, such as those that can be reliably reproduced across separate unimodal

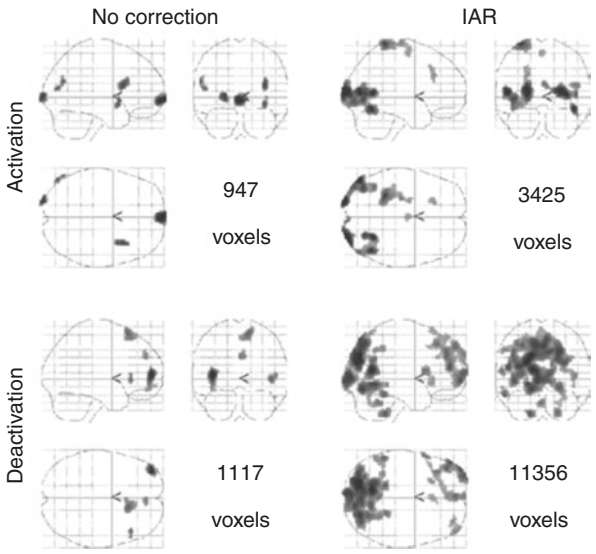

Fig. 9.8 Dependence of fMRI correlates of the alpha rhythm on the quality of image acquisition artefact correction. Glass brains were obtained using the power in the alpha band as a regressor convolved with the HRF ($p = 0.005$, uncorrected). Left: Without any artefact correction. Right: Using IAR image acquisition artefact removal. (Modified from Grouiller et al. (2007))

sessions (in contrast to spontaneous phenomena such as interictal epileptic discharges that can only be detected on EEG, for example, or indeed the multimodal variability of individual responses to a reproducible stimulus) considering the wisdom, that is, potential added value of performed synchronous EEG-fMRI recordings.

Acknowledgements We would like to thank Daniel Margulies and Matthias Reinacher for proofreading the manuscript. This work was supported by the German Federal Ministry of Education and Research BMBF (Berlin Neuroimaging Center, Bernstein Center for Computational Neuroscience) and the German Research Foundation DFG (Berlin School of Mind and Brain, CRC 1315, CRC 936 and RI 2073/6-1), EU H2020 VirtualBrainCloud 826421, Human Brain Project 785907 and ERC 683049, Berlin Institute of Health & Foundation Charité and Johanna Quandt Excellence Initiative.

References

Allen PJ, Josephs O, Turner R (2000) A method for removing imaging artifact from continuous EEG recorded during functional MRI. Neuroimage 12(2):230–239

Anami K, Mori T, Tanaka F, Kawagoe Y, Okamoto J, Yarita M, Ohnishi T, Yumoto M, Matsuda H, Saitoh O (2003) Stepping stone sampling for retrieving artifact-free electroencephalogram during functional magnetic resonance imaging. Neuroimage 19(2 Pt 1):281–295

Baudewig J, Bittermann HJ, Paulus W, Frahm J (2001) Simultaneous EEG and functional MRI of epileptic activity: a case report. Clin Neurophysiol 112:1196–1200

Becker R, Ritter P, Moosmann M, Villringer A (2005) Visual evoked potentials recovered from fMRI scan periods. Hum Brain Mapp 26(3):221–230

Bell AJ, Sejnowski TJ (1995) An information-maximization approach to blind separation and blind deconvolution. Neural Comput 7(6):1129–1159

Benar C, Aghakhani Y, Wang Y, Izenberg A, Al Asmi A, Dubeau F, Gotman J (2003) Quality of EEG in simultaneous EEG–fMRI for epilepsy. Clin Neurophysiol 114(3):569–580

Chen JCC, Forsyth A, Dubowitz DJ, Muthukumaraswamy SD (2020) On the quality, statistical efficiency, and safety of simultaneously recorded multiband fMRI/EEG. Brain Topogr 33:303–316. https://doi.org/10.1007/s10548-020-00761-w

Chowdhury MEH, Mullinger KJ, Glover P, Bowtell R (2014) Reference layer artefact subtraction (RLAS): a novel method of minimizing EEG artefacts during simultaneous fMRI. Neuroimage 84:307–319. https://doi.org/10.1016/j.neuroimage.2013.08.039

Ertl M, Kirsch V, Leicht G, Karch S, Olbrich S, Reiser M, Hegerl U, Pogarell O, Mulert C (2010) Avoiding the ballistocardiogram (BCG) artifact of EEG data acquired simultaneously with fMRI by pulse-triggered presentation of stimuli. J Neurosci Methods 186(2):231–241. https://doi.org/10.1016/j.jneumeth.2009.11.009

Felblinger J, Slotboom J, Kreis R, Jung B, Boesch C (1999) Restoration of electrophysiological signals distorted by inductive effects of magnetic field gradients during MR sequences. Magn Reson Med 41(4):715–721

Foged MT, Lindberg U, Vakamudi K et al (2017) Safety and EEG data quality of concurrent high-density EEG and high-speed fMRI at 3 tesla. PLoS One 12(5):e0178409

Freyer F, Becker R, Anami K, Curio G, Villringer A, Ritter P (2009) Ultrahigh-frequency EEG during fMRI: pushing the limits of imaging-artifact correction. Neuroimage 48:94

Gallichan D, Marques JP, Gruetter R (2016) Retrospective correction of involuntary microscopic head movement using highly accelerated fat image navigators (3D FatNavs) at 7T. Magn Reson Med 75(3):1030. https://doi.org/10.1002/mrm.25670

Garreffa G, Carni M, Gualniera G, Ricci GB, Bozzao L, De Carli D, Morasso P, Pantano P, Colonnese C, Roma V et al (2003) Real-time MR artifacts filtering during continuous EEG/fMRI acquisition. Magn Reson Imaging 21(10):1175–1189

Giraud AL, Kleinschmidt A, Poeppel D, Lund TE, Frackowiak RS, Laufs H (2007) Endogenous cortical rhythms determine cerebral specialization for speech perception and production. Neuron 56(6):1127–1134

Goldman RI, Stern JM, Engel J Jr, Cohen MS (2000) Acquiring simultaneous EEG and functional MRI. Clin Neurophysiol 111(11):1974–1980

Goldman RI, Stern JM, Engel J Jr, Cohen MS (2002) Simultaneous EEG and fMRI of the alpha rhythm. Neuroreport 13:2487–2492

Goncalves SI, de Munck JC, Pouwels PJ, Schoonhoven R, Kuijer JP, Maurits NM, Hoogduin JM, Van Someren EJ, Heethaar RM, Lopes da Silva FH (2005) Correlating the alpha rhythm to BOLD using simultaneous EEG/fMRI: inter-subject variability. Neuroimage 30:203

Grouiller F, Vercueil L, Krainik A, Segebarth C, Kahane P, David O (2007) A comparative study of different artefact removal algorithms for EEG signals acquired during functional MRI. Neuroimage 38(1):124–137

Hanson LG, Lund TE, Hanson CG (2007) Encoding of electrophysiology and other signals in MR images. J Magn Reson Imaging 25(5):1059–1066

Hill RA, Chiappa KH, Huang-Hellinger F, Jenkins BG (1995) EEG during MR imaging: differentiation of movement artifact from paroxysmal cortical activity. Neurology 45:1942–1943

Hoffmann A, Jager L, Werhahn KJ, Jaschke M, Noachtar S, Reiser M (2000) Electroencephalography during functional echo-planar imaging echo-planar imaging: detection of epileptic spikes using post-processing methods. Magn Reson Med 44(5):791–798

Horovitz SG, Skudlarski P, Gore JC (2002) Correlations and dissociations between BOLD signal and P300 amplitude in an auditory oddball task: a parametric approach to combining fMRI and ERP. Magn Reson Imaging 20:319–325

Horovitz SG, Rossion B, Skudlarski P, Gore JC (2004) Parametric design and correlational analyses help integrating fMRI and electrophysiological data during face processing. Neuroimage 22:1587–1595

Huang-Hellinger FR, Breiter HC, McCormack GM, Cohen MS, Kwong KK, Savoy RL, Weisskoff RM, Davis TL, Baker JR, Belliveau JW et al (1995) Simultaneous functional magnetic resonance imaging and electrophysiological recording. Hum Brain Mapp 3:13–23

Hyvarinen A (1999) Fast and robust fixed-point algorithms for independent component analysis. IEEE Trans Neural Netw 10:626–634

Iannetti GD, Niazy RK, Wise RG, Jezzard P, Brooks JC, Zambreanu L, Vennart W, Matthews PM, Tracey I (2005) Simultaneous recording of laser-evoked brain potentials and continuous, high-field functional magnetic resonance imaging in humans. Neuroimage 28(3):708–719

Ives JR, Warach S, Schmitt F, Edelman RR, Schomer DL (1993) Monitoring the patient's EEG during echo planar MRI. Electroencephalogr Clin Neurophysiol 87:417–420

Jorge J, Grouiller F, Ipek Ö et al (2015a) Simultaneous EEG-fMRI at ultra-high field: artifact prevention and safety assessment. Neuroimage 105:132–144. https://doi.org/10.1016/j.neuroimage.2014.10.055

Jorge J, Grouiller F, Gruetter R, van der Zwaag W, Figueiredo P (2015b) Towards high-quality simultaneous EEG-fMRI at 7T: detection and reduction of EEG artifacts due to head motion. Neuroimage 120:143–153. https://doi.org/10.1016/j.neuroimage.2015.07.020

Kim H-C, Yoo S-S, Lee J-H (2015) Recursive approach of EEG-segment-based principal component analysis substantially reduces cryogenic pump artifacts in simultaneous EEG–fMRI data. Neuroimage 104:437–451. https://doi.org/10.1016/j.neuroimage.2014.09.049.

Krakow K, Woermann FG, Symms MR, Allen PJ, Lemieux L, Barker GJ, Duncan JS, Fish DR (1999) EEG-triggered functional MRI of interictal epileptiform activity in patients with partial seizures. Brain 122:1679–1688

Krakow K, Allen PJ, Symms MR, Lemieux L, Josephs O, Fish DR (2002) EEG recording during fMRI experiments: image quality. Hum Brain Mapp 10(1):10–158. https://doi.org/10.1002/(sici)1097-0193(200005)10:1%3C10::aid-hbm20%3E3.0.co;2-t

Kruggel F, Wiggins CJ, Herrmann CS, von Cramon DY (2000) Recording of the event-related potentials during functional MRI at 3.0 tesla field strength. Magn Reson Med 44:277–282

Kyathanahally SP, Wang Y, Calhoun VD, Deshpande G (2017) Investigation of true high frequency electrical substrates of fMRI-based resting state networks using parallel independent component analysis of simultaneous EEG/fMRI data. Front Neuroinform 11:74

Laufs H, Kleinschmidt A, Beyerle A, Eger E, Salek-Haddadi A, Preibisch C, Krakow K (2003) EEG-correlated fMRI of human alpha activity. Neuroimage 19:1463–1476

Lemieux L, Allen PJ, Franconi F, Symms MR, Fish DR (1997) Recording of EEG during fMRI experiments: patient safety. Magn Reson Med 38(6):943–952

Lemieux L, Krakow K, Fish DR (2001) Comparison of spike-triggered functional MRI BOLD activation and EEG dipole model localization. Neuroimage 14:1097–1104

Luo Q, Huang X, Glover GH (2014) Ballistocardiogram artifact removal with a reference layer and standard EEG cap. J Neurosci Methods 233:137–149. https://doi.org/10.1016/J.JNEUMETH.2014.06.021

Mandelkow H, Halder P, Boesiger P, Brandeis D (2006) Synchronization facilitates removal of MRI artefacts from concurrent EEG recordings and increases usable bandwidth. Neuroimage 32(3):1120–1126

Mantini D, Perrucci MG, Cugini S, Ferretti A, Romani GL, Del Gratta C (2007) Complete artifact removal for EEG recorded during continuous fMRI using independent component analysis. Neuroimage 34(2):598–607

Maziero D, Velasco TR, Hunt N, Payne E, Lemieux L, Salmon CEG, Carmichael DW (2016) Towards motion insensitive EEG-fMRI: correcting motion-induced voltages and gradient artefact instability in EEG using an fMRI prospective motion correction (PMC) system. Neuroimage 138:13–27. https://doi.org/10.1016/j.neuroimage.2016.05.003

McIntosh JR, Yao J, Hong L, Faller J, Sajda P (2019) Ballistocardiogram artifact reduction in simultaneous EEG-fMRI using deep learning, arXiv: quantitative methods

Moosmann M, Ritter P, Krastel I, Brink A, Thees S, Blankenburg F, Taskin B, Obrig H, Villringer A (2003) Correlates of alpha rhythm in functional magnetic resonance imaging and near infrared spectroscopy. Neuroimage 20:145–158

Mullinger K, Brookes M, Stevenson C, Morgan P, Bowtell R (2008) Exploring the feasibility of simultaneous electroencephalography/functional magnetic resonance imaging at 7 T. Magn Reson Imaging 26(2008):968–977

Mullinger KJ, Castellone P, Bowtell R (2013) Best current practice for obtaining high quality EEG data during simultaneous fMRI. J Vis Exp 76:e50283. https://doi.org/10.3791/50283

Negishi M, Abildgaard M, Nixon T, Constable RT (2004) Removal of time-varying gradient artifacts from EEG data acquired during continuous fMRI. Clin Neurophysiol 115(9):2181–2192

Neuner I, Arrubla J, Felder J, Shah NJ (2014) Simultaneous EEG–fMRI acquisition at low, high and ultra-high magnetic fields up to 9.4 T: perspectives and challenges. Neuroimage 102(2014):71–79

Niazy RK, Beckmann CF, Iannetti GD, Brady JM, Smith SM (2005) Removal of FMRI environment artifacts from EEG data using optimal basis sets. Neuroimage 28(3):720–737

Nierhaus T, Gundlach C, Goltz D, Thiel SD, Pleger B, Villringer A (2013) Internal ventilation system of MR scanners induces specific EEG artifact during simultaneous EEG-fMRI. Neuroimage 74:70–76

Opitz B, Mecklinger A, Von Cramon DY, Kruggel F (1999) Combining electrophysiological and hemodynamic measures of the auditory oddball. Psychophysiology 36:142–147

Ordidge RJ, Helpern JA, Qing ZX, Knight RA, Nagesh V (1994) Correction of motional artifacts in diffusion-weighted MR images using navigator echoes. Magn Reson Imaging 12:455–460

Ritter P, Villringer A (2006) Simultaneous EEG–fMRI. Neurosci Biobehav Rev 30:823–838

Ritter P, Freyer F, Becker R, Anami K, Curio G, Villringer A (2006) Recording of ultrafast (600 Hz) EEG oscillations with amplitudes in the nanovolt range during fMRI-acquisition periods. In: 14th Scientific Meeting ISMRM, Seattle, WA, USA, 6–12 May 2006

Ritter P, Becker R, Graefe C, Villringer A (2007) Evaluating gradient artifact correction of EEG data acquired simultaneously with fMRI. Magn Reson Imaging 25(6):923–932

Ritter P, Freyer F, Curio G, Villringer A (2008a) High frequency (600 Hz) population spikes in human EEG delineate thalamic and cortical fMRI activation sites. Neuroimage 42(2):483–490

Ritter P, Moosmann M, Villringer A (2008b) Rolandic alpha and beta EEG rhythms' strengths are inversely related to fMRI-BOLD signal in primary somatosensory and motor cortex. Hum Brain Mapp 30(4):1168–1187

Rothlübbers S, Relvas V, Leal A, Murta T, Lemieux L, Figueiredo P (2015) Characterisation and reduction of the EEG artefact caused by the helium cooling pump in the MR environment: validation in epilepsy patient data. Brain Topogr 28(2):208–220. https://doi.org/10.1007/s10548-014-0408-0

Salek-Haddadi A, Merschhemke M, Lemieux L, Fish DR (2002) Simultaneous EEG-correlated ictal fMRI. Neuroimage 16:32–40

Salek-Haddadi A, Lemieux L, Merschhemke M, Friston KJ, Duncan JS, Fish DR (2003) Functional magnetic resonance imaging of human absence seizures. Ann Neurol 53:663–667

Schmid MC, Oeltermann A, Juchem C, Logothetis NK, Smirnakis SM (2006) Simultaneous EEG and fMRI in the macaque monkey at 4.7 tesla. Magn Reson Imaging 24:335–342

Schrooten M, Vandenberghe R, Peeeters R, Dupont P (2019) Quantitative analyses help in choosing between simultaneous vs. separate EEG and fMRI. Front Neurosci 12:1009

Schubert R, Ritter P, Wustenberg T, Preuschhof C, Curio G, Sommer W, Villringer A (2008) Spatial attention related SEP amplitude modulations covary with BOLD signal in S1—a simultaneous EEG–fMRI study. Cereb Cortex 18:2686–2700

Seeck M, Lazeyras F, Michel CM, Blanke O, Gericke CA, Ives J, Delavelle J, Golay X, Haenggeli CA, de Tribolet N, Landis T (1998) Non-invasive epileptic focus localization using EEG-triggered functional MRI and electromagnetic tomography. Electroencephalogr Clin Neurophysiol 106:508–512

Sijbers J, Michiels I, Verhoye M, Van Audekerke J, Van der LA, Van Dyck D (1999) Restoration of MR-induced artifacts in simultaneously recorded MR/EEG data. Magn Reson Imaging 17(9):1383–1391

Sommer M, Meinhardt J, Volz HP (2003) Combined measurement of event-related potentials (ERPs) and fMRI. Acta Neurobiol Exp (Wars) 63:49–53

Steyrl D, Müller-Putz GR (2019) Artifacts in EEG of simultaneous EEG-fMRI: pulse artifact remainders in the gradient artifact template are a source of artifact residuals after average artifact subtraction. J Neural Eng 16(1):016011

Steyrl D, Krausz G, Koschutnig K, Edlinger G, Müller-Putz GR (2018) Online reduction of artifacts in EEG of simultaneous EEG-fMRI using reference layer adaptive filtering (RLAF). Brain Topogr 31:129–149. https://doi.org/10.1007/s10548-017-0606-7

Symms MR, Allen PJ, Woermann FG, Polizzi G, Krakow K, Barker GJ, Fish DR, Duncan JS (1999) Reproducible localization of interictal epileptiform discharges using EEG-triggered fMRI. Phys Med Biol 44:N161–N1N8

Uji M, Wilson R, Francis ST, Mullinger KJ, Mayhew SD (2018) Exploring the advantages of multiband fMRI with simultaneous EEG to investigate coupling between gamma frequency neural activity and the BOLD response in humans. Hum Brain Mapp 39(4):1673–1687

Van Audekerkea J, Peeters R, Verhoye M, Sijbers J, Van der LA (2000) Special designed RF-antenna with integrated non-invasive carbon electrodes for simultaneous magnetic resonance imaging and electroencephalography acquisition at 7T. Magn Reson Imaging 18(7):887–891

van der Meer JN, Pampel A, Van Someren EJW, Ramautar JR, van der Werf YD, Gomez-Herrero G, Lepsien J, Hellrung L, Hinrichs H, Möller HE, Walter M (2016) Carbon-wire loop based artifact correction outperforms post-processing EEG/fMRI corrections—a validation of a real-time simultaneous EEG/fMRI correction method. Neuroimage 125:880–894. https://doi.org/10.1016/j.neuroimage.2015.10.064

Wan X, Iwata K, Riera J, Kitamura M, Kawashima R (2006) Artifact reduction for simultaneous EEG/fMRI recording: adaptive FIR reduction of imaging artifacts. Clin Neurophysiol 117(3):681–692

Warach S, Ives JR, Schlaug G, Patel MR, Darby DG, Thangaraj V, Edelman RR, Schomer DL (1996) EEG-triggered echo-planar functional MRI in epilepsy. Neurology 47:89–93

Image Quality Issues

10

David Carmichael

10.1 fMRI Pulse Sequences

The requirement of a fMRI pulse sequence is BOLD sensitivity, which means predominantly T2*-weighted[1] sequences such as GE-EPI, although spin echo sequences such as spin echo EPI (SE-EPI) can also be used (Bandettini et al. 1994; Norris et al. 2002; Schmidt et al. 2005).

SE-EPI suffers from reduced volume coverage relative to GE-EPI due to the longer echo times required and generally shows smaller signal changes (Bandettini et al. 1994; Schmidt et al. 2005). Spin echo sequences do not suffer from signal dropout and therefore perform much better in areas of large through-plane susceptibility gradients (Norris et al. 2002). There is mixed opinion as to whether or in which parts of the brain spin echo sequences may be advantageous (Parkes et al. 2005; Schmidt et al. 2005), but they are likely to be most usefully employed at field strengths of >3 T (Duong et al. 2002; Nair and Duong 2004; Koopmans et al. 2012), where they are considered to be more spatially specific because larger veins (which are displaced from the active region) contribute little to the fMRI signal. However, despite the increased availability of ultra-high-field 7T MRI systems, GE-EPI is still the most frequently used pulse sequence. Some considerable research has recently been devoted to using steady-state free precession sequences for fMRI (Miller et al. 2003, 2004, 2006; Zhong et al. 2007). While these sequences have shown promise, they are generally employed for niche applications (Miller et al. 2006). It is also worth noting that hybrid approaches using spin and gradient echoes such as GRASE

[1] The transverse relaxation time including a contribution from slowly changing or constant background magnetic fields.

D. Carmichael (✉)
Department of Biomedical Engineering, School of Biomedical Engineering and Imaging Sciences, King's College London, London, UK
e-mail: david.carmichael@kcl.ac.uk

C. Mulert, L. Lemieux (eds.), *EEG - fMRI*,
https://doi.org/10.1007/978-3-031-07121-8_10

(Feinberg et al. 1995; Fernandez-Seara et al. 2005) are also capable of being used to obtain high-quality fMRI data.

The most significant recent alteration to fMRI data acquisition is the combination of now readily available high-density RF receiver coils; these can be used in combination with simultaneous multi-slice (SMS) excitation (Larkman et al. 2001; Nunes et al. 2006; Setsompop et al. 2012). In this approach, a modified RF pulse is used so that after each excitation pulse, data from a number of slices (the SMS factor) are obtained. This means that each raw image (one for each receiver coil) has slices overlaid or aliased together. Each coil has a different weighting of signal from different slices owing to their differing spatial sensitivity in the slice direction. Image reconstruction, given knowledge of this coil spatial sensitivity, can then be used to reassign signal to the correct slice. To enhance this method, an additional gradient in the slice direction is typically employed that spatially offsets each slice image (Setsompop et al. 2012) as shown in Fig. 10.1. This approach has the advantage of reducing the sequence TR or increasing the slice coverage or reducing the slice thickness allowing these parameters to be optimised for different applications. This has now become widely available and has been used in large-scale projects such as the human connectome (Uğurbil et al. 2013). The advantage of SMS is that the excitation of more of the sample for each period of data acquisition means there is not an intrinsic SNR penalty (in contrast to in-plane parallel imaging). However, noise can be enhanced particularly when more slices are excited together and therefore have a greater degree of signal aliasing (more slices signal is mixed) that must be disentangled using the available variability in RF receiver coil sensitivity. This can cause noise enhancement and the mixing of signal from different slices leading to the possibility of measured signal changes in slices obtained in the same readout but that are remote from the active brain area (Todd et al. 2016). Recent work has shown that for individual fMRI results (McDowell and Carmichael 2018; Sahib et al. 2016) and group studies (Todd et al. 2016), SMS factors of 4 or more used to reduce the TR are not beneficial. A possible exception is for certain resting-state acquisitions (Hutter et al. 2018); this will be discussed further in the physiological noise section.

Three-dimensional echo-planar imaging also termed echo volume imaging (EVI) has also been the subject of renewed interest in part owing to the increased sophistication of image acquisition and reconstruction methodology (e.g. Kirilina et al. 2016; Poser et al. 2010). In EVI, the entire object is excited and spatial encoding is achieved via gradients in a single long echo train. For practical reasons, it is typically not possible, or desirable, to obtain all of the data in a single long readout owing to signal decay and strong sensitivity to distortions (described in a later section). Therefore, the entire object is excited but the data readout is segmented into several parts with different spatial encoding. This data then has to be put back together, and it is this process that is very sensitive to phase errors that can be introduced by subject motion, physiological noise or scanner instabilities (Lutti et al. 2013). It is also worth noting that conceptually at high SMS factors, the sequence becomes more like EVI as a larger proportion of the object is imaged in each readout, with the key difference being that the data acquisition and reconstruction are in the spatial domain for SMS rather than signal or k-space domain for segmented 3D

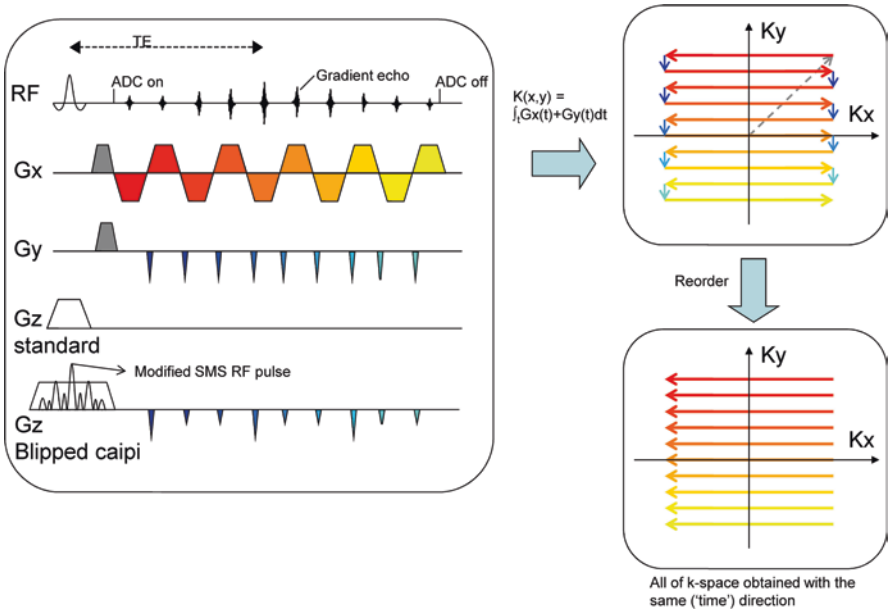

Fig. 10.1 (**a**–**c**) Standard blipped Cartesian EPI pulse sequence and corresponding k-space trajectory. The blipped EPI pulse sequence is shown (**a**); the standard encoding scheme for 2D EPI is shown. On the bottom line, the adjustments used for SMS are shown with a multi-slice RF excitation and additional gradients that cause the slices to be offset. In this example, the additional gradient blips in the slice direction will cause a relative shift for each slice of one-third of the field of view. On the *top line* is the RF showing the slice-selective excitation pulse followed by a series of gradient echoes. Each of the gradient echoes is formed by a readout gradient of opposite polarity. Additionally, for each gradient reversal, a different phase encode line is readout by the application of a phase-encoding gradient during the read gradient reversal. ADC is the analogue-to-digital converter that is switched on to record the signal. At the bottom, modifications of the RF and Gz gradients for SMS with blipped-CAIPI are shown. (**b**) The k-space trajectory is shown; the position in k-space is determined by the gradient area. The colour of the gradient corresponds to the k-space trajectory. Initially, the *grey* gradients take us to the k-space corner, and then the readout gradient alternately traverses from *right* to *left* while the phase-encoding blips make the jumps from *top* to *bottom* at the end of each readout gradient. It is worth noting that the order that k-space is acquired in the phase-encoding direction can be reversed (here the blips are negative), and this will alter the distortion (see Fig. 10.3 and consider the effect on the k-space trajectory of opposite-sign phase-encoding blips). (**c**) Alternate lines of data are reversed in direction prior to reconstruction. This effectively means that each line of k-space data should look as if it has been obtained under the same polarity of gradient (otherwise each line appears as if time was reversed). Any mismatch between positive and negative gradients creates a mismatch along the Ky direction in alternate lines and causes an N/2 ghost

echo-planar imaging (Stirnberg et al. 2017). An extreme version of the use of receiver coils to encode spatial position has also been developed and used for EEG-fMRI (Jacobs et al. 2014) where spatial encoding is only used in the readout direction and encoding in the other directions is entirely performed by the receiver coils (Zahneisen et al. 2011).

A final option for the fMRI pulse sequence worthy of consideration is to utilise a multi-echo readout. Here, after each excitation multiple images are obtained of *the same* slice. This will extend the time taken to image a slice leading to a long TR; however, it is also compatible with SMS that can be used to maintain the desired TR and temporal sampling. The main benefit of a multi-echo fMRI sequence is that it allows for noise and signal components to be separated. This is achieved by examining the signal change in each voxel obtained at each echo time. The fMRI signal is mediated by the exponential decay defined by the T2*, whereas many noise sources cause an alteration of signal that is constant at each echo. Therefore, by fitting the multiple echo data to obtain a map of T2* at each time point for subsequent analysis, the effects of noise on these maps can be strongly attenuated as compared to the T2*-weighted images themselves (Kundu et al. 2017).

10.2 GE-EPI

The sequence of choice for most fMRI applications is GE-EPI, due to its high speed and a high signal-to-noise ratio (SNR) per unit time. An image can typically be obtained in 20–50 ms using modern hardware, giving whole brain coverage in 2–4 s (Schmitt et al. 1998; Mansfield 1977; Ordidge 1999; Turner and Ordidge 2000). With SMS, this whole brain coverage can be achieved in as little as a few hundred milliseconds.

In the following section, we will restrict our discussion to Cartesian k-space trajectory EPI because it is the most frequently used and generally offers highly competitive performance in terms of speed and artefact level. Other k-space trajectories commonly used for EPI include spirals where both read and phase-encoding gradients are equivalent in pulse shape and amplitude but offset in phase and oscillate in a sinusoidal manner (Ahn et al. 1986; Glover and Law 2001; Preston et al. 2004; Sangill et al. 2006). This can reduce image distortion, for example, due to faster traversal of k-space (especially compared to the phase-encoding direction of Cartesian EPI), but may not necessarily yield an overall increase in performance over the whole brain (Block and Frahm 2005).

An EPI sequence diagram is shown in Fig. 10.1. A gradient echo is formed when the transverse magnetisation is dephased and then rephased by linear magnetic field gradients alone (unlike a spin echo). The EPI experiment involves a single RF excitation pulse followed by a train of these echoes that are read out by applying a series of gradients with equal areas and opposite magnitude. Each echo has a different net phase-encoding gradient due to the extra gradients (blips) applied between the readout gradient reversals (Wielopolski et al. 1998). In EPI, all of the PE steps are acquired in one TR, making it a fast technique. This implementation of EPI is termed ‘single shot’ because it requires only one RF excitation of the magnetisation to obtain an entire image data set.

The echo time (TE) is centred on the middle PE step, where the net phase-encoding gradient is zero. It is clear that as each echo is at a different position in time, the magnetisation will have experienced different amounts of dephasing from any local magnetic field differences. These are caused by interfaces between materials of different magnetic

susceptibility, such as the head and air. Any inconsistency between successive echoes, obtained at different times, has associated problems that will be discussed at greater length later. EPI can suffer from a number of other problems that are directly related to its strategy of full k-space coverage in a single shot. EPI readouts are naturally longer than for other pulse sequences, because a greater distance through k-space must be travelled in one go (see Fig. 10.1). This is why 3D echo-planar sequences are split into segments. Additional problems are associated with having reversed the direction travelled through k-space in alternate lines (see Schmitt et al. 1998 for an additional description of EPI artefacts and their causes). Here, we first look to explain the most common sources of EPI artefact in a qualitative manner, and we describe the range of methods available to moderate their effects before going on to determine how the addition of EEG equipment may exacerbate these image quality issues.

10.2.1 Image Blurring

Blurring of image detail occurs because of T2*-/T2-related signal decay over the length of the acquisition (i.e. not all points in k-space are sampled at the same effective TE). For EPI, the large time difference between adjacent k-space data points, particularly in the phase-encoding direction, causes greater signal decay and thus increased blurring. This can be thought of as the effective application of a filter in k-space described by the signal decay during the readout with the blurring caused in the image described by the Fourier transform of this filter, which is called the point spread function (PSF) (see Fig. 10.2). In the tissue with a shorter T2*, due to stronger local susceptibility-related magnetic fields that are increased by utilising higher main magnetic field strengths, this problem is increased. Blurring will thus also be increased where stronger local susceptibility-related magnetic fields are produced by EEG equipment. Reduced blurring is achieved by shorter readout lengths or higher-resolution images without increased readout duration. Methods to shorten readouts include multishot segmented EPI (Menon et al. 1997; Wielopolski et al. 1998), related pulse sequences that split the readout into shorter segments without requiring multishots (Bornert and Jensen 1994; Carmichael et al. 2005; Feinberg et al. 2002; Priest et al. 2004; Rzedzian 1987) and parallel imaging (PI) methods (Carlson and Minemura 1993; Griswold et al. 2002; Hutchinson and Raff 1988; Pruessmann et al. 1999; Sodickson and Manning 1997). Alternatively, improved shimming (Cusack et al. 2005; Gruetter 1993; Gruetter and Tkac 2000; Mackenzie et al. 1987; van Gelderen et al. 2007; Ward et al. 2002; Wilson et al. 2003; Wilson and Jezzard 2003) can also locally decrease blurring by increasing local field homogeneity. In most fMRI experiments, including EEG-fMRI, blurring is not a primary consideration for pulse sequence optimisation. This is due to the usual spatial extent of activation exceeding the voxel size and because the optimisation of SNR, temporal resolution and image dropout is usually more critical. However, it is important to remember that the resolution is degraded, especially in the phase-encoding direction in GE-EPI, and in some cases where small structures are interrogated—such as high-resolution mapping of cortical columns within visual areas—some minimisation of blurring may be beneficial.

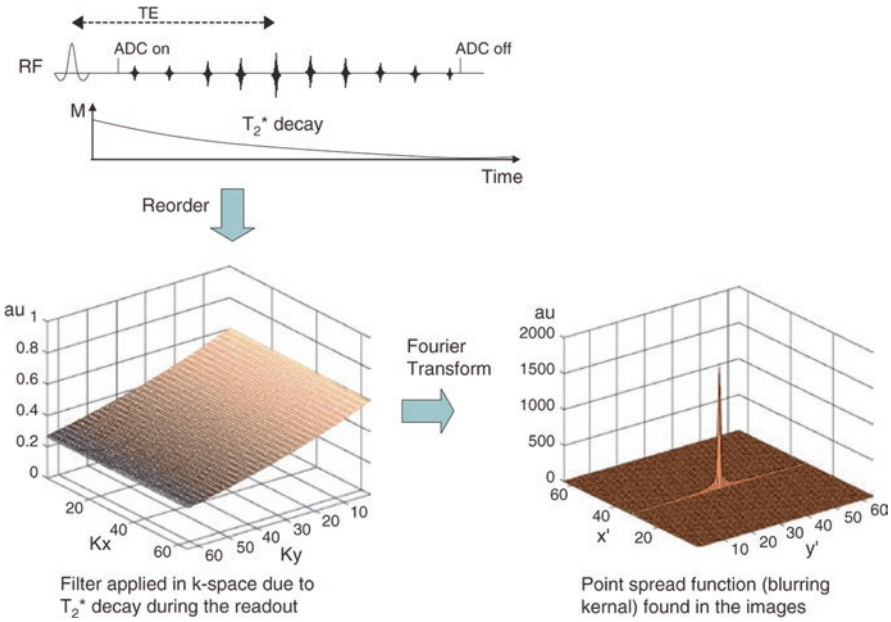

Fig. 10.2 Blurring in EPI images. Due to the properties of the Fourier transform, we can separately consider each of the different components that modulate the underlying k-space signal produced by an object (which are all multiplied together in actual data). Each of these components can be thought of as a filter. The effect seen in the image is blurring from a convolution of the object by the Fourier transform of each k-space filter. There is a large amount of signal decay during the long EPI readout (*top*), which can thus be considered independently of other signal modulations (e.g. those imposed by imaging gradients or the object itself). When the data is reordered in k-space, the signal decay makes a 2D function in k-space that is an effective filter, as shown in the *bottom left*. The Fourier transform of this filter determines the point spread function, which describes the blurring of the data from each voxel

10.2.2 Geometric Distortion

Due to the time difference between the acquisitions of adjacent k-space data points in the phase-encoding direction (or correspondingly the low (PE) bandwidth, which is simply the reciprocal), local magnetic field perturbations from various sources (Jezzard and Clare 1999; Wielopolski et al. 1998) have the time to cause significant local phase accumulation relative to that produced by the phase-encoding gradients (i.e. the local magnetic field gradient area is large relative to the size of the phase-encoding blips). This causes an apparent shift in the data from the local position in the image, with the shift in position proportional to the size of the local difference in the local static magnetic field (B_0) (Jezzard and Balaban 1995). In addition to a simple shift of data from one position to another, data from one position may be stretched over a larger area or squashed into a smaller area. In Fig. 10.3, the process is described in terms of k-space coverage. At different positions within the brain, there is a local magnetic field gradient that has an additive effect, positive or

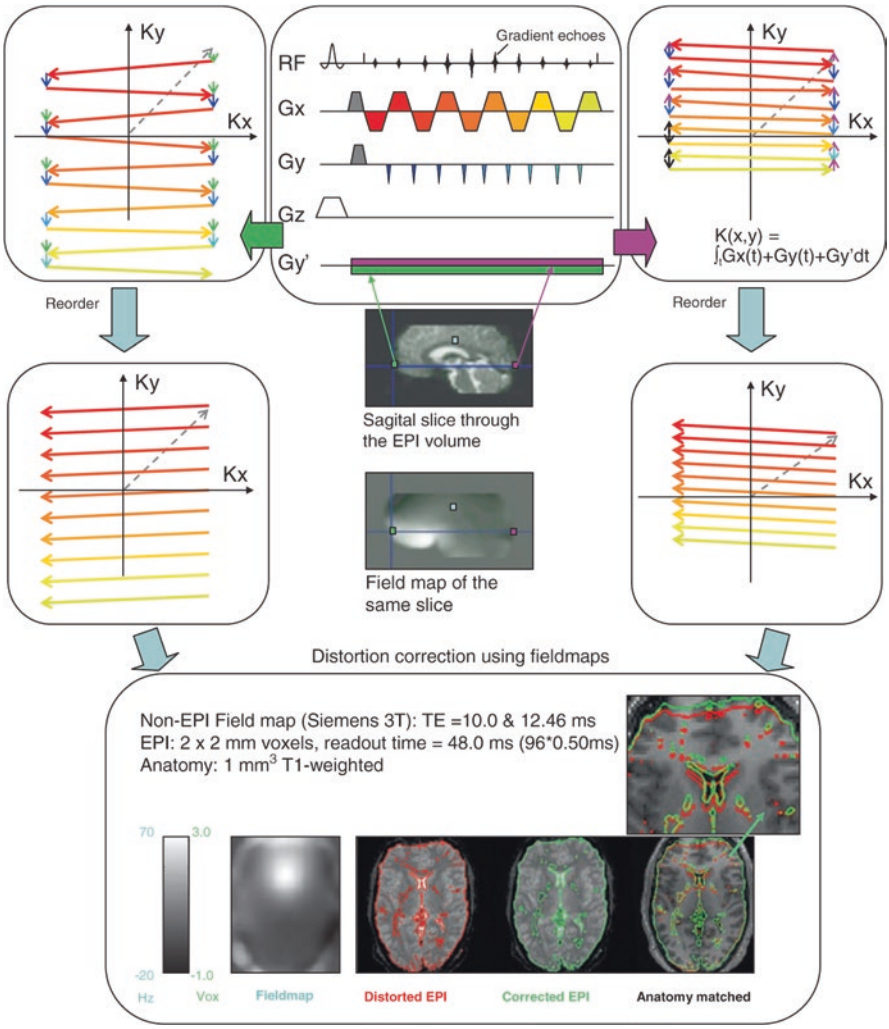

Fig. 10.3 Distortion in EPI images. When an extra local in-plane gradient is present in the phase-encoding direction due to susceptibility artefacts, the effective local k-space trajectory is altered. If the local gradient adds to the PE blips (as on the *left*), then the distance between the lines and k-space area covered is increased, and this will cause the data to be spread over a larger area. This will make the local image data appear stretched. Alternatively, if local gradients have opposite polarity to the PE blips (as on the *right*), the k-space trajectory has less distance between the lines and covers a smaller area, and so the local image data will appear squashed. Field map-based distortion correction is shown at the *bottom*. The field map was obtained using a standard gradient echo sequence and two complex images at different echo times, which were masked, phase unwrapped and smoothed. This can be converted into units of displacement (here in voxels), and then the EPI image can be unwarped using the voxel displacement. This improves the match to the anatomical image that does not suffer from distortion

negative, on the phase-encoding gradients. This can be conceptualised as causing a different k-space trajectory for magnetisation at a different spatial position. In one spatial position, the phase encoding (Ky) covers a greater effective k-space area and the lines are further apart. This corresponds to squeezing the data into a smaller area. Alternatively, the lines are forced closer together, with the effect of stretching the data in the image. Distortion will be increased where stronger local susceptibility-related magnetic fields are produced by EEG equipment and are also increased with the magnetic field strength of the scanner.

The simplest method of reducing distortion is to shorten the time between the phase-encoding blips by switching the read gradients faster and with greater amplitude, thereby requiring an increased readout bandwidth (with a concomitant reduction in SNR). This corresponds to reducing the time taken to travel through the k-space trajectory in Fig. 10.1. Unfortunately, the rate and maximum amplitude of the read gradient switching is limited by physiological constraints; rapidly varying magnetic fields can induce currents in nerves large enough to cause stimulation (Cohen et al. 1990; Mansfield and Harvey 1993). In addition, the desired gradient waveform is only accurately produced when both its amplitude and switching rate lie within certain limits. Therefore, one option that is available is to reduce the number and increase the size of the phase-encoding steps in the acquisition window, necessitating the recovery of a full set of image information by some other means. There are a number of different techniques that are used to perform this function, and they can be classified into two approaches. First, there is interleaved segmented EPI (Butts et al. 1994; Hennel and Nedelec 1995) (for two segments, every other line of the standard k-space coverage is read out, and then the remaining lines are read out in a separate acquisition), although this entails a penalty in temporal resolution that would be unacceptable for many fMRI applications. Various strategies have been suggested to read out the segments consecutively. One of the simplest is to use a 45° RF pulse and acquisition followed directly by a 90° RF pulse and acquisition (Rzedzian 1987) or to take pairs of images with different spatial profiles imposed and then reconstruct the data (Carmichael et al. 2005; Feinberg et al. 2002; Priest et al. 2004). The second approach uses differing degrees of prior information to recreate full images from reduced data sets. Partial Fourier methods that exploit the conjugate symmetry of k-space have been used (Feinberg et al. 1986), but they do not always significantly reduce distortion and can introduce increased blurring. Methods, collectively known as parallel imaging (PI), have allowed a considerable increase in acquisition speed in-plane as opposed to in the slice direction (Carlson and Minemura 1993; Hutchinson and Raff 1988; Pruessmann et al. 1999; Sodickson and Manning 1997). These all rely on the parallel use of receiver coils with different spatially varying sensitivities. Some calibration of the sensitivity functions of these coils gives information that is complementary to standard Fourier encoding. This allows a reduction in the density with which k-space must be sampled, reducing the distortion by the factor of speed-up (reduction in sampling density) employed in the PE direction. The penalty for all of these methods is a reduction in SNR and a potential increase in image reconstruction artefacts that can outweigh the benefits (Lutcke et al. 2006). Lastly, there are methods for correcting the distortion. These rely on

mapping the underlying B_0 field, which means that the distortion can be spatially calibrated and corrected. Methods for B_0 mapping are numerous (e.g. Gruetter and Tkac 2000; Lamberton et al. 2007; Mansfield 1984; Poser et al. 2006; Priest et al. 2006), but most methods simply perform two scans at different TEs. The local phase difference between the images is proportional to the local magnetic field. The phase difference can then be translated into a pixel shift map to visualise and correct these distortions, as shown in Fig. 10.3 (Chen and Wyrwicz 1999; Hutton et al. 2002; Jezzard and Balaban 1995; Munger et al. 2000; Reber et al. 1998; Schmithorst et al. 2001; Zaitsev et al. 2004). The main limitation of this method is that information from regions where the data is squashed into a smaller area cannot be fully recovered. This can be overcome if images are obtained with alternate directions for k-space traversal (in the PE direction), effectively switching the areas that are squashed to being stretched and vice versa (Morgan et al. 2004; Weiskopf et al. 2005). However, differences between alternate volumes can be hard to eliminate, and an effective reduction in temporal resolution or volume coverage is likely. Distortions can still pose a problem for standard fMRI and EEG-fMRI studies, particularly when high structural fidelity is required, such as when fMRI is used to assist in presurgical mapping of eloquent cortex, or where presurgical EEG-fMRI results from epilepsy patients are evaluated against structural images obtained post-resection.

10.2.3 Signal Dropout

Dropout, like distortion, is due to strong local magnetic field gradients interfering with the image acquisition process. There are two related but distinct mechanisms by which signal dropout can occur. The primary mechanism is due to local fields across the slice (through the imaging plane). The local magnetic fields cause magnetisation at different positions across the slice width to produce signals with corresponding frequencies. These signals from different positions will, with time, accumulate differing phases and so cancel; the net effect is a more rapid signal decay (see Fig. 10.4). If the signal decays substantially before the centre of k-space has been traversed, where the main low-frequency components of the signal are encoded, the majority of the signal is not sampled, and so the region will appear dark. The second mechanism is dropout due to in-plane gradients; if the in-plane gradients are strong enough, they will alter the k-space trajectory (i.e. an extreme example of what we saw previously for distortion). For dropout to occur, the trajectory must be altered radically such that the central region of k-space is not covered (see Fig. 10.4) (Deichmann et al. 2002, 2003; Weiskopf et al. 2006, 2007). It must also be remembered that in-plane gradients are still problematic even when dropout does not occur. This is because the effective TE (the point at which the centre of k-space is sampled) is shifted in time to earlier or later in the readout. An earlier TE will mean that there is strong signal but little BOLD contrast, whereas a later TE will have strong contrast but the signal will have decayed too much. Both in-plane and through-plane local susceptibility-related gradients can be increased where stronger magnetic fields are produced by EEG equipment.

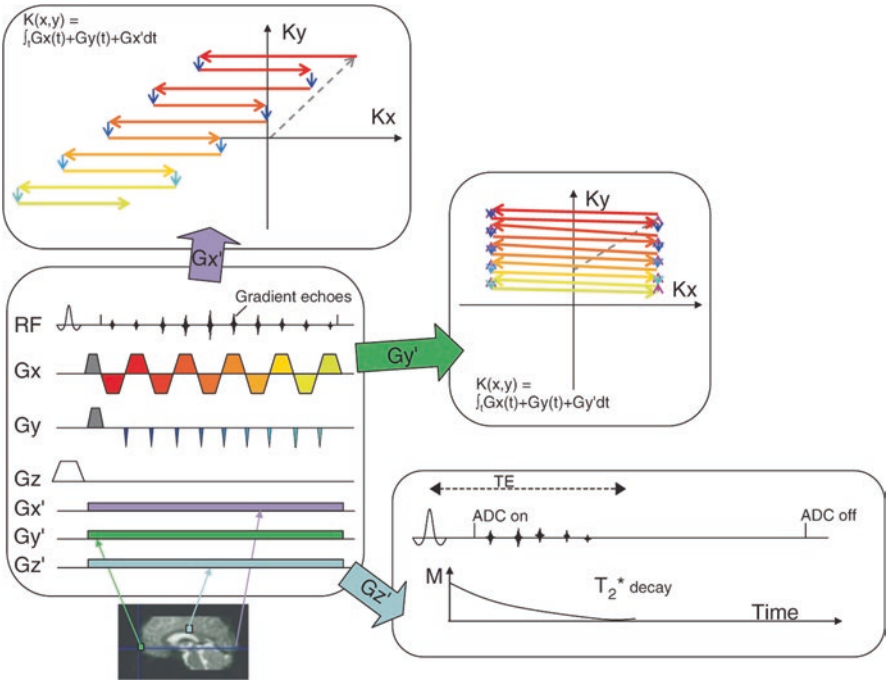

Fig. 10.4 Dropout in EPI images. Different mechanisms that cause signal dropout in EPI images are shown. An extra local gradient is present due to susceptibility artefacts (Gx', Gy' or Gz'). In the case of a local gradient Gz' from one particular position, this causes faster T_2* decay via through-plane dephasing, such that the signal has decayed before the centre of k-space has been sampled. Dropout can also occur when the local in-plane gradients Gx' or Gy' cause an alteration in the k-space trajectory such that the centre of k-space is not sampled. Note that even if the k-space centre is sampled, this will occur either much earlier or later in the echo train, leading to a greatly reduced BOLD sensitivity

There are a number of approaches that can be adopted to minimise dropout, primarily concerned with through-slice effects. The first consideration is the TE; reducing the TE means that the centre of k-space will be covered sooner, before the signal has largely decayed, and so reduces dropout. However, the BOLD sensitivity is reduced with TE. The balance required is to minimise the TE without strongly reducing the BOLD sensitivity (Deichmann et al. 2002). At 1.5 T, this means that a TE of around 50 ms is typically used, shortening to around 30 ms at 3 T. Another initial very simple approach is to decrease the slice thickness, reducing the frequency range across the slice, and hence the degree of phase dispersion that will occur (Frahm et al. 1993; Merboldt et al. 2000). Some penalty is incurred in terms of signal for well-shimmed areas (i.e. areas with a uniform local magnetic field) due to decreased voxel volume, whereas poorly shimmed areas will benefit from a large increase in signal. There is also a penalty in terms of volume coverage, although gaps between slices can be increased. The balance between these different factors will depend on the particular experiment, regions of primary interest, the sequence

and the scanner. It is in this context that SMS sequences have a distinct advantage because they allow for thinner slices to be obtained in the same TR and, at least with modest SMS factors (typically ≤ 3), there is not a large SNR penalty. Therefore, although SMS sequences are often used to reduce the TR to increase temporal sampling, they are a very useful method to mitigate signal dropouts by reducing slice thickness while maintaining the TR and SNR.

In addition to making the slices thinner, the orientation of the slices can also be altered to minimise dropout (Cho et al. 1988; Deichmann et al. 2002; Weiskopf et al. 2006). Since the primary loss is due to gradients across the slice, by changing the slice tilt, the size of the local gradients perpendicular to the slice plane can be reduced. However, slice tilting is often used to reduce the size of in-plane gradients that are causing dropout or reduced BOLD sensitivity. The increased through-plane gradients are then compensated with a z-shim (discussed below).

In addition to optimising TE, slice thickness and slice tilt, significant dropout can still occur, particularly in orbitofrontal regions and the temporal poles (Deichmann et al. 2003). The local B_0 gradients produced by putting a subject into the magnet field can be compensated for by using a pulse sequence with an additional preparatory gradient of opposite polarity but similar area, which is generally referred to as a z-shim (Constable and Spencer 1999; Frahm et al. 1988; Ordidge et al. 1994a). There are two main effects from utilising a z-shim. Firstly, in areas of the brain that are not affected by strong local gradients, the T_2* is effectively increased, and so this can reduce the BOLD sensitivity when using the same TE sequence. This suggests that only a moderate z-shim can be used without a significant penalty in sensitivity over much of the brain (Deichmann et al. 2002). Secondly, in areas where the z-shim compensates for local gradients, a large improvement in dropout is achieved with a correspondingly large improvement in sensitivity to BOLD signal changes. Unfortunately, it is normally difficult to achieve a z-shim improvement in one area without a decrease of performance in another, and so the optimal choice of z-shim (and slice tilt combination) will depend on the regions of most interest for a particular study (Deichmann et al. 2002; Weiskopf et al. 2006, 2007). One way to achieve a more optimal z-shim for a greater range of areas is to use a multi-echo EPI readout (Poser et al. 2006). This means that images can be obtained at several different TEs and with different compensation gradient polarities or directions. The images can then be combined very simply (e.g. by addition) or by a weighting scheme devised from calibrating BOLD sensitivity to maximise the benefits (Constable and Spencer 1999; Poser et al. 2006). There can be some cost in terms of the time taken to obtain the data from each slice, which in turn may reduce volume coverage, making a simple reduction in slice width an attractive and simpler choice. However, multi-echo EPI sequences have a very high ratio of data acquisition time over scan time and so can offer a very efficient alternative strategy. Dropout is often the greatest problem in both fMRI and EEG-fMRI studies. Dropouts can be made worse (or at least BOLD sensitivity may be reduced) where EEG equipment produces increased magnetic field inhomogeneity within the brain.

10.2.4 Image Ghosting

In EPI, ghosting is normally produced by a mismatch between echoes formed by read gradients of opposite polarity. In Fig. 10.1, the process of reordering k-space is demonstrated; alternate lines are reversed (flipped about the origin) in order to have traversed k-space in the same direction for each line. Any inconsistency between lines acquired under positive- or negative-polarity gradients will cause an error in the image reconstruction (i.e. a flipped positive gradient line should be the same as a negative line if the phase encoding is the same). As alternate lines are affected, a ghost (a partial repeat of the image) will appear displaced in the phase-encoding direction by half the field of view. While this is often referred to as the 'Nyquist ghost', this is misleading as it is not a data undersampling error but a mismatch between alternate PE k-space lines, and thus the term N/2 ghost is more accurate. Gradient inconsistencies, eddy currents and susceptibility gradients can all contribute to this mismatch (Feinberg and Oshio 1994; Fischer and Ladebeck 1998; Reeder et al. 1997; Wan et al. 1997; Wielopolski et al. 1998). Ghosting can be affected by EEG equipment where susceptibility-related fields are responsible. Hardware improvements to increase gradient shape accuracy and reduce eddy currents, for example, or corrections to account for these inconsistencies can all reduce the artefact level (Fischer and Ladebeck 1998). One method frequently employed to correct these mismatches in alternate lines is to employ a reference scan (or navigator echo) (Hu and Le 1996; Ordidge et al. 1994b; Wan et al. 1997). The echo train used for the EPI acquisition is performed without PE gradients. A series of echoes is formed that can alternately be reversed in time. Any shift in the TE between them (in k-space) will produce a corresponding linear phase shift in image space. This allows the phase of the Fourier-transformed echoes to be compared and the difference between them used to correct all subsequent acquisitions. A further improvement can often be made to ghosting performance if the actual k-space trajectory is measured (Duyn et al. 1998; Josephs et al. 2000). One key consideration for fMRI is the stability of the ghost, because temporal changes due to drift or correction of imaging hardware can lead to false-positive activation and a reduction in temporal SNR (TSNR) (see Sect. 10.4.1). Ghosting can still provide significant image artefacts, particularly at higher field strengths and where EEG equipment decreases magnetic field homogeneity.

10.2.5 RF Interference

MRI systems are specifically designed to be maximally sensitive to RF signals around a particular frequency called the Larmor frequency of the system. RF signals are highly prevalent, particularly in the typical environment of a scanner in a busy hospital or research laboratory surrounded by a wide range of electronic equipment. To record the relatively weak RF signals from the sample without any of these confounding signals from the local RF background, the magnet is placed within a Faraday cage. This is an enclosed conductive metal sheet or fine mesh that is

connected to earth, and when external static or electromagnetic radiation is incident on the cage, electric currents are generated (and dissipated via the earth) which nullify the signal within the enclosed region. To make this approach effective, a good earth and complete enclosure of a room is required. This suggests an obvious weakness of MRI systems: access in and out of the room is essential, necessitating a door; gradient and RF systems require connection through the cage. The two weak points of the Faraday cage are thus the door and filter panel. Typically, attenuation of RF to 100 dB is specified, although in practice this can be difficult to achieve. Finally, equipment for stimulus presentation, physiological monitoring or indeed EEG equipment within the scanner room requires extra consideration. Firstly, by introducing these extra active components within the cage, any RF or electrostatic discharges they may produce will cause interference and degrade image quality. Secondly, equipment with any kind of highly conductive wire or cable crossing from the outside to inside the cage (i.e. via a waveguide) is a potential route for RF to be brought into the room. A more detailed description of methods for addressing these issues is given in Chap. 7. RF interference is generally visible in one of two forms in images: an increase in the overall background noise in an image more easily quantified as a corresponding decrease in SNR, attributable to incoherent broadband RF, and/or spatially localised bright spots in the image, attributable to coherent RF at distinct frequencies, as in Fig. 10.8c. In most structural imaging, the RF, due to its (slice-independent) constant frequency, will appear at the same position on each slice. For EPI, this is somewhat complicated by the fact that each readout direction is reversed, resulting in the N/2 ghost of the RF artefact due to local phase inconsistencies. A repeat of the artefact in the readout direction is often produced. fMRI is particularly sensitive to RF interference because it causes a local fluctuation in the signal intensity, which can dramatically increase the temporal variance and thus severely affect sensitivity to activation. This may result in false-positive activation, particularly if any of the equipment is switched on during image acquisition. We address detection and monitoring of RF performance in more detail in Sect. 10.5.3.

10.3 Other Sources of Image Artefact in fMRI

10.3.1 Bulk Head Motion

The recorded EEG and fMRI time series are both highly sensitive to motion. The greatest effort should be put into minimising subject movement via better head restraint and increased comfort (Laufs et al. 2008). This is especially important for patient studies in general (Hamandi et al. 2004; Salek-Haddadi et al. 2003) and when recording the highly motion-sensitive EMG. The use of a vacuum head cushion (Benar et al. 2003) has been found to minimise both motion-induced artefacts on the images and motion-induced currents contaminating the electrophysiological signal. Additionally, bite bars, inflating cuffs and subject-specific moulded cushions are also used in some centres. The use of sedative agents to

suppress motion needs careful consideration, as 'neuroactive' substances can alter net synaptic activity in a region-specific manner and thus fMRI signal intensity (Kleinschmidt et al. 1999). Under certain circumstances, sedation must be considered, such as when studying very young children with fMRI (Jacobs et al. 2007).

MRI motion correction via image realignment typically entails affine coregistration and is normally effective at dealing with small differences in head position through a scan (Ashburner and Friston 2004); example traces can be seen in Fig. 10.5. However, it should be remembered that the effects of motion can last longer than the period of movement itself; for example, the effective TR seen by the tissue moved into a different slice will be different, leading to signal fluctuations lasting for several TR periods (Friston et al. 1996). By including the motion realignment parameters, and preferably an expansion to take into account these extra effects, motion-related variance can be effectively modelled within general linear model (GLM) analyses (Friston et al. 1996; Lund et al. 2005). If large motion

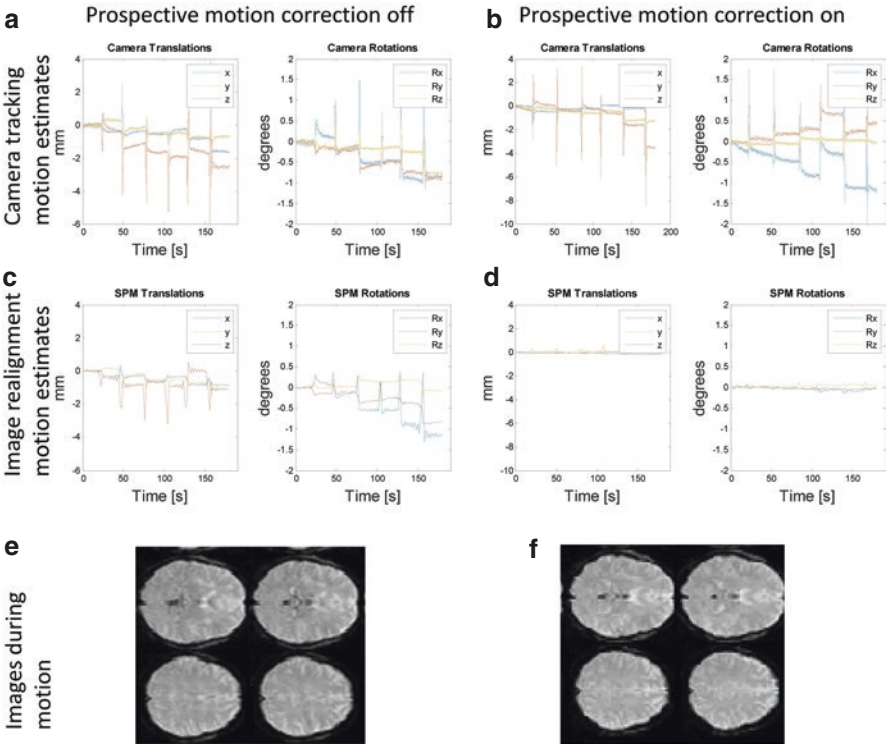

Fig. 10.5 (**a–f**) Motion traces from an optical camera tracking system are shown. Large motion events are seen when the subjects are asked to cross their legs in the camera tracking data (**a**, **b**); this is partially represented in the motion estimates from the realignment parameters (**c**). With prospective motion correction (**b**, **d**, **f**), the motion is largely corrected resulting in relatively small deviations in the realignment parameters (**d**) and improved image quality (**f**)

events occur, it is worth considering nulling their effects. Again, the preferred method is to include extra regressors (one for each large motion event) into the GLM to account for this variance (Lemieux et al. 2007; Salek-Haddadi et al. 2006) (as opposed to removal of data from the time series). Valuable data sets can often be recovered if motion effects are modelled sufficiently at the analysis stage (Lemieux et al. 2007).

There is a fundamental limitation with realignment-based motion correction algorithms in that it relies on the assumption that these parameters are accurately capturing motion events. This assumption is clearly broken in a number of situations such as movements that are faster than the frequency that can be captured by sampling rate such as sudden jerks or tremor; in Fig. 10.5, motion traces during leg crossing show discrepancies between the head motion and realignment parameters although they correctly capture the trend in the motion.

There are an increasing number of image-based post-processing algorithms that aim to extract noise components including motion directly from the data, and this is an extensive field of research. However, it is clear from a wide range of studies that extracting these parameters whether based on the bio-physiological plausibility of signal changes (Tierney et al. 2016) or by using spatial or temporal criteria to define noisy voxels (Behzadi et al. 2007), improved noise modelling can be achieved resulting in an improvement over scan-nulling (Tierney et al. 2016). There are a number of reviews on these approaches that have predominantly been developed for resting-sate fMRI; for further details, see Parkes et al. (2018). These methods are highly relevant here because where association and comparison between EEG and fMRI signals are used, temporally coherent artefacts will co-occur in both data types with ample potential to confound an analysis. However, this problem can also be used to provide improved motion characterisation by using identified motion-related EEG artefacts to inform fMRI motion correction (Wong et al. 2016).

Of course prevention is often better than cure, and there have been exciting developments in the application of prospective motion correction for EEG-fMRI (Daniel et al. 2019; Maziero et al. 2016). Motion correction can be performed using navigator echoes (Ordidge et al. 1994b; Gallichan et al. 2016), which relies on the Fourier shift theorem whereby a spatial shift of the image can be detected and corrected by measurement of the phase shift within MRI k-space data. An approach that has been used increasingly involves the use of a camera and markers attached to the subject to track motion with a short delay. This information can then be used to update the scanner acquisition so that the imaging slice remains in the patient frame of reference. This largely removes the problem of substantial signal changes where the tissue within a slice receives multiple excitations (within a TR) because it has moved into a different slice plane between the pulses. This was often thought by the community to be detrimental to EEG correction strategies; however, it has been shown that high-quality prospective fMRI motion correction facilitates EEG correction rather than hampering it because it is the motion that introduces the non-stationarity into the correction algorithms rather than its correction (Maziero et al. 2015).

10.3.2 Physiological Noise

Some 'noise' is physiological and related to global or local changes in brain state that happen spontaneously. These signals were previously considered as being purely noise in terms of cognitive, paradigm-driven experiments. However, increasingly, these spontaneous changes are being treated as signals of interest (Biswal et al. 1995; Fox and Raichle 2007; Laufs et al. 2003). EEG-fMRI allows some interpretation of these spatial patterns in terms of brain state (Laufs et al. 2008), and this will be addressed in more detail in subsequent chapters.

Cardiac and respiratory cycles also can cause confounding signal changes. These occur due to motion of the whole head and from changes in pressure within the skull resulting in pulsatile motion of the brain. Due to the temporal resolution of fMRI normally being below that of the cardiac signals, aliasing occurs and must be accounted for; otherwise these effects can look like low-frequency BOLD-related signal changes. Methods are available to derive regressors from EEG/EOG/ECG signals for subsequent entry into standard GLM analysis to remove any confounding signal variance from these sources (Glover et al. 2000; Liston et al. 2006).

As introduced in the motion section, an alternative and often effective strategy is to derive the influence of physiological noise on the fMRI time courses via estimation from the data itself. Here, there are a wide variety of methods to choose from, but they can be categorised into a number of approaches. Firstly, independent component analysis can be used followed by component classification to derive the temporal signatures of physiological noise components (e.g. Pruim et al. 2015) that can be incorporated into a model such as a GLM as effects of no interest or the data reconstructed with those components removed. Secondly, noise models can be derived from spatial criteria. In simplest form, the brain tissue not BOLD active (e.g. CSF and white matter) can be used (Behzadi et al. 2007; Bright et al. 2017) and signals averaged that contain a significant relationship to physiological noise. This can be finessed by instead using temporal criteria where highly variable voxels are used that will contain a mix of physiological and motion-related variance (tCompCor (Behzadi et al. 2007)) additionally with a biophysical interpretation (Tierney et al. 2016). Thirdly, the use of multi-echo data can be used to separate physiological noise components if they do not contribute to exponential T2* behaviour (Kundu et al. 2017). While effective, this does not account for some aspects such as respiration-related effects that are mediated via the same mechanisms as fMRI signals (Power et al. 2018). Lastly, with the advent of fast fMRI sequences, the aspects of physiological noise that occur at a different temporal frequency can be removed via direct filtering of the signal over frequency ranges where physiological noise occurs but where fMRI signal does not, for example, cardiac-related noise.

10.4 The Impact of EEG Recording on MR Image Quality

In Chaps. 8 and 9, the effects of MRI on the EEG signal were discussed; here, we instead look at the potential influence of the EEG system on MRI image quality. As previously described, fMRI relies on good SNR, a high degree of temporal stability,

and can be affected by artefacts due to the way that GE-EPI data is acquired. The presence of an EEG system can interact with both the static and rotating magnetic fields required for signal excitation and reception (Mullinger et al. 2007), which can have a subsequent impact on image quality (Krakow et al. 2000), as described below. Fortunately, these effects can be minimised by careful design of the EEG equipment.

10.4.1 Main Static Magnetic Field (B_0) Effects

MRI utilises a very strong, highly uniform main magnetic field, which is perturbed by the presence of any material with a magnetic susceptibility (χ). This degree of disturbance depends on the main field strength and the magnetic susceptibility ($\Delta B_0 = \chi B_0$). The high strength of the main field dictates that even weakly magnetic material such as water ($\chi = \sim 1 \times 10^{-7}$) can cause a local change in the magnetic field that can increase the distortion, dropout and ghosting described above. The main magnetic field can be readily measured from two gradient echo images with a different TE. The local difference between the phases of the images is due to the local magnetic fields, and so the offset of the field in Hz can be calculated (as for distortion correction). Even the weakly magnetic materials typically used in an MRI-compatible EEG cap have susceptibility values capable of introducing artefacts. The effect of two different commercially available MRI caps (both employing Ag/AgCl ring electrodes, 5 kΩ resistors, copper-braided wires and Abralyte 200 conductive gel) on the B_0 field in a uniform phantom taken from Mullinger et al. is shown in Fig. 10.5. There are clear localised regions of decreased homogeneity caused by the electrodes of the cap that are made worse with higher field strength. Taken over the volume, there is an increase in the number of pixels with a large field offset (Mullinger et al. 2007). However, in the same study, a similar measurement over the human brain at 3 T did not yield such a clear difference between cap on/cap off. A range of materials are available for the electrode heads, connecting wires, current-limiting resistors added for safety reasons (Lemieux et al. 1997), adhesives and gels, although a balance must be struck between EEG performance and the imaging requirements. Two factors determine the severity and impact of artefact caused by these components at a given field strength: its susceptibility and its position relative to both imaging and brain geometry. The relative geometry of the head and the electrodes is fixed by the experimental requirement of good EEG coverage (Debener et al. 2008). The available evidence suggests that plastic AgCl-coated electrodes can yield a small improvement in B_0 performance, although Ag/AgCl electrodes can also perform similarly in terms of image quality (Stevens et al. 2007) and may provide improved EEG quality. Both of these electrode types caused B_0 field perturbations over 10–15 mm at 4 T (Stevens et al. 2007) and so should not unduly affect signals from the brain when imaging the human head. It should be noted that in paediatric applications (Arichi et al. 2017) with the brain closer to the electrodes, this artefact may still be problematic. In addition, at ultra-high field ≥7 T, artefacts are

increased and so may extend into the brain. Alternatives to the commonly used metallic EEG electrode materials (silver, silver chloride, gold) such as carbon may also yield low artefact levels (Krakow et al. 2000), while Sn or brass plated with Ni and then Au can cause greater problems (Baumann and Noll 1999; Stevens et al. 2007). The susceptibility of most electrode gels is broadly similar to the tissue (due to the conductivity required for EEG), giving limited scope for improvement in susceptibility-related artefacts caused by the gel/air interface. The choice of material for the safety resistors needs more careful selection, as many resistors use ferro- or diamagnetic materials, for example, in the end caps connecting the terminating wires to the resistive material (Krakow et al. 2000). In the tests of Mullinger et al. (2007), the interface between the plastic surface of the phantom and the EEG electrodes and gel is likely to be the source of the greater variance in B_0. This interface is not present in the human head (see Fig. 10.6), where B_0 variation appears to be reduced compared to within the phantom. Increased inhomogeneity in B_0 will be seen as increased EPI image artefacts, with dropout, distortion and potentially ghosting produced. However, provided that the materials used for EEG electrodes and gel are carefully chosen and tested, there is only a small increase in B_0 inhomogeneity within the human brain, limiting the impact on image quality.

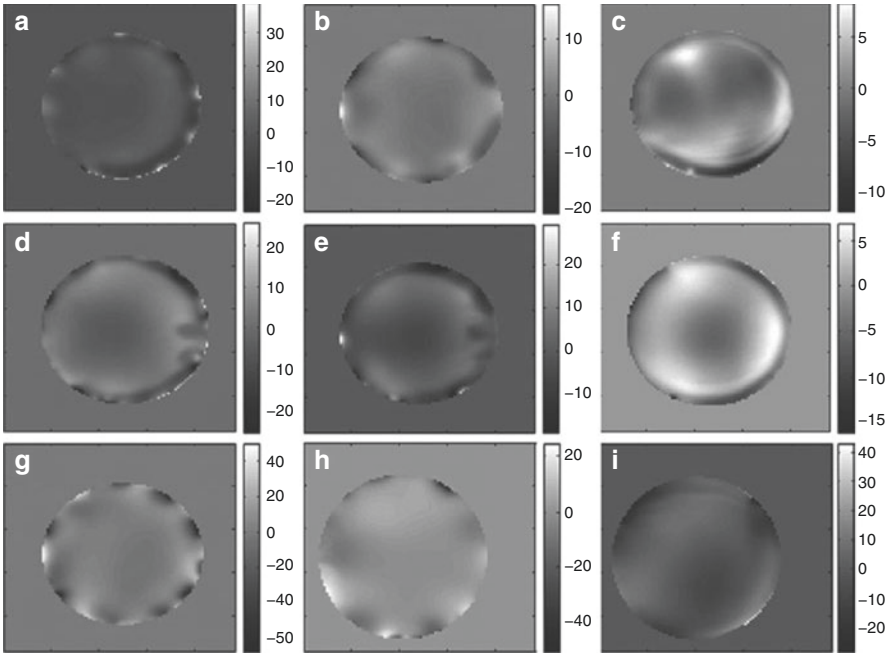

Fig. 10.6 (**a–i**) B_0 field maps (in Hz) acquired from the phantom. Maps are shown after removal of large-scale field variations (due to the global shim) to view primarily the effect of the EEG cap at 1.5 T (**a–c**), 3 T (**d–f**) and 7 T (**g–i**) with the 64-electrode cap (*left*), 32-electrode cap (*centre*) and no cap (*right*) on. Reproduced with permission from Mullinger et al. (2007)

10.4.2 Transverse Rotational Magnetic Field (B_1) Effects

MRI signal excitation and reception use a rotating RF field at the Larmor frequency, as described in Sect. 10.3.1. To excite the sample, an RF field is applied that causes the magnetisation to be rotated from the longitudinal axis into the transverse plane. This magnetisation then subsequently creates a rotating RF field that can then be detected by the RF coil. Any non-uniformity in the excitation profile makes it difficult to excite all of the magnetisation within the object (i.e. the flip angle will not be uniformly 90° across the object), and so some regions will suffer a corresponding signal reduction. Via the principle of reciprocity (Hoult and Lauterbur 1976), the B_1 field created by the coil for signal excitation is the same as the sensitivity of the coil (the MRI correlate of an EEG gain matrix) for signal detection. This means that the object will have a spatial variation in signal detection performance with the same pattern as for signal excitation.[2] Furthermore, the introduction of any conductive or dielectric material (i.e. the head or an EEG electrode) causes a change in the B_1 field (Sled and Pike 1998). This is because the field induces surface currents in the material that act to minimise the field produced within the object (i.e. they shield the object from the field). It is useful to consider the effects on two length scales: firstly, a global effect from the introduction of the EEG system can generally be considered a loss of coil efficiency and so SNR (see the section on the impact on SNR); secondly, local changes in the B_1 field are produced by local current flow which acts to reduce the B_1 field. This will produce areas with a reduced flip angle for signal excitation and so a reduced signal and a corresponding drop in sensitivity for signal reception.

The B_1 performance for the two EEG caps described in the previous section in a phantom can be seen in Fig. 10.7. The EEG cap has an effect on B_1 that appears to increase with field strength and is worse around the ECG wire. This is likely to be due to the increased coupling of the longer length ECG wire to the RF field, with the induction of greater currents than for the shorter EEG wires. The B_1 perturbation produced by the electrodes themselves appears weak, at least at the lower field strengths. Increased electrode impedance decreases the perturbation in the B_1 field: Krakow et al. demonstrated that both plastic coated with AgCl and carbon electrodes, which offer greater impedance than metallic electrode materials, gave less artefact (Krakow et al. 2000). However, in a different comparison of electrodes at 4 T, where B_1 was independently assessed, similar shielding was produced by three different electrode types, with shielding reduced to 5% at 10–11 mm from the electrode (Stevens et al. 2007). In addition, secondary currents can flow in the safety resistors and cause artefacts, so these must be chosen carefully. Electrode wires can cause B_1 perturbations, even when safety resistors are present (Mullinger et al. 2007); higher impedance alternatives such as carbon can reduce this artefact (Krakow et al. 2000). These considerations have been revisited owing to interest in performing EEG-fMRI at

[2] This assumes that the same coil is used for both signal excitation and reception. It is increasingly common for different coils to be used for each purpose, with each imposing a different pattern.

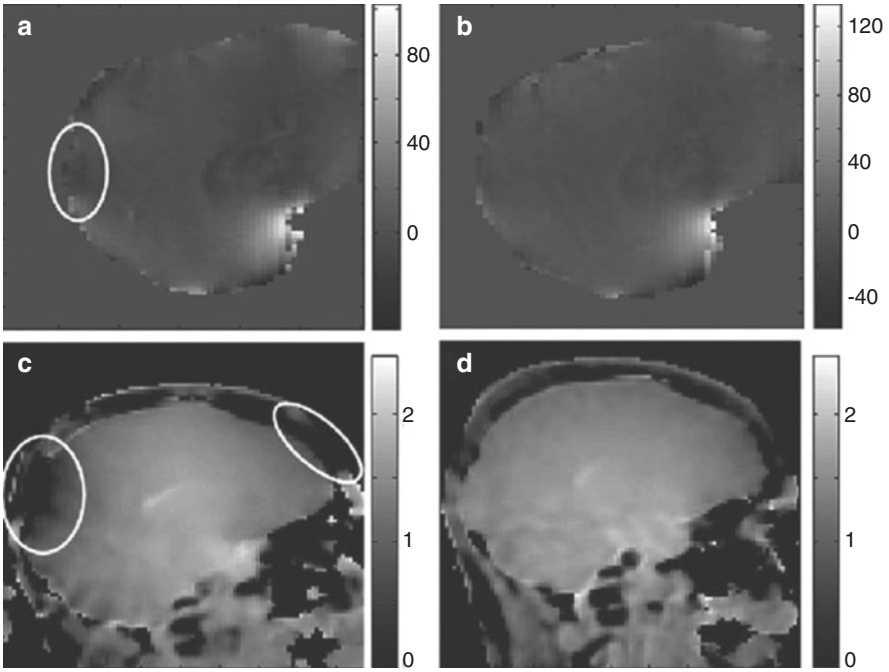

Fig. 10.7 (**a–d**) B_0 and B_1 maps obtained in the human head. Effects of 32-electrode cap at 3 T on B_0 maps (in Hz) (**a**, **b**) and flip angle maps (normalised to average flip angle) (**c**, **d**). (**a**, **c**) Acquired with the cap on (regions affected are *highlighted*); (**b**, **d**) with no cap. Reproduced with permission from Mullinger et al. (2007)

7 T, for example, with improved design of EEG cap wiring (Jorge et al. 2015) or changes in wiring material to increase its impedance at RF.

RF pulses that aim to produce a uniform flip angle despite local variation in B_1 (frequently referred to as 'adiabatic' pulses) do exist (Garwood et al. 1989; Garwood and Delabarre 2001) but are more commonly employed for global signal inversion or refocusing and normally require greater RF power than standard excitation pulses (de Graaf et al. 1996). Certainly, investigation of EEG-fMRI performance with spatially selective 90° pulses that exhibit acceptable off-resonance behaviour such as derivatives of the BIR4 pulse (de Graaf et al. 1996; Shen and Rothman 1997) is merited and may be essential to limit artefacts at higher field strengths. B_1 perturbations will produce regional intensity variation in EPI images without increased distortion. One simple method to determine whether B_1 or B_0 field effects are responsible for regionally reduced performance (where B_0 and B_1 mapping sequences are not available) is to compare spin echo 2DFT images with the EPI; where both exhibit changes in image intensity, the problem can be assigned to a local B_1 effect.

10.4.3 Impact on SNR

The overall effect of the introduction of the EEG system is a reduction in SNR. Locally, this can be due to reduced signal related to decreased B_0 and B_1 homogeneity. Globally, there will be an average reduction in B_1 sensitivity due to the introduction of EEG equipment from shielding effects, and increased noise from increased RF coil impedance, with a concomitant global reduction in SNR. The shielding effect is a reduction in B_1 in the head from induced current flow in the EEG electrodes. To understand the increase in noise, the system can be considered as a whole with a highly resonant RF coil circuit having its impedance increased by the introduction of the head and then further increased by the introduction of EEG components. While the increase in impedance (a reduction in the coil efficiency usually measured by the Q factor) is one effect, it is also possible that the whole system (coil with head and EEG system inside) suffers from a split or shifted resonant frequency. In this case, a quite dramatic reduction in coil performance can result. A reduction in SNR within the images will be seen, but, where the same coil is used for RF transmission, there will also be a large increase in the transmitted power required for a particular RF excitation and increased local electric fields with the associated safety risks (Lemieux et al. 1997).

In the image quality study of Krakow et al. (2000), only the increase in electronic noise due to the introduction of the EEG amplifier was investigated, and no noise increase was detected when properly shielded. While this approach will detect any RF interference, it does not determine the amount of SNR loss due to a reduction in the RF coil performance via the mechanisms described above. One previous study observed a reduction in SNR that was proportional to the number of electrodes in the cap (Scarff et al. 2004), while an innovative ink cap that uses conductive ink rather than conventional wires had little apparent effect on the SNR (Vasios et al. 2006). More recently, tests of two commercially available caps at different field strengths on five subjects found a reduction of 4–28% in the TSNR. A smaller SNR reduction was found on the 3 T system, although this could be due to cap design and may not lead to a large difference in detected activation (Bonmassar et al. 2001). While some decrease in TSNR (see Sect. 10.5.1) could be caused by increased movement due to the greater discomfort of wearing an EEG cap, it is likely that this is also because of cap-coil interaction. It is worth noting that reducing the appearance of B_1-related artefacts is worthwhile even when they do not appear to greatly affect signal from the brain, because reducing this interaction will improve the overall SNR performance via reduced loading/detuning of the RF coil. It should be noted that SNR reductions may not always lead to a reduction in fMRI sensitivity (Luo and Glover 2012) if noise sources, predominantly physiological, are similarly scaled. However, as discussed below, it is increasingly possible to separate the signal and noise, and therefore reductions in SNR will then impact fMRI results.

10.5 fMRI Quality Assurance (QA)

The large demands placed on MRI hardware by scanning at close to the maximum gradient switching rate and amplitude for extended periods, coupled with the sensitivity of fMRI to any temporal signal changes, mean that careful, regular fMRI

QA is important to ensure that scanner performance is maximised and any faults are quickly detected. In this section, some of the key QA measurements are described. In many respects, the principle is more important than any specific tests; the more that careful, regular, quantitative monitoring of the system is performed, the better. In particular, we focus on tests aimed more generally at fMRI QA but which constitute a good basic set of tests of fMRI data quality that can be performed both with and without the EEG equipment. A summary of this can be found in Table 10.1.

Table 10.1 Examples of QA procedures

Scans	Suggested frequency	Example parameters	Example measurements	What to look out for	Possible cause
Spin echo 2DFT	Daily	192 × 128 matrix, TE = minimum, TR = 3 s, 5 central slices	SNR	Change or fluctuations in value	Non-specific
EPI (as used for EEG-fMRI)	Weekly	TR = 2000 ms, TE = 30 ms, 200 volumes, 27 slices	Temporal mean	Strong repeats of the image (ghosts)	Gradient performance, timing and pre-emphasis, phase correction errors
			Temporal SD reformatted as coronal sections	Lines in the slice direction/ strong images	RF interference/B_0 and possible gradient drift
			Weisskoff plot	Change in plot	Non-specific
			RDC	Change in value	Non-specific
EPI (as used for EEG-fMRI) with and without EEG cap	Monthly	TR = 2000 ms, TE = 30 ms, 200 volumes, 27 slices		Compare with the measurements without EEG equipment	EEG system fault
Repeat run	Monthly	Place slices outside the phantom and set the transmit gain to zero. Run for >10 min, i.e. 400 volumes	Play the images back as a movie with a volume in each frame	Changes in background noise level, any structure in the noise	Coherent noise patterns within certain slices suggest spiking from the gradients or electrostatic discharges from another source. Higher signal in a consistent spatial position indicates RF interference

10.5.1 Quantification of SNR and Temporal SNR

The receiver bandwidth determines the frequencies and levels of signal and noise obtained (given a certain object imaged at a specified resolution), since most of the signal is normally concentrated at low frequencies, whereas the noise is distributed across the frequency range. However, given that a certain bandwidth is used for a specific scan protocol, then the SNR describes the quality of the data and can be very sensitive, if non-specific, to the performance of most components of the system. A phantom should be used that approximates the size and loading (RF interaction) of the human head. A phantom made of gel to eliminate flow effects is also desirable for testing fMRI temporal stability. Highly accurate and easily reproducible positioning of the phantom is important within both the RF coil and the main magnetic field isocentres (i.e. the SNR measured should not change when the test is performed by a different person!). Where different RF coils are routinely employed, each should be regularly tested. Different methods can be used to take a measurement of the signal and noise. However, most simple SNR tests (such as those described here) make the assumptions that the background noise follows a Raleigh distribution in the magnitude image and that the spatial distribution of noise is homogeneous. These criteria are not met in most images from array receiver coils or where image filtering or corrections have been applied (Constantinides et al. 1997; Dietrich et al. 2007). To sample the signal, an image of the object must be obtained and the average signal within it calculated, typically by averaging the signal over a large (>75%) area. Noise can be measured in a similar manner by taking several background regions in the image and averaging them, although care must be taken to avoid regions exhibiting any artefact from the object, such as Gibbs ringing (Haacke et al. 1999), ghosting, or if any correction or filter is applied. An alternative approach to measure the noise is to obtain a further image using identical parameters, take the difference, and calculate the standard deviation within the same region of interest (ROI) (i.e. the area defined on the first image for the signal). This method can be affected by any temporal instability and, as such, is usefully viewed to detect any structure in the noise; if edges are visible, centre frequency or gradient drift may be indicated, or if a low SNR version of the object is apparent, RF/receiver instabilities can be responsible. Also, the value obtained from each SNR measurement method will be different by a constant factor due to the rectification of Gaussian noise when a background noise region is used. Different sequences may be employed for SNR

calculation, but a fully relaxed 2DFT spin echo sequence is a highly reliable method and is complimentary to an fMRI-specific EPI run. While standard SNR measurement is sensitive to many aspects of scanner performance, it does not generally test temporal fluctuations that can affect fMRI. In contrast to the static SNR, the TSNR includes contributions from fluctuations from scanner drift from the gradients as they heat and from the main magnetic field, ghost fluctuations due to timing errors, etc. The TSNR is simply the mean signal in a voxel divided by its variance over time. This measure of SNR can be more reliable where PI reconstruction methods and/or image filters are applied (Dietrich et al. 2007). A number of values in addition to the TSNR can be calculated and monitored from an EPI time series obtained from a phantom. One such standardised set of measurements (used by the FBIRN consortium) that can be automated is freely available (http://www.nbirn.net) and well described (Friedman and Glover 2006). These standardised QA measurements are important for cross-centre comparison (Friedman et al. 2007).

10.5.2 The Weisskoff Test

The Weisskoff test is a simple method for assessing scanner stability (Weisskoff 1996) and is included within the FBIRN procedure (Friedman and Glover 2006). In its original formulation, two ROIs are obtained inside and outside the phantom for each point in time and compared as the region is linearly changed in size. Taking the average mean and standard deviation produced, the standard deviation should be reduced with the square root of number of voxels in the ROI if purely Johnson noise is present from the scanner hardware and sample. The calculation can then be repeated only where the relative fluctuation from time point to time point is calculated again as the regions are linearly changed in size. Any difference between the two curves generated is attributable to extra temporal fluctuations in the images from scanner instabilities. The performance of the scanner can thus be characterised for a particular phantom and scanning sequence and the performance assessed over time. A derivative single value measure can also be obtained from this test called the radius of decorrelation (RDC), which can be thought of as being the point at which statistical independence between voxels is lost; practically speaking, it is where the two curves described above begin to deviate (see Fig. 10.8).

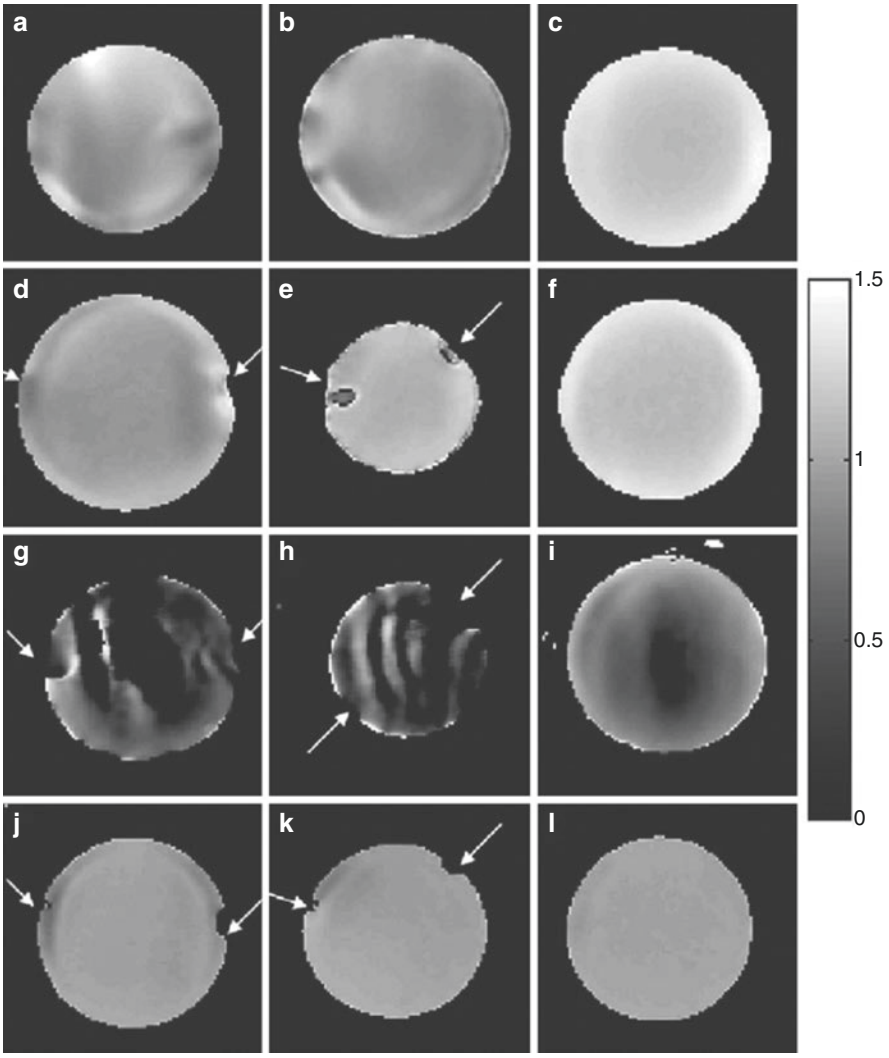

Fig. 10.8 (**a–l**) Flip angle maps (B_1) acquired from a phantom. Flip angle maps of the phantom (normalised to average flip angle) with the 64-electrode cap (*left*), the 32-electrode cap (*centre*) and no cap (*right*). **a–c** show maps acquired at 3 T from similar slices to those shown in Fig. 10.1. The maps shown in the rest of the figure are taken from more inferior slices and show the effect of B_1 perturbations occurring in proximity to the ECG and EOG wires (*arrowed*) at 3 T (**d–f**), 7 T (**g–i**) and 1.5 T (**j–l**). A more inferior slice is shown for the 64-electrode cap compared with the 32-electrode cap, as the paths of the EOG and ECG wires were different on these caps. Thresholding in low-signal areas leads to the generation of significantly sized areas in the 7 T maps where the flip angle cannot be characterised. Reproduced with permission from Mullinger et al. (2007)

10.5.3 Coherent Noise Testing

While RF interference can affect other measurements such as SNR and the RDC, specific testing is useful because the introduction of EEG equipment into the scanner environment increases the potential for this problem to occur. As an additional test to those suggested above, viewing a 3D volume of the temporal variance (e.g. taking the magnitude image time series and calculating the temporal standard deviation for each voxel) is highly instructive. With the data displayed such that the slice direction is in the image plane (e.g. axial images reformatted as coronal sections), RF interference will be seen as stripes running along the slice direction because the source of the signal is the same frequency independent of the RF or imaging gradients and so it will appear in the same place. Very few other artefacts have a similar appearance (apart from possibly some flow effects). Another useful and simple test for detecting noise changes is to simply scan while not receiving signal from the object. This is normally achieved by setting the RF transmit gain to zero, and/or from imaging slices outside the object, and often requires any automated prescanning to be skipped or performed manually (because most clinical scanners will detect that no signal is present and the centre frequency setting, for example, will fail). By looking at a long time series of images containing pure noise, any transient increases or changes in time due to RF interference or electrostatic discharges (often called spike noise) can be relatively easily detected visually. Finally, the equipment should be tested in all possible states. For example, where different gain settings, sampling frequencies or numbers of channels may be used in an EEG amplifier, it is worthwhile checking each operational state because RF noise might be generated or its frequency shifted in one particular configuration. An example of RF noise from a malfunctioning EEG amplifier is shown in Fig. 10.9.

Subject Data QA Procedures

Owing to the advent of large-scale projects to obtain fMRI data in thousands of subjects, there has been significant work aiming to perform fMRI QA on data that has been obtained in subjects (Alfaro-Almagro et al. 2018; Marcus et al. 2013). In general, the approach taken has been to utilise measures already introduced in this chapter such as TSNR and summary measures of motion realignment parameters to evaluate data quality. These are readily available to use and therefore can be applied to monitor data quality in participant studies in addition to regular QA procedures.

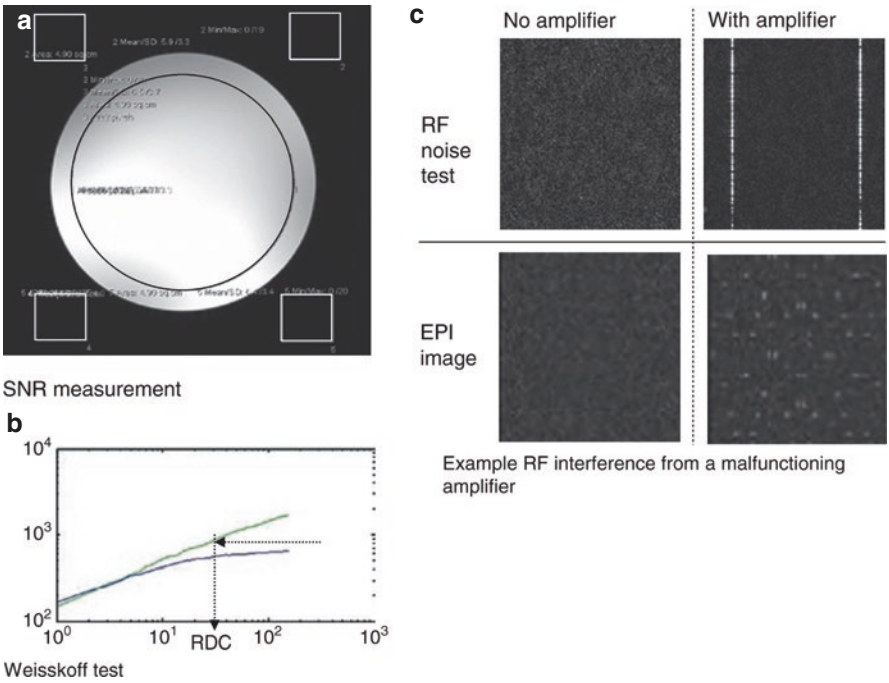

Fig. 10.9 (**a–c**) Examples of QA measurements. An example SNR measurement is shown (**a**) with the mean and standard deviation in the regions of the signal and noise compared. An example Weisskoff plot is shown (**b**), including the radius of decorrelation. Finally, an example of the appearance of RF noise in images obtained with the RF transmitter effectively turned off is shown (**c**)

10.6 Summary and Conclusions

Image quality is at the core of any successful investigation of brain activity using fMRI. Therefore, it is crucial to understand the mechanisms of the image formation process and its possible pitfalls, particularly when special equipment is in the vicinity of the MRI instrument, such as that used for EEG recording. In general, properly designed and tested EEG equipment should not adversely degrade image quality. The optimisation of fMRI sequences and the application of rigorous QA protocols will ensure optimal image acquisition and minimise the risks of false-negative or false-positive findings. It is likely that exact parameter choices are application and hardware dependent. However, there is increased evidence for the utility of faster fMRI sequences in a range of applications, and at least for modest TR reductions, there is a consensus that fMRI results are improved. Physiological and subject motion-related noise remains a challenge for all fMRI studies including EEG-fMRI. However, there are an increasing range of strategies available based on both image post-processing and acquisition developments that in concert can substantially reduce their impact.

Acknowledgements I would like to thank the following contributors to this chapter: Danilo Mazeiro and Mirja Steinbrenner for helping make figures; Ralf Deichmann (Brain Imaging Centre, Frankfurt) for his useful comments about EPI artefacts, Jack Wells (Department for Medical Physics, UCL, London), Philip Allen (Department of Clinical Neurophysiology, National Hospital for Neurology and Neurosurgery, London) and Nikolaus Weiskopf for careful reading of the manuscript; Chloe Hutton and Nikolaus Weiskopf (Wellcome Trust Centre for Neuroimaging, UCL, London) for providing the distortion correction part of Fig. 10.3 and the Weisskoff plot script for Fig. 10.8b; Alison Duncan (AMRIG, UCL, London) for providing Fig. a; and Richard Bowtell (Sir Peter Mansfield Magnetic Resonance Centre, Nottingham, UK) and the International Journal of Psychophysiology (https://doi.org/10.1016/j.ijpsycho.2007.06.008) for allowing the reproduction of Figs. 10.5, 10.6, and 10.7.

References

Ahn CB, Kim JH, Cho ZH (1986) High speed spiral scan echo planar imaging. IEEE Trans Med Imaging 5(1):2–5

Alfaro-Almagro F, Jenkinson M, Bangerter NK, Andersson JLR, Griffanti L, Douaud G, Smith SM (2018) Image processing and Quality Control for the first 10,000 brain imaging datasets from UK Biobank. NeuroImage 166:400–424. https://doi.org/10.1016/j.neuroimage.2017.10.034

Arichi T, Whitehead K, Barone G, Pressler R, Padormo F, Edwards AD, Fabrizi L (2017) Localization of spontaneous bursting neuronal activity in the preterm human brain with simultaneous EEG-fMRI. elife 6:27841. https://doi.org/10.7554/eLife.27814

Ashburner J, Friston K (2004) Rigid body registration. In: Frackowiak RSJ, Friston KJ, Frith CD, Dolan RJ, Price CJ, Zeki S, Ashburner J, Penny W (eds) Human brain function. Elsevier, Amsterdam, pp 635–653

Bandettini PA, Wong EC, Jesmanowicz A, Hinks RS, Hyde JS (1994) Spin-echo and gradient-echo EPI of human brain activation using BOLD contrast: a comparative study at 1.5 T. NMR Biomed 7:12–20

Baumann SB, Noll DC (1999) A modified electrode cap for EEG recordings in MRI scanners. Clin Neurophysiol 110:2189–2193

Behzadi Y, Restom K, Liau J, Liu TT (2007) A component based noise correction method (CompCor) for BOLD and perfusion based fMRI. NeuroImage 37(1):90–101. https://doi.org/10.1016/j.neuroimage.2007.04.042

Benar C, Aghakhani Y, Wang Y, Izenberg A, Al Asmi A, Dubeau F, Gotman J (2003) Quality of EEG in simultaneous EEG–fMRI for epilepsy. Clin Neurophysiol 114:569–580

Biswal B, Yetkin FZ, Haughton VM, Hyde JS (1995) Functional connectivity in the motor cortex of resting human brain using echo-planar MRI. Magn Reson Med 34:537–541

Block KT, Frahm J (2005) Spiral imaging: a critical appraisal. J Magn Reson Imaging 21:657–668

Bonmassar G, Hadjikhani N, Ives JR, Hinton D, Belliveau JW (2001) Influence of EEG electrodes on the BOLD fMRI signal. Hum Brain Mapp 14:108–115

Bornert P, Jensen D (1994) Single-shot-double-echo EPI. Magn Reson Imaging 12:1033–1038

Bright MG, Tench CR, Murphy K (2017) Potential pitfalls when denoising resting state fMRI data using nuisance regression. NeuroImage 154:159–168. https://doi.org/10.1016/j.neuroimage.2016.12.027

Butts K, Riederer SJ, Ehman RL, Thompson RM, Jack CR (1994) Interleaved echo planar imaging on a standard MRI system. Magn Reson Med 31:67–72

Carlson JW, Minemura T (1993) Imaging time reduction through multiple receiver coil data acquisition and image reconstruction. Magn Reson Med 29:681–687

Carmichael DW, Priest AN, De Vita E, Ordidge RJ (2005) Common SENSE (sensitivity encoding using hardware common to all MR scanners): a new method for single-shot segmented echo planar imaging. Magn Reson Med 54:402–410

Chen NK, Wyrwicz AM (1999) Correction for EPI distortions using multi-echo gradient-echo imaging. Magn Reson Med 41:1206–1213
Cho ZH, Kim DJ, Kim YK (1988) Total inhomogeneity correction including chemical shifts and susceptibility by view angle tilting. Med Phys 15:7–11
Cohen MS, Weisskoff RM, Rzedzian RR, Kantor HL (1990) Sensory stimulation by time-varying magnetic fields. Magn Reson Med 14:409–414
Constable RT, Spencer DD (1999) Composite image formation in z-shimmed functional MR imaging. Magn Reson Med 42:110–117
Constantinides CD, Atalar E, McVeigh ER (1997) Signal-to-noise measurements in magnitude images from NMR phased arrays. Magn Reson Med 38:852–857
Cusack R, Russell B, Cox SM, De Panfilis C, Schwarzbauer C, Ansorge R (2005) An evaluation of the use of passive shimming to improve frontal sensitivity in fMRI. NeuroImage 24:82–91
Daniel AJ, Smith JA, Spencer GS, Jorge J, Bowtell R, Mullinger KJ (2019) Exploring the relative efficacy of motion artefact correction techniques for EEG data acquired during simultaneous fMRI. Hum Brain Mapp 40(2):578–596. https://doi.org/10.1002/hbm.24396
de Graaf RA, Nicolay K, Garwood M (1996) Single-shot, B1-insensitive slice selection with a gradient-modulated adiabatic pulse, BISS-8. Magn Reson Med 35:652–657
Debener S, Mullinger KJ, Niazy RK, Bowtell RW (2008) Properties of the ballistocardiogram artefact as revealed by EEG recordings at 1.5, 3 and 7 T static magnetic field strength. Int J Psychophysiol 67:189–199
Deichmann R, Josephs O, Hutton C, Corfield DR, Turner R (2002) Compensation of susceptibility-induced BOLD sensitivity losses in echo-planar fMRI imaging. NeuroImage 15:120–135
Deichmann R, Gottfried JA, Hutton C, Turner R (2003) Optimized EPI for fMRI studies of the orbitofrontal cortex. NeuroImage 19:430–441
Dietrich O, Raya JG, Reeder SB, Reiser MF, Schoenberg SO (2007) Measurement of signal-to-noise ratios in MR images: influence of multichannel coils, parallel imaging, and reconstruction filters. J Magn Reson Imaging 26:375–385
Duong TQ, Yacoub E, Adriany G, Hu X, Ugurbil K, Vaughan JT, Merkle H, Kim SG (2002) High-resolution, spin-echo BOLD, and CBF fMRI at 4 and 7 T. Magn Reson Med 48:589–593
Duyn JH, Yang Y, Frank JA, van der Veen JW (1998) Simple correction method for k-space trajectory deviations in MRI. J Magn Reson 132:150–153
Feinberg DA, Oshio K (1994) Phase errors in multi-shot echo planar imaging. Magn Reson Med 32:535–539
Feinberg DA, Hale JD, Watts JC, Kaufman L, Mark A (1986) Halving MR imaging time by conjugation: demonstration at 3.5 kG. Radiology 161:527–531
Feinberg DA, Kiefer B, Johnson G (1995) GRASE improves spatial resolution in single shot imaging. Magn Reson Med 33:529–533
Feinberg DA, Reese TG, Wedeen VJ (2002) Simultaneous echo refocusing in EPI. Magn Reson Med 48:1–5
Fernandez-Seara MA, Wang Z, Wang J, Rao HY, Guenther M, Feinberg DA, Detre JA (2005) Continuous arterial spin labeling perfusion measurements using single shot 3D GRASE at 3 T. Magn Reson Med 54:1241–1247
Fischer H, Ladebeck R (1998) Echo-planar imaging image artefacts. In: Schmitt F, Stehling MK, Turner R (eds) Echo-planar imaging. Springer, Berlin, pp 180–200
Fox MD, Raichle ME (2007) Spontaneous fluctuations in brain activity observed with functional magnetic resonance imaging. Nat Rev Neurosci 8:700–711
Frahm J, Merboldt KD, Hanicke W (1988) Direct FLASH MR imaging of magnetic field inhomogeneities by gradient compensation. Magn Reson Med 6:474–480
Frahm J, Merboldt KD, Hanicke W (1993) Functional MRI of human brain activation at high spatial resolution. Magn Reson Med 29:139–144
Friedman L, Glover GH (2006) Report on a multicenter fMRI quality assurance protocol. J Magn Reson Imaging 23:827–839
Friedman L, Stern H, Brown GG, Mathalon DH, Turner J, Glover GH, Gollub RL, Lauriello J, Lim KO, Cannon T, Greve DN, Bockholt HJ, Belger A, Mueller B, Doty MJ, He J, Wells W, Smyth

P, Pieper S, Kim S, Kubicki M, Vangel M, Potkin SG (2007) Test-retest and between-site reliability in a multicenter fMRI study. Hum Brain Mapp 29:958–972
Friston KJ, Williams S, Howard R, Frackowiak RS, Turner R (1996) Movement-related effects in fMRI time-series. Magn Reson Med 35:346–355
Gallichan D, Marques JP, Gruetter R (2016) Retrospective correction of involuntary microscopic head movement using highly accelerated fat image navigators (3D FatNavs) at 7T. Magn Reson Med 75(3):25670. https://doi.org/10.1002/mrm.25670
Garwood M, Delabarre L (2001) The return of the frequency sweep: designing adiabatic pulses for contemporary NMR. J Magn Reson 153:155–177
Garwood M, Ugurbil K, Rath AR, Bendall MR, Ross BD, Mitchell SL, Merkle H (1989) Magnetic resonance imaging with adiabatic pulses using a single surface coil for RF transmission and signal detection. Magn Reson Med 9:25–34
Glover GH, Law CS (2001) Spiral-in/out BOLD fMRI for increased SNR and reduced susceptibility artifacts. Magn Reson Med 46:515–522
Glover GH, Li TQ, Ress D (2000) Image-based method for retrospective correction of physiological motion effects in fMRI: RETROICOR. Magn Reson Med 44:162–167
Griswold MA, Jakob PM, Heidemann RM, Nittka M, Jellus V, Wang J, Kiefer B, Haase A (2002) Generalized autocalibrating partially parallel acquisitions (GRAPPA) 121. Magn Reson Med 47:1202–1210
Gruetter R (1993) Automatic, localized in vivo adjustment of all first- and second-order shim coils. Magn Reson Med 29:804–811
Gruetter R, Tkac I (2000) Field mapping without reference scan using asymmetric echo-planar techniques. Magn Reson Med 43:319–323
Haacke EM, Brown RW, Thompson MR, Venkatesan R (1999) The continuous and discrete Fourier transforms. In: Magnetic resonance imaging: physical principles and sequence design. Wiley, New York, pp 207–230
Hamandi K, Salek-Haddadi A, Fish DR, Lemieux L (2004) EEG/functional MRI in epilepsy: the queen square experience. J Clin Neurophysiol 21:241–248
Hennel F, Nedelec JF (1995) Interleaved asymmetric echo-planar imaging. Magn Reson Med 34:520–524
Hoult DI, Lauterbur PC (1976) The signal to noise ratio of the nuclear magnetic resonance experiment. J Magn Reson 34:425–433
Hu X, Le TH (1996) Artifact reduction in EPI with phase-encoded reference scan. Magn Reson Med 36:166–171
Hutchinson M, Raff U (1988) Fast MRI data acquisition using multiple detectors. Magn Reson Med 6:87–91
Hutter J, Price AN, Cordero-Grande L, Malik S, Ferrazzi G, Gaspar A, Hajnal JV (2018) Quiet echo planar imaging for functional and diffusion MRI. Magn Reson Med 79(3):1447–1459. https://doi.org/10.1002/mrm.26810
Hutton C, Bork A, Josephs O, Deichmann R, Ashburner J, Turner R (2002) Image distortion correction in fMRI: a quantitative evaluation. NeuroImage 16:217–240
Jacobs J, Kobayashi E, Boor R, Muhle H, Stephan W, Hawco C, Dubeau F, Jansen O, Stephani U, Gotman J, Siniatchkin M (2007) Hemodynamic responses to interictal epileptiform discharges in children with symptomatic epilepsy. Epilepsia 48:2068–2078
Jacobs J, Stich J, Zahneisen B, Assländer J, Ramantani G, Schulze-Bonhage A, LeVan P (2014) Fast fMRI provides high statistical power in the analysis of epileptic networks. NeuroImage 88:282–294. https://doi.org/10.1016/j.neuroimage.2013.10.018
Jezzard P, Balaban RS (1995) Correction for geometric distortion in echo planar images from B0 field variations 50. Magn Reson Med 34:65–73
Jezzard P, Clare S (1999) Sources of distortion in functional MRI data. Hum Brain Mapp 8:80–85
Jorge J, Grouiller F, Ipek Ö, Stoermer R, Michel CM, Figueiredo P, Gruetter R (2015) Simultaneous EEG-fMRI at ultra-high field: artifact prevention and safety assessment. NeuroImage 105:132–144. https://doi.org/10.1016/j.neuroimage.2014.10.055

Josephs O, Weiskopf N, Deichmann R, Turner R (2000) Trajectory measurement and generalised reconstruction in rectilinear EPI. In: Proc 8th Int Meet ISMRM, Denver, CO, USA, 1–7 April 2000

Kirilina E, Lutti A, Poser BA, Blankenburg F, Weiskopf N (2016) The quest for the best: The impact of different EPI sequences on the sensitivity of random effect fMRI group analyses. NeuroImage 126:49–59. https://doi.org/10.1016/j.neuroimage.2015.10.071

Kleinschmidt A, Bruhn H, Kruger G, Merboldt KD, Stoppe G, Frahm J (1999) Effects of sedation, stimulation, and placebo on cerebral blood oxygenation: a magnetic resonance neuroimaging study of psychotropic drug action. NMR Biomed 12:286–292

Koopmans PJ, Boyacioğlu R, Barth M, Norris DG (2012) Whole brain, high resolution spin-echo resting state fMRI using PINS multiplexing at 7 T. NeuroImage 62(3):1939–1946. https://doi.org/10.1016/J.NEUROIMAGE.2012.05.080

Krakow K, Allen PJ, Symms MR, Lemieux L, Josephs O, Fish DR (2000) EEG recording during fMRI experiments: image quality. Hum Brain Mapp 10:10–15

Kundu P, Voon V, Balchandani P, Lombardo MV, Poser BA, Bandettini PA (2017) Multi-echo fMRI: a review of applications in fMRI denoising and analysis of BOLD signals. NeuroImage 154:59–80. https://doi.org/10.1016/J.NEUROIMAGE.2017.03.033

Lamberton F, Delcroix N, Grenier D, Mazoyer B, Joliot M (2007) A new EPI-based dynamic field mapping method: application to retrospective geometrical distortion corrections. J Magn Reson Imaging 26:747–755

Larkman DJ, Hajnal JV, Herlihy AH, Coutts GA, Young IR, Ehnholm G (2001) Use of multicoil arrays for separation of signal from multiple slices simultaneously excited. J Magn Reson Imaging 13(2):313–317

Laufs H, Krakow K, Sterzer P, Eger E, Beyerle A, Salek-Haddadi A, Kleinschmidt A (2003) Electroencephalographic signatures of attentional and cognitive default modes in spontaneous brain activity fluctuations at rest. Proc Natl Acad Sci U S A 100:11053–11058

Laufs H, Daunizeau J, Carmichael DW, Kleinschmidt A (2008) Recent advances in recording electrophysiological data simultaneously with magnetic resonance imaging. NeuroImage 40:515–528

Lemieux L, Allen PJ, Franconi F, Symms MR, Fish DR (1997) Recording of EEG during fMRI experiments: patient safety. Magn Reson Med 38:943–952

Lemieux L, Salek-Haddadi A, Lund TE, Laufs H, Carmichael D (2007) Modelling large motion events in fMRI studies of patients with epilepsy. Magn Reson Imaging 25:894–901

Liston AD, Lund TE, Salek-Haddadi A, Hamandi K, Friston KJ, Lemieux L (2006) Modelling cardiac signal as a confound in EEG–fMRI and its application in focal epilepsy studies. NeuroImage 30:827–834

Lund TE, Norgaard MD, Rostrup E, Rowe JB, Paulson OB (2005) Motion or activity: their role in intra- and inter-subject variation in fMRI. NeuroImage 26:960–964

Luo Q, Glover GH (2012) Influence of dense-array EEG cap on fMRI signal. Magn Reson Med 68(3):807–815. https://doi.org/10.1002/mrm.23299

Lutcke H, Merboldt KD, Frahm J (2006) The cost of parallel imaging in functional MRI of the human brain. Magn Reson Imaging 24:1–5

Lutti A, Thomas DL, Hutton C, Weiskopf N (2013) High-resolution functional MRI at 3 T: 3D/2D echo-planar imaging with optimized physiological noise correction. Magn Reson Med 69(6):1657–1664. https://doi.org/10.1002/mrm.24398

Mackenzie IS, Robinson EM, Wells AN, Wood B (1987) A simple field map for shimming. Magn Reson Med 5:262–268

Mansfield P (1977) Multi-planar image formation using NMR spin echoes. J Phys C 10:L55–L58

Mansfield P (1984) Spatial mapping of the chemical shift in NMR. Magn Reson Med 1:370–386

Mansfield P, Harvey PR (1993) Limits to neural stimulation in echo-planar imaging. Magn Reson Med 29:746–758

Marcus DS, Harms MP, Snyder AZ, Jenkinson M, Wilson JA, Glasser MF (2013) Human connectome project informatics: quality control, database services, and data visualization. NeuroImage 80:202–219. https://doi.org/10.1016/j.neuroimage.2013.05.077

Maziero D, Sturzbecher M, Velasco TR, Rondinoni C, Castellanos AL, Carmichael DW, Salmon CEG (2015) A comparison of independent component analysis (ICA) of fMRI and electrical source imaging (ESI) in focal epilepsy reveals misclassification using a classifier. Brain Topogr 28(6):4. https://doi.org/10.1007/s10548-015-0436-4

Maziero D, Velasco TR, Hunt N, Payne E, Lemieux L, Salmon CEG, Carmichael DW (2016) Towards motion insensitive EEG-fMRI: Correcting motion-induced voltages and gradient artefact instability in EEG using an fMRI prospective motion correction (PMC) system. NeuroImage 138:13–27. https://doi.org/10.1016/j.neuroimage.2016.05.003

McDowell AR, Carmichael DW (2018) Optimal repetition time reduction for single subject event-related functional magnetic resonance imaging. Magn Reson Med. https://doi.org/10.1002/mrm.27498

Menon RS, Thomas CG, Gati JS (1997) Investigation of BOLD contrast in fMRI using multi-shot EPI. NMR Biomed 10:179–182

Merboldt KD, Finsterbusch J, Frahm J (2000) Reducing inhomogeneity artifacts in functional MRI of human brain activation-thin sections vs gradient compensation. J Magn Reson 145:184–191

Miller KL, Hargreaves BA, Lee J, Ress D, deCharms RC, Pauly JM (2003) Functional brain imaging using a blood oxygenation sensitive steady state. Magn Reson Med 50:675–683

Miller KL, Hargreaves BA, Lee J, Ress D, deCharms RC, Pauly JM (2004) Functional brain imaging with BOSS FMRI. Conf Proc IEEE Eng Med Biol Soc 7:5234–5237

Miller KL, Smith SM, Jezzard P, Pauly JM (2006) High-resolution FMRI at 1.5T using balanced SSFP. Magn Reson Med 55:161–170

Morgan PS, Bowtell RW, McIntyre DJ, Worthington BS (2004) Correction of spatial distortion in EPI due to inhomogeneous static magnetic fields using the reversed gradient method. J Magn Reson Imaging 19:499–507

Mullinger K, Debener S, Coxon R, Bowtell R (2007) Effects of simultaneous EEG recording on MRI data quality at 1.5, 3 and 7 tesla. Int J Psychophysiol 67:178–188

Munger P, Crelier GR, Peters TM, Pike GB (2000) An inverse problem approach to the correction of distortion in EPI images. IEEE Trans Med Imaging 19:681–689

Nair G, Duong TQ (2004) Echo-planar BOLD fMRI of mice on a narrow-bore 9.4 T magnet. Magn Reson Med 52:430–434

Norris DG, Zysset S, Mildner T, Wiggins CJ (2002) An investigation of the value of spin-echo-based fMRI using a Stroop color-word matching task and EPI at 3 T. NeuroImage 15:719–726

Nunes R, Hajnal J et al. (2006) Simultaneous slice excitation and reconstruction for single shot EPI. Afni.Nimh.Nih.Gov. http://afni.nimh.nih.gov/sscc/staff/rwcox/ISMRM_2006/ISMRM2006-3340/files/00293.pdf

Ordidge R (1999) The development of echo-planar imaging (EPI): 1977–1982. MAGMA 9:117–121

Ordidge RJ, Gorell JM, Deniau JC, Knight RA, Helpern JA (1994a) Assessment of relative brain iron concentrations using T2-weighted and T2*-weighted MRI at 3 Tesla. Magn Reson Med 32:335–341

Ordidge RJ, Helpern JA, Qing ZX, Knight RA, Nagesh V (1994b) Correction of motional artifacts in diffusion-weighted MR images using navigator echoes. Magn Reson Imaging 12:455–460

Parkes LM, Schwarzbach JV, Bouts AA, Deckers RH, Pullens P, Kerskens CM, Norris DG (2005) Quantifying the spatial resolution of the gradient echo and spin echo BOLD response at 3 Tesla. Magn Reson Med 54:1465–1472

Parkes L, Fulcher B, Yücel M, Fornito A (2018) An evaluation of the efficacy, reliability, and sensitivity of motion correction strategies for resting-state functional MRI. NeuroImage 171:415–436. https://doi.org/10.1016/j.neuroimage.2017.12.073

Poser BA, Versluis MJ, Hoogduin JM, Norris DG (2006) BOLD contrast sensitivity enhancement and artifact reduction with multiecho EPI: parallel-acquired inhomogeneity-desensitized fMRI. Magn Reson Med 55:1227–1235

Poser BA, Koopmans PJ, Witzel T, Wald LL, Barth M (2010) Three dimensional echo-planar imaging at 7 Tesla. NeuroImage 51(1):261–266. https://doi.org/10.1016/j.neuroimage.2010.01.108

Power JD, Plitt M, Gotts SJ, Kundu P, Voon V, Bandettini PA, Martin A (2018) Ridding fMRI data of motion-related influences: Removal of signals with distinct spatial and physical bases in multiecho data. Proc Natl Acad Sci 115(9):2105–2114. https://doi.org/10.1073/pnas.1720985115
Preston AR, Thomason ME, Ochsner KN, Cooper JC, Glover GH (2004) Comparison of spiral-in/out and spiral-out BOLD fMRI at 1.5 and 3 T. NeuroImage 21:291–301
Priest AN, Carmichael DW, De Vita E, Ordidge RJ (2004) Method for spatially interleaving two images to halve EPI readout times: two reduced acquisitions interleaved (TRAIL). Magn Reson Med 51:1212–1222
Priest AN, De Vita E, Thomas DL, Ordidge RJ (2006) EPI distortion correction from a simultaneously acquired distortion map using TRAIL. J Magn Reson Imaging 23:597–603
Pruessmann KP, Weiger M, Scheidegger MB, Boesiger P (1999) SENSE: sensitivity encoding for fast MRI 18. Magn Reson Med 42:952–962
Pruim RHR, Mennes M, van Rooij D, Llera A, Buitelaar JK, Beckmann CF (2015) ICA-AROMA: a robust ICA-based strategy for removing motion artifacts from fMRI data. NeuroImage 112:267–277. https://doi.org/10.1016/j.neuroimage.2015.02.064
Reber PJ, Wong EC, Buxton RB, Frank LR (1998) Correction of off resonance-related distortion in echo-planar imaging using EPI-based field maps. Magn Reson Med 39:328–330
Reeder SB, Atalar E, Bolster BD Jr, McVeigh ER (1997) Quantification and reduction of ghosting artifacts in interleaved echo-planar imaging. Magn Reson Med 38:429–439
Rzedzian R (1987) High speed, high resolution, spin echo imaging by mosaic scan and MESH. In: Proc 6th Annu Meet SMRM, New York, 17–21 Aug 1987
Sahib AK, Mathiak K, Erb M, Elshahabi A, Klamer S, Scheffler K, Ethofer T (2016) Effect of temporal resolution and serial autocorrelations in event-related functional MRI. Magn Reson Med 76(6):1805–1813. https://doi.org/10.1002/mrm.26073
Salek-Haddadi A, Lemieux L, Merschhemke M, Diehl B, Allen PJ, Fish DR (2003) EEG quality during simultaneous functional MRI of interictal epileptiform discharges. Magn Reson Imaging 21:1159–1166
Salek-Haddadi A, Diehl B, Hamandi K, Merschhemke M, Liston A, Friston K, Duncan JS, Fish DR, Lemieux L (2006) Hemodynamic correlates of epileptiform discharges: an EEG–fMRI study of 63 patients with focal epilepsy. Brain Res 1088:148–166
Sangill R, Wallentin M, Ostergaard L, Vestergaard-Poulsen P (2006) The impact of susceptibility gradients on cartesian and spiral EPI for BOLD fMRI. MAGMA 19:105–114
Scarff CJ, Reynolds A, Goodyear BG, Ponton CW, Dort JC, Eggermont JJ (2004) Simultaneous 3-T fMRI and high-density recording of human auditory evoked potentials. NeuroImage 23:1129–1142
Schmidt CF, Boesiger P, Ishai A (2005) Comparison of fMRI activation as measured with gradient- and spin-echo EPI during visual perception. NeuroImage 26:852–859
Schmithorst VJ, Dardzinski BJ, Holland SK (2001) Simultaneous correction of ghost and geometric distortion artifacts in EPI using a multiecho reference scan. IEEE Trans Med Imaging 20:535–539
Schmitt F, Stehling MK, Turner R (eds) (1998) Echo-planar imaging. Springer, Berlin
Setsompop K, Gagoski BA, Polimeni JR, Witzel T, Wedeen VJ, Wald LL (2012) Blipped-controlled aliasing in parallel imaging for simultaneous multislice echo planar imaging with reduced g-factor penalty. Magn Reson Med 67(5):1210–1224. https://doi.org/10.1002/mrm.23097
Shen J, Rothman DL (1997) Adiabatic slice-selective excitation for surface coils. J Magn Reson 124:72–79
Sled JG, Pike GB (1998) Standing-wave and RF penetration artifacts caused by elliptic geometry: an electrodynamic analysis of MRI. IEEE Trans Med Imaging 17:653–662
Sodickson DK, Manning WJ (1997) Simultaneous acquisition of spatial harmonics (SMASH): fast imaging with radiofrequency coil arrays. Magn Reson Med 38:591–603
Stevens TK, Ives JR, Klassen LM, Bartha R (2007) MR compatibility of EEG scalp electrodes at 4 Tesla. J Magn Reson Imaging 25:872–877
Stirnberg R, Huijbers W, Brenner D, Poser BA, Breteler M, Stöcker T (2017) Rapid whole-brain resting-state fMRI at 3 T: efficiency-optimized three-dimensional EPI versus repetition time-

matched simultaneous-multi-slice EPI. NeuroImage 163:81–92. https://doi.org/10.1016/j.neuroimage.2017.08.031
Tierney TM, Weiss-Croft LJ, Centeno M, Shamshiri EA, Perani S, Baldeweg T, Carmichael DW (2016) FIACH: a biophysical model for automatic retrospective noise control in fMRI. NeuroImage 124:1009–1020. https://doi.org/10.1016/j.neuroimage.2015.09.034
Todd N, Moeller S, Auerbach EJ, Yacoub E, Flandin G, Weiskopf N (2016) Evaluation of 2D multiband EPI imaging for high-resolution, whole-brain, task-based fMRI studies at 3T: sensitivity and slice leakage artifacts. NeuroImage 124:32–42. https://doi.org/10.1016/j.neuroimage.2015.08.056
Turner R, Ordidge RJ (2000) Technical challenges of functional magnetic resonance imaging. IEEE Eng Med Biol Mag 19:42–54
Uğurbil K, Xu J, Auerbach EJ, Moeller S, Vu AT, Duarte-Carvajalino JM (2013) Pushing spatial and temporal resolution for functional and diffusion MRI in the human connectome project. NeuroImage 80:80–104. https://doi.org/10.1016/j.neuroimage.2013.05.012
van Gelderen P, de Zwart JA, Starewicz P, Hinks RS, Duyn JH (2007) Real-time shimming to compensate for respiration-induced B0 fluctuations. Magn Reson Med 57:362–368
Vasios CE, Angelone LM, Purdon PL, Ahveninen J, Belliveau JW, Bonmassar G (2006) EEG/(f) MRI measurements at 7 Tesla using a new EEG cap ("InkCap"). NeuroImage 33:1082–1092
Wan X, Gullberg GT, Parker DL, Zeng GL (1997) Reduction of geometric and intensity distortions in echo-planar imaging using a multireference scan. Magn Reson Med 37:932–942
Ward HA, Riederer SJ, Jack CR Jr (2002) Real-time autoshimming for echo planar timecourse imaging. Magn Reson Med 48:771–780
Weiskopf N, Klose U, Birbaumer N, Mathiak K (2005) Single-shot compensation of image distortions and BOLD contrast optimization using multi-echo EPI for real-time fMRI. NeuroImage 24:1068–1079
Weiskopf N, Hutton C, Josephs O, Deichmann R (2006) Optimal EPI parameters for reduction of susceptibility-induced BOLD sensitivity losses: a whole-brain analysis at 3 T and 1.5 T. NeuroImage 33:493–504
Weiskopf N, Hutton C, Josephs O, Turner R, Deichmann R (2007) Optimized EPI for fMRI studies of the orbitofrontal cortex: compensation of susceptibility-induced gradients in the readout direction. MAGMA 20:39–49
Weisskoff RM (1996) Simple measurement of scanner stability for functional NMR imaging of activation in the brain. Magn Reson Med 36:643–645
Wielopolski PA, Schmitt F, Stehling MK (1998) Echo-planar pulse sequences. In: Schmitt F, Stehling MK, Turner R (eds) Echo-planar imaging. Springer, Berlin, pp 65–134
Wilson JL, Jezzard P (2003) Utilization of an intra-oral diamagnetic passive shim in functional MRI of the inferior frontal cortex. Magn Reson Med 50:1089–1094
Wilson JL, Jenkinson M, Jezzard P (2003) Protocol to determine the optimal intraoral passive shim for minimisation of susceptibility artifact in human inferior frontal cortex 3. NeuroImage 19:1802–1811
Wong C-K, Zotev V, Misaki M, Phillips R, Luo Q, Bodurka J (2016) Automatic EEG-assisted retrospective motion correction for fMRI (aE-REMCOR). NeuroImage 129:133–147. https://doi.org/10.1016/j.neuroimage.2016.01.042
Zahneisen B, Grotz T, Lee KJ, Ohlendorf S, Reisert M, Zaitsev M, Hennig J (2011) Three-dimensional MR-encephalography: fast volumetric brain imaging using rosette trajectories. Magn Reson Med 65(5):1260–1268. https://doi.org/10.1002/mrm.22711
Zaitsev M, Hennig J, Speck O (2004) Point spread function mapping with parallel imaging techniques and high acceleration factors: fast, robust, and flexible method for echo-planar imaging distortion correction. Magn Reson Med 52:1156–1166
Zhong K, Leupold J, Hennig J, Speck O (2007) Systematic investigation of balanced steady-state free precession for functional MRI in the human visual cortex at 3 Tesla. Magn Reson Med 57:67–73

EEG-fMRI at Ultrahigh Magnetic Fields: $B_0 \geq 3$ Tesla

11

Giorgio Bonmassar, Laura Lewis, and Karen Mullinger

11.1 Introduction

Functional MRI (fMRI) can be used to map regional changes in cerebral blood flow and blood-oxygenation-level-dependent (BOLD) signals associated with the neuronal activity (Belliveau et al. 1991; Kwong et al. 1992; Ogawa et al. 1992). In 2003, the US Food and Drug Administration raised the value of the static field of "no significant risk" for MRI to 8 Tesla (T), potentially opening up this technology to large numbers of laboratories in the USA. Regulatory agencies in Europe and Asia have reached similar conclusions, and as a result, the number of ultrahigh-field (UHF) systems worldwide is growing rapidly. Furthermore, commercial clinical systems for UHF 7 Tesla imaging are now entering the pipeline for FDA approval, leading to increased interest and accessibility of high-field systems.

G. Bonmassar (✉)
AbiLab, Athinoula A. Martinos Center for Biomedical Imaging, Department of Radiology, Massachusetts General Hospital, Boston, MA, USA

Department of Radiology, Harvard Medical School, Boston, MA, USA
e-mail: giorgio.bonmassar@mgh.harvard.edu

L. Lewis
AbiLab, Athinoula A. Martinos Center for Biomedical Imaging, Department of Radiology, Massachusetts General Hospital, Boston, MA, USA

Department of Radiology, Harvard Medical School, Boston, MA, USA

Department of Biomedical Engineering, Boston University, Boston, MA, USA
e-mail: ldlewis@bu.edu

K. Mullinger
Sir Peter Mansfield Imaging Centre, School of Physics and Astronomy, University of Nottingham, Nottingham, UK

Centre for Human Brain Health, School of Psychology, University of Birmingham, Birmingham, UK
e-mail: karen.mullinger@nottingham.ac.uk

C. Mulert, L. Lemieux (eds.), *EEG - fMRI*,
https://doi.org/10.1007/978-3-031-07121-8_11

The increased static field B_0 of high-field scanners enables improved signal-to-noise ratio (SNR), offering the possibility of increasing spatial resolution and reducing scan times (Yacoub et al. 2001; Wiesinger et al. 2006; Harel et al. 2006). This high SNR has now enabled 7T fMRI studies to resolve activity patterns across cortical layers, within small subcortical nuclei, and at faster timescales (Polimeni et al. 2010; Newton et al. 2012; deMartino et al. 2013; Lewis et al. 2016; Huber et al. 2018), allowing imaging of neural activity patterns that are challenging to detect at 3T. EEG-fMRI at high field, therefore, has the potential to provide important new insights for neuroscience. In this chapter, we outline the safety issues raised and the challenges involved in performing EEG at high-field MRI or at static magnetic fields greater than 3T, as well as the potential advantages of this approach.

11.2 Safety Considerations

11.2.1 Physical Principles and Relevant Safety Guidelines

The physical principles and mechanisms that arise from the interaction of EEG and MRI data acquisition systems are described in the Chap. 7, where the reader will also find the safety guidelines that should be taken in consideration for the simultaneous recording of EEG and fMRI data. In summary, those guidelines concern heat deposition inside the body (FDA 2003; IEC 2002); heating of objects, such as EEG electrodes, placed in contact with the body; and tissue contact currents, such as those induced in conducting objects placed in contact with or close proximity to the body. This section focuses on safety considerations at high field; while the mechanisms that may result in health hazards are the same as for more standard field strengths, some of the effects are amplified by the stronger field. While the allowed SAR is constant across field strengths, the SAR of sequences employed in high-field MRI scanning is generally higher than that at lower field strengths. Moreover, although the safety record to date at standard field strengths has been good, with no reported incidents to our knowledge, the experience at high field is much more limited.

At high static magnetic fields ($B_0 \geq 3$ T), MRI employs a correspondingly higher RF for signal excitation and reception because of the linear relation between Larmor frequency and B_0 field strength. Since SAR increases as the square of the Larmor frequency, problems associated with exposure to RF may worsen (Ibrahim et al. 2001). In addition, at $B_0 = 7$ T, the Larmor frequency for water protons is 300 MHz (i.e., approximately corresponding to a 1 m wavelength in empty space). Hence, at higher frequencies or in different media, the size of the biological object can be comparable to or larger than the effective wavelength; this may cause problems because dielectric resonant effects cause an inhomogeneous excitation field $B+$ (i.e., the circularly polarized component of the transverse magnetic field) (Sled and Pike 1998). As is the case at lower field strengths, localized peaks in SAR caused by interactions between the RF coil and tissue/sample properties may be a safety issue when using sequences close to volume-average SAR limits and depending on how the scanner-reported SAR is estimated. Analytical studies using homogeneous spheres to simulate the human head (Bottomley et al. 1985; Bottomley and Andrew

1978; Glover et al. 1985; Keltner et al. 1991; Mansfield and Morris 1982) have shown that as the frequency of the $B+$ field increases, homogeneity tends to decrease, and correspondingly the peak (local) SAR may be increased.

11.2.2 Safety Studies at High Fields

MRI-compatible temperature probes have been used for in vitro measurements (Kangarlu et al. 2003; Sharan et al. 2003), sometimes in the presence of metallic implants (Carmichael et al. 2008; Chou et al. 1997). Temperature measurements have also been carried out to test the safety of EEG caps at high field specifically. These tests have included investigating the effect of different wire lengths on RF heating (Stevens et al. 2007b). This study showed that the extent of heating at the tip of wire was dependent on the ratio of the wire length to the RF wavelength and that care must be taken not to set up a resonance effect in the wires of the EEG system. A commercially available 32-channel EEG cap has also been tested for heating effects at 7 T by Mullinger et al. (2008b). The results of this study showed that for the particular setup used in this case, it was safe to record EEG at 7 T, although the authors highlighted the need to test new combinations of equipment, as heating effects may vary depending on the experimental setup. Vasios et al. (2006) also investigated the heating effects of a custom-made EEG cap, the "InkCap," which was designed to reduce potential RF heating effects by using distributed impedance in the conductive structures of the cap, thus reducing RF interactions. They compared the heating effects observed with this cap to those produced by commercially available EEG caps at 7 T. This study demonstrated that, at all the locations considered, the InkCap exhibited lower or equal heating effects to those recorded from the commercially available caps.

While measurements are useful and necessary for a direct evaluation of RF heating, they do have limitations. For example, in vitro models are not always anatomically accurate (e.g., they may be based on spherical phantoms). Also, temperature probes such as the fluoroscopic optical fibers are only able to provide measurements at a small number of locations (determined by the number of channels on the instrument) and only over a limited part of the test object or body (on the order of 1 mm^3) (Nitz et al. 2005). This limitation can be partly addressed using simulations that can provide estimates of the electromagnetic fields and SAR. Bioheating models predicted temperature rises throughout the volume of interest and for a range of test object configurations that may not be amenable for experimental testing.

SAR simulation studies on anatomically accurate head models have been performed using the finite difference time domain (FDTD) method (Jin 1999), and several numerical head models have been presented in the literature (Gandhi and Chen 1999; Kainz et al. 2005). While $2 \times 2 \times 2.5$ mm^3 volume elements provide sufficient accuracy when evaluating whole-head SAR in MRI (Collins and Smith 2003), this approximation is no longer valid when peak 10 g averaged SAR is considered the main dosimetric parameter. Moreover, the spatial resolution limits proper modeling of the anatomical structures of the human head (Angelone et al. 2006), which can result in a lack of or limitations in the accuracy of EM estimation at radiofrequency in those anatomical structures. A realistic geometric model included an anatomically

accurate head and torso model (Makris et al. 2008; Massire et al. 2012; Serano et al. 2015), a 256-channel hdEEG sensor cap, an RF transmit (Tx) coil (Bonmassar et al. 2013), and a phased-array RF receive (Rx) coil model; see Fig. 11.1. Simulations were carried out for a frequency of 300 MHz with perfectly matched layer boundary conditions (Berenger 1994) using the FDTD technique (Cangellaris and Wright 1991; Dimbylow and Gandhi 1991). The resulting $B1$-field maps reproduced the typical central brightening observed at 7 T. The amount of exposure to electromagnetic fields is determined using computational models of dosimetry tested with direct measurements. Numerical simulations and measurements have also been performed using medical implants (Chou and Guy 1979; Gangarosa et al. 1987) and EEG electrodes during MRI (Angelone et al. 2004; Carmichael et al. 2007, 2008; Ho 2001; Mirsattari et al. 2004; Rezai et al. 2002). These studies show the presence of local heating, usually concentrated near the implant/electrode, and a dependence on the dimensions, orientation, shape, and location of the implant/electrode. Safety studies (Armenean et al. 2004; Lazeyras et al. 2001; Lemieux et al. 1997; Mirsattari et al. 2004) specifically designed to address the safety of EEG-fMRI have been performed at 1.5 T on human subjects. These studies demonstrated that any temperature increase

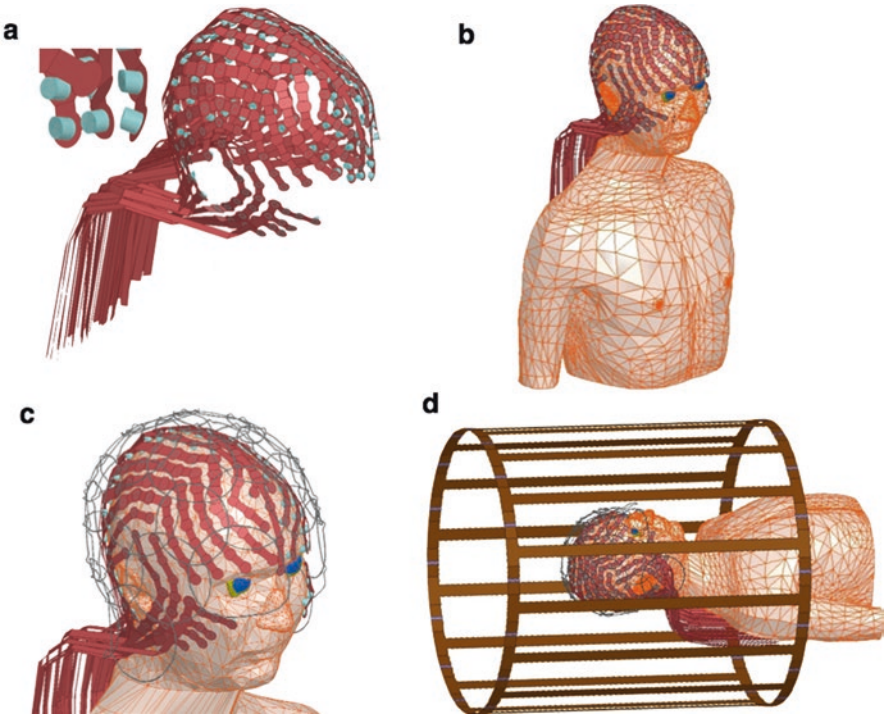

Fig. 11.1 Representation of a high-resolution head model ($1 \times 1 \times 1$ mm^3) and a co-registered EEG InkNet. (**a**) Computational model of 256-channel high-density EEG (hdEEG) cap. (**b**) Anatomical model (head and torso) with the hdEEG cap; (**c**) anatomical model with the hdEEG cap and the RF receive array coil model. (**d**) Anatomical model with the hdEEG cap and the MRI RF receive and transmit coil models. (Reprinted from Atefi et al. (2018))

and induced currents could be limited to the allowed limit if adequate measures are taken and protocols followed (e.g., limiting scanning to low SAR sequences such as gradient-echo EPI, using only head RF coils, fMRI acquisition, and prespecified MR instrumentation). Some studies have addressed these issues at higher field strength, with Angelone et al. (2006) investigating these effects through simulations and Atefi et al. (2018) investigating these effects through direct temperature measurements at 7 T; both studies used a head transmit coil.

As a result of the same mechanism that leads to inhomogeneous RF excitation, enhanced local E fields are a common feature at high fields (Bottomley and Andrew 1978; Glover et al. 1985; Mansfield and Morris 1982), and so there is potentially a greater risk of extreme peaks in SAR near the electrodes/leads (Angelone et al. 2004). In simulations at 7 T, it was noticed that local SAR depends on the number of electrodes, the lead layout (e.g., different ways for the EEG wires to escape the coil), the pulse sequences, the RF transmit coil type, and the head morphology. A study using an eight-tissue model showed that whole-head SAR could increase by a factor of up to four when EEG is recorded using copper leads and 128 EEG electrodes compared to without EEG (see also the Chap. 7) (Angelone et al. 2004) due to a large increase in the resistive load experienced by the RF coil. Interestingly, 3 T results (Fig. 11.2) showed that peak SAR (pSAR, 0.1 g SAR, and 1 g SAR) increases nonlinearly, rather than exponentially as previously reported (Angelone et al. 2004) as a function of lead conductivity. The simulations with a 256-channel hdEEG cap model with copper leads showed a sixfold increase in peak 1 g SAR in the head model compared to the case without the cap. However, the Angelone et al.'s (2004) study also showed (Fig. 11.3) the absence of a local hot spot irrespective of RF coil type or a number of EEG electrodes used.

Furthermore, it is well known (Wiggins et al. 2005) that leads or cables with lengths of the same order as the RF wavelength may result in excessive heating associated with resonance effects and coil detuning (Konings et al. 2000). This effect was demonstrated by Stevens (Stevens et al. 2007b), who showed that if the wire length was equal to a quarter of the RF wavelength, then a resonant effect could be set up and image artifacts created. The use of RF chokes on longer wires may be an effective way to overcome this problem (Stevens et al. 2007a). When the number of EEG leads is very high, the dense array of wires may even reduce the local SAR (Angelone et al. 2004), typically in the occipital lobe. The effect of lead resistivity on tissue EM fields has also been investigated. However, the material of the EEG electrodes alone has a small influence compared to the overall EEG electrode/lead configuration (Fig. 11.4) and that the use of current-limiting resistors between EEG electrodes and leads, which are designed to reduce the risk of RF burns due to contact currents at the skin/electrode interface (Lemieux et al. 1997), does not have a significant impact on the electric field inside the body (Angelone et al. 2006). However, it may be that at higher fields with decreasing resonant lengths, the use of distributed impedance becomes more important.

While it has been shown that scanner-supplied SAR estimates are not a reliable indicator of localized heating due to conductive objects such as implants across scanners, temperature change has been shown to be proportionally related to SAR for a fixed scanning configuration (Baker et al. 2004). Furthermore, SAR is

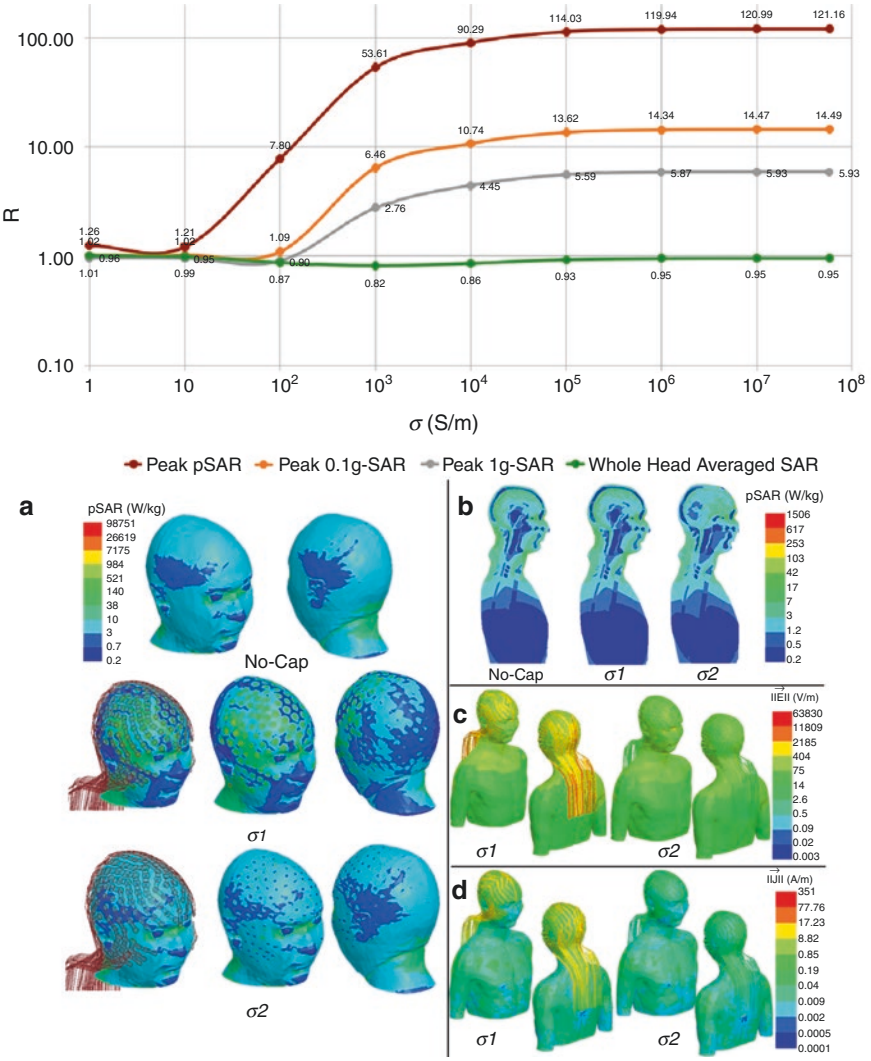

Fig. 11.2 SAR dependence on lead conductivity at 3 T. (Top) Values of R for nine InkNet lead conductivities for peak single-point SAR (pSAR), peak 0.1 g SAR, peak 1 g SAR, and SAR averaged over the whole head. (Bottom) Results of numerical simulations for the head model with No-Cap and with a hdEEG cap with σ1 = 5.8.107 S/m and σ2 = 40 S/m. Images show (**a**) single-point SAR (pSAR)on the head surface, (**b**) pSAR in mid sagittal plane, (**c**) electric field magnitude, and (**d**) current density magnitude. (Reprinted from Atefi et al. (2018))

currently the only available relevant index for practical use (Shellock 2007). A possible solution is to use large safety margins in combination with carefully defined experimental protocols, for example, by using MR sequences with the SAR well below power levels that cause heating close to safety guideline limits (Carmichael et al. 2007, 2008; Lemieux et al. 1997; Vasios et al. 2006).

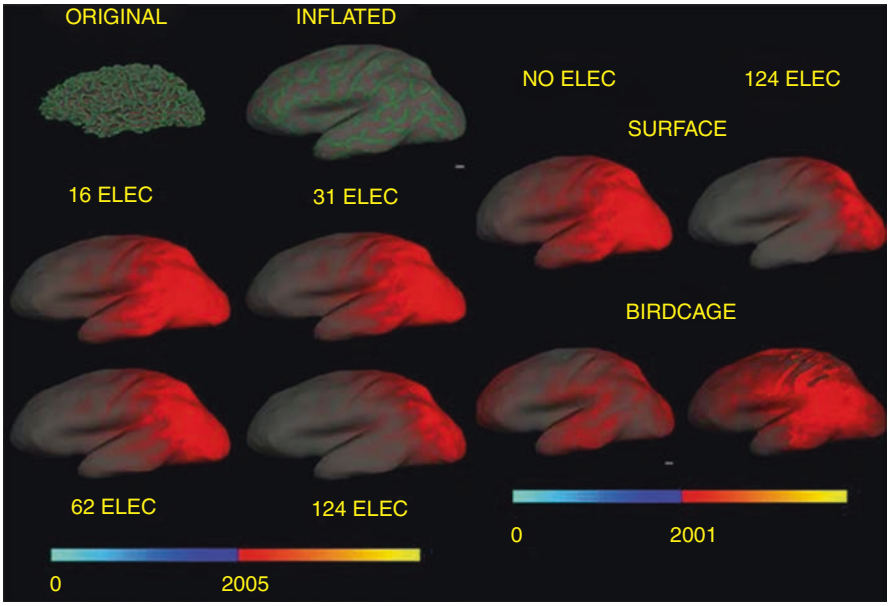

Fig. 11.3 Top left: The original pial and inflated surface of a human brain automatically segmented from MRI images. Bottom left: SAR distribution in the inflated cortical surface with a different number of electrodes using a surface coil. Right: SAR distribution for a surface (top) and a birdcage coil (bottom) using 124 electrodes compared with a no electrode configuration. (Reprinted from Angelone et al. (2004))

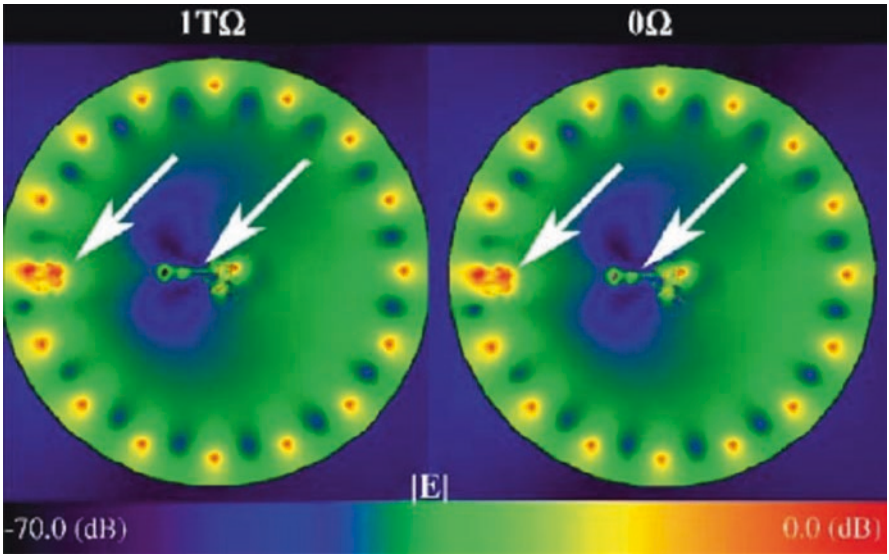

Fig. 11.4 Top: Magnitude of the electric field distribution for two models with 1 TΩ (left) and 0 V resistors (right). Axial slice corresponding to the plane on top of the head model. The electric field distribution is modified along the copper leads (arrows) but is not affected by the presence of the resistors and is the same even in these two extreme cases (scale: 0–70 dB with 0 dB = 104 V/m). (Reprinted from Angelone et al. (2006))

11.2.3 Safe Imaging with High-Density EEG Nets

EEG is increasingly performed with high-density (≥64 channel) systems (Figs. 11.1 and 11.2), to enable improved head coverage and source localization of neural signals. The previously described InkCap has now been adapted into a 256-channel geodesic net, the InkNet (Fig. 11.5a), which enables high-quality imaging at 7T while simultaneously acquiring high-density EEG signals. Poulsen et al.'s (2016) study showed that that high-resistance, conductive inks

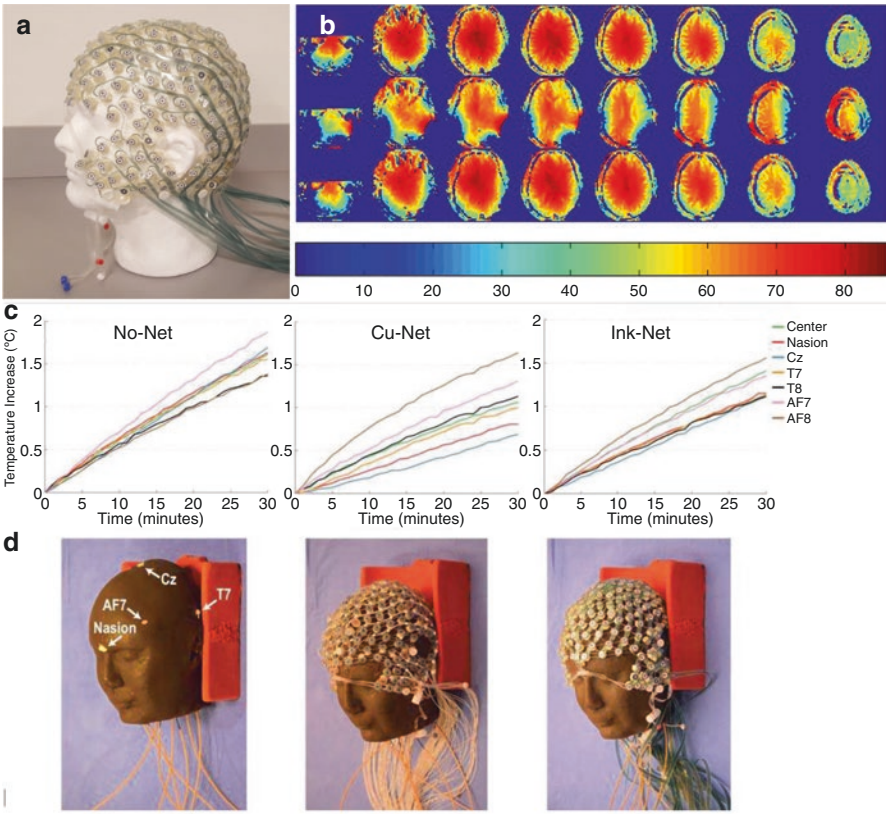

Fig. 11.5 The InkNet (**a**) allows acquisition of high-density (256-channel) EEG while preserving high image quality and avoiding unsafe heating levels at 7 T. (**b**) Flip angle at 3 T under each of the three conditions show large signal loss artifacts from the presence of copper wires in the Cu-Net condition (middle rows). In contrast, the InkNet maps (lower rows) are comparable to No-Net (upper rows). Maps are in neurological convention. The target FA is 60°. (**c**) Temperature increase (middle) during a high SAR TSE sequence at 7 T to induce heating in an anthropomorphic head phantom wearing: No-Net (left), Cu-Net (middle), and InkNet (right). (**d**) Phantom with no-net (left), Cu-Net (middle), and inknet (right) with seven temperature probes (orange-encased optical fibers) inserted from the base of the neck column indicated positions, along with homologous positions AF8 and T8 on the right side, and head center. Thermally conductive grease, used to ensure good probe contact with the phantom tissue, can be seen at each location (Poulsen et al. 2016)

printed on polymer thick film (PTF) substrate could be effectively applied to the construction of electrodes and leads for a dEEG system with up to 256 channels. The prototype 256-channel InkNet was demonstrated to be safe to use during scanning at 7T field strength (Fig. 11.5c), by showing no extra heating compared to a phantom with no EEG electrodes. The InkNet also exhibited no visible MRI or fMRI artifact or signal loss as tested in humans at 3T, whereas using a 256-channel MR-conditional EEG net with conventional copper leads showed a considerable signal loss (Fig. 11.5b) and reduced fMRI SNR (Poulsen et al. 2016).

11.3 EEG Recording and Quality

EEG recording quality poses a major challenge at high magnetic fields. While the methods described in the Chap. 9 that are used to minimize pulse- or motion-related artifacts on EEG at the source should still be employed, the laws of physics tell us that the residual artifact will be amplified in high-field conditions. These residuals can overpower the neural signals of interest, leading to important challenges and potential confounds.

11.3.1 Pulse-Related Artefact

Pulse artifact noise removal is one of the most important steps for the successful integration of simultaneously recorded EEG and fMRI data at high field. As discussed in the Chap. 9, the exact origin of the pulse artifact is still poorly understood. The ballistocardiogram (BCG) has been recognized for over 50 years: it is produced when blood from the heart is pumped upward along the ascending aorta. When the heart pumps blood, the major motion is along the axis parallel to the spine as a rocking movement of the patient's body at each heartbeat (Reilly 1992). This type of noise is of small amplitude, is not present in every subject, and is easy to eliminate outside of the MRI environment by using damping foam or by placing the subject in a position other than supine during EEG recordings.

The first EEG recordings obtained inside MRI scanners were also characterized by pulse-related noise (Huang-Hellinger et al. 1995); this was interpreted as being due to pulsatile whole-body, head, or scalp motion, time-locked to the cardiac cycle (Ives et al. 1993; Nakamura et al. 2006; Schomer et al. 2000). In addition to the ballistic effect, it has also been suggested that the Hall effect, whereby a voltage is induced by the flow of conducting blood in the proximity of electrodes, may contribute to the artifact (Debener et al. 2008; Wendt et al. 1988). Collectively these cardiac-related artifact sources are known as the pulse artifact (PA, see Chap. 8 for more detail). The PA artifact magnitude increases greatly with field strength (Fig. 11.6), as does its spatial variability (Debener et al. 2008). Furthermore, recent work has shown that the PA artifact variability is driven by a number of factors (Jorge et al. 2019). While head position and orientation play a part, the contribution

Fig. 11.6 Pulse artifact (PA) amplitude increases substantially at the high magnetic field. An example EEG trace recorded at 3 T vs. a trace recorded at 7 T is shown. The BCG corresponds to the large peaks locked to the cardiac cycle; the amplitude of this noise is greatly increased in the 7 T recording

of heartbeat variability and the respiratory cycle has been shown to also be significant. This increased artifact amplitude combined with the sources of PA artifact variability means that the residual noise after standard PA removal techniques will also be greater at higher field strengths and can even swamp the neurally generated EEG signals of interest.

These artifacts can be partially reduced through hardware choices. Using a novel cap design based on conductive ink technology and specifically designed for use at 7 T, Vasios et al. observed a 3.5-fold reduction of the pulse-related artifact compared to EEG recorded using a carbon fiber electrode set (Vasios et al. 2006). Furthermore, the authors suggested that the design of the new net offers greater comfort, tends to reduce subject movement, and allows for longer measurement times. In addition, altering cable length and geometry can contribute to reducing artifacts (Jorge et al. 2015). Alternatively, as discussed in Chap. 8, methods to monitor head motion with additional hardware may be employed as a method to remove the PA artifact overcoming some of the problems associated with artifact variability (Jorge et al. 2019); see also Sect. 11.3.3.

11.3.2 Other Noise Sources at High Field

A second, related, major challenge for high-field EEG-fMRI is that any effects of motion induce far greater amplitude noise than at lower field. Electromotive forces induced in loops formed by the EEG recording system and subject by body movement are proportional to field strength, so it is particularly important to keep subjects as still as possible during combined EEG-fMRI experiments carried out at high field. This increase also underlies an issue discussed by Mullinger et al. (2008a) and Purdon et al. (2005b) that the amplifiers and cables within the magnetic field must be isolated from any vibration. In addition, vibrations may be reduced by switching off cryogenic cooling compression pumps during EEG recording (Mullinger et al. 2008a). Finally, the scanner itself may pose increased motion issues, as scanning at 7 T often generates strong vibrations, with consequent noise in the EEG. A 7 T scanning, therefore, introduces motion artifacts not just from the human subject but from the cryogenic pump, scanner, and other equipment (Fig. 11.7).

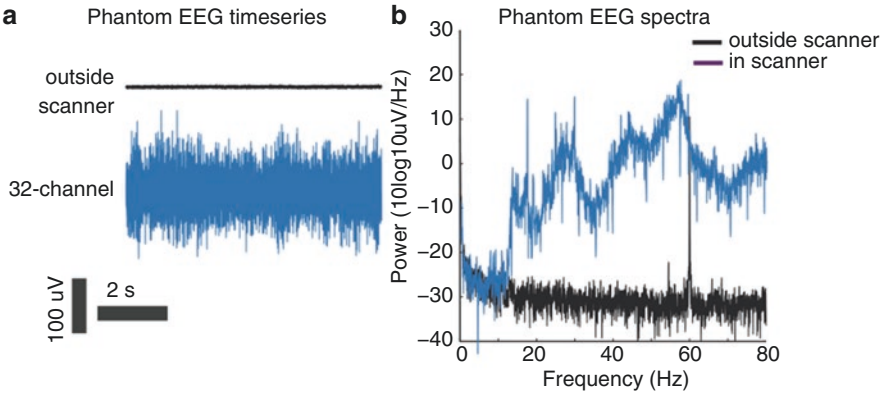

Fig. 11.7 Vibration-induced EEG noise at 7 T. (**a**) EEG time series measurements are taken from a phantom, either outside the scanner room or at the center of the 7 T scanner bore. (**b**) High-amplitude noise is seen inside the scanner—since no human subject is present, these artifacts are driven entirely by vibration and other scanner-related motion, independently of any subject-generated motion or PA

Studies have demonstrated that subject motion can introduce EEG noise that can, in turn, cause artifactual conclusions to be drawn from the fMRI data, because the motion is correlated across these two data sources (Fellner et al. 2016; Flanagan et al. 2009; Jansen et al. 2012). Special care must, therefore, be taken at 7 T to be aware of and control for the effects of motion. A particular concern is that even if attempts are made to remove noise introduced by motion, the residuals from this process will be larger at 7 T and can overwhelm the neural signals (Jorge et al. 2015). As a result, a concerted effort is currently underway to develop methods to remove motion artifacts from EEG data.

11.3.3 EEG Noise Removal Strategies at High Field

Because major sources of noise at high field include both the subject-generated PA and subject- and scanner-generated motion-driven noise, special care is needed in removing EEG artifacts.

In light of increased understanding of the problems of motion-induced artifacts (Fellner et al. 2016; Flanagan et al. 2009; Jansen et al. 2012) and the interaction of subject movement with PA (Jorge et al. 2019) and gradient artifacts (Zhang et al. 2019), which is only exacerbated with increased field strength, a new wave of approaches are being developed to remove these artifacts. These techniques involve acquiring a separate signal that captures the ongoing noise or monitors motion in the scanner (on the timescale of the EEG signal) but crucially does not measure the neural activity. The additional signals recorded can then be used to monitor and, in some cases, remove motion-related artifacts from the EEG signal through simple subtraction or, more commonly, signal processing

techniques such as linear regression. PA possible approaches include (1) isolating a set of electrodes from the head and connecting these through a conductive reference layer so that they record solely noise primarily related to motion (Chowdhury et al. 2014; Luo et al. 2014; Steyrl et al. 2017; Xia et al. 2014), (2) using additional conductive loops that are spatially close to the EEG electrodes to detect motion (Cohen et al. 2019; Jorge et al. 2015; Abbott et al. 2014); (3) using an optical motion-tracking system to monitor motion (LeVan et al. 2013; Maziero et al. 2016), and (4) recording vibration directly, which then requires modeling to remove the corresponding EEG noise (Bonmassar et al. 1999). The artifacts (i.e., gradient, PA, and motion combinations) which have been shown to be removed using such motion monitoring devices vary across the different methods. However, for the artifact removals that have been tested, methods employing the use of specific hardware to monitor motion have been shown widely to surpass only using conventional post-processing methods (see Fig. 11.8 and Jorge et al. 2015; LeVan et al. 2013; Luo et al. 2014; Maziero et al. 2016; van der Meer et al. 2016). Further discussion of these methods for PA correction in general is provided in Chap. 8. The relative merits of the current techniques for motion artifact correction in terms of performance and practicality are also becoming clearer (Daniel et al. 2019). If hardware approaches are unavailable,

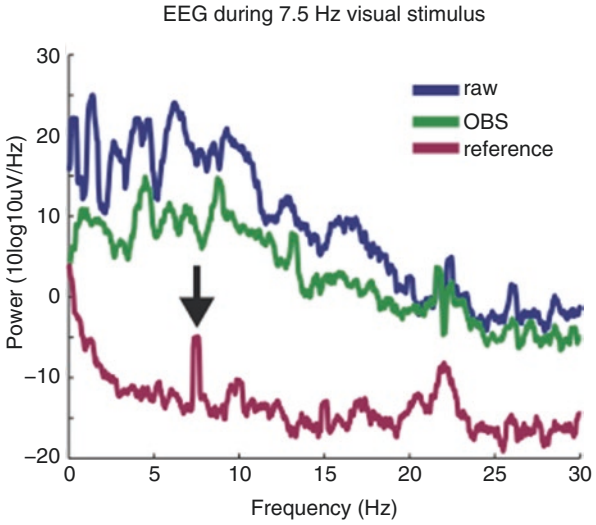

Fig. 11.8 Comparing the performance of noise removal techniques at 7 T. Spectra are of an occipital EEG channel during the presentation of a 7.5 Hz flickering checkerboard, which is expected to induce a corresponding peak of visually induced activity in the EEG spectrum at 7.5 Hz. The "raw" trace (blue) shows the spectrum after gradient artifact removal, but no further cleaning; the "OBS" trace (green) shows the spectrum with an optimal basis set cleaning (Nitz et al. 2005); and the "reference" trace (purple) shows the spectrum after regression of reference channels (Luo et al. 2014). While previous reports have shown that each method can work well at 3 T, only the reference-based approach recovers the 7.5 Hz signal in these data (black arrow), due to the additional, noncardiac noise present in the 7 T signals

data-driven approaches that aim to isolate noise processes automatically without the use of reference signals, such as those based on independent components analysis or harmonic regression, can also help to reduce EEG noise at high fields (Abreu et al. 2016; Krishnaswamy et al. 2015).

11.4 Image Quality

As described in Chap. 9, EEG equipment placed inside or close to the field of view may degrade image quality through two mechanisms: perturbation of the fields used for image generation (RF, gradient and static), causing image distortion or signal loss, and the introduction of RF interference by the EEG amplification and digitization electronics, resulting in noise in the images. The former may be more problematic in high-field scanners, particularly the effects resulting from interactions with the static field. In addition, RF shielding can occur due to the interaction of the electromagnetic field from the wires and EEG electrodes and may depend on the wires' radii and orientations, the surrounding tissue conductivity, and the total number of wire leads (Young and Wait 1989). Shielding and $B1$ nonuniformity may get worse if the leads or electrode electrical lengths approach resonance, which may be more likely as the field strength increases. These effects may reduce the electric field in one location while increasing it in others, with possible image quality and safety implications (Angelone et al. 2004).

The interaction of copper EEG leads with the $B1+$ field has been investigated at 1.5, 3, and 7 T using 32- and 64-channel EEG systems with braided copper wire leads (Mullinger et al. 2008b). Significant artifacts were only observed close to the wires leading to the ECG and EOG electrodes, which are longer than the EEG leads. Even with signal loss problems that arise from the presence of the longer copper leads, the same group has demonstrated that it is possible to record BOLD signals from areas affected (Mullinger et al. 2008b). However, most of the $B0$ distortions observed were limited to the outer 1 cm of the phantom and human head and were thus outside the brain, and these artifacts were mainly caused by the EEG electrodes. Although the field perturbations increased with field strength, due to their localized nature, it was concluded that fMRI data would not be significantly degraded, even at high field, as the skull and scalp are ~1 cm thick on average (Luo et al. 2014). The $B1+$ distortions due to the longer leads on the cap posed a more significant problem since they were observed at all field strengths, though they were significantly worse at higher field strengths. The precise cause of this artifact remains to be investigated, although the longer lead lengths are believed to be a contributing factor, and RF chokes such as those described by Stevens et al. (2007b) may alleviate this problem. Importantly, the temporal SNR in the presence of the 64-channel cap at 7 T was shown to be greater than that of images collected with no cap present at 3 T.

A detailed study of the effect of electrode composition on $B0$ and $B1$ artifacts at 4 T has been carried out by Stevens et al. (2007a, b), and it showed that electrodes

containing any ferromagnetic material unsurprisingly produce large magnetic susceptibility artifacts. However, the spatial extent of the artifacts produced when diamagnetic materials are used is generally small, with Ag/AgCl producing the smallest artifact suggesting adequate EPI image quality even at 7 T (Mullinger et al. 2008b). A special EEG cap has been developed specifically for application at high field (Angelone et al. 2006). The cap is based on conductive ink microstrips which have a resistance per unit length of 2 kΩ/m, with electrodes made of Ag-/AgCl-printed rings and two motion sensors placed on the temporal regions of the cap. The performance was assessed by FDTD simulations, temperature measurements, and EEG recordings during structural and functional MRI recordings at 7 T using 12 healthy human volunteers. EM field and SAR estimates were obtained by simulation for different values of the microstrip resistivity (Fig. 11.4) with a circularly polarized 16-rod birdcage coil (Angelone et al. 2004). Measurements on a phantom and human subjects (Angelone et al. 2006) demonstrated superior EEG and image quality compared to a cap based on carbon fiber at 7 T (Angelone et al. 2004).

11.5 Example of an Application of EEG-fMRI at 7 T: Auditory Steady-State Response (ASSR)

In the field of audiology, electrophysiological measurements play an important role when tests designed to obtain behavioral measurements are performed on individuals who are unable to respond to audible stimuli. In particular, newborns, very young children, elderly people, or incapacitated patients benefit from the use of such measurements. Although auditory brainstem responses (ABR) are considered the gold standard in diagnostic testing, a recent review presented a collection of studies linking the ASSR threshold in infants and children to the pure tone hearing threshold (Cone-Wesson et al. 2002). The ASSR stimulation frequency may reflect the activity of underlying generators (Stach 2002): low frequency (0–20 Hz) with late-latency responses and middle-frequency (20–60 Hz) stimuli are associated with middle-latency responses and high-frequency (>60 Hz) stimuli with brain stem responses. The ASSR is an evoked response modulated by pure tones in amplitude (AM) or frequency (FM). Commonly, the tones are switched *on* and *off* repeatedly during the session in order to determine an average reading. In adults, the strongest responses occur at a rate of approximately 40/s (Galambos et al. 1981). The ASSR amplitude at 40 Hz is usually much larger than any component of the ABR and is, therefore, easier to record, especially in noisy environments such as MRI. For example, a 40 Hz modulation frequency sets off an increase of EEG activity in the delta (up to 3 Hz) and theta (4–7 Hz) bands during periods of sleep and correlates significantly with decreased amplitude. In this section, we present high-field ERP-fMRI physiological recordings from eight healthy volunteers performed by Purdon et al. (Fig. 11.9).

In this study, stimuli consisted of 1 ms clicks or noise bursts at 40 Hz in a 30 s *on*/*off* pattern for a total of 15 min per run. The stimuli were delivered by a

laptop computer running Presentation 0.76 (Neurobehavioral Systems, Albany, CA) and by a custom-built, electrically shielded electrostatic headphone system with a frequency response to 20 kHz and an acoustic noise attenuation of >30 dB above 800 Hz. Functional MRI acquisitions were arranged according to a "long-TR" auditory fMRI design, with TR = 1 s (fifteen 4 mm slices, 1 mm skip, coronal orientation) and a 9 s gap between volumes, allowing hemodynamic responses elicited by acoustic scanner noise to subside before the next volume acquisition. EEG acquisitions were interleaved with image acquisitions using the high-field one EEG recording system see Appendix 2 in this chapter with a high dynamic range to prevent saturation during imaging (1 kHz sampling rate, DC to 500 Hz bandwidth). EEG electrodes were placed in adjacent bipolar pairs along a coronal plane using resistive carbon fiber leads (Angelone et al. 2004). Motion sensors were placed above preauricular points for motion artifact rejection. ASSRs were computed from M2-Cz in the frequency domain using multitaper spectral analysis (Percival and Walden 1993) (bandwidth = 0.4 Hz) from 4 s windows centered 4 s prior to each volume acquisition. For each EEG recording window, the amplitude (square root of the power) at 40 Hz was computed to produce a 40 Hz amplitude time series. The fMRI time series were then analyzed using a linear model consisting of the 40 Hz amplitude time series plus a sixth-order polynomial (nuisance effect), fitted using the *3d Deconvolve* method in AFNI (Cox RW 1996). The fluctuations in 40 Hz amplitude were found to be correlated with (4 s delayed) BOLD changes throughout the auditory system, including the cochlear nucleus, the inferior colliculus (IC), the medial geniculate nucleus, and the Heschl's gyrus (HG), suggesting that brainstem structures play an important role in generating or modulating the 40 Hz ASSR. Figure 11.9 shows the BOLD fMRI activity at 7 T in HG and IC, along with the time series fit between fMRI (blue) and ASSR amplitude (red) for the indicated voxel. These studies demonstrate that time-varying ERP measurements can be made concurrently with fMRI and that these time-varying measurements can be correlated with the BOLD signal at 7 T.

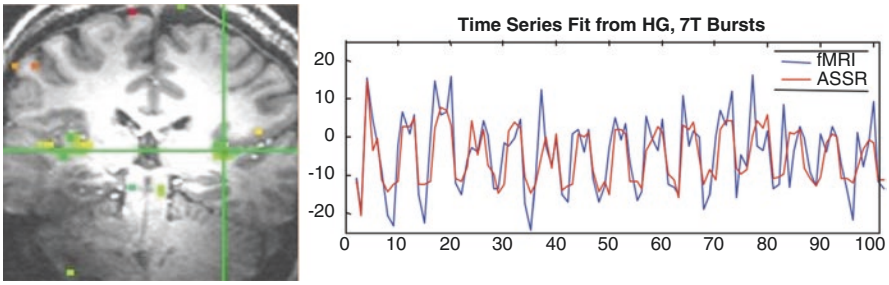

Fig. 11.9 EEG-fMRI study of steady-state auditory responses (ASSR) at 7 T. (Left) Activation map. (Right) Time series fit from Heschl's gyrus (HG). Spontaneous fluctuations in ASSR match spontaneous fluctuations in the BOLD signal. (Reprinted from Purdon et al. (2005a))

11.6 Conclusions

In this chapter, we have presented the issues and challenges brought about by using EEG/MRI at high fields, including safety, noise reduction, and hardware considerations.

In relation to safety, we have seen that investigators have mostly focused on RF-induced heating, reflecting the MR regulatory guidelines on maximum SAR exposure. While the results of investigations on the safety of recording EEG while scanning at high field suggest that it can be done safely, it is important to limit those conclusions to the specific experimental conditions described in those studies, and site-specific safety assessments are always advised prior to application, whether using commercially marketed or "homemade" equipment. We can, therefore, expect the body of evidence on the safety and data quality aspects to increase with growing interest in combining the two modalities at high field to ensure that its promise of the greater signal is fully exploited. These remarks equally apply to the issues of EEG and MRI data quality, which—although promising results have already been obtained—remain a technical challenge.

Acknowledgment The authors would like to thank the National Institute of Health for supporting this research under the National Institute of Biomedical Imaging and Bioengineering under Grant # R01EB024343.

References

Abbott DF, Masterton RAJ, Archer JS, Fleming SW, Warren AEL, Jackson GD (2014) Constructing carbon fiber motion-detection loops for simultaneous EEG-fMRI. Front Neurol 5:260. https://doi.org/10.3389/fneur.2014.00260

Abreu R, Leite M, Jorge J, Grouiller F, van der Zwaag W, Leal A, Figueiredo P (2016) Ballistocardiogram artifact correction taking into account physiological signal preservation in simultaneous EEG-fMRI. NeuroImage. https://doi.org/10.1016/j.neuroimage.2016.03.034

Angelone LM, Potthast A, Segonne F, Iwaki S, Belliveau JW, Bonmassar G (2004) Metallic electrodes and leads in simultaneous EEG-MRI: specific absorption rate (SAR) simulation studies. Bioelectromagnetics 25(4):285–295

Angelone LM, Vasios CE, Wiggins G, Purdon PL, Bonmassar G (2006) On the effect of resistive EEG electrodes and leads during 7 T MRI: simulation and temperature measurement studies. Magn Reson Imaging 24(6):801–812

Armenean C, Perrin E, Armenean M, Beuf O, Pilleul F, Saint-Jalmes H (2004) RF-induced temperature elevation along metallic wires in clinical magnetic resonance imaging: influence of diameter and length. Magn Reson Med 52(5):1200–1206

Atefi SR, Serano P, Poulsen C, Angelone LM, Bonmassar G (2018) Numerical and experimental analysis of radiofrequency-induced heating versus lead conductivity during EEG-MRI at 3 T. IEEE Trans Electromagn Compat 2018:1–8

Baker KB, Tkach JA, Nyenhuis JA, Phillips M, Shellock FG, Gonzalez-Martinez J, Rezai AR (2004) Evaluation of specific absorption rate as a dosimeter of MRI-related implant heating. J Magn Reson Imaging 20(2):315–320

Belliveau JW, Kennedy DN, McKinstry RC, Buchbinder BR, Weisskoff RM, Cohen MS, Vevea JM, Brady TJ, Rosen BR (1991) Functional mapping of the human visual cortex by magnetic resonance imaging. Science 254:716–719

Berenger JP (1994) A perfectly matched layer for the absorption of electromagnetic waves. Comput Phys 114:185–200

Bonmassar G, Anami K, Ives J, Belliveau JW (1999) Simultaneous EEG/fMRI recordings: 64-channel VEPs and 3T fMRI. NeuroImage 9:S254

Bonmassar G, Serano P, Angelone LM (2013) Specific absorption rate in a standard phantom containing a deep brain stimulation lead at 3 Tesla MRI. In: Neural engineering (NER), 2013 6th international IEEE/EMBS conference on

Bottomley PA, Andrew ER (1978) RF magnetic field penetration, phase shift and power dissipation in biological tissue: Implications for NMR imaging. Phys Med Biol 23:630–643

Bottomley P, Redington R, Edelstein W (1985) Estimating radiofrequency power deposition in body NMR imaging. Magn Reson Med 2:336–349

Cangellaris AC, Wright SM (1991) Analysis of the numerical error caused by the stair-stepped approximation of a conducting boundary in FDTD simulations of electromagnetic phenomena. IEEE Trans Antennas Propag 39:1518–1525

Carmichael DW, Pinto S, Limousin-Dowsey P, Thobois S, Allen PJ, Lemieux L, Yousry T, Thornton JS (2007) Functional MRI with active, fully implanted, deep brain stimulation systems: safety and experimental confounds. NeuroImage 37(2):508–517

Carmichael DW, Thornton JS, Rodionov R, Thornton R, McEvoy A, Allen PJ, Lemieux L (2008) Safety of localizing epilepsy monitoring intracranial electroencephalograph electrodes using MRI: radiofrequency-induced heating. J Magn Reson Imaging 28(5):1233–1244

Chou CK, Guy AW (1979) Carbon-loaded Teflon electrodes for chronic EEG recordings in microwave research. J Microw Power 14(4):399–404

Chou CK, McDougall JA, Chan KW (1997) RF heating of implanted spinal fusion stimulator during magnetic resonance imaging. IEEE Trans Biomed Eng 44(5):367–373

Chowdhury MEH, Mullinger KJ, Glover P, Bowtell R (2014) Reference layer artefact subtraction (RLAS): a novel method of minimizing EEG artefacts during simultaneous fMRI. NeuroImage 84:307–319

Cohen N, Tsizin E, Fried I, Fahoum F, Hendler T, Gazit T, Medvedovsky M (2019) Conductive gel bridge sensor for motion tracking in simultaneous EEG-fMRI recordings. Epilepsy Res 149:117–122

Collins CM, Smith MB (2003) Spatial resolution of numerical models of man and calculated specific absorption rate using the FDTD method: a study at 64 MHz in a magnetic resonance imaging coil. J Magn Reson Imaging 18(3):383–388

Cone-Wesson B, Rickards F, Poulis C, Parker J, Tan L, Pollard J (2002) The Auditory Steady-State Response: Clinical Observations and Applications in Infants and Children. J Am Acad Audiol 13:270–282

Cox RW (1996). AFNI: software for analysis and visualization of functional magnetic resonance neuroimages. Comput Biomed Res 29(3):162–173. https://doi.org/10.1006/cbmr.1996.0014

Daniel AJ, Smith JA, Spencer GS, Jorge J, Bowtell R, Mullinger KJ (2019) Exploring the relative efficacy of motion artefact correction techniques for EEG data acquired during simultaneous fMRI. Hum Brain Mapp 40(2):578–596

Debener S, Mullinger KJ, Niazy RK, Bowtell RW (2008) Properties of the ballistocardiogram artefact as revealed by EEG recordings at 1.5, 3 and 7 T static magnetic field strength. Int J Psychophysiol 67(3):189–199

De Martino F, Zimmermann J, Muckli L, Ugurbil K, Yacoub E, Goebel R (2013) Cortical Depth Dependent Functional Responses in Humans at 7T: Improved Specificity with 3D GRASE. PLoS ONE 8(3):e60514

Dimbylow PJ, Gandhi OP (1991) Finite-difference time-domain calculations of SAR in a realistic heterogeneous model of the head for plane-wave exposure from 600 MHz to 3 GHz. Phys Med Biol 36(8):1075–1089

FDA (2003) Criteria for significant risk investigations of magnetic resonance diagnostic devices. Center for Devices and Radiological Health, Silver Spring

Fellner MC, Volberg G, Mullinger KJ, Goldhacker M, Wimber M, Greenlee MW, Hanslmayr S (2016) Spurious correlations in simultaneous EEG-fMRI driven by in-scanner movement. NeuroImage 133:354–366

Flanagan D, Abbott DF, Jackson GD (2009) How wrong can we be? The effect of inaccurate mark-up of EEG/fMRI studies in epilepsy. Clin Neurophysiol 120(9):1637–1647
Gandhi OP, Chen XB (1999) Specific absorption rates and induced current densities for an anatomy-based model of the human for exposure to time-varying magnetic fields of MRI. Magn Reson Med 41(4):816–823
Gangarosa RE, Minnis JE, Nobbe J, Praschan D, Genberg RW (1987) Operational safety issues in MRI. Magn Reson Imaging 5(4):287–292
Galambos R, Makeig S, Talmachoff PJ (1981) A 40-Hz Auditory Potential Recorded from the Human Scalp. Proc Natl Acad Sci 78(4):2643–2647
Glover GH, Hayes CE, Pelc NJ, Edelstein WA, Mueller OM, Hart HR, Hardy CJ, O'Donnell M, Barber WD (1985) Comparison of linear and circular polarization for magnetic resonance imaging. J Magn Reson 64:255–270
Harel N, Ugurbil K, Uludag K, Yacoub E (2006) Frontiers of Brain Mapping Using MRI. J Magn Reson Imaging, 23(6):945–957
Ho HS (2001) Safety of metallic implants in magnetic resonance imaging. J Magn Reson Imaging 14(4):472–477
Huang-Hellinger FR, Breiter HC, Mc Cormack G, Cohen MS, Kwong KK, Sutton JP, Savoy RL, Weisskoff RM, Davis TL, Baker JR, Belliveau JW, Rosen BR (1995) Simultaneous functional magnetic resonance imaging and electrophysiological recording. Hum Brain Mapp 3:13–23
Huber L, Tse DHY, Wiggins CJ, Uludag K, Kashyap S, Jangraw DC, Bandettini PA, Poser BA, Ivanov D (2018) Ultra-high resolution blood volume fMRI and BOLD fMRI in humans at 9.4 T: Capabilities and challenges. NeuroImage 178:769–779
Ibrahim TS, Abduljalil AM, Baertlein BA, Lee R, Robitaill PM (2001) Analysis of B1 field profiles and SAR values for multi-strut transverse electromagnetic RF coils in high field MRI applications. Phys Med Biol 46(10):2545–2555
IEC (2002) International Standard, medical equipment - part 2-33: particular requirements for the safety of the magnetic resonance equipment for medical diagnosis, 2nd revision. International Electrotechnical Commission, Geneva, pp 29–31
Ives JR, Warach S, Schmitt F, Edelman RR, Schomer DL (1993) Monitoring the patient's EEG during echo-planar MRI. Electroencephalogr Clin Neurophysiol 87:417–420
Jansen M, White TP, Mullinger KJ, Liddle EB, Gowland PA, Francis ST, Bowtell R, Liddle PF (2012) Motion-related artefacts in EEG predict neuronally plausible patterns of activation in fMRI data. NeuroImage 59(1):261–270
Jin J-M (1999) Electromagnetic analysis and design in magnetic resonance imaging. CRC Press, Boca Raton
Jorge J, Grouiller F, Ipek O, Stoermer R, Michel CM, Figueiredo P, van der Zwaag W, Gruetter R (2015) Simultaneous EEG-fMRI at ultra-high field: artifact prevention and safety assessment. NeuroImage 105:132–144
Jorge J, Bouloc C, Brechet L, Michel CM, Gruetter R (2019) Investigating the variability of cardiac pulse artifacts across heartbeats in simultaneous EEG-fMRI recordings: a 7T study. NeuroImage 191:21–35
Kainz W, Christ A, Kellom T, Seidman S, Nikoloski N, Beard B, Kuster N (2005) Dosimetric comparison of the specific anthropomorphic mannequin (SAM) to 14 anatomical head models using a novel definition for the mobile phone positioning. Phys Med Biol 50(14):3423–3445
Kangarlu A, Shellock FG, Chakeres DW (2003) 8.0-Tesla human MR system: temperature changes associated with radiofrequency-induced heating of a head phantom. J Magn Reson Imaging 17(2):220–226
Keltner JR, Carlson JW, Roos MS, Wong STS, Wong TL, Budinger TF (1991) Electromagnetic fields of surface coil in vivo NMR at high frequencies. Magn Reson Med 22:467–480
Krishnaswamy P, Bonmassar G, Poulsen C, Pierce ET, Purdon PL, Brown EN (2015) Reference-free removal of EEG-fMRI ballistocardiogram artifacts with harmonic regression. NeuroImage 128:398–412
Konings MK, Bartels LW, Smits HF, Bakker CJ (2000) Heating around intravascular guidewires by resonating RF waves. J Magn Reson Imaging 12(1):79–85

Kwong KK, Belliveau JW, Stern C, Chesler DA, Goldberg IE, Poncelet BP, Kennedy DN, Weisskoff RM, Cohen MS, Turner R, Cheng H-M, Brady TJ, Rosen BR (1992) Functional MR imaging of primary visual and motor cortex. In: Tenth annual meeting of the society for magnetic resonance imaging. Society of Magnetic Resonance Imaging, New York

Lazeyras F, Zimine I, Blanke O, Perrig SH, Seeck M (2001) Functional MRI with simultaneous EEG recording: feasibility and application to motor and visual activation. J Magn Reson Imaging 13(6):943–948

Lemieux L, Allen PJ, Franconi F, Symms MR, Fish DR (1997) Recording of EEG during fMRI experiments: patient safety. Magn Reson Med 38(6):943–952

LeVan P, Maclaren J, Herbst M, Sostheim R, Zaitsev M, Hennig J (2013) Ballistocardiographic artifact removal from simultaneous EEG-fMRI using an optical motion-tracking system. NeuroImage 75:1–11

Lewis LD, Setsompop K, Rosen BR, Polimeni JR (2016) Fast fMRI can detect oscillatory neural activity in humans. PNAS 113(43):6679–6685

Luo QF, Huang XS, Glover GH (2014) Ballistocardiogram artifact removal with a reference layer and standard EEG cap. J Neurosci Methods 233:137–149

Makris N, Angelone L, Tulloch S, Sorg S, Kaiser J, Kennedy D, Bonmassar G (2008) MRI-based anatomical model of the human head for specific absorption rate mapping. Med Biol Eng Comput 46(12):1239–1251

Mansfield P, Morris PG (1982) NMR imaging in biomedicine. Academic, New York

Massire A, Cloos MA, Luong M, Amadon A, Vignaud A, Wiggins CJ, Boulant N (2012) Thermal simulations in the human head for high field MRI using parallel transmission. J Magn Reson Imaging 35(6):1312–1321

Maziero D, Velasco TR, Hunt N, Payne E, Lemieux L, Salmon CEG, Carmichael DW (2016) Towards motion insensitive EEG-fMRI: correcting motion-induced voltages and gradient artefact instability in EEG using an fMRI prospective motion correction (PMC) system. NeuroImage 138:13–27

Mirsattari SM, Lee DH, Jones D, Bihari F, Ives JR (2004) MRI compatible EEG electrode system for routine use in the epilepsy monitoring unit and intensive care unit. Clin Neurophysiol 115(9):2175–2180

Mullinger K, Brookes M, Stevenson C, Morgan P, Bowtell R (2008a) Exploring the feasibility of simultaneous electroencephalography/functional magnetic resonance imaging at 7 T. Magn Reson Imaging 26(7):968–977

Mullinger K, Debener S, Coxon R, Bowtell R (2008b) Effects of simultaneous EEG recording on MRI data quality at 1.5, 3 and 7 tesla. Int J Psychophysiol 67(3):178–188

Nakamura W, Anami K, Mori T, Saitoh O, Cichocki A, Amari S (2006) Removal of ballistocardiogram artifacts from simultaneously recorded EEG and fMRI data using independent component analysis. IEEE Trans Biomed Eng 53(7):1294–1308

Newton AT, Rogers BP, Gore JC, Morgan (2012) VL Improving measurement of functional connectivity through decreasing partial volume effects at 7T, NeuroImage 59(3): 2511–2517

Nitz WR, Brinker G, Diehl D, Frese G (2005) Specific absorption rate as a poor indicator of magnetic resonance-related implant heating. Investig Radiol 40(12):773–776

Ogawa S, Tank DW, Menon R, Ellermann JM, Kim S-G, Merkle H, Ugurbil K (1992) Intrinsic signal changes accompanying sensory stimulation: Functional brain mapping with magnetic resonance imaging. Proc Natl Acad Sci U S A 89:5951–5955

Percival DB, Walden AT (1993) Spectral analysis for physical applications. Cambridge University Press, Cambridge UK

Poulsen C, Wakeman DG, Atefi SR, Luu P, Konyn A, Bonmassar G (2016) Polymer thick film technology for improved simultaneous dEEG/MRI recording: safety and MRI data quality. Magn Reson Med 77(2):895–903

Polimeni JR, Fischl B, Greve DN, Wald LL (2010) Laminar analysis of 7 T BOLD using an imposed spatial activation pattern in human V1. NeuroImage 52(4):1334–1346

Purdon PL, Purdon AM, Jaaskelainen I, Iwaki S, Angelone LM, Belliveau JW, Brown EN, Bonmassar G (2005a) Concurrent EEG-fMRI of the 40-Hz auditory steady-state response at

3 and 7 Tesla. 11th Annual Meeting of the Organization for Human Brain Mapping, Toronto, Canada, Neuroimage

Purdon PP, Millan H, Bonmassar G (2005b) High-field one: an open-source hardware and software platform for acquisition and real-time processing of electrophysiology during MRI. Neuroinformatics 175(2):165–186

Reilly JP (1992) Principles of nerve and heart excitation by time-varying magnetic fields. Ann N Y Acad Sci 649:96–117

Rezai AR, Finelli D, Nyenhuis JA, Hrdlicka G, Tkach J, Sharan A, Rugieri P, Stypulkowski PH, Shellock FG (2002) Neurostimulation systems for deep brain stimulation: in vitro evaluation of magnetic resonance imaging-related heating at 1.5 tesla. J Magn Reson Imaging 15(3):241–250

Schomer DL, Bonmassar G, Lazeyras F, Seeck M, Blum A, Anami K, Schwartz D, Belliveau JW, Ives J (2000) EEG-Linked functional magnetic resonance imaging in epilepsy and cognitive neurophysiology. J Clin Neurophysiol 17(1):43–58

Stach BA (2002) The auditory steady-state response. The Hearing Journal 55(9):10–18

Serano P, Angelone LM, Katnani H, Eskandar E, Bonmassar G (2015) A novel brain stimulation technology provides compatibility with MRI. Sci Rep 5:9805

Sharan A, Rezai AR, Nyenhuis JA, Hrdlicka G, Tkach J, Baker K, Turbay M, Rugieri P, Phillips M, Shellock FG (2003) MR safety in patients with implanted deep brain stimulation systems (DBS). Acta Neurochir Suppl 87:141–145

Shellock FG (2007) Comments on MR heating tests of critical implants. J Magn Reson Imaging 26(5):1182–1185

Sled JG, Pike GB (1998) Standing-wave and RF penetration artifacts caused by elliptic geometry: an electrodynamic analysis of MRI. IEEE Trans Med Imaging 17(4):653–662

Stevens T, Ives J, Bartha R (2007a) Avoiding resonant lengths of wire with RF Chokes at 4 Tesla. International Society for Magnetic Resonance in Medicine, Berlin

Stevens T, Ives J, Bartha R (2007b) Energy coupling between RF electric fields and conductive wires: image artifacts and heating. International Society for Magnetic Resonance in Medicine, Berlin

Steyrl D, Krausz G, Koschutnig K, Edlinger G, Muller-Putz GR (2017) Reference layer adaptive filtering (RLAF) for EEG artifact reduction in simultaneous EEG-fMRI. J Neural Eng 14(2):026003

van der Meer JN, Pampel A, Van Someren EJW, Ramautar JR, van der Werf YD, Gomez-Herrero G, Lepsien J, Hellrung L, Hinrichs H, Moller HE, Walter M (2016) Carbon-wire loop based artifact correction outperforms post-processing EEG/fMRI corrections-A validation of a real-time simultaneous EEG/fMRI correction method. NeuroImage 125:880–894

Vasios CE, Angelone LM, Purdon PL, Ahveninen J, Belliveau JW, Bonmassar G (2006) EEG/(f) MRI measurements at 7 Tesla using a new EEG cap ("InkCap"). NeuroImage 33(4):1082–1092

Wendt RE, Wilcott MR, Nitz W, Murphy PH, Bryan RN (1988) MR imaging of susceptibility-induced magnetic field inhomogeneities. Radiology 168(3):837–841

Wiesinger F, Van De Moortele PF, Adriany G, Zanche ND, Ugurbil K, Pruessmann KP (2006) Potential and feasibility of parallel MRI at high field. NMR in Biomedicine 19(3):368–378

Wiggins GC, Potthast A, Triantafyllou C, Wiggins CJ, Wald LL (2005) Eight-channel phased array coil and detunable TEM volume coil for 7 T brain imaging. Magn Reson Med 54(1):235–240

Xia HJ, Ruan D, Cohen MS (2014) Separation and reconstruction of BCG and EEG signals during continuous EEG and fMRI recordings. Front Neurosci 8:163

Yacoub E, Shmuel A, Pfeuffer J, Van De Moortele PF, Adriany G, Anderson P, Vaughan JT, Merkle H, Ugurbil K, Hu X (2001) Imaging brain function in humans at 7 Tesla. Magn Reson Med 45(4):588–594

Young, JL, Wait, JR (1989). Shielding properties of an ensemble of thin, infinitely long, parallel wires over a lossy half space. IEEE Transactions on Electromagnetic Compatibility (ISSN 0018-9375), vol. 31, 1989; p. 238–244.

Zhang S, Hennig J, LeVan P (2019) Direct modelling of gradient artifacts for EEG-fMRI denoising and motion tracking. J Neural Eng 16(5):056010

Experimental Design and Data Analysis Strategies

12

Jonathan Wirsich, Andrew P. Bagshaw, Maxime Guye, Louis Lemieux, and Christian-G. Bénar

12.1 Introduction

As described in earlier chapters, EEG and fMRI are two powerful, noninvasive tools for studying human brain activity. Since they have complementary spatiotemporal properties, with EEG providing millisecond temporal resolution and fMRI millimetre spatial resolution, there has been a drive over the last two decades to record them simultaneously, a technique referred to as simultaneous EEG–fMRI or simply EEG–fMRI. The combined data promise to provide a more complete view of brain activity and hopefully improve understanding of the spatiotemporal dynamics of brain processes.

J. Wirsich
EEG and Epilepsy Unit, University Hospitals and Faculty of Medicine of Geneva, Geneva, Switzerland
e-mail: Jonathan.Wirsich@unige.ch

A. P. Bagshaw
Centre for Human Brain Health and School of Psychology, University of Birmingham, Birmingham, UK
e-mail: a.p.bagshaw@bham.ac.uk

M. Guye
Aix Marseille Univ, CNRS, CRMBM, Centre for Magnetic Resonance in Biology en Medicine, Marseille, France
e-mail: Maxime.GUYE@univ-amu.fr

L. Lemieux
UCL Queen Square Institute of Neurology, London, UK
e-mail: louis.lemieux@ucl.ac.uk

C.-G. Bénar (✉)
Aix Marseille Univ, INSERM, INS, Inst Neurosci Syst, Marseille, France
e-mail: christian.benar@univ-amu.fr

C. Mulert, L. Lemieux (eds.), *EEG - fMRI*,
https://doi.org/10.1007/978-3-031-07121-8_12

The earliest attempts to combine EEG and fMRI avoided the technical issues of recording EEG in the MRI scanner by acquiring the two datasets separately and combining the results. As discussed in the Chap. 1, this approach is particularly suitable when the brain phenomena or effects of interest are predictable in time (e.g. externally triggered) and reproducible across sessions (i.e. the expected signal changes are unaffected by the experimental conditions). Furthermore, serially acquired multimodal data are best suited for analyses of effects averaged across sessions. Conversely, the data obtained from simultaneous acquisitions do not have any such constraints and can be used to study individual events, on the condition that data quality is not compromised by possible interactions between the EEG and MR systems. Simultaneous recordings generally add an extra layer of complexity to the experimental setup (see the Chaps. 8 and 9) but there is a potential time saving compared to serial acquisitions.

The applications of simultaneous EEG–fMRI can be grouped into two categories, according to the nature of brain activity under study. First, the technique has been used to investigate spontaneous transient events or fluctuations in EEG power, for example, interictal epileptic discharges, sleep spindles or the alpha rhythm. In this case, simultaneous recordings are necessary, since the activity of interest varies unpredictably (i.e. it is not under experimental control) and without external manifestation other than in the EEG or fMRI. Comparable datasets could therefore not be obtained with certainty across separate unimodal sessions.

Second, EEG–fMRI has been used in cognitive and sensory neuroscience applications where the activity of interest is induced by an experimental stimulus. In this situation, EEG–fMRI is necessary if one is interested in part of the signal that varies unpredictably, i.e. inter-event variation, or to eliminate potential inter-session confounds such as habituation, learning, attention, fatigue, etc.

This chapter's starting assumption is the availability, in the mind of the potential user of EEG–fMRI, of a hypothesis or question regarding the link between a particular feature or set of features of the EEG signal and haemodynamic changes. This chapter's main purpose is therefore to give the reader an overview of the different ways in which EEG–fMRI data can be acquired and analysed to address this type of question. While there is now a consensus on the most efficient way in which EEG–fMRI can be acquired, i.e. via continuous recording in contrast to interleaved acquisitions, the most effective way in which to integrate the data remains an active area of research.

12.2 Data Acquisition and Experimental Design

Ignoring any technical consideration, all multimodal data acquisitions should be performed simultaneously. However, data quality is a crucial issue in determining degree of multimodal acquisition synchrony. The MR scanner is a very challenging environment for EEG recordings, and both data acquisition processes can severely affect the other's performance through electromagnetic interactions (see the Chaps. 8 and 9). Recording good-quality EEG inside the scanner and during scanning

requires special measures to be taken to minimize any effect on MR image quality (Krakow et al. 2000; see the Chap. 10) and to ensure patient safety (Lemieux et al. 1997; see the Chap. 7).

As highlighted in the Chap. 7, and as identified in the initial work of Ives and colleagues (Ives et al. 1993), EEG data recorded during fMRI scanning suffers from two major artefacts. The MR image acquisition artefact obscures the physiological EEG whenever scanning occurs, while the pulse-related artefact (often called ballistocardiogram or BCG, although the mechanism is not known precisely) is continuously present in most subjects placed within the scanner's static magnetic field (Allen et al. 1998) (see the Chap. 8). The magnitude of the pulse artefact is strongly affected by the static (B_0) field strength of the scanner, which also needs to be considered when designing an experiment since it can lead to significant reductions in EEG signal quality at high field (>3 T) and is particularly problematic at ultra-high field (7 T) (Neuner et al. 2013; Jorge et al. 2015a, b; Abreu et al. 2016).

These two artefacts constitute the two most important practical barriers to recording continuous EEG data during fMRI. Another artefact arises from vibrations of the scanner's cooling helium pump. While this artefact can be avoided by turning off the pump, partial artefact reduction methods are available for recording with a running pump (Rothlubbers et al. 2013, 2015; Kim et al. 2015). The artefact can also be reduced by suppressing vibrations by minimizing the distance between amplifier and RF coil (Jorge et al. 2015b). The internal ventilation system of the scanner might also add additional vibration artefacts in the gamma range of the EEG signal (Nierhaus et al. 2013).

The first simultaneous recordings used triggered or sparse acquisition and relied only on periods during which the EEG was uncontaminated by the artefact resulting from gradient switching. We will discuss this strategy in greater detail in Sect. 12.2.1 (see also the Chap. 17). When it was shown that this artefact (even though it is impressively large) could be reduced significantly using signal processing methods, this launched the current interest in continuous recordings and increased the possibilities offered by simultaneous EEG–fMRI. This is discussed in Sect. 12.2.2. Both acquisition modes permit the investigation of two main types of activity, spontaneous and stimulus-related, although there can be constraints imposed by the data acquisition strategy on the experimental design. This issue is discussed in Sect. 12.2.3.

12.2.1 Interleaved EEG and fMRI Acquisitions: Triggered and Sparse Scanning

In the first report of EEG recorded in the MRI scanner, Ives and colleagues identified some of the major technical issues associated with the technique, namely the presence of artefacts on the EEG associated with the heartbeat and scanning (Ives et al. 1993) (see the Chaps. 8 and 9). The first use of EEG-fMRI in two patients with epilepsy used an interleaved data acquisition scheme to minimize the impact of the scanning artefact on EEG, by triggering an echoplanar image (EPI) acquisition a

few seconds after the observation of a paroxysmal discharge on the EEG (Warach et al. 1996). The trigger delay was chosen to capture images at the presumed peak time of the spike-related haemodynamic response (see Fig. 12.1) and resulted in a set of post-spike images (epileptic activity image set). Following the general approach in fMRI of contrasting brain states, images were also acquired following periods devoid of epileptic form discharges (normal background or control image set). Activation maps were obtained by comparing control images to epileptic activity images (voxel-wise *t*-tests; see in this section) or by cross-correlation analysis (Bandettini et al. 1993). The sequence of acquisition of the post-spike and control images can be random, according to the spontaneous EEG (Symms et al. 1999), or via sequential blocks of post-spike and control images, with the administration of a spike-suppressing drug in-between (Seeck et al. 1998). This acquisition technique, called spike-triggered fMRI, is a form of *interleaved multimodal imaging*.

The application of online pulse artefact reduction can lead to an increase in spike detection reliability (Allen et al. 1998; Salek-Haddadi et al. 2003b). Spike-triggered fMRI went on to be used by a number of groups who were interested in revealing the haemodynamic correlates of epileptic activity (Seeck et al. 1998; Krakow et al. 1999; Patel et al. 1999; Symms et al. 1999; Al-Asmi et al. 2003). However, although spike-triggered fMRI represented a technical breakthrough, it has a number of drawbacks. Firstly, it is only applicable to the study of large, clear EEG events that can easily be detected visually in the EEG, allowing scan acquisition to be initiated reliably. Secondly, it required a highly trained observer to monitor the EEG for the duration of the scanning session to identify events of interest. Thirdly, degradation of the EEG quality during scanning and the resulting lack of information on the subject's state means that only a short train of images (slices or volumes) could be acquired per event, limiting the total amount of data that can be acquired (per unit

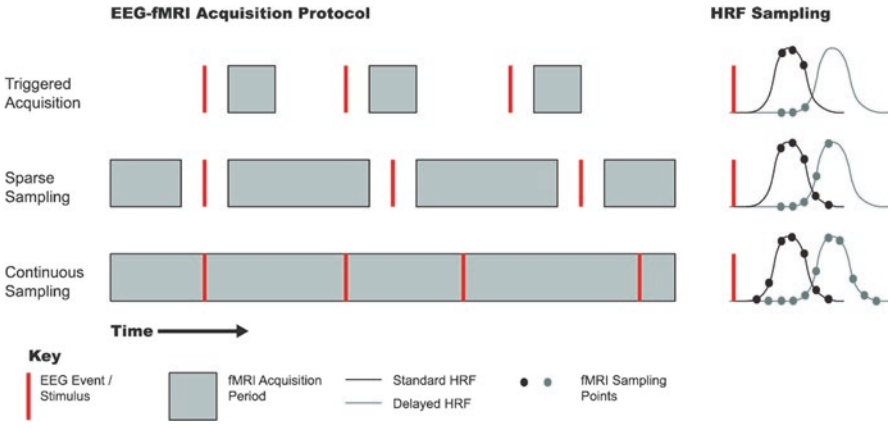

Fig. 12.1 Illustration of triggered, sparse (interleaved) and continuous acquisition schemes and their effect on the sampling of the event-related BOLD change. (*Left*) Relationship between the fMRI acquisition strategy and the EEG events of interest. (*Right*) BOLD change sampling for each of the acquisition techniques, for standard and delayed HRF

time), with a resulting impact on the statistical power (Krakow et al. 2001). Moreover, the sensitivity of the technique relies entirely on the assumption that the post-discharges can sample the peak of the spike-related BOLD change, and that no epileptic activity occurred during the acquisition of the control images. Finally, this acquisition mode does not provide continuous sampling of the MR signal, making it impossible to model slow drifts in the fMRI signal, which can also lead to reduced detection power.

An alternative interleaved acquisition mode, that we will refer to as *interleaved periodic EEG–fMRI*, was subsequently implemented to study other EEG phenomena, for example, evoked potentials and spontaneous activity such as the alpha rhythm. By having a relatively long scan repetition time (TR) but acquiring a few slices spaced evenly within each TR (e.g. six slices with a TR of 4 s), the majority of each scan period is free from gradient switching, resulting in periods of clean EEG (Goldman et al. 2000). A similar strategy is to acquire all slices at the beginning of each TR, leaving a silent period with artefact-free EEG (Bonmassar et al. 1999; Kruggel et al. 2000; Feige et al. 2005). A final variant is to acquire a prolonged period of fMRI, for example, 30 s, followed by an equivalent period without fMRI during which EEG is acquired. This approach is particularly suited for slowly varying phenomena, such as sleep patterns (Portas et al. 2000; Bonmassar et al. 2001). Periodic interleaved schemes are not suitable for the study of spontaneous brief discharges, which can occur undetected during periods of scanning.

While sparse sampling techniques opened up the use of EEG–fMRI to the study of a wider range of EEG phenomena, they still had a number of disadvantages. Although statistical power was increased relative to spike triggering, sampling of the haemodynamic timecourse is limited (see Fig. 12.1). For example, if the stimulation is time-locked to the fMRI, the same points on the HR would be sampled at each TR, leading to suboptimal characterization of the timecourse. Similarly, if the timecourse of the BOLD changes differs markedly from the presumed (i.e. canonical) response, detection power would be considerably reduced, a problem that also affects the spike-triggered approach (Fig. 12.1). Perhaps the greatest disadvantage of sparse sampling protocols is the constraint on the experimental method in terms of timing of the stimuli and fMRI acquisition. Typically, considerably fewer slices are acquired compared to a conventional fMRI acquisition, effectively reducing the efficiency of the experimental design. Recent developments in fast EPI sequences (e.g. simultaneous multi-slice/multi-band acquisition) can overcome this limitation, however, and allow full brain coverage (Uji et al. 2018).

Given these disadvantages, sparse sampling and spike-triggered protocols have now been superseded with the advent of continuous EEG–fMRI, although they are still sometimes employed (Christmann et al. 2007; Scheeringa et al. 2011), particularly in the investigation of auditory stimuli when a silent period is beneficial (Belin et al. 1999; Scarff et al. 2004) or to examine high-frequency activity on the EEG where a period without gradient artefact can help (Uji et al. 2018).

12.2.2 Simultaneous EEG and fMRI Acquisitions: Continuous Scanning

Continuous scanning—i.e. uninterrupted acquisition of fMRI volumes, as is the case in conventional fMRI experiments—is the preferred option in terms of fMRI data acquisition strategy in the majority of experimental situations. By acquiring the maximum amount of data per unit time, statistical (detection) power and characterization of the HRF are optimized (see Fig. 12.1). A number of hardware and software technical developments allow adequate EEG quality during MR scanning for most applications. The most widely used techniques for the removal of artefacts on the EEG are based on modifications of the template subtraction method developed by Allen and colleagues for pulse and scanning artefact reduction (Allen et al. 1998, 2000) (see the Chaps. 8 and 9). A number of commercially available EEG recording and artefact correction systems allow continuous scanning. Studies have demonstrated that EEG data quality from continuous recording can be as good as that from sparse sampling paradigms, at least at low frequencies (<20 Hz), thereby allowing analysis of a wide range of EEG phenomena (Salek-Haddadi et al. 2003a; Becker et al. 2005; Comi et al. 2005; Debener et al. 2005; Sammer et al. 2005; Im et al. 2006; Bagshaw and Warbrick 2007; Bénar et al. 2007).

12.2.3 Experimental Protocol

EEG–fMRI experimental protocols reflect the two main types of EEG phenomena, namely spontaneous brain activity in the resting state (i.e. in the absence of any experimental manipulation or stimulation) and stimulus-driven paradigms, where the interest is focused on the brain response to particular stimuli.

12.2.3.1 Resting-State EEG–fMRI: Spontaneous Brain Activity

The first simultaneous EEG–fMRI studies concentrated on two types of spontaneous activity, interictal epileptic spikes (Ives et al. 1993; Warach et al. 1996; Seeck et al. 1998; Krakow et al. 1999; Al-Asmi et al. 2003) and alpha waves (Goldman et al. 2002; Laufs et al. 2003a; Moosmann et al. 2003). EEG–fMRI has also found application in the study of a number of other types of spontaneous activity: generalized spike-and-wave discharges (Archer et al. 2003; Aghakhani et al. 2004; Gotman et al. 2005; Laufs et al. 2006a; Hamandi et al. 2008), ictal epileptic discharges (Jackson and Opdam 2000; Salek-Haddadi et al. 2002; Federico et al. 2005; Kobayashi et al. 2006) and sleep paroxysms (Laufs et al. 2006b; Schabus et al. 2007; Stern et al. 2011; Caporro et al. 2012). For reviews, see (Salek-Haddadi et al. 2003a; Gotman et al. 2006; Stern 2006; Laufs and Duncan 2007; Zijlmans et al. 2007; Formaggio et al. 2011; Pittau et al. 2012; Centeno and Carmichael 2014). EEG–fMRI has also been used to study the neural correlates of sleep (Lovblad et al. 1999; Portas et al. 2000; Czisch et al. 2002, 2004; Tanaka et al. 2003; Fukunaga et al. 2006; Horovitz et al. 2007; Wirsich et al. 2018)—see review of methods in (Duyn 2012)—and arousal level (Matsuda et al. 2002; Foucher et al. 2004). It has

been applied extensively to the investigation of "resting state" networks and their relationship with electrophysiological activity (Laufs et al. 2003b; Mantini et al. 2007b; Scheeringa et al. 2008; Sadaghiani et al. 2010; Hiltunen et al. 2014; Neuner et al. 2014; Mayhew and Bagshaw 2017). Spontaneous activity has also been used to explore the connectivity dynamics of brain networks, integrating both electrophysiological and haemodynamic measurements (Britz et al. 2010; Musso et al. 2010; Tagliazucchi et al. 2012b; Chang et al. 2013; Labounek et al. 2015), while recent studies have started to integrate concurrent EEG-fMRI data on a whole-brain graph theoretical level (Deligianni et al. 2014; Wirsich et al. 2017). Such combinational approaches have advantageously informed investigations of functional connectivity alterations related to brain pathology, particularly in Epilepsy (Centeno and Carmichael 2014; Khoo et al. 2017; Ridley et al. 2017; Abreu et al. 2019). Specific effects on connectivity dynamics of transient activities (such as interictal epileptiform discharges (IEDs)) or brain states have also been evidenced (Xiao et al. 2016; Omidvarnia et al. 2017; Shamshiri et al. 2017; Tangwiriyasakul et al. 2018; Qin et al. 2019). Resting-state functional connectivity will be addressed in more detail in Sect. 12.3.6.

As compared to the stimulus-dependent approaches discussed later, where physiological noise is normally orthogonal to the evoked signal of interest, a continuous analysis of resting state data requires additional care to be taken (Tagliazucchi et al. 2013; Tagliazucchi and Laufs 2014) to control for the impact of physiological (i.e. non-neuronal, primarily cardiac and respiratory) noise (Abreu et al. 2017). In resting-state studies subjects are often asked to keep their eyes closed, as well as to stay still. Keeping the eyes closed is clearly relevant for alpha-wave studies and also permits eye blink artefacts on the EEG to be avoided. The advantage of keeping the eyes closed is not so straightforward for the study of other brain rhythms. This is a parameter of the protocol that needs consideration, as there could be interactions between having eyes open/closed (Wu et al. 2010; McAvoy et al. 2012; Mo et al. 2013), arousal level and the activity of interest. It has thus been shown that fluctuations of physiological rhythms can have an impact on the results of EEG-fMRI studies (Tyvaert et al. 2008). Moreover, for epileptic spikes, there can be a higher spike yield in low arousal or sleep states (Malow et al. 1997), which can be a confounding effect as the response could originate from regions involved in the fluctuation of the arousal level, in the generation of alpha waves or in visual areas. The possibility that subjects will enter sleep inadvertently should also be considered if subjects' eyes are closed since it has been suggested that many resting-state studies supposedly conducted during wakefulness are contaminated by the intrusion of sleep (Tagliazucchi and Laufs 2014).

12.2.3.2 Stimulus-Driven Paradigms

While the advantages of simultaneous EEG–fMRI are obvious for the study of spontaneous activity, this is less clear for paradigms involving experimental manipulation of the subject's brain state (Josephs et al. 1997), for example, in evoked response studies involving repetitions of the same set of stimuli. As noted in the Chap. 1, one must consider the possibility of separate EEG and fMRI recording

sessions before embarking on simultaneous acquisitions in such situations. In particular, one must consider whether the EEG recording could take place in a separate session by replicating the experimental protocol performed in the scanner since simultaneous recordings have major drawbacks relative to separate EEG and fMRI sessions. For example, simultaneous recording significantly lengthens the fMRI session because of the time needed to apply the EEG cap or electrodes and to set up the EEG system in the fMRI environment (even though simultaneous recording shortens the total acquisition time for a given subject). In addition, simultaneous recording results in a less comfortable setup for the subject, which may limit the total scanning time and in extreme cases can result in premature termination of the session.

However, as noted in the Chap. 1, there are situations where simultaneous recordings are necessary. Firstly, to ensure that signals correspond to the same conditions and brain states, for example, in terms of lighting, ambient noise, confinement, arousal, attention, emotional state, strategy, etc. This can be of particular interest for attention (Okon-Singer et al. 2011; Walz et al. 2013; Wang et al. 2016; Bayer et al. 2018), memory and learning protocols (Hanslmayr et al. 2011; Hoppstadter et al. 2015; Herweg et al. 2016), as well as for auditory paradigms (Mulert et al. 2004; Li et al. 2017). Secondly, for the study of individual events (Fell 2007), which are the only "true" events (in contrast to averages), allowing a deeper study of the relationship between fMRI and EEG and behaviour (Debener et al. 2005; Eichele et al. 2005; Bénar et al. 2007; Nguyen and Cunnington 2014; Walz et al. 2014; Wirsich et al. 2014). Thirdly, monitoring of EEG markers of general brain state (e.g. arousal) may inform the analysis of responses to stimuli and help to explain inter- and intra-individual response variability (Matsuda et al. 2002; Mayhew et al. 2013a, b). Finally, the EEG can serve as a "control" modality when one needs to compare the fMRI recordings with other modalities that can also be recorded simultaneously with EEG, such as MEG and/or intracranial EEG (Dubarry et al. 2014), near-infrared spectroscopy (Machado et al. 2011), etc. The simultaneously acquired EEG signals can then serve to assess the extent to which the activity of interest (e.g. evoked potentials or background activity) is reproducible across sessions.

In addition to paradigms that are based on repetitive stimuli, continuous naturalistic stimuli such as movie watching have been used in EEG-fMRI experiments (Morillon et al. 2010; Whittingstall et al. 2010; Lehongre et al. 2013). The continuous nature of this stimulus makes analysis strategies based on single-trial variability or averaging unsuitable. Instead the type of analysis approaches used in resting state analysis is more appropriate (see Sect. 12.2.3.1). It is equally possible to correlate brain activity timecourses across subjects as the naturalistic stimulus is normally the same for all participants (Simony et al. 2016). Another interesting stimulus-driven paradigm is the utilization of biofeedback (Zich et al. 2015). As this paradigm relies on presenting the instantaneous and clean EEG signal back to the subject this approach requires efficient online gradient artefact rejection in particular (Jorge et al. 2015b; Zich et al. 2015; Steyrl et al. 2018).

12.3 Analysis of Simultaneously Acquired EEG–fMRI Data

Since it is a relatively underused instrument, EEG–fMRI studies have often had an exploratory flavour, although they are hypothesis-driven at the level of each dataset. This is particularly the case in the study of spontaneous brain activity (epileptic discharges, rhythms, etc.) aimed at identifying the spatiotemporal patterns of haemodynamic change related to the EEG phenomena of interest, with the primary question generally being "do any parts of the brain activate/deactivate in relation to a specific EEG phenomenon?" This has mainly been done through analyses of the correlation of the BOLD timeseries with a postulated EEG-derived model of haemodynamic changes, implemented in the form of general linear models (GLM). In the language of the Chap. 1, this analytical approach can be characterized as being asymmetric and hypothesis-driven (EEG-informed GLM). The above question can be rephrased to be more specific as: "assuming a fixed and well-characterized response to a brief neuronal (EEG) event, what are the brain regions, if any, which activate/deactivate in relation to the observed EEG events?" In the case of epilepsy, for example, this question can be answered using the timing of epileptic discharges for the spike-triggered acquisition mode discussed previously and in analyses of EEG–fMRI data that assume a fixed HRF (see below).

Another question that has often been explored is "what is the 'optimal' EEG-derived model of haemodynamic changes?". Interest in this question has been motivated by the suspicion that the relationship between neuronal activity and haemodynamic changes for spontaneous brain activity reflected on the EEG may deviate from the norm (represented by the "canonical" HRF), particularly in pathological systems. Unfortunately, no ground truth against which models can be formally evaluated is generally available in human studies, and in practice this question has been explored by using relatively flexible HRF basis sets or families of GLMs to map out the spatiotemporal variability of the EEG-related BOLD changes, including the shape of the HRF. For stimulus-based studies, the analysis of EEG–fMRI has focused on exploring the relationship between specific features of the EEG signal and the time-locked BOLD signal. These can be addressed within the GLM framework using parametric designs. Even more exploratory approaches have also been proposed that rely on the identification of patterns in the multivariate data based on general assumptions relating to the statistical properties of the signals, such as principal component analysis (PCA) and independent component analysis (ICA). The above relates to the analysis of individual datasets and will be discussed in more detail in the remainder of this section.

Note that the methods available for group studies where an atomically consistent effect can be hypothesized across subjects, such as evoked responses and EEG rhythms, will not be reviewed here since the details are not specific to EEG–fMRI; we refer the reader to the Chap. 15 for further reading. However, there is one aspect of the analysis of group EEG–fMRI data that demands particular attention, namely the potential for exceedingly unbalanced designs resulting from the widely varying experimental efficiencies of recordings of spontaneous brain activity. A discussion of this point can be found in (Friston et al. 2005), and an example application in generalized epilepsy in (Hamandi et al. 2008).

12.3.1 Model-Based Analysis of fMRI Time-Series Data

The basic strategy for the analysis of fMRI data aims at identifying the voxels at which the BOLD signal is significantly correlated with a postulated timecourse and therefore can be reframed as the problem of identifying the sources of signal variance.

12.3.1.1 Preprocessing

It has been shown that a large proportion of the variance in fMRI timeseries can be attributed to head motion (Friston et al. 1996). Therefore, the first step of the fMRI processing pipeline usually consists of the spatial realignment of the serially acquired scans (Friston et al. 1995). This step is commonly followed by spatial smoothing to boost the signal of interest according to the matched filter principle and to make the data conform better to the assumptions of Gaussian random field (GRF) theory, which is used to make inferences in the classical statistical framework (see below). The amount of smoothing must be chosen by considering the expected spatial scale of the haemodynamic changes and the need for the degree of data smoothness to be substantially greater than the voxel size (see Penny and Friston, Classical and Bayesian Inference in fMRI, in: Human Brain Function; see Josephs and Henson (1999) for a detailed discussion of event-related fMRI data analysis).

The rest of the analysis pipeline focuses on the derivation of maps consisting of voxels for which changes in the BOLD signal can be related to the aspect of brain activity which is of interest to the investigator.

12.3.1.2 The General Linear Model (GLM) and Statistical Inference

The most commonly used fMRI data analysis strategy relies on fitting a general linear model (GLM) to the data (Worsley and Friston 1995). A GLM consists of a set of equations expressing the predicted fMRI signal timecourse as a weighted sum of linear terms representing the effects of interest and confounds (i.e. effects of no interest such as movement). The GLM is therefore an expression of the assumption that fMRI changes can be linearly related to the experimental effects at every voxel. In the absence of prior localization-related hypotheses about this relationship, as is commonly the case in most fMRI studies, the same GLM (set of linear equations) is estimated (i.e. fitted to the data) at every brain voxel, resulting in estimated weights. The localizing information provided by fMRI derives from the variability of resulting weights across voxels.

This section provides a brief introduction to the GLM, focusing on model specification and statistical inference; explanations of model estimation and statistical models can be found in (Worsley et al. 2002; Lindquist 2008) or in open source software manuals (e.g. http://www.fil.ion.ucl.ac.uk/spm/doc/manual.pdf). Note that the GLM approach is closely related to the often-used correlation analysis and represents a generalization of the latter that is capable of handling multiple linear regressions corresponding to multiple effects of interest.

In the following we will focus exclusively on classical estimation and inference; the reader is invited to consult (Friston et al. 2002) for a comparative discussion of the classical and Bayesian approaches.

Building a GLM

The fMRI signal at any given voxel is represented as a vector of serial observations, y_i, $i = 1 \ldots N$, where N is the total number of observations (scans). Each observation y_i is modelled as a weighted sum of x_k ($k = 1 \ldots K$) "regressors", where K is the number of effects represented in the model, and the residual (zeromean) error e_i,

$$e: \; y_i \; = \; \beta_1 x_{i1} \; + \; \beta_2 x_{i2} \; + \; \ldots \; + \beta_K x_{iK} \; + \; e_i, \tag{12.1}$$

where β_j are the unknown weights for each of the K effects; the βs are usually referred to as the model parameters. Expressed in vector and matrix form, we have

$$Y \; = \; \mathrm{X}\beta \; + \; e. \tag{12.2}$$

The matrix **X** represents the modelled effects and is known as the design matrix. The aim of the GLM estimation procedure is to estimate the model parameters, i.e. vector β, at every voxel.

Regressors are usually categorized as effects of interest or effects of no interest (i.e. confounds). The objective of this dichotomy is to separate signal from noise in all its forms, such as noise associated with instrumental, physiological or other effects (body motion) not related to the specific experimental question.

Regressors of interest therefore model the part of the fMRI signal that relates to the experimental events or conditions (stimuli, responses, epileptic spikes, EEG alpha power, etc). Regressors representing the effects of interest are typically obtained by convolving impulses or boxcar functions, which are mathematical representations of the events or conditions of interest, with a model of the event-related fMRI response such as the canonical haemodynamic response function (HRF) or other basis set (e.g. inclusion of additional time and dispersion derivatives; Fourier expansion; finite impulse response). The choice of a specific mathematical representation for the events of interest is dictated by the nature of the events. In the case of a very brief external stimuli or spontaneous epileptic spikes, the events are typically represented by a stick (delta) function (epileptic spikes span approximately 100 ms, which is very short in terms of fMRI; although this duration can vary in a subject, the effect of spike length is rarely taken into account (Bagshaw et al. 2005) and spikes are typically represented as "'zero-duration"' events). In contrast, runs (or bursts) of epileptic spikes may be represented as series of individual stick functions, each presenting a spike, or as variable-duration blocks. For continually varying brain activity, such as brain rhythms, the EEG signal power may be used as a mathematical representation of the neuronal activity. The choice of haemodynamic basis set reflects a number of considerations: for example, one may wish to estimate the shape of the event-related BOLD change rather than assume any particular shape, in which case a flexible model is required using a basis set consisting of multiple functions over a shorter or longer time window than the canonical HRF; alternatively, by restricting the basis set to a single function, effects that match this

function can be detected with maximum sensitivity; see Josephs and Henson (1999). Each of these choices corresponds to a model to be tested, expressing a specific set of assumptions about the relationship between stimulus (when present), neuronal response and haemodynamic signal. This will be the subject of further discussion in forthcoming sections on specific EEG-derived modelling strategies.

Regressors of no interest are introduced to attempt to model the remainder of the fMRI signal. Examples of such regressors are: structured noise, which may include movement-related signal changes, and can be modelled using there alignment parameters of the fMRI timeseries; and slow fluctuations due to drift in scanner sensitivity, which can be modelled as a sum of low-frequency sine and cosine waves. When modelled accurately, the inclusion of such effects can be important, as it permits a more reliable estimation of the coefficients of the GLM corresponding to the effects of interest and increases the level of confidence in the findings (Lund et al. 2005). For example, if the regressor of interest varies slowly and is not orthogonal to the slow drifts, part of the energy of the slow drift could be wrongly attributed to the regressor of interest (i.e. the corresponding coefficient would be overestimated).

Within the classical framework, parameter estimation proceeds using *ordinary least squares*, a standard methodology which aims to minimize the residual sum of squares, i.e. the sum of the squared difference between the predicted signal change and the observations (sum of e terms in Eq. (12.1)). For the GLM, this procedure guarantees maximum likelihood estimates, which is an important, often-cited statistical concept. It means that the estimated parameter values are the most probable given the data.

An important issue when building a GLM is that of correlation (i.e. non-orthogonality) between regressors, which can result in loss of sensitivity. This may be particularly problematic in models that contain several event-related parametric factors and require an orthogonalization procedure (Eichele et al. 2005). Another issue concerns the linearity between EEG and fMRI that is implied in the construction of a parametric regressor. Such linearity may not be guaranteed (Vazquez and Noll 1998; Wager et al. 2005; Wan et al. 2006), but the large literature using the linear model suggests that it is a reasonable assumption. Moreover, linear analysis may still capture some nonlinear effects (Deneux and Faugeras 2006). Additional regressors can also be added to a GLM (with the parameters elevated to the power of 2, 3, etc.) in order to model nonlinear effects (Friston et al. 1998).

Statistics

The goal of statistical inference in fMRI within the GLM framework is to test whether the amplitude of β (or a combination of coefficients) is significantly different from zero. A linear combination of coefficients is called a contrast. For example, in a task involving an active condition (corresponding to β_1) and a reference condition (corresponding to β_2), the contrast would be $(\beta_1 - \beta_2)$.[1] The statistical significance of such a contrast can be tested with a t statistic:

[1] Corresponding to contrast vector [1, –1] in the language of the SPM software.

$$T = (\beta_1 - \beta_2) / std\ (\beta_1 - \beta_2) \sim (\beta_1 - \beta_2) / S(\beta_1 - \beta_2) \tag{12.3}$$

where std (β) is the estimated standard deviation of β, which is proportional to the sum of the squares of the residuals, $S(\beta)$. Taking the simple case of a GLM with a single regressor of interest and its corresponding parameter, β, we can use such a t statistic

$$T = \beta / std\ (\beta) \tag{12.4}$$

To test the hypothesis, $\beta > 0$. This is the simplest contrast and is commonly used to test whether a predicted experimental effect (e.g. associated with a simple ON-OFF stimulus) is likely to be present in the data.

Another option is to test whether at least one coefficient within a set is different from zero. This can be necessary when the activity of interest is modelled by several regressors, such as in models using a basis set consisting of more than one function. For example, in order to test for departures of the haemodynamic response from the canonical HRF, it can be useful to include the derivative of the HRF into the model in addition to the canonical HRF to map brain regions for which the BOLD signal can be represented by any linear combination of the canonical HRF and its temporal derivative. This can be accomplished using an F test, which is essentially a generalization of the t test that allows us to test a hypothesis on a subset, β_1, of the parameters β; for example, that $\beta_1 = 0$. An F statistic can be devised by considering the full model and the reduced version of the model that is obtained if the hypothesis is true ($\beta_1 = 0$). Representing the reduced model by the subset of parameters, β_2, the appropriate F statistics:

$$F = \frac{\frac{\left[S(\beta_2) - S(\beta)\right]}{p - p_2}}{\frac{S(\beta)}{N - p}}, \tag{12.5}$$

where $S(\beta)$ is the squares of the residuals for the full model (and $S(\beta_2)$ for the reduced model), p is the rank of the design matrix for the full model (and p_2 for the reduced model) and N is the number of scans. An explanation of the implementation of Eq. (12.5) in the SPM software using contrast matrices can be found in (Penny and Friston 2004) and in online SPM documentation.[2] An example of its application using a Fourier basis set can be found in the Chap. 17 (Fig. 12.1).

Significance of BOLD Changes

The above process results in 3D maps representing the t or F statistic of the effect of interest at every voxel: the so-called statistical parametric maps or SPMs. The statistics are derived independently for each voxel, which can easily number in the tens of thousands in the brain—hence the "massively univariate analysis" terminology often used in the context of fMRI. However, the significance of the deviations

[2] https://www.fil.ion.ucl.ac.uk/spm/doc/books/hbf2/.

from the null hypothesis (i.e. the conversion of t statistics to Z scores) must be assessed in relation to the maximum score or the size of an activated region. Crucially, only the false-positive rate (type I errors) can be controlled. Type II error control is generally neglected since it is difficult to specify a quantitative alternative hypothesis in fMRI as is required for a power calculation. To put it simply, the lack of activation does not prove that there is no underlying brain activity.

Numerous means of calculating significance thresholds for functional MR images have been developed. Seminal work was based on the theory of random Gaussian fields (Worsley et al. 1992). This is a parametric framework that controls for the fact that, in the null hypothesis of no significant effect, the maximum value of the map can be above the threshold with a p value of α (typically, $\alpha = 0.05$). Such a threshold is corrected for the large multiple comparison problem that arises when simultaneously testing a large number of voxels and corresponds to the family-wise error rate (FWE). The importance of correction for multiple comparisons and controlling for false positives has been emphasized (Bennett et al. 2009; Bennett and Miller 2010). Another option, within the same framework, is to use a threshold based on the extent of a given cluster of activated voxels above an uncorrected threshold with a low p value (typically, $\alpha = 0.001$) (Poline et al. 1997; Cao 1999). The thresholds obtained with random field theory are typically high and require a large level of image smoothing (typically with a filter FWHM of 10–15 mm). To be noted, the specificity of cluster thresholding has been criticized (Woo et al. 2014; Eklund et al. 2016). A second alternative is to use the threshold that allows a given portion of activated voxels to be false detections. This is the "false detection rate" (FDR), which is a less conservative than the family-wise statistic on the maximum (Genovese et al. 2002). We note that the classical interpretation of FDR has been challenged (Chumbley and Friston 2008). A third alternative is to derive the distribution of the statistic in the null hypothesis directly from the data, for example, by shuffling the labels of active and control conditions (Bullmore et al. 2001). This is the nonparametric framework, which allows the structure of the data (spatiotemporal correlations) to be taken into account explicitly, and which handles the multiple comparison issue in a straightforward manner (Nichols and Holmes 2002; Meriaux et al. 2006).

12.3.2 EEG-Derived GLM: Use of Event on sets and Illustration in Epilepsy

The study of spontaneous brain activity using EEG–fMRI raises a number of important issues related to GLM building, namely the identification and categorization of events of interest, the mathematical representation of those events and the choice of a basis set for the HRF, as well as model comparison. Due to fluctuations in the background EEG, defining the baseline (control state) is also a challenge.

Since the first applications of EEG–fMRI were in patients with epilepsy, the first attempts at data integration were geared towards the study of subclinical (without behavioural manifestations), randomly occurring, epileptic discharges (for reviews

on the seminal studies, see Salek-Haddadi et al. (2003a), Gotman et al. (2004), Lemieux (2004), Gotman et al. (2006); for more recent reviews see Centeno and Carmichael (2014), van Graan et al. (2015)). The aim of this strategy is to find regions of BOLD change linked to the discharges, which can potentially help in presurgical evaluation (Pittau et al. 2014). The timing of interictal epileptiform discharges (IED) is used in an event-related fMRI analysis to create regressors representing the effects of interest, by convolving the event onsets represented as delta functions[3] with a model of the event-related haemodynamic change in the form of a haemodynamic basis set (Fig. 12.2).

One difficulty of EEG-fMRI in epilepsy is that every patient is a particular case, and clinical results are needed for individual patients. This implies that processing has to be performed at the single-subject level, contrary to task-related analyses that can use large cohorts. In addition, the spatiotemporal aspects of IEDs vary greatly between patients and can also vary in time for any given patient. Therefore, although conceptually simple, this approach relies on the detection of those events—a subjective process—and their categorization. Visual or automatic detection of epileptic spikes can be challenging and can impact statistical results (Flanagan et al. 2009). Classification of spikes is important because each regressor corresponds to a hypothesis that can be phrased as follows: there are brain regions in which the BOLD signal change *averaged across the events* is nonzero. This implies that the events grouped into each regressor are haemodynamically consistent. It has thus been proposed to cluster interictal discharges based on the waveforms as observed on the sensors (Pedreira et al. 2014). It is to be noted that consistency at the level of the sensors does not guarantee consistency at the voxel

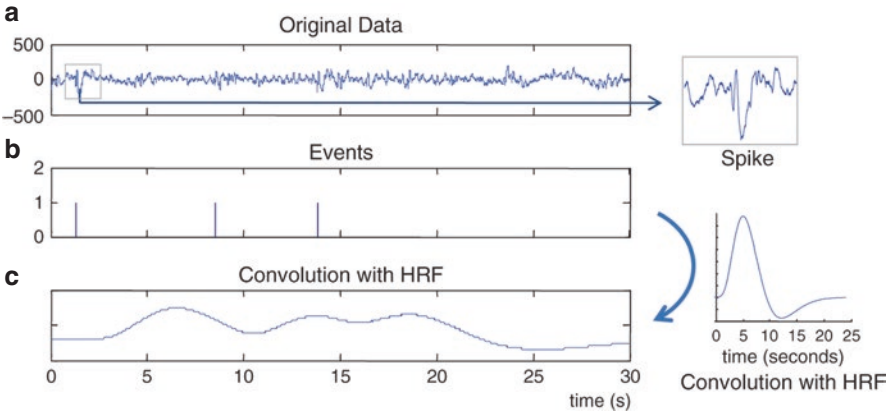

Fig. 12.2 (**a–c**) Modelling of fMRI signal timecourse using event timing alone and basis set consisting of a single function. (**a**) Each event (here, interictal epileptic spikes) is marked by visual inspection of the EEG data recorded in the scanner. (**b**) On set vector: series of identical impulse ("delta") functions. (**c**) Corresponding regressor for a general linear model (GLM) obtained by convolving the events with a canonical HRF

[3] Usually implemented as a stick function of unitary amplitude.

level, nor in terms of haemodynamic responses. Another option is to use detections based on ICA components (Ossadtchi et al. 2004; Malinowska et al. 2014), which can potentially separate processes corresponding to separate regions as suggested by their dipolar nature (Delorme et al. 2012)—although this is not guaranteed. A last option is to use reconstruction at the source level in order to build regressors (Vulliemoz et al. 2010). More sophisticated approaches can take into account various morphological aspects of the IED, such as duration and amplitude (Mirsattari et al. 2006; LeVan et al. 2010). It has also been proposed to filter the EEG by the topography of interictal spikes and/or artefacts, in order to improve signal-to-noise ratio (Siniatchkin et al. 2007; Grouiller et al. 2011; Tousseyn et al. 2014).

The haemodynamic basis set can consist of a single function such as the canonical or standard HRF, or a multiplicity of functions such as assets of time-shifted standard HRFs, the finite impulse response (FIR) and Fourier basis sets (Josephs et al. 1997; Josephs and Henson 1999; Bagshaw et al. 2004). As alluded to in the previous section, models based on a single function are optimal for the detection of BOLD changes that match that function (this is the "matched filter" principle), whereas models based on basis sets with multiple functions can be used to assess the shape of the event-related BOLD changes and to map interregional variations in the timecourse of the changes.

Variability in the timecourse of the IED-related BOLD changes has been shown to impact on detection efficiency (Kang et al. 2003; Bagshaw et al. 2004; Lu et al. 2006; Salek-Haddadi et al. 2006; Lemieux et al. 2008; Grouiller et al. 2010; Storti et al. 2013). BOLD changes time-locked with EEG events may appear earlier or later than predicted by the standard model, in epilepsy and in response to normal brain rhythms (Feige et al. 2005; de Munck et al. 2007; Lemieux et al. 2008), sometimes even prior to scalp EEG changes (Hawco et al. 2007; Pittau et al. 2011). Such observations may be seen as highlighting a limitation of the scalp EEG as a basis for modelling whole-brain activity, but also as an example of the added value of the combined method. However, the lack of a proper assessment of response variability using the specific modelling approaches used in the above studies in relation to event-related BOLD effects in healthy brains limits our ability to interpret the observed deviations as being specifically related to epilepsy (Rollings et al. 2016). In particular, the often-cited study by Aguirre on the variability of the response to a reaction-time motor task is based on a Fourier basis set consisting of only three sines and three cosines, which is less flexible than most models used in the above epilepsy studies (Aguirre et al. 1998). More work is needed, including animal and computational models, in order to understand the basis of variability in the HRF in terms of physiological processes (Mirsattari et al. 2006; Vanzetta et al. 2010; Voges et al. 2012; Saillet et al. 2016).

The above issues are ultimately related to model selection, which is a fundamental problem of science and is particularly troublesome in the classical statistical framework, which usually favours complex models over simple models since the former tend to "mechanically" explain a greater proportion of the

variance.[4] Nonetheless, it is relatively common practice to compare models in EEG–fMRI, particularly when exploring the relationship between EEG and fMRI. This is often done by selecting the way in which regressors expressing different model variants are incorporated into GLMs. By incorporating all effects of interest within a single, embedded model, one can test for the significance of the variance explained by specific factors through appropriate *F* contrasts (see Salek-Haddadi et al. (2006) and Liston et al. (2006b) for illustrations). An alternative is to build a set of separate GLMs. In this approach, statistical correction factors must be applied to account for multiple models, and selection of the result ("best" model and associated map) requires the application of an additional criterion, such as the extent of activation or *t* score (Bagshaw et al. 2004). The Bayesian inference methodology offers an elegant framework for dealing with parameter estimation and model comparison and has been used in HRF estimation (Marrelec et al. 2003). Estimation and detection normally impose the need to use two different datasets in order to avoid overfitting of the noise, although an interesting avenue (again permitted within the Bayesian framework) is to jointly estimate the HRF and detect activated voxels (Lu et al. 2006; Makni et al. 2008; Chaari et al. 2013).

Evidently, the data acquisition and analysis strategies described above are fundamentally different from conventional "activation" fMRI experiments in that there is no explicit reference or control state. In the resting state, fluctuations in brain rhythms are accompanied by typical BOLD patterns (Goldman et al. 2002; Laufs et al. 2003b; Mantini et al. 2007b). Therefore, background EEG may be used to improve models of the baseline fMRI signal fluctuations (Tyvaert et al. 2008) in addition to the usual confounding effects of respiration, the cardiac cycle, motion and instrument-related effects (e.g. low-frequency drifts).

The exquisite temporal resolution of EEG recorded simultaneously with fMRI also offers the possibility of modelling MR signal changes in the latter at a much faster timescale than the BOLD effect, namely the neuroelectric MR effect (sometimes referred to as neuronal current MR imaging) (Bodurka and Bandettini 2002; Hagberg et al. 2006). By precisely marking the onset of generalized spike and wave in relation to the acquisition of individual MR slices, Liston et al. employed a basis set consisting of a series of FIRs to study MR signal changes at a 30-ms timescale (Liston et al. 2004). Using a phase-cycled stimulus-induced rotary saturation approach with spin-lock preparation Kiefer et al. recently showed that this neuroelectric effect is related to IEDs and can be used to inform source reconstruction of IED (Kiefer et al. 2016).

[4] The Bayesian approach is probably preferable as it allows inclusion of an "Occam factor" in the comparison, i.e. a penalization of model with many parameters.

12.3.3 EEG-Derived GLM: Parametric Design and Single Trial

The use of single-trial variability and spectral information, which are widely applied in sensory and cognitive neuroscience applications, leads to event-related designs similar to those described above in epilepsy, differing mainly in the nature of the EEG information that is included in the GLM analysis.

A strategy employed to investigate the coupling between the EEG and fMRI signals is the manipulation of one or several parameters within the protocol and the comparison of the corresponding fluctuations in the EEG and fMRI signals. As described in the Chap. 1, this type of study may be done in separate or simultaneous data acquisition sessions depending on the experimental conditions and the type of inference that one wishes to make. For example, by varying the intertrial interval or stimulation intensity, one is able to divide the trials into groups, resulting in one EEG and one fMRI analysis per group. One can then test whether the two signals fluctuate similarly across groups (Horovitz et al. 2004). This approach has been applied for evoked potentials (Liebenthal et al. 2003), ERP fluctuations of face selectivity (Sadeh et al. 2010), high-frequency (gamma) activity (Foucher et al. 2003) and even ultra-high-frequency (600 Hz) responses (Ritter et al. 2008).

The inclusion of parameters derived from a single-trial analysis of the EEG data, i.e. from the individual EEG responses to the stimuli, offers the possibility of exploring the relationship between EEG and haemodynamic signals much more deeply; for example, the BOLD correlates of the ERP amplitude (Debener et al. 2005; Eichele et al. 2005; Bénar et al. 2007; Walz et al. 2014; Wirsich et al. 2014), latency (Bénar et al. 2007; Walz et al. 2014) or the amplitude of high-frequency oscillations (Mulert et al. 2007). See Fig. 12.3 for a description of parametric analysis and Fig. 12.4 for an application.

The analysis of single-trial data is hampered by a low signal-to-noise ratio compared to averaged responses. Single-trial analysis techniques designed to improve signal-to-noise ratio based on feature extraction can be used fruitfully in combined EEG–fMRI analysis (Mayhew et al. 2006; Philiastides and Sajda 2006), as well as in all fields of EEG processing, for example, brain–computer interfaces (Cincotti et al. 2003). Several aspects of the activity can help to characterize intertrial fluctuations: temporal structure, its time–frequency structure (Quian Quiroga and Garcia 2003; Wang et al. 2007; Benar et al. 2009), its spatial configuration across sensors or a combination of these (Ranta-aho et al. 2003).

Various techniques have been proposed to improve the signal-to-noise ratio of single trials. Instead of relying on single trial fluctuations of one electrode it has been proposed to use combined electrode measures (Fuglo et al. 2012), wavelet denoising (Eichele et al. 2005; Bagshaw and Warbrick 2007) or independent component analysis (ICA) (Debener et al. 2005; De Vos et al. 2012; Warbrick et al. 2014). When applied on an individual level, ICA can give inconsistent results across subjects depending on the quality of the data and of the decomposition. This can be

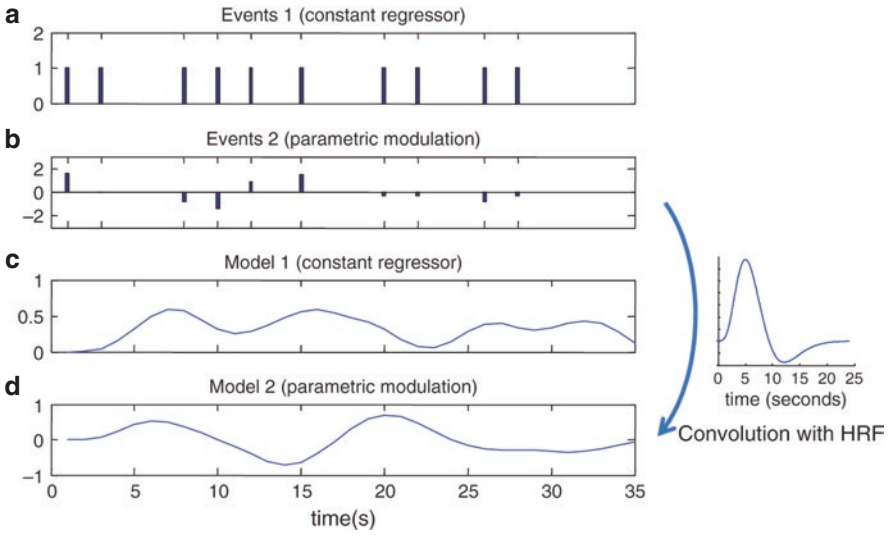

Fig. 12.3 (**a–d**) Modelling of fMRI data using parametric modulation. (**a**) Vector of event on sets as in Fig. 12.2; (**b**) EEG event feature vector (e.g. amplitude, duration). (**c**, **d**) Corresponding regressor obtained by convolution of (**a**) and (**b**), respectively, with the canonical HRF. When combined in a single GLM, statistical maps can be obtained showing voxels for which each effect explains a significant amount of additional variance by defining appropriate contrasts (Salek-Haddadi et al. 2006)

improved by analysing the ICA on a group level (Eichele et al. 2011) which allows several single trial estimates of different components in an EEG-fMRI paradigm to be extracted (Wirsich et al. 2014). Alternatively, to improve the single trial quality, it has been demonstrated that a classifier can learn the single trial content that best discriminates two different stimuli. On a trained model the classifier output of each single trial can be used as a regressor in an EEG-Derived GLM (Parra et al. 2002; Goldman et al. 2009; Walz et al. 2014). This approach can not only be used in combination with a GLM but also in combination with an fMRI encoder (Muraskin et al. 2017).

ICA is a good approach as a purely data-driven way of exploring new data or when using only one stimulus type. Still, hypothesis-driven approaches like classification of single trials will provide more specific and interpretable estimates (Calhoun and Sui 2016). Future directions may fuse these approaches by adding a priori information into source separation (Porcaro et al. 2010).

Source localization or spatial filtering can also serve as a way of denoising, with the additional potential advantage, given an appropriate model, of providing spatial information on the processes of interest (Brookes et al. 2008). This is a very promising approach, as it would permit the fMRI signal to be correlated with the source of EEG data originating from the same region (Grouiller et al. 2011), thereby removing one source of ambiguity.

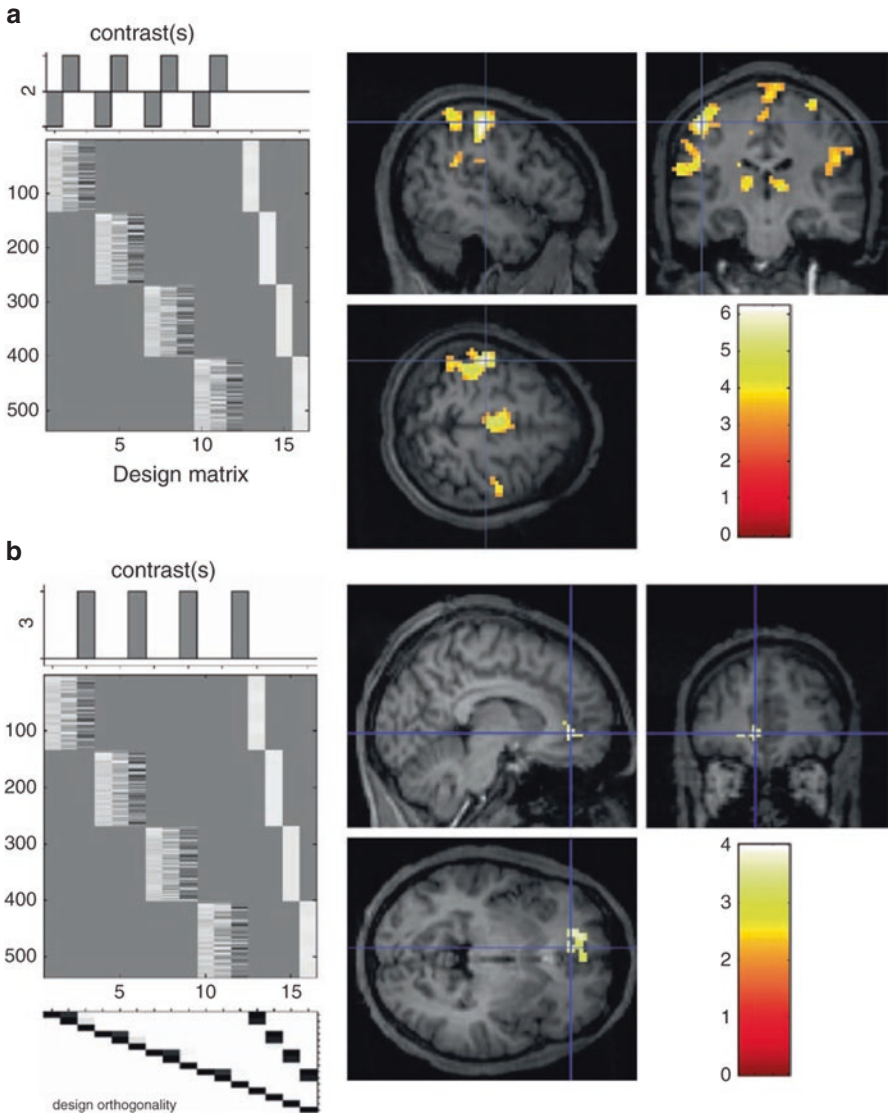

Fig. 12.4 (**a**, **b**) EEG–fMRI study in an auditory odd ball experiment. Comparison of fMRI activation for (**a**) rare events and (**b**) parametric modulation based on P300 amplitude at Cz (subject 1 of Bénar et al. 2007). The detailed design matrix is presented on the left column. There are four runs and three regressors per run: frequent events, rare events and parametric modulation (see Fig. 12.3). In (**a**) the contrast is "rare–frequent". In (**b**) the contrast only includes the parametric regressor

12.3.4 EEG-Derived GLM: EEG Spectrum

One of the most important uses of EEG–fMRI to date has been in identifying the brain regions that co-vary with changes in brain rhythms and more generally EEG spectral power. Although oscillatory activity has been studied since the earliest days of EEG (Berger 1929), locating the cortical generators of this activity using EEG alone is difficult because of the ill-posed nature of the inverse problem (Geselowitz 1967). fMRI provides an alternative method that has the potential advantage over EEG of being capable of recording activity directly from subcortical structures or more recently, due to ultra-high field, from different cortical laminae (Yacoub et al. 2008; Kashyap et al. 2018; Fracasso et al. 2018, for review: Dumoulin et al. 2018).

Studies of spectral power can be split into two basic categories: those which examine spontaneous fluctuations and those which use an experimental manipulation to modify spectral power in a specific frequency range. The analytical approach is essentially the same for both types of data and is conceptually similar to what has been discussed previously. Typically, EEG data are filtered into short epochs of the order of a second, and power in one or more frequency bands is quantified for each epoch. In most applications, the power timeseries is convolved with a postulated kernel function representing the BOLD change per impulse input (usually the standard haemodynamic response function) and entered as a regressor in a GLM analysis (Fig. 12.5). The choice of EEG channel or group of channels for the power calculation requires careful consideration (e.g. see Laufs et al. (2003a)). This kind

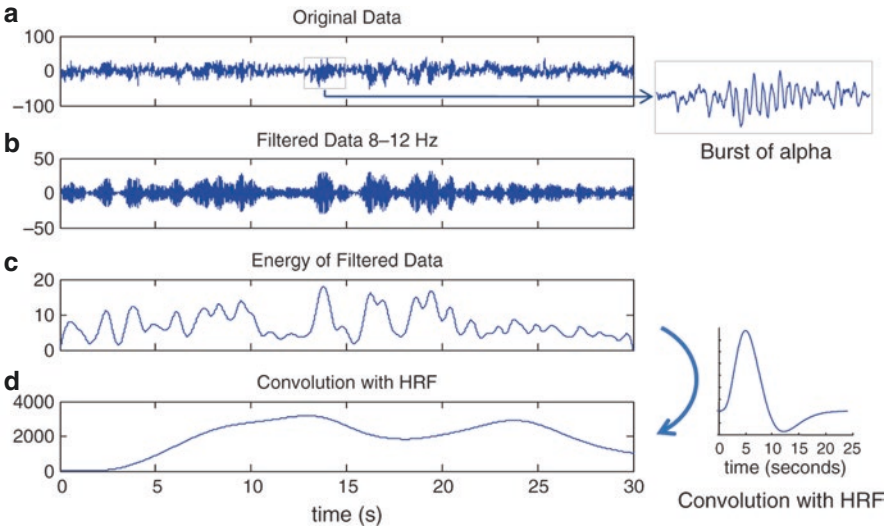

Fig. 12.5 (**a–d**) Modelling of fMRI timeseries using the energy within a frequency band. (**a**) Original EEG data, where several alpha wave bursts can be seen. (**b**, **c**) Energy in the 8–12 Hz band, using a sliding window Fourier transform (Goldman et al. 2002). (**d**) Regressor obtained by convolving energy with canonical HRF

of study is particularly demanding on EEG quality because of the potential for artefacts to corrupt the power spectrum (see the Chaps. 8 and 9).

Early examples of this type of study were based on interleaved acquisitions, with posterior alpha power extracted from simultaneously acquired EEG–fMRI data (Goldman et al. 2002; Laufs et al. 2003a). Although this technique was originally applied to the study of the power of the alpha rhythm (Moosmann et al. 2003; Feige et al. 2005; Goncalves et al. 2006; de Munck et al. 2007, 2009; Sadaghiani et al. 2010) and to alpha phase synchronization (Jann et al. 2009; Sadaghiani et al. 2012), it can also be used to examine oscillations at higher or lower frequency. Laufs et al. (2003b) also quantified beta power and included that as a regressor in the fMRI analysis and noted the similarity between the regions identified and those associated with the default mode network (DMN) (Raichle and Snyder 2007). Mantini and colleagues found different spatial patterns of fMRI response across EEG frequency bands (Mantini et al. 2007b), while Scheeringa et al. related frontal theta power to the DMN (Scheeringa et al. 2008). Studies on event-related synchronization and desynchronization (ERD/ERS Pfurtscheller and Lopes da Silva (1999)) using EEG–fMRI have focused on the BOLD correlates of low-frequency oscillations in the theta and delta range (<7 Hz) during hyperventilation (Makiranta et al. 2004) and mental arithmetic (Makiranta et al. 2004; Sammer et al. 2007), as well as fundamental questions about neurovascular coupling related to the alpha and beta bands (Mullinger et al. 2013). During a face integration task Kottlow et al. showed that global field synchronization of the gamma band is correlated to the BOLD signal (Kottlow et al. 2012), while BOLD activity was also found to correlate with the auditory gamma response (Mulert et al. 2010). Scheeringa et al. demonstrated frequency specific independent BOLD-EEG associations for high and low frequencies during a visual attention task (Scheeringa et al. 2011). By studying cortical depth representation of the relation between trial-by-trial variation in BOLD and EEG power during a visual attention task, different profiles over laminar depths in the visual cortex were assigned for α, β and γ-oscillations (Scheeringa et al. 2012). Scheeringa and Fries were able to further our understanding of the relationship between specific rhythms and layer-specific anatomical projections (Scheeringa and Fries 2019). Feed forward projections (predominantly originating from supragranular layers and terminating in granular layer (layer 4)) being mainly ruled by gamma-band influences, and feedback projections (predominantly originating from infragranular layers and terminating outside granular layer) being mainly ruled by alpha- and/or beta-band influences (Scheeringa and Fries 2019).

Some work has been done at lower frequencies of the order of 1 Hz or less (Khader et al. 2007). For example, by using ICA decomposition of the EEG, it has been demonstrated that the BOLD signal correlated with infraslow EEG (0.01–0.1 Hz) power (Hiltunen et al. 2014). Parkes and colleagues used the same methodology to examine the BOLD correlates of the post-movement beta rebound (Parkes et al. 2006). See the Chap. 15 for a review of the findings. The presented approaches all assume a static linear relationship between BOLD activity and EEG frequencies. More recent work demonstrate a dynamic relationship of alpha and BOLD activity

on a trial to trial basis (Mayhew et al. 2013a) and during the resting state (Mayhew and Bagshaw 2017). Taking advantage of the capability of EEG to easily track vigilance states derived from a combination of different EEG bands, Falahpour et al. created a correlated vigilance template for fMRI resting state activity (Falahpour et al. 2018).

Using an approach similar to (Liston et al. 2006b), Mandelkow et al. attempted to detect fast (neuronal current-related) signal changes linked to alpha power, but were hampered by the pulse artefact (Mandelkow et al. 2007). More generally, difficulties that can arise from narrow-band filtering are presented in Sect. 12.5.3.2. It has been also shown that some of the BOLD-alpha coactivations are correlated to respiration (Yuan et al. 2013), suggesting the importance of removing physiological artefacts in both EEG and fMRI signals (Perlbarg et al. 2007). It is also worth remembering that even with the most advanced and effective methods for artefact correction, residual artefacts can still corrupt the EEG signal and lead to spurious but plausible EEG-BOLD correlations (Jansen et al. 2012; Fellner et al. 2016).

12.3.5 Multivariate Analysis

The analysis technique outlined above is based on the interrogation of the fMRI signal through the same EEG-derived model at each and every voxel and is therefore often referred to as a *massively univariate* approach. An alternative approach is the identification of meaningful patterns (e.g. across multiple voxels or EEG channels) based on more generic assumptions for the properties of signals and their generators (Martinez-Montes et al. 2004). Multivariate methods have the advantage of reducing the dimensionality of the data and also potentially finding subtle patterns that are "diluted" across many voxels.

Several multivariate techniques have been proposed for the analysis of biophysical signals: PCA (Rosler and Manzey 1981; Lai and Fang 1999; Dien et al. 2007), singular value decomposition (SVD), nonlinear PCA (Friston et al. 1999; Thirion and Faugeras 2003), canonical component analysis (Vitrai et al. 1984; De Clercq et al. 2006), partial least squares (PLS) analysis (McIntosh and Lobaugh 2004), ICA (Makeig et al. 1997; Kobayashi et al. 1999; Vigario et al. 2000; Jung et al. 2001; James and Gibson 2003) and parallel factor analysis (Miwakeichi et al. 2004).

The most commonly applied multivariate technique for EEG-fMRI is ICA (Jutten and Herault 1991; Comon 1994). It can be used to decompose EEG signals (N channels × P timepoints) into a set of fixed topographies (across the N channels) and a corresponding timecourse, with the constraint that the timecourses are maximally independent (temporal ICA). Spatial ICA, whereby a constraint of maximally independent spatial patterns is employed, has also been used successfully to identify "sources" in fMRI. The fact that the ICA constraint is applied along the spatial dimension for fMRI data mainly stems from the fact that this is the largest dimension (contrary to EEG where it is time), and ICA requires many points in

order to give stable results. Several algorithms have been proposed for computing such decompositions (Bell and Sejnowski 1995; Cardoso 1999; Hyvarinen and Oja 2000).

ICA can be used to identify and subsequently remove artefacts on the EEG traces (Benar et al. 2003; Srivastava et al. 2005; Briselli et al. 2006; Nakamura et al. 2006; Bagshaw and Warbrick 2007; Debener et al. 2007; Mantini et al. 2007a), or on the fMRI signal (McKeown et al. 2005; Bagshaw and Warbrick 2007). This approach is potentially very useful, but one of the major difficulties is the identification of the components to be removed (LeVan et al. 2006; Ting et al. 2006; Perlbarg et al. 2007; Tohka et al. 2008; Viola et al. 2009). Moreover, the activity to be removed (e.g. the pulse-related artefact) may not have a stable spatiotemporal pattern, which violates one of the basic assumptions of ICA, rendering the process suboptimal (Wallstrom et al. 2004; Debener et al. 2008). Conversely, ICA has been used to identify signals representing activity of interest (McKeown et al. 1998; Jung et al. 2001; Duann et al. 2002; Rodionov et al. 2007). As discussed in Sect. 12.3.3 this has two attractions: signal denoising, which is very useful for single-trial analysis (Bagshaw and Warbrick 2007; De Vos et al. 2012; Warbrick et al. 2014; Wirsich et al. 2014), and separation of activity from different sources (with a source corresponding to a brain region or to a synchronous network). Such an approach has been used for single-trial EEG–fMRI studies (Debener et al. 2005). Beyond single trials this ICA approach can also be used to extract cleaned continuous EEG timecourses which are then fused with fMRI using a GLM (Labounek et al. 2019). A more extreme form of this use of ICA is to constrain the decomposition to optimize the detection of a particular feature of interest (e.g., an evoked potential peak or frequency band (Porcaro et al. 2010)). A joint ICA approach has also been proposed with both EEG and fMRI signals considered together (Calhoun et al. 2006; Eichele et al. 2007; Moosmann et al. 2007; Bridwell et al. 2013). Apart from fusing the modalities at signal level, ICA has been used to fuse EEG- and fMRI-derived functional connectivity (Wirsich et al. 2020a).

We note in passing that ICA has also been employed to extract and compare fMRI dynamics to EEG spectral power timecourses or states in an attempt to relate band-specific EEG dynamics or EEG states to large-scale fMRI networks (Britz et al. 2010; Lamos et al. 2018).

Another multivariate approach to the fusion problem is to perform a spatial decomposition of the EEG data into different microstates (Lehmann and Skrandies 1984) by using clustering analysis (Britz et al. 2010; Musso et al. 2010), ICA (Yuan et al. 2012) or time-frequency decomposition (Schwab et al. 2015). Onsets of these microstate features can then be correlated to the BOLD timecourses. Decoders of EEG and fMRI activity that learn task-specific multivariate and multimodal patterns of activation have also been applied (Muraskin et al. 2017), while Meir-Hasson et al. used EEG-fMRI recordings and a machine learning approach in order to identify EEG fingerprints that predict BOLD activity of deep brain structures (Meir-Hasson et al. 2014). For a more general review of multivariate machine learning approaches to integrate EEG and fMRI data see (Dähne et al. 2015).

12.3.6 EEG-informed fMRI Functional Connectivity

The models discussed so far only consider local BOLD activation and deactivation linked to metrics derived from EEG recordings. A different perspective is to model the brain as a network as derived from the interregional communication of local brain activity (i.e. functional connectivity, FC (Biswal et al. 2010)). FC in fMRI was first demonstrated in the motor cortex (Biswal et al. 1995) and has since then been generalized to the temporal correlation of different brain regions including the construction of a whole-brain connectivity graph (Achard et al. 2006).

As discussed in the preceding section the relationship between EEG frequency content and BOLD activity during rest is complex, as reflected by the existence of several intrinsic functionally connected networks (the so-called intrinsically connected networks, ICNs, or resting state networks, RSNs), for example. Here we discuss the EEG signatures influencing the magnitude of fMRI-derived FC. This section focuses on results from simultaneous EEG-fMRI only, a general discussion between M/EEG and fMRI connectivity can be found in Sadaghiani and Wirsich (2020).

Since fMRI-FC is generally measured by the temporal correlation over a 10–20 min resting-state recording, EEG power cannot readily be integrated by using a GLM. Different approaches have been proposed to access the dynamic modulations of FC. To link FC changes in a conditional setting, the psychophysiological and modulatory interactions (PPI) approach can be used (Friston et al. 1997). This allows the EEG modulation of the fluctuating connectivity changes to be investigated using a GLM. For example, by using PPI, Scheeringa et al. showed that high and low alpha power states modulate the ongoing connectivity between the visual cortex and the rest of the brain (Scheeringa et al. 2012).

Another approach is to subdivide the timecourses into a series of windows, allowing dynamic functional connectivity analyses. Resting-state functional connectivity has been explored in this dynamic way by using sliding window and time-frequency coherence analysis (Chang and Glover 2010). Applying measures from pairwise BOLD connectivity and frequency specific EEG power in a 2-min sliding window approach, Tagliazuchi et al. showed that alpha and beta power are associated with decreased FC whereas long-range connections were correlated with gamma power (Tagliazucchi et al. 2012b). Considering the different resting state networks of the brain, Chang et al. used a sliding window of 40 s to demonstrate that dynamic FC between the dorsal attention network (DAN) and the default mode network (DMN) is anticorrelated to alpha power whereas theta power is correlated positively (Chang et al. 2013). For a review of time-varying analysis in resting state fMRI, see Hutchison et al. (2013) and Keilholz (2014).

As an alternative approach, using an ICA model Allen et al. showed that fMRI-FC dynamically operates in different reoccuring states that are correlated to co-occuring band-specific EEG power (Allen et al. 2018; Lamos et al. 2018). Furthermore, Keinänen et al. demonstrated that infraslow EEG dynamics are correlated with the fMRI dynamic intra-network FC of the default mode network (Keinänen et al. 2018). Abreu et al. used machine learning methods applied to

EEG-informed dynamic FC and identified different states of fMRI connectivity overtime in patients suffering from focal epilepsy (Abreu et al. 2019). It is also possible to use EEG-based FC measures to inform the BOLD signal, although this has been less widely done. Due to the superior temporal resolution of EEG, FC can be calculated over the duration of the acquisition of one fMRI volume, which enables the use of the previously described GLM approach to predict the BOLD signal based on EEG connectivity (Biazoli Jr. et al. 2013).

Analysing EEG-fMRI dynamics becomes a particularly powerful tool when exploring the co-occurring shifts based on well-studied EEG markers of attention or sleepiness (Tagliazucchi et al. 2013). Tagliazucchi et al. showed that fMRI-FC changes dynamically with the individual drowsiness of subjects (Tagliazucchi et al. 2012b). In addition, Tagliazucchi et al. built a classifier based on EEG sleep stages to learn fMRI functional connectivity patterns associated with sleep (Tagliazucchi et al. 2012a). This classifier was then successfully applied to automatically analyse only fMRI data from a larger cohort (Tagliazucchi and Laufs 2014), suggesting the presence of sleep in ostensibly waking scans. Taken as a primary effect of interest, the duration of sleep stages derived from concurrent EEG-fMRI can also be used in a GLM as a regressor of no interest (not different than, for example, movement parameters) when looking at static FC differences during sleep deprivation (Wirsich et al. 2018). Damaraju et al. used different sleep stages, that were derived from concurrent EEG recordings in the scanner, to show that dynamic fMRI-FC states are depending on the sleep state (Damaraju et al. 2020).

FC-based analyses are not limited to asymmetric analysis based on the use of EEG to inform fMRI measures (or vice versa). Data can also be integrated at a higher level of connectivity-based abstraction. These advanced integration approaches use source reconstruction of the electrophysiological data to map the same 3D brain space as the fMRI data (see Chap. 2). Brookes et al. demonstrated that electrophysiological connectivity derived from the source reconstructed power envelopes of MEG recordings is comparable to fMRI-FC (Brookes et al. 2011), while Deligianni et al. showed that this is equally true when comparing EEG-FC (envelope power) with fMRI during a concurrent EEG-fMRI experiment (Deligianni et al. 2014). More recently it has been shown that concurrent EEG is not only partly correlated to fMRI, but also to structural connectivity estimated using diffusion weighted imaging (Deligianni et al. 2016; Wirsich et al. 2017). Wirsich et al. (2017) demonstrated that functional connectivity as measured by amplitude-corrected imaginary part of the coherency and based on source reconstructed EEG improves the estimation of the functional-structural connectivity relationship as opposed to an fMRI-only model (Wirsich et al. 2017). See Fig. 12.6.

As with many other aspects of EEG-fMRI, additional work is needed to understand how metrics derived from one modality map onto those derived from the other. For example, a change in the temporal correlation between regions measured with fMRI may not necessarily be reflected in the power spectrum of EEG. Wirsich et al. demonstrated that not only EEG power is related to dynamic FC but there exists also a general link between dynamic FC derived from either EEG or fMRI during resting state (Wirsich et al. 2020b). Equally, during different cognitive tasks,

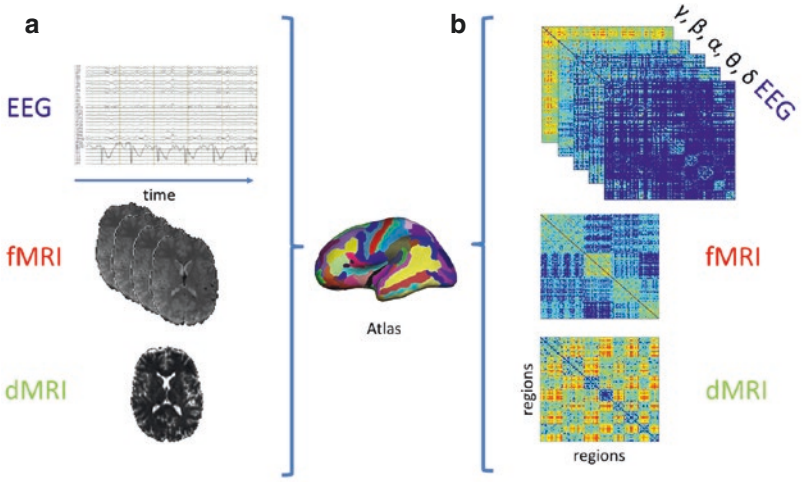

Fig. 12.6 Illustration of multimodal data integration of brain connectivity using concurrent EEG-fMRI and diffusion MRI (dMRI). (**a**) Source reconstructed EEG signal, BOLD activity and fibre tracks derived from dMRI are mapped onto a common anatomical atlas. (**b**) Between each region pair connectivity is derived from temporal correlation of the BOLD timeseries (fMRI) and amplitude-corrected imaginary part of the coherency of the EEG timeseries (band separated). Diffusion connectivity is estimated by counting the number of connecting fibre tracks between each region. The resulting trimodal connectivity matrices are significantly correlated to each other (for more detail see Wirsich et al. 2017).

Abreu et al. observed correlated dynamic FC states derived from both fMRI and concurrently recorded EEG (Abreu et al. 2020).

This dynamic relationship might be particularly critical in conditions where electrophysiological events are specific markers of pathological status such is the case in epilepsy. Using simultaneous intracranial EEG (icEEG) recordings and fMRI in patients suffering from drug-resistant focal epilepsy Ridley et al. have demonstrated opposite patterns of FC as measured by the two modalities simultaneously in the epileptic networks when applying the same connectivity analysis method (Ridley et al. 2017).

12.3.7 Use of intracerebral EEG in the context of concurrent fMRI recordings

During presurgical evaluation of patients with epilepsy, invasive recordings can be performed in order to define the brain region that needs to be resected to render the patient seizure-free. These recordings, performed solely on clinical grounds, provide a formidable opportunity to gather data in humans with unique spatial specificity and signal-to-noise ratio far beyond that available with noninvasive, scalp recordings. There are two types of invasive EEG recordings: electrocorticography,

which places electrode grids at the surface of the brain, and stereo electroencephalography (or "depth EEG"), which implants electrodes directly within the brain tissues, allowing deep brain structures to be targeted (Wennberg et al. 1998; Bartolomei et al. 2017). In addition to their clinical importance in guiding surgical planning, these invasive recordings represent a unique opportunity to validate the findings of noninvasive methods by providing a "ground truth" to EEG/MEG source localization and EEG-fMRI analysis (Benar et al. 2006; van Houdt et al. 2012; Zhang et al. 2012; Grova et al. 2016).

A recently developed avenue consists of recording fMRI simultaneously with intracranial EEG. This permits fMRI analysis to be performed based on patterns (e.g. epileptic form discharges) identified on the EEG recorded intracranially in the same way as described previously for scalp EEG-fMRI and has found application in epilepsy (Vulliemoz et al. 2011; Cunningham et al. 2012; Beers et al. 2015; Chaudhary et al. 2016; Ridley et al. 2017), cognition (Saignavongs et al. 2017) and brain stimulation (Bhattacharyya et al. 2017). Safety issues are of course of paramount importance and must be addressed (Carmichael et al. 2010, 2012), while a remaining concern is the signal loss at the electrode location due to magnetic field distortion (Carmichael et al. 2012). However, this could be overcome in the future with new electrode designs (Bonmassar et al. 2012).

12.4 EEG and fMRI Localization: Modes of Integration

We have already seen how EEG and fMRI can be correlated using EEG-derived GLMs and how multivariate methods and functional connectivity can extract further spatial and temporal information from the signals. In many of the approaches, the EEG is used purely as a timemarker of brain state, in the same way as external stimuli or responses in conventional cognitive fMRI studies. We now step back from simultaneous acquisitions to explore further how the two modalities can be integrated with the specific aim of localizing the generators of the underlying brain activity. For example, how can EEG source imaging be combined with fMRI to enhance localization?

As discussed in the Chap. 1, methods for the fusion of localization information obtained from EEG and fMRI analysis can be categorized according to the degree to which the relationship between the two signals forms part of a model and the role that each modality plays in the model. Coregistration of independently derived EEG and fMRI localization probably represents the least model-dependent mode of data fusion. In the preceding sections we have already described the mechanics of an asymmetric form of integration, namely the prediction of fMRI signal changes based on EEG. Finally, we discuss the so-called symmetric source reconstruction algorithms.

12.4.1 Comparison of Independently Derived Results

One of the most common strategies for multimodal integration has been to treat the EEG and fMRI datasets separately and compare the results in space (fusion a posteriori; Kruggel et al. 2001; Liebenthal et al. 2003; Foucher et al. 2004; Makiranta

et al. 2004; Becker et al. 2005; Henning et al. 2005; Otzenberger et al. 2005; Sammer et al. 2005). The simplest way to combine EEG source reconstruction and fMRI data is to compare the localization results obtained separately (e.g. from the analysis of averaged events) by coregistration and projection onto a common anatomical space (Opitz et al. 1999).

Prior to any attempt at further integration it is probably wise to use this approach as a first step. Spatial concordance cannot be expected in many circumstances due to the fundamentally different natures of the two signals (Disbrow et al. 2000; Nunez and Silberstein 2000; Ritter and Villringer 2006). Nonetheless, a good degree of spatial concordance can provide cross-validation and reassurance that the two methods are sensitive to similar phenomena and activity (Lemieux et al. 2001a; Bénar et al. 2006; Wirsich et al. 2014).

In situations with a few well-separated activated regions, good spatial concordance (see Fig. 12.7) allows one to consider the use of the timecourse of the EEG sources to estimate the chronometry of activation (Rossell et al. 2003; O'Hare et al. 2007). However, the EEG inverse problem can become ambiguous and/or inaccurate for a small number of electrodes, a large number of activated regions, for spatially extended sources, for regions close to one another, or those with highly correlated timecourses (Supek and Aine 1993; Huang et al. 1998). As a consequence, it seems intuitively obvious that guiding the EEG inverse problem within formation coming from fMRI, as presented in the next sections, will be helpful. As discussed in the Sect. 12.3.6, fMRI based whole-brain connectivity can also be readily compared to EEG source reconstructed connectivity (Deligianni et al. 2014; Wirsich et al. 2017).

12.4.2 fMRI as a Spatial Constraint for EEG Source Reconstruction

The good spatial coverage and localizing capability of fMRI on the one hand and the ambiguity of the EEG inverse problem on the other have inspired some investigators to develop methods based on the use of fMRI information as a prior constraint that informs EEG source localization (fMRI-informed EEG analysis).

In a dipolar framework, this can be done by applying constraints based on the fMRI activation clusters, in the form of either solution spacemasks or initialization of the estimates (Menon et al. 1997; Ahlfors et al. 1999; Toma et al. 2002; Bledowski et al. 2004). In a distributed sources framework, it is possible to give more weight to regions with fMRI activation (Liu et al. 1998; Babiloni et al. 2000), although tuning of the weighting parameter is not straightforward. The strength of the fMRI-derived constraints on source modelling is an important consideration: a hard constraint whereby solution dipoles are limited to the region of activation is probably inappropriate in most situations due to the potential discrepancy between EEG generator and BOLD localization—for example, in cases with regions that respond selectively to one or other of the modalities, perhaps because the task induces a change in neuronal synchrony that does not result in altered metabolic demand.

Careful consideration of the effect of constraints on the solution requires validation when possible. This is a potentially difficult problem, as the number of sources

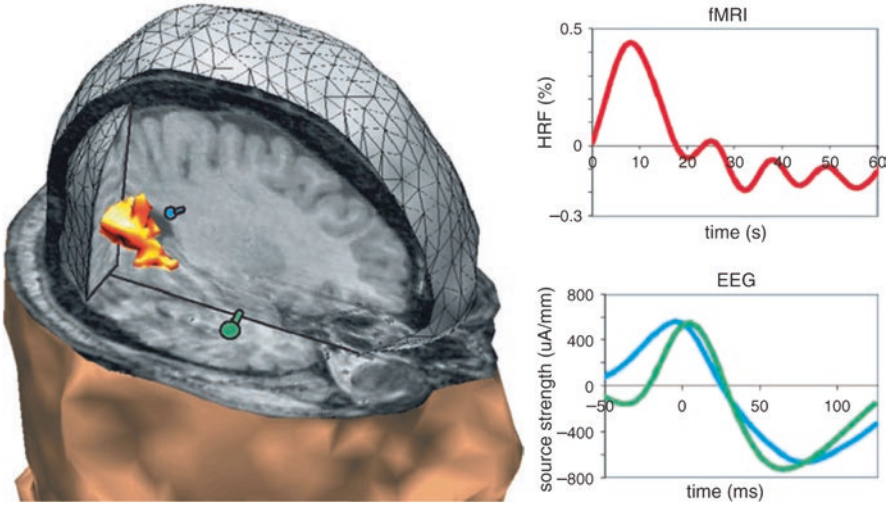

Fig. 12.7 Comparison of epileptic spike EEG dipole source localization and fMRI activation (subject 1 of Benar et al. 2002). Here, only one of the two dipoles (blue) matches the fMRI cluster. The evolution of the dipole strength at the concordant dipole location may provide additional time resolution

is a very sensitive parameter in EEG dipolar source localization: for example, placing a model dipole in a region that is silent on EEG could capture part of the signal from other sources. Conversely, not placing a dipole in an actual EEG source that is not seen by fMRI could result in a "spilling" of its activity to the other dipoles. Generally speaking, leaking of activity between spatially close sources is unavaoidable due to the ill-posed nature of the inverse problem and to smoothing arising from the inverse operator (Palva et al. 2018) and it is therefore necessary to carefully quantify the effects of mismatches over EEG–fMRI integration techniques (Liu et al. 2006).

By enabling the fMRI constraint to be incorporated probabilistically, Bayesian modelling (Baillet and Garnero 1997; Schmidt et al. 1999; Trujillo-Barreto et al. 2001; Phillips et al. 2005) integrates fMRI-activated regions in the form of statistical priors, which also forms a natural framework for the evaluation of distributed sources. Moreover, the Bayesian formalism provides a mechanism for model comparison/combination (Trujillo-Barreto et al. 2004) and to assess whether a given fMRI constraint is compatible with the EEG data, for example (Daunizeau et al. 2005; Grova et al. 2008). Applied to resting state data where no activation prior is available, information of intrinsic networks can be alternatively used (Lei et al. 2012). For a detailed review see (Lei et al. 2015).

12.4.3 Towards Symmetrical Models of EEG and fMRI Fusion

There have been a few examples of alternatives to the "classical" model of EEG-derived fMRI modelling employed in the vast majority of studies of spontaneous brain activity (see the Chaps. 15, 16, 17, 18, and 19) and evoked responses. For

example, fMRI has been used to inform the interpretation of spontaneously occurring events or patterns in simultaneously recorded EEG. Liston et al. (2006a) used a spike clustering method and projection of the entire EEG record onto a set of equivalent sources. They were able to provide additional evidence that spike-like events, not previously identified by expert observers, were probably low-amplitude spikes since their BOLD signature matched that of the visually identified spikes. Outside of the field of epilepsy, Mantini et al. were able to demonstrate the electrophysiological signatures of six spatially characterized resting state networks (identified using data-driven fMRI analysis) by studying the correlation between the BOLD signal in those networks and the simultaneously recorded EEG across frequency bands (Mantini et al. 2007b), while Feige et al. used a deconvolution approach to examine the temporal relationship between spontaneous electrophysiological and haemodynamic activity (Feige et al. 2017).

The asymmetry in the role of each modality may reflect a historical bias towards more detailed characterization of scalp EEG, compared to the BOLD signal. The ultimate aim of neuroimaging is a model of all neurosignals and their relationship to neuronal activity, upon which an assessment of the true value of any given modality (in relation to specific brain activity) could be based. A path to such a model has been proposed that removes this asymmetry in biophysical models of neurosignals, with neural activity as input. Towards this goal, an asymmetrical Bayesian source estimation framework has been introduced that integrates fMRI and EEG data (Trujillo-Barreto et al. 2001). The theoretical promise is that such models would take full advantage of the available information, with resulting improved sensitivity. For example, a weak prediction from each modality may reach significance in the joint analysis. Using dynamic causal modelling (DCM, Friston et al. 2003), Nguyen et al. added EEG as a contextual modulator to improve model selection (Nguyen et al. 2014). Another example of the added value of joint analysis was given in the Sec. 12.3.6 where symmetrical EEG-fMRI connectivity has been used in a linear model to better estimate the underlying structural connectivity (Wirsich et al. 2017). Those complementary contributions of joint EEG and fMRI connectivity can also be decomposed by using ICA (Wirsich et al. 2020a). Another interesting symmetric path is to compute the mutual information between EEG and fMRI (Ostwald et al. 2010; Ostwald and Bagshaw 2011; Caballero-Gaudes et al. 2013). Progresses arising in neurocomputational/biophysical modelling could be of help in the future (Voges et al. 2012).

Wirsich et al. estimated averaged connectivity over a 20-min timecourse (Wirsich et al. 2017), whereas dynamic symmetrical models offer much greater precision but rely on accurate coupling models, which remain the subject of investigation. In their current implementation, heuristic forms of the coupling function have been used and the Bayesian approach can be used to account for discordant EEG and fMRI-activated regions (Daunizeau et al. 2007) (see the Chap. 27 for further discussion of this approach). As the coupling of EEG and fMRI is partly determined by the underlying structure of the brain, Schirner et al. were able to show that EEG source activity of simultaneous recording can be used to improve neurophysiological simulations derived from structural connectivity, resulting in a better match between simulated and empirical BOLD activity (Schirner et al. 2018). This may point towards the

need for symmetrical models geared towards EEG-fMRI data fusion to also incorporate anatomical information.

12.5 Unresolved Problems and Caveats

Ultimately, the entire EEG–fMRI enterprise aims to improve our ability to characterize neuronal activity and in the process improve our understanding of the relationship between the two types of signals. We have explored a range of data acquisition and analysis strategies that allow the investigator to investigate the BOLD correlates of certain aspects of the EEG and more generally the sources of the EEG and fMRI signals. Despite some success at revealing novel information, there are unresolved issues, both conceptual and practical, which need addressing.

12.5.1 Relationship Between Neuronal Activity, EEG and fMRI Signals

As discussed in the Chap. 2, scalp EEG is primarily a measure of the synchronous post synaptic activity of cortical pyramidal neurons (Lopes da Silva and Van Rotterdam 2005; Nunez and Srinivasan 2005) and is largely insensitive to deep structures such as the hippocampus and thalamus (Merlet and Gotman 2001; Gavaret et al. 2004). Changes in synchrony can have a large effect on the scalp EEG signal even if the overall neuronal firing rate and hence metabolic load is not altered. Moreover, the closed morphology of certain deep structures such as amygdala or thalamus greatly reduces the measurable external field. However, several studies report sensitivity to signals from deep structures, and the final word may not have been said about the ability of EEG or MEG to record from the subcortex (Schnitzler et al. 2006; Attal et al. 2007; Attal and Schwartz 2013; Koessler et al. 2015; Pizzo et al. 2019; Seeber et al. 2019). Additionally, relationships between scalp EEG and BOLD signals have been demonstrated for different subcortical structures (Meir-Hasson et al. 2014; Schwab et al. 2015). Scalp EEG is a biased measure of brain activity, dependent not only on the location of the generating region but also the exact temporal relationship between cell populations. As discussed in the Chap. 3, fMRI reflects changes in bloodflow, oxygenation and volume. Indirectly, BOLD fMRI is a measure of energy consumption or metabolic demand (Arthurs and Boniface 2002; Logothetis and Wandell 2004). Combined intracerebral microelectrode and fMRI measurements have shown that the BOLD signal is correlated with variations in neuronal firing rate and to a greater extent with variations in local field potentials. In particular, strong correlations have been reported between gamma band electrical activity (>35 Hz) and BOLD signals (Logothetis et al. 2001; Niessing et al. 2005; Lachaux et al. 2007) (see the Chap. 4). Based on such observations and heuristic arguments, Kilner et al. postulated a linear relationship between the ratio of high-to low-frequency EEG signal power and BOLD (Kiefer et al. 2016). However, the observation of haemodynamic signals locked to stimulus timing but

without sensory input or expression in the form of the local measures of neuronal activity potentially raises questions about the causal assumption simplified in the GLM and the relationship between neural activity and BOLD (Sirotin and Das 2009). The fact that BOLD signal changes have been observed following optogenetic activation of astrocytes, in the absence of neuronal activation, also points towards the potential complexity of the relationship between EEG and fMRI (Takata et al. 2018).

The linear nature of most fMRI modelling strategies requires the identification of aspects of the EEG signal that are predicted to vary linearly in relation to the BOLD signal to be most efficient, an assumption that has not been investigated to any great extent. Evidently, this is a simple starting assumption in most cases and has been the subject of much work in relation to evoked or event-related responses. Studies based on animal models have suggested a linear coupling between the amplitude of epileptic spikes and the haemodynamic response (Mirsattari et al. 2006; Vanzetta et al. 2010). Nonlinear effects have been observed in response to sensory stimuli (Birn and Bandettini 2005; Wan et al. 2006), and epilepsy using the Volterra series in the GLM framework (Salek-Haddadi et al. 2006), and there is certainly considerable scope for more investigation of this issue, particularly in relation to the relative nonlinearities of EEG and fMRI (Arthurs et al. 2007; Liu et al. 2010).

fMRI data at the resolution of cortical-layers (laminar fMRI) using ultra-high field MRI could help to better understand such complex BOLD responses in certain tasks or during IEDs. Different laminar involvements (granular vs supragranular) have been identified depending on the propagated or "de novo" nature of IEDs defined by microelectrodes recordings in epileptic patients (Ulbert et al. 2004). This suggests that such laminar differentiation could help to better understand spatiotemporal organization of IEDs. In addition, the second part of IEDs is often dominated by an inhibitory nature (particularly in spike-and-wave discharges) that could have different effects on BOLD signal compared to excitation. Using visual-task laminar fMRI at 7 T a laminar dependent BOLD modulation related to the type of input (i.e. excitatory vs. inhibitory) has been evidenced (Fracasso et al. 2018). Thus, future availability of EEG-fMRI at 7 T will probably provide new insights to a better understanding of neuronal activity, EEG and fMRI (Mullinger et al. 2013; Neuner et al. 2014; Grouiller et al. 2015).

12.5.2 Specific Issues Related to Spontaneous Brain Activity

12.5.2.1 HRF

In conventional event-related cognitive fMRI experiments in healthy subjects, models based on the standard or canonical HRF (possibly with the addition of extra terms to allow for some variability) have proven successful. Nonetheless, as noted earlier, significant variability has been observed in responses to normal stimuli in healthy brains.

Spontaneous brain activity may be associated with neurophysiological processes that have no correlates on scalp EEG (e.g. in deep structures, or those which are too

weak to be detected on the scalp, or lack sufficient synchrony). For example, imagine that a certain brain state involves two processes, both associated with haemodynamic changes: one reflected on scalp EEG, and the other not reflected on EEG. A fixed temporal relationship between the two processes would lead to an apparent timeshift in the HRF. The relationship between the synchronous activity of cortical pyramidal cells in pathological areas and bloodflow may also deviate from the norm (see Salek-Haddadi et al. 2006 for a detailed discussion of this issue).

A number of studies have investigated the haemodynamic changes related to interictal epileptiform activity and revealed considerable variability in this response across subjects (Lemieux et al. 2001b; Benar et al. 2002; Gotman et al. 2004), with some evidence of delayed (Bagshaw et al. 2004; Lu et al. 2006; Grouiller et al. 2007) responses, as well as super linearity at short event durations (Bagshaw et al. 2005). For the alpha rhythm, the presence of a travelling wave was suggested by flexible HRF modelling (de Munck et al. 2007). One interesting observation has been BOLD changes consistent with an onset occurring prior to the observation of the discharge on scalp EEG (Hawco et al. 2007; Lemieux et al. 2008; Pittau et al. 2011) something that has also been seen in relation to the alpha (Feige et al. 2005) and other rhythms (Feige et al. 2017), and in epileptic seizures in humans and animal models (Makiranta et al. 2004; Federico et al. 2005). This suggests the potential importance of defining subject-specific HRFs (Kang et al. 2003; Grouiller et al. 2010; Storti et al. 2013), although potential methodological confounds related to the temporal blurring associated with the HRF must also be considered (Rollings et al. 2016).

Nonetheless, these observations highlight the potential limitations of using EEG as a basis to model BOLD fMRI and the issue of the choice of an optimal basis set. Multivariate techniques such as ICA have the advantage that there is no need to define a model of the BOLD response. They are therefore useful tools for exploratory data analysis and allow the assumptions of the HRF model to be directly tested. How these considerations translate to resting state recordings is also largely unknown. For example, it has been shown that simple HRF models might be an oversimplification as in some brain regions resting fMRI activity precedes EEG power rises (Feige et al. 2017).

12.5.2.2 Experimental Efficiency of Paradigm-less fMRI

In conventional, paradigm-driven fMRI studies, such as cognitive studies, one has the opportunity to optimize the experimental design (Dale 1999). Moreover, the classical procedure is to rely on a contrast between an active and a baseline condition. For spontaneous activity, the timecourse of the activity of interest is essentially random, with important consequences for experimental efficiency and consequently the technique's yield and clinical potential. For example, in focal epilepsy, localizing information is obtained in roughly 60% of cases in whom interictal spikes are observed over EEG–fMRI sessions lasting between 20 and 60 min (see the Chaps. 17, 18, and 19), even though these are cases selected for their relatively high levels of EEG activity. Part of this can probably be attributed to most early epilepsy studies taking place at 1.5 T, with some evidence that at 3 T results are more reproducible

and it is less likely that there will be no activation/deactivation if spikes are observed (Gholipour et al. 2011).

The lack of experimental control has also highlighted the question of fMRI baseline by blurring the boundary between "activated" and control states. Despite the fundamental difficulties associated with a lack of experimental control, we anticipate that the study of the brain's resting state using functional imaging will continue to constitute an active area of investigation.

12.5.3 The Impact of Data Acquisition and Processing Artefacts on fMRI Data Analysis

12.5.3.1 Artefacts in the Signals

A prudent approach to fMRI analysis is to devise models that incorporate as much knowledge of the factors that may influence the signal as possible. In this regard, the EEG and ECG can provide information not normally available in conventional fMRI experiments. Although movements pose a considerable problem in simultaneous EEG–fMRI, by giving rise to artefacts in both the EEG and the fMRI timeseries, the combination of EEG and fMRI makes it possible to assess the occurrence of motion events in a way that is not normally possible in fMRI without EEG, through the inspection of the EEG traces in relation to the fMRI scan realignment parameters. This can be useful in cases where motion is expected to be correlated with events of interest, such as seizures, and can be an important form of bias assessment (Salek-Haddadi et al. 2003c).

Other important potential sources of fMRI signal variance are respiration and heartbeat-related artefacts. Considerable work has been done to remove these, which are generally aliased in the fMRI signal but can be captured to a large extent in the ECG and in corporate into models of the fMRI signal (Glover et al. 2000; Liston et al. 2006b; Perlbarg et al. 2007). With the more widespread use of faster fMRI sequences this is likely to become less of an issue if only because the artefacts will no longer be aliased and hence easier to remove.

A very important pitfall is that some of these artefacts can be correlated (e.g. heartbeat and respiration artefacts) (Mandelkow et al. 2007), or, even worse, correlated with the protocol itself. For example, the subject can move the head when responding, or close the eyes after the response. This can lead to signal changes in both EEG and fMRI that will be correlated with the protocol and may be mistaken for a brain activation in response to the protocol. The net result of stimulus (or effect of interest)-related confounds is a reduction of sensitivity when properly incorporated into the fMRI model or possible false activation otherwise (Lund et al. 2005). Again, the availability of simultaneous physiological recordings can help to devise models that account for effects related to such confounds.

12.5.3.2 Artefacts Introduced by EEG Preprocessing

The results of any signal processing method must always be considered very carefully, as every method can produce spurious results if its assumptions are not

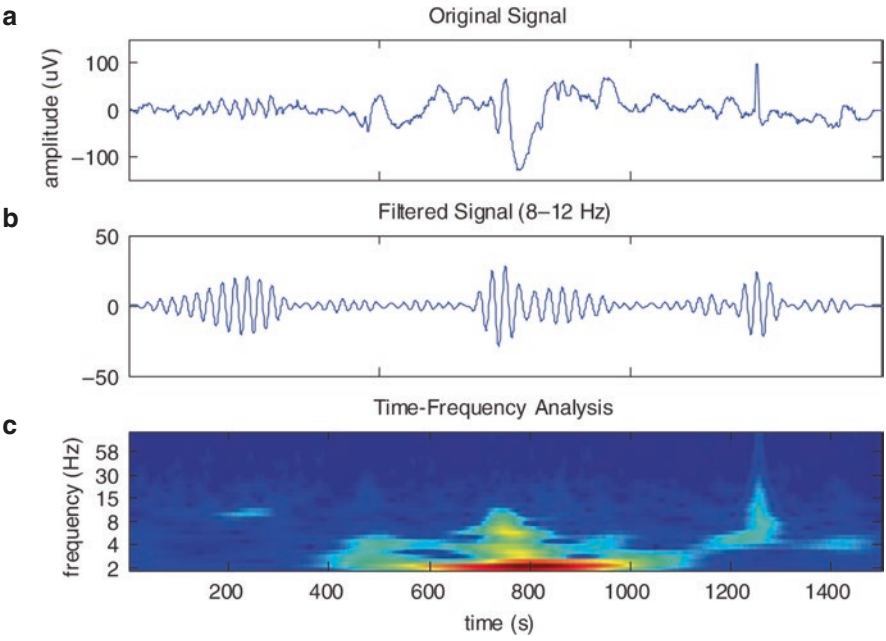

Fig. 12.8 (**a**–**c**) Pitfall of narrow-band filtering. (**a**) Original composite signal, with an alpha oscillation (around 200 ms), an epileptic spike (around 800 ms) and a synthetic spiky artefact (around 1,300 ms). (**b**) All signals seem oscillatory when filtered in a narrow band. (**c**) Time-frequency analysis allows the different signals to be differentiated

fulfilled. As a consequence, such confounds must be tracked down at every step. A generally misleading effect is the fact that each EEG channel is recorded with respect to a reference electrode (Lehmann and Skrandies 1984). This means that any measure of relation between channels (coherence, phase locking, etc.) can be confounded by this common signal.

Another major source of confound is the fact that transient activity filtered in a limited bandwidth can be mistaken for actual oscillatory data (see Fig. 12.8). This means that if one wants to perform a frequency-band-related analysis in EEG–fMRI, the data have to be checked carefully for artefacts. This can be quite easy for bands corresponding to low frequencies, but can prove more difficult for small artefacts (i.e. small spikes) that can be hidden in the data but produce a disastrous effect on high-frequency activity estimation.

Similarly, as mentioned in the section on multivariate analysis, there can be cross-talk issues in ICA decomposition. Indeed, if part of the signal of interest is not captured by its own component but rather spills onto artefact-related components, it will be removed in the ICA procedure (Wallstrom et al. 2004). This can in theory also happen for high-frequency activity, which represents a weak signal in EEG, or for protocol-related activity that is only present in a small time window in each trial. An additional consideration to account for when extracting connectivity-based measures of EEG is

the crosstalk introduced by primary source leakage (Nolte et al. 2004; Schoffelen and Gross 2009; Colclough et al. 2016) and other ghost interactions (Palva et al. 2018).

12.6 Summary and Outlook

The possibility of recording EEG inside the MRI scanner allows one to introduce fine temporal information from the EEG into the analysis of the fMRI signal at the single-trial level and allows the investigation of the haemodynamic correlates of spontaneous phenomena best observed on EEG, such as epileptic discharges, sleep or dynamic fluctuations in brain rhythms. The technique's limitations reflect those of EEG and fMRI taken individually. While the most widely used analysis method to date has been the general linear model, data-driven techniques such as ICA provide a framework for further exploratory studies with fewer assumptions.

Future directions could arise from the use of fast fMRI sequences, which allow a finer temporal sampling of the haemodynamic response (Jacobs et al. 2014; Foged et al. 2017), or recording with other modalities such as PET (Grouiller et al. 2015). Another promising avenue is computational modelling (Voges et al. 2012) that allows information from other modalities such as diffusion weighted imaging to be integrated into a coherent framework. Modelling can be combined with Bayesian inference in order to fuse data and estimate "hidden" parameters of activation (Jirsa et al. 2017).

Acknowledgements The authors wish to thank Jean Gotman and Christophe Grova for their comments and corrections to the manuscript of the first edition.

References

Abreu R, Leite M, Jorge J, Grouiller F, van der Zwaag W, Leal A, Figueiredo P (2016) Ballistocardiogram artifact correction taking into account physiological signal preservation in simultaneous EEG-fMRI. NeuroImage 135:45–63

Abreu R, Nunes S, Leal A, Figueiredo P (2017) Physiological noise correction using ECG-derived respiratory signals for enhanced mapping of spontaneous neuronal activity with simultaneous EEG-fMRI. NeuroImage 154:115–127

Abreu R, Leal A, Figueiredo P (2019) Identification of epileptic brain states by dynamic functional connectivity analysis of simultaneous EEG-fMRI: a dictionary learning approach. Sci Rep 9(1):638

Abreu R, Simoes M, Castelo-Branco M (2020) Pushing the limits of EEG: estimation of large-scale functional brain networks and their dynamics validated by simultaneous fMRI. Front Neurosci 14:323

Achard S, Salvador R, Whitcher B, Suckling J, Bullmore E (2006) A resilient, low-frequency, small-world human brain functional network with highly connected association cortical hubs. J Neurosci 26(1):63–72

Aghakhani Y, Bagshaw AP, Benar CG, Hawco C, Andermann F, Dubeau F, Gotman J (2004) fMRI activation during spike and wave discharges in idiopathic generalized epilepsy. Brain 127(Pt 5):1127–1144

Aguirre GK, Zarahn E, D'Esposito M (1998) The variability of human, BOLD hemodynamic responses. NeuroImage 8(4):360–369

Ahlfors SP, Simpson GV, Dale AM, Belliveau JW, Liu AK, Korvenoja A, Virtanen J, Huotilainen M, Tootell RB, Aronen HJ, Ilmoniemi RJ (1999) Spatiotemporal activity of a cortical network for processing visual motion revealed by MEG and fMRI. J Neurophysiol 82(5):2545–2555

Al-Asmi A, Bénar CG, Gross DW, Khani YA, Andermann F, Pike B, Dubeau F, Gotman J (2003) fMRI activation in continuous and spike-triggered EEG-fMRI studies of epileptic spikes. Epilepsia 44(10):1328–1339

Allen PJ, Polizzi G, Krakow K, Fish DR, Lemieux L (1998) Identification of EEG events in the MR scanner: the problem of pulse artifact and a method for its subtraction. NeuroImage 8(3):229–239

Allen PJ, Josephs O, Turner R (2000) A method for removing imaging artifact from continuous EEG recorded during functional MRI. NeuroImage 12(2):230–239

Allen EA, Damaraju E, Eichele T, Wu L, Calhoun VD (2018) EEG signatures of dynamic functional network connectivity states. Brain Topogr 31(1):101–116

Fracasso A, Luijten PR, Dumoulin SO, Petridou N (2018) Laminar imaging of positive and negative BOLD in human visual cortex at 7 T. NeuroImage 164100-111 S1053811917301490. https://doi.org/10.1016/j.neuroimage.2017.02.038

Archer JS, Abbott DF, Waites AB, Jackson GD (2003) fMRI "deactivation" of the posterior cingulate during generalized spike and wave. NeuroImage 20(4):1915–1922

Arthurs OJ, Boniface S (2002) How well do we understand the neural origins of the fMRI BOLD signal? Trends Neurosci 25(1):27–31

Arthurs OJ, Donovan T, Spiegelhalter DJ, Pickard JD, Boniface SJ (2007) Intracortically distributed neurovascular coupling relationships within and between human somatosensory cortices. Cereb Cortex 17(3):661–668

Attal Y, Schwartz D (2013) Assessment of subcortical source localization using deep brain activity imaging model with minimum norm operators: a MEG study. PLoS One 8(3):e59856

Attal Y, Bhattacharjee M, Yelnik J, Cottereau B, Lefèvre J, Okada Y, Bardinet E, Chupin M, Baillet S (2007) Modeling and detecting deep brain activity with MEG & EEG. In: Conference proceedings: annual international conference of the IEEE engineering in medicine and biology society. IEEE Engineering in Medicine and Biology Society, Piscataway, pp 4937–4940

Babiloni F, Carducci F, Cincotti F, Del Gratta C, Roberti GM, Romani GL, Rossini PM, Babiloni C (2000) Integration of high resolution EEG and functional magnetic resonance in the study of human movement-related potentials. Methods Inf Med 39(2):179–182

Bagshaw AP, Warbrick T (2007) Single trial variability of EEG and fMRI responses to visual stimuli. NeuroImage 38(2):280–292

Bagshaw AP, Aghakhani Y, Benar CG, Kobayashi E, Hawco C, Dubeau F, Pike GB, Gotman J (2004) EEG-fMRI of focal epileptic spikes: analysis with multiple haemodynamic functions and comparison with gadolinium-enhanced MR angiograms. Hum Brain Mapp 22(3):179–192

Bagshaw AP, Hawco C, Benar CG, Kobayashi E, Aghakhani Y, Dubeau F, Pike GB, Gotman J (2005) Analysis of the EEG-fMRI response to prolonged bursts of interictal epileptiform activity. NeuroImage 24(4):1099–1112

Baillet S, Garnero L (1997) A Bayesian approach to introducing anatomo-functional priors in the EEG/MEG inverse problem. IEEE Trans Biomed Eng 44(5):374–385

Bandettini PA, Jesmanowicz A, Wong EC, Hyde JS (1993) Processing strategies for time-course data sets in functional MRI of the human brain. Magn Reson Med 30(2):161–173

Bartolomei F, Lagarde S, Wendling F, McGonigal A, Jirsa V, Guye M, Benar C (2017) Defining epileptogenic networks: contribution of SEEG and signal analysis. Epilepsia 58(7):1131–1147

Bayer M, Rubens MT, Johnstone T (2018) Simultaneous EEG-fMRI reveals attention-dependent coupling of early face processing with a distributed cortical network. Biol Psychol 132:133–142

Becker R, Ritter P, Moosmann M, Villringer A (2005) Visual evoked potentials recovered from fMRI scan periods. Hum Brain Mapp 26(3):221–230

Beers CA, Williams RJ, Gaxiola-Valdez I, Pittman DJ, Kang AT, Aghakhani Y, Pike GB, Goodyear BG, Federico P (2015) Patient specific hemodynamic response functions associated with

interictal discharges recorded via simultaneous intracranial EEG-fMRI. Hum Brain Mapp 36(12):5252–5264
Belin P, Zatorre RJ, Hoge R, Evans AC, Pike B (1999) Event-related fMRI of the auditory cortex. NeuroImage 10(4):417–429
Bell AJ, Sejnowski TJ (1995) An information-maximization approach to blind separation and blind deconvolution. Neural Comput 7(6):1129–1159
Benar CG, Gross DW, Wang Y, Petre V, Pike B, Dubeau F, Gotman J (2002) The BOLD response to interictal epileptiform discharges. NeuroImage 17(3):1182–1192
Benar C, Aghakhani Y, Wang Y, Izenberg A, Al-Asmi A, Dubeau F, Gotman J (2003) Quality of EEG in simultaneous EEG-fMRI for epilepsy. Clin Neurophysiol 114(3):569–580
Benar CG, Grova C, Kobayashi E, Bagshaw AP, Aghakhani Y, Dubeau F, Gotman J (2006) EEG-fMRI of epileptic spikes: concordance with EEG source localization and intracranial EEG. NeuroImage 30(4):1161–1170
Bénar CG, Grova C, Kobayashi E, Bagshaw AP, Aghakhani Y, Dubeau F, Gotman J (2006) EEG-fMRI of epileptic spikes: concordance with EEG source localization and intracranial EEG. NeuroImage 30(4):1161–1170
Bénar CG, Schon D, Grimault S, Nazarian B, Burle B, Roth M, Badier JM, Marquis P, Liegeois-Chauvel C, Anton JL (2007) Single-trial analysis of oddball event-related potentials in simultaneous EEG-fMRI. Hum Brain Mapp 28(7):602–613
Benar CG, Papadopoulo T, Torresani B, Clerc M (2009) Consensus matching pursuit for multi-trial EEG signals. J Neurosci Methods 180(1):161–170
Bennett CM, Miller MB (2010) How reliable are the results from functional magnetic resonance imaging? Ann N Y Acad Sci 1191:133–155
Bennett CM, Wolford GL, Miller MB (2009) The principled control of false positives in neuroimaging. Soc Cogn Affect Neurosci 4(4):417–422
Berger H (1929) Über das Elektroenkephalogramm des Menschen. Arch Psychiatr Nervenkr 87:527–570
Bhattacharyya PK, Mullin J, Lee BS, Gonzalez-Martinez JA, Jones SE (2017) Safety of externally stimulated intracranial electrodes during functional MRI at 1.5T. Magn Reson Imaging 38:182–188
Biazoli CE Jr, Sturzbecher M, White TP, Dos Santos Onias HH, Andrade KC, de Araujo DB, Sato JR (2013) Application of partial directed coherence to the analysis of resting-state EEG-fMRI data. Brain Connect 3(6):563–568
Birn RM, Bandettini PA (2005) The effect of stimulus duty cycle and "off" duration on BOLD response linearity. NeuroImage 27(1):70–82
Biswal B, Yetkin FZ, Haughton VM, Hyde JS (1995) Functional connectivity in the motor cortex of resting human brain using echo-planar MRI. Magn Reson Med 34(4):537–541
Biswal BB, Mennes M, Zuo XN, Gohel S, Kelly C, Smith SM, Beckmann CF, Adelstein JS, Buckner RL, Colcombe S, Dogonowski AM, Ernst M, Fair D, Hampson M, Hoptman MJ, Hyde JS, Kiviniemi VJ, Kotter R, Li SJ, Lin CP, Lowe MJ, Mackay C, Madden DJ, Madsen KH, Margulies DS, Mayberg HS, McMahon K, Monk CS, Mostofsky SH, Nagel BJ, Pekar JJ, Peltier SJ, Petersen SE, Riedl V, Rombouts SA, Rypma B, Schlaggar BL, Schmidt S, Seidler RD, Siegle GJ, Sorg C, Teng GJ, Veijola J, Villringer A, Walter M, Wang L, Weng XC, Whitfield-Gabrieli S, Williamson P, Windischberger C, Zang YF, Zhang HY, Castellanos FX, Milham MP (2010) Toward discovery science of human brain function. Proc Natl Acad Sci U S A 107(10):4734–4739
Bledowski C, Prvulovic D, Hoechstetter K, Scherg M, Wibral M, Goebel R, Linden DE (2004) Localizing P300 generators in visual target and distractor processing: a combined event-related potential and functional magnetic resonance imaging study. J Neurosci 24(42):9353–9360
Bodurka J, Bandettini PA (2002) Toward direct mapping of neuronal activity: MRI detection of ultraweak, transient magnetic field changes. Magn Reson Med 47(6):1052–1058
Bonmassar G, Anami K, Ives J, Belliveau JW (1999) Visual evoked potential (VEP) measured by simultaneous 64-channel EEG and 3T fMRI. Neuroreport 10(9):1893–1897

Bonmassar G, Schwartz DP, Liu AK, Kwong KK, Dale AM, Belliveau JW (2001) Spatiotemporal brain imaging of visual-evoked activity using interleaved EEG and fMRI recordings. NeuroImage 13(6):1035–1043

Bonmassar G, Fujimoto K, Golby AJ (2012) PTFOS: flexible and absorbable intracranial electrodes for magnetic resonance imaging. PLoS One 7(9):e41187

Bridwell DA, Wu L, Eichele T, Calhoun VD (2013) The spatiospectral characterization of brain networks: fusing concurrent EEG spectra and fMRI maps. NeuroImage 69:101–111

Briselli E, Garreffa G, Bianchi L, Bianciardi M, Macaluso E, Abbafati M, Grazia Marciani M, Maraviglia B (2006) An independent component analysis-based approach on ballistocardiogram artifact removing. Magn Reson Imaging 24(4):393–400

Britz J, Van De Ville D, Michel CM (2010) BOLD correlates of EEG topography reveal rapid resting-state network dynamics. NeuroImage 52(4):1162–1170

Brookes MJ, Mullinger KJ, Stevenson CM, Morris PG, Bowtell R (2008) Simultaneous EEG source localisation and artifact rejection during concurrent fMRI by means of spatial filtering. NeuroImage 40(3):1090–1104

Brookes MJ, Woolrich M, Luckhoo H, Price D, Hale JR, Stephenson MC, Barnes GR, Smith SM, Morris PG (2011) Investigating the electrophysiological basis of resting state networks using magnetoencephalography. Proc Natl Acad Sci U S A 108(40):16783–16788

Bullmore E, Long C, Suckling J, Fadili J, Calvert G, Zelaya F, Carpenter TA, Brammer M (2001) Colored noise and computational inference in neurophysiological (fMRI) time series analysis: resampling methods in time and wavelet domains. Hum Brain Mapp 12(2):61–78

Caballero-Gaudes C, Van de Ville D, Grouiller F, Thornton R, Lemieux L, Seeck M, Lazeyras F, Vulliemoz S (2013) Mapping interictal epileptic discharges using mutual information between concurrent EEG and fMRI. NeuroImage 68:248–262

Calhoun VD, Sui J (2016) Multimodal fusion of brain imaging data: a key to finding the missing link(s) in complex mental illness. Biol Psychiatry Cogn Neurosci Neuroimaging 1(3):230–244

Calhoun VD, Adali T, Pearlson GD, Kiehl KA (2006) Neuronal chronometry of target detection: fusion of hemodynamic and event-related potential data. NeuroImage 30(2):544–553

Cao J (1999) The size of the connected components of excursion sets of chi2, t and F fields. Adv Appl Probab 31:577–593

Caporro M, Haneef Z, Yeh HJ, Lenartowicz A, Buttinelli C, Parvizi J, Stern JM (2012) Functional MRI of sleep spindles and K-complexes. Clin Neurophysiol 123(2):303–309

Cardoso JF (1999) High-order contrasts for independent component analysis. Neural Comput 11(1):157–192

Carmichael DW, Thornton JS, Rodionov R, Thornton R, McEvoy AW, Ordidge RJ, Allen PJ, Lemieux L (2010) Feasibility of simultaneous intracranial EEG-fMRI in humans: a safety study. NeuroImage 49(1):379–390

Carmichael DW, Vulliemoz S, Rodionov R, Thornton JS, McEvoy AW, Lemieux L (2012) Simultaneous intracranial EEG-fMRI in humans: protocol considerations and data quality. NeuroImage 63(1):301–309

Centeno M, Carmichael DW (2014) Network connectivity in epilepsy: resting state fMRI and EEG-fMRI contributions. Front Neurol 5:93

Chaari L, Vincent T, Forbes F, Dojat M, Ciuciu P (2013) Fast joint detection-estimation of evoked brain activity in event-related FMRI using a variational approach. IEEE Trans Med Imaging 32(5):821–837

Chang C, Glover GH (2010) Time-frequency dynamics of resting-state brain connectivity measured with fMRI. NeuroImage 50(1):81–98

Chang C, Liu Z, Chen MC, Liu X, Duyn JH (2013) EEG correlates of time-varying BOLD functional connectivity. NeuroImage 72:227–236

Chaudhary UJ, Centeno M, Thornton RC, Rodionov R, Vulliemoz S, McEvoy AW, Diehl B, Walker MC, Duncan JS, Carmichael DW, Lemieux L (2016) Mapping human preictal and ictal haemodynamic networks using simultaneous intracranial EEG-fMRI. Neuroimage Clin 11:486–493

Christmann C, Koeppe C, Braus DF, Ruf M, Flor H (2007) A simultaneous EEG-fMRI study of painful electric stimulation. NeuroImage 34(4):1428–1437

Chumbley JR, Friston KJ (2008) False discovery rate revisited: FDR and topological inference using Gaussian random fields. NeuroImage 44(1):62–70

Cincotti F, Mattia D, Babiloni C, Carducci F, Salinari S, Bianchi L, Marciani MG, Babiloni F (2003) The use of EEG modifications due to motor imagery for brain-computer interfaces. IEEE Trans Neural Syst Rehabil Eng 11(2):131–133

Colclough GL, Woolrich MW, Tewarie PK, Brookes MJ, Quinn AJ, Smith SM (2016) How reliable are MEG resting-state connectivity metrics? NeuroImage 138:284–293

Comi E, Annovazzi P, Silva AM, Cursi M, Blasi V, Cadioli M, Inuggi A, Falini A, Comi G, Leocani L (2005) Visual evoked potentials may be recorded simultaneously with fMRI scanning: a validation study. Hum Brain Mapp 24(4):291–298

Comon P (1994) Independent component analysis, a new concept. Signal Process 36(3):287–314

Cunningham CB, Goodyear BG, Badawy R, Zaamout F, Pittman DJ, Beers CA, Federico P (2012) Intracranial EEG-fMRI analysis of focal epileptiform discharges in humans. Epilepsia 53(9):1636–1648

Czisch M, Wetter TC, Kaufmann C, Pollmacher T, Holsboer F, Auer DP (2002) Altered processing of acoustic stimuli during sleep: reduced auditory activation and visual deactivation detected by a combined fMRI/EEG study. NeuroImage 16(1):251–258

Czisch M, Wehrle R, Kaufmann C, Wetter TC, Holsboer F, Pollmacher T, Auer DP (2004) Functional MRI during sleep: BOLD signal decreases and their electrophysiological correlates. Eur J Neurosci 20(2):566–574

Dähne S, Bießmann F, Samek W, Haufe S, Goltz D, Gundlach C, Villringer A, Fazli S, Müller KR (2015) Multivariate machine learning methods for fusing multimodal functional neuroimaging data. Proc IEEE 103(9):1507–1530

Dale AM (1999) Optimal experimental design for event-related fMRI. Hum Brain Mapp 8(2-3):109–114

Damaraju E, Tagliazucchi E, Laufs H, Calhoun VD (2020) Connectivity dynamics from wakefulness to sleep. NeuroImage 220:117047

Daunizeau J, Grova C, Mattout J, Marrelec G, Clonda D, Goulard B, Pelegrini-Issac M, Lina JM, Benali H (2005) Assessing the relevance of fMRI-based prior in the EEG inverse problem: a Bayesian model comparison approach. IEEE Trans Signal Process 53(9):3461–3472

Daunizeau J, Grova C, Marrelec G, Mattout J, Jbabdi S, Pelegrini-Issac M, Lina JM, Benali H (2007) Symmetrical event-related EEG/fMRI information fusion in a variational Bayesian framework. NeuroImage 36(1):69–87

De Clercq W, Vergult A, Vanrumste B, Van Paesschen W, Van Huffel S (2006) Canonical correlation analysis applied to remove muscle artifacts from the electroencephalogram. IEEE Trans Biomed Eng 53(12):2583–2587

de Munck JC, Goncalves SI, Huijboom L, Kuijer JP, Pouwels PJ, Heethaar RM, Lopes da Silva FH (2007) The hemodynamic response of the alpha rhythm: an EEG/fMRI study. NeuroImage 35(3):1142–1151

de Munck JC, Goncalves SI, Mammoliti R, Heethaar RM, Lopes da Silva FH (2009) Interactions between different EEG frequency bands and their effect on alpha-fMRI correlations. NeuroImage 47(1):69–76

De Vos M, Thorne JD, Yovel G, Debener S (2012) Let's face it, from trial to trial: comparing procedures for N170 single-trial estimation. NeuroImage 63(3):1196–1202

Debener S, Ullsperger M, Siegel M, Fiehler K, von Cramon DY, Engel AK (2005) Trial-by-trial coupling of concurrent electroencephalogram and functional magnetic resonance imaging identifies the dynamics of performance monitoring. J Neurosci 25(50):11730–11737

Debener S, Strobel A, Sorger B, Peters J, Kranczioch C, Engel AK, Goebel R (2007) Improved quality of auditory event-related potentials recorded simultaneously with 3-T fMRI: removal of the ballistocardiogram artefact. NeuroImage 34(2):587–597

Debener S, Mullinger KJ, Niazy RK, Bowtell RW (2008) Properties of the ballistocardiogram artefact as revealed by EEG recordings at 1.5, 3 and 7 T static magnetic field strength. Int J Psychophysiol 67(3):189–199

Deligianni F, Centeno M, Carmichael DW, Clayden JD (2014) Relating resting-state fMRI and EEG whole-brain connectomes across frequency bands. Front Neurosci 8:258
Deligianni F, Carmichael DW, Zhang GH, Clark CA, Clayden JD (2016) NODDI and tensor-based microstructural indices as predictors of functional connectivity. PLoS One 11(4):e0153404
Delorme A, Palmer J, Onton J, Oostenveld R, Makeig S (2012) Independent EEG sources are dipolar. PLoS One 7(2):e30135
Deneux T, Faugeras O (2006) Using nonlinear models in fMRI data analysis: model selection and activation detection. NeuroImage 32(4):1669–1689
Dien J, Khoe W, Mangun GR (2007) Evaluation of PCA and ICA of simulated ERPs: Promax vs. Infomax rotations. Hum Brain Mapp 28(8):742–763
Disbrow EA, Slutsky DA, Roberts TP, Krubitzer LA (2000) Functional MRI at 1.5 tesla: a comparison of the blood oxygenation level-dependent signal and electrophysiology. Proc Natl Acad Sci U S A 97(17):9718–9723
Duann JR, Jung TP, Kuo WJ, Yeh TC, Makeig S, Hsieh JC, Sejnowski TJ (2002) Single-trial variability in event-related BOLD signals. NeuroImage 15(4):823–835
Dubarry AS, Badier JM, Trebuchon-Da Fonseca A, Gavaret M, Carron R, Bartolomei F, Liegeois-Chauvel C, Regis J, Chauvel P, Alario FX, Benar CG (2014) Simultaneous recording of MEG, EEG and intracerebral EEG during visual stimulation: from feasibility to single-trial analysis. NeuroImage 99:548–558
Duyn JH (2012) EEG-fMRI methods for the study of brain networks during sleep. Front Neurol 3:100
Eichele T, Specht K, Moosmann M, Jongsma ML, Quiroga RQ, Nordby H, Hugdahl K (2005) Assessing the spatiotemporal evolution of neuronal activation with single-trial event-related potentials and functional MRI. Proc Natl Acad Sci U S A 102(49):17798–17803
Eichele T, Calhoun VD, Moosmann M, Specht K, Jongsma ML, Quiroga RQ, Nordby H, Hugdahl K (2007) Unmixing concurrent EEG-fMRI with parallel independent component analysis. Int J Psychophysiol 67(3):222–234
Eichele T, Rachakonda S, Brakedal B, Eikeland R, Calhoun VD (2011) EEGIFT: group independent component analysis for event-related EEG data. Comput Intell Neurosci 2011:129365
Eklund A, Nichols TE, Knutsson H (2016) Cluster failure: why fMRI inferences for spatial extent have inflated false-positive rates. Proc Natl Acad Sci U S A 113(28):7900–7905
Yacoub E, Harel N, Uğurbil K (2008) High-field fMRI unveils orientation columns in humans. Proceedings of the National Academy of Sciences 105(30):10607–10612. https://doi.org/10.1073/pnas.0804110105
Falahpour M, Chang C, Wong CW, Liu TT (2018) Template-based prediction of vigilance fluctuations in resting-state fMRI. NeuroImage 174:317–327
Federico P, Abbott DF, Briellmann RS, Harvey AS, Jackson GD (2005) Functional MRI of the pre-ictal state. Brain 128(8):1811–1817
Feige B, Scheffler K, Esposito F, Di Salle F, Hennig J, Seifritz E (2005) Cortical and subcortical correlates of electroencephalographic alpha rhythm modulation. J Neurophysiol 93(5):2864–2872
Feige B, Spiegelhalder K, Kiemen A, Bosch OG, Tebartz van Elst L, Hennig J, Seifritz E, Riemann D (2017) Distinctive time-lagged resting-state networks revealed by simultaneous EEG-fMRI. NeuroImage 145(Pt A):1–10
Fell J (2007) Cognitive neurophysiology: beyond averaging. NeuroImage 37(4):1069–1072
Fellner MC, Volberg G, Mullinger KJ, Goldhacker M, Wimber M, Greenlee MW, Hanslmayr S (2016) Spurious correlations in simultaneous EEG-fMRI driven by in-scanner movement. NeuroImage 133:354–366
Flanagan D, Abbott DF, Jackson GD (2009) How wrong can we be? The effect of inaccurate mark-up of EEG/fMRI studies in epilepsy. Clin Neurophysiol 120(9):1637–1647
Foged MT, Lindberg U, Vakamudi K, Larsson HBW, Pinborg LH, Kjaer TW, Fabricius M, Svarer C, Ozenne B, Thomsen C, Beniczky S, Paulson OB, Posse S (2017) Safety and EEG data quality of concurrent high-density EEG and high-speed fMRI at 3 Tesla. PLoS One 12(5):e0178409
Formaggio E, Storti SF, Bertoldo A, Manganotti P, Fiaschi A, Toffolo GM (2011) Integrating EEG and fMRI in epilepsy. NeuroImage 54(4):2719–2731

Foucher JR, Otzenberger H, Gounot D (2003) The BOLD response and the gamma oscillations respond differently than evoked potentials: an interleaved EEG-fMRI study. BMC Neurosci 4:22
Foucher JR, Otzenberger H, Gounot D (2004) Where arousal meets attention: a simultaneous fMRI and EEG recording study. NeuroImage 22(2):688–697
Friston KJ, Ashburner J, Frith CD, Poline JB, Heather JD, Frackowiak RSJ (1995) Spatial registration and normalization of images. Hum Brain Mapp 3(3):165–189
Friston KJ, Williams S, Howard R, Frackowiak RS, Turner R (1996) Movement-related effects in fMRI time-series. Magn Reson Med 35(3):346–355
Friston KJ, Buechel C, Fink GR, Morris J, Rolls E, Dolan RJ (1997) Psychophysiological and modulatory interactions in neuroimaging. NeuroImage 6(3):218–229
Friston KJ, Josephs O, Rees G, Turner R (1998) Nonlinear event-related responses in fMRI. Magn Reson Med 39(1):41–52
Friston K, Phillips J, Chawla D, Buchel C (1999) Revealing interactions among brain systems with nonlinear PCA. Hum Brain Mapp 8(2-3):92–97
Friston KJ, Penny W, Phillips C, Kiebel S, Hinton G, Ashburner J (2002) Classical and Bayesian inference in neuroimaging: theory. NeuroImage 16(2):465–483
Friston KJ, Harrison L, Penny W (2003) Dynamic causal modelling. NeuroImage 19(4):1273–1302
Friston KJ, Stephan KE, Lund TE, Morcom A, Kiebel S (2005) Mixed-effects and fMRI studies. NeuroImage 24(1):244–252
Fuglo D, Pedersen H, Rostrup E, Hansen AE, Larsson HB (2012) Correlation between single-trial visual evoked potentials and the blood oxygenation level dependent response in simultaneously recorded electroencephalography-functional magnetic resonance imaging. Magn Reson Med 68(1):252–260
Fukunaga M, Horovitz SG, van Gelderen P, de Zwart JA, Jansma JM, Ikonomidou VN, Chu R, Deckers RH, Leopold DA, Duyn JH (2006) Large-amplitude, spatially correlated fluctuations in BOLD fMRI signals during extended rest and early sleep stages. Magn Reson Imaging 24(8):979–992
Gavaret M, Badier JM, Marquis P, Bartolomei F, Chauvel P (2004) Electric source imaging in temporal lobe epilepsy. J Clin Neurophysiol 21(4):267–282
Genovese CR, Lazar NA, Nichols T (2002) Thresholding of statistical maps in functional neuroimaging using the false discovery rate. NeuroImage 15(4):870–878
Geselowitz DB (1967) On bioelectric potentials in an inhomogeneous volume conductor. Biophys J 7(1):1–11
Gholipour T, Moeller F, Pittau F, Dubeau F, Gotman J (2011) Reproducibility of interictal EEG-fMRI results in patients with epilepsy. Epilepsia 52(3):433–442
Glover GH, Li TQ, Ress D (2000) Image-based method for retrospective correction of physiological motion effects in fMRI: RETROICOR. Magn Reson Med 44(1):162–167
Goldman RI, Stern JM, Engel J Jr, Cohen MS (2000) Acquiring simultaneous EEG and functional MRI. Clin Neurophysiol 111(11):1974–1980
Goldman RI, Stern JM, Engel J Jr, Cohen MS (2002) Simultaneous EEG and fMRI of the alpha rhythm. Neuroreport 13(18):2487–2492
Goldman RI, Wei CY, Philiastides MG, Gerson AD, Friedman D, Brown TR, Sajda P (2009) Single-trial discrimination for integrating simultaneous EEG and fMRI: identifying cortical areas contributing to trial-to-trial variability in the auditory oddball task. NeuroImage 47(1):136–147
Goncalves SI, de Munck JC, Pouwels PJ, Schoonhoven R, Kuijer JP, Maurits NM, Hoogduin JM, Van Someren EJ, Heethaar RM, Lopes da Silva FH (2006) Correlating the alpha rhythm to BOLD using simultaneous EEG/fMRI: inter-subject variability. NeuroImage 30(1):203–213
Gotman J, Bénar CG, Dubeau F (2004) Combining EEG and FMRI in epilepsy: methodological challenges and clinical results. J Clin Neurophysiol 21(4):229–240
Gotman J, Grova C, Bagshaw A, Kobayashi E, Aghakhani Y, Dubeau F (2005) Generalized epileptic discharges show thalamocortical activation and suspension of the default state of the brain. Proc Natl Acad Sci U S A 102(42):15236–15240

Gotman J, Kobayashi E, Bagshaw AP, Benar CG, Dubeau F (2006) Combining EEG and fMRI: a multimodal tool for epilepsy research. J Magn Reson Imaging 23(6):906–920

Grouiller F, Vercueil L, Krainik A, Segebarth C, Kahane P, David O (2007) Evaluation of the hemodynamic response function for interictal epileptiform discharges. In: Proc. 13th annual meeting of the Organization for Human Brain Mapping, Chicago, USA

Grouiller F, Vercueil L, Krainik A, Segebarth C, Kahane P, David O (2010) Characterization of the hemodynamic modes associated with interictal epileptic activity using a deformable model-based analysis of combined EEG and functional MRI recordings. Hum Brain Mapp 31(8):1157–1173

Grouiller F, Thornton RC, Groening K, Spinelli L, Duncan JS, Schaller K, Siniatchkin M, Lemieux L, Seeck M, Michel CM, Vulliemoz S (2011) With or without spikes: localization of focal epileptic activity by simultaneous electroencephalography and functional magnetic resonance imaging. Brain 134(10):2867–2886

Grouiller F, Delattre BM, Pittau F, Heinzer S, Lazeyras F, Spinelli L, Iannotti GR, Seeck M, Ratib O, Vargas MI, Garibotto V, Vulliemoz S (2015) All-in-one interictal presurgical imaging in patients with epilepsy: single-session EEG/PET/(f)MRI. Eur J Nucl Med Mol Imaging 42(7):1133–1143

Grova C, Daunizeau J, Kobayashi E, Bagshaw AP, Lina JM, Dubeau F, Gotman J (2008) Concordance between distributed EEG source localization and simultaneous EEG-fMRI studies of epileptic spikes. NeuroImage 39(2):755–774

Grova C, Aiguabella M, Zelmann R, Lina JM, Hall JA, Kobayashi E (2016) Intracranial EEG potentials estimated from MEG sources: A new approach to correlate MEG and iEEG data in epilepsy. Hum Brain Mapp 37(5):1661–1683

Hagberg GE, Bianciardi M, Maraviglia B (2006) Challenges for detection of neuronal currents by MRI. Magn Reson Imaging 24(4):483–493

Hamandi K, Laufs H, Noth U, Carmichael DW, Duncan JS, Lemieux L (2008) BOLD and perfusion changes during epileptic generalised spike wave activity. NeuroImage 39(2):608–618

Hanslmayr S, Volberg G, Wimber M, Raabe M, Greenlee MW, Bauml KH (2011) The relationship between brain oscillations and BOLD signal during memory formation: a combined EEG-fMRI study. J Neurosci 31(44):15674–15680

Hawco CS, Bagshaw AP, Lu Y, Dubeau F, Gotman J (2007) BOLD changes occur prior to epileptic spikes seen on scalp EEG. NeuroImage 35(4):1450–1458

Henning S, Merboldt KD, Frahm J (2005) Simultaneous recordings of visual evoked potentials and BOLD MRI activations in response to visual motion processing. NMR Biomed 18(8):543–552

Herweg NA, Apitz T, Leicht G, Mulert C, Fuentemilla L, Bunzeck N (2016) Theta-alpha oscillations bind the hippocampus, prefrontal cortex, and striatum during recollection: evidence from simultaneous EEG-fMRI. J Neurosci 36(12):3579–3587

Hiltunen T, Kantola J, Abou Elseoud A, Lepola P, Suominen K, Starck T, Nikkinen J, Remes J, Tervonen O, Palva S, Kiviniemi V, Palva JM (2014) Infra-slow EEG fluctuations are correlated with resting-state network dynamics in fMRI. J Neurosci 34(2):356–362

Hoppstadter M, Baeuchl C, Diener C, Flor H, Meyer P (2015) Simultaneous EEG-fMRI reveals brain networks underlying recognition memory ERP old/new effects. NeuroImage 116:112–122

Horovitz SG, Rossion B, Skudlarski P, Gore JC (2004) Parametric design and correlational analyses help integrating fMRI and electrophysiological data during face processing. NeuroImage 22(4):1587–1595

Horovitz SG, Fukunaga M, de Zwart JA, van Gelderen P, Fulton SC, Balkin TJ, Duyn JH (2007) Low frequency BOLD fluctuations during resting wakefulness and light sleep: a simultaneous EEG-fMRI study. Hum Brain Mapp 29(6):671–682

Huang M, Aine CJ, Supek S, Best E, Ranken D, Flynn ER (1998) Multi-start downhill simplex method for spatio-temporal source localization in magnetoencephalography. Electroencephalogr Clin Neurophysiol 108(1):32–44

Hutchison RM, Womelsdorf T, Allen EA, Bandettini PA, Calhoun VD, Corbetta M, Della Penna S, Duyn JH, Glover GH, Gonzalez-Castillo J, Handwerker DA, Keilholz S, Kiviniemi V, Leopold

DA, de Pasquale F, Sporns O, Walter M, Chang C (2013) Dynamic functional connectivity: promise, issues, and interpretations. NeuroImage 80:360–378
Hyvarinen A, Oja E (2000) Independent component analysis: algorithms and applications. Neural Netw 13(4-5):411–430
Im CH, Liu Z, Zhang N, Chen W, He B (2006) Functional cortical source imaging from simultaneously recorded ERP and fMRI. J Neurosci Methods 157(1):118–123
Ulbert I, Heit G, Madsen J, Karmos G, Halgren E (2004) Laminar Analysis of Human Neocortical Interictal Spike Generation and Propagation: Current Source Density and Multiunit Analysis In Vivo. Epilepsia 45(s4):48–56. https://doi.org/10.1111/j.0013-9580.2004.04011.x
Ives JR, Warach S, Schmitt F, Edelman RR, Schomer DL (1993) Monitoring the patient's EEG during echo planar MRI. Electroencephalogr Clin Neurophysiol 87(6):417–420
Jackson GD, Opdam HI (2000) Ictal fMRI: methods and models. Adv Neurol 83:203–211
Jacobs J, Stich J, Zahneisen B, Asslander J, Ramantani G, Schulze-Bonhage A, Korinthenberg R, Hennig J, LeVan P (2014) Fast fMRI provides high statistical power in the analysis of epileptic networks. NeuroImage 88:282–294
James CJ, Gibson OJ (2003) Temporally constrained ICA: an application to artifact rejection in electromagnetic brain signal analysis. IEEE Trans Biomed Eng 50(9):1108–1116
Jann K, Dierks T, Boesch C, Kottlow M, Strik W, Koenig T (2009) BOLD correlates of EEG alpha phase-locking and the fMRI default mode network. NeuroImage 45(3):903–916
Jansen M, White TP, Mullinger KJ, Liddle EB, Gowland PA, Francis ST, Bowtell R, Liddle PF (2012) Motion-related artefacts in EEG predict neuronally plausible patterns of activation in fMRI data. NeuroImage 59(1):261–270
Jirsa VK, Proix T, Perdikis D, Woodman MM, Wang H, Gonzalez-Martinez J, Bernard C, Benar C, Guye M, Chauvel P, Bartolomei F (2017) The virtual epileptic patient: individualized whole-brain models of epilepsy spread. NeuroImage 145(Pt B):377–388
Jorge J, Grouiller F, Gruetter R, van der Zwaag W, Figueiredo P (2015a) Towards high-quality simultaneous EEG-fMRI at 7 T: detection and reduction of EEG artifacts due to head motion. NeuroImage 120:143–153
Jorge J, Grouiller F, Ipek O, Stoermer R, Michel CM, Figueiredo P, van der Zwaag W, Gruetter R (2015b) Simultaneous EEG-fMRI at ultra-high field: artifact prevention and safety assessment. NeuroImage 105:132–144
Josephs O, Henson RN (1999) Event-related functional magnetic resonance imaging: modelling, inference and optimization. Philos Trans R Soc Lond Ser B Biol Sci 354(1387):1215–1228
Josephs O, Turner R, Friston K (1997) Event-related fMRI. Hum Brain Mapp 5(4):243–248
Jung TP, Makeig S, Westerfield M, Townsend J, Courchesne E, Sejnowski TJ (2001) Analysis and visualization of single-trial event-related potentials. Hum Brain Mapp 14(3):166–185
Jutten C, Herault J (1991) Blind separation of sources. 1. An adaptive algorithm based on neuromimetic architecture. Signal Process 24(1):1–10
Kang JK, Benar C, Al-Asmi A, Khani YA, Pike GB, Dubeau F, Gotman J (2003) Using patient-specific hemodynamic response functions in combined EEG-fMRI studies in epilepsy. NeuroImage 20(2):1162–1170
Keilholz SD (2014) The neural basis of time-varying resting-state functional connectivity. Brain Connect 4(10):769–779
Keinänen T, Rytky S, Korhonen V, Huotari N, Nikkinen J, Tervonen O, Palva JM, Kiviniemi V (2018) Fluctuations of the EEG-fMRI correlation reflect intrinsic strength of functional connectivity in default mode network. J Neurosci Res 96(10):1689–1698
Khader P, Schicke T, Roder B, Rosler F (2007) On the relationship between slow cortical potentials and BOLD signal changes in humans. Int J Psychophysiol 67(3):252–261
Khoo HM, von Ellenrieder N, Zazubovits N, Dubeau F, Gotman J (2017) Epileptic networks in action: synchrony between distant hemodynamic responses. Ann Neurol 82(1):57–66
Kiefer C, Abela E, Schindler K, Wiest R (2016) Focal epilepsy: MR imaging of nonhemodynamic field effects by using a phase-cycled stimulus-induced rotary saturation approach with spin-lock preparation. Radiology 280(1):237–243

Kim HC, Yoo SS, Lee JH (2015) Recursive approach of EEG-segment-based principal component analysis substantially reduces cryogenic pump artifacts in simultaneous EEG-fMRI data. NeuroImage 104:437–451

Kobayashi K, James CJ, Nakahori T, Akiyama T, Gotman J (1999) Isolation of epileptiform discharges from unaveraged EEG by independent component analysis. Clin Neurophysiol 110(10):1755–1763

Kobayashi E, Hawco CS, Grova C, Dubeau F, Gotman J (2006) Widespread and intense BOLD changes during brief focal electrographic seizures. Neurology 66(7):1049–1055

Koessler L, Cecchin T, Colnat-Coulbois S, Vignal JP, Jonas J, Vespignani H, Ramantani G, Maillard LG (2015) Catching the invisible: mesial temporal source contribution to simultaneous EEG and SEEG recordings. Brain Topogr 28(1):5–20

Kottlow M, Jann K, Dierks T, Koenig T (2012) Increased phase synchronization during continuous face integration measured simultaneously with EEG and fMRI. Clin Neurophysiol 123(8):1536–1548

Krakow K, Woermann FG, Symms MR, Allen PJ, Lemieux L, Barker GJ, Duncan JS, Fish DR (1999) EEG-triggered functional MRI of interictal epileptiform activity in patients with partial seizures. Brain 122(9):1679–1688

Krakow K, Allen PJ, Symms MR, Lemieux L, Josephs O, Fish DR (2000) EEG recording during fMRI experiments: image quality. Hum Brain Mapp 10(1):10–15

Krakow K, Lemieux L, Messina D, Scott CA, Symms MR, Duncan JS, Fish DR (2001) Spatio-temporal imaging of focal interictal epileptiform activity using EEG-triggered functional MRI. Epileptic Disord 3(2):67–74

Kruggel F, Wiggins CJ, Herrmann CS, von Cramon DY (2000) Recording of the event-related potentials during functional MRI at 3.0 Tesla field strength. Magn Reson Med 44(2):277–282

Kruggel F, Herrmann CS, Wiggins CJ, von Cramon DY (2001) Hemodynamic and electroencephalographic responses to illusory figures: recording of the evoked potentials during functional MRI. NeuroImage 14(6):1327–1336

Labounek R, Lamos M, Marecek R, Brazdil M, Jan J (2015) Exploring task-related variability in fMRI data using fluctuations in power spectrum of simultaneously acquired EEG. J Neurosci Methods 245:125–136

Labounek R, Bridwell DA, Marecek R, Lamos M, Mikl M, Bednarik P, Bastinec J, Slavicek T, Hlustik P, Brazdil M, Jan J (2019) EEG spatiospectral patterns and their link to fMRI BOLD signal via variable hemodynamic response functions. J Neurosci Methods 318:34–46

Lachaux JP, Fonlupt P, Kahane P, Minotti L, Hoffmann D, Bertrand O, Baciu M (2007) Relationship between task-related gamma oscillations and BOLD signal: New insights from combined fMRI and intracranial EEG. Hum Brain Mapp 28(12):1368–1375

Lai SH, Fang M (1999) A novel local PCA-based method for detecting activation signals in fMRI. Magn Reson Imaging 17(6):827–836

Lamos M, Marecek R, Slavicek T, Mikl M, Rektor I, Jan J (2018) Spatial-temporal-spectral EEG patterns of BOLD functional network connectivity dynamics. J Neural Eng 15(3):036025

Laufs H, Duncan JS (2007) Electroencephalography/functional MRI in human epilepsy: what it currently can and cannot do. Curr Opin Neurol 20(4):417–423

Laufs H, Kleinschmidt A, Beyerle A, Eger E, Salek-Haddadi A, Preibisch C, Krakow K (2003a) EEG-correlated fMRI of human alpha activity. NeuroImage 19(4):1463–1476

Laufs H, Krakow K, Sterzer P, Eger E, Beyerle A, Salek-Haddadi A, Kleinschmidt A (2003b) Electroencephalographic signatures of attentional and cognitive default modes in spontaneous brain activity fluctuations at rest. Proc Natl Acad Sci U S A 100(19):11053–11058

Laufs H, Lengler U, Hamandi K, Kleinschmidt A, Krakow K (2006a) Linking generalized spike-and-wave discharges and resting state brain activity by using EEG/fMRI in a patient with absence seizures. Epilepsia 47(2):444–448

Laufs H, Walker MC, Lund TE (2006b) EEG-fMRI of sleep spindles and K-complexes at 3T. Clin Neurophysiol 117:148–149

Lehmann D, Skrandies W (1984) Spatial analysis of evoked potentials in man–a review. Prog Neurobiol 23(3):227–250

Lehongre K, Morillon B, Giraud AL, Ramus F (2013) Impaired auditory sampling in dyslexia: further evidence from combined fMRI and EEG. Front Hum Neurosci 7:454
Lei X, Hu J, Yao D (2012) Incorporating FMRI functional networks in EEG source imaging: a Bayesian model comparison approach. Brain Topogr 25(1):27–38
Lei X, Wu T, Valdes-Sosa PA (2015) Incorporating priors for EEG source imaging and connectivity analysis. Front Neurosci 9:284
Lemieux L (2004) Electroencephalography-correlated functional MR imaging studies of epileptic activity. Neuroimaging Clin N Am 14(3):487–506
Lemieux L, Allen PJ, Franconi F, Symms MR, Fish DR (1997) Recording of EEG during fMRI experiments: patient safety. Magn Reson Med 38(6):943–952
Lemieux L, Krakow K, Fish DR (2001a) Comparison of spike-triggered functional MRI BOLD activation and EEG dipole model localization. NeuroImage 14(5):1097–1104
Lemieux L, Salek-Haddadi A, Josephs O, Allen P, Toms N, Scott C, Krakow K, Turner R, Fish DR (2001b) Event-related fMRI with simultaneous and continuous EEG: description of the method and initial case report. NeuroImage 14(3):780–787
Lemieux L, Laufs H, Carmichael D, Paul JS, Walker MC, Duncan JS (2008) Noncanonical spike-related BOLD responses in focal epilepsy. Hum Brain Mapp 29(3):329–345
LeVan P, Urrestarazu E, Gotman J (2006) A system for automatic artifact removal in ictal scalp EEG based on independent component analysis and Bayesian classification. Clin Neurophysiol 117(4):912–927
LeVan P, Tyvaert L, Gotman J (2010) Modulation by EEG features of BOLD responses to interictal epileptiform discharges. NeuroImage 50(1):15–26
Li Q, Liu G, Wei D, Guo J, Yuan G, Wu S (2017) The spatiotemporal pattern of pure tone processing: a single-trial EEG-fMRI study. NeuroImage 187:184–191
Liebenthal E, Ellingson ML, Spanaki MV, Prieto TE, Ropella KM, Binder JR (2003) Simultaneous ERP and fMRI of the auditory cortex in a passive oddball paradigm. NeuroImage 19(4):1395–1404
Lindquist MA (2008) The statistical analysis of fMRI data. Stat Sci 23(4):439–464
Liston AD, Salek-Haddadi A, Kiebel SJ, Hamandi K, Turner R, Lemieux L (2004) The MR detection of neuronal depolarization during 3-Hz spike-and-wave complexes in generalized epilepsy. Magn Reson Imaging 22(10):1441–1444
Liston AD, De Munck JC, Hamandi K, Laufs H, Ossenblok P, Duncan JS, Lemieux L (2006a) Analysis of EEG-fMRI data in focal epilepsy based on automated spike classification and Signal Space Projection. NeuroImage 31(3):1015–1024
Liston AD, Lund TE, Salek-Haddadi A, Hamandi K, Friston KJ, Lemieux L (2006b) Modelling cardiac signal as a confound in EEG-fMRI and its application in focal epilepsy studies. NeuroImage 30(3):827–834
Liu AK, Belliveau JW, Dale AM (1998) Spatiotemporal imaging of human brain activity using functional MRI constrained magnetoencephalography data: Monte Carlo simulations. Proc Natl Acad Sci U S A 95(15):8945–8950
Liu Z, Kecman F, He B (2006) Effects of fMRI-EEG mismatches in cortical current density estimation integrating fMRI and EEG: a simulation study. Clin Neurophysiol 117(7):1610–1622
Liu Z, Rios C, Zhang N, Yang L, Chen W, He B (2010) Linear and nonlinear relationships between visual stimuli, EEG and BOLD fMRI signals. NeuroImage 50(3):1054–1066
Logothetis NK, Wandell BA (2004) Interpreting the BOLD signal. Annu Rev Physiol 66:735–769
Logothetis NK, Pauls J, Augath M, Trinath T, Oeltermann A (2001) Neurophysiological investigation of the basis of the fMRI signal. Nature 412(6843):150–157
Lopes da Silva FH, Van Rotterdam A (2005) Biophysical aspects of EEG and magnetoencephalogram generation. In: Niedermeyer E, Lopes da Silva FH (eds) Electroencephalography: basic principles, clinical applications, and related fields. Lippincott Williams Wilkins, Baltimore
Lovblad KO, Thomas R, Jakob PM, Scammell T, Bassetti C, Griswold M, Ives J, Matheson J, Edelman RR, Warach S (1999) Silent functional magnetic resonance imaging demonstrates focal activation in rapid eye movement sleep. Neurology 53(9):2193–2195

Lu Y, Bagshaw AP, Grova C, Kobayashi E, Dubeau F, Gotman J (2006) Using voxel-specific hemodynamic response function in EEG-fMRI data analysis. NeuroImage 32(1):238–247
Lund TE, Norgaard MD, Rostrup E, Rowe JB, Paulson OB (2005) Motion or activity: their role in intra- and inter-subject variation in fMRI. NeuroImage 26(3):960–964
Machado A, Lina JM, Tremblay J, Lassonde M, Nguyen DK, Lesage F, Grova C (2011) Detection of hemodynamic responses to epileptic activity using simultaneous Electro-EncephaloGraphy (EEG)/Near Infra Red Spectroscopy (NIRS) acquisitions. NeuroImage 56(1):114–125
Makeig S, Jung TP, Bell AJ, Ghahremani D, Sejnowski TJ (1997) Blind separation of auditory event-related brain responses into independent components. Proc Natl Acad Sci U S A 94(20):10979–10984
Makiranta MJ, Ruohonen J, Suominen K, Sonkajarvi E, Salomaki T, Kiviniemi V, Seppanen T, Alahuhta S, Jantti V, Tervonen O (2004) BOLD-contrast functional MRI signal changes related to intermittent rhythmic delta activity in EEG during voluntary hyperventilation-simultaneous EEG and fMRI study. NeuroImage 22(1):222–231
Makni S, Idier J, Vincent T, Thirion B, Dehaene-Lambertz G, Ciuciu P (2008) A fully Bayesian approach to the parcel-based detection-estimation of brain activity in fMRI. NeuroImage 41(3):941–969
Malinowska U, Badier JM, Gavaret M, Bartolomei F, Chauvel P, Benar CG (2014) Interictal networks in magnetoencephalography. Hum Brain Mapp 35(6):2789–2805
Malow BA, Kushwaha R, Lin X, Morton KJ, Aldrich MS (1997) Relationship of interictal epileptiform discharges to sleep depth in partial epilepsy. Electroencephalogr Clin Neurophysiol 102(1):20–26
Mandelkow H, Halder P, Brandeis D, Soellinger M, de Zanche N, Luechinger R, Boesiger P (2007) Heart beats brain: the problem of detecting alpha waves by neuronal current imaging in joint EEG-MRI experiments. NeuroImage 37(1):149–163
Mantini D, Perrucci MG, Cugini S, Ferretti A, Romani GL, Del Gratta C (2007a) Complete artifact removal for EEG recorded during continuous fMRI using independent component analysis. NeuroImage 34(2):598–607
Mantini D, Perrucci MG, Del Gratta C, Romani GL, Corbetta M (2007b) Electrophysiological signatures of resting state networks in the human brain. Proc Natl Acad Sci U S A 104(32):13170–13175
Marrelec G, Benali H, Ciuciu P, Pelegrini-Issac M, Poline JB (2003) Robust Bayesian estimation of the hemodynamic response function in event-related BOLD fMRI using basic physiological information. Hum Brain Mapp 19(1):1–17
Martinez-Montes E, Valdes-Sosa PA, Miwakeichi F, Goldman RI, Cohen MS (2004) Concurrent EEG/fMRI analysis by multiway partial least squares. NeuroImage 22(3):1023–1034
Matsuda T, Matsuura M, Ohkubo T, Ohkubo H, Atsumi Y, Tamaki M, Takahashi K, Matsushima E, Kojima T (2002) Influence of arousal level for functional magnetic resonance imaging (fMRI) study: simultaneous recording of fMRI and electroencephalogram. Psychiatry Clin Neurosci 56(3):289–290
Mayhew SD, Bagshaw AP (2017) Dynamic spatiotemporal variability of alpha-BOLD relationships during the resting-state and task-evoked responses. NeuroImage 155:120–137
Mayhew SD, Iannetti GD, Woolrich MW, Wise RG (2006) Automated single-trial measurement of amplitude and latency of laser-evoked potentials (LEPs) using multiple linear regression. Clin Neurophysiol 117(6):1331–1344
Mayhew SD, Hylands-White N, Porcaro C, Derbyshire SW, Bagshaw AP (2013a) Intrinsic variability in the human response to pain is assembled from multiple, dynamic brain processes. NeuroImage 75:68–78
Mayhew SD, Ostwald D, Porcaro C, Bagshaw AP (2013b) Spontaneous EEG alpha oscillation interacts with positive and negative BOLD responses in the visual-auditory cortices and default-mode network. NeuroImage 76:362–372
McAvoy M, Larson-Prior L, Ludwikow M, Zhang D, Snyder AZ, Gusnard DL, Raichle ME, d'Avossa G (2012) Dissociated mean and functional connectivity BOLD signals in visual cortex during eyes closed and fixation. J Neurophysiol 108(9):2363–2372

McIntosh AR, Lobaugh NJ (2004) Partial least squares analysis of neuroimaging data: applications and advances. NeuroImage 23:250–263

McKeown MJ, Makeig S, Brown GG, Jung TP, Kindermann SS, Bell AJ, Sejnowski TJ (1998) Analysis of fMRI data by blind separation into independent spatial components. Hum Brain Mapp 6(3):160–188

McKeown M, Hu YJ, Jane Wang Z (2005) ICA denoising for event-related fMRI studies. Conf Proc IEEE Eng Med Biol Soc 1:157–161

Meir-Hasson Y, Kinreich S, Podlipsky I, Hendler T, Intrator N (2014) An EEG finger-print of fMRI deep regional activation. NeuroImage 102(1):128–141

Menon V, Ford JM, Lim KO, Glover GH, Pfefferbaum A (1997) Combined event-related fMRI and EEG evidence for temporal-parietal cortex activation during target detection. Neuroreport 8(14):3029–3037

Meriaux S, Roche A, Dehaene-Lambertz G, Thirion B, Poline JB (2006) Combined permutation test and mixed-effect model for group average analysis in fMRI. Hum Brain Mapp 27(5):402–410

Merlet I, Gotman J (2001) Dipole modeling of scalp electroencephalogram epileptic discharges: correlation with intracerebral fields. Clin Neurophysiol 112(3):414–430

Mirsattari SM, Wang Z, Ives JR, Bihari F, Leung LS, Bartha R, Menon RS (2006) Linear aspects of transformation from interictal epileptic discharges to BOLD fMRI signals in an animal model of occipital epilepsy. NeuroImage 30(4):1133–1148

Miwakeichi F, Martinez-Montes E, Valdes-Sosa PA, Nishiyama N, Mizuhara H, Yamaguchi Y (2004) Decomposing EEG data into space-time-frequency components using parallel factor analysis. NeuroImage 22(3):1035–1045

Mo J, Liu Y, Huang H, Ding M (2013) Coupling between visual alpha oscillations and default mode activity. NeuroImage 68:112–118

Moosmann M, Ritter P, Krastel I, Brink A, Thees S, Blankenburg F, Taskin B, Obrig H, Villringer A (2003) Correlates of alpha rhythm in functional magnetic resonance imaging and near infrared spectroscopy. NeuroImage 20(1):145–158

Moosmann M, Eichele T, Nordby H, Hugdahl K, Calhoun VD (2007) Joint independent component analysis for simultaneous EEG-fMRI: principle and simulation. Int J Psychophysiol 67(3):212–221

Morillon B, Lehongre K, Frackowiak RS, Ducorps A, Kleinschmidt A, Poeppel D, Giraud AL (2010) Neurophysiological origin of human brain asymmetry for speech and language. Proc Natl Acad Sci U S A 107(43):18688–18693

Mulert C, Jager L, Schmitt R, Bussfeld P, Pogarell O, Moller HJ, Juckel G, Hegerl U (2004) Integration of fMRI and simultaneous EEG: towards a comprehensive understanding of localization and time-course of brain activity in target detection. NeuroImage 22(1):83–94

Mulert C, Hepp P, Leicht G, Karch S, Lutz J, Moosmann M, Reiser M, Hegerl U, Pogarell O, Möller H-J, Jäger L (2007) High frequency oscillations in the gamma-band and the corresponding BOLD signal: Trial-by-trial coupling of EEG and fMRI reveals the involvement of the thalamic reticular nucleus (TRN). 13th Annual Meeting of the Organization for Human Brain Mapping Chicago, Illinois

Mulert C, Leicht G, Hepp P, Kirsch V, Karch S, Pogarell O, Reiser M, Hegerl U, Jager L, Moller HJ, McCarley RW (2010) Single-trial coupling of the gamma-band response and the corresponding BOLD signal. NeuroImage 49(3):2238–2247

Mullinger KJ, Mayhew SD, Bagshaw AP, Bowtell R, Francis ST (2013) Poststimulus undershoots in cerebral blood flow and BOLD fMRI responses are modulated by poststimulus neuronal activity. Proc Natl Acad Sci U S A 110(33):13636–13641

Muraskin J, Brown TR, Walz JM, Tu T, Conroy B, Goldman RI, Sajda P (2017) A multimodal encoding model applied to imaging decision-related neural cascades in the human brain. NeuroImage 180(Pt A):211–222

Musso F, Brinkmeyer J, Mobascher A, Warbrick T, Winterer G (2010) Spontaneous brain activity and EEG microstates. A novel EEG/fMRI analysis approach to explore resting-state networks. NeuroImage 52(4):1149–1161

Nakamura W, Anami K, Mori T, Saitoh O, Cichocki A, Amari S (2006) Removal of ballistocardiogram artifacts from simultaneously recorded EEG and fMRI data using independent component analysis. IEEE Trans Biomed Eng 53(7):1294–1308

Neuner I, Warbrick T, Arrubla J, Felder J, Celik A, Reske M, Boers F, Shah NJ (2013) EEG acquisition in ultra-high static magnetic fields up to 9.4 T. NeuroImage 68:214–220

Neuner I, Arrubla J, Werner CJ, Hitz K, Boers F, Kawohl W, Shah NJ (2014) The default mode network and EEG regional spectral power: a simultaneous fMRI-EEG study. PLoS One 9(2):e88214

Nguyen VT, Cunnington R (2014) The superior temporal sulcus and the N170 during face processing: single trial analysis of concurrent EEG-fMRI. NeuroImage 86:492–502

Nguyen VT, Breakspear M, Cunnington R (2014) Fusing concurrent EEG-fMRI with dynamic causal modeling: application to effective connectivity during face perception. NeuroImage 102(1):60–70

Nichols TE, Holmes AP (2002) Nonparametric permutation tests for functional neuroimaging: a primer with examples. Hum Brain Mapp 15(1):1–25

Nierhaus T, Gundlach C, Goltz D, Thiel SD, Pleger B, Villringer A (2013) Internal ventilation system of MR scanners induces specific EEG artifact during simultaneous EEG-fMRI. NeuroImage 74:70–76

Niessing J, Ebisch B, Schmidt KE, Niessing M, Singer W, Galuske RA (2005) Hemodynamic signals correlate tightly with synchronized gamma oscillations. Science 309(5736):948–951

Nolte G, Bai O, Wheaton L, Mari Z, Vorbach S, Hallett M (2004) Identifying true brain interaction from EEG data using the imaginary part of coherency. Clin Neurophysiol 115(10):2292–2307

Nunez PL, Silberstein RB (2000) On the relationship of synaptic activity to macroscopic measurements: does co-registration of EEG with fMRI make sense? Brain Topogr 13(2):79–96

Nunez P, Srinivasan R (2005) Electric fields of the brain. Oxford University Press, New York

O'Hare AJ, Dien J, Waterson LD, Savage CR (2007) Activation of the posterior cingulate by semantic priming: a co-registered ERP/fMRI study. Brain Res 1189:97–114

Okon-Singer H, Podlipsky I, Siman-Tov T, Ben-Simon E, Zhdanov A, Neufeld MY, Hendler T (2011) Spatio-temporal indications of sub-cortical involvement in leftward bias of spatial attention. NeuroImage 54(4):3010–3020

Omidvarnia A, Pedersen M, Vaughan DN, Walz JM, Abbott DF, Zalesky A, Jackson GD (2017) Dynamic coupling between fMRI local connectivity and interictal EEG in focal epilepsy: a wavelet analysis approach. Hum Brain Mapp 38(11):5356–5374

Opitz B, Mecklinger A, Friederici AD, von Cramon DY (1999) The functional neuroanatomy of novelty processing: integrating ERP and fMRI results. Cereb Cortex 9(4):379–391

Ossadtchi A, Baillet S, Mosher JC, Thyerlei D, Sutherling W, Leahy RM (2004) Automated interictal spike detection and source localization in magnetoencephalography using independent components analysis and spatio-temporal clustering. Clin Neurophysiol 115(3):508–522

Ostwald D, Bagshaw AP (2011) Information theoretic approaches to functional neuroimaging. Magn Reson Imaging 29(10):1417–1428

Ostwald D, Porcaro C, Bagshaw AP (2010) An information theoretic approach to EEG-fMRI integration of visually evoked responses. NeuroImage 49(1):498–516

Otzenberger H, Gounot D, Foucher JR (2005) P300 recordings during event-related fMRI: a feasibility study. Brain Res Cogn Brain Res 23(2-3):306–315

Palva JM, Wang SH, Palva S, Zhigalov A, Monto S, Brookes MJ, Schoffelen JM, Jerbi K (2018) Ghost interactions in MEG/EEG source space: a note of caution on inter-areal coupling measures. NeuroImage 173:632–643

Parkes LM, Bastiaansen MC, Norris DG (2006) Combining EEG and fMRI to investigate the post-movement beta rebound. NeuroImage 29(3):685–696

Parra L, Alvino C, Tang A, Pearlmutter B, Yeung N, Osman A, Sajda P (2002) Linear spatial integration for single-trial detection in encephalography. NeuroImage 17(1):223–230

Patel MR, Blum A, Pearlman JD, Yousuf N, Ives JR, Saeteng S, Schomer DL, Edelman RR (1999) Echo-planar functional MR imaging of epilepsy with concurrent EEG monitoring. AJNR Am J Neuroradiol 20(10):1916–1919

Pedreira C, Vaudano AE, Thornton RC, Chaudhary UJ, Vulliemoz S, Laufs H, Rodionov R, Carmichael DW, Lhatoo SD, Guye M, Quian Quiroga R, Lemieux L (2014) Classification of EEG abnormalities in partial epilepsy with simultaneous EEG-fMRI recordings. NeuroImage 99:461–476

Penny W, Friston KJ (2004) Chapter 47 - classical and bayesian inference. In: Frackowiak RSJ, Friston KJ, Frith CD et al (eds) Human brain function, 2nd edn. Academic, Burlington, pp 911–968

Perlbarg V, Bellec P, Anton JL, Pelegrini-Issac M, Doyon J, Benali H (2007) CORSICA: correction of structured noise in fMRI by automatic identification of ICA components. Magn Reson Imaging 25(1):35–46

Pfurtscheller G, Lopes da Silva FH (1999) Event-related EEG/MEG synchronization and desynchronization: basic principles. Clin Neurophysiol 110(11):1842–1857

Philiastides MG, Sajda P (2006) Temporal characterization of the neural correlates of perceptual decision making in the human brain. Cereb Cortex 16(4):509–518

Phillips C, Mattout J, Rugg MD, Maquet P, Friston KJ (2005) An empirical Bayesian solution to the source reconstruction problem in EEG. NeuroImage 24(4):997–1011

Pittau F, Levan P, Moeller F, Gholipour T, Haegelen C, Zelmann R, Dubeau F, Gotman J (2011) Changes preceding interictal epileptic EEG abnormalities: comparison between EEG/fMRI and intracerebral EEG. Epilepsia 52(6):1120–1129

Pittau F, Dubeau F, Gotman J (2012) Contribution of EEG/fMRI to the definition of the epileptic focus. Neurology 78(19):1479–1487

Pittau F, Grouiller F, Spinelli L, Seeck M, Michel CM, Vulliemoz S (2014) The role of functional neuroimaging in pre-surgical epilepsy evaluation. Front Neurol 5:31

Pizzo F, Roehri N, Medina Villalon S, Trebuchon A, Chen S, Lagarde S, Carron R, Gavaret M, Giusiano B, McGonigal A, Bartolomei F, Badier JM, Benar CG (2019) Deep brain activities can be detected with magnetoencephalography. Nat Commun 10(1):971

Poline JB, Worsley KJ, Evans AC, Friston KJ (1997) Combining spatial extent and peak intensity to test for activations in functional imaging. NeuroImage 5(2):83–96

Porcaro C, Ostwald D, Bagshaw AP (2010) Functional source separation improves the quality of single trial visual evoked potentials recorded during concurrent EEG-fMRI. NeuroImage 50(1):112–123

Portas CM, Krakow K, Allen P, Josephs O, Armony JL, Frith CD (2000) Auditory processing across the sleep-wake cycle: simultaneous EEG and fMRI monitoring in humans. Neuron 28(3):991–999

Qin Y, Jiang S, Zhang Q, Dong L, Jia X, He H, Yao Y, Yang H, Zhang T, Luo C, Yao D (2019) BOLD-fMRI activity informed by network variation of scalp EEG in juvenile myoclonic epilepsy. Neuroimage Clin 22:101759

Quian Quiroga R, Garcia H (2003) Single-trial event-related potentials with wavelet denoising. Clin Neurophysiol 114(2):376–390

Raichle ME, Snyder AZ (2007) A default mode of brain function: a brief history of an evolving idea. NeuroImage 37(4):1083–1090. discussion 1097-1089

Ranta-aho PO, Koistinen AS, Ollikainen JO, Kaipio JP, Partanen J, Karjalainen PA (2003) Single-trial estimation of multichannel evoked-potential measurements. IEEE Trans Biomed Eng 50(2):189–196

Scheeringa R, Fries P (2019) Cortical layers rhythms and BOLD signals. NeuroImage 197689-698 S1053811917309096. https://doi.org/10.1016/j.neuroimage.2017.11.002

Ridley B, Wirsich J, Bettus G, Rodionov R, Murta T, Chaudhary U, Carmichael D, Thornton R, Vulliemoz S, McEvoy A, Wendling F, Bartolomei F, Ranjeva JP, Lemieux L, Guye M (2017) Simultaneous intracranial EEG-fMRI shows inter-modality correlation in time-resolved connectivity within normal areas but not within epileptic regions. Brain Topogr 30(5):639–655

Ritter P, Villringer A (2006) Simultaneous EEG-fMRI. Neurosci Biobehav Rev 30(6):823–838

Ritter P, Freyer F, Curio G, Villringer A (2008) High-frequency (600 Hz) population spikes in human EEG delineate thalamic and cortical fMRI activation sites. NeuroImage 42(2):483–490

Rodionov R, De Martino F, Laufs H, Carmichael DW, Formisano E, Walker M, Duncan JS, Lemieux L (2007) Independent component analysis of interictal fMRI in focal epilepsy: comparison with general linear model-based EEG-correlated fMRI. NeuroImage 38(3):488–500

Rollings DT, Assecondi S, Ostwald D, Porcaro C, McCorry D, Bagary M, Soryal I, Bagshaw AP (2016) Early haemodynamic changes observed in patients with epilepsy, in a visual experiment and in simulations. Clin Neurophysiol 127(1):245–253

Rosler F, Manzey D (1981) Principal components and varimax-rotated components in event-related potential research: some remarks on their interpretation. Biol Psychol 13:3–26

Rossell SL, Price CJ, Nobre AC (2003) The anatomy and time course of semantic priming investigated by fMRI and ERPs. Neuropsychologia 41(5):550–564

Rothlubbers S, Relvas V, Leal A, Figueiredo P (2013) Reduction of EEG artefacts induced by vibration in the MR-environment. Conf Proc IEEE Eng Med Biol Soc 2013:2092–2095

Rothlubbers S, Relvas V, Leal A, Murta T, Lemieux L, Figueiredo P (2015) Characterisation and reduction of the EEG artefact caused by the helium cooling pump in the MR environment: validation in epilepsy patient data. Brain Topogr 28(2):208–220

Sadaghiani S, Wirsich J (2020) Intrinsic connectome organization across temporal scales: New insights from cross-modal approaches. Netw Neurosci 4(1):1–29

Sadaghiani S, Scheeringa R, Lehongre K, Morillon B, Giraud AL, Kleinschmidt A (2010) Intrinsic connectivity networks, alpha oscillations, and tonic alertness: a simultaneous electroencephalography/functional magnetic resonance imaging study. J Neurosci 30(30):10243–10250

Sadaghiani S, Scheeringa R, Lehongre K, Morillon B, Giraud AL, D'Esposito M, Kleinschmidt A (2012) alpha-band phase synchrony is related to activity in the fronto-parietal adaptive control network. J Neurosci 32(41):14305–14310

Sadeh B, Podlipsky I, Zhdanov A, Yovel G (2010) Event-related potential and functional MRI measures of face-selectivity are highly correlated: a simultaneous ERP-fMRI investigation. Hum Brain Mapp 31(10):1490–1501

Saignavongs M, Ciumas C, Petton M, Bouet R, Boulogne S, Rheims S, Carmichael DW, Lachaux JP, Ryvlin P (2017) Neural activity elicited by a cognitive task can be detected in single-trials with simultaneous intracerebral EEG-fMRI recordings. Int J Neural Syst 27(1):1750001

Saillet S, Quilichini PP, Ghestem A, Giusiano B, Ivanov AI, Hitziger S, Vanzetta I, Bernard C, Benar CG (2016) Interneurons contribute to the hemodynamic/metabolic response to epileptiform discharges. J Neurophysiol 115(3):1157–1169

Salek-Haddadi A, Lemieux L, Fish DR (2002) Role of functional magnetic resonance imaging in the evaluation of patients with malformations caused by cortical development. Neurosurg Clin N Am 13(1):63–69

Salek-Haddadi A, Friston KJ, Lemieux L, Fish DR (2003a) Studying spontaneous EEG activity with fMRI. Brain Res Brain Res Rev 43(1):110–133

Salek-Haddadi A, Lemieux L, Merschhemke M, Diehl B, Allen PJ, Fish DR (2003b) EEG quality during simultaneous functional MRI of interictal epileptiform discharges. Magn Reson Imaging 21(10):1159–1166

Salek-Haddadi A, Lemieux L, Merschhemke M, Friston KJ, Duncan JS, Fish DR (2003c) Functional magnetic resonance imaging of human absence seizures. Ann Neurol 53(5):663–667

Salek-Haddadi A, Diehl B, Hamandi K, Merschhemke M, Liston A, Friston K, Duncan JS, Fish DR, Lemieux L (2006) Hemodynamic correlates of epileptiform discharges: an EEG-fMRI study of 63 patients with focal epilepsy. Brain Res 1088(1):148–166

Sammer G, Blecker C, Gebhardt H, Kirsch P, Stark R, Vaitl D (2005) Acquisition of typical EEG waveforms during fMRI: SSVEP, LRP, and frontal theta. NeuroImage 24(4):1012–1024

Sammer G, Blecker C, Gebhardt H, Bischoff M, Stark R, Morgen K, Vaitl D (2007) Relationship between regional hemodynamic activity and simultaneously recorded EEG-theta associated with mental arithmetic-induced workload. Hum Brain Mapp 28(8):793–803

Scarff CJ, Reynolds A, Goodyear BG, Ponton CW, Dort JC, Eggermont JJ (2004) Simultaneous 3-T fMRI and high-density recording of human auditory evoked potentials. NeuroImage 23(3):1129–1142

Schabus M, Dang-Vu TT, Albouy G, Balteau E, Boly M, Carrier J, Darsaud A, Degueldre C, Desseilles M, Gais S, Phillips C, Rauchs G, Schnakers C, Sterpenich V, Vandewalle G, Luxen A, Maquet P (2007) Hemodynamic cerebral correlates of sleep spindles during human non-rapid eye movement sleep. Proc Natl Acad Sci U S A 104(32):13164–13169

Scheeringa R, Bastiaansen MC, Petersson KM, Oostenveld R, Norris DG, Hagoort P (2008) Frontal theta EEG activity correlates negatively with the default mode network in resting state. Int J Psychophysiol 67(3):242–251

Scheeringa R, Fries P, Petersson KM, Oostenveld R, Grothe I, Norris DG, Hagoort P, Bastiaansen MC (2011) Neuronal dynamics underlying high- and low-frequency EEG oscillations contribute independently to the human BOLD signal. Neuron 69(3):572–583

Scheeringa R, Petersson KM, Kleinschmidt A, Jensen O, Bastiaansen MC (2012) EEG alpha power modulation of fMRI resting-state connectivity. Brain Connect 2(5):254–264

Schirner M, McIntosh AR, Jirsa V, Deco G, Ritter P (2018) Inferring multi-scale neural mechanisms with brain network modelling. elife 7:e28927

Schmidt DM, George JS, Wood CC (1999) Bayesian inference applied to the electromagnetic inverse problem. Hum Brain Mapp 7(3):195–212

Schnitzler A, Timmermann L, Gross J (2006) Physiological and pathological oscillatory networks in the human motor system. J Physiol Paris 99(1):3–7

Schoffelen JM, Gross J (2009) Source connectivity analysis with MEG and EEG. Hum Brain Mapp 30(6):1857–1865

Schwab S, Koenig T, Morishima Y, Dierks T, Federspiel A, Jann K (2015) Discovering frequency sensitive thalamic nuclei from EEG microstate informed resting state fMRI. NeuroImage 118:368–375

Seeber M, Cantonas LM, Hoevels M, Sesia T, Visser-Vandewalle V, Michel CM (2019) Subcortical electrophysiological activity is detectable with high-density EEG source imaging. Nat Commun 10(1):753

Dumoulin SO, Fracasso A, van der Zwaag W, Siero JCW, Petridou N (2018) Ultra-high field MRI: Advancing systems neuroscience towards mesoscopic human brain function. NeuroImage 168345-357 S1053811917300289. https://doi.org/10.1016/j.neuroimage.2017.01.028

Seeck M, Lazeyras F, Michel CM, Blanke O, Gericke CA, Ives J, Delavelle J, Golay X, Haenggeli CA, de Tribolet N, Landis T (1998) Non-invasive epileptic focus localization using EEG-triggered functional MRI and electromagnetic tomography. Electroencephalogr Clin Neurophysiol 106(6):508–512

Shamshiri EA, Tierney TM, Centeno M, St Pier K, Pressler RM, Sharp DJ, Perani S, Cross JH, Carmichael DW (2017) Interictal activity is an important contributor to abnormal intrinsic network connectivity in paediatric focal epilepsy. Hum Brain Mapp 38(1):221–236

Simony E, Honey CJ, Chen J, Lositsky O, Yeshurun Y, Wiesel A, Hasson U (2016) Dynamic reconfiguration of the default mode network during narrative comprehension. Nat Commun 7:12141

Siniatchkin M, Moeller F, Jacobs J, Stephani U, Boor R, Wolff S, Jansen O, Siebner H, Scherg M (2007) Spatial filters and automated spike detection based on brain topographies improve sensitivity of EEG-fMRI studies in focal epilepsy. NeuroImage 37(3):834–843

Kashyap S, Ivanov D, Havlicek M, Poser BA, Uludağ K (2018) Impact of acquisition and analysis strategies on cortical depth-dependent fMRI. NeuroImage 168332-344 S1053811917304147. https://doi.org/10.1016/j.neuroimage.2017.05.022

Srivastava G, Crottaz-Herbette S, Lau KM, Glover GH, Menon V (2005) ICA-based procedures for removing ballistocardiogram artifacts from EEG data acquired in the MRI scanner. NeuroImage 24(1):50–60

Stern JM (2006) Simultaneous electroencephalography and functional magnetic resonance imaging applied to epilepsy. Epilepsy Behav 8(4):683–692

Stern JM, Caporro M, Haneef Z, Yeh HJ, Buttinelli C, Lenartowicz A, Mumford JA, Parvizi J, Poldrack RA (2011) Functional imaging of sleep vertex sharp transients. Clin Neurophysiol 122(7):1382–1386

Steyrl D, Krausz G, Koschutnig K, Edlinger G, Muller-Putz GR (2018) Online reduction of artifacts in EEG of simultaneous EEG-fMRI using reference layer adaptive filtering (RLAF). Brain Topogr 31(1):129–149

Storti SF, Formaggio E, Bertoldo A, Manganotti P, Fiaschi A, Toffolo GM (2013) Modelling hemodynamic response function in epilepsy. Clin Neurophysiol 124(11):2108–2118

Supek S, Aine CJ (1993) Simulation studies of multiple dipole neuromagnetic source localization: model order and limits of source resolution. IEEE Trans Biomed Eng 40(6):529–540

Symms MR, Allen PJ, Woermann FG, Polizzi G, Krakow K, Barker GJ, Fish DR, Duncan JS (1999) Reproducible localization of interictal epileptiform discharges using EEG-triggered fMRI. Phys Med Biol 44(7):161–168

Tagliazucchi E, Laufs H (2014) Decoding wakefulness levels from typical fMRI resting-state data reveals reliable drifts between wakefulness and sleep. Neuron 82(3):695–708

Tagliazucchi E, von Wegner F, Morzelewski A, Borisov S, Jahnke K, Laufs H (2012a) Automatic sleep staging using fMRI functional connectivity data. NeuroImage 63(1):63–72

Tagliazucchi E, von Wegner F, Morzelewski A, Brodbeck V, Laufs H (2012b) Dynamic BOLD functional connectivity in humans and its electrophysiological correlates. Front Hum Neurosci 6:339

Tagliazucchi E, von Wegner F, Morzelewski A, Brodbeck V, Borisov S, Jahnke K, Laufs H (2013) Large-scale brain functional modularity is reflected in slow electroencephalographic rhythms across the human non-rapid eye movement sleep cycle. NeuroImage 70:327–339

Takata N, Sugiura Y, Yoshida K, Koizumi M, Hiroshi N, Honda K, Yano R, Komaki Y, Matsui K, Suematsu M, Mimura M, Okano H, Tanaka KF (2018) Optogenetic astrocyte activation evokes BOLD fMRI response with oxygen consumption without neuronal activity modulation. Glia 66:2013–2023

Tanaka H, Fujita N, Takanashi M, Hirabuki N, Yoshimura H, Abe K, Nakamura H (2003) Effect of stage 1 sleep on auditory cortex during pure tone stimulation: evaluation by functional magnetic resonance imaging with simultaneous EEG monitoring. AJNR Am J Neuroradiol 24(10):1982–1988

Tangwiriyasakul C, Perani S, Centeno M, Yaakub SN, Abela E, Carmichael DW, Richardson MP (2018) Dynamic brain network states in human generalized spike-wave discharges. Brain 141(10):2981–2994

Thirion B, Faugeras O (2003) Dynamical components analysis of fMRI data through kernel PCA. NeuroImage 20(1):34–49

Ting KH, Fung PC, Chang CQ, Chan FH (2006) Automatic correction of artifact from single-trial event-related potentials by blind source separation using second order statistics only. Med Eng Phys 28(8):780–794

Tohka J, Foerde K, Aron AR, Tom SM, Toga AW, Poldrack RA (2008) Automatic independent component labeling for artifact removal in fMRI. NeuroImage 39(3):1227–1245

Toma K, Matsuoka T, Immisch I, Mima T, Waldvogel D, Koshy B, Hanakawa T, Shill H, Hallett M (2002) Generators of movement-related cortical potentials: fMRI-constrained EEG dipole source analysis. NeuroImage 17(1):161–173

Tousseyn S, Dupont P, Robben D, Goffin K, Sunaert S, Van Paesschen W (2014) A reliable and time-saving semiautomatic spike-template-based analysis of interictal EEG-fMRI. Epilepsia 55(12):2048–2058

Trujillo-Barreto NJ, Martínez-Montes E, Melie-García L, Valdés-Sosa PA (2001) A Symmetrical Bayesian Model for fMRI and EEG/MEG Neuroimage Fusion. Int J Bioelectromag 3:1

Trujillo-Barreto NJ, Aubert-Vazquez E, Valdes-Sosa PA (2004) Bayesian model averaging in EEG/MEG imaging. NeuroImage 21(4):1300–1319

Tyvaert L, Levan P, Grova C, Dubeau F, Gotman J (2008) Effects of fluctuating physiological rhythms during prolonged EEG-fMRI studies. Clin Neurophysiol 119(12):2762–2774

Uji M, Wilson R, Francis ST, Mullinger KJ, Mayhew SD (2018) Exploring the advantages of multiband fMRI with simultaneous EEG to investigate coupling between gamma frequency neural activity and the BOLD response in humans. Hum Brain Mapp 39(4):1673–1687

van Graan LA, Lemieux L, Chaudhary UJ (2015) Methods and utility of EEG-fMRI in epilepsy. Quant Imaging Med Surg 5(2):300–312

van Houdt PJ, Ossenblok PP, Colon AJ, Boon PA, de Munck JC (2012) A framework to integrate EEG-correlated fMRI and intracerebral recordings. NeuroImage 60(4):2042–2053

Vanzetta I, Flynn C, Ivanov AI, Bernard C, Bénar CG (2010) Investigation of linear coupling between single-event blood flow responses and interictal discharges in a model of experimental epilepsy. J Neurophysiol 103(6):3139–3152

Vazquez AL, Noll DC (1998) Nonlinear aspects of the BOLD response in functional MRI. NeuroImage 7(2):108–118

Vigario R, Sarela J, Jousmaki V, Hamalainen M, Oja E (2000) Independent component approach to the analysis of EEG and MEG recordings. IEEE Trans Biomed Eng 47(5):589–593

Viola FC, Thorne J, Edmonds B, Schneider T, Eichele T, Debener S (2009) Semi-automatic identification of independent components representing EEG artifact. Clin Neurophysiol 120(5):868–877

Vitrai J, Czobor P, Simon G, Varga L, Marosfi S (1984) Beyond principal component analysis: canonical component analysis for data reduction in classification of EPs. Int J Biomed Comput 15(2):93–111

Voges N, Blanchard S, Wendling F, David O, Benali H, Papadopoulo T, Clerc M, Benar C (2012) Modeling of the neurovascular coupling in epileptic discharges. Brain Topogr 25(2):136–156

Vulliemoz S, Rodionov R, Carmichael DW, Thornton R, Guye M, Lhatoo SD, Michel CM, Duncan JS, Lemieux L (2010) Continuous EEG source imaging enhances analysis of EEG-fMRI in focal epilepsy. NeuroImage 49(4):3219–3229

Vulliemoz S, Carmichael DW, Rosenkranz K, Diehl B, Rodionov R, Walker MC, McEvoy AW, Lemieux L (2011) Simultaneous intracranial EEG and fMRI of interictal epileptic discharges in humans. NeuroImage 54(1):182–190

Wager TD, Vazquez A, Hernandez L, Noll DC (2005) Accounting for nonlinear BOLD effects in fMRI: parameter estimates and a model for prediction in rapid event-related studies. NeuroImage 25(1):206–218

Wallstrom GL, Kass RE, Miller A, Cohn JF, Fox NA (2004) Automatic correction of ocular artifacts in the EEG: a comparison of regression-based and component-based methods. Int J Psychophysiol 53(2):105–119

Walz JM, Goldman RI, Carapezza M, Muraskin J, Brown TR, Sajda P (2013) Simultaneous EEG-fMRI reveals temporal evolution of coupling between supramodal cortical attention networks and the brainstem. J Neurosci 33(49):19212–19222

Walz JM, Goldman RI, Carapezza M, Muraskin J, Brown TR, Sajda P (2014) Simultaneous EEG-fMRI reveals a temporal cascade of task-related and default-mode activations during a simple target detection task. NeuroImage 102(1):229–239

Wan X, Riera J, Iwata K, Takahashi M, Wakabayashi T, Kawashima R (2006) The neural basis of the hemodynamic response nonlinearity in human primary visual cortex: implications for neurovascular coupling mechanism. NeuroImage 32(2):616–625

Wang Z, Maier A, Leopold DA, Logothetis NK, Liang H (2007) Single-trial evoked potential estimation using wavelets. Comput Biol Med 37(4):463–473

Wang W, Viswanathan S, Lee T, Grafton ST (2016) Coupling between theta oscillations and cognitive control network during cross-modal visual and auditory attention: supramodal vs modality-specific mechanisms. PLoS One 11(7):e0158465

Warach S, Ives JR, Schlaug G, Patel MR, Darby DG, Thangaraj V, Edelman RR, Schomer DL (1996) EEG-triggered echo-planar functional MRI in epilepsy. Neurology 47(1):89–93

Warbrick T, Arrubla J, Boers F, Neuner I, Shah NJ (2014) Attention to detail: why considering task demands is essential for single-trial analysis of BOLD correlates of the visual P1 and N1. J Cogn Neurosci 26(3):529–542

Wennberg R, Quesney F, Olivier A, Rasmussen T (1998) Electrocorticography and outcome in frontal lobe epilepsy. Electroencephalogr Clin Neurophysiol 106(4):357–368

Whittingstall K, Bartels A, Singh V, Kwon S, Logothetis NK (2010) Integration of EEG source imaging and fMRI during continuous viewing of natural movies. Magn Reson Imaging 28(8):1135–1142

Wirsich J, Benar C, Ranjeva JP, Descoins M, Soulier E, Le Troter A, Confort-Gouny S, Liegeois-Chauvel C, Guye M (2014) Single-trial EEG-informed fMRI reveals spatial dependency of BOLD signal on early and late IC-ERP amplitudes during face recognition. NeuroImage 100:325–336

Wirsich J, Ridley B, Besson P, Jirsa V, Benar C, Ranjeva JP, Guye M (2017) Complementary contributions of concurrent EEG and fMRI connectivity for predicting structural connectivity. NeuroImage 161:251–260

Wirsich J, Rey M, Guye M, Benar C, Lanteaume L, Ridley B, Confort-Gouny S, Casse-Perrot C, Soulier E, Viout P, Rouby F, Lefebvre MN, Audebert C, Truillet R, Jouve E, Payoux P, Bartres-Faz D, Bordet R, Richardson JC, Babiloni C, Rossini PM, Micallef J, Blin O, Ranjeva JP, Pharmacog C (2018) Brain networks are independently modulated by donepezil, sleep, and sleep deprivation. Brain Topogr 31(3):380–391

Wirsich J, Amico E, Giraud AL, Goni J, Sadaghiani S (2020a) Multi-timescale hybrid components of the functional brain connectome: a bimodal EEG-fMRI decomposition. Netw Neurosci 4(3):658–677

Wirsich J, Giraud AL, Sadaghiani S (2020b) Concurrent EEG- and fMRI-derived functional connectomes exhibit linked dynamics. NeuroImage 219:116998

Woo CW, Krishnan A, Wager TD (2014) Cluster-extent based thresholding in fMRI analyses: pitfalls and recommendations. NeuroImage 91:412–419

Worsley KJ, Friston KJ (1995) Analysis of fMRI time-series revisited–again. NeuroImage 2(3):173–181

Worsley KJ, Evans AC, Marrett S, Neelin P (1992) A three-dimensional statistical analysis for CBF activation studies in human brain. J Cereb Blood Flow Metab 12(6):900–918

Worsley KJ, Liao CH, Aston J, Petre V, Duncan GH, Morales F, Evans AC (2002) A general statistical analysis for fMRI data. NeuroImage 15(1):1–15

Wu L, Eichele T, Calhoun VD (2010) Reactivity of hemodynamic responses and functional connectivity to different states of alpha synchrony: a concurrent EEG-fMRI study. NeuroImage 52(4):1252–1260

Xiao F, An D, Lei D, Li L, Chen S, Wu X, Yang T, Ren J, Gong Q, Zhou D (2016) Real-time effects of centrotemporal spikes on cognition in rolandic epilepsy: An EEG-fMRI study. Neurology 86(6):544–551

Sirotin YB, Das A (2009) Anticipatory haemodynamic signals in sensory cortex not predicted by local neuronal activity. Nature 457(7228):475–479. https://doi.org/10.1038/nature07664

Yuan H, Zotev V, Phillips R, Drevets WC, Bodurka J (2012) Spatiotemporal dynamics of the brain at rest–exploring EEG microstates as electrophysiological signatures of BOLD resting state networks. NeuroImage 60(4):2062–2072

Yuan H, Zotev V, Phillips R, Bodurka J (2013) Correlated slow fluctuations in respiration, EEG, and BOLD fMRI. NeuroImage 79:81–93

Zhang J, Liu W, Chen H, Xia H, Zhou Z, Wang L, Mei S, Liu Q, Li Y (2012) EEG-fMRI validation studies in comparison with icEEG: a review. Int J Psychophysiol 84(3):233–239

Zich C, Debener S, Kranczioch C, Bleichner MG, Gutberlet I, De Vos M (2015) Real-time EEG feedback during simultaneous EEG-fMRI identifies the cortical signature of motor imagery. NeuroImage 114:438–447

Zijlmans M, Huiskamp G, Hersevoort M, Seppenwoolde JH, van Huffelen AC, Leijten FS (2007) EEG-fMRI in the preoperative work-up for epilepsy surgery. Brain 130(9):2343–2353

Real-Time fMRI Neurofeedback with Simultaneous EEG

13

Vadim Zotev, Ahmad Mayeli, Chung-Ki Wong, and Jerzy Bodurka

13.1 Introduction

Modern neuroimaging modalities (e.g., fMRI, EEG, MEG, fNIRS) offer broad opportunities for noninvasive brain neuromodulation based on neuroimaging signals measured in real time. The most common among such neuromodulation approaches is neurofeedback (nf). It allows a person to view a real-time neuroimaging signal reflecting an ongoing activity of his/her own brain and volitionally control this activity. EEG neurofeedback (EEG-nf) makes it possible to modulate electrophysiological brain activity as registered by scalp EEG electrodes. Real-time fMRI neurofeedback (rtfMRI-nf) enables volitional regulation of blood-oxygenation-level-dependent (BOLD) activity of a target brain region as measured by BOLD fMRI. Advances in simultaneous EEG-fMRI (e.g., Mulert and Lemieux 2010) have opened up new exciting possibilities in the field of neuromodulation.

V. Zotev (✉)
Laureate Institute for Brain Research, Tulsa, OK, USA

Mind Research Network, Albuquerque, NM, USA
e-mail: vzotev@mrn.org

A. Mayeli
Laureate Institute for Brain Research, Tulsa, OK, USA

University of Pittsburgh, Pittsburgh, PA, USA
e-mail: mayelia@upmc.edu

C. -K. Wong
Laureate Institute for Brain Research, Tulsa, OK, USA

OAM Photonics LLC, Albuquerque, NM, USA
e-mail: ckwong@oamphotonics.com

J. Bodurka
Laureate Institute for Brain Research, Tulsa, OK, USA
e-mail: jbodurka@laureateinstitute.org

C. Mulert, L. Lemieux (eds.), *EEG - fMRI*,
https://doi.org/10.1007/978-3-031-07121-8_13

Combination of concurrent EEG and fMRI measurements allows implementation of three different neuromodulation paradigms: (1) EEG-nf with simultaneous fMRI, (2) rtfMRI-nf with simultaneous EEG, and (3) simultaneous rtfMRI-nf and EEG-nf, which we abbreviate as rtfMRI-EEG-nf. Each of these paradigms can provide unique insights into human brain function and lead to development of new clinical neurofeedback applications. In this chapter, we focus on the last two paradigms and discuss their technical challenges, pioneering applications, neuroscience findings, and future directions.

Implementations of rtfMRI-nf have been made possible by the development of real-time functional magnetic resonance imaging (rtfMRI), a technique in which fMRI image processing, particularly the spatial image alignment required for head motion correction, keeps up with fMRI data acquisition (Cox et al. 1995). An rtfMRI signal from a selected brain region, updated at a rate of fMRI acquisition (repetition time *TR*), can be displayed to a person inside the MRI scanner, for example, in the form of a thermometer-style variable-height bar on a screen. The participant therefore has an opportunity to regulate his/her own brain activity by controlling the rtfMRI-nf signal in (what is experienced as) real time while performing a mental task engaging the target region. For reviews of rtfMRI-nf, see, for example, Birbaumer et al. (2013), deCharms (2008), Sitaram et al. (2017), Thibault et al. (2018), and Weiskopf (2012).

The main advantage of rtfMRI-nf compared to other types of neurofeedback (EEG-nf, MEG-nf, fNIRS-nf) is its ability to target BOLD activities of small precisely defined regions anywhere in the brain, including deep subcortical areas. This ability derives from the tomographic nature of MRI, as well as relatively high spatial resolution, whole-brain coverage, and improved sensitivity of measured signal to neuronal activity that can be achieved in modern fMRI (e.g., Bellgowan et al. 2006; Bodurka et al. 2004; de Zwart et al. 2004). In contrast, EEG, MEG, and fNIRS are each characterized by limited spatial depth sensitivity and relatively low source localization accuracy. This advantage of rtfMRI-nf is particularly important in studies of emotion regulation. Early proof-of-concept applications of rtfMRI-nf already targeted activities of deep brain regions, such as the amygdala (Posse et al. 2003) and subdivisions of the anterior cingulate cortex (ACC, Weiskopf et al. 2003). Among numerous more recent rtfMRI-nf studies, about 50% were designed to achieve regulation of BOLD activities of specific subcortical or deep cortical regions, particularly the amygdala, the insula, and the ACC (Thibault et al. 2018). Another important advantage of using rtfMRI for neurofeedback is sufficiently uniform whole-brain fMRI imaging coverage provided by modern MRI instrumentation, pulse sequences, and image reconstruction techniques. This allows a detailed fMRI investigation of network interactions between a target region and other regions throughout the brain (e.g., Zotev et al. 2011, 2013).

The rtfMRI-nf with simultaneous EEG is a very promising new multimodal brain research paradigm (Zotev et al. 2016, 2018a, b), which offers major research opportunities while presenting only minor technical difficulties beyond those of EEG-fMRI and rtfMRI-nf. When discussing this paradigm, we consider EEG recordings during rtfMRI to be passive, meaning that no EEG information is used in real time as part of the experimental procedure, and all EEG data analyses are

performed offline after the experiment. (The simultaneous multimodal rtfMRI-EEG-nf is discussed in Sect. 13.4.) The two modalities work together as follows. The rtfMRI-nf procedure enables direct modulation of BOLD activity of a deep subcortical target brain region, such as the amygdala. This modulation enhances interactions within the corresponding brain network, which depends on the mental task being performed along with rtfMRI-nf and includes both subcortical and cortical brain regions (e.g., Zotev et al. 2011, 2013). Electrophysiological activities of the engaged cortical regions can be efficiently probed by the simultaneous scalp EEG. This approach makes it possible to study associations between BOLD activities of target brain regions and various EEG activity metrics and patterns. Because EEG and fMRI data are acquired simultaneously, and EEG electrodes can be made visible in MR images if necessary, no co-registration issues arise in EEG-fMRI, in contrast, for example, to MEG-MRI data integration with its well-known co-registration problem (e.g., Zotev et al. 2008a, b).

The rtfMRI-nf with simultaneous EEG paradigm allows investigation of fundamental relationships between hemodynamic and electrophysiological processes in the human brain. It can enhance EEG-fMRI research in the following ways. First, it can provide greater sensitivity to specific EEG-fMRI effects of interest compared to conventional resting-state or task-based EEG-fMRI paradigms, because activity of a relevant brain region (or regions) is modulated more directly. Second, it can improve experimental power, because sufficient rtfMRI-nf training (when practical) can reduce both within-subject and between-subject variabilities in EEG-fMRI results. Therefore, this approach may be particularly well suited and beneficial in hypothesis-driven studies of weak EEG-fMRI phenomena. In such studies, both rtfMRI-nf implementation and experimental protocol should be optimized to enhance the procedure's capability to detect EEG-fMRI effects of interest (Zotev et al. 2018a). Alternatively, EEG data acquired during rtfMRI can be used in a more exploratory fashion to investigate EEG correlates of a preselected rtfMRI-nf procedure (Zotev et al. 2016, 2018b). Such investigation can be important from the clinical applications perspective, because it can help to identify promising target measures for stand alone EEG-nf. Effects of such EEG-nf could potentially complement or even approximate those of the rtfMRI-nf, thus enabling development of more affordable, portable, and accessible neurofeedback treatment options.

While the rtfMRI-nf with simultaneous EEG approach aims to evaluate electrophysiological processes during rtfMRI-nf training, the EEG-nf with simultaneous fMRI technique can be used to study hemodynamic processes accompanying EEG-nf training (e.g., Cavazza et al. 2014; Kinreich et al. 2012; Shtark et al. 2015; Zich et al. 2015). Scientifically, the two methods complement each other and can approach the same EEG-fMRI phenomenon from different directions. However, implementations of EEG-nf with simultaneous fMRI (or rtfMRI-EEG-nf) face a formidable technical challenge. To provide a reliable EEG-nf signal during fMRI, one has to achieve an accurate automatic removal of EEG-fMRI artifacts, as well as common EEG artifacts, from the EEG data in real time. In EEG recordings during fMRI, the theta and alpha EEG bands are severely contaminated with cardioballistic (CB) and random motion-related artifacts, while the beta and gamma EEG bands are contaminated with MRI gradient-switching (MR) artifacts. These

artifacts occur in addition to common EEG artifacts (eye-blinking, saccadic, muscle, electrode pop, reference, etc.). The main advantage of the rtfMRI-nf with simultaneous EEG approach is that all mentioned artifacts are identified and removed in *offline* EEG-fMRI analysis. This allows careful visual inspection of the entire EEG dataset at every analysis step and application of the most advanced EEG artifact removal techniques available, including independent component analysis (ICA), without real-time constraints. Moreover, one can utilize motion-related artifacts in EEG data acquired during fMRI to improve accuracy of retrospective fMRI motion correction (Wong et al. 2016, 2018; Zotev et al. 2012).

This chapter is organized as follows. In Sect. 13.2, we discuss rtfMRI-nf of the amygdala activity and its EEG correlates, with a focus on frontal alpha EEG asymmetry. Section 13.3 is devoted to rtfMRI-nf of the thalamus activity and its effects on alpha EEG rhythm. In Sect. 13.4, we review implementations and initial applications of rtfMRI-EEG-nf. Section 13.5 describes a real-time ICA procedure for improved EEG-nf during fMRI. Conclusions are summarized in Sect. 13.6.

13.2 Regulation of Amygdala BOLD Activity and Frontal EEG Asymmetry

The amygdala plays a fundamental role in emotion processing. Regulation of emotions involves interactions between the amygdala and areas of the prefrontal cortex (PFC), capable of exerting modulatory control over the amygdala activity. Emotion regulation employs essentially the same cognitive capacities as the executive function (i.e., attention, working memory, inhibition, planning, task shifting), except that they are used to control emotions. The executive function/emotion regulation (EF/ER) system includes the dorsolateral PFC (DLPFC), the ventrolateral PFC (VLPFC), and the medial PFC regions (Liberzon and Abelson 2016). The DLPFC also plays a central role in integrating motivation and executive function during goal pursuit (Spielberg et al. 2012). In major depressive disorder (MDD), emotion regulation deficits lead to exaggerated amygdala responses to negative or threat-related stimuli and blunted amygdala responses to positive emotional stimuli (e.g., Murray et al. 2011). MDD is also characterized by deficient approach motivation, associated with MDD patients' diminished reward responsiveness and reduced ability to engage in goal-oriented behaviors (e.g., Henriques and Davidson (2000)).

We have conducted the first study in which electrophysiological correlates of rtfMRI-nf training were evaluated using simultaneous EEG (Zotev et al. 2016). In the study, MDD patients learned to upregulate BOLD activity of their left amygdala using rtfMRI-nf during a positive emotion induction task based on retrieval of happy autobiographical memories (Fig. 13.1). The purpose of the amygdala activity upregulation was to strengthen the amygdala response to positive emotion and enhance recall of happy memories. The left amygdala (LA) was chosen as the target for rtfMRI-nf (Zotev et al. 2011, 2016) following the hypothesis that the right amygdala (RA) is involved in a rapid automatic detection of an emotional stimulus, while the left amygdala is engaged in a more sustained emotional stimulus

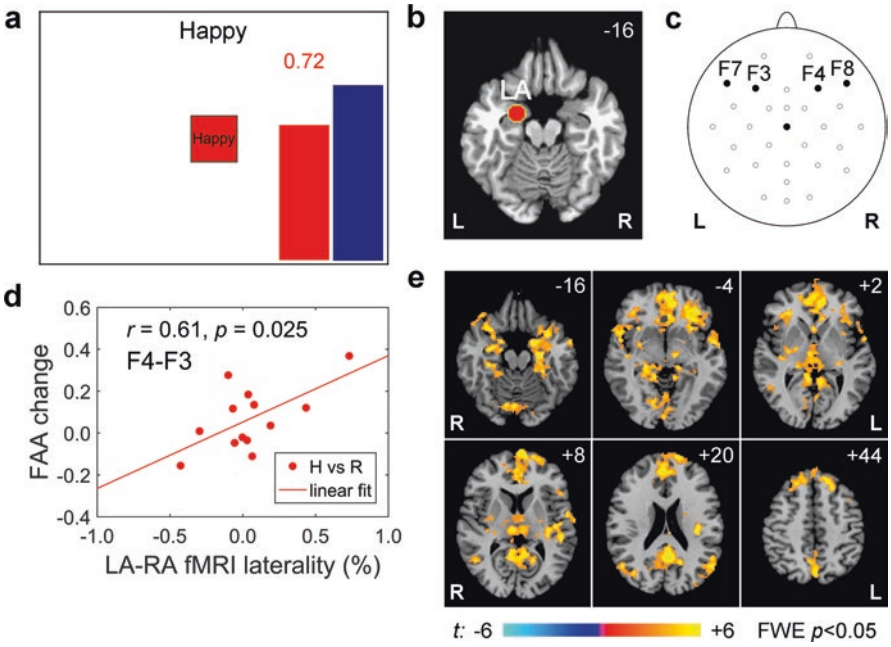

Fig. 13.1 Real-time fMRI neurofeedback of the amygdala activity with simultaneous EEG. (**a**) Real-time GUI display screen with variable-height red rtfMRI-nf bar and blue target bar. (**b**) Left amygdala (LA) target ROI for the rtfMRI-nf. (**c**) EEG electrodes used to study frontal EEG asymmetry. (**d**) Correlation between average laterality of the amygdala fMRI activity and average changes in frontal alpha EEG asymmetry (FAA, F4 vs F3) during the Happy Memories with rtfMRI-nf task (H) relative to the Rest baseline (R) for the experimental group (EG). (**e**) EEG-based PPI interaction effect indicating more positive temporal correlations between FAA and fMRI activities during the Happy Memories with rtfMRI-nf task compared to the Count task for the EG. The left hemisphere (L) is to the reader's right. The maps are shown in the Talairach space with *z*-coordinate specified for each slice. After Zotev et al. (2016)

evaluation (Wright et al. 2001). EEG recordings were conducted simultaneously with fMRI. EEG data analyses in the described study were exploratory, and no assumptions about EEG activity were made at the study design stage.

The experimental session included four rtfMRI-nf runs, each consisting of alternating 40 s long blocks of Happy Memories with rtfMRI-nf, Count, and Rest conditions (Zotev et al. 2011, 2016). A Transfer run without nf was added to evaluate transfer of training effects. For the experimental group (EG, $n = 13$), the rtfMRI-nf signal was based on average BOLD activity for a spherical target region of interest (ROI) in the LA area (Fig. 13.1b), measured in real time as fMRI percent signal change with respect to the Rest baseline. For the control group (CG, $n = 11$), the (sham) rtfMRI-nf signal was based on BOLD activity of a different brain region, presumably not involved in emotion processing (Zotev et al. 2011). The nf signal was displayed to a participant inside the scanner as a variable-height red bar on the screen (Fig. 13.1a), with the bar height updated every 2 s. During the Happy

Memories conditions with rtfMRI-nf, the participant was instructed to feel happy by recalling happy autobiographical events, while simultaneously trying to control and raise the level of the red rtfMRI-nf bar to a target level. All the experiments described in this chapter were conducted on the General Electric Discovery MR750 3T MRI scanner at the Laureate Institute for Brain Research (LIBR). A single-shot gradient-recalled echo-planar imaging (EPI) sequence was used for fMRI data acquisition. The rtfMRI-nf was implemented using a custom real-time MRI monitoring and control system (Bodurka and Bandettini 2008) utilizing real-time features of AFNI (Cox 1996). EEG recordings were performed simultaneously with fMRI using a 32-channel MR-compatible EEG system from the Brain Products, GmbH, as described previously (Zotev et al. 2012, 2016).

The EEG recordings during fMRI made it possible to examine mean task-dependent variations in EEG power and EEG coherence that accompanied the rtfMRI-nf training. During the Happy Memories with rtfMRI-nf task, the MDD patients in the EG were able to successfully upregulate BOLD activity of the LA target ROI, while the corresponding RA activity levels were somewhat lower. Thus, the rtfMRI-nf procedure increased laterality of the amygdala BOLD activity. The most significant EEG effects were observed for the upper alpha EEG band, which was defined individually for each participant as [IAF…IAF+2] Hz, where IAF is an individual alpha peak frequency. Mean variations in the upper alpha EEG power also exhibited laterality: the power showed stronger reductions during the rtfMRI-nf task for the prefrontal and temporal EEG channels on the left, compared to those on the right for the EG (Zotev et al. 2016). This observation suggested that frontal alpha EEG asymmetry was a relevant measure for characterizing EEG effects of the rtfMRI-nf procedure. Frontal alpha EEG asymmetry is commonly defined as FAA = $\ln(P(\text{right})) - \ln(P(\text{left}))$, where P is alpha EEG power for the corresponding prefrontal EEG channels on the right and on the left. Here, we discuss FAA for channels F4 on the right and F3 on the left (Fig. 13.1c) for the upper alpha EEG band. The mean FAA changes during the rtfMRI-nf task relative to the Rest baseline were positive for the EG and negative for the CG (Zotev et al. 2016). The EG vs CG group difference in the FAA changes was significant, provided that intersubject variability in depression severity was taken into account. The MDD patients' depression severity was assessed using the Hamilton Depression Rating Scale (HDRS, Hamilton 1960). Remarkably, the average individual FAA changes during the rtfMRI-nf task for the EG showed a strong dependence on trait depression severity and a significant positive correlation with the HDRS depression severity ratings (Zotev et al. 2016). Enhancements in upper alpha EEG coherence (EEG coherence slope across the four rtfMRI-nf runs) exhibited positive correlations with the HDRS ratings for pairs of frontotemporal EEG channels on the left, but not for those on the right. Correlation between the average individual laterality (left vs right) of such EEG coherence enhancement among frontotemporal EEG channels and the HDRS ratings was also positive and significant (Zotev et al. 2016).

These EEG findings provide important insights regarding effects of the rtfMRI-nf training from the EEG research perspective. A local reduction in alpha EEG power indicates activation of the underlying cortical area (Cook et al. 1998;

Goldman et al. 2002). The observed reductions in upper alpha power revealed activations of the left prefrontal and temporal cortical regions, including the left DLPFC and left VLPFC, during the rtfMRI-nf task for the EG. EEG studies have demonstrated relative hypoactivity (elevated alpha power) of the left prefrontal regions in depressed individuals—a finding that was hypothesized to indicate diminished trait approach motivation in depression (e.g., Henriques and Davidson 1991, 2000; Smith et al. 2018). Note that approach motivation is a construct within the positive valence systems domain of the research domain criteria (RDoC) matrix (e.g., Morris and Cuthbert 2012). The activation of the left prefrontal regions (reduced alpha power) during the rtfMRI-nf training can be interpreted as suggesting an enhancement in approach motivation with a possibility for correction of approach motivation deficits. Indeed, rtfMRI-nf training in general is a goal-oriented behavior that requires approach motivation on the part of a participant to be successful. In our study, for example, the MDD patients were asked to raise the rtfMRI-nf bar to reach the target level (Fig. 13.1a). They also induced happy emotion, which is associated with approach motivation. Moreover, the amygdala itself is a part of the brain network instantiating approach motivation, together with the left DLPFC, VLPFC (orbitofrontal cortex), ACC, and basal ganglia regions (Spielberg et al. 2012). Therefore, the described rtfMRI-nf procedure conceivably has the potential to correct approach motivation deficits in MDD patients by combining three essential elements: goal pursuit, happy emotion, and modulation of the amygdala activity and its network interactions.

The FAA, defined above, is believed to reflect functional and anatomical differences between the approach and avoidance motivation systems (e.g., Elliot and Covington 2001). It is commonly interpreted according to the approach-withdrawal hypothesis (e.g., Davidson 1992, 1998; Harmon-Jones and Gable 2018). This hypothesis posits that the approach motivation system engages activity of the left prefrontal regions, particularly the left DLPFC, leading to reduced alpha EEG power on the left and more positive FAA, while the avoidance motivation system recruits activity of the right prefrontal regions, especially the right DLPFC, leading to reduced alpha power on the right and more negative FAA. Because most clinical EEG exams are resting-state exams, most FAA studies in the literature focused on resting FAA. However, the very definition of resting state implies absence of any emotion or motivation. Thus, resting FAA studies can only examine spontaneous activities of the two motivation systems (presumably reflecting trait motivational characteristics), which can be obscured by random and hard-to-control variations in emotional, motivational, and physiological states. It has been demonstrated that FAA levels measured during an emotional challenge provide results more consistent with predictions of the approach-withdrawal hypothesis than resting FAA (Stewart et al. 2014). In the described study, we did not evaluate resting FAA at all. Instead, we focused on mean FAA changes between control conditions (Rest, Count) and the rtfMRI-nf task, as well as temporal FAA variations. Investigation of mean FAA changes yielded two important results, as mentioned above. First, the FAA changes distinguished between effects of the actual LA-targeting rtfMRI-nf (EG) and those of the sham rtfMRI-nf (CG), suggesting a stronger approach motivation for the EG

and/or a stronger avoidance motivation for the CG. Note that avoidance motivation during the rtfMRI-nf training may be associated with stress, confusion, frustration, etc. that might accompany performance of the difficult nf task, particularly for the CG. Second, the FAA changes showed significant positive correlation with trait depression severity (HDRS) for the EG, discussed below. These findings demonstrate that the mean FAA changes associated with performance of the rtfMRI-nf task are sensitive to both specific rtfMRI-nf effects and severity of depressive symptoms.

We interpret the positive correlation between the average individual FAA changes associated with the rtfMRI-nf and the HDRS depression severity as an indication of a short-term correction (reversal) of FAA abnormalities specific to MDD. This correction occurs during performance of the rtfMRI-nf task and is related to the above-mentioned capacity of the rtfMRI-nf procedure to enhance approach motivation while increasing BOLD activity of the amygdala and the motivation-related circuitry. More specifically, average individual FAA levels during the control conditions (Rest, Count) exhibited negative correlations with the HDRS ratings (Zotev et al. 2016). This dependence is similar to the negative correlation between FAA levels and depression severity often observed in resting and task-based FAA studies (e.g., Smith et al. 2018; Stewart et al. 2014; Thibodeau et al. 2006). During the rtfMRI-nf task, the corresponding average individual FAA levels for the EG were more positive and uncorrelated with the HDRS ratings (Zotev et al. 2016). As a result, the average individual *changes* in FAA between the Rest baseline and the rtfMRI-nf task were more positive in MDD patients with higher depression severity, yielding the positive correlation with the HDRS ratings. Similarly, MDD patients with higher depression severity exhibited more positive laterality of the EEG coherence enhancement among frontotemporal EEG channels across the four nf runs. These EEG results suggest that the beneficial short-term effects of the rtfMRI-nf training in terms of normalizing FAA are stronger in MDD patients with more severe depression. Consistent with these findings, the study by Stewart et al. (2014) revealed that MDD patients showed larger positive FAA changes between avoidance-related and approach-related tasks than did participants without history of depression.

EEG-fMRI data analyses in the described study demonstrated, for the first time, correlations between FAA variations and simultaneously measured BOLD activity (Fig. 13.1d, e). The average individual FAA changes between the Rest baseline and the rtfMRI-nf task for the EG exhibited significant positive correlation with the amygdala BOLD laterality (Fig. 13.1d), that is, the difference in mean BOLD activities between the LA and RA (Zotev et al. 2016). To examine task-specific temporal correlations between FAA and BOLD activities across the brain, we conducted a psychophysiological interaction (PPI) analysis (Friston et al. 1997) adapted for EEG-fMRI (Zotev et al. 2014, 2016, 2018a). An EEG-based PPI correlation regressor was defined by convolution of the FAA time course with the hemodynamic response function (HRF) (Fig. 13.2a). An EEG-based PPI interaction regressor was defined by first multiplying the FAA time course by a selected contrast function (+1 for Happy Memories, −1 for Count, 0 for Rest conditions) (Fig. 13.2b) and then

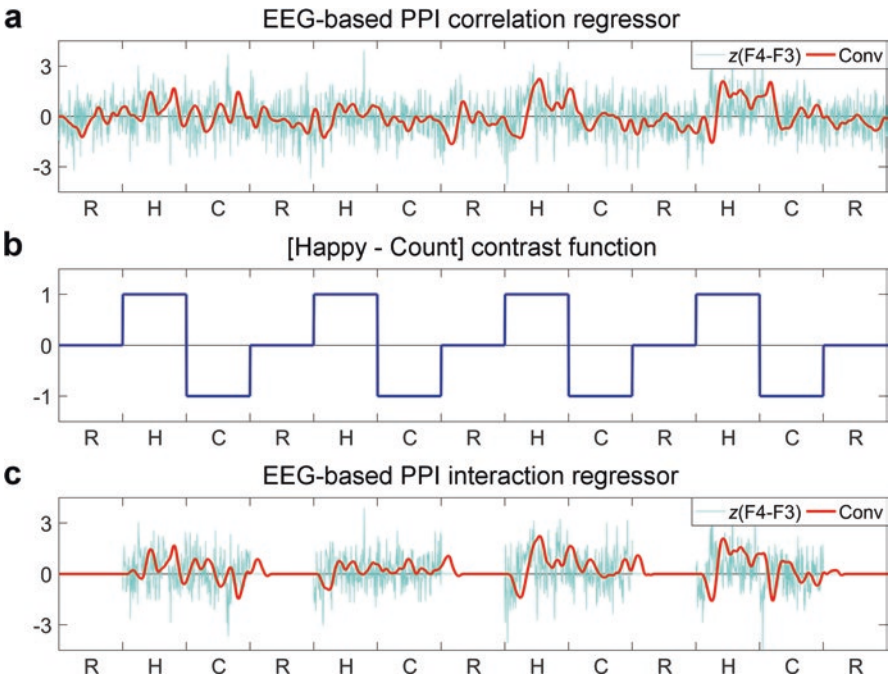

Fig. 13.2 Definition of regressors for EEG-informed psychophysiological interaction (PPI) analysis of fMRI data. (**a**) Convolution of a time course of EEG activity (FAA converted to *z*-scores) with the hemodynamic response function (HRF) yields an EEG-based PPI correlation regressor. (**b**) Contrast function for the Happy Memories (H) vs Count (C) conditions for one experimental run. (**c**) Convolution of the time course of EEG activity, multiplied by the contrast function, with the HRF yields an EEG-based PPI interaction regressor for the specified condition contrast. After Zotev et al. (2016)

convolving the resulting waveform with the HRF (Fig. 13.2c). The two EEG-based PPI regressors (correlation and interaction) were used in a general linear model (GLM)-based PPI analysis of the fMRI data. Thus, the PPI analysis was similar to a conventional fMRI-only PPI analysis, except that the initial deconvolution step (used to estimate neuronal activity from an fMRI time course, Gitelman et al. 2003) was not used, and the actual neuronal activity (FAA) time course was employed to define the two regressors. The PPI interaction effect for the EG was positive and significant for the LA region (Fig. 13.1e), indicating a more positive temporal correlation between the FAA (convolved with the HRF) and the LA BOLD activities during the rtfMRI-nf task relative to the control task (Zotev et al. 2016). The corresponding PPI interaction effect for the CG was negative, with a significant EG vs CG group difference. Beyond the LA, the PPI interaction for the EG was positive and significant for many brain regions involved in emotion regulation (Fig. 13.1e), particularly the left VLPFC (lateral orbitofrontal cortex, BA 47), the left DLPFC (BA 8), the medial frontopolar cortex (BA 10/9), the left rostral ACC (BA 32/24), and other cortical and subcortical areas (Zotev et al. 2016).

The positive correlation between the average FAA changes and the amygdala BOLD laterality (Fig. 13.1d) means, within the approach-avoidance framework, that the stronger approach motivation during the rtfMRI-nf task was associated with the higher BOLD activity of the target amygdala region (LA) relative to the nontarget region (RA). The positive PPI interaction effects for the EG (Fig. 13.1e) indicate that volitional regulation of the amygdala BOLD activity using the rtfMRI-nf was accompanied by enhanced temporal correlations between the FAA and BOLD activities of the amygdala, the EF/ER system, and other involved regions.

From the neuroscience perspective, these EEG-fMRI correlation results demonstrate that FAA is a meaningful measure of emotion/motivation that can indirectly reflect activity of the amygdala. Importantly, this conclusion retrospectively validates the main assumption behind hundreds of EEG studies of emotion/motivation that relied on FAA. Even though correlations between FAA and various psychological metrics had been reported in the literature, our study (Zotev et al. 2016) was the first to directly relate FAA to brain activity measured simultaneously by another neuroimaging modality (fMRI). Note, however, that our conclusion regarding the meaning of FAA only applies to FAA variations associated with emotion regulation, and not to resting FAA, which was not examined in our study.

From the clinical applications perspective, the EEG-fMRI results suggest that EEG-nf aimed at upregulation of FAA (e.g., Allen et al. 2001; Cavazza et al. 2014; Peeters et al. 2014; Quaedflieg et al. 2016) would be compatible with the described rtfMRI-nf procedure for upregulation of the LA BOLD activity. Note that the FAA-based EEG-nf approach has conceptual similarities to the repetitive transcranial magnetic stimulation (rTMS) treatments for MDD. Such treatments commonly involve either stimulation of the left DLPFC activity using high-frequency rTMS, or inhibition of the right DLPFC activity using low-frequency rTMS, or both (e.g., Fitzgerald et al. 2006). Obviously, clinical effectiveness of the FAA-based EEG-nf compared to that of the amygdala rtfMRI-nf (e.g., Young et al. 2017; Zotev et al. 2018b) remains to be evaluated. Nevertheless, simplicity, portability, and low cost of a standalone FAA-based EEG-nf could make it a valuable addition to the rtfMRI-nf in treatment of depression.

13.3 Regulation of Thalamic BOLD Activity and Alpha EEG Rhythm

The thalamus is often referred to as the grand central station of the human brain (e.g., Taber et al. 2004). Most sensory inputs are routed through the thalamus before reaching the cortex. Thalamic nuclei have extensive neuronal connections to various cortical areas and subcortical structures. Electrical stimulation of a single thalamic nucleus using deep brain stimulation (DBS) electrodes allows modulation (activation or inhibition) of a large network of brain regions with inherent connectivity to that nucleus (e.g., Zumsteg et al. 2006). Therefore, thalamic nuclei are promising targets for noninvasive and spatially precise neuromodulation by means of rtfMRI-nf. Such modulation is especially interesting when combined with EEG recordings.

Activities of thalamocortical neurons are known to play important roles in generation of alpha oscillations (e.g., Hughes and Crunelli 2005; Crunelli et al. 2018). However, exact mechanisms of generation, modulation, and propagation of alpha EEG rhythm remain poorly understood. Resting EEG-fMRI studies have revealed positive temporal correlations between posterior alpha EEG power and BOLD activities of dorsal thalamic regions (e.g., de Munck et al. 2007; DiFrancesco et al. 2008; Goldman et al. 2002; Omata et al. 2013), particularly those of the mediodorsal (MD) and anterior (AN) thalamic nuclei (Liu et al. 2012). However, this phenomenon is relatively weak in resting state and rather difficult to explain. Scalp EEG cannot probe electrical oscillations in the thalamus because of the limited depth sensitivity, while the MD and AN nuclei do not have extensive neuronal connections to parietal or occipital cortical regions. This scientific problem can be addressed using rtfMRI-nf with simultaneous EEG.

We have performed the first study in which rtfMRI-nf was used for volitional regulation of BOLD activity of the thalamus (Zotev et al. 2018a). The target ROI consisted of the MD and AN thalamic nuclei, which are parts of the limbic thalamus (Taber et al. 2004). Healthy participants learned to upregulate the target BOLD activity while recalling happy autobiographical memories (Fig. 13.3). We selected this task because both the MD and AN are activated during autobiographical memory retrieval (e.g., Spreng et al. 2009; Svoboda et al. 2006). EEG recordings were conducted simultaneously with fMRI. The study was designed to test the hypothesis that direct modulation of the MD and AN BOLD activities using the rtfMRI-nf would enhance their temporal correlations with posterior alpha EEG power. Another exploratory goal of the study was to identify cortical regions supporting such correlation effects.

The experimental session included four rtfMRI-nf runs, each consisting of alternating 40 s long blocks of Happy Memories with rtfMRI-nf, Attend, and Count conditions (Zotev et al. 2018a). A Transfer run without nf was added to evaluate transfer of training effects beyond the actual training. For the experimental group (EG, $n = 15$), the rtfMRI-nf signal was based on average BOLD activity for the AN/MD target ROI (Fig. 13.3b), measured in real time as fMRI percent signal change with respect to the Attend baseline. For the control group (CG, $n = 14$), the sham feedback signal was computer-generated and independent of any brain activity. The nf signal was displayed to the participant inside the scanner as a variable-height red bar on the screen (Fig. 13.3a), as described in Sect. 13.2. During the Happy Memories with rtfMRI-nf conditions, the participant was asked to evoke happy autobiographical memories, while simultaneously trying to control and raise the level of the red rtfMRI-nf bar as high as possible. The fluctuating nf bar was also displayed, but not controlled, during the Attend and Count conditions to reduce variations in visual attention levels among the conditions (Zotev et al. 2018a). The experiment was performed using the same rtfMRI-nf system and EEG-fMRI setup as outlined in Sect. 13.2.

The described experimental procedure allowed us to investigate mean task-dependent variations in alpha EEG activity and compare them to mean thalamic BOLD activity. During the Happy Memories with rtfMRI-nf task, the participants

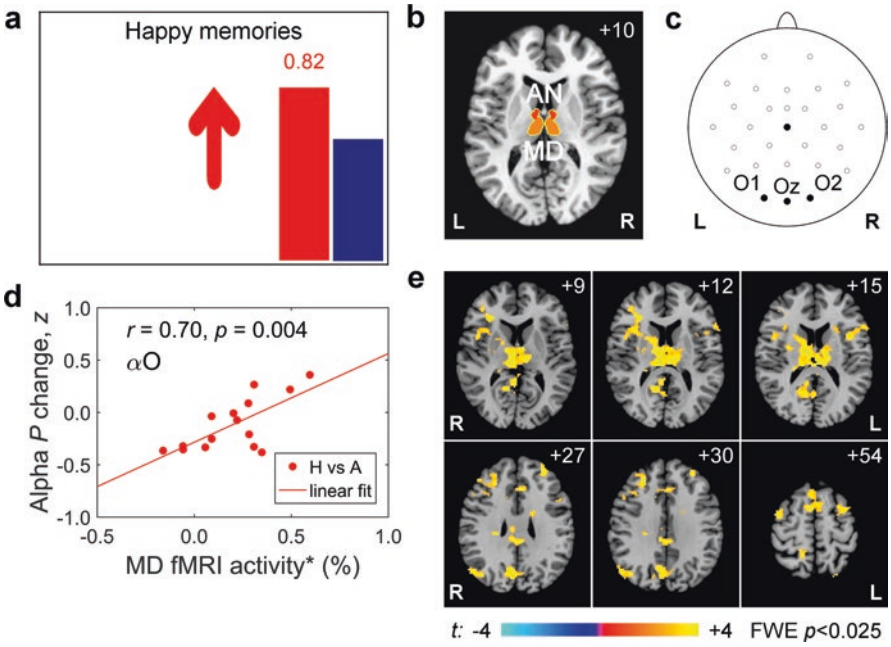

Fig. 13.3 Real-time fMRI neurofeedback of the thalamus activity with simultaneous EEG. (**a**) Real-time GUI display screen with variable-height red rtfMRI-nf bar and blue zero-level bar. (**b**) Target ROI for the rtfMRI-nf encompassing the anterior nucleus (AN) and the mediodorsal nucleus (MD) of the thalamus. (**c**) EEG electrodes used to study occipital EEG activity. (**d**) Correlation between average fMRI activity of the MD (orthogonalized with respect to V1/V2 time course) and average changes in normalized occipital alpha EEG power (z-scores) during the Happy Memories with rtfMRI-nf task (H) relative to the Attend baseline (A) for the experimental group (EG). (**e**) Group difference in EEG-based PPI interaction effects indicating more positive temporal correlations between the occipital alpha power and fMRI activity during the Happy Memories with rtfMRI-nf task compared to the Attend baseline for the EG relative to the control group (CG). The left hemisphere (L) is to the reader's right. The maps are shown in the Talairach space with z-coordinate specified for each slice. After Zotev et al. (2018a)

in the EG were able to successfully upregulate BOLD activities of the AN and MD thalamic nuclei (Zotev et al. 2018a). Importantly, fMRI functional connectivity between the MD and the medial inferior precuneus (BA 31) was significantly stronger during the rtfMRI-nf task for the EG compared to the CG. Because alpha EEG power is modulated by visual attention, we used average fMRI time course of the visual cortex V1/V2 as a covariate of no interest in fMRI and EEG-fMRI data analyses. The alpha EEG band was defined individually for each participant as [IAF − 2…IAF + 2] Hz, where IAF is an individual alpha peak frequency. Amplitude modulation of EEG activity in this alpha band was studied by considering an alpha activity envelope for each channel. Temporal correlations between such alpha envelopes were enhanced during the rtfMRI-nf task relative to the Attend baseline for the EG. Individual enhancements in the alpha envelope correlations, averaged across all EEG channel pairs, exhibited significant positive correlation with the

corresponding individual MD BOLD activity levels for the EG (Zotev et al. 2018a). Next, we considered average normalized occipital alpha EEG power, $\alpha O = \ln(P(O1)) + \ln(P(O2)) + \ln(P(Oz))$, where P is EEG power for the occipital electrodes (Fig. 13.3c) in the defined alpha band. Individual changes in the occipital alpha power between the Attend baseline and the rtfMRI-nf task showed significant positive correlation with the corresponding MD BOLD activity levels (Fig. 13.3d). Such positive alpha-BOLD correlation effect for the EG was also significant for the Transfer run without nf (Zotev et al. 2018a).

The significant positive correlation between the enhancement in correlated modulation of alpha EEG activity throughout the EEG array and mean BOLD activity of the MD during the rtfMRI-nf task demonstrates that the MD plays a major role in modulating alpha EEG rhythm. The corresponding correlation for the AN BOLD activity was not significant. A possible reason for this difference is that the AN has connections predominantly to subcortical regions, so its ability to influence activities of large cortical areas is less pronounced than that of the MD, which has extensive neuronal connections to the prefrontal cortex (Taber et al. 2004). The significant positive correlation between mean values of the MD BOLD activity and mean occipital alpha EEG power changes (Fig. 13.3d) is consistent with the positive temporal correlations between temporal fluctuations in the same activities observed in resting EEG-fMRI.

EEG-fMRI temporal correlation analyses in our study demonstrated that performance of the rtfMRI-nf task was associated with enhanced temporal correlations between occipital alpha EEG power and BOLD activities in the thalamus and other brain regions (Fig. 13.3e). EEG-based PPI analyses were conducted separately for two condition contrasts, Happy vs Attend and Happy vs Count, and were similar to the PPI analysis illustrated in Fig. 13.2. An EEG-based PPI correlation regressor was defined by convolution of a time course of the normalized occipital alpha EEG power (converted to z-scores) with the HRF. An EEG-based PPI interaction regressor for the Happy vs Attend contrast was defined by first multiplying the alpha power time course by the contrast function (+1 for Happy Memories, −1 for Attend, 0 for Count conditions) and then convolving the resulting waveform with the HRF. An EEG-based PPI interaction regressor for the Happy vs Count contrast was defined in a similar way using the corresponding contrast function (+1 for Happy Memories, −1 for Count, 0 for Attend conditions). The PPI interaction effects for both contrasts were positive for the MD and AN ROIs for the EG, meaning that temporal correlations between the occipital alpha EEG power (convolved with the HRF) and BOLD activities of these regions were more positive during the rtfMRI-nf task than during the control tasks (Attend, Count). The corresponding PPI interaction effects for the CG were negative, with significant EG vs CG group differences for both ROIs and both contrasts (Zotev et al. 2018a). The PPI interaction effect for the Happy vs Attend contrast also showed significant positive EG vs CG group differences for the medial pulvinar, caudate body, DLPFC (BA 9), supplementary motor area (SMA, BA 6), ACC (BA 32), precuneus/PCC (BA 31, 30), angular gyrus (BA 39), and other regions (Fig. 13.3e). The PPI interaction effect for the Happy vs Count contrast exhibited significant EG vs CG group differences for the

ventrolateral nucleus (VL), medial pulvinar, caudate body, putamen, DLPFC (BA 9), SMA (BA 6), cingulate gyrus (BA 24, 32), precuneus (BA 19), middle temporal gyrus (BA 39), and other regions (Zotev et al. 2018a).

The whole-brain PPI results indicate that temporal correlation between the occipital alpha EEG power and BOLD activity was enhanced during the rtfMRI-nf task compared to the Attend condition (for the EG relative to the CG) for the posterior DMN nodes, including the precuneus/PCC (BA 31, 30) and the right angular gyrus (BA 39) (Fig. 13.3e). When compared to the Count condition, the temporal correlation during the rtfMRI-nf task was enhanced for temporoparietal regions (BA 39, 19) in close proximities to the lateral DMN nodes. These results suggest that the positive alpha-BOLD correlation effects observed for the dorsal thalamus and other subcortical regions may be supported by the posterior DMN nodes. These nodes are activated during autobiographical memory retrieval (e.g., Spreng et al. 2009) and show increased localized alpha power in the process (e.g., Knyazev et al. 2015). Because these are cortical regions, their activities are reliably probed by scalp EEG.

Our results also highlight the important role of functional connectivity between the MD thalamic nucleus and the precuneus. The locus within the medial inferior precuneus (BA 31) that exhibited the most significant EG vs CG group difference in the PPI interaction effects for the Happy vs Attend contrast (Fig. 13.3e) was very close to the location that showed the most significant positive EG vs CG group difference in fMRI functional connectivity with the MD during the rtfMRI-nf task (Zotev et al. 2018a). This region is adjacent to the parieto-occipital sulcus. MEG source localization studies have shown that the strongest dipole-modeled sources of posterior alpha rhythm are distributed around the parieto-occipital sulcus and around the calcarine sulcus (Hari et al. 1997; Manshanden et al. 2002). The parieto-occipital alpha sources (BA 31, 7, 19) are involved in cognitive and memory functions (e.g., Tuladhar et al. 2007; Seibert et al. 2011), while the calcarine alpha sources (V1/V2) are engaged in more basic visual functions. The stronger interaction between the MD and the inferior precuneus during the rtfMRI-nf task means the stronger ability of the MD to influence the parieto-occipital sources of alpha rhythm. Therefore, it is the interaction between the MD and the inferior precuneus, reflected in their fMRI functional connectivity, that may modulate the observed positive temporal association between the posterior alpha EEG power and the MD BOLD activity. Indeed, the correlation between the MD-precuneus functional connectivity and the PPI interaction effect for the MD was positive and significant for the Transfer run for the EG (supplement in Zotev et al. 2018a).

Our study clearly demonstrates that the positive alpha-BOLD correlation effect for deep subcortical regions is not limited to the dorsal thalamus, but can be also observed for the basal ganglia. The PPI analyses revealed enhanced temporal correlations between posterior alpha EEG power and BOLD activities of the caudate and putamen. These regions, together constituting the dorsal striatum, play important roles in learning, including learning from feedback (e.g., Grahn et al. 2008).

They are engaged during the rtfMRI-nf training. The fact that resting EEG-fMRI studies have not shown pronounced alpha-BOLD correlations for these regions reflects the absence of learning in resting state. Furthermore, our results indicate that posterior alpha EEG power exhibited, during the rtfMRI-nf task, enhanced temporal correlations with BOLD activities of the basal ganglia-thalamocortical circuits. These circuits are closed loops that enable parallel processing and integration (Alexander et al. 1991; Grahn et al. 2008). The PPI results revealed two such circuits: the prefrontal (dorsolateral) circuit (DLPFC → caudate → globus pallidus/substantia nigra → MDpc → DLPFC) and the motor circuit (SMA → putamen → globus pallidus/substantia nigra → VLo → SMA) (Zotev et al. 2018a). Therefore, not only do these basal ganglia-thalamocortical circuits contribute prominently to the rtfMRI-nf learning cycle (Birbaumer et al. 2013), but they also show temporal correlations with posterior alpha EEG power. In contrast, the PPI results did not reveal significant effects in the amygdala, suggesting that the amygdala, though providing some input to the MD, is not actively involved in generation or modulation of alpha oscillations.

From the neuroscience perspective, our EEG-fMRI results confirm the fundamental role of the thalamus, especially the mediodorsal nucleus (MD), in modulation of alpha EEG rhythm. Our findings suggest that the positive temporal correlations between thalamic BOLD activity and posterior alpha EEG power are supported by the posterior DMN nodes. In particular, the positive alpha-BOLD correlation effect for the MD is modulated by the interaction between the MD and the inferior precuneus, reflected in their fMRI functional connectivity. A promising direction for future EEG-fMRI research involves application of rtfMRI-nf based on a difference in BOLD activities of two selected nuclei of the thalamus. Such approach could help to elucidate functional differences between thalamic nuclei and understand their effects on EEG activity.

From the clinical applications perspective, the rtfMRI-nf targeting BOLD activities of the AN/MD can be used to correct autobiographical memory disturbances in MDD and posttraumatic stress disorder (PTSD), for example, by increasing these BOLD activities during retrieval of happy autobiographical memories and/or reducing them in response to traumatic memories or depressive rumination. The capability of the described rtfMRI-nf procedure to modify functional connectivity between the MD and the posterior DMN may be relevant in treatment of MDD, where such connectivity is abnormally elevated during rest (e.g., Hamilton et al. 2015). The rtfMRI-nf of thalamic BOLD activity can also potentially be used as a neurorehabilitation tool in treatment of neurological disorders affecting the thalamus, such as Korsakoff's syndrome (e.g., Taber et al. 2004). Our EEG-fMRI findings suggest that EEG-nf targeting posterior alpha EEG activity (e.g., Hanslmayr et al. 2005; Nicholson et al. 2016; Zoefel et al. 2011) during a memory task would be compatible with the rtfMRI-nf of the AN/MD BOLD activity. Therefore, both types of neurofeedback can be employed in combination, for example, to enhance treatment of autobiographical memory disturbances in MDD and PTSD.

13.4 Simultaneous Real-Time fMRI and EEG Neurofeedback

Simultaneous multimodal real-time fMRI and EEG neurofeedback (rtfMRI-EEG-nf) is a combination of simultaneously provided rtfMRI-nf and EEG-nf that enables simultaneous regulation of both hemodynamic and electrophysiological brain activities (Zotev et al. 2014). Promising target measures for rtfMRI-EEG-nf can be identified in rtfMRI-nf with simultaneous EEG studies, as illustrated in Sects. 13.2 and 13.3, as well as in EEG-nf with simultaneous fMRI studies. To successfully implement rtfMRI-EEG-nf, one has to overcome two major technical challenges. First, rtfMRI and EEG data streams need to be synchronized, processed, and integrated in real time to allow simultaneous display of two neurofeedback signals from the two imaging modalities. Second, EEG-fMRI and common EEG artifacts must be accurately removed from real-time EEG data to provide a reliable EEG-nf signal during fMRI, as explained in Sect. 13.1. The main promise of rtfMRI-EEG-nf is the potential for achieving greater clinical effectiveness in treatment of neurological and psychiatric disorders than can be achieved with rtfMRI-nf or EEG-nf administered separately.

We have developed the first multimodal real-time control system for integration of simultaneous rtfMRI and EEG data streams to provide rtfMRI-EEG-nf (Zotev et al. 2014). The system is designed to operate with the General Electric Discovery MR750 3T MRI scanner and a 128-channel MR-compatible EEG system from the Brain Products, GmbH. The EEG system's clock is synchronized with the MRI scanner's clock using Brain Products' SyncBox device. MRI slice markers (TTL pulses) are sent from the scanner to the EEG system via a parallel port and recorded together with the EEG data. These markers are used to synchronize real-time EEG data processing with an fMRI pulse sequence. The multimodal real-time control system extends the functionality of the original real-time MRI monitoring and control system (Bodurka and Bandettini 2008) and includes a fully integrated pipeline for processing simultaneously acquired EEG data. The system uses real-time features of AFNI (Cox 1996) and real-time capabilities of the BrainVision RecView software (Brain Products, GmbH). fMRI data are converted from DICOM to AFNI format in real time using a custom real-time software, which runs on the MRI scanner's host computer and utilizes the Dimon AFNI program. The converted data are exported via a TCP/IP socket to a computer running real-time AFNI (Zotev et al. 2014). The AFNI real-time plugin is used to perform fMRI motion correction and compute mean fMRI signal values for selected ROIs for each acquired fMRI volume. EEG data are acquired using the BrainVision Recorder software and transferred to the RecView software, where MR and CB artifacts are partially removed in real time using built-in automated procedures for average artifact subtraction (AAS, Allen et al. 1998, 2000). The Remote Data Access (RDA) feature of the RecView is then used to export the processed EEG data via a TCP/IP socket from the EEG computer to the real-time computer. Further EEG data processing includes automated data inspection, moving-window FFT analysis, and computation of EEG powers for selected channels in selected frequency bands. The rtfMRI and EEG data streams are finally integrated in the multimodal graphical user interface (mGUI)

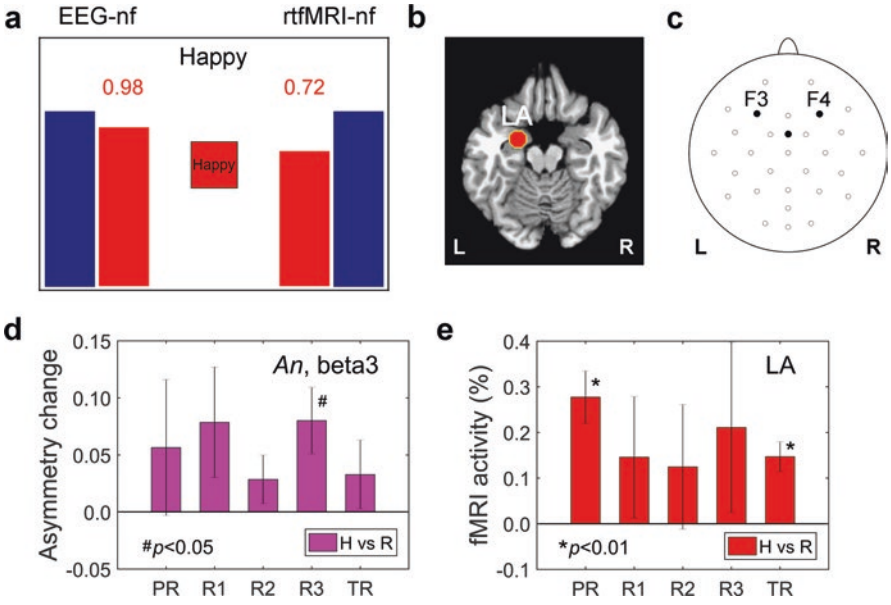

Fig. 13.4 Simultaneous multimodal real-time fMRI and EEG neurofeedback. (**a**) Real-time multimodal GUI display screen with variable-height red EEG-nf bar on the left and red rtfMRI-nf bar on the right. The blue bars are target levels. (**b**) Left amygdala (LA) target ROI for the rtfMRI-nf. (**c**) EEG electrodes F3 and F4 used to provide the EEG-nf. (**d**) Mean changes in frontal high-beta (beta3) EEG asymmetry during the Happy Memories with rtfMRI-EEG-nf task (H) relative to the Rest baseline (R). The group results are shown for four nf runs (PR, R1, R2, R3) and for Transfer run without nf (TR). (**e**) Corresponding mean fMRI activity levels for the LA. After Zotev et al. (2014)

software running two processing threads and receiving data from two sockets. The mGUI computes rtfMRI-nf and EEG-nf signal values and generates graphics for real-time display (Fig. 13.4a). The multimodal real-time control system includes custom software modules written in Python, including NumPy, and in Perl, including Perl/Tk (Zotev et al. 2014).

We have conducted a pilot, proof-of-concept study demonstrating the feasibility of simultaneous regulation of both hemodynamic and electrophysiological brain activities using rtfMRI-EEG-nf (Zotev et al. 2014). In the study, six healthy participants performed a happy emotion induction task based on retrieval of happy autobiographical memories, while simultaneously trying to control and raise two variable-height neurofeedback bars on the screen (Fig. 13.4a). The multimodal real-time control system described above was used to provide the rtfMRI-EEG-nf. The system was configured for 32-channel EEG. The rtfMRI-nf signal was updated every 2 s, while the EEG-nf signal was updated every 0.4 s. The LA target ROI for the rtfMRI-nf (Fig. 13.4b) was the same as described in Sect. 13.2. Frontal EEG asymmetry in the high-beta band for channels F3 and F4 (Fig. 13.4c) was employed as a target measure for the EEG-nf. It was defined as $A = [P(\text{F3}) - P(\text{F4})] / [P(\text{F3})$

+ P(F4)], where P is EEG power in the high-beta (beta 3) band [21…30] Hz. Note that the right-hand side in this definition has an opposite sign compared to that in the FAA definition (Sect. 13.2), because excitatory cortical activity is associated with increased high-beta EEG power (e.g., Cook et al. 1998). We used the relative asymmetry A as the target for EEG-nf, because its distribution over a finite (rather than infinite) interval makes it convenient for real-time applications. In offline statistical analyses, normalized asymmetry $An = \text{atanh}(A) = [\ln(P(\text{F3})) - \ln(P(\text{F4}))]/2$ was employed instead. We selected upregulation of the high-beta EEG asymmetry as a goal of the EEG-nf procedure for the following reasons. First, resting frontal EEG asymmetry in the high-beta band is more negative in MDD patients compared to healthy controls due to increased high-beta activity in the right prefrontal regions observed in MDD (Pizzagalli et al. 2002). Alleviation of depressive symptoms is associated with a stronger reduction in high-beta power on the right than on the left (Paquette et al. 2009), leading to more positive resting high-beta EEG asymmetry. Second, because frontal EEG power asymmetry is a differential measure, it is less sensitive to global EEG phenomena and various artifacts than EEG signal power from a single electrode. Third, EEG signals measured in the high-beta band during fMRI are less affected by residual CB and random motion artifacts than signals in the alpha and theta EEG bands (Zotev et al. 2014).

During the rtfMRI-EEG-nf task, the study participants were able to successfully upregulate both the rtfMRI-nf and EEG-nf signals (Zotev et al. 2014), as evidenced by positive group mean values of both target measures for each of the four nf runs (Fig. 13.4d, e). Task-dependent temporal correlations between the normalized frontal high-beta EEG asymmetry An and BOLD activity were evaluated using an EEG-based PPI analysis, similar to the one illustrated in Fig. 13.2. Positive PPI interaction effects for the Happy vs Count condition contrast were observed for the LA, left insula (BA 22), right orbitofrontal cortex (BA 47), right dorsomedial prefrontal cortex (BA 9), right superior temporal gyrus (BA 41), and other regions. This means that temporal correlations between the An time course and BOLD activities of these regions were enhanced during the rtfMRI-EEG-nf task relative to the control task. In particular, the positive PPI interaction effect for the LA region indicates that the high-beta EEG asymmetry and the LA BOLD activity were indeed modulated together in real time.

More recently, another implementation of a hybrid neurofeedback platform combining EEG and fMRI was reported by the INRIA group (Mano et al. 2017). It was developed for operation with a Siemens MAGNETOM 3T Verio MRI scanner and a 64-channel MR-compatible EEG system from the Brain Products, GmbH. The platform's architecture is generally similar to the one we described above. The fMRI subsystem utilizes MATLAB programs to export fMRI data from the MRI host computer in real time (adapted from FieldTrip) and perform real-time motion correction (adapted from SPM8), while the EEG subsystem relies on the real-time EEG processing capabilities of the BrainVision RecView software (Mano et al. 2017). The authors also reported a study in which healthy participants learned to regulate laterality of the primary motor cortex activity using either unimodal (EEG-nf or rtfMRI-nf) or bimodal (rtfMRI-EEG-nf) neurofeedback during a motor imagery

task (Perronnet et al. 2017). EEG and fMRI laterality indices for motor cortex activity were used as neurofeedback target measures. The results showed that the rtfMRI-EEG-nf was more effective at activating the motor cortex when compared to the EEG-nf, but not when compared to the rtfMRI-nf (Perronnet et al. 2017). This work demonstrated the importance of careful side-by-side performance comparisons for different types of neurofeedback.

The two rtfMRI-EEG-nf studies mentioned above (Perronnet et al. 2017; Zotev et al. 2014) had one important feature in common: real-time removal of MR and CB artifacts was based, in both studies, on the AAS procedures implemented in the BrainVision RecView software. However, the AAS algorithms only allow approximate artifact removal, so residual MR and CB artifacts are left in the processed EEG data, particularly in real-time applications. Moreover, random motion EEG-fMRI artifacts and various common EEG artifacts, which can be quite persistent during performance of a difficult task, cannot be corrected by such algorithms at all.

One possible way to improve suppression of residual CB and random motion EEG artifacts inside an MRI scanner is to employ a real-time artifact regression using reference artifact signals induced in wire loops added to an EEG cap (Masterton et al. 2007). This approach can be very practical in applications utilizing EEG signals from only few electrodes to provide EEG-nf. Recently, we implemented an enhanced real-time EEG-fMRI artifact removal procedure for improved EEG-nf during fMRI (Zotev et al. 2020). We modified a standard 32-channel MR-compatible EEG cap by adding four reference contours (wire loops with resistors). Geometries of these contours were optimized so that recorded artifacts closely approximate random motion and CB artifacts registered by EEG channels F3 and F4. A real-time regression of the reference artifact waveforms was performed within the RecView software after the AAS procedure for MR artifacts and prior to the AAS procedure for CB artifacts. This approach allowed us to provide a reliable EEG-nf based on frontal alpha EEG asymmetry (FAA for channels F3 and F4), as well as a more accurate EEG-nf based on frontal high-beta EEG asymmetry. Building on these advances, we conducted the first emotion self-regulation study in which MDD patients used rtfMRI-EEG-nf to simultaneously modulate two fMRI and two EEG activity measures relevant to major depression (Zotev et al. 2020; Zotev and Bodurka 2020).

Another promising strategy to achieve improved real-time EEG artifact suppression during fMRI is implementation of real-time ICA for EEG data, as described in the following section.

13.5 Real-Time Independent Component Analysis for EEG-fMRI

The main signal processing challenge in simultaneous EEG-fMRI is the need for accurate removal of artifacts emerging during acquisition of EEG data in MRI environment (e.g., Mulert and Lemieux 2010). This problem is even more complicated in real-time applications, such as EEG-nf with simultaneous fMRI or the

rtfMRI-EEG-nf discussed above (Sect. 13.4). The AAS (Allen et al. 1998, 2000) is a common approach for reducing both MR and CB artifacts, which takes into account their quasiperiodic temporal properties. The AAS involves generation of an average artifact template and subtraction of this template from the artifact-contaminated EEG data. This method is implemented for real-time MR and CB artifact suppression in the BrainVision RecView software. It has been used in several real-time EEG-fMRI studies (e.g., Becker et al. 2011; Cavazza et al. 2014; Kinreich et al. 2012; Mano et al. 2017; Zich et al. 2015; Zotev et al. 2014). Although the AAS is quite successful at reducing these types of artifacts, some residual MR and CB artifacts remain due to temporal variabilities in these artifacts' properties. Furthermore, as mentioned in Sect. 13.4, the AAS can only attenuate MR and CB artifacts and cannot correct random motion-related and common EEG artifacts. Different hardware-based approaches have been proposed for improved correction of random motion, MR, and CB artifacts. They include the use of an additional motion sensor (Bonmassar et al. 2002), reference wire loops (Masterton et al. 2007; van der Meer et al. 2016; Zotev et al. 2020), and a reference conductive layer with reference electrodes (Dunseath and Alden 2010; Luo et al. 2014). However, these methods cannot handle common EEG artifacts (Sect. 13.1), such as ocular or muscle artifacts.

We have introduced a novel method combining the AAS and ICA for real-time reduction of both fMRI-related and common physiological artifacts in EEG data recorded simultaneously with fMRI (Mayeli et al. 2016). ICA is a mathematical technique for determining hidden factors and sources from random variables, measurements, and signals (e.g., Hyvärinen et al. 2001). It has been widely used in offline EEG and EEG-fMRI analyses for attenuating residual MR and CB artifacts, as well as various common EEG artifacts (Sect. 13.1). ICA decomposes an observed multivariate vector into groups of stochastically independent vectors. Several principles and procedures have been developed to maximize statistical independence among extracted sources, which led to different ICA methods (e.g., Infomax, FastICA, SOBI, Robust ICA, JADE, ORICA). These methods provide powerful techniques for detecting and reducing EEG artifacts. Unlike other artifact correction approaches (e.g., the AAS or optimal basis sets), ICA can be applied for detection of nearly all types of artifacts. It can also be combined with other artifact correction methods.

In order to achieve reliable results from an ICA decomposition, the number of samples submitted to an ICA algorithm should be some multiple k of n^2, where n is the number of EEG channels and $k > 20$ as a rule of thumb (Onton et al. 2005). This requirement makes application of ICA in real time rather challenging. To overcome this limitation, Mayeli et al. (2016) used a moving-window ICA decomposition. The second-order blind identification (SOBI, Belouchrani et al. 1997) technique, based on a blind identification using a joint diagonalization of several covariance matrices, was selected for ICA because of its higher convergence rate compared to other ICA methods. In the proposed real-time algorithm, MR and CB artifacts are first reduced using the real-time AAS in the RecView software, and the EEG data are downsampled to 250 S/s. The moving-window ICA decomposition is

commenced when the total number of acquired EEG data points per channel reaches 10,000 (40 s). The ICA is performed for 22 EEG channels for the 40 s time window. The window is shifted every 4 s when the next 1000 data points are acquired, and the ICA is repeated. Power spectrum density, topographic map, kurtosis, and energy are extracted from the last 4-s data interval for each IC. Based on extracted features and predefined threshold values, the algorithm classifies ICs as either neuronal activity or four types of artifacts (Mayeli et al. 2016). Specifically, ocular (eye-blinking) artifact mainly affects frontopolar EEG channels and is characterized by high energy and largest spectrum density at very low frequencies. Random motion artifact has very high energy and kurtosis values and exhibits high spectrum density at low frequencies. Residual CB artifact is identified based on its high spectrum density in the theta EEG band, high energy, and predominantly bipolar topography. Finally, muscle and residual MR artifacts are recognized by large spectrum density at higher (beta and gamma band) frequencies (Mayeli et al. 2016). After removing ICs related to these artifacts, an inverse ICA transform is applied to reconstruct the corrected EEG signal.

The real-time ICA algorithm was implemented in a software module written in Python and utilizing NumPy functionality. The ICA module was integrated with the multimodal real-time control system used to provide rtfMRI-EEG-nf (Zotev et al. 2014). The real-time ICA performance was tested in resting-state EEG-fMRI experiments involving six healthy participants. Several evaluation metrics were employed to compare the real-time ICA artifact correction to an offline ICA correction. The results showed that the real-time algorithm could effectively reduce all four types of artifacts without removing any neuronal signal (Mayeli et al. 2016). The proposed methodology can be further improved in several ways. For instance, machine learning techniques could be utilized for automatic artifact detection and IC classification. Also, GPU-based data processing would further increase the algorithm speed leading to more accurate real-time identification and removal of EEG and EEG-fMRI artifacts.

Recently, Hsu and colleagues applied another ICA method, named Online Recursive ICA (ORICA, Akhtar et al. 2012), for correcting EEG artifacts in real time (Hsu et al. 2014, 2016). However, the feasibility of using this approach for real-time removal of MR, CB, and random motion artifacts from EEG data acquired during fMRI needs to be investigated.

13.6 Conclusions

The discussed applications of the real-time fMRI neurofeedback with simultaneous EEG approach (Sects. 13.2 and 13.3) demonstrate that it is a powerful tool for neuroscience research. Its main strength compared to other neuromodulation techniques is that it enables direct targeted noninvasive modulation of BOLD activities of deep brain regions and investigation of related EEG activities measured simultaneously with high temporal resolution. This allows comprehensive analysis of spatiotemporal dynamic relationships between concurrent hemodynamic and

electrophysiological processes in the human brain. Therefore, this approach can be used to address fundamental problems in neuroscience (Sect. 13.3). From the clinical perspective, rtfMRI-nf can help to elucidate neural interactions within brain circuits involved in emotion regulation and identify novel, more efficient clinical targets for treatment of affective disorders. Investigation of electrophysiological processes accompanying rtfMRI-nf training of emotion regulation using simultaneous EEG can lead to development of more affordable and portable EEG-only neurofeedback therapies for depression and other neuropsychiatric disorders.

The simultaneous multimodal rtfMRI-EEG-nf approach (Sect. 13.4) has stimulated active development efforts, which led to important technical advances in real-time EEG-fMRI data integration and artifact removal, including implementation of real-time ICA for EEG-fMRI (Sect. 13.5). Conceivably, rtfMRI-EEG-nf can have stronger therapeutic effects than either rtfMRI-nf or EEG-nf, because it can simultaneously and consistently target disorder-specific brain activities, identified by two very different imaging modalities—fMRI and EEG. The first application of rtfMRI-EEG-nf in a patient population yielded promising results (Zotev et al. 2020). However, clinical potential of this emerging neuromodulation technique remains to be explored.

References

Akhtar MT, Jung TP, Makeig S, Cauwenberghs G (2012) Recursive independent component analysis for online blind source separation. IEEE Int Symp Circuits Syst:2813–2816

Alexander GE, Crutcher MD, DeLong MR (1991) Basal ganglia-thalamocortical circuits: parallel substrates for motor, oculomotor, "prefrontal" and "limbic" functions. Prog Brain Res 85:119–146

Allen JJB, Harmon-Jones E, Cavender JH (2001) Manipulation of frontal EEG asymmetry through biofeedback alters self-reported emotional responses and facial EMG. Psychophysiology 38:685–693

Allen PJ, Polizzi G, Krakow K, Fish DR, Lemieux L (1998) Identification of EEG events in the MR scanner: the problem of pulse artifact and a method for its subtraction. NeuroImage 8:229–239

Allen PJ, Josephs O, Turner R (2000) A method for removing imaging artifact from continuous EEG recorded during functional MRI. NeuroImage 12:230–239

Becker R, Reinacher M, Freyer F, Villringer A, Ritter P (2011) How ongoing neuronal oscillations account for evoked fMRI variability. J Neurosci 31:11016–11027

Bellgowan PSF, Bandettini PA, van Gelderen P, Martin A, Bodurka J (2006) Improved BOLD detection in the medial temporal region using parallel imaging and voxel volume reduction. NeuroImage 29:1244–1251

Belouchrani A, Abed-Meraim K, Cardoso JF, Moulines E (1997) A blind source separation technique using second-order statistics. IEEE Trans Signal Process 45:434–444

Birbaumer N, Ruiz S, Sitaram R (2013) Learned regulation of brain metabolism. Trends Cogn Sci 17:295–302

Bodurka J, Bandettini P (2008) Real time software for monitoring MRI scanner operation. NeuroImage 41(Suppl. 1):S85

Bodurka J, Ledden PJ, van Gelderen P, Chu R, de Zwart JA, Morris D, Duyn JH (2004) Scalable multichannel MRI data acquisition system. Magn Reson Med 51:165–171

Bonmassar G, Purdon PL, Jääskeläinen IP, Chiappa K, Solo V, Brown EN, Belliveau JW (2002) Motion and ballistocardiogram artifact removal for interleaved recording of EEG and EPs during MRI. NeuroImage 16:1127–1141

Cavazza M, Aranyi G, Charles F, Porteous J, Gilroy S, Klovatch I, Jackont G, Soreq E, Keynan NJ, Cohen A, Raz G, Hendler T (2014) Towards empathic neurofeedback for interactive storytelling. In: Finlayson MA, Meister JC, Bruneau EG (eds) 5th workshop on computational models of narrative (CMN'14). Schloss Dagstuhl, Wadern, pp 42–60

Cook IA, O'Hara R, Uijtdehaage SHJ, Mandelkern M, Leuchter AF (1998) Assessing the accuracy of topographic EEG mapping for determining local brain function. Electroencephalogr Clin Neurophysiol 107:408–414

Cox RW (1996) AFNI: software for analysis and visualization of functional magnetic resonance neuroimages. Comput Biomed Res 29:162–173

Cox RW, Jesmanowicz A, Hyde JS (1995) Real-time functional magnetic resonance imaging. Magn Reson Med 33:230–236

Crunelli V, Lorincz ML, Connelly WM, David F, Hughes SW, Lambert RC, Leresche N, Errington AC (2018) Dual function of thalamic low-vigilance state oscillations: rhythm-regulation and plasticity. Nat Rev Neurosci 19:107–118

Davidson RJ (1992) Anterior cerebral asymmetry and the nature of emotion. Brain Cogn 20:125–151

Davidson RJ (1998) Affective style and affective disorders: perspectives from affective neuroscience. Cognit Emot 12:307–330

deCharms RC (2008) Applications of real-time fMRI. Nat Rev Neurosci 9:720–729

de Munck JC, Gonçalves SI, Huijboom L, Kuijer JPA, Pouwels PJW, Heethaar RM, Lopes da Silva FH (2007) The hemodynamic response of the alpha rhythm: an EEG/fMRI study. NeuroImage 35:1142–1151

de Zwart JA, Ledden PJ, van Gelderen P, Bodurka J, Chu R, Duyn JH (2004) Signal-to-noise ratio and parallel imaging performance of a 16-channel receive-only brain coil array at 3.0 Tesla. Magn Reson Med 51:22–26

DiFrancesco MW, Holland SK, Szaflarski JP (2008) Simultaneous EEG/functional magnetic resonance imaging at 4 tesla: correlates of brain activity to spontaneous alpha rhythm during relaxation. J Clin Neurophysiol 25:255–264

Dunseath WJR, Alden TA (2010) Apparatus and method for acquiring a signal. U.S. Patent 7715894

Elliot AJ, Covington MV (2001) Approach and avoidance motivation. Ed Psychol Rev 13:73–92

Fitzgerald PB, Benitez J, de Castella A, Daskalakis ZJ, Brown TL, Kulkarni J (2006) A randomized, controlled trial of sequential bilateral repetitive transcranial magnetic stimulation for treatment-resistant depression. Am J Psychiatry 163:88–94

Friston KJ, Buechel C, Fink GR, Morris J, Rolls E, Dolan RJ (1997) Psychophysiological and modulatory interactions in neuroimaging. NeuroImage 6:218–229

Gitelman DR, Penny WD, Ashburner J, Friston KJ (2003) Modeling regional and psychophysiologic interactions in fMRI: the importance of hemodynamic deconvolution. NeuroImage 19:200–207

Goldman RI, Stern JM, Engel J Jr, Cohen MS (2002) Simultaneous EEG and fMRI of the alpha rhythm. NeuroReport 13:2487–2492

Grahn JA, Parkinson JA, Owen AM (2008) The cognitive functions of the caudate nucleus. Prog Neurobiol 86:141–155

Hamilton M (1960) A rating scale for depression. J Neurol Neurosurg Psychiatry 23:56–62

Hamilton JP, Farmer M, Fogelman P, Gotlib IH (2015) Depressive rumination, the default-mode network, and the dark matter of clinical neuroscience. Biol Psychiatry 78:224–230

Hanslmayr S, Sauseng P, Doppelmayr M, Schabus M, Klimesch W (2005) Increasing individual upper alpha power by neurofeedback improves cognitive performance in human subjects. Appl Psychophysiol Biofeedback 30:1–10

Hari R, Salmelin R, Mäkelä JP, Salenius S, Helle M (1997) Magnetoencephalographic cortical rhythms. Int J Psychophysiol 26:51–62

Harmon-Jones E, Gable PA (2018) On the role of asymmetric frontal cortical activity in approach and withdrawal motivation: an updated review of the evidence. Psychophysiology 55:e12879

Henriques JB, Davidson RJ (1991) Left frontal hypoactivation in depression. J Abnorm Psychol 100:535–545

Henriques JB, Davidson RJ (2000) Decreased responsiveness to reward in depression. Cogn Emotion 14:711–724

Hsu SH, Mullen T, Jung TP, Cauwenberghs G (2014) Online recursive independent component analysis for real-time source separation of high-density EEG. IEEE Eng Med Biol Soc 36:3845–3848

Hsu SH, Mullen T, Jung TP, Cauwenberghs G (2016) Real-time adaptive EEG source separation using online recursive independent component analysis. IEEE Trans Neural Syst Rehabil Eng 24:309–319

Hughes SW, Crunelli V (2005) Thalamic mechanisms of EEG alpha rhythms and their pathological implications. Neuroscientist 11:357–372

Hyvärinen A, Karhunen J, Oja E (2001) Independent component analysis. Wiley, New York

Kinreich S, Podlipsky I, Intrator N, Hendler T (2012) Categorized EEG neurofeedback performance unveils simultaneous fMRI deep brain activation. In: Langs G et al (eds) Machine learning and interpretation in neuroimaging. Springer, Berlin, pp 108–115

Knyazev GG, Savostyanov AN, Bocharov AV, Dorosheva EA, Tamozhnikov SS, Saprigyn AE (2015) Oscillatory correlates of autobiographical memory. Int J Psychophysiol 95:322–332

Liberzon I, Abelson JL (2016) Context processing and the neurobiology of post-traumatic stress disorder. Neuron 92:14–30

Liu Z, de Zwart JA, Yao B, van Gelderen P, Kuo LW, Duyn JH (2012) Finding thalamic BOLD correlates to posterior alpha EEG. NeuroImage 63:1060–1069

Luo Q, Huang X, Glover GH (2014) Ballistocardiogram artifact removal with a reference layer and standard EEG cap. J Neurosci Methods 233:137–149

Mano M, Lecuyer A, Bannier E, Perronnet L, Noorzadeh S, Barillot C (2017) How to build a hybrid neurofeedback platform combining EEG and fMRI. Front Neurosci 11:140

Manshanden I, de Munck JC, Simon NR, Lopes da Silva FH (2002) Source localization of MEG sleep spindles and the relation to sources of alpha band rhythms. Clin Neurophysiol 113:1937–1947

Masterton RAJ, Abbott DF, Fleming SW, Jackson GD (2007) Measurement and reduction of motion and ballistogram artefacts from simultaneous EEG and fMRI recordings. NeuroImage 37:202–211

Mayeli A, Zotev V, Refai H, Bodurka J (2016) Real-time EEG artifact correction during fMRI using ICA. J Neurosci Methods 274:27–37

Morris SE, Cuthbert BN (2012) Research Domain Criteria: cognitive systems, neural circuits, and dimensions of behavior. Dialogues Clin Neurosci 14:29–37

Mulert C, Lemieux L (eds) (2010) EEG-fMRI: physiological basis, technique, and applications. Springer, Berlin

Murray EA, Wise SP, Drevets WC (2011) Localization of dysfunction in major depressive disorder: prefrontal cortex and amygdala. Biol Psychiatry 69:e43–e54

Nicholson AA, Ros T, Frewen PA, Densmore M, Théberge J, Kluetsch RC, Jetly R, Lanius RA (2016) Alpha oscillation neurofeedback modulates amygdala complex connectivity and arousal in posttraumatic stress disorder. NeuroImage Clin 12:506–516

Omata K, Hanakawa T, Morimoto M, Honda M (2013) Spontaneous slow fluctuation of EEG alpha rhythm reflects activity in deep-brain structures: a simultaneous EEG-fMRI study. PLoS ONE 8:e66869

Onton J, Delorme A, Makeig S (2005) Frontal midline EEG dynamics during working memory. NeuroImage 27:341–356

Paquette V, Beauregard M, Beaulieu-Prevost D (2009) Effect of psychoneurotherapy on brain electromagnetic tomography in individuals with major depressive disorder. Psychiatry Res Neuroimaging 174:231–239

Peeters F, Oehlen M, Ronner J, van Os J, Lousberg R (2014) Neurofeedback as a treatment for major depressive disorder – a pilot study. PLoS ONE 9:e91837

Perronnet L, Lecuyer A, Mano M, Bannier E, Lotte F, Clerc M, Barillot C (2017) Unimodal versus bimodal EEG-fMRI neurofeedback of a motor imagery task. Front Hum Neurosci 11:193

Pizzagalli DA, Nitschke JB, Oakes TR, Hendrick AM, Horras KA, Larson CL, Abercrombie HC, Schaefer SM, Koger JV, Benca RM, Pascual-Marqui RD, Davidson RJ (2002) Brain electrical tomography in depression: the importance of symptom severity, anxiety, and melancholic features. Biol Psychiatry 52:73–85

Posse S, Fitzgerald D, Gao K, Habel U, Rosenberg D, Moore GJ, Schneider F (2003) Real-time fMRI of temporolimbic regions detects amygdala activation during single-trial self-induced sadness. NeuroImage 18:760–768

Quaedflieg CWEM, Smulders FTY, Meyer T, Peeters F, Merckelbach H, Smeets T (2016) The validity of individual frontal alpha asymmetry EEG neurofeedback. Soc Cogn Affect Neurosci 11:33–43

Seibert TM, Hagler DJ, Brewer JB (2011) Early parietal response in episodic retrieval revealed with MEG. Hum Brain Mapp 32:171–181

Shtark MB, Verevkin EG, Kozlova LI, Mazhirina KG, Pokrovskii MA, Petrovskii ED, Savelov AA, Starostin AS, Yarosh SV (2015) Synergetic fMRI-EEG brain mapping in alpha-rhythm voluntary control mode. Bull Exp Biol Med 158:644–649

Sitaram R, Ros T, Stoeckel L, Haller S, Scharnowski F, Lewis-Peacock J, Weiskopf N, Blefari ML, Rana M, Oblak E, Birbaumer N, Sulzer J (2017) Closed-loop brain training: the science of neurofeedback. Nat Rev Neurosci 18:86–100

Smith EE, Cavanagh JF, Allen JJB (2018) Intracranial source activity (eLORETA) related to scalp-level asymmetry scores and depression status. Psychophysiology 55:e13019

Spielberg JM, Miller GA, Warren SL, Engels AS, Crocker LD, Banich MT, Sutton BP, Heller W (2012) A brain network instantiating approach and avoidance motivation. Psychophysiology 49:1200–1214

Spreng RN, Mar RA, Kim ASN (2009) The common neural basis of autobiographical memory, prospection, navigation, theory of mind, and the default mode: a quantitative meta-analysis. J Cogn Neurosci 21:489–510

Stewart JL, Coan JA, Towers DN, Allen JJB (2014) Resting and task-elicited prefrontal EEG alpha asymmetry in depression: support for the capability model. Psychophysiology 51:446–455

Svoboda E, McKinnon MC, Levine B (2006) The functional neuroanatomy of autobiographical memory: a meta-analysis. Neuropsychologia 44:2189–2208

Taber KH, Wen C, Khan A, Hurley RA (2004) The limbic thalamus. J Neuropsychiatry Clin Neurosci 16:127–132

Thibault RT, MacPherson A, Lifshitz M, Roth RR, Raz A (2018) Neurofeedback with fMRI: a critical systematic review. NeuroImage 172:786–807

Thibodeau R, Jorgensen RS, Kim S (2006) Depression, anxiety, and resting frontal EEG asymmetry: a meta-analytic review. J Abnorm Psychol 115:715–729

Tuladhar AM, ter Huurne N, Schoffelen JM, Maris E, Oostenveld R, Jensen O (2007) Parieto-occipital sources account for the increase in alpha activity with working memory load. Hum Brain Mapp 28:785–792

van der Meer JN, Pampel A, Van Someren EJW, Ramautar JR, van der Werf YD, Gomez-Herrero G, Lepsien J, Hellrung L, Hinrichs H, Möller HE, Walter M (2016) Carbon-wire loop based artifact correction outperforms post-processing EEG/fMRI corrections—a validation of a real-time simultaneous EEG/fMRI correction method. NeuroImage 125:880–894

Weiskopf N (2012) Real-time fMRI and its application to neurofeedback. NeuroImage 62:682–692

Weiskopf N, Veit R, Erb M, Mathiak K, Grodd W, Goebel R, Birbaumer N (2003) Physiological self-regulation of regional brain activity using real-time functional magnetic resonance imaging (fMRI): methodology and exemplary data. NeuroImage 19:577–586

Wong CK, Zotev V, Misaki M, Phillips R, Luo Q, Bodurka J (2016) Automatic EEG-assisted retrospective motion correction for fMRI (aE-REMCOR). NeuroImage 129:133–147

Wong CK, Luo Q, Zotev V, Phillips R, Chan KWC, Bodurka J (2018) Automatic cardiac cycle determination directly from EEG-fMRI data by multi-scale peak detection method. J Neurosci Methods 304:168–184

Wright CI, Fischer H, Whalen PJ, McInerney SC, Shin LM, Rauch SL (2001) Differential prefrontal cortex and amygdala habituation to repeatedly presented emotional stimuli. NeuroReport 12:379–383

Young KD, Siegle GJ, Zotev V, Phillips R, Misaki M, Yuan H, Drevets WC, Bodurka J (2017) Randomized clinical trial of real-time fMRI amygdala neurofeedback for major depressive disorder: effects on symptoms and autobiographical memory recall. Am J Psychiatry 174:748–755

Zich C, Debener S, Kranczioch C, Bleichner MG, Gutberlet I, De Vos M (2015) Real-time EEG feedback during simultaneous EEG-fMRI identifies the cortical signature of motor imagery. NeuroImage 114:438–447

Zoefel B, Huster RJ, Herrmann CS (2011) Neurofeedback training of the upper alpha frequency band in EEG improves cognitive performance. NeuroImage 54:1427–1431

Zotev VS, Volegov PL, Matlashov AN, Espy MA, Mosher JC, Kraus RH Jr (2008b) Parallel MRI at microtesla fields. J Magn Reson 192:197–208

Zotev VS, Matlashov AN, Volegov PL, Savukov IM, Espy MA, Mosher JC, Gomez JJ, Kraus RH Jr (2008a) Microtesla MRI of the human brain combined with MEG. J Magn Reson 194:115–120

Zotev V, Krueger F, Phillips R, Alvarez RP, Simmons WK, Bellgowan P, Drevets WC, Bodurka J (2011) Self-regulation of amygdala activation using real-time fMRI neurofeedback. PLoS ONE 6:e24522

Zotev V, Yuan H, Phillips R, Bodurka J (2012) EEG-assisted retrospective motion correction for fMRI: E-REMCOR. NeuroImage 63:698–712

Zotev V, Phillips R, Young KD, Drevets WC, Bodurka J (2013) Prefrontal control of the amygdala during real-time fMRI neurofeedback training of emotion regulation. PLoS ONE 8:e79184

Zotev V, Phillips R, Yuan H, Misaki M, Bodurka J (2014) Self-regulation of human brain activity using simultaneous real-time fMRI and EEG neurofeedback. NeuroImage 85:985–995

Zotev V, Yuan H, Misaki M, Phillips R, Young KD, Feldner MT, Bodurka J (2016) Correlation between amygdala BOLD activity and frontal EEG asymmetry during real-time fMRI neurofeedback training in patients with depression. NeuroImage Clin 11:224–238

Zotev V, Misaki M, Phillips R, Wong CK, Bodurka J (2018a) Real-time fMRI neurofeedback of the mediodorsal and anterior thalamus enhances correlation between thalamic BOLD activity and alpha EEG rhythm. Hum Brain Mapp 39:1024–1042

Zotev V, Phillips R, Misaki M, Wong CK, Wurfel BE, Krueger F, Feldner M, Bodurka J (2018b) Real-time fMRI neurofeedback training of the amygdala activity with simultaneous EEG in veterans with combat-related PTSD. NeuroImage Clin 19:106–121

Zotev V, Mayeli A, Misaki M, Bodurka J (2020) Emotion self-regulation training in major depressive disorder using simultaneous real-time fMRI and EEG neurofeedback. NeuroImage Clin 27:102331

Zotev V, Bodurka J (2020) Effects of simultaneous real-time fMRI and EEG neurofeedback in major depressive disorder evaluated with brain electromagnetic tomography. NeuroImage Clin 28:102459

Zumsteg D, Lozano AM, Wieser HG, Wennberg RA (2006) Cortical activation with deep brain stimulation of the anterior thalamus for epilepsy. Clin Neurophysiol 117:192–207

Non-invasive Brain Stimulation with Multimodal Acquisitions

14

Alexander T. Sack, Teresa Schuhmann, and Tom A. de Graaf

14.1 Brain Imaging: Possibilities and Limitations

Brain imaging today includes a range of methodologies that can reveal various aspects of the physiological basis of cognition, perception and behaviour. Foremost among them are functional magnetic resonance imaging (fMRI) and electroencephalography (EEG). In this chapter, we mainly focus on fMRI and how it can be meaningfully combined with brain stimulation approaches. Towards the end, we return to EEG, its combination with brain stimulation and fMRI and the unique contributions offered by such multimodal research.

fMRI is a non-invasive imaging method, capable of visualising brain areas that are active during different behavioural or cognitive functions. As such, fMRI provides evidence for local (task-dependent) changes in brain activity, but it is limited in revealing direct causal relationships between these brain activity changes and their behavioural or cognitive consequences. Is the observed change in brain activity functionally relevant for the task? To answer this question, the experimental design must somehow be inverted. Where in functional neuroimaging the cognition or behaviour is the independent variable and brain activity the dependent variable, we wish to turn this around. We should manipulate brain activity, making this the experimental factor, and observe the effects of this manipulation on cognition or behaviour. If the experimentally induced brain activity change has effects on task performance, only then can one conclude that the brain activity involved is functionally relevant. The direction of behavioural effects moreover provides information on the potential specific role of the targeted brain region in the task at hand. To achieve this sort of controlled experimental setup, a method of transient and local brain

A. T. Sack (✉) · T. Schuhmann · T. A. de Graaf
Section Brain Stimulation and Cognition, Department of Cognitive Neuroscience, Faculty of Psychology and Neuroscience, Maastricht University, Maastricht, the Netherlands
e-mail: a.sack@maastrichtuniversity.nl; t.schuhmann@maastrichtuniversity.nl; tom.degraaf@maastrichtuniversity.nl

C. Mulert, L. Lemieux (eds.), *EEG - fMRI*,
https://doi.org/10.1007/978-3-031-07121-8_14

activity manipulation is required. Such methods exist and are collectively referred to as functional brain interference or brain stimulation techniques.

14.2 Invasive and Non-invasive Brain Stimulation

Brain stimulation techniques (also referred to as brain perturbation, brain interference or neuromodulation techniques) can be divided into invasive and non-invasive approaches. Some invasive methods, such as cooling and microstimulation, are mainly limited to animal studies, while other invasive (deep brain) stimulations are used in humans but only in patient populations. In contrast, transcranial low-intensity electrical current stimulation (tES) and transcranial magnetic stimulation (TMS) are *non-invasive* brain stimulation techniques (NIBS), which can be safely used in both human volunteers and patients. NIBS allows for controlled manipulation of brain activity in several ways. TES is thought to modulate cortical excitability during application and—depending on stimulation parameters—can also outlast the stimulation itself. Depending on the parameters and form of tES, it can (1) enhance or decrease cortical excitability or (2) align/amplify local oscillations. TMS, depending on the parameters of the application, can (1) induce transient disruptions of neural activity ('virtual lesions'), (2) enhance or decrease cortical excitability, (3) transiently stimulate ('activate') neural populations or (4) even align/amplify local oscillations. In all cases, by transiently changing activity in the stimulated brain area and revealing a subsequent change in a particular behaviour, NIBS can be regarded as a unique research approach to investigate causal structure-function relationships.

14.2.1 The Physics and Physiology of Single-Pulse Transcranial Magnetic Stimulation (TMS)

Any TMS device consists of a bank of capacitors capable of producing high discharge currents and an electromagnetic stimulating coil to apply magnetic pulses of up to several Tesla. The intense and rapidly changing currents are discharged into the coil, thereby creating a strong and time-varying magnetic field (pulse). This pulse can reach its peak in a few hundred microseconds and induce an electric field in the neuronal tissue underneath the coil. The strength of the induced electric field depends mainly on the rate of change of the magnetic field. Due to the electrical conductivity of the living tissue, the induced electric field results in electrical (eddy) currents in the cortex, in a parallel but opposite direction to the current in the coil (Lenz's law). These currents can cause depolarisation and induce action potentials, in the underlying neurons.

Physical parameters of the magnetic field (e.g. rise time and spatial field distribution) determine the temporal-spatial characteristics of the magnetic pulse sent into the brain, but the induced electric field characteristics in neural tissue depend on some additional factors. The shape of the skull, the distance from

TMS coil to the gyrating cortical layers, the shape of coil and intensity of stimulation and whether pulses are monophasic or biphasic all influence the final effective strength and extent of stimulation at the cortical level. Moreover, the magnetic field strength decreases exponentially with distance and the cortical surface is convoluted. Magnetic coils have different possible geometric shapes, affecting focality and induced current direction. All these characteristics, of stimulation coils and the underlying neuronal tissue, interact to determine the actualised neuronal depolarisation of mostly superficial levels of the brain (within a few cm of the coil). And that is considering the effects of one magnetic pulse only.

14.2.2 From Single-Pulse to Repetitive TMS: Stimulation Protocols

TMS pulses can be applied one at a time (single-pulse TMS), in pairs separated by a variable interval (paired-pulse TMS) or in multiples, ranging from triple-pulse or even quintuple-pulse TMS. Importantly, for these application methods, the pulses are usually locked to an external event (e.g. task onset), therefore potentially revealing information about the chronometry of a perceptual or cognitive process (e.g. Schuhmann et al. 2009, 2012; de Graaf et al. 2014). We can, therefore, refer to these approaches as chronometric, or event-related, TMS. By applying chronometric TMS at variable times during task execution, it is possible to investigate not only whether a given brain region is necessary for the tested behaviour but also at what time point (with a temporal resolution of 5–10 ms) the neural activity at the stimulation site is critical for successful task performance (chronometry of functional relevance; see also Walsh and Pascual-Leone 2003).

TMS pulses can also be applied rhythmically, for a longer duration, in either ‘conventional’ or ‘patterned’ protocols of repetitive stimulation (repetitive TMS, rTMS, Rossi et al. 2009). The important feature of both conventional and patterned rTMS protocols is that they can modulate the excitability of the stimulated area for some time after the TMS application itself. The nature of these after-effects, whether they are inhibitory or excitatory, mainly depends on the frequency of stimulation. In conventional rTMS protocols, single TMS pulses are applied in a regular rhythm, with a core distinction between low-frequency rTMS (stimulation frequency of 1 Hz or less) and high-frequency rTMS (stimulation frequency >1 Hz). Patterned rTMS refers to repetitive application of short high-frequency bursts of rTMS, interleaved by short pauses of no stimulation. In theta burst stimulation (TBS), short bursts of 50 Hz rTMS are repeated with a rate in the theta range (5 Hz) as a continuous (cTBS) or intermittent (iTBS) train (Di Lazzaro 2008; Huang et al. 2005). Both 1 Hz rTMS and cTBS have been found to produce lasting inhibitory after-effects, whereas high-frequency rTMS and iTBS can induce lasting facilitatory after-effects on motor corticospinal output in healthy participants. These, however, are group-level effects that may differ between participants (e.g. Maeda et al. 2000) and seem dependent on idiosyncratic brain

mechanisms (e.g. Chechlacz et al. 2015). The inter- and even intra-individual variability of responses to rTMS is one of the reasons that combining TMS with brain imaging can be so valuable.

The ability of rTMS to induce longer-lasting excitability changes has opened the door for the clinical applications of TMS in treating various neuropsychiatric disorders, for example, by 'down- or up-regulating' pathologically hyper- or hypoactive brain areas (Brighina et al. 2003; Haraldsson et al. 2004; Hoffman 2003; Hoffman and Becker 2005; Martin et al. 2003; Paus and Barrett 2004).

14.2.3 Clinical Applications of TMS

Over the past 20 years, an increasing number of studies of the potential therapeutic effects of TMS have been published (Lefaucheur et al. 2014). Disorders including addiction (Camprodon et al. 2007; Eichhammer et al. 2003), obsessive compulsive disorder (Martin et al. 2003; Sachdev et al. 2001), pain (Khedr et al. 2005; Lefaucheur et al. 2001), schizophrenia (Chibbaro et al. 2005; Lee et al. 2005) and depression (George et al. 1995; Pascual-Leone et al. 1996) have been studied; however, of all the psychiatric disorders, TMS in major depressive disorder (MDD) has been studied most thoroughly.

To treat depression, repetitive TMS is applied to the dorsolateral prefrontal cortex (DLPFC). Numerous studies stimulated either left DLPFC with high-frequency TMS or right DLPFC with low-frequency TMS, with diverse results (for review see, for example, Schonfeldt-Lecuona et al. 2010). O'Reardon et al. (2007) published a large multicentre trial of daily left prefrontal TMS in medication-free patients with MDD, reporting encouraging results. In contrast, Herwig and colleagues found no difference in responder rates or depression rating scales between real TMS and sham treatment groups in their multicentre trial (Herwig et al. 2007). Early meta-analyses of the antidepressant effect of rTMS (Burt et al. 2002; Gross et al. 2007; Holtzheimer et al. 2001; Kozel and George 2002; Martin et al. 2003; McNamara et al. 2001) also revealed mixed results, with differences between findings perhaps relating to small sample sizes as well as heterogeneous designs.

The validity of TMS for the treatment of depression in clinical practice thus remained unclear for quite some time. While TMS certainly seemed to have beneficial effects with therapeutic potential, the inconsistency of results needed explanation, so that consensus could be reached on which TMS protocols are effective for which types of depression patients (see also Ridding and Rothwell 2007). Nevertheless, in 2008, the first rTMS device (NeuroStar TMS Therapy System) received FDA approval for the treatment of resistant major refractory depression in adults. Since then, FDA approval has been awarded to multiple manufacturers for the same rTMS protocols, always stimulating the left frontal cortex with excitatory protocols, daily for several weeks excluding weekends. Since the standard excitatory rTMS protocol takes relatively long to complete (a

single session takes 37 min), it is of interest that patterned rTMS (the iTBS protocol described above) received FDA approval as well in summer 2018. iTBS to treat depression achieves similar effects in only a fraction of the time (6 min).

An extensive consensus review on the therapeutic potential and efficacy of TMS was published by Lefaucheur et al. (2014). They concluded that, at that time, there was 'definite efficacy' for the antidepressant effects of high-frequency left DLPFC rTMS in the treatment of depression and 'probably efficacy' for low-frequency right DLPFC rTMS.

TMS was also considered 'definitely effective' in the treatment of neuropathic pain and 'probably effective' in the treatment of motor stroke and schizophrenia (Lefaucheur et al. 2014), sometimes through interesting mechanisms. Indeed, clinical studies employed rTMS to alleviate behavioural or cognitive deficits in patients suffering from brain injury, lesions and stroke (see, for example, Brighina et al. 2003; Koch et al. 2008; Oliveri et al. 1999, 2001). By suppressing the intact hemisphere of stroke patients, the damaged hemisphere is (to an extent) released from the strong interhemispheric inhibition. This allows the damaged hemisphere to express its remaining functionality. TMS studies based on this logic have delivered encouraging results, demonstrating that the counterintuitive strategy of decreasing neural excitability of the healthy hemisphere actually improves deficits following unilateral brain damage to the other hemisphere (Brighina et al. 2003; Cazzoli et al. 2010; Koch et al. 2008; Nyffeler et al. 2009; Oliveri et al. 2000a, b, 2001; Shindo et al. 2006; Song et al. 2009).

14.3 The Multimodal Approach: Combinations of Brain Stimulation and Brain Imaging

Brain imaging and brain stimulation offer highly complementary methods for studying the healthy and diseased human brain. It is, therefore, sensible to combine these approaches in human fundamental and clinical neuroscience. But NIBS and functional imaging can be combined in different ways. Brain imaging can take place *before* brain stimulation, to guide and/or individually calibrate the brain stimulation protocols. Brain imaging and brain stimulation can be implemented *simultaneously*, for instance, to chart brain dynamics using TMS pulses as 'system probes' or to reveal the neural bases for TMS-induced changes in cognition or behaviour. In some cases, the latter can be achieved also by brain imaging *after* brain stimulation, if NIBS protocols are used to induce neuronal changes that last sufficiently long to capture them with functional imaging immediately after. Both the simultaneous combination and the different sequential experimental combinations can be considered 'multimodal approaches' (see Fig. 14.1). All are useful for the investigation of functional brain-behaviour relationships, though they have different applications, advantages and limitations.

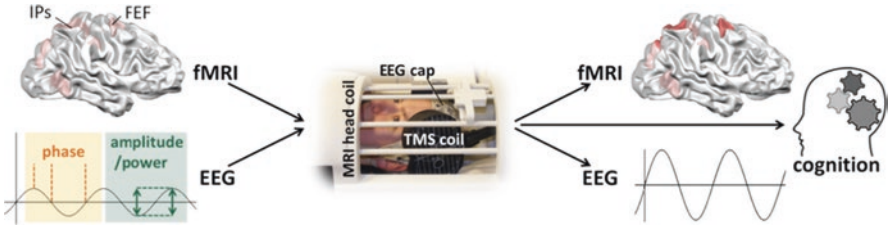

Fig. 14.1 The multimodal approach. Information from individual EEG and fMRI can be used to inform subsequent non-invasive brain stimulation (NIBS), for instance, using fMRI activations to guide the cortical stimulation target or using individual EEG oscillatory activity to calibrate/tailor TMS or TES stimulation protocols. Alternatively, NIBS can be administered simultaneously with brain imaging, such as EEG and fMRI, or even all together. Lastly, the neural effects of, or responses to, NIBS could be evaluated using brain imaging to better understand the neural basis of NIBS effects on cognition and behaviour

14.3.1 Brain Imaging Before Brain Stimulation

When applying TMS in cognitive studies, the brain areas of interest do not always have a behavioural signature output, as is the case for TMS over the motor cortex or visual cortex. For these brain regions, and associated cognitive research questions, it is not straightforward to determine the precise scalp location where TMS pulses should be administered. Functional imaging before TMS can be used to address this problem by precisely localising a task-related area of cortical activation for subsequent use with a frameless stereotaxic TMS neuronavigation system, thus optimising the exact coil positioning for TMS. In this way, the combination of brain imaging and subsequent brain stimulation permits the assessment of whether, in a given participant, this task-related functional activity (shown using brain imaging) is actually functionally relevant to that individual's successful task performance (Andoh et al. 2006; Sack et al. 2006; Thiel et al. 2005). There are now several commercially available stereotaxic systems for TMS neuronavigation. Most of them allow for fMRI-TMS co-registration procedures so that events occurring around the head of the participant in real space are registered online and visualised in real time at correct positions relative to the participant's anatomical reconstruction of the brain. By superimposing the functional data on the anatomical reconstruction of the brain, the TMS coil can be neuronavigated to a specific functional activation area of every participant (see Sack et al. 2009) (Fig. 14.2).

Using such neuronavigation systems, TMS coil positioning can become highly accurate, targeting anatomical or functional 'hotspots' in individual participants with millimetre precision. This is relevant since, despite the limited spatial resolution of the applied magnetic field, spatial TMS coil shifts in the order of millimetres have been shown to sometimes result in a complete loss of behavioural or cognitive impairment effects (Beckers and Homberg 1992; d'Alfonso et al. 2002). Comparing different localisation strategies for TMS-based primary motor cortex mappings in terms of accuracy and efficiency, Sparing et al. (2008) found that fMRI-guided stimulation was most precise (accuracy was concluded to be in the millimetre

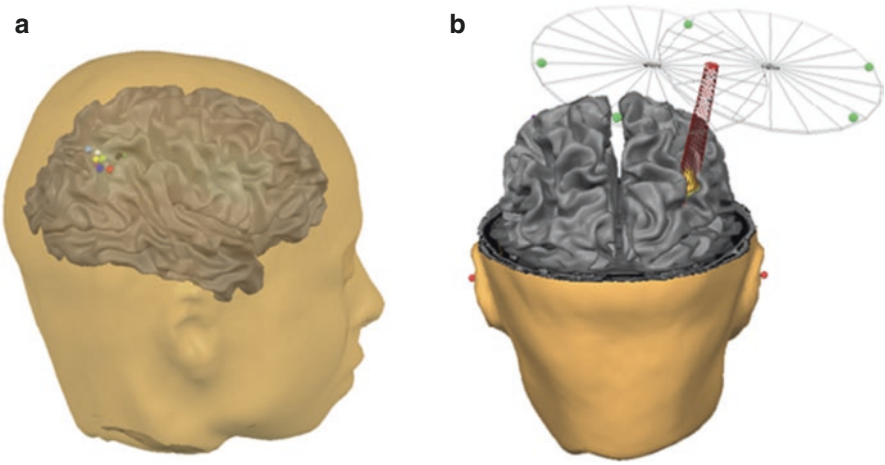

Fig. 14.2 fMRI-Guided TMS Neuronavigation. Panel (**a**) shows several colour-coded fMRI activity clusters superimposed on a reconstruction of the cortical surface, projected within a transparent mesh of a reconstructed head in Talairach space. Each of these clusters represents an individual fMRI 'hotspot', that is, strongest task-related activity, of an individual participant obtained in a separate fMRI measurement. The spatial distribution between these individual fMRI activity clusters accounts for the inter-individual variability in structure-function correspondence. Panel (**b**) shows a snapshot of the BrainVoyager TMS neuronavigation system used to guide TMS coil positioning based on one of these activity clusters of a given participant. The red beam indicates where the magnetic field of TMS is strongest and is navigated in real time to the here orange colour-coded individual fMRI hotspot of this particular participant. The exact positioning of the TMS coil and thus the target area for the magnetic brain stimulation is therefore individually defined based on the fMRI data obtained in a separate session prior to TMS

range). Feredoes et al. (2007) used fMRI to localise TMS sites for disruption of short-term verbal information retention.

Sack et al. (2009) investigated the behavioural impact of right parietal TMS on a number comparison task, when TMS localisation was based on (1) individual fMRI-guided TMS neuronavigation, (2) individual MRI-guided TMS neuronavigation, (3) group functional Talairach coordinates or (4) the 10–20 EEG position P4. They quantified the behavioural effect of each TMS localisation approach, calculated the standardised experimental effect sizes and conducted a statistical power analysis, which revealed that the individual fMRI-guided TMS neuronavigation yielded the strongest behavioural effect size (Sack et al. 2009). This increased effect size of TMS when using (f)MRI-guided coil positioning has also been shown in the context of clinical TMS applications for various psychiatric disorders (Ahdab et al. 2010; De Ridder et al. 2011; Herbsman et al. 2009). Development of cortical targeting approaches is still ongoing, with different approaches making different trade-offs between practical and cost feasibility on the one hand and maximising successful cortical targeting on the other hand. To provide a recent example, Duecker et al. (2014) describe an approach that uses pre-existing functional target locations (i.e. published coordinates/location of an fMRI-based group functional hotspot for a task

for interest), back-projected onto individual anatomical data after sophisticated cortex-based alignment of those data to an anatomical template. This approach finds a middle ground, marrying some of the benefits of functional localisation and the consideration of individual anatomy, without requiring fMRI measurements in single participants which may not always be available.

14.3.2 Brain Imaging After Brain Stimulation

Certain brain stimulation protocols, such as rTMS, TBS or anodal/cathodal tDCS, are capable of modulating neural excitability of a region beyond the stimulation duration. Functional imaging can then be used to investigate these prolonged NIBS after-effects. Imaging the immediate and longer-lasting after-effects of NIBS is paramount for revealing the underlying neurobiological mechanisms that cause the observed behavioural changes and clinical treatment effects of TMS stimulation.

An elegant example of this approach comes from Hubl et al. (2008). Here, the right frontal eye field (FEF) was stimulated outside the MR scanner using continuous theta burst rTMS (TBS). Then fMRI was used to map the TBS-induced effects and assess their temporal persistence across the brain during a saccade task. The results showed a TBS-induced suppression of local BOLD activity that appeared 20–35 min (but not immediately) after stimulation (Hubl et al. 2008). Suppression, albeit weaker, was also evident in more remote regions, including the (pre)supplementary and parietal eye fields. Similarly, Cardenas-Morales et al. (2011) used fMRI for exploring the after-effects of iTBS over the primary motor cortex. A recent example demonstrates how this approach is also valuable to understand more cognitive and emotional brain mechanisms and their interplay. Engelen et al. (2018) presented volunteers with short movie clips of actors displaying either neutral or angry whole-body actions, measuring brain activity with fMRI. The left amygdala did not differentiate these stimuli, unless areas in the action network (inferior parietal lobule, ventral premotor cortex) were first inhibited by continuous TBS. The effects of TBS and emotion were also clear from other action network regions, confirming complex dynamics between emotional and action brain systems uniquely revealed by the combination of TBS and subsequent fMRI.

A similar approach has been used to better understand the clinical efficacy of NIBS. For instance, several studies have used functional imaging to visualise TMS after-effects in prefrontal cortex (PFC), to explore the mechanisms underlying therapeutic applications for depression (Fitzgerald et al. 2007). These studies suggest that prefrontal rTMS in normal and depressed participants has profound effects on both local and remote brain regions implicated in depression, including bilateral frontal, limbic and paralimbic areas (Fitzgerald et al. 2007; Kimbrell et al. 1999, 2002; Pogarell et al. 2006, 2007; Speer et al. 2000, 2009; Teneback et al. 1999). Importantly, these rTMS-induced effects appear to be frequency dependent, with low-frequency rTMS leading to bilateral reduction in frontal activation (Fitzgerald et al. 2007).

14.3.3 Simultaneous Brain Stimulation and Brain Imaging

While useful, functional imaging after TMS application remains fundamentally limited in elucidating the neuronal effects of TMS. Concurrent TMS and neuroimaging offers a broader range of 'in vivo' information regarding the actual and immediate effects of TMS on cortical activation, both local and remote. Simultaneous TMS and imaging can thus be used to online track the TMS effects in the brain or probe intracerebral connectivity (Bestmann et al. 2003b, 2004, 2005; Bohning et al. 1999, 2000b; Ruff et al. 2006; Sack et al. 2007). Therefore, even in the absence of overt behaviour, TMS during fMRI facilitates the imaging of pathways of activity spreading within and between brain networks. The simultaneous approach allows the investigation of local and remote brain responses to TMS, and/or the local and remote brain correlates of TMS-induced changes in cognition/behaviour, at a neurophysiological level. Thus, it can be determined, in vivo, which brain areas—either directly or transsynaptically affected by TMS—passively respond to TMS and/or actively underlie the observed TMS-induced behavioural changes during task execution. However, the simultaneous combination of TMS and functional imaging poses great technical challenges. Therefore, it is routinely used by only few research groups, and the number of simultaneous TMS/fMRI publications is still considerably small (see Reithler et al. 2011 for an overview).

Besides the need for specific hardware (e.g. an MR-compatible TMS system), simultaneous TMS and BOLD fMRI require appropriate temporal synchronisation between MRI acquisition and TMS pulse application. Furthermore, the discharge, and even mere presence, of MR-compatible TMS coils in the bore of the magnet produces artefacts in the echo-planar imaging (EPI) images that need to be resolved before the synchronised combination of functional imaging and brain stimulation becomes feasible. We now first briefly outline relevant technical and implementation considerations and then discuss some instructive examples of simultaneous TMS-fMRI experiments that highlight the unique insights offered by this multimodal approach.

14.3.3.1 Technical Challenges and Practical Implementation

The use of TMS inside the MR scanner during simultaneous TMS/fMRI studies requires several modifications to TMS hardware, specific TMS/fMRI interleaved experimental designs and the consideration or removal of several artefacts. Most importantly, the standard TMS coils routinely used outside the MR scanner are not appropriate for simultaneous TMS/fMRI studies. Instead, specific MR-compatible non-ferromagnetic TMS coils are required in strengthened casing. To fit in the scanner environment, these coils generally have no handle, and positioning requires adaptive solutions since frameless stereotaxy is challenging. A common solution is to fit the coil with MR markers that allow post hoc reconstruction of coil positioning and triangulation of the cortical target. The MR-compatible TMS coil is connected to the stimulator outside the RF-shielded cabin via a cable running through a wave guide. Therefore, the RF shield of the MR scanner is pierced by the TMS cable, which acts as an antenna transmitting RF noise into the scanner. Special RF noise

filters then need to be installed for simultaneous TMS/fMRI studies as an additional hardware component. Without an RF filter, the TMS set-up causes a loss of 20–80% in signal-to-fluctuation-noise ratio of EPI images. An RF filter largely prevents this loss, at the cost of around 7% of functional TMS efficacy (Bungert et al. 2012a).

Despite the installation of an RF filter, the MR image quality is often still decreased in simultaneous TMS and fMRI studies. This is because the mere presence of a TMS coil in the scanner can result in static magnetic field inhomogeneities, which particularly affect EPI scans (commonly used for fMRI). Baudewig et al. (2000) systematically investigated the type and extent of the artefacts induced by the TMS coil during MR measurements. The authors revealed that although the anatomical images were unaffected, there were pronounced signal losses and geometric distortions in EPI acquisitions perpendicular to the plane of the coil. However, these artefacts could be markedly reduced, particularly artefacts remote from the coil, by using an EPI orientation parallel to the coil plane. With such EPI orientation, signal losses and geometric distortions attenuate with increasing distance from the coil and so are restricted to the area very close to the coil. In this scenario, it is unlikely that functional images of the human cortex are strongly affected, given a scalp-cortex distance of >1 cm.

After having addressed the technical challenges discussed above, one can progress to the most important step: applying TMS pulses during actual MR EPI data acquisition. But actually, it must be noted that simultaneous TMS/fMRI is not advisable in the strictest sense. In practice, TMS pulses and MRI acquisitions are interleaved, to avoid the artefacts produced by the TMS-induced currents. This way, fMRI scans can remain artefact-free even though TMS is applied in the MR environment. ‘Simultaneous’ or ‘concurrently combined’ TMS/fMRI thus generally refers to *interleaved* TMS and fMRI measurements. But for all intents and purposes, this may be considered ‘simultaneous’, since the temporal characteristics and resolution of the BOLD signal render the delay ineffectual. To achieve interleaved TMS-fMRI, the MR sequence must send a trigger signal to the TMS apparatus (for instance, through a computer) with every RF pulse excitation. Timing is critical, since distortions may still occur up to 100 ms after administration of a TMS pulse (Bestmann et al. 2003a; Shastri et al. 1999), although this will differ between labs. These lasting artefacts are purportedly related to residual currents in the TMS coil and to currents induced by the vibrations in the TMS coil following a pulse (Shastri et al. 1999). With better vibration absorption in the TMS coil, the delay between TMS pulse and MR image acquisition may be reduced considerably.

There are various methods for temporally interleaving TMS and MRI for simultaneous experiments. For example, TMS pulses and MR images can be interleaved by insertion of temporal gaps after each volume (Ruff et al. 2006; Sack et al. 2007). Sack et al. (2007) applied bursts of rTMS at ~13.3 Hz, in an acquisition gap of 560 ms between subsequent MR volumes. In this study, a delay of 200 ms from the last TMS pulse to the beginning of the next MR volume acquisition protected the subsequent MR acquisition from pulse-related artefacts. Alternatively, TMS pulses can be separated, not by placing them at between functional volume acquisitions but by interleaving them after each slice within one volume (Bestmann et al. 2004, 2005;

Bohning et al. 2000a). This method still requires a sufficient delay between TMS pulses and slice acquisition so that subsequent slices are not perturbed. Finally, single slices might also be deliberately perturbed by the TMS pulse and then be identified and replaced, either by interpolation between pre- and post-pulse acquisitions of the same slice or by including affected slices as covariates in a general linear model analysis. Since the latter approach does involve TMS *during* EPI, researchers should check with their hardware manufacturers whether this procedure is advised. When employing any of these methods with modified EPI sequences to optimise interleaved TMS/fMRI measurements, it is also recommended to introduce oversampling of the phase-encoding direction of EPI images in order to shift the so-called ghosting artefact outside the volume of interest.

One additional problem for simultaneous (interleaved) TMS/fMRI studies was discussed by Weiskopf et al. (2009), who reported that leakage currents may be generated when switching stimulation intensities. In a phantom measurement, these leakage currents in the TMS coil varied parametrically with the TMS output intensity (its capacitor charge) and induced magnetic field inhomogeneities which led to false-positive fMRI findings. In other words, BOLD signal increased parametrically with TMS intensity in their phantom measurement (Weiskopf et al. 2009). Following this report, a technical solution has been pioneered which introduces a relay in parallel (and diodes in series) with the TMS coil. When the relay is closed, leakage current primarily flows through this relay, rather than the TMS coil. A trigger signal then briefly opens the relay so that a TMS pulse can be applied. However, although these (or similar) solutions are now standard in MR-compatible TMS systems, appropriate test measurements should be run in order to identify any remaining artefacts or false positives due to leakage current.

In sum, even an MRI-compatible TMS coil affects the magnetic field (Bungert et al. 2012b), and TMS pulses perturb MR images within a certain timeframe. Several solutions were proposed to limit or circumvent the latter and development is still ongoing. Such development is not limited to the problem of artefacts alone but expands to new design of MR coils to be used with concurrent TMS (Navarro de Lara et al. 2017) or reliable cortical target localisation in concurrent TMS/fMRI, for example (Hubl et al. 2008). Below, we discuss why the benefits of multimodal imaging justify these efforts.

14.3.3.2 TMS Affects Networks, Not Just a Local Region

Generally, studies using concurrent TMS-fMRI have shown that TMS affects the BOLD signal in the targeted site and moreover task dependently. This is encouraging, given the widespread assumption that TMS affects excitability/activity in the region directly underneath the coil, and that this activity change reflects behavioural effects of TMS (see Reithler et al. 2011, for an exhaustive overview). However, one of the most important additional insights from combined TMS and functional imaging studies is that locally applied TMS not affects neural activity at the stimulation site but also affects remote and interconnected brain regions (Bestmann et al. 2003b; Blankenburg et al. 2008; Bohning et al. 2000a; Denslow et al. 2005; Ruff et al. 2006; Rushworth et al. 2002; Sack et al. 2007). This includes cortical as well as

subcortical brain areas, as revealed by early application to the human motor system (Baudewig et al. 2001; Bestmann et al. 2004; Bohning et al. 1999, 2000a). It seems that application of TMS in essence inserts energy into a system; TMS to an isolated neuronal population will excite not only that population, but a connected brain area will propagate the inserted energy throughout its anatomical (Boorman et al. 2007) and functional (Sack 2006) network. It is precisely the value of TMS-fMRI that this spread of TMS excitation can be tracked throughout the brain.

Bohning et al. (1999) showed that the BOLD signal resulting from TMS correlated to the TMS intensity both in local (targeted) and remote brain areas. Moreover, Bohning et al. (2000a) could show that TMS-induced finger movements resulted in BOLD signals throughout the brain that were similar to BOLD signals resulting from voluntary finger tapping. This constituted an early demonstration of the validity of using TMS-fMRI to probe functional/anatomical networks in the brain. Bestmann et al. (2004) confirmed this notion, stimulating with high-frequency rTMS the left primary sensorimotor cortex (M1/S1) at supra- and subthreshold intensities (no finger movements induced in the latter condition) and measuring the BOLD signals throughout the brain. A network of distinct cortical and subcortical motor system structures was activated in response to the TMS, again involving the same regions activated by voluntary finger movements. Interestingly, this was the case even for subthreshold stimulation, showing that TMS can probe an anatomical network even in the absence of overt behavioural response, although subthreshold stimulation in the absence of induced muscle contractions mainly led to enhanced BOLD responses in supplementary and premotor cortices and not in the local M1/S1 region that was actually stimulated (see Hanakawa et al. 2009 for similar intensity-dependent remote activation changes based on spTMS and Caparelli et al. 2010, for remote effects in the visual system).

This suggests that the local BOLD effects, directly underneath the coil, may constitute a special case: they depend on actually induced muscle contractions, while remote connected motor network regions also involved in voluntary movements are activated by M1/S1 TMS even subthreshold (Bestmann et al. 2004; Denslow et al. 2005). Based on modelling work, Esser et al. (2005) suggest that TMS locally stimulates both excitatory and inhibitory neural populations (ergo the net activation and thus BOLD is weaker here) but remotely results mainly in excitatory responses which are easier to detect. However, the matter is not settled, given the still ill-defined intricacies of TMS effects on local neural circuits and moreover the connection between such effects and the BOLD signal (Logothetis 2008; Logothetis et al. 2010). Still, the anatomical and especially functional specificity of the observed remote network effects argues against a non-specific (water ripple-like) spread of TMS-induced activity. Moreover, the observed networks closely resemble the brain systems involved in natural tasks involving the same regions. For a more elaborate review of these issues, see Reithler et al. (2011).

14.3.3.3 TMS Network Effects Depend on Brain State

Focal TMS can lead to both local and remote neural effects, within anatomically or functionally connected networks. However, several combined TMS/fMRI studies

have also found that these effects are state or task dependent. In other words, the state of the brain at the moment of TMS, as induced by task demands or external sensory stimulation, or even by naturally occurring fluctuations, can influence the local and remote network response to TMS. Bestmann et al. (2008) applied TMS over the left dorsal premotor cortex (PMd) at two intensities (low vs. high) and two motor states (grip vs. no-grip). The authors revealed a significant crossover interaction between motor state and TMS intensity over left PMd, arising in right M1 and right PMd. TMS over left PMd during rest (no-grip) led to an activation decrease in right PMd and M1. Such contralateral decrease following TMS has been observed in most (Bestmann et al. 2004; Kemna and Gembris 2003) but not all simultaneous TMS/fMRI studies over the motor cortex (Bohning et al. 2000a; Hanakawa et al. 2009). Importantly, during (left-handed) grip, left PMd TMS actually induced a contralateral *in*crease in activation, with stronger functional coupling following high-intensity TMS as compared to low intensity. This reversal of effects (activation increases/decreases) is likely caused by differences in the initial brain states, in relation to interregional mutual inhibition/facilitation mechanisms (see also O'Shea et al. (2007)).

Recently, state dependence has been demonstrated in more cognitive contexts. Sack et al. (2007) revealed that TMS over right IPS only resulted in right-hemispheric frontoparietal network effects when participants were engaged in a cognitive (spatial judgement) task that required the proper functioning of the targeted brain region. When a control task (colour judgement) did not rely on the parietal cortex, these network effects of TMS were not found (Sack et al. 2007). State-dependent responses to TMS have been shown in the context of spatial attention as well (Bestmann et al. 2007), also concurrently with fMRI (Heinen et al. 2011). Attention is subserved by a frontoparietal functional network, and disruption of this network by TMS can affect attention performance (Dambeck et al. 2006; Duecker et al. 2013; Hilgetag et al. 2001). Simultaneous fMRI revealed BOLD decreases in this network as a whole, associated with TMS-induced attentional bias (Ricci et al. 2012).

Furthermore, recent TMS/fMRI studies showed directional influences of right parietal activity on regions in other networks, like the ventral attention network and fusiform cortex (Leitão et al. 2015), and even frontal cortices, possibly in relation to post-decisional processes or monitoring in the context of a signal detection task (Leitão et al. 2017). These recent examples demonstrate how simultaneous TMS/fMRI continues to provide valuable insights into the neural mechanisms underlying TMS effects on not only motor and perceptual systems but also higher-order cognition such as attention and even memory (Hawco et al. 2017). Collectively, these findings indicate that TMS-induced neural activity is particularly likely to spread to nodes of a (currently active) functional network and that activity does not necessarily spread to regions that are only anatomically connected to the target site.

14.3.3.4 TMS Network Effects Are Functionally Relevant

The demonstration of remote neural effects of TMS raises the question of whether (and to what extent) these indirect remote effects are also relevant, and functionally related, to the TMS-induced behavioural changes. In other words, are reported

behavioural effects of TMS solely attributable to TMS-induced neural activity changes at that target site, or might these behavioural effects relate to a widely distributed network effect? Frontal eye fields (FEF) are the frontal node of the frontoparietal attention network discussed above. Heinen et al. (2011) stimulated right FEF with TMS, in the MR scanner, while participants viewed both face and motion stimuli. When face stimuli were attended, the TMS pulses induced BOLD increases in the fusiform face area. When motion stimuli were attended, the TMS pulses induced BOLD increases in motion area MT+. Here, the FEF-TMS effects on performance correlated with the BOLD changes in local region FEF but also the BOLD changes in remote region MT+.

Ruff et al. (2006, 2008, 2009) also applied TMS to right FEF simultaneously with fMRI. They revealed remote BOLD effects in two bilateral sets of occipital brain regions within retinotopic visual areas V1–V4. Right FEF-TMS led to BOLD increases for peripheral visual field representations, but BOLD decreases for the central visual field. If these remote BOLD effects of TMS were functionally relevant, then assuming that higher BOLD signal equals higher contrast sensitivity, the authors hypothesised that FEF-TMS should enhance peripheral, relative to central, vision. Interestingly, these behavioural predictions were later confirmed by the authors in a psychophysical study outside the MR scanner. This suggests that, indeed, remote effects of TMS can be functionally relevant.

Does that mean that the local and remote BOLD modulations by TMS, discussed above, reflect the operation of, and TMS-impairment of, a functional network? Sack et al. (2007) applied TMS over right and left parietal cortex during whole-brain BOLD fMRI of spatial cognition performance. The authors found that right, but not left, parietal TMS (1) behaviourally impaired spatial cognition and (2) induced BOLD changes across a right-hemispheric network of frontoparietal regions, including right superior parietal lobule (SPL) and ipsilateral middle frontal gyrus (MFG), in specifically the spatial cognition and not a control task. Only SPL had been stimulated by TMS, so it is accurate to state that parietal TMS impaired spatial cognition performance. But when correlating the TMS-induced behavioural impairment (increases in reaction times) to the TMS-induced changes in BOLD activity, the correlations were in fact equally high for the stimulated SPL and the remote MFG. This strongly suggests that the behavioural deficits are not exclusively caused by neural activity changes at the site of stimulation but rather caused by neural network effects. If so, TMS to the other regions in the network could have equivalent effects on behaviour, which can be systematically tested in follow-up experiments (e.g. de Graaf et al. 2009).

Based on such insights, one might turn this logic around, stimulating cortical areas connected to remote areas precisely *because* those remote regions are hypothesised to be causally relevant, and not directly targetable by TMS, for instance, because they are subcortical. In a breakthrough demonstration, Walsh and Pascual-Leone (2003) stimulated the lateral parietal cortex, based on evidence that hippocampus may interact intensively with the lateral parietal cortex in a wide cortico-hippocampal network to support associative memory function. However, the causal relevance of cortico-hippocampal interactivity had not directly been

demonstrated. Walsh and Pascual-Leone (2003) showed that lateral parietal modulation by TMS increased functional connectivity in this network and moreover led to improvements in associative memory. And in fact, when it comes to the dominant current clinical application of TMS, left frontal TMS to treat depression, at least some of the beneficial effects may arise from the remote modulation of limbic system activity through its connections to the stimulated frontal cortex (Fitzgerald et al. 2007).

14.4 New Developments

Out of the various interesting recent developments, we would like to briefly discuss two (1) closed-loop neuroscience and (2) TMS-fMRI-EEG multimodal implementations. As fMRI developed to become more widespread, EEG itself experienced a resurgence, particularly when it comes to the study of neuronal oscillations and their role in perception, cognition and behaviour. Although we focused on the combination of TMS-fMRI in this chapter and discussed its value at length, these last two new developments involve brain stimulation applied simultaneously with EEG.

14.4.1 Closed-Loop Neuroscience

Closed-loop neuroscience is an umbrella term that refers to a range of paradigmatic approaches (Zrenner et al. 2016). In the current context, the notion of closed-loop brain stimulation and brain imaging is most important. Brain stimulation changes the state of the brain, but its effects or its efficacy, have in turn been shown to depend on brain state at the time of stimulation. We have discussed this above for TMS-fMRI combinations, but it holds true for EEG as well. For instance, the power (Romei et al. 2008a, b) and phase (Dugué et al. 2011) of ongoing alpha oscillations predict the cortical response to occipital TMS pulses, as indexed by perception of TMS-induced visual experiences called phosphenes. This role of oscillatory phase seems to hold even when it is experimentally controlled by simultaneously applied transcranial alternating current stimulation (tACS). Schilberg et al. (2018) demonstrated this in the motor cortex. This relevance of oscillatory phase might be exploited, for instance, by controlling it with tACS (e.g. Graaf et al. 2020). Goldsworthy et al. (2016) found that the lasting effects of repetitive TMS (continuous theta burst stimulation) depended on the phase of concurrent tACS at which TMS bursts were administered. But oscillatory phase, or any other observable brain state index, can also be measured and analysed in real time to guide brain stimulation. The idea of closed-loop stimulation is that functionally relevant brain state indices are monitored and analysed in real time, and brain stimulation (i.e. TMS pulses) is applied at state-dependent, experimentally controlled, moments in time. Indeed, Zrenner et al. (2018) recently showed that a real-time EEG-TMS set-up enabled stronger lasting effects of a repetitive TMS protocol on motor excitability,

by the repeated administration of bursts of pulses at certain phases of the ongoing sensorimotor mu rhythm.

14.4.2 Simultaneous TMS-fMRI-EEG

In this chapter, we discussed at length how TMS and fMRI can be combined in different ways and how specifically the simultaneous combination of TMS/fMRI allows a very immediate evaluation of how TMS affects the brain locally and remotely by stimulating a specific brain region and simultaneously monitoring whole-brain network changes in activity. But we also showed how such effects were state and task dependent. This is why the closed-loop approach seems promising.

However, simultaneous TMS-fMRI studies ignore the temporal dynamics and rhythmic oscillations of brain activity reflecting (spontaneous) fluctuations between low and high excitable states during which incoming stimuli are less or more efficiently processed and neural signals are less or more propagated within brain networks. In order to understand and unravel these dynamics in detail, the simultaneous combination of EEG with fMRI and TMS makes an invaluable contribution. The core approach is to use EEG to track ongoing oscillatory activity, indexing brain state at the time of a TMS pulse. fMRI then measures the brain-wide response to the TMS pulse. We pioneered and successfully implemented this approach methodologically and showed it to be feasible and safe for human research already in 2013 (Peters et al. 2013).

In our most recent publication (Peters et al. 2020), we demonstrated for the first time how this simultaneous TMS-fMRI-EEG set-up can be applied to fundamental questions within cognitive neuroscience by revealing how TMS as a system probe evokes (sub-)cortical network responses depending on EEG-indexed brain state. To this end, we assessed how trial-by-trial pre-TMS EEG alpha and low-beta power fluctuations influenced motor network activations induced by subthreshold triple-pulse TMS to the right dorsal premotor cortex. Strong pre-TMS alpha power resulted in decreased TMS-induced BOLD activations throughout the bilateral cortico-subcortical motor system (including striatum and thalamus), suggesting shunted network connectivity. In contrast to alpha activity, strong pre-TMS beta power did not impede TMS signal propagation but instead tended to facilitate signal propagation in motor circuits. Such facilitatory effects corroborate and extend recent insights in the key role of beta activity in coordinating communication in the human motor system (Peters et al. 2020). This study clearly demonstrates how concurrent TMS-EEG-fMRI allows to non-invasively chart the communication mechanisms within larger, dynamically interacting networks and subsystems in the brain. The here described simultaneous TMS-fMRI-EEG approach provides a versatile framework also for future studies on the propagation of TMS-induced activity in functional cortico-(sub)cortical networks, allowing to test a wide range of theories through flexible adaptation to the oscillatory band or TMS protocol of interest and its applicability to different network nodes with varying functional relevance. This ability of concurrent TMS-fMRI-EEG also links to the above-described new

development in the field of closed-loop neuroscience as it holds the potential to inform and evaluate future EEG-triggered TMS applications aiming to apply TMS at predefined oscillatory brain states that either will or will not lead to specific remote brain activations by either facilitating or shunting signal propagation from the cortical TMS stimulation site.

14.5 Conclusions

The combination of brain stimulation with brain imaging offers unique experimental possibilities for understanding the functional architecture of the healthy and diseased human brain. Brain imaging before brain stimulation is useful for the identification (in individual participants or patients) of an exact NIBS target site. Brain imaging after brain stimulation is useful for identifying the spatial pattern and persistency of NIBS-induced neural activity changes that last beyond the stimulation itself (NIBS after-effects). Finally, brain imaging during brain stimulation allows one to stimulate a specific brain region while simultaneously monitoring whole-brain changes in brain activity and behaviour, allowing causal brain-behaviour inferences across the entire brain. Simultaneous, or more precisely interleaved, TMS/fMRI studies appear to converge on the following conclusions: (1) focal TMS applied to a brain region has not only local but rather network effects, (2) these network effects of TMS are state and task dependent and (3) these network effects are functionally relevant.

These results seem to have troubling implications for the interpretation of purely behavioural TMS (without concurrent imaging) studies. After all, without, and sometimes even with, concurrent imaging, we cannot determine whether behavioural effects of TMS are due to its local neural effects and the local *and* remote neural effects which reflect modulation of a functional network, or whether the behavioural effects are even attributable to the remote neural effects *rather than* effects in the stimulated region? For the latter, there is currently no conclusive evidence, and as discussed elsewhere (Sack 2010), brain stimulation experiments remain highly valuable also without neuroimaging. But these questions and insights prompt us to move away from modular views of brain function and TMS disruption thereof, forcing us to consider a new conceptualisation that involves functional interactions between various remote, connected brain regions, together constituting networks of integrated, functionally relevant activity. Of course, a very positive consequence of this body of work is that TMS imaging can be used to investigate and reveal exactly these mechanisms, to show how interactions within and between brain networks may support perception and cognition. Simultaneous TMS imaging substantially adds information and insight to purely behavioural TMS experiments, without taking away any of the original relevance of such work. In fact, this enterprise can only be enriched by work employing further complementary techniques in combination with brain stimulation, for instance, MR spectroscopy (Stagg et al. 2009), functional near-infrared spectroscopy (Hada et al. 2006; Kozel et al. 2009; Mochizuki et al. 2006) and diffusion-weighted imaging (DWI) of white matter bundles (Boorman et al. 2007; Kloppel et al. 2008).

To complete this viewpoint, and support the system-level investigations outlined above, investigations at a more fine-grained level will likely be required as well. This is achieved most informatively through invasive animal research (e.g. see Funke and Benali 2010), helping us understand the neurophysiological mechanisms underlying the local and remote effects observed in human research. Work with cats (Allen et al. 2007; Aydin-Abidin et al. 2006; de Labra et al. 2007; Moliadze et al. 2005, 2003; Pasley et al. 2009; Valero-Cabre et al. 2007, 2005), rodents (Aydin-Abidin et al. 2008; Trippe et al. 2009) and monkeys (Ohnishi et al. 2004; Hayashi et al. 2004) has already delivered important contributions in this regard, although not yet into the remote effects of TMS. Also, considering the intrinsic intricacies of neural circuits, a multimodal approach with complementary methods (Logothetis 2008) will likely be required to achieve a cross-level understanding of TMS effects in the brain.

The role and potential of TMS in research and therapeutic settings have, thanks in part to the advances described here, not only been validated but actually increased over the years. With the multimodal research facilities now in place in several labs over the world and the analysis on several levels from animal work to human whole-brain analysis to computational modelling, we are starting to improve our understanding of TMS-induced changes in the brain and behaviour. As such, TMS has begun to provide unique insights into the causal relations and interactions within and between system-level networks in the human brain, all in vivo and non-invasively. With the introduction of simultaneous TMS-fMRI-EEG, a new chapter in the book of multimodal imaging has been opened. The new frontier in non-invasive neuroscience research is to integrate the connectome (brain networks) with the 'dynome' (brain dynamics) in order to unravel the mechanisms of communication within larger, dynamically interacting networks and subsystems in the brain and to understand how *(spatial) network and (temporal) oscillation mechanisms interact.* Ultimately, we remain confident that better understanding of the neural effects of TMS will lead to more informed clinical applications. Further effective and well-controlled therapeutic interventions may thus become possible in the near future.

References

Ahdab R, Ayache SS, Brugieres P et al (2010) Comparison of "standard" and "navigated" procedures of TMS coil positioning over motor, premotor and prefrontal targets in patients with chronic pain and depression. Neurophysiol Clin 40:27–36

Allen EA, Pasley BN, Duong T et al (2007) Transcranial magnetic stimulation elicits coupled neural and hemodynamic consequences. Science 317:1918–1921

Andoh J, Artiges E, Pallier C et al (2006) Modulation of language areas with functional mr image-guided magnetic stimulation. NeuroImage 29:619–627

Aydin-Abidin S, Moliadze V, Eysel UT et al (2006) Effects of repetitive TMS on visually evoked potentials and EEG in the anaesthetized cat: dependence on stimulus frequency and train duration. J Physiol 574:443–455

Aydin-Abidin S, Trippe J, Funke K et al (2008) High- and low-frequency repetitive transcranial magnetic stimulation differentially activates c-fos and zif268 protein expression in the rat brain. Exp Brain Res 188:249–261

Baudewig J, Paulus W, Frahm J (2000) Artifacts caused by transcranial magnetic stimulation coils and eeg electrodes in t(2)*-weighted echo-planar imaging. Magn Reson Imaging 18:479–484
Baudewig J, Siebner HR, Bestmann S et al (2001) Functional MRI of cortical activations induced by transcranial magnetic stimulation (TMS). Neuroreport 12:3543–3548
Beckers G, Homberg V (1992) Cerebral visual motion blindness: Transitory akinetopsia induced by transcranial magnetic stimulation of human area v5. Proc Biol Sci 249:173–178
Bestmann S, Baudewig J, Frahm J (2003a) On the synchronization of transcranial magnetic stimulation and functional echo-planar imaging. J Magn Reson Imaging 17:309–316
Bestmann S, Baudewig J, Siebner HR et al (2003b) Subthreshold high-frequency TMS of human primary motor cortex modulates interconnected frontal motor areas as detected by interleaved fMRI-TMS. NeuroImage 20:1685–1696
Bestmann S, Baudewig J, Siebner HR et al (2004) Functional MRI of the immediate impact of transcranial magnetic stimulation on cortical and subcortical motor circuits. Eur J Neurosci 19:1950–1962
Bestmann S, Baudewig J, Siebner HR et al (2005) Bold MRI responses to repetitive TMS over human dorsal premotor cortex. NeuroImage 28:22–29
Bestmann S, Ruff CC, Blakemore C, Driver J, Thilo KV (2007) Spatial attention changes excitability of human visual cortex to direct stimulation. Curr Biol 17(2):134–139. https://doi.org/10.1016/j.cub.2006.11.063
Bestmann S, Swayne O, Blankenburg F et al (2008) Dorsal premotor cortex exerts state-dependent causal influences on activity in contralateral primary motor and dorsal premotor cortex. Cereb Cortex 18:1281–1291
Blankenburg F, Ruff CC, Bestmann S et al (2008) Interhemispheric effect of parietal TMS on somatosensory response confirmed directly with concurrent tms-fmri. J Neurosci 28:13202–13208
Bohning DE, Shastri A, McConnell KA et al (1999) A combined tms/fmri study of intensity-dependent TMS over motor cortex. Biol Psychiatry 45:385–394
Bohning DE, Shastri A, McGavin L et al (2000a) Motor cortex brain activity induced by 1-hz transcranial magnetic stimulation is similar in location and level to that for volitional movement. Investig Radiol 35:676–683
Bohning DE, Shastri A, Wassermann EM et al (2000b) Bold-f MRI response to single-pulse transcranial magnetic stimulation (TMS). J Magn Reson Imaging 11:569–574
Boorman ED, O'Shea J, Sebastian C et al (2007) Individual differences in white-matter microstructure reflect variation in functional connectivity during choice. Curr Biol 17:1426–1431
Brighina F, Bisiach E, Oliveri M et al (2003) 1 hz repetitive transcranial magnetic stimulation of the unaffected hemisphere ameliorates contralesional visuospatial neglect in humans. Neurosci Lett 336:131–133
Bungert A, Chambers CD, Long E, Evans CJ (2012a) On the importance of specialized radiofrequency filtering for concurrent TMS/MRI. J Neurosci Methods 210(2):202–205. https://doi.org/10.1016/j.jneumeth.2012.07.023
Bungert A, Chambers CD, Phillips M, Evans CJ (2012b) Reducing image artefacts in concurrent TMS/fMRI by passive shimming. NeuroImage 59(3):2167–2174. https://doi.org/10.1016/j.neuroimage.2011.10.013
Burt T, Lisanby SH, Sackeim HA (2002) Neuropsychiatric applications of transcranial magnetic stimulation: a meta analysis. Int J Neuropsychopharmacol 5:73–103
Camprodon JA, Martinez-Raga J, Alonso-Alonso M et al (2007) One session of high frequency repetitive transcranial magnetic stimulation (rTMS) to the right prefrontal cortex transiently reduces cocaine craving. Drug Alcohol Depend 86:91–94
Caparelli EC, Backus W, Telang F, Wang G-J, Maloney T, Goldstein RZ et al (2010) Simultaneous TMS-fMRI of the visual cortex reveals functional network, even in absence of phosphene sensation. Open Neuroimaging J 4(1):100–110. https://doi.org/10.2174/1874440001004010100
Cardenas-Morales L, Gron G, Kammer T (2011) Exploring the after-effects of theta burst magnetic stimulation on the human motor cortex: a functional imaging study. Hum Brain Mapp 32:1948–1960

Cazzoli D, Muri RM, Hess CW et al (2010) Treatment of hemispatial neglect by means of rTMS–a review. Restor Neurol Neurosci 28:499–510

Chechlacz M, Humphreys GW, Sotiropoulos SN, Kennard C, Cazzoli D (2015) Structural organization of the corpus callosum predicts attentional shifts after continuous theta burst stimulation. J Neurosci *35*(46):15353–15368

Chibbaro G, Daniele M, Alagona G et al (2005) Repetitive transcranial magnetic stimulation in schizophrenic patients reporting auditory hallucinations. Neurosci Lett 383:54–57

d'Alfonso AA, van Honk J, Schutter DJ et al (2002) Spatial and temporal characteristics of visual motion perception involving v5 visual cortex. Neurol Res 24:266–270

Dambeck N, Sparing R, Meister IG, Wienemann M (2006) Interhemispheric imbalance during visuospatial attention investigated by unilateral and bilateral TMS over human parietal cortices. Brain Res 1072(1):194–199

de Graaf TA, Jacobs C, Roebroeck A et al (2009) Fmri effective connectivity and TMS chronometry: complementary accounts of causality in the visuospatial judgment network. PLoS One 4:e8307

de Graaf TA, Koivisto M, Jacobs C, Sack AT (2014) The chronometry of visual perception: review of occipital TMS masking studies. Neurosci Biobehav Rev 45:295–304

de Labra C, Rivadulla C, Grieve K et al (2007) Changes in visual responses in the feline dLGN: selective thalamic suppression induced by transcranial magnetic stimulation of v1. Cereb Cortex 17:1376–1385

De Ridder D, Vanneste S, Kovacs S et al (2011) Transcranial magnetic stimulation and extradural electrodes implanted on secondary auditory cortex for tinnitus suppression. J Neurosurg 114:903–911

Denslow S, Lomarev M, George MS et al (2005) Cortical and subcortical brain effects of transcranial magnetic stimulation (TMS)-induced movement: An interleaved tms/functional magnetic resonance imaging study. Biol Psychiatry 57:752–760

Di Lazzaro V (2008) The physiological basis of the effects of intermittent theta burst stimulation of the human motor cortex. J Physiol 586:3871–3871

Duecker F, Formisano E, Sack AT (2013) Hemispheric differences in the voluntary control of spatial attention: direct evidence for a right-hemispheric dominance within frontal cortex. J Cogn Neurosci 25(8):1332–1342. https://doi.org/10.1162/jocn_a_00402

Duecker F, Frost MA, Graaf TA, Graewe B, Jacobs C, Goebel R, Sack AT (2014) The cortex-based alignment approach to TMS coil positioning. J Cogn Neurosci 26(10):2321–2329. https://doi.org/10.1162/jocn_a_00635

Dugué L, Marque P, VanRullen R (2011) The phase of ongoing oscillations mediates the causal relation between brain excitation and visual perception. J Neurosci 31(33):11889–11893

Eichhammer P, Johann M, Kharraz A et al (2003) High-frequency repetitive transcranial magnetic stimulation decreases cigarette smoking. J Clin Psychiatry 64:951–953

Engelen T, Zhan M, Sack AT, de Gelder B (2018) Dynamic interactions between emotion perception and action preparation for reacting to social threat: a combined cTBS-fMRI study. eNeuro 5(3):17. https://doi.org/10.1523/ENEURO.0408-17.2018

Esser SK, Hill SL, Tononi G (2005) Modeling the effects of transcranial magnetic stimulation on cortical circuits. J Neurophysiol 94:622–639

Feredoes E, Tononi G, Postle BR (2007) The neural bases of the short-term storage of verbal information are anatomically variable across individuals. J Neurosci 27:11003–11008

Fitzgerald PB, Sritharan A, Daskalakis ZJ et al (2007) A functional magnetic resonance imaging study of the effects of low frequency right prefrontal transcranial magnetic stimulation in depression. J Clin Psychopharmacol 27:488–492

Funke K, Benali A (2010) Cortical cellular actions of transcranial magnetic stimulation. Restor Neurol Neurosci 28:399–417

George MS, Wassermann EM, Williams WA et al (1995) Daily repetitive transcranial magnetic stimulation (rTMS) improves mood in depression. Neuroreport 6:1853–1856

Goldsworthy M, Vallence A, Yang R, Pitcher J, Ridding M (2016) Combined transcranial alternating current stimulation and continuous theta burst stimulation: a novel approach for neuroplasticity induction. Eur J Neurosci 43(4):572 579

Graaf TA, Thomson A, Janssens S, Bree S, Oever S, Sack AT (2020) Does alpha phase modulate visual target detection? Three experiments with tACS phase-based stimulus presentation. Eur J Neurosci 2020:1–15

Gross M, Nakamura L, Pascual-Leone A et al (2007) Has repetitive transcranial magnetic stimulation (rTMS) treatment for depression improved? A systematic review and meta-analysis comparing the recent vs. The earlier rTMS studies. Acta Psychiatr Scand 116:165–173

Hada Y, Abo M, Kaminaga T et al (2006) Detection of cerebral blood flow changes during repetitive transcranial magnetic stimulation by recording hemoglobin in the brain cortex, just beneath the stimulation coil, with near-infrared spectroscopy. NeuroImage 32:1226–1230

Hanakawa T, Mima T, Matsumoto R et al (2009) Stimulus-response profile during single-pulse transcranial magnetic stimulation to the primary motor cortex. Cereb Cortex 19:2605–2615

Haraldsson HM, Ferrarelli F, Kalin NH et al (2004) Transcranial magnetic stimulation in the investigation and treatment of schizophrenia: a review. Schizophr Res 71:1–16

Hawco C, Armony JL, Daskalakis ZJ, Berlim MT, Chakravarty MM, Pike GB, Lepage M (2017) Differing time of onset of concurrent TMS-fMRI during associative memory encoding: a measure of dynamic connectivity. Front Hum Neurosci 11:404. https://doi.org/10.3389/fnhum.2017.00404

Hayashi T, Ohnishi T, Okabe S et al (2004) Long-term effect of motor cortical repetitive transcranial magnetic stimulation. Ann Neurol 56:77–85

Heinen K, Ruff CC, Bjoertomt O, Schenkluhn B, Bestmann S, Blankenburg F et al (2011) Concurrent TMS-fMRI reveals dynamic interhemispheric influences of the right parietal cortex during exogenously cued visuospatial attention. Eur J Neurosci 33(5):991–1000. https://doi.org/10.1111/j.1460-9568.2010.07580.x

Herbsman T, Avery D, Ramsey D et al (2009) More lateral and anterior prefrontal coil location is associated with better repetitive transcranial magnetic stimulation antidepressant response. Biol Psychiatry 66:509–515

Herwig U, Fallgatter AJ, Hoppner J et al (2007) Antidepressant effects of augmentative transcranial magnetic stimulation: Randomised multicentre trial. Br J Psychiatry 191:441–448

Hilgetag CC, Théoret H, Pascual-Leone A (2001) Enhanced visual spatial attention ipsilateral to rTMS-induced "virtual lesions" of human parietal cortex. Nat Neurosci. https://doi.org/10.1038/nn0901-953

Hoffman RE (2003) Variations on the chemical shift of TMS. J Magn Reson 163:325–331

Hoffman RE, Becker ED (2005) Temperature dependence of the 1h chemical shift of tetramethylsilane in chloroform, methanol, and dimethylsulfoxide. J Magn Reson 176:87–98

Holtzheimer PE, Russo J, Avery DH (2001) A meta-analysis of repetitive transcranial magnetic stimulation in the treatment of depression. Psychopharmacol Bull 35:149–169

Huang Y-Z, Edwards MJ, Rounis E et al (2005) Theta burst stimulation of the human motor cortex. Neuron 45:201–206

Hubl D, Nyffeler T, Wurtz P et al (2008) Time course of blood oxygenation level-dependent signal response after theta burst transcranial magnetic stimulation of the frontal eye field. Neuroscience 151:921–928

Kemna LJ, Gembris D (2003) Repetitive transcranial magnetic stimulation induces different responses in different cortical areas: a functional magnetic resonance study in humans. Neurosci Lett 336:85–88

Khedr EM, Kotb H, Kamel NF et al (2005) Longlasting antalgic effects of daily sessions of repetitive transcranial magnetic stimulation in central and peripheral neuropathic pain. J Neurol Neurosurg Psychiatry 76:833–838

Kimbrell TA, Little JT, Dunn RT et al (1999) Frequency dependence of antidepressant response to left prefrontal repetitive transcranial magnetic stimulation (rTMS) as a function of baseline cerebral glucose metabolism. Biol Psychiatry 46:1603–1613

Kimbrell TA, Ketter TA, George MS et al (2002) Regional cerebral glucose utilization in patients with a range of severities of unipolar depression. Biol Psychiatry 51:237–252

Kloppel S, Baumer T, Kroeger J et al (2008) The cortical motor threshold reflects microstructural properties of cerebral white matter. NeuroImage 40:1782–1791

Koch G, Oliveri M, Cheeran B et al (2008) Hyperexcitability of parietal-motor functional connections in the intact left-hemisphere of patients with neglect. Brain 131:3147–3155
Kozel FA, George MS (2002) Meta-analysis of left prefrontal repetitive transcranial magnetic stimulation (rTMS) to treat depression. J Psychiatr Pract 8:270–275
Kozel FA, Tian F, Dhamne S et al (2009) Using simultaneous repetitive transcranial magnetic stimulation/functional near infrared spectroscopy (rTMS/fNIRS) to measure brain activation and connectivity. NeuroImage 47:1177–1184
Lee SH, Kim W, Chung YC et al (2005) A double blind study showing that two weeks of daily repetitive TMS over the left or right temporoparietal cortex reduces symptoms in patients with schizophrenia who are having treatment-refractory auditory hallucinations. Neurosci Lett 376:177–181
Lefaucheur JP, Drouot X, Nguyen JP (2001) Interventional neurophysiology for pain control: Duration of pain relief following repetitive transcranial magnetic stimulation of the motor cortex. Neurophysiol Clin 31:247–252
Lefaucheur J-P, André-Obadia N, Antal A, Ayache SS, Baeken C, Benninger DH et al (2014) Evidence-based guidelines on the therapeutic use of repetitive transcranial magnetic stimulation (rTMS). Clin Neurophysiol 125(11):2150–2206. https://doi.org/10.1016/j.clinph.2014.05.021
Leitão J, Thielscher A, Tünnerhoff J, Noppeney U (2015) Concurrent TMS-fMRI reveals interactions between dorsal and ventral attentional systems. J Neurosci 35(32):11445–11457. https://doi.org/10.1523/JNEUROSCI.0939-15.2015
Leitão J, Thielscher A, Lee H, Tuennerhoff J, Noppeney U (2017) Transcranial magnetic stimulation of right inferior parietal cortex causally influences prefrontal activation for visual detection. Eur J Neurosci 17:309. https://doi.org/10.1111/ejn.13743
Logothetis NK (2008) What we can do and what we cannot do with fMRI. Nature 453:869–878
Logothetis NK, Augath M, Murayama Y et al (2010) The effects of electrical microstimulation on cortical signal propagation. Nat Neurosci 13:1283–1291
Maeda F, Keenan JP, Tormos JM, Topka H, Pascual-Leone A (2000) Interindividual variability of the modulatory effects of repetitive transcranial magnetic stimulation on cortical excitability. Exp Brain Res 133(4):425–430
Martin JL, Barbanoj MJ, Perez V et al (2003) Transcranial magnetic stimulation for the treatment of obsessive-compulsive disorder. Cochrane Database Syst Rev 3:CD003387
McNamara B, Ray JL, Arthurs OJ et al (2001) Transcranial magnetic stimulation for depression and other psychiatric disorders. Psychol Med 31:1141–1146
Mochizuki H, Ugawa Y, Terao Y et al (2006) Cortical hemoglobin-concentration changes under the coil induced by single-pulse TMS in humans: a simultaneous recording with near-infrared spectroscopy. Exp Brain Res 169:302–310
Moliadze V, Zhao Y, Eysel U et al (2003) Effect of transcranial magnetic stimulation on single-unit activity in the cat primary visual cortex. J Physiol 553:665–679
Moliadze V, Giannikopoulos D, Eysel UT et al (2005) Paired-pulse transcranial magnetic stimulation protocol applied to visual cortex of anaesthetized cat: effects on visually evoked single-unit activity. J Physiol 566:955–965
Navarro de Lara LI, Tik M, Woletz M, Frass-Kriegl R, Moser E, Laistler E, Windischberger C (2017) High-sensitivity TMS/fMRI of the human motor cortex using a dedicated multichannel MR coil. NeuroImage 150:262–269. https://doi.org/10.1016/j.neuroimage.2017.02.062
Nyffeler T, Cazzoli D, Hess CW et al (2009) One session of repeated parietal theta burst stimulation trains induces long-lasting improvement of visual neglect. Stroke 40:2791–2796
O'Reardon JP, Solvason HB, Janicak PG et al (2007) Efficacy and safety of transcranial magnetic stimulation in the acute treatment of major depression: a multisite randomized controlled trial. Biol Psychiatry 62:1208–1216
O'Shea J, Sebastian C, Boorman ED et al (2007) Functional specificity of human premotor-motor cortical interactions during action selection. Eur J Neurosci 26:2085–2095
Ohnishi T, Hayashi T, Okabe S et al (2004) Endogenous dopamine release induced by repetitive transcranial magnetic stimulation over the primary motor cortex: an [11c]raclopride positron emission tomography study in anesthetized macaque monkeys. Biol Psychiatry 55:484–489

Oliveri M, Rossini PM, Traversa R et al (1999) Left frontal transcranial magnetic stimulation reduces contralesional extinction in patients with unilateral right brain damage. Brain 122(Pt 9):1731–1739

Oliveri M, Caltagirone C, Filippi MM et al (2000a) Paired transcranial magnetic stimulation protocols reveal a pattern of inhibition and facilitation in the human parietal cortex. J Physiol 529(Pt 2):461–468

Oliveri M, Rossini PM, Filippi MM et al (2000b) Time-dependent activation of parieto-frontal networks for directing attention to tactile space. A study with paired transcranial magnetic stimulation pulses in right-brain-damaged patients with extinction. Brain 123(Pt 9):1939–1947

Oliveri M, Bisiach E, Brighina F et al (2001) rTMS of the unaffected hemisphere transiently reduces contralesional visuospatial hemineglect. Neurology 57:1338–1340

Pascual-Leone A, Rubio B, Pallardo F et al (1996) Rapid-rate transcranial magnetic stimulation of left dorsolateral prefrontal cortex in drug-resistant depression. Lancet 348:233–237

Pasley BN, Allen EA, Freeman RD (2009) State-dependent variability of neuronal responses to transcranial magnetic stimulation of the visual cortex. Neuron 62:291–303

Paus T, Barrett J (2004) Transcranial magnetic stimulation (TMS) of the human frontal cortex: implications for repetitive TMS treatment of depression. J Psychiatry Neurosci 29:268–279

Peters JC, Reithler J, Schuhmann T, de Graaf TA, Uludag K, Goebel R, Sack AT (2013) On the feasibility of concurrent human TMS-EEG-fMRI measurements. J Neurophysiol 109(4):1214–1227

Peters JC, Reithler J, de Graaf TA, Schuhmann T, Goebel R, Sack AT (2020) Concurrent human TMS-EEG-fMRI enables monitoring of oscillatory brain state-dependent gating of cortico-subcortical network activity. Nat Commun Biol 3(1):40

Pogarell O, Koch W, Popperl G et al (2006) Striatal dopamine release after prefrontal repetitive transcranial magnetic stimulation in major depression: preliminary results of a dynamic [123i] ibzm spect study. J Psychiatr Res 40:307–314

Pogarell O, Koch W, Popperl G et al (2007) Acute prefrontal rTMS increases striatal dopamine to a similar degree as d-amphetamine. Psychiatry Res 156:251–255

Reithler J, Peters JC, Sack AT (2011) Multimodal transcranial magnetic stimulation: using concurrent neuroimaging to reveal the neural network dynamics of noninvasive brain stimulation. Prog Neurobiol 94:149–165

Ricci R, Salatino A, Li X, Funk AP, Logan SL, Mu Q et al (2012) Imaging the neural mechanisms of TMS neglect-like bias in healthy volunteers with the interleaved TMS/fMRI technique: preliminary evidence. Front Hum Neurosci 6:326. https://doi.org/10.3389/fnhum.2012.00326

Ridding MC, Rothwell JC (2007) Is there a future for therapeutic use of transcranial magnetic stimulation? Nat Rev Neurosci 8:559–567

Romei V, Brodbeck V, Michel C, Amedi A, Pascual-Leone A, Thut G (2008a) Spontaneous fluctuations in posterior alpha-band EEG activity reflect variability in excitability of human visual areas. Cereb Cortex 18(9):2010–2018

Romei V, Rihs T, Brodbeck V, Thut G (2008b) Resting electroencephalogram alpha-power over posterior sites indexes baseline visual cortex excitability. Neuroreport 19(2):203–208

Rossi S, Hallett M, Rossini PM et al (2009) Safety, ethical considerations, and application guidelines for the use of transcranial magnetic stimulation in clinical practice and research. Clin Neurophysiol 120:2008–2039

Ruff CC, Blankenburg F, Bjoertomt O et al (2006) Concurrent TMS-fMRI and psychophysics reveal frontal influences on human retinotopic visual cortex. Curr Biol 16:1479–1488

Ruff CC, Bestmann S, Blankenburg F et al (2008) Distinct causal influences of parietal versus frontal areas on human visual cortex: evidence from concurrent tms-fmri. Cereb Cortex 18:817–827

Ruff CC, Driver J, Bestmann S (2009) Combining TMS and fMRI: from 'virtual lesions' to functional-network accounts of cognition. Cortex 45:1043–1049

Rushworth MF, Hadland KA, Paus T et al (2002) Role of the human medial frontal cortex in task switching: a combined FMRI and TMS study. J Neurophysiol 87:2577–2592

Sachdev PS, McBride R, Loo CK et al (2001) Right versus left prefrontal transcranial magnetic stimulation for obsessive-compulsive disorder: a preliminary investigation. J Clin Psychiatry 62:981–984

Sack AT (2006) Transcranial magnetic stimulation, causal structure-function mapping and networks of functional relevance. Curr Opin Neurobiol 16:593–599

Sack AT (2010) Does TMS need functional imaging? Cortex 46:131–133

Sack AT, Kohler A, Linden DE et al (2006) The temporal characteristics of motion processing in hmt/v5+: combining FMRI and neuronavigated TMS. NeuroImage 29:1326–1335

Sack AT, Kohler A, Bestmann S et al (2007) Imaging the brain activity changes underlying impaired visuospatial judgments: Simultaneous FMRI, TMS, and behavioral studies. Cereb Cortex 17:2841–2852

Sack AT, Cohen Kadosh R, Schuhmann T et al (2009) Optimizing functional accuracy of TMS in cognitive studies: a comparison of methods. J Cogn Neurosci 21:207–221

Schilberg L, Engelen T, Oever S, Schuhmann T, de Gelder B, de Graaf TA, Sack AT (2018) Phase of beta-frequency tACS over primary motor cortex modulates corticospinal excitability. Cortex 103:142–152

Schonfeldt-Lecuona C, Cardenas-Morales L, Freudenmann RW et al (2010) Transcranial magnetic stimulation in depression–lessons from the multicentre trials. Restor Neurol Neurosci 28:569–576

Schuhmann T, Schiller NO, Goebel R, Sack AT (2009) The temporal characteristics of functional activation in Broca's area during overt picture naming. Cortex 45(9):1111–1116

Schuhmann T, Schiller NO, Goebel R, Sack AT (2012) Speaking of which: dissecting the neurocognitive network of language production in picture naming. Cereb Cortex 22(3):701–709

Shastri A, George MS, Bohning DE (1999) Performance of a system for interleaving transcranial magnetic stimulation with steady-state magnetic resonance imaging. Electroencephalogr Clin Neurophysiol Suppl 51:55–64

Shindo K, Sugiyama K, Huabao L et al (2006) Long-term effect of low-frequency repetitive transcranial magnetic stimulation over the unaffected posterior parietal cortex in patients with unilateral spatial neglect. J Rehabil Med 38:65–67

Song W, Du B, Xu Q et al (2009) Low-frequency transcranial magnetic stimulation for visual spatial neglect: a pilot study. J Rehabil Med 41:162–165

Sparing R, Buelte D, Meister IG et al (2008) Transcranial magnetic stimulation and the challenge of coil placement: a comparison of conventional and stereotaxic neuronavigational strategies. Hum Brain Mapp 29:82–96

Speer AM, Kimbrell TA, Wassermann EM et al (2000) Opposite effects of high and low frequency rTMS on regional brain activity in depressed patients. Biol Psychiatry 48:1133–1141

Speer AM, Benson BE, Kimbrell TK et al (2009) Opposite effects of high and low frequency RTMS on mood in depressed patients: relationship to baseline cerebral activity on pet. J Affect Disord 115:386–394

Stagg CJ, Wylezinska M, Matthews PM et al (2009) Neurochemical effects of theta burst stimulation as assessed by magnetic resonance spectroscopy. J Neurophysiol 101:2872–2877

Teneback CC, Nahas Z, Speer AM et al (1999) Changes in prefrontal cortex and paralimbic activity in depression following two weeks of daily left prefrontal TMS. J Neuropsychiatry Clin Neurosci 11:426–435

Thiel A, Haupt WF, Habedank B et al (2005) Neuroimaging-guided rTMS of the left inferior frontal gyrus interferes with repetition priming. NeuroImage 25:815–823

Trippe J, Mix A, Aydin-Abidin S et al (2009) Theta burst and conventional low-frequency RTMS differentially affect GABAergic neurotransmission in the rat cortex. Exp Brain Res 199:411–421

Valero-Cabre A, Payne BR, Rushmore J et al (2005) Impact of repetitive transcranial magnetic stimulation of the parietal cortex on metabolic brain activity: a 14c-2dg tracing study in the cat. Exp Brain Res 163:1–12

Valero-Cabre A, Payne BR, Pascual-Leone A (2007) Opposite impact on 14c-2-deoxyglucose brain metabolism following patterns of high and low frequency repetitive transcranial magnetic stimulation in the posterior parietal cortex. Exp Brain Res 176:603–615

Walsh V, Pascual-Leone A (2003) Transcranial magnetic stimulation: a neurochronometrics of mind. MIT Press, Cambridge

Weiskopf N, Josephs O, Ruff CC et al (2009) Image artifacts in concurrent transcranial magnetic stimulation (TMS) and fmri caused by leakage currents: modeling and compensation. J Magn Reson Imaging 29:1211–1217

Zrenner C, Belardinelli P, Müller-Dahlhaus F, Ziemann U (2016) Closed-Loop Neuroscience and Non-Invasive Brain Stimulation: A Tale of Two Loops. Front Cell Neurosci 7;10:92. https://doi.org/10.3389/fncel.2016.00092. PMID: 27092055; PMCID: PMC4823269

Zrenner C, Desideri D, Belardinelli P, Ziemann U (2018) Real-time EEG-defined excitability states determine efficacy of TMS-induced plasticity in human motor cortex. Brain Stimul 11(2):374–389. https://doi.org/10.1016/j.brs.2017.11.016. Epub 2017 Nov 24. PMID: 29191438.

Part III

Applications of EEG-fMRI

Brain Rhythms

15

Rene Scheeringa and Helmut Laufs

15.1 Multimodal Studies of Brain Rhythms

Ever since the very first measurements by Hans Berger, we know that the brain produces rhythmic electrophysiological activity that can be measured by EEG (Berger 1929). Since then, many different rhythmic phenomena have been studied not only by EEG but also by MEG and invasive intracranial recordings in patient populations and animals. This has yielded a wide body of knowledge on which types of rhythmic activity can be recorded, under which circumstances they occur, how they can be modulated by task demands, how they relate to clinical conditions and what their putative functional role is (Buzsáki 2006; Lopes da Silva 2013). The electrophysiological recording techniques are however in one way or another all limited in their spatial resolution and coverage. Microelectrodes can directly measure electrophysiological activity with unrivalled resolution in animals and patient populations but are highly invasive and are in practice, limited to only a few regions. Another invasive technique, ECoG can measure electrophysiological activity in up to a roughly a hemisphere but is limited in coverage to the cortical surface and has a resolution in the order of cortical macro-columns (Scheeringa and Fries 2017). Noninvasive recordings like EEG and MEG measure

R. Scheeringa (✉)
Erwin L. Hahn Institute for Magnetic Resonance Imaging, UNESCO-Weltkulturerbe Zollverein, University Duisburg-Essen, Essen, Germany

Department of Neurology and Brain Imaging Center, Johann Wolfgang Goethe-Universität, Frankfurt am Main, Germany

Radboud University Nijmegen, Donders Institute for Brain, Cognition and Behaviour, Donders Centre for Cognitive Neuroimaging, Nijmegen, The Netherlands
e-mail: rene.scheeringa@donders.ru.nl

H. Laufs
Department of Neurology, Christian-Albrechts-University Kiel, Kiel, Germany
e-mail: helmut@laufs.com; h.laufs@neurologie.uni-kiel.de

C. Mulert, L. Lemieux (eds.), *EEG - fMRI*,
https://doi.org/10.1007/978-3-031-07121-8_15

population-level neural activity at scalp level and can in principle cover close to the entire brain but are in general limited to a resolution of roughly an entire cortical region, while its sensitivity for detecting signals is not uniformly distributed over the cortex. Furthermore, it requires rhythmic synchrony over a larger piece of the cortex, typically fully synchronous activity of ~10,000–50,000 neurons is thought to be needed to yield a detectable EEG response (Murakami and Okada 2006). In terms of coverage and resolution, fMRI is much less restricted. Recent advancements in high resolution now make it possible to acquire data at submillimetre resolution from the entire brain in a few seconds (Polimeni et al. 2010; Zahneisen et al. 2015). It measures neural activity indirectly through the haemodynamic response that follows it. As a consequence, its temporal resolution is in the order of seconds; it does not allow us to measure the vast majority of rhythmic neural activity. Combining the measurement of EEG and fMRI therefore holds the promise to study neural activity related to brain rhythms throughout the entire brain at in principle up to submillimetre resolution, while preserving the millisecond resolution necessary to measure those brain rhythms with EEG. In this chapter, we discuss how these combined measurements of EEG and fMRI to study brain rhythms can and has been approached. While discussing this, we will make a distinction between studies that combine these measurements to study spontaneous endogenously generate measurements during resting state and those that study changes in brain rhythms that are related to task conditions. In the context of resting state studies, we also include a discussion of endogenously generated brain rhythms during sleep and those related to epilepsy. This distinction ”resting state” and “task-related” brain rhythms is mainly made based on historical grounds. Many of the first studies that combined EEG-fMRI studies focused on the link between spontaneous rhythmic activity during resting state, in particular the alpha rhythm (Goldman et al. 2002; Laufs et al. 2003a; Moosmann et al. 2003). The first studies that focused on task-related changes followed in general a few years later (Sammer et al. 2007, 2005; Scheeringa et al. 2009). The approaches to combining EEG and fMRI in resting state and task contexts are on some aspects very similar, but there are also some notable differences.

15.1.1 Considerations for the Study of Rest

Accurately determining the temperature of whiskey in a shot glass is not a trivial task. Lowering the tip of the thermometer into the fluid will introduce both thermal and kinetic energy, thus biasing the measurement. Additionally, the alcohol is volatile and hence the volume not constant. Similarly, experimentally assessing spontaneous resting brain activity is a virtually impossible task. The general scientific approach of externally manipulating (independent variable) the system under observation in order to obtain informative measurements (dependent variable) about the object of interest may suspend the resting state; in other words, it may cause the object of interest to change and evade. In any case, the alive brain obviously never truly remains at rest, as this would prohibit (re)active functioning. In this chapter,

the term "resting state" will refer to a state of "endogenous brain activity" that is spontaneously ongoing, not intentionally induced externally nor voluntarily generated by the subject.

The study of resting state brain activity becomes especially interesting if one perceives neural processes as being mainly intrinsic—weighting, gating and subsequently integrating new and external information into the brain—as opposed to a rather absolute resting state that contrasts with momentary activity driven by external demands (Raichle and Snyder 2007). Unless one is creating a contextual setting with respect to which "rest" is defined (Fair et al. 2007; Raichle et al. 2001; Raichle and Snyder 2007), then paradigmatic, repetitive stimulation by definition precludes rest. This suggests that the method of choice is the analysis of ongoing spontaneous brain activity rather than averaged or induced brain activity.

The most prominent property of this activity are neuronal ensemble oscillations or "rhythms".

These resting state oscillations can be perturbed by spontaneous, brief pathological or physiological interruptions, the study of which further nourishes interest in the resting state and spontaneous variations of it. Conversely, knowledge of resting state brain activity can improve our understanding of task-induced brain activity. This may need to be seen in the context of the underlying spontaneous brain activity: perceiving rest as a momentary state (i.e. a brief epoch of ongoing endogenous activity); it has been proposed that intrinsic fluctuations within cortical systems can account for (intertrial) variability in human behaviour through its addition to the purely task-induced activity (Fox et al. 2007).

Also, there is evidence that sets of brain regions, "networks", which typically exhibit coherent activity in a task context, facilitating binding (Mesulam 1990, 1998; Munk and Neuenschwander 2000), are also intermittently active during rest (see the first paragraph of this section).

Their degree of prominence or even absence during rest is related to the (patho) physiological brain state on both short ("microstate") and long (psychiatric condition) timescales (Lehmann et al. 2005). In Alzheimer's disease, for example, both electrophysiological and imaging experiments of spontaneous brain activity have pointed to disease-associated variability of resting state networks (Sorg et al. 2007; Stam et al. 2005).

15.1.2 From Unimodal to Multimodal Approaches to the Resting State

Endogenous changes in resting state activity can be observed across vigilance and sleep stages but also as pathologic activity in the form of epileptic activity. Both types of activity (changes) can be detected and characterised using electroencephalography (EEG), the gold standard method for determining sleep stages (Rechtschaffen and Kales 1968) and epileptiform activity noninvasively (Gibbs et al. 1935). While the EEG indicates the occurrence of a state, it does not reveal much about its nature.

Resting state fMRI has been around for more than two decades now (Biswal et al. 1995) but has largely gained traction in the last 10–15 years growing into an entire field of research on its own. One of the major developments in this field is the identification of 10–15 large-scale networks of brain regions that covary in neural activity during wakeful rest (Damoiseaux et al. 2006; Smith et al. 2009). This has spurred a large body of research into these networks in both healthy subjects and clinical populations (Castellanos et al. 2013).

Concurrent measurements of EEG and blood oxygenation level-dependent (BOLD) functional magnetic resonance imaging (fMRI) allow us to simultaneously assess brain activity from two angles (see the Chap. 12). One modality can be used to inform the other. In this manner, spontaneous neural oscillations can be studied without external manipulation. For example, the EEG data can describe endogenous modulations of vigilance or can serve to identify spontaneous events such as sleep spindles and epileptic discharges (see Chaps. 16, 17, 18, and 19). The EEG can be treated as the independent variable, forming a regressor that can be used to interrogate the fMRI data, the dependent variable. The reverse is also possible, and attempts at data fusion are also being made where all of the data are used equally as dependent and independent variables simultaneously (see the Chap. 28).

In the paragraphs below, we will first discuss the unimodal approaches to studying spontaneous neural activity during resting state. These will be followed by multimodal simultaneous EEG–fMRI approaches to the study of resting state.

15.1.3 Unimodal Approaches to Resting State

15.1.3.1 Resting State in fMRI

The observation that cortical regions can show systematic patterns of correlations in the absence of any physical stimulation or experimental manipulation was already observed in the early years of fMRI research. Biswal et al. (1995) reported that during rest there was a strong correlation of the BOLD signal measured in the sensorimotor cortices in both hemispheres. In the more than two decades that followed resting state, fMRI has become one of the main neuroimaging tools used in fundamental research on healthy subjects as well as in research in clinical populations (Bijsterbosch 2017). Research in healthy subjects has demonstrated that there are roughly ten large scale resting state brain networks that can be reliably measured in healthy subjects (Damoiseaux et al. 2006; Smith et al. 2009).

In the early work by Biswal et al. (1995), a strong correspondence was already observed between the resting state correlation maps and the fMRI-BOLD-activation map during a bilateral finger tapping task. This foreshadowed that there might be a strong correspondence between the brain regions within a resting state network that exhibit co-fluctuations in spontaneous activity and brain regions that regularly co-activate (or deactivate) in a task context. Smith et al. (2009) investigated this more systematically. They analysed the datasets of 30,000 subjects in a wide variety of task settings from the BrainMap database of functional imaging studies (Fox and Lancaster 2002; Laird et al. 2005) to investigate which brain regions show covary in

activation and deactivation across subjects and task settings. They observed that the networks of brain regions that consistently covary in task-induced activation changes are the very same networks as the large-scale brain networks observed in resting state fMRI. This suggests that task-related activations observed in fMRI at least in part reflect changes in neural activity that also underlie the spontaneous covariation of activity within brain networks during resting state.

15.1.3.2 Spontaneous Neural Activity in Electrophysiology

The occurrence of spontaneous brain activity reflected electrophysiology can already be traced back to the very first EEG recordings by Hans Berger who identified the most prominent EEG rhythm during awake resting state: an 8–12 Hz rhythm, the "alpha rhythm", which can be measured at posterior regions of the scalp. He noticed its desynchronisation with ceasing vigilance and with engagement in an attention-demanding task on the other (Berger 1929), while it increased in amplitude when subjects closed their eyes. Despite this observation, spontaneous brain activity during relaxed wakefulness ("awake rest") has historically been less well characterised, even though it is recorded in day-to-day clinical practice. Although many EEG studies (too numerous to mention) have been performed since the work of Berger, these have mainly been resting state examinations in a clinical context and in sleep research. A methodological milestone was achieved in the form of invasive, single-cell and multiunit recordings (Steriade 1995). In crude summary, human EEG activity within a certain frequency band cannot be directly linked to specific (mal)function without taking into account its amplitude, spatial distribution, reactivity, intra- and interindividual variability, and generally speaking the context in which it is observed (Laufs et al. 2006c; Nunez et al. 2001; Urrestarazu et al. 2007). Accordingly, a variety of EEG oscillations, from ultraslow (direct current/below 0.1 Hz) to ultrafast (around 1000 Hz), have been observed and mostly assigned Greek letters ranging from alpha to omega (Curio 2000). Invasive EEG experiments (Steriade 2005) and noninvasive source localisation methods (Lopes da Silva 2004; Michel et al. 2004) have shed light on specific brain regions involved in the generation and maintenance of various brain oscillations.

More recetly, there have been attempts to investigate whether the networks of brain regions underlying neural oscillations we observe with EEG and in particularly MEG (Brookes et al. 2011a, b; De Pasquale et al. 2010). Because, unlike the signals measured with EEG, magnetic signals recorded with MEG are undisturbed by the tissue located in between the source location and the sensors, higher spatial accuracy can be achieved. Therefore, source-level MEG has been the primary method of choice to identify the networks underlying the spontaneous fluctuations in oscillations measured at the sensor level. In one such a study, Brookes et al. (2011b) set out to directly test whether the resting state networks observed in fMRI could also be recreated from source-level MEG power estimates. The observed that when similar ICA based approaches are employed to extract resting state networks from fMRI and source-level MEG power, very similar networks can indeed be observed. Further investigation to the frequency-specific nature of the networks observed in MEG revealed that these networks wore most strongly expressed in beta

band and to a lesser extent alpha band power-to-power correlations between brain regions within a network.

15.1.4 Multimodal Studies of Rest

15.1.4.1 Direct and Indirect Measurement of Neural Activity by (f)MRI

Simultaneous recordings of EEG and fMRI are often thought of as an endeavour in combining the best of both worlds: it combines the direct measurement of neural activity at high temporal resolution of EEG with the high spatial resolution and in principle whole brain coverage that can be achieved with BOLD-based fMRI. Although we can measure BOLD from practically any location in the brain the main disadvantages are that it is an indirect, delayed and temporally low-pass filtered measure of brain activity. If we were able to measure direct neural activity with the same spatial accuracy and coverage and noninvasively as with the BOLD signal haemodynamic methods like fMRI would become obsolete. Over the years, there have been several such attempts to measure the neural activity directly with MRI. These attempts make use of the fact that neural activity leads to small local currents that can result in a phase shift or signal loss of the recorded MRI signals. Phantom and in vitro experiments have demonstrated these effects are in principle detectable (Bodurka and Bandettini 2002; Bodurka et al. 1999; Petridou et al. 2006; Sundaram et al. 2016), but in vivo measurements have remained controversial (Bandettini et al. 2005; Luo et al. 2011; Parkes et al. 2007; Sundaram et al. 2010; Tang et al. 2008). Recently, this approach has regained new attention by a study by Truong et al. (2019) that reports being able to make changes in alpha activity in eyes-closed versus eyes-open conditions. This approach might open up a new technique to directly measure neural activity directly with MRI, but in the foreseeable future, it is unlikely to replace BOLD-based fMRI research.

With fMRI we measure neural activity indirectly by measuring the haemodynamic response to changes in neural activity. This haemodynamic signal is in general assumed to be too slow to directly measure fast changes in neural activity and can be seen as a low-pass filter of the neural activity. If pushed to its extremes though, Lewis et al. (2016) showed that that it might be possible to measure the oscillatory nature of neural activity up to 0.75 Hz, which is substantially higher than previously thought. This brings slow frequency phenomena like slow steady-state-evoked potentials, slow event-related potentials and slow-wave sleep possibly within the realm of detectability with fMRI. Most oscillations and evoked potentials however occur on a time-scale that is orders of magnitude faster than can be measured with fMRI. Therefore, when multimodal recordings of EEG and fMRI are done, the oscillatory activity in task and rest itself is not related to the BOLD signal, but the variation in the amplitude (or power) of the oscillations over time or trials is used to correlate with the haemodynamic signal. In order to match the temporal delay and low-pass filter characteristics of the haemodynamic response, this oscillatory signal is convolved with a model of the haemodynamic response to obtain to

obtain an EEG-based regressor that to be used in a general linear model (GLM) for fMRI analysis.

15.1.4.2 Functional Imaging Studies of "Brain Oscillations"

Unimodal fMRI studies of rest are primarily based on data-driven analysis approaches (functional connectivity; principal or independent component analysis, PCA/ICA). Over a dozen consistent resting state networks have been identified (Fox and Raichle 2007). The interpretation of signal changes in these resting state networks remains difficult when assessed unimodally and (necessarily) in the absence of a task and distinct context. Objectively assessing a subject's state during data acquisition (e.g. via external observation or a post hoc interview) remains a difficult and inaccurate task, especially when subjects drift between wakefulness and drowsiness. An additional perspective on brain activity at rest can be obtained via a second measure, that of EEG. This can give information on the subject's "state of mind", especially the level of vigilance. If functionally well-established EEG features can be correlated with fMRI, then the associated fMRI maps can be better interpreted. The meaning of the fMRI maps will most likely parallel the meaning of the associated EEG (Laufs et al. 2006c). On the other hand, EEG–fMRI can help to elucidate the brain processes that underlie specific, less-understood EEG phenomena if the related fMRI signal changes have been observed and interpreted previously, for example, in the context of a task (Laufs et al. 2007; Schabus et al. 2007).

15.1.4.3 Endogenous Brain Oscillations in Healthy Subjects

Neuronal oscillations in different EEG frequency bands and associated topographies have been identified in the context of different types of active mental activity. Spontaneous brain activity during relaxed wakefulness ("awake rest") has inherently been less well characterised, despite the fact that it is recorded in day-to-day clinical practice and was the first condition to have been assessed with EEG (Berger 1929). The most prominent EEG rhythm during the awake resting state was described by Hans Berger: he termed the posterior 8–12 Hz oscillations the "alpha rhythm" and noticed its desynchronisation with ceasing vigilance on the one hand and with engagement in an attention-demanding task on the other (Berger 1929).

Unsurprisingly, the first EEG–fMRI investigations studying healthy volunteers at rest were concerned with the BOLD correlates of this very prominent EEG alpha rhythm. In line with neurophysiological animal studies, Goldman et al., Moosmann et al. and (similarly) later Mantini et al. noted that thalamic BOLD activity was positively correlated with posterior alpha oscillations on scalp EEG. They identified an inverse correlation of the alpha EEG with the occipital-parietal areas, reflecting the alpha oscillations' scalp topography (Goldman et al. 2002; Mantini et al. 2007; Moosmann et al. 2003). Laufs et al., and again similarly Mantini et al., also found that a frontal-parietal network was associated with alpha desynchronisation (Laufs et al. 2003a; Mantini et al. 2007). In line with Berger's observations, they claimed to have visualised endogenously waxing and waning attention with fluctuating alpha desynchronisation indexed by activity changes in a frontal-parietal network, which had previously and independently been established as being an attentional

system (Laufs et al. 2003a, 2006c). An almost identical network had been found to be engaged during a variety of attention-demanding tasks, especially mental arithmetic (Gruber et al. 2001): a form of brain activity that is also classically known to suppress the alpha rhythm (Berger 1929); see Fig. 15.1.

In a strict sense, apart from any (thalamic) activation associated with alpha power increases (Feige et al. 2005; Goldman et al. 2002; Mantini et al. 2007; Moosmann et al. 2003), none of the studies mentioned above revealed notable coherent (cortical) correlates of scalp EEG alpha oscillations; instead, by identifying inverse relationships, brain regions that increase their activity in the *absence* of marked alpha activity were identified (Laufs et al. 2006c). Once again, in congruence with Hans Berger's observations, when they reanalysed their data, Laufs et al. found indications that the occipitally pronounced, inversely alpha-associated pattern occurred in association with a decline in vigilance. This finding was supported by a corresponding enhanced spectral density in the theta (4–7 Hz) band, as typically observed during drowsiness. Furthermore, positron emission tomography (PET) data had shown activation in occipital brain regions during light sleep when contrasted against wakefulness (Kjaer et al. 2002). The absence of a single average cortical BOLD signal pattern correlated positively with alpha power across studies may be explained by (spatially) nonuniform brain activity at the population level during periods of

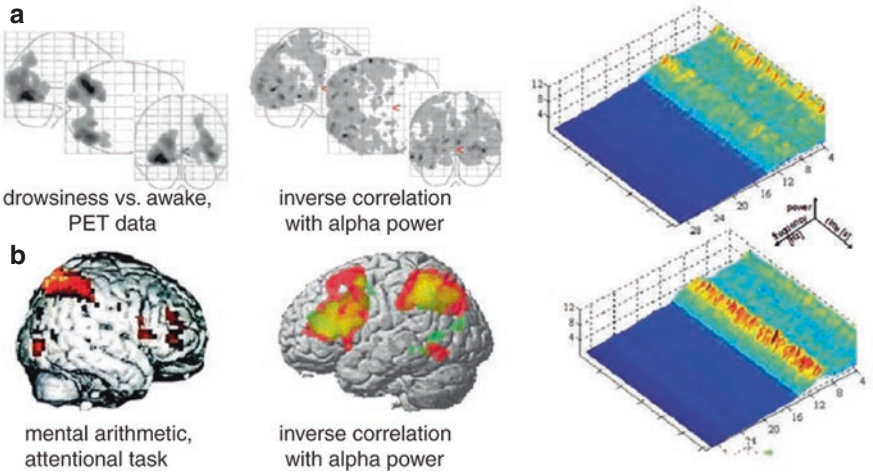

Fig. 15.1 (**a**, **b**) Functionally characterised imaging patterns (*left*), inversely alpha-correlated fMRI maps (*middle*) and associated averaged EEG spectra (*right*). A single EEG feature can be associated with a variety of fMRI maps. (**a**) Using PET, Kjaer et al. found higher signals in bilateral occipital brain regions during drowsiness compared to at rest (Kjaer et al. 2002). Similar occipital and additional parietal fMRI signal changes were inversely associated with alpha power in a group of resting subjects showing EEG features of drowsiness (Laufs et al. 2006c). (**b**) A bilateral frontal-parietal network is known to support attention-demanding tasks, especially mental arithmetic (Gruber et al. 2001). In awake, resting subjects, the fMRI signals in a set of brain regions very similar to that involved during mental arithmetic increase with desynchronised alpha oscillations (Laufs et al. 2003a; Mantini et al. 2007)

prominent alpha oscillations, which fMRI group analysis must fail to detect (Friston et al. 1999; Laufs et al. 2006c). This can be caused by different brain regions that relate to the posterior alpha rhythms in different subjects that are in different mental states.

Another reason why different regions correlate with alpha band activity in different subjects is that different brain regions actually underly the generation of the alpha band variation in different subjects. The posterior alpha rhythm generated in the visual cortex is not the only neural activity that is reflected in changes in the alpha band at EEG channel level. It is reasonable to assume that many parts of the cortex generates some neural activity in the alpha frequency range, and what is measured at channel level with EEG is a weighted sum of all this activity. This weighted sum can change over conditions and mental states within a subject but can systematically differ over subjects due to anatomical differences in both neural and non-neural anatomy. Techniques that focus on unmixing this channel level mixture of alpha band activity can therefore contribute in separating the alpha source of interest from other sources of noninterest. Source analysis techniques like beamformer approaches (Brookes et al. 2009; Hanslmayr et al. 2011; Zumer et al. 2014) or blind source separation techniques like ICA have been applied to achieve this separation of sources in the alpha range and also in other frequency bands (Scheeringa et al. 2008, 2011, 2012). An example of this approach in the context of the posterior alpha rhythm during resting state is a study by Scheeringa et al. (2012) who applied ICA on the EEG data in order to select a central posterior independent components with a peak in the alpha band. When correlating variation in alpha power in this component with the BOLD signal across the entire brain, they did observe the expected negative correlation in the visual system.

15.1.4.4 Similar Electrical Oscillations, Different fMRI Networks

The example discussed in the previous section showed that endogenous electrical oscillations, namely, posterior alpha power during relaxed wakefulness, can be associated with different fMRI maps (haemodynamic networks). Slight methodological or analytical differences between the cited studies can only partially explain this effect. It is more likely that different (dynamic) brain states were studied and reflected in several EEG features, among which only one, the suppression of occipital alpha oscillations, was included in the abovementioned analyses. This feature must be common to the different identified brain states and represents only an indirect measure. This suggests that, for a more detailed assessment of neural oscillations, broader EEG spectral properties and more comprehensive EEG spatial information must be incorporated into such analyses. Statistical considerations also require the parallel evaluation of, for example, multiple EEG frequency bands, especially if the bands are correlated with one another (Laufs et al. 2006c; Mantini et al. 2007): if only one of several correlated EEG features is used as a regressor in a general linear model (GLM), the attribution of the associated fMRI variance to a frequency band will be unspecific. For instance, if alpha and theta power are highly correlated, then the utilisation of either the theta or the alpha regressor in an fMRI analysis may yield very similar fMRI maps.

In an attempt to analyse a broader EEG frequency content (although not across space), Laufs et al. simultaneously correlated occipital theta, alpha and different beta frequency bands with fMRI data in a GLM (Laufs et al. 2003b). They found that activity in the beta-2 (17–23 Hz) frequency band correlates with the DMN (Raichle et al. 2001). No significant theta band correlations were found in the fMRI data in that study (Laufs et al. 2003b). PET meta-analyses had originally identified the DMN (see Fig. 15.2) (Mazoyer et al. 2001). This describes a set of brain regions that show greater activity at rest than during states of reduced consciousness and states of extroverted perception and action. Thus, their activities are highest during an idling or intermediate activity state following which the brain can then either engage in more activity (e.g. a task) or less activity (e.g. sleep)—hence its name (Raichle et al. 2001). While most resting state networks were later identified by data-driven fMRI experiments, the DMN was described in PET and fMRI meta analyses as a group of areas that consistently exhibited decreases from relative

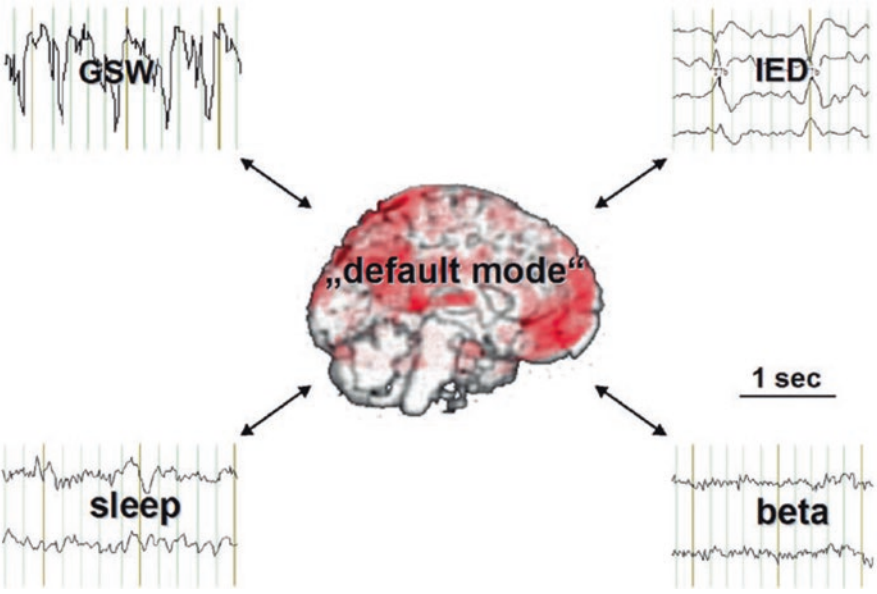

Fig. 15.2 A single fMRI map can be associated with a variety of EEG features at rest. Generalised *spike* and *wave* (*GSW*) discharges on EEG, typical rhythmic EEG oscillations during absence seizures with loss of consciousness, are associated with decreased fMRI signal in the precuneus, dorsal prefrontal cortices and the temporoparietal junction, regions of the "default mode network" (Archer et al. 2003; De Tiege et al. 2007; Gotman et al. 2005; Hamandi et al. 2006; Laufs et al. 2006a; Salek-Haddadi et al. 2003). Interictal epileptic discharges (*IEDs*) occurring frequently on EEG in temporal lobe epilepsy, characterised by complex partial seizures during which consciousness is impaired, are associated with fMRI signal decreases in "default mode" brain regions (Kobayashi et al. 2006b; Laufs et al. 2006a). During *sleep*, especially sleep stage II, central alpha power was found to be inversely associated with fMRI signal changes in regions constituting the DMN (Laufs et al. 2007). *Beta* band EEG oscillations are associated with fMRI signal fluctuations in "default mode" brain regions (Laufs et al. 2003b; Mantini et al. 2007)

baselines of a wide variety of goal-directed behavioural tasks (Raichle et al. 2001). This allowed a meaning to be assigned to this network.

The identification of the "default mode" regions via a regressor derived from spontaneous EEG (beta-2 power) oscillations during wakefulness suggested that this network is dynamically active even when "at rest". Band specificity was demonstrated by making EEG the dependent variable: an fMRI signal time course taken from a representative region within the DMN (left temporoparietal junction) was correlated with specific EEG sub-bands and best fitted to the beta-2 oscillations (Laufs et al. 2003b).

Mantini et al. further extended this EEG–fMRI integration to an awake and at rest condition. They incorporated EEG bands between 1 and 50 Hz, averaged across the entire scalp, into their analysis. They correlated the fMRI time courses of resting state networks (identified by means of ICA) with these bands (Mantini et al. 2007). There was again an almost exclusively inverse correlation between the fMRI signals and the EEG frequency band (delta, theta, alpha, beta, gamma) power for four out of six identified resting state networks. This may indicate that at the group level, a commonality of brain states could only be detected in the form of desynchronisation of brain oscillations at different frequencies. The most specific and positive EEG–fMRI correlation was revealed for the 30–50 Hz gamma band. This will require validation given that the BOLD signal changes occurred in the frontal lobe near areas typically bound to EPI signal dropout and that 30–50 Hz EEG may contain increased noise.

As discussed above, occipital beta-2 power was found to correlate positively with the DMN (Laufs et al. 2003b). Mantini et al. additionally found that spatially averaged alpha power covaried with BOLD activity in the default mode network (Mantini et al. 2007). Scheeringa et al. identified a very similar network during eyes-open rest that was inversely correlated with frontal theta power, the latter derived by applying ICA on the EEG data (Scheeringa et al. 2008).

In an approach similar to Mantini et al. (2007), Sadaghiani et al. (2010) set out to investigate how two resting state networks, the dorsal attention network and the tonic alertness network relate frequency-specific changes in EEG power. They demonstrated that the dorsal attention network is, as was observed by Mantini et al. (2007), negatively related to the alpha and beta band power. The tonic alertness network, a network that just like the dorsal attention network is often active in task settings, however showed a positive correlation with both alpha and beta powers. Instead of averaging within frequency bands, the correlations in this studies were calculated for each frequency bin of the EEG power analysis separately. This revealed within the alpha range a separation in the exact frequency range the two networks correlated with EEG power. The dorsal attention network correlated negatively with alpha in the 7–10 Hz range, while the tonic alertness network correlated positively with alpha in the 10–12 Hz. These frequencies overlapped with what are historically identified as the lower and upper alpha bands, respectively (Klimesch 1999).

The studies discussed in this paragraph demonstrate how the state of the subject (eyes open, resting in the context of a cognitive task) as well as the analytical

strategy pursued (frontal EEG power, single frequency band, ICA or channel level) can affect EEG–fMRI correspondence. This is to some extent inherent to the measurement of EEG in resting state, since it is often hard to ensure all subjects are in the same mental state where different brain networks can relate to the same oscillatory EEG phenomenon but where selecting the same oscillatory EEG feature in all subjects can also be a challenge.

15.1.4.5 Similar fMRI Networks, Different Electrical Oscillations

As argued in the section above, similar electrical oscillations can correlate with different fMRI oscillations. On the other hand, the "default mode" fMRI resting state oscillations have been found to correlate with power in different EEG frequency bands, including (during eyes-closed rest) with spatially averaged alpha and beta (Mantini et al. 2007), posterior beta-2 (Laufs et al. 2003b), and (during eyes open rest) inversely with frontal theta oscillations (Scheeringa et al. 2008); see Fig. 15.2.

Based on fMRI functional connectivity analysis, Horovitz et al. suggested that the dynamic resting state activity persists in this network during reduced vigilance (Horovitz et al. 2008). A single-case EEG–fMRI study related activity in the DMN during sleep stage II (Rechtschaffen and Kales 1968) primarily to decreased central alpha power (Laufs et al. 2007). While PET data (Maquet 2000) congruent with the "default mode" concept (Raichle et al. 2001) identified a relative decrease in activity in that network during sleep compared to wakefulness, it is now clear that this network sustains its activity despite decreasing vigilance and possibly functions at a lower energy level. The association of decreased activity in the DMN with other EEG features (focal and generalised epileptic activity) will be discussed below.

15.1.4.6 Brain Rhythms and Connectivity

Where the previous studies correlated the strength of oscillations with the strength of the BOLD signal, several studies have now also used multimodal measurements to investigate connectivity between brain regions. Two types of approaches can be distinguished: In the first approach the strength of specific brain rhythms can be used to predict changes in BOLD-based fMRI connectivity. The second approach is the reversed of the first, where the level of BOLD activation in brain regions or brain networks is used to predict connectivity measures in EEG.

In an example of the first approach Scheeringa et al. investigated whether connectivity of the primary visual cortex with the rest of the brain depended on the strength of occipital alpha oscillations. For this they applied ICA on the EEG data and selected a central posterior alpha component. In previous EEG studies, this posterior alpha component was reliably related to visual processing, with a likely source location in the early visual cortex (Makeig et al. 2004a, b). In line with this, a negative correlation with BOLD was also observed in early visual cortex. For investigating whether connectivity of this region with regions in the rest of the brain was modulated by the strength of alpha band oscillations, a connectivity analysis similar to the psychophysiological interaction (Friston et al. 1997) was used, which tested whether the regression slope between the seed in early visual cortex and the rest of the brain was different for when alpha amplitude was high compared to when

it was low. They observed that fMRI-based connectivity between early visual regions and later extra-striate regions in the visual stream was lower when alpha amplitude was high. This indicates that an increase in alpha amplitude in a brain region correlates with that region being functionally uncoupled from other brain regions, which is in line with the notion that alpha is related to functional inhibition of brain regions (Jensen and Mazaheri 2010; Klimesch et al. 2007).

In electrophysiology, increased connectivity is often thought to be expressed in increased phase synchrony in electrophysiological signals originating from different brain regions (Fries 2015; Jensen et al. 2014; Varela et al. 2001). Also for the alpha band increased phase synchrony is thought to be related to increased connectivity between regions (Jensen et al. 2014). This phase synchrony is thought to be under active attentional control. In a reanalysis of the resting state data discussed above, Sadaghiani et al. (2012) investigated whether fluctuations in global phase locking between would be related to a network related to attention or cognitive control. For this they calculated the phase locking value in a sliding window of 10 s for the upper alpha band and correlated this with the BOLD signal in the entire brain. This revealed a network of frontoparietal brain regions that is commonly associated with adaptive control.

Taken together, with these two studies, Sadaghiani et al. (2012) and Sadaghiani et al. (2010) were able to relate three different attentional control networks to different aspects of global alpha band oscillations. The dorsal attention network was inversely related to the lower alpha band, the tonic alertness network related positively with the upper alpha band, while global phase synchrony in this frequency band related positively to a brain network related to adaptive cognitive control. These findings suggest that the influence these three brain networks involved in attention and cognitive control have on neural processing in the cortex is reflected in different aspects of alpha band activity.

15.1.4.7 Brain Oscillations and Networks During Sleep

EEG is the central tool in sleep research, and oscillations serve to define sleep stages (Rechtschaffen and Kales 1968). EEG–fMRI is therefore an ideal tool to extend investigations of awake, resting brain oscillations to states of reduced vigilance. This will only be briefly touched on here because a separate chapter of this book is dedicated to EEG–fMRI and sleep (see the Chap. 16). Due to their limited temporal resolution, EEG–PET studies have to assess sleep stage-related mean brain activity over many minutes (Maquet 2000) but cannot identify within-state activity or metabolic correlates of brief sleep-specific oscillations and events such as sleep spindles, vertex sharp waves or K-complexes. While the first EEG–fMRI study of spontaneous sleep without visual or acoustic stimulation was still performed in the spirit of these PET studies (Kaufmann et al. 2006), since then, sleep stage-specific EEG frequency patterns have been studied in a single case alongside an event-related analysis of sleep spindles and K-complexes (Laufs et al. 2007). A larger study confirmed and extended the findings of sleep spindle-associated bilateral thalamic, superior temporal and sensorimotor cortical activations (Schabus et al. 2007). Both studies discussed temporal lobe activation as a possible indication of memory

processing during sleep, but due to the nature of resting state investigations, there was no probing task, and so this interpretation presently remains speculative. This is an example of a shortcoming of resting state studies, even when concurrent EEG information is available.

Delta oscillations are a prominent and characteristic feature of deeper non-rapid eye movement sleep stages (Rechtschaffen and Kales 1968), but correlating these EEGs with fMRI oscillations during sleep stages III and IV in the single case study did not reveal significant fMRI networks. Possible explanations for this include ignoring the phase of the oscillations and inappropriately limited exploitation of their spatial distribution, and it indicates that more sophisticated analysis strategies should be used in future studies (Laufs et al. 2007).

15.1.4.8 Endogenous Brain Oscillations in Patients with Epilepsy

Epilepsy is a special case of EEG–fMRI resting state studies, and three chapters of this book are dedicated to it (Chaps. 17, 18, and 19). This is why this chapter restricts itself to pathology-specific brain rhythms as well as further examples of EEG patterns associated with the brain networks discussed above.

Historically, the development of EEG recording during fMRI was driven by the motivation to localise the source of epileptic activity via haemodynamic correlates of the spontaneously occurring, unpredictable EEG events. Patients at rest were examined in order to create an event-related model for interrogating the fMRI data, and additional paradigms appeared dispensable at the time (Gotman et al. 2006; Laufs and Duncan 2007). The objective of the studies was not the resting state but to contrast epileptic activity against an implicit baseline. As it turned out, however, generalised epileptic activity in the form of 3/s spike and wave complexes affects activity in the DMN (Archer et al. 2003; De Tiege et al. 2007; Gotman et al. 2005; Hamandi et al. 2006; Laufs et al. 2006a; Salek-Haddadi et al. 2003). The behavioural correlate of the prototype for such generalised discharges are absence seizures, which are characterised by impaired consciousness. Other conditions of impaired consciousness have already been associated with a decrease in activity in default mode brain regions (Laureys et al. 2004), and the fMRI maps associated with absence seizures can be interpreted in an analogous way (Gotman et al. 2005; Laufs et al. 2006d). Surprisingly, even frequent focal interictal epileptic discharges in patients with temporal lobe epilepsy were associated with a relative signal decrease in the DMN, although behavioural changes are not obvious during focal interictal epileptic activity (Kobayashi et al. 2006a; Laufs et al. 2006a). Assuming that decreased activity in the DMN during focal epileptic activity represents another instance of impaired consciousness, this may explain cognitive deficits observed in epilepsy patients with frequent interictal discharges and complex partial seizures characterised by a loss of consciousness (Laufs et al. 2006a). Thus, resting state EEG–fMRI can identify impaired brain function. Altered brain rhythms—changes in ongoing EEG activity such as focal theta or delta slowing—may indicate pathology and can be used to localise the epileptogenic area in EEG–fMRI analyses (Laufs et al. 2006b; Siniatchkin et al. 2007). Studies relating ongoing brain activity itself to epileptic pathology are underway.

15.2 Multimodal Approaches in a Task Setting

15.2.1 General Considerations

As mentioned above, the brain regions that form the different resting state networks are also regularly found to coactivate in task settings (Smith et al. 2009). Furthermore, MEG research has indicated that these resting state networks are also expressed in covariations in oscillatory power, in particular in the beta band (Brookes et al. 2011a). From this, the question arises which brain regions and networks of brain regions relate to the task effects in oscillations measured by MEG and EEG. Since fMRI can measure neural activity from the entire brain, simultaneously recorded EEG and fMRI can be applied to address this question. Although measuring EEG and fMRI simultaneously in a task setting is technically more challenging than measurements during resting state, they also provide several advantages compared to measurements during resting state.

The first advantage is that by virtue of introducing a task with different conditions and stages (e.g. cue, encoding, retrieval and response phases of a task), there is more control of the mental state and mental activities of the subject compared to resting state. This also helps us in interpreting the relation we find (or do not find) between the EEG feature of interest and the fMRI results. Furthermore, the different stages and conditions allow us to do ask more focused questions and do more focused analyses. It allows us, for instance, to investigate in which brain regions neural activity relates to a parametric increase in frontal theta power with working memory load during the maintenance phase of a working memory task (Scheeringa et al. 2009), as is detailed in the examples below.

Another advantage from a methodological point of view is that when an EEG task effect is well established and characterized by earlier research or through an earlier independent measurement, we can use this effect to "denoise" the EEG from spurious brain activity we are not interested in or non-brain noise sources like eye blinks and MRI-related artifacts. Two well-tested approaches here are blind source separation techniques like ICA (Debener et al. 2006, 2005; Scheeringa et al. 2011, 2016, 2009) or beamformer-based source analysis (Brookes et al. 2009; Zumer et al. 2014). In the first approach, we can select one or more components that show the task effect of interest, while removing all other components that model activity and artifacts of noninterest. The beamformer approach makes use of the noise-suppressing properties of this source analysis method. In this approach, a spatial filter is constructed for each source location under consideration. This spatial filter is constructed in such a way that signals coming from the source location in question are maximally let through, while simultaneously maximally suppressing activity not coming from this location. By selecting the source location where the task effects is maximal, we can maximally suppress activity coming from other sources that are influencing the measurement at channel level. In this case, the noise-suppressing features of the beamforming approach are of more interest here than getting the exact source location of the effect of interest.

While one may analyse the simultaneously recorded EEG and fMRI completely separately, this would negate the benefits of doing simultaneous measurements apart from those associated with both measurements having been carried out in exactly the same environment, in addition to the inevitable, albeit potentially negligible depending on the application, impact on data quality highlighted in previous chapters. The true advantage of simultaneous EEG and fMRI in a task context is that it allows us to statistically relate the two modalities across individual responses in way that is not possible across separate, unimodal sessions. In this context, there are two sources of (co)variation that can exploited. We can investigate whether EEG and fMRI covary in their responses over trials or whether they covary in their effects over subjects.

The first step when using variation over trials to study how EEG and fMRI relate is to obtain the best possible estimate of single trial variation in the oscillatory EEG effect of interest (Debener et al. 2006). This can greatly benefit from the ICA or beamformer denoising approaches discussed above. Subsequently the single trial estimates of the strength of the oscillatory activity can be used as a parametric modulation of the condition and phase of the trial it was measured. By including both the EEG-based parametric and task regressors in the statistical design, it is possible to test whether there is a link of the BOLD signal with the single trial variation EEG oscillations up and above the task modulation. If a link between EEG and fMRI is observed it does however not necessarily imply that there is also a link between the task effects in both modalities. Some of the variation of the EEG response could be related to non-task-related processes or spurious activity from noise sources that were not fully removed in the denoising stage. If there however is a link between the EEG task effect and the regions where the BOLD signal correlates with variation EEG power over trials, an fMRI-task effect that is in line with the task effect in EEG should be present. This can then subsequently be explicitly tested for.

Given a sufficient large number of subjects (dependent on the strength of the expected correlation), the strength in a task effect in EEG can be correlated with the same task effect in fMRI. For example, the variations over subjects in attention-related effects in alpha, beta or gamma band power can be correlated with attention effects for the same contrast in fMRI over subjects (Scheeringa et al. 2016). In this case, variation over subjects is the source of variance we use to establish a link between EEG and fMRI. By doing this analysis in multimodal measurements and not separate unimodal measurements in the same subjects, we capture both trait and mental state influences on variation in the effects over subjects. With separate measurements, only trait-like influences, that is the extent to which subjects demonstrate the same task response in EEG and fMRI over repeated measures, can be used as a source of variance.

15.2.2 Multimodal Measurements in a Task Context: Examples

In a task setting, many different brain regions usually show a task effects in fMRI, while in EEG a variety of task effects can be observed in multiple frequency bands over different parts of the scalp. An important question that can be addressed with

simultaneously recorded EEG and fMRI is which of these brain regions relate to which oscillatory effects observed in EEG. One example in which such a problem was addressed is in a working memory study by Scheeringa et al. (2009). In this experiment, the goal was to find the brain networks related to working memory induced parametric increases in posterior alpha and frontal theta power during working memory maintenance. The recorded EEG data did indeed reveal parametric increases in frontal theta and right posterior alpha power with working memory load. Trial-by-trial correlations revealed two separate nonoverlapping collections of brain regions that correlated negatively with alpha and theta power. More importantly some of these regions correlating with the alpha regressor and most of the regions correlating with the theta regressor showed a parametric decrease in activity with working memory load, in line with the negative correlation with the regressors and the parametric increase in EEG power. For the alpha band, these regions were in the primary visual cortex and right middle temporal gyrus which is in line with reduced sensory processing during working memory maintenance. The regions that were found to be related to frontal theta together formed the default mode network. This suggests that frontal theta power is indicative of deactivation of the default mode network during tasks, than it is to active task processes or working memory maintenance as was previously hypothesised (Gevins et al. 1997; Jensen 2006; Jensen and Lisman 1998; Jensen and Tesche 2002; Onton et al. 2005). The fact that two separate nonoverlapping collections of brain regions were observed to relate to two brain rhythms that demonstrated a load-dependent increase in power during working maintenance illustrates that EEG-informed analysis of fMRI data can differentiate between regions showing a similar task effect in fMRI alone.

Another example of how integrated EEG-fMRI can aid the interpretation of the results in buth modalities is a study by Hanslmayr et al. (2011) who investigated memory formation during a task in which a list of words needed to be remembered. For both fMRI and EEG they computed the subsequent memory effect were comparing the responses for later remembered versus later forgotten words In the EEG they observed lower beta power and higher theta power for later remembered compared to later forgotten words. Source analysis revealed a putative source location in the left inferior frontal cortex for beta and bilaterally in the medial temporal lobe for theta. Interestingly, increased fMRI activity for remembered words was found in the left inferior prefrontal cortex and the right parahippocampal gyrus, overlapping with putative the source locations for the beta and theta effects. Only for beta however a negative correlation between BOLD and trial-by-trial variation in EEG power was observed in the left inferior prefrontal cortex, while no correlation was reported for theta in the medial temporal lobe. This negative correlation for beta in the left inferior frontal gyrus combined with the increased BOLD and decreased beta power in the same regions provides strong evidence that this region is directly related to the subsequent memory effect in beta power. This is in line with a negative relation between beta power and the BOLD signal observed in other regions of the cortex (Scheeringa et al. 2011, 2016; Yuan et al. 2010). For the theta effect the case is weaker. Although the increase and theta is thought to originate from a region close to the observed fMRI effect, no positive correlations over trials were observed here.

What this study, combined with the study by Scheeringa et al. (2009) does illustrate is that both fMRI activation and deactivations observed with fMRI can be related to the changes observed in specific brain rhythms. For the working memory all effects were related to deactivations, where here a beta decrease was related to an increase in BOLD. Also for theta a positive relation between BOLD and EEG power was more likely to be observed given the overlap in fMRI activation and source location. If this would have been observed, this would have suggested that the neural processes underlying frontal theta power are different from those generating theta power in the medial temporal lobe, although both are reflected in changes in neural synchrony in the same frequency range. Combined EEG-fMRI can potentially contribute to distinguishing these processes.

15.2.3 Linking Neuronal Oscillations to Haemodynamic Changes

A question that often arises is whether the regions that correlate with oscillations are also the source location of the observed oscillatory effects with EEG at scalp level. Since the EEG-fMRI analyses discussed here are correlational in nature, this is not necessarily the case. It is however sometimes possible to make a good case for this. For instance in the working memory study by Scheeringa et al. (2009) the medial frontal part of the default mode network that correlated with frontal theta is also the likely source location since it is in line with source analyses that have located it in or near the medial frontal cortex (Ishii et al. 1999; Martinez-Montes et al. 2004; Miwakeichi et al. 2004; Scheeringa et al. 2008). Furthermore other candidate regions, neither negatively nor positively correlating with frontal theta were observed. Since the parametric decrease in fMRI activity with working memory load also mirrored the increase in frontal theta increase, the medial frontal part of the default mode network is the most likely source location for the medial frontal theta rhythm observed here. This conclusion does however depend on the presence of a direct link between oscillatory activity and BOLD at the source location.

For investigating the link between oscillatory activity and the BOLD signal, the gold standard is provided by studies that record haemodynamic signals and simultaneously with intracranial recordings in or very near the same patch of cortex. This kind of research is most readily and systematically carried out in animals (Goense and Logothetis 2008; Logothetis et al. 2001; Niessing et al. 2005; Shmuel et al. 2006; Viswanathan and Freeman 2007), but occasional recordings in patients with implanted electrodes have been reported (Vulliemoz et al. 2011). The first study that accomplished the technically challenging endeavour of measuring fMRI and intracranial electrophysiology simultaneously was Logothetis et al. (2001). In a landmark study where BOLD, local field potentials and multi-unit activity simultaneously in the same patch of visual cortex, they observed that during visual stimulation the

BOLD signal better matched the response pattern in LFP amplitude than that of multi-unit activity, particularly in the gamma frequency range. This notion that gamma band activity in particular closely follows the BOLD response was further strengthened by work from Niessing et al. (2005); who measured haemodynamic signals simultaneously with local field potentials and spiking activity. Like Logothetis et al., they observed that LFP amplitude, especially in the high gamma range, was a better predictor of the BOLD signal than the spiking rate. They however extended their analysis to other frequencies and observed a pattern of negative correlations between BOLD and LFP for low-frequency bands (predominantly delta and theta) and positive correlations in high-frequency bands (beta and gamma). The notion of negative correlation is largely in line with most EEG-fMRI studies that found negative correlations between oscillatory power and BOLD in low frequency in low-frequency bands (Goldman et al. 2002; Laufs et al. 2003a; Moosmann et al. 2003; Scheeringa et al. 2008, 2009; Zumer et al. 2014). It also supports the idea that multiple-frequency bands must be taken into account to understand how neural oscillation relate to the BOLD signal.

These studies however all involve invasive recordings in animals, and the question arises whether the pattern how low and high frequencies relate to fMRI also hold in healthy human subjects. Scheeringa et al. (2011) set out to investigate this with simultaneous recorded EEG and fMRI. In order to investigate this, they chose a task that induced strong fMRI activation in early visual cortex (Hoogenboom et al. 2006) and that reliably induced decreases in alpha and beta power and an increase in gamma power in MEG and EEG recordings (Hoogenboom et al. 2010, 2006; Koch et al. 2009; Muthukumaraswamy and Singh 2013; van Pelt et al. 2012) that source analyses located in early visual cortex as well. Furthermore, these responses resembled those observed in intracranial recordings in early visual cortex in animals (Fries et al. 2008). By correlating the variation in the different frequency bands with the BOLD signal over trials, they observed that alpha and beta correlated negatively with the BOLD signal while gamma correlated positively with BOLD. In addition, they observed that gamma band variations over trials did not correlate with those in the alpha and beta band, indicating that the neural processes underlying these EEG phenomena independently contributed to changes in the BOLD signal. This study thus largely supports the findings in animals on how different frequency bands relate to the BOLD signal and the notion that multiple frequency bands need to be taken into account to understand the relation between BOLD and neural oscillations.

The finding that gamma-related neural processes independently contribute to the BOLD signal from processes related to alpha and beta oscillations is in itself not surprising considering the fact that they are thought to play different roles in information processing in the brain. Intracranial recordings in animals have demonstrated that the gamma band activity predominately reflects a feedforward flow of information from lower order brain regions, while alpha and beta oscillations relate to the feedback flow in the opposite direction (Bastos et al. 2015;

Michalareas et al. 2016; van Kerkoerle et al. 2014). On an anatomical level, feedforward and feedback information is carried over laminar-specific connections between brain regions (Douglas and Martin 2004; Gilbert 1983; Markov and Kennedy 2013; Markov et al. 2014). In general, feedforward anatomical connections originate in supragranular (layers II and III) layers and projects to the granular layer (layer IV). Feedback connections originate in infragranular layers (layers V and VI) and project back to both infra- and supragranular layers. In line with this, recordings in animals have revealed that gamma band activity is strongest in granular and supragranular layers (Buffalo et al. 2011; Maier et al. 2010; van Kerkoerle et al. 2014) while beta band activity is strongest in infragranular layers (Maier et al. 2011). Both infra- and supragranular sources have been observed for alpha band oscillations (Bollimunta et al. 2008, 2011; Haegens et al. 2015; Spaak et al. 2012).

Invasive laminar electrophysiology in healthy humans is not possible. Although there are developments to measure at laminar resolution with MEG (Troebinger et al. 2014), most advances in measuring laminar level neural activity over the past decade have come from high-resolution fMRI (voxel size <1 mm^3). Where the first laminar fMRI studies were focused on technical development, over the last few years, it has become a viable tool in cognitive research (De Martino et al. 2015; Kok et al. 2016; Lawrence et al. 2019, 2018; Muckli et al. 2015; Scheeringa et al. 2016). Since neural oscillations have been linked to cortical layers, the question arises whether the relation they have with BOLD is also layer specific. In a follow-up study from the experiment discussed above, Scheeringa et al. (Scheeringa et al. 2016) investigated with combined EEG/fMRI whether alpha, beta and gamma band oscillations correlate with BOLD measured in different layers of the early visual cortex. Their results were largely in line with invasive recordings in animals. Gamma power correlated with BOLD at middle and superficial layers, while beta correlated negatively with BOLD in deep layers and alpha correlated with both deep and superficial layers. This study demonstrates that combining laminar fMRI with EEG can provide a means to study laminar-specific feedforward and feedback processes in healthy human subjects (Fig. 15.3).

CHECKLIST INTERPRETATION RELATION EEG & FMRI			
Are task effects observed in EEG and fMRI related?	**YES**	**NO**	**UNKNOWN**
1. Does the EEG feature correlate with fMRI over trials?			
2. Do the changes over conditions in EEG resemble the changes over conditions in fMRI?*			
3. Do the task effects in EEG and fMRI correlate over subjects?			
4. Are the correlations over trials and subjects and the changes over conditions not contradicting?**			
Is an EEG-related brain regions also the source location?	**YES**	**NO**	**UNKNOWN**
5. Does source analysis of the EEG feature locate it to the same or close to the observed region?			
6. Have source analysis analyses on EEG or MEG in the past revealed the same region for this effect?			
7. Are there no other plausible source regions where fMRI relates to the EEG feature?			
8. Have intracranial recordings in animals and/or humans demonstrated the same or a similar effect in the region in question?			
9. Is the observed EEG-fMRI relation in line with how the EEG feature (at source level) relates to fMRI in other studies?			

Fig. 15.3 Checklist for interpreting results obtained from simultaneous recorded EEG and fMRI. The crucial question that most often arises when combining EEG and fMRI in a task setting is which of the regions that show a task effect (activation or deactivation) relate to the task induced changes in EEG features (e.g. changes in frequency-specific power, but also evoked potentials) that are observed. In this checklist, questions are listed that can help to address this issue. The more the questions 1–4 are answered with "yes", the stronger the case is for a relation between the task effects in both modalities. Assuming that a relation between task effects in EEG and fMRI is established through questions 1–4, whether the brain region in question is also the source location of the EEG feature. Questions 5–9 address this question, and the more they are answered with "yes", the stronger the case for a region being the source location of the EEG feature is. *Question 2: For instance, if EEG power increases monotonically working load (as in Scheeringa et al. 2009), a brain region related to this is expected to have either a monotonic increase or decrease with working memory load. **Question 4: For example, when EEG power increases with working memory load and a negative correlation is observed over trials (Question 1), if a region related to the working memory in EEG can be expected to show a monotonic decrease in fMRI activity with working memory load and a negative correlation of the effect of working memory load in both modalities over subjects

15.3 Conclusions

The studies discussed above indicate that neural oscillations and the BOLD signal are clearly related. Although sometimes a case for a direct link at source level is very plausible, simultaneous EEG and fMRI will not provide the ultimate proof of this, and it is however not always immediately clear whether there is a direct link, and it remains possible there are fMRI insensitive neural processes reflected in the EEG and EEG insensitive processes reflected in fMRI measurements. Both in resting state and in task contexts, in many cases, combined measurements can provide new insights that neither technique alone is not able to provide. We can now investigate how brain rhythms measured by EEG in rest relate differentially how networks of brain activity across the entire brain and vice versa which features measured by electrophysiology relate to specific brain networks and brain regions. With fMRI being measured at ever higher resolution which allows for the measurement of different cortical layers and small subcortical nuclei, this relation can be mapped in ever greater detail.

References

Archer JS, Abbott DF, Waites AB, Jackson GD (2003) fMRI "deactivation" of the posterior cingulate during generalized spike and wave. NeuroImage 20(4):1915–1922

Bandettini PA, Petridou N, Bodurka J (2005) Direct detection of neuronal activity with MRI: Fantasy, possibility, or reality? Appl Magn Reson 29:65–88

Bastos AM, Vezoli J, Bosman CA, Schoffelen JM, Oostenveld R, Dowdall JR, De Weerd P, Kennedy H, Fries P (2015) Visual areas exert feedforward and feedback influences through distinct frequency channels. Neuron 85:390–401

Berger H (1929) Über das elektrenkephalogramm des menschen. Arch Psychiatr Nervenkr 87:527–570

Bijsterbosch J (2017) Introduction to resting state fMRI functional connectivity, 1st edn. Oxford University Press, Oxford

Biswal B, Yetkin FZ, Haughton VM, Hyde JS (1995) Functional connectivity in the motor cortex of resting human brain using echo-planar MRI. Magn Reson Med 34:537–541

Bodurka J, Bandettini PA (2002) Toward direct mapping of neuronal activity: MRI detection of ultraweak, transient magnetic field changes. Magn Reson Med 47:1052–1058

Bodurka J, Jesmanowicz A, Hyde JS, Xu H, Estkowski L, Li SJ (1999) Current-induced magnetic resonance phase imaging. J Magn Reson 137:265–271

Bollimunta A, Chen Y, Schroeder CE, Ding M (2008) Neuronal mechanisms of cortical alpha oscillations in awake-behaving macaques. J Neurosci 28:9976–9988

Bollimunta A, Mo J, Schroeder CE, Ding M (2011) Neuronal mechanisms and attentional modulation of corticothalamic alpha oscillations. J Neurosci 31:4935–4943

Brookes MJ, Vrba J, Mullinger KJ, Geirsdottir GB, Yan WX, Stevenson CM, Bowtell R, Morris PG (2009) Source localisation in concurrent EEG/fMRI: applications at 7T. NeuroImage 45:440–452

Brookes MJ, Hale JR, Zumer JM, Stevenson CM, Francis ST, Barnes GR, Owen JP, Morris PG, Nagarajan SS (2011a) Measuring functional connectivity using MEG: methodology and comparison with fcMRI. NeuroImage 56:1082–1104

Brookes MJ, Woolrich M, Luckhoo H, Price D, Hale JR, Stephenson MC, Barnes GR, Smith SM, Morris PG (2011b) Investigating the electrophysiological basis of resting state networks using magnetoencephalography. Proc Natl Acad Sci U S A 108:16783–16788

Buffalo EA, Fries P, Landman R, Buschman TJ, Desimone R (2011) Laminar differences in gamma and alpha coherence in the ventral stream. Proc Natl Acad Sci U S A 108:11262–11267

Buzsáki G (2006) Rhythms of the brain. Oxford University Press, Oxford

Castellanos FX, Di Martino A, Craddock RC, Mehta AD, Milham MP (2013) Clinical applications of the functional connectome. NeuroImage 80:527–540

Curio G (2000) Ain't no rhythm fast enough: EEG bands beyond beta. J Clin Neurophysiol 17(4):339–340

Damoiseaux JS, Rombouts SARB, Barkhof F, Scheltens P, Stam CJ, Smith SM, Beckmann CF (2006) Consistent resting-state networks across healthy subjects. Proc Natl Acad Sci U S A 103:13848–13853

De Martino F, Moerel M, Ugurbil K, Goebel R, Yacoub E, Formisano E (2015) Frequency preference and attention effects across cortical depths in the human primary auditory cortex. Proc Natl Acad Sci U S A 112:16036–16041

De Pasquale F, Della Penna S, Snyder AZ, Lewis C, Mantini D, Marzetti L, Belardinelli P, Ciancetta L, Pizzella V, Romani GL, Corbetta M (2010) Temporal dynamics of spontaneous MEG activity in brain networks. Proc Natl Acad Sci U S A 107:6040–6045

De Tiege X, Harrison S, Laufs H, Boyd SG, Clark CA, Gadian DG, Neville BG, Vargha-Khadem F, Cross HJ (2007) Impact of interictal secondary-generalized activity on brain function in epileptic encephalopathy: an EEG–fMRI study. Epilepsy Behav 11(3):460–465

Debener S, Ullsperger M, Siegel M, Fiehler K, von Cramon DY, Engel AK (2005) Trial-by-trial coupling of concurrent electroencephalogram and functional magnetic resonance imaging identifies the dynamics of performance monitoring. J Neurosci 25:11730–11737

Debener S, Ullsperger M, Siegel M, Engel AK (2006) Single-trial EEG-fMRI reveals the dynamics of cognitive function. Trends Cogn Sci 10:558–563

Douglas RJ, Martin KA (2004) Neuronal circuits of the neocortex. Annu Rev Neurosci 27:419–451

Fair DA, Schlaggar BL, Cohen AL, Miezin FM, Dosenbach NU, Wenger KK, Fox MD, Snyder AZ, Raichle ME, Petersen SE (2007) A method for using blocked and event-related fMRI data to study "resting state" functional connectivity. NeuroImage 35(1):396–405

Feige B, Scheffler K, Esposito F, Di Salle F, Hennig J, Seifritz E (2005) Cortical and subcortical correlates of electroencephalographic alpha rhythm modulation. J Neurophysiol 93(5):2864–2872

Fox PT, Lancaster JL (2002) Opinion: mapping context and content: the BrainMap model. Nat Rev Neurosci 3:319–321

Fox MD, Raichle ME (2007) Spontaneous fluctuations in brain activity observed with functional magnetic resonance imaging. Nat Rev Neurosci 8(9):700–711

Fox MD, Snyder AZ, Vincent JL, Raichle ME (2007) Intrinsic fluctuations within cortical systems account for intertrial variability in human behavior. Neuron 56(1):171–184

Fries P (2015) Rhythms for cognition: communication through coherence. Neuron 88:220–235

Fries P, Scheeringa R, Oostenveld R (2008) Finding gamma. Neuron 58:303–305

Friston KJ, Buechel C, Fink GR, Morris J, Rolls E, Dolan RJ (1997) Psychophysiological and modulatory interactions in neuroimaging. NeuroImage 6:218–229

Friston KJ, Holmes AP, Price CJ, Buchel C, Worsley KJ (1999) Multisubject fMRI studies and conjunction analyses. NeuroImage 10(4):385–396

Gevins A, Smith ME, McEvoy L, Yu D (1997) High-resolution EEG mapping of cortical activation related to working memory: effects of task difficulty, type of processing, and practice. Cereb Cortex 7:374–385

Gibbs FA, Davis H, Lennox WG (1935) The electro-encephalogram in epilepsy and in conditions of impaired consciousness. Arch NeurPsychcol 34(6):1133–1148

Gilbert CD (1983) Microcircuitry of the visual cortex. Annu Rev Neurosci 6:217–247

Goense JB, Logothetis NK (2008) Neurophysiology of the BOLD fMRI signal in awake monkeys. Curr Biol 18:631–640

Goldman RI, Stern JM, Engel J Jr, Cohen MS (2002) Simultaneous EEG and fMRI of the alpha rhythm. Neuroreport 13(18):2487–2492

Gotman J, Grova C, Bagshaw A, Kobayashi E, Aghakhani Y, Dubeau F (2005) Generalized epileptic discharges show thalamocortical activation and suspension of the default state of the brain. Proc Natl Acad Sci U S A 102(42):15236–15240

Gotman J, Kobayashi E, Bagshaw AP, Benar CG, Dubeau F (2006) Combining EEG and fMRI: a multimodal tool for epilepsy research. J Magn Reson Imaging 23(6):906–920

Gruber O, Indefrey P, Steinmetz H, Kleinschmidt A (2001) Dissociating neural correlates of cognitive components in mental calculation. Cereb Cortex 11(4):350–359

Haegens S, Barczak A, Musacchia G, Lipton ML, Mehta AD, Lakatos P, Schroeder CE (2015) Laminar profile and physiology of the alpha rhythm in primary visual, auditory, and somatosensory regions of neocortex. J Neurosci 35:14341–14352

Hamandi K, Salek-Haddadi A, Laufs H, Liston A, Friston K, Fish DR, Duncan JS, Lemieux L (2006) EEG–fMRI of idiopathic and secondarily generalized epilepsies. NeuroImage 31(4):1700–1710

Hanslmayr S, Volberg G, Wimber M, Raabe M, Greenlee MW, Bauml KH (2011) The relationship between brain oscillations and BOLD signal during memory formation: a combined EEG-fMRI study. J Neurosci 31:15674–15680

Hoogenboom N, Schoffelen JM, Oostenveld R, Parkes LM, Fries P (2006) Localizing human visual gamma-band activity in frequency, time and space. NeuroImage 29:764–773

Hoogenboom N, Schoffelen JM, Oostenveld R, Fries P (2010) Visually induced gamma-band activity predicts speed of change detection in humans. NeuroImage 51:1162–1167

Horovitz SG, Fukunaga M, de Zwart JA, van Gelderen P, Fulton SC, Balkin TJ, Duyn JH (2008) Low frequency BOLD fluctuations during resting wakefulness and light sleep: a simultaneous EEG-fMRI study. Hum Brain Mapp 29(6):671–682

Ishii R, Shinosaki K, Ukai S, Inouye T, Ishihara T, Yoshimine T, Hirabuki N, Asada H, Kihara T, Robinson SE, Takeda M (1999) Medial prefrontal cortex generates frontal midline theta rhythm. Neuroreport 10:675–679

Jensen O (2006) Maintenance of multiple working memory items by temporal segmentation. Neuroscience 139:237–249

Jensen O, Lisman JE (1998) An oscillatory short-term memory buffer model can account for data on the Sternberg task. J Neurosci 18:10688–10699

Jensen O, Mazaheri A (2010) Shaping functional architecture by oscillatory alpha activity: gating by inhibition. Front Hum Neurosci 4:186

Jensen O, Tesche CD (2002) Frontal theta activity in humans increases with memory load in a working memory task. Eur J Neurosci 15:1395–1399

Jensen O, Gips B, Bergmann TO, Bonnefond M (2014) Temporal coding organized by coupled alpha and gamma oscillations prioritize visual processing. Trends Neurosci 37:357–369

Kaufmann C, Wehrle R, Wetter TC, Holsboer F, Auer DP, Pollmacher T, Czisch M (2006) Brain activation and hypothalamic functional connectivity during human non-rapid eye movement sleep: an EEG/fMRI study. Brain 129(3):655–667

Kjaer TW, Law I, Wiltschiotz G, Paulson OB, Madsen PL (2002) Regional cerebral blood flow during light sleep: a H(2)(15)O-PET study. J Sleep Res 11(3):201–207

Klimesch W (1999) EEG alpha and theta oscillations reflect cognitive and memory performance: a review and analysis. Brain Res Brain Res Rev 29:169–195

Klimesch W, Sauseng P, Hanslmayr S (2007) EEG alpha oscillations: the inhibition-timing hypothesis. Brain Res Rev 53:63–88

Kobayashi E, Bagshaw AP, Benar CG, Aghakhani Y, Andermann F, Dubeau F, Gotman J (2006a) Temporal and extratemporal BOLD responses to temporal lobe interictal spikes. Epilepsia 47(2):343–354

Kobayashi E, Bagshaw AP, Grova C, Dubeau F, Gotman J (2006b) Negative BOLD responses to epileptic spikes. Hum Brain Mapp 27(6):488–497

Koch SP, Werner P, Steinbrink J, Fries P, Obrig H (2009) Stimulus-induced and state-dependent sustained gamma activity is tightly coupled to the hemodynamic response in humans. J Neurosci 29:13962–13970

Kok P, Bains LJ, van Mourik T, Norris DG, de Lange FP (2016) Selective activation of the deep layers of the human primary visual cortex by top-down feedback. Curr Biol 26:371–376
Laird AR, Lancaster JL, Fox PT (2005) BrainMap: the social evolution of a human brain mapping database. Neuroinformatics 3:65–78
Laufs H, Duncan JS (2007) Electroencephalography/functional MRI in human epilepsy: what it currently can and cannot do. Curr Opin Neurol 20(4):417–423
Laufs H, Kleinschmidt A, Beyerle A, Eger E, Salek-Haddadi A, Preibisch C, Krakow K (2003a) EEG-correlated fMRI of human alpha activity. NeuroImage 19:1463–1476
Laufs H, Krakow K, Sterzer P, Eger E, Beyerle A, Salek-Haddadi A, Kleinschmidt A (2003b) Electroencephalographic signatures of attentional and cognitive default modes in spontaneous brain activity fluctuations at rest. Proc Natl Acad Sci U S A 100(19):11053–11058
Laufs H, Hamandi K, Salek-Haddadi A, Kleinschmidt AK, Duncan JS, Lemieux L (2006a) Temporal lobe interictal epileptic discharges affect cerebral activity in "default mode" brain regions. Hum Brain Mapp 28(10):1923–1932
Laufs H, Hamandi K, Walker MC, Scott C, Smith S, Duncan JS, Lemieux L (2006b) EEG–fMRI mapping of asymmetrical delta activity in a patient with refractory epilepsy is concordant with the epileptogenic region determined by intracranial EEG. Magn Reson Imaging 24(4):367–371
Laufs H, Holt JL, Elfont R, Krams M, Paul JS, Krakow K, Kleinschmidt A (2006c) Where the BOLD signal goes when alpha EEG leaves. NeuroImage 31(4):1408–1418
Laufs H, Lengler U, Hamandi K, Kleinschmidt A, Krakow K (2006d) Linking generalized spike-and-wave discharges and resting state brain activity by using EEG/fMRI in a patient with absence seizures. Epilepsia 47(2):444–448
Laufs H, Walker MC, Lund TE (2007) "Brain activation and hypothalamic functional connectivity during human non-rapid eye movement sleep: an EEG/fMRI study"—its limitations and an alternative approach. Brain 130(7):e75
Laureys S, Owen AM, Schiff ND (2004) Brain function in coma, vegetative state, and related disorders. Lancet Neurol 3(9):537–546
Lawrence SJD, van Mourik T, Kok P, Koopmans PJ, Norris DG, de Lange FP (2018) Laminar organization of working memory signals in human visual cortex. Curr Biol 28:e3434
Lawrence SJ, Norris DG, de Lange FP (2019) Dissociable laminar profiles of concurrent bottom-up and top-down modulation in the human visual cortex. elife 8:44422
Lehmann D, Faber PL, Galderisi S, Herrmann WM, Kinoshita T, Koukkou M, Mucci A, Pascual-Marqui RD, Saito N, Wackermann J et al (2005) EEG microstate duration and syntax in acute, medication-naive, first-episode schizophrenia: a multi-center study. Psychiatry Res 138(2):141–156
Lewis LD, Setsompop K, Rosen BR, Polimeni JR (2016) Fast fMRI can detect oscillatory neural activity in humans. Proc Natl Acad Sci U S A 113:E6679–E6685
Logothetis NK, Pauls J, Augath M, Trinath T, Oeltermann A (2001) Neurophysiological investigation of the basis of the fMRI signal. Nature 412(6843):150–157
Lopes da Silva F (2004) Functional localization of brain sources using EEG and/or MEG data: volume conductor and source models. Magn Reson Imaging 22(10):1533–1538
Lopes da Silva F (2013) EEG and MEG: relevance to neuroscience. Neuron 80:1112–1128
Luo QF, Jiang X, Gao JH (2011) Detection of neuronal current MRI in human without BOLD contamination. Magn Reson Med 66:492–497
Maier A, Adams GK, Aura C, Leopold DA (2010) Distinct superficial and deep laminar domains of activity in the visual cortex during rest and stimulation. Front Syst Neurosci 4:31
Maier A, Aura CJ, Leopold DA (2011) Infragranular sources of sustained local field potential responses in macaque primary visual cortex. J Neurosci 31:1971–1980
Makeig S, Debener S, Onton J, Delorme A (2004a) Mining event-related brain dynamics. Trends Cogn Sci 8:204–210
Makeig S, Delorme A, Westerfield M, Jung TP, Townsend J, Courchesne E, Sejnowski TJ (2004b) Electroencephalographic brain dynamics following manually responded visual targets. PLoS Biol 2:e176

Mantini D, Perrucci MG, Del Gratta C, Romani GL, Corbetta M (2007) Electrophysiological signatures of resting state networks in the human brain. Proc Natl Acad Sci U S A 104(32):13170–13175

Maquet P (2000) Functional neuroimaging of normal human sleep by positron emission tomography. J Sleep Res 9(3):207–231

Markov NT, Kennedy H (2013) The importance of being hierarchical. Curr Opin Neurobiol 23:187–194

Markov NT, Vezoli J, Chameau P, Falchier A, Quilodran R, Huissoud C, Lamy C, Misery P, Giroud P, Ullman S, Barone P, Dehay C, Knoblauch K, Kennedy H (2014) Anatomy of hierarchy: feedforward and feedback pathways in macaque visual cortex. J Comp Neurol 522:225–259

Martinez-Montes E, Valdes-Sosa PA, Miwakeichi F, Goldman RI, Cohen MS (2004) Concurrent EEG/fMRI analysis by multiway partial least squares. NeuroImage 22:1023–1034

Mazoyer B, Zago L, Mellet E, Bricogne S, Etard O, Houde O, Crivello F, Joliot M, Petit L, Tzourio-Mazoyer N (2001) Cortical networks for working memory and executive functions sustain the conscious resting state in man. Brain Res Bull 54(3):287–298

Mesulam MM (1990) Large-scale neurocognitive networks and distributed processing for attention, language, and memory. Ann Neurol 28(5):597–613

Mesulam MM (1998) From sensation to cognition. Brain 121(6):1013–1052

Michalareas G, Vezoli J, van Pelt S, Schoffelen JM, Kennedy H, Fries P (2016) Alpha-beta and gamma rhythms subserve feedback and feedforward influences among human visual cortical areas. Neuron 89:384–397

Michel CM, Murray MM, Lantz G, Gonzalez S, Spinelli L, Grave de Peralta R (2004) EEG source imaging. Clin Neurophysiol 115(10):2195–2222

Miwakeichi F, Martinez-Montes E, Valdes-Sosa PA, Nishiyama N, Mizuhara H, Yamaguchi Y (2004) Decomposing EEG data into space-time-frequency components using parallel factor analysis. NeuroImage 22:1035–1045

Moosmann M, Ritter P, Krastel I, Brink A, Thees S, Blankenburg F, Taskin B, Obrig H, Villringer A (2003) Correlates of alpha rhythm in functional magnetic resonance imaging and near infrared spectroscopy. NeuroImage 20(1):145–158

Muckli L, De Martino F, Vizioli L, Petro LS, Smith FW, Ugurbil K, Goebel R, Yacoub E (2015) Contextual feedback to superficial layers of V1. Curr Biol 25:2690–2695

Munk MH, Neuenschwander S (2000) High-frequency oscillations (20 to 120 Hz) and their role in visual processing. J Clin Neurophysiol 17(4):341–360

Murakami S, Okada Y (2006) Contributions of principal neocortical neurons to magnetoencephalography and electroencephalography signals. J Physiol 575:925–936

Muthukumaraswamy SD, Singh KD (2013) Visual gamma oscillations: the effects of stimulus type, visual field coverage and stimulus motion on MEG and EEG recordings. NeuroImage 69:223–230

Niessing J, Ebisch B, Schmidt KE, Niessing M, Singer W, Galuske RA (2005) Hemodynamic signals correlate tightly with synchronized gamma oscillations. Science 309(5736):948–951

Nunez PL, Wingeier BM, Silberstein RB (2001) Spatial-temporal structures of human alpha rhythms: theory, microcurrent sources, multiscale measurements, and global binding of local networks. Hum Brain Mapp 13(3):125–164

Onton J, Delorme A, Makeig S (2005) Frontal midline EEG dynamics during working memory. NeuroImage 27:341–356

Parkes LM, de Lange FP, Fries P, Toni I, Norris DG (2007) Inability to directly detect magnetic field changes associated with neuronal activity. Magn Reson Med 57:411–416

Petridou N, Plenz D, Silva AC, Loew M, Bodurka J, Bandettini PA (2006) Direct magnetic resonance detection of neuronal electrical activity. Proc Natl Acad Sci U S A 103:16015–16020

Polimeni JR, Fischl B, Greve DN, Wald LL (2010) Laminar analysis of 7T BOLD using an imposed spatial activation pattern in human V1. NeuroImage 52:1334–1346

Raichle ME, Snyder AZ (2007) A default mode of brain function: a brief history of an evolving idea. NeuroImage 37(4):1083–1090

Raichle ME, MacLeod AM, Snyder AZ, Powers WJ, Gusnard DA, Shulman GL (2001) A default mode of brain function. Proc Natl Acad Sci U S A 98(2):676–682

Rechtschaffen A, Kales AA (1968) A manual of standardized terminology, techniques and scoring system for sleep stages of human subjects. US Public Health Service, Washington, pp 1463–1476

Sadaghiani S, Scheeringa R, Lehongre K, Morillon B, Giraud AL, Kleinschmidt A (2010) Intrinsic connectivity networks, alpha oscillations, and tonic alertness: a simultaneous electroencephalography/functional magnetic resonance imaging study. J Neurosci 30:10243–10250

Sadaghiani S, Scheeringa R, Lehongre K, Morillon B, Giraud AL, D'Esposito M, Kleinschmidt A (2012) alpha-band phase synchrony is related to activity in the fronto-parietal adaptive control network. J Neurosci 32:14305–14310

Salek-Haddadi A, Lemieux L, Merschhemke M, Friston KJ, Duncan JS, Fish DR (2003) Functional magnetic resonance imaging of human absence seizures. Ann Neurol 53(5):663–667

Schabus M, Dang-Vu TT, Albouy G, Balteau E, Boly M, Carrier J, Darsaud A, Degueldre C, Desseilles M, Gais S et al (2007) Hemodynamic cerebral correlates of sleep spindles during human non-rapid eye movement sleep. Proc Natl Acad Sci U S A 104(32):13164–13169

Scheeringa R, Bastiaansen MC, Petersson KM, Oostenveld R, Norris DG, Hagoort P (2008) Frontal theta EEG activity correlates negatively with the default mode network in resting state. Int J Psychophysiol 67(3):242–251

Siniatchkin M, van Baalen A, Jacobs J, Moeller F, Moehring J, Boor R, Wolff S, Jansen O, Stephani U (2007) Different neuronal networks are associated with spikes and slow activity in hypsarrhythmia. Epilepsia 48(12):2312–2321. https://doi.org/10.1111/j.1528-1167.2007.01195.x

Sorg C, Riedl V, Muhlau M, Calhoun VD, Eichele T, Laer L, Drzezga A, Forstl H, Kurz A, Zimmer C et al (2007) Selective changes of resting-state networks in individuals at risk for Alzheimer's disease. Proc Natl Acad Sci U S A 104(47):18760–18765

Stam CJ, Montez T, Jones BF, Rombouts SA, van der Made Y, Pijnenburg YA, Scheltens P (2005) Disturbed fluctuations of resting state EEG synchronization in Alzheimers disease. Clin Neurophysiol 116(3):708–715

Steriade M (1995) Brain activation, then (1949) and now: coherent fast rhythms in corticothalamic networks. Arch Ital Biol 134(1):5–20

Steriade M (2005) Sleep, epilepsy and thalamic reticular inhibitory neurons. Trends Neurosci 28(6):317–324

Urrestarazu E, Chander R, Dubeau F, Gotman J (2007) Interictal high-frequency oscillations (100–500 Hz) in the intracerebral EEG of epileptic patients. Brain 130(Pt 9):2354–2366

Sammer G, Blecker C, Gebhardt H, Bischoff M, Stark R, Morgen K, Vaitl D (2007) Relationship between regional hemodynamic activity and simultaneously recorded EEG-theta associated with mental arithmetic-induced workload. Hum Brain Mapp 28:793–803

Sammer G, Blecker C, Gebhardt H, Kirsch P, Stark R, Vaitl D (2005) Acquisition of typical EEG waveforms during fMRI: SSVEP, LRP, and frontal theta. NeuroImage 24:1012–1024

Scheeringa R, Fries P (2017) Cortical layers, rhythms and BOLD signals. NeuroImage 197:689–698

Scheeringa R, Fries P, Petersson KM, Oostenveld R, Grothe I, Norris DG, Hagoort P, Bastiaansen MC (2011) Neuronal dynamics underlying high- and low-frequency EEG oscillations contribute independently to the human BOLD signal. Neuron 69:572–583

Scheeringa R, Koopmans PJ, van Mourik T, Jensen O, Norris DG (2016) The relationship between oscillatory EEG activity and the laminar-specific BOLD signal. Proc Natl Acad Sci U S A 113:6761–6766

Scheeringa R, Petersson KM, Kleinschmidt A, Jensen O, Bastiaansen MC (2012) EEG alpha power modulation of fMRI resting-state connectivity. Brain Connect 2:254–264

Scheeringa R, Petersson KM, Oostenveld R, Norris DG, Hagoort P, Bastiaansen MC (2009) Trial-by-trial coupling between EEG and BOLD identifies networks related to alpha and theta EEG power increases during working memory maintenance. NeuroImage 44:1224–1238

Shmuel A, Augath M, Oeltermann A, Logothetis NK (2006) Negative functional MRI response correlates with decreases in neuronal activity in monkey visual area V1. Nat Neurosci 9:569–577

Smith SM, Fox PT, Miller KL, Glahn DC, Fox PM, Mackay CE, Filippini N, Watkins KE, Toro R, Laird AR, Beckmann CF (2009) Correspondence of the brain's functional architecture during activation and rest. Proc Natl Acad Sci U S A 106:13040–13045

Spaak E, Bonnefond M, Maier A, Leopold DA, Jensen O (2012) Layer-specific entrainment of gamma-band neural activity by the alpha rhythm in monkey visual cortex. Curr Biol 22:2313–2318

Sundaram P, Nummenmaa A, Wells W, Orbach D, Orringer D, Mulkern R, Okada Y (2016) Direct neural current imaging in an intact cerebellum with magnetic resonance imaging. NeuroImage 132:477–490

Sundaram P, Wells WM, Mulkern RV, Bubrick EJ, Bromfield EB, Munch M, Orbach DB (2010) Fast human brain magnetic resonance responses associated with epileptiform spikes. Magn Reson Med 64:1728–1738

Tang L, Avison MJ, Gatenby JC, Gore JC (2008) Failure to direct detect magnetic field dephasing corresponding to ERP generation. Magn Reson Imaging 26:484–489

Troebinger L, Lopez JD, Lutti A, Bestmann S, Barnes G (2014) Discrimination of cortical laminae using MEG. NeuroImage 102(2):885–893

Truong TK, Roberts KC, Woldorff MG, Song AW (2019) Toward direct MRI of neuro-electromagnetic oscillations in the human brain. Magn Reson Med 81:3462–3475

van Kerkoerle T, Self MW, Dagnino B, Gariel-Mathis MA, Poort J, van der Togt C, Roelfsema PR (2014) Alpha and gamma oscillations characterize feedback and feedforward processing in monkey visual cortex. Proc Natl Acad Sci U S A 111:14332–14341

van Pelt S, Boomsma DI, Fries P (2012) Magnetoencephalography in twins reveals a strong genetic determination of the peak frequency of visually induced gamma-band synchronization. J Neurosci 32:3388–3392

Varela F, Lachaux JP, Rodriguez E, Martinerie J (2001) The brainweb: phase synchronization and large-scale integration. Nat Rev Neurosci 2:229–239

Viswanathan A, Freeman RD (2007) Neurometabolic coupling in cerebral cortex reflects synaptic more than spiking activity. Nat Neurosci 10:1308–1312

Vulliemoz S, Carmichael DW, Rosenkranz K, Diehl B, Rodionov R, Walker MC, McEvoy AW, Lemieux L (2011) Simultaneous intracranial EEG and fMRI of interictal epileptic discharges in humans. NeuroImage 54:182–190

Yuan H, Liu T, Szarkowski R, Rios C, Ashe J, He B (2010) Negative covariation between task-related responses in alpha/beta-band activity and BOLD in human sensorimotor cortex: an EEG and fMRI study of motor imagery and movements. NeuroImage 49:2596–2606

Zahneisen B, Ernst T, Poser BA (2015) SENSE and simultaneous multislice imaging. Magn Reson Med 74:1356–1362

Zumer JM, Scheeringa R, Schoffelen JM, Norris DG, Jensen O (2014) Occipital alpha activity during stimulus processing gates the information flow to object-selective cortex. PLoS Biol 12:e1001965

Sleep

16

Michael Czisch and Renate Wehrle

Abbreviations

ACC	Anterior cingulate cortex
(r)CBF	(Regional) cerebral blood flow
DMN	Default mode network
EMG	Electromyography
EOG	Electrooculography
EPI	Echo planar imaging
IPL	Inferior parietal lobule
KC	K-complex
MEG	Magnetencephalography
mPFC	Medial prefrontal cortex
NBR	Negative BOLD response
RSN	Resting state network
PCC	Posterior cingulate cortex
PET	Positron emission tomography
PFC	Prefrontal cortex
PGO	Ponto-geniculo-occipital (waves)
PHG	Parahippocampal gyrus
PSG	Polysomnography
RSpC	Retrosplenial cortex
SPECT	Single photon emission computer tomography
STG	Superior temporal gyrus
SWS	Slow-wave sleep

To appear in: Mulert & Lemieux, EEG–fMRI

M. Czisch (✉) · R. Wehrle
Max Planck Institute of Psychiatry, Munich, Germany
e-mail: czisch@psych.mpg.de

C. Mulert, L. Lemieux (eds.), *EEG - fMRI*,
https://doi.org/10.1007/978-3-031-07121-8_16

16.1 FMRI in Sleep Research

16.1.1 Sleep

The time spent asleep consumes about one third of our lifetime. In contrast to anesthesia or a comatose state, the perceptual disengagement from the environment and alteration ("loss") of consciousness can be reversed during sleep upon intense stimulation. A large body of knowledge on sleep-related processes has been collected in the last decades; however, the precise functions of sleep have yet to be disclosed.

Most of our current understanding of cortical activity across the different stages of vigilance is derived from EEG recordings. Concomitant to falling asleep, the changes in brain activity on a cellular level—namely switching from tonic to burst mode firing with increased periods of hyperpolarization—induce typical changes in EEG (Steriade 2003; Carskadon and Dement 2017). Altered surface EEG during sleep in humans has first been documented as early as 1929 by Berger (1929), later followed by Loomis' description of specific characteristics in sleep recordings like K-complexes (KCs) and sleep spindles (Loomis et al. 1938). The misconception of sleep as a cessation of brain activity as compared to the reticular activation during wakefulness was finally overthrown in 1953, when Eugene Aserinsky and Nathaniel Kleitman first described an active brain state accompanied by rapid eye movements (REM) recurring at regular intervals within sleep (Aserinsky and Kleitman 1953). Awakenings from this state of high cortical activity go along with higher incidences of vivid dream reports that putatively accompany the activated cortical states. REM sleep shares many features with wakefulness and is therefore also referred to as "paradoxical sleep." A further characteristic of REM sleep is the loss of voluntary muscle control. Based on these distinct features, international standards for scoring sleep stages have been established which rely not only on EEG but also include electrooculogram (EOG) and electromyogram (EMG) criteria (Rechtschaffen and Kales 1968; Silber et al. 2007). For clinical purposes, this electrophysiological triad is usually extended by acquisition of cardiovascular activity (electrocardiogram, pulse oximetry), breathing parameters (thoracic and abdominal movements, effective breathing), snoring, and EMG recordings of particular muscle groups (e.g., anterior tibialis muscle). This multimodal recording (polysomnography, PSG) represents the standard way of registering sleep in humans.

The increasing depth of sleep is conventionally subdivided into stages characterized by specific EEG criteria: switching from predominance of high-frequency rhythms (gamma, beta, and alpha) during active wakefulness to frequency slowing toward theta, delta, and slow oscillations, including distinct graphoelements like KCs and sleep spindles (Fig. 16.1).

The stages of NREM sleep are paralleled by increasing arousal thresholds. NREM sleep makes up for about 80% of the total sleep time, and about 50% of the night is spent in light NREM sleep stage 2.

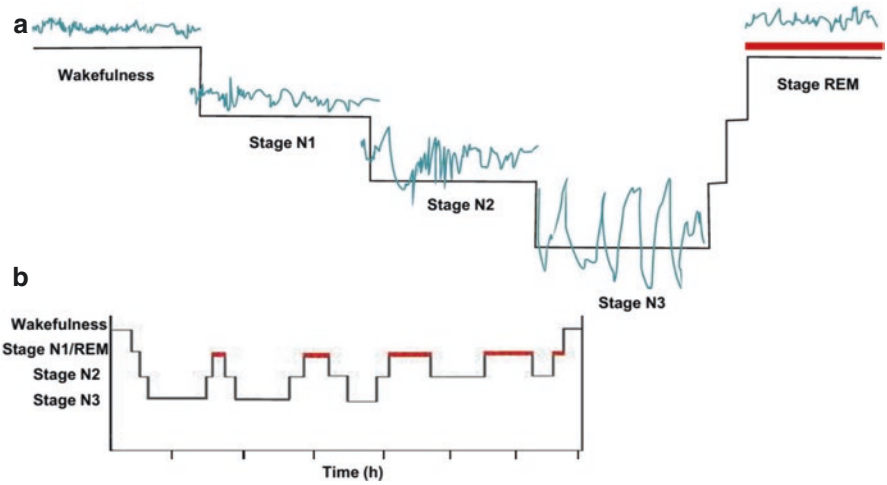

Fig. 16.1 Sleep EEG and sleep cycles in human sleep. Figure (**a**) depicts typical EEG activity during the different vigilance stages: wakefulness is characterized by high-frequency (gamma, beta) activity that is shifting toward slower theta rhythms in sleep stage N1. Theta is also the background activity during sleep stage N2, which in addition is interspersed with sleep spindles (12–15 Hz) and K-complexes. Sleep stage N3, also termed slow wave sleep, is dominated by increasing amounts of delta activity. During REM sleep, the cortical activation with high-frequency activities similar to wakefulness prevails. Figure (**b**) summarizes the continuous alternation of sleep cycles during the course of the night, with typical decreases of slow wave sleep and increases of REM sleep across a night

Timing and amount of sleep is regulated both by a homeostatic (increased sleep pressure after prolonged wakefulness) and by a circadian process (tendency to fall asleep according to constantly fluctuating physiological rhythms). Based on these rhythms, paced by the suprachiasmatic nucleus, sleep is organized in progressive alternations of the NREM sleep stages N1 to N3 and REM sleep, in cycles lasting about 90 min on average. NREM sleep stage N3, also termed slow-wave sleep (SWS) because of the prevailing delta slow oscillatory EEG activity reflecting homeostatic sleep pressure, predominates in the first sleep cycles. REM sleep episodes prevail in the second half of the night (Pace-Schott and Hobson 2002; Carskadon and Dement 2017).

Spectral EEG composition during sleep shows characteristic topographic and coherence patterns (Achermann and Borbely 1998; Finelli et al. 2001b; De Gennaro et al. 2005). A prominent example of typical regional-specific patterns is given by the hyperfrontality of slow oscillations. Additionally, homeostatic sleep pressure and individual genetic factors influence sleep structure and the spectral power distribution (Finelli et al. 2001a; Tucker et al. 2007; Ambrosius et al. 2008; Tarokh et al. 2011).

Parallel to the changes in neuronal activity, arousal thresholds, consciousness states, and the processing of information are dramatically altered during sleep: The

reduced responsiveness to environmental stimuli with first signs of sleep oscillations is partially mediated by attenuated transmission via the thalamus, which serves as central input gate for sensory stimuli. Event-related EEG components typical of more complex information processing during wakefulness are replaced by waveforms with similar behavior and longer latencies (e.g., a P450 component). Some large-amplitude ERP components specifically appear in NREM sleep and possibly reflect inhibitory processes (for review, see Bastuji and Garcia-Larrea 1999; Colrain and Campbell 2007). Still, strongly deviant or highly relevant stimuli may lead to awakenings. Contrary to NREM sleep, most late cortical potentials and the ability to discriminate complex stimuli are partially restored during REM sleep. The apparent lack of integrating external information in REM sleep is not mediated by thalamocortical inhibition but assumed to occur due to altered prefrontal activity and generally altered connectivity patterns, possibly dominated by intrinsical loops (Llinas and Pare 1991). Inhibition of sensory information has been further linked to NREM sleep spindles that can reduce postsynaptic potentials of thalamic neurons. External stimulation may elicit KCs as a typical sleep-related expression of stimulus response, giving KCs a special role within the sleep slow waves (Halasz 2016). As during the deepening of NREM sleep cortical cells "join" the rhythms, widespread synchronous slow oscillations dominate and thus alter neuronal functionality (Steriade 2006).

16.1.2 Imaging Sleep

Various neuroimaging methods do qualify for addressing sleep-specific questions, and each method has its own advantages and drawbacks. Several excellent reviews condense findings on neuroimaging in sleep and illustrate their impact on sleep and brain research and characterization of sleep disorders (Drummond et al. 2004; Dang-Vu et al. 2007; Nofzinger and Maquet 2017). In brief, the first studies applied positron emissions tomography with fluorodeoxyglucose (FDG-PET), a radioactive tracer that averages neuronal glucose uptake over about half an hour. The long decay times allow for application of the tracer in the general setting of a common sleep laboratory, with a delayed read-out in the PET scanner during which the subject may even be awake. Temporal resolution of the PET imaging procedure was later enhanced by application of $H_2{}^{15}O$-PET. This tracer also opened the possibility to repeatedly scan an individual but introduced the drawback that participants now need to sleep inside the PET scanner. A related method, single photon emission computed tomography (SPECT), provides similar information as PET and could, e.g., document dissociated states of motor arousal and persisting cortical sleep during sleepwalking (Bassetti et al. 2000).

As a further method, high-density EEG can reveal important spatial information as, e.g., on the site of origin and the traveling of slow oscillations, on experience-dependent local alterations in slow-wave activity, or even brain maturation (Massimini et al. 2003; Huber et al. 2006; Kurth et al. 2010). Closely related to

EEG, magnetencephalography (MEG) measures the magnetic fields induced by the electrical neuronal currents which form the EEG response. Temporal resolution of MEG is in the millisecond range, but signals from deep brain structures cannot be recorded straightforwardly. MEG was applied in sleep research to investigate, e.g., REM sleep saccades (Ioannides et al. 2004) or brain rhythms like sleep spindles (Klinzing et al. 2016).

Taken together, PET, SPECT, MEG, and high-density EEG studies have consistently confirmed hypotheses from animal studies that sleep is not a single invariable brain state but that brain activity strongly depends on sleep stages: compared to wakefulness, NREM sleep is characterized by a global decrease in cerebral metabolism and blood flow and furthermore by regional CBF decreases in the pons, the mesencephalon, thalamus, basal ganglia and basal forebrain, hypothalamus, and various other cortical regions including the prefrontal cortex (PFC) and anterior cingulate cortex (ACC). For REM sleep, on the other hand, high neuronal activity was consistently reported. Activity increased, e.g., in the pontine tegmentum, thalamus, amygdala, hippocampus, and ACC, as compared to both wakefulness and NREM sleep, but less activity compared to wakefulness was reported in the dorsolateral PFC, posterior cingulate cortex (PCC), precuneus, and inferior parietal cortex.

16.1.3 EEG and fMRI in Sleep Research

In some fMRI experiments in sleeping subjects without using concomitant EEG recordings, missing behavioral reactions are being used to indicate that the participant had fallen asleep. However, unequivocal sleep can only be confirmed with concomitant EEG recordings, as sleep is basically defined by EEG criteria. Acquisition of simultaneous EEG recordings during fMRI is therefore mandatory to differentiate the characteristics of altered brain activity during sleep. Additional EOG and EMG recordings are needed to allow for classical scoring of all sleep stages according to international guidelines (Rechtschaffen and Kales 1968; Silber et al. 2007).

The introduction of nonmagnetic EEG recording systems which can be operated in strong magnetic fields, and improvement in EEG postprocessing techniques enabled researchers to routinely acquire simultaneous EEG/fMRI at clinical field strengths (up to 3 Tesla) or even in ultrahigh field scanners up to 9.4 Tesla (Abbasi et al. 2015; Jorge et al. 2015). Thus, it is possible to obtain fMRI data during polysomnographically verified, unambiguous sleep.

The higher spatial and temporal resolution of simultaneous fMRI and EEG measurements in comparison to other imaging methods offers impressive new ways to target sleep-related phenomena that have so far been restricted to invasive measurements in animal models.

Apart from serving to define the sleep stages, sleep electrophysiology hosts a variety of valuable information: characteristic EEG graphoelements like KCs and

sleep spindles, arousals and fluctuating microstates, changing spectral compositions, evoked potentials, rapid eye movements. Studying the associated brain activity with fMRI is only feasible by the help of simultaneous electrophysiological recordings in sufficient high quality.

Nevertheless, some research questions may still benefit from utilizing each method separately:

- Studies focusing only on electrophysiological measures (without fMRI) might be preferable when targeting continuous all-night recordings, when studying participants other than good sleepers, when studying intervention effects on sleep, especially on sleep structure, and finally in sleep disorders, especially when increased motor activity is involved.
- Studies focusing on fMRI (without EEG recording) might be preferable when targeting specific cerebral functions possibly influenced by sleep, e.g., memory consolidation, when studying influences of sleep restriction or sleep deprivation (Drummond and Brown 2001; Spoormaker et al. 2012b; Peters et al. 2014) and when studying dysfunctional states related to sleep. The interplay of brain areas disclosing aspects of the functional significance of sleep may also well be studied using fMRI without simultaneous EEG acquisition.

16.2 fMRI During Sleep: Technical Challenges

Many aspects of polysomnographic sleep fMRI experiments share common problems with simultaneous EEG/fMRI recordings in general and are being described extensively elsewhere in this book (see the Chaps. 1, 7, 8, and 9). Nevertheless, specific difficulties arise when investigating sleep. Depending on hardware and software facilities available and linked to specific research questions, several of the following topics may arise:

16.2.1 Sleep Recording

16.2.1.1 Multimodality of Sleep Recording

As outlined in the introduction, the proper definition of sleep in humans is based not only on EEG but also further on EOG and EMG criteria. This poses additional requirements on the hardware facilities, like availability of additional electrodes and channels, with special wiring for longer cables. Potential benefit can be gained from bipolar recordings, e.g., of EMG recordings. Furthermore, postprocessing techniques must offer satisfying solutions to gain high quality of all the electrophysiological data recorded, as otherwise events of interest cannot be unambiguously distinguished. Effective solutions to eliminate ECG distortions are of major importance. Special requirements for high-frequency signals like EMG may be needed (van Duinen et al. 2005; Wehrle et al. 2005; van Rootselaar et al. 2007) (Fig. 16.2).

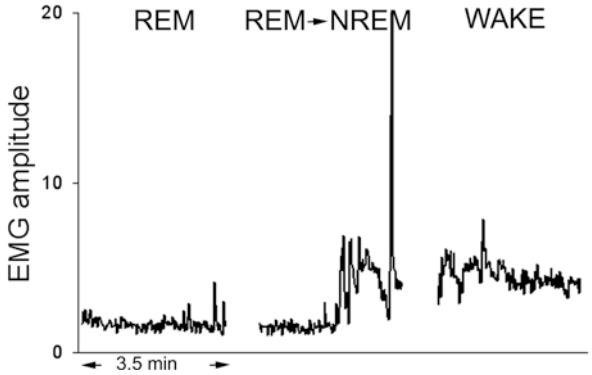

Fig. 16.2 REM EMG. Variance of chin EMG recordings during fMRI scanning is given, as seen in three consecutive scans of the same participant. In contrast to the elevated EMG levels during NREM sleep (middle, after arousal) and wakefulness (right), unambiguous REM sleep displays muscle atonia (left) with only short muscle twitches interspersed (Wehrle et al. 2005, reprinted with kind permission of Lippincott, Walters & Kluwers)

16.2.1.2 Referentiation of Recordings

Classic sleep recording or ERP studies tend to use mastoid electrodes as a reference site. However, sufficient good quality of recordings at this electrode position may turn out to be difficult because of high susceptibility to cardioballistic artifacts. In addition, headphones needed for proper sound protection do often cover these electrode sites and may cause subjective discomfort or pain. It seems advisable not to use mastoid positions as primary reference during data acquisition. EOG recording quality may additionally benefit from using nasion or Fpz derivation for reference, instead of the mastoid reference.

16.2.1.3 Extended Recording Time: Electrophysiological Recordings

Signal quality of most electrophysiological recording devices usually deteriorates over time. Increased sweating may reduce adequate contact of electrodes. Some electrode sites strongly deteriorate during extended sessions but cannot be reattached or replaced in sleeping subjects without awakening.

16.2.2 MR Imaging

16.2.2.1 Extended Recording Time: fMRI Recordings

MR image quality is also affected when the scanner is operating for an extended period of time. In general, adjustment of field homogeneity by shimming procedures is done once at the very beginning of the session, but may degrade over time due to participants' movements, but also due to hardware instabilities. Coils are continuously delivering magnetic field gradients with extremely short rise times and large amplitudes for several hours. This leads to temperature instabilities in these coils. Furthermore, the

stability of the main magnetic field cannot be guaranteed over an extended period of time, leading to intensity drifts in the images. This especially holds true if the helium cryogenic compressor of the magnet is transiently switched off during the experiment to minimize artifacts on EEG. Depending on imaging parameters, physiological artifacts with BOLD activity correlated to cardiac or respiratory noise may be increased and should be accounted for, especially for resting state experiments (see below).

16.2.2.2 Movement

Participants' movements tend to be increased in sleep studies. Body movements are a common phenomenon during the process of falling asleep in the form of the common hypnagogic myocloni, as well as around REM sleep. During these periods, the compelling urge to move may lead to arousal and awakening of the subject or disrupt fMRI recordings.

16.2.3 Effect on Participant

16.2.3.1 Participant Not Falling or Staying Asleep

fMRI procedures per se induce highly adverse effects on sleep. Due to the inevitable strong head fixation which also forces the participant to stay in a supine position and due to the narrow tunnel and noisy environment, many people raise concerns regarding the chance of falling asleep under these conditions. Noisy environments inherently deteriorate sleep architecture, with increases in sleep latency, sleep fragmentation, and sleep stage changes, resulting in reduction of total amount of sleep. Waxing and waning of drowsiness may easily be obtained during extended recording sessions, but consolidated sleep is more difficult to record.

16.2.3.2 Extended Recording Time: Subjective Discomfort

Not only is it difficult to fall asleep but also to stay asleep in the scanner. Even if participants manage to reach stable sleep, fMRI sessions cannot be extended endlessly to obtain whole-night recordings. The participant's comfort should be particularly considered when placing the subject in the scanner, as aching electrodes or strong head fixation will possibly make it difficult to fall or to stay asleep. One should also be prepared that participants may be disoriented or feel uneasy after awakening in the magnet. In such situations, the complex experimental setup hampers rapid removal of participants from the scanner.

16.2.4 Effect on Study Protocols

16.2.4.1 Drop-Out Rate

The issues listed above indicate that the overall drop-out in sleep studies is higher as compared to classical fMRI studies performed during daytime. It seems noteworthy to point out that one's expectations regarding the time needed to acquire reasonable data sets should be adjusted to these limiting factors.

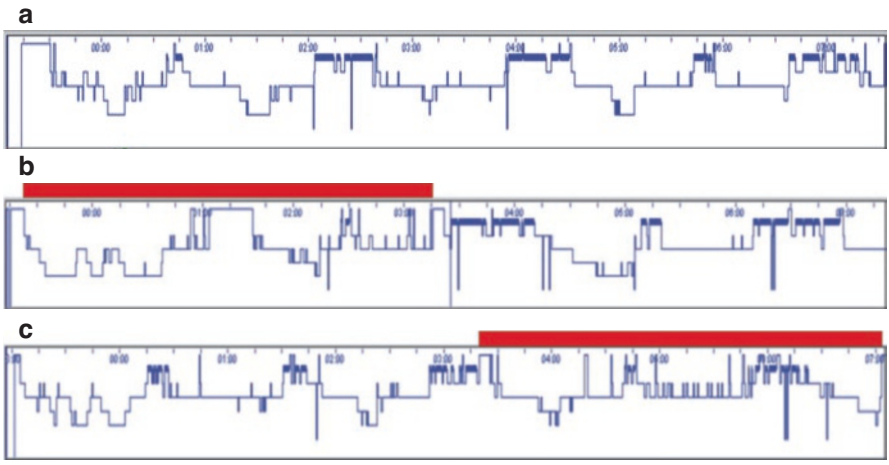

Fig. 16.3 REM suppression. Effect of fMRI procedures on sleep architecture. Head restrainment and scanner noise, applied without interference of magnetic fields, were applied in the sleep lab during one half of the night. The figure gives distribution of sleep stages across a whole night of a single subject: baseline night without any interference (**a**), MR simulation during first half (**b**), and second half (**c**) of the night, indicated by the red bar. Adverse effects especially on REM sleep include delayed REM onset and strong fragmentation of REM sleep periods, thus decreasing the overall amount of REM sleep to less than 50% of the baseline condition

16.2.4.2 Specific Suppression of Sleep Stages

Drop-out rates also depend on the sleep stage under investigation, because acoustic noise not only reduces the overall amount of sleep but predominantly affects specific sleep stages, namely, REM sleep (Fig. 16.3).

To test the detrimental influence of the scanning procedures on sleep architecture, the fMRI environment was mimicked in a sleep lab situation (Wehrle et al., unpublished). For this, the participant's head was fixated inside a sham MR coil, restricting the body posture to supine position, while repetitive scanner noise with comparable loudness level was replayed. Such procedures were shown to have severe effects on sleep structure, specifically fragmenting and reducing REM sleep. REM sleep with concomitant muscle atonia may represent a vulnerable sleep stage, highly sensitive to uncomfortable and apparently dangerous environments, and thus hard to be acquired in the MR scanner (see also Khubchandani et al. 2005). Furthermore, attempts to move one's body that often occur before and during REM sleep are not possible in the scanner.

16.2.4.3 Selection Bias

So far, subjects who are not able to sleep on their back or who are sensitive to environmental disturbances have not been studied at all. Selection of individuals finally able to sleep inside the scanner might introduce a bias by recruiting only subjects who might display specifically sleep-protective mechanisms.

16.2.4.4 No Control Over Sleep State

There is no guarantee or control about whether participants do or do not fall asleep during scanning or whether the sleep stage aimed at can be scanned for a sufficient long time. fMRI studies during sleep thus may face a methodological drawback, making it difficult to obtain possible within-subject effects based on repeated measurement as, e.g., in intervention studies.

16.2.4.5 No Whole-Night Recordings

If participants manage to fall asleep in the scanner, usually one or two sleep cycles can be recorded. Information on a whole night of sleep with the entire sleep progression throughout the night as usually obtained in sleep laboratory recordings is hardly feasible in fMRI studies.

16.2.4.6 Fluctuation of Microstates

Furthermore, fluctuating microstates within sleep cannot be voluntary influenced. Baseline activity is presumably not even stable during wakefulness (Goncalves et al. 2006). During sleep, all studies so far point out very prominent BOLD signal changes related to even short-lived EEG elements within sleep; thus, the continuous change in baseline states must be expected to be increased during sleep. Depending on the timescales of fMRI recordings during sleep, this methodological issue should be taken into account in analyzing sleep data.

16.2.5 Possible Solutions

16.2.5.1 Habituation

Habituation to noisy or uncomfortable sleeping environments is a common physiological adaptation process and can certainly be extended to the extreme situation of sleeping in an fMRI scanner. The participants should be accustomed to the experimental setup to increase the probability of sleep.

16.2.5.2 Sleep Deprivation

One method to counteract the arousing effects of fMRI procedures is to apply sleep deprivation previous to the fMRI experiment. The elevated sleep pressure will shorten sleep latency and increase sleep continuity. Total sleep deprivation also induces changes in the composition of EEG spectral power during recovery sleep; however, the spatial distributions as typical for individual participants were shown to be basically preserved (Finelli et al. 2001a). Sleep deprivation further affects mood, possibly making subjects more sensitive for any experimental discomfort.

16.2.5.3 MR Recording Techniques

Some of the first fMRI studies used interleaved recordings, where echo planar imaging (EPI) acquisitions are separated by periods of undisturbed EEG (Portas et al. 2000), or minimized gradient noise by application of pulse sequences avoiding fast gradient switching. The BURST method (Hennig and Hodapp 1993) was

successfully applied during REM sleep (Lovblad et al. 1999), and a "silent" gradient fast echo experiment was performed in NREM sleep (Czisch et al. 2002). Unfortunately, a drawback of these MR techniques lies in low signal-to-noise ratios as compared to EPI and in restriction to only a few slices due to sequence timing. Reduction of the slope of the gradient flanks however reduced MR-induced artifacts in the EEG recordings, which allowed correction of gradient artifacts by elimination of discrete distorted EEG frequency bins (Hoffmann et al. 2000). With EPI imaging, postprocessing correction algorithms are available based on high sampling rates of EEG recordings (~5 kHz) synchronized to the MR scanner clock (Mandelkow et al. 2006). In this way, any artifact caused by the rapid switching of the MR gradients is always sampled identically in the EEG. Based on the assumption of a stationary gradient artifact and a "random" EEG signal, an artifact template is calculated (often using a sliding window) and subtracted from the distorted EEG, resulting in an interpretable EEG signal. Commercial EEG systems allow for an online artifact correction during the fMRI experiment and thus for a close monitoring of the subject's sleep state.

Heart rate and respiration are dependent on the sleep stage and may influence the fMRI analysis. Especially in resting state experiments without an external paradigm, correction for cardiac and respiratory artefacts is needed. A number of correction strategies have been proposed, based on simultaneously acquired physiological signals (Glover et al. 2000), on signal fluctuations outside the grey matter compartment (Behzadi et al. 2007), or on denoising by excluding ICA components not showing the expected frequency profile or localization (Salimi-Khorshidi et al. 2014).

16.3 FMRI in Sleep: Results

The following chapter will focus on functional MRI studies performed during unambiguous sleep, based on the mandatory simultaneous use of polysomnographic recordings. Related research lines like morphological MRI studies in sleep disorders (sleep apnea, narcolepsy, hypersomnia, etc.), and studies utilizing fMRI to investigate cognitive functions related to sleep or sleep deprivation performed without paralleled EEG measurements will not or only marginally be discussed here.

16.3.1 Sensory Processing During Sleep

Arousal thresholds are higher during sleep, nevertheless we can be aroused by external stimuli—the brain's capacity to selectively process and evaluate stimuli according to their relevance must be preserved to a certain degree. Thalamocortical transmission of stimuli is altered during sleep, and combined EEG/fMRI opens up the possibility to study the underlying neuronal mechanisms of such changes in sensory processing in humans.

16.3.1.1 NREM Sleep

Several fMRI studies investigated the reactivity of the human brain in sleep. In most cases, acoustic stimuli were applied, as they appear best suited to investigate cerebral activation to stimulation in sleeping participants.

Acoustic Stimulation

Many studies applied a classic block design with, e.g., 20 or 30 s of continuous stimulation versus rest, which yields strong activation of auditory cortex during wakefulness.

Investigating the effect of sleep stage 1 on auditory cortex reactivity upon presentation of pure tones revealed a reduced activation as compared to wakefulness in the temporal gyrus during drowsiness and falling asleep (Tanaka et al. 2003). Similarly, publications investigating sensory processing in sleeping children, without concomitant polysomnography, report a positive BOLD response to different auditory stimuli in several areas including the bilateral superior temporal gyrus during sleep (Wilke et al. 2003; Redcay et al. 2007).

Portas and colleagues investigated the effects of two types of acoustic stimuli: a neutral beep tone and the subject's own name that carries high personal affective significance (Portas et al. 2000), using a 17-s interleaved design, with sleep classified in the undisturbed EEG traces before and after the fMRI blocks. As expected, the individual's own name provoked significantly more complete awakenings than neutral tones, confirming the arousing capacity of this stimulus type. The fMRI analysis revealed a remarkable similar activation pattern in wakefulness and sleep, with bilateral activation of the auditory cortex, thalamus, and caudate nucleus; however, the interleaved study protocol, lacking EEG information during stimulation, implies that transient arousal reactions upon stimulation may also have influenced the results. Finally, interaction analysis of stimulus type and sleep state revealed increased activation of the left amygdala and left PFC for name versus tone stimuli specifically during the trials where participants have been sleeping.

When applying stimuli without arousing or affective components in a 30-s block design and with simultaneous EEG information, the auditory cortex showed almost abolished positive BOLD response during NREM sleep (Czisch et al. 2002, 2004). Surprisingly, a negative BOLD response (NBR) was shown during extended acoustic stimulation in sleep, with a maximum amplitude and extent during sleep stage 2. Sleep stage 1 was characterized by a transition phase showing intermediate responses with positive BOLD signals in the auditory cortex and emerging transmodal NBR in the occipital cortex. Analysis of the EEG revealed a concomitant increase in slow-wave activity (KCs and EEG delta waves) during 30-s stimulus presentation as compared to the resting baseline within light NREM sleep. The amplitude of the NBR was best correlated to the relative increase in the KC density during stimulation, whereas relative increases in total delta power showed closer association to the spatial extent of the NBR. This finding corroborates a presumed decreased neuronal activity, as increased sleep depth is characterized by increased EEG slow-wave activity that presumably reflects prolonged periods of neuronal hyperpolarization. Similar findings were obtained during generalized epileptic seizures with slow EEG activity (Fig. 16.4).

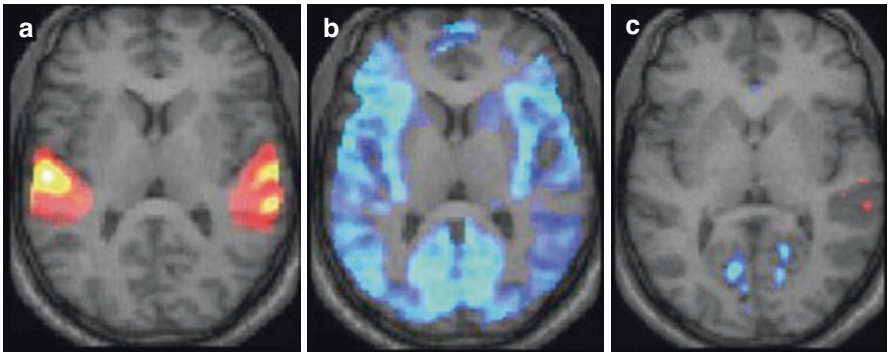

Fig. 16.4 NREM stimulation. Effects of block-design acoustic stimulation on brain reactivity across sleep. Acoustic stimulation for 30sec during wakefulness induces activation of the bilateral auditory cortex (**a**), which decreases during sleep stage 1 (data not shown). During light NREM sleep stage 2, continuous acoustic stimulation induces a relative decrease in BOLD signals in widespread cortical areas (**b**), reflecting induced increases in K-complexes (slow EEG activity). During slow wave sleep with background slow EEG activity, no further changes are elicited upon acoustic stimulation (**c**) (partly reprinted from Czisch et al. 2004 with kind permission of Blackwell Publishing Ltd)

In contrast, the thalamic time curves indicated an initial positive BOLD response which, despite ongoing acoustic stimulation, returned to baseline levels after a few seconds. This effect also was most pronounced in the very first stimulation epoch, suggesting an initial thalamic reaction to sensory stimuli assessing the potential meaning of the stimuli, followed by reduced activity of the thalamus probably due to habituation processes.

This was further explored in an event-related fashion with an acoustic oddball design applying frequent and rare tones during NREM sleep (Czisch et al. 2009). Negative BOLD response in several cortical areas including motor cortex and amygdala was confirmed for rare tones, accompanied by sleep-specific late negative slow deflection in the ERP. Rare tones followed by evoked KCs were however associated with a more wake-like activation, indicating that the brain may be transiently more responsive preceding a KC, a finding corroborated by the data from Dang-Vu et al. (2011). In contrast, tones presented during the presence of EEG spindles elicited hardly any brain activation, well in line with the notion that external signal processing is strongly diminished during spindle activity, given their own thalamocortical interplay (Dang-Vu et al. 2011). Spontaneous brain activity like sleep spindles and KCs modifies the response and decoding of sensory input, a finding corroborated by altered activity dynamics with increased variance of activity in sensory cortices during NREM sleep (Davis et al. 2016).

Visual Stimulation

Performing fMRI in children frequently requires sedation to minimize movement artefacts. To investigate the infant's ability to regulate their CBF response, Born and colleagues used visual stimulation with flashing stroboscopic light in sedated

children (Born et al. 1998, 2002a). Upon stimulation, a consistent NBR in the occipital cortex was reported. Negative BOLD response upon sensory stimulation has been reported in further studies with sedated children (Martin et al. 1999; Altman and Bernal 2001) and sleeping children (Redcay et al. 2007). Redcay et al. also analyzed functional connectivity of the sensory areas and report preserved networks during sleep. In 2002, Born and colleagues reported similar cortical stimulation-induced decreases, now investigating healthy adult volunteers with simultaneous EEG recordings during natural SWS (Born et al. 2002b). As during sedation, a NBR was observed in the occipital cortex, which was located more rostrodorsal as compared to the BOLD increase regularly observed during wakefulness. In an independent sample, Born and colleagues successfully studied further subjects, now applying $H_2{}^{15}O$-PET imaging. They were able to reproduce the fMRI results detecting a reduced relative rCBF upon stimulation in the occipital cortex. These findings are discussed in the context of neuronal inhibition of the visual cortex upon stimulation. As our findings using acoustic stimuli during NREM sleep describe a similar reduced BOLD response in visual areas, this reduction may be regarded as a general or cross-modal sleep protective response independent of the modality of the stimuli.

Olfactory Stimulation

Another interesting aspect of sleep that may be investigated with fMRI is the putative role in consolidation of newly acquired memories. Olfactory stimuli, which have been associated to a learning session during daytime, have been applied by Rasch and colleagues during subsequent SWS in order to reactivate specific memories during sleep (Rasch et al. 2007). Olfactory afferents can project directly to higher-order regions including the hippocampus and may thus putatively modulate hippocampus-dependent declarative memories. Reapplication of olfactory stimuli during sleep actually was shown to enhance recall of the hippocampus-dependent declarative memory, but not hippocampus-independent tasks like finger tapping. To test whether olfactory-induced reactivations are indeed related to increased activity in the hippocampal system, the authors re-exposed subjects to the same odor cues in fMRI sessions during SWS following the learning sessions. During sleep, renewed application of the olfactory stimulus induced a bilateral increase in hippocampal region of interest, which exceeded the relative changes found during wakefulness, supporting data from animal studies that patterns of hippocampal neuronal activity involved during learning are reactivated in the SWS.

16.3.1.2 REM Sleep

Most studies so far investigated the processing of external stimuli during stages of NREM sleep. Neuroimaging as well as EEG recordings indicate high thalamocortical activity in both wakefulness and REM sleep; nevertheless, sensory integration of external stimuli does not occur during REM sleep (Maquet 2000; Hobson and Pace-Schott 2002). To study the altered processing of external stimulation during REM sleep with fMRI, acoustic stimulation using non-arousing stimuli was applied in

healthy subjects (Wehrle et al. 2007). When contrasting acoustic stimulation versus the resting baseline in unambiguous REM sleep, we observed two distinct patterns of activity when separating the fMRI sessions depending on the number of concomitant rapid eye movements: during the tonic REM sleep background with the classical high-frequency EEG and low muscle tone, but with only a limited number of phasic rapid eye movement bursts, the cortical activation obtained upon acoustic stimulation resembled the regular positive BOLD response as observed during wakefulness, with however strongly reduced BOLD amplitudes compared to the ones obtained to wakefulness. As opposed to these findings, acoustic stimulation during phasic REM sleep epochs with a high number of rapid eye movements showed a diffusive negative BOLD response including the thalamus. No activation of the auditory cortex was observed. This is in line with evoked potential studies during human REM sleep, where evoked responses are strongly suppressed and may differ depending on the actual presence or absence of rapid eye movements (Sallinen et al. 1996; Takahara et al. 2002). In addition, a parallel reduction in the number of rapid eye movements and in thalamocortical signal intensity during external stimulation was observed. Investigation of temporal correlations of BOLD activity to time curves derived from thalamic regions of interest suggested a highly synchronized activity of thalamocortical areas specific during periods with rapid eye movements (Fig. 16.5).

These findings support an increased thalamocortical intrinsic activation associated with phasic REM sleep bursts. The high activity of the brain especially during

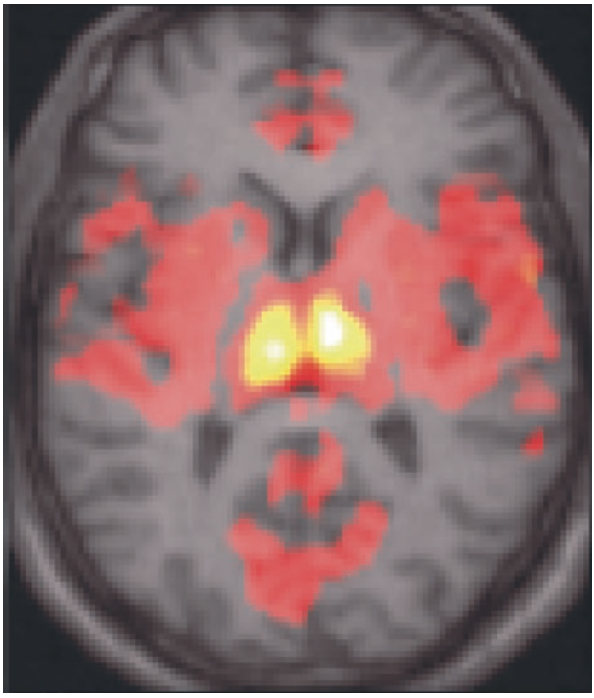

Fig. 16.5 REM stimulation. Cortical activation correlated to—supposedly intrinsic—thalamic activity associated to phasic REM periods. During times of high number of rapid eye movements, the brain's reactivity to external stimulation is strongly suppressed (reprinted from Wehrle et al. 2007 with kind permission of Blackwell Publishing Ltd)

phasic REM sleep may be regarded as a functionally isolated "closed loop" as proposed by Llinas and Pare (1991), reflecting an intrinsically highly active brain state. These phasic periods are embedded in a tonic REM sleep background with increased capacities to process external stimulation.

16.3.2 EEG-Informed fMRI

fMRI was successfully applied to study unperturbed sleep, without applying any additional external stimulation. The first studies were an important milestone as they have proven the general applicability of fMRI measurements during sleep by replicating and extending previous findings based on using radioactive tracer-dependent neuroimaging. The fMRI approach allows for improved resolution and better classification of sleep substates and associated neuronal activities—especially important when single EEG graphoelements like spindles or delta oscillations are investigated.

16.3.2.1 Falling Asleep

Staging of sleep according either to the older Rechtschaffen and Kales (1968) scoring guidelines or the new AASM classification (Silber et al. 2007) represents the gold standard in sleep research. Kaufmann et al. (2006) described specific activation changes in the process of falling asleep by setting the BOLD response in relation to the respective sleep stages.

Technical limitations restricted the MR repetition time to a rather long duration of 10s but thus minimized cardiac artefacts in the fMRI analysis as compared to faster repetition rates (Kaufmann et al. 2006, 2007; Laufs et al. 2007).

Consistent with the majority of previously published findings, the cerebral activity as reflected in the BOLD signal decreased throughout NREM sleep as compared to wakefulness. The signal changes comprised cortical regions, the limbic lobe, the thalamus, the caudate nucleus, and midbrain structures such as the hypothalamus. In extension of previous reports, the fMRI approach allowed for a more detailed analysis of sleep stage-specific patterns which are involved in the successive discontinuation of wakefulness, suggesting that a synchronized sleeping state can only be established if these regions interact in a well-balanced manner: Structures with reduced activation as compared to wakefulness already during sleep stage 1 were the anterior thalamic nuclei, the PCC, and the cuneus. In addition, during sleep stage 2, which is usually associated with the loss of self-conscious awareness, signal reduction was obtained in frontal and more ACC areas, along with the inferior parietal and superior temporal gyrus, the insula, and dorsal thalamic nuclei (Fig. 16.6).

Consolidated SWS showed a further reduction of activity in the frontal and inferior parietal gyrus, the insula, the caudate nucleus, and the ACC. This cascade of successive downregulation during the consolidation of NREM sleep may be a prerequisite for establishing deep sleep.

By relating the fMRI data during NREM sleep to the spectral EEG power in the alpha frequency range, activity in the thalamus was obtained. This effect is well in line with neuroimaging correlates of alpha activity found during wakefulness

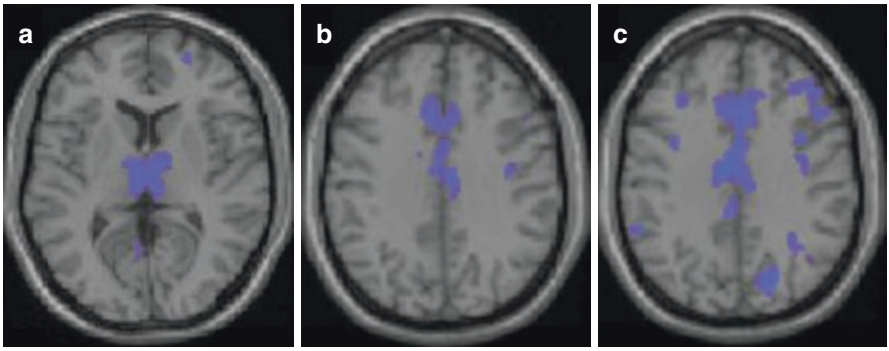

Fig. 16.6 NREM BOLD decreases. Effect of sleep stages according to Rechtschaffen and Kales (1968) on relative BOLD signal changes during falling asleep. Transition from wakefulness to sleep stage 1 is accompanied by signal decreases in the thalamus (**a**). Further deepening of sleep toward sleep stage 2 is accompanied among other by prominent decreases in anterior cingulate areas (**b**), which increases and includes further cortical areas when proceeding to slow wave sleep (**c**) (Kaufmann et al. 2006; reprinted with kind permission of Oxford University Press)

(Goldman et al. 2002; Moosmann et al. 2003; Feige et al. 2005). Signal decreases in occipital regions were often reported associated to alpha rhythms in wakefulness, but an equivalent signal decrease when evaluated against the EEG background of sleep could not be obtained.

16.3.2.2 Graphoelements: Spindles, K-Complexes, and Slow Oscillations

Apart from relating BOLD signals to sleep stages, fMRI allows for studying BOLD correlates of characteristic graphoelements within sleep in event-related statistical designs. Although cerebral activity is generally decreased during NREM sleep as compared to wakefulness, distinct regional and temporal activation with respect to the sleep stage-specific baseline can be observed.

Schabus and colleagues investigated the cerebral correlates of sleep spindles, transient oscillations in the beta frequency range defining NREM sleep stage 2 (Schabus et al. 2007). Two distinct types of spindles with presumably functional differences have been described earlier, namely slow (<13 Hz) and fast (>13 Hz) spindles, with a predominance over frontal and centro-parietal areas, respectively (Fig. 16.7).

The authors first identified an activation pattern common for both spindle types, comprising the thalamus, ACC, left insula, and the bilateral superior temporal gyrus. When separating the spindle types, activity related to slow spindles largely corresponded to the common pattern, including activation of the superior frontal gyrus. In contrast, fast spindles showed additional recruitment in the supplementary motor area, sensorimotor, and mid-cingulate cortex. Differential comparison to slow spindles revealed increased responses for fast spindles in the left hippocampus, the orbital and middle frontal, mesial PFC, sensorimotor cortex, and anterior insula. Peak activation for slow spindles was located in the mediodorsal nucleus of the thalamus, and for fast spindles in the ventral posterior and pulvinar thalamic nuclei,

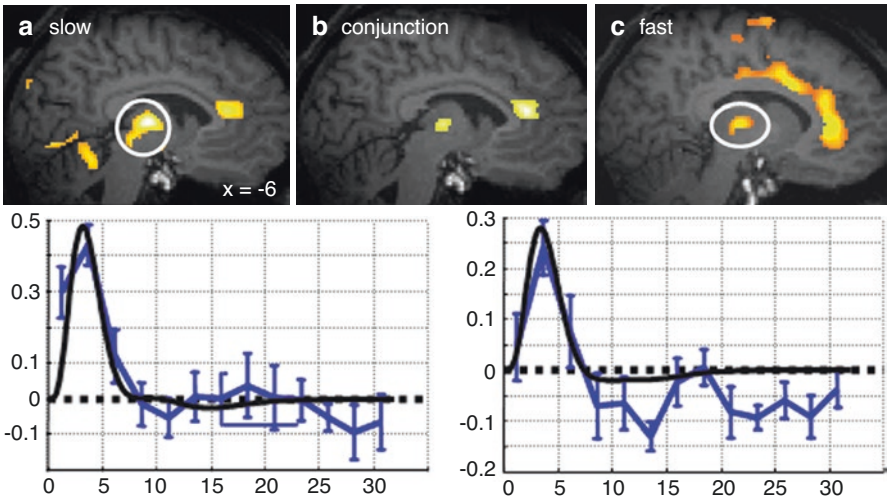

Fig. 16.7 NREM spindle correlates. BOLD correlates to onset of slow (**a**) and fast (**c**) sleep spindles and conjunction of both spindle types (**b**). Note that thalamic activation characterizes both types of spindles, whereas the fast spindle type is associated with an activation in cingulate and somatosensory cortical areas (Schabus et al. 2007; reprinted with permission, Copyright (2007) National Academy of Sciences, U.S.A.)

that anatomically project to sensorimotor and posterior parietal cortices. Thalamic activation in both spindle types is well in line with neurophysiological evidence that spindles are generated in the thalamus and arise by inhibition of thalamocortical neurons and post-inhibitory rebound spiking in thalamocortical cells in large cortical regions (Schabus et al. 2007; Andrade et al. 2011). Interestingly, hippocampal-cortical functional connectivity was found strongest during NREM sleep stage 2 and within sleep stage 2 mostly increased during sleep spindles (Andrade et al. 2011).

Spindle-coupled reactivation of brain activity as linked to previously declarative learning tasks can be traced during NREM sleep (Bergmann et al. 2012). Memory network connectivity increases during NREM sleep also could be found to correlate with following memory performance (van Dongen et al. 2011). BOLD analysis linked to K-complexes suggests some degree of information processing by activation of sensory areas during KCs, however with limited involvement of anterior insula. This may reflect the reactive, information processing as well as the sleep-protective role of KCs (Jahnke et al. 2012).

Animal cellular data show that NREM sleep is organized by slow oscillations (SO), derived from periods with intense neuronal firing alternating with hyperpolarization phases (Steriade 2006). SOs could also be evidenced in humans (Achermann and Borbely 1997; Massimini et al. 2003). Dang-Vu and colleagues investigated the BOLD response associated with SO (Dang-Vu et al. 2008). Negative BOLD responses were not reported. Positive brain responses associated with SO could be verified in subcortical structures, including the brainstem, hypothalamus, and thalamus. Significant activations were also located in primary and associative neocortical

areas and in limbic regions, including the hippocampus. These findings again highlight core structures underlying the organization of NREM sleep phenomena.

16.3.2.3 REM Sleep

Circadian timing in the early morning hours and suppressing effects of the study circumstances as outlined in the introduction are among the main reasons why fMRI studies of REM sleep are less often performed.

Nevertheless, in fact the first study using truly combined EEG and fMRI methods in sleep research published 1999 by Lovblad and colleagues reported REM sleep data (Lovblad et al. 1999). The authors investigated BOLD signal changes during REM sleep as compared to the NREM background preceding the REM sleep episode. Technically, they applied a silent BURST sequence to minimize acoustic noise and gradient induced EEG artifacts, which allowed for continuous sampling of data over several hours. Muscle atonia could not be reliably detected and sleep stage classification was modified, focusing on rapid eye movements and absence of KCs to distinguish REM sleep from sleep stage 2 and missing responses to calling the subject's name via the intercom system. In their study, Lovblad et al. successfully examined two (out of a total of five) participants during REM sleep. An increased activation of the occipital cortex and reduced activity in the frontal lobes during REM sleep as compared to the BOLD amplitudes during NREM sleep was reported. These findings are in agreement with previous PET studies highlighting a deactivation in the frontal cortex and an increased activation in secondary, but not in primary visual cortex during REM sleep (Maquet et al. 1996; Braun et al. 1997, 1998; Nofzinger et al. 1997).

Later, REM sleep data could also be acquired using a regular EPI protocol (Wehrle et al. 2005, 2007), with unambiguous REM sleep based on muscle atonia and presence of rapid eye movements (Fig. 16.8).

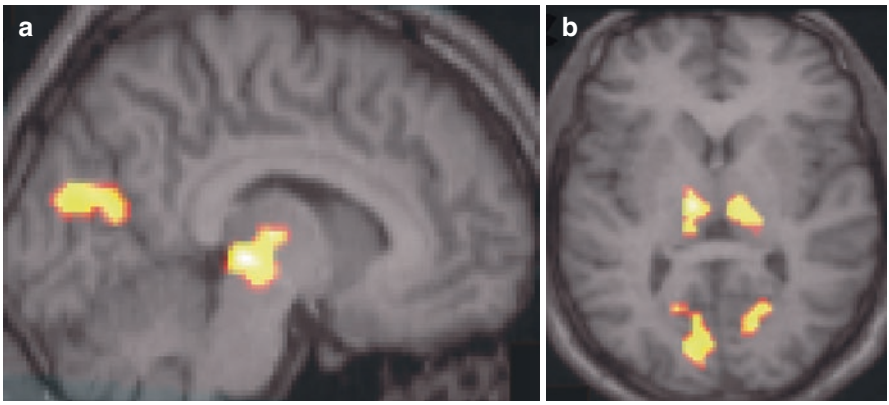

Fig. 16.8 REM rapid eye movement correlates. BOLD activity correlated to rapid eye movements during REM sleep. Within REM sleep, the number of rapid eye movements per fMRI volume was calculated. BOLD signal intensity corresponding to eye movements in REM sleep shows activation in bilateral posterior thalamus and in occipital areas; midline view (**a**), axial view (**b**) (Wehrle et al. 2005; reprinted with kind permission of Lippincott, Walters & Kluwers)

BOLD activation in direct temporal relationship to rapid eye movements within REM sleep revealed bilateral activation in the thalamus and the secondary visual cortex, a pattern remarkably consistent with PGO activity in animal models. PGO waves have long been described in animal models using invasive techniques and have been proposed to precede eye movements and to be the generators of REM sleep in mammals.

Taken together, these findings emphasize that spontaneous sleep is not a state of brain quiescence but organized in exact progressions of highly specific brain network activities.

16.3.2.4 Lucid REM Sleep

Simultaneous recording of EEG and fMRI during sleep also opens the possibility to assess brain activity related to specific dream contents. Dreams are defined as mentations occurring mainly (but not exclusively) during REM sleep and which are remembered and can be reported by the sleeper after awakening. Previous data as derived from PET allow to set the REM sleep-specific pattern of regional brain activity into relation with the often bizarre and emotional content of typical dreams (Desseilles et al. 2011). However, the precise timing of dream events is normally concealed in an experimental setting, making it extremely difficult to analyze correlations of dream imaginary with fMRI BOLD signal fluctuations. Horikawa et al. (2013) investigated dream-like mentations during the sleep-onset (hypnagogic) period testing for the similarity of the hypnagogic BOLD signal fluctuations to the awake response to a set of about 20 prerecorded visual items. They exploited a machine learning decoder trained on a number of brain regions relevant for visual processing. While their analysis revealed an accuracy of 70–80% for decoding the sleep imagery, it should be noted that most events were actually sampled during the sleep-wake transition period S1.

In a series of experiment in lucid dreamers, we studied aspects of REM sleep mentations and sleep consciousness. Lucid dreaming is defined as a state in which the subject gains insight into his state of mind during dreaming and may alter dream contents. Notably, lucid dreaming is a trainable skill. From an experimental perspective, lucid dreaming is of interest since it allows to establish means of communication with the sleeping subjects, e.g., by predefined eye movements. We asked lucid dreamers to dream about hand clenching during their lucid dream and to communicate the change of the hands with eye movement cascades (Dresler et al. 2011). The experimental design therefore copied an extremely stable fMRI motor task in wakefulness, but shifting the imagined execution of the hand movements into the dream state. We observed a similar pattern of brain activation both during the imagined tasks execution during wakefulness and in lucid REM sleep, showing for the first time the functional representation of dreamed motion.

Lucid dreaming can also be exploited to study specific aspect of consciousness. Conscious awareness can be classified in three subtypes (Cicogna and Bosinelli 2001): the phenomenal experience of objects and events, the meta-awareness of the mental life, and self-awareness. As compared to common REM sleep dreams,

lucid dreaming is defined as a state of meta-awareness or higher-order consciousness. Using this concept, we investigated differences in BOLD signal amplitudes related to the onset and the fading of a lucid dream, as compared to the regular background of REM sleep (Dresler et al. 2012). Doing so, a network of brain regions showed higher activity in lucid dreams, namely, the bilateral precuneus, cuneus, parietal lobules, and prefrontal and occipitotemporal cortices activated. Our data complement reports showing increase EEG gamma band power in fronto-lateral brain regions upon onset of lucidity (Voss et al. 2009). Thus, lucid dreams represents itself as a state of proper REM sleep augmented be local and distinct increases of brain activity. In addition, the brain regions identified in our fMRI study show some remarkable resemblance to brain regions which underwent strongest volumetric expansion during evolution (Van Essen and Dierker 2007). Following the interpretation of lucid dreaming representing a state of higher-order consciousness, it may be speculated that higher order consciousness is a defining human feature. Our studies on lucid dreaming may also have implications for psychiatric research. The differences observed between REM sleep and lucid dreaming resemble differences between psychotic patients and healthy controls (Dresler et al. 2015) (Fig. 16.9).

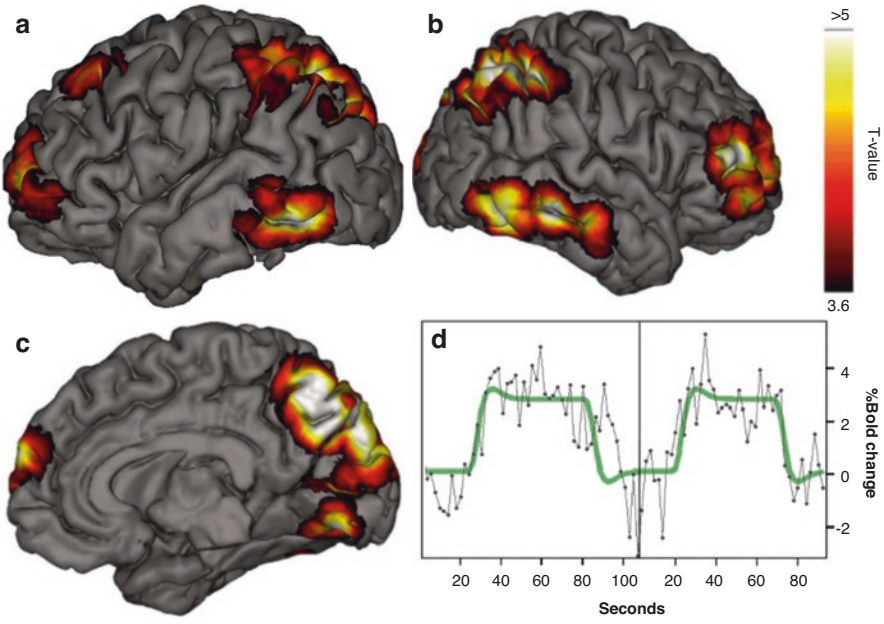

Fig. 16.9 Lucid dreaming. Activity related to lucid dreaming. Color-coded clusters represent areas significantly activated during lucid epochs in REM sleep ($p_{FDR} < 0.005$): left hemisphere (**a**), right hemisphere (**b**), midline view (**c**). Predicted (green) and fitted (black) fMRI data of the peak activation in the right precuneus, showing combined analysis of two independent lucid epochs in a single subject (boxed) (**d**) (Dresler et al. 2012; reprinted with kind permission of Oxford University Press)

16.3.3 Network Analysis

Today, resting state fMRI is used for detecting spontaneous low-frequency BOLD signal oscillations (<0.1 Hz), which not only occur during active wakefulness but also persist during human sleep and other states of impaired consciousness. Using either seed based cross-correlation analysis or independent component analysis (ICA), specific brain networks can be detected. Network analyses such as a graph theoretical approaches enable us to break down the complex intra- and inter-network interplay into a handful of markers characterizing the brain's state. Not only the static functional connectivity but also its temporal features have recently been investigated.

One of the most discussed resting state networks is the default mode network (DMN), being related to autobiographical memory retrieval, day dreaming, and other mentations which are directed to internal states (Gusnard et al. 2001; Raichle et al. 2001; Spreng and Grady 2010).

Falling asleep and passing through different NREM sleep stages not only is accompanied by reduced sensory processing but also by gradually decreased consciousness and self-awareness. Studying the DMN across sleep stages thus provides interesting insights into the sleep induced state of altered consciousness and allows for comparison with pharmaceutical or pathological induced loss of consciousness. Studying young healthy subjects across the first sleep cycle of the night, continuously acquiring resting state fMRI data and polysomnography, showed a gradual decline of the DMN network integrity, with various brain regions losing their integration in the DMN (Sämann et al. 2011). The first regions to drop out of the DMN are the parahippocampal gyrus and the thalamus, already at light sleep stages 1 and 2. The long range FC between the posterior cingulated cortex (PCC) and retrosplenial cortex (RspC), and the anterior cingulated cortex (ACC) progressively declines as well, while other brain regions, such as the inferior parietal lobule, show stable incorporation into the DMN. These findings demonstrate that functional connectivity strongly depends on the vigilance state and may cover a large dynamic range (Fig. 16.10). Similar results have been found for intrinsic networks in adults and in children (Horovitz et al. 2008, 2009; Larson-Prior et al. 2009; Chow et al. 2013; Manning et al. 2013; Wilson et al. 2015), with increases in variability during sleep, and however slightly varying results for the—less stable?—transition to sleep and light sleep (Horovitz et al. 2009; Larson-Prior et al. 2011). Even shorter than usual analysis epoch lengths of 30 s appear sufficient for detection of DMN alterations during sleep (Wilson et al. 2015). It should be noted that some authors also reported negative findings (Koike et al. 2011). Investigation of thalamocortical and intra-thalamic functional connectivity shows specific thalamocortical increases only for sensorimotor connections and increases intra-thalamic connectivity during sleep (Hale et al. 2016). The decline in RSN integrity has recently been modeled with consistent results, showing that while occurrence of local slow-wave activity at sleep onset due to reduced cholinergic input may not yet affect RSN, at very low levels of cholinergic modulation (deep sleep), global slow waves arise and RSN merge and become undifferentiated (Deco et al. 2014).

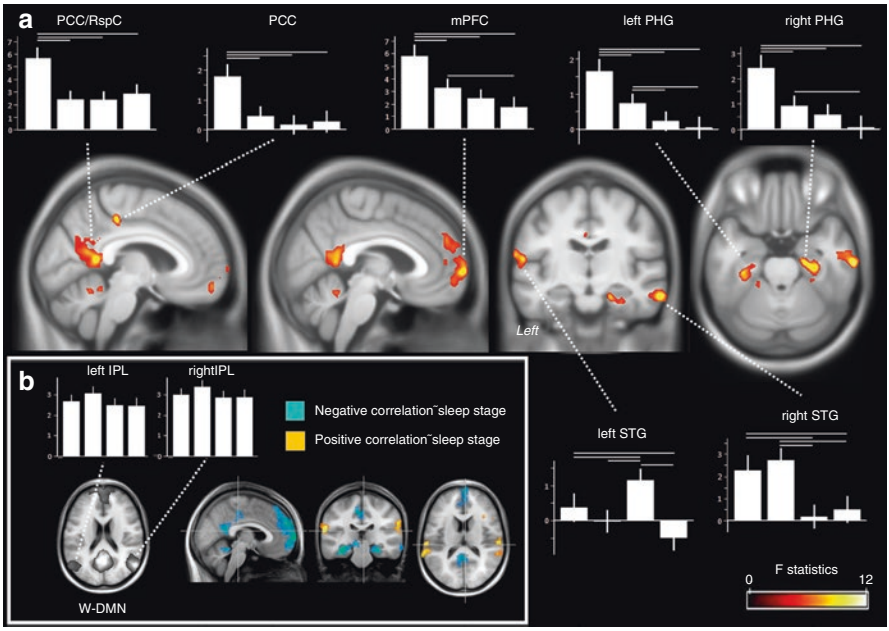

Fig. 16.10 DMN in sleep. Sleep stage-dependent areas of the DMN and its anti-correlated network (ACN). (**a**) Clusters represent areas with significant main effect of sleep stage on focal DMN strength ($P_{\text{cluster.FWE}} < 0.05$). Graph bars represent the strength (contrast estimates) for each sleep stage (left to right: wakefulness (W), stage N1, stage N2, and SWS) as extracted from the peak voxels; horizontal lines indicate significant post hoc comparisons as assessed by T contrasts. Note different dynamics and different final level reached. (**b**) Highly similar areas as compared with (**a**) appeared in the comparison of W against sleep (combined N1, N2, and SWS). Note the additional appearance of two significant clusters in the posterior ACN nodes, reflecting the increase from negative Z values (anticorrelation) during wakefulness to vanishing contribution during SWS. Graph bars represent average contrast values extracted from the bilateral IPL cluster as defined in wakefulness. Note stable contribution of these nodes to the DMN across the NREM sleep stages (Sämann et al. 2011; reprinted with kind permission of Oxford University Press)

Interestingly, the uncoupling of DMN as during NREM sleep is being "recoupled" during REM sleep. Higher-order association areas, including DMN regions, and sensorimotor areas become anticorrelated and fluctuate rhythmically (Chow et al. 2013).

Using graph theoretical analysis, the alterations in the whole-brain functional organization during NREM sleep were studied (Spoormaker et al. 2010). Based on an atlas segmentation of the brain, 90 cortical and subcortical structures and their interplay were studied using a maximum overlap discrete wavelet transformation to the ROI's functional time series. Overall network metrics such as small-world organization (a marker of network efficiency) revealed significant differences between sleep stages (SWS > wakefulness > S1/S2), mainly driven by increased local clustering and a regular network structure in SWS and a shift toward a more random structure in S1/S2. Thalamocortical connectivity was drastically reduced upon sleep

onset, while cortico-cortical connectivity initially increased (similar to Larson-Prior et al. 2011), but broke down in subsequent SWS. Especially long-range connections were affected rather than local short connections. This also became evident in a hierarchical cluster analysis on functional connectivity (Spoormaker et al. 2012a). Here, disintegration of a frontoparietal network again starts in stage 1, whereas in SWS the number of local submodules increased. IPL, although persisting in the DMN during sleep, was found to be less connected to the frontal cortex in sleep. Intra-thalamic synchronization stayed high during sleep stage 1, while the thalamo-cortical connectivity fades (Larson-Prior et al. 2011; Spoormaker et al. 2012a). These data thus reveal a transition from a globally integrated functional network present during wakefulness toward a more disintegrated network falling apart into local submodules in deep sleep. Similar, functional segregation of a given system into subsystems was reported for several RSN upon sleep (Boly et al. 2012). This configuration in SWS may support optimal local processing of information in segregated modules, likely related to memory consolidation processes. In addition, a decline in frontoparietal temporal autocorrelation during sleep was reported, extending the spatial findings of DMN disintegration described above to temporal aspects (Tagliazucchi et al. 2013). Timing of information transfer within the networks, separated for higher- and lower-frequency activity, shows a reversal of cortical-hippocampal signaling in slow-wave sleep, well in line with a two-stage reciprocal communication underlying memory consolidation (Mitra et al. 2016). Besides, even within sleep stages, functional connectivity is not stable: Early 12-min segments in an SWS epoch showed smaller functional DMN connectivity than later ones (Watanabe et al. 2014).

These features of the brain network can be interpreted in the light of reduced consciousness during sleep: Impaired thalamocortical connectivity may suppress transmission of sensory input, while reduced general connectivity in deep NREM sleep limits information integration across remote brain regions. Frontoparietal clusters, being part of strongly interconnected hubs in the network during wakefulness enabling cognitive functions, also reduced the functional connectivity. Setting these results in perspective with other studies on altered states of consciousness, remarkable similarities in the brain network organization become evident: Subjects undergoing propofol-induced loss of consciousness also show a breakdown of the long-range PCC/ACC functional coupling and integration of the thalamus into the brain network as in sleep (Boveroux et al. 2010; Schröter et al. 2012). Even more compelling, patients suffering from different grades of trauma-induced loss of consciousness (minimal responsive state, vegetative state, and coma) show a similar decline in the DMN architecture, with gradually reduced PCC/ACC functional connectivity correlating with the patient's impairment (Vanhaudenhuyse et al. 2010).

It should be noted that alterations in functional network organization are not restricted to sleep per se but can also be provoked by increased sleep pressure: Reduced connectivity in DMN and ACN was reported after partial as well as after total sleep deprivation for one night (Sämann et al. 2010; De Havas et al. 2012). Sleep deprivation for 36 h induced decreased thalamo-hippocampal and thalamo-cortical connectivity (Shao et al. 2013). Similarly, daytime sleepiness correlated

with reduced thalamocortical and DMN connectivity: functional connectivity (Ward et al. 2013; Killgore et al. 2015). Finally, patients suffering from primary insomnia show increase DMN connectivity in a number of connections during wakefulness, as compared with good sleepers (Regen et al. 2016).

In summary, an influence of vigilance fluctuations on RSN organization is well documented. The fact that not only sleep but even increased sleepiness alters RSN connectivity is alarming: differences observed, e.g., in patient populations as compared with healthy controls might be caused or modulated by comorbid sleep disorders rather than signifying a feature of the primary disorder. This potential confound should always be considered. Ideally, resting state fMRI experiments should be augmented by concomitant measures of the vigilance levels, such as EEG or pupillometry (Schneider et al. 2016). Or, post hoc analysis of RSN data may be used to evaluate if the subject did fall asleep during the run. Support vector machine classifiers based on resting state fMRI in large data sets collected in polysomnographically verified sleep can be applied (Tagliazucchi et al. 2012; Altmann et al. 2016). The importance of such a post hoc test for vigilance has been impressively documented by occurrence of sleep in a third of over 1000 tested RSN experiment which were recorded during wakefulness (Tagliazucchi and Laufs 2014).

16.3.4 Animal Data

Our knowledge of the neurophysiology of sleep is for the most part based on experiments in animal models, where invasive protocols can be applied to derive detailed knowledge of the cellular mechanisms underlying sleep.

However, applying fMRI during natural sleep in animals is an extremely demanding task. Usually, animal welfare considerations allow application of MRI only in anesthetized animals. Sedation is also needed to minimize movements in addition to stereotactic fixation of the animal's head. Anesthesia of course prevents applicability of fMRI of complex behavioral tasks which can only be measured in conscious and cooperating animals.

To study unsedated animals, lengthy training periods are necessary to habituate the animal to the experimental fMRI environment. This even more holds true for natural sleep, during which the animal needs to relax and fall asleep in the restricted and extremely loud experimental setup. These considerations render the application of fMRI in animal models less attractive, especially in rodents where invasive recordings and histological analysis are easily feasible.

Nevertheless, Khubchandani and colleagues managed to conduct the only fMRI study on natural sleep in animals so far (Khubchandani et al. 2005). The authors used nonmagnetic silver wire electrodes, implanted on the skull of rats using polycarbonate screws for EEG measurements sewn to the muscle of the external canthus of the eye for EOG or implanted in the neck muscle used for EMG. Sleep-wakefulness scoring was performed differentiating low-frequency EEG with decreased EOG and EMG amplitudes as criteria for sleep, whereas high-frequency EEG with concomitant increased EOG and EMG classified

wakefulness. To immobilize the animal during the MR procedure, a mold of dental cement was attached to the skull and fixed in the animal holder during measurements. Training consisted of habituation to the scanner noise as well as to the body restraint up to several hours. Surprisingly, no gradient-induced artifacts or influences of the static magnetic field on the electrophysiological recordings have been reported at 4.7 T (Khubchandani et al. 2003). Prior to the final sleep recording, the rats were sleep deprived for 24 h. The authors applied a gradient echo fast imaging method, restricted to 3 planes passing the preoptic area. Based on image subtraction, the authors describe an increase in the signal intensities in the medial preoptic area during NREM sleep, interpreted as sleep-inducing action of this area. More consistent with imaging data from humans, concomitant signal decreases in a frontoparietal network as compared to images obtained during wakefulness were reported.

Recent experiments in rodent tried to circumvent the problems of fMRI studies during natural sleep in animals and investigated "sleep-like" states under pharmaceutical sedation using, e.g., propofol (Hudetz et al. 2016; no EEG) or urethane (Zhurakovskaya et al. 2016), as a proxy for natural sleep. Investigating differences between slow-wave activity and fast-wave activity under urethane sedation in rats, and by using the animal's respiration rate as an assay of current brain state, Wilson et al. (Wilson et al. 2011) report FC between the piriform cortex and both limbic and neocortical areas to be enhanced during slow-wave states. These results are in contradiction to the results described above in human sleep.

16.4 Summary and Outlook

The first pioneering works applying simultaneous electrophysiological readings for characterizing sleep in the MR environment were published as early as 1999 (Lovblad et al. 1999; Portas et al. 2000), mostly using stimulation protocols. The focus then shifted toward neural correlates of specific graphoelements within sleep stages like sleep spindles, slow oscillations or rapid eye movements in an event-related fashion, thus further exploiting the high temporal resolution of electrophysiological recordings and the benefits of fMRI methodology (Dang-Vu et al. 2005; Wehrle et al. 2005; Schabus et al. 2007). Recently, focus advanced toward network analyses. This progress was made possible by constantly improved EEG hardware components allowing for multimodal recordings, by increased capacities of modern MR systems for continuous data collection, and by advanced online and postprocessing algorithms simplifying classification of sleep stages during the fMRI experiment.

In future times, hardware and software developments will further enable research groups to apply more demanding experimental designs, with, e.g., fast and silent fMRI in ultrahigh field scanners.

fMRI with its intrinsic methodological advantages will essentially contribute to sleep research by targeting specific research questions. Functional changes that putatively differ across lifetime might also be addressed by neuroimaging methods

in the future. The proposed role of sleep for daytime functioning like memory consolidation and neuronal plasticity may be further disclosed, probably differentiating processes based on NREM and REM sleep-specific networks. Additional lines of research include new insights by modulation of sleep in the form of sleep deprivation and of pharmacological modulation of sleep stages. Access to information on sleep and sleepiness during fMRI will help to disentangle signal fluctuations based on vigilance alterations from direct effects of interventional influences. Direct assessment of cerebral correlates linked to sleep-related disorders in the uncomfortable experimental environment may especially benefit from improved noise cancellation methods and less restrictions to body posture. Future studies will bring new insights into spontaneous brain activity and into successful or dysfunctional cerebral compensation processes associated to sleep-related disturbances.

Acknowledgments We gratefully thank all enduring participants. Part of the authors' work performed at the Max Planck Institute in Munich was supported by a grant from the Deutsche Forschungsgemeinschaft (DFG WE 2250/6-I,II). We want to thank Florian Holsboer, Thomas Pollmächer, Dorothee P. Auer, and Thomas Wetter for the support. We owe special debts to M. Dresler, C. Kaufmann, P. G. Sämann, and V. I. Spoormaker for all their endless and engaged contributions, and A. Mann and R. Schirmer for their excellent technical support.

References

Abbasi O et al (2015) Time-frequency analysis of resting state and evoked EEG data recorded at higher magnetic fields up to 9.4 T. J Neurosci Methods 255:1–11. https://doi.org/10.1016/j.jneumeth.2015.07.011

Achermann P, Borbely AA (1997) Low-frequency (<1 Hz) oscillations in the human sleep electroencephalogram. Neuroscience 81(1):213–222

Achermann P, Borbely AA (1998) Temporal evolution of coherence and power in the human sleep electroencephalogram. J Sleep Res 7(1):36–41

Altman NR, Bernal B (2001) Brain activation in sedated children: auditory and visual functional MR imaging. Radiology 221(1):56–63. https://doi.org/10.1148/radiol.2211010074

Altmann A et al (2016) Validation of non-REM sleep stage decoding from resting state fMRI using linear support vector machines. NeuroImage 125:544–555. https://doi.org/10.1016/j.neuroimage.2015.09.072

Ambrosius U et al (2008) Heritability of sleep electroencephalogram. Biol Psychiatry 64(4):344–348. https://doi.org/10.1016/j.biopsych.2008.03.002

Andrade KC et al (2011) Sleep spindles and hippocampal functional connectivity in human NREM sleep. J Neurosci 31(28):10331–10339. https://doi.org/10.1523/JNEUROSCI.5660-10.2011

Aserinsky E, Kleitman N (1953) Regularly occurring periods of eye motility, and concomitant phenomena, during sleep. Science 118(3062):273–274

Bassetti C et al (2000) SPECT during sleepwalking. Lancet 2000:484–485. https://doi.org/10.1016/S0140-6736(00)02561-7

Bastuji H, Garcia-Larrea L (1999) Evoked potentials as a tool for the investigation of human sleep. Sleep Med Rev 3(1):23–45

Behzadi Y et al (2007) A component based noise correction method (CompCor) for BOLD and perfusion based fMRI. NeuroImage 37(1):90–101. https://doi.org/10.1016/j.neuroimage.2007.04.042

Berger H (1929) Über das Elektrenkephalogramm des Menschen. Arch Psychiatr Nervenkr 87:527–570

Bergmann TO et al (2012) Sleep spindle-related reactivation of category-specific cortical regions after learning face-scene associations. NeuroImage 59(3):2733–2742. https://doi.org/10.1016/j.neuroimage.2011.10.036

Boly M et al (2012) Hierarchical clustering of brain activity during human nonrapid eye movement sleep. Proc Natl Acad Sci U S A 109(15):5856–5861. https://doi.org/10.1073/pnas.1111133109

Born AP et al (1998) Visual activation in infants and young children studied by functional magnetic resonance imaging. Pediatr Res 44(4):578–583. https://doi.org/10.1203/00006450-199810000-00018

Born AP et al (2002a) Cortical deactivation induced by visual stimulation in human slow-wave sleep. NeuroImage 17(3):1325–1335

Born AP et al (2002b) Visual cortex reactivity in sedated children examined with perfusion MRI (FAIR). Magn Reson Imaging 20(2):199–205

Boveroux P et al (2010) Breakdown of within- and between-network resting state functional magnetic resonance imaging connectivity during propofol-induced loss of consciousness. Anesthesiology 113(5):1038–1053. https://doi.org/10.1097/ALN.0b013e3181f697f5

Braun AR et al (1997) Regional cerebral blood flow throughout the sleep-wake cycle. An H2(15) O PET study. Brain 120(7):1173–1197

Braun AR et al (1998) Dissociated pattern of activity in visual cortices and their projections during human rapid eye movement sleep. Science 279(5347):91–95

Carskadon MA, Dement WC (2017) Normal human sleep: an overview. In: Kryger M, Roth T, Dement WC (eds) Principles and practice of sleep medicine, 6th edn. Elsevier, Philadelphia, pp 15–24

Chow HM et al (2013) Rhythmic alternating patterns of brain activity distinguish rapid eye movement sleep from other states of consciousness. Proc Natl Acad Sci U S A 110(25):10300–10305. https://doi.org/10.1073/pnas.1217691110

Cicogna PC, Bosinelli M (2001) Consciousness during dreams. Conscious Cogn 10(1):26–41. https://doi.org/10.1006/ccog.2000.0471

Colrain IM, Campbell KB (2007) The use of evoked potentials in sleep research. Sleep Med Rev 11(4):277–293. https://doi.org/10.1016/j.smrv.2007.05.001

Czisch M et al (2002) Altered processing of acoustic stimuli during sleep: reduced auditory activation and visual deactivation detected by a combined fMRI/EEG study. NeuroImage. https://doi.org/10.1006/nimg.2002.1071

Czisch M et al (2004) Functional MRI during sleep: BOLD signal decreases and their electrophysiological correlates. Eur J Neurosci. https://doi.org/10.1111/j.1460-9568.2004.03518.x

Czisch M et al (2009) Acoustic oddball during NREM sleep: a combined EEG/fMRI study. PLoS One 4(8):e6749. https://doi.org/10.1371/journal.pone.0006749

Dang-Vu TT et al (2005) Cerebral correlates of delta waves during non-REM sleep revisited. NeuroImage 28(1):14–21. https://doi.org/10.1016/j.neuroimage.2005.05.028

Dang-Vu TT et al (2007) Neuroimaging in sleep medicine. Sleep Med 8(4):349–372. https://doi.org/10.1016/j.sleep.2007.03.006

Dang-Vu TT et al (2008) Spontaneous neural activity during human slow wave sleep. Proc Natl Acad Sci U S A 105(39):15160–15165. https://doi.org/10.1073/pnas.0801819105

Dang-Vu TT et al (2011) Interplay between spontaneous and induced brain activity during human non-rapid eye movement sleep. Proc Natl Acad Sci U S A 108(37):15438–15443. https://doi.org/10.1073/pnas.1112503108

Davis B et al (2016) Progression to deep sleep is characterized by changes to BOLD dynamics in sensory cortices. NeuroImage 130:293–305. https://doi.org/10.1016/j.neuroimage.2015.12.034

De Gennaro L et al (2005) An electroencephalographic fingerprint of human sleep. NeuroImage 26(1):114–122. https://doi.org/10.1016/j.neuroimage.2005.01.020

De Havas JA et al (2012) Sleep deprivation reduces default mode network connectivity and anti-correlation during rest and task performance. NeuroImage 59(2):1745–1751. https://doi.org/10.1016/j.neuroimage.2011.08.026

Deco G et al (2014) Modeling resting-state functional networks when the cortex falls asleep: local and global changes. Cereb Cortex 24(12):3180–3194. https://doi.org/10.1093/cercor/bht176

Desseilles M et al (2011) Cognitive and emotional processes during dreaming: a neuroimaging view. Conscious Cogn 20(4):998–1008. https://doi.org/10.1016/j.concog.2010.10.005
Dresler M et al (2011) Dreamed movement elicits activation in the sensorimotor cortex. Curr Biol 21(21):1833–1837. https://doi.org/10.1016/j.cub.2011.09.029
Dresler M et al (2012) Neural correlates of dream lucidity obtained from contrasting lucid versus non-lucid REM sleep: a combined EEG/fMRI case study. Sleep 35(7):1017–1020. https://doi.org/10.5665/sleep.1974
Dresler M et al (2015) Neural correlates of insight in dreaming and psychosis. Sleep Med Rev 20:92–99. https://doi.org/10.1016/j.smrv.2014.06.004
Drummond SP, Brown GG (2001) The effects of total sleep deprivation on cerebral responses to cognitive performance. Neuropsychopharmacology 25(5):68–73. https://doi.org/10.1016/S0893-133X(01)00325-6
Drummond SPA et al (2004) Functional imaging of the sleeping brain: review of findings and implications for the study of insomnia. Sleep Med Rev 8(3):227–242. https://doi.org/10.1016/j.smrv.2003.10.005
Feige B et al (2005) Cortical and subcortical correlates of electroencephalographic alpha rhythm modulation. J Neurophysiol 93(5):2864–2872. https://doi.org/10.1152/jn.00721.2004
Finelli LA, Achermann P, Borbely AA (2001a) Individual "fingerprints" in human sleep EEG topography. Neuropsychopharmacology 25(5):S57–S62. https://doi.org/10.1016/S0893-133X(01)00320-7
Finelli LA, Borbely AA, Achermann P (2001b) Functional topography of the human nonREM sleep electroencephalogram. Eur J Neurosci 13(12):2282–2290
Glover GH, Li TQ, Ress D (2000) Image-based method for retrospective correction of physiological motion effects in fMRI: RETROICOR. Magn Reson Med 44(1):162–167
Goldman RI et al (2002) Simultaneous EEG and fMRI of the alpha rhythm. Neuroreport 13(18):2487–2492. https://doi.org/10.1097/01.wnr.0000047685.08940.d0
Goncalves SI et al (2006) Correlating the alpha rhythm to BOLD using simultaneous EEG/fMRI: inter-subject variability. NeuroImage 30(1):203–213. https://doi.org/10.1016/j.neuroimage.2005.09.062
Gusnard DA et al (2001) Medial prefrontal cortex and self-referential mental activity: relation to a default mode of brain function. Proc Natl Acad Sci U S A 98(7):4259–4264. https://doi.org/10.1073/pnas.071043098
Halasz P (2016) The K-complex as a special reactive sleep slow wave - a theoretical update. Sleep Med Rev 29:34–40. https://doi.org/10.1016/j.smrv.2015.09.004
Hale JR et al (2016) Altered thalamocortical and intra-thalamic functional connectivity during light sleep compared with wake. NeuroImage 125:657–667. https://doi.org/10.1016/j.neuroimage.2015.10.041
Hennig J, Hodapp M (1993) Burst imaging. MAGMA 1:39–48
Hobson JA, Pace-Schott EF (2002) The cognitive neuroscience of sleep: neuronal systems, consciousness and learning. Nat Rev 3(9):679–693. https://doi.org/10.1038/nrn915
Hoffmann A et al (2000) Electroencephalography during functional echo-planar imaging: detection of epileptic spikes using post-processing methods. Magn Reson Med 44(5):791–798
Horikawa T et al (2013) Neural decoding of visual imagery during sleep. Science 340(6132):639–642. https://doi.org/10.1126/science.1234330
Horovitz SG et al (2008) Low frequency BOLD fluctuations during resting wakefulness and light sleep: a simultaneous EEG-fMRI study. Hum Brain Mapp 29(6):671–682. https://doi.org/10.1002/hbm.20428
Horovitz SG et al (2009) Decoupling of the brain's default mode network during deep sleep. Proc Natl Acad Sci U S A 106(27):11376–11381. https://doi.org/10.1073/pnas.0901435106
Huber R et al (2006) Arm immobilization causes cortical plastic changes and locally decreases sleep slow wave activity. Nat Neurosci 9(9):1169–1176. https://doi.org/10.1038/nn1758
Hudetz AG et al (2016) Propofol anesthesia reduces Lempel-Ziv complexity of spontaneous brain activity in rats. Neurosci Lett 628:132–135. https://doi.org/10.1016/j.neulet.2016.06.017

Ioannides AA et al (2004) MEG tomography of human cortex and brainstem activity in waking and REM sleep saccades. Cereb Cortex 14(1):56–72
Jahnke K et al (2012) To wake or not to wake? The two-sided nature of the human K-complex. NeuroImage 59(2):1631–1638. https://doi.org/10.1016/j.neuroimage.2011.09.013
Jorge J et al (2015) Towards high-quality simultaneous EEG-fMRI at 7 T: detection and reduction of EEG artifacts due to head motion. NeuroImage 120:143–153. https://doi.org/10.1016/j.neuroimage.2015.07.020
Kaufmann C et al (2006) Brain activation and hypothalamic functional connectivity during human non-rapid eye movement sleep: an EEG/fMRI study. Brain. https://doi.org/10.1093/brain/awh686
Kaufmann C et al (2007) Beyond noise: reply to Laufs et al. [2]. Brain 130(7):e76. https://doi.org/10.1093/brain/awm085
Khubchandani M et al (2003) Stereotaxic assembly and procedures for simultaneous electrophysiological and MRI study of conscious rat. Magn Reson Med 49(5):962–967. https://doi.org/10.1002/mrm.10441
Khubchandani M et al (2005) Functional MRI shows activation of the medial preoptic area during sleep. NeuroImage 26(1):29–35. https://doi.org/10.1016/j.neuroimage.2005.01.002
Killgore WDS et al (2015) Daytime sleepiness is associated with altered resting thalamocortical connectivity. Neuroreport 26(13):779–784. https://doi.org/10.1097/WNR.0000000000000418
Klinzing JG et al (2016) Spindle activity phase-locked to sleep slow oscillations. NeuroImage 134:607–616. https://doi.org/10.1016/j.neuroimage.2016.04.031
Koike T et al (2011) Connectivity pattern changes in default-mode network with deep non-REM and REM sleep. Neurosci Res 69(4):322–330. https://doi.org/10.1016/j.neures.2010.12.018
Kurth S et al (2010) Mapping of cortical activity in the first two decades of life: a high-density sleep electroencephalogram study. J Neurosci 30(40):13211–13219. https://doi.org/10.1523/JNEUROSCI.2532-10.2010
Larson-Prior LJ et al (2009) Cortical network functional connectivity in the descent to sleep. Proc Natl Acad Sci U S A 106(11):4489–4494. https://doi.org/10.1073/pnas.0900924106
Larson-Prior LJ et al (2011) Modulation of the brain's functional network architecture in the transition from wake to sleep. Prog Brain Res 193:277–294. https://doi.org/10.1016/B978-0-444-53839-0.00018-1
Laufs H, Walker MC, Lund TE (2007) 'Brain activation and hypothalamic functional connectivity during human non-rapid eye movement sleep: an EEG/fMRI study'–its limitations and an alternative approach. Brain 2007:e75. https://doi.org/10.1093/brain/awm084
Llinas RR, Pare D (1991) Of dreaming and wakefulness. Neuroscience 44(3):521–535
Loomis A, Harvey N, Hobart G (1938) Distribution of disturbance patterns in the human electroencephalogram, with special reference to sleep. J Neurophysiol 1:413–430
Lovblad KO et al (1999) Silent functional magnetic resonance imaging demonstrates focal activation in rapid eye movement sleep. Neurology 53(9):2193–2195
Mandelkow H et al (2006) Synchronization facilitates removal of MRI artefacts from concurrent EEG recordings and increases usable bandwidth. NeuroImage 32(3):1120–1126. https://doi.org/10.1016/j.neuroimage.2006.04.231
Manning JH, Courchesne E, Fox PT (2013) Intrinsic connectivity network mapping in young children during natural sleep. NeuroImage 83:288–293. https://doi.org/10.1016/j.neuroimage.2013.05.020
Maquet P (2000) Functional neuroimaging of normal human sleep by positron emission tomography. J Sleep Res 9(3):207–231
Maquet P et al (1996) Functional neuroanatomy of human rapid-eye-movement sleep and dreaming. Nature 383(6596):163–166. https://doi.org/10.1038/383163a0
Martin E et al (1999) Visual processing in infants and children studied using functional MRI. Pediatr Res 46(2):135–140
Massimini M, Rosanova M, Mariotti M (2003) EEG slow (approximately 1 Hz) waves are associated with nonstationarity of thalamo-cortical sensory processing in the sleeping human. J Neurophysiol 89(3):1205–1213. https://doi.org/10.1152/jn.00373.2002

Mitra A et al (2016) Human cortical-hippocampal dialogue in wake and slow-wave sleep. Proc Natl Acad Sci U S A 113(44):E6868–E6876. https://doi.org/10.1073/pnas.1607289113
Moosmann M et al (2003) Correlates of alpha rhythm in functional magnetic resonance imaging and near infrared spectroscopy. NeuroImage 20(1):145–158
Nofzinger EA, Maquet P (2017) What brain imaging reveals about sleep generation and maintenance. In: Principles and practice of sleep medicine. Elsevier, Amsterdam, pp 118–131
Nofzinger EA et al (1997) Forebrain activation in REM sleep: an FDG PET study. Brain Res 770(1-2):192–201
Pace-Schott EF, Hobson JA (2002) The neurobiology of sleep: genetics, cellular physiology and subcortical networks. Nat Rev 3(8):591–605. https://doi.org/10.1038/nrn895
Peters AC et al (2014) One night of partial sleep deprivation affects habituation of hypothalamus and skin conductance responses. J Neurophysiol 112(6):1267–1276. https://doi.org/10.1152/jn.00657.2013
Portas CM et al (2000) Auditory processing across the sleep-wake cycle: simultaneous EEG and fMRI monitoring in humans. Neuron 28(3):991–999
Raichle ME et al (2001) A default mode of brain function. Proc Natl Acad Sci U S A 98(2):676–682. https://doi.org/10.1073/pnas.98.2.676
Rasch B et al (2007) Odor cues during slow-wave sleep prompt declarative memory consolidation. Science 315(5817):1426–1429. https://doi.org/10.1126/science.1138581
Rechtschaffen A, Kales A (1968) A manual of standardized terminology, techniques and scoring system for sleep stages of human subjects. Arch Gen Psychiatry 20(2):246–247
Redcay E, Kennedy DP, Courchesne E (2007) fMRI during natural sleep as a method to study brain function during early childhood. NeuroImage 38(4):696–707. https://doi.org/10.1016/j.neuroimage.2007.08.005
Regen W et al (2016) Objective sleep disturbances are associated with greater waking resting-state connectivity between the retrosplenial cortex/hippocampus and various nodes of the default mode network. J Psychiatry Neurosci 41(5):295–303. https://doi.org/10.1503/jpn.140290
Salimi-Khorshidi G et al (2014) Automatic denoising of functional MRI data: combining independent component analysis and hierarchical fusion of classifiers. NeuroImage 90:449–468. https://doi.org/10.1016/j.neuroimage.2013.11.046
Sallinen M, Kaartinen J, Lyytinen H (1996) Processing of auditory stimuli during tonic and phasic periods of REM sleep as revealed by event-related brain potentials. J Sleep Res 5(4):220–228
Sämann PG et al (2010) Increased sleep pressure reduces resting state functional connectivity. MAGMA 23(5–6):375–389. https://doi.org/10.1007/s10334-010-0213-z
Sämann PG et al (2011) Development of the brain's default mode network from wakefulness to slow wave sleep. Cereb Cortex 21(9):2082–2093. https://doi.org/10.1093/cercor/bhq295
Schabus M et al (2007) Hemodynamic cerebral correlates of sleep spindles during human non-rapid eye movement sleep. Proc Natl Acad Sci U S A 104(32):13164–13169. https://doi.org/10.1073/pnas.0703084104
Schneider M et al (2016) Spontaneous pupil dilations during the resting state are associated with activation of the salience network. NeuroImage 139:189–201. https://doi.org/10.1016/j.neuroimage.2016.06.011
Schröter MS et al (2012) Spatiotemporal reconfiguration of large-scale brain functional networks during propofol-induced loss of consciousness. J Neurosci 32(37):12832–12840. https://doi.org/10.1523/JNEUROSCI.6046-11.2012
Shao Y et al (2013) Decreased thalamocortical functional connectivity after 36 hours of total sleep deprivation: evidence from resting state FMRI. PLoS One 8(10):e78830. https://doi.org/10.1371/journal.pone.0078830
Silber MH et al (2007) The visual scoring of sleep in adults. J Clin Sleep Med 3(2):121–131
Spoormaker VI et al (2010) Development of a large-scale functional brain network during human non-rapid eye movement sleep. J Neurosci 30(34):11379–11387. https://doi.org/10.1523/JNEUROSCI.2015-10.2010
Spoormaker VI, Gleiser PM, Czisch M (2012a) Frontoparietal connectivity and hierarchical structure of the brain's functional network during sleep. Front Neurol 3:80. https://doi.org/10.3389/fneur.2012.00080

Spoormaker VI et al (2012b) Effects of rapid eye movement sleep deprivation on fear extinction recall and prediction error signaling. Hum Brain Mapp. https://doi.org/10.1002/hbm.21369
Spreng RN, Grady CL (2010) Patterns of brain activity supporting autobiographical memory, prospection, and theory of mind, and their relationship to the default mode network. J Cogn Neurosci 22(6):1112–1123. https://doi.org/10.1162/jocn.2009.21282
Steriade M (2003) The corticothalamic system in sleep. Front Biosci 8:878–899
Steriade M (2006) Grouping of brain rhythms in corticothalamic systems. Neuroscience 137(4):1087–1106. https://doi.org/10.1016/j.neuroscience.2005.10.029
Tagliazucchi E, Laufs H (2014) Decoding wakefulness levels from typical fMRI resting-state data reveals reliable drifts between wakefulness and sleep. Neuron 82(3):695–708. https://doi.org/10.1016/j.neuron.2014.03.020
Tagliazucchi E et al (2012) Automatic sleep staging using fMRI functional connectivity data. NeuroImage 63(1):63–72. https://doi.org/10.1016/j.neuroimage.2012.06.036
Tagliazucchi E et al (2013) Breakdown of long-range temporal dependence in default mode and attention networks during deep sleep. Proc Natl Acad Sci U S A 110(38):15419–15424. https://doi.org/10.1073/pnas.1312848110
Takahara M, Nittono H, Hori T (2002) Comparison of the event-related potentials between tonic and phasic periods of rapid eye movement sleep. Psychiatry Clin Neurosci 56(3):257–258. https://doi.org/10.1046/j.1440-1819.2002.00999.x
Tanaka H et al (2003) Effect of stage 1 sleep on auditory cortex during pure tone stimulation: evaluation by functional magnetic resonance imaging with simultaneous EEG monitoring. AJNR Am J Neuroradiol 24(10):1982–1988
Tarokh L, Carskadon MA, Achermann P (2011) Trait-like characteristics of the sleep EEG across adolescent development. J Neurosci 31(17):6371–6378. https://doi.org/10.1523/JNEUROSCI.5533-10.2011
Tucker AM, Dinges DF, Van Dongen HPA (2007) Trait interindividual differences in the sleep physiology of healthy young adults. J Sleep Res 16(2):170–180. https://doi.org/10.1111/j.1365-2869.2007.00594.x
van Dongen EV et al (2011) Functional connectivity during light sleep is correlated with memory performance for face-location associations. NeuroImage 57(1):262–270. https://doi.org/10.1016/j.neuroimage.2011.04.019
van Duinen H et al (2005) Surface EMG measurements during fMRI at 3T: accurate EMG recordings after artifact correction. NeuroImage 27(1):240–246. https://doi.org/10.1016/j.neuroimage.2005.04.003
Van Essen DC, Dierker DL (2007) Surface-based and probabilistic atlases of primate cerebral cortex. Neuron 56(2):209–225. https://doi.org/10.1016/j.neuron.2007.10.015
van Rootselaar A-F et al (2007) fMRI analysis for motor paradigms using EMG-based designs: a validation study. Hum Brain Mapp 28(11):1117–1127. https://doi.org/10.1002/hbm.20336
Vanhaudenhuyse A et al (2010) Default network connectivity reflects the level of consciousness in non-communicative brain-damaged patients. Brain 133(1):161–171. https://doi.org/10.1093/brain/awp313
Voss U et al (2009) Lucid dreaming: a state of consciousness with features of both waking and non-lucid dreaming. Sleep 32(9):1191–1200
Ward AM et al (2013) Daytime sleepiness is associated with decreased default mode network connectivity in both young and cognitively intact elderly subjects. Sleep 36(11):1609–1615. https://doi.org/10.5665/sleep.3108
Watanabe T et al (2014) Network-dependent modulation of brain activity during sleep. NeuroImage 98:1–10. https://doi.org/10.1016/j.neuroimage.2014.04.079
Wehrle R et al (2005) Rapid eye movement-related brain activation in human sleep: a functional magnetic resonance imaging study. Neuroreport 16(8):853–857. https://doi.org/10.1097/00001756-200505310-00015
Wehrle R et al (2007) Functional microstates within human REM sleep: first evidence from fMRI of a thalamocortical network specific for phasic REM periods. Eur J Neurosci. https://doi.org/10.1111/j.1460-9568.2007.05314.x

Wilke M, Holland SK, Ball WSJ (2003) Language processing during natural sleep in a 6-year-old boy, as assessed with functional MR imaging. AJNR Am J Neuroradiol 24(1):42–44
Wilson DA et al (2011) State-dependent functional connectivity of rat olfactory system assessed by fMRI. Neurosci Lett 497(2):69–73. https://doi.org/10.1016/j.neulet.2011.04.031
Wilson RS et al (2015) Influence of epoch length on measurement of dynamic functional connectivity in wakefulness and behavioural validation in sleep. NeuroImage 112:169–179. https://doi.org/10.1016/j.neuroimage.2015.02.061
Zhurakovskaya E et al (2016) Global functional connectivity differences between sleep-like states in Urethane anesthetized rats measured by fMRI. PLoS One 11(5):e0155343. https://doi.org/10.1371/journal.pone.0155343

EEG–fMRI in Adults with Focal Epilepsy

17

Umair J. Chaudhary, Matthew C. Walker, and Louis Lemieux

17.1 Introduction

The application of EEG-correlated fMRI (EEG–fMRI) in adults with focal epilepsy has two principal aims: to improve our understanding of the generators of epileptiform activity and to improve the surgical treatment of epilepsy. EEG–fMRI has been used to study scalp *interictal* epileptiform discharges (IEDs) (Coan et al. 2016; Kobayashi et al. 2006b; Markoula et al. 2018; Pittau et al. 2017; Salek-Haddadi et al. 2006; Thornton et al. 2011; Zijlmans et al. 2007) and seizures (Abreu et al. 2005; Chaudhary et al. 2012a; Di Bonaventura et al. 2006b; Diekmann and Hoppner 2014; Donaire et al. 2009a; Donaire et al. 2009b;Federico et al. 2005a; Fernandez et al. 2011; Hamandi et al. 2006; Kobayashi et al. 2006c; Marrosu et al. 2009; Morano et al. 2017; Morocz et al. 2003; Salek-Haddadi et al. 2002; Salek-Haddadi et al. 2009; Sierra-Marcos et al. 2013; Thornton et al. 2010b; Tyvaert et al. 2008; Tyvaert et al. 2009; Usami et al. 2016; Vaudano et al. 2012; Vaudano et al. 2013). The relative abundance of IEDs (and the lack of associated clinical manifestations) drove the initial development of EEG–fMRI with a view to studying the fMRI signal changes associated with epileptic activity (Hill et al. 1995; Ives et al. 1993). Previously, fMRI had been employed to study the haemodynamic correlates of seizures, relying on visual observation of the patient for interpretation of the BOLD

U. J. Chaudhary
Neurology Department, Queen Elizabeth Hospital, University Hospitals Birmingham NHS Foundation Trust, Birmingham, United Kingdom

National Hospital for Neurology and Neurosurgery, Queen Square, London, United Kingdom
e-mail: umair.chaudhary@ucl.ac.uk

M. C. Walker · L. Lemieux (✉)
UCL Queen Square Institute of Neurology, UCL, London, UK
e-mail: m.walker@ucl.ac.uk; louis.lemieux@ucl.ac.uk

C. Mulert, L. Lemieux (eds.), *EEG - fMRI*,
https://doi.org/10.1007/978-3-031-07121-8_17

signal changes. Ictal BOLD changes are, however, generally widespread, long lasting and difficult to interpret, particularly without concurrent EEG (Detre et al. 1995; Jackson et al. 1994; Krings et al. 2000; Salek-Haddadi et al. 2003a).

Analysis of scalp IEDs is not without its problems. Scalp IEDs may reflect propagated activity rather than the source. Furthermore, even when the scalp IEDs are representative of the source or sources, there are no unique solutions to the generator location problem, and such solutions depend upon critical assumptions (such as the number of sources). EEG–fMRI is free from such assumptions and may therefore give a more accurate indication of the source or sources of IEDs.

EEG–fMRI may also help with surgical evaluation, and this chapter will mainly deal with this subject. The assessment of curative resective surgery is aimed at identifying the epileptogenic zone (Rosenow and Luders 2001). This relies upon the convergence of presurgical investigations, including clinical history, seizure semiology, long-term video EEG, neuroimaging and neuropsychometry. Discordance between these may lead to a lesser chance of surgical success and the need for further investigation (e.g. further non-invasive imaging, invasive EEG recordings). The relative weight that is lent to each of these investigations varies depending on the lobar localisation and the pathogenesis of the epilepsy and in many instances is either controversial or undetermined. The role of EEG–fMRI in the presurgical assessment of people with focal epilepsy has expanded over the last decade; there have been studies specifically addressing this issue and these are discussed below. One of the main criticisms that can be levelled at EEG–fMRI (indeed a criticism that can be levelled at other investigations such as magnetoencephalography) is that majority of studies to date have assessed interictal rather than ictal activity. This raises two questions: what does interictal activity represent, and how does it relate to the epileptogenic zone? We will therefore address the nature of an interictal spike and the relevance of interictal activity to presurgical evaluations before discussing in detail the possible roles of EEG–fMRI.

Up to now, most ictal EEG–fMRI data have been obtained due to the fortuitous occurrence of a seizure or seizures in the course of what was intended to be interictal EEG–fMRI investigation, with the exception of few studies with strict selection criteria on seizure frequency and the use of activation procedures in patients with reflex epilepsy. Ictal EEG–fMRI offers the chance to address the main limitation of previous studies into the BOLD changes that occur in conjunction with spontaneous seizures, namely the lack of EEG. However, the technique is limited by the relative rarity and unpredictability of seizures, time constraints and safety considerations due to the confined space of the magnet bore and limited access.

As described in the Chap. 12, regions of BOLD increase or decrease related to events of interest such as epileptiform activity can be identified using EEG-derived linear models of the fMRI time course, in what is effectively a correlation analysis. The main steps in this approach are EEG event detection and classification; choice of a mathematical representation for the events (e.g. unitary spike, block, etc.); choice of haemodynamic basis set for convolution with the mathematic representation, resulting in an event-related linear model of the event; inclusion of nuisance effects. Individual spikes can be conceived as zero-duration events, at least on the timescale of fMRI, and are therefore usually represented as a mathematical spike with no scope for EEG-derived dynamics to be included in the models of the BOLD

time course. However, a number of haemodynamic function basis sets are available for convolution, from the so-called canonical HRF to series of gamma functions, each corresponding to a different set of assumptions and therefore liable to reveal different activation patterns. This is in contrast to (extended) seizures, for which the choice of event mathematical representations is greater (fixed amplitude block, series of spikes, etc.), in addition to the choice of haemodynamic basis sets. Some of these modelling issues will be discussed in greater detail in this chapter.

17.2 Interictal EEG–fMRI

17.2.1 What Is an Interictal Spike?

Epileptiform interictal EEG abnormalities include spikes, which are fast electrographic transients lasting less than 70 ms; and sharp waves, which last 70–120 ms (de Curtis and Avanzini 2001). That these are pathological is supported by their very rare occurrence (<1%) in healthy individuals (Gregory et al. 1993) and their strong association with epilepsy (Marsan and Zivin 1970). Spikes and sharp waves are often followed by a slow wave lasting hundreds of milliseconds. As discussed below, this slow wave probably represents a period of relative refractoriness. It has been established from concomitant field potential and intracellular recordings that the intracellular correlate of the interictal spike is the paroxysmal depolarising shift (Matsumoto and Marsan 1964), a slow depolarising potential with a high-frequency (>200 Hz) burst of action potentials. A number of pathological mechanisms have been proposed to underlie the interictal spike, including the intrinsic burst properties of neurons and the synchronisation of neuronal populations.

The interictal spike is terminated by the activation of hyperpolarising GABA(A) and GABA(B) receptor-mediated currents and calcium-dependent potassium currents (de Curtis and Avanzini 2001; McCormick and Contreras 2001). Therefore, interictal spikes activate hyperpolarising currents, resulting in a post-spike refractory period during which neuronal activity is inhibited (de Curtis and Avanzini 2001). The effective activation of these currents by the interictal spike raises the possibility that spikes can be anti-ictogenic. There is evidence that this may be the case or at least that spikes are intrinsically different from a seizure.

A seizure is not the evolution of spike discharges but can begin as a distinct high-frequency rhythm. Spike discharges can precede the seizure with progressively less effective after hyperpolarisations in mesial temporal lobe epilepsy (King and Spencer 1995), but ictal activity remains a distinct phenomenon. Furthermore, increased interictal spiking occurs after the seizure, raising the possibility that this is a compensatory antiepileptic response (de Curtis and Avanzini 2001). Experiments in entorhinal cortex-hippocampal slice preparations have confirmed the antiepileptic potential of spikes. Spike discharges generated in the CA3 region inhibited epileptic activity in the entorhinal cortex, so that sectioning of the Schaffer collaterals led to potentiation of entorhinal cortex seizure activity (Barbarosie and Avoli 1997). This leads to two important conclusions: first, interictal spikes can have an inhibitory effect; second, they can have this effect remote from where the spikes arise.

Since interictal spikes are not a normal characteristic of the brain, they are necessarily indicative of pathology. However, they are not necessarily indicative of the area from which seizures arise. This raises an important question: do all the spiking cortex (in addition to the area in which a seizure arises) have to be removed for a successful surgical outcome; in other words, once the ictogenic area has been removed, can the irritative zone generate seizures? If this were so, then identifying the full extent of the irritative zone would be critical to directing surgery and to predicting surgical outcome.

It appears that the irritative zone has different implications for different aetiologies and lobar localisations. Furthermore, not all spikes are equal and certain patterns appear to carry greater weight, perhaps being more indicative of cortex that can initiate seizures as well as maintain interictal discharges.

17.2.2 Interictal Epileptiform Activity in Presurgical Assessment

This relevance of interictal activity depends on lobe and aetiology. The predictive value of IEDs in temporal lobe epilepsy has been the subject of numerous conflicting studies. Nevertheless, a number of conclusions can be drawn about interictal activity and temporal lobe epilepsy. The side that most consistently has interictal spikes has a high chance (>90%) of being the side from which seizures arise (Blume et al. 1993; Blume 2001). However, in a single recording session, this probability drops to approximately 75% (Blume 2001). This is similar for scalp, depth and subdural recordings. Reassuringly, the most consistent spikes recorded with subdural electrodes have a >90% chance of arising from the same lobe and >70% chance of arising from the same gyrus as the seizures (Blume et al. 2001a; Blume 2001). Although subdural electrodes have a limited coverage, these translate into a high chance that seizures arise ipsilateral to and in the vicinity of interictal spikes. Furthermore, repeated recordings lead to improved specificity. Prominent contralateral interictal activity and/or interictal activity discordant with the ictal onset zone carry a decreased chance of surgical success (Duncan 2007, 2011; Palmer et al. 1999; Schulz et al. 2000).

These results suggest that localising interictal activity in temporal lobe epilepsy may give accurate information on the epileptogenic zone and an indication of prognosis following surgical resection. The data for interictal activity in patients with extratemporal lobe seizures are less promising. This is because of frequent propagation (often to other lobes) and larger irritative and epileptogenic zones. However, MEG studies and source localisation with high-density scalp EEG have revealed that, even in extratemporal studies, there can be a considerable concordance between interictal activity and ictal onset zone (Herrendorf et al. 2000; Stefan et al. 2003). Indeed, it has been suggested that highly localised MEG activity in some instances may obviate the requirement for intracranial EEG recordings.

The use of scalp EEG to identify interictal activity has another consequence. It is suggested that synchronous or nearly synchronous activation of as much as 10–20 cm^2 of gyral cortex is necessary to give a spike detectable by scalp electrodes

(Tao et al. 2005, 2007). The immediate conclusion is that any method that relies on scalp EEG activity will only detect activations involving large cortical areas. Alternatively, a positive consequence of this filtering may be the effective selection of more significant and relevant interictal activity.

Therefore, interictal activity commonly overlaps with the seizure onset zone but is often more extensive. Does it reveal cortex beyond the ictal onset zone that needs to be resected in order to obtain a successful surgical outcome? Studies in patients with encephalomalacia suggest that resection of spiking cortex is necessary for a good surgical outcome (Kazemi et al. 1997), while studies of patients with mesial temporal lobe epilepsy are controversial (Schwartz et al. 1997). Certainly removal of the whole area with epileptogenic potential is necessary for surgical success, i.e. removal of epileptogenic zone (Luders et al. 2006; Rosenow and Luders 2001). Indeed, a note of caution needs to be made in the interpretation of many studies in that larger resections are, a priori, likely to be associated with better surgical outcome; the challenge is to remove as little cortex as necessary to have a successful outcome. Certain spikes seem to be of greater importance, such as leading discharges—those that occur on a millisecond basis prior to others (Alarcon et al. 1997). Further, paroxysmal fast and runs of repetitive spikes have greater significance than isolated spikes in cortical dysplasia (Widdess-Walsh et al. 2007). All spikes are therefore not equal.

What implications do these findings have for the application of EEG–fMRI in focal epilepsy?

1. There may be a difference in its utility between temporal and extratemporal lobe epilepsies.
2. EEG–fMRI may be of greater localising value in certain aetiologies.
3. Scalp EEG–fMRI may be limited to the most significant spikes involving the largest cortical areas.
4. The area revealed by EEG–fMRI is likely to be larger than the epileptogenic zone.
5. Scalp EEG–fMRI is unlikely to be able to differentiate spikes that are of greatest importance (e.g. leading spikes) because of the temporal resolution of fMRI.

These indicate that EEG–fMRI may have utility as an additional presurgical investigation, perhaps to guide intracranial EEG placement. Even in this respect, certain problems remain. Many patients (see below) may not have suitable discharges on scalp EEG and therefore cannot be used in EEG–fMRI studies. However, with developing analysis techniques, lack of interictal discharges on scalp EEG during simultaneous EEG-fMRI has been addressed to some extent (Grouiller et al. 2010) using spike topography correlation maps. In addition, the scalp EEG spikes are likely to represent only a proportion of spikes that are occurring in a region, and since EEG–fMRI in effect compares BOLD signal at the time of scalp spikes with that at the time of no spikes on scalp EEG, then the power of this method may be reduced, resulting in a failure to detect significant BOLD changes. These factors may substantially reduce the impact of EEG–fMRI on presurgical investigation. For this reason, the search for other EEG features (such as focal fast activity or focal

slow) or other EEG analyses that may correlate with activity in the epileptogenic zone recorded with intracranial electrodes is also the subject of research.

17.2.3 Methodology

17.2.3.1 Data Acquisition

The technological aspects of EEG–fMRI data acquisitions are discussed in the Chaps. 7, 8, 9, 10, and 11, and the different data acquisition modes (and data analysis) are discussed in the Chap. 12. Here, we will focus on the main methodological aspects of studies on patients with epilepsy. In brief, EEG–fMRI has mainly been performed on conventional MR scanners using BOLD-weighted EPI sequences, with field strengths in the range 1.5–3 T, and using EEG recording equipment specifically designed for EEG–fMRI. The so-called "MR-compatible" EEG devices are designed to minimise the electromagnetic interactions between the two data acquisition systems (artefacts in the EEG and images), ensure data synchrony (commonly achieved by recording a scanner clock-derived signal as one of the EEG or auxiliary channels), record the ECG and minimise the additional health risks to the subject.

Patients are generally at rest in the MR scanner. Manipulation of drug levels has been used in some studies to modulate the rate of IED, creating "control" and "active" states with corresponding sets of scans acquired in separate, successive sessions. Special attention to mechanical means of head immobilisation is recommended, as patients are more prone to motion than healthy volunteers. Initial EEG–fMRI in epilepsy studies universally utilised "spike- or EEG-triggered fMRI", employing a form of interleaved multimodal acquisition, whereby two sets of fMRI datasets were acquired in one session: one set consisting of (single or burst) scans acquired following the detection of an event of interest (e.g. IED) on EEG, and another set of scans acquired following periods of normal background (control state). Spike-triggered fMRI was a way of avoiding the problem of image acquisition artefact, which is caused by the switching magnetic gradients and obscures the EEG. Following technological developments that made it possible to remove or reduce the image acquisition artefact, continuous EEG–fMRI became possible, providing good-quality EEG data throughout the scanning process. This is now the favoured acquisition mode due to its ability to visualise the entire EEG, which may increase sensitivity but also has advantages from the point of view of fMRI modelling. For example, in spike-triggered fMRI, scans were acquired roughly from 4 s following an event of interest, based on the assumption that the BOLD change would peak at around 5–6 s post-spike; the lack of temporal continuity in the control scan dataset hinders baseline modelling. It also has the advantage of not requiring online identification of spikes.

17.2.3.2 Data Analysis

The primary aim of EEG–fMRI data analysis is usually the identification of regions of IED-related BOLD change, and the time course of those changes is an important secondary aim. This is the conventional brain-mapping problem of event-related

fMRI, with the difference that the experimental design is totally unknown until after the data have been acquired and the EEG has been reviewed, in contrast to conventional paradigm-driven fMRI studies.

The most commonly used fMRI mapping approach is based on building a general linear model (GLM) of the BOLD time course (see the Chap. 12 for a further explanation of the GLM-based approach to fMRI analysis). For data acquired using the spike-triggered scheme, the two sets of scans ("spike" and "control") were simply compared voxel-wise using a *t* test. For continuous EEG–fMRI, one must attempt to model the entire fMRI time series, which is a greater challenge. In summary, the main steps of the GLM building process to identify areas of interest in epilepsy are: (1) identification of events of interest (spikes, runs of spikes, other pathological discharges); (2) classification of the events of interest (grouping according to morphology, field topography); (3) mathematical representation of the events of interest (as "zero-duration/delta function" events, blocks of event runs, etc.); (4) choice of a model of the HRF for convolution: canonical HRF with inclusion of temporal and dispersion derivatives; or another basis set (e.g. Fourier over block). The result is a set of regressors representing the BOLD changes predicted to occur in relation to the IED.

The reliable identification of EEG events of interest requires dedicated review software to reduce or remove pulse-related and image acquisition artefacts (see the Chaps. 8 and 9). EEG event markers are defined in real time and in relation to the fMRI scan series, thanks to scan time markers on the EEG record provided by the scanner–EEG synchronisation mechanism. The resulting event markers form the basis of the modelling of the effects of interest.

The baseline is the other, equally important, side of the statistical comparison that is applied at every brain voxel to reveal BOLD changes linked to the effect or effects of interest (spikes). In EEG terms, the intervals between the marked events of interest are usually considered to constitute the control state. In fact, this "baseline state" is subject to multiple sources of signal variation: physiological (neurological and other) and artefactual (head motion or scanner related). For example, we know from intracranial EEG recordings that the scalp EEG is a very biased and limited representation of physiological or pathological brain activity, reflecting a fundamental limitation of EEG–fMRI. Nonetheless, the effects of confounding factors on the fMRI signal may be added to the model, such as motion and cardiac via the ECG (see Salek-Haddadi et al. 2003b).

The parameters (mathematical weight of each regressor) of the resulting GLM are then estimated at each voxel and can be tested against the null hypothesis (i.e. parameter estimate not significantly different from zero). The *z* scores for each effect are then mapped across the scanned brain to produce statistical parametric maps (SPM).

An important point to keep in mind is that, given a particular EEG record, one may have a large number of possible GLMs, each effectively corresponding to a different set of questions or hypotheses about the relationship between EEG and BOLD. For example, different EEG observers are likely to identify and classify events differently; this will produce different GLMs. Given a set of EEG events, one may choose to focus on detecting the brain regions for which the spike-related

BOLD time course has a fixed shape (e.g. canonical HRF) or to identify brain regions for which the spike-related BOLD time course can have any of a wide variety of shapes (e.g. using the Fourier basis set). The former maximises sensitivity to a specific pattern (the same response is expected irrespective of position), while the latter can be used to both estimate the shape of the time course and identify inter-regional variations in the relationship between event of interest and BOLD signal (i.e. the time course of the BOLD change can vary across the brain).

The principal outputs of fMRI model estimations are statistical maps and time plots of the estimated event-related responses. For example, localisation of the regional BOLD changes is often assessed in relation to the epileptogenic or irritative zones (known or presumed) to provide evidence of validity or potential clinical utility (e.g. as a potential non-invasive adjunct to current localisation techniques). The interpretation of the maps can be facilitated by co-registering them with more anatomically accurate MR images, such as those obtained from T1-weighted volumetric sequences, and the use of atlases (also often based on volumetric sequences or on photographic atlases) for anatomical labelling. However, both methods are prone to error due to differences in the physics of image formation for the two types of sequence, which can result in significant co-registration errors and mislocalisation/labelling (see Gholipour et al. 2007; Gholipour et al. 2008a; Gholipour et al. 2008b for reviews). Concordance of the BOLD maps has been assessed in relation to the presumed or known irritative zone/seizure onset zone/epileptogenic zone at various scales, from lobar (BOLD cluster located in the same lobe) to millimetric (by measurement in Cartesian space or along the cortical surface). BOLD maps usually show a complex pattern of multiple clusters and various criteria have been employed to assess the spatial agreement between BOLD clusters and the presumed or known irritative zone/seizure onset zone/epileptogenic zone. These criteria include localisation of the most statistically significant BOLD cluster, localisation of the cluster corresponding to the earliest BOLD increase or localisation of the most statistically significant BOLD cluster with a cut-off threshold for predefined spatial and statistical thresholds. One of the approaches is to classify BOLD maps as concordant (all BOLD clusters within the independently defined epileptogenic zone); concordant plus (statistically most significant BOLD cluster is concordant but other BOLD clusters are discordant); some concordance (statistically most significant BOLD cluster is discordant but one of the other BOLD clusters is concordant; discordant (all BOLD clusters are discordant) (Chaudhary et al. 2012a, 2013, 2016; Di Bonaventura et al. 2006b; Donaire et al. 2009b, 2013; Gotman et al. 2005; Hamandi et al. 2004; Salek-Haddadi et al. 2006; Thornton et al. 2011).

The interpretation of the shape of the BOLD change over time is of interest from two points of view: the assessment of deviations from the "canonical" HRF observed during physiological tasks and the direction of the epilepsy-related BOLD changes relative to baseline. The first can be addressed by modelling the BOLD changes related to spikes (considered as zero-duration events) using a flexible basis set such as the Fourier expansion ((Josephs et al. 1997); also see the Chap. 12). The first application of continuous EEG–fMRI illustrated the interest in using a flexible modelling approach to plot the spike-related BOLD time course (see Fig. 17.1).

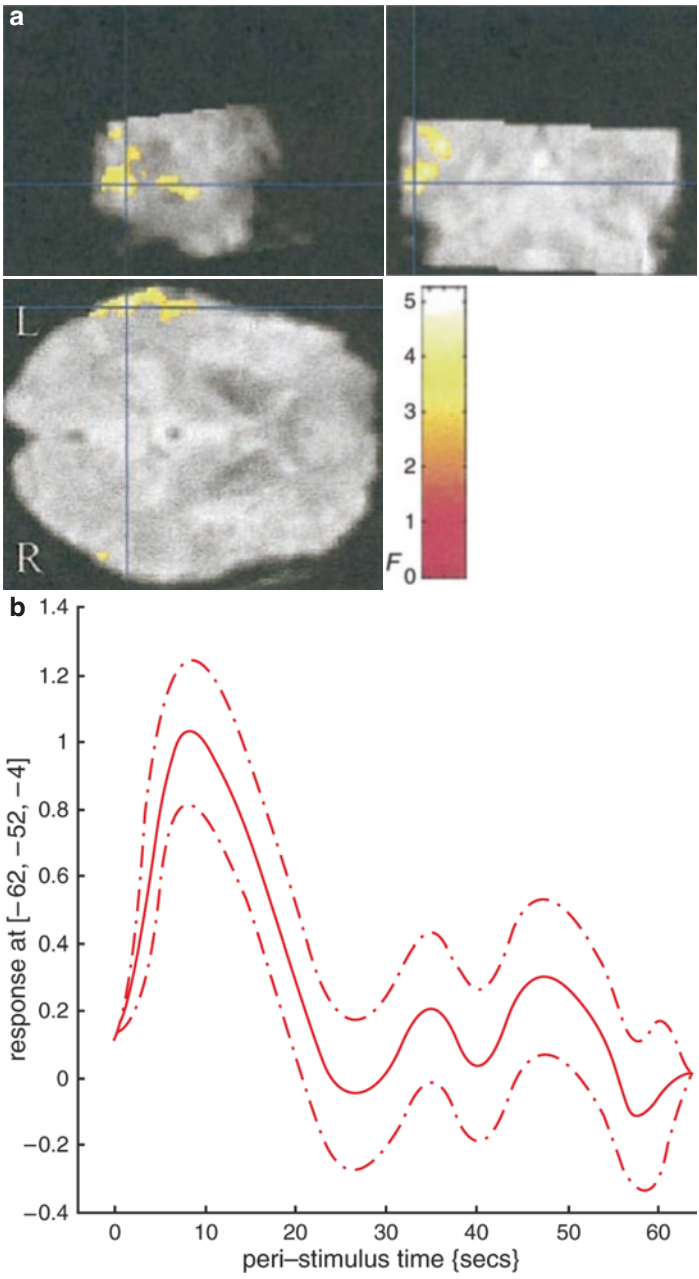

Fig. 17.1 (**a**, **b**) Interictal continuous EEG–fMRI. Fifty-year-old patient with chronic encephalitis of the left hemisphere and intractable partial and secondary generalised seizures. Thirty-seven high-amplitude (>200 μV) stereotyped sharp waves maximal at T3 (left mid-temporal) focal were the most prominent feature. (**a**) SPM{F} of the spike-related events in the continuous EEG–fMRI experiment projected onto orthogonal slices of the mean EPI, showing activation localisation in the left temporal region. The F contrast was a unit matrix across a 16-term Fourier basis set used to model the event-related change. The crosshair is placed at the global statistical maximum. (**b**) Estimated time course of IED-related BOLD signal at global maximum (adapted from (Lemieux et al. 2001))

Given the generally biphasic nature of the HRF, with its initial peak followed by an undershoot, assigning a sign to such transient changes is largely a matter of convention. One possibility is to call an "activation" any region that reaches statistical significance for a *t* test over the regressor built by convolution of the canonical (or similar) HRF with the chosen mathematical representation of the event of interest and a "deactivation" any region for which this is the case for the inverted HRF; for more flexible models of transient changes that do not rely on the canonical HRF, an alternative is to use the sign of the largest deviation from zero over the fitted response's duration.

17.2.4 Relevance of the Observed BOLD Changes

The observation that local field potentials in the brain correlate with a positive fMRI BOLD signal is important for the interpretation of EEG–fMRI findings in focal epilepsy (Logothetis et al. 2001). Importantly, it was the field potentials and not the single unit spiking (action potential) activity that correlated best with the BOLD signal. Therefore, the generator of BOLD signal correlates well with the generator of the EEG signal, which is also generated by field potentials and not by action potentials. However, EEG and BOLD measure different aspects of brain activity—electrical signal vs. metabolic signal—and these may be generated by different cells. In addition, EEG reflects neuronal synchrony (see the Chaps. 2 and 4). BOLD activation is therefore likely to represent the source and possibly the propagation of IEDs. Although BOLD activations are often maximal in the spiking temporal lobe, there are often widespread activations in disparate (including contralateral) temporal and extratemporal regions (Kobayashi et al. 2006a). These incongruent activations probably represent the propagation of interictal activity. Moreover, early positive BOLD changes prior to the epileptic discharges have also been demonstrated, suggesting that these early changes may reflect increased neuronal activity in the spike field prior to the EEG spike (Jacobs et al. 2009).

IED-related BOLD changes can occur in the form of activation (positive BOLD) and deactivation (negative BOLD). What do BOLD deactivations represent? Local deactivations could represent vascular steal. However, there is evidence that negative BOLD signals correlate with GABA concentrations and relative neuronal inactivity (Northoff et al. 2007; Shmuel et al. 2006), leading to the possibility that negative BOLD can result from cortical inhibition. These propositions are critical for the interpretation of EEG–fMRI in focal epilepsy, because interictal spikes are the result of excitatory synaptic activity but result in both local and more distant inhibition (see above). This would, to some extent, explain the association of IEDs with not only local positive BOLD signals but also local and distant negative BOLD signals. A further explanation of BOLD deactivations associated with IEDs is the possibility that interictal activity may disrupt resting-state brain activity, such as the so-called default mode network (Gotman et al. 2005; Laufs et al. 2007; Salek-Haddadi et al. 2006; Thornton et al. 2010a,

2011). Spike-associated BOLD activations are more frequently concordant with the independently defined electroclinical localisation than BOLD deactivations, which are more often discordant (Liu et al. 2008; Salek-Haddadi et al. 2006; Thornton et al. 2010a, 2011). BOLD activations are also likely to overlap with or be adjacent to intracranial lesions (Al-Asmi et al. 2003; Di Bonaventura et al. 2006b; Krakow et al. 1999a; Salek-Haddadi et al. 2006; Thornton et al. 2010a, 2011; Tyvaert et al. 2008). Nevertheless, (Benar et al. 2006) found that the negative BOLD responses may represent EEG activity measured using intracranial EEG and, in some instances, may provide concordant information. A relationship between BOLD deactivations and type of IED (i.e. spike followed by a slow wave: slow wave is an electrographic correlate of neuronal inhibition) and location of epileptic focus (i.e. larger cortical areas in posterior quadrant) has also been suggested (Pittau et al. 2013).

17.2.5 Clinical Utility

For an assessment of clinical utility, three further questions need to be addressed: (1) What is the yield of EEG–fMRI in unselected patients undergoing presurgical assessment? (2) How closely does EEG–fMRI correlate with intracranial investigation? (3) What is the added value of EEG–fMRI in presurgical assessment?

Over the last two decade, these questions have been addressed to some extent. One study that addressed replicability in focal epilepsy (Krakow et al. 1999b), six out of ten patients had activations that were confirmed on a subsequent scan. The largest "unselected" group of patients with focal epilepsy was 63 patients (25 males), four of whom were excluded (mainly due to excessive head movement). These patients were, however, included in this study only if they had frequent interictal discharges (spikes, polyspikes, sharp waves) on a recent EEG. Examination of other studies reveals that a similar criterion was used (Al-Asmi et al. 2003; Kobayashi et al. 2006a; Lazeyras et al. 2000b) or sometimes that even more stringent criteria were used (Krakow et al. 1999b). Even with this criterion in this study, 25 of the patients (42%) had no IEDs. Of the remaining 34, 11 had no change in BOLD signal. Therefore, out of the original 63 patients, EEG–fMRI revealed activations/deactivations in 23 (37%). This is comparable to other studies, such as a study of 38 patients with intractable partial epilepsy in which only 31 studies from 48 could be analysed, mainly because of a lack of IEDs, and there was a significant fMRI activation in only 12 (25% of all studies and 39% of those that could be analysed). Therefore, even when frequent interictal discharges are present on a previous EEG, there is a significant chance that no further information will be revealed by EEG–fMRI. A number of studies have analysed the features of IEDs associated with a BOLD signal change; these are frequent epileptiform discharges, runs of epileptiform discharges, higher amplitude discharges and discharges with similar morphology (Al-Asmi et al. 2003; Kobayashi et al. 2006a; Krakow et al. 1999b;

Salek-Haddadi et al. 2006). Continuous fMRI has enabled posthoc analysis rather than manual triggering and so increases the yield (Al-Asmi et al. 2003), and the yield may be better at 3 T rather than 1.5 T (Federico et al. 2005a). Since one of the main problems is the lack of IEDs, then it is important to be more inclusive (i.e. less rigorous) of possible interictal EEG abnormalities or to use a method that relies less on correlation with scalp EEG such as independent component analysis (ICA) of the fMRI data (Rodionov et al. 2007; van Houdt et al. 2015). Another approach is to analyse other scalp EEG activity such as focal slow, which has been shown in a small number of patients to have a strong concordance with site of lesion and intracranial EEG investigation (Federico et al. 2005a; Laufs et al. 2006). The tendency of expert observers to exclude discharges that are not clearly epileptiform, as encountered in clinical practice, may also limit the technique's sensitivity. The detection of more subtle IEDs using a more integrative analysis of the EEG and fMRI may provide an avenue for improvement (Liston et al. 2006). This has been used with some success but is an area that requires further research.

The other question is whether the canonical HRF is the best model for IED-related changes or whether deviant, noncanonical BOLD signal changes yield useful additional information; systematic investigation of this issue suggests that in adults, noncanonical changes are relatively rare and likely to be discordant and are therefore likely to decrease the specificity of the method (Lemieux et al. 2008; Salek-Haddadi et al. 2006). This is in line with the observation that the yield of EEG–fMRI (i.e. proportion of cases in whom IEDs are captured that show significant activations) has not drastically increased following the transition from spike-triggered (with its assumption of a canonical spike-related response) at roughly 50–60% to continuous EEG–fMRI (capable of capturing a much greater number of events and greater modelling capability) at roughly 60–70%, although no satisfactory comparison exists. Although the use of multiple haemodynamic response functions in fMRI analysis may increase the yield to 80% (Kobayashi et al. 2006a), this may also be at the expense of specificity, and further studies are required. It is important to note that deviations from the canonical response have not been subjected to the same scrutiny for normal stimuli in healthy subjects as it has been in epilepsy. Therefore, the specificity of deviant responses to epilepsy is unknown.

A critical issue is the degree of concordance of intracranial EEG with scalp EEG–fMRI. Two potential problems when addressing this issue are the limited coverage by intracranial EEG, and the fact that the fMRI BOLD (at 1.5 T) originates mainly from relatively large veins that drain the neuronally activated area (Lai et al. 1993), resulting in a discrepancy between signal location and active cortex. Notwithstanding this, multiple later studies have shown a significant concordance between intracranial EEG-based localisation of epileptic focus and IED-related BOLD changes in epileptic focus using EEG-fMRI (Al-Asmi et al. 2003; Benar et al. 2006; Khoo et al. 2017; Lazeyras et al. 2000a; Pittau et al. 2012; Thornton et al. 2010a, 2011; van Houdt et al. 2013; Zijlmans et al. 2007).

Does EEG–fMRI give added value? A study comparing EEG–fMRI with scalp EEG source localisation has demonstrated a good degree of concordance at the

lobar level (Lemieux et al. 2001). A study of five patients compared scalp EEG source localisation, EEG–fMRI and intracranial EEG (Benar et al. 2006). EEG–fMRI compared favourably against EEG source localisation. Within an error of 20 mm, the percentage matches between BOLD activations and intracranial EEG were better than those between EEG source localisation and intracranial EEG. Importantly, BOLD and EEG source localisation identified distinct areas of intracranial EEG activity. This study did not consider surgical outcome or concordance with ictal intracranial recordings, but it indicates that EEG–fMRI and EEG source localisation can give distinct information. Another scalp EEG-fMRI study has demonstrated that localisation of BOLD changes, for epileptic discharges on scalp EEG, can provide more refined localisation of the epileptic focus as compared to scalp EEG alone (Pittau et al. 2012).

Another aspect of added value is if the EEG–fMRI can improve the prediction of surgical success. Thornton and colleagues demonstrated that localisation of maximal BOLD changes was concordant the surgically resected area in patient who became seizure free; in comparison, patients who had significant BOLD changes outside the resected area had reduced seizure frequency only (Thornton et al. 2010a). More specifically, a retrospective study in patients with temporal lobe epilepsy undergoing presurgical evaluation has demonstrated that epileptiform discharges related BOLD maps concordant with resected area were independently related to good surgical outcome. The EEG-fMRI BOLD maps had a sensitivity of 81% and specificity of 79% to identify patients with good surgical outcome, with positive and negative predictive values of 81% and 79%, respectively (Coan et al. 2016).

An alternative approach to determining added value is to consider patients who have been turned down for surgery. A study of 29 patients rejected for surgery because of an inability to localise a single source with EEG were selected for EEG–fMRI study (Zijlmans et al. 2007). All of these patients were noted to have frequent IEDs (>10 in 40 min) on a previous EEG. Of these 29 patients, a significant BOLD response was observed in 15. Eight patients had a BOLD signal that was topographically related to interictal discharges. For four patients (14%), there was felt to be enough information to proceed to intracranial studies. Two had intracranial studies and in both there was concordance between BOLD activation and ictal onset zone, but only one was operated on, the other patient had seizure onset zone closer to eloquent cortex. The operated patient had a significant improvement in seizure frequency (Engel grade II), but was not rendered seizure-free.

Prospective role of EEG-fMRI in clinical decision-making, i.e. (1) to decide about surgical candidacy; or (2) to guide the placement of intracranial electrodes; and (3) possibly, in the future, removing the need for intracranial electrodes remains under explored. Two studies (Kowalczyk et al. 2020; Markoula et al. 2018) have explored the impact of EEG-fMRI on epilepsy surgery decision-making. These studies show that when results of EEG-fMRI were presented in a multidisciplinary meeting after the initial decision about epilepsy surgery was made based on conventional techniques, EEG-fMRI results had a critical or supportive impact to modify initial surgical plan. These changes in epilepsy surgical plan included

modification of surgical candidacy, placement of intracranial EEG electrodes and need for additional non-invasive tests prior to proceeding further in epilepsy surgery pathway.

An interesting concept proposed by EEG-fMRI studies is the possibility of presence of a common node. Piriform cortex ipsilateral to the epileptic focus has shown IED-related BOLD changes in patients with heterogenous focal epilepsies (Flanagan et al. 2014; Garganis et al. 2013; Laufs et al. 2011). Full clinical potential of this area in propagation of epileptic activity, epilepsy surgery success and therapeutic electric stimulation remains to be elucidated in future, yet it provides insights for future research in epilepsy.

17.2.6 The Influence of Lesions

It is likely that different lesions will have different effects on the BOLD signal generated by IEDs. This question has not been systematically studied, and there are only small case series. An important consideration is EEG–fMRI in patients with malformations of cortical development, as these (in particular focal cortical dysplasia) comprise a significant proportion of MRI-negative cases at the time of initial evaluation for epilepsy surgery (McGonigal et al. 2007). From a large study of patients with focal epilepsy, four of eight patients with malformations of cortical development had concordant activations (the other four had no activations) (Salek-Haddadi et al. 2006). This concordance of BOLD changes with the location of malformation of cortical development and epileptic focus (on intracranial EEG) has been confirmed in later studies in larger proportion of patients (Federico et al. 2005b; Pittau et al. 2017; Thornton et al. 2011; Tyvaert et al. 2008; Watanabe et al. 2014). However, BOLD changes were also seen distributed above/around the malformation of cortical development and in distant cortical regions in a network fashion, discordant with the epileptic focus, corroborating the evidence for epileptic network theory. This valuable information provided by EEG-fMRI in patients with malformation of cortical development (especially focal cortical dysplasia) can potentially be used for prognostic purposes for predicting seizure freedom after surgery.

In an investigation of 14 patients with either nodular or band heterotopia, out of 26 studies, 23 were analysed and 22 had a significant BOLD change (Kobayashi et al. 2006b). Sixty-seven percent of the nodular heterotopia group activations and 100% of the band heterotopia group activations were in the heterotopia and/or surrounding cortex. Deactivations were also associated with the heterotopia but less robustly.

Polymicrogyria is a widespread abnormality associated with epilepsy. Evidence from intracranial EEG investigation and experimental work suggests that the epileptogenic region can be outside the predominant structural abnormality. An EEG–fMRI study revealed significant BOLD changes in 89% of the studies with 61.5% (8/13) of the maximal activations involving the lesion (Kobayashi et al. 2005).

These studies suggest that malformations of cortical development can be the main source of epileptiform activity, that such activity is detectable by EEG–fMRI and that it may be associated with BOLD activations more than deactivations. This holds promise for the analysis of patients with apparently normal structural imaging.

What about other lesions? It would be important to consider vascular lesions because of potential problems. The problem with lesions containing blood vessels is that there may be considerable BOLD signal loss. It is therefore not surprising that in five patients with cavernoma, EEG–fMRI showed no responses within the lesion or its immediate periphery (Kobayashi et al. 2007). Reassuringly, two patients had perilesional BOLD changes, but the others had distant activations. This raises the distinct prospect that vascular lesions may be less suitable for EEG–fMRI studies.

17.2.7 Simultaneous intracranial EEG-fMRI

Scalp EEG-fMRI largely depends on scalp EEG and thus inherits the low sensitivity limitation of scalp EEG to identify epileptiform discharges. There have been developments to circumvent the low sensitivity of scalp EEG by using topographic voltage maps or voxel based changes in haemodynamic responses in patients with focal epilepsy (Grouiller et al. 2011; Lopes et al. 2012). On the other hand, epileptiform discharges related to BOLD response is still not seen despite the presence of epileptiform discharges in a significant proportion of cases, or the distribution of epileptiform discharges related to BOLD changes remains unexplained (Salek-Haddadi et al. 2006). Simultaneous recording of intracranial EEG and fMRI (icEEG-fMRI) may help to answer some of these questions.

Intracranial implantation of electrodes (subdural grids, depth electrodes or stereo-encephalography) is performed to localise the epileptic focus and eloquent cortex during presurgical assessment in patients with refractory focal epilepsy (Cardinale et al. 2019; Isnard et al. 2018; Luders and Comair 2000). Intracranial EEG has higher electrophysiological sensitivity and regional specificity, particularly for depth electrodes, as compared to scalp EEG (Luders et al. 2006).

Initial safety studies have demonstrated that icEEG-fMRI can be performed without posing any significant additional health risks, provided a strict protocol is followed. Some signal degradation is observed nearer (~1 cm) to the intracranial electrode contact; however, this signal degradation is orientation dependent (Boucousis et al. 2012; Carmichael et al. 2008, 2010, 2012). In icEEG-fMRI studies, performed on a limited number of patients, significant BOLD changes associated with epileptiform discharges on intracranial EEG were observed, often concordant with the intracranial EEG electrode contacts showing epileptiform discharges (Aghakhani et al. 2015; Chaudhary et al. 2012b; Cunningham et al. 2012; Vulliemoz et al. 2011). In addition, BOLD changes associated with epileptiform discharges were also seen in remote areas which were not sampled by intracranial

EEG in some cases. This finding of a widespread BOLD network associated with focal epileptiform discharges on intracranial EEG suggests a wider underlying haemodynamic network (Chaudhary et al. 2012b, 2014, 2021; Vulliemoz et al. 2011), and may suggest an explanation for the persistence of seizures after surgery in some patients.

17.3 Ictal EEG–fMRI

Ictal is derived from the Latin word *ictus*, which is used to describe a sudden neurologic event like stroke or an epileptic seizure. Ictal is used to describe anything pertaining to epileptic seizures that is a manifestation of excessive and/or hypersynchronous, self-limited activity of neurons in the brain (Blume et al. 2001b).

As mentioned previously, due to the practical difficulties and risks associated with acquiring MR scans during seizures, ictal EEG–fMRI had a much lesser impact than interictal EEG–fMRI initially. Over the last decade, there has been significant increase in capturing seizures during simultaneous EEG-fMRI. These studies have encompassed both generalised and focal epilepsy, and mapping ictal BOLD changes using simultaneous EEG-fMRI has potentially offered an alternative to ictal SPECT in carefully selected patients.

Nonetheless, ictal EEG–fMRI may play an important role in epilepsy research and clinical applications, as it provides the opportunity to explore haemodynamic and electrophysiological changes associated with a seizure, which is the defining event of epilepsy and central to the clinical evaluation of patients with drug-resistant epilepsy (Chaudhary et al. 2013).

In the following, we discuss the limitations and review the clinical applications of ictal EEG–fMRI in patients with focal epilepsy.

17.3.1 Limitations of Ictal EEG–fMRI

Certain methodological and procedural factors have core importance in ictal EEG–fMRI, limiting its applicability, and they deserve careful consideration at this stage of the discussion.

17.3.1.1 Unpredictable Nature of Seizures

Due to the difficulty of predicting the occurrence and the relative rarity of spontaneous seizures, ictal EEG–fMRI has been reported in patients with either frequent or inducible seizures, or as fortuitous occurrences of spontaneous seizures in studies of interictal activity, thereby severely limiting the practical utility of ictal EEG–fMRI. Daily absence seizures, pseudo absence seizures, tonic and atonic seizures, focal electrographic seizures, focal seizures with minimal motion and inducible seizures of reading epilepsy, musicogenic epilepsy, writing epilepsy and startle epilepsy have been investigated (Abreu et al. 2005; Aghakhani et al. 2004;

Chaudhary et al. 2012a; Di Bonaventura et al. 2006b; Diekmann and Hoppner 2014; Donaire et al. 2009a; Federico et al. 2005a; Fernandez et al. 2011; Hamandi et al. 2006; Kobayashi et al. 2006c; Marrosu et al. 2009; Morano et al. 2017; Morocz et al. 2003; Salek-Haddadi et al. 2002, 2009; Sierra-Marcos et al. 2013; Szaflarski et al. 2010; Tenney et al. 2018; Thornton et al. 2010b; Tyvaert et al. 2008; Usami et al. 2016; Vaudano et al. 2012, 2014, 2017; Zhang et al. 2014). Moreover, it is not always possible to record spontaneous ictal events in all selected patients; e.g. only one third to half of all patients recruited in above studies had ictal events. While the likelihood of recording seizures generally increases with acquisition time, this is limited to roughly 90–120 min by resource and patient comfort considerations. Thus, by applying strict selection criteria based on seizure frequency, seizure types and seizure-related motion, yield of ictal EEG-fMRI can be increased.

17.3.1.2 Seizure-Related Motion

Seizure-related motion is a fundamental feature affecting the image quality and leads to false-positive or false-negative results in EEG–fMRI (Hajnal et al. 1994; Jansen et al. 2012; Lund et al. 2005). Thus, by selecting cases in whom stereotypical seizures have less motion, an effort has been made to minimise this problem. In addition, vacuum cushions significantly reduce motion-related noise on the EEG and fMRI (Benar et al. 2003). Adjusting the subject's axial position can also reduce gradient artefact (Mullinger et al. 2011). After acquisition, fMRI scans can be corrected for motion by slice-timing correction, realignment, spatial smoothing and later incorporation of the estimated rigid body realignment parameters (Fig. 17.2) as confounding covariates in the design matrix to remove any residual artefacts (Chaudhary et al. 2012a; Salek-Haddadi et al. 2009; Tyvaert et al. 2008). Another approach to counteracting the signal changes, secondary to motion events during image acquisition, is scan nulling, where additional regressors for each motion event are modelled in the design matrix. Scan nulling reduces the effect of motion significantly (Lemieux et al. 2007). However, this approach of using scan nulling, practically subtracts the motion affected scans from any further signal processing. Prospective motion correction (Maclaren et al. 2013; Todd et al. 2015) may prove useful to obtain meaningful information from data corrupted by seizure-related motion during simultaneous ictal EEG-fMRI. Seizure-related motion also affects EEG quality (see Fig. 17.2), prospective motion correction can also be used to improve EEG quality during large amplitude motion (Maziero et al. 2016).

17.3.2 Detection of Ictal Activity

In some instances, ictal EEG activity is easy to differentiate from interictal EEG activity (Kobayashi et al. 2006c; Salek-Haddadi et al. 2002) (Fig. 17.2). However, there are instances where clinical seizure onset may precede ictal rhythms on scalp EEG or vice versa (Ray et al. 2007; Tao et al. 2007). Various methods can be

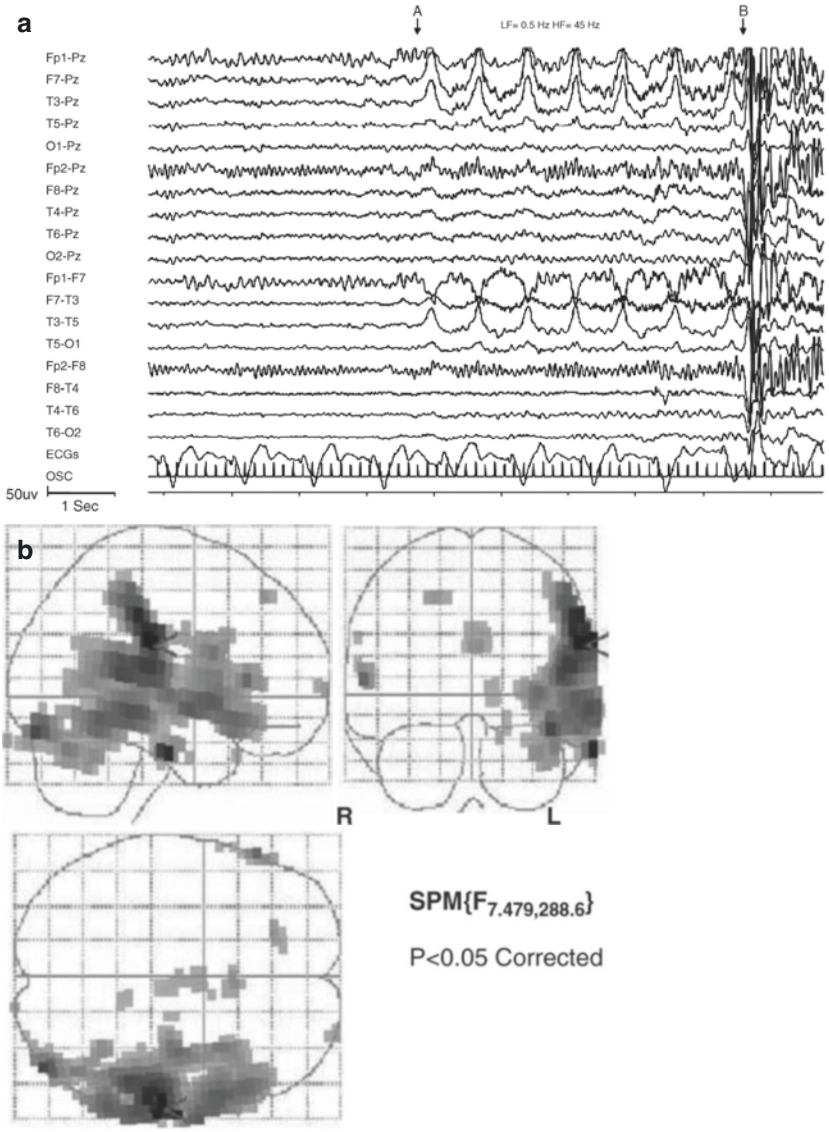

Fig. 17.2 (**a–c**) Ictal EEG–fMRI. A 47-year-old right-handed patient with a two-year history of intractable generalised tonic-clonic seizures. An electrographic seizure started approximately 3 min into the acquisition, with focal rhythmic delta activity emerging abruptly and being unilaterally maximum over the F7/T3 electrodes (see Fig. 17.1); it lasted for the next 15 s prior to evolving into a localised (F7/T3) 5 Hz theta rhythm and decaying slowly over the next 26 s. Brief EEG motion artefact was evident 5 s into the seizure. (**a**) EEG segment showing seizure onset (point *A*) and motion artefact on EEG (point *B*). (**b**) SPM showing seizure-related BOLD activation result of F test across 16-term Fourier basis set; cluster is shown on spatially normalised "glass brain". *Red arrowhead* shows global statistical maximum. (**c**) Regional ictal BOLD signal change (*green*, maximum change in cluster; *blue*, estimated change averaged over whole cluster; *red*, fitted sine function) in relation to motion as assessed by an fMRI time series realignment process (*red*, *green*, *blue*, X, Y and Z translations, and the corresponding rotations below). Note the negative BOLD signal prior to seizure onset (adapted from Salek-Haddadi et al. 2002)

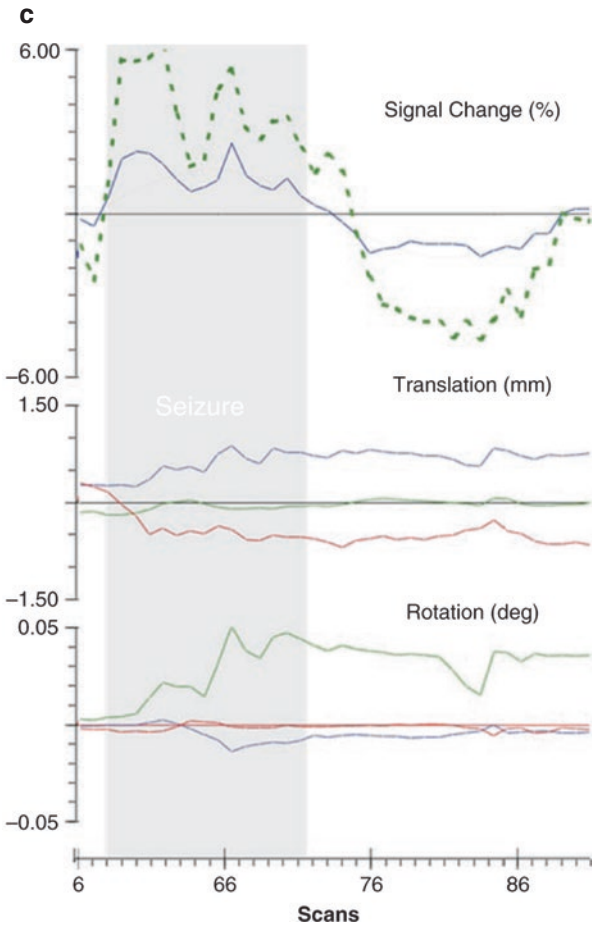

Fig. 17.2 (continued)

employed to detect clinical seizures, such as button pressing by the patient specially when seizure are triggered by a known stimulus, observing and identifying clinical changes inside the scanner similar to typical clinical seizure, following a verbal signal from the patient and using simultaneous video EEG recording in the scanner (Chaudhary et al. 2012a; Di Bonaventura et al. 2006b; Donaire et al. 2009a; Salek-Haddadi et al. 2009; Thornton et al. 2010b; Tyvaert et al. 2008). Although subject to uncertainty and imprecision, when precise synchronisation with the EEG recording is unavailable, these time markers can be used as a basis for modelling the associated BOLD changes.

17.3.3 Statistical Analysis of Ictal Haemodynamic Changes

As for interictal studies, the usual data preprocessing and modelling steps are commonly applied to the ictal fMRI time series; a high-pass filter is applied to the data

and design matrix, according to the noise characteristics of the scanner and the inclusion of autoregressive models to estimate the intrinsic temporal autocorrelation structure of the data. However, modelling the effects of interest linked to ictal activity is a priori a much more challenging task than for interictal activity for a number of reasons: the long durations of the events of interest give scope for yet-unknown patterns of signal change, affecting the choice of a mathematical representation for the events of interest and haemodynamic basis set; the potentially greater degree of inter-event variability makes it more difficult to classify and group events; the possibility of pathological activity not reflected on scalp EEG or linked to behavioural changes (baseline problem); the potential for greater head and body motion. In addition, any interictal activity should be incorporated into the model.

Different EEG patterns have been used so far in various studies for modelling purposes, which include slow wave discharges (Salek-Haddadi et al. 2009), sharp rhythmic activity, sharp fast activity, rhythmic bilateral discharges, slow waves, spikes, polyspikes and spike wave discharges (Chaudhary et al. 2012a; Di Bonaventura et al. 2006b; Donaire et al. 2009a; Salek-Haddadi et al. 2002, 2003c, 2009; Sierra-Marcos et al. 2013; Thornton et al. 2010b; Tyvaert et al. 2008).

In the framework of general linear model, the choice of representing an ictal event and of basis set to explore ictal haemodynamic patterns have been variable across different research groups. This includes modelling a single duration ictal event convolved with a Fourier basis set spanning the entire event, thereby allowing for an almost arbitrary BOLD signal time course at any given location (Salek-Haddadi et al. 2002;Thornton et al. 2010b); representing events (spikes and onset of ictal activity) identified on EEG as stick functions and convolved with a canonical haemodynamic response function and its first temporal derivative (Salek-Haddadi et al. 2009); modelling ictal events taking into account event duration and convolved with four haemodynamic response functions (Tyvaert et al. 2008); segmenting seizure into 10 s blocks, convolved with a time variant canonical haemodynamic response function and contrasted with a baseline block and/or a contagious block (Donaire et al. 2009a; Sierra-Marcos et al. 2013) dividing seizure into phases based on their spatio-temporal and clinical evolution (i.e. ictal onset, ictal established and late ictal) and convolved with a canonical haemodynamic response function and its temporal and dispersion derivatives (Chaudhary et al. 2012a; Thornton et al. 2010b). The inclusion of regressors to account for motion-related fMRI signal effects and close examination of the temporal relationship between motion and signal change are generally advisable, and case selection based on a maximum allowable degree of motion is also possible, although the choice of a specific threshold value is problematic (see Chaudhary et al. for review (Chaudhary et al. 2013)).

In order to avoid operator driven selection bias for identification of seizure onset on EEG, data driven approach: Independent Component Analysis has also been used to explore seizure related haemodynamic changes. It implies minimum constraints on the shape, latency and duration of haemodynamic response function (LeVan et al. 2010; Thornton et al. 2010b).

17.3.4 Application of Ictal EEG–fMRI

Despite the issues highlighted above, EEG–fMRI has been successful in revealing interesting patterns of BOLD signal change related to ictal events captured on scalp EEG in a small number of cases.

17.3.4.1 Localisation Potential of Ictal EEG–fMRI

Ictal EEG–fMRI has shown the potential to localise the epileptogenic zone. The first case report showed a region of significant BOLD change concordant with the electrographic focus (Salek-Haddadi et al. 2002). The use of a flexible basis set revealed BOLD time-course variations across the activated region, and a suggestion of change prior to the EEG onset, but their pathological significance is unclear due to the level of inter-regional variability observed in healthy subjects (Aguirre et al. 1998). The large amplitude of the BOLD activation was deemed consistent with the levels of blood flow changes commonly observed using PET and SPECT (Salek-Haddadi et al. 2002).

In patients with focal epilepsy, multiple case reports (Chassagnon et al. 2009; Di Bonaventura et al. 2006a; Federico et al. 2005a; Kobayashi et al. 2006c; Marrosu et al. 2009) and larger case series (Chaudhary et al. 2012a; Di Bonaventura et al. 2006b; Donaire et al. 2009a; LeVan et al. 2010; Salek-Haddadi et al. 2009; Sierra-Marcos et al. 2013; Thornton et al. 2010b; Tyvaert et al. 2008, 2009) have shown that ictal EEG–fMRI results were consistent with the independently derived, electroclinically determined epileptogenic zone and intracranial recordings where available. Seizure-related BOLD maps are usually rich in terms of multiple clusters of haemodynamic change within a single map. Therefore, concordance of these maps is usually evaluated based on the location of statistically most significant or clinically most relevant cluster (Chaudhary et al. 2013). However, haemodynamic changes at the onset of seizure (Fig. 17.3) are found to be most concordant with the epileptogenic zone/seizure onset zone (Chaudhary et al. 2012a; Donaire et al. 2009a; Sierra-Marcos et al. 2013; Thornton et al. 2010b). A similar pattern of ictal haemodynamic changes localised to the epileptogenic zone/seizure onset zone at the ictal onset on intracranial EEG (i.e. gold standard tool to localise seizure onset; Fig. 17.4) has also been shown using simultaneous intracranial EEG-fMRI (Chaudhary et al. 2016). Based on these studies, it appears that BOLD changes linked to ictal events can provide non-invasive BOLD localisation at sub-lobar which can be useful for guiding implantation of intracranial electrodes in patients with refractory epilepsy undergoing presurgical evaluation.

17.3.4.2 Mechanism of Epilepsy

In reading epilepsy (Salek-Haddadi et al. 2006), ictal EEG–fMRI revealed activations in cortical and subcortical areas, concordant with EEG changes. This observation points towards the early recruitment of subcortical structures, which may propagate and synchronise cortical activity. This has provided further evidence for a cortico-subcortical network in seizure generation.

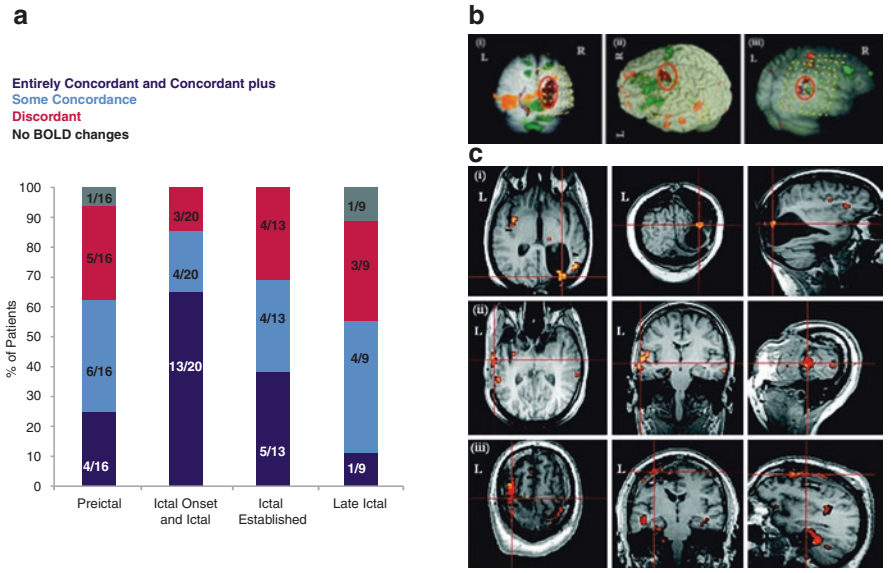

Fig. 17.3 Ictal and preictal BOLD changes and their comparison with the seizure onset zone and cortical resection. (**a**) Bar chart showing level of concordance of BOLD changes with the presumed seizure onset zone, during ictal and preictal phases. (**b**) SPMs of F-statistics overlaid on 3D rendered brain in individual space, showing the relationship between preictal (orange) and ictal onset-related BOLD changes (green), implanted electrodes and structural lesion (red). (i) Patient #10: The global-maximum cluster in the right occipito-temporal region for the preictal and *Ictal* phase was within the presumed seizure onset zone and was 1.8 cm and 2.5 cm respectively from the invasively-defined seizure onset zone. (ii) Patient #16: The global-maximum cluster in the left superior/middle frontal gyrus for the *Ictal* phase was within the presumed seizure onset zone at 1.5 cm from the invasively-defined seizure onset zone. For the preictal phase another cluster in medial superior frontal gyrus was within the presumed seizure onset zone at 2.5 cm from the invasively-defined seizure onset zone. (iii) Patient #1: For the *Ictal-onset* phase, the second most statistically significant BOLD cluster in right inferior parietal lobe was within the presumed seizure onset zone at 1.9 cm from the invasively-defined seizure onset zone. The global-maximum preictal cluster in the right parietal region was within the presumed seizure onset zone at 3cm from the invasively-defined seizure onset zone. (**c**) Ictal onset-related maps overlaid on co-registered post-surgical T1-volume. Cross-hair shows the BOLD-cluster within the presumed seizure onset zone. (i) Patient #1 had a cortical resection including the right parietal tuber and overlapping ictal onset-related cluster (cross-hair: ILAE Class-I at 1.5 year). (ii) Patient #4 underwent left anterior temporal lobe resection which did not involve the ictal onset-related global-maximum cluster in superior temporal gyrus (cross-hair; ILAE Class-III at 1 year). (iii) Patient #16 had a resection including right posterior superior frontal gyrus/middle frontal gyrus and part of supplementary motor area and ictal onset-related global-maximum cluster (cross-hair; ILAE Class-I at 1 year). Adapted from Chaudhary et al. (2012a)

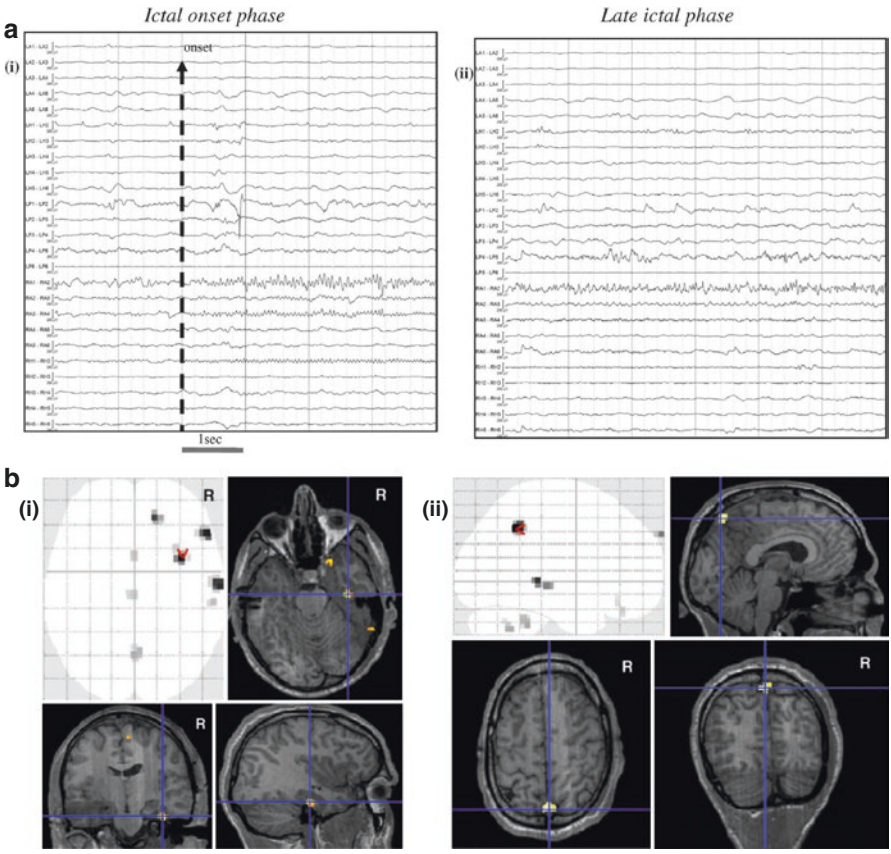

Fig. 17.4 Seizure-related BOLD changes based on visual segmentation of seizure (models 1 and 2). (**a**) Representative sample of EEG recorded during icEEG-fMRI, (1) EEG showing Ictal onset phase consisted of fast activity in beta range involving RA contacts 1–4 and RH contacts 1–2. (2) EEG showing Late-ictal phase consisted of fast activity in gamma range involving RA contacts 1–2 and LPH contacts 4–5. (**b**) BOLD changes overlaid on glass brain and on a co-registered T1-volume. (1) Ictal onset phase-related BOLD clusters were seen in the right fusiform gyrus (global statistical maximum: cross-hair) in addition to other clusters in the right temporal lobe and the precuneus. (2) Late-ictal phase-related BOLD clusters were seen in the precuneus (global statistical maximum: cross-hair) in addition to other clusters in the right temporal lobe and the posterior cingulate. Adapted from Chaudhary et al. (2016)

In patients with different types of malformations of cortical development, different BOLD patterns have been seen for ictal and interictal activity in lesions, overlying cortex and distant areas ((Tyvaert et al. 2008); see Fig. 17.5). BOLD responses were found to be significantly greater for ictal compared to interictal activity. Studies in patients with focal cortical dysplasia demonstrated BOLD activations involving the lesion during both interictal and ictal recording. In contrast, patients with band heterotopias had BOLD activations with interictal epileptic activity involving the lesion and areas distant to the lesion, whereas ictal BOLD increases

involved the lesion only. Similarly, patients with nodular heterotopia also showed some discordance between BOLD changes with ictal and interictal epileptic activity; ictal activity originated in the overlying cortex, whereas spike-related BOLD changes were congruent with the nodular heterotopia and distant cortex (Tyvaert et al. 2008). However, others have found a mixture of BOLD increases and decreases irrespective of the presence of structural abnormality (Chaudhary et al. 2012a; Hamandi et al. 2006; Jacobs et al. 2008, 2009; Laufs et al. 2007; Thornton et al. 2010b; Vaudano et al. 2009). It is possible that that cerebral blood flow can be compromised in areas of structural abnormalities leading to demand perfusion mismatch or dysregulated neurovascular coupling resulting in variable patterns of BOLD activity during seizure; however, many aspects of the interaction between BOLD and neuronal activity still remains to be elucidated (Logothetis and Pfeuffer 2004; Pasley et al. 2007; Raichle et al. 2001; Sakatani et al. 2007; Schridde et al. 2008; Shmuel et al. 2002, 2006; Shulman et al. 2007).

Ictal scalp EEG-fMRI can reveal temporal evolution of hemodynamic changes, i.e. preictal: prior to the seizure onset on scalp EEG, at the seizure onset and during

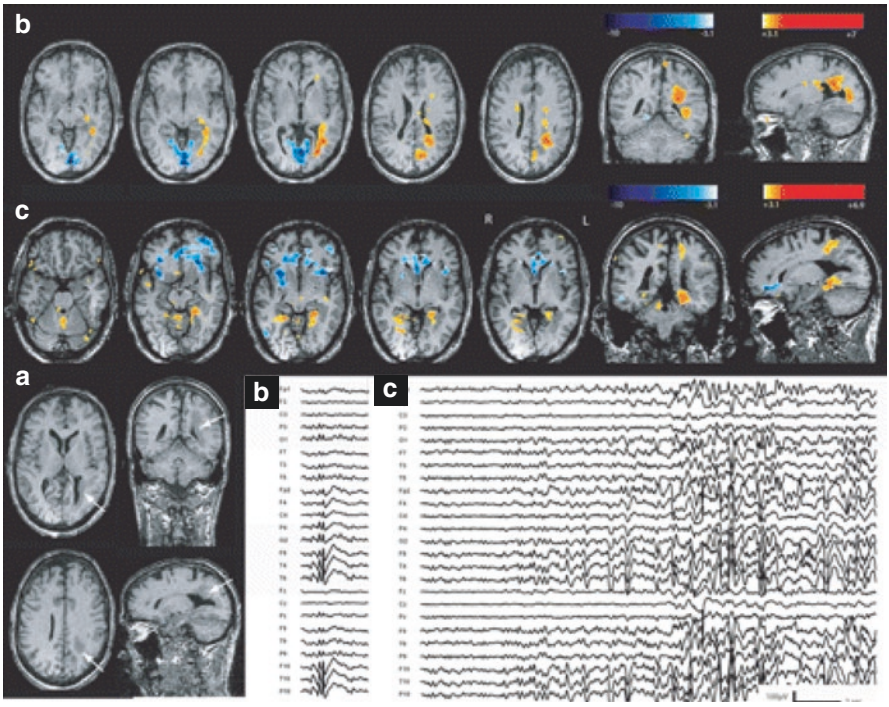

Fig. 17.5 Nodular heterotopia. (**a**) Anatomical MRI showed a right occipitotemporal nodular heterotopia over the occipital horn (head of white arrows). Abnormal overlying cortex over the whole posterior quadrant. (**b**) Increase of BOLD signal involved essentially the nodular heterotopia during right posterior temporoparietal spikes. Deactivation was confined in the cuneus. (**c**) Activation during the seizure involved only the overlying cortex; the nodular heterotopia was not involved. On the EEG, the seizure started by a right posterior temporoparietal sharp rhythmic activity. Adapted from Tyvaert et al. (2008)

seizure propagation (Chaudhary et al. 2012a; Donaire et al. 2009a; Federico et al. 2005a; Sierra-Marcos et al. 2013; Thornton et al. 2010b; Vaudano et al. 2012, 2013). Preictal changes (Fig. 17.6) involve epileptogenic and also more widespread areas including irritative zones and/or resting state network-related areas (Bartolomei et al. 2004; Gnatkovsky et al. 2008; Huberfeld et al. 2011; Schwartz et al. 2011; Trombin et al. 2011; Truccolo et al. 2011; Wendling et al. 2005; Zhao et al. 2007). These haemodynamic changes suggest recruitment and interaction of neuronal and

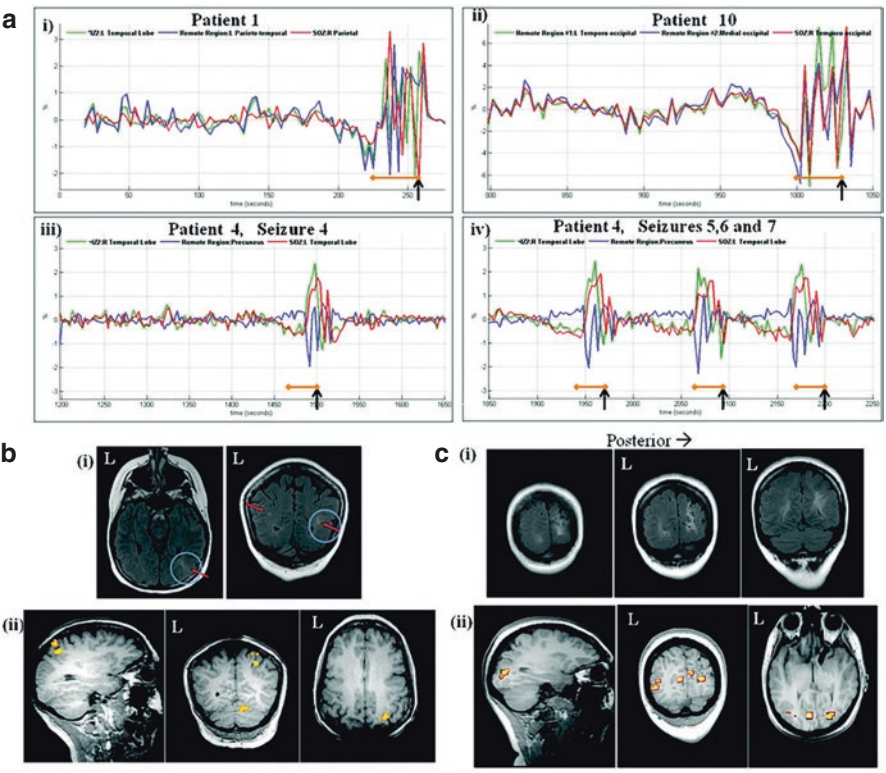

Fig. 17.6 Preictal time courses and BOLD changes. (**a**) Time courses of preictal BOLD clusters for patients #1, 4 and 10. Prior to the seizure onset on scalp-EEG, multiple areas including the seizure onset zone, irritative zone and remote regions showed a consistent BOLD decrease (Median onset: –31 s; 95% confidence-interval: –35.7 to –26.3) followed by an increase (Median onset: –16 s (95% confidence-interval: –18.1 to –13.9) suggesting recruitment of a widespread preictal network. Black arrow = seizure onset; orange bar = 30 s preictal window. *Patient #1 had a second irritative zone (IZ2) showing IEDs on MEG. Patient #4 had a second irritative zone (IZ2) showing IEDs on MEG. (**b**) Patient #1. (i) Multiple tubers were seen in right parietal lobe (epileptogenic: encircled) and left temporal lobe. (ii) The preictal map (overlaid on co-registered T1-volume) was classified as *Concordant-plus* showing global-maximum cluster in right parietal lobe within the presumed seizure onset zone. (**c**) Patient #10. (i) Long standing ischaemic damage with malformation of gyri in right occipito-parietal region extending into right posterior temporal lobe on MRI-scan. (ii) The preictal map (overlaid on co-registered T1-volume) had *Some-concordance* showing global-maximum BOLD cluster in left medial parieto-occipital region and another cluster in right lateral parieto-occipital region within the presumed seizure onset zone (Chaudhary et al. 2012a)

metabolic network at/prior to the seizure onset, i.e. initial BOLD decreases representing active inhibitory circuits which are surpassed by the increasing neuronal activity (represented by BOLD increases) as seizure evolves. These preictal haemodynamic changes may represent the ictal rhythm which is yet not synchronised enough to be represented on scalp EEG due to its inherent limitations (Chaudhary et al. 2012a; Ray et al. 2007; Tao et al. 2005), preictal discharges (Huberfeld et al. 2011), fast oscillatory activity (Wendling et al. 2005) or activity from glial cells (Moore and Cao 2008). Ictal haemodynamic changes during seizure propagation are seen in the symptomatogenic areas such as clinical semiology related areas (Chaudhary et al. 2012a), musicogenic seizure-related network (Marrosu et al. 2009; Morocz et al. 2003), reading epilepsy-related network (Salek-Haddadi et al. 2009; Vaudano et al. 2012) suggesting recruitment of these areas as epileptic activity spreads. Seizure-related BOLD decreases in the default mode network are thought to suggest changes in awareness (Chaudhary et al. 2012a).

17.4 Conclusions

EEG–fMRI, with its capacity to reveal 3D, whole-brain maps of haemodynamic changes related to pathological EEG patterns, is a unique tool for the study of epilepsy. While the technique's yield (though comparable to that of MEG) remains limited, it has provided new localising information and revealed previously unseen brain networks in a large proportion of the patients. The combination of fMRI with EEG allows the application of powerful hypothesis-driven fMRI analysis techniques to reveal haemodynamic changes specifically correlated with pathological EEG patterns such as IED. However, this means that this approach to EEG–fMRI also suffers from some of the limitations of EEG, in particular its limited sensitivity, which can result in a poor baseline against which postulated BOLD changes can be assessed. The application of more sophisticated EEG analysis techniques may lead to more objective and reliable GLMs. Efforts are being made to both improve our understanding of the relationship between epileptiform discharges and BOLD signals; and use EEG-fMRI as an additional localizing tool for patients undergoing presurgical evaluation for refractory epilepsy, with the ultimate aim of better understanding the mechanism of generation of epileptic activity.

References

Abreu P, Ribeiro M, Forni A, Pires I, Sousa G (2005) Writing epilepsy: a neurophysiological, neuropsychological and neuroimaging study. Epilepsy Behav 6:463–466

Aghakhani Y, Bagshaw AP, Benar CG et al (2004) fMRI activation during spike and wave discharges in idiopathic generalized epilepsy. Brain 127:1127–1144

Aghakhani Y, Beers CA, Pittman DJ, Gaxiola-Valdez I, Goodyear BG, Federico P (2015) Co-localization between the BOLD response and epileptiform discharges recorded by simultaneous intracranial EEG-fMRI at 3 T. Neuroimage Clin 7:755–763

Aguirre GK, Zarahn E, D'esposito M (1998) The variability of human, BOLD hemodynamic responses. NeuroImage 8:360–369

Alarcon G, Garcia Seoane JJ, Binnie CD et al (1997) Origin and propagation of interictal discharges in the acute electrocorticogram. Implications for pathophysiology and surgical treatment of temporal lobe epilepsy. Brain 120(12):2259–2282

Al-Asmi A, Benar CG, Gross DW et al (2003) fMRI activation in continuous and spike-triggered EEG-fMRI studies of epileptic spikes. Epilepsia 44:1328–1339

Barbarosie M, Avoli M (1997) CA3-driven hippocampal-entorhinal loop controls rather than sustains in vitro limbic seizures. J Neurosci 17:9308–9314

Bartolomei F, Wendling F, Regis J, Gavaret M, Guye M, Chauvel P (2004) Pre-ictal synchronicity in limbic networks of mesial temporal lobe epilepsy. Epilepsy Res 61:89–104

Benar C, Aghakhani Y, Wang Y et al (2003) Quality of EEG in simultaneous EEG-fMRI for epilepsy. Clin Neurophysiol 114:569–580

Benar CG, Grova C, Kobayashi E et al (2006) EEG-fMRI of epileptic spikes: concordance with EEG source localization and intracranial EEG. NeuroImage 30:1161–1170

Blume WT (2001) Current trends in electroencephalography. Curr Opin Neurol 14:193–197

Blume WT, Borghesi JL, Lemieux JF (1993) Interictal indices of temporal seizure origin. Ann Neurol 34:703–709

Blume WT, Holloway GM, Wiebe S (2001a) Temporal epileptogenesis: localizing value of scalp and subdural interictal and ictal EEG data. Epilepsia 42:508–514

Blume WT, Luders HO, Mizrahi E, Tassinari C, van Emde BW, Engel J Jr (2001b) Glossary of descriptive terminology for ictal semiology: report of the ILAE task force on classification and terminology. Epilepsia 42:1212–1218

Boucousis SM, Beers CA, Cunningham CJ et al (2012) Feasibility of an intracranial EEG-fMRI protocol at 3T: risk assessment and image quality. NeuroImage 63:1237–1248

Cardinale F, Rizzi M, Vignati E et al (2019) Stereoelectroencephalography: retrospective analysis of 742 procedures in a single centre. Brain 142:2688–2704

Carmichael DW, Hamandi K, Laufs H, Duncan JS, Thomas DL, Lemieux L (2008) An investigation of the relationship between BOLD and perfusion signal changes during epileptic generalised spike wave activity. Magn Reson Imaging 26:870–873

Carmichael DW, Thornton JS, Rodionov R et al (2010) Feasibility of simultaneous intracranial EEG-fMRI in humans: a safety study. NeuroImage 49:379–390

Carmichael DW, Vulliemoz S, Rodionov R, Thornton JS, McEvoy AW, Lemieux L (2012) Simultaneous intracranial EEG-fMRI in humans: protocol considerations and data quality. NeuroImage 63:301–309

Chassagnon S, Hawko CS, Bernasconi A, Gotman J, Dubeau F (2009) Coexistence of symptomatic focal and absence seizures: video-EEG and EEG-fMRI evidence of overlapping but independent epileptogenic networks. Epilepsia 50:1821–1826

Chaudhary UJ, Carmichael DW, Rodionov R et al (2012a) Mapping preictal and ictal haemodynamic networks using video-electroencephalography and functional imaging. Brain 135:3645–3663

Chaudhary UJ, Carmichael DW, Rodionov R et al (2012b) Conference Abstract: Mapping the irritative zone using simultaneous intracranial EEG-fMRI and comparison with postsurgical outcome. Epilepsia 53:14

Chaudhary UJ, Centeno M, Carmichael DW, Diehl B, Walker MC, Duncan JS, Lemieux L (2021) Mapping Epileptic Networks Using Simultaneous Intracranial EEG-fMRI. Frontiers in Neurology 12693504. https://doi.org/10.3389/fneur.2021.693504

Chaudhary UJ, Duncan JS, Lemieux L (2013) Mapping hemodynamic correlates of seizures using fMRI: a review. Hum Brain Mapp 34:447–466

Chaudhary UJ, Perani S, Carmichael D et al (2014) Conference Abstract: Epileptic network using scalp and intracranial EEG-fMRI and postsurgical outcome. Epilepsy Curr 14:88–89

Chaudhary UJ, Centeno M, Thornton RC et al (2016) Mapping human preictal and ictal haemodynamic networks using simultaneous intracranial EEG-fMRI. Neuroimage Clin 11:486–493

Coan AC, Chaudhary UJ, Frederic G et al (2016) EEG-fMRI in the presurgical evaluation of temporal lobe epilepsy. J Neurol Neurosurg Psychiatry 87:642–649

Cunningham CB, Goodyear BG, Badawy R et al (2012) Intracranial EEG-fMRI analysis of focal epileptiform discharges in humans. Epilepsia 53:1636–1648

de Curtis M, Avanzini G (2001) Interictal spikes in focal epileptogenesis. Prog Neurobiol 63:541–567

Detre JA, Sirven JI, Alsop DC, O'Connor MJ, French JA (1995) Localization of subclinical ictal activity by functional magnetic resonance imaging: correlation with invasive monitoring. Ann Neurol 38:618–624

Di Bonaventura C, Carnfi M, Vaudano AE et al (2006a) Ictal hemodynamic changes in late-onset rasmussen encephalitis. Ann Neurol 59:432–433

Di Bonaventura C, Vaudano AE, Carni M et al (2006b) EEG/fMRI study of ictal and interictal epileptic activity: methodological issues and future perspectives in clinical practice. Epilepsia 47(5):52–58

Diekmann V, Hoppner AC (2014) Cortical network dysfunction in musicogenic epilepsy reflecting the role of snowballing emotional processes in seizure generation: an fMRI-EEG study. Epileptic Disord 16:31–44

Donaire A, Bargallo N, Falcon C et al (2009a) Identifying the structures involved in seizure generation using sequential analysis of ictal-fMRI data. NeuroImage 47:173–183

Donaire A, Falcon C, Carreno M et al (2009b) Sequential analysis of fMRI images: a new approach to study human epileptic networks. Epilepsia 50:2526–2537

Donaire A, Capdevila A, Carreno M et al (2013) Identifying the cortical substrates of interictal epileptiform activity in patients with extratemporal epilepsy: an EEG-fMRI sequential analysis and FDG-PET study. Epilepsia 54:678–690

Duncan JS (2007) Epilepsy surgery. Clin Med 7:137–142

Duncan JS (2011) Selecting patients for epilepsy surgery: synthesis of data. Epilepsy Behav 20:230–232

Federico P, Abbott DF, Briellmann RS, Harvey AS, Jackson GD (2005a) Functional MRI of the pre-ictal state. Brain 128:1811–1817

Federico P, Archer JS, Abbott DF, Jackson GD (2005b) Cortical/subcortical BOLD changes associated with epileptic discharges: an EEG-fMRI study at 3 T. Neurology 64:1125–1130

Fernandez S, Donaire A, Maestro I et al (2011) Functional neuroimaging in startle epilepsy: involvement of a mesial frontoparietal network. Epilepsia 52:1725–1732

Flanagan D, Badawy RA, Jackson GD (2014) EEG-fMRI in focal epilepsy: local activation and regional networks. Clin Neurophysiol 125:21–31

Garganis K, Kokkinos V, Zountsas B (2013) EEG-fMRI findings in late seizure recurrence following temporal lobectomy: a possible contribution of area tempestas. Epilepsy Behav Case Rep 1:157–160

Gholipour A, Kehtarnavaz N, Briggs R, Devous M, Gopinath K (2007) Brain functional localization: a survey of image registration techniques. IEEE Trans Med Imaging 26:427–451

Gholipour A, Kehtarnavaz N, Briggs RW et al (2008a) Validation of non-rigid registration between functional and anatomical magnetic resonance brain images. IEEE Trans Biomed Eng 55:563–571

Gholipour A, Kehtarnavaz N, Gopinath K, Briggs R, Panahi I (2008b) Average field map image template for Echo-Planar image analysis. Conf Proc IEEE Eng Med Biol Soc 2008:94–97

Gnatkovsky V, Librizzi L, Trombin F (2008) Fast activity at seizure onset is mediated by inhibitory circuits in the entorhinal cortex in vitro. Ann Neurol 64:674–686

Gotman J, Grova C, Bagshaw A, Kobayashi E, Aghakhani Y, Dubeau F (2005) Generalized epileptic discharges show thalamocortical activation and suspension of the default state of the brain. Proc Natl Acad Sci U S A 102:15236–15240

Gregory RP, Oates T, Merry RT (1993) Electroencephalogram epileptiform abnormalities in candidates for aircrew training. Electroencephalogr Clin Neurophysiol 86:75–77

Grouiller F, Vercueil L, Krainik A, Segebarth C, Kahane P, David O (2010) Characterization of the hemodynamic modes associated with interictal epileptic activity using a deformable model-based analysis of combined EEG and functional MRI recordings. Hum Brain Mapp 31:1157–1173

Grouiller F, Thornton RC, Groening K et al (2011) With or without spikes: localization of focal epileptic activity by simultaneous electroencephalography and functional magnetic resonance imaging. Brain 134:2867–2886
Hajnal JV, Myers R, Oatridge A, Schwieso JE, Young IR, Bydder GM (1994) Artifacts due to stimulus correlated motion in functional imaging of the brain. Magn Reson Med 31:283–291
Hamandi K, Salek-Haddadi A, Fish DR, Lemieux L (2004) EEG/functional MRI in epilepsy: the queen square experience. J Clin Neurophysiol 21:241–248
Hamandi K, Salek-Haddadi A, Laufs H et al (2006) EEG-fMRI of idiopathic and secondarily generalized epilepsies. NeuroImage 31:1700–1710
Herrendorf G, Steinhoff BJ, Kolle R et al (2000) Dipole-source analysis in a realistic head model in patients with focal epilepsy. Epilepsia 41:71–80
Hill RA, Chiappa KH, Huang-Hellinger F, Jenkins BG (1995) EEG during MR imaging: differentiation of movement artifact from paroxysmal cortical activity. Neurology 45:1942–1943
Huberfeld G, Menendez P, Pallud J et al (2011) Glutamatergic pre-ictal discharges emerge at the transition to seizure in human epilepsy. Nat Neurosci 14:627–634
Isnard J, Taussig D, Bartolomei F et al (2018) French guidelines on stereoelectroencephalography (SEEG). Neurophysiol Clin 48:5–13
Ives JR, Warach S, Schmitt F, Edelman RR, Schomer DL (1993) Monitoring the patient's EEG during echo planar MRI. Electroencephalogr Clin Neurophysiol 87:417–420
Jackson GD, Connelly A, Cross JH, Gordon I, Gadian DG (1994) Functional magnetic resonance imaging of focal seizures. Neurology 54:524–527
Jacobs J, Rohr A, Moeller F et al (2008) Evaluation of epileptogenic networks in children with tuberous sclerosis complex using EEG-fMRI. Epilepsia 49:816–825
Jacobs J, LeVan P, Moeller F et al (2009) Hemodynamic changes preceding the interictal EEG spike in patients with focal epilepsy investigated using simultaneous EEG-fMRI. NeuroImage 45:1220–1231
Jansen M, White TP, Mullinger KJ et al (2012) Motion-related artefacts in EEG predict neuronally plausible patterns of activation in fMRI data. NeuroImage 59:261–270
Josephs O, Turner R, Friston K (1997) Event-related f MRI. Hum Brain Mapp 5:243–248
Kazemi NJ, So EL, Mosewich RK et al (1997) Resection of frontal encephalomalacias for intractable epilepsy: outcome and prognostic factors. Epilepsia 38:670–677
Khoo HM, Hao Y et al (2017) The hemodynamic response to interictal epileptic discharges localizes the seizure-onset zone. Epilepsia 58:811–823
King D, Spencer S (1995) Invasive electroencephalography in mesial temporal lobe epilepsy. J Clin Neurophysiol 12:32–45
Kobayashi E, Bagshaw AP, Jansen A et al (2005) Intrinsic epileptogenicity in polymicrogyric cortex suggested by EEG-fMRI BOLD responses. Neurology 64:1263–1266
Kobayashi E, Bagshaw AP, Benar CG et al (2006a) Temporal and extratemporal BOLD responses to temporal lobe interictal spikes. Epilepsia 47:343–354
Kobayashi E, Bagshaw AP, Grova C, Gotman J, Dubeau F (2006b) Grey matter heterotopia: what EEG-fMRI can tell us about epileptogenicity of neuronal migration disorders. Brain 129:366–374
Kobayashi E, Hawco CS, Grova C, Dubeau F, Gotman J (2006c) Widespread and intense BOLD changes during brief focal electrographic seizures. Neurology 66:1049–1055
Kobayashi E, Bagshaw AP, Gotman J, Dubeau F (2007) Metabolic correlates of epileptic spikes in cerebral cavernous angiomas. Epilepsy Res 73:98–103
Kowalczyk MA, Omidvarnia A, Abbott DF, Tailby C, Vaughan DN, Jackson GD (2020) Clinical benefit of presurgical EEG-fMRI in difficult-to-localize focal epilepsy: a single-institution retrospective review. Epilepsia 61:49–60
Krakow K, Wieshmann UC, Woermann FG et al (1999a) Multimodal MR imaging: functional, diffusion tensor, and chemical shift imaging in a patient with localization-related epilepsy. Epilepsia 40:1459–1462
Krakow K, Woermann FG, Symms MR et al (1999b) EEG-triggered functional MRI of interictal epileptiform activity in patients with partial seizures. Brain 122(9):1679–1688

Krings T, Topper R, Reinges MH et al (2000) Hemodynamic changes in simple partial epilepsy: a functional MRI study. Neurology 54:524–527
Lai S, Hopkins AL, Haacke EM et al (1993) Identification of vascular structures as a major source of signal contrast in high resolution 2D and 3D functional activation imaging of the motor cortex at 1.5T: preliminary results. Magn Reson Med 30:387–392
Laufs H, Hamandi K, Walker MC et al (2006) EEG-fMRI mapping of asymmetrical delta activity in a patient with refractory epilepsy is concordant with the epileptogenic region determined by intracranial EEG. Magn Reson Imaging 24:367–371
Laufs H, Hamandi K, Salek-Haddadi A, Kleinschmidt AK, Duncan JS, Lemieux L (2007) Temporal lobe interictal epileptic discharges affect cerebral activity in "default mode" brain regions. Hum Brain Mapp 28:1023–1032
Laufs H, Richardson MP, Salek-Haddadi A et al (2011) Converging PET and fMRI evidence for a common area involved in human focal epilepsies. Neurology 77:904–910
Lazeyras F, Blanke O, Perrig S et al (2000a) EEG-triggered functional MRI in patients with pharmacoresistant epilepsy. J Magn Reson Imaging 12:177–185
Lazeyras F, Blanke O, Zimine I, Delavelle J, Perrig SH, Seeck M (2000b) MRI, (1)H-MRS, and functional MRI during and after prolonged nonconvulsive seizure activity. Neurology 55:1677–1682
Lemieux L, Salek-Haddadi A, Josephs O et al (2001) Event-related fMRI with simultaneous and continuous EEG: description of the method and initial case report. NeuroImage 14:780–787
Lemieux L, Salek-Haddadi A, Lund TE, Laufs H, Carmichael D (2007) Modelling large motion events in fMRI studies of patients with epilepsy. Magn Reson Imaging 25:894–901
Lemieux L, Laufs H, Carmichael D, Paul JS, Walker MC, Duncan JS (2008) Noncanonical spike-related BOLD responses in focal epilepsy. Hum Brain Mapp 29:329–345
LeVan P, Tyvaert L, Moeller F, Gotman J (2010) Independent component analysis reveals dynamic ictal BOLD responses in EEG-fMRI data from focal epilepsy patients. NeuroImage 49:366–378
Liston AD, de Munck JC, Hamandi K et al (2006) Analysis of EEG-fMRI data in focal epilepsy based on automated spike classification and Signal Space Projection. NeuroImage 31:1015–1024
Liu Y, Yang T, Yang X et al (2008) EEG-fMRI study of the interictal epileptic activity in patients with partial epilepsy. J Neurol Sci 268:117–123
Logothetis NK, Pfeuffer J (2004) On the nature of the BOLD fMRI contrast mechanism. Magn Reson Imaging 22:1517–1531
Logothetis NK, Pauls J, Augath M, Trinath T, Oeltermann A (2001) Neurophysiological investigation of the basis of the fMRI signal. Nature 412:150–157
Lopes R, Lina JM, Fahoum F, Gotman J (2012) Detection of epileptic activity in fMRI without recording the EEG. NeuroImage 60:1867–1879
Luders H, Comair YG (2000) Epilepsy surgery. Lippincott Williams & Wilkins, Philadelphia
Luders HO, Najm I, Nair D, Widdess-Walsh P, Bingman W (2006) The epileptogenic zone: general principles. Epileptic Disord 8(2):1–9
Lund TE, Norgaard MD, Rostrup E, Rowe JB, Paulson OB (2005) Motion or activity: their role in intra- and inter-subject variation in fMRI. NeuroImage 26:960–964
Maclaren J, Herbst M, Speck O, Zaitsev M (2013) Prospective motion correction in brain imaging: a review. Magn Reson Med 69:621–636
Markoula S, Chaudhary UJ, Perani S et al (2018) The impact of mapping interictal discharges using EEG-fMRI on the epilepsy presurgical clinical decision making process: a prospective study. Seizure 61:30–37
Marrosu F, Barberini L, Puligheddu M et al (2009) Combined EEG/fMRI recording in musicogenic epilepsy. Epilepsy Res 84:77–81
Marsan CA, Zivin LS (1970) Factors related to the occurrence of typical paroxysmal abnormalities in the EEG records of epileptic patients. Epilepsia 11:361–381
Matsumoto H, Marsan CA (1964) Cortical cellular phenomena in experimental epilepsy: interictal manifestations. Exp Neurol 9:286–304

Maziero D, Velasco TR, Hunt N et al (2016) Towards motion insensitive EEG-fMRI: correcting motion-induced voltages and gradient artefact instability in EEG using an fMRI prospective motion correction (PMC) system. NeuroImage 138:13–27
McCormick DA, Contreras D (2001) On the cellular and network bases of epileptic seizures. Annu Rev Physiol 63:815–846
McGonigal A, Bartolomei F, Regis J et al (2007) Stereoelectroencephalography in presurgical assessment of MRI-negative epilepsy. Brain 130:3169–3183
Moore CI, Cao R (2008) The hemo-neural hypothesis: on the role of blood flow in information processing. J Neurophysiol 99:2035–2047
Morano A, Carni M, Casciato S et al (2017) Ictal EEG/fMRI study of vertiginous seizures. Epilepsy Behav 68:51–56
Morocz IA, Karni A, Haut S, Lantos G, Liu G (2003) fMRI of triggerable aurae in musicogenic epilepsy. Neurology 60:705–709
Mullinger KJ, Yan WX, Bowtell R (2011) Reducing the gradient artefact in simultaneous EEG-fMRI by adjusting the subject's axial position. NeuroImage 54:1942–1950
Northoff G, Walter M, Schulte RF et al (2007) GABA concentrations in the human anterior cingulate cortex predict negative BOLD responses in fMRI. Nat Neurosci 10:1515–1517
Palmer CA, Geyer JD, Keating JM et al (1999) Rasmussen's encephalitis with concomitant cortical dysplasia: the role of GluR3. Epilepsia 40:242–247
Pasley BN, Inglis BA, Freeman RD (2007) Analysis of oxygen metabolism implies a neural origin for the negative BOLD response in human visual cortex. NeuroImage 36:269–276
Pittau F, Dubeau F, Gotman J (2012) Contribution of EEG/fMRI to the definition of the epileptic focus. Neurology 78:1479–1487
Pittau F, Fahoum F, Zelmann R, Dubeau F, Gotman J (2013) Negative BOLD response to interictal epileptic discharges in focal epilepsy. Brain Topogr 26:627–640
Pittau F, Ferri L, Fahoum F, Dubeau F, Gotman J (2017) Contributions of EEG-fMRI to assessing the epileptogenicity of focal cortical dysplasia. Front Comput Neurosci 11:8
Raichle ME, MacLeod AM, Snyder AZ, Powers WJ, Gusnard DA, Shulman GL (2001) A default mode of brain function. Proc Natl Acad Sci U S A 98:676–682
Ray A, Tao JX, Hawes-Ebersole SM, Ebersole JS (2007) Localizing value of scalp EEG spikes: a simultaneous scalp and intracranial study. Clin Neurophysiol 118:69–79
Rodionov R, De MF, Laufs H et al (2007) Independent component analysis of interictal fMRI in focal epilepsy: comparison with general linear model-based EEG-correlated fMRI. NeuroImage 38:488–500
Rosenow F, Luders H (2001) Presurgical evaluation of epilepsy. Brain 124:1683–1700
Sakatani K, Murata Y, Fujiwara N et al (2007) Comparison of blood-oxygen-level-dependent functional magnetic resonance imaging and near-infrared spectroscopy recording during functional brain activation in patients with stroke and brain tumors. J Biomed Opt 12:062110
Salek-Haddadi A, Merschhemke M, Lemieux L, Fish DR (2002) Simultaneous EEG-Correlated Ictal fMRI. NeuroImage 16:32–40
Salek-Haddadi A, Friston KJ, Lemieux L, Fish DR (2003a) Studying spontaneous EEG activity with fMRI. Brain Res Brain Res Rev 43:110–133
Salek-Haddadi A, Lemieux L, Merschhemke M, Diehl B, Allen PJ, Fish DR (2003b) EEG quality during simultaneous functional MRI of interictal epileptiform discharges. Magn Reson Imaging 21:1159–1166
Salek-Haddadi A, Lemieux L, Merschhemke M, Friston KJ, Duncan JS, Fish DR (2003c) Functional magnetic resonance imaging of human absence seizures. Ann Neurol 53:663–667
Salek-Haddadi A, Diehl B, Hamandi K et al (2006) Hemodynamic correlates of epileptiform discharges: an EEG-fMRI study of 63 patients with focal epilepsy. Brain Res 1088:148–166
Salek-Haddadi A, Mayer T, Hamandi K et al (2009) Imaging seizure activity: a combined EEG/EMG-fMRI study in reading epilepsy. Epilepsia 50:256–264
Schridde U, Khubchandani M, Motelow JE, Sanganahalli BG, Hyder F, Blumenfeld H (2008) Negative BOLD with large increases in neuronal activity. Cereb Cortex 18:1814–1827

Schulz R, Luders HO, Hoppe M, Tuxhorn I, May T, Ebner A (2000) Interictal EEG and ictal scalp EEG propagation are highly predictive of surgical outcome in mesial temporal lobe epilepsy. Epilepsia 41:564–570

Schwartz TH, Bazil CW, Walczak TS, Chan S, Pedley TA, Goodman RR (1997) The predictive value of intraoperative electrocorticography in resections for limbic epilepsy associated with mesial temporal sclerosis. Neurosurgery 40:302–309

Schwartz TH, Hong SB, Bagshaw AP, Chauvel P, Benar CG (2011) Preictal changes in cerebral haemodynamics: review of findings and insights from intracerebral EEG. Epilepsy Res 97:252–266

Shmuel A, Yacoub E, Pfeuffer J et al (2002) Sustained negative BOLD, blood flow and oxygen consumption response and its coupling to the positive response in the human brain. Neuron 36:1195–1210

Shmuel A, Augath M, Oeltermann A, Logothetis NK (2006) Negative functional MRI response correlates with decreases in neuronal activity in monkey visual area V1. Nat Neurosci 9:569–577

Shulman RG, Rothman DL, Hyder F (2007) A BOLD search for baseline. NeuroImage 36:277–281

Sierra-Marcos A, Maestro I, Falcon C et al (2013) Ictal EEG-fMRI in localization of epileptogenic area in patients with refractory neocortical focal epilepsy. Epilepsia 54:1688–1698

Stefan H, Hummel C, Scheler G et al (2003) Magnetic brain source imaging of focal epileptic activity: a synopsis of 455 cases. Brain 126:2396–2405

Szaflarski JP, DiFrancesco M, Hirschauer T et al (2010) Cortical and subcortical contributions to absence seizure onset examined with EEG/fMRI. Epilepsy Behav 18:404–413

Tao JX, Ray A, Hawes-Ebersole S, Ebersole JS (2005) Intracranial EEG substrates of scalp EEG interictal spikes. Epilepsia 46:669–676

Tao JX, Baldwin M, Ray A, Hawes-Ebersole S, Ebersole JS (2007) The impact of cerebral source area and synchrony on recording scalp electroencephalography ictal patterns. Epilepsia 48:2167–2176

Tenney JR, Kadis DS, Agler W et al (2018) Ictal connectivity in childhood absence epilepsy: associations with outcome. Epilepsia 59:971–981

Thornton R, Laufs H, Rodionov R et al (2010a) EEG correlated functional MRI and postoperative outcome in focal epilepsy. J Neurol Neurosurg Psychiatry 81:922–927

Thornton RC, Rodionov R, Laufs H et al (2010b) Imaging haemodynamic changes related to seizures: comparison of EEG-based general linear model, independent component analysis of fMRI and intracranial EEG. NeuroImage 53:196–205

Thornton R, Vulliemoz S, Rodionov R et al (2011) Epileptic networks in focal cortical dysplasia revealed using electroencephalography-functional magnetic resonance imaging. Ann Neurol 70:822–837

Todd N, Josephs O, Callaghan MF, Lutti A, Weiskopf N (2015) Prospective motion correction of 3D echo-planar imaging data for functional MRI using optical tracking. NeuroImage 113:1–12

Trombin F, Gnatkovsky V, de CM. (2011) Changes in action potential features during focal seizure discharges in the entorhinal cortex of the in vitro isolated guinea pig brain. J Neurophysiol 106:1411–1423

Truccolo W, Donoghue JA, Hochberg LR et al (2011) Single-neuron dynamics in human focal epilepsy. Nat Neurosci 14:635–641

Tyvaert L, Hawco C, Kobayashi E, LeVan P, Dubeau F, Gotman J (2008) Different structures involved during ictal and interictal epileptic activity in malformations of cortical development: an EEG-fMRI study. Brain 131:2042–2060

Tyvaert L, LeVan P, Dubeau F, Gotman J (2009) Noninvasive dynamic imaging of seizures in epileptic patients. Hum Brain Mapp 30:3993–4011

Usami K, Matsumoto R, Sawamoto N et al (2016) Epileptic network of hypothalamic hamartoma: an EEG-fMRI study. Epilepsy Res 125:1–9

van Houdt PJ, de Munck JC, Leijten FSS et al (2013) EEG-fMRI correlation patterns in the presurgical evaluation of focal epilepsy: a comparison with electrocorticographic data and surgical outcome measures. NeuroImage 75:238–248

van Houdt PJ, Ossenblok PP, Colon AJ et al (2015) Are epilepsy-related fMRI components dependent on the presence of interictal epileptic discharges in scalp EEG? Brain Topogr 28:606–618
Vaudano AE, Laufs H, Kiebel SJ et al (2009) Causal hierarchy within the thalamo-cortical network in spike and wave discharges. PLoS One 4:e6475
Vaudano AE, Carmichael DW, Salek-Haddadi A et al (2012) Networks involved in seizure initiation. A reading epilepsy case studied with EEG-fMRI and MEG. Neurology 79:249–253
Vaudano AE, Avanzini P, Tassi L et al (2013) Causality within the epileptic network: an EEG-fMRI study validated by intracranial EEG. Front Neurol 4:185
Vaudano AE, Ruggieri A, Vignoli A et al (2014) Epilepsy-related brain networks in ring chromosome 20 syndrome: an EEG-fMRI study. Epilepsia 55:403–413
Vaudano AE, Olivotto S, Ruggieri A et al (2017) Brain correlates of spike and wave discharges in GLUT1 deficiency syndrome. Neuroimage Clin 13:446–454
Vulliemoz S, Carmichael DW, Rosenkranz K et al (2011) Simultaneous intracranial EEG and fMRI of interictal epileptic discharges in humans. NeuroImage 54:182–190
Watanabe S, An D, Safi-Harb M, Dubeau F, Gotman J (2014) Hemodynamic response function (HRF) in epilepsy patients with hippocampal sclerosis and focal cortical dysplasia. Brain Topogr 27:613–619
Wendling F, Hernandez A, Bellanger JJ, Chauvel P, Bartolomei F (2005) Interictal to ictal transition in human temporal lobe epilepsy: insights from a computational model of intracerebral EEG. J Clin Neurophysiol 22:343–356
Widdess-Walsh P, Jeha L, Nair D, Kotagal P, Bingaman W, Najm I (2007) Subdural electrode analysis in focal cortical dysplasia: predictors of surgical outcome. Neurology 69:660–667
Zhang Z, Liao W, Wang Z et al (2014) Epileptic discharges specifically affect intrinsic connectivity networks during absence seizures. J Neurol Sci 336:138–145
Zhao M, Suh M, Ma H, Perry C, Geneslaw A, Schwartz TH (2007) Focal increases in perfusion and decreases in hemoglobin oxygenation precede seizure onset in spontaneous human epilepsy. Epilepsia 48:2059–2067
Zijlmans M, Huiskamp G, Hersevoort M, Seppenwoolde JH, van Huffelen AC, Leijten FS (2007) EEG-fMRI in the preoperative work-up for epilepsy surgery. Brain 130:2343–2353

EEG-fMRI in Generalised Epilepsy: Adults

18

Patrick Carney and Graeme Jackson

18.1 Idiopathic Generalised Epilepsy

18.1.1 Definition and Classification of Generalised Epilepsy Syndromes

Generalised epilepsies are common and account for up to 20% of epilepsy diagnoses particularly in younger age groups (Jallon and Latour 2005; Olafsson et al. 2005). Although generalised epilepsies commonly present in childhood, they may present de novo in early or late adulthood and may persist into adulthood following onset in adolescents (Jallon and Latour 2005). First defined by the ILAE in

P. Carney (✉)
Box Hill Hospital, Level 2, Box Hill, VIC, Australia

Eastern Health Clinical School, Faculty of Medicine, Nursing and Health Sciences, Monash University, Clayton, VIC, Australia

The Florey Institute for Neuroscience and Mental Health, Melbourne Brain Centre, Parkville, VIC, Australia
e-mail: Patrick.carney2@easternhealth.org.au

G. Jackson
Florey Institute of Neuroscience and Mental Health, Heidelberg, VIC, Australia

Austin Hospital, Melbourne University, Heidelberg, VIC, Australia
e-mail: graeme.jackson@florey.edu.au

C. Mulert, L. Lemieux (eds.), *EEG - fMRI*,
https://doi.org/10.1007/978-3-031-07121-8_18

1989 (ILAE 1989), as idiopathic generalised epilepsies (IGE), they referred to epilepsies in which "all seizures are initially generalized, with an EEG expression that is a generalized, bilateral, synchronous, symmetrical discharge", and in addition, patients were considered to be "normal" between seizures; "a normal interictal state, without neurologic or neuroradiologic signs". The cause was unknown other than a "possible hereditary predisposition". More recent classification documents have used the term "genetic generalised epilepsies" (GGE) (Berg et al. 2010; Scheffer et al. 2017) which reflects a desire by the classification committee highlight the strong evidence in support of a genetic aetiology. Resistance to this view comes mostly from the limited number of known genes causing GGE (Mullen et al. 2018) and the potential stigma that arises from the term "genetic" which indicates inheritance and therefore may lead to negative perceptions of a patient with epilepsy. At present, the terms IGE, GGE and GE are all acceptable and interchangeable. We will use the term idiopathic generalised epilepsy (IGE) in this document. In the classification document of 2010 (Berg et al. 2010), generalised epilepsies are referred to as "Generalized epileptic seizures are conceptualized as originating at some point within, and rapidly engaging, bilaterally distributed networks. Such bilateral networks can include cortical and subcortical structures, but do not necessarily include the entire cortex". This observation reflects thinking on potential mechanisms of seizure generation and is key to how we might use EEG-fMRI to better understand the mechanisms and impacts of generalised seizures (Carney and Jackson 2014).

18.1.2 Diagnosing IGE

An approach to the diagnosis of IGE is considered as part of a broad approach to the diagnosis of epilepsy in the 2017 classification paper (Scheffer et al. 2017). In the initial classification, a greater emphasis was placed on EEG and neuroimaging findings, whereas in the new classification, the starting point for classification is the seizure type; the seizure is generalised in type, as opposed to focal or unknown. This enables consideration of epilepsy diagnosis and then, where possible, classification of the epilepsy syndrome. The well-recognised and ILAE-approved syndromes of GE are listed in Table 18.1.

Table 18.1 Epilepsy syndromes defined by the ILAE (*AS* absence seizure, *TCS* tonic-clonic seizure, *MS* myoclonic seizure, *EM* eyelid myoclonia, *MAS* myoclonic absence seizure, *MA* myoclonic atonic seizure)(Scheffer et al. 2017; ILAE 1985)

Epilepsy syndrome	Common seizure types	Age of onset
Childhood absence epilepsy	AS, TCS (less common)	4–10 years
Juvenile absence epilepsy	AS, TCS, MS	>10 years
Juvenile myoclonic epilepsy	MS, TCS, AS	>10 years
Epilepsy with eyelid myoclonias	EM, AS, TCS	
Epilepsy with myoclonic absence	MAS, AS, TCS	
Epilepsy with myoclonic atonic seizures	MA, AS, TCS	
Epilepsy with generalised TCS alone	TCS	

18.1.3 IGE Comorbidity

Given the conceptualisation of IGE as a large scale network disorder with abnormal network behaviour underpinning seizure generation, it is important to consider what the impact of abnormal network behaviour might have on other cognitive processes, not just during seizures but in the interictal period. A systemic review of cognitive studies in IGE highlighted the presence of pervasive cognitive impairments across a number of domains including executive function, processing speed and working memory which potentially impact on educational and vocational abilities (Loughman et al. 2014). Although there are likely to be effects of seizure burden and medication on cognitive outcome, it would appear that even in well-controlled epilepsy, cognitive outcomes may be impaired (Henkin et al. 2005). Mood disorders are also common in the epilepsies with a likely bidirectional relationship between the risk of epilepsy and severity and the presence of depression suggesting common underlying pathophysiological mechanisms (Josephson et al. 2017). The use of functional imaging, including EEG fMRI, provides a specific mechanism to study network performance and potentially establishes the link between functional networks and cognitive and affective performance.

18.2 Cortical and Subcortical Generators of Generalised Spike and Wave Activity

The hallmark feature of IGE is the generalised spike and wave discharge (GSW). GSW are defined by a low-amplitude surface negative spike followed by a dome-like slow wave (Avoli et al. 2001). Discharges can display marked variability in morphology with single discharges as well as polyspike activity. Onset is typically symmetrical, but asymmetric onset and apparent "focal" features are well described (Holmes et al. 2004). To understand the mechanism of generation of spike and wave activity, one needs to consider both the cellular networks involved in seizure generation and the large-scale functional networks that whole brain functional MRI demonstrates.

At a cellular level thalamocortical networks appear to be the major seizure generating apparatus (Kostopoulos 2000; Steriade 2005). The thalamus displays rhythmic firing and has extensive reciprocal connections to the cortex, with excitatory neurons (glutamatergic) arising from the dorsal thalamus conveying information to the cortex and excitatory cortical neurons project back to the thalamus (Steriade 2005; Blumenfeld 2002). In addition there is an inhibitory brake on this pathway. Inhibition occurs as a consequence of cortical and thalamic connections to the reticular nucleus of the thalamus which then projects back on to the anterior thalamus and cortex releasing gamma-aminobutyric acid (GABA)—an inhibitory neurotransmitter (Steriade 2005). This excitatory activity is the likely generator of the "spike", while reciprocal inhibition creates the after going slow "wave" (Blumenfeld 2005).

Thalamocortical networks provide us with a cellular pathway for the generation of seizures and interictal discharges, while a number of experimental pathways have been used to then explain how seizures may arise. Early experimental models of spike and wave activity gave rise to opposing theories on the pre-eminence of the thalamus or cortex in seizure generation (for review, see Blumenfeld 2005). These contrasting theories were united by the *generalised cortico-reticular theory* of Gloor, in which spike and wave arose from interactions between ascending inputs from the thalamus and a diffusely hyper-excitable cortex (Gloor 1968). More recently, the *cortical focus theory* has suggested that a cortical focus is required to initiate generalised activity (Meeren et al. 2005). This draws strongly on evidence from genetic absence epilepsy models in rats (Meeren et al. 2002; Pinault 2003; Pinault and O'Brien 2005) where an apparent cortical focus at the onset of a seizure is then followed by oscillations within the thalamocortical network. It is this view that is encompassed in the 2010 classification commission document which refers to generalised seizures originating "at some point within, and rapidly engaging, bilaterally distributed networks" (Berg et al. 2010).

These models indicate the importance of studying the structural and functional relationships between large-scale brain networks in humans if we are to understand the mechanisms of spike and wave activity. EEG-fMRI presents an opportunity to understand the relevance of these models to the human condition.

18.3 What EEG fMRI Has to Tell Us About Generators of Generalised Spike and Wave in Adults

Although the focus of this chapter is to consider insights into adult IGE provided by EEG-fMRI, it is impossible to do this without also referring to the extensive paediatric literature. In this section, we will discuss specifically the network insights provided by EEG-fMRI into the generation of interictal epileptiform discharges in both adults and children.

18.3.1 EEG-fMRI Provides a Topographic Map of Structures Involved in the Generation of GSW

18.3.1.1 The Thalamus and Cortex in GSW

The thalamus plays a central role as a relay station for information transfer in the brain, demonstrating strong reciprocal connections to the cortex, and not surprisingly has been consistently identified as a major region of positive BOLD change during interictal epileptiform activity (GSW discharges) and ictal discharges (absence seizures) in adults (Aghakhani et al. 2004; Benuzzi et al. 2015; Gotman et al. 2005; Laufs et al. 2006; Moeller et al. 2010a; Pugnaghi et al. 2014; Hamandi et al. 2008; Szaflarski et al. 2010a) and children (Bai et al. 2008, 2010; Berman et al. 2010; Carney et al. 2010, 2012; Killory et al. 2011; Li et al. 2009; Moeller et al. 2008a, b, 2010b, c) with generalised epilepsy syndromes.

The dominant theories of generation of GSW discussed above highlight the important interaction of the thalamus and cortex, and not surprisingly, changes in BOLD involving the thalamus and cortex are seen consistently. Thalamic change is most commonly seen as an increase in BOLD during interictal and ictal events across EEG-fMRI studies mentioned above. Cortical BOLD change however shows greater variability. There is a consistent negative BOLD change seen in the mesial and lateral parietal cortex, encompassing the precuneus and posterior cingulate mesially, and the angular and supramarginal gyrus laterally. These structures together are the key structures of the "default mode network" (DMN) (Raichle et al. 2001). The DMN has been identified as a key cognitive network subserving non-task-related cognitive processing and is consistently seen not only in EEG-fMRI studies of generalised epilepsy but also focal epilepsies and in a range of other functional imaging studies (Centeno and Carmichael 2014). The reason for negative BOLD change in this region is not clear with a number of theories proposed (Carney and Jackson 2014). BOLD change in other regions of the cortex is much more variable with both positive and negative changes seen involving primary (Berman et al. 2010; Carney et al. 2012) and association cortex without a consistent pattern that can be attributed to age, syndrome type (Aghakhani et al. 2004; Gotman et al. 2005) or nature of discharge (AS v interictal discharge) (Szaflarski et al. 2010a; Carney et al. 2010; Li et al. 2009). Hence, although both the thalamus and cortex are consistently identified as regions of BOLD change in response to both ictal and interictal generalised epileptic activity, exactly what this tells us about the mechanism of discharge generation is not so clear.

18.3.1.2 The Thalamus

Thalamic involvement in epileptic discharges in IGE is a consistent finding regardless of age, discharge type (interictal spike and wave or absence seizure) or epilepsy syndrome. An important question is to what extent particular subnuclei of the thalamus may be involved and what is the temporal relationship of BOLD signal change with regard to seizure onset thus providing insight into the potential generators of spike and wave.

There are significant limitations using EEG-fMRI when it comes to identifying thalamic subunits. An early step in the analysis of EEG-fMRI involves spatial smoothing to boost the signal of interest meaning that the resolution may be less than the size of relevant thalamic nuclei. In one study (Tyvaert et al. 2009), thalamic regions of interest were selected by a neurosurgeon with expertise in thalamic stereotaxy. In this population of adults with a range of IGE syndromes, the time course of the BOLD signal indicated a role for the posterior nuclei in discharge initiation or propagation while the anterior nuclei were more likely to play a role in discharge maintenance. Using a data-driven approach, Masterton et al. (2013) has observed two components of the spatial extent of epileptiform discharges; one located in the midline may reflect the local venous drainage into thalamostriate veins, while the other component involves the lateral thalamic nuclei and lentiform nuclei bilaterally (see Fig. 18.1) suggesting a more extensive thalamostriate network.

As discussed above, understanding the timing of thalamic versus cortical BOLD change is important for how we might better understand the generation of GSW and AS. Analysis of BOLD signal provides an opportunity to better understand these

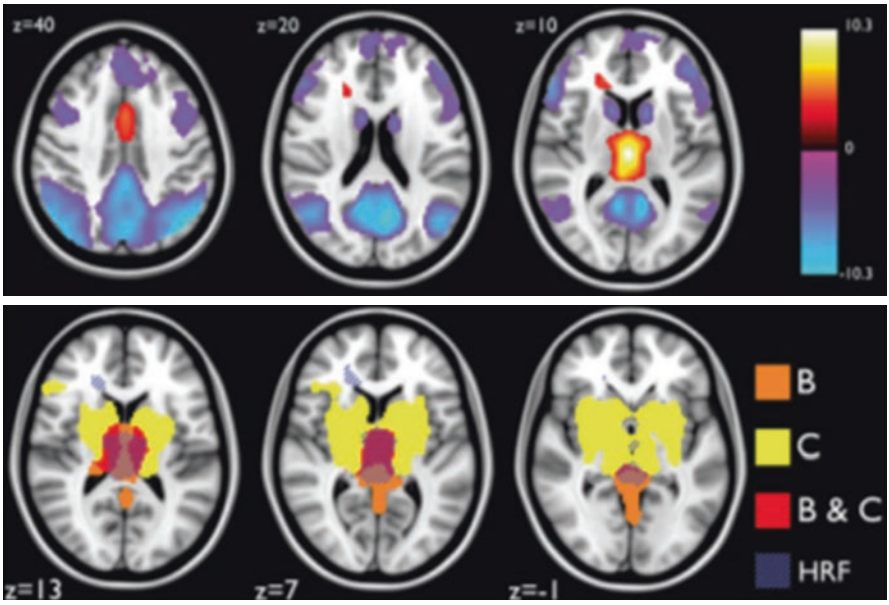

Fig. 18.1 Absence epilepsy subnetworks revealed by event-related independent components analysis (eICA). Panel 1 shows three axial sections of a group activation event-related analysis, while Image 2 shows thalamic activations identified using eICA. In panel 1, colours indicate activations (warm colours) and deactivations (cool colours). Panel 2 illustrates the areas of thalamic activation detected by the canonical HRF analysis, and components B and C of the eICA analysis. Significant activations from component B are represented by the orange-coloured areas, component C by the yellow-coloured areas, and areas where activation was detected in both components are represented by the red coloured areas. (Figure adapted from Masterton et al. 2013)

timing relationships although several methodological issues must be considered. The acquisition of a whole volume of MRI data usually occurs at a TR of approximately 3 s depending on the protocol used. Nonetheless, a number of methods have been used to extract relevant timing information, in spite of these limitations, which give some insight into thalamic BOLD change with regard to GSW activity. Methods have included selecting specific regions of interest and studying the time course within those regions (Bai et al. 2010; Carney et al. 2010; Moeller et al. 2008a), using independent components analysis (ICA) (Moeller et al. 2010a; Masterton et al. 2013) or using a shifting haemodynamic response function (HRF) (Szaflarski et al. 2010a; Bai et al. 2010; Moeller et al. 2008a; Benuzzi et al. 2012). Studies have shown BOLD change may precede event onset (Moeller et al. 2008b) although more commonly occur congruent with event onset (Szaflarski et al. 2010a; Carney et al. 2010; Benuzzi et al. 2012) but may also follow event onset (Bai et al. 2010). There is some debate whether the time course is canonical or that it deviates significantly form the canonical response. Our observation has been that the BOLD response is canonical, in contrast to the other elements consistently identified during spike and wave discharges (which we have dubbed the core network (Carney et al. 2010)), and we have speculated that the thalamus therefore appears to behave physiologically and reactively to the onset of epileptiform activity, although it may be critical to sustaining the seizure (Carney et al. 2012).

Non-Thalamic Subcortical Contributions

The study by Masterton above indicates the potential for non-thalamic subcortical involvement in GSW. Although several subcortical structures have been identified, including the reticular structures of the pons (Carney et al. 2010) and cerebellum (Bai et al. 2010; Benuzzi et al. 2012), the most commonly identified subcortical nuclei has been the caudate nuclei which commonly show symmetrical negative BOLD change in response to AS and GSW. The relevance of BOLD change in the caudate is not certain however it may be that changes in the caudate are related to connections with the prefrontal cortex. Zhang et al. (2008) used functional connectivity analysis to assess resting state correlations in the brain and showed correlations between the prefrontal cortex and the caudate nucleus. It may be that changes in the dorsolateral frontal cortex may interact with the caudate.

18.3.1.3 Cortical BOLD: The Importance of the Default Mode Network

Even in the very early studies of generalised epilepsies using spike-triggered EEG-fMRI, there was evidence of BOLD signal reductions in the DMN (Archer et al. 2003). The observation of task-induced activity decreases in parietal and frontal cortical regions was first made during a meta-analysis of PET studies of visual processing (Shulman and Fiez 1997). This network of regions was later termed the DMN (Raichle et al. 2001) and was identified as a distinct network in several other studies (Binder et al. 1999; Mazoyer et al. 2001). The DMN is involved in internalized cognitive activity including random thoughts and free associations of ideas and memories (Mazoyer et al. 2001; Andreasen et al. 1995). One might expect DMN signal change to distinguish between adult and paediatric EEG-fMRI studies as the DMN is known to show functional differences in children over differing developmental ages, with paediatric networks demonstrating a fundamentally different structure to adults, and are not just a precursors to the adult form (Power et al. 2010; Fair et al. 2009). Despite these functional differences, DMN change appears to be similar in adult and paediatric studies.

Several key observations have been made regarding the pattern and timing of BOLD change in the DMN in GSW and AS:

1. It appears consistent across age groups, syndrome classification and discharge type (AS v GSW) in individuals and in group analysis.
2. Studies analysing the timing of BOLD change in the DMN suggest this most commonly precedes the epileptiform event, importantly also occurring before thalamic BOLD increases, in both adults and children (Bai et al. 2010; Carney et al. 2010; Moeller et al. 2008a; Benuzzi et al. 2012; Szaflarski et al. 2010b).
3. The time course of BOLD change is complex often with an initial increase in BOLD, and therefore blood flow, followed by a reduction in BOLD signal closer to the timing of event onset before slowly returning to baseline. This pattern in some studies has deviated from the usual canonical or physiological BOLD response (Bai et al. 2010; Carney et al. 2010; Moeller et al. 2008a; Benuzzi et al. 2012; Szaflarski et al. 2010b).

The significance of DMN change is uncertain. In a review article, we have argued that DMN changes reflect a pre-emptive state of the brain which "permits"

or facilitate the occurrence of epileptiform events (Carney and Jackson 2014). We argue that "fluctuating states of awareness contribute to an environment conducive to the generation of epileptiform activity. Within that 'conducive' environment a further 'trigger' is required to initiate an epileptiform event". This is contrary to the argument that the DMN may be "switched off" during a generalised discharge, thus being the substrate for loss of awareness during and absence seizure(Gotman et al. 2005; Blumenfeld 2012; Danielson et al. 2011), or that frontal BOLD might be an initiating event for a generalised discharge (Archer et al. 2003; Vaudano et al. 2009). One of the arguments in support DMN BOLD change not being an indicator of loss of awareness comes from the fact that BOLD change appeared to be largely the same whether an absence, with loss of awareness or a brief burst of GSW, where awareness was retained. The Blumenfeld lab that published extensively on cognitive change associated with EEG-fMRI suggested that the defining feature of an absence seizure versus GSW may be the extent or intensity of BOLD and EEG change in already recognised networks (Li et al. 2009; Guo et al. 2016). Whether BOLD change is the product of, or a necessary requirement for, generalised epileptiform activity is not clear. Nonetheless, it is a consistent feature across a range of studies and is clearly an important component of the network of structures necessary to generated generalised epileptic activity.

Cortical Change in Adults Beyond the DMN

Given the likely role of thalamocortical networks in the generation of generalised epileptic activity, it would be expected that corresponding regions of positive BOLD would also be seen in EEG-fMRI studies; however, the opposite is the case. Cortical BOLD increases occur but they are not seen consistently or reproducibly between patients, although often these cortical patterns are reproducible within events in a single patient (Moeller et al. 2010b). Our interest in this variable cortical phenomenon leads to the observation of changes in the dorsolateral prefrontal cortex (activations, or deactivations) appeared related to severity of the underlying epilepsy syndrome (Carney et al. 2012). Zhang et al.(Zhang et al. 2015) used a novel "EEG-informed fMRI analysis" to study event-related discharges which showed activation in the medial frontal cortex, and to a lesser extent in the insular and sensory motor cortex, which linked strongly to activations in the medial dorsal nuclei of the thalamus. Other studies in adults have shown variable patterns of activation and deactivation in a range of primary and secondary/association cortical regions (Aghakhani et al. 2004; Gotman et al. 2005; Moeller et al. 2010c). We have also considered whether genetic factors may play a role in differences in the pattern of BOLD change. In unpublished data shown in Fig. 18.2, we studied BOLD change in sib pairs (young adults and children) with generalised epilepsy and showed the strongest correlation between BOLD change in matched voxels was seen in monozygotic twins with concordant epilepsy syndrome and with the weakest correlation in siblings with discordant syndromes. At this stage, it is not clear what can be inferred about cortical change beyond the DMN in GGE.

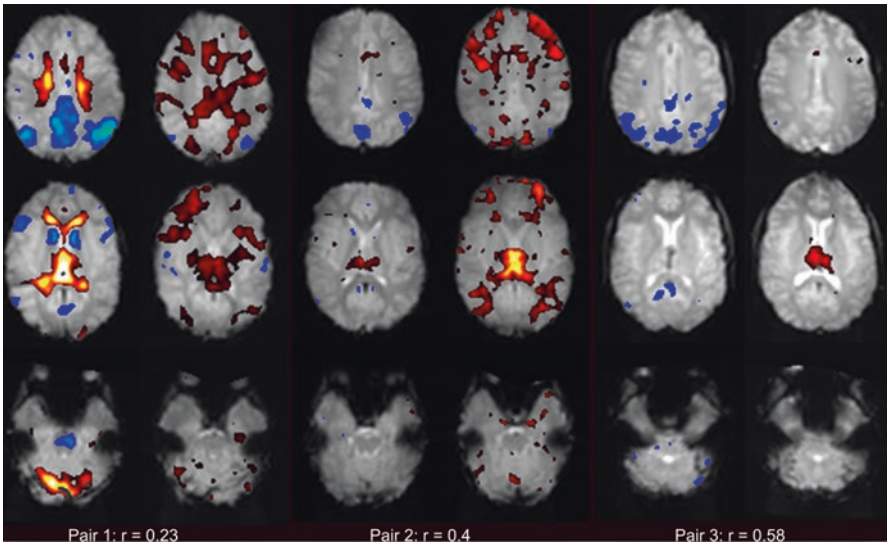

Fig. 18.2 Is BOLD change genetically determined? Correlation of BOLD change across all voxels was compared between siblings pairs (unpublished data). Axial sections showing BOLD change in cortical and subcortical regions for three sibling pairs. A comparison was then performed between siblings comparing raw BOLD signal between homologous voxels. A mean "r" value was the generated from the paired voxel values. The correlations between activation maps for the sibling pairs and reproducibility cohort are shown. Monozygotic twins with juvenile absence epilepsy (19 years) had a similarly high correlation of 0.58. A non-twin sibling pair with same syndrome (eyelid myoclonia with absence, ages 5 and 6) had a correlation of 0.4, whereas the sibling pair with different syndromes (CAE and ETCSA ages 8 and 6) had the lowest correlation of 0.23. Colour map images of positive BOLD (red to white; 0 to +10) and negative BOLD (blue to green 0 to −10) displayed on the subjects mean EPI image ($p < 0.001$ uncorrected)

18.3.1.4 Cortical Change in Lennox-Gastaut Syndrome

One situation where cortical BOLD change may be instructive is in patients with Lennox-Gastaut syndrome (LGS) in comparison to IGE. LGS has superficial similarities to GGE given the presence of generalised spike and wave activity, but this is where the similarity ends. LGS may arise in the context of an identifiable structural abnormality or may be cryptogenic and likely genetic (Arzimanoglou et al. 2009). The diagnostic clinical triad includes:

1. Multiple seizure types including tonic seizures.
2. Intellectual disability of varying severity.
3. Characteristic EEG findings of diffuse slowing, slow spike and wave (in contrast to fast spike wave seen in GGE) and the presence of paroxysmal bursts of fast activity which may occur spontaneously, often in sleep, and commonly in association with tonic seizures.

In LGS, changes in the DMN during SSW are typical of those seen in GSW of IGE, that is, predominantly negative BOLD change (Archer et al. 2014a; Pillay et al. 2013). Interestingly, the pons may be deactivated during GSW (Carney et al. 2010)

but shows a prominent increase in activity with SSW during fMRI regardless of the aetiology of LGS (that is structural or lesion negative/presumed genetic) (Pillay et al. 2013; Siniatchkin et al. 2011). The pattern of BOLD change associated with generalised paroxysmal fast activity (GPFA) is quite different with diffuse increase in BOLD activity involving association cortices showing simultaneous activation of attention and DMN networks in both children and adults (Archer et al. 2014a; Pillay et al. 2013; Archer et al. 2014b). This observation is unique given the DMN and attentional networks are usually anti-correlated given their opposing cognitive functions and appears to occur in both lesional and lesion-negative patients (Archer et al. 2014b).

In an abstract presented at the American Epilepsy Society in 2013 (Carney et al. 2014), we compared the patterns and time course of BOLD change between LGS and GGE. The DMN showed a similar pattern of deactivation during SSW and GSW with the major difference in BOLD change occurring in primary cortical areas, which show little change during GSW, but prominent deactivation during SSW. This was highlighted in the time course analysis of selected regions of interest (Fig. 18.3). The pons is deactivated during GSW but has rising activity prior to SSW. We hypothesise

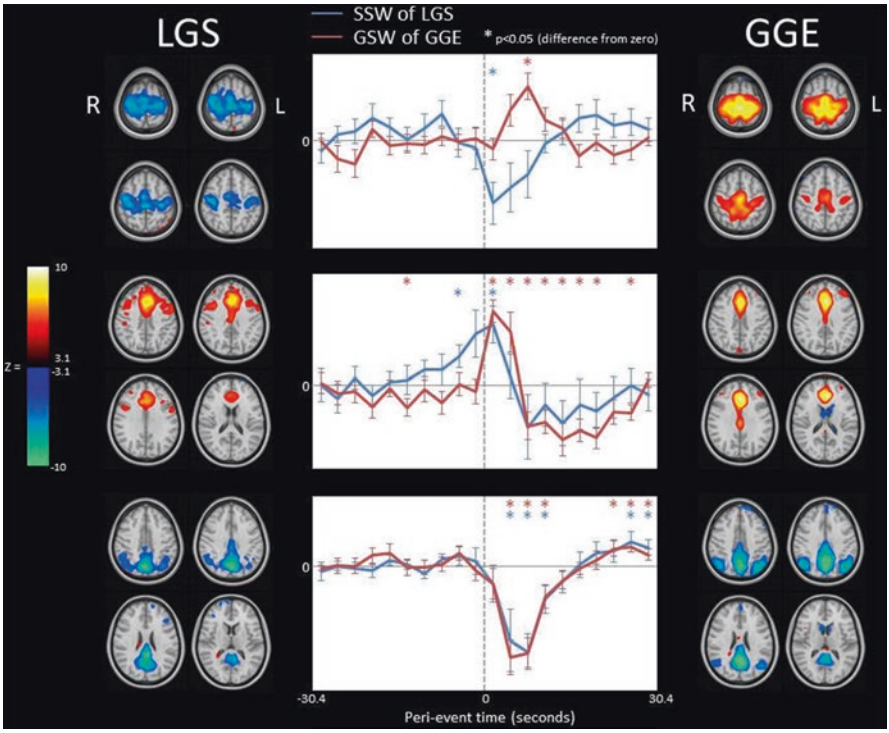

Fig. 18.3 Lennox-Gastaut syndrome compared to genetic generalised epilepsy. Group eICA of LGS compared to IGE(GGE) reveals the primary motor cortex is activated during the GSW of IGE but deactivated during the SSW of LGS. In this figure components of interest are displayed along with their associated average event-related time courses. To aid interpretation, the colour scale of *spatial* maps has been adjusted to show regions of initial signal decrease in cool colours and initial increase in warm colours

that although there are superficial similarities, it is likely that there are fundamental differences in how epileptic activity is generated in LGS versus GGE.

18.3.1.5 Connectivity Analysis Insights into the Mechanisms of GSW

Functional as well as structural methods of connectivity have been employed using a number of differing techniques to identify how the brain networks may be impaired in patients with epilepsy. Although not strictly EEG-fMRI, these studies often use EEG recorded events during EEG-fMRI studies to enable event-related or event-free analysis of connectivity (Xiao et al. 2017). In these studies, it would appear that significant perturbations of normal cortical and subcortical network relationships are common in IGE when compared to matched controlled populations. This may be influenced by the presence or absence of interictal activity (Luo et al. 2012; Masterton et al. 2012), the duration of disease, background seizure frequency (Liu et al. 2017) and accentuated by cognitive tasks (Vollmar et al. 2011). The observation by Vollmar and colleagues (Vollmar et al. 2011) that cognitive task performance in adults with JME leads to stronger activation of primary and supplementary motor areas, persistent activation of medial frontal regions and deactivation of the DMN (enhanced in those with active epilepsy) provides insight into how impairment of normal network organisation may be a substrate for neuropsychological impairment. Connectivity analysis provides insight into how brain function in patients with GGE may differ from the normal resting state between seizures and interictal discharges.

18.4 Conclusions

EEG-fMRI has proved to be a rich tool to explore the mechanisms which underpin the generation of seizures and interictal activity in adults with IGE enabling the non-invasive exploration of the underlying topography of seizure generation. In step with the extensive animal-model literature, EEG-fMRI has confirmed the importance of the thalamus as a central relay for interictal activity. However, perhaps more importantly, it has led to observations, such as the negative cortical BOLD change in the DMN, which have forced researchers to re-evaluate what thalamocortical relationships are and how they might contribute to seizure generation and the symptoms and signs of generalised seizures. Although lacking the temporal resolution of electrophysiological studies, EEG-fMRI has enabled insights into the spatial and temporal relationships, providing a means of understanding of how animal models may apply to the human condition. The increasing use of functional connectivity, often guided by in scanner EEG, will allow these spatial and temporal relationships to be further explored.

References

Aghakhani Y, Bagshaw AP, Benar CG et al (2004) fMRI activation during spike and wave discharges in idiopathic generalized epilepsy. Brain 127:1127–1144

Andreasen NC, O'Leary DS, Cizadlo T et al (1995) Remembering the past: two facets of episodic memory explored with positron emission tomography. Am J Psychiatry 152:1576–1585

Archer JS, Abbott DF, Waites AB, Jackson GD (2003) fMRI "deactivation" of the posterior cingulate during generalized spike and wave. Neuroimage 20:1915–1922

Archer JS, Warren AE, Stagnitti MR, Masterton RA, Abbott DF, Jackson GD (2014a) Lennox-Gastaut syndrome and phenotype: secondary network epilepsies. Epilepsia 55:1245–1254

Archer JS, Warren AE, Jackson GD, Abbott DF (2014b) Conceptualizing Lennox-Gastaut syndrome as a secondary network epilepsy. Front Neurol 5:225

Arzimanoglou A, French J, Blume WT et al (2009) Lennox-Gastaut syndrome: a consensus approach on diagnosis, assessment, management, and trial methodology. Lancet Neurol 8:82–93

Avoli M, Rogawski MA, Avanzini G (2001) Generalized epileptic disorders: an update. Epilepsia 42:445–457

Bai X, Berman R, Negishi M, Novotny EJ, Constable RT, Blumenfeld H (2008) Timing and correlation of fMRI network changes in typical childhood absence seizures. In: Neurosciences. Society for Neuroscience, Washington, DC

Bai X, Vestal M, Berman R et al (2010) Dynamic time course of typical childhood absence seizures: EEG, behavior, and functional magnetic resonance imaging. J Neurosci 30:5884–5893

Benuzzi F, Mirandola L, Pugnaghi M et al (2012) Increased cortical BOLD signal anticipates generalized spike and wave discharges in adolescents and adults with idiopathic generalized epilepsies. Epilepsia 53:622–630

Benuzzi F, Ballotta D, Mirandola L et al (2015) An EEG-fMRI study on the termination of generalized spike-and-wave discharges in absence epilepsy. PLoS One 10:e0130943

Berg AT, Berkovic SF, Brodie MJ et al (2010) Revised terminology and concepts for organization of seizures and epilepsies: report of the ILAE Commission on classification and terminology, 2005-2009. Epilepsia 51:676–685

Berman R, Negishi M, Vestal M et al (2010) Simultaneous EEG, fMRI, and behavior in typical childhood absence seizures. Epilepsia 51:2011

Binder JR, Frost JA, Hammeke TA, Bellgowan PS, Rao SM, Cox RW (1999) Conceptual processing during the conscious resting state. A functional MRI study. J Cogn Neurosci 11:80–95

Blumenfeld H (2002) The thalamus and seizures. Arch Neurol 59:135–137

Blumenfeld H (2005) Cellular and network mechanisms of spike-wave seizures. Epilepsia 46(Suppl 9):21–33

Blumenfeld H (2012) Impaired consciousness in epilepsy. Lancet Neurol 11:814–826

Carney PW, Jackson GD (2014) Insights into the mechanisms of absence seizure generation provided by EEG with functional MRI. Front Neurol 5:162

Carney PW, Masterton RA, Harvey AS, Scheffer IE, Berkovic SF, Jackson GD (2010) The core network in absence epilepsy. Differences in cortical and thalamic BOLD response. Neurology 75:904–911

Carney PW, Masterton RA, Flanagan D, Berkovic SF, Jackson GD (2012) The frontal lobe in absence epilepsy: EEG-fMRI findings. Neurology 78:1157–1165

Carney PW, Archer J, Warren AE, Abbott DF, Jackson GD (2014) Primary cortex and pons behave differently during spike and wave discharges of Genetic Generalised Epilepsy versus Lennox-Gastaut Syndrome. AES 2013 Annual meeting—online abstract supplement. Epilepsy Curr 14:1–475

Centeno M, Carmichael DW (2014) Network connectivity in epilepsy: resting state fMRI and EEG-fMRI contributions. Front Neurol 5:93

Danielson NB, Guo JN, Blumenfeld H (2011) The default mode network and altered consciousness in epilepsy. Behav Neurol 24:55–65

Fair DA, Cohen AL, Power JD et al (2009) Functional brain networks develop from a "local to distributed" organization. PLoS Comput Biol 5:e1000381

Gloor P (1968) Generalized cortico-reticular epilepsies. Some considerations on the pathophysiology of generalized bilaterally synchronous spike and wave discharge. Epilepsia 9:249–263
Gotman J, Grova C, Bagshaw A et al (2005) Generalized epileptic discharges show thalamocortical activation and suspension of the default state of the brain. Proc Natl Acad Sci U S A 102:15236–15240
Guo JN, Kim R, Chen Y et al (2016) Impaired consciousness in patients with absence seizures investigated by functional MRI, EEG, and behavioural measures: a cross-sectional study. Lancet Neurol 15:1336–1345
Hamandi K, Laufs H, Noth U, Carmichael DW, Duncan JS, Lemieux L (2008) BOLD and perfusion changes during epileptic generalised spike wave activity. Neuroimage 39:608–618
Henkin Y, Sadeh M, Kivity S, Shabtai E, Kishon-Rabin L, Gadoth N (2005) Cognitive function in idiopathic generalized epilepsy of childhood. Dev Med Child Neurol 47:126–132
Holmes MD, Brown M, Tucker DM, Holmes MD, Brown M, Tucker DM (2004) Are "generalized" seizures truly generalized? Evidence of localized mesial frontal and frontopolar discharges in absence. [see comment]. Epilepsia 45:1568–1579
ILAE (1985) Proposal for classification of epilepsies and epileptic syndromes. Commission on classification and terminology of the international league against epilepsy. Epilepsia 26:268–278
ILAE (1989) Proposal for revised classification of epilepsies and epileptic syndromes. Commission on classification and terminology of the international league against epilepsy. Epilepsia 30:389–399
Jallon P, Latour P (2005) Epidemiology of idiopathic generalized epilepsies. Epilepsia 46(Suppl 9):10–14
Josephson CB, Lowerison M, Vallerand I et al (2017) Association of depression and treated depression with epilepsy and seizure outcomes: a multicohort analysis. JAMA Neurol 74:533–539
Killory BD, Bai X, Negishi M et al (2011) Impaired attention and network connectivity in childhood absence epilepsy. Neuroimage 56:2209–2217
Kostopoulos GK (2000) Spike-and-wave discharges of absence seizures as a transformation of sleep spindles: the continuing development of a hypothesis. Clin Neurophysiol 111(Suppl 2):S27–S38
Laufs H, Lengler U, Hamandi K, Kleinschmidt A, Krakow K (2006) Linking generalized spike-and-wave discharges and resting state brain activity by using EEG/fMRI in a patient with absence seizures. Epilepsia 47:444–448
Li Q, Luo C, Yang T et al (2009) EEG-fMRI study on the interictal and ictal generalized spike-wave discharges in patients with childhood absence epilepsy. Epilepsy Res 87:160–168
Liu F, Wang Y, Li M et al (2017) Dynamic functional network connectivity in idiopathic generalized epilepsy with generalized tonic-clonic seizure. Hum Brain Mapp 38:957–973
Loughman A, Bowden SC, D'Souza W (2014) Cognitive functioning in idiopathic generalised epilepsies: a systematic review and meta-analysis. Neurosci Biobehav Rev 43:20–34
Luo C, Li Q, Xia Y et al (2012) Resting state basal ganglia network in idiopathic generalized epilepsy. Hum Brain Mapp 33:1279–1294
Masterton RA, Carney PW, Jackson GD (2012) Cortical and thalamic resting-state functional connectivity is altered in childhood absence epilepsy. Epilepsy Res 99:327–334
Masterton RAJ, Carney PW, Abbott DF, Jackson GD (2013) Absence epilepsy subnetworks revealed by event-related independent components analysis of functional magnetic resonance imaging. Epilepsia 54:801–808
Mazoyer B, Zago L, Mellet E et al (2001) Cortical networks for working memory and executive functions sustain the conscious resting state in man. Brain Res Bull 54:287–298
Meeren HK, Pijn JP, Van Luijtelaar EL, Coenen AM, Lopes da Silva FH (2002) Cortical focus drives widespread corticothalamic networks during spontaneous absence seizures in rats. J Neurosci 22:1480–1495
Meeren H, van Luijtelaar G, Lopes da Silva F, Coenen A (2005) Evolving concepts on the pathophysiology of absence seizures: the cortical focus theory. Arch Neurol 62:371–376
Moeller F, Siebner HR, Wolff S et al (2008a) Changes in activity of striato-thalamo-cortical network precede generalized spike wave discharges. Neuroimage 39:1839–1849

Moeller F, Siebner HR, Wolff S et al (2008b) Simultaneous EEG-fMRI in drug-naive children with newly diagnosed absence epilepsy. Epilepsia 49:1510–1519
Moeller F, Levan P, Gotman J (2010a) Independent component analysis (ICA) of generalized spike wave discharges in fMRI: comparison with general linear model-based EEG-fMRI. Hum Brain Mapp 32(2):209–217
Moeller F, Levan P, Muhle H et al (2010b) Absence seizures: individual patterns revealed by EEG-fMRI. Epilepsia 51:11
Moeller F, Muhle H, Wiegand G, Wolff S, Stephani U, Siniatchkin M (2010c) EEG-fMRI study of generalized spike and wave discharges without transitory cognitive impairment. Epilepsy Behav 18:313–316
Mullen SA, Berkovic SF, Commission IG (2018) Genetic generalized epilepsies. Epilepsia 59:1148–1153
Olafsson E, Ludvigsson P, Gudmundsson G, Hesdorffer D, Kjartansson O, Hauser WA (2005) Incidence of unprovoked seizures and epilepsy in Iceland and assessment of the epilepsy syndrome classification: a prospective study. Lancet Neurol 4:627–634
Pillay N, Archer JS, Badawy RA, Flanagan DF, Berkovic SF, Jackson G (2013) Networks underlying paroxysmal fast activity and slow spike and wave in Lennox-Gastaut syndrome. Neurology 81:665–673
Pinault D (2003) Cellular interactions in the rat somatosensory thalamocortical system during normal and epileptic 5-9 Hz oscillations. J Physiol 552:881–905
Pinault D, O'Brien TJ (2005) Cellular and network mechanisms of genetically-determined absence seizures. Thalamus Relat Syst 3:181–203
Power JD, Fair DA, Schlaggar BL, Petersen SE (2010) The development of human functional brain networks. Neuron 67:735–748
Pugnaghi M, Carmichael DW, Vaudano AE et al (2014) Generalized spike and waves: effect of discharge duration on brain networks as revealed by BOLD fMRI. Brain Topogr 27:123–137
Raichle ME, MacLeod AM, Snyder AZ, Powers WJ, Gusnard DA, Shulman GL (2001) A default mode of brain function. Proc Natl Acad Sci U S A 98:676–682
Scheffer IE, Berkovic S, Capovilla G et al (2017) ILAE classification of the epilepsies: position paper of the ILAE commission for classification and terminology. Epilepsia 58:512–521
Shulman GI, Fiez JA (1997) Common blood flow changes across visual tasks: II. Decreases in cerebral cortex. J Cogn Neurosci 9:5
Siniatchkin M, Coropceanu D, Moeller F, Boor R, Stephani U (2011) EEG-fMRI reveals activation of brainstem and thalamus in patients with Lennox-Gastaut syndrome. Epilepsia 52:766–774
Steriade M (2005) Sleep, epilepsy and thalamic reticular inhibitory neurons. Trends Neurosci 28:317–324
Szaflarski JP, DiFrancesco M, Hirschauer T et al (2010a) Cortical and subcortical contributions to absence seizure onset examined with EEG/fMRI. Epilepsy Behav 18:404–413
Szaflarski JP, Lindsell CJ, Zakaria T, Banks C, Privitera MD (2010b) Seizure control in patients with idiopathic generalized epilepsies: EEG determinants of medication response. Epilepsy Behav 17:525–530
Tyvaert L, Chassagnon S, Sadikot A, LeVan P, Dubeau F, Gotman J (2009) Thalamic nuclei activity in idiopathic generalized epilepsy: an EEG-fMRI study. Neurology 73:2018–2022
Vaudano AE, Laufs H, Kiebel SJ et al (2009) Causal hierarchy within the Thalamo-cortical network in spike and wave discharges. PLoS One 4(8):e6475
Vollmar C, O'Muircheartaigh J, Barker GJ et al (2011) Motor system hyperconnectivity in juvenile myoclonic epilepsy: a cognitive functional magnetic resonance imaging study. Brain 134:1710–1719
Xiao F, An D, Zhou D (2017) Functional MRI-based connectivity analysis: a promising tool for the investigation of the pathophysiology and comorbidity of epilepsy. Seizure 44:37–41
Zhang D, Snyder AZ, Fox MD, Sansbury MW, Shimony JS, Raichle ME (2008) Intrinsic functional relations between human cerebral cortex and thalamus. J Neurophysiol 100:1740–1748
Zhang CH, Sha Z, Mundahl J et al (2015) Thalamocortical relationship in epileptic patients with generalized spike and wave discharges—a multimodal neuroimaging study. NeuroImage Clin 9:117–127

EEG-fMRI in Children with Epilepsy

19

Michael Siniatchkin, Friederike Moeller, and Francois Dubeau

Abbreviations

BECTS	Benign epilepsy with centro-temporal spikes
BOLD	Blood oxygenation level dependent
EEG	Electroencephalography
fMRI	Functional magnetic resonance imaging
HRF	Haemodynamic response function

19.1 EEG-fMRI in Children with Epilepsy

Childhood epilepsies differ from adult epilepsies regarding aetiology, pathogenesis, seizure semiology and EEG patterns and prognosis (Roger et al. 2005). The immature brain is more prone to develop seizures, and epileptic discharges are more frequent and less localized in children than in adults (Holmes 1997). The clinical

M. Siniatchkin (✉)
Protestant Clinics Bethel, University Clinic of Child and Adolescent Psychiatry and Psychotherapy, University of Bielefeld, Bielefeld, Germany
e-mail: Michael.siniatchkin@evkb.de

F. Moeller
Great Ormond Street Hospital for Children, London, UK
e-mail: Friederike_moeller@gosh.nhs.uk

F. Dubeau
Department of Neurology and Neurosurgery, Montreal Neurological Hospital and Institute, McGill University, Montreal, QC, Canada
e-mail: francois.dubeau@muhc.mcgill.ca

C. Mulert, L. Lemieux (eds.), *EEG - fMRI*,
https://doi.org/10.1007/978-3-031-07121-8_19

manifestations are also age-correlated and can vary within patients throughout their maturation process (Ben-Ari 2006). Some epileptic syndromes are seen only in infants or children such as the West syndrome and severe myoclonic epilepsy of infancy, the idiopathic occipital epilepsies and the benign epilepsy with centro-temporal spikes (Roger et al. 2005). Most of our understanding of the networks involved in the generation and propagation of epileptic activity in the immature brain derives from animal models and little from the study of human epilepsies.

Combining EEG and fMRI to study the haemodynamic correlates of spontaneous brain discharges, such as interictal epileptiform discharges (IED), provides a unique opportunity to investigate in vivo epileptogenic networks in patients with epilepsy (previous chapters and Moeller et al. 2013a; Maloney et al. 2015). It is a non-invasive technique that can be applied serially, or longitudinally, to children of all ages and that could add essential information on the maturation process and on developmental changes due to epilepsy. However, the use of EEG-fMRI in the paediatric population is associated with a host of methodological issues regarding data acquisition and analysis.

19.2 Methodological Issues Specific to Paediatric EEG-fMRI Studies

19.2.1 Patient Selection and Scanning

One of the most challenging aspects of performing fMRI in children is to obtain a sufficient cooperation from their part so that adequate data can be collected. There are two main aspects to this issue: first, minimizing anxiety so that the child will agree to enter the scanner and remain in the scanner for the entirety of the exam, and second ensuring that the child stays motionless throughout the entire study (20–30 mins on average). Generally, sedation may be used for children undergoing EEG-fMRI, especially in very young children and children with developmental delay (Moeller et al. 2013a). In non-sedated children, usually older and without developmental delay, anxiety may be reduced if a relative or someone familiar to the child is in the MR room during data acquisition, if EEG-fMRI is simulated first and the child trained for the test and, finally, if external stimulation (video and audio tapes), is used as early as possible before the test to distract the child (Rosenberg et al. 1997; Gaillard et al. 2001; Poldrack et al. 2002; Centeno et al. 2016). In some cases, relaxation techniques may help (Quirk et al. 1989).

Even well prepared or sedated, children are subject to motion (head and body movements) during the acquisition time. For instance, to reduce the effect of head motion on EEG-fMRI results, algorithms are used to improve quality and sensitivity of fMRI analysis (Bednarz and Kana 2018). Despite these difficulties, a survey of the literature reveals that EEG-fMRI studies have been conducted successfully in more than 1000 children with epilepsy to date. In our experience, so far, the recordings are well tolerated and the fMRI data of good quality can be obtained (see below).

19.2.2 Modelling IED-Related BOLD Changes in Children: Variability and Developmental Changes

The haemodynamic response function (HRF) to external stimuli is known to change over the course of normal development, most notably during infancy (Schapiro et al. 2004). Whereas auditory and visual stimulation results in positive BOLD responses (activations) in adults, several studies have reported negative BOLD responses (deactivations) to the same sensory stimulation in infants (for review, Poldrack et al. 2002). Despite a great deal of variability, there is a general pattern of BOLD responses in different stages of development: until 8 weeks, a significant proportion of children show no BOLD changes, older infants and children demonstrate negative BOLD responses in most cases until the age of 3 years (Morita et al. 2000; Martin et al. 1999). In children older than 3 years, positive BOLD responses dominate and persist throughout maturation.

The term 'HRF' designates the BOLD time course in response to a brief stimulus. In the field of EEG-fMRI in epilepsy, HRF commonly refers to the BOLD change associated with brief discharges such as focal spikes. The effects of epilepsy and brain maturation on the shape of the HRF (amplitude, polarity and latency) are not well characterized. Jacobs et al. (2007) underline the impact of age on the IED-related BOLD changes and demonstrated that children with focal lesional epilepsy show deactivations more frequently than activations in the irritative zone compare to adults with the same type of epilepsy. In another study, the same group (Jacobs et al. 2008a) analysed the latency of the IED-related positive and negative BOLD changes using a Fourier basis set in 37 children with focal epilepsy (age range of 3 months–18 years). Peak time of the positive BOLD changes in the youngest children (0–2 years) was significantly longer (mean, 7.74 s) than in older age groups. Moreover, the negative BOLD changes peaked later compared with HRF for positive BOLD responses in all age groups. The influence of age on the HRF in children may be explained by a different vascular response to neural activity compare to adults, by a higher synaptic density and increased rates of synaptogenesis resulting in higher energy demand in the cortex of infants and young children or by an increased venous capacitance effect usually found in the paediatric age group (Meek et al. 1998).

Changes in brain state (vigilance, drowsiness and sleep), the effect of anaesthetics or sedative drugs and of the antiepileptic medication itself probably modulate the BOLD signal and, hence, influence the fMRI results: for instance, more negative BOLD responses are observed if children are sedated during the EEG-fMRI studies (Altman and Bernal 2001; Bell et al. 2005; Born et al. 1998; Moehring et al. 2008). Whatever the mechanism and explanation, the choice of basis set for fMRI modelling may be particularly important in paediatric studies with possible implications for the technique's yield (Jacobs et al. 2007). Modelling variability in the amplitude and field of the IED may further improve the yield of EEG-fMRI results (Kowalczyk et al. 2020).

19.3 Results of EEG-fMRI Studies in Paediatric Epilepsy

19.3.1 Self-Limited Focal Epilepsies

Self-limited focal epilepsies represent a group of epileptic disorders that show well-defined focal epileptiform EEG patterns which undergo strong developmental influences (Dalla Bernardina et al. 2005). Early applications of EEG-fMRI in children focused on the benign epilepsy with centro-temporal spikes (BECTS) or Rolandic epilepsy (Archer et al. 2003). Seizures in BECTS begin typically with paraesthesia and jerking in the mouth, face and hand, usually with a preserved level of consciousness, supporting their origin of epileptic activity in the sensorimotor cortex. Accordingly, the EEG-fMRI studies in patients with BECTS have shown IED-associated BOLD signal changes in the sensorimotor cortex, whereas distant BOLD signal changes were interpreted as propagated activity (Archer et al. 2003, Boor et al. 2003, 2007; Lengler et al. 2007; Siniatchkin et al. 2007a; Masterton et al. 2013, see Fig. 19.1). Note that even in patients with well-localized IEDs, electrical source analysis was needed in order to differentiate between BOLD signal changes related to the initiation of epileptic activity from BOLD effects which can be attributed to the propagated activity (Boor et al. 2007). The BOLD response to focal IED in BECTS was different to the canonical shape of the HRF underlining the importance of more variable HRF in paediatric studies (Masterton et al. 2010). Interestingly, these early studies revealed some indications for possible interaction between the epileptic and the cognitive networks which may be responsible for cognitive deficits and psychiatric symptoms in patients with BECTS. In addition to activations in the

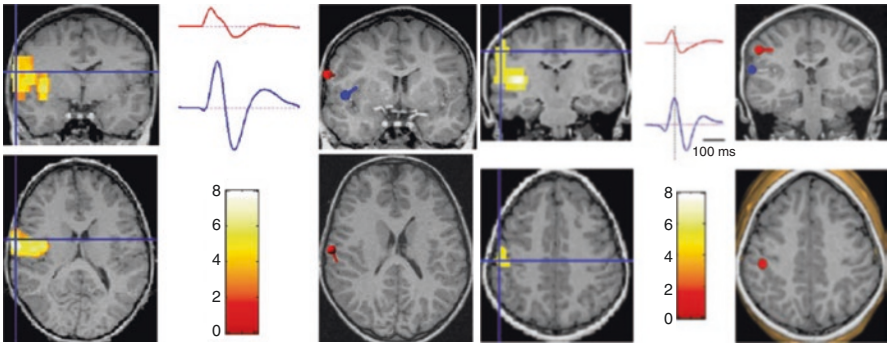

Fig. 19.1 Examples of two patients with benign epilepsy with centro-temporal spikes (Boor et al. 2007). For each patient, the left picture shows results of event-related EEG-fMRI study. Only significant activations (FWE corrected, $p < 0.05$) are presented. The right picture demonstrates localization of equivalent current dipoles (calculated with BESA) for generators of epileptic activity (red) and propagated activity (blue). Note a good concordance between dipole localization and activation in the centro-temporal region in both patients. The figure illustrates how the combination of EEG source imaging and fMRI may disclose physiological significance of activated brain regions and separate areas of initiation and propagation of epileptic activity

sensorimotor cortex, Archer et al. (2003) also described fMRI deactivation in both medial frontal regions, adjacent to the cingulate sulcus ($p = 0.004$, corrected), a location consistent with areas involved in attention and concentration, which may provide a link with the aforementioned psychological deficits. The effects of centro-temporal spikes on cognition were demonstrated in a study of Xiao et al. (2016). The authors performed a dynamic analysis of functional connectivity in 22 medication-naïve patients with BECTS and differentiated between the pre-spike-, spike- and post-spike-related activities. The analysis of dynamic changes revealed positive correlations between bilateral rolandic areas and the left inferior frontal gyrus (Broca area), the left inferior parietal lobe and the supramarginal gyrus (areas responsible for receptive language function) as well as the right inferior frontal gyrus and left caudate. Anti-correlations were found in the default mode network. The authors suggested rolandic IED directly disrupt the functional brain networks responsible for language, behaviour and cognition in children with BECTS (Xiao et al. 2016). IED-related and IED-independent disturbance of functional connectivity in cognitive networks of patients with BECTS has been supported in a number of recent connectivity studies (Li et al. 2017, 2019).

It seems likely that antiepileptic drugs exert an influence on IED-related neuronal networks as revealed by EEG-fMRI and on the interaction between these networks and networks of cognitive function. Zhang et al. (2018) demonstrated a clear and significant IED-associated activation in the Rolandic cortex in 11 children with BECTS, whereas activation strength and the overall area of activation were diminished in the levetiracetam-medicated group of 12 children with BECTS. Moreover, the drug-naïve group showed deactivation in the regions engaged in higher cognition networks compared with the levetiracetam-medicated group (Zhang et al. 2018). These findings may shed a light on the pharmacological mechanism of levetiracetam therapy on BECTS.

In other benign epilepsies (benign occipital lobe epilepsies of a Gastaut type and Panayiotopoulos type), Leal et al. (2006, 2007) found an activation pattern in different cortical occipital and parietal areas corresponding well to the localization of interictal epileptiform discharges. The authors suggested that EEG-fMRI provides a more satisfactory mapping of the irritative zone than those obtained from EEG source analysis. Moreover, Moeller et al. (2013a) investigated ten patients with atypical benign partial epilepsy (ABPE or pseudo-Lennox syndrome) using simultaneous EEG-fMRI recording. Focal BOLD signal changes concordant with the spike field and distant cortical and subcortical BOLD signal changes were detected. The group analysis revealed a thalamic activation. This study demonstrated that ABPE is characterized by patterns similar to studies in Rolandic epilepsy (focal BOLD signal changes in the spike field) as well as patterns observed in continuous spikes and waves during slow sleep (CSWS) (distant BOLD signal changes in cortical and subcortical structures; see below), thereby underscoring that idiopathic focal epilepsies of childhood form a spectrum of overlapping syndromes.

19.3.2 Symptomatic and Cryptogenic Focal Epilepsies

An important motivation to perform EEG-fMRI studies in epilepsy is to use this method to map the epileptogenic and irritative zones for surgical purposes and any areas responsible for functional deficits. In adults, attempts have been made to reveal the epileptogenic zone using EEG-fMRI within a preoperative workup for epilepsy surgery in a selected group of patients (Zijlmans et al. 2007; Thornton et al. 2010, 2011; Grouiller et al. 2011; Coan et al. 2016; Sebastiano et al. 2020). EEG-fMRI studies in lesional pharmacoresistant epilepsies are of a particular interest, especially from a clinical point of view. However, before the method finds a place in the clinical routine, validation studies demonstrating correspondence between lesions and BOLD signal changes are needed (Al-Asmi et al. 2003; Salek-Haddadi et al. 2006). It could be hypothesized that different lesions may cause activation of different epileptogenic networks which will be specifically displayed by EEG-fMRI (Kobayashi et al. 2005, 2007). Also, the EEG-fMRI method may be a useful tool to study and understand lesional, peri-lesional and remote regions (Kobayashi et al. 2006a, b; Thornton et al. 2011; Coan et al. 2016). Few studies have been performed in children with lesional, or non-lesional, pharmacoresistant epilepsies, often due to developmental delay and need for sedation. As there is only limited evidence for added clinical value of EEG-fMRI, it may not seem ethical for children to undergo sedation for the investigation. While some listed studies have included single paediatric patients, only few studies have investigated specific groups of children with focal epilepsy.

De Tiege et al. (2007a, b) presented the first study of EEG-fMRI in six children with symptomatic and non lesional pharmacoresistant focal epilepsy (Fig. 19.2). In four children (66%), activations colocalised with the presumed location of the epileptic focus, and in a fifth, colocalisation was seen for both activation and deactivation. Moreover, EEG-fMRI results were concordant with either invasive EEG recording (1 patient), with brain lesion (2 patients) or with ictal SPECT (2 patients), suggesting a potential role of this method in children to map non-invasively the haemodynamic changes associated with epileptic activity and delineate the epileptogenic zone.

Jacobs et al. (2007) analysed 13 children with pharmacoresistant lesional focal epilepsy (Fig. 19.3). In 84% of the studies, BOLD responses were localized in the lesion or presumed irritative zone. In contrast to studies in adults (Salek-Haddadi et al. 2006), deactivations in the lesion and the irritative zone were more common than activations. In another study of Jacobs et al. (2008b), five children with tuberous sclerosis complex (TSC) and pharmacoresistant focal epilepsy were studied in a 3 T MR scanner. A BOLD response was found in at least one tuber localized in the lobe responsible for spikes generation and presumed seizure onset zone (according to EEG-video monitoring) in all patients. In four patients, the same tubers were involved in generation of topographically different spikes and the BOLD changes were always multifocal, sometimes involving tubers distant from the spike field. The study of Jacobs et al. (2008b) demonstrated extended epileptogenic networks in patients with TSC which were more expanded than networks described in PET and SPECT studies (Chugani et al. 1998).

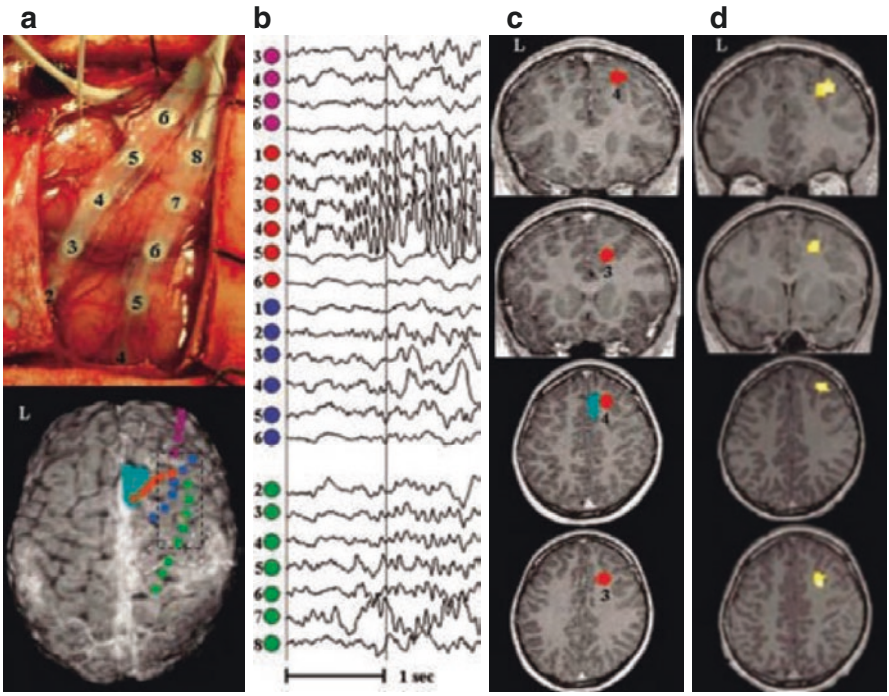

Fig. 19.2 Example of the close spatial correspondence between intracranial EEG recordings and EEG-fMRI activations in a child suffering from focal epilepsy. (**a**) Surface position of three subdural strips (green, blue and violet circles) and the depth electrodes (red circle) relative to the brain lesion (focal cortical dysplasia in green). (**b**) A sample of the intracranial recording showing that seizures started at contacts one to four of the depth electrodes (red circle). (**c**) Location of contacts three and four of the depth electrode (red circle) involved in seizure onset on coronal and axial brain scan. (**d**) Colocalized activations found with EEG-fMRI. (From De Tiege et al., 2007 with permission)

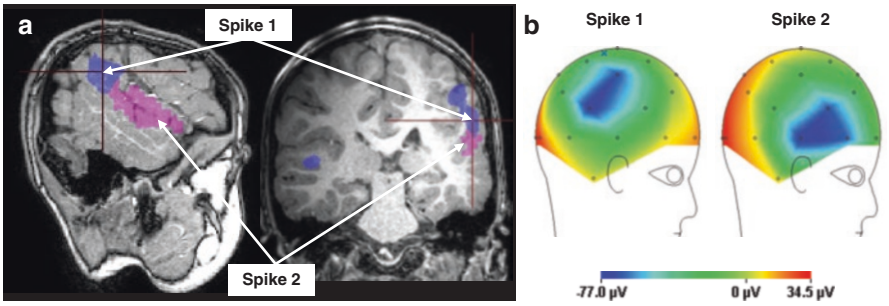

Fig. 19.3 EEG-fMRI results (**a**) in 8 eight-years-old boy with a right-hemispheric extended perisylvian polymicrogyria and focal seizures. The patient has two types of interictal epileptiform discharges (Spike 1 and Spike 2): in the right centro-parietal and right temporal areas (**b**). Note a good correspondence between bioelectrical activity and cortical deactivation. In this patient, and as in many other cases, the locations of the negative BOLD response were consistent with those of the lesion and epileptiform discharges. (From Jacobs et al. 2007 with permission)

In a group of six children with unambiguous focus localisation (validated through ictal EEG, PET and ictal SPECT), the hemodynamic changes corresponded to the epileptogenic zone in four children. Combined source analysis in these patients suggested that distant BOLD signal changes might be explained by propagated epileptic activity (Groening et al. 2009). The study of Groening et al. (2009) provided evidence that electrical source analysis shows better sensitivity in localization of the epileptogenic zone in children than EEG-fMRI. Moreover, the source analysis revealed clear advantages separating the brain areas of the initial epileptic activity from areas involved into the propagated activity. The advantages of the source analysis were illustrated by Elshoff et al. (2012). In this study, results of electrical source analysis were compared with results of EEG-fMRI recordings retrospectively in nine patients who suffered from pharmacoresistant focal epilepsy and underwent epileptic surgery with the favourable outcome (Engel class I and IIb). While the results of the source analysis were concordant with the resection area in all patients, EEG-fMRI revealed areas of activation within the resection area in only four cases.

The additive value of EEG-fMRI and electrical source imaging (ESI) for presurgical evaluation was demonstrated by a comprehensive study of Centeno et al. (2017). Fifty-three children with drug-resistant epilepsy underwent EEG-fMRI. Fifty-two of 53 patients had significant maps of activation: 47 of 53 for EEG-fMRI, 44 of 53 for ESI and 34 of 53 for both. The epileptogenic zone was well characterized in 29 patients; 26 had an EEG-fMRI activation that was correct in 11, 22 patients had ESI localization that was correct in 17 and 12 patients had combined EEG-fMRI and ESI that was correct in 11. Seizure outcome following resection was correctly predicted by EEG-fMRI activations in 8 of 20 patients and by the ESI maximum in 13 of 16 patients. The combined EEG-fMRI/ESI region entirely predicted outcome in 9 of 9 patients, including 3 with no lesion visible on MRI. The study demonstrated that EEG-fMRI combined with ESI provides a simple unbiased localization that may predict surgery better than each individual test, including MRI-negative patients (Centeno et al. 2017).

In summary, EEG-fMRI studies may represent a valuable additional investigation localise epileptogenic zone in some patients with pharmacoresistant focal epilepsies. However, the sensitivity of EEG-fMRI studies in children is lower than in adults. To improve sensitivity, methodological optimization of spike detection and MR data acquisition is necessary. The correspondence between the areas of activation and epileptogenic zone was found only in some children. At the moment, the EEG-fMRI represents only one option among others (EEG source reconstruction, PET, SPECT, etc.) in the presurgical setup. Further methodological and validation studies are needed in order to evaluate and improve the yield of the technique in children with focal epilepsies. Some studies have revealed a higher sensitivity by performing recordings with a fast fMRI sequence called MREG (magnetic resonance encephalography) which provides a temporal resolution of around 100 ms (Jacobs et al. 2014) or by analysing spike-specific topographic maps—instead of clear spikes—which may recognize even hidden spikes and improve time series necessary for analysis (Grouiller et al. 2011).

19.3.3 Idiopathic Generalized Epilepsies

Idiopathic generalized epilepsy (IGE) is characterized by EEG patterns with generalized spike wave discharges (GSW) typically arising from normal background activity. Early EEG-fMRI studies investigated adult patients with idiopathic generalized epilepsy who showed short GSW paroxysms (Aghakhani et al. 2004; Gotman et al. 2005; Hamandi et al. 2006). These studies have confirmed that the thalamus is activated during GSW but also showed deactivation in the medial frontal cortex, precuneus, lateral parietal and frontal cortex—i.e. areas of the so-called default mode network (DMN). It has been proposed that the DMN constitutes a necessary favourable neurometabolic environment for cognitive functions, represents a physiological baseline for processes of attention and working memory and supports dynamical integration of cognitive and emotional processing (Raichle and Mintun 2006). Abnormal activity in the DMN and disturbed connectivity between the structures involved may influence task performance and contribute to pathogenesis of neuropsychiatric disorders such as attention-deficit hyperactivity, Alzheimer's disease, autism, schizophrenia or depression (Broyd et al. 2009). Moreover, altered activity in the DMN has been associated with fluctuations and disturbance of consciousness (Boly et al. 2008). It has been suggested that disruption of the resting state activity by pathological processes (e.g. those that give rise to spike) may be related to alterations in cognitive function and a possible mechanism which may underlie cognitive deficits in epilepsy (Gotman et al. 2005).

Labate et al. (2005) presented results of an EEG-fMRI study in an untreated 7-year-old girl with new onset idiopathic generalized epilepsy (IGE), frequent absence seizures and eyelid myoclonia. Bursts of 3-Hz spike wave and polyspike wave epileptiform discharges registered in a 3 T MR scanner were associated with prominent, bilateral activation in the thalamus ($p < 0.05$, corrected) and less pronounced areas of cortical activation and deactivation. A few years later, Moeller and colleagues investigated absence seizures in drug naïve children with newly diagnosed epilepsy and confirmed a thalamic activation along with deactivation in the DMN areas and the caudate nucleus (Moeller et al. 2008a, see Figs. 19.4 and 19.5). These few observations on absence seizures in children extend the findings on generalized spike wave paroxysms performed in adults with idiopathic generalized epilepsy (see Chap. 18 and Aghakhani et al. 2004; Gotman et al. 2005; Hamandi et al. 2006; Laufs et al. 2007). These data seem to suggest that the age of subjects and antiepileptic medication (all studies in adults have been done in treated patients and often with drug-resistant idiopathic generalized epilepsy) does not influence the haemodynamic and metabolic responses during spike-and-wave activity and, hence, possibly reflect stable and typical neuronal networks. Additionally, in a group analysis, Carney and colleagues showed that the brainstem is also involved during absence seizures (Carney et al. 2010). Subgroups of absence patterns with either predominantly positive or negative BOLD signal changes in the dorsolateral prefrontal cortex seem to exist and might have phenotypic and genetic implications (Carney et al. 2012). Tenney et al. demonstrated that pretreatment ictal connectivity

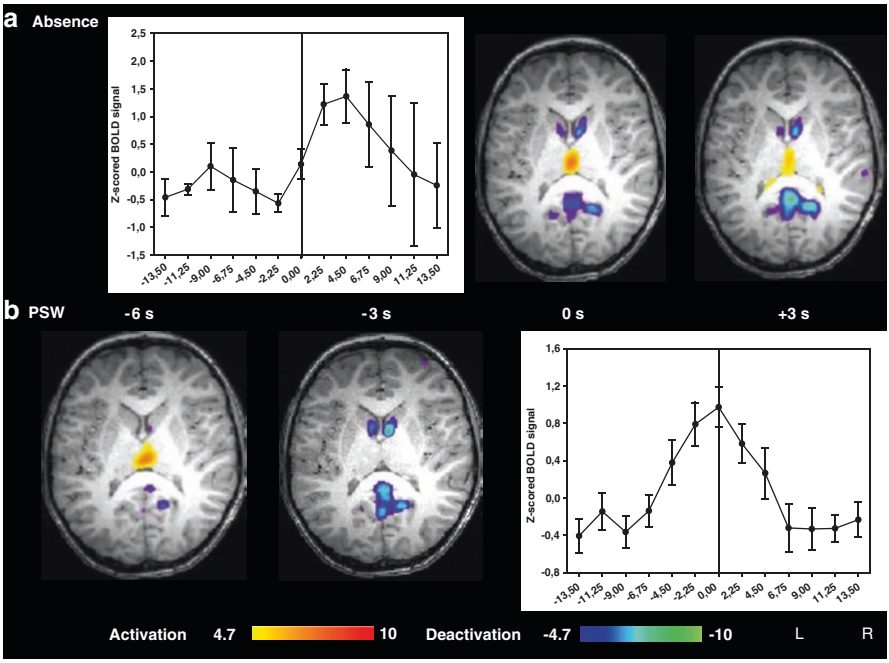

Fig. 19.4 Involvement of the typical neuronal network (thalamic activation and deactivation in precuneus, frontoparietal cortex and caudate nucleus) associated with generalized epileptiform discharges in a 8-year-old boy with juvenile absence epilepsy. This patient presented with both 3/s absence seizures and generalized irregular polyspike-wave paroxysms (PSW). The figure represents BOLD change patterns at 3 and 6 s prior to epileptiform discharges (−3 and −6), at the beginning of the discharge (0) and 3 s after the discharge (3). The diagram demonstrates the time course of the normalized BOLD signal extracted from the voxel in the thalamus with the maximal t-value (for a more detailed description, see Moeller et al., 2007). *X*-axis shows the time (s) around the beginning of a generalized paroxysm (point 0). Note that with 3/s spike-and-wave discharge, the changes of BOLD signal in the striato-thalamo-cortical network occurs at the beginning of the discharge. In contrast, this network already shows changes 6 s before PSW are seen in the surface EEG

differences in children with CAE are associated with response to antiepileptic treatment (Tenney et al. 2018).

But how are absences initiated and terminated? A sliding window analysis of human absences showed that areas of the DMN and the caudate nucleus were involved significantly earlier than the thalamus. Early patient-specific BOLD signal changes could mirror a cortical focus (Moeller et al. 2010a). In a dynamic group analysis of absence seizure, Bai and colleagues could show that BOLD signal changes in the medial frontal and orbitofrontal cortex preceded the onset of absence seizures up to 14 s whereas negative BOLD signal changes in default mode areas were seen up to 20 s after the end of absence seizures (Bai et al. 2010). It seems likely that human absence seizures start in prefrontal cortical areas and then secondarily involve thalamocortical synchronisation. This observation was supported by

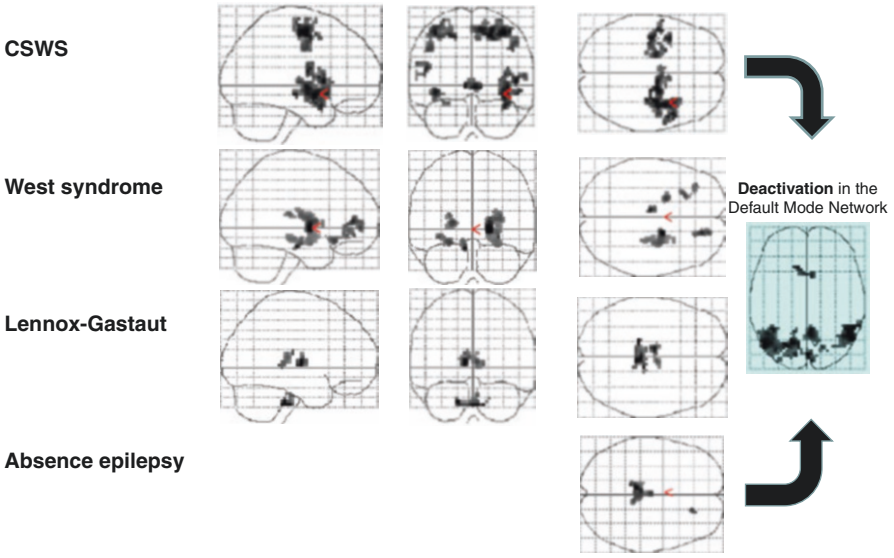

Fig. 19.5 Pattern (glass brain) of activation and deactivation (blue) in groups of epilepsy patients suffering from continuous spikes and waves during slow sleep (CSWS), West syndrome, Lennox-Gastaut syndrome and absence epilepsy. (From Moeller et al. 2008a; Siniatchkin et al. 2007b, 2010, 2011)

source analysis demonstrating two leading sources of activity during an absence seizure: a source in the frontal cortex and in the thalamus (Moeller et al. 2013a). Another study analysed the end of absence seizures (Benuzzi et al. 2015). The authors suggested that the termination of absence seizures is associated with a decrease in BOLD signal over the bilateral dorsolateral frontal cortex and a BOLD signal increase over the precuneus-posterior cingulate region bilaterally. These changes are opposite to the onset of absence seizures as described above.

There are inconsistent results regarding the question whether BOLD signal changes might occur prior to GSW: while BOLD signal changes preceding GSW have been reported in some adult patients with GSW, in children with polyspike wave paroxysms and a group of patients with absence seizures (Moeller et al. 2008b; Bai et al. 2010), no preceding BOLD signal changes have been detected in other studies (Moeller et al. 2008a, 2011). Early parietal BOLD responses prior to absences support the hypothesis that changes in activity within the default mode areas could facilitate the occurrence of GSW (Vaudano et al. 2009; Carney et al. 2010). Further studies are needed in order to investigate preceding haemodynamic changes before GSW seen on the scalp EEG in detail. Now, it can be suggested that the conflicting results may be attributed to differences in the analysis or different samples of patients.

Studying children with absence seizures, Bai et al. (2011) found an increased interhemispheric connectivity in the orbitofrontal cortex indicating increased synchronous activity between both hemispheres at rest. Increased connectivity was also

found in the network of basal ganglia when compared with healthy controls. This increased connectivity was even more pronounced during periods with GSW discharges (Luo et al. 2012). However, decreased functional connectivity was described for the thalamus (Masterton et al. 2012), the DMN (Luo et al. 2011) and the attention network (Killory et al. 2011) in children with absence seizures. These findings might explain impaired interictal attention in these children. Decreased connectivity in the DMN areas was negatively correlated with epilepsy duration (Luo et al. 2011). Furthermore, Yang and colleagues showed that this decreased connectivity within the default mode network, the cognitive control network and the attention network was more pronounced during interictal GSW (Yang et al. 2012). However, the studies on functional connectivity in patients with absence seizure are contradictory. For example, an interictal functional connectivity study in adult patients with different types of IGE did not show pathological connectivity in areas that are known to interact during GSW (Moeller et al. 2011).

EEG-fMRI studies with simultaneous testing during absences suggest that absences that are associated with a stronger cognitive impairment are associated with more widespread BOLD signal changes than absences with no or mild cognitive impairment (Berman et al. 2010). However, in a case report in a girl with long-lasting GSW paroxysms without concomitant cognitive impairment, the same networks were activated as in absences with clinical manifestation (Moeller et al. 2010b). More recently, it was shown that impaired consciousness in absence seizures seems to be related to the intensity of physiological changes in GSW associated networks of the brain. Increased EEG and fMRI amplitude at the onset of seizures are associated with behavioural impairment. These findings suggest that a vulnerable state may exist at the initiation of some seizures leading to greater physiological changes and altered consciousness (Guo et al. 2016).

It is of note that the same thalamocortical network is associated with primary and secondary GSW paroxysms, with ictal and interictal generalized discharges independent of age and antiepileptic medication. However, not all GSW seem to be associated with this network. Photoparoxysmal response (PPR) is an electroencephalographic trait characterized by the occurrence of epileptiform discharges in response to visual stimulation. An EEG-fMRI study in children with PPR showed an involvement of the parietal and frontal cortex but not the thalamus in most of the subjects during generalized PPR (Moeller et al. 2009a). It seems likely that PPR mainly a cortical phenomenon. However, in a patient in whom photic stimulation evoked a generalized tonic-clonic seizure, an excessive increase in BOLD signal in the visual cortex together with the involvement of the thalamus in the network was detected (Moeller et al. 2009b).

In summary, EEG-fMRI represents a valuable method to study pathogenetic mechanisms of ictal and interictal GSW. EEG-fMRI was able to describe a specific fingerprints of activation associated with GSW. Furthermore, the method could to investigate the temporal dynamics of paroxysms providing a deep insight into epileptogenesis in the IGE and also shed some light on the link between absences and impaired awareness.

19.3.4 Epileptic Encephalopathies

Epileptic encephalopathies (EE) refer to a group of severe epileptic disorders characterized by spontaneous, recurrent seizures that result in cognitive and behavioural disturbances. In most cases, EE represent challenging, difficult to treat conditions and are associated with unfavourable outcome. Despite of great impact of EE on the development, very little is known about pathogenetic mechanisms and, in particular, about neuronal networks underlying EE. One important feature of most EE is that different etiological factors (e.g. genetic background, lesions, malformations, neurometabolic abnormalities) result in a similar clinical expression (similar type of seizures, similar interictal abnormalities). This may indicate that different aetiologies, depending on the developmental stage, engage encephalopathy-specific pathogenetic pathways that constitute specific neuronal networks responsible for each particular EE. Based on this suggestion, different EEG-fMRI studies have tried to specify fingerprints of EE on the network level which would explain clinical similarity despite of etiological heterogeneity.

West syndrome is a prototype of severe epileptic encephalopathy of infancy consisting of tonic spasms, psychomotor developmental delay and the characteristic EEG pattern of hypsarrhythmia—a low structured mix of a multifocal spike and sharp wave activity and high voltage slow waves (Dulac 2001; Hrachovy and Frost 2003). Early PET studies have revealed a hypsarrhythmia underlying network which has included brain areas of focal cortical hypometabolism and subcortical hypermetabolism in putamen and brainstem (Chugani et al. 1992; Chiron et al. 1993; Metsähonkala et al. 2002). It was unclear, however, whether this network is associated with epileptiform discharges or high amplitude slow activity, as both pathological phenomena may be epileptogenic in West syndrome. In an EEG-fMRI study, Siniatchkin et al. (2007b) investigated infants with West syndrome and showed that the epileptiform discharges cause positive BOLD signal changes in the cerebral cortex (especially in the occipital areas), whereas the high-amplitude slow wave activity in hypsarrhythmia is commonly associated with BOLD signal changes in brainstem, putamen and thalamus (Figs. 19.5 and 19.6). There were no negative BOLD signal changes in relation to hypsarrhythmia, especially no deactivations in the DMN. Moreover, the activation pattern seems to be specific for West syndrome as it was not observed in infants with focal epilepsies. Interesting is that the subsequent source analysis which was performed in the same sample of subjects for high amplitude slow activity revealed similar electrical sources in the occipital cortex, putamen and brainstem as shown by fMRI and even described the functional hierarchy between the sources: activity in the brainstem seems to influence other sources and represent the key pathogenetic feature of West syndrome (Japaridze et al. 2013). The brainstem pathology is the best to explain both the clinical seizures which might result from intermittent interference of descending brainstem pathways controlling spinal reflex activity and characteristic EEG features of hypsarrhythmia which might be related to the activity in the ascending pathways from the same brainstem areas that project widely to the cerebral cortex (Frost and Hrachovy 2005).

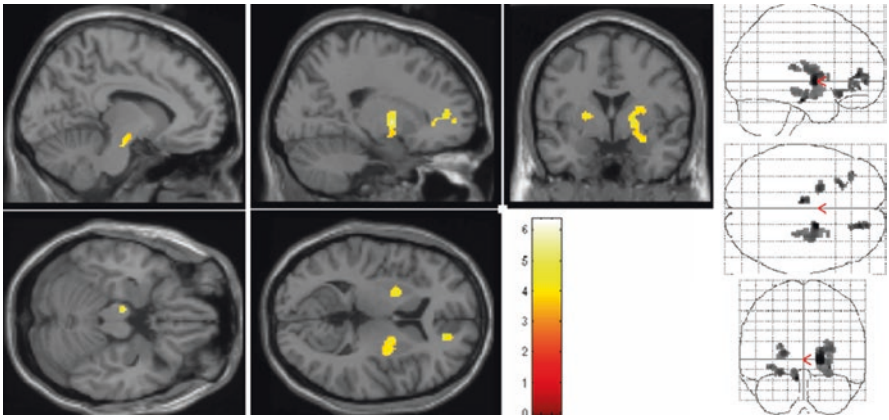

Fig. 19.6 Results of group analysis in children with West syndrome. (From Siniatchkin et al. 2007b with permission). High-voltage slow wave activity within the hypsarrhythmia was associated with BOLD signal increase in brain voxels representing putamen and brain stem

And it seems likely that the activity in the brainstem represents the common pathogenetic pathway in West and *Lennox-Gastaut syndrome* (LGS). West syndrome often evolves into LGS, an epileptic encephalopathy characterized by different types of seizures (tonic, tonic-clonic and atonic seizures as well as atypical absences), typical EEG changes (slow spike wave complexes ranging from 1 to 2.5/s, runs of rapid spikes and polyspikes) and accompanying developmental delay (Arzimanoglou et al. 2009). An EEG-fMRI study in children with both lesional and non-lesional cases of LGS revealed activation of brainstem and thalamus associated with epileptiform discharges (Siniatchkin et al. 2011; Fig. 19.5). Because the brainstem exerts control over the gating function of the thalamus through its influence on the reticular thalamic nucleus, activity in brainstem (reticular formation and raphe serotoninergic pathways) and thalamus may lead to diffuse changes of cortical excitability which predispose the neocortex to multifocal epileptic activity (Hrachovy and Frost 2003). Surprisingly, a recently published study described an increased functional connectivity between brain areas belonging to the DMN in children with multifocal epileptic activity including young patients with the LGS (Siniatchkin et al. 2018). This increased functional connectivity shows that the brain of LGS patients is prone for increased synchrony predisposing them to multifocal epileptic activity. Additionally, the study of Siniatchkin et al. (2011) demonstrated that especially the centromedian and anterior part of the thalamus constitute the LGs specific network. A significant role of thalamocortical pathways in LGS was demonstrated previously: centromedian thalamic nucleus stimulation in patients with refractory LGS have been an effective treatment strategy (Velasco et al. 2006). The anterior thalamus has been frequently and successfully used as a target for deep brain stimulation in patients with multifocal and secondary generalized epileptic activity (Samadani and Baltuch 2007). Increased connectivity of specific thalamocortical circuits could potentially be a target for thalamic deep brain stimulation

(Warren et al. 2017). However, while brainstem and thalamus seems to be a key players in LGS, Warren et al. could demonstrate that generalised paroxysmal fast activity is most likely driven by the prefrontal cortex, with propagation occurring first to the brainstem and then from brainstem to thalamus (Warren et al. 2019). These therapeutic options underline the significance of the thalamus in the pathogenesis of LGS and multifocal IEDs.

When analysing different EEG patterns, Pillay and colleagues demonstrated that paroxysmal fast activity is associated with coactivation of the default mode and attention network as well as subcortical structures (brainstem, thalamus and basal ganglia). By comparison, the slow spike wave complexes showed predominantly deactivations in cortical and subcortical areas which often show a non-canonical hemodynamic response (Pillay et al. 2013; Archer et al. 2014). Functional connectivity studies demonstrate abnormal cognitive network interactions which the author proposed to lead to epileptic encephalopathy (Warren et al. 2016).

Epileptic encephalopathy with *continuous spikes and waves during slow sleep (CSWS)* is an age-related disorder characterized by acquired variable neuropsychological impairment, epilepsy with heterogeneous seizure types and the presence of the interictal electroencephalographic (EEG) findings of intense subcontinuous spike wave complexes that usually occupy more than 85% of non-REM sleep (Tassinari et al. 2005). CSWS can be attributed to different aetiologies (symptomatic cases with various structural brain lesions and MRI-negative cases with probable genetic background, for example, in the form of Landau-Kleffner syndrome LKS or atypical benign partial epilepsy of childhood) and in the majority of cases is associated with manifold acquired psychomotor and cognitive deficits and even regressions. The first EEG-fMRI study on CSWS was published by De Tiege et al. (2007a, b). The authors investigated a 9-year-old girl suffering from partial seizures and who developed CSWS and neuropsychological deficits. Epileptiform activity was associated with focal activations in the right superior frontal, postcentral and superior temporal cortex as well as deactivations in the lateral and medial frontoparietal cortices, posterior cingulate gyrus and cerebellum. In concordance with this study, Siniatchkin et al. (2010) investigated 12 children with CSWS of different aetiologies using simultaneous recordings of EEG and fMRI. The study revealed a typical network of brain activation in patients: positive BOLD signal changes involved bilateral perisylvian regions (well corresponding with PET and MEG/EEG studies), cingulate gyrus as well as bilateral frontal and parietal cortex and thalamus (Fig. 19.5). Electrical source analysis demonstrated a similar involvement of the perisylvian brain regions, independent of aetiology and area of spike generation. Moreover, source reconstruction provided evidence that the typical pattern of brain activation is more likely to be related to a specific pattern of propagation of epileptic activity during CSWS. Negative BOLD signal changes were found in precuneus, lateral parietal cortex and medial frontal cortex. These structures are usually involved in a pattern of deactivation that occurs during the initiation of task-related activity and represent the DMN which is active in the resting brain with a high degree of functional connectivity (Raichle et al. 2001). The authors hypothesized that one of the possible mechanisms how epileptic activity in patients with CSWS

causes cognitive deficits, is interruption of the activity and connectivity within the DMN. Note that areas of hypometabolism revealed by PET studies resemble those of deactivation in EEG-fMRI studies representing remote inhibition of the default mode network (Ligot et al. 2014). It is an elegant hypothesis explaining cognitive deficits by inhibition/deactivation in the DMN. However, this hypothesis still has to be proven by correlating neuropsychological and neuroimaging data.

The *Dravet syndrome* or severe myoclonic epilepsy of infancy (SMEI) is an intractable epileptic encephalopathy of early childhood which is caused by a mutation in the *SCN1A* gene in 80% of patients. In an EEG-fMRI study, 10 carriers of mutations in the *SCN1A* gene were investigated (Moehring et al. 2013). However, despite the common aetiology, the study revealed different individual neuronal networks underlying interictal epileptiform discharges. The only common feature of brain activation consisted of positive BOLD signal changes in the DMN areas found seven patients. But even these activations were inconsistent and were note detected in the group analysis. Although the attempt to describe a common syndrome-specific network for SMEI patients was not successful, the results correspond with other neuroimaging studies which have demonstrated pathogenetic heterogeneity in SMEI patients (Ferrie et al. 1997; Korinthenberg et al. 2004).

Myoclonic astatic epilepsy (MAE) of early childhood, first described by Doose and colleagues, is a difficult to treat generalized electroclinical syndrome characterized by age of onset mostly between 2 and 6 years, myoclonic, astatic, drop attacks, generalized tonic-clonic seizure and short absences. Simultaneous EEG-fMRI recordings were performed in 13 children with MAE (Moeller et al. 2014). Activation was detected in the thalamus (all patients), premotor cortex (6 patients) and putamen (6 patients). Deactivation was found in the default mode network areas (7 patients). The group analysis confirmed activations in the thalamus, premotor cortex, putamen and cerebellum and deactivations in the DMN. In addition to the thalamocortical network which is commonly found in idiopathic generalized epilepsies, GSW in MAE patients are characterized by BOLD signal changes in brain structures associated with motor function. The involvement of these structures might predispose to the typical seizure semiology of myoclonic jerks observed in MAE.

19.4 Summary and Future Perspectives

EEG-fMRI in paediatric epilepsies is a promising tool for the investigation of neuronal networks involved in the generation of interictal epileptiform discharges absence seizures. This technique is successfully applied in awake, sleeping or sedated children with focal and generalised epilepsies and in all age groups. It is of note that similar results were obtained in subjects with focal epilepsies and primary as well as secondary generalized epilepsies both during wakefulness and sleep, in medicated and non-medicated children and with or without sedation, albeit in small groups up to now. Several studies in the paediatric epilepsy population have demonstrated the capability of EEG-fMRI to provide new information on the neuronal networks involved in different types of epileptiform activity.

The combination of EEG and fMRI should help to study brain function in a variety of epileptic syndromes, providing more insight into state of the brain during epileptic activity. Finally, the clinical value of EEG-fMRI has to be validated. EEG-fMRI maps must be compared with data from established investigations including intracranial EEG recordings, other methods of functional neuroimaging (PET, SPECT), and EEG source analysis. A major problem is to determine whether BOLD signal changes represent areas of the initial epileptic activity or areas of propagation. Ultimately, informative results will come from comparisons with epilepsy surgery outcome studies.

References

Aghakhani Y, Bagshaw AP, Benar CG, Hawco C, Andermann F, Dubeau F, Gotman J (2004) fMRI activation during spike and wave discharges in idiopathic generalized epilepsy. Brain 127:1127–1144

Al-Asmi A, Benar CG, Gross DW, Aghakhani Y, Andermann F, Pike B, Dubeau F, Gotman J (2003) fMRI activation in continuous and spike-triggered EEG-fMRI studies of epileptic spikes. Epilepsia 44:1328–1339

Altman NR, Bernal B (2001) Brain activation in sedated children: auditory and visual functional MR imaging. Radiology 221:56–63

Archer JS, Briellman RS, Abbott DF, Syngeniotis A, Wellard RM, Jackson GD (2003) Benign epilepsy with centro-temporal spikes: spike triggered fMRI shows somato-sensory cortex activity. Epilepsia 44:200–204

Archer JS, Warren AE, Stagnitti MR, Masterton RA, Abbott DF, Jackson GD (2014) Lennox-Gastaut syndrome and phenotype: secondary network epilepsies. Epilepsia 55(8):1245–54

Arzimanoglou A, French J, Blume WT, Cross JH, Ernst JP, Feucht M, Genton P, Guerrini R, Kluger G, Pellock JM, Perucca E, Wheless JW (2009) Lennox-gastaut syndrome: a consensus approach on diagnosis, assessment, management, and trial methodology. Lancet Neurol 8:82–93

Bai X, Vestal M, Berman R, Negishi M, Spann M, Vega C, Desalvo M, Novotny EJ, Constable RT, Blumenfeld H (2010) Dynamic time course of typical childhood absence seizures: EEG, behavior, and functional magnetic resonance imaging. J Neurosci 30(17):5884–93.

Bai X, Guo J, Killory B, Vestal M, Berman R, Negishi M, Danielson N, Novotny EJ, Constable RT, Blumenfeld H (2011) Resting functional connectivity between the hemispheres in childhood absence epilepsy. Neurology 76:1960–1967

Bednarz HM, Kana RK (2018) Advances, challenges, and promises in pediatric neuroimaging of neurodevelopmental disorders. Neurosci Biobehav Rev 90:50–69

Bell EC, Willson MC, Wilman AH, Dave S, Silverstone PH (2005) Differential effects of chronic lithium and valproate on brain activation in healthy volunteers. Hum Psychopharmacol 20:415–424

Ben-Ari Y (2006) Basic developmental rules and their implication for epilepsy in the immature brain. Epileptic Disord 8:91–102

Benuzzi F, Ballotta D, Mirandola L, Ruggieri A, Vaudano AE, Zucchelli M, Ferrari E, Nichelli PF, Meletti S (2015) An EEG-fMRI study on the termination of generalized spike-and-wave discharges in absence epilepsy. PLoS One 10(7):e0130943

Berman R, Negishi M, Vestal M, Spann M, Chung MH, Bai X, Purcaro M, Motelow JE, Danielson N, Dix-Cooper L, Enev M, Novotny EJ, Constable RT, Blumenfeld H (2010) Simultaneous EEG, fMRI, and behavior in typical childhood absence seizures. Epilepsia 51:2011–2022

Boly M, Phillips C, Tshibanda L, Vanhaudenhuyse A, Schabus M, Dang-Vu TT, Moonen G, Hustinx R, Maquet P, Laureys S (2008) Intrinsic brain activity in altered states of consciousness: how conscious is the default mode of brain function? Ann N Y Acad Sci 1129:119–129

Boor S, Vucurevic G, Pfleiderer C, Stoeter P, Kutschke G, Boor R (2003) EEG-related functional MRI in benign childhood epilepsy with centrotemporal spikes. Epilepsia 44:688–692

Boor R, Jacobs J, Bauermann T, Scherg M, Boor S, Vucurevic G, Kutschke G, Stoeter P (2007) Combined spike-related functional MRI and multiple source analysis in the non-invasive spike localization of benign rolandic epilepsy. Clin Neurophysiol 118(4):901–909

Born P, Leth H, Miranda MJ, Rostrup E, Stensqaard A, Peitersen B, Larsson HB, Lou HC (1998) Visual activation in infants and young children studied by functional magnetic resonance imaging. Pediatr Res 44:578–583

Broyd SJ, Demanuele C, Debener S, Helps SK, James CJ, Sonuga-Barke EJ (2009) Default-mode brain dysfunction in mental disorders: a systematic review. Neurosci Biobehav Rev 33:279–296

Carney PW, Masterton RA, Harvey AS, Scheffer IE, Berkovic SF, Jackson GD (2010) The core network in absence epilepsy. Differences in cortical and thalamic BOLD response. Neurology 75:904–911

Carney PW, Masterton RA, Flanagan D, Berkovic SF, Jackson GD (2012) The frontal lobe in absence epilepsy: EEG-fMRI findings. Neurology 78:1157–1165

Centeno M, Tierney TM, Perani S, Shamshiri EA, StPier K, Wilkinson C, Konn D, Banks T, Vulliemoz S, Lemieux L, Pressler RM, Clark CA, Cross JH, Carmichael DW (2016) Optimising EEG-fMRI for localisation of focal epilepsy in children. PLoS One 11(2):e0149048

Centeno M, Tierney TM, Perani S, Shamshiri EA, Pier KS, Wilkinson C, Konn D, Vulliemoz S, Grouiller F, Lemieux L, Pressler RM, Clark CA, Cross JH, Carmichael DW (2017) Combined electroencephalography-functional magnetic resonance imaging and electrical source imaging improves localization of pediatric focal epilepsy. Ann Neurol 82:278–287

Chiron C, Dulac O, Bulteau C, Nuttin C, Depas G, Raynaud C, Syrota A (1993) Study of regional cerebral blood flow in west syndrome. Epilepsia 34:707–715

Chugani HT, Shewmon DA, Sankar R (1992) Infantile spasms: II. Lenticular nuclei and brain stem activation on positron emission tomography. Ann Neurol 31:212–219

Chugani DC, Chugani HT, Muzik O, Shah JR, Shah AK, Canady A, Mangner TJ, Chakraborty PK (1998) Imaging epileptogenic tubers in children with tuberous sclerosis complex using alpha-[11C]methyl-L-tryptophan positron emission tomography. Ann Neurol 44:858–866

Coan AC, Chaudhary UJ, Grouiller F, Campos BM, De Ciantis A, Vulliemoz S, Diehl B, Beltramini GC, Carmichael DW, Thornton RC, Covolan RJ, Cendes F, Lemieux L (2016) EEG-fMRI in the presurgical evaluation of temporal lobe epilepsy. J Neurol Neurosurg Psychiatry 87:642–649

Dalla Bernardina B, Sgro V, Fejerman N (2005) Epilepsy with centro-temporal spikes and related syndromes. In: Roger J, Bureau M, Dravet C, Genton P, Tassinari CA, Wolf P (eds) Epileptic syndromes in infancy, childhood and adolescence. John Libbey Eurotext, Montrouge, pp 203–226

De Tiege X, Harrison S, Laufs H, Boyd SG, Clark CA, Allen P, Neville BG, Vargha-Khadem F, Cross JH (2007a) Impact of interictal epileptic activity on normal brain function in epileptic encephalopathy: an electroencephalography—functional magnetic resonance imaging study. Epilepsy Behav 11:460–465

De Tiege X, Laufs H, Boyd SG, Harkness W, Allen PJ, Clark CA, Connelly A, Cross JH (2007b) EEG-fMRI in children with pharmacoresistant focal epilepsy. Epilepsia 48:385–389

Dulac O (2001) What is west syndrome? Brain Dev 23:447–452

Elshoff L, Groening K, Grouiller F, Wiegand G, Wolff S, Michel C, Stephani U, Siniatchkin M (2012) The value of EEG-fMRI and EEG source analysis in the presurgical setup of children with refractory focal epilepsy. Epilepsia 53:1597–1606

Ferrie CD, Mardsen PK, Maisey MN, Robinson RO (1997) Cortical and subcortical glucose metabolism in childhood epileptic encephalopathies. J Neurol Neurosurg Psychiatry 63:181–187

Frost JD Jr, Hrachovy RA (2005) Pathogenesis of infantile spasms: a model based on developmental desynchronization. J Clin Neurophysiol 22(1):25–36

Gaillard WD, Grandin CB, Xu B (2001) Developmental aspects of pediatric fMRI: considerations for image acquisition, analysis, and interpretation. Neuroimage 13:239–249

Gotman J, Grova C, Bagshaw A, Kobayashi E, Aghakhani Y, Dubeau F (2005) Generalized epileptic discharges show thalamocortical activation and suspension of the default state of the brain. Proc Natl Acad Sci U S A 102:15236–15240

Groening K, Brodbeck V, Moeller F, Wolff S, van Baalen A, Michel CM, Jansen O, Boor R, Wiegand G, Stephani U, Siniatchkin M (2009) Combination of EEG-fMRI and EEG source analysis improves interpretation of spike-associated activation networks in paediatric pharmacoresistant focal epilepsies. Neuroimage 46:827–833

Grouiller F, Thornton RC, Groening K, Spinelli L, Duncan JS, Schaller K, Siniatchkin M, Lemieux L, Seeck M, Michel CM, Vulliemoz S (2011) With or without spikes: localization of focal epileptic activity by simultaneous electroencephalography and functional magnetic resonance imaging. Brain 134:2867–2886

Guo JN, Kim R, Chen Y, Negishi M, Jhun S, Weiss S, Ryu JH, Bai X, Xiao W, Feeney E, Rodriguez-Fernandez J, Mistry H, Crunelli V, Crowley MJ, Mayes LC, Constable RT, Blumenfeld H (2016) Impaired consciousness in patients with absence seizures investigated by functional MRI, EEG, and behavioural measures: a cross-sectional study. Lancet Neurol 1:1336–1345

Hamandi K, Salek-Haddadi A, Laufs H, Liston A, Friston K, Fish DR, Duncan JS, Lemieux L (2006) EEG-fMRI of idiopathic and secondary generalized epilepsies. Neuroimage 31:1700–1710

Holmes GL (1997) Epilepsy in the developing brain: lessons from the laboratory and clinic. Epilepsia 38:12–30

Hrachovy RA, Frost JD (2003) Infantile epileptic encephalopathy with hypsarrhythmia (infantile spasms/ west syndrome). J Clin Neurophysiol 20:408–425

Jacobs J, Kobayashi E, Boor R, Muhle H, Wolff S, Hawco C, Dubeau F, Jansen O, Stephani U, Gotman J, Siniatchkin M (2007) Hemodynamic responses to interictal epileptiform discharges in children with symptomatic epilepsy. Epilepsia 48:2068–2078

Jacobs J, Hawco C, Kobayashi E, Boor R, LeVan P, Stephani U, Siniatchkin M, Gotman J (2008a) Variability of the hemodynamic response function with age in children with epilepsy. Neuroimage 40:601–614

Jacobs J, Rohr A, Moeller F, Boor R, Kobayashi E, Stephani U, Gotman J, Siniatchkin M (2008b) Evaluation of epileptogenic networks in children with tuberous sclerosis complex using EEG-fMRI. Epilepsia 49:816–825

Jacobs J, Stich J, Zahneisen B, Assländer J, Ramantani G, Schulze-Bonhage A, Korinthenberg R, Henning J, LeVan P (2014) Fast fMRI provides high statistical power in the analysis of epileptic networks. Neuroimage 88:282–294

Japaridze N, Muthuraman M, Moeller F, Boor R, Anwar AR, Deuschl G, Stephani U, Raethjen J, Siniatchkin M (2013) Neuronal networks in west syndrome as revealed by source analysis and renormalized partial directed coherence. Brain Topogr 26(1):157–170

Killory BD, Bai X, Negishi M, Vega C, Spann MN, Vestal M, Guo J, Berman R, Danielson N, Trejo J, Shisler D, Novotny EJ Jr, Constable RT, Blumenfeld H (2011) Impaired attention and network connectivity in childhood absence epilepsy. Neuroimage 56:2209–2217

Kobayashi E, Bagshaw AP, Jansen A, Andermann F, Andermann E, Gotman J, Dubeau F (2005) Intrinsic epileptogenicity in polymicrogyric cortex suggested by EEG-fMRI BOLD responses. Neurology 12:1263–1266

Kobayashi E, Bagshaw AP, Grova C, Gotman J, Dubeau F (2006a) Grey matter heterotopia: what EEG-fMRI can tell us about epileptogenicity of neuronal migration disorders. Brain 129:366–374

Kobayashi E, Bagshaw AP, Benar CG, Aghakhani Y, Andermann F, Dubeau F, Gotman J (2006b) Temporal and extratemporal BOLD responses to temporal lobe interictal spikes. Epilepsia 47:343–354

Kobayashi E, Bagshaw AP, Gotman J, Dubeau F (2007) Metabolic correlates of epileptic spikes in cerebral cavernous angiomas. Epilepsy Res 73:98–103

Korinthenberg R, Bauer-Scheid C, Burkart P, Martens-Le Bouar H, Kassubek J, Juengling FD (2004) 18FDG-PET in epilepsies of infantile onset with pharmacoresistant generalized tonic-clonic seizures. Epilepsy Res 60:53–61

Kowalczyk MA, Omidvarnia A, Dhollander T, Jackson GD (2020) Dynamic analysis of fMRI activation during epileptic spikes can help identify the seizure origin. Epilepsia 61:2558. https://doi.org/10.1111/epi.16695

Labate A, Briellmann RS, Abbott DF, Waites AB, Jackson GD (2005) Typical childhood absence seizures are associated with thalamic activation. Epileptic Disord 7:373–377

Laufs H, Hamandi K, Salek-Haddadi A, Kleinschmidt AK, Duncan JS, Lemieux L (2007) Temporal lobe interictal epileptic discharges affect cerebral activity in "default mode" brain regions. Hum Brain Mapp 28:1023–1032

Leal A, Dias A, Vieira JP, Secca M, Jordao C (2006) The BOLD effect of interictal spike activity in childhood occipital lobe epilepsy. Epilepsy 47:1536–1542

Leal A, Nunes S, Martins A, Secca M, Jordao C (2007) Brain mapping of epileptic activity in a case of idiopathic occipital lobe epilepsy (Panayiotopoulos syndrome). Epilepsia 48:1179–1183

Lengler U, Kafadar I, Neubauer BA, Krakow K (2007) fMRI correlates of interictal epileptic activity in patients with idiopathic benign focal epilepsy of childhood. A simultaneous EEG-functional MRI study. Epilepsy Res 75:29–38

Li R, Ji GJ, Yu Y, Ding MP, Tang YL, Chen H, Liao W (2017) Epileptic discharge related functional connectivity within and between networks in benign epilepsy with centrotemporal spikes. Int J Neural Syst 27:1750018

Li R, Wang L, Chen H, Guo X, Liao W, Tang YL, Chen H (2019) Abnormal dynamics of functional connectivity density in children with benign epilepsy with centrotemporal spikes. Brain Imaging Behav 13:985–994

Ligot N, Archambaud F, Trotta N, Goldman S, Van Bogaert P, Chiron C, De Tiege X (2014) Default mode network hypometabolism in epileptic encephalopathies with CSWS. Epilepsy Res 108:861–871

Luo C, Li Q, Lai Y, Xia Y, Qin Y, Liao W, Li S, Zhou D, Yao D, Gong Q (2011) Altered functional connectivity in default mode network in absence epilepsy: a resting-state fMRI study. Hum Brain Mapp 32:438–449

Luo C, Li Q, Xia Y, Lei X, Xue K, Yao Z, Lai Y, Martínez-Montes E, Liao W, Zhou D, Valdes-Sosa PA, Gong Q, Yao D (2012) Resting state basal ganglia network in idiopathic generalized epilepsy. Hum Brain Mapp 33:1279–1294

Maloney TC, Tenney JR, Szaflarski JP, Vannest J (2015) Simultaneous electroencephalography and functional magnetic resonance imaging and the identification of epileptic networks in children. J Pediatr Epilepsy 4:174–183

Martin E, Joeri P, Loenneker T, Ekatodramis D, Vitacco D, Henning J, Marcar VL (1999) Visual processing in infants and children studied using functional MRI. Pediatr Res 46:135–140

Masterton RA, Harvey AS, Archer JS, Lillywhite LM, Abbott DF, Scheffer IE, Jackson GD (2010) Focal epileptiform spikes do not show a canonical BOLD response in patients with benign rolandic epilepsy (BECTS). Neuroimage 51:252–260

Masterton RA, Carney PW, Jackson GD (2012) Cortical and thalamic resting-state functional connectivity is altered in childhood absence epilepsy. Epilepsy Res 99:327–334

Masterton RA, Jackson GD, Abbott DF (2013) Mapping brain activity using event-related independent component analysis (eICA): specific advantages for EEG-fMRI. Neuroimage 70:164–174

Meek JH, Firbank M, Elwell CE, Atkinson J, Braddick O, Wyatt JS (1998) Regional hemodynamic responses to visual stimulation in awake infants. Pediatr Res 43:840–843

Metsähonkala L, Gaily E, Rantala H, Salmi E, Valanne L, Aarimaa T, Liukkonen E, Holopainen I, Granström ML, Erkinjuntti M, Grönroos T, Sillanpaa M (2002) Focal and global cortical hypometabolism in patients with newly diagnosed infantile spasms. Neurology 58:1646–1651

Moehring J, Moeller F, Jacobs J, Siebner H, Wolff S, Jansen O, Stephani U, Siniatchkin M (2008) The influence of sleep on BOLD response in children with epilepsy. Neurosci Lett 443:61–66

Moehring J, von Spiczak S, Moeller F, Helbig I, Wolff S, Jansen O, Muhle H, Boor R, Stephani U, Siniatchkin M (2013) Variability of EEG-fMRI findings in patients with SCN1A-positive dravet syndrome. Epilepsia 54(5):918–926

Moeller F, Siebner H, Wolff S, Muhle H, Boor R, Granert O, Jansen O, Stephani U, Siniatchkin M (2008a) EEG-fMRI in children with untreated childhood absence epilepsy. Epilepsia 49:1510–1519

Moeller F, Siebner H, Wolff S, Muhle H, Boor R, Granert O, Jansen O, Stephani U, Siniatchkin M (2008b) Changes in activity of striato-thalamo-cortical network precede generalized spike wave discharges. Neuroimage 39:1839–1849

Moeller F, Siebner HR, Ahlgrimm N, Wolff S, Muhle H, Granert O, Boor R, Jansen O, Gotman J, Stephani U, Siniatchkin M (2009a) fMRI activation during spike and wave discharges evoked by photic stimulation. Neuroimage 48:682–695

Moeller F, Siebner HR, Wolff S, Muhle H, Granert O, Jansen O, Stephani U, Siniatchkin M (2009b) Mapping brain activity on the verge of a photically induced generalized tonic-clonic seizure. Epilepsia 50:1632–1637

Moeller F, Levan P, Muhle H, Stephani U, Dubeau F, Siniatchkin M, Gotman J (2010a) Absence seizures: individual patterns revealed by EEG-fMRI. Epilepsia 51:2000–2010

Moeller F, Muhle H, Wiegand G, Wolff S, Stephani U, Siniatchkin M (2010b) EEG-fMRI study of generalized spike and wave discharges without transitory cognitive impairment. Epilepsy Behav 18(3):313–316

Moeller F, Levan P, Gotman J (2011) Independent component analysis (ICA) of generalized spike wave discharges in fMRI: comparison with general linear model-based EEG-fMRI. Hum Brain Mapp 2:209–217

Moeller F, Stephani U, Siniatchkin M (2013a) Simultaneous EEG and fMRI recordings (EEG-fMRI) in children with epilepsy. Epilepsia 54(6):971–982

Moeller F, Groening K, Moehring J, Muhle H, Wolff S, Jansen O, Stephani U, Siniatchkin M (2014) EEG-fMRI in myoclonic astatic epilepsy (Doose syndrome). Neurology 82(17):1508–1513

Morita T, Kochiyama T, Yamada H, Konishi Y, Yonekura Y, Matsumura M, Sadato N (2000) Difference in the metabolic response to photic stimulation of the lateral geniculate nucleus and the primary visual cortex of infants: a fMRI study. Neurosci Res 38:63–70

Pillay N, Archer JS, Badawy RA, Flanagan DF, Berkovic SF, Jackson G (2013) Networks underlying paroxysmal fast activity and slow spike and wave in Lennox-Gastaut syndrome. Neurology 81(7):665–673

Poldrack RA, Pare-Blagoev EJ, Grant PE (2002) Pediatric functional magnetic resonance imaging: progress and challenges. Top Magn Reson Imaging 13:61–70

Quirk ME, Letendre AJ, Ciottone RA, Langley JF (1989) Evaluation of three psychologic interventions to reduce anxiety during MR imaging. Radiology 173:759–762

Raichle ME, MacLeod AM, Snyder AZ, Powers WJ, Gusnard DA, Shulman GL (2001) A default mode of brain function. PNAS 98(2):676–82

Raichle ME, Mintun MA (2006) Brain work and brain imaging. Annu Rev Neurosci 29:449–476

Roger J, Bureau M, Dravet C, Genton P, Tassinari CA, Wolf P (2005) Epileptic syndromes in infancy, childhood and adolescence. John Libbey Eurotext Ltd, Montrouge

Rosenberg DR, Sweeney JA, Gillen JS (1997) Magnetic resonance imaging of children without sedation: preparation with simulation. J Am Acad Child Adolesc Psychiatry 36:853–859

Salek-Haddadi A, Diehl B, Hamandi K, Merschhemke M, Liston A, Friston K, Duncan JS, Fish DR, Lemieux L (2006) Hemodynamic correlates of epileptiform discharges: an EEG-fMRI study of 63 patients with focal epilepsy. Brain Res 1088:148–166

Samadani U, Baltuch GH (2007) Anterior thalamic nucleus stimulation for epilepsy. Acta Neurochir Suppl 97(pt2):343–346

Schapiro MB, Schmithorst VJ, Wilke M, Byars AW, Strawsburg RH, Holland SK (2004) BOLD fMRI signal increases with age in selected brain regions in children. Neuroreport 15:2575–2578

Sebastiano DR, Tassi L, Duran D, Visani E, Gozzo F, Cardinale F, Nobili L, Del Sole A, Rubino A, Dotta S, Schiaffi E, Garbelli R, Franceschetti S, Spreafico R, Panzica F (2020) Identifying the epileptogenic zone by four non-invasive imaging technique versus stereo-EEG in MRI-negative pre-surgery epilepsy patients. Clin Neurophysiol 131:1815–1823

Siniatchkin M, Moeller F, Jacobs J, Stephani U, Boor R, Wolff S, Jansen O, Siebner H, Scherg M (2007a) Spatial filters and automated spike detection based on brain topographies improve sensitivity of EEG-fMRI studies in focal epilepsy. Neuroimage 37:834–843

Siniatchkin M, van Baalen A, Jacobs J, Moeller F, Moehring J, Boor R, Wolff S, Jansen O, Stephani U (2007b) Different neuronal networks are associated with spikes and slow activity in Hypsarrhythmia. Epilepsia 48:2312–2321

Siniatchkin M, Groening K, Moehring J, Moeller F, Boor R, Brodbeck V, Michel CM, Rodionov R, Lemieux L, Stephani U (2010) Neuronal networks in children with continuous spikes and waves during slow sleep. Brain 133:2798–2813

Siniatchkin M, Coropceanu D, Moeller F, Boor R, Stephani U (2011) EEG-fMRI reveals activation of brainstem and thalamus in patients with Lennox-Gastaut syndrome. Epilepsia 52(4):766–774

Siniatchkin M, Moehring J, Kroeher B, Galka A, von Ondarza G, Moeller F, Wolff S, Tagliazucchi E, Steinmann E, Boor R, Stephani U (2018) Multifocal epilepsy in children is associated with increased long-distance functional connectivity: an explorative EEG-fMRI study. Eur J Paediatr Neurol 22(6):1054–1065

Tassinari CA, Rubboli G, Volpi L, Billard C, Bureau M (2005) Electrical status epilepticus during slow sleep (ESES or CSWS) including acquired epileptic aphasia (Landau-Kleffner syndrome). In: Rodger J, Bureau M, Dravet C, Genton P, Tassinari CA, Wolf P (eds) Epileptic syndromes in infancy, childhood and adolescence, 4th edn. John Libbey Eurotext, Montrouge, pp 295–314

Tenney JR, Kadis DS, Agler W, Rozhkov L, Altaye M, Xiang J, Vannest J, Glauser TA (2018) Ictal connectivity in childhood absence epilepsy: Associations with outcome. Epilepsia 59(5):971–981

Thornton R, Laufs H, Rodionov R, Cannadathu S, Carmichael DW, Vulliemoz S, Salek-Haddadi A, McEvoy AW, Smith SM, Lhatoo S, Elwes RD, Guye M, Walker MC, Lemieux L, Duncan JS (2010) EEG correlated functional MRI and postoperative outcome in focal epilepsy. J Neurol Neurosurg Psychiatry 81:922–927

Thornton R, Vulliemoz S, Rodionov R, Carmichael DW, Chaudhary UJ, Diehl B, Laufs H, Vollmar C, McEvoy AW, Walker MC, Bartolomei F, Guye M, Chauvel P, Duncan JS, Lemieux L (2011) Epileptic networks in focal cortical dysplasia revealed using electroencephalography-functional magnetic resonance imaging. Ann Neurol 70:822–837

Vaudano AE, Laufs H, Kiebel SJ, Carmichael DW, Hamandi K, Guye M, Thornton R, Rodionov R, Friston KJ, Duncan JS, Lemieux L (2009) Causal hierarchy within the thalamo-cortical network in spike and wave discharges. PLoS One 4:e6475

Velasco AL, Velasco F, Jimenez F, Velasco M, Castro G, Carrillo-Ruiz JD, Fanghänel G, Boleaga B (2006) Neuromodulation of the centromedian thalamic nuclei in the treatment of generalized seizures and the improvement of the quality of life in patients with Lennox-Gastaut syndrome. Epilepsia 47(7):1203–1212

Warren AE, Abbott DF, Vaughan DN, Jackson GD, Archer JS (2016) Abnormal cognitive network interactions in Lennox-Gastaut syndrome: a potential mechanism of epileptic encephalopathy. Epilepsia 57(5):812–822

Warren AEL, Abbott DF, Jackson GD, Archer JS (2017) Thalamocortical functional connectivity in Lennox-Gastaut syndrome is abnormally enhanced in executive-control and default-mode networks. Epilepsia 58(12):2085–2097

Warren AEL, Harvey AS, Vogrin SJ, Bailey C, Davidson A, Jackson GD, Abbott DF, Archer JS (2019) The epileptic network of Lennox-Gastaut syndrome: cortically driven and reproducible across age. Neurology 93(3):e215–e226

Xiao F, An D, Lei L, Chen S, Wu X, Yang T, Ren J, Gong Q, Zhou D (2016) Real-time effects of centrotemporal spikes on cognition in rolandic epilepsy: an EEG-fMRI study. Neurology 86:544–551

Yang T, Luo C, Li Q, Guo Z, Liu L, Gong Q, Yao D, Zhou D (2012) Altered resting-state connectivity during interictal generalized spike-wave discharges in drug-naïve childhood absence epilepsy. Hum Brain Mapp 33:2081

Zhang Q, Xang F, Hu Z, Xu Q, Bernhardt BC, Quan W, Li Q, Zhang Z, Lu G (2018) Antiepileptic drug of levetiracetam decreases centrotemporal spike-associated activation in rolandic epilepsy. Front Neurosci 12:796

Zijlmans M, Huiskamp G, Hersevoort M, Seppenwoolde JH, van Huffelen AC, Leijten FSS (2007) EEG-fMRI in the preoperative work-up for epilepsy surgery. Brain 130:2343–2353

EEG-fMRI in Psychiatry

20

Gebhard Sammer and Christoph Mulert

20.1 Introduction

Our understanding of the brain and brain disorders is substantially related to the methods that are available for investigating the brain and both fMRI and EEG have substantially contributed and continue to contribute to current concepts of normal and disturbed brain function. Accordingly, an important question is which current issues or specific research questions in psychiatry can be better addressed and really benefit from using simultaneous EEG-fMRI in comparison to using these methods alone or in separate. What reasons justify the additional effort for the implementation of safe recordings, the achievement of high-quality EEG and fMRI data and the additional effort for the solution of specific artefact problems and analysis problems? Research approaches that justify simultaneous EEG-fMRI in psychiatry generally go beyond the research insights of "where does it happen in the brain?". They encompass aspects of the underlying neural mechanisms that, for instance, could include a relevant role of neuronal oscillations or brain rhythms that can be addressed with the EEG, but not only with fMRI. For example, it is highly relevant to distinguish between the phasic activity of dopaminergic neurons related to reward (in the frequency range from 15 to 30 Hz) and the tonic activity of dopaminergic neurons (in the frequency range from 2 to 10 Hz). To illustrate this, drug addiction is related to the rapid, spike-like effects of certain dopaminergic drugs that mimic the

G. Sammer (✉) · C. Mulert
Centre of Psychiatry, Justus Liebig University, Giessen, Germany
e-mail: gebhard.sammer@uni-giessen.de

C. Mulert, L. Lemieux (eds.), *EEG - fMRI*,
https://doi.org/10.1007/978-3-031-07121-8_20

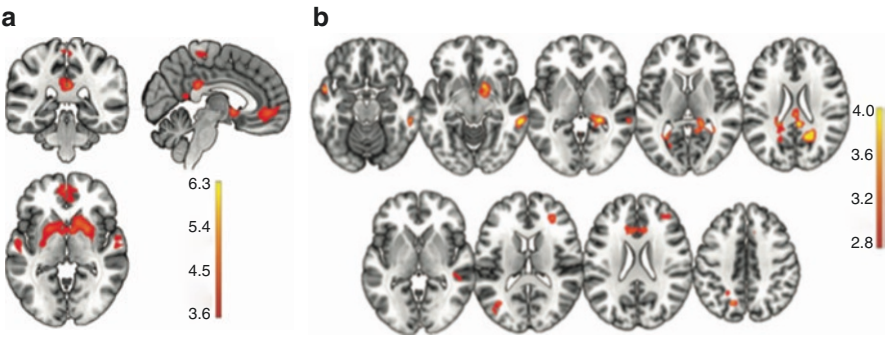

Fig. 20.1 Simultaneous EEG-fMRI for analyzing reward-related beta−/ and loss-related theta frequency range activity (**a**) conventional fMRI analysis: brain areas showing greater BOLD response for gain vs loss feedback (single-voxel $P < 0.001$, $P(\text{FDR}) < 0.05$ at the cluster level). (**b**) EEG–fMRI fusion analysis results (single-voxel $P < 0.005$, $k = 100$): Areas showing high-beta-band-associated activations for the contrast gain > loss feedback including the ventral striatum / Ncl. Accumbens (top row) and theta-band-associated activations for the contrast loss > gain (bottom row) including the anterior cingulate cortex. The opposite contrasts did not yield significant results in any of the above cases. *BOLD* blood-oxygen-level dependent, *EEG* electroencephalography, *FDR* false discovery rate, *fMRI* functional magnetic resonance imaging. (Reprinted from Andreou, C., H. Frielinghaus, J. Rauh, M. Mussmann, S. Vauth, P. Braun, G. Leicht and C. Mulert (2017). "Theta and high-beta networks for feedback processing: a simultaneous EEG-fMRI study in healthy male subjects." Transl Psychiatry,7(1), e1016; https://doi.org/10.1038/tp.2016.287, Copyright (2017), with permission from Springer Nature. Open access article under the CC BY license (https://creativecommons.org/licenses/by/4.0/))

physiological phasic activity of dopaminergic neurons, while the risk of drug addiction is lower with drugs that mimic the tonic activity of dopaminergic neurons. Using EEG, phasic beta activity after reward can be distinguished from theta activity after loss, and disturbances in psychiatric conditions have been described (Andreou et al. 2015) to be related to psychopathological aspects like impulsivity. At the same time, prominent subcortical structures in the dopaminergic reward system cannot be assessed directly with the EEG, and changes in these regions have been identified in various psychiatric disorders using fMRI (Deserno et al. 2016; Clark et al. 2019). Accordingly, the simultaneous EEG-fMRI offers the possibility to search for more comprehensive findings, for example, to investigate the phasic activity in the beta frequency range for reward in subcortical structures such as the ventral striatum and the nucleus accumbens (Andreou et al. 2017) under different psychiatric conditions (see Fig. 20.1). Similar approaches are addressed below.

20.2 Anxiety Disorder

Understanding fear is important for treating phobia. It is of particular interest whether different types of fear produce different or similar physiological activation patterns. Michałowski et al. (2017) compared spider, blood/injection and

social anxiety in the same study. FMRI, EEG and ECG were recorded simultaneously as physiological parameters. The technical equipment consisted of a Siemens 3 T Trio MRI scanner and 64-channel BrainAmps. Subjects were tested for social anxiety, mutilation and spider phobia using scales. The task was a picture presentation paradigm using fear-related material from different picture collections. The P1 component and the late positive potential (LPP) were calculated for the EEG. FMRI-GLM analysis was calculated for regions of interest associated with the processing of anxiety stimuli. The main results showed an increased P1 amplitude in anxious subjects, which means increased vigilance. Images of spiders and angry faces were associated with larger LPPs than neutral images. This effect was more pronounced in the spider and social fear groups. The FMRI analysis showed that the increased responses to anxiety-related stimuli are mainly due to certain anxieties and not to general anxiety. However, no joint EEG-fMRI analysis was reported. The advantage of simultaneously recorded signals in this study is evident in the advantage of the close temporal relationship of the results.

Drug abuse or addiction are often associated with psychiatric disorders. The impact of such comorbidity on the underlying disease or brain function is of great interest for both diagnosis and treatment. Karch et al. (2008) examined the influence of trait anxiety (STAI) on performance monitoring in healthy subjects and in alcohol-dependent patients using an auditory go/no-go task. Evoked potentials (P300 component) were recorded during the EPI acquisition using a 62-channel BrainAmp in a 1.5 Tesla Siemens Sonata MR scanner. Here too, the data from fMRI and EEG were analysed separately. The main results showed differences in haemodynamic activation patterns between the high and low anxiety groups in frontal brain regions related to inhibition of the go/no-go task response. No results were found for the P300 ERPs.

20.3 Attention Deficit Hyperactivity Disorder (ADHD)

There is broad agreement that the behaviour of people with Attention Deficit Hyperactivity Disorder (ADHD) is characterized by increased variability in many aspects of their behaviour (Killeen 2019). Selective attention and sustained attention are as much a focus of research as impulsive behaviour. Although many biological changes from molecular to behavioural levels have been reported, the pathophysiology of ADHD is far from clear. Probably due to a changed attention function, the oscillations in the lower theta and alpha frequency band are increased, the activity in the higher alpha frequency band is reduced (Lenartowicz et al. 2016). A simultaneous EEG-fMRI study of EEG alpha frequency band activity was performed to investigate whether fronto-parieto-occipital connectivity is impaired in ADHD. Male teenagers with ADHD were compared to healthy controls. They had to do a spatial working memory task. The EEG was recorded with a high-resistance

HydroCel with 256 channels from Electrical Geodesics in a 3 T Siemens Trio MR scanner. An alpha event-related desynchronization (ERD) was calculated from the EEG data. EEG-fMRI analysis was calculated as a psychophysiological interaction analysis (PPI) as implemented in FSL for alpha-ERD activity, and connectivity was estimated for either the right lateral occipital cortex, the right upper occipital cortex and the right frontal eye fields. Alpha-ERD was associated with fronto-parieto-occipital connectivity in participants with ADHD, which is likely indicative of a compensatory attention response.

Karch et al. (2014) emphasized the importance of executive dysfunction in patients with ADHD. A small sample of adults with ADHD and healthy controls participated in the study. The MR scanner was a 1.5 T Siemens Sonata. The EEG was recorded with a 62-channel BrainAmp. The subjects performed a voluntary selection task using an auditory go/no-go paradigm during the recording. The joint EEG-fMRI analysis was performed by trial-by-trial coupling of EEG and fMRI for N2 amplitude at Fz and P3 amplitude at FCz. While no results were found for P3, reduced N2-related BOLD responses were found in the ADHD group. In a previous study with the same design and the same technical equipment, but without EEG-based analysis, the results showed increased frontal and parietal activity during the voluntary selection task. Frontal activation was less in ADHD patients during free reactions (Karch et al. 2010).

20.4 Depression, Posttraumatic Stress Disorder (PTSD) and Neurofeedback

Neurofeedback is assumed to offer a great possibility to enhance the treatment of neurological or psychiatric diseases, particularly epilepsy, major depression, posttraumatic stress disorder or the attention deficit hyperactive disorder. For example, EEG-neurofeedback is the first attempt of neurofeedback dating about four decades ago, being used in epilepsy, attention deficit hyperactivity disorder and for cognitive enhancement. Subjects “see” or “hear” their own brain activity in “real time” by being usually presented a low pass filtered representation of the brain signal of interest. The task of the subjects is to shape their brain waves in the intended way. More recently, neurofeedback using BOLD signals is emergently studied for therapeutically use, preferably in depression but also in the context of diseases related to altered amygdala functioning and the processing of salient stimuli, as, for instance, in phobia, obsessive compulsive disorder or addiction.

After trying the neurofeedback method in healthy volunteers (Zotev et al. 2014), a similar method was examined in a smaller group ($N = 13$) of patients diagnosed with major depression (Zotev et al. 2016). The participants were able to successfully acquire the neurofeedback of the left amygdala. Self-regulated haemodynamic amygdala activation was associated with simultaneously recorded

surface EEG patterns. Upper alpha band asymmetry correlated with severity of major depression and amygdala-BOLD laterality. Zotev et al. (2018) expanded their approach to real-time fMRI neurofeedback (rtfMRI-nf) to train top-down modulation of amygdala activity in veterans with combat-related PTSD. The technical environment was a 3 T General Electric MR750 MRI scanner, a standard 8-channel receive-only head coil array in combination with a 32-channel BrainAmp. Here too, the participants had to learn to control the left amygdala BOLD signal. The feedback signal consisted of two bars, one representing changes in the left amygdala BOLD signal and the other calculated as relative EEG power asymmetry for F3 and F4 in the high beta band. As required in neurofeedback studies, the experimental group was compared to a group that received sham feedback instead. The results showed improved functional connectivity between the left amygdala and DLPFC during training, which corresponded to a simultaneously recorded left-lateralized improvement in the coherence in the upper EEG alpha frequency. These findings correlated with a decrease in clinical PTSD values, but there was no significant difference from the control group receiving sham neurofeedback. Successful self-regulation of the amygdala was also described by Keynan et al. (2016). They derived an "electrical amygdala fingerprint" from the simultaneous EEG-fMRI recorded during amygdala neurofeedback sessions. This parameter, inspired by fMRI, has been found to predict the haemodynamic activity of the amygdala so that it can even be used to self-regulate the amygdala at the bedside. Zotev et al. (2020) expanded their approach to real-time fMRI neurofeedback and combined it with EEG neurofeedback (rtfMRI-EEG-nf). This should allow participants to regulate their haemodynamic (BOLD fMRI) and electrophysiological (EEG) regional brain activities. This method was applied to self-regulation training for emotions in a small sample of patients with major depression (MDD). Eight patients received neurofeedback during a happy emotion induction task and were asked to simultaneously regulate the left amygdala, left rostral anterior cingulate cortex and frontal EEG asymmetries in the alpha and high beta bands. Another eight patients received sham neurofeedback. In the neurofeedback group, the participants were able to successfully regulate their brain activity and reported an improvement in their mood.

Using an approach to pharmacological fMRI, McMillan et al. (2020) recorded EEG-fMRI after ketamine infusion in patients with major depression. The study was carried out using a randomized, double-blind, active, placebo-controlled crossover design. The EEG was recorded in a 3 T Siemens Skyra MR scanner, the 64-channel EEG was recorded using BrainCap MR and BrainAmp MR Plus amplifiers (Brain Products, Germany) during a resting state and a breath hold task. The advantage of the EEG-informed pharmacological MRI analysis was that it showed different time courses of the ketamine-induced neuronal activity (Fig. 20.2).

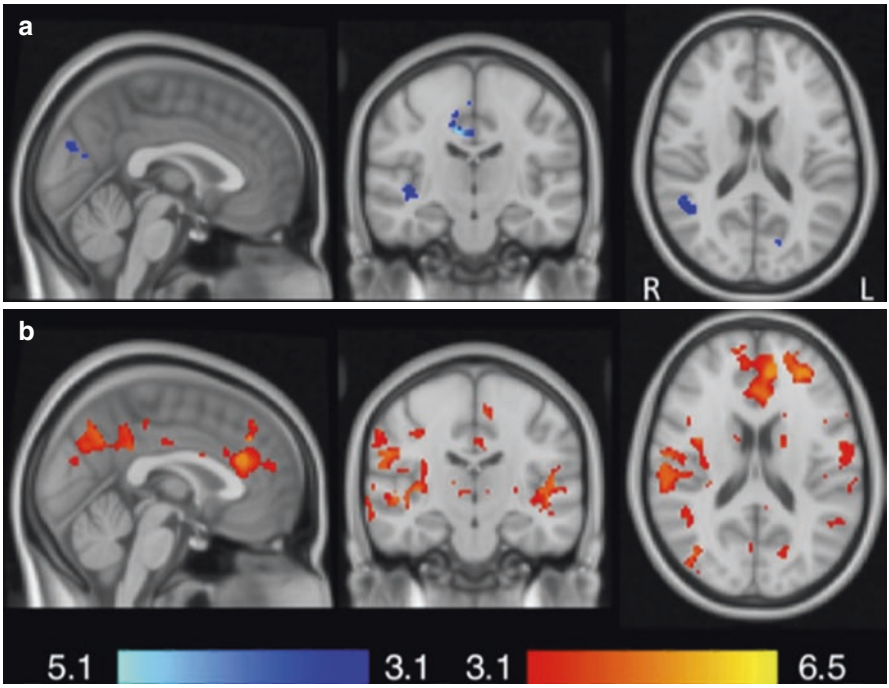

Fig. 20.2 Group statistical Z maps of modelled ketamine BOLD response for time courses of band-limited virtual sensor EEG power for (**a**) the low beta frequency band and (**b**) the high gamma frequency band, showing significant effects of ketamine ($Z \geq 3.1$, $p < 0.05$, FWE cluster corrected). Physiological noise and motion regressors were included in the model. A grey matter mask was applied to all maps. (Reprinted from McMillan R, Sumner R, Forsyth A, Campbell D, Malpas G, Maxwell E, Deng C, Hay J, Ponton R, Sundram F, Muthukumaraswamy S. (2020) "Simultaneous EEG/fMRI recorded during ketamine infusion in patients with major depressive disorder." Prog Neuropsychopharmacol Biol Psychiatry. pp. 8, Apr 20;99:109838. doi: 10.1016/j.pnpbp.2019.109838, Copyright (2019) with permission from Elsevier Inc.)

20.5 Schizophrenia

There were two papers that tested the hypothesis of altered brain networking characteristics in patients with schizophrenia using simultaneous EEG-fMRI. There is evidence that schizophrenia is a neurodevelopmental disorder characterized by a variant migration of neurons. The examination of neural networks in schizophrenia compared to HC tests such a model. One method for examining brain networks is based on EEG oscillations. Assuming that neural oscillations, or more precisely the oscillatory activity resulting from the neural mass activity, indicate the formation of transient brain networks that connect or integrate distributed brain regions, simultaneous EEG-fMRI recordings make it possible to link this oscillation activity with spatial haemodynamic activation patterns.

Baenninger et al. (2016, 2017) investigated whether psychotic patients (including patients diagnosed with schizophrenia, schizoaffective disorder and brief psychotic disorder) showed differences in brain regions that are involved in integrative mechanisms, as indicated by EEG oscillations. The study was carried out at two research sites, where different technical devices, different scanning and analysis software and parameter settings for the preprocessing of the data were involved. EEG-fMRI was collected at resting. The data were adapted for the main analysis, which was based on the EEG global field synchronization measure (calculated for several frequency bands), which represents the common-phase synchronization across electrodes. Global field synchronization parameters were used as parametric modulators for the first-level fMRI analysis to identify EEG-fMRI coupled clusters. The results showed that the associations between BOLD and global field synchronization in EEG-delta, alpha1 and beta were different in patients compared to HC. This has been found for extrastriate visual areas, for alpha1 oscillations and areas associated with the default mode network areas for the delta and beta frequency bands. Within the same theoretical framework it is known that the auditory gamma response is reduced in schizophrenia. Leicht et al. (2016) examined an EEG-gamma-mediated brain network using an EEG-informed fMRI analysis in subjects prone to psychosis and compared them to HC. The subjects performed an auditory selective attention task during the EEG-fMRI recording. The technical equipment consisted of a 64-channel BrainAmp and a 3 T Siemens Trio MR scanner. Based on time series representing the auditory evoked gamma response, regressors for the EEG-informed fMRI-GLM analysis were calculated for each subject before analysis at the group level. Reduced activity was observed in subjects at high risk of psychosis compared to HC in a network associated with gamma oscillation activity. The gamma-related network comprised bilaterally the auditory cortex, the thalamus, the anterior cingulate cortex and the dorsolateral prefrontal cortex.

Among other things, schizophrenia is associated with a change in perception and hallucinations. The event-related EEG potential has proven to be an excellent tool for examining the perception of all modalities. Modulations of ERPs by schizophrenia have been studied intensively. Ford et al. (2016) were interested in haemodynamic correlates of auditory event-related potential (AEP). They compared N100 and P200 components of the AEP between a group of patients with schizophrenia or schizoaffective disorder and an HC group. AEPs were recorded while listening to 1000 Hz tones. When using an fMRI block design, the blocks either consisted of the listening task or belonged to a resting condition. The MR scanner was a 3 T Siemens Skyra, EEG was recorded with a 32-channel BrainAmp. The joint analysis of ERP and BOLD data was carried out using a joint independent component analysis. As a result, joint independent components in both groups showed a bilateral relationship of N100 to activation of the auditory cortex. For P200, joint-independent components positively correlated with haemodynamic activation in the superior and mid temporal gyrus in the frontal and parietal regions. A negative correlation of P200 was found with the medial prefrontal cortex, the precuneus and the visual cortex. A group difference was only found for P200-linked components (Fig. 20.3).

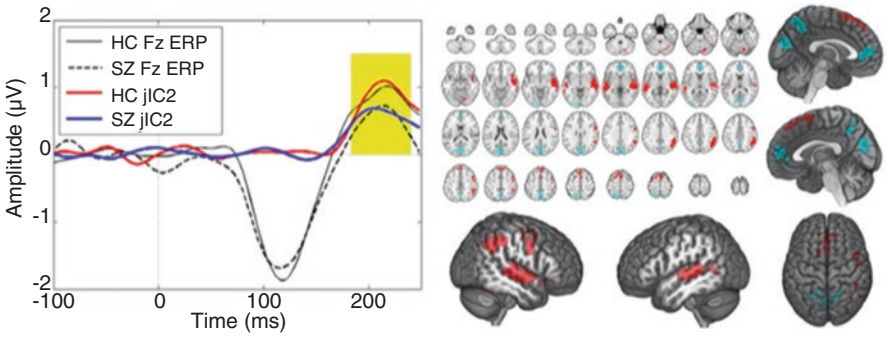

Fig. 20.3 Results from the fMRI/ERP joint ICA analysis at electrode Fz, showing the "P200" joint independent component (JIC). On the left are shown average ERP waveforms for healthy controls (HC) (black solid line) and participants with schizophrenia (SZ) (black dotted line) overlaid onto the temporal aspect of the "P200" JIC for HC (red) and SZ (blue). On the right, regions depicted in red reflect areas where the "P200" JIC is positively correlated with BOLD activation, and those in cyan reflect areas where there is negative covariation between P200 amplitude and BOLD activation. (Reprinted from Ford JM, Roach BJ, Palzes VA, Mathalon DH (2016) Using concurrent EEG and fMRI to probe the state of the brain in schizophrenia. Neuroimage Clin. pp. 434, Aug 10;12:429–41. doi: 10.1016/j.nicl.2016.08.009, Copyright (2016) with permission from Elsevier Inc. Open access article under the CC BY-NC-ND license (http://creativecommons.org/licenses/by-nc-nd/4.0/))

Another study on auditory processing in schizophrenia was carried out by Kirino et al. (2019). Kirino et al. (2019) summarize that mismatch negativity (MMN), an event-related potential generated by hearing stimuli that deviate from standard auditory stimuli, is reduced in patients with schizophrenia and might serve as a biological candidate marker for schizophrenia. They recorded EEGs during event-related fMRI and compared the data between 12 patients with schizophrenia and 15 healthy volunteers. The MMN was triggered by stimulus omission. A Philips Achieva 3.0 Tesla MRI scanner was used together with a BrainAmp and Easycap. The upper temporal gyrus in the right hemisphere correlated positively with the MMN amplitude at Fz in patients with schizophrenia. Apart from many other results in the individual modalities of this study, no further correlations with MMN were reported.

Another prominent theory of schizophrenia concerns dopamine. Altered dopamine transmission is associated with psychiatric disorders such as schizophrenia, depression or ADHD. In particular, the corticostriatal and meso-striatal dopamine systems, the former being involved in working memory including executive function and the latter mediating reward processing, seem to play a crucial role in these diseases. It is therefore of interest whether there are any effects of COMT polymorphism on brain function during reward processing. This question was asked by Boecker-Schlier et al. (2016). They investigated the effects of the COMT Val158Met genetic polymorphism, the variation in environmental conditions and the association with neuronal reward correlates, focusing on adversity in childhood. Healthy participants performed a monetary incentive delay task. The simultaneous EEG-fMRI was recorded in a 3 T Siemens Trio MR scanner using a 64-channel BrainAmp.

Although EEG-fMRI was recorded at the same time, EEG and fMRI were analyzed separately and no analysis was carried out together. Activation in the reward system during win trials revealed a gene x environment interaction. Higher childhood family adversity is related to increased reward sensitivity and reduced efficiency in reward processing particularly in genetically at-risk individuals. A similar study by the same research group (Boecker et al. 2014) examined the effects of adversity in early life on the processing of neuronal rewards later in life, including ADHD symptoms, in a larger sample ($N = 162$) of healthy young adults. As in the previous study, the subjects performed an incentive delay task. The technical environment for scanners and EEG was the same as in the study above. The contingent negative variation (CNV) was calculated for the EEG; for the fMRI, a GLM region of interest approach was carried out for the regions that are assigned to the reward system. Correlations between ROI measurements, CNV, adversity and lifelong ADHD symptoms were found. The authors proposed a different long-term impact of adversity in early life on reward processing, which implies hypo-responsiveness during reward anticipation and hyper-responsiveness when receiving a reward. In this context, another current EEG-fMRI study is of interest. Sperl et al. (2019) wanted to investigate whether fronto-medial oscillations in the EEG theta frequency band can support a fronto-medial to amygdala brain network. These networks have been suggested to play an important role in learning fear reactions. Simultaneous recordings were made 24 h after fear conditioning and fear extinction. 21 healthy subjects took part in a 2-day paradigm of fear conditioning and extinction. The measurements were recorded in a 3 T Siemens Prisma MR scanner using a 32-channel BrainAmp. Using an EEG-informed analysis approach, frontal midline theta and values indicating human fear and extinction recall were included in the fMRI-GLM analysis. This analysis revealed a relationship between the theta EEG, fear extinction recall and the right amygdala, suggesting that a high recall of the conditioned and extinguished fear as indicated by EEG theta power was related to a high fear extinction recall as indicated by fMRI amygdala activation. An inverse relationship has been reported for theta-EEG and vmPFC, which is likely to correlate with a putative inhibitory role of vmPFC in anxiety during early recall of extinction.

The fMRI or EEG at rest seems to reflect the basic requirements for undisturbed brain function. Studies have shown changes in resting state networks in various diseases, including schizophrenia. While a consistent spatial-temporal coupling between neuronal oscillations and resting state networks is strongly associated with successful cognitive processing in healthy controls, Razavi et al. (2013) tested the hypothesis that this coupling is changed in schizophrenia. BrainAmps, consisting of 92 channels, were used in a 3 T Siemens Magnetom Trio MR scanner. Covariance maps between the EEG frequency bands and the resting state networks were calculated for the patient and the control group. A topographical analysis of variance was carried out for group comparisons. It was concluded that the results showed an altered coupling between resting state networks and the simultaneous oscillation activity in patients with a schizophrenia spectrum disorder.

There is a lot of discussion about the effects of nicotine on cognitive brain function, especially in the context of the dopamine model of schizophrenia. Mobascher

et al. (2012) investigated the influence of 1 mg nasal nicotine on the P300 obtained during an odd ball-type visual task. The EEG-FMRI was measured in a 3 T Siemens Trio MR scanner using 32-channel EEG BrainAmps. The EEG-informed analysis was calculated as an fMRI-GLM analysis, with individual experimental P300 amplitudes added as information about the BOLD amplitudes. As a main result, an effect of the drug on the task-induced activity of the anterior cingulate cortex was reported. The benefit of using EEG-fMRI was justified by the lack of effects in separately analyzed EEG and fMRI measurements with nicotine. In addition, no effect of the group was found at all.

The anaesthetic ketamine is known to cause psychotic symptoms and also change cognitive processing (Uno and Coyle 2019). Ketamine is a non-competitive NMDA receptor antagonist, thus modulates glutamatergic neurotransmission. EEG studies have shown that ketamine attenuates P300 amplitude and mismatch negativity (MMN) in healthy volunteers (see Uno and Coyle 2019 for an overview). As a result, ketamine has been repeatedly discussed in connection with schizophrenic diseases. Forsyth et al. (2018) investigated the modulation of neural activity by ketamine and midazolam, the latter being a short-acting benzodiazepine that targets GABAA receptors. A group of 30 male volunteers participated in 3 sessions. Ketamine, midazolam and placebo were administered in a three-way, placebo-controlled, crossover design. 64-channel BrainAmps and a 3 T Siemens Skyra MR scanner were used for data recording. The so-called fractional amplitude of low-frequency fluctuations (fALFF) was taken into account for the fMRI analysis. fALFF measures the portion of low-frequency fluctuations within a certain frequency band in the entire recorded frequency range. The EEG-informed analysis used performance estimates from several EEG frequency bands, which were derived from occipital and frontal bipolar recordings. These average power values for each frequency of interest were introduced into the regression model. With ketamine, a widespread reduction in fALFF and various effects on the EEG frequency bands could be shown. The relationship between EEG parameters and haemodynamic activation was also different, but the authors emphasized the explanatory nature of the study. In the same study, a second paper was published that focuses exclusively on ketamine and implements a different analytical approach (McMillan et al. 2019). For the EEG-informed fMRI analysis, ketamine-induced changes for several EEG frequency bands were identified. The time series of power values for each frequency band of interest were included in the respective GLM model. In summary, the authors concluded that the EEG-informed fMRI analysis can increase confidence that MR imaging of the pharmacological intervention is directly related to the underlying neuronal activity. Similarly, Zacharias et al. (2020) investigated whether a prefrontal decrease in functional connectivity induced by ketamine was associated with reduced vigilance indicated by EEG. In a proof-of-concept study with subanaesthetic S-ketamine in healthy volunteers, fMRI and EEG were simultaneously recorded during rest using a 3 T Siemens Trio scanner, BrainAmp amplifiers and an EasyCap. The results showed a relationship between EEG activity and network connectivity in standard mode, which is consistent with the hypothesis of a reduced alertness state induced by ketamine.

20.6 Obsessive-Compulsive Disorder (OCD)

Intrusive thoughts are characteristic in obsessive-compulsive disorder (OCD). Compulsions are executed to avoid expected negative implications. Ritualized behaviours are established to reduce anxiety and distress related to the obsessions. The frontostriatal model of OCD suggests that increased frontal activity directs attention to potential threats that lead to compulsions. Therefore, in patients with OCD pronounced error related activity, as is represented by the error related negativity (ERN), can be found. Such error-related activity is primarily associated with the anterior cingulate cortex. Grützmann et al. (2016) aimed to examine the neural correlates of performance monitoring, which are indicated by improved ERN in obsessive-compulsive disorder. Patients with OCD were compared to healthy volunteers. The subjects performed a version of the flanker interference task using arrows. The EEG was recorded with a 32-channel BrainAmp in a 1.5 T Siemens Sonata MR scanner. ERN amplitudes of single trials were estimated using an ICA-based method described in this article. These parameters were used to calculate intra-individual correlations between ERN and local BOLD responses for correct and incorrect attempts. Group analyses revealed increased ERN amplitudes, an increased activation of the anterior cingulate cortex and the right amygdala in response to erroneous responses in the OCD group, as well as an increased intra-individual correlation of the activation, which is represented by the ERN and the pre-supplementary motor area (pre-SMA). Another study on conflict monitoring and error processing using informed EEG-fMRI analysis (3 T Philips Achieva, 64-channel BrainAmps) in healthy subjects only, using a flanker task, showed also that stronger ERN amplitudes were related to activation in the anterior cingulate cortex and the pre-SMA (cluster-level tests). Latter was associated with conjoint activation of ERN and N2 (Iannaccone et al. 2015). For EEG-informed fMRI analysis, GLM conflict condition regressor was modulated by single trial ERP amplitudes.

20.7 Dementia

Dementia and Alzheimer's in particular are widespread and are therefore being intensively investigated in many ways. Cognitive decline is a primary symptom of pathological aging. As a result, there are numerous studies on the underlying pathomechanism, prevention strategies and treatments to slow down cognitive decline. Two studies with EEG-fMRI examined the influence of pharmacological interventions on brain function with donepezil in healthy volunteers. Donepezil is an acetyl-cholinesterase inhibitor that increases the availability of the acetylcholine neurotransmitter, which is known to be an important neurotransmitter for cognitive processing. The acetyl-cholinesterase inhibitors donepezil as well as rivastigmine and galantamine are currently approved drugs in the pharmacotherapy of Alzheimer's disease. Balsters et al. (2011) examined the effects of AChEI (donepezil) on perception in healthy older participants. A peculiarity of this study is that it was probably the first simultaneous EEG / fMRI study to examine the effects of a pharmacological agent. A smaller sample of 14

participants aged between 55 and 76 years was examined, comparing baseline, donepezil and placebo in separate test sessions within the same subjects. The technical equipment consisted of a 32-channel BrainAmp and a Philips 3 T Achieva MR scanner. Cognitive testing was performed using a paired associates learning task. Main analysis was performed using EEG power measures for the usually used EEG frequency bands in an EEG-informed GLM-fMRI analysis approach. An age regressor was included in the GLM model. It was reported that donepezil affected paired association learning, resting alpha, beta, and delta band power. EEG-informed fMRI analysis suggested that oscillatory alteration in the delta band was associated with hippocampal activity, effects on the alpha band were related to frontal-parietal network, and beta was associated with default-mode activation. A more recent study on donepezil aimed to investigate the effects of donepezil, memantine, and modafinil before and after sleep deprivation (Wirsich et al. 2018). Sleep deprivation was implemented as a model of cognitive impairment. Eleven healthy subjects participated in five sessions. EEG was recorded using 64-channel BrainAmps within a Siemens 3 T Magnetom Verio. A functional connectome was constructed from fMRI data, which was based on correlations of the wavelet time series between the regions defined by an anatomical atlas. An expert identified sleep stages using the EEG. The sleep stage categories were assigned to the fMRI volumes, while the duration information was retained by being introduced as covariates in the network-based statistical approach of the connectome. A change in network connectivity was only seen with donepezil, separate from the changes caused by sleep deprivation or sleep.

The first EEG-fMRI study in Alzheimer's patients—and these are still rare—examined the relationship between the performance of the alpha band power and the haemodynamic default mode network (Brueggen et al. 2017). Fourteen patients with AD were compared to 14 matching healthy controls. EEG (32-channel BrainAmp) and fMRI (3 T Siemens MR scanner) were recorded simultaneously. An EEG-informed fMRI analysis was calculated by inserting a regressor into the GLM model that contained the alpha band performance information derived only from the occipital electrodes. Group comparisons of alpha activity were not statistically significant. A reduced positive association between alpha and haemodynamic activity in multiple brain regions in AD patients was reported for the default mode network and the thalamus. However, it should be noted that the statistical threshold was set to $p < 0.01$ without statistical correction for multiple comparisons.

From above, it can be seen that progress has been made in using the simultaneous EEG-fMRI measurement in the past 10 years. The method has been applied to a wider range of psychiatric disorders and has treated more subtle changes in the brain. Progress has also been made in the development and reliability of methods that bring EEG and fMRI together. However, the large number of methods and implementations could also prove to be a disadvantage in terms of the replicability crisis. Another point is that comprehensive models for psychiatric disorders are still lacking, and therefore the ability to identify reliable and specific biomarkers for psychiatric disorders is reduced. With the progress made so far and still to be expected in the EEG-fMRI method, a better understanding and better diagnosis of psychiatric disorders can certainly be expected.

References

Andreou C, Kleinert J, Steinmann S, Fuger U, Leicht G, Mulert C (2015) Oscillatory responses to reward processing in borderline personality disorder. World J Biol Psychiatry 16(8):575–586

Andreou C, Frielinghaus H, Rauh J, Mussmann M, Vauth S, Braun P, Leicht G, Mulert C (2017) Theta and high-beta networks for feedback processing: a simultaneous EEG-fMRI study in healthy male subjects. Transl Psychiatry 7(1):e1016

Baenninger A, Diaz Hernandez L, Rieger K, Ford JM, Kottlow M, Koenig T (2016) Inefficient preparatory fMRI-BOLD network activations predict working memory dysfunctions in patients with schizophrenia. Front Psych 7:29. https://doi.org/10.3389/fpsyt.2016.00029. eCollection 2016. Erratum in: front psychiatry. 2016;7:141. PubMed PMID: 27047395; PubMed Central PMCID: PMC4796005

Baenninger A, Palzes VA, Roach BJ, Mathalon DH, Ford JM, Koenig T (2017) Abnormal coupling between default mode network and delta and beta band brain electric activity in psychotic patients. Brain Connect 7(1):34–44. https://doi.org/10.1089/brain.2016.0456. Epub 2017 Jan 24. PubMed PMID: 27897031; PubMed Central PMCID: PMC5312599

Balsters JH, O'Connell RG, Martin MP, Galli A, Cassidy SM et al (2011) Donepezil impairs memory in healthy older subjects: behavioural, EEG and simultaneous EEG/fMRI biomarkers. PLoS One 6(9):e24126. https://doi.org/10.1371/journal.pone.0024126

Boecker R, Holz NE, Buchmann AF, Blomeyer D, Plichta MM, Wolf I, Baumeister S, Meyer-Lindenberg A, Banaschewski T, Brandeis D, Laucht M (2014) Impact of early life adversity on reward processing in young adults: EEG-fMRI results from a prospective study over 25 years. PLoS One 9(8):e104185. https://doi.org/10.1371/journal.pone.0104185. Correction in: PLoS One. 2014; 9(10): e112155. PMCID: PMC4131910

Boecker-Schlier R, Holz NE, Buchmann AF, Blomeyer D, Plichta MM, Jennen-Steinmetz C, Wolf I, Baumeister S, Treutlein J, Rietschel M, Meyer-Lindenberg A, Banaschewski T, Brandeis D, Laucht M (2016) Interaction between COMT Val(158)met polymorphism and childhood adversity affects reward processing in adulthood. Neuroimage 132:556–570. https://doi.org/10.1016/j.neuroimage.2016.02.006. Epub 2016 Feb 12. PMID: 26879624

Brueggen K, Fiala C, Berger C, Ochmann S, Babiloni C, Teipel SJ (2017) Early changes in alpha band power and DMN BOLD activity in Alzheimer's disease: a simultaneous resting state EEG-fMRI study. Front Aging Neurosci 9:319. https://doi.org/10.3389/fnagi.2017.00319. eCollection 2017. PubMed PMID: 29056904; PubMed Central PMCID: PMC5635054, 9

Clark L, Boileau I, Zack M (2019) Neuroimaging of reward mechanisms in gambling disorder: an integrative review. Mol Psychiatry 24(5):674–693

Deserno L, Schlagenhauf F, Heinz A (2016) Striatal dopamine, reward, and decision making in schizophrenia. Dialogues Clin Neurosci 18(1):77–89

Ford JM, Roach BJ, Palzes VA, Mathalon DH (2016) Using concurrent EEG and fMRI to probe the state of the brain in schizophrenia. Neuroimage Clin 12:429–441. https://doi.org/10.1016/j.nicl.2016.08.009. eCollection 2016. PubMed PMID: 27622140; PubMed Central PMCID: PMC5008052, 12, 429

Forsyth A, McMillan R, Campbell D, Malpas G, Maxwell E, Sleigh J, Dukart J, Hipp JF, Muthukumaraswamy SD (2018) Comparison of local spectral modulation, and temporal correlation, of simultaneously recorded EEG/fMRI signals during ketamine and midazolam sedation. Psychopharmacology (Berl) 235(12):3479–3493. https://doi.org/10.1007/s00213-018-5064-8. Epub 2018 Nov 14, 235, 3479. PubMed PMID: 30426183

Grützmann R, Endrass T, Kaufmann C, Allen E, Eichele T, Kathmann N (2016) Presupplementary motor area contributes to altered error monitoring in obsessive-compulsive disorder. Biol Psychiatry 80(7):562–571. https://doi.org/10.1016/j.biopsych.2014.12.010. Epub 2014 Dec 18. PMID: 25659234

Iannaccone R, Hauser TU, Staempfli P, Walitza S, Brandeis D, Brem S (2015) Conflict monitoring and error processing: new insights from simultaneous EEG-fMRI. Neuroimage 105:395–407.

https://doi.org/10.1016/j.neuroimage.2014.10.028. Epub 2014 Oct 22. PubMed PMID: 25462691

Karch S, Jäger L, Karamatskos E, Graz C, Stammel A, Flatz W, Lutz J, Holtschmidt-Täschner B, Genius J, Leicht G, Pogarell O, Born C, Möller HJ, Hegerl U, Reiser M, Soyka M, Mulert C (2008) Influence of trait anxiety on inhibitory control in alcohol-dependent patients: simultaneous acquisition of ERPs and BOLD responses. J Psychiatr Res 42(9):734–745. https://doi.org/10.1016/j.jpsychires.2007.07.016. Epub 2007 Sep 10. PMID: 17826793

Karch S, Thalmeier T, Lutz J, Cerovecki A, Opgen-Rhein M, Hock B, Leicht G, Hennig-Fast K, Meindl T, Riedel M, Mulert C, Pogarell O (2010) Neural correlates (ERP/fMRI) of voluntary selection in adult ADHD patients. Eur Arch Psychiatry Clin Neurosci 260(5):427–440. https://doi.org/10.1007/s00406-009-0089-y. Epub 2009 Nov 12. PubMed PMID: 19907927

Karch S, Voelker JM, Thalmeier T, Ertl M, Leicht G, Pogarell O, Mulert C (2014) Deficits during voluntary selection in adult patients with ADHD: new insights from single-trial coupling of simultaneous EEG/fMRI. Front Psych 5:41. https://doi.org/10.3389/fpsyt.2014.00041. eCollection 2014. PubMed PMID: 24795657; PubMed Central PMCID: PMC4001047

Keynan JN, Meir-Hasson Y, Gilam G, Cohen A, Jackont G, Kinreich S, Ikar L, Or-Borichev A, Etkin A, Gyurak A, Klovatch I, Intrator N, Hendler T (2016) Limbic activity modulation guided by functional magnetic resonance imaging-inspired electroencephalography improves implicit emotion regulation. Biol Psychiatry 80(6):490–496. https://doi.org/10.1016/j.biopsych.2015.12.024. Epub 2016 Jan 6. PubMed PMID: 26996601

Killeen PR (2019) Models of Attention-deficit hyperactivity disorder. Behav Processes 162:205–214. https://doi.org/10.1016/j.beproc.2019.01.001. [Epub ahead of print] Review. PubMed PMID:30677472

Kirino E, Hayakawa Y, Inami R, Inoue R, Aoki S (2019) Simultaneous fMRI-EEG-DTI recording of MMN in patients with schizophrenia. PLoS One 14(5):e0215023. https://doi.org/10.1371/journal.pone.0215023. PMID: 31071097; PMCID: PMC6508624

Leicht G, Vauth S, Polomac N, Andreou C, Rauh J, Mußmann M, Karow A, Mulert C (2016) EEG-informed fMRI reveals a disturbed gamma-band-specific network in subjects at high risk for psychosis. Schizophr Bull 42(1):239–249. https://doi.org/10.1093/schbul/sbv092. Epub 2015 Jul 10. PubMed PMID: 26163477; PubMed Central PMCID: PMC4681551

Lenartowicz A, Lu S, Rodriguez C, Lau EP, Walshaw PD, McCracken JT, Cohen MS, Loo SK (2016) Alpha desynchronization and frontoparietal connectivity during spatial working memory encoding deficits in ADHD: a simultaneous EEGfMRI study. Neuroimage Clin 11:210–223. https://doi.org/10.1016/j.nicl.2016.01.023. PMCID: PMC4761724

McMillan R, Forsyth A, Campbell D, Malpas G, Maxwell E, Dukart J, Hipp J, Muthukumaraswamy S (2019) Temporal dynamics of the pharmacological MRI response to subanaesthetic ketamine in healthy volunteers: a simultaneous EEG/fMRI study. J Psychopharmacol 33(2):219–229. https://doi.org/10.1177/0269881118822263. [Epub ahead of print] PubMed PMID: 30663520

McMillan R, Sumner R, Forsyth A, Campbell D, Malpas G, Maxwell E, Deng C, Hay J, Ponton R, Sundram F, Muthukumaraswamy S (2020) Simultaneous EEG/fMRI recorded during ketamine infusion in patients with major depressive disorder. Prog Neuropsychopharmacol Biol Psychiatry 99:109838. https://doi.org/10.1016/j.pnpbp.2019.109838. Epub 2019 Dec 13. PMID: 31843628

Michałowski JM, Matuszewski J, Droździel D, Koziejowski W, Rynkiewicz A, Jednoróg K, Marchewka A (2017) Neural response patterns in spider, blood-injection-injury and social fearful individuals: new insights from a simultaneous EEG/ECG-fMRI study. Brain Imaging Behav 11(3):829–845. https://doi.org/10.1007/s11682-016-9557-y. PubMed PMID: 27194564

Mobascher A, Warbrick T, Brinkmeyer J, Musso F, Stoecker T, Jon Shah N, Winterer G (2012) Nicotine effects on anterior cingulate cortex in schizophrenia and healthy smokers as revealed by EEG-informed fMRI. Psychiatry Res 204(2–3):168–177. https://doi.org/10.1016/j.pscychresns.2012.09.005. Epub 2012 Nov 6. PubMed PMID: 23137805

Razavi N, Jann K, Koenig T, Kottlow M, Hauf M et al (2013) Shifted coupling of EEG driving frequencies and fMRI resting state networks in schizophrenia Spectrum disorders. PLoS One 8(10):e76604. https://doi.org/10.1371/journal.pone.0076604

Sperl MFJ, Panitz C, Rosso IM, Dillon DG, Kumar P, Hermann A, Whitton AE, Hermann C, Pizzagalli DA, Mueller EM (2019) Fear extinction recall modulates human frontomedial theta and amygdala activity. Cereb Cortex 29(2):701–715. https://doi.org/10.1093/cercor/bhx353. PMID: 29373635; PMCID: PMC6659170

Uno Y, Coyle JT (2019) Glutamate hypothesis in Schizophrenia. Psychiatry Clin Neurosci 73(5):204–215. https://doi.org/10.1111/pcn.12823. [Epub ahead of print] PubMed PMID: 30666759

Wirsich J, Rey M, Guye M, Bénar C, Lanteaume L, Ridley B, Confort-Gouny S, Cassé-Perrot C, Soulier E, Viout P, Rouby F, Lefebvre MN, Audebert C, Truillet R, Jouve E, Payoux P, Bartrés-Faz D, Bordet R, Richardson JC, Babiloni C, Rossini PM, Micallef J, Blin O, Ranjeva JP (2018) Brain networks are independently modulated by donepezil, sleep, and sleep deprivation. Brain Topogr 31(3):380–391. https://doi.org/10.1007/s10548-017-0608-5. Epub 2017 Nov 23. PubMed PMID: 29170853

Zacharias N, Musso F, Müller F, Lammers F, Saleh A, London M, de Boer P, Winterer G (2020) Ketamine effects on default mode network activity and vigilance: a randomized, placebo-controlled crossover simultaneous fMRI/EEG study. Hum Brain Mapp 41(1):107–119. https://doi.org/10.1002/hbm.24791. Epub 2019 Sep 18. PMID: 31532029; PMCID: PMC7268043

Zotev V, Phillips R, Yuan H, Misaki M, Bodurka J (2014) Self-regulation of human brain activity using simultaneous real-time fMRI and EEG neurofeedback. Neuroimage 85(Pt 3):985–995. https://doi.org/10.1016/j.neuroimage.2013.04.126. Epub 2013 May 11. PubMed PMID: 23668969

Zotev V, Yuan H, Misaki M, Phillips R, Young KD, Feldner MT, Bodurka J (2016) Correlation between amygdala BOLD activity and frontal EEG asymmetry during real-time fMRI neurofeedback training in patients with depression. Neuroimage Clin 11:224–238. https://doi.org/10.1016/j.nicl.2016.02.003. eCollection 2016. PubMed PMID: 26958462; PubMed Central PMCID: PMC4773387

Zotev V, Phillips R, Misaki M, Wong CK, Wurfel BE, Krueger F, Feldner M, Bodurka J (2018) Real-time fMRI neurofeedback training of the amygdala activity with simultaneous EEG in veterans with combat-related PTSD. Neuroimage Clin 19:106–121. https://doi.org/10.1016/j.nicl.2018.04.010. eCollection 2018. PubMed PMID: 30035008; PubMed Central PMCID: PMC6051473

Zotev V, Mayeli A, Misaki M, Bodurka J (2020) Emotion self-regulation training in major depressive disorder using simultaneous real-time fMRI and EEG neurofeedback. Neuroimage Clin 27:102331. https://doi.org/10.1016/j.nicl.2020.102331. Epub ahead of print. PMID: 32623140

Combining Electroencephalography and Functional Magnetic Resonance Imaging in Pain Research

21

G. D. Iannetti and A. Mouraux

21.1 Introduction

In 1976, Carmon et al. showed, for the first time, that radiant heat pulses generated by a CO_2 laser stimulator could, when directed to the skin, elicit brain potentials in the ongoing human electroencephalogram (EEG). Such laser pulses have been later demonstrated to activate Aδ and C skin nociceptors in a *selective* and *synchronous* fashion (see Plaghki and Mouraux 2003, for a review). Since this first report, numerous studies have relied on laser-evoked brain potentials (LEPs) to assess the function of nociceptive somatosensory pathways, with the objective to gain insight into the neural processes that underlie the perception of pain. In the late 80s, a number of studies have used multi-channel EEG recordings to examine the topographical distribution of LEPs (e.g. Treede et al. 1988) and model their underlying neural sources, thus starting to identify the different brain areas activated by nociceptive somatosensory input (Bromm and Chen 1995; Tarkka and Treede 1993). A consistent finding across these studies is that LEPs are well explained by the combination of a midline source (usually assigned to the anterior part of the cingulate cortex, ACC) and a pair of bilateral opercular sources (usually assigned to secondary somatosensory (SII) and/or insular cortex). In several subsequent studies (Tarkka and Treede 1993; Valentini et al. 2012), an additional parietal source was added to the model, and assigned to the primary somatosensory cortex (SI) contralateral to the stimulated side (see Garcia-Larrea et al. 2003, for a review).

G. D. Iannetti (✉)
Neuroscience and Behaviour Laboratory, IstitutoItaliano di Tecnologia, Rome, Italy

Department of Neuroscience Physiology and Pharmacology, University College London, London, UK

A. Mouraux
Institute of Neuroscience, Université Catholique de Louvain, Brussels, Belgium
e-mail: andre.mouraux@uclouvain.be

C. Mulert, L. Lemieux (eds.), *EEG - fMRI*,
https://doi.org/10.1007/978-3-031-07121-8_21

These early findings have been later corroborated by a large number of studies using magnetoencephalography (MEG, e.g. Ploner et al. 2002), direct intracerebral recording of local field potentials (e.g. Frot and Mauguiere 2003), and neuroimaging methods that sample neural activity indirectly by measuring stimulus-evoked changes in regional cerebral blood flow (PET and functional magnetic resonance imaging (fMRI); Davis et al. 1998; Peyron et al. 1999). Several meta analyses have reviewed the existing data on EEG, MEG, PET, and fMRI responses to nociceptive stimulation (Apkarian et al. 2005; Garcia-Larrea et al. 2003; Peyron et al. 1999) and have confirmed the existence of a common set of brain regions responding to nociceptive stimuli, including bilateral thalamus, bilateral SII, bilateral insula, anterior cingulate cortex, prefrontal cortex, and, less consistently, contralateral SI cortex. A number of investigators have hypothesized that this network of brain areas, sometimes referred to as the "pain matrix" (Melzack 1999), reflects brain activities that are specifically involved in the processing of nociceptive input, and therefore may constitute a "cerebral signature for pain" (e.g. Tracey and Mantyh 2007).

However, the actual functional significance of brain responses elicited by nociceptive stimuli remains, to date, a matter of debate (Iannetti and Mouraux 2010; Mouraux and Iannetti 2018). Clear experimental evidence in support of the notion that these brain responses reflect truly nociceptive-specific brain processes is lacking. On the contrary, there is an accumulating evidence suggesting that these responses are very indirectly related to pain perception. For example, when nociceptive laser stimuli are presented at short and constant inter-stimulus intervals (thus increasing the temporal expectancy of the stimulus, and hence reducing its surprise content), a clear dissociation between the magnitude of LEPs and the magnitude of perceived pain can be observed, both using scalp EEG (Iannetti et al. 2008) and intracerebral EEG within the insular cortex (Liberati et al. 2018). Similarly, when brain responses to nociceptive stimuli are compared directly with those elicited by stimuli belonging to other sensory modalities (Kunde and Treede 1993; Somervail et al. 2021, 2022; Liberati et al. 2016; Lui et al. 2008; Mouraux and Iannetti 2009), results show that the two responses are strikingly similar, and therefore, that the greater part of the brain responses to nociceptive stimuli may actually reflect supramodal brain processes (i.e. brain processes that are elicited by sudden sensory stimuli regardless of sensory modality).

One reason for the poor understanding of the functional significance of nociceptive-related EEG and fMRI brain responses is the limited spatial resolution of EEG and the limited temporal resolution of fMRI. These intrinsic limitations make it difficult to tease out physiologically distinct brain activities contributing to the measured responses, as these appear lumped in space when sampled with EEG and lumped in time when sampled with fMRI. Therefore, because EEG signals contain the temporal information that is missing in fMRI signals, and because fMRI signals contain the spatial resolution that is missing in EEG signals (i.e. both methods provide complementary spatial–temporal information), the scientific community has shown an interest in the simultaneous recording of EEG and fMRI responses (Iannetti and Wise 2007). Here, we will show that combining EEG and fMRI is not sufficient to sample neural activity with the temporal resolution of

EEG and the spatial resolution of fMRI. Nevertheless, we will also show that when methods are used to analyze the recorded signals at the level of single trials, combining these two neuroimaging methods to perform EEG-informed BOLD fMRI modelling can provide novel physiological information about the cortical processing of nociceptive input.

In the following sections we will (1) examine the general issues related to the simultaneous collection of EEG and fMRI responses to nociceptive stimuli, (2) examine the practical issues related to the simultaneous collection of EEG and fMRI responses to nociceptive stimuli, (3) review the studies that have attempted to combine such recordings, and (4) illustrate, with some recent results, how single-trial estimation of EEG data can drive the analysis of fMRI data and thus provide novel physiological information.

21.2 Combining EEG and fMRI in Pain Research: General Issues

The spatial and temporal resolution of a given functional neuroimaging technique is defined as its ability to distinguish two distinct events in space and time, respectively.

Scalp EEG detects changes in scalp potential that are generated mainly by the summation of post-synaptic activity occurring in regularly oriented cortical neurons, thus providing a direct measure of spontaneous and stimulus-evoked neuronal activity on a millisecond time scale (Speckmann and Elger 1999). Since the skin, skull, and meningeal layers interposed between the brain and the recording electrodes distort and exert a spatial low-pass filtering on neuronal currents, the recorded signals have a spatial resolution in the order of centimetres, thus preventing the discrimination between distinct but spatially neighbouring neural sources of activity (Nunez and Srinivasan 2006). This issue is particularly relevant when considering the large EEG responses evoked by transient nociceptive stimuli, as these are thought to originate mostly from non-superficial brain structures like the operculo-insular cortex and the cingulate cortex, thus making the recorded signal particularly affected by volume conduction.

In contrast, blood oxygen level-dependent (BOLD) fMRI samples neural activity indirectly, by detecting changes in blood oxygenation that are linked, but not equivalent, to changes in neuronal activity (Kwong et al. 1992; Ogawa et al. 1992). It is often stated that fMRI, unlike EEG, has an excellent spatial resolution, in the order of millimetres. However, it is important to mention that the actual spatial resolution of BOLD-fMRI is compromised by the fact that the hemodynamic response to neural activity is not necessarily restricted to the locus of this neural activity, a notion that has been described previously as "watering the entire garden for the sake of one thirsty flower" (Malonek and Grinvald 1996). Furthermore, when performing analyses at the group level, inter-subject spatial registration requires the warping of single subject data, a procedure that can lead to distortions and even displacements of activity between neighbouring cerebral lobes (Ozcan et al. 2005). The temporal resolution of fMRI is limited by the variable delay between the onset of neural

activity and the subsequent hemodynamic response, as well as by the long-lasting nature of this hemodynamic response (both in the order of several seconds; Menon and Goodyear 2001). Furthermore, the temporal profile of the hemodynamic response may vary across subjects and brain regions (Lee et al. 1995; Robson et al. 1998). Consequently, the temporal resolution of BOLD-fMRI is very low, making it extremely difficult to unravel neural processes separated in time by less than a few seconds.

When considering these physiological properties, it becomes apparent that achieving optimal spatial–temporal resolution by exploiting the higher temporal resolution of EEG and the higher spatial resolution of BOLD-fMRI is not obvious, because *EEG and fMRI do not necessarily sample the same neural activity*.

The lack of correspondence between neural activity sampled by EEG and fMRI is particularly striking when comparing EEG and fMRI responses elicited by sensory stimuli. Sensory event-related potentials (ERPs) are short-lasting EEG responses, mainly related to transient changes in the peripheral sensory input. Sensory ERPs only reflect the fraction of stimulus-triggered brain activity that is (1) synchronous enough to summate into a measurable scalp potential, (2) spatially organized into an "open-field" configuration, and (3) time-locked and phase-locked to the onset of the stimulus (Regan 1989). For example, (1) the neural activity triggered by a slowly rising thermal stimulus will not yield a measurable ERP because the neural activity it elicits is not synchronous enough; (2) the neural activity originating from a "closed field" structure such as a subcortical nucleus will not yield a measurable ERP because the electrical fields generated by each neuron cancel each other; and (3) the neural activity consisting of stimulus-triggered modulations of the magnitude of ongoing EEG oscillations (i.e. event-related synchronization (ERS) and desynchronization (ERD)) will not yield a measurable ERP because these oscillations are not phase-locked to the onset of the stimulus. In contrast, the BOLD-fMRI signal is relatively independent of the synchronicity of the afferent volley, the spatial configuration of the underlying source, and most importantly, it integrates stimulus-triggered neural activity over a much longer time scale.

This mismatch between the neural activity sampled by ERPs and the fMRI can mislead the interpretation of combined ERP and fMRI recordings, even when data are not collected in the same experimental session. For example, a commonly used approach to combine ERP and fMRI data is to exploit the spatial resolution of fMRI in order to define better the neural generators of scalp ERPs (Christmann et al. 2002; Mulert et al. 2004). Indeed, the problem of estimating the location and extent of electrical sources contributing to a given scalp ERP signal (i.e. the EEG "inverse problem"; Nunez and Srinivasan 2006) is fundamentally ill-posed since the scalp ERP can be explained by an infinite number of source configurations. Therefore, to obtain a unique solution, constraints must be imposed on the model (Michel et al. 2004). With this aim, a number of investigators have used the location of stimulus-induced BOLD-fMRI responses as a "functional constraint" (i.e. fMRI-constrained ERP source localization). However, it is important to take into account that only a fraction of the stimulus-triggered neural activity contributes to

the scalp ERP, and that this fraction probably constitutes only a subset of the neural activities reflected in the BOLD-fMRI response. Therefore, although fMRI-constrained ERP source localization can certainly be a means to improve the solution of the EEG inverse problem by constraining the placement of dipolar sources in brain areas that are metabolically active, it can still produce false-positive results by allowing the misplacement of dipolar sources in brain regions that are metabolically active, but that do not contribute to the ERP response.

When considering nociceptive somatosensory input, the fact that the BOLD-fMRI signal integrates neural activity over a long time scale is likely to generate a significant mismatch between nociceptive-related neural activity that is sampled by EEG and fMRI. The perceptual correlate of a single strong nociceptive stimulus is long-lasting and multi-dimensional. Besides its sensory-discriminative dimension, it also encompasses motivational and emotional dimensions. Because ERPs almost exclusively reflect transient changes in neural activity, they capture only the initial part of the long-lasting neural response related to the perception of pain. In contrast, since fMRI data integrates neural responses over a longer time scale, they might reflect more closely the neural activity related to the perception as a whole.

The contribution of different populations of peripheral nociceptive afferents to the recorded brain response is likely to increase further the mismatch between the neural activity sampled by EEG and fMRI. This is due to the fact that nociceptive stimuli activate two different classes of peripheral nociceptors: small myelinated Aδ nociceptors and unmyelinated C nociceptors. While the activation of Aδ nociceptors results in sharp, short-lasting "pricking" sensations, the activation of C nociceptors conveys dull, long-lasting "burning" or "aching" sensations that spread well beyond the spatial limits of the stimulus. For this reason, brief and intense laser stimuli elicit a typical dual sensation of "first" (Aδ-related) and "second" (C-related) pain (Lewis and Ponchin 1937). Yet, for reasons that remain poorly understood, co-activation of Aδ- and C-nociceptors using laser stimulation predominantly elicits LEPs related to the activation of Aδ nociceptors (Mouraux et al. 2004; but see Hu et al. 2014). This leads to the possibility of an important mismatch between the brain activity underlying LEPs (which is strictly related to the activation of Aδ nociceptors and thus, to the perception of "first pain") and the brain activity underlying the BOLD-fMRI response (which could reflect a combination of brain activity related to the activation of both Aδ and C nociceptors).

For all these reasons, before addressing the problem of *how* EEG and fMRI responses to nociceptive stimulation can be concomitantly recorded, it is thus crucial to discuss *why* this should be done, and in which instances it may yield physiological information unobtainable using data collected in separate experimental sessions. Sampling EEG and fMRI data in a truly simultaneous fashion is technically challenging. The experimental setup is complex, and issues related to subject safety and quality of collected data must be addressed using dedicated EEG hardware (Lemieux et al. 1997). Magnetic susceptibility effects and radiofrequency interaction associated with EEG electrodes and wires cause signal dropouts and geometric distortions on MR images (Bonmassar et al. 2001). Degradation of image signal-to-noise ratio due to electromagnetic noise emitted by the EEG

recording headbox has also been described (Krakow et al. 2000). Most importantly, the collected EEG data is contaminated by severe MR-induced artifacts. These consist mainly of "pulse" artifacts caused by cardiac pulse-related movements and blood flow effects within the scanner static magnetic field, and "imaging" artifacts caused by radio-frequency and gradient switching during image acquisition. Pulse artifacts are regular, have relatively low amplitude, and occur even when MR images are not being acquired. In contrast, imaging artifacts are large and obscure the EEG completely (Allen et al. 2000). The removal of these artifacts, although feasible, is a complex and time-demanding procedure (Niazy et al. 2005). In addition, the increased subject discomfort related to combining the EEG setup with the constraints of the MR environment reduces the possible duration of the experimental session, and thus limits the complexity of the experimental design. For all these reasons, repeating the same experimental paradigm in two separate experimental sessions, is, in most cases, a more rewarding strategy (Iannetti et al. 2005a).

Nevertheless, as detailed more extensively in other sections of this book, the simultaneous recording of EEG and fMRI unleashes its potential in two particular circumstances: (1) when the neural activity under investigation displays a certain level of *unpredictability*, and (2) when the experimental design introduces important *time-dependent effects* such as habituation, learning, or between-session variability in the effect of a given pharmacological compound.

Outside the field of pain research, typical examples of such circumstances are studies examining ictal and interictal activities in epileptic patients (Hamandi et al. 2008), sleep stages (Wehrle et al. 2007), and spontaneous fluctuations of ongoing EEG rhythms (Laufs et al. 2003). Also, combining EEG and fMRI within a single recording session may be useful when examining the time-dependent effect of drugs on the processing of sensory input and, in particular, the effect of anaesthetic agents on the processing of nociceptive input (e.g. Rogers et al. 2004). Finally, when studies focus on brain responses that are strongly dependent of cognitive variables such as the focus of selective attention or the general level of arousal, the peculiar attentional context and the additional sensory stimulation inherent to a working MR scanner can introduce important, non-task-related differences when comparing data collected in separate sessions.

In the field of pain research (see also Sect. 21.5), the intrinsic variability of the brain responses to nociceptive stimulation can actually be exploited using simultaneous and *continuous* (i.e. not interleaved) acquisition of EEG and fMRI data to assess physiologically meaningful between-trial variations of EEG and BOLD-fMRI brain responses, and examine their relationship with behavioural measures (e.g. intensity of pain perception, reaction-time latency). In addition, simultaneous (but not necessarily continuous) acquisition of EEG and fMRI data can be important in the evaluation of drug effects, when a significant within-subject, between-session variation in the response to the drug (e.g. the potential development of tolerance to opioids) is expected.

21.3 Combining EEG and fMRI in Pain Research: Practical Issues

21.3.1 Selectivity of the Nociceptive Input in EEG-fMRI Studies

Noxious heat stimulation of the skin is most frequently used in EEG and fMRI studies of nociception, because they selectively activate nociceptive-specific transduction mechanisms in heat-sensitive free nerve endings located in the superficial layers of the skin (Julius and Basbaum 2001). If the temperature of the skin is raised above the thermal activation threshold of Aδ- and C-fiber nociceptors (Treede et al. 1995), the stimulus will be transduced into a nociceptive afferent volley. Noxious heat can be delivered using either thermal conduction (contact thermodes) or thermal radiation (infrared lasers). Alternative methods to activate Aδ- and C-fiber free nerve endings include mechanical pinprick stimulation to activate mechano-sensitive nociceptors (Iannetti et al. 2013) (Slugg et al. 2004), contact cold stimulation (De Keyser et al. 2018), and intraepidermal electrical stimulation (Inui et al. 2002; Mouraux et al. 2010).

Whatever the techniques used to sample neural activity, it is important to ascertain that the brain responses elicited by the nociceptive stimulus are truly related to the processing of nociceptive input (and not to the processing of another type of sensory input). For this reason, heat nociceptive stimulation is preferred to electrical or mechanical noxious stimulation, as the latter concomitantly activate low-threshold mechano-receptors and corresponding Aβ fibers (for a discussion on this topic see Baumgartner et al. 2005 and Plaghki and Mouraux 2003).For the same reason, radiant heat stimulation is preferred to contact heat stimulation, as contact thermodes unavoidably activate non-nociceptive Aβ-fiber afferents: the contact of the thermode with the skin results in the activation of slowly-adapting non-nociceptive mechanoreceptors, and changing the location of the thermode from trial to trial results in additional phasic tactile input (Greffrath et al. 2007). Because the activation of Aβ-fiber afferents induced by contact thermodes is not strictly synchronous with the onset of the thermal stimulus, and because the averaging procedures used to reveal ERPs cancels out signal changes that are not strictly time-locked to the stimulus onset, its contribution to contact-heat evoked potentials may be considered as negligible (CHEPs; Chen et al. 2001).In contrast, when contact thermodes are used to elicit BOLD-fMRI brain responses, the contribution of both tonic and phasic non-nociceptive Aβ-fiber input could become significant, because the BOLD signal integrates neural activity over a much longer time scale (see also Sect. 21.2), and it has been shown that even long-lasting tonic stimuli may elicit a significant "sustained" BOLD response (Bandettini et al. 1997).

Another advantage of radiant over conductive heat is that infrared laser stimulators heat the skin much faster (up to 10,000 °C/s; Plaghki and Mouraux 2003) than contact thermodes (currently up to 70 °C/s for thermodes specifically designed for the recording of CHEPs; Baumgartner et al. 2005). Therefore, because nociceptors are activated much more synchronously by fast-rising laser stimuli than by slow-rising contact heat stimuli, laser stimuli currently elicit ERPs much more reliably than contact thermodes (Baumgartner et al. 2005; Iannetti et al. 2006; see also Sect. 21.2).

21.3.2 Delivery of Nociceptive Stimuli in EEG/fMRI Environment

When performing pain-related EEG/fMRI studies, an important issue to consider is that the equipment involved in the delivery of the nociceptive stimulus must be compatible with the strong magnetic field of the MR scanner. Short-wavelength laser pulses (e.g. Nd:YAP lasers: $\lambda = 1.34$ μm) can be easily transmitted through inexpensive optic fibers. Recently, optic fibers capable of transmitting longer-wavelength CO_2 pulses ($\lambda = 10.6$ μm) have been made available, but are comparatively much more expensive (Plaghki and Mouraux 2003). Using such fibers, laser stimuli can be delivered inside the scanner room, while keeping the laser source outside. A number of contact thermodes have been developed to deliver noxious heat within the MR environment (e.g. Wise et al. 2002). Furthermore, both transcutaneous and intraepidermal electrical stimuli are easily delivered in the MR scanner room, provided that safety measures related to the presence of electric currents are considered. Finally, several laboratories (e.g. Lui et al. 2008) have built custom pneumatically driven devices to deliver noxious mechanical stimuli inside the MR scanner room.

Taking these different factors into consideration, it appears that noxious heat pulses generated by infrared laser stimulators constitute, at present, the preferred method of producing nociceptive sensory input for the concurrent recording of EEG and fMRI because they (1) are entirely selective for nociceptors, (2) elicit a nociceptive afferent volley that is synchronous enough to elicit reliable ERPs, and (3) can be delivered safely inside the scanner using optic fibers.

21.3.3 Experimental Design

Interleaved vs. *continuous EEG-fMRI acquisition*. The main source of contamination of the EEG by MR-related artifacts is represented by the radio-frequency and gradient switching that occurs during image acquisition. For this reason, several studies aiming at recording ERPs and fMRI within the same experimental session rely on an *interleaved* experimental design. In such a design, the introduction of short pauses in the acquisition of MR images (e.g. 3 s of image acquisition alternated with 3 s without image acquisition) allows the recording of EEG data unaffected by the dynamic imaging artifact. However, interleaving EEG and fMRI acquisition has important practical and theoretical limitations, mainly represented by an inefficient sampling of the neural activity and the consequent hemodynamic response, and by a reduction in the flexibility of the stimulus presentation paradigm (Garreffa et al. 2004; Nebel et al. 2005).The alternative is to acquire EEG and fMRI data simultaneously and *continuously* using an event-related experimental design, and then rely on offline signal-processing methods to remove the contaminating artifacts (Niazy et al. 2005).

Inter-stimulus interval. The rate of stimulus presentation can affect very significantly not only the magnitude, but also the functional significance of the EEG responses elicited by nociceptive stimuli. When the inter-stimulus interval (ISI) is kept constant across trials, it has been shown that the shorter the ISI, the smaller the recorded EEG response (Raij et al. 2003; Truini et al. 2004). For this reason some investigators have recommended the use of ISIs larger than 4 s (Raij et al. 2003).

However, it has also been shown that when the ISI is randomized across trials, thus making the occurrence of the nociceptive stimulus *unpredictable*, the magnitude of the EEG response is unaffected by stimulus repetition even at ISIs as short as 280 ms (Mouraux et al. 2004; Mouraux and Iannetti 2008). Consequently, if fMRI and EEG responses to nociceptive stimulation are sampled in an interleaved manner, it is crucial to present the nociceptive stimuli using the same ISI and stimulation paradigm, or else the functional significance of the brain responses sampled using EEG and fMRI may be very different.

Number of stimuli. Another practical issue to consider when designing the experiment is the number of nociceptive stimuli required to elicit reliable EEG and fMRI responses. Most studies recording ERPs elicited by nociceptive stimulation average a total of 20–40 stimuli (Treede et al. 2003). When using an event-related design, a similar number of stimuli is usually used to assess fMRI responses to nociceptive stimulation. The magnitude of EEG responses to nociceptive stimuli can vary greatly as a function of the parameters of the nociceptive stimulus and the stimulated body district. For example, fast-rising nociceptive stimuli yield a more synchronous afferent volley, thus providing a stronger spatial–temporal summation at central synapses that enhances intensity of perceived pain and increases the magnitude of measured brain responses (Iannetti et al. 2004). Similarly, and because of the shorter conduction distance and the higher density of skin nociceptors, nociceptive stimuli delivered to a proximal body district (e.g. the trigeminal territory) yield brain responses of significantly shorter latency and larger amplitude than nociceptive stimuli delivered to a distal body district (e.g. the foot; Truini et al. 2005; see for example Fig. 21.1 in Valentini et al. 2012).

Displacement of the stimulus. To avoid nociceptor fatigue or sensitization, and to allow passive cooling of the skin, the laser beam must be moved slightly after each stimulus (Treede et al. 2003). This is usually achieved by having an experimenter who manually displaces the laser beam inside the scanner room. However, although common in fMRI studies, this approach is far from being optimal because (1) it is necessary to provide the experimenter with some form of cue about when the beam has to be displaced, thus making the procedure prone to mistakes, and (2) it makes it difficult to define the exact location of stimulated spots. For these reasons, the development of computer-controlled MR-compatible devices to displace automatically the laser beam would be desirable, particularly when the time interval between two consecutive stimuli is short (Lee et al. 2008).

21.4 Studies Combining EEG and fMRI in Pain Research

This section will focus on four studies that have collected simultaneously EEG and BOLD-fMRI responses to nociceptive stimulation (Christmann et al. 2007; Iannetti et al. 2005a; Mayhew et al. 2013; Mobascher et al. 2009).

Iannetti et al. (2005a) demonstrated for the first time the feasibility of recording reliable laser-evoked EEG and fMRI responses in a truly simultaneous and continuous fashion (i.e. using a single and *continuous* acquisition of EEG and fMRI data). They showed that the latency, the amplitude, and the scalp distribution of LEPs recorded

during fMRI acquisition are not significantly different from the latency, the amplitude, and the scalp distribution of LEPs recorded outside the MR scanner (Fig. 21.1). This finding has two important implications. First, because of the observed similarities, it indicates that in most experimental designs, multi-modal integration of LEP and fMRI results can be carried out using data collected in separate, single-modality experiments. Second, because it shows that reliable LEPs can be recorded during a truly simultaneous collection of fMRI data, it demonstrates the possibility of performing EEG-driven analysis of fMRI data in pain research (see Sect. 21.5).

Christmann et al. (2007) recorded EEG and fMRI responses elicited by the electrical transcutaneous stimulation of the right thumb, and observed a good concordance

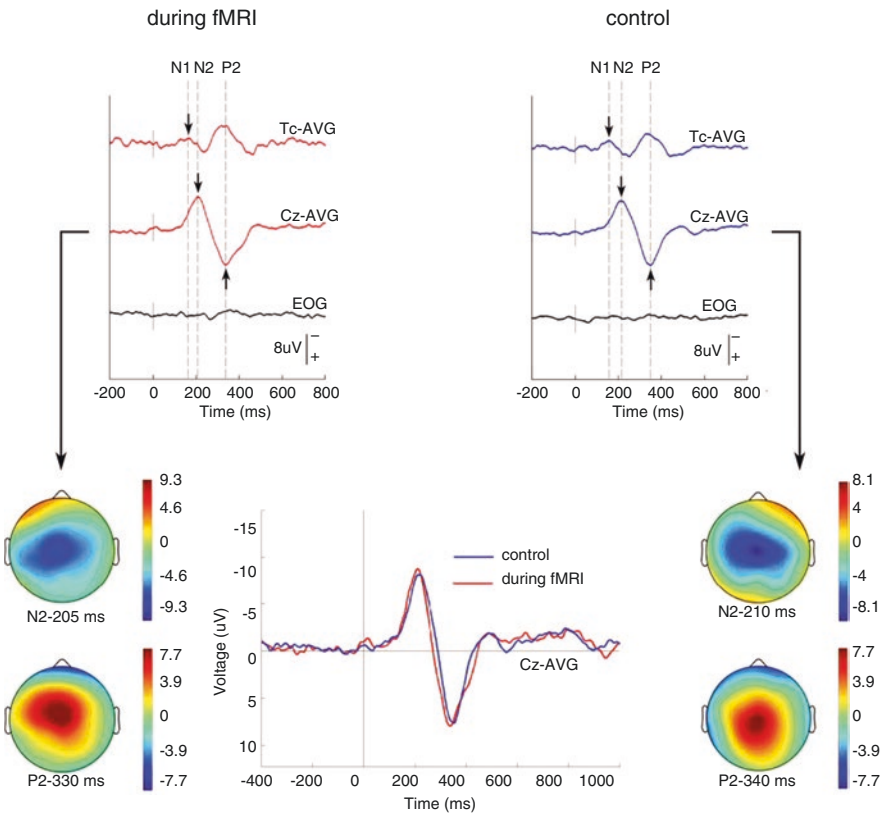

Fig. 21.1 Comparison between the grand-average waveforms (data from seven subjects) and scalp topographies of LEPs recorded during simultaneous and continuous fMRI at 3 T (left panel) and LEPs recorded in a control session outside the scanner room (right panel). The same recording equipment and experimental paradigm were used in both sessions. LEPs were elicited by stimulation (Nd:YAP laser) of the right-hand dorsum. Negativity is plotted upwards. Recordings from the vertex (Cz) and the temporal electrode contralateral to the stimulated side (Tc) are computed against average reference (AVG). Electro-oculogram was recorded to monitor eye-blinks. Arrows indicate early N1 and late N2–P2 components. Scalp topographies are shown at N2 and P2 peak latencies. Note the similarity between latencies, amplitudes, and scalp topographies of N2 and P2 waves obtained in the fMRI and in the control session (lower panel). (Reproduced from Iannetti et al., 2005, with permission)

between the strength and the location of the fMRI response and the modelled sources contributing to the ERP. However, for the reasons outlined in Sect. 21.3, the significance of this study is beset by two important limitations related to stimulus selectivity and experimental design. The first is due to the fact that the authors employed high-intensity electrical stimuli. Because non-nociceptive afferent fibers have a lower electrical activation threshold than nociceptive afferent fibers, these stimuli activated the full spectrum of peripheral fibers and were thus not selective for nociceptive afferents. The second is due to the fact that the authors, to avoid the contamination of EEG by MR-imaging artifacts, collected EEG and fMRI data in an *interleaved* manner. Therefore, both neuroimaging modalities did not sample the same neural activity, thus making the direct comparison of both responses less meaningful.

In summary, neither the study of Iannetti et al. (2005a) nor the study of Christmann et al. (2007) provide novel physiological information that could not have been obtained by recording EEG and fMRI brain responses in two separate experimental sessions.

Mobascher et al. (2009) simultaneously recorded EEG and fMRI-BOLD responses to painful laser stimuli in a group of 20 participants. Interestingly, they exploited the trial-by-trial variability in the elicited EEG responses to assess how different components of the laser-evoked EEG response may relate to stimulus-evoked changes in fMRI-BOLD activity. They found that variations in the amplitude of the laser-evoked P2 potential was related to variations in BOLD signal mainly in the ACC, as well as in deep structures such as the amygdala and thalamus. Mayhew et al. (2013) used a similar EEG-driven analysis of fMRI-BOLD signals, as well as an fMRI-driven analysis of EEG responses, exploiting natural trial-by-trial variability to characterize the relationship between fluctuations in pain ratings, fluctuations in pain-evoked EEG responses, and fluctuations in fMRI-BOLD signals. They showed that variability in pain-evoked fMRI responses is correlated with pain-evoked EEG responses. They also showed that pre-stimulus resting-state fMRI activity predicts the subsequent magnitude of stimulus-evoked pain ratings and EEG responses. Additionally, the power of the ongoing EEG alpha-band oscillation was related to this resting-state fMRI activity. The approaches developed in these two studies will be further discussed in Sect. 21.5.

21.5 Future Directions: EEG-Driven Analysis of fMRI-BOLD Responses to Nociceptive Stimulation

Whatever the neuroimaging modality, the magnitude of the activity elicited by the selective stimulation of nociceptive afferents displays a significant amount of trial-to-trial variability (Iannetti et al. 2005b; Purves and Boyd 1993). Most often, since this variability cannot be explained by identified experimental factors, it is discarded as physiologically meaningless noise. However, both the peripheral and central sources of this variability are likely to contain information that is physiologically relevant. Two peripheral factors contribute particularly to the variability of brain responses to nociceptive stimuli, namely the different number of afferents stimulated from trial to trial, and the significant variance in the conduction velocity of primary nociceptive afferents (Treede et al. 1998). Furthermore, an increasing

number of studies have shown that a great part of the variability of any given brain response results from dynamic fluctuations of the ongoing cortical activity (Arieli et al. 1996), possibly related to fluctuations of vigilance, expectation, and attentional focus, or changes in task strategy. Therefore, exploring the trial-to-trial variability of EEG and fMRI brain responses, as well as exploring its relationship with behavioural variables (e.g. intensity of perception, reaction-time latency), might provide important insights into the functional significance of the different processes that underlie these brain responses.

In the following section, we will show how the trial-to-trial variability of EEG responses can be used to drive the analysis of simultaneously recorded fMRI responses, and thereby establish relationships between temporally distinct peaks of the EEG response and spatially distinct clusters of the fMRI-BOLD response (Fig. 21.2).

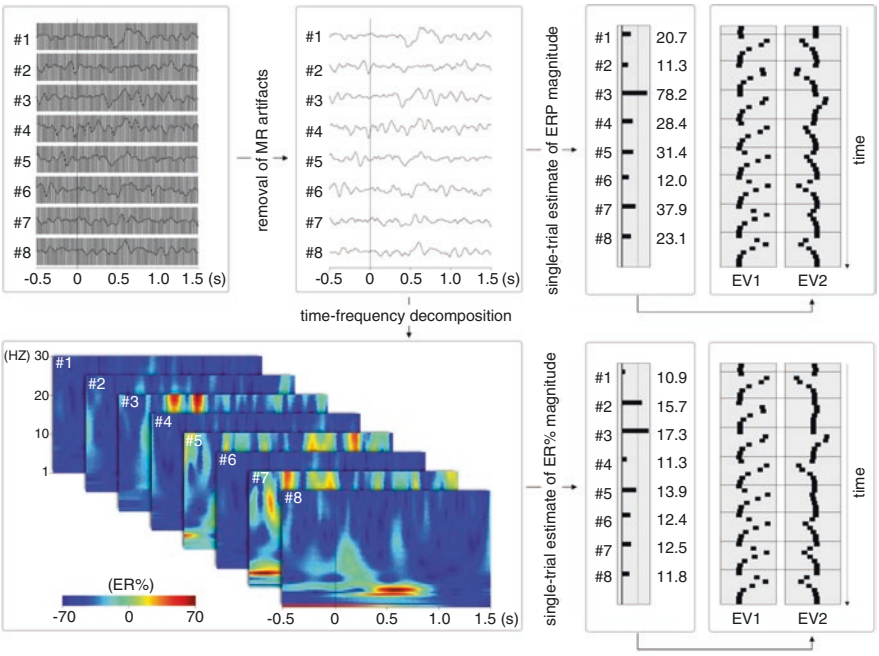

Fig. 21.2 Single-trial EEG-driven analysis of BOLD-fMRI brain responses to nociceptive stimulation. EEG and BOLD-fMRI data are recorded simultaneously and continuously. The peristimulus EEG recordings (−0.5 to +1.0 s relative to stimulus onset) are contaminated by severe MR-related artifacts. These artifacts are efficiently removed using a method based on a principal component analysis (Niazy et al. 2005). Once MR-related artifacts have been removed, different approaches can be used to quantify, within each single epoch, the magnitude of both phase-locked (i.e. ERPs; see also Fig. 21.3) and non-phase-locked (i.e. ERS and ERD; see also Fig. 21.4) EEG responses. Single-trial estimates of the magnitude of laser-evoked EEG responses are consequently used as regressors in the general linear model analysis of fMRI timeseries, to identify voxels whose BOLD signal time course correlates with the trial-to-trial variability of laser-evoked EEG responses. Two regressors are used for each single-subject analysis, one representing the mean amplitude of the EEG response (EV1) and the other representing the trial-to-trial variability of the EEG response (EV2)

We will (1) examine different methods to estimate the magnitude of stimulus-evoked EEG responses at the level of single trials, and (2) show how these different methods have been used recently to drive the analysis of simultaneously acquired fMRI data.

21.5.1 Single-Trial Estimation of the Magnitude of Stimulus-Evoked EEG Responses

A simple way to obtain a single-trial estimate of the magnitude of stimulus-evoked EEG responses consists of visually identifying and measuring a defined peak of activity within each single EEG epoch. This approach has been shown to be reasonably effective for nociceptive ERPs, as these are particularly of large amplitude (Iannetti et al. 2005b; Purves and Boyd 1993). However, this method has three important limitations: (1) it is prone to the introduction of involuntary biases by the observer, (2) it leads to an overestimation of response magnitude, since some single-trial estimates are likely to reflect the spurious detection of uncorrelated noise resembling the searched-for visual template, and (3) the obtained results are difficult to replicate, as they are observer-dependent.

Recently, Mayhew et al. (2006) showed that a multiple linear regression approach can be used to obtain an unbiased and accurate estimate of the latency and amplitude of single-trial nociceptive ERPs. In this method, a basis set of regressors and their temporal derivatives are obtained from the average ERP waveform. This basis set is then regressed against each single EEG epoch, thus providing a quantitative measure of latency and amplitude of the different peaks of the ERP waveform (Hu et al. 2010, 2011) (Fig. 21.3b). This methods has been subsequently refined by a preliminary wavelet filtering (Hu et al. 2010) and additional regressors to also model single-trial shape variability (Hu et al. 2011).

However, ERPs reflect only a fraction of the EEG response to a given stimulus. Indeed, the stimulus also triggers transient increases (ERS) and decreases (ERD) of the power of ongoing EEG oscillations. Identifying ERS and ERD requires to estimate the average time-varying power of EEG oscillations. This can be obtained by performing a joint time–frequency decomposition of EEG epochs using, for example, the continuous wavelet transform (see Fig. 21.4). ERS and ERD are subsequently identified by averaging time–frequency maps across trials. To estimate the magnitude of ERS and ERD at the level of single trials, approaches similar to those used to obtain single-trial estimates of the amplitude and latency of ERPs have been developed (Hu et al. 2015). Importantly, this approach has the potential to identify nociceptive-related EEG responses that correlate more closely with fMRI responses, because a number of studies have suggested that the BOLD-fMRI signal could, at least in other sensory modalities, be more tightly related with the occurrence of longer-lasting ERD and ERS.

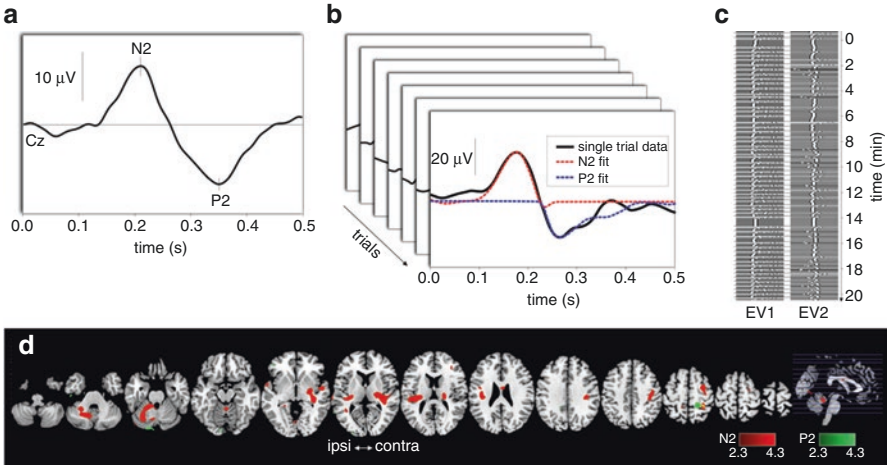

Fig. 21.3 Correlation between the trial-to-trial variability of LEPs and the simultaneously recorded BOLD-fMRI signal. EEG and fMRI responses to nociceptive laser stimuli were recorded simultaneously and continuously in five subjects. For each subject, 60 laser stimuli were applied to the left-hand dorsum, and 60 laser stimuli to the right-hand dorsum. Panel **a** shows the LEP waveform obtained by averaging peri-stimulus EEG epochs across trials (electrode Cz vs. nose reference, data from one representative subject). The response is characterized by a negative deflection (N2) followed by a positive deflection (P2). The average LEP waveform was used to create a set of four regressors formed by the N2 waveform, the P2 waveform, and their temporal derivatives (Mayhew et al. 2006). A multiple linear regression of the basis set of the four regressors against each single EEG epoch was used to model each single-trial ERP, and thus obtain an estimate of the amplitude and latency of N2 and P2 peaks in each single trial (panel **b**). The black waveform corresponds to a single representative EEG epoch. The red and green waveforms correspond to the automated fittings of the N2 and P2 deflections. The single-trial estimates of N2 and P2 amplitudes were subsequently used to create regressors and thereby investigate the correlation between the trial-to-trial variability of the N2 and P2 EEG peaks and the simultaneously and continuously recorded BOLD signal, using two separate single-subject analyses (one for each peak). For each analysis, two regressors were used (panel **c**). The first (EV1) represented the average amplitude of the peak of interest. The second (EV2) represented the trial-to-trial variability of the peak of interest. Panel **d** shows the results obtained at group level (the hemisphere ipsilateral to the stimulated side is shown on the left). Voxels whose BOLD signal time course was significantly correlated with the trial-to-trial variability of the N2 EEG peak are shown in red, while voxels whose time course was significantly correlated with the trial-to-trial variability of the P2 EEG peak are shown in green. Analysis was done using a mixed effects analysis and cluster-based thresholding ($z > 2.3$, $p < 0.05$). Note how the variability of the N2 peak correlates with the BOLD signal time course of voxels located in the ipsilateral and contralateral posterior insula. Also note how the variability of both the N2 and P2 peaks correlate with the BOLD signal time course of voxels located in the vicinity of the hand area of the contralateral primary somatosensory cortex

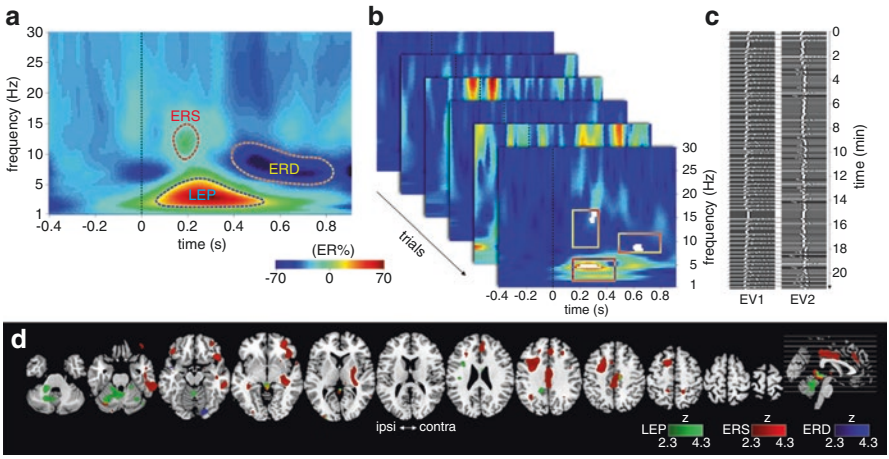

Fig. 21.4 Correlation between the trial-to-trial variability of laser-evoked EEG responses identified in the time–frequency domain and the simultaneously recorded BOLD-fMRI signal. EEG and BOLD-fMRI responses to nociceptive laser stimuli were recorded simultaneously and continuously in five subjects. For each subject, 60 laser stimuli were applied to the left-hand dorsum, and 60 laser stimuli to the right-hand dorsum. A time–frequency decomposition of each single EEG epoch (electrode Cz vs. nose reference) was performed using the continuous wavelet transform to generate a map of EEG oscillation power as a function of time and frequency. The maps are expressed as the percentage of change (ER%) relative to a pre-stimulus reference interval (−400 to −100 ms). Across-trial averaging of these maps (panel **a**) reveals both phase-locked LEPs and nonphase-locked laser-induced modulations of the power of ongoing EEG oscillations (ERS and ERD). Three time–frequency regions of interest (ROIs) were defined, centred around the locations of the three main foci of activity. (ROI-LEP: 150–450 ms and 1–5 Hz, ROI-ERS: 150–300 ms and 8–17 Hz; ROI-ERD: 500–800 ms and 8–12 Hz). Within each ROI, the mean of the 10% of pixels displaying the greatest increase (ROI-LEP and ROI-ERS) or decrease (ROI-ERD) in amplitude was calculated for each single EEG epoch (panel **b**). Single-trial estimates of LEP, ERS, and ERD magnitude were subsequently used to create regressors and thereby investigate the correlation between the trial-to-trial variability of each of the three laser-evoked EEG responses and the simultaneously recorded BOLD signal, using three separate single-subject analyses. For each analysis, two regressors were used (panel **c**). The first (EV1) represented the average amplitude of the EEG response. The second (EV2) represented the trial-to-trial variability of the EEG response. Panel **d** shows the results obtained at the group level (the hemisphere ipsilateral to the stimulated side is shown on the left). Voxels whose BOLD signal time course was significantly correlated with the trial-to-trial variability of ROI-LEP, ROI-ERS, and ROI-ERD are shown respectively in green, red, and blue. Analysis was done using a mixed effects analysis and cluster-based thresholding ($z > 2.3$, $p < 0.05$)

21.5.2 Correlation Between EEG and fMRI Responses at Single-Trial Level

The analysis steps required to extract physiologically relevant information embedded in the trial-to-trial variability of simultaneously acquired EEG and fMRI brain responses to nociceptive stimulation are outlined in Fig. 21.2. After the removal of the pulse and imaging artifact (Niazy et al. 2005), EEG signals are filtered and

segmented into peri-stimulus epochs. A continuous wavelet transform can be used to build a time–frequency matrix, expressing single-trial signal amplitude as a function of time and frequency. A single-trial estimate of EEG response magnitude is then obtained either from the original signal in the time domain (e.g. the amplitude of the N2 and P2 peaks at the vertex, estimated using a multiple linear regression approach; see Fig. 21.3b) or in the time–frequency domain (e.g. the percent increase or decrease of oscillation amplitude corresponding to a focus of ERS or ERD, estimated within a defined time–frequency region of interest; see Fig. 21.4b). These single-trial estimates of the magnitude of the EEG response are used to build a function of the predicted hemodynamic response, which is finally included as an additional column in the design matrix of the general linear model used to analyze the fMRI timeseries. This method allows identifying voxels whose variations in BOLD signal time course is predicted by the trial-to-trial variability of the measured EEG response. The same approach could be used to correlate the trial-to-trial variability of laser-evoked EEG responses with the fMRI-BOLD signal decomposed into a set of spatially independent maps and time courses using a spatial Probabilistic Independent Component Analysis (PICA; Beckmann and Smith 2004). PICA decomposes the fMRI data into a linear combination of independent spatio-temporal components (ICs), each hypothesized to reflect independent physical or physiological sources of BOLD signal change (Fig. 21.5). The approach has the advantage of allowing to correlate single-trial variability of EEG responses to physiologically relevant independent patterns of BOLD-fMRI activity (see also Bagshaw and Warbrick 2007). Finally, the same approach can be applied to the exploration of single-trial information that is not derived from the EEG, such as the energy of the eliciting sensory stimulus or the intensity of the perceived sensation (Niazy 2006). Such EEG-informed BOLD modelling approaches were recently exploited successfully in two EEG/fMRI studies on pain perception (Mayhew et al. 2013; Mobascher et al. 2009). Mobascher et al. (2009) delivered brief painful laser stimuli to the left-hand dorsum of 20 participants while simultaneously recording EEG and BOLD-fMRI. They then constructed two BOLD predictors using single-trial estimates of the N2 and P2 components of LEPs. The N2 regressor did not explain additional variance in BOLD signals throughout the brain. However, the regressor derived from the single-trial estimates of P2 amplitude did explain variance in set of brain regions including the ACC, the precuneus, the right operculo-insular region, the thalamus, and the right amygdala (Fig. 21.6). By showing that the P2 wave is related to activity originating from these specific brain structures, these findings provide new insight into the functional significance of the different components of nociceptive ERPs and, more generally, on how nociceptive input is processed in the human brain. Mayhew et al. (2013) recorded simultaneously EEG/fMRI data in 16 patients, while they were receiving brief contact heat stimuli, to investigate the relationship between single-trial BOLD responses, EEG responses, pre-stimulus amplitude of alpha-band EEG oscillations, pre-stimulus resting-state BOLD activity, and pain perception. They observed that pre- and peri-stimulus BOLD signals in the so-called default mode network (DMN) was related to the magnitude of the pain-evoked brain response sampled using fMRI and EEG, as well as subjective pain ratings. Pre-stimulus amplitude of alpha-band EEG oscillations was correlated with

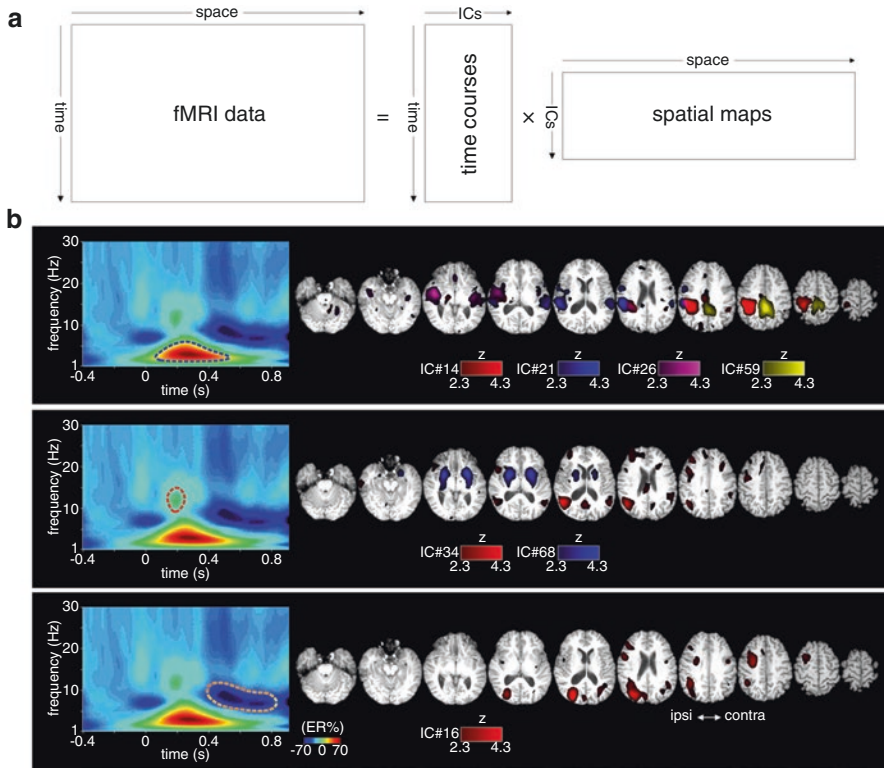

Fig. 21.5 Correlation between the trial-to-trial variability of laser-evoked EEG responses and the BOLD-fMRI signal decomposed into a set of spatially independent maps and time courses using a spatial Probabilistic Independent Component Analysis (PICA; Beckmann and Smith 2004). EEG and BOLD-fMRI responses to nociceptive laser stimuli were recorded simultaneously and continuously in five subjects. For each subject, 60 laser stimuli were applied to the left-hand dorsum, and 60 laser stimuli to the right-hand dorsum. PICA was used to decompose the fMRI data into a linear combination of independent spatio-temporal components (ICs), each reflecting an independent physical or physiological source of BOLD signal change (panel **a**). A time–frequency decomposition of EEG epochs (electrode Cz vs. nose reference) was used to obtain single-trial estimates of phase-locked (LEP) and non-phase-locked (ERS and ERD) EEG responses (see Fig. 21.4 for details). These single-trial estimates were subsequently used to create regressors and thereby investigate the correlation between the trial-to-trial variability of each of these three laser-evoked EEG responses and the time course of each IC. Panel **b** shows the results obtained in one representative subject. The spatial maps of ICs whose time courses were significantly ($p < 0.01$) correlated with the trial-to-trial variability of the LEP response, the ERS response, and the ERD response are shown in the upper, middle, and lower row, respectively. Note how the variability of the LEP response (panel **b**, top row) correlates with the temporal profile of ICs located in the contralateral insular cortex (purple), secondary somatosensory cortex (blue), and in the hand area of the primary somatosensory cortex (red), while the ERS response (panel **b**, middle row) correlates with the temporal profile of ICs located in the deep insular cortex bilaterally. In contrast, the variability of the ERD response (panel **b**, bottom row) correlates with the temporal profile of ICs located in posterior brain regions (red)

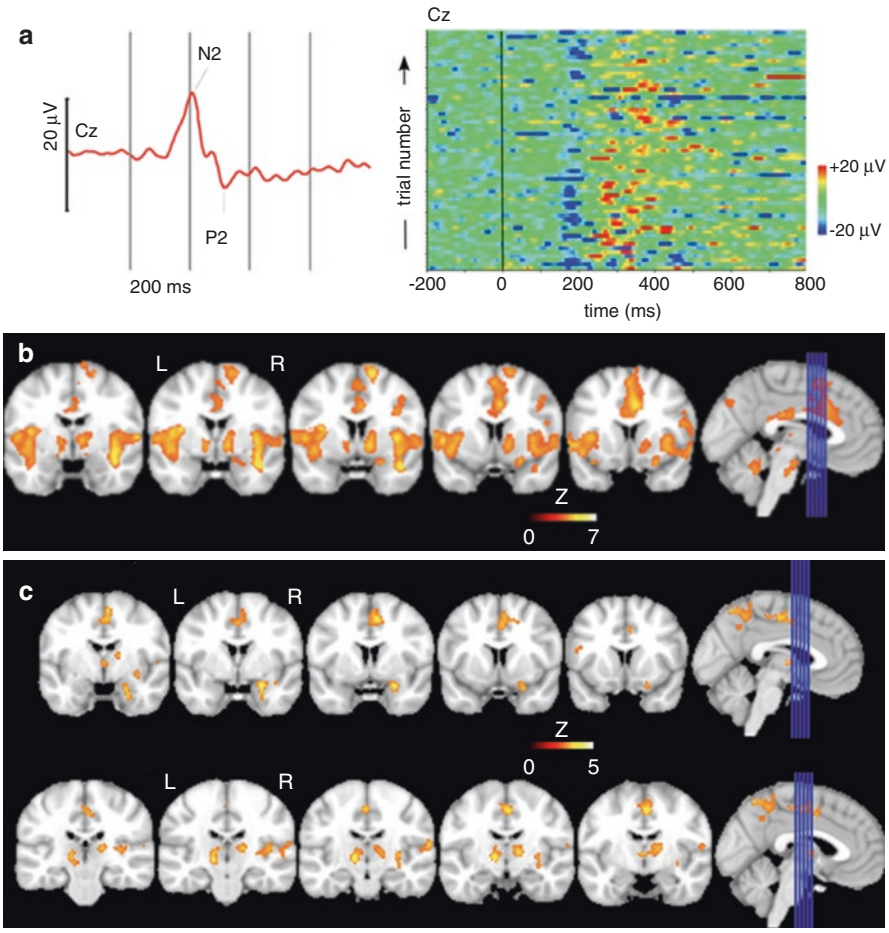

Fig. 21.6 EEG-informed modelling of pain-evoked BOLD-fMRI brain responses. Simultaneous EEG and fMRI data were collected in 20 participants exposed to transient laser heat stimuli delivered to the left-hand dorsum. (**a**) LEPs sampled using EEG. The left graph shows the group-level average response recorded at electrode Cz. The right graph shows single-trial EEG responses recorded in a single participant. Note the trial-by-trial variability in magnitude and latency of the negative N2 wave (blue response approximately 200 ms after stimulus onset) and the positive P2 wave (red response approximately 300–400 ms after stimulus onset). (**b**) Whole-brain analysis of the fMRI-BOLD response to laser stimulation. (**c**) Whole-brain analysis of the fMRI-BOLD signal variance explained by the trial-to-trial variations in P2 amplitude. Note that there is only partial overlap between the cortical and subcortical regions shown in **b** and **c**, indicating that the P2 wave could be related to a subset of the brain regions typically activated by painful stimuli. (Adapted from Mobascher et al. (2009))

the amplitude of both the DMN-related BOLD signals, and stimulus-evoked EEG responses. Taken together, these results provide new insight into the dynamics of ongoing brain activity and how these may influence the processing of nociceptive input and pain perception.

Acknowledgments G.D. Iannetti is supported by the European Research Council (Consolidator Grant PAINSTRAT) and the Wellcome Trust (COLL JLARAXR).

References

Allen PJ, Josephs O, Turner R (2000) A method for removing imaging artifact from continuous EEG recorded during functional MRI. Neuroimage 12:230–239

Apkarian AV, Bushnell MC, Treede RD, Zubieta JK (2005) Human brain mechanisms of pain perception and regulation in health and disease. Eur J Pain 9:463–484

Arieli A, Sterkin A, Grinvald A, Aertsen A (1996) Dynamics of ongoing activity: explanation of the large variability in evoked cortical responses. Science 273:1868–1871

Bagshaw AP, Warbrick T (2007) Single trial variability of EEG and fMRI responses to visual stimuli. Neuroimage 38:280–292

Bandettini PA, Kwong KK, Davis TL, Tootell RB, Wong EC, Fox PT, Belliveau JW, Weisskoff RM, Rosen BR (1997) Characterization of cerebral blood oxygenation and flow changes during prolonged brain activation. Hum Brain Mapp 5:93–109

Baumgartner U, Cruccu G, Iannetti GD, Treede RD (2005) Laser guns and hot plates. Pain 116:1–3

Beckmann CF, Smith SM (2004) Probabilistic independent component analysis for functional magnetic resonance imaging. IEEE Trans Med Imaging 23:137–152

Bonmassar G, Hadjikhani N, Ives JR, Hinton D, Belliveau JW (2001) Influence of EEG electrodes on the BOLD fMRI signal. Hum Brain Mapp 14:108–115

Bromm B, Chen AC (1995) Brain electrical source analysis of laser evoked potentials in response to painful trigeminal nerve stimulation. Electroencephalogr Clin Neurophysiol 95:14–26

Carmon A, Mor J, Goldberg J (1976) Evoked cerebral responses to noxious thermal stimuli in humans. Exp Brain Res 25:103–107

Chen AC, Niddam DM, Arendt-Nielsen L (2001) Contact heat evoked potentials as a valid means to study nociceptive pathways in human subjects. Neurosci Lett 316:79–82

Christmann C, Ruf M, Braus DF, Flor H (2002) Simultaneous electroencephalography and functional magnetic resonance imaging of primary and secondary somatosensory cortex in humans after electrical stimulation. Neurosci Lett 333:69–73

Christmann C, Koeppe C, Braus DF, Ruf M, Flor H (2007) A simultaneous EEG-fMRI study of painful electric stimulation. Neuroimage 34:1428–1437

Davis KD, Kwan CL, Crawley AP, Mikulis DJ (1998) Event-related fMRI of pain: entering a new era in imaging pain. Neuroreport 9:3019–3023

De Keyser R, van den Broeke EN, Courtin A, Dufour A, Mouraux A (2018) Event-related brain potentials elicited by high-speed cooling of the skin: a robust and non-painful method to assess the spinothalamic system in humans. Clin Neurophysiol 129:1011–1019

Frot M, Mauguiere F (2003) Dual representation of pain in the operculo-insular cortex in humans. Brain 126:438–450

Garcia-Larrea L, Frot M, Valeriani M (2003) Brain generators of laser-evoked potentials: from dipoles to functional significance. Neurophysiol Clin 33:279–292

Garreffa G, Bianciardi M, Hagberg GE, Macaluso E, Marciani MG, Maraviglia B, Abbafati M, Carni M, Bruni I, Bianchi L (2004) Simultaneous EEG-fMRI acquisition: how far is it from being a standardized technique? Magn Reson Imaging 22:1445–1455

Greffrath W, Baumgartner U, Treede RD (2007) Peripheral and central components of habituation of heat pain perception and evoked potentials in humans. Pain 132:301–311

Hamandi K, Laufs H, Noth U, Carmichael DW, Duncan JS, Lemieux L (2008) BOLD and perfusion changes during epileptic generalised spike wave activity. Neuroimage 39:608–618

Hu L, Mouraux A, Hu Y, Iannetti GD (2010) A novel approach for enhancing the signal-to-noise ratio and detecting automatically event-related potentials (ERPs) in single trials. NeuroImage 50(1):99–111. S105381190901297X. https://doi.org/10.1016/j.neuroimage.2009.12.010

Hu L, Liang M, Mouraux A, Wise RG, Hu Y, Iannetti GD (2011) Taking into account latency amplitude and morphology: improved estimation of single-trial ERPs by wavelet filtering

and multiple linear regression. J Neurophysiol 106(6):3216–3229. https://doi.org/10.1152/jn.00220.2011
Hu L, Cai MM, Xiao P, Luo F, Iannetti GD (2014) Human brain responses to concomitant stimulation of Aδ and C nociceptors. J Neurosci 34(34):11439–11451. https://pubmed.ncbi.nlm.nih.gov/25143623/
Hu L, Zhang ZG, Mouraux A, Iannetti GD (2015) Multiple linear regression to estimate time-frequency electrophysiological responses in single trials. Neuroimage 111:442–453
Iannetti GD, Mouraux A (2010) From the neuromatrix to the pain matrix (and back). Exp Brain Res 205:1–12
Iannetti GD, Leandri M, Truini A, Zambreanu L, Cruccu G, Tracey I (2004) Adelta nociceptor response to laser stimuli: selective effect of stimulus duration on skin temperature, brain potentials and pain perception. Clin Neurophysiol 115:2629–2637
Iannetti GD, Niazy RK, Wise RG, Jezzard P, Brooks JC, Zambreanu L, Vennart W, Matthews PM, Tracey I (2005a) Simultaneous recording of laser-evoked brain potentials and continuous, high-field functional magnetic resonance imaging in humans. Neuroimage 28:708–719. https://pubmed.ncbi.nlm.nih.gov/16112589/
Iannetti GD, Zambreanu L, Cruccu G, Tracey I (2005b) Operculoinsular cortex encodes pain intensity at the earliest stages of cortical processing as indicated by amplitude of laser-evoked potentials in humans. Neuroscience 131:199–208
Iannetti GD, Zambreanu L, Tracey I (2006) Similar nociceptive afferents mediate psychophysical and electrophysiological responses to heat stimulation of glabrous and hairy skin in humans. J Physiol 577:235–248
Iannetti GD, Wise RG (2007) BOLD functional MRI in disease and pharmacological studies: room for improvement? Magn Reson Imaging 25(6):978–988. https://pubmed.ncbi.nlm.nih.gov/17499469/
Iannetti G, Hughes NP, Lee MC, Mouraux A (2008) The determinants of laser-evoked EEG responses: pain perception or stimulus saliency? J Neurophysiol 100:815–828
Iannetti GD, Baumgartner U, Tracey I, Treede RD, Magerl W (2013) Pinprick-evoked brain potentials: a novel tool to assess central sensitization of nociceptive pathways in humans. J Neurophysiol 110:1107–1116
Inui K, Tran TD, Hoshiyama M, Kakigi R (2002) Preferential stimulation of Adelta fibers by intraepidermal needle electrode in humans. Pain 96:247–252
Julius D, Basbaum AI (2001) Molecular mechanisms of nociception. Nature 413:203–210
Krakow K, Allen PJ, Symms MR, Lemieux L, Josephs O, Fish DR (2000) EEG recording during fMRI experiments: image quality. Hum Brain Mapp 10:10–15
Kunde V, Treede RD (1993) Topography of middle-latency somatosensory evoked potentials following painful laser stimuli and non-painful electrical stimuli. Electroencephalogr Clin Neurophysiol 88:280–289
Kwong KK, Belliveau JW, Chesler DA, Goldberg IE, Weisskoff RM, Poncelet BP, Kennedy DN, Hoppel BE, Cohen MS, Turner R et al (1992) Dynamic magnetic resonance imaging of human brain activity during primary sensory stimulation. Proc Natl Acad Sci U S A 89:5675–5679
Laufs H, Krakow K, Sterzer P, Eger E, Beyerle A, Salek-Haddadi A, Kleinschmidt A (2003) Electroencephalographic signatures of attentional and cognitive default modes in spontaneous brain activity fluctuations at rest. Proc Natl Acad Sci U S A 100:11053–11058
Lee AT, Glover GH, Meyer CH (1995) Discrimination of large venous vessels in time-course spiral blood-oxygen-level-dependent magnetic-resonance functional neuroimaging. Magn Reson Med 33:745–754
Lee MC, Mouraux A, Iannetti GD (2008) Characterizing the cortical activity related to the emergence of a conscious painful experience. In: 6th FENS Forum of European Neuroscience, Geneva, Switzerland
Lemieux L, Allen PJ, Franconi F, Symms MR, Fish DR (1997) Recording of EEG during fMRI experiments: patient safety. Magn Reson Med 38:943–952
Lewis T, Ponchin EE (1937) The double pain response of the human skin to a single stimulus. Clin Sci 3:67–76
Liberati G, Klocker A, Safronova MM, Ferrao Santos S, Ribeiro Vaz JG, Raftopoulos C, Mouraux A (2016) Nociceptive local field potentials recorded from the human insula are not specific for nociception. PLoS Biol 14:e1002345

Liberati G, Algoet M, Klocker A, Ferrao Santos S, Ribeiro-Vaz JG, Raftopoulos C, Mouraux A (2018) Habituation of phase-locked local field potentials and gamma-band oscillations recorded from the human insula. Sci Rep 8:8265

Lui F, Duzzi D, Corradini M, Serafini M, Baraldi P, Porro CA (2008) Touch or pain? Spatio-temporal patterns of cortical fMRI activity following brief mechanical stimuli. Pain 138:362

Malonek D, Grinvald A (1996) Interactions between electrical activity and cortical microcirculation revealed by imaging spectroscopy: implications for functional brain mapping. Science 272:551–554

Mayhew SD, Iannetti GD, Woolrich MW, Wise RG (2006) Automated single-trial measurement of amplitude and latency of laser-evoked potentials (LEPs) using multiple linear regression. Clin Neurophysiol 117:1331–1344

Mayhew SD, Hylands-White N, Porcaro C, Derbyshire SWG, Bagshaw AP (2013) Intrinsic variability in the human response to pain is assembled from multiple, dynamic brain processes. Neuroimage 75:68–78

Melzack R (1999) From the gate to the neuromatrix. Pain Suppl 6:S121–S126

Menon RS, Goodyear BG (2001) Spatial and temporal resolution in fMRI. In: Jezzard P, Matthews PM, Smith SM (eds) Functional MRI an introduction to methods. Oxford University Press, Oxford, pp 145–158

Michel CM, Murray MM, Lantz G, Gonzalez S, Spinelli L, Grave De Peralta R (2004) EEG source imaging. Clin Neurophysiol 115:2195–2222

Mobascher A, Brinkmeyer J, Warbrick T, Musso F, Wittsack HJ, Saleh A, Schnitzler A, Winterer G (2009) Laser-evoked potential P2 single-trial amplitudes covary with the fMRI BOLD response in the medial pain system and interconnected subcortical structures. Neuroimage 45:917–926

Mouraux A, Iannetti G (2009) Laser-evoked potentials do not reflect nociceptive-specific brain activity. In: 6th FENS Forum of European Neuroscience, July 12–16, Geneva, Switzerland. https://pubmed.ncbi.nlm.nih.gov/19339457/

Mouraux A, Iannetti GD (2008) A review of the evidence against the "first come first served" hypothesis. Comment on Truini et al. [Pain 2007;131:43-7]. Pain 136:219–221. author reply 222-213. https://pubmed.ncbi.nlm.nih.gov/19339457/

Mouraux A, Iannetti GD (2018) The search for pain biomarkers in the human brain. Brain 141:3290–3307

Mouraux A, Guerit JM, Plaghki L (2004) Refractoriness cannot explain why C-fiber laser-evoked brain potentials are recorded only if concomitant Adelta-fiber activation is avoided. Pain 112:16–26

Mouraux A, Iannetti GD, Plaghki L (2010) Low intensity intra-epidermal electrical stimulation can activate Aδ-nociceptors selectively. Pain 150:199–207

Mulert C, Jäger L, Schmitt R, Bussfeld P, Pogarell O, Möller HJ, Juckel G, Hegerl U (2004) Integration of fMRI and simultaneous EEG: towards a comprehensive understanding of localization and time-course of brain activity in target detection. Neuroimage 22:83–94

Nebel K, Stude P, Wiese H, Muller B, de Greiff A, Forsting M, Diener HC, Keidel M (2005) Sparse imaging and continuous event-related fMRI in the visual domain: a systematic comparison. Hum Brain Mapp 24:130–143

Niazy RK (2006) Simultaneous electroencephalography and functional MRI: methods and applications. Doctoral Dissertation. Univeristy of Oxford, Oxford

Niazy RK, Beckmann CF, Iannetti GD, Brady JM, Smith SM (2005) Removal of FMRI environment artifacts from EEG data using optimal basis sets. Neuroimage 28:720–737

Nunez PL, Srinivasan R (2006) Electric fields of the brain. In: The Neurophysics of EEG, 2nd edn. Oxford University Press, New York

Ogawa S, Tank DW, Menon R, Ellermann JM, Kim SG, Merkle H, Ugurbil K (1992) Intrinsic signal changes accompanying sensory stimulation: functional brain mapping with magnetic resonance imaging. Proc Natl Acad Sci U S A 89:5951–5955

Ozcan M, Baumgartner U, Vucurevic G, Stoeter P, Treede RD (2005) Spatial resolution of fMRI in the human parasylvian cortex: comparison of somatosensory and auditory activation. Neuroimage 25:877–887

Peyron R, Garcia-Larrea L, Gregoire MC, Costes N, Convers P, Lavenne F, Mauguiere F, Michel D, Laurent B (1999) Haemodynamic brain responses to acute pain in humans: sensory and attentional networks. Brain 122(Pt 9):1765–1780

Plaghki L, Mouraux A (2003) How do we selectively activate skin nociceptors with a high power infrared laser? Physiology and biophysics of laser stimulation. Neurophysiol Clin 33:269–277
Ploner M, Gross J, Timmermann L, Schnitzler A (2002) Cortical representation of first and second pain sensation in humans. Proc Natl Acad Sci U S A 99:12444–12448
Purves AM, Boyd SG (1993) Time-shifted averaging for laser evoked potentials. Electroencephalogr Clin Neurophysiol 88:118–122
Raij TT, Vartiainen NV, Jousmaki V, Hari R (2003) Effects of interstimulus interval on cortical responses to painful laser stimulation. J Clin Neurophysiol 20:73–79
Regan D (1989) Human brain electrophysiology. In: Evoked potentials and evoked magnetic fields in science and medicine. Elsevier, New York
Robson MD, Dorosz JL, Gore JC (1998) Measurements of the temporal fMRI response of the human auditory cortex to trains of tones. Neuroimage 7:185–198
Rogers R, Wise RG, Painter DJ, Longe SE, Tracey I (2004) An investigation to dissociate the analgesic and anesthetic properties of ketamine using functional magnetic resonance imaging. Anesthesiology 100:292–301
Slugg RM, Campbell JN, Meyer RA (2004) The population response of A- and C-fiber nociceptors in monkey encodes high-intensity mechanical stimuli. J Neurosci 24:4649–4656
Somervail R, Zhang F, Novembre G, Bufacchi RJ, Guo Y, Crepaldi M, Hu L, Iannetti GD (2021) Waves of change: brain sensitivity to differential not absolute stimulus intensity is conserved across humans and rats. Cerebral Cortex 31(2):949–960. https://doi.org/10.1093/cercor/bhaa267
Somervail R, Bufacchi RJ, Salvatori C, Neary-Zajiczek L, Guo Y, Novembre G, Iannetti GD (2022) Brain responses to surprising stimulus offsets: phenomenology and functional significance. Cerebral Cortex 32(10):2231–2244. https://doi.org/10.1093/cercor/bhab352
Speckmann E, Elger C (1999) Introduction to the neurophysiological basis of the EEG and DC potentials. In: Niedermeyer E, Lopes da Silva F (eds) Electroencephalography. Basic principles, clinical applications, and related fields. Lippincott Williams & Wilkins, Baltimore, pp 15–27
Tarkka IM, Treede RD (1993) Equivalent electrical source analysis of pain-related somatosensory evoked potentials elicited by a CO2 laser. J Clin Neurophysiol 10:513–519
Tracey I, Mantyh PW (2007) The cerebral signature for pain perception and its modulation. Neuron 55:377–391
Treede RD, Kief S, Holzer T, Bromm B (1988) Late somatosensory evoked cerebral potentials in response to cutaneous heat stimuli. Electroencephalogr Clin Neurophysiol 70:429–441
Treede RD, Meyer RA, Raja SN, Campbell JN (1995) Evidence for two different heat transduction mechanisms in nociceptive primary afferents innervating monkey skin. J Physiol 483(Pt 3):747–758
Treede RD, Meyer RA, Campbell JN (1998) Myelinated mechanically insensitive afferents from monkey hairy skin: heat-response properties. J Neurophysiol 80:1082–1093
Treede RD, Lorenz J, Baumgartner U (2003) Clinical usefulness of laser-evoked potentials. Neurophysiol Clin 33:303–314
Truini A, Rossi P, Galeotti F, Romaniello A, Virtuoso M, De Lena C, Leandri M, Cruccu G (2004) Excitability of the Adelta nociceptive pathways as assessed by the recovery cycle of laser evoked potentials in humans. Exp Brain Res 155:120–123
Truini A, Galeotti F, Romaniello A, Virtuoso M, Iannetti GD, Cruccu G (2005) Laser-evoked potentials: normative values. Clin Neurophysiol 116:821–826
Valentini E, Hu L, Chakrabarti B, Hu Y, Aglioti SM, Iannetti GD (2012) The primary somatosensory cortex largely contributes to the early part of the cortical response elicited by nociceptive stimuli. Neuroimage 59:1571–1581
Wehrle R, Kaufmann C, Wetter TC, Holsboer F, Auer DP, Pollmacher T, Czisch M (2007) Functional microstates within human REM sleep: first evidence from fMRI of a thalamocortical network specific for phasic REM periods. Eur J Neurosci 25:863–871
Wise RG, Rogers R, Painter D, Bantick S, Ploghaus A, Williams P, Rapeport G, Tracey I (2002) Combining fMRI with a pharmacokinetic model to determine which brain areas activated by painful stimulation are specifically modulated by remifentanil. Neuroimage 16:999–1014

Simultaneous Electroencephalography and Functional Magnetic Resonance Imaging of the Human Auditory System

22

Johannes Vosskuhl, Christoph S. Herrmann, André Brechmann, and Henning Scheich

22.1 Introduction

When trying to examine the physiological correlates of cognitive functions, human neuroscience is restricted to non-invasive measures when dealing with healthy subjects. Correlates of cognitive brain processes are present in electromagnetic fields and hemodynamic responses which can be recorded with electroencephalography (EEG) and functional magnetic resonance imaging (fMRI), respectively. While EEG offers a temporal resolution on the millisecond time scale, intracranial sources of activity must be inferred from extracranial recordings—a phenomenon referred to as the inverse problem. FMRI offers a spatial resolution on the millimeter scale but suffers from a suboptimal temporal resolution, since the blood oxygen dependent (BOLD) signal is an indirect hemodynamic consequence of electrical brain activity.

Combining EEG and fMRI promises to integrate the good temporal resolution of EEG with the good spatial resolution of fMRI (for reviews, see Debener et al. 2006; Herrmann and Debener 2008; Huster et al. 2012; Menon and Crottaz-Herbette

J. Vosskuhl
Experimental Psychology Lab, Department of Psychology, European Medical School, Carl von Ossietzky University, Oldenburg, Germany
e-mail: j.vosskuhl@uol.de

C. S. Herrmann (✉)
Experimental Psychology Lab, Department of Psychology, European Medical School, Carl von Ossietzky University, Oldenburg, Germany

Research Center Neurosensory Science, University of Oldenburg, Oldenburg, Germany
e-mail: christoph.herrmann@uol.de

A. Brechmann · H. Scheich
Center for Behavioural Brain Science, Magdeburg, Germany

Leibniz-Institute for Neurobiology, Magdeburg, Germany
e-mail: andre.brechmann@lin-magdeburg.de; henning.scheich@lin-magdeburg.de

C. Mulert, L. Lemieux (eds.), *EEG - fMRI*,
https://doi.org/10.1007/978-3-031-07121-8_22

2005). However, it has to be noted that some authors have questioned the implicit assumption that both measures pick up more or less the same neural activity. A number of studies have demonstrated that EEG and BOLD responses do not reflect identical neural activity, which has resulted in the notion of "EEG signals without fMRI correlates" and vice versa (Huster et al. 2012; Ritter and Villringer 2006). Such a case could occur when two sources of an EEG signal merely synchronize at no metabolic cost. Then, a change in the EEG signal would be measured without a BOLD signal change. The opposite case can happen if two neural sources change their activity, which would result in a detectable BOLD signal, but their electrical trace on the scalp cancels out.

EEG and fMRI setups are both complicated technical environments requiring sophisticated hard- and software as well as skilled personnel for operation. Thus, even slight disturbances such as a nearby electromechanical device in EEG or metal parts inside the MR scanner may result in severe artifacts and corrupted signal quality. Therefore, the recording of EEG signals inside the MR scanner certainly compromises EEG signal quality (e.g., Warbrick and Bagshaw 2008) and can also affect the quality of MR images (e.g., Mullinger et al. 2008).

Two types of artifacts obscure EEG data when recording inside an MR scanner. The first is the so-called cardioballistic artifact. It is related to the cardiac cycle and scales in amplitude proportionally to the magnetic field strength (Debener et al. 2008). It is commonly agreed that the cardioballistic artifact is related to the pulsatile movement of the head and/or the pulsatile movement of EEG electrodes. It is, therefore, also referred to as the pulse artifact. EEG electrodes and EEG leads are conductive, and the movement of conductive material in a static magnetic field induces a current which is picked up by the EEG. Numerous articles deal with this artifact and meanwhile offer effective mechanisms to correct for it (see e.g. Bonmassar et al. 2002; Debener et al. 2007; Ellingson et al. 2004; Niazy et al. 2005). Two fundamentally different approaches have been established for the correction of the cardioballistic, artifact: First, the subtraction of an artifact template separately for each channel, second, separating the source of the cardioballistic artifact from internal (EEG) sources using for example independent component analysis (ICA). A comparison of these two major approaches revealed that both are successful in correcting the artifact but the first cluster of methods appeared to be more convenient to use, especially for unexperienced users (see Vanderperren et al. 2010 for more details). Currently, a technical approach to the problem has been suggested where additional carbon wire loops are used as additional sensors to track and correct these artifacts (van der Meer et al. 2016).

The second type of artifact is caused by the MRI gradient switching and radio frequency (RF) pulses and is referred to as gradient artifact (GA). This artifact is limited to the time required to acquire these images. For many purposes, the GA can be avoided by recording EEG and fMRI data interleaved with each other (see "sparse sampling" below). However, even in the case of temporally overlapping EEG recording and acquisition of MR slices, the artifact can be corrected by adequate software algorithms (see e.g. Allen et al. 2000; Felblinger et al. 1999; Ritter et al. 2007; Sijbersa et al. 2000).

A different category of artifacts has meanwhile been described, which is related to specific scanner hardware such as the helium pump (Rothlübbers et al. 2014) or the ventilation system (Nierhaus et al. 2013). Both of which are less well investigated and thus correction methods are less well developed (See Rothlübbers et al. (2014) and van der Meer et al. (2016) for methods to correct the helium pump artifact). Generally, if possible, ventilation inside the scanner bore and the helium pump should be switched off during EEG-fMRI measurements.

Using the above-mentioned techniques has become fairly convenient as some of them have been implemented in widely available software packages. Despite the feasibility and elegance of simultaneously recording EEG and BOLD responses and the potential insights to be gained with this method, it should be noted that many research questions do not require such a technically challenging approach. Whenever it is sufficient to have subjects perform a task twice, it is much more convenient to have them do the two types of recordings separately. In many cases, even one of the two measurements may suffice to answer relevant research questions.

22.2 Specifics of Auditory Recordings

The scanner environment is especially unsuitable for auditory experiments requiring a number of special hardware and software solutions. At least the following three problems are specific to auditory experiments and shall be addressed in the sequel:

- The static magnetic field interferes with auditory equipment.
- The transient magnetic fields generate noise, which interferes with auditory perception and in turn with cognitive processing.
- The scanner noise generates a BOLD response which needs to be differentiated from the auditory response to the acoustic stimuli.

Further details of problems with auditory experiments inside MR scanners are discussed in valuable review articles (McJury and Shellock 2000; Moelker and Pattynama 2003; Palmer et al. 2006; Peelle 2014).

22.2.1 Interference of the Static Magnetic Field

To begin with, there is a strong magnetic field, which precludes the use of standard auditory equipment such as headphones. The static magnetic fields of commercially available scanners currently range from 1 to 7 Tesla. No ferromagnetic devices can be brought into the scanner, since they would be attracted by the magnet and could potentially result in accidents. Thus, standard headphones with metallic leads cannot be operated inside a scanner. In addition, the transient magnetic fields used for slice selection and readout would induce currents in metallic leads, which in turn would produce undesired sounds in the headphones. A preliminary but suboptimal

solution has been the design of air-pressure devices as they are also used in magnetoencephalography. Unfortunately, these devices sometimes show problems such as asymmetric levels.

Today, a number of special sound delivery devices have been designed and made commercially available, which can cope with the hostile conditions and are sufficiently precise for auditory experiments (Baumgart et al. 1998; Palmer et al. 1998; Norman-Haignere and McDermott 2016). These devices use non-magnetic copper wires and piezoelectric or electrostatic earphones, thus overcoming the problems of air-pressure headphones.

22.2.2 Interference of Transient Magnetic Fields

More importantly, the sound which is created by the scanner interferes with the perception of auditory stimuli. The flow of electric current induces a magnetic field surrounding the conductor. If the conductor lies within a magnetic field, a force acts upon the conductor, which is the so-called Lorentz force. This is the case for the gradient coil of an MR scanner which generates the transient magnetic fields for slice selection and readout. This Lorentz force deforms the gradient coils. That deformation propagates to the surrounding air, generating a noise similar to the case when the membrane of a loudspeaker is being moved (Mansfield et al. 1998). This scanner noise scales with the field strength of the scanner (Price et al. 2001) and usually exceeds 100 dB sound pressure level requiring a shielding from the subjects' ears by earplugs and/or appropriate headphones to avoid damage to the hearing system. Note, however, that hearing protection, even if perfect at the outer ear, does not prevent bone conduction of the scanner noise.

Thus, even with significant suppression by hearing protection, the remaining noise still interferes with auditory perception in different ways. Scanner noise may physically mask experimental stimuli if presented simultaneously, thus preventing subjects from perceiving stimuli when presented during fMRI measurement. Additionally, more cognitive effort must be engaged to process the presented stimuli as can be seen from research on speech in noise (Scott and McGettigan 2013). In their review, Scott and McGettigan illustrate how speech-in-noise stimuli recruit additional prefrontal and parietal areas when compared with unmasked speech stimuli. A scenario that seems directly transferrable to auditory experiments in noisy environments such as an MRI-scanner. Furthermore, it has been suggested that continuous echo planar imaging (EPI) noise when compared with sparse imaging may reduce left lateralized activity in the superior temporal gyrus during word processing (Gaab et al. 2007). However, this interpretation could not be confirmed in a sound intensity categorization task that was shown to be left lateralized independent of the used fMRI sequence, i.e. continuous EPI vs. low-noise FLASH sequence (Angenstein et al. 2016).

Scanner noise not only affects cognitive performance but also physiological signals from the brain. It has been demonstrated that the noise of the MR scanner's EPI sequences results in significant changes of subjects' auditory MEG responses

during an auditory experiment (Herrmann et al. 2000) and similar findings have been obtained for ERPs (Novitski et al. 2001, 2003). Thus, specific experimental paradigms suited for recording inside an MR scanner have to be designed. A few studies offering solutions to these problems will be reviewed below.

22.2.3 BOLD Response to Scanner Noise

A further problem for auditory fMRI experiments is the fact that the scanner noise itself results in a BOLD response. Bandettini et al. (1998) contrasted images that were taken after a scanning period with others that were preceded by silence. The results showed an activation of primary auditory cortex due to the scanner noise. Subsequently, it was shown for an auditory discrimination task that the percentage of time during which MR scanner noise was present due to slice acquisition modulates the BOLD response in auditory cortex (Shah et al. 1999). By investigating the time course of scanner noise activating auditory cortices, Hall et al. (2000) were able to demonstrate that primary and secondary auditory cortex showed peaks at 4–5 s after stimulus onset, which decayed after a further 5–8 s. This time course indicates that noise contamination in auditory designs can be substantially reduced by using long repetition times of about 9–13 s.

The additional BOLD response induced by scanner noise results in a higher level of baseline activation in auditory cortices. The BOLD response induced by experimental stimuli is then added onto a higher baseline which may result in relatively weaker responses (e.g. in % signal change), or even ceiling effects.

It should be noted that the scanner noise poses a problem also for non-auditory experiments. For example, BOLD responses in visual cortex have been reported to decrease by 50% during the presence of scanner noise (Cho et al. 1998).

The manifold effects of scanner noise on the outcome of auditory experiments in the MRI, as well as different ideas to solve and circumvent the problem can be found in Peelle (2014). Here, we will describe the most common approaches and review their success.

22.2.4 Sparse Sampling

A potential solution to the problem of scanner noise exists in presenting stimuli during silent periods of the scanning protocol, as suggested by Hall et al. (2000). The scanner noise is only audible when the scanner actually scans a volume of the brain. However, the scanning procedure need not be continuous but can be performed intermittently in order to leave silent periods for stimulation. Since the BOLD response lags the electrical brain response by about 6 s (Fig. 22.1a), this offers the possibility to present an auditory stimulus in silence. The lagging BOLD response of the same trial is then recorded subsequently generating the described noise. This approach was initially developed for auditory fMRI acquisition. However, it also offers to record the EEG response during silence and thus in the absence of gradient

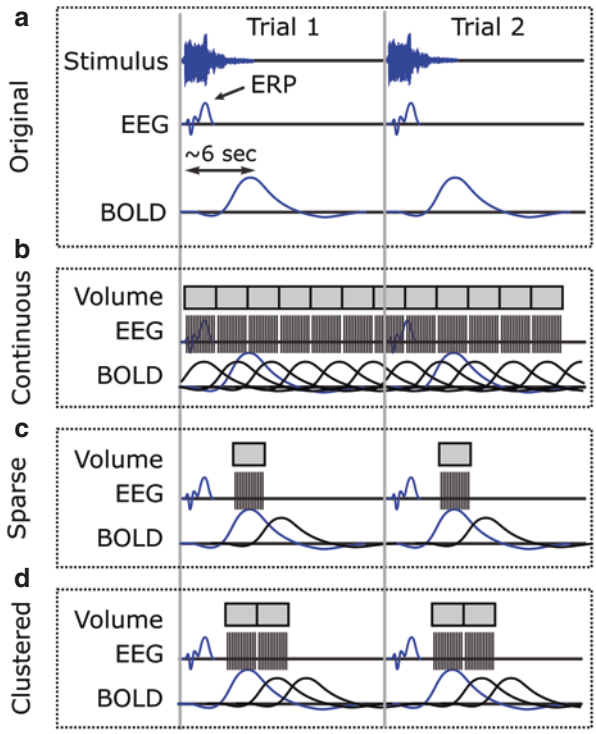

Fig. 22.1 Overview of different MRI acquisition techniques. Panel **a** shows two trials of an auditory experiment (Stimulus in top row) and the respective schematic neural responses in the EEG (ERP in blue, middle row) and the BOLD response (blue, bottom row). The original responses are copied into panels **b**-**d**, which represent different paradigms of fMRI. **b** illustrates continuous EPI scanning with volumes measured consecutively. The ERP is masked by gradient artifacts in the EEG (black comb-shaped) throughout the measurement. The BOLD response to the stimulus is potentially obscured by BOLD responses to the scanner noise (black). **c** shows a sparse sampling method where one volume is measured around the peak of the expected BOLD response. Here both the ERP and the stimulus-related BOLD response are mainly untouched by gradient artifact or scanner noise-related BOLD responses. Part **d** represents clustered sampling with two volumes

artifacts. This procedure is illustrated in Fig. 22.1c and has been called as sparse sampling (Hall et al. 1999) or clustered acquisition (Edmister et al. 1999). Note that "clustered" acquisition is sometimes used interchangeably with "sparse sampling". We will refer to sparse sampling every time where only one volume is measured between two silent periods and "clustered" whenever more than one volume is measured between two silent periods (Fig. 22.1d).

A historical perspective on the development of sparse sampling fMRI is given in Talavage and Hall (2012).

Sparse sampling has become a widely used solution to the problem of scanner noise interference in auditory experiments revealing numerous phenomena of auditory cortex (Behler and Uppenkamp 2016; Gaab et al. 2003; Li et al. 2017; Müller et al. 2003; Tae et al. 2014; Tanaka et al. 2000).

The parameter space for sparse sampling fMRI is considerably big. Thus, finding the optimal parameters is dependent of the research question at hand. Nevertheless, it has been suggested to use medium repetition times between 2 and 6 s (Liem et al. 2012; Perrachione and Ghosh 2013) to optimize statistical power, even though acoustic contamination by the scanner noise is not fully avoided at this rate.

One of the major caveats of the traditional sparse sampling method is that the volume is measured at always the same time-point relative to the stimulus onset. Assuming a stable hemodynamic response to the stimuli, sparse sampling thus prohibits insights into the shape and response latency of the hemodynamic response and can even lead to a significant underestimation of the effects, if the measured volume does not coincide with the peak hemodynamic response (Peelle 2014). Jittering the onset times of the measured volume has been suggested to circumvent this problem (Belin et al. 1999). With a sufficiently high number of trials, a reliable temporal profile of the hemodynamic response can be estimated.

Further developments of the sparse sampling method include the measurement of not only one but several volumes before a silent period (Fig. 22.1d). This clustered image acquisition technique increases statistical power in comparison to the standard sparse sampling account with only one volume measured per repetition (Zaehle et al. 2007) and allows for insights into dynamics of the hemodynamic response. The implementation, as proposed by Zaehle et al. (2007) suffers from a decay of T1-magnetization over the number of volumes measured before the silent period. This in turn poses problems to analysis and interpretation of these data.

This problem is overcome in a more sophisticated variant of sparse sampling, the so-called interleaved silent steady-state imaging (Schwarzbauer et al. 2006) by keeping the T1 magnetization constant using silent excitation pulses in the silent periods.

The described innovative approaches, even though overcoming some problems for auditory fMRI, do not overcome the problems of EEG recordings during auditory fMRI experiments. Only the traditional sparse sampling method with just one measured volume allows for EEG measurements free of the gradient artifact between volumes. Pulse artifacts, however, will still be measured and have to be corrected for.

22.2.5 Silent fMRI Acquisition

A different solution to the problem of scanner noise interfering with auditory experiment lies in suppressing the noise in the first place. As described above, the noise results from the transient magnetic fields—the so-called gradients—and is louder when the transient is stronger (Moelker et al. 2003). On the one hand, this poses a problem due to the constantly increasing field strengths of MR scanners. On the other hand, it offers a handle on how to tackle the problem. The noise is generated by the Lorentz forces due to gradient currents. Hennel et al. (1999) used this knowledge to suggest an approach for the reduction of scanner noise. Instead of rectangular gradient slopes, they used sinusoidal, reducing the number of harmonics in the

spectrum and a longer gradient duration which reduced the steepness of the gradient. This resulted in a reduction of scanner noise by 40 dBA for spin-echo and gradient-echo pulse sequences whose harmonics are audible (the fundamental gradient frequencies below 100 Hz are hardly audible). However, it was not as successful for faster EPI or FLASH (fast low angle shot) sequences whose fundamental gradient frequency is already in the audible range and suppression of the harmonics is not as effective. Another approach is to use simultaneous multislice excitation (SIMEX) sequences which acquire multiple slices with one multifrequency RF pulse, resulting in fewer pulses per scan (Loenneker et al. 2001). While the SIMEX sequences were applied as block design, Yang et al. (2000) carried out an event-related silent sequence revealing 54% signal increase when compared with a conventional technique and suggesting tonotopic maps within Heschl's gyrus. Amaro et al. (2002) compared conventional and silent acquisition protocols as well as a block design and an event-related design, demonstrating that the silent event-related design yielded maximal BOLD responses to a single auditory cue. Low-noise FLASH sequences were applied to demonstrate central functions of the auditory system, such as sound-level dependence (Brechmann et al. 2002) and sound intensity categorization (Angenstein et al. 2016).

Current methodological developments include further manipulations in the EPI sequence (Peelle et al. 2010; Schmitter et al. 2008) but also the design of new techniques for acquiring T2 weighted images to show the BOLD signal (Solana et al. 2016). This method uses the rotating ultra-fast imaging sequence (Madio and Lowe 1995) for image-acquisition and reduces the noise level by ~40 dBA relative to a standard EPI sequence at almost no costs on data quality (Solana et al. 2016). At the same time, the method is considered promising for concurrent EEG measurements (Solana et al. 2016).

22.2.6 Adjusting Auditory Stimulus Frequencies

The sound that is produced by the scanner resembles a complex tone (cf. Fig. 22.2). A typical EPI sequence has a spectral peak at the switching periodicity of the magnetic transients plus harmonics and sub-harmonics, which lie within the frequency range of 500–5000 Hz (Counter et al. 2000; Hedeen and Edelstein 1997). Unfortunately, this is also the frequency range of human speech and of many auditory stimuli. Thus, the scanner noise could selectively influence those stimuli which fall into the same frequency range by a process called masking (Brosch et al. 1999). Novitski et al. (2006) were able to demonstrate this effect recording MEG in a pitch change detection task comparing a silent background with simulated scanner noise. The authors were able to demonstrate that the amplitude of the mismatch negativity (MMN), which reflects the automatic detection of the pitch change, is only affected by scanner noise when it spectrally overlaps with the auditory stimulus. This is a potential explanation of findings by Le et al. (2001) who discovered that the perception of sine tones was reduced when they spectrally overlapped with scanner noise.

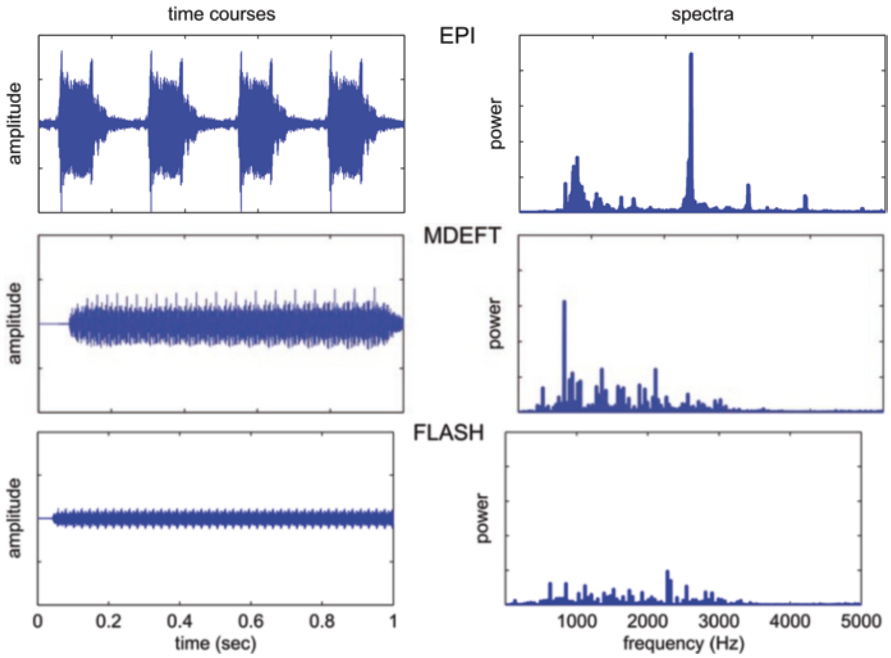

Fig. 22.2 Time courses (left column) and frequency spectra (right column) of three different scanning protocols. Echo planar imaging (EPI) has a sharp peak in the audible frequency range. MDEFT (modified driven equilibrium Fourier tomography) has a lower cut-off frequency and reduced power. Low-noise FLASH is the most silent of the three sequences

Importantly, these results offer another approach to auditory fMRI experiments. Either, MR sequences could be designed such as not to overlap with the auditory stimuli in an experiment. However, this approach is probably only feasible in research environments where MR physicists are capable of programming their own sequences. In clinical sites, another approach is promising. The scanner noise of the available scanning sequences can easily be recorded on a digital sound recorder (See Fig. 22.2 for such recordings). Note that caution has to be applied not to bring ferromagnetic devices too close to the scanner! A Fourier transform can yield the frequency spectrum of the scanner noise, and stimuli can be designed to lie outside the main peaks of the spectrum.

This approach seems especially appropriate when the design of the experiment excludes the possibility to apply sparse sampling. This would, for example, be the case when trying to implement n-back working memory tasks with fixed latencies (see e.g. Brechmann et al. 2007) or when investigating auditory streaming which requires a certain amount of time to build up (see e.g. Micheyl et al. 2007).

22.2.7 Active Noise Cancellation

Another approach to reduce the influence of the scanner noise on fMRI experiments is to manipulate the noise, so it is perceived less by the subject. The principle

includes the cancellation of scanner noise by measuring the acoustic characteristics and designing a "destructive" sound signal that is played to the subject in the scanner. The destructive signal must be designed so that it cancels out scanner noise at the subject, thus reducing the perceived scanner noise by approximately 20–35 dB (Hall et al. 2009; Li et al. 2011). Challenges for the technique are the MR-compatible measurement of sounds close to the subject inside of the scanner, and playing the destructive sound at a high temporal precision (Peelle 2014).

22.3 Simultaneous EEG and fMRI in Auditory Experiments

In order to avoid the abovementioned obstacles of recording EEG inside an MRI scanner, a number of early studies have recorded EEG and BOLD responses from the same subjects in two separate EEG and fMRI recording sessions.

Menon and Crottaz-Herbette (2005) analyzed the P3, an event-related potential (ERP), in response to rare target stimuli in order to investigate processes of auditory target detection. They were able to demonstrate that the dipole locations of the inverse solution for the P3 coincided with the maximum BOLD activations within the temporo-parietal cortex. Subsequently, a second group analyzed the P3a, an ERP response to novel auditory stimuli, and found foci in the superior temporal gyrus (Opitz et al. 1999). Later in the same year, a third group analyzed the P3 in response to auditory as well as visual targets and was able to describe a whole network of brain regions involved in target processing (Linden 1999). This research has led to the method of "fMRI-constrained source modeling" for EEG as well as MEG (Fujimaki et al. 2002). Numerous studies have applied similar approaches in auditory experiments (e.g. Opitz et al. 1999; Doeller et al. 2003; Crottaz-Herbette and Menon 2006).

A further important approach is to carry out parametric studies separately in EEG and fMRI and to correlate the EEG and BOLD responses in order to find out which of them covary with respect to the same parameter. This approach has been applied by Horovitz et al. (2002) in an auditory oddball paradigm, revealing that the BOLD response in some brain regions (e.g. supramarginal gyrus and right medial frontal gyrus) covary with P3 amplitude, while others (ACC) are activated by targets but do not show this covariation. Using a combination of EEG, fMRI, and diffusion-weighted images, Coffey et al. (2017) integrated knowledge about the frequency following response, a mechanism of sound encoding in the brain, from different modalities in previous research. The authors correlated the frequency following responses in the EEG, with BOLD activity measured in a separate session using identical experimental procedures. Their data confirm a hypothesized cortical contribution to this lower level process of sound encoding in the human brain, which was mostly investigated in the brainstem.

One of the criticisms of separate recording protocols results from the fact that it seems impossible to control whether a subject performs in the same manner in both experiments (Debener et al. 2006). For separate recordings, it seems necessary to test for the order of session effects. In numerous psychophysiological studies, these tests

have revealed significant differences depending on whether subjects performed an experiment for the first time or repeated a known experimental paradigm in a second session. This is easily conceivable for paradigms explicitly investigating learning and memory processes. One should note that the most basic perceptual and cognitive operations may also show adaptation over time, such that temporal aspects of sessions or order of trials should be taken into account. A further criticism is that even minor changes of an experimental setup can result in significant changes of subjects' behavioral and physiological responses. For example, changing a subject from a seated upright position, as common in EEG recordings, into a supine position, as necessary for fMRI scanners, may influence physiological responses and overt behavior.

In order to overcome the problems of separate recordings, EEG and BOLD responses have been recorded simultaneously. The first such study in the auditory system applied the above-mentioned approach of correlating the parametric variation of an ERP component with the BOLD response in a simultaneous recording (Liebenthal et al. 2003). The authors were able to identify brain regions in which the BOLD response covaried with the strength of the MMN. Subsequently, another group set out to investigate the P3 during target processing, revealing an enhancement for targets concurrent with increased BOLD activity in the temporoparietal junction, frontal areas, and the insulae (Mulert et al. 2004). Scarff et al. (2004) have used simultaneous recording of EEG and BOLD responses in order to compare the anatomical locations of the N1 generators. Source reconstruction of ERP data revealed dipole locations in the superior temporal gyrus which coincided with the center of gravity of the BOLD responses. However, the authors also reported some differences between ERP dipoles and BOLD activity in terms of asymmetry and the inferior-superior axis of the brain. Otzenberger et al. (2005) further extended previous findings by showing that different P3 components such as the target-P3 and novelty-P3 could be discriminated in a simultaneous recording, a finding that has been replicated by Strobel et al. (2008). Combined ERP-BOLD analyses of the N1 and P3 components were also established in a sample of children (Rusiniak et al. 2013).

Another study has investigated the influence of task difficulty on MMN amplitude and fMRI activation (Sabri et al. 2006). The authors were able to show that the superior temporal gyrus and sulcus were more strongly activated in the difficult auditory task. By combining a current source density reconstruction of ERP data and simultaneously recorded BOLD responses, Mulert et al. (2005) were able to demonstrate that both measures revealed the dependence upon the sound level of auditory stimuli. Debener et al. (2007) showed how three different methods for artifact removal in simultaneous recordings differentially affect auditory N1 amplitude and signal-to-noise ratio (SNR).

In addition to data aggregation, the analysis of single-trial data is another successful approach in EEG-fMRI analysis. Due to the parallel acquisition of EEG and BOLD responses, parameters of the two measurements can be correlated across single trials potentially leading to a better understanding of the coupling of the two (Debener et al. 2006). It has been convincingly demonstrated that the amplitude of ERP components varies systematically over time reflecting cognitive processes and that this variation can be used to identify those brain regions where the BOLD contrast shows the

same variation (Eichele et al. 2005). In a similar vein, Bénar et al. (2007) were able to demonstrate that the amplitude of P3 correlated positively with BOLD activity in the ACC which is believed to reflect attentional processes. In addition, a negative correlation of P3 latency with BOLD activity in medial frontal regions probably reflects processes of action planning or performance monitoring, since P3 latency was at the same time negatively correlated with subjects' reaction times.

The spatio-temporal dynamics of pure time processing has been investigated using single-trial EEG-fMRI analysis (Li et al. 2017). The authors were able to map pure-tone processing in three temporal stages, characterized by ERP components, in areas from the midbrain, auditory, and motor cortex. The BOLD activity of these areas correlates with the amplitude of specific ERP components.

The previous studies mostly used relatively simple approaches to EEG-MRI data analysis, which typically do not make use of the full amount of data measured. These methods either use the fMRI data to more precisely map reconstructed sources of EEG activity or they integrate EEG findings into the fMRI analysis by means of e.g. a correlation between ERPs and the BOLD signal (Horovitz et al. 2002; Liebenthal et al. 2003; Rusiniak et al. 2013).

With the increase in computational power, new, more sophisticated methods have been established in the field, which make use of the full spectrum of multivariate data in multimodal measurements. For the approach of the so-called joint ICA (Calhoun et al. 2005, 2009), data from different modalities are combined in one ICA in order to identify hidden factors in the combined data. This data-driven method does not assume a model of the relationship between factors (such as a HRF) and is thus able to uncover non-linear relationships between experimental conditions (Calhoun et al. 2009). Further details about the different ways of EEG-fMRI data analysis can be found, for example, in the intelligible review by Huster et al. (2012).

Using joint ICA on EEG-fMRI data from an auditory oddball task, Calhoun et al. (2005) associated the N1 ERP component with primary and secondary auditory regions in the temporal lobe as well as multiple motor regions related to motor planning. N2 is related to more widespread temporal activity and motor regions responsible for movement execution including cerebellar activity. The P3 peak then is accompanied by additional activation of somatosensory and brain stem activation. The authors especially highlight the finding of brain stem activation related to the P3 peak because it is very hard to detect in a unimodal ERP analysis of the data due to its small size and remoteness to the EEG electrodes. In this context, it might be worth mentioning that Calhoun et al. (2005) used only one EEG-electrode (Cz) in their joint ICA. Their results might have been even more detailed if more EEG data had been incorporated.

22.4 Evaluation Methods of Concurrent Auditory EEG-fMRI

In comparison to the correction of the MR-related artifacts in EEG-data, which can now be achieved with an acceptable accuracy, the influence of scanner noise seems to be a much bigger problem for the experimental outcomes of an auditory EEG-fMRI experiment. MR-scanning, unlike other techniques, is an inherently noisy

method, and even though ambitions were taken to reduce the level of scanner noise, it seems unlikely that MR-experimentation will become completely silent in the near future. Therefore, it appears useful to test the current approaches to auditory EEG-fMRI for their effectiveness and to assess their quality. We will now review three studies comparing different auditory (EEG-)fMRI procedures by replicating established findings from auditory experiments.

A classic finding about the amplitude of the N1 component is its increase in amplitude with higher stimulus intensities (Beagley and Knight 1967; Rapin et al. 1966). If that relationship could be replicated in concurrent EEG-fMRI measurements, this would give a rough guideline about the influence of scanner noise on the EEG-response to auditory stimulation. Using a standard EPI-sequence, this relationship was not found in EEG-fMRI (Mulert et al. 2005) even though in the same article this relationship could be replicated using the same paradigm outside the scanner (Mulert et al. 2005). One explanation for this result is the scanner noise. Since stimuli were presented in scanner noise, the physical parameters of the acoustic stimulation were dramatically different: first, the relative loudness difference between the stimuli is reduced; second, the inter-stimulus intervals are reduced, assuming that the pulse-like noise of an EPI-sequence is considered a stimulus. A solution to both problems was suggested by Thaerig et al. (2008) who measured the BOLD response with a silent (~ 54 dB sound pressure level) FLASH sequence which produces a relatively continuous noise. The authors presented frequency-modulated tones at two intensity levels and found an increased N1 amplitude for the louder sound (Fig. 22.3, upper panel). In addition, they also reported a BOLD activation pattern typical for frequency-modulated sounds, which was descriptively more pronounced for the louder sounds (One exemplary subject is shown in Fig. 22.3, lower panel). Their experiment provides evidence that silent fMRI with a continuous noise pattern allows for concurrent measurements of auditory EEG and fMRI without major dropouts in signal quality in both domains.

A different, well-established finding in auditory neuroscience is the tonotopic mapping in the auditory cortices. In an attempt to map the influence of scanner noise on tonotopic mapping, Langers et al. (2014) used frequency-sweep stimuli which were presented during continuous, traditional EPI, sparse sampling EPI, and a clustered EPI with 2 volumes measured between two silent periods. Overall, they report highly similar tonotopic maps for all three types of measurement. Yet, they also found a reduction in signal intensity in those parts of the tonotopic maps, which overlap in frequency with the scanner noise. This effect was strongest in the continuous and clustered EPI measurements. Since all standard EPI sequences show similar frequency spectra, this effect of masking was to be expected. These results support the idea that sparse EPI techniques, even though in principal they do not differ from standard EPI with respect to their peak sound intensity, are suitable to measure BOLD signals in primary auditory cortex.

One study has compared standard, sparse sampling and quiet EPI methods with each other as well as one continuous EPI sequence which was matched in frequency of the readout gradient to the sparse sampling EPI sequence (Peelle et al. 2010). To compare the signal quality between methods, the authors used speech stimuli and,

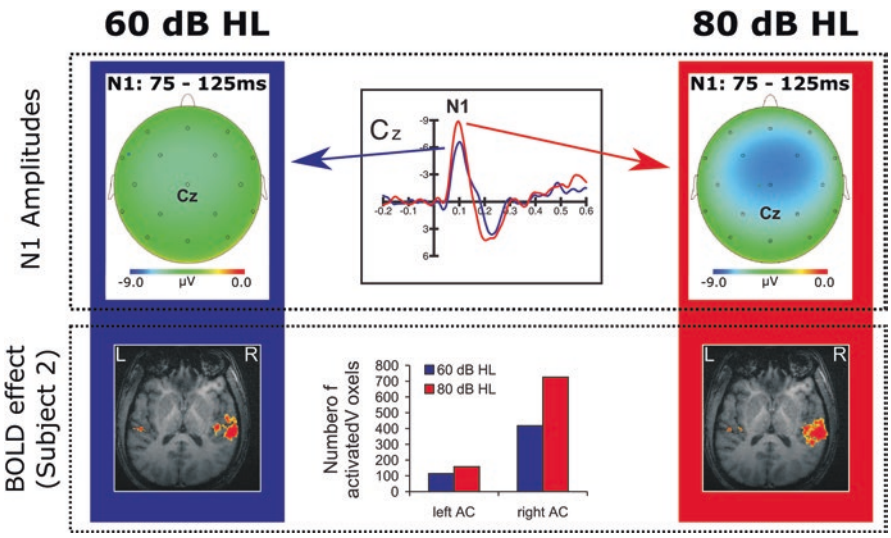

Fig. 22.3 The upper panel shows the auditory event-related potentials from the EEG-fMRI experiment from Thaerig et al. (2008). The central plot depicts the ERP from stimuli presented at 60 dB (blue) and 80 dB (red). The N1 component shows the typical dependence upon sound level, i.e. larger amplitudes for higher sound pressure. Topographic maps (left and right upper plots) reveal the good resemblance of ERPs recorded outside the scanner. The lower panel shows the BOLD response from the same experiment from one exemplary subject. The number of activated voxels is increased for stimuli presented at 80 dB when compared to 60 dB, as can be seen from the bar plots in the lower central bar plot. (Adapted from Thaerig et al. 2008)

as a baseline, noise, which was matched in frequency band and amplitude envelope to the speech stimuli. When they compared sequences on the baseline condition, it turned out that quiet EPI yields the largest responses in primary auditory cortex. When analyzing the contrast speech > baseline, i.e. high-level auditory processing, they found comparable results for all four tested sequences with a decrease in BOLD sensitivity in the quiet EPI sequence. Further, the authors note that the standard EPI sequence requires higher listening effort when compared with the quiet sequence most probably due to the higher level of masking scanner noise.

22.5 Conclusion

Overall, sparse sampling of standard EPI sequences provides a good option for EEG-fMRI of higher level auditory processing. During silent periods, stimuli can be presented in relative silence, and EEG can be recorded without gradient artifacts. Sparse sampling, however, comes at the cost of reduced statistical power because of a reduced number of measurement points, and pulse artifacts in EEG still occur. For experiments of higher order processes, such as language comprehension or learning, continuous measurements using either quiet EPI, or other quiet sequences sensitive to the BOLD signal, seem to be more appropriate. Even though scanner

artifacts in the EEG-data are more severe in this case, this caveat seems acceptable for a better time resolution of the hemodynamic effects, as well as higher statistical power in the fMRI.

References

Allen PJ, Josephs O, Turner R (2000) A method for removing imaging artifact from continuous EEG recorded during functional MRI. Neuroimage 12:230–239

Amaro E, Williams SCR, Shergill SS et al (2002) Acoustic noise and functional magnetic resonance imaging: current strategies and future prospects. J Magn Reson Imaging 16:497–510

Angenstein N, Stadler J, Brechmann A (2016) Auditory intensity processing: effect of MRI background noise. Hear Res 333:87–92

Bandettini PA, Jesmanowicz A, Van Kylen J et al (1998) Functional MRI of brain activation induced by scanner acoustic noise. Magn Reson Med 39:410–416

Baumgart F, Kautisch T, Tempelmann C et al (1998) Electrodynamic headphones and woofers for application in magnetic resonance imaging scanners. Med Phys 25:2068–2070

Beagley HA, Knight JJ (1967) Changes in auditory evoked response with intensity. J Laryngol Otol 81:861–873

Behler O, Uppenkamp S (2016) The representation of level and loudness in the central auditory system for unilateral stimulation. Neuroimage 139:176–188

Belin P, Zatorre RJ, Hoge R et al (1999) Event-related fMRI of the auditory cortex. Neuroimage 10:417–429

Bénar CG, Schön D, Grimault S et al (2007) Single-trial analysis of oddball event-related potentials in simultaneous EEG-fMRI. Hum Brain Mapp 28:602–613

Bonmassar G, Purdon PL, Jääskeläinen IP et al (2002) Motion and ballistocardiogram artifact removal for interleaved recording of EEG and EPs during MRI. Neuroimage 16:1127–1141

Brechmann A, Baumgart F, Scheich H (2002) Sound-level-dependent representation of frequency modulations in human auditory cortex: a low-noise fMRI study. J Neurophysiol 87:423–433

Brechmann A, Gaschler-Markefski B, Sohr M et al (2007) Working memory-specific activity in auditory cortex: potential correlates of sequential processing and maintenance. Cereb Cortex 17:2544–2552

Brosch M, Schulz A, Scheich H (1999) Processing of sound sequences in macaque auditory cortex: response enhancement. J Neurophysiol 82:1542–1559

Calhoun V, Adali T, Pearlson G, Kiehl K (2005) Neuronal chronometry of target detection: fusion of hemodynamic and event-related potential DATA. IEEE Work Mach Learn Signal Process 30:239–244

Calhoun VD, Liu J, Adali T (2009) A review of group ICA for fMRI data and ICA for joint inference of imaging, genetic, and ERP data. Neuroimage 45:163–172

Cho ZH, Chung SC, Lim DW, Wong EK (1998) Effects of the acoustic noise of the gradient systems on fMRI: a study on auditory, motor, and visual cortices. Magn Reson Med 39:331–336

Coffey EBJ, Musacchia G, Zatorre RJ (2017) Cortical correlates of the auditory frequency-following and onset responses: EEG and fMRI evidence. J Neurosci 37:830–838

Counter SA, Olofsson A, Borg E et al (2000) Analysis of magnetic resonance imaging acoustic noise generated by a 4.7 T experimental system. Acta Otolaryngol 120:739–743

Crottaz-Herbette S, Menon V (2006) Where and when the anterior cingulate cortex modulates attentional response: combined fMRI and ERP evidence. J Cogn Neurosci 18:766–780

Debener S, Ullsperger M, Siegel M, Engel AK (2006) Single-trial EEG-fMRI reveals the dynamics of cognitive function. Trends Cogn Sci 10:558–563

Debener S, Strobel A, Sorger B et al (2007) Improved quality of auditory event-related potentials recorded simultaneously with 3-T fMRI: removal of the ballistocardiogram artefact. Neuroimage 34:587–597

Debener S, Mullinger KJ, Niazy RK, Bowtell RW (2008) Properties of the ballistocardiogram artefact as revealed by EEG recordings at 1.5, 3 and 7 T static magnetic field strength. Int J Psychophysiol 67:189–199

Doeller CF, Opitz B, Mecklinger A et al (2003) Prefrontal cortex involvement in preattentive auditory deviance detection: neuroimaging and electrophysiological evidence. Neuroimage 20:1270–1282

Edmister WB, Talavage TM, Ledden PJ, Weisskoff RM (1999) Improved auditory cortex imaging using clustered volume acquisitions. Hum Brain Mapp 7:89–97

Eichele T, Specht K, Moosmann M et al (2005) Assessing the spatiotemporal evolution of neuronal activation with single-trial event-related potentials and functional MRI. Proc Natl Acad Sci 102:17798–17803

Ellingson ML, Liebenthal E, Spanaki MV et al (2004) Ballistocardiogram artifact reduction in the simultaneous acquisition of auditory ERPS and fMRI. Neuroimage 22:1534–1542

Felblinger J, Slotboom J, Kreis R et al (1999) Restoration of electrophysiological signals distorted by inductive effects of magnetic field gradients during MR sequences. Magn Reson Med 41:715–721

Fujimaki N, Hayakawa T, Nielsen M et al (2002) An fMRI-constrained MEG source analysis with procedures for dividing and grouping activation. Neuroimage 17:324–343

Gaab N, Gaser C, Zaehle T et al (2003) Functional anatomy of pitch memory - an fMRI study with sparse temporal sampling. Neuroimage 19:1417–1426

Gaab N, Gabrieli JDE, Glover GH (2007) Assessing the influence of scanner background noise on auditory processing. I. an fMRI study comparing three experimental designs with varying degrees of scanner noise. Hum Brain Mapp 28:703–720

Hall DA, Haggard MP, Akeroyd MA et al (1999) "Sparse" temporal sampling in auditory fMRI. Hum Brain Mapp 7:213–223

Hall DA, Summerfield AQ, Gonçalves MS et al (2000) Time-course of the auditory BOLD response to scanner noise. Magn Reson Med 43:601–606

Hall DA, Chambers J, Akeroyd MA et al (2009) Acoustic, psychophysical, and neuroimaging measurements of the effectiveness of active cancellation during auditory functional magnetic resonance imaging. J Acoust Soc Am 125:347–359

Hedeen RA, Edelstein WA (1997) Characterization and prediction of gradient acoustic noise in MR imagers. Magn Reson Med 37:7–10

Hennel F, Girard F, Loenneker T (1999) "Silent" MRI with soft gradient pulses. Magn Reson Med 42:6–10

Herrmann CS, Debener S (2008) Simultaneous recording of EEG and BOLD responses: a historical perspective. Int J Psychophysiol 67:161–168

Herrmann CS, Oertel U, Wang Y et al (2000) Noise affects auditory and linguistic processing differently. Neuroreport 11:227–230

Horovitz SG, Skudlarski P, Gore JC (2002) Correlations and dissociations between BOLD signal and P300 amplitude in an auditory oddball task: a parametric approach to combining fMRI and ERP. Magn Reson Imaging 20:319–325

Huster RJ, Debener S, Eichele T, Herrmann CS (2012) Methods for simultaneous EEG-fMRI: an introductory review. J Neurosci 32:6053–6060

Langers DRM, Sanchez-Panchuelo RM, Francis ST et al (2014) Neuroimaging paradigms for tonotopic mapping (II): the influence of acquisition protocol. Neuroimage 100:663–675

Le TH, Patel S, Roberts TP (2001) Functional MRI of human auditory cortex using block and event-related designs. Magn Reson Med 45:254–260

Li M, Rudd B, Lim TC, Lee J-H (2011) In situ active control of noise in a 4 T MRI scanner. J Magn Reson Imaging 34:662–669

Li Q, Liu G, Wei D et al (2017) The spatiotemporal pattern of pure tone processing: a single-trial EEG-fMRI study. Neuroimage 156:1–8

Liebenthal E, Ellingson ML, Spanaki MV et al (2003) Simultaneous ERP and fMRI of the auditory cortex in a passive oddball paradigm. Neuroimage 19:1395–1404

Liem F, Lutz K, Luechinger R et al (2012) Reducing the interval between volume acquisitions improves "sparse" scanning protocols in event-related auditory fMRI. Brain Topogr 25:182–193
Linden DEJ (1999) The functional neuroanatomy of target detection: an fMRI study of visual and auditory oddball tasks. Cereb Cortex 9:815–823
Loenneker T, Hennel F, Ludwig U, Hennig J (2001) Silent BOLD imaging. MAGMA 13:76–81
Madio DP, Lowe IJ (1995) Ultra-fast imaging using low flip angles and fids. Magn Reson Med 34:525–529
Mansfield P, Glover PM, Beaumont J (1998) Sound generation in gradient coil structures for MRI. Magn Reson Med 39:539–550
McJury M, Shellock FG (2000) Auditory noise associated with MR procedures: a review. J Magn Reson Imaging 12:37–45
Menon V, Crottaz-Herbette S (2005) Combined EEG and fMRI studies of human brain function. Int Rev Neurobiol 66:291–321
Micheyl C, Carlyon RP, Gutschalk A et al (2007) The role of auditory cortex in the formation of auditory streams. Hear Res 229:116–131
Moelker A, Pattynama PMT (2003) Acoustic noise concerns in functional magnetic resonance imaging. Hum Brain Mapp 20:123–141
Moelker A, Wielopolski PA, Pattynama PMT (2003) Relationship between magnetic field strength and magnetic-resonance-related acoustic noise levels. MAGMA 16:52–55
Mulert C, Jäger L, Schmitt R et al (2004) Integration of fMRI and simultaneous EEG: towards a comprehensive understanding of localization and time-course of brain activity in target detection. Neuroimage 22:83–94
Mulert C, Jäger L, Propp S et al (2005) Sound level dependence of the primary auditory cortex: simultaneous measurement with 61-channel EEG and fMRI. Neuroimage 28:49–58
Müller BW, Stude P, Nebel K et al (2003) Sparse imaging of the auditory oddball task with functional MRI. Neuroreport 14:1597–1601
Mullinger K, Debener S, Coxon R, Bowtell R (2008) Effects of simultaneous EEG recording on MRI data quality at 1.5, 3 and 7 tesla. Int J Psychophysiol 67:178–188
Niazy RK, Beckmann CF, Iannetti GD et al (2005) Removal of FMRI environment artifacts from EEG data using optimal basis sets. Neuroimage 28:720–737
Nierhaus T, Gundlach C, Goltz D et al (2013) Internal ventilation system of MR scanners induces specific EEG artifact during simultaneous EEG-fMRI. Neuroimage 74:70–76
Norman-Haignere S, McDermott JH (2016) Distortion products in auditory fMRI research: measurements and solutions. Neuroimage 129:401–413
Novitski N, Alho K, Korzyukov O et al (2001) Effects of acoustic gradient noise from functional magnetic resonance imaging on auditory processing as reflected by event-related brain potentials. Neuroimage 14:244–251
Novitski N, Anourova I, Martinkauppi S et al (2003) Effects of noise from functional magnetic resonance imaging on auditory event-related potentials in working memory task. Neuroimage 20:1320–1328
Novitski N, Maess B, Tervaniemi M (2006) Frequency specific impairment of automatic pitch change detection by fMRI acoustic noise: an MEG study. J Neurosci Methods 155:149–159
Opitz B, Mecklinger A, Friederici AD, Von Cramon DY (1999) The functional neuroanatomy of novelty processing: integrating ERP and fMRI results. Cereb Cortex 9:379–391
Otzenberger H, Gounot D, Foucher JR (2005) P300 recordings during event-related fMRI: a feasibility study. Cogn Brain Res 23:306–315
Palmer AR, Bullock DC, Chambers JD (1998) A high-output, high-quality sound system for use in auditory. Neuroimage 7:S359
Palmer AR, Chambers J, Hall DA (2006) New fMRI methods for hearing and speech. Acoust Sci Technol 27:125–133
Peelle JE (2014) Methodological challenges and solutions in auditory functional magnetic resonance imaging. Front Neurosci 8:1–13
Peelle JE, Eason RJ, Schmitter S et al (2010) Evaluating an acoustically quiet EPI sequence for use in fMRI studies of speech and auditory processing. Neuroimage 52:1410–1419

Perrachione TK, Ghosh SS (2013) Optimized design and analysis of sparse-sampling fMRI experiments. Front Neurosci 7:1–18
Price DL, De Wilde JP, Papadaki AM et al (2001) Investigation of acoustic noise on 15 MRI scanners from 0.2 T to 3 T. J Magn Reson Imaging 13:288–293
Rapin I, Schimmel H, Tourk LM et al (1966) Evoked responses to clicks and tones of varying intensity in waking adults. Electroencephalogr Clin Neurophysiol 21:335–344
Ritter P, Villringer A (2006) Simultaneous EEG-fMRI. Neurosci Biobehav Rev 30:823–838
Ritter P, Becker R, Graefe C, Villringer A (2007) Evaluating gradient artifact correction of EEG data acquired simultaneously with fMRI. Magn Reson Imaging 25:923–932
Rothlübbers S, Relvas V, Leal A et al (2014) Characterisation and reduction of the EEG artefact caused by the helium cooling pump in the MR environment: validation in epilepsy patient data. Brain Topogr 28:208–220
Rusiniak M, Lewandowska M, Wolak T et al (2013) A modified oddball paradigm for investigation of neural correlates of attention: a simultaneous ERP-fMRI study. MAGMA 26:511–526
Sabri M, Liebenthal E, Waldron EJ et al (2006) Attentional modulation in the detection of irrelevant deviance: a simultaneous ERP/fMRI study. J Cogn Neurosci 18:689–700
Scarff CJ, Reynolds A, Goodyear BG et al (2004) Simultaneous 3-T fMRI and high-density recording of human auditory evoked potentials. Neuroimage 23:1129–1142
Schmitter S, Diesch E, Amann M et al (2008) Silent echo-planar imaging for auditory FMRI. MAGMA 21:317–325
Schwarzbauer C, Davis MH, Rodd JM, Johnsrude I (2006) Interleaved silent steady state (ISSS) imaging: a new sparse imaging method applied to auditory fMRI. Neuroimage 29:774–782
Scott SK, McGettigan C (2013) The neural processing of masked speech. Hear Res 303:58–66
Shah NJ, Jäncke L, Grosse-Ruyken ML, Müller-Gärtner HW (1999) Influence of acoustic masking noise in fMRI of the auditory cortex during phonetic discrimination. J Magn Reson Imaging 9:19–25
Sijbersa J, Van Audekerke J, Verhoye M et al (2000) Reduction of ECG and gradient related artifacts in simultaneously recorded human EEG/MRI data. Magn Reson Imaging 18:881–886
Solana AB, Menini A, Sacolick LI et al (2016) Quiet and distortion-free, whole brain BOLD fMRI using T2-prepared RUFIS. Magn Reson Med 75:1402–1412
Strobel A, Debener S, Sorger B et al (2008) Novelty and target processing during an auditory novelty oddball: a simultaneous event-related potential and functional magnetic resonance imaging study. Neuroimage 40:869–883
Tae WS, Yakunina N, Kim TS et al (2014) Activation of auditory white matter tracts as revealed by functional magnetic resonance imaging. Neuroradiology 56:597–605
Talavage TM, Hall DA (2012) How challenges in auditory fMRI led to general advancements for the field. Neuroimage 62:641–647
Tanaka H, Fujita N, Watanabe Y et al (2000) Effects of stimulus rate on the auditory cortex using fMRI with “sparse” temporal sampling. Neuroreport 11:2045–2049
Thaerig S, Behne N, Schadow J et al (2008) Sound level dependence of auditory evoked potentials: simultaneous EEG recording and low-noise fMRI. Int J Psychophysiol 67:235–241
van der Meer JN, Pampel A, Van Someren EJW et al (2016) Carbon-wire loop based artifact correction outperforms post-processing EEG/fMRI corrections-a validation of a real-time simultaneous EEG/fMRI correction method. Neuroimage 125:880–894
Vanderperren K, De Vos M, Ramautar JR et al (2010) Removal of BCG artifacts from EEG recordings inside the MR scanner: a comparison of methodological and validation-related aspects. Neuroimage 50:920–934
Warbrick T, Bagshaw AP (2008) Scanning strategies for simultaneous EEG-fMRI evoked potential studies at 3 T. Int J Psychophysiol 67:169–177
Yang Y, Engelien A, Engelien W et al (2000) A silent event-related functional MRI technique for brain activation studies without interference of scanner acoustic noise. Magn Reson Med 43:185–190
Zaehle T, Schmidt CF, Meyer M et al (2007) Comparison of “silent” clustered and sparse temporal fMRI acquisitions in tonal and speech perception tasks. Neuroimage 37:1195–1204

Visual System

23

Robert Becker, Stephen Mayhew, Petra Ritter, and Arno Villringer

23.1 Simultaneous EEG-fMRI of the Visual System: Signal Quality

Combining both EEG and fMRI is still a challenging task. A large number of studies on the feasibility of EEG-fMRI for the visual system have been performed because it is an accessible and well-described system.

A general question while performing EEG-fMRI experiments is whether typical neural patterns of the visual system as measured by EEG, such as alpha oscillation or visual evoked potentials (VEPs), are modified by the strong static magnetic field inside the MR environment. Despite two studies reporting changed evoked

R. Becker (✉)
Department of Psychology, Neurolinguistics, University of Zurich, Zurich, Switzerland
e-mail: email@robertbecker.info

S. Mayhew
School of Psychology, Center for Human Brain Health, University of Birmingham, Birmingham, UK
e-mail: s.d.mayhew@bham.ac.uk

P. Ritter
Charité—Universitätsmedizin Berlin, Berlin, Germany

Section Brain Simulation, Department of Neurology, Berlin Institute of Health, Humboldt-Universität zu Berlin, Berlin, Germany

Berlin Institute of Health (BIH), Berlin, Germany

Bernstein Center for Computational Neuroscience, Berlin, Germany
e-mail: petra.ritter@bih-charite.de

A. Villringer
Department of Neurology, Max Planck Institute for Human Cognitive and Brain Sciences, Leipzig, Germany
e-mail: villringer@cbs.mpg.de

C. Mulert, L. Lemieux (eds.), *EEG - fMRI*,
https://doi.org/10.1007/978-3-031-07121-8_23

potentials during exposure to the strong magnetic field of the MR environment (Bunkrad et al. 1989; Sammer et al. 2005), most other studies have reported typical evoked potentials (EPs) within the magnetic field, although without systematic comparison to non-MR EPs. Typical configurations have been shown for VEPs (Bonmassar et al. 1999; Kruggel et al. 2000; Muri et al. 1998; Negishi et al. 2004; Comi et al. 2005; Becker et al. 2005, Assecondi et al. 2010; Vanderperren et al. 2010, see also Fig. 23.1) and for visual oddball P300 potentials (Otzenberger et al. 2005; Negishi et al. 2004). The recording of VEPs at high MR B_0 fields (4.7 T) was demonstrated for monkeys (Schmid et al. 2006). EEG source localization was also shown to be feasible for EEG data from inside the MR tomograph by Bonmassar et al. (2001) and Im et al. (2006). Depending on whether EPs were recorded in an interleaved manner (i.e. during non-acquisition intervals of the MR sequence) or

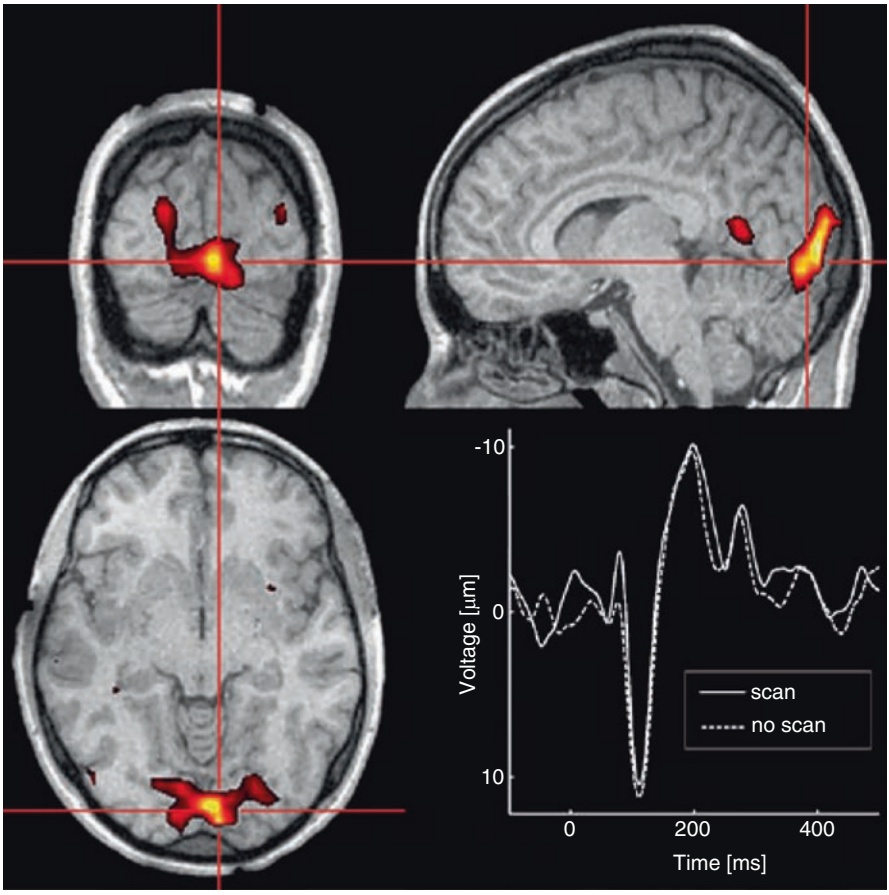

Fig. 23.1 The effect of MR gradient artifact removal on the average VEP for one subject (*bottom right*). Accompanying slices (*top row and bottom left*) show the corresponding fMRI activations. (From Becker et al. 2005)

continuously, the data had to be corrected for either the ballistocardiogram (BCG) or for both BCG and MR imaging artifacts.

Another question is whether the imaging of metabolic responses is impaired by the EEG equipment inside the MR environment. Lazeyras et al. (2001) found that functional imaging during visual stimulation yielded similar activations for fMRI with simultaneous EEG acquisition and for fMRI acquisition alone.

In general, it can be stated that average VEPs can be recorded reliably in the scanner using conventional artifact removal techniques. Depending on the magnetic field strength, single-trial analysis or the analysis of non-averaged data may be hampered by BCG residuals. Because it is a complex signal that varies in both time and space, it may not always be completely removable (Debener et al. 2008). The signal quality of such VEPs can be enhanced by application of further preprocessing such as by using independent component analyses (ICA) based procedures (Porcaro et al. 2010; Scheeringa et al. 2011a) or beamforming (Brookes et al. 2008).

23.2 fMRI-Informed EEG of the Visual System

With the aid of EEG it is possible to analyze temporally highly resolved dynamics of evoked responses during visual stimulation. However, due to the inverse problem, an exact and unconstrained localization of these evoked responses is not possible (Helmholtz 1853). Since the visual areas in humans are densely clustered at the occipital pole, and an increasing number of generators may be concurrently active with subsequent stages of processing, the differentiation of neural sources by EEG source localization in the visual system is additionally intricate (Vanni et al. 2004). Thus, the motivation for using EEG-fMRI for this purpose is to benefit from the high spatial resolution of fMRI and improve the localization of visual evoked responses in the visual system. In this section, we focus on EEG-fMRI that performs source localization constrained by or compared to fMRI. Strictly evaluated, unconstrained EEG dipole modelling with fMRI does not fall into this category of fMRI-informed EEG, but it is included to maintain topical integrity.

23.2.1 Localising VEPs

In a typical pattern-onset stimulation, the first component (called C1, with a peak latency of around 60–100 ms) is commonly believed to be generated by striate cortex. However, the origin of the following component, P1 (peaking around 100–130 ms), is more uncertain, and possibly reflects extrastriate generators as well as generators within primary visual areas (Di Russo et al. 2002). Thus, one motivation for fMRI-informed EEG is to shed more light on the question of generator sites for EP components. The idea behind fMRI-informed EEG is to constrain the location of the dipole by identifying regions that exhibit significantly increased BOLD activity (e.g. caused by visual stimulation) while keeping the orientation and strength of the dipole flexible for further dipole fitting (also called “seeding”). An

unconstrained EEG-fMRI study by Di Russo et al. (2002) showed a promising substantial overlap between activated fMRI sites and EEG dipoles. Also, Bonmassar et al. (2001), who performed unconstrained and fMRI-constrained source localization over the entire EP window during a checkerboard pattern reversal task, found that the sources were consistently located in the calcarine sulcus with a more focal distribution in the fMRI-constrained localization approach, along with a slightly lower dipole power than in the unconstrained analysis.

An EEG-fMRI study by Di Russo et al. (2002) used unconstrained EEG dipole modelling to localise sources of early visual evoked components, tracing the pathway from the primary visual cortex (earliest component, C1) via extrastriate areas (P1/posterior N1 component) to higher-cognitive areas, such as in the parietal lobe (anterior N1). Dipoles were fitted sequentially, according to the peak latencies of observed components. The comparison with fMRI activations for the same experimental setup yielded generally good agreement between activated fMRI sites and EEG dipoles. However, they also stated that localising generators for components later than C1/P1 becomes an increasingly difficult task, because the number of putative temporally and spatially overlapping generators accumulates in subsequent processing stages.

In an fMRI-constrained manner, Di Russo et al. (2007) localized generators of steady-state visual evoked potentials (SSVEPS), and reported that the visual areas V1 (primary visual cortex) and V5/MT (middle temporal) were the two major generators that contributed to SSVEPS. Interestingly, two out of the four fMRI activation sites were shown to only marginally contribute to the explained variance of the dipole model when seeded, and were thus discarded. The resulting two-dipole seeded model corresponded well to the unseeded two-dipole model although it explained slightly less variance.

In contrast to the seeding approach used in the aforementioned studies, Vanni et al. (2004) also integrated the orientation of the fMRI-activated cortical areas (using 3D anatomical information from high-resolution structural MRI). The authors noted that high spatial concordance of anatomical and functional MR scans is crucial to this approach because dipole position and orientation may otherwise be distorted, leading to incorrect initial forward models. Orientation is especially susceptible to any misalignment. The goal was to identify the hierarchical cortical processing of visual stimulation. While it was possible to separate visual areas V1, V2 and V3 spatially by fMRI, the fMRI-constrained dipole modelling did not always succeed in assigning each of these areas a distinct dipole. For example, V2 sources were often collapsed together with either V1 or V3 sources.

A tacit assumption that is normally accepted when seeding fMRI-constrained dipoles is that the fMRI activation sites used to constrain the dipole solution are regions that show positive BOLD responses. The rationale for doing so was questioned by Whittingstall et al. (2007), who first performed fMRI-unconstrained source localization for visual checkerboard stimulation. When comparing results to BOLD fMRI activations they found that the early N75 component dipole localization reflected the peak positive BOLD response in or near V1, while, in contrast to Di Russo et al. (2002), the P100 (or P1) localization result yielded a region that also

exhibited significant voxels with negative BOLD responses (NBR). The authors argued that this negative response, especially when interpreted as an inhibitory process and not mere vascular stealing, may also play an important role in the processing of visual stimuli. However, it is not clear whether the P100 can be regarded as originating from inhibitory processes. Studies in monkeys indicate that, depending on the exact type of stimulation (i.e. flash stimulation or pattern reversal), the simian homologue of the P100 may reflect either at least partially inhibitory processes (i.e. net hyperpolarisation from stellate cells in primary visual cortex) or excitatory processes (i.e. net depolarisation of pyramidal neurons) (Schroeder et al. 1991).

23.2.2 Visual Attention and Other Cognitive Processes

Localising EP components that reflect attention or other cognitive processes such as target detection with the help of EEG or fMRI is attractive because the underlying neuroanatomy is less well known than it is for processing in primary visual areas. A seminal study on direct neuronal and vascular-metabolic activity associated with attentional effects in the visual system was performed not with EEG-fMRI but with EEG-PET by Heinze et al. (1994). By using separate PET and EEG sessions, they studied the effect of visual selective attention with PET-constrained dipole modelling. They found a close correspondence between unconstrained and PET-constrained EEG dipoles reflecting the effect of visual attention in the P1 EP component. Both the PET activation and the EEG dipole were located in the fusiform gyrus. These results were confirmed by an EEG-fMRI study performed by Mangun et al. (1998) without dipole modelling, which showed that there was a comparable visual spatial attention-related increase in BOLD activity in the posterior fusiform and middle occipital gyri accompanied by a modulated P1 component of the EPs. There was no BOLD modulation of the calcarine sulcus (i.e. in primary visual area V1).

However, there is debate over whether primary visual areas like V1 can also be modulated by top-down mediated attention. Martinez et al. (1999) examined this question with EEG-fMRI and found a divergence between fMRI and EP results. The fMRI results did show a modulation of primary visual cortex activity by attention, whereas the attentional effect in the EP occurred 70 ms after stimulus onset, and corresponding fMRI-unconstrained dipoles indicated that extrastriate region V3 was the putative generator site. In a follow-up study, Di Russo et al. (2003) tried to answer the question of whether the attentional effect in V1, as found by fMRI, could possibly be explained by re-entrant modulatory activity from higher visual areas like V3. They showed that the effect of visual attention did not involve modulation of the early visual evoked component (i.e. C1 around 70 ms, which was shown to be localized in V1). However, they found responses later than the N1 component (150–225 ms range) that were also localized to V1. Since this component also behaved similarly to the early C1 component in terms of reversing polarity upon changing between upper and lower visual field stimulation, the authors argued that there was evidence of an attention-dependent modulation of V1. This would point

in a similar direction to the findings of Martinez et al. (1999), with the twist here that the influence of attention in primary visual cortex was paralleled by both the fMRI activations and the late time window EP-dipole sources. Di Russo et al. (2003) used an fMRI "semiconstrained" dipole analysis, which in contrast to a fully seeded model also allowed changes in the initial positions of dipoles, which were defined by significant fMRI activation sites.

Another example of a well-examined cognitive process is the detection of an infrequent target during a (visual) oddball task that elicits the so-called P3 component arising roughly 300–600 ms after the target stimulus. Attempts have been made to localise it via EEG dipole modelling studies, but with inconsistent results (Bledowski et al. 2004). Sometimes this component is divided into P3a and P3b components. While P3a is said to mainly reflect the processing of distractor events, P3b is what is classically referred to as P3 and reflects the detection of novel, infrequent events in general. fMRI studies have shown the involvement of regions like the anterior cingulate cortex (ACC) and the supramarginal gyrus (SMG) (Ardekani et al. 2002). Similar regions were also reported by Linden et al. (1999) for uninformed EEG-fMRI during a visual and auditory oddball task. Bledowski et al. (2004) were interested in separating the P3a and P3b responses. They performed a separate-session three-stimulus visual oddball task (frequent, infrequent distractor and infrequent target) with fMRI-informed source localization of P3a and P3b responses, and found that a broadly distributed network of sources accounted for the respective P3a and P3b responses. Their approach was to start from a common set of six pairs of fMRI seeds for both target and distractor conditions. Analysis of the time courses of resulting dipole moments indicated that the insula and the precentral sulcus seemed to be contributing more to the P3a component than to the P3b. Crottaz-Herbette and Menon (2006) used a different fMRI-informed EEG localization approach. By performing a two-stimulus (frequent standard and infrequent target) auditory and visual oddball task, each resulting in a modality-dependent set of fMRI seeds for dipole fitting, they identified the ACC as being the main contributor to the N2b–P3a effect in both sensory modalities. For the visual oddball P3b component, they noted the involvement of inferior parietal areas (this was also reported by Bledowski et al. 2004).

Concerning the different results for generators of the P3 component, it should be said that, with an increasing number of assumed dipoles, dipole fitting often yields highly satisfactory results in terms of explaining the variance of EP waveforms. However, equally efficient solutions may exhibit quite different positions of dipoles. Thus, fMRI constraints are used to constrain the solution space. If the fMRI constraints differ prior to dipole fitting, the positions of the dipoles should also differ.

Apart from the visual oddball studies addressed above, there are also studies focusing on other higher-cognitive processes, like the processing of perceptual illusions or transitions, figure-ground separation, or the construction of objects from incomplete information. An innovative electrophysiological paradigm was used by Appelbaum et al. (2006), who separated the neuronal processes for the figure and background regions of a visual stimulus by "tagging" them with distinct spectral properties; in other words, they were textures characterized by different temporal frequencies. The resulting separate time courses of the figure and background

components were subjected to cortical current density (CCD) analysis constrained by fMRI activations. These source reconstructions suggested that the figure region information was routed to the lateral occipital cortex (LOC), but that this was not the case for the processing of background region information.

Schoth et al. (2007) used the rotating Necker cube as a visual stimulus, which, in contrast to other illusionary multistable stimuli, has a predictable transition point between its different modes of perception. In this study, fMRI activations of the rotating Necker cube were used as constraints for current density reconstruction of the VEP related to the arising perceptual transition. It revealed initial processing in Brodmann area 18 and subsequent spreading along the visual dorsal stream.

Concerning the topic of higher-cognitive perceptual processes, Sehatpour et al. (2006) employed EEG-fMRI to identify neural networks that are active during "perceptual closure", which means the filling in of required information for a partially fragmented or distorted visual image in order to actively construct a recognisable object again. The major contributor to perceptual closure, as found by fMRI, was LOC. Without using a priori information from fMRI activations, EEG source analysis of the accompanying Ncl ("negativity related to closure") EP component yielded similar regions within the LOC to those found by fMRI.

Croize et al. (2004) used a combined MEG, EEG and fMRI approach together with unconstrained source localization to examine visuospatial short-term memory processing. While there was largely good agreement between localized EEG current densities and MEG dipoles with fMRI activation sites, only the MEG covered a memory-encoding component in a late time window (around 400 ms) corresponding to right premotor areas. as observed by fMRI. The authors argued that this may be due to the well-known differential sensitivities of EEG and MEG to either radial or tangential sources, respectively.

Summarising the above studies, it can be said that complementing the EEG dipole models with the associated changes in fMRI activity largely confirmed the results of unconstrained dipole fitting in EEG studies. Also, the use of fMRI-guided dipoles seemed to lead to efficient models in terms of low residual variance. However, a direct comparison of the unconstrained vs. the constrained model approach was not always provided. When it was, the constrained model tended to explain slightly less variance. Some fMRI seeds also had to be discarded due to their inefficiency at explaining the variance of the EP waveform. In our view, findings of non-overlapping activity are as interesting as findings of overlapping activity, which however appear to be emphasized in published studies.

23.3 EEG-Informed fMRI of the Visual System

In contrast to the previously described approach of fMRI-informed EEG, the approach of EEG-informed fMRI implies deriving information from the EEG that can be used to identify regions that exhibit BOLD responses co-varying with the selected parameter. There are many candidate EEG response features including the: amplitude and latency of VEPs; magnitude of event-related synchronization/desynchronization

(ERS/ERD) of oscillatory power and spontaneous fluctuations in oscillatory power. There are also many analytic options for data integration, for a review of approaches see (Abreu et al. 2018), but the common goal is that instead of constraining a dipole solution, to create a new model of predicted BOLD activity, which can then be tested.

23.3.1 Spontaneous EEG Oscillations

The posterior alpha oscillation (8–13 Hz) and its relationship to the activity of the visual system is long established (Berger 1929). However, although alpha is the most prominent spontaneous neural oscillation, a clear localization of its generators has not been achieved. Long neglected as merely a marker of cortical idling, it is now hypothesized that alpha provides a mechanism for gating and regulating the flow of information both within and between brain networks by selectively inhibiting task-irrelevant pathways (Jensen and Mazaheri 2010). Alpha provides a useful measure of arousal and cortical excitability (Romei et al. 2008; Olbrich et al. 2009). A number of studies have investigated the functional importance of alpha by studying the association of within and between subject variations in alpha with variation of subsequent behavioral and brain responses. Findings suggest that pre-stimulus alpha power modulates the detection of visual targets and amplitude of VEPs (Hanslmayr et al. 2007; Linkenkaer-Hansen et al. 2004; Becker et al. 2008). Therefore, examining pre-stimulus and spontaneous alpha activity is important for achieving a full understanding of event-related processes.

Across many EEG-fMRI studies, a close relationship between posterior alpha oscillation and fMRI-BOLD signal changes has been reported (Goldman et al. 2002; Laufs et al. 2003a, b, 2006; Moosmann et al. 2003; Goncalves et al. 2006; Feige et al. 2005; de Munck et al. 2007; Wu et al. 2010; Liu et al. 2010; Zhan et al. 2014; Mayhew and Bagshaw 2017). In those EEG-informed fMRI studies, the EEG parameter of interest was the amplitude of the alpha oscillation. Typically, the envelope of the oscillatory alpha power was calculated over each fMRI TR period, convolved with the hemodynamic response function (HRF) and used as a predictor for each BOLD signal time point. Despite the similar approaches used, the results were not completely consistent with marked inter-subject variability in size and extent of alpha-BOLD correlations. However, a negative correlation between alpha power and the BOLD signal in occipital and parietal areas is widely observed (Goldman et al. 2002; Moosmann et al. 2003; Feige et al. 2005; de Munck et al. 2007; Wu et al. 2010; Liu et al. 2010; Zhan et al. 2014; Mayhew and Bagshaw 2017). Positive, alpha-BOLD correlations in the thalamus are also observed (Goldman et al. 2002; Moosmann et al. 2003; de Munck et al. 2007; Liu et al. 2010; Mayhew and Bagshaw 2017, see Fig. 23.2); however, a recent study found negative correlations within the visual thalamus and pulvinar as well as positive correlations in the anterior and medial dorsal nuclei (Liu et al. 2010). Another study found that the phase of pre-stimulus oscillations at 7 Hz predicted task-related changes in functional connectivity between higher and lower level visual areas, as measured by fMRI (Hanslmayr et al. 2013). These results support the concept of the alpha oscillation acting as a gating mechanism for input to the visual system.

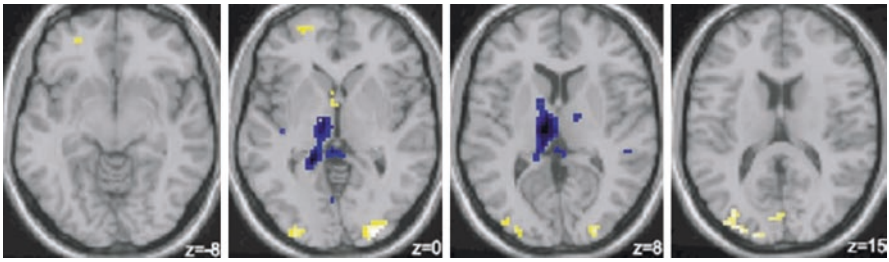

Fig. 23.2 Results from a correlation analysis between alpha amplitude and BOLD signal. (Modified from Moosmann et al. 2003). Group analysis of six subjects, $p < 0.05$, corrected for multiple comparisons. *Yellow*: Significantly negative correlations. *Blue*: Significantly positive correlations

In contrast, some studies (Laufs et al. 2003a, b, 2006; Goncalves et al. 2006) have also reported frontoparietal negative correlations for some subjects, which is consistent with recent reports of a more global, and modality-independent role of alpha oscillation in vigilance and alertness (Matsuda et al. 2002; Henning et al. 2006; Sadaghiani et al. 2010). Mayhew and Bagshaw (2017) used 16 s sliding window analysis, rather than static correlations over the entire scan duration, to reveal substantial spatiotemporal variability of resting-state alpha-BOLD relationships within-subjects. Alpha-BOLD correlations passed through many different configurations such that the static network was fully represented in only ~10% of 16 s epochs, showing that the static network loses its coherence such that its different regional components correlate with alpha during different periods of time (Mayhew and Bagshaw 2017).

de Munck et al. (2007) were specifically interested in whether the time course of the metabolic correlate of the alpha oscillation follows the temporal assumptions of the HRF. The correlations between the BOLD signal and the alpha power in the occipital and parietal regions showed similar temporal lags as previously supposed when using the canonical HRF, while the correlation in the thalamus was less delayed (by several seconds).

In these types of studies, simultaneous EEG-fMRI acquisition is crucial to relate spontaneously fluctuating EEG activity to concurrent BOLD signals.

Recent extensions to this work have begun to elucidate how measures of spontaneous alpha oscillations, extracted from pre-stimulus data, modulate subsequent fMRI responses (Scheeringa et al. 2011b; Becker et al. 2011; Mayhew et al. 2013; Mayhew and Bagshaw 2017). Scheeringa et al. found that the amplitude of the BOLD response to visual checkerboard stimuli presented at the trough of alpha cycle was larger than the response to stimuli at the peak of the cycle (Scheeringa et al. 2011b). Becker et al. (2011) and Mayhew et al. (2013) found that the amplitude of the BOLD response to visual stimuli was also correlated with the magnitude of pre-stimulus alpha power, to the extent that variations in alpha activity explained variability in both positive and negative BOLD amplitudes (Becker et al. 2011; Mayhew et al. 2013). Specifically, trials preceded by high levels of alpha power were observed to show smaller positive BOLD responses than trials of low alpha power. These latter two studies also evidence subtle differences in the alpha-BOLD

relationship between task and rest but are consistent with the concept of posterior alpha representing a marker of the excitability and responsiveness of the visual cortex. In interpreting such studies one must always bear in mind that scalp EEG measures the summed activity of all nearby synchronous post-synaptic potentials, and therefore the concept of the existence of a single posterior alpha oscillation may be an over simplification and that different alpha sources may predominate depending on particular behavioral circumstances (see Shaw 2003; Sokoliuk et al. 2018). Further clarification and classification of spontaneous oscillations will be required to better understand the patterns of dynamic behavior that alpha exhibits and how this is influenced by brain state and experimental context.

Another approach to investigating spontaneous activity with EEG-fMRI was pursued by Mantini et al. (2007), who decomposed BOLD activity into independent clusters, reflecting so-called resting-state networks (RSNs). They then temporally correlated the BOLD signal in these networks with the EEG spectral activity as averaged across all electrodes and found distinct spectral-correlation patterns for each RSN. An extension of this approach preserves distinct and topographically specific EEG oscillations and examine their relationship to RSN BOLD activity. Results from such an approach are shown in Fig. 23.3. This shows the topography and time courses of two different RSNs (a visual network and the default mode

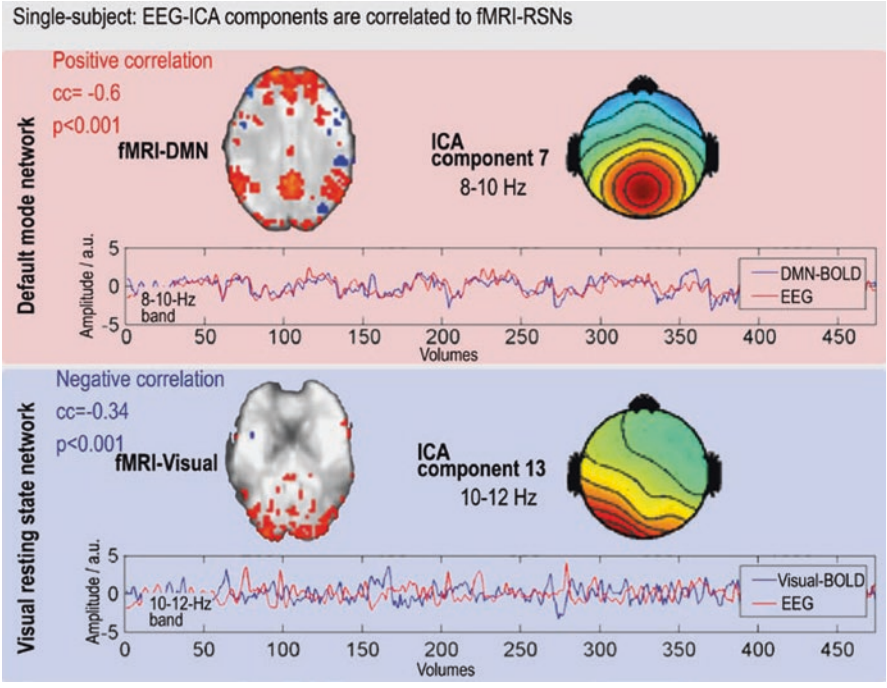

Fig. 23.3 Correlation between two different BOLD RSNs (default mode network at the *top* and visual component at the *bottom*) and the EEG-ICA components for a single subject. (Modified from Ritter et al. 2008)

network; Raichle et al. 2001) and those of two distinct spontaneous EEG components (as identified via ICA) that correlate maximally with the RSNs. This result demonstrates that spatially and spectrally neighboring EEG components can exhibit different relationships with different RSNs (Ritter et al. 2008). More recent work used Hidden Markov Modelling, a data driven method to identify fast (<1 s) transient network dynamics in EEG data. They found that the fMRI correlates of these transient networks showed highly reproducible spatial patterns with strong similarity to established configurations of intrinsic connectivity networks (Hunyadi et al. 2019).

23.3.2 Task-Related EEG Activity

Concerning EEG-informed fMRI studies of task-related activity, a number of studies have correlated and/or integrated single-trial visually evoked EEG activity with BOLD responses, extending work in other sensory and cognitive systems (Debener et al. 2005; Benar et al. 2007; Eichele et al. 2005; Mayhew et al. 2010a). Initial studies used separate session recordings and by measuring the variability in average ERP and BOLD amplitudes were able to investigate between-subject correlations in EEG and fMRI responses (Horovitz et al. 2004; Knyazeva et al. 2006a, b; Yeşilyurt et al. 2010). Due to the developments in both EEG hardware and preprocessing techniques, more recent studies have been able to collect simultaneous EEG-fMRI recordings of many aspects of visual processing. This approach enables single-trial analysis where parametric measures of EEG response variability are used to inform the fMRI analysis at the within-subject level (Mayhew et al. 2010b; Novitskiy et al. 2011; Walz et al. 2014; Warbrick et al. 2014).

For example, Horovitz et al. (2004) parametrically varied the noise level in a picture and correlated the resulting effect on the N170 peak EP amplitude with fMRI activations, and identified a highly significant correlation with the fusiform gyrus. The authors concluded that this supports the idea of the fusiform gyrus, contributing to the generation of the N170 EP component, since both entities show corresponding effects of experimental manipulation of the noise level. Another approach was employed by Philiastides and Sajda (2007), who used parameters estimated from a previous EEG study to model the BOLD response during different stages of a perceptual decision task in an fMRI experiment, which allowed them to identify distinct cortical networks for each stage.

Bagshaw and Warbrick (2007) analyzed EEG and fMRI single-trial data from separate sessions and reported a robust correlation between the experimentally manipulated latency variabilities of EEG and BOLD single trials, which hints that the observed variability may share a common neural origin. Further, simultaneous single-trial studies were required to obtain more direct evidence for that assumption, as discussed below.

Other studies used EEG parameters for correlation analyses across subjects to identify the relationship between inter-hemispheric coherence and involved visual areas. Knyazeva et al. (2006a) showed that visual area V4 was more active during

stimulation with iso-oriented gratings than during stimulation with orthogonally oriented gratings. EEG analysis showed that stimulation with iso-oriented gratings was also accompanied by increased inter-hemispheric coherence of occipital electrodes in the beta band. Additionally, there was a significant correlation of inter-hemispheric coherence across subjects with visual area V4. The results were taken as evidence for the involvement of this extrastriate site in early perceptual grouping, since iso-oriented gratings obey the Gestalt principles (in this case collinearity and common fate). In another study, Knyazeva et al. (2006b) used different spatial frequencies of stimulation and a similar analysis and experimental approach as that used in the aforementioned study. They showed that independent of spatial frequency, inter-hemispheric lower beta-band synchronization was highly correlated with the activation of ventral extrastriate areas, while synchronization of the higher beta band corresponded to more dorsal extrastriate areas.

Yeşilyurt et al. (2010) used ultra-short stimuli (0.1-5 ms) to minimize non-linear effects in the BOLD data and used separate session recordings to study whether VEP and BOLD responses were similarly modulated by stimulus intensity and duration. They found that the mean N1 peak amplitude linearly covaried with BOLD across subjects, but the P1 did not (Yeşilyurt et al. 2010).

The N1 and P1 components have been the subject of many other EEG-fMRI studies of the processing of visual stimuli. Novitskiy et al. (2011) separately examined the BOLD correlates of the P1 (50–150 ms) and P1 (150–250 ms) components of single-trial VEPs using the integration by prediction approach (Novitskiy et al. 2011). This study required subjects to respond to 150 ms checkerboard wedges presented to different quadrants of the visual field, separate by 1–2.5 s. They used a GLM to model the BOLD correlates of the difference between the N1 and P1 amplitudes in the hemispheres, both contralateral and ipsilateral to the stimuli. They found that N1 and P1 correlated with BOLD in similar regions of the temporal-parietal junction and the dorsal stream. These correlations were spatially distant from the visual cortex activations seen to the main effect, constant amplitude GLM regressors, therefore suggesting that VEP amplitude did not explain additional variance in the primary visual response. Mayhew et al. (2010b) reported a similar finding, whereby VEPs were measured from a 4 Hz stimulus in a 30 s block design were found to correlate with BOLD amplitudes only in peripheral areas of the activation, away from the most significant BOLD response in the calcarine.

Warbrick et al. (2014) used integration by prediction of single-trial VEP amplitudes to show that the BOLD correlations with P1 and N1 components were sensitive to task manipulations and were informative about different attentional and response components of the task. Their paradigm featured separate conditions of passively viewing, silently counting, or actively responding to a visual oddball paradigm. They reported that the regions of BOLD correlation with P1 mostly reflected sensory encoding of stimulus features for passive and counting conditions. The BOLD correlates of N1 were more informative for the respond condition, suggesting that its activity reflected the discrimination between stimulus types, and processes involved in integrating sensory information with response selection.

Whittingstall et al. (2008) compared the spatial co-localization of EEG and fMRI sources rather than studying covariations of response amplitudes. Using a 2 Hz partial field visual checkerboard stimuli they evoked positive BOLD responses that were co-localized with the VEP N75 dipole source and NBR that were spatially congruent with the P100 dipole. This suggests that different biophysical relationships could exist between different neural and hemodynamic response parameters.

Much work has been performed developing pre-processing techniques and establishing the quality of VEPs acquired in the hostile scanner environment in the presence of ballistocardiogram and gradient artifacts (Assecondi et al. 2010; Vanderperren et al. 2010). Further work has focused on improving extraction and measurement of parameters of visually evoked activity and the separation of signal from the large amounts of noise during simultaneous fMRI recordings. One approach uses an adaptation of ICA called functional source separation to extract evoked EEG activity by exploiting a-priori knowledge of the signal of interest, e.g. the peak latency of the VEP P100 component (Porcaro et al. 2010). Other approaches have moved beyond using simple EEG amplitudes as response features and instead used a sliding window linear classification of VEP data to discriminate standard vs. oddball VEP responses and used these data as GLM regressors to reveal the temporal sequence of fMRI correlations in the early (<275 ms), middle (275–500 ms), and late (>500 ms) phases of the response (Walz et al. 2014). A similar method was used to separate early and late temporal components of the neural response to visual pattern perception during a learning task (Mayhew et al. 2012). Further work applied information theory to combine EEG and fMRI time-domain features by quantifying the information in their joint probability distribution (Ostwald et al. 2010), allowing a differentiation to be made between signal features which were informative about the external stimulus and those which are informative about other signal features. This multitude of approaches highlight that the field is yet to reach a consensus concerning the most appropriate way to combine EEG and fMRI data and few approaches offer truly integrated analysis. One possibility in this regard is the joint-ICA approach which allows fusion of EEG and fMRI information in common data space and a single spatiotemporal solution (Moosmann et al. 2008). Dynamic causal modelling (DCM) has also been applied to fuse EEG-fMRI data during a face perception task (Nguyen et al. 2014). Here the model space of the DCM construction was constrained to visual regions shown by a GLM analysis to be recruited by the task, and single-trial N170 amplitudes were found to act as modulators of the effective connectivity between the fusiform face area and other visual areas. They also report that model evidence for the DCMs including the N170 information was more than those models without it (Nguyen et al. 2014).

23.4 Uninformed EEG–fMRI and Other Approaches

Aside from fMRI-informed EEG and EEG-informed fMRI, combined EEG–fMRI studies can also be performed in a mutually "uninformed" way, where each modality is analyzed separately. These studies will be discussed in the following section,

with the exception of EEG-fMRI studies with unconstrained source localization, which are actually uninformed but have been already described in the section on fMRI-informed EEG.

23.4.1 Event-Related Oscillations (EROs)

Foucher et al. (2003) related EPs and event-related gamma band activity to the BOLD signal and postulated a closer correspondence between BOLD and gamma than between BOLD and the EP response, arguing that non-phase-locked EEG responses should be considered when modelling the hemodynamic response. During a visual oddball task, a weaker P3 component was produced during target than during novel detection, while BOLD activity increased. This was paralleled by a stronger spectral response in the gamma range (32–38 Hz) in EEG.

Another study by Fiebach et al. (2005) also examined effects of event-related gamma band activity during a different task. Using a visual lexical decision task, parallel behavior between gamma and BOLD was observed: upon the presentation of pseudo-words, BOLD activity in defined areas, gamma band response and phase synchrony between electrodes increased, while these effects were inverted but still parallel upon the presentation of words. Of course, this experimental task differs fundamentally from that above; however, it is still worthwhile discussing such diverging results in the context of a universal relationship between oscillatory activity and BOLD responses.

23.4.2 Visual Attention and Other Cognitive Processes

Gazzaley et al. (2005) reported top-down modulated magnitude and speed of neural activity as measured with EEG and fMRI. Amplitudes of evoked responses in both EEG and fMRI (neural activity) were modulated by an attentional paradigm showing faces and scenes, respectively. For fMRI, there was higher activity in the parahippocampal place area for the remember scenes vs. the ignore scenes condition, and higher activity in the fusiform face area for the remember faces vs. the ignore faces condition. Concerning the EEG results, the EP difference waveform for this contrast also yielded a significant amplitude as well as latency effect for the face-selective N170 component, which had not been reported before. Mangun et al. (1998) showed that there was a visual spatial attention-related increase in BOLD activity in the posterior fusiform and middle occipital gyri accompanied by a modulated P1 component of the ERPs. They did not report on later effects of attention, and in contrast to the aforementioned studies they found no consistent activation of V1.

Muller et al. (2005) used a multistable visual motion paradigm where subjects responded to spontaneous transitions of the perceptual mode of the stimulus. Transitions between different modes were marked by alpha and beta activity decreases and delta increases in the EEG before transition. Regions of increased

BOLD activity included right anterior insula, MT, and supplementary motor area, while thalamus and right superior temporal gyrus showed decreases in BOLD activity.

The neural mechanisms of visual spatial attention have been investigated by a number of recent EEG-fMRI studies employing single-trial analyses (Zumer et al. 2014; Liu et al. 2016; Green et al. 2017). In these studies, the response of interest was oscillatory EEG power measured during a pre-stimulus cue period. During this cue, subjects were instructed to covertly allocate their spatial attention (e.g. to the left or right visual field) in order to report a subsequent visual stimulus target presented there. Liu et al. (2016) found that single-trial attentional modulations of alpha power were inversely correlated with BOLD in parietal and medial frontal regions that also showed activation on average to the attentional task. They also observed positive alpha-BOLD correlates in regions of the default mode network, suggesting that attentional fluctuations in alpha track the response pattern of the task-positive and task-negative networks (Liu et al. 2016).

Zumer et al. (2014) used a working memory paradigm where subjects processed hemifield faces and ignored landscapes and vice versa. They also found that single-trial alpha power correlated with attention network BOLD signal, and furthermore that alpha contralateral to the attended object predicted the BOLD signal representing that object in ventral object-selective regions. They also report an inverse alpha-BOLD correlation in unattended ipsilateral visual cortex. This provides further evidence that alpha reflects gating processes between the visual cortex and the ventral stream. Green et al. (2017) extended these works by studying attentional modulations in gamma power, as well as alpha, and also subcortical EEG-BOLD correlates. They also found an inverse alpha-BOLD correlation in visual regions ipsilateral to the cued location, interpreted as a suppression of task-irrelevant cortex. Positive gamma-BOLD correlations were seen in contralateral visual cortex regions representing the attended visual field. Importantly they found that both alpha and gamma correlated with BOLD in the pulvinar nucleus (Green et al. 2017), demonstrating that subcortical activity can be studied via correlations between BOLD and scalp EEG.

23.5 Investigating Neurovascular Coupling in the Visual System by EEG–fMRI

Investigating the coupling relationship between neural activity and BOLD signal has occupied investigators since the beginning of fMRI-based research and much of this work has taken place in the visual modality. Simultaneous EEG-fMRI is a powerful tool for investigating a wide range of neurovascular coupling questions as it not only allows relation of BOLD response amplitudes to parameters of EEG activity (e.g. EPs or EROs) but also enables examination of which response parameters (e.g. EP amplitude at different latencies, or different frequency EROs) are most correlated with BOLD.

In a pioneering study, Logothetis et al. (2001) found a higher correspondence between local field potentials (LFPs) and the BOLD signal than between multiunit activity (MUA) and BOLD. This seminal work has been supported by many other studies (Viswanathan and Freeman 2007; Rauch et al. 2008; Magri et al. 2012) leading to conclusions that both EEG and BOLD primary reflect synaptic population inputs, since EEG reflects synchronized extracellular dendritic currents rather than action potentials. This is a promising result for EEG-fMRI analysis which commonly assume a linear coupling between neural activity and BOLD. Some studies support a mostly linear relationship (Singh et al. 2003) but others suggest a more complex coupling can occur (Liu et al. 2010), as we will explain below with exemplary studies on the visual system.

Huettel et al. (2004) attempted to link intracranially recorded human visual event-related local field potentials (ER LFPs) and BOLD fMRI in separate sessions by experimentally manipulating stimulus duration. They found a divergence between consistently (non-linearly) increasing BOLD activity in calcarine and fusiform cortex for longer stimulation, and differing EP responses from these two regions (i.e. an onset-sustained response that was partially dependent on stimulus duration as well as a pure onset response that was independent of stimulus duration). This supports the notion that the BOLD signal integrates information on a longer timescale, which complicates the estimation of the direct neural basis from BOLD measurements. Janz et al. (2001) showed that the adaptation effect for repetitive stimulation from a checkerboard reversal, as seen in the BOLD signal, is not plainly mirrored and cannot be accounted for completely by adaptation effects as observed in the accompanying VEP. This would speak against a straightforward inference from BOLD to EEG and vice versa, thus demanding adjusted approaches in order to model the hemodynamic response as a consequence of electrophysiological properties.

Wan et al. (2006) also examined the non-linearity of the visual event-related BOLD and EP responses with concurrent EEG–fMRI by modulating stimulus frequency and contrast. Interestingly, when estimating neuronal efficacy from BOLD rather than using this parameter directly, a comparison of it to mean power of electrical activity (which is non-linear by nature) resulted in a linear correlation between both indices of neural activity, indicating that the observed non-linearity may have a neural basis.

Guy et al. (1999) studied EEG and fMRI responses to periodic stimulation. A new measure created by correlating the EEG with the VEP template was created (VEPEG) and compared with the fMRI BOLD signal. Both measures mirrored the fundamental frequency of the stimulus presentation and both of them exhibited a post-stimulus negativation, which may point to similar neural processes after stimulus offset. Singh et al. (2003) examined the effect of changing the frequency of a checkerboard flash stimulation on BOLD and EP responses, and found a robust correlation between strength of SSVEPs (amplitudes) and BOLD response activations.

Henning et al. (2005) found a divergence between EEG and fMRI effects when applying different types of visual stimulation, such as pattern reversal, motion onset

and motion reversal of a starfield stimulus. While EPs (especially N2 components) were the most enhanced by motion onset, fMRI activation (with its maximum in visual area MT) was largest for motion reversal. They argue that this may be due to both modalities reflecting different processes. In the light of a more complete description of neural activity, it would have been of interest to investigate whether non-phase-locked EEG responses could explain the divergent effects.

Coupling between neural activity and BOLD have often been reported to be strongest in the gamma-frequency band (Logothetis et al. 2001) but given that interactions between oscillatory frequency bands are well known (Canolty et al. 2006; Osipova et al. 2008) and BOLD represents the integral of all underlying metabolic demand, the nuanced link between BOLD and broadband activity is of great interest.

Although not capable of simultaneous recordings, studies comparing between subject variability in mean MEG and BOLD responses have greatly contributed to understanding of neurovascular coupling. Although close spatial correspondence between sources of oscillatory ERD/ERS and BOLD responses is consistently reported (Brookes et al. 2005; Muthukumaraswamy and Singh 2008), several studies report differential modulation of MEG and BOLD responses with changes in visual stimulus parameters (Muthukumaraswamy and Singh 2008, 2009; Swettenham et al. 2013). For instance, no changes in BOLD amplitude with the spatial frequency of visual gratings were observed despite a 300% increase in gamma ERS (Muthukumaraswamy and Singh 2009). Such studies illustrate the complexity of this issue, that neurovascular coupling may not be consistent and generalizable and instead vary with stimulus parameters.

EEG-fMRI has been used to consolidate our understanding of neurovascular coupling by providing replications of Logothetis' original work non-invasively in humans. Scheeringa et al. (2011a) measured BOLD and broadband range of oscillatory EEG responses to a contracting visual grating stimuli and reported: positive correlations between gamma ERS and BOLD; and negative correlations between BOLD and both alpha and beta ERD. In addition they found these correlations were independent and that gamma was the strongest predictor of BOLD (Scheeringa et al. 2011a). More recent work using electrocorticography (ECoG) presented contrasting and intriguing results that BOLD was most closely related to asynchronous visual responses in the gamma range, called broadband gamma (Winawer et al. 2013), rather than oscillatory narrowband gamma that has been more commonly studied, e.g. by Scheeringa et al. (2011a) and Muthukumaraswamy and Singh (2009).

EEG-fMRI has also been applied for interrogation of BOLD response origins by the addition of concurrent arterial spin labelling for the measurement of cerebral blood flow (Mullinger et al. 2013, 2014). This provides deeper neurophysiological insight by allowing study of more of the underlying biophysical components that make up the complex BOLD signal and allows investigation the origin of less well known and relatively poorly understood components, such as NBR and post-stimulus undershoots (PSU). PSUs occur on cessation of stimulation where the BOLD signal falls below baseline amplitude before returning to resting levels. PSUs were originally thought to reflect purely vascular effects such as slow recovery of cerebral blood volume (Buxton et al. 1998) but recent work has shown that

the amplitude of BOLD and cerebral blood flow PSUs correlate with alpha power in the post-stimulus response period (Mullinger et al. 2017) and are associated with decreased oxygen metabolism. This suggests an inhibitory neural origin of PSUs and is concordant with recent MEG work that suggests that this response period may have a functional purpose (Hunt et al. 2019).

In general, more complex biophysical models of the relationship between EEG and fMRI activity are needed to clarify the origins of different BOLD response components and reported divergent relationships across different stimulus parameters. One step in this direction is the forward model of Sotero and Trujillo-Barreto (2008), which was able to reproduce VEPs and concurrent BOLD patterns as well as the spontaneous alpha oscillation with its accompanying typical BOLD activity. A biophysical model that could actually produce the overlaps as well as the observed divergences between EEG and fMRI would be of great value, since this would contribute to a better understanding of the nature of both modalities and enable better integration of their complementary information.

23.6 Outlook

The following section attempts to sum up what has been achieved so far and at the same time discuss what is still missing. First, we critically examine whether the frequently stated expectation of EEG-fMRI, that of providing both high spatial and temporal resolution of brain activity, has been met with respect to studies of the visual system.

Without restricting ourselves to the visual system, EEG-fMRI experiments yield two kinds of measures: one highly temporally resolved measure from the EEG and another spatially highly resolved signal from the fMRI measurement. What we ultimately desire to obtain is one merged, composite signal that has both high spatial and temporal resolution. However, what we normally obtain is a temporal correlation between BOLD activity and an HRF-convolved EEG time course (EEG-informed fMRI) or a spatial co-localization between a BOLD cluster and an EEG source (fMRI-informed EEG). These types of temporal or spatial overlaps hint at relevant connections between the two modalities but do not necessarily represent causal relations.

The use of fMRI constraints for EEG source modelling suffers from the problem that fMRI clusters do not always reflect neural activity that contributes to EEG scalp potentials. Thus, it is prone to errors caused by inappropriate modelling of assumed sources of brain activity. Of course, substantial overlap between unconstrained EEG dipoles and fMRI activations has been shown. If we use an appropriate model, we can attribute the temporal dynamics of an EEG dipole to an fMRI cluster.

In EEG-informed fMRI, regions are identified that show a correlation between BOLD activity and a certain EEG parameter. Here, relationships between EEG parameters and BOLD activity other than linear correlations should also be considered. Also, the critical assumption that the chosen EEG parameter indexes neuronal activity may not always be justified (e.g. in the case of BCG contamination of EEG parameters).

Concerning examinations of neurovascular coupling, depending on the examined EEG parameter—EP amplitudes, single-trial activity, spontaneous, or event-related oscillatory activity—the characterization of the EEG-BOLD relationship will vary, which is also reflected in the results of the studies on neurovascular coupling in the visual system discussed above. Even a complete description of all conceivable EEG parameters may not appropriately reflect the neural processes of a certain region, leading to suboptimal modelling of BOLD responses.

Given the option of directly measuring neuronal activity with the help of MRI (sometimes termed "direct" (f)MRI), the concurrent use of EEG would be finally made obsolete, since the MR signal would then provide high temporal and spatial resolution for one and the same measure. The visual system has already been used several times as a starting point for such attempts, but contradictory conclusions have been drawn about its feasibility, since either favorable but indirect results (Bianciardi et al. 2004; Konn et al. 2004) or rather discouraging results have been obtained when using concurrent EEG for validation (Mandelkow et al. 2007).

Having summarized the results of EEG-fMRI studies in the visual system, in our opinion, the great strength of EEG-fMRI lies in its ability to dissect the composite metabolic response of the BOLD signal and tease apart components most related to different periods of temporal activity, contributions of different frequency bands, or modulations of network functional connectivity. Although yet to be fully and consistently exploited it has the potential to actually merge both modalities in order to obtain one single measure, as in direct fMRI. In addition, by using simultaneous EEG-fMRI, we are able to observe interactions between the two complementary measures of brain activity, which can reveal new insights into fundamental questions of brain function, such as how spontaneous oscillations affect the way that events are processed.

References

Abreu R, Leal A, Figueiredo P (2018) EEG-informed fMRI: a review of data analysis methods. Front Hum Neurosci 12:29

Appelbaum LG et al (2006) Cue-invariant networks for figure and background processing in human visual cortex. J Neurosci 26(45):11695–11708

Ardekani BA et al (2002) Functional magnetic resonance imaging of brain activity in the visual oddball task. Brain Res Cogn Brain Res 14(3):347–356

Assecondi S, Vanderperren K, Novitskiy N, Ramautar JR, Fias W, Staelens S, Stiers P, Sunaert S, Van Huffel S, Lemahieu I (2010) Effect of the static magnetic field of the MR-scanner on ERPs: evaluation of visual, cognitive and motor potentials. Clin Neurophysiol 121:672–685

Bagshaw AP, Warbrick T (2007) Single trial variability of EEG and fMRI responses to visual stimuli. Neuroimage 38(2):280–292

Becker R et al (2005) Visual evoked potentials recovered from fMRI scan periods. Hum Brain Mapp 26(3):221–230

Becker R et al (2008) Influence of ongoing alpha rhythm on the visual evoked potential. Neuroimage 39(2):707–716

Becker R, Reinacher M, Freyer F, Villringer A, Ritter P (2011) How ongoing neuronal oscillations account for evoked fMRI variability. J Neurosci 31:11016–11027

Benar CG et al (2007) Single-trial analysis of oddball event-related potentials in simultaneous EEG–fMRI. Hum Brain Mapp 28(7):602–613
Berger H (1929) Über das Elektrenkephalogram des Menschen. Arch Psychiatr Nervenkr 87:527–570
Bianciardi M et al (2004) Combination of BOLD–fMRI and VEP recordings for spin-echo MRI detection of primary magnetic effects caused by neuronal currents. Magn Reson Imaging 22(10):1429–1440
Bledowski C et al (2004) Localizing P300 generators in visual target and distractor processing: a combined event-related potential and functional magnetic resonance imaging study. J Neurosci 24(42):9353–9360
Bonmassar G et al (1999) Visual evoked potential (VEP) measured by simultaneous 64-channel EEG and 3T fMRI. Neuroreport 10(9):1893–1897
Bonmassar G et al (2001) Spatiotemporal brain imaging of visual-evoked activity using interleaved EEG and fMRI recordings. Neuroimage 13(6 Pt 1):1035–1043
Brookes MJ, Gibson AM, Hall SD, Furlong PL, Barnes GR, Hillebrand A, Singh KD, Holliday IE, Francis ST, Morris PG (2005) GLM-beamformer method demonstrates stationary field, alpha ERD and gamma ERS co-localisation with fMRI BOLD response in visual cortex. Neuroimage 26:302–308
Brookes MJ, Mullinger KJ, Stevenson CM, Morris PG, Bowtell R (2008) Simultaneous EEG source localisation and artifact rejection during concurrent fMRI by means of spatial filtering. Neuroimage 40:1090–1104
Bunkrad M et al (1989) Visual evoked cortical potentials modified by a NMR magnetic field of 0.24 tesla. Fortschr Ophthalmol 86(6):702–705
Buxton RB, Frank LR, Wong EC, Siewert B, Warach S, Edelman RR (1998) A general kinetic model for quantitative perfusion imaging with arterial spin labeling. Magn Reson Med 40:383–396
Canolty RT, Edwards E, Dalal SS, Soltani M, Nagarajan SS, Kirsch HE, Berger MS, Barbaro NM, Knight RT (2006) High gamma power is phase-locked to theta oscillations in human neocortex. Science 313:1626–1628
Comi E et al (2005) Visual evoked potentials may be recorded simultaneously with fMRI scanning: a validation study. Hum Brain Mapp 24(4):291–298
Croize AC et al (2004) Dynamics of parietofrontal networks underlying visuospatial short-term memory encoding. Neuroimage 23(3):787–799
Crottaz-Herbette S, Menon V (2006) Where and when the anterior cingulate cortex modulates attentional response: combined fMRI and ERP evidence. J Cogn Neurosci 18(5):766–780
de Munck JC et al (2007) The hemodynamic response of the alpha rhythm: an EEG/fMRI study. Neuroimage 35(3):1142–1151
Debener S et al (2005) Trial-by-trial coupling of concurrent electroencephalogram and functional magnetic resonance imaging identifies the dynamics of performance monitoring. J Neurosci 25(50):11730–11737
Debener S et al (2008) Properties of the ballistocardiogram artefact as revealed by EEG recordings at 1.5, 3 and 7 T static magnetic field strength. Int J Psychophysiol 67(3):189–199
Di Russo F et al (2002) Cortical sources of the early components of the visual evoked potential. Hum Brain Mapp 15(2):95–111
Di Russo F et al (2003) Source analysis of event-related cortical activity during visuo-spatial attention. Cereb Cortex 13(5):486–499
Di Russo F et al (2007) Spatiotemporal analysis of the cortical sources of the steady-state visual evoked potential. Hum Brain Mapp 28(4):323–334
Eichele T et al (2005) Assessing the spatiotemporal evolution of neuronal activation with single-trial event-related potentials and functional MRI. Proc Natl Acad Sci U S A 102(49):17798–17803
Feige B et al (2005) Cortical and subcortical correlates of electroencephalographic alpha rhythm modulation. J Neurophysiol 93(5):2864–2872

Fiebach CJ et al (2005) Neuronal mechanisms of repetition priming in occipitotemporal cortex: spatiotemporal evidence from functional magnetic resonance imaging and electroencephalography. J Neurosci 25(13):3414–3422
Foucher JR et al (2003) The BOLD response and the gamma oscillations respond differently than evoked potentials: an interleaved EEG–fMRI study. BMC Neurosci 4:22
Gazzaley A et al (2005) Top-down enhancement and suppression of the magnitude and speed of neural activity. J Cogn Neurosci 17(3):507–517
Goldman RI et al (2002) Simultaneous EEG and fMRI of the alpha rhythm. Neuroreport 13(18):2487–2492
Goncalves SI et al (2006) Correlating the alpha rhythm to BOLD using simultaneous EEG/fMRI: inter-subject variability. Neuroimage 30(1):203–213
Green JJ, Boehler CN, Roberts KC, Chen LC, Krebs RM, Song AW, Woldorff MG (2017) Cortical and subcortical coordination of visual spatial attention revealed by simultaneous EEG-fMRI recording. J Neurosci 37:7803–7810
Guy CN et al (1999) fMRI and EEG responses to periodic visual stimulation. Neuroimage 10(2):125–148
Hanslmayr S, Aslan A, Staudigl T, Klimesch W, Herrmann CS, Bauml KH (2007) Prestimulus oscillations predict visual perception performance between and within subjects. Neuroimage 37:1465–1473
Hanslmayr S, Volberg G, Wimber M, Dalal SS, Greenlee MW (2013) Prestimulus oscillatory phase at 7 Hz gates cortical information flow and visual perception. Curr Biol 23(22):2273–2278
Heinze HJ et al (1994) Combined spatial and temporal imaging of brain activity during visual selective attention in humans. Nature 372(6506):543–546
Helmholtz H (1853) Über einige Gesetze der Vertheilung elektrischer Ströme in körperlichen Leitern mit Anwendung auf die thierisch-elektrischen Versuche. Ann Phys 165(6):211–233
Henning S et al (2005) Simultaneous recordings of visual evoked potentials and BOLD MRI activations in response to visual motion processing. NMR Biomed 18(8):543–552
Henning S et al (2006) Task- and EEG-correlated analyses of BOLD MRI responses to eyes opening and closing. Brain Res 1073–1074:359–364
Horovitz SG et al (2004) Parametric design and correlational analyses help integrating fMRI and electrophysiological data during face processing. Neuroimage 22(4):1587–1595
Huettel SA et al (2004) Linking hemodynamic and electrophysiological measures of brain activity: evidence from functional MRI and intracranial field potentials. Cereb Cortex 14(2):165–173
Hunt BAE, Liddle EB, Gascoyne LE, Magazzini L, Routley BC, Singh KD, Morris PG, Brookes MJ, Liddle PF (2019) Attenuated post-movement Beta rebound associated with schizotypal features in healthy people. Schizophr Bull 45:883–891
Hunyadi B, Woolrich MW, Quinn AJ, Vidaurre D, De Vos M (2019) A dynamic system of brain networks revealed by fast transient EEG fluctuations and their fMRI correlates. Neuroimage 185:72–82
Im CH et al (2006) Functional cortical source imaging from simultaneously recorded ERP and fMRI. J Neurosci Methods 157(1):118–123
Janz C et al (2001) Coupling of neural activity and BOLD fMRI response: new insights by combination of fMRI and VEP experiments in transition from single events to continuous stimulation. Magn Reson Med 46(3):482–486
Jensen O, Mazaheri A (2010) Shaping functional architecture by oscillatory alpha activity: gating by inhibition. Front Hum Neurosci 4:186
Knyazeva MG et al (2006a) Imaging of a synchronous neuronal assembly in the human visual brain. Neuroimage 29(2):593–604
Knyazeva MG et al (2006b) Interhemispheric integration at different spatial scales: the evidence from EEG coherence and FMRI. J Neurophysiol 96(1):259–275
Konn D et al (2004) Initial attempts at directly detecting alpha wave activity in the brain using MRI. Magn Reson Imaging 22(10):1413–1427

Kruggel F et al (2000) Recording of the event-related potentials during functional MRI at 3.0 tesla field strength. Magn Reson Med 44(2):277–282
Laufs H et al (2003a) EEG-correlated fMRI of human alpha activity. Neuroimage 19(4):1463–1476
Laufs H et al (2003b) Electroencephalographic signatures of attentional and cognitive default modes in spontaneous brain activity fluctuations at rest. Proc Natl Acad Sci U S A 100(19):11053–11058
Laufs H et al (2006) Where the BOLD signal goes when alpha EEG leaves. Neuroimage 31(4):1408–1418
Lazeyras F et al (2001) Functional MRI with simultaneous EEG recording: feasibility and application to motor and visual activation. J Magn Reson Imaging 13(6):943–948
Linden DE et al (1999) The functional neuroanatomy of target detection: an fMRI study of visual and auditory oddball tasks. Cereb Cortex 9(8):815–823
Linkenkaer-Hansen K, Nikulin VV, Palva S, Ilmoniemi RJ, Palva JM (2004) Prestimulus oscillations enhance psychophysical performance in humans. J Neurosci 24:10186–10190
Liu Z, Rios C, Zhang N, Yang L, Chen W, He B (2010) Linear and nonlinear relationships between visual stimuli, EEG and BOLD fMRI signals. Neuroimage 50:1054–1066
Liu Y, Bengson J, Huang H, Mangun GR, Ding M (2016) Top-down modulation of neural activity in anticipatory visual attention: control mechanisms revealed by simultaneous EEG-fMRI. Cereb Cortex 26:517–529
Logothetis NK et al (2001) Neurophysiological investigation of the basis of the fMRI signal. Nature 412(6843):150–157
Magri C, Schridde U, Murayama Y, Panzeri S, Logothetis NK (2012) The amplitude and timing of the BOLD signal reflects the relationship between local field potential power at different frequencies. J Neurosci 32:1395–1407
Mandelkow H et al (2007) Heart beats brain: the problem of detecting alpha waves by neuronal current imaging in joint EEG-MRI experiments. Neuroimage 37(1):149–163
Mangun GR et al (1998) ERP and fMRI measures of visual spatial selective attention. Hum Brain Mapp 6(5–6):383–389
Mantini D et al (2007) Electrophysiological signatures of resting state networks in the human brain. Proc Natl Acad Sci U S A 104(32):13170–13175
Martinez A et al (1999) Involvement of striate and extrastriate visual cortical areas in spatial attention. Nat Neurosci 2(4):364–369
Matsuda T et al (2002) Influence of arousal level for functional magnetic resonance imaging (fMRI) study: simultaneous recording of fMRI and electroencephalogram. Psychiatry Clin Neurosci 56(3):289–290
Mayhew SD, Bagshaw AP (2017) Dynamic spatiotemporal variability of alpha-BOLD relationships during the resting-state and task-evoked responses. Neuroimage 155:120–137
Mayhew SD, Dirckx SG, Niazy RK, Iannetti G, Wise RG (2010a) EEG signatures of auditory activity correlate with simultaneously recorded fMRI responses in humans. Neuroimage 49:849–864
Mayhew SD, Macintosh BJ, Dirckx SG, Iannetti GD, Wise RG (2010b) Coupling of simultaneously acquired electrophysiological and haemodynamic responses during visual stimulation. Magn Reson Imaging 28:1066–1077
Mayhew SD, Li S, Kourtzi Z (2012) Learning acts on distinct processes for visual form perception in the human brain. J Neurosci 32:775–786
Mayhew SD, Ostwald D, Porcaro C, Bagshaw AP (2013) Spontaneous EEG alpha oscillation interacts with positive and negative BOLD responses in the visual auditory cortices and default-mode network. Neuroimage 76:362–372
Moosmann M et al (2003) Correlates of alpha rhythm in functional magnetic resonance imaging and near infrared spectroscopy. Neuroimage 20(1):145–158
Moosmann M, Eichele T, Nordby H, Hugdahl K, Calhoun VD (2008) Joint independent component analysis for simultaneous EEG-fMRI: principle and simulation. Int J Psychophysiol 67:212–221

Muller TJ et al (2005) The neurophysiological time pattern of illusionary visual perceptual transitions: a simultaneous EEG and fMRI study. Int J Psychophysiol 55(3):299–312
Mullinger KJ, Mayhew SD, Bagshaw AP, Bowtell R, Francis ST (2013) Poststimulus undershoots in cerebral blood flow and BOLD fMRI responses are modulated by poststimulus neuronal activity. Proc Natl Acad Sci U S A 110:13636–13641
Mullinger KJ, Mayhew SD, Bagshaw AP, Bowtell R, Francis ST (2014) Evidence that the negative BOLD response is neuronal in origin: a simultaneous EEG-BOLD-CBF study in humans. Neuroimage 94:263–274
Mullinger KJ, Cherukara MT, Buxton RB, Francis ST, Mayhew SD (2017) Post-stimulus fMRI and EEG responses: evidence for a neuronal origin hypothesised to be inhibitory. Neuroimage 157:388–399
Muri RM et al (1998) Recording of electrical brain activity in a magnetic resonance environment: distorting effects of the static magnetic field. Magn Reson Med 39(1):18–22
Muthukumaraswamy SD, Singh KD (2008) Spatiotemporal frequency tuning of BOLD and gamma band MEG responses compared in primary visual cortex. Neuroimage 40:1552–1560
Muthukumaraswamy SD, Singh KD (2009) Functional decoupling of BOLD and gamma-band amplitudes in human primary visual cortex. Hum Brain Mapp 30:2000–2007
Negishi M et al (2004) Removal of time-varying gradient artifacts from EEG data acquired during continuous fMRI. Clin Neurophysiol 115(9):2181–2192
Nguyen VT, Breakspear M, Cunnington R (2014) Fusing concurrent EEG-fMRI with dynamic causal modeling: application to effective connectivity during face perception. Neuroimage 102(Pt 1):60–70
Novitskiy N, Ramautar JR, Vanderperren K, De Vos M, Mennes M, Mijovic B, Vanrumste B, Stiers P, Van den Bergh B, Lagae L, Sunaert S, Van Huffel S, Wagemans J (2011) The BOLD correlates of the visual P1 and N1 in single-trial analysis of simultaneous EEG-fMRI recordings during a spatial detection task. Neuroimage 54:824–835
Olbrich S, Mulert C, Karch S, Trenner M, Leicht G, Pogarell O, Hegerl U (2009) EEG-vigilance and BOLD effect during simultaneous EEG/fMRI measurement. Neuroimage 45:319–332
Osipova D, Hermes D, Jensen O (2008) Gamma power is phase-locked to posterior alpha activity. PLoS One 3:e3990
Ostwald D, Porcaro C, Bagshaw AP (2010) An information theoretic approach to EEG-fMRI integration of visually evoked responses. Neuroimage 49:498–516
Otzenberger H, Gounot D, Foucher JR (2005) P300 recordings during event-related fMRI: a feasibility study. Brain Res Cogn Brain Res 23(2–3):306–15. https://doi.org/10.1016/j.cogbrainres.2004.10.017. Epub 2004 Dec 29. PMID: 15820638.
Philiastides MG, Sajda P (2007) EEG-informed fMRI reveals spatiotemporal characteristics of perceptual decision making. J Neurosci 27(48):13082–13091
Porcaro C, Ostwald D, Bagshaw AP (2010) Functional source separation improves the quality of single trial visual evoked potentials recorded during concurrent EEG-fMRI. Neuroimage 50:112–123
Raichle ME et al (2001) A default mode of brain function. Proc Natl Acad Sci U S A 98(2):676–682
Rauch A, Rainer G, Logothetis NK (2008) The effect of a serotonin-induced dissociation between spiking and perisynaptic activity on BOLD functional MRI. Proc Natl Acad Sci U S A 105:6759–6764
Ritter P et al (2008) Relation between spatially and spectrally confined EEG rhythms and fMRI resting state networks. In: 14th Ann Meet OHBM, Melbourne, Australia, 15–19 June 2008
Romei V, Brodbeck V, Michel C, Amedi A, Pascual-Leone A, Thut G (2008) Spontaneous fluctuations in posterior alpha-band EEG activity reflect variability in excitability of human visual areas. Cereb Cortex 18:2010–2018

Sadaghiani S, Scheeringa R, Lehongre K, Morillon B, Giraud AL, Kleinschmidt A (2010) Intrinsic connectivity networks, alpha oscillations, and tonic alertness: a simultaneous electroencephalography/functional magnetic resonance imaging study. J Neurosci 30:10243–10250

Sammer G et al (2005) Acquisition of typical EEG waveforms during fMRI: SSVEP, LRP, and frontal theta. Neuroimage 24(4):1012–1024

Scheeringa R, Fries P, Petersson K-M, Oostenveld R, Grothe I, Norris DG, Hagoort P, Bastiaansen MCM (2011a) Neuronal dynamics underlying high- and low-frequency EEG oscillations contribute independently to the human BOLD signal. Neuron 69:572–583

Scheeringa R, Mazaheri A, Bojak I, Norris DG, Kleinschmidt A (2011b) Modulation of visually evoked cortical FMRI responses by phase of ongoing occipital alpha oscillations. J Neurosci 31:3813–3820

Schmid MC et al (2006) Simultaneous EEG and fMRI in the macaque monkey at 4.7 tesla. Magn Reson Imaging 24(4):335–342

Schoth F et al (2007) Cerebral processing of spontaneous reversals of the rotating Necker cube. Neuroreport 18(13):1335–1338

Schroeder CE et al (1991) Striate cortical contribution to the surface-recorded pattern-reversal VEP in the alert monkey. Vision Res 31(7–8):1143–1157

Sehatpour P et al (2006) Spatiotemporal dynamics of human object recognition processing: an integrated high-density electrical mapping and functional imaging study of "closure" processes. Neuroimage 29(2):605–618

Shaw JC (2003) More on alpha rhythm characteristics. In: The brain's alpha rhythms and the mind. Elsevier, Amsterdam, pp 15–32

Singh M et al (2003) Correlation between BOLD–fMRI and EEG signal changes in response to visual stimulus frequency in humans. Magn Reson Med 49(1):108–114

Sokoliuk R, Mayhew SD, Aquino KM, Wilson R, Brookes MJ, Francis ST, Hanslmayr S, Mullinger KJ (2018) Two spatially distinct posterior alpha sources fulfill different functional roles in attention. J Neurosci 39(36):7183–7194

Sotero RC, Trujillo-Barreto NJ (2008) Biophysical model for integrating neuronal activity, EEG, fMRI and metabolism. Neuroimage 39(1):290–309

Swettenham JB, Muthukumaraswamy SD, Singh KD (2013) BOLD responses in human primary visual cortex are insensitive to substantial changes in neural activity. Front Hum Neurosci 7:76

Vanderperren K, De Vos M, Ramautar JR, Novitskiy N, Mennes M, Assecondi S, Vanrumste B, Stiers P, Van den Bergh BR, Wagemans J, Lagae L, Sunaert S, Van Huffel S (2010) Removal of BCG artifacts from EEG recordings inside the MR scanner: a comparison of methodological and validation-related aspects. Neuroimage 50:920–934

Vanni S et al (2004) Sequence of pattern onset responses in the human visual areas: an fMRI constrained VEP source analysis. Neuroimage 21(3):801–817

Viswanathan A, Freeman RD (2007) Neurometabolic coupling in cerebral cortex reflects synaptic more than spiking activity. Nat Neurosci 10:1308–1312

Walz JM, Goldman RI, Carapezza M, Muraskin J, Brown TR, Sajda P (2014) Simultaneous EEG-fMRI reveals a temporal cascade of task-related and default-mode activations during a simple target detection task. Neuroimage 102(Pt 1):229–239

Wan X et al (2006) The neural basis of the hemodynamic response nonlinearity in human primary visual cortex: implications for neurovascular coupling mechanism. Neuroimage 32(2):616–625

Warbrick T, Arrubla J, Boers F, Neuner I, Shah NJ (2014) Attention to detail: why considering task demands is essential for single-trial analysis of BOLD correlates of the visual P1 and N1. J Cogn Neurosci 26:529–542

Whittingstall K et al (2007) Evaluating the spatial relationship of event-related potential and functional MRI sources in the primary visual cortex. Hum Brain Mapp 28(2):134–142

Whittingstall K, Kevin W, Wilson D, Doug W, Schmidt M, Matthias S, Stroink G, Gerhard S (2008) Correspondence of visual evoked potentials with FMRI signals in human visual cortex. Brain Topogr 21:86–92

Winawer J, Kay KN, Foster BL, Rauschecker AM, Parvizi J, Wandell BA (2013) Asynchronous broadband signals are the principal source of the BOLD response in human visual cortex. Curr Biol 23:1145–1153

Wu L, Eichele T, Calhoun VD (2010) Reactivity of hemodynamic responses and functional connectivity to different states of alpha synchrony: a concurrent EEG-fMRI study. Neuroimage 52:1252–1260

Yeşilyurt B, Whittingstall K, Uğurbil K, Logothetis NK, Uludağ K (2010) Relationship of the BOLD signal with VEP for ultrashort duration visual stimuli (0.1 to 5 ms) in humans. J Cereb Blood Flow Metab 30:449–458

Zhan Z, Xu L, Zuo T, Xie D, Zhang J, Yao L, Wu X (2014) The contribution of different frequency bands of fMRI data to the correlation with EEG alpha rhythm. Brain Res 1543:235–243

Zumer JM, Scheeringa R, Schoffelen JM, Norris DG, Jensen O (2014) Occipital alpha activity during stimulus processing gates the information flow to object-selective cortex. PLoS Biol 12:e1001965

Cognition

24

Susanne Karch and Christoph Mulert

24.1 Advantages and Disadvantages of Simultaneous EEG–fMRI Recordings of Cognitive Functions

In cognitive neuroscience, there has been growing interest in simultaneous and combined EEG–fMRI recordings in cognitive paradigms in order to obtain datasets with high spatial and temporal resolution (Benar et al. 2007). There are several reasons why simultaneous EEG–fMRI acquisition seems to make sense in the investigation of cognition: mental processes don't need to be identical even if an identical cognitive paradigm is conducted several times. Differences in the participant's mood, vigilance, and familiarity with the task, for example, have proved to be important for cognitive processes as well as for the underlying brain activity (Debener et al. 2006; Matsuda et al. 2002; Menon and Crottaz-Herbette 2005). Often, the same stimuli cannot be used twice, for example, stimuli used in learning and memory experiments or planning tasks. Simultaneous EEG–fMRI recordings have the advantage of an identical environment, the same conditions of stimulation, and subject state, for example, time of the day, time spent on the task, and level of arousal. In addition, this method appears to be advantageous for distinct samples, for example, children or aged people, in order to avoid multiple sessions involving extended periods of time (Menon and Crottaz-Herbette 2005). Multiple session might not be feasible, reliable, or practical in clinical studies, for example, focusing on the effect of medication on cognitive processes (Menon and Crottaz-Herbette 2005). Additionally, various processing stages of cognitive tasks, for example, stimulus encoding and evaluation,

S. Karch (✉)
Department of Psychiatry and Psychotherapy, University Munich, Munich, Germany
e-mail: Susanne.Karch@med.uni-muenchen.de

C. Mulert
Centre of Psychiatry, Justus Liebig University, Giessen, Germany
e-mail: Christoph.Mulert@psychiat.med.uni-giessen.de

C. Mulert, L. Lemieux (eds.), *EEG - fMRI*,
https://doi.org/10.1007/978-3-031-07121-8_24

memory, selection of action, and guiding decisions, can be decomposed ("*mental chronometry*"; Linden 2007; Posner 1978) using EEG and fMRI. In tasks focusing on higher cognitive functions (e.g., executive functions, memory), both nonspecific processes (e.g., attention, arousal) and specific abilities (e.g., planning, cognitive flexibility, encoding) are required for successful task execution. EEG–fMRI data may be useful to distinguish neural correlates of specific and nonspecific aspects of cognitive functioning. Furthermore, EEG–fMRI studies allow for combining localization of cognition-related brain structures with neurophysiological mechanisms, for example, functional coherence of brain regions.

24.2 Attention

Attention is the cognitive process of maintaining the mental focus on one or several aspects of the environment while ignoring other things in order to deal effectively with the information in the attentional focus. Diverse aspects of cognitive functioning are part of this concept, for example, the ability to maintain a consistent behavioral response during continuous and repetitive activity (sustained attention) and in the face of distraction or competing stimuli, respectively (selective attention). This concept also refers to the capacity of mental flexibility allowing individuals to shift their focus of attention and to alter between tasks with different cognitive requirements (alternating attention) and to respond simultaneously to multiple task demands (divided attention) (Sohlberg and Mateer 1989).

The examination of neural responses is crucial for the evaluation of the functional efficiency of brain functions. In electroencephalographic investigations, attention frequently has been examined by using the so-called oddball paradigm as well as mismatch-associated paradigms. One of the most important aspects of electrophysiological responses is the so-called P300 component, a positive component about 300–600 ms after the presentation of a stimulus. The P300 has proved to be abnormal in many clinical conditions including aging, schizophrenia, depression, Alzheimer's disease, and psychopathy (Ford et al. 1994; Kawasaki et al. 2004; McCarley et al. 1991; Polich and Corey-Bloom 2005; Polich and Herbst 2000; van der Stelt et al. 2004). For that reason, neural generators of ERPs have attracted considerable interest (Bledowski et al. 2004a).

24.2.1 Oddball Paradigm

The *oddball paradigm* has been associated with attention and information processing capacity. During this task, participants detect and respond to infrequent target events embedded in a series of repetitive events (Sutton et al. 1965). The detection of novel, salient information is crucial in order to facilitate the adaptation to a rapidly changing environment (Sokolov 1963). The oddball paradigm entails top-down regulated attention on a stimulus. Sometimes novel stimuli which do not require a behavioral response (deviants) are presented additionally in this task. The presentation of deviants enables a breaking of ongoing focused attention and the attraction of attention (Bledowski et al. 2004a).

Aberrant electrophysiological responses associated with rare, task-relevant stimuli have been reported about 300–500 ms after the presentation of the task, especially in frontocentral and parietal brain regions (P3/P300). This event-related potential (ERP) is thought to reflect the mental processes underlying the allocation of attentional resources to an incoming stimulus and its evaluation, as well as decision-making and memory updating (Calhoun et al. 2006). There are two components of the P300: P3a and P3b. The P3a has a more frontal distribution and is thought to be associated with an orienting response (Friedman et al. 2001). Variations related to the P3b appear a little later and primarily have a parietal distribution. The P3b is associated with context updating, context disclosure, event categorization, and processing capacity (Donchin and Coles 1988; Kok 2001).

Intracranial recordings for the identification P3-related neural generators supported the view that the P3a is primarily related to paralimbic areas as well as frontal, parietal, and cingulate brain regions (Halgren et al. 1998). The integration of context information (P3b) engaged frontotemporal cortices, association cortices, and the hippocampus. Brain responses to oddball tasks have been extensively studied using fMRI (e.g., Halgren et al. 1998; Horovitz et al. 2002; Kiehl et al. 2005b; Linden et al. 1999; McCarthy et al. 1997; Menon et al. 1997). It is assumed that oddball paradigms elicit activations in a widespread cortical network including the anterior temporal gyrus, the inferior and superior parietal lobe, the anterior and posterior cingulate cortex, the thalamus, and lateral frontal brain regions. Some studies found a rightward lateralization in frontal, temporal, and parietal regions (Kiehl et al. 2005a; Stevens et al. 2005).

It has been demonstrated that the electrophysiological results of the oddball paradigm that has been performed in the MRI scanner are not directly comparable to those that were acquired in studies outside the MRI. Chun et al. (2016) revealed a delay N1, P300 latency, and RT inside the MRI scanner (Chun et al. 2016). These variations should be considered in the evaluation of these results.

In order to improve the understanding of target-associated brain activity, a precise localization of the generators of the P3 was aimed for in several studies. The comparison of fMRI findings with those of an independent localization of event-related potentials using low resolution electromagnetic tomography (LORETA) (Mulert et al. 2004) revealed highly concordant responses in the temporoparietal junction, the supplementary motor area (SMA)/anterior cingulate cortex (ACC), the insula, and the middle frontal gyrus. BOLD activations of the motor cortex were not represented in the P300 potential. Concerning the time course of brain responses, the activation seemed to start in the temporal lobe and the temporoparietal junction and the latest activity in the frontal cortex and SMA (Mulert et al. 2004).

Bledowski et al. intended to distinguish neuroanatomical correlates related to generators of the P3a component, which is mainly evoked by distractor events, from those of the P3b, which has been associated with the detection of rare events in general (targets and distractors) using EEG and fMRI acquired in separate sessions. Results of a visual oddball paradigm with three different conditions (frequent, rare, and distractor) revealed that targets elicited a posterior P3b; distractor stimuli were followed by a frontocentral P3a ERP. Both conditions produced BOLD responses in the temporoparietal junction and the right prefrontal gyrus. Furthermore, target processing led to bilateral presylvian responses, whereas the frontal eye fields, bilateral superior parietal

cortices, and left prefrontal cortex contributed to distractor processing (Bledowski et al. 2004b). An fMRI-based EEG model was designed to directly relate the datasets: fMRI-constrained seeding points were located in the prefrontal cortex, precentral sulcus, inferior parietal lobe, posterior parietal cortex, inferior temporal cortex, anterior insula, right superior temporal sulcus, as well as cingulate gyrus. The results revealed that all sources had contributed to the target and distractor condition: frontal areas and the insula contributed mainly to the P3a which was compatible to a more anterior distribution on the scalp. By contrast, the P3b was mainly produced by higher visual and supramodal association areas (e.g., parietal and inferior temporal areas) (Bledowski et al. 2004b). Altogether, the results confirmed previous reports about a supramodal target detection system. Beyond this, some task-specific subsystems associated to P3a and P3b components seemed to exist (Bledowski et al. 2004a, b) (Fig. 24.1).

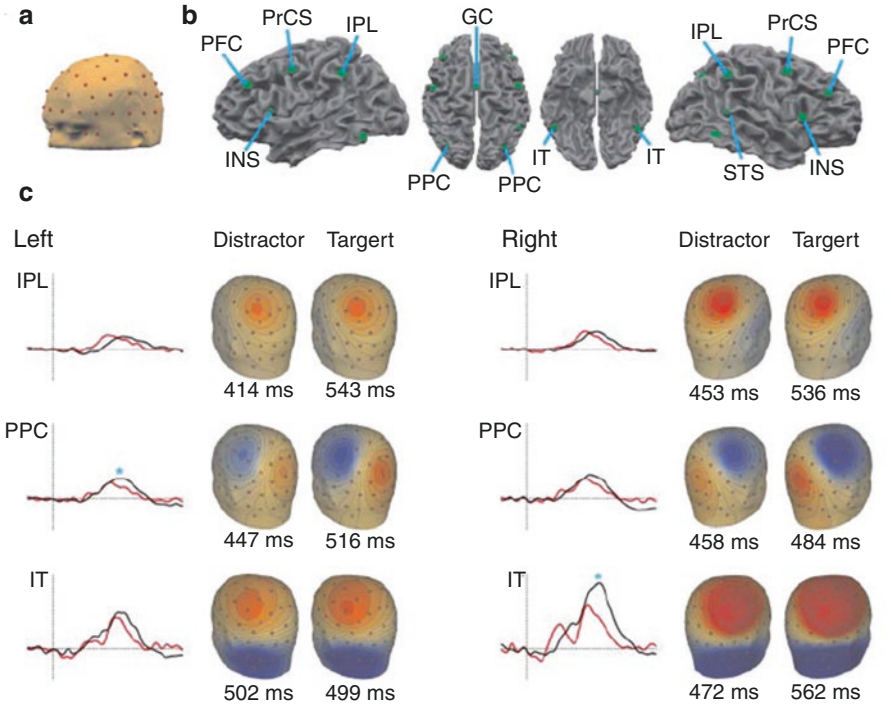

Fig. 24.1 Combined EEG and fMRI study using a novelty paradigm; dipoles were seated into BOLD clusters. Source activity in target and distractor condition. (**a**) A surface of a standard head (MNI template) with standard 81 electrode configuration. (**b**) Position of the regional sources on a surface reconstruction of the MNI template brain. (**c**) Source activity waves and topographical maps of scalp voltage of the main current flow direction of each regional source for the target and distractor conditions (abbreviations: * indicates significant differences between regional source peak amplitude in the target and distractor conditions; *PFC* prefrontal cortex, *INS* anterior insula, *PrCS* precentral sulcus, *IPL* inferior parietal lobe, *GC* cingulate gyrus, *PPC* posterior parietal cortex; *IT* inferior temporal sulcus, *STS* superior temporal sulcus) (Bledowski et al. 2004a; Copyright (2004) Society for Neuroscience)

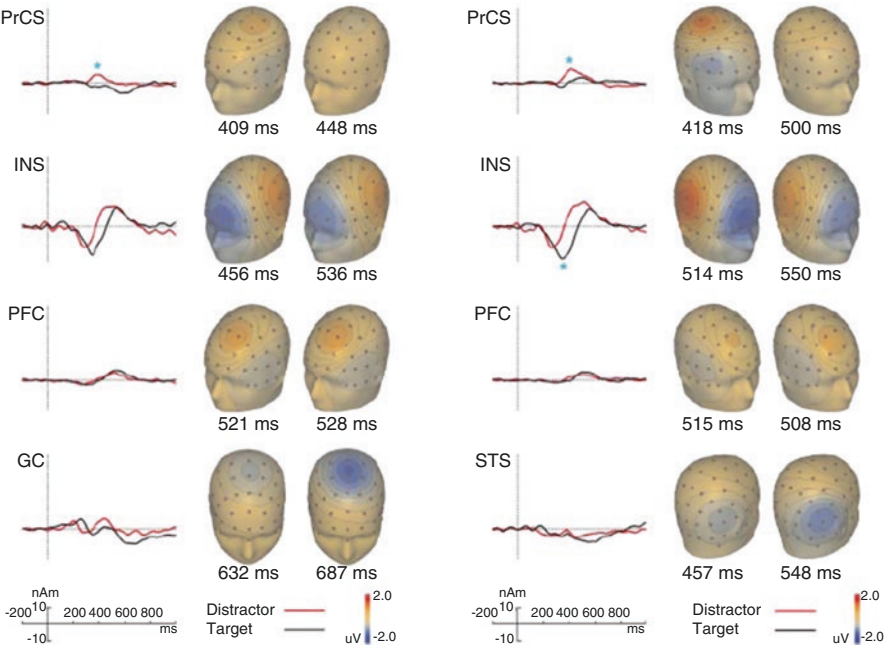

Fig. 24.1 (continued)

The study of Crottaz-Herbette and Menon (2006) was especially concerned about the influence of the ACC in attentional control. A simple auditory and visual oddball task was used to examine whether, and to which extent, early attentional effects were influenced by top-down processes from the ACC. The importance of the ACC in attentional control has been demonstrated before, for example, in tasks requiring selective attention or the inhibition of prepotent responses (Botvinick et al. 2001; Bush et al. 2000; Milham and Banich 2005). As expected, the presentation of infrequent stimuli led to significantly greater responses in the ACC as well as an enhanced contribution of the SMA, inferior parietal cortex, basal ganglia, cerebellum, and left premotor cortex. Modality-specific variations were produced especially in the primary sensory cortices. Although attention-related activation of the ACC was similar in both modalities, its connectivity was remarkably specific: the auditory task produced an enhanced effective connectivity between the ACC and the Heschl gyrus, left middle and superior temporal gyri, the left and right precentral and postcentral gyri, the supramarginal gyrus, the caudate, the thalamus, and the cerebellum. During the visual oddball task, the ACC showed an increased connectivity with the striate cortex, the precuneus/cuneus, and the posterior cingulate gyrus. ERP recordings confirmed that oddball tasks elicit prominent frontocentral and central N2 and P3a signals. The fMRI-constrained dipole modeling showed that the ACC is the major generator of the N2b–P3a components of the ERP. Summarized, a top-down attentional modulation of early sensory processing by the ACC is suggested. These results provide evidence for a model of attentional control based on

dynamic bottom-up and top-down interactions between the ACC and primary sensory regions (Crottaz-Herbette and Menon 2006).

Calhoun et al. performed a spatial independent component analysis (ICA) of the hemodynamic change data and a temporal ICA of the ERPs to derive a spatiotemporal decomposition. The results provided evidence for initial auditory processing and corresponding preparatory motor activity. These initial activations were followed by N2-related activations in association areas and motor execution regions. The early P3a was associated with enhanced neural responses of thalamic regions and posterior superior parietal lobe areas, as well as decreases in orbitofrontal brain regions. The late P3b showed associations with posterior temporal and temporoparietal lobe regions in addition to lateral prefrontal areas (Calhoun et al. 2006).

Walz et al. (2013) demonstrated that the ACC is strongly associated with early and late EEG components. Late components are also related to brainstem, right middle frontal gyrus, and right orbitofrontal cortex. Variability in insula and temporoparietal junction is reflected in reaction time variability. In addition, the authors demonstrated some evidence for reciprocal effective connections between the brainstem and cortical regions (Walz et al. 2013).

The analysis of fluctuations in the brain regions involved in a simple visual oddball task demonstrated a temporal cascade of transient activations: right frontal regions and lateral occipital cortex were involved post stimulus and early in the trial. These brain regions have been linked, for example, to attentional orienting and decision certainty. The behavioral responses were followed by responses in brain areas that have often been associated to default-mode network and introspection (e.g., precuneus, posterior cingulate cortex) (Walz et al. 2014). These results may indicate that both task-dependent and default-mode networks are transiently engaged with a specific temporal ordering (Walz et al. 2014).

Warbrick et al. (2014) demonstrated that task demands influenced BOLD correlates during a visual oddball paradigm: the P1 component reflected changes in the sensory encoding of stimulus features and seemed to be more relevant for the passive and count condition. The N1 was more informative for the respond condition and seemed to be relevant for processes involved in the integration of sensory information with response selection (Warbrick et al. 2014).

The effect of trial-by-trial variability on neurofunctional parameters, for instance, due to variations in arousal, has been explored in several studies (Benar et al. 2007; Debener et al. 2007; Eichele et al. 2005): information about changes in event-related EEG activity of each trial was used as a parameter for fMRI analysis. Eichele et al. (2005) separated three independent stages during oddball processing: the main sources of early ERP components (P2; ~170 ms) were located in temporal and frontal lobes and is assumed to indicate matching processes between sensory input and a neuronal representation of stimuli selected for further processing. Later, electrophysiological responses (N2) were related to the anterior frontomedian cortex and parahippocampal regions and appeared to be linked with the detection of a mismatch and memory processes, rather than attentional processes (Eichele et al. 2005). As expected, the most extensive BOLD responses were related to the P300 about 320 ms after stimulus presentation in frontal, temporal, and parietal brain regions,

especially in the right hemisphere. Similar changes have been associated with a mechanism elicited when a memory representation of the recent stimulus context is updated as opposed to the detection of deviancy (Eichele et al. 2005) (Fig. 24.2).

Furthermore, there was some evidence for a relation of P3 latency, cognitive functions, and BOLD responses: single-trial P3 latency correlated clearly with the reaction time. Significant fMRI activations for the modulation by P300 amplitude and latency were obtained both at the single subject level and the group level: P300 parameters seemed to be associated with fMRI activations in the anterior medial frontal region, the parietal–occipital junction, and the anterior medial frontal region. However, a large variability in the patterns of activations across subjects was observed. Whether the modulation of the ERP reflected a modulation of neural activity visible in the fMRI, or both EEG and fMRI signals were jointly modulated by the same factors, for example, the level of attention was not clear (Benar et al. 2007).

Walz et al. (2015) examined the effect of alpha activity before the presentation of stimuli on the neuronal responses during an oddball task. A higher alpha power state before the stimulus presentation was related to stronger decision-related BOLD responses in brain regions that seem to be related to the late processing stream.

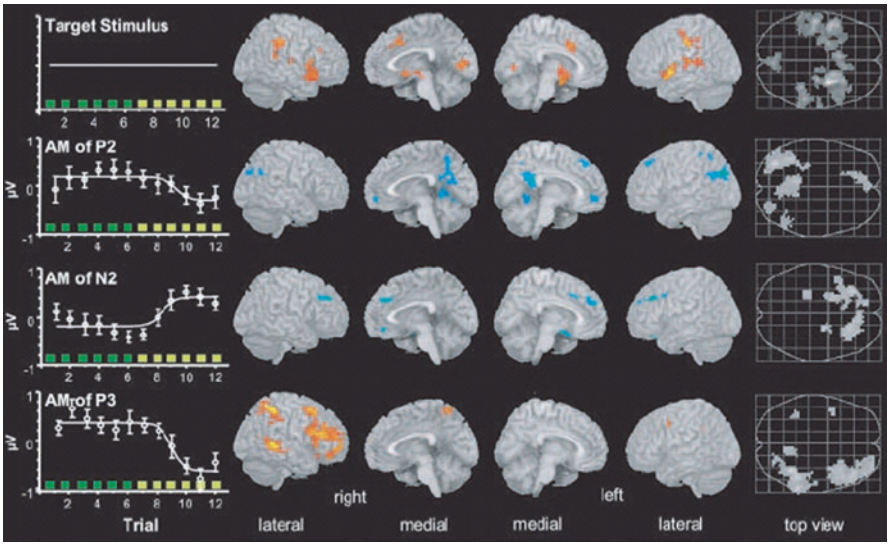

Fig. 24.2 Simultaneous EEG–fMRI experiment using an oddball paradigm. Amplitude modulation (AM)-correlated fMRI results. Render views and maximum-intensity projections of the general target-related activation and positive (red) and negative (blue) correlations with the respective AM. Each correlation may show for each voxel the maximum *t* value from the four electrodes (Fz, FC1, FC2, Cz). To the left of each rendering of the AM-correlated fMRI, the average AM (empty circles ± SEM) and the fitted sigmoid curves are shown. Top row, target-related activation, $P < 0.05$ (FWE), cluster size >10; second row, P2 (170 ms); third row, N2 (200 ms); and fourth row, P3 (320 ms). All AM-related activations were thresholded at $P < 0.001$ (uncorrected), cluster extent threshold $P < 0.01$ (Eichele et al. 2005; Copyright (2005) National Academy of Sciences, USA)

Primary sensory regions have not been affected by this alpha activity. Phase analysis provided support for a thalamocortical loop in attentional modulations. This may indicate that cortical alpha rhythms modulate task-associated responses very early in the processing stream (Walz et al. 2015).

Warbrick et al. (2012) applied EEG–fMRI methods for pharmacoimaging. Their results showed that EEG-informed fMRI data can help to examine the effect of nicotine on attention-related brain responses in more detail than conventional analyses (Warbrick et al. 2012). A clinical application of EEG–fMRI–based pharmacoimaging in patients with schizophrenia used a double-blind, placebo-controlled crossover design to compare the results of patients and controls after the application of 1 mg nasal nicotine and with those without the application of nicotine. Nicotine application was related to increased P300-informed brain responses in patients and controls especially in the anterior cingulate and medial frontal brain regions. Nicotine-related brain responses of patients and healthy subjects were comparable (Mobascher et al. 2012).

In summary, the feasibility of tracking single-trial variations of both amplitude and latency of an EEG wave during fMRI scanning was proved. The use of simultaneous EEG–fMRI can be seen as a bridge between the well-established field of evoked cognitive potentials and the fast growing field of fMRI studies; the study contributes to this goal by linking the fluctuations of the features of a well-known ERP component to the fMRI signal. It also permits the extraction of new information from evoked activity with a very high spatial resolution (Benar et al. 2007).

24.2.2 Mismatch Negativity

The mismatch negativity reflects the registration of differences between an actual presented stimulus and the representation of stimuli in memory (Näätänen and Winkler 1999). The mismatch detection has been associated with preattentive change detection and is considered to be more or less automatic. Mismatch-generating processes have often been associated with the initiation of an involuntary switch to information outside the focus of attention (Giard et al. 1990; Schroger and Wolff 1996). In a sequence of frequently repeated standard stimuli, infrequent auditory stimuli are rarely interspersed during mismatch experiments. In contrast to oddball paradigms, no behavioral response is required. The mismatch negativity is linked to the mismatch between sensory input from a deviant stimulus and neural correlates of sensory information, representing the features of a repeatedly presented standard stimuli (Näätänen and Winkler 1999).

Electrophysiologically, mismatch leads to a negative deflection, the so-called mismatch negativity (MMN), peaking roughly between 100 and 250 ms after deviance onset (Näätänen et al. 1978). The MMN is commonly calculated by subtracting the ERP elicited from the standard information from the ERP produced by the deviant stimulus. The MMN is often followed by a P3a component announcing a voluntary or involuntary switch of attention to salient or novel events. It is elicited

when a certain threshold of difference between characteristic of the stimulus and the memory trace to the preceding stimuli is exceeded (Katayama and Polich 1998). Imaging studies (Mathiak et al. 2002; Opitz et al. 1999) as well as intracranial recordings (Javitt et al. 1992; Kropotov et al. 1995) provided evidence that the main MMN generators are located in the transverse temporal gyrus and the STG. In addition, frontal brain regions are thought to be involved as well, for example, the inferior frontal gyrus (IFG) (Downar et al. 2002; Opitz et al. 2002). Frontal brain regions seemed to be activated at a later stage than temporal regions and contributed to the switch of attention (Rinne et al. 2000). Downar et al. (2002) assumed that the IFG could be relevant for the evaluation of the potential importance of the stimuli presented.

Using EEG and fMRI responses, Opitz et al. (2002) examined the influence of the degree of variation of deviants from standard stimuli on neural parameters. Significant BOLD activations were observed during the presentation of medium and large deviants in the STG and in the opercular part of the right IFG. Temporal lobe activations were more pronounced for large than for medium deviants, whereas the reverse was true for the IFG. Small deviants failed to produce any reliable response during fMRI: they could only be detected during silence. Hemodynamic changes of the STG correlated with the change-related ERP signal between 90 and 120 ms (early MMN), while the IFG response correlated with the MMN in a late time window (140–170 ms). The authors concluded that the right fronto-opercular cortex is part of the neural network generating the MMN and could be attributed to an involuntary amplification or contrast enhancement mechanism (Opitz et al. 2002). The prefrontal cortex might be associated with change detection (Opitz et al. 2002; Rinne et al. 2000).

An EEG–fMRI experiment of Liebenthal et al. (2003) revealed MMN recorded in both large and small deviant conditions, especially in frontal sites. An increased negativity in Fz was linked with enhanced BOLD responses in the right STG bordering the superior temporal sulcus and on the right posterior superior temporal plane. Smaller peaks were found in the right posterior STG, the Heschl gyri, the left planum temporale, and the left STG. Altogether, the results of MMN generators on the superior temporal plane were consistent with dipole analysis and magnetoencephalographic recordings (Giard et al. 1990; Opitz et al. 2002). In addition, generators in each temporal region were hypothesized: one generator near the primary auditory areas on the superior temporal plane is thought to be the first to respond, probably corresponding to the N1 component. The later generator is meant to be located more anteriorly and laterally and seems to be associated with the MMN (Liebenthal et al. 2003). The results of the study support the idea that frequency deviancy detection is linked with generators in the right lateral part of the STG. However, a confident differentiation of N1- and MMN-associated brain responses and P3a-related responses was not possible.

Doeller et al. (2003) used a dipole analysis constrained by fMRI: The dipole analysis revealed an early MMN amplitude and activity of the STG that increased with pitch deviance. However, the right IFG and the late MMN amplitude showed

an inverted u-shape like pattern. The right prefrontal cortex seemed to be relevant for the auditory pitch discrimination, especially, when the differentiability of pitch deviants and standards are low. The authors concluded that these prefrontal mechanisms are probably associated with a top-down modulation of the deviance detection system in the STG (Doeller et al. 2003).

Apart from the magnitude of deviance, the modulation of attention might also matter for mismatch detection. Sabri et al. (2006) accomplished a simultaneous EEG–fMRI experiment in which the difficulty of the primary task was modulated. The results demonstrated an enhanced deviant-induced MMN in the easy task compared to the difficult task, whereas the N1 and P3a components were smaller. The frontocentral negativity varied across conditions regarding the temporal dimension: in the difficult task, the negativity was observed 60–110 ms after the stimulus presentation, indicating a link to the N1 component. In addition, a strong positivity was observed 210–340 ms after the stimulus. In the easy task, the significant negativity rather seemed to be associated with the MMN and was observed 110–170 ms after stimulus presentation. So, the underlying electrophysiological processes might be discriminative. Apart from frontal regions, passive deviancy detection, as reflected by the MMN, was connected with activations in the dorsal part of the STG, and involuntary shifting of attention, as reflected by the P3a, was observed in the dorsal and ventral parts of the superior temporal cortex, respectively. The authors suggested that the dorsal STG regions were primarily affected by the passive detection of mismatch between the memory influenced by standard tones and the incoming deviant, whereas the ventral region appeared to be modulated by involuntary shifts of attention to task-irrelevant auditory features (Sabri et al. 2006).

Presumably, mismatch detection can be associated with hemodynamic responses of superior temporal as well as frontal brain regions. EEG–fMRI studies have provided evidence for a functional dissociation of these regions and have given further insight into the chronology of brain responses. Another factor to possibly have an influence on mismatch detection is the focus of attention; this was investigated in a further study.

24.2.3 Preparatory Attention

Most of the classic studies of preparatory attention are based on the contingent negative variation (CNV). This negative potential is generated in the interval preceding and stimulus that needs further processing (Gomez et al. 2006). CNV is suggested to be an index of cortical arousal during anticipatory attention, preparation, motivation, and information processing (Nagai et al. 2004; Tecce 1972). Neurophysiological theories suggest that the CNV reflects a subthreshold activation of the cortex, preparing the cortex for processing the next stimulus and response (Rockstroh et al. 1982), as well as integrating cognitive and motor components (Nagai et al. 2004). The CNV can be induced when a warning stimulus is presented before the target stimulus during a reaction time task. There are several dissociable

components of the CNV: the early phase of the CNV, maximal at midline electrodes, encompasses an orienting response. Later variations of the CNV, maximal at the vertex, rather reflect motor preparation. Neuroimaging studies have shown a contribution of primary motor cortex, ACC, SMA, frontoparietal regions, and subcortical centers (Gomez et al. 2003; Ioannides et al. 1994).

In an EEG–fMRI study, increased BOLD responses in the thalamus, somatomotor cortex, midcingulate, SMA, and insular cortices during the period of CNV generation were demonstrated (Nagai et al. 2004). Additionally, single-trial analysis indicated that the thalamic, anterior cingulate and supplementary motor activity was modulated by the amplitude of the CNV. Thus, thalamocortical interactions appeared to regulate the CNV amplitude (Nagai et al. 2004) (Fig. 24.3).

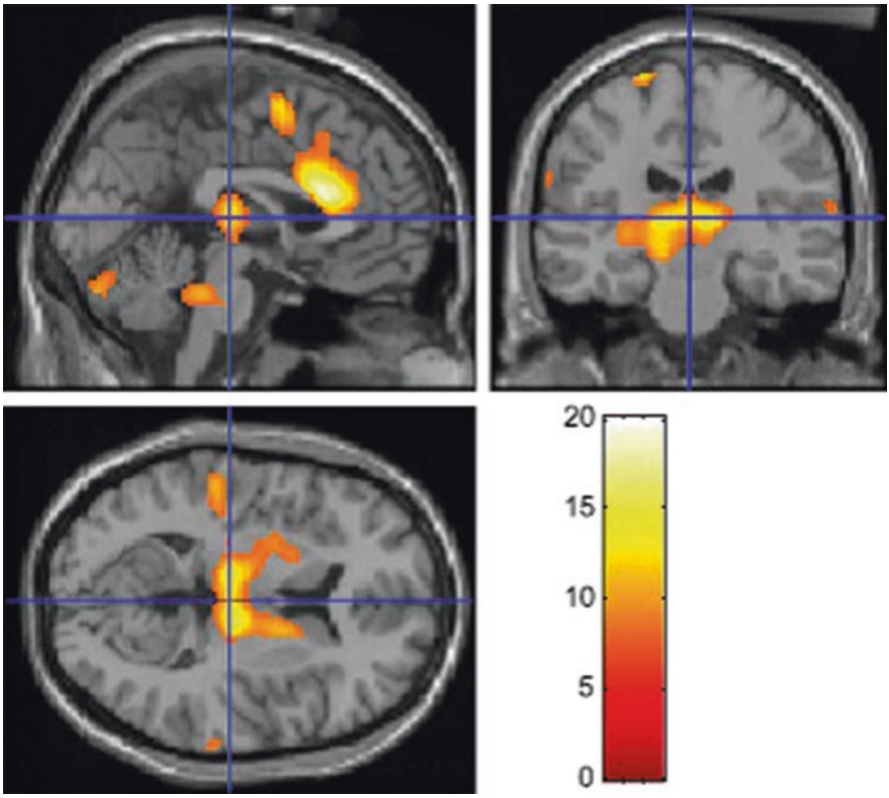

Fig. 24.3 Brain regions modulated by CNV amplitude. In five subjects, CNV was recorded simultaneously with acquisition of fMRI data. A fixed-effect analysis was used to determine across these subjects' regional brain activity correlating with trial-by-trial changes in measured CNV amplitude (derived from the integral over 3.5 s of baseline-corrected EEG data). *F* tests of regions were activity-related significant ($P < 0.05$, corrected) and highlighted bilateral thalamus, ACC/SMA, pons, and cerebellum. The distribution of this activity is plotted on orthogonal sections of a template brain, illustrating the location of thalamic involvement extending into basal ganglia (Reprint from Nagai et al. 2004; Copyright (2004) with permission from Elsevier)

24.3 Executive functions

Executive functioning describes a set of cognitive abilities that control and regulate other abilities and behaviors necessary for goal-directed behavior. Various abilities are included, for example, the ability to initiate and stop actions, to monitor and evaluate performance in relation to goals, to flexibly change and revise plans and behavior as needed, and to solve problems (Ylvisaker and DeBonis 2000). They are necessary for appropriate, socially responsible and effectively self-serving behavior (Lezak 1983).

Neuroimaging research proved that executive functioning is mediated by the prefrontal lobes of the cerebral cortex. Even though, different executive functions are associated with different regions of the frontal lobe (Braver et al. 2001; Carlson et al. 1998; D'Esposito et al. 1998; Stuss and Levine 2002; Watanabe et al. 2002). Apart from that, a wide cerebral network including temporal, parietal and subcortical structures and thalamic pathways is activated (e.g., Lewis et al. 2004; Watanabe et al. 2002). Along with the broad heterogeneity of executive functions, various experimental paradigms and tests have been used to acquire these processes.

24.3.1 Cognitive Flexibility

Cognitive flexibility comprises the ability to shift the attention from one perceptual parameter to another. The ability to flexibly adapt mental activity and behavior according to upcoming environmental requirements is crucial for successful behavior. Flexible responses can be investigated, for example, when using the *Wisconsin Card Sorting Test (WCST)* (Grant and Berg 1948). This test comprises a fairly easy task (rearranging of cards with simple symbols according to various criteria, e.g., color). However, no instructions are given on how to complete the task. Feedback provided after each match enables the subject to acquire the correct rule of classification.

ERP studies revealed a posterior P3b wave along with the performance in WCST-like tasks (Barcelo et al. 2000). Stimulus presentation elicited an enhanced synchronization between prefrontal, temporal, and posterior association cortex comprising different frequency ranges (Gonzalez-Hernandez et al. 2002). Functional neuroimaging studies verified the influence of frontal lobes (e.g., Konishi et al. 2002; Lie et al. 2006), as well as temporal and parietal regions (Lie et al. 2006) during the performance of the WCST. Up to now, there have been no combined or simultaneous EEG–fMRI studies addressing cognitive flexibility and set-shifting abilities. Still, a functional segregation of neural responses related to task components like set-shifting, working memory, inhibitory control, or feedback was attempted in several fMRI studies (e.g., Konishi et al. 1999; Lie et al. 2006; Monchi et al. 2001): rule changing in WCST-like tests seemed to be followed by responses in the inferior prefrontal area (Konishi et al. 1999), whereas positive and negative feedback led to an increased activation in the dorsolateral prefrontal cortex (DLPFC) (Monchi et al. 2001). Beyond that, negative feedback

indicating the need for a mental shift produced an enhanced contribution of a cortical basal ganglia loop (ventrolateral prefrontal cortex, caudate nucleus, thalamus) (Monchi et al. 2001).

24.3.2 Performance Monitoring

Important aspects of performance monitoring are controlling and dynamic adjustment of behavior within changing environmental requirements. Performance monitoring involves the detection of errors as well as the subsequent adjustment of behavior reinforcing adaptive behavior (Holroyd et al. 2002).

Erroneous actions, in particular, are highly informative for the adjustments of future behavior (Ridderinkhof et al. 2004). Erroneous responses are associated with negativity at frontocentral midline sites peaking about 100 ms after an error was made, the so-called negativity associated with errors (Ne)/error-related negativity (ERN) (Falkenstein et al. 1991; Gehring et al. 1993). Initially, the ERN/Ne was interpreted in context of the *error-monitoring system*: the ERN/Ne was meant to reflect the detection of errors or an attempt to inhibit errors (Gehring et al. 1993; Scheffers and Coles 2000; Scheffers et al. 1996). Then again, the ERN/Ne was interpreted in the context of the *conflict monitoring system* being essential for the detection of a high degree of response competition and the recruitment of top-down control from the DLPFC, which again is important in order to improve task performance and to reduce conflict (Botvinick et al. 1999, 2001; Carter et al. 1998; Cohen et al. 2000).

Imaging studies revealed a contribution of the ACC in error processing and response conflict (Braver et al. 2001; Carter et al. 1998; Ullsperger and von Cramon 2001). Disagreement exists about the precise location within the ACC: some studies reported a contribution of the caudal ACC during response conflict and the activation of the rostral ACC along with error processing (Braver et al. 2001; Kiehl et al. 2000). Other studies suggested conflict and error-related brain activations in the caudal ACC (Carter et al. 1998; Menon et al. 2001). Frontomedian areas appear to be associated with error-induced behavioral changes (e.g., posterior slowing) (Garavan et al. 2002). In addition, the DLPFC, the (pre-)SMA, (Kiehl et al. 2000; Menon et al. 2001), and the basal ganglia (Holroyd and Coles 2002) contributed to the modulation of the ERN/Ne.

Combined EEG–fMRI analyses of a *Go/NoGo paradigm* were used to further distinguish error and conflict-related brain responses (Mathalon et al. 2003). The results showed the expected ERN/Ne during error trials, especially at Cz as well as a nogo-related N2. Rostral, caudal, and motor ACC were activated during both conditions: these responses were more pronounced during the nogo trials compared to error trials, and a tight coupling between inhibition- and error-related brain responses could be demonstrated. The correlation of EEG and fMRI data revealed that error and conflict monitoring, at least partially, recruit the same brain regions, for example, caudal ACC. These results were consistent with the idea of medial frontal lobe monitoring in error and conflict monitoring. In addition, both processes engage

some distinct neural circuitry: error-specific responses were shown in the rostral ACC, the BA 10, and posterior cingulate. Conflict monitoring also recruited the DLPFC and inferior parietal lobule. Thus, error and conflict monitoring may be dissociable, subserved by overlapping and distinct ACC regions (Mathalon et al. 2003) (Fig. 24.4).

Another study used a speeded *flanker task* to analyze neural correlates of ERN and post-error slowing (Debener et al. 2005). During this task, participants were instructed to respond according to the direction of an arrow that was presented on a screen. The arrow was flanked by further arrows directing in the same (compatible trials) or the opposite direction (incompatible trials). A profound ERN was shown in frontocentral sites, especially for the incongruent error trials. Further analysis showed an association between high single-trial amplitudes and short reaction times for the incompatible errors, whereas incompatible correct trials were related to a small negativity. In addition, the ERN was systematically associated with ensuing behavioral adjustment: higher ERN amplitudes were related to longer reaction times in post-error trials. Single-trial amplitudes also covaried with enhanced BOLD responses in the rostral cingulate zone. Therefore, these results supported the view that the rostral cingulate zone is one source of the ERN and seems to be involved in controlling subsequent adjustment (Debener et al. 2005; Holroyd et al. 2004; Ridderinkhof et al. 2004; Ullsperger and von Cramon 2004).

A study using a modified flanker task demonstrated that higher ERN amplitudes are related to increased responses in the ACC, rostral cingulate zone (RCZ), and pre-SMA; whereas N2 amplitudes were linked to responses of the pre-SMA (Iannaccone et al. 2015). Conjunction analysis of EEG-informed fMRI revealed common activation of ERN and N2 in the pre-SMA that provided some evidence for shared conflict-related processes of the ERN and N2 (Iannaccone et al. 2015). By contrast, a spatial dissociation of conflict- and error-related responses along the medial frontal wall was shown (Iannaccone et al. 2015).

Performance monitoring also includes the anticipation and inhibition of behavioral responses. *Response anticipation* was assessed by comparing responses after a cue was given to prepare versus a cue indicating relax; *response conflict* was examined by comparing incongruent and congruent trials (Fan et al. 2007). As expected, response anticipation facilitated response execution: the responses were faster when a warning signal was presented before the actual target. In addition, response anticipation was associated with altered electrophysiological responses, especially in midline electrodes (CNV), as well as enhanced cue-associated fMRI activations encompassing a distributed right lateralized thalamo-cortico-striatal network and brain area regions significant for executive control. In addition, a greater anticipation-related gamma power and decreased responses in theta-, alpha-, and beta-bands, especially in frontal brain regions and the superior parietal lobe has been demonstrated. The authors assumed that the increased gamma band activity and decreased alpha band activity in regions associated with attention, sensory processing, and motor preparation support the assumption that the PFC exerts top-down control of task-relevant brain regions in response anticipation. Response conflict during

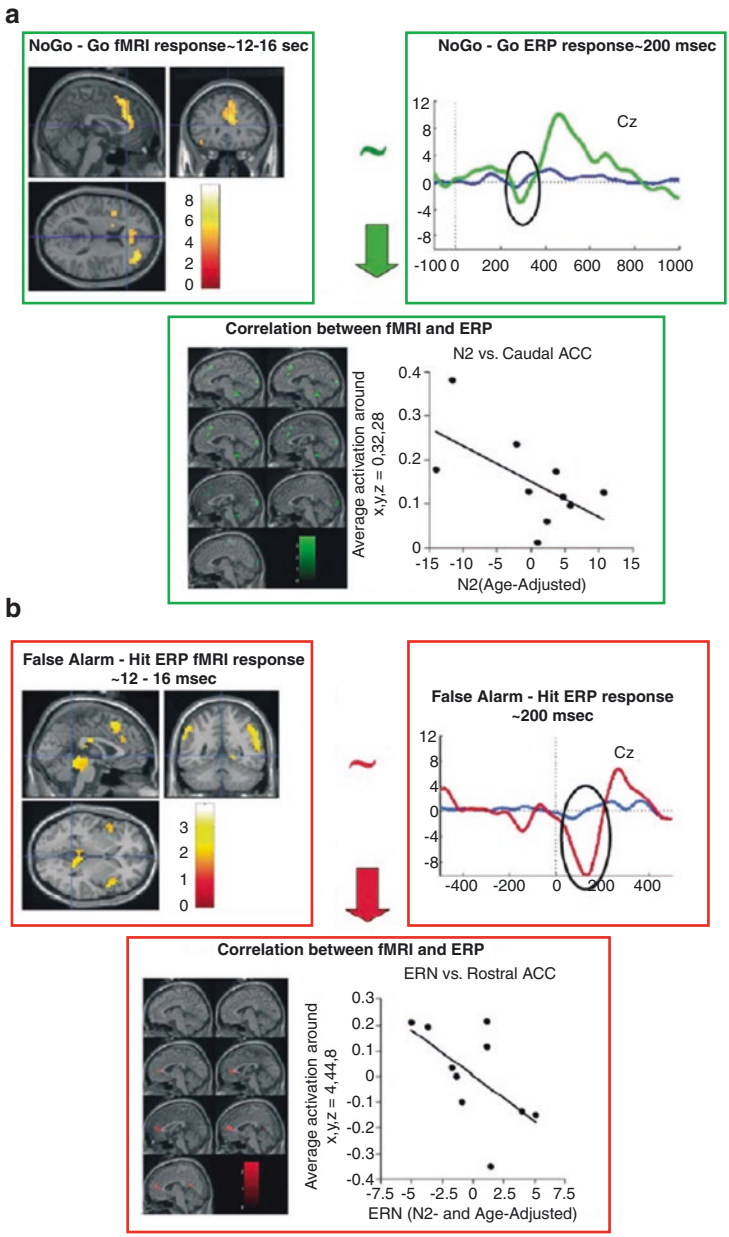

Fig. 24.4 (**a**) fMRI, ERP and fMRI–ERP correlations for correct rejections (NoGo)—hits (Go) comparisons. Three-planar view for fMRI ($P < 0.001$, uncorrected; upper left), ERPs overlaid correct rejections and hits from Cz (upper right), fMRI and ERP correlations ($P < 0.05$, uncorrected) focusing on the ACC (lower left), scatter plot showing that subjects with larger age-adjusted N2 scores have greater caudal ACC activation. (**b**) fMRI, ERP, and fMRI–ERP correlations for false alarms (NoGo)—hits (Go) comparisons. Three-planar view for fMRI ($P < 0.05$, uncorrected; upper left), ERPs overlaid false alarms and hits from Cz (upper right), fMRI, and ERP correlations ($P < 0.05$, uncorrected) focusing on the ACC (lower left), scatter plot showing that subjects with larger age-adjusted N2 scores have greater rostral ACC activation (Reprint from Mathalon et al. 2003; Copyright (2003) with permission from Elsevier)

uncued trials also led to an enhanced contribution of brain regions linked to executive control. Neural responses were enhanced compared to the response anticipation task (cued trials). In summary, common regions of a dorsal frontoparietal network and the ACC seemed to be engaged in the flexible control of a wide range of executive processes. Response anticipation modulated overall activity in the executive control network but did not interact with response conflict processing (Fan et al. 2007) (Fig. 24.5).

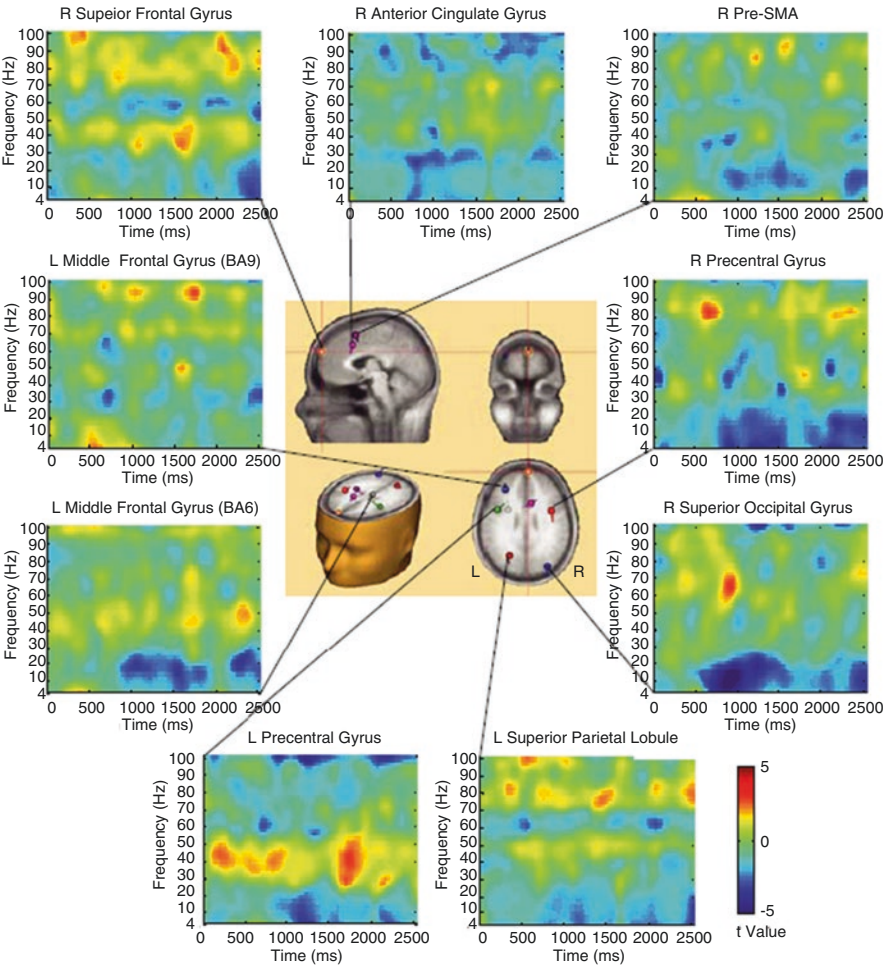

Fig. 24.5 Power change difference diagrams for the ready minus relax cue contrast as a function of time–frequency and the dipoles of ERP data. The center panel shows the dipole locations. The small balls and bars represent the locations and orientations of the dipoles, respectively. The right superior frontal gyrus shows greater gamma (>30 Hz) power maintained over the cue-target interval, whereas the right superior occipital gyrus shows a power decrease in theta (4–8 Hz), alpha (8–12 Hz), and beta (12–30 Hz) bands. The cue onset is at 0 ms, and the target onset is at 2500 ms (Fan et al. 2007; Copyright (2007) Society for Neuroscience)

24.3.3 Decision-Making

The influence of mental effort on decision-making processes was examined in a simultaneous EEG–fMRI experiment of with a forced choice reaction task: the subjects were instructed to accomplish this task under both high and low effort conditions (Mulert et al. 2008). Mental effort significantly affected the N1 potential but did not show any influence on the P300 potential. In the high-effort condition, single-trial coupling of EEG with fMRI demonstrated N1-related BOLD activity in the ACC and auditory cortex (Mulert et al. 2008). Comparing the N1-specific activity of the high-effort condition and the control condition (passive listening), significant activation was found only in the ACC. Hence, early ACC activation is suggested to be important for effort-related decision-making (Mulert et al. 2008). The application of this paradigm in subjects with high-risk state of psychosis revealed that neuronal responses in a network of brain regions (e.g., auditory cortices, thalamus, frontal brain regions including ACC, DLPFC) associated with the evoked gamma-band response were significantly lower in high-risk subjects compared to healthy controls, and the task performance was decreased (Leicht et al. 2016). Given the fact that a disturbed evoked gamma band response has shown to be altered in patients with schizophrenia, these results may indicate a potential applicability for the prediction of transition of high-risk subjects to schizophrenia (Leicht et al. 2016).

An EEG-informed fMRI study of emotional decisions were examined using a gambling paradigm. The results of the study indicated that during win versus loss, stimuli activations in the caudate, the ventral striatum, the orbitofrontal cortex, and the cingulate were shown (Guo et al. 2017). The integration of EEG and fMRI data revealed wide activation areas including the posterior cingulate and the orbitofrontal cortex. In addition, activation in the ventral striatum and medial prefrontal cortex was related to EEG power features especially theta (Guo et al. 2017).

24.3.4 Behavioral Inhibition

The ability to inhibit responses that are inappropriate in the current context is crucial for interactions in the social context (Logan et al. 1984; Shallice 1988). Inhibition capacity can be assessed, for example, with *Go/NoGo* tasks: these tasks require the subjects to respond to one type of stimulus and to withhold a response to another stimulus.

Electrophysiologically, the response inhibition process seems to be associated with a negative deflection that reaches a frontocentral maximum about 200 ms after the presentation of the respective stimuli (N2) (Falkenstein et al. 1999). More recently, it has been speculated that N2 reflects response conflict rather than inhibitory control (Donkers and van Boxtel 2004; Nieuwenhuis et al. 2003). The nogo-P3, a positive-going peak observed approx. 300–600 ms after stimulus, is assumed to be related to response inhibition (Kamarajan et al. 2005). Inhibition-related hemodynamic responses included the ACC (Braver et al. 2001; Casey et al. 1997; Durston et al. 2002; Liddle et al. 2001), the middle and inferior cingulate cortex, anterior

insula (Braver et al. 2001; Watanabe et al. 2002), the (pre-) SMA (Garavan et al. 2002; Ullsperger and von Cramon 2001), and parietal brain regions (Garavan et al. 2002; Watanabe et al. 2002). BOLD reactivity was usually stronger in the right hemisphere than in the left hemisphere (Garavan et al. 1999; Kelly et al. 2004).

Deficits in response inhibition capacities in schizophrenic patients were associated with increased go-related activations and decreased nogo-associated variations compared to controls (Ford et al. 2004). Enhanced inhibition-related hemodynamic responses were shown in controls compared to schizophrenic patients in a network of brain regions including medial and lateral frontal regions, the precuneus, the inferior parietal lobe, the gyrus postcentralis, the STG, and the insula. Altogether, these results indicated that go responses were more arduous and deliberate for patients with schizophrenia than for healthy subjects, whereas response inhibition was easier. The combined evaluation of ERPs and BOLD responses revealed a positive association of P300 amplitudes with BOLD responses in the ACC, DLPFC, inferior parietal lobe, and caudate nucleus in healthy subjects. In patients, there was a modest correlation between parietocentral nogo-P3 and ACC activations. Overall, the results indicated that healthy subjects set up prepotent response biases during go trials. The effort expended to overcome this tendency during inhibition is reflected in the nogo-P3 amplitude and the recruitment of neural structures associated with executive control. Patients with schizophrenia, however, did not show strong response biases. In addition, the DLPFC, the inferior parietal lobe, and the striatum did not contribute significantly to task execution in patients (Ford et al. 2004).

The combination of EEG and fMRI helped to generate a hypothesis about different cognitive strategies of psychiatric populations, and neural structures recruited to implement them (Ford et al. 2004).

The examination of response inhibition capacity in alcohol-dependent patients showed that self-rated anxiety considerably influenced cognitive functions and their neural correlates: patients with high self-rated anxiety showed significantly elevated activations during response inhibition, especially in the middle/superior frontal gyrus, and the right IFG compared to patients with low ratings on these scales. In addition, enhanced activations were shown in temporoparietal brain regions. The integration of EEG and fMRI data produced a positive correlation between P300 amplitudes at frontocentral locations and medial frontal, insular as well as right temporoparietal BOLD responses in healthy subjects. In patients, associations between ERPs and hemodynamic responses were less clear: patients with small anxiety ratings showed positive relations between the insula and frontocentral P300 amplitudes. Contrary to the control subjects, there was no association with medial frontal and temporoparietal regions. Patients with increased anxiety scores, however, revealed correlations between enhanced P300 latencies in FCz and right frontal and inferior parietal activations. Altogether, these results provided evidence that alcohol-dependent patients and healthy subjects recruit different brain regions during behavioral inhibition. In addition, comorbid symptoms of trait anxiety considerably influenced the pattern of brain functions related to cognitive functions in alcohol-dependent subjects (Karch et al. 2007).

Ko et al. (2016) examined the inhibitory control capacity in a realistic stop-signal task. For that purpose, the results of a scenario with visual symbols (1) and a battlefield scenario with the task instruction to shoot at terrorists (2) were compared. During the battlefield scenario, the stop signal led to higher BOLD responses and synchronization of the theta–alpha activities in the right temporoparietal junction (rTPJ). The authors assumed that the higher activation of rTPJ in the battlefield scenario may be related to morality judgments or attentional reorienting (Ko et al. 2016).

Data-Driven Analysis

Most of the EEG–fMRI studies focus on measuring known ERP components in single trials and correlate the resulting time series with the fMRI–BOLD signal. Data-driven analyses provide the opportunity to select automatically task-specific electrophysiological independent components in order to examine the relationship between trial by trial variability and BOLD responses (Schmuser et al. 2014). Aim of this method is to show that the variability of the chosen ERP component is specific for the targeted neurophysiological process. Positive correlations of fMRI–BOLD signal with EEG-derived regressors in frontostriatal regions which were more pronounced in an early phase compared to a late phase of task execution were demonstrated in a visual Go/NoGo task. The authors concluded that different phases of task execution can be distinguished with this method (Schmuser et al. 2014).

Differences regarding the interindividual variability of response inhibition may also constitute a key to pathological processes underlying impulse control disorders (Schmuser et al. 2016). A data-driven classification in two groups according neurophysiological responses to the Nogo stimuli revealed differences on questionnaires regarding attention deficit/hyperactivity disorder, differences regarding reaction time and intraindividual RT variability, variations regarding the activations in the left inferior frontal cortex/insula, left putamen as well as regarding the P3 amplitudes (Schmuser et al. 2016). The authors concluded that the interindividual difference in an electrophysiological correlate of response inhibition is correlated with distinct, potentially compensatory neural activity. It was assumed that these results may indicate the existence of dissociable phenotypes of response inhibition that possibly provides protection against impulsivity-related dysfunction (Schmuser et al. 2016).

24.3.5 Working Memory

Working memory (WM) refers to processes used for temporal storing and manipulating information (Baddeley 1992). Baddeley and Hitch (1974) proposed a WM model based on the assumption of three basic components. Information is stored by silently rehearsing sounds or words in a continuous loop (*phonological loop*). The *visuospatial sketchpad* is engaged when performing visual or spatial tasks. The *central executive* is responsible for the supervision of information integration and for coordinating both systems (Baddeley and Hitch 1974). Later on, the concept was

extended by adding the *episodic buffer*, that is meant to contain images integrating phonological, visual and spatial information, and possibly information not covered in other systems (Baddeley 1992).

The DLPFC, the IFG, the ACC, and temporoparietal brain regions are suggested to account for WM processes (D'Esposito et al. 2000; Veltman et al. 2003). The phonological store is thought to be constituted by left parietal activations, whereas the rehearsal process is constituted by left prefrontal activations (Paulesu et al. 1993).

Bledowski et al. (2006) conducted a WM task to further analyze the *mental chronometry* of WM retrieval on the basis of an fMRI-constrained source analysis in order to distinguish various subprocesses of WM abilities. The results indicated early BOLD activations within the inferior temporal cortex associated with the electrophysiological N1 and P3a component, which were followed by responses of the posterior parietal cortex. Late responses were also observed in the ventrolateral prefrontal cortex as well as the medial frontal and premotor areas. The authors proposed that these neural responses might reflect various cognitive stages during task processing, for example, perceptual evaluation (inferotemporal), storage buffer operations (posterior parietal cortex), active retrieval (ventrolateral prefrontal cortex), and action selection (medial frontal and premotor cortex) (Bledowski et al. 2006).

Michels et al. (2010) used EEG-constrained fMRI analysis by introducing power value of an oscillation into the general linear model (GLM) as a covariate and identified the distribution patterns corresponding to theta and alpha activities under different loads (see Fig. 24.6). For theta power, these brain areas were mainly the medial prefrontal cortex and posterior parietal cortex (PPC). For alpha power, they were the DLPFC, PPC, and some other brain regions (Michels et al. 2010). In addition, the results indicate that low as well as high oscillatory activity are linked to neuronal activity during cognitive demanding processes (Michels et al. 2010).

An influence of memory load on the intensity and time course of EEG oscillations on WM was also demonstrated by a joint independent component analysis of EEG oscillations and fMRI activation (Zhao et al. 2017): time-locked activity of theta and beta were modulated by memory load in the early stimuli evaluation stage, corresponding to the enhanced activation in the frontal and parietal lobe, which were involved in stimulus discrimination, information encoding and delay-period activity (Zhao et al. 2017). During response selection, load-dependent changes in alpha and gamma activity are related to enhanced BOLD responses in frontal, temporal, and parietal lobes, which played important roles in attention, information extraction, and memory retention (Zhao et al. 2017).

Executive dysfunction and deficits in working memory are common in various psychiatric diseases, for example, schizophrenia (Catafau et al. 1994; Goldman-Rakic 1994). Functional MRI studies focusing on WM tasks in schizophrenic patients found abnormal activations especially in the PFC (Johnson et al. 2006; Manoach et al. 2000; Tan et al. 2005). A combined EEG–fMRI study was designed to distinguish the effect of early perceptual stages from later, memory-related operations on WM capacities of schizophrenic patients (Haenschel et al. 2007). Perceptual and cognitive stages of WM performance were separated using ERP analysis. The

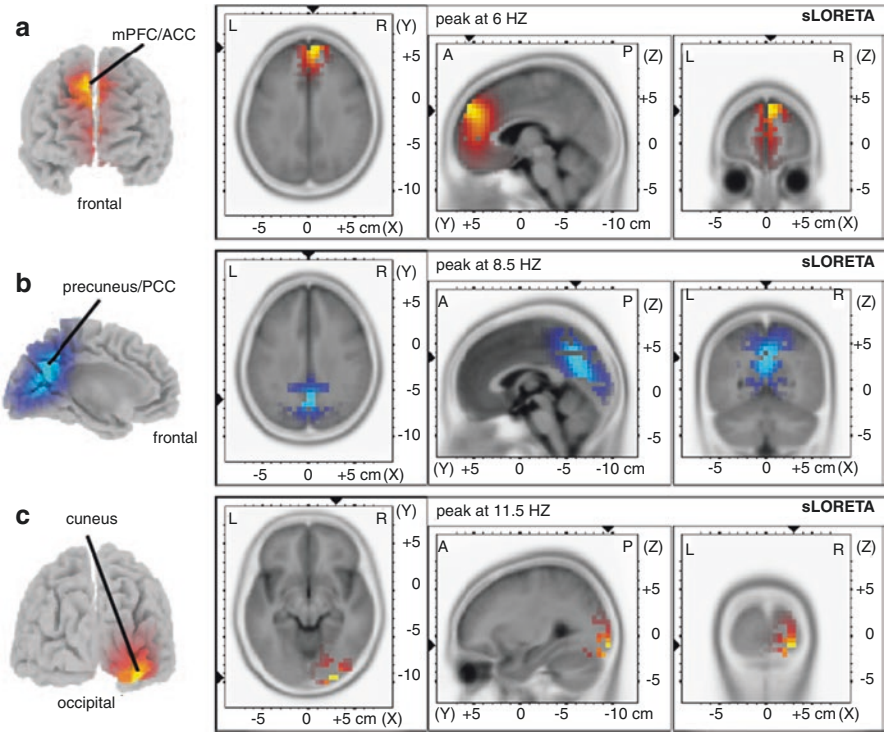

Fig. 24.6 EEG source localization (sLORETA) activation maps for the contrast of a cognitive more demanding task (five consonants) vs. an easier task (two consonants). (**a**) Theta (5–7 Hz) band power increased ($p < 0.1$) with load at the border of the MPFC and the ACC. (**b**) Alpha1 (8–10 Hz) showed decreased (blue) activity ($p < 0.05$, corrected for multiple comparisons) at the border of the precuneus and the PCC with an increase of load. (**c**) Alpha2 (10–13 Hz) showed positive load modulations ($p < 0.05$, corrected for multiple comparisons) in the right middle occipital gyrus (cuneus, BA 18). The t values are plotted onto an MRI template (Michels et al. 2010)

results suggested that early aspects, indicated by the P1 amplitude, and late aspects of encoding and retrieval, represented by P370 amplitude, were reduced in patients compared to healthy controls. Furthermore, unlike healthy subjects, patients did not show a gradual increment of P1 along with increasing task demands. In patients, the P1 reduction was mirrored by reduced activation of visual areas. Altogether, the findings showed the relevance of early sensory deficits for higher level cognitive dysfunctions in schizophrenia (Haenschel et al. 2007).

The application of EEG–fMRI in boys with ADHD using a spatial WM scenario demonstrated that alpha ERD during encoding was associated with occipital activation and fronto-parieto-occipital functional connectivity (Lenartowicz et al. 2016; see Fig. 24.7). The authors concluded that this may indicate that the alpha ERD involves and perhaps arises as a result of top-down network interactions (Lenartowicz et al. 2016). Participants with primarily inattentive type ADHD demonstrated weaker occipital activations whereas their fronto-parieto-occipital

connectivity was stronger. This may indicate a compensatory response of the attentional system in modulating activity within occipital cortex. These results are interpreted as a unique, encoding-related ADHD deficit in fronto-parieto-occipital connectivity (Lenartowicz et al. 2016).

Several aspects of executive functioning, for example, verbal fluency and cognitive flexibility, have not been addressed in EEG–fMRI studies so far. Functional dissociations of brain regions connected with flexible responses to task demands have been examined in functional MRI studies independent of EEG recordings. Regarding behavioral inhibition and decision-making, EEG–fMRI studies were conducted to further distinguish neural correlates of different aspects of cognition, for example, conflict-related and error-related tasks as well as response anticipation and response conflict. In addition, various processing stages of WM retrieval were

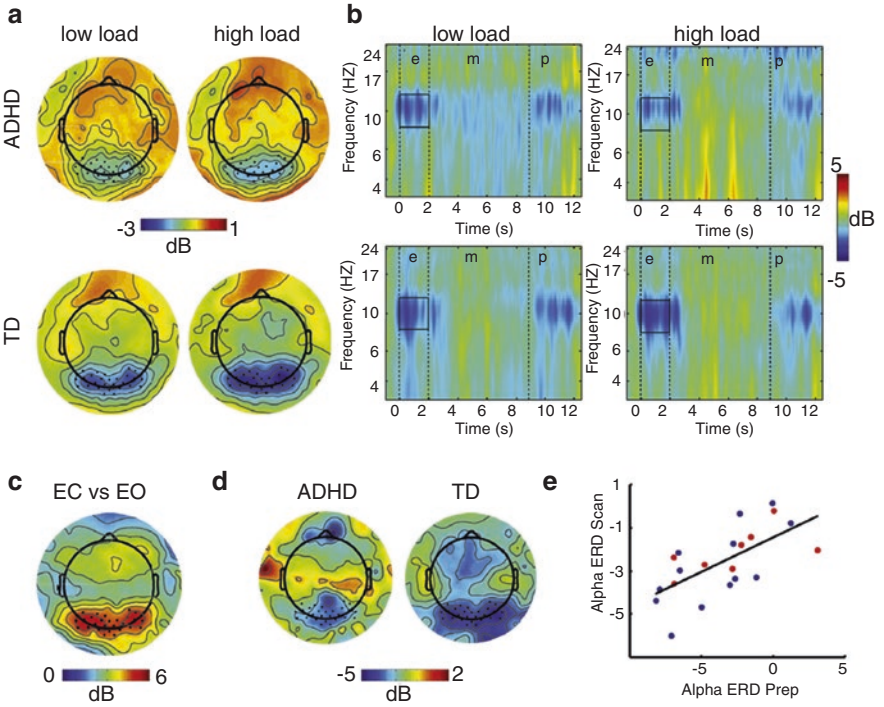

Fig. 24.7 Alpha ERD during spatial working memory encoding (**a**, **b**) performed during fMRI was observed in both ADHD and typical developing (TD) participants, was distributed spatially over occipital electrodes (**a**) and temporally throughout the 2-s encoding interval (**b**). Alpha ERD was greater for higher load and in TD participants. A comparison of peak alpha power during pre-scan eyes-open (EO) and eyes-closed (EC) conditions (**c**) was used to identify electrodes of interest for alpha ERD analyses. Alpha ERD was also weaker in ADHD than in TD participants during preparatory practice, (**d**) pre-scanning and was significantly correlated with alpha ERD during scanning (**e**), indicating that between-subject variability was preserved in the concurrent EEG–fMRI recordings. *TD* typically developing, *ADHD* attention-deficit hyperactivity disorder, *ERD* event-related desynchronization (Lenartowicz et al. 2016)

decomposed (mental chronometry) using combined EEG–fMRI measurements. Furthermore, the brain activity of healthy subjects was compared to those associated with deficient executive processes in psychiatric patients: these studies provided evidence for distinct patterns of neural responses.

24.4 Memory

There are three main stages in the formation and retrieval of memory:

1. *encoding*: processing and combining of received information
2. *storing* of encoded information
3. *retrieval:* calling back stored information

Irrespective of these criteria, memory processes can be classified according to the amount of information being processed, the duration of storage, and the kind of information being stored. The *sensory memory* stores impressions of sensory information for the initial 200–500 ms after its presentation. Some of the information is transferred to the *short-term memory* and can be recalled for several seconds up to 1 min. In the *long-term memory*, much larger quantities of information can be stored, and the information is potentially stored for an unlimited time period. In contrast to the sensory and the short-term memory, the information in the long-term memory is stored semantically. Long-term memory can be divided into the *declarative* and the *procedural memory* (Anderson 1976). The declarative memory contains information that is explicitly stored and retrieved, for example, contact-independent facts (*semantic memory*) or personal memories such as emotions and personal associations (*episodic memory*). The procedural memory, however, primarily contains cognitive und motor skills which have been formed primarily via repetition and without explicit learning.

Medial temporal lobes are assumed to reliably contribute to memory processes (Cabeza and Nyberg 2000; Yancey and Phelps 2001). Neurobiological responses during effective encoding and the formation of new declarative memories have been observed in medial temporal lobe structures, including the hippocampus and surrounding parahippocampal cortices (Brewer et al. 1998; Ofen et al. 2007; Otten et al. 2002). The *storage of information* appeared to be related to a network of cortical brain regions, for example, association cortices. *Retrieval processes* seemed to be associated with enhanced responses of the prefrontal cortex and temporal regions (Cabeza and Nyberg 2000; de Zubicaray et al. 2007; Habib and Nyberg 2007; Henson 2005), intraparietal sulcus and precuneus (Henson et al. 2005), as well as the parietal cortex (de Zubicaray et al. 2007; Heun et al. 2004).

Iidaka et al. (2006) aimed at disentangling the conscious recollection of information from familiarity-based judgments using fMRI and ERP. For this purpose, an old/new recognition task was designed. In addition, the level of processing was modulated in order to test whether retrieval activity in the cortical and subcortical structures was affected by the depth of processing during memory encoding. During

the encoding phase of the experiment, pictures were presented; in the deep-encoding condition, the subjects judged whether the picture was man-made or a natural object; in the shallow-encoding condition, the subjects judged whether the object was presented on the left or right side of the screen. The findings of the study were consistent with those of former studies supposing a frontoparietal involvement during retrieval success. In addition, parietal activity associated with retrieval success produced by deeply encoded items was greater than that produced by the shallowly encoded item. In addition, the study provided some evidence that the left prefrontal cortex activation is primarily associated with the conscious and successful recognition of old items. In contrast, the right inferior parietal area was more likely to be related to familiarity-based judgment than to recollection-based judgment. The retrieval success was modulated by the functional connectivity in the left hemisphere (Iidaka et al. 2006).

It has been demonstrated that recognition memory is underlied by two independent processes: (1) recollection: a conscious retrieval of contextual information that is related to the late parietal old new effect; (2) familiarity: a contextual feeling of knowing that is associated with early mid-frontal old/new effect. An EEG-informed fMRI analysis demonstrated that activation in the right DLPFC and the right intraparietal sulcus was associated with the early frontal old/new effect. By contrast, activation in the right posterior hippocampus, parahippocampal cortex, and retrosplenial cortex was associated with the amplitude of the late parietal old new effect (Hoppstadter et al. 2015).

An EEG-informed fMRI analysis during a face recognition task enabled a spatiotemporal characterization of the complete cognitive process of face recognition. These results were improved in comparison with EEG and/or fMRI-only analyses (Wirsich et al. 2014).

Altogether, these studies demonstrated the possibility to distinguish BOLD responses associated with different aspects of task execution and related to a differential temporal architecture using the integration of EEG–fMRI.

24.5 Limitations and Outlook

Present EEG–fMRI studies focusing on cognitive processes provided further information, for example, about the localization of various aspects of cognitive processing and ERP components. Therefore, variable methods were used, for example, the comparison of BOLD responses and localization of ERPs based on LORETA analysis (Mulert et al. 2004), fMRI-constrained dipole models (Bledowski et al. 2004b; Crottaz-Herbette and Menon 2006), and single-trial analysis (Debener et al. 2006; Eichele et al. 2005). Single-trial analysis, additionally, enabled examinations about how aspects like habituation influenced task execution. Determining the influence of arousal and the default mode on cognitive functioning might belong to important aspects of further EEG–fMRI assessments, for instance, the question if and to what extent the default mode of brain activity, as represented by BOLD–fMRI, does account for event-related trial-by-trial fluctuations (Debener et al. 2006).

Working memory studies revealed a chronological dissociation of prefrontal and parietal brain regions suggesting parallel as well as serial retrieval processes (Bledowski et al. 2006). In addition, a functional dissociation of various aspects of cognitive functioning was attempted in several studies: partial overlapping and distinct brain regions were related to error processing and conflict monitoring (Mathalon et al. 2003) as well as response conflict and response anticipation (Fan et al. 2007). Furthermore, associations of BOLD responses and oscillations in various frequency bands were assessed (Meltzer et al. 2007; Sammer et al. 2007).

So far, the number of simultaneous EEG–fMRI studies focusing on the examination of cognitive processes is limited: combined evaluations of electrophysiological and hemodynamic information, sometimes acquired through diverse samples, are still the majority. Conclusions to be possibly drawn from these studies, are limited because some of the main advantages of simultaneous studies are not achieved, for example, both parameters are not acquired under the same conditions probably resulting in differences regarding factors potentially influencing cognitive abilities like motivation, learning, habituation, and arousal.

Most of the existing simultaneous and combined EEG–fMRI studies investigating cognitive abilities focus on attention processes. Investigations dealing with other aspects of cognitive functioning such as executive functions and memory processes are rare. One reason for this might be the fact that neurobiological aspects of attention take center stage in electrophysiological studies. These attention-related electrophysiological studies formed the basis for many EEG–fMRI measurements. Methodological difficulties might be the reason why some cognitive functions have rarely been analyzed: memory processes, for example, fundamentally rely on subcortical brain functions, for example, the hippocampus. By contrast, the EEG is particular sensitive to post-synaptic potentials which are generated in superficial layers of the cortex. Electrical activity of deep structures contributes far less to the EEG signal. Thus, memory-related functional changes in deep brain structures cannot be recorded reliably with electroencephalography. Another reason for the limited number of studies focusing on cognitive functions other than attention might be that executive functions, for example, comprise a number of different components; various tasks are used to acquire these processes. Functional results often vary clearly between tasks; small variations between task demands may already produce clear functional differences. Another problem arises through the examination of planning processes and the management of new problems: problems cease to be novel after the first administration of the test; therefore, they cannot be determined reliably using methods which depend on the iterative presentation of similar tasks (e.g., functional MRI, ERPs) (Burgess 1997; Denckla 1996). Lezak (1983) assumed that the examination of goal setting, structuring, and decision-making is difficult in the highly structured context of studies. In addition, due to the high complexity of executive tasks, basic nonexecutive processes like attention, memory, and motor skills might be triggered during task execution (Burgess 1997), various subprocesses are likely, and similar behaviors can have quite different causes (Jurado and Rosselli 2007).

Due to the limited number of studies regarding cognitive functions other than attention, this overview is one-sided. Various aspects of cognitive functioning were not accounted for according to their significance in cognitive psychology and research, respectively. The text was strongly determined by the number of EEG–fMRI studies presented in literature so far. Often, only some aspects of a cognitive domain were accounted for during these studies.

Despite several difficulties to be considered in the evaluation of executive functions, the examination of these processes might be particularly interesting: interactions between primary sensory areas, unimodal and multimodal association cortices and prefrontal regions, as well as between various parts of the prefrontal cortex are assumed to be of some importance in executive functioning. EEG–fMRI could contribute to the functional dissociation of these processes and their underlying brain responses. The assignment of subprocesses of cognitive functioning to various brain regions can be investigated using temporal information ("*mental chronometry*"). In addition, interactions between various sensoric and cognitive subprocesses, for example, encoding, comparison of new information with those stored in memory, and response preparation could be explored.

Another promising approach is the implementation of EEG–fMRI studies in the evaluation of neuropsychiatric diseases. Apart from structural deficits, a functional disintegration of various brain structures and functions is thought to belong to the main neurobiological basis of these diseases. These deficits in brain functions and functional interactions might be evaluated using EEG–fMRI studies and could contribute considerably to a further understanding of neurobiological aspects of these diseases. However, the examination of neurologic and psychiatric patients as well as children reveals limitations: EEG–fMRI investigations tend to be more stressful than single EEG and functional MRI recordings. Furthermore, the recordings are more time consuming, for example, the time required is significantly influenced by the number of electrodes. Due to the extraordinary technical complexity, at present, the practicability in the daily clinical routine is limited. As a consequence, only three studies with psychiatric patients have been published so far. The relevance of this approach, however, was demonstrated, for example, in a study of Haenschel et al. (2007). Their results indicated that working memory deficits of schizophrenic patients were not solely the consequence of dysfunction in prefrontal brain regions. More likely, early visual deficits contributed to these deficits.

References

Anderson JR (1976) Language, memory and thought. Erlbaum, Mahwah

Baddeley A (1992) Working memory. Science 255(5044):556–559

Baddeley AD, Hitch GJ (1974) Working memory. In: Bower GAA (ed) The psychology of learning and motivation. Academic, New York, pp 47–89

Barcelo F, Munoz-Cespedes JM, Pozo MA, Rubia FJ (2000) Attentional set shifting modulates the target P3b response in the Wisconsin card sorting test. Neuropsychologia 38(10):1342–1355

Benar CG, Schon D, Grimault S, Nazarian B, Burle B, Roth M, Anton JL (2007) Single-trial analysis of oddball event-related potentials in simultaneous EEG-fMRI. Hum Brain Mapp 28(7):602–613

Bledowski C, Prvulovic D, Goebel R, Zanella FE, Linden DE (2004a) Attentional systems in target and distractor processing: a combined ERP and fMRI study. NeuroImage 22(2):530–540

Bledowski C, Prvulovic D, Hoechstetter K, Scherg M, Wibral M, Goebel R, Linden DE (2004b) Localizing P300 generators in visual target and distractor processing: a combined event-related potential and functional magnetic resonance imaging study. J Neurosci 24(42):9353–9360

Bledowski C, Cohen Kadosh K, Wibral M, Rahm B, Bittner RA, Hoechstetter K, Linden DE (2006) Mental chronometry of working memory retrieval: a combined functional magnetic resonance imaging and event-related potentials approach. J Neurosci 26(3):821–829

Botvinick M, Nystrom LE, Fissell K, Carter CS, Cohen JD (1999) Conflict monitoring versus selection-for-action in anterior cingulate cortex. Nature 402(6758):179–181

Botvinick MM, Braver TS, Barch DM, Carter CS, Cohen JD (2001) Conflict monitoring and cognitive control. Psychol Rev 108(3):624–652

Braver TS, Barch DM, Gray JR, Molfese DL, Snyder A (2001) Anterior cingulate cortex and response conflict: effects of frequency, inhibition and errors. Cereb Cortex 11(9):825–836

Brewer JB, Zhao Z, Desmond JE, Glover GH, Gabrieli JD (1998) Making memories: brain activity that predicts how well visual experience will be remembered. Science 281(5380):1185–1187

Burgess P (1997) Theory and methodology in executive function research. In: Rabbitt P (ed) Methodology of frontal executive function. Psychology Press, Hove, pp 81–116

Bush G, Luu P, Posner MI (2000) Cognitive and emotional influences in anterior cingulate cortex. Trends Cogn Sci 4(6):215–222

Cabeza R, Nyberg L (2000) Imaging cognition II: an empirical review of 275 PET and fMRI studies. J Cogn Neurosci 12(1):1–47

Calhoun VD, Adali T, Pearlson GD, Kiehl KA (2006) Neuronal chronometry of target detection: fusion of hemodynamic and event-related potential data. NeuroImage 30(2):544–553

Carlson S, Martinkauppi S, Rama P, Salli E, Korvenoja A, Aronen HJ (1998) Distribution of cortical activation during visuospatial n-back tasks as revealed by functional magnetic resonance imaging. Cereb Cortex 8(8):743–752

Carter CS, Braver TS, Barch DM, Botvinick MM, Noll D, Cohen JD (1998) Anterior cingulate cortex, error detection, and the online monitoring of performance. Science 280(5364):747–749

Casey BJ, Castellanos FX, Giedd JN, Marsh WL, Hamburger SD, Schubert AB, Rapoport JL (1997) Implication of right frontostriatal circuitry in response inhibition and attention-deficit/hyperactivity disorder. J Am Acad Child Adolesc Psychiatry 36(3):374–383

Catafau AM, Parellada E, Lomena FJ, Bernardo M, Pavia J, Ros D, Gonzalez-Monclus E (1994) Prefrontal and temporal blood flow in schizophrenia: resting and activation technetium-99m-HMPAO SPECT patterns in young neuroleptic-naive patients with acute disease. J Nucl Med 35(6):935–941

Chun J, Peltier SJ, Yoon D, Manschreck TC, Deldin PJ (2016) Prolongation of ERP latency and reaction time (RT) in simultaneous EEG/fMRI data acquisition. J Neurosci Methods 268:78–86. https://doi.org/10.1016/j.jneumeth.2016.05.011

Cohen JD, Botvinick M, Carter CS (2000) Anterior cingulate and prefrontal cortex: who's in control? Nat Neurosci 3(5):421–423

Crottaz-Herbette S, Menon V (2006) Where and when the anterior cingulate cortex modulates attentional response: combined fMRI and ERP evidence. J Cogn Neurosci 18(5):766–780

D'Esposito M, Aguirre GK, Zarahn E, Ballard D, Shin RK, Lease J (1998) Functional MRI studies of spatial and nonspatial working memory. Brain Res Cogn Brain Res 7(1):1–13

D'Esposito M, Postle BR, Rypma B (2000) Prefrontal cortical contributions to working memory: evidence from event-related fMRI studies. Exp Brain Res 133(1):3–11

de Zubicaray G, McMahon K, Eastburn M, Pringle AJ, Lorenz L, Humphreys MS (2007) Support for an auto-associative model of spoken cued recall: evidence from fMRI. Neuropsychologia 45(4):824–835

Debener S, Ullsperger M, Siegel M, Fiehler K, von Cramon DY, Engel AK (2005) Trial-by-trial coupling of concurrent electroencephalogram and functional magnetic resonance imaging identifies the dynamics of performance monitoring. J Neurosci 25(50):11730–11737

Debener S, Ullsperger M, Siegel M, Engel AK (2006) Single-trial EEG-fMRI reveals the dynamics of cognitive function. Trends Cogn Sci 10(12):558–563

Debener S, Strobel A, Sorger B, Peters J, Kranczioch C, Engel AK, Goebel R (2007) Improved quality of auditory event-related potentials recorded simultaneously with 3-T fMRI: removal of the ballistocardiogram artefact. NeuroImage 34(2):587–597

Denckla MB (1996) A theory and model of executive function: a neuropsychological perspective. In: Lyon G, Krasnegor N (eds) Attention, memory, and executive function. Paul Brooks, Towson

Doeller CF, Opitz B, Mecklinger A, Krick C, Reith W, Schroger E (2003) Prefrontal cortex involvement in preattentive auditory deviance detection: neuroimaging and electrophysiological evidence. NeuroImage 20(2):1270–1282

Donchin E, Coles MGH (1988) Is the P300 component a manifestation of context updating? Behav Brain Sci 11:355–372

Donkers FC, van Boxtel GJ (2004) The N2 in go/no-go tasks reflects conflict monitoring not response inhibition. Brain Cogn 56(2):165–176

Downar J, Crawley AP, Mikulis DJ, Davis KD (2002) A cortical network sensitive to stimulus salience in a neutral behavioral context across multiple sensory modalities. J Neurophysiol 87(1):615–620

Durston S, Thomas KM, Worden MS, Yang Y, Casey BJ (2002) The effect of preceding context on inhibition: an event-related fMRI study. NeuroImage 16(2):449–453

Eichele T, Specht K, Moosmann M, Jongsma ML, Quiroga RQ, Nordby H, Hugdahl K (2005) Assessing the spatiotemporal evolution of neuronal activation with single-trial event-related potentials and functional MRI. Proc Natl Acad Sci U S A 102(49):17798–17803

Falkenstein M, Hohnsbein J, Hoormann J, Blanke L (1991) Effects of crossmodal divided attention on late ERP components. II. Error processing in choice reaction tasks. Electroencephalogr Clin Neurophysiol 78(6):447–455

Falkenstein M, Hoormann J, Hohnsbein J (1999) ERP components in Go/Nogo tasks and their relation to inhibition. Acta Psychol 101(2-3):267–291

Fan J, Kolster R, Ghajar J, Suh M, Knight RT, Sarkar R, McCandliss BD (2007) Response anticipation and response conflict: an event-related potential and functional magnetic resonance imaging study. J Neurosci 27(9):2272–2282

Ford JM, White P, Lim KO, Pfefferbaum A (1994) Schizophrenics have fewer and smaller P300s: a single-trial analysis. Biol Psychiatry 35(2):96–103

Ford JM, Gray M, Whitfield SL, Turken AU, Glover G, Faustman WO, Mathalon DH (2004) Acquiring and inhibiting prepotent responses in schizophrenia: event-related brain potentials and functional magnetic resonance imaging. Arch Gen Psychiatry 61(2):119–129

Friedman D, Cycowicz YM, Gaeta H (2001) The novelty P3: an event-related brain potential (ERP) sign of the brain's evaluation of novelty. Neurosci Biobehav Rev 25(4):355–373

Garavan H, Ross TJ, Stein EA (1999) Right hemispheric dominance of inhibitory control: an event-related functional MRI study. Proc Natl Acad Sci U S A 96(14):8301–8306

Garavan H, Ross TJ, Murphy K, Roche RA, Stein EA (2002) Dissociable executive functions in the dynamic control of behavior: inhibition, error detection, and correction. NeuroImage 17(4):1820–1829

Gehring WJ, Goss B, Coles MG, Meyer DE, Donchin E (1993) A neural system for error detection and compensation. Psychol Sci 4:385–390

Giard MH, Perrin F, Pernier J, Bouchet P (1990) Brain generators implicated in the processing of auditory stimulus deviance: a topographic event-related potential study. Psychophysiology 27(6):627–640

Goldman-Rakic PS (1994) Working memory dysfunction in schizophrenia. J Neuropsychiatry Clin Neurosci 6(4):348–357

Gomez CM, Marco J, Grau C (2003) Preparatory visuo-motor cortical network of the contingent negative variation estimated by current density. NeuroImage 20(1):216–224

Gomez CM, Marco-Pallares J, Grau C (2006) Location of brain rhythms and their modulation by preparatory attention estimated by current density. Brain Res 1107(1):151–160
Gonzalez-Hernandez JA, Pita-Alcorta C, Cedeno I, Bosch-Bayard J, Galan-Garcia L, Scherbaum WA, Figueredo-Rodriguez P (2002) Wisconsin Card Sorting Test synchronizes the prefrontal, temporal and posterior association cortex in different frequency ranges and extensions. Hum Brain Mapp 17(1):37–47
Grant DA, Berg EA (1948) A behavioral analysis of degree of reinforcement and ease of shifting to new responses in a Weigl-type card-sorting problem. J Exp Psychol 38:404–411
Guo Q, Zhou T, Li W, Dong L, Wang S, Zou L (2017) Single-trial EEG-informed fMRI analysis of emotional decision problems in hot executive function. Brain Behav 7(7):e00728. https://doi.org/10.1002/brb3.728
Habib R, Nyberg L (2007) Neural correlates of availability and accessibility in memory. Cereb Cortex 18:1720–1726
Haenschel C, Bittner RA, Haertling F, Rotarska-Jagiela A, Maurer K, Singer W, Linden DE (2007) Contribution of impaired early-stage visual processing to working memory dysfunction in adolescents with schizophrenia: a study with event-related potentials and functional magnetic resonance imaging. Arch Gen Psychiatry 64(11):1229–1240
Halgren E, Marinkovic K, Chauvel P (1998) Generators of the late cognitive potentials in auditory and visual oddball tasks. Electroencephalogr Clin Neurophysiol 106(2):156–164
Henson R (2005) A mini-review of fMRI studies of human medial temporal lobe activity associated with recognition memory. Q J Exp Psychol B 58(3-4):340–360
Henson RN, Hornberger M, Rugg MD (2005) Further dissociating the processes involved in recognition memory: an FMRI study. J Cogn Neurosci 17(7):1058–1073
Heun R, Jessen F, Klose U, Erb M, Granath DO, Grodd W (2004) Response-related fMRI of veridical and false recognition of words. Eur Psychiatry 19(1):42–52
Holroyd CB, Coles MG (2002) The neural basis of human error processing: reinforcement learning, dopamine, and the error-related negativity. Psychol Rev 109(4):679–709
Holroyd CB, Coles MG, Nieuwenhuis S (2002) Medial prefrontal cortex and error potentials. Science 296(5573):1610–1611
Holroyd CB, Larsen JT, Cohen JD (2004) Context dependence of the event-related brain potential associated with reward and punishment. Psychophysiology 41(2):245–253
Hoppstadter M, Baeuchl C, Diener C, Flor H, Meyer P (2015) Simultaneous EEG-fMRI reveals brain networks underlying recognition memory ERP old/new effects. NeuroImage 116:112–122. https://doi.org/10.1016/j.neuroimage.2015.05.026
Horovitz SG, Skudlarski P, Gore JC (2002) Correlations and dissociations between BOLD signal and P300 amplitude in an auditory oddball task: a parametric approach to combining fMRI and ERP. Magn Reson Imaging 20(4):319–325
Iannaccone R, Hauser TU, Staempfli P, Walitza S, Brandeis D, Brem S (2015) Conflict monitoring and error processing: new insights from simultaneous EEG-fMRI. NeuroImage 105:395–407. https://doi.org/10.1016/j.neuroimage.2014.10.028
Iidaka T, Matsumoto A, Nogawa J, Yamamoto Y, Sadato N (2006) Frontoparietal network involved in successful retrieval from episodic memory. Spatial and temporal analyses using fMRI and ERP. Cereb Cortex 16(9):1349–1360
Ioannides AA, Fenwick PB, Lumsden J, Liu MJ, Bamidis PD, Squires KC, Fenton GW (1994) Activation sequence of discrete brain areas during cognitive processes: results from magnetic field tomography. Electroencephalogr Clin Neurophysiol 91(5):399–402
Javitt DC, Schroeder CE, Steinschneider M, Arezzo JC, Vaughan HG Jr (1992) Demonstration of mismatch negativity in the monkey. Electroencephalogr Clin Neurophysiol 83(1):87–90
Johnson MR, Morris NA, Astur RS, Calhoun VD, Mathalon DH, Kiehl KA, Pearlson GD (2006) A functional magnetic resonance imaging study of working memory abnormalities in schizophrenia. Biol Psychiatry 60(1):11–21
Jurado MB, Rosselli M (2007) The elusive nature of executive functions: a review of our current understanding. Neuropsychol Rev 17(3):213–233

Kamarajan C, Porjesz B, Jones KA, Choi K, Chorlian DB, Padmanabhapillai A, Begleiter H (2005) Alcoholism is a disinhibitory disorder: neurophysiological evidence from a Go/No-Go task. Biol Psychol 69(3):353–373

Karch S, Jager L, Karamatskos E, Graz C, Stammel A, Flatz W, Mulert C (2007) Influence of trait anxiety on inhibitory control in alcohol-dependent patients: simultaneous acquisition of ERPs and BOLD responses. J Psychiatr Res 42(9):734–745

Katayama J, Polich J (1998) Stimulus context determines P3a and P3b. Psychophysiology 35(1):23–33

Kawasaki T, Tanaka S, Wang J, Hokama H, Hiramatsu K (2004) Abnormalities of P300 cortical current density in unmedicated depressed patients revealed by LORETA analysis of event-related potentials. Psychiatry Clin Neurosci 58(1):68–75

Kelly AM, Hester R, Murphy K, Javitt DC, Foxe JJ, Garavan H (2004) Prefrontal-subcortical dissociations underlying inhibitory control revealed by event-related fMRI. Eur J Neurosci 19(11):3105–3112

Kiehl KA, Liddle PF, Hopfinger JB (2000) Error processing and the rostral anterior cingulate: an event-related fMRI study. Psychophysiology 37(2):216–223

Kiehl KA, Stevens MC, Celone K, Kurtz M, Krystal JH (2005a) Abnormal hemodynamics in schizophrenia during an auditory oddball task. Biol Psychiatry 57(9):1029–1040

Kiehl KA, Stevens MC, Laurens KR, Pearlson G, Calhoun VD, Liddle PF (2005b) An adaptive reflexive processing model of neurocognitive function: supporting evidence from a large scale (n = 100) fMRI study of an auditory oddball task. NeuroImage 25(3):899–915

Ko LW, Shih YC, Chikara RK, Chuang YT, Chang EC (2016) Neural Mechanisms of Inhibitory Response in a Battlefield Scenario: A Simultaneous fMRI-EEG Study. Front Hum Neurosci 10:185. https://doi.org/10.3389/fnhum.2016.00185

Kok A (2001) On the utility of P3 amplitude as a measure of processing capacity. Psychophysiology 38(3):557–577

Konishi S, Nakajima K, Uchida I, Kikyo H, Kameyama M, Miyashita Y (1999) Common inhibitory mechanism in human inferior prefrontal cortex revealed by event-related functional MRI. Brain 122(Pt 5):981–991

Konishi S, Hayashi T, Uchida I, Kikyo H, Takahashi E, Miyashita Y (2002) Hemispheric asymmetry in human lateral prefrontal cortex during cognitive set shifting. Proc Natl Acad Sci U S A 99(11):7803–7808

Kropotov JD, Naatnen R, Sevostianov AV, Alho K, Reinikainen K, Kropotova OV (1995) Mismatch negativity to auditory stimulus change recorded directly from the human temporal cortex. Psychophysiology 32(4):418–422

Leicht G, Vauth S, Polomac N, Andreou C, Rauh J, Mussmann M, Mulert C (2016) EEG-informed fMRI reveals a disturbed gamma-band-specific network in subjects at high risk for psychosis. Schizophr Bull 42(1):239–249. https://doi.org/10.1093/schbul/sbv092

Lenartowicz A, Lu S, Rodriguez C, Lau EP, Walshaw PD, McCracken JT, Loo SK (2016) Alpha desynchronization and fronto-parietal connectivity during spatial working memory encoding deficits in ADHD: a simultaneous EEG-fMRI study. Neuroimage Clin 11:210–223. https://doi.org/10.1016/j.nicl.2016.01.023

Lewis SJ, Dove A, Robbins TW, Barker RA, Owen AM (2004) Striatal contributions to working memory: a functional magnetic resonance imaging study in humans. Eur J Neurosci 19(3):755–760

Lezak MD (1983) Neuropsychological assessment. Oxford University Press, New York

Liddle PF, Kiehl KA, Smith AM (2001) Event-related fMRI study of response inhibition. Hum Brain Mapp 12(2):100–109

Lie CH, Specht K, Marshall JC, Fink GR (2006) Using fMRI to decompose the neural processes underlying the Wisconsin Card Sorting Test. NeuroImage 30(3):1038–1049

Liebenthal E, Ellingson ML, Spanaki MV, Prieto TE, Ropella KM, Binder JR (2003) Simultaneous ERP and fMRI of the auditory cortex in a passive oddball paradigm. NeuroImage 19(4):1395–1404

Linden DEJ (2007) What, when, where in the brain? Exploring mental chronometry with brain imaging and electrophysiology. Rev Neurosci 18(2):159–171
Linden DE, Prvulovic D, Formisano E, Vollinger M, Zanella FE, Goebel R, Dierks T (1999) The functional neuroanatomy of target detection: an fMRI study of visual and auditory oddball tasks. Cereb Cortex 9(8):815–823
Logan GD, Cowan WB, Davis KA (1984) On the ability to inhibit simple and choice reaction time responses: a model and a method. J Exp Psychol Hum Percept Perform 10(2):276–291
Manoach DS, Gollub RL, Benson ES, Searl MM, Goff DC, Halpern E, Rauch SL (2000) Schizophrenic subjects show aberrant fMRI activation of dorsolateral prefrontal cortex and basal ganglia during working memory performance. Biol Psychiatry 48(2):99–109
Mathalon DH, Whitfield SL, Ford JM (2003) Anatomy of an error: ERP and fMRI. Biol Psychol 64(1-2):119–141
Mathiak K, Rapp A, Kircher TT, Grodd W, Hertrich I, Weiskopf N, Ackermann H (2002) Mismatch responses to randomized gradient switching noise as reflected by fMRI and whole-head magnetoencephalography. Hum Brain Mapp 16(3):190–195
Matsuda T, Matsuura M, Ohkubo T, Ohkubo H, Atsumi Y, Tamaki M, Kojima T (2002) Influence of arousal level for functional magnetic resonance imaging (fMRI) study: simultaneous recording of fMRI and electroencephalogram. Psychiatry Clin Neurosci 56(3):289–290
McCarley RW, Faux SF, Shenton ME, Nestor PG, Holinger DP (1991) Is there P300 asymmetry in schizophrenia? Arch Gen Psychiatry 48(4):380–383
McCarthy G, Luby M, Gore J, Goldman-Rakic P (1997) Infrequent events transiently activate human prefrontal and parietal cortex as measured by functional MRI. J Neurophysiol 77(3):1630–1634
Meltzer JA, Negishi M, Mayes LC, Constable RT (2007) Individual differences in EEG theta and alpha dynamics during working memory correlate with fMRI responses across subjects. Clin Neurophysiol 118(11):2419–2436
Menon V, Crottaz-Herbette S (2005) Combined EEG and fMRI studies of human brain function. Int Rev Neurobiol 66:291–321
Menon V, Ford JM, Lim KO, Glover GH, Pfefferbaum A (1997) Combined event-related fMRI and EEG evidence for temporal-parietal cortex activation during target detection. Neuroreport 8(14):3029–3037
Menon V, Adleman NE, White CD, Glover GH, Reiss AL (2001) Error-related brain activation during a Go/NoGo response inhibition task. Hum Brain Mapp 12(3):131–143
Michels L, Bucher K, Luchinger R, Klaver P, Martin E, Jeanmonod D, Brandeis D (2010) Simultaneous EEG-fMRI during a working memory task: modulations in low and high frequency bands. PLoS One 5(4):e10298. https://doi.org/10.1371/journal.pone.0010298
Milham MP, Banich MT (2005) Anterior cingulate cortex: an fMRI analysis of conflict specificity and functional differentiation. Hum Brain Mapp 25(3):328–335
Mobascher A, Warbrick T, Brinkmeyer J, Musso F, Stoecker T, Jon Shah N, Winterer G (2012) Nicotine effects on anterior cingulate cortex in schizophrenia and healthy smokers as revealed by EEG-informed fMRI. Psychiatry Res 204(2-3):168–177. https://doi.org/10.1016/j.pscychresns.2012.09.005
Monchi O, Petrides M, Petre V, Worsley K, Dagher A (2001) Wisconsin Card Sorting revisited: distinct neural circuits participating in different stages of the task identified by event-related functional magnetic resonance imaging. J Neurosci 21(19):7733–7741
Mulert C, Jager L, Schmitt R, Bussfeld P, Pogarell O, Moller HJ, Hegerl U (2004) Integration of fMRI and simultaneous EEG: towards a comprehensive understanding of localization and time-course of brain activity in target detection. NeuroImage 22(1):83–94
Mulert C, Seifert C, Leicht G, Kirsch V, Ertl M, Karch S, Jager L (2008) Single-trial coupling of EEG and fMRI reveals the involvement of early anterior cingulate cortex activation in effortful decision making. NeuroImage 42(1):158–168. https://doi.org/10.1016/j.neuroimage.2008.04.236

Näätänen R, Winkler I (1999) The concept of auditory stimulus representation in cognitive neuroscience. Psychol Bull 125(6):826–859
Näätänen R, Gaillard AW, Mantysalo S (1978) Early selective-attention effect on evoked potential reinterpreted. Acta Psychol 42(4):313–329
Nagai Y, Critchley HD, Featherstone E, Fenwick PB, Trimble MR, Dolan RJ (2004) Brain activity relating to the contingent negative variation: an fMRI investigation. NeuroImage 21(4):1232–1241
Nieuwenhuis S, Yeung N, van den Wildenberg W, Ridderinkhof KR (2003) Electrophysiological correlates of anterior cingulate function in a go/no-go task: effects of response conflict and trial type frequency. Cogn Affect Behav Neurosci 3(1):17–26
Ofen N, Kao YC, Sokol-Hessner P, Kim H, Whitfield-Gabrieli S, Gabrieli JD (2007) Development of the declarative memory system in the human brain. Nat Neurosci 10(9):1198–1205
Opitz B, Mecklinger A, Friederici AD, von Cramon DY (1999) The functional neuroanatomy of novelty processing: integrating ERP and fMRI results. Cereb Cortex 9(4):379–391
Opitz B, Rinne T, Mecklinger A, von Cramon DY, Schroger E (2002) Differential contribution of frontal and temporal cortices to auditory change detection: fMRI and ERP results. NeuroImage 15(1):167–174
Otten LJ, Henson RN, Rugg MD (2002) State-related and item-related neural correlates of successful memory encoding. Nat Neurosci 5(12):1339–1344
Paulesu E, Frith CD, Frackowiak RS (1993) The neural correlates of the verbal component of working memory. Nature 362(6418):342–345
Polich J, Corey-Bloom J (2005) Alzheimer's disease and P300: review and evaluation of task and modality. Curr Alzheimer Res 2(5):515–525
Polich J, Herbst KL (2000) P300 as a clinical assay: rationale, evaluation, and findings. Int J Psychophysiol 38(1):3–19
Posner MI (1978) Chronometric explorations of mind. Oxford University Press, New York
Ridderinkhof KR, Ullsperger M, Crone EA, Nieuwenhuis S (2004) The role of the medial frontal cortex in cognitive control. Science 306(5695):443–447
Rinne T, Alho K, Ilmoniemi RJ, Virtanen J, Naatanen R (2000) Separate time behaviors of the temporal and frontal mismatch negativity sources. NeuroImage 12(1):14–19
Rockstroh B, Elbert T, Birbaumer N, Lutzenberger W (1982) Slow brain potentials and behavior. Urban & Schwarzenberg, Baltimore
Sabri M, Liebenthal E, Waldron EJ, Medler DA, Binder JR (2006) Attentional modulation in the detection of irrelevant deviance: a simultaneous ERP/fMRI study. J Cogn Neurosci 18(5):689–700
Sammer G, Blecker C, Gebhardt H, Bischoff M, Stark R, Morgen K, Vaitl D (2007) Relationship between regional hemodynamic activity and simultaneously recorded EEG-theta associated with mental arithmetic-induced workload. Hum Brain Mapp 28(8):793–803
Scheffers MK, Coles MG (2000) Performance monitoring in a confusing world: error-related brain activity, judgments of response accuracy, and types of errors. J Exp Psychol Hum Percept Perform 26(1):141–151
Scheffers MK, Coles MG, Bernstein P, Gehring WJ, Donchin E (1996) Event-related brain potentials and error-related processing: an analysis of incorrect responses to go and no-go stimuli. Psychophysiology 33(1):42–53
Schmuser L, Sebastian A, Mobascher A, Lieb K, Tuscher O, Feige B (2014) Data-driven analysis of simultaneous EEG/fMRI using an ICA approach. Front Neurosci 8:175. https://doi.org/10.3389/fnins.2014.00175
Schmuser L, Sebastian A, Mobascher A, Lieb K, Feige B, Tuscher O (2016) Data-driven analysis of simultaneous EEG/fMRI reveals neurophysiological phenotypes of impulse control. Hum Brain Mapp 37(9):3114–3136. https://doi.org/10.1002/hbm.23230
Schroger E, Wolff C (1996) Mismatch response of the human brain to changes in sound location. Neuroreport 7(18):3005–3008

Shallice T (1988) From neuropsychology to mental structure. Cambridge University Press, Cambridge
Sohlberg M, Mateer CA (1989) Introduction to cognitive rehabilitation: theory and practice. Guilford Press, New York
Sokolov EN (1963) Higher nervous functions: the orienting reflex. Annu Rev Physiol 35:545–580
Stevens MC, Calhoun VD, Kiehl KA (2005) Hemispheric differences in hemodynamics elicited by auditory oddball stimuli. NeuroImage 26(3):782–792
Stuss DT, Levine B (2002) Adult clinical neuropsychology: lessons from studies of the frontal lobes. Annu Rev Psychol 53:401–433
Sutton S, Zubin J, John ER (1965) Evoked potential correlates of stimulus uncertainty. Science 150:1187–1188
Tan HY, Choo WC, Fones CS, Chee MW (2005) fMRI study of maintenance and manipulation processes within working memory in first-episode schizophrenia. Am J Psychiatry 162(10):1849–1858
Tecce JJ (1972) Contingent negative variation (CNV) and psychological processes in man. Psychol Bull 77(2):73–108
Ullsperger M, von Cramon DY (2001) Subprocesses of performance monitoring: a dissociation of error processing and response competition revealed by event-related fMRI and ERPs. NeuroImage 14(6):1387–1401
Ullsperger M, von Cramon DY (2004) Neuroimaging of performance monitoring: error detection and beyond. Cortex 40(4-5):593–604
van der Stelt O, Frye J, Lieberman JA, Belger A (2004) Impaired P3 generation reflects high-level and progressive neurocognitive dysfunction in schizophrenia. Arch Gen Psychiatry 61(3):237–248
Veltman DJ, Rombouts SA, Dolan RJ (2003) Maintenance versus manipulation in verbal working memory revisited: an fMRI study. NeuroImage 18(2):247–256
Walz JM, Goldman RI, Carapezza M, Muraskin J, Brown TR, Sajda P (2013) Simultaneous EEG-fMRI reveals temporal evolution of coupling between supramodal cortical attention networks and the brainstem. J Neurosci 33(49):19212–19222. https://doi.org/10.1523/JNEUROSCI.2649-13.2013
Walz JM, Goldman RI, Carapezza M, Muraskin J, Brown TR, Sajda P (2014) Simultaneous EEG-fMRI reveals a temporal cascade of task-related and default-mode activations during a simple target detection task. NeuroImage 102(Pt 1):229–239. https://doi.org/10.1016/j.neuroimage.2013.08.014
Walz JM, Goldman RI, Carapezza M, Muraskin J, Brown TR, Sajda P (2015) Prestimulus EEG alpha oscillations modulate task-related fMRI BOLD responses to auditory stimuli. NeuroImage 113:153–163. https://doi.org/10.1016/j.neuroimage.2015.03.028
Warbrick T, Mobascher A, Brinkmeyer J, Musso F, Stoecker T, Shah NJ, Winterer G (2012) Nicotine effects on brain function during a visual oddball task: a comparison between conventional and EEG-informed fMRI analysis. J Cogn Neurosci 24(8):1682–1694. https://doi.org/10.1162/jocn_a_00236
Warbrick T, Arrubla J, Boers F, Neuner I, Shah NJ (2014) Attention to detail: why considering task demands is essential for single-trial analysis of BOLD correlates of the visual P1 and N1. J Cogn Neurosci 26(3):529–542. https://doi.org/10.1162/jocn_a_00490
Watanabe J, Sugiura M, Sato K, Sato Y, Maeda Y, Matsue Y, Kawashima R (2002) The human prefrontal and parietal association cortices are involved in NO-GO performances: an event-related fMRI study. NeuroImage 17(3):1207–1216
Wirsich J, Benar C, Ranjeva JP, Descoins M, Soulier E, Le Troter A, Guye M (2014) Single-trial EEG-informed fMRI reveals spatial dependency of BOLD signal on early and late IC-ERP amplitudes during face recognition. NeuroImage 100:325–336. https://doi.org/10.1016/j.neuroimage.2014.05.075

Yancey SW, Phelps EA (2001) Functional neuroimaging and episodic memory: a perspective. J Clin Exp Neuropsychol 23(1):32–48

Ylvisaker M, DeBonis D (2000) Executive function impairment in adolescence: TBI and ADHD. Top Lang Disord 20(2):29–57

Zhao X, Li X, Yao L (2017) Localized fluctuant oscillatory activity by working memory load: a simultaneous EEG-fMRI study. Front Behav Neurosci 11:215. https://doi.org/10.3389/fnbeh.2017.00215

Neuronal Models for EEG–fMRI Integration

25

Dora Hermes and Jeroen C. W. Siero

25.1 From Correlating Measurements to Models of Neuronal Population Activity

Imagine studying a machine that produces packages. This machine requires supplies to make the packages and energy to fuel the machine. The mechanisms of the machine can be studied by counting the number of packages that it has produced, by counting the supplies needed or by calculating the energy that it has consumed. In general, these three measures will be correlated, since more packages will require more energy and supplies. However, the machine will use energy when it is turned on and measurements of energy usage will not give an accurate indication of when a package is produced. Also, the number of supplied may not always match the packages produced, since some supplies may last a longer time compared to others.

Similarly, there are many different ways to study the human brain with each measurement providing a complementary view of brain function. Integrating different measurements can thus provide additional information about brain function. Two of the most common measurements of human brain function are field potentials and the blood oxygen–level-dependent (BOLD) response. Field potentials can be measured at varying scales with electroencephalography (EEG), magnetoencephalography (MEG), electrocorticography (ECoG), stereo EEG (sEEG), or extracellularly placed electrodes (local field potential, LFP). Field potentials measure the electrical activity of neuronal populations and have a timescale of milliseconds. The

D. Hermes (✉)
Department of Physiology & Biomedical Engineering, Mayo Clinic, Rochester, MN, USA
e-mail: hermes.dora@mayo.edu

J. C. W. Siero
Department of Radiology, University Medical Center Utrecht, Utrecht, Netherlands

Spinoza Centre for Neuroimaging Amsterdam, Royal Netherlands Academy of Arts and Sciences, Amsterdam, Netherlands
e-mail: J.C.W.Siero@umcutrecht.nl

C. Mulert, L. Lemieux (eds.), *EEG - fMRI*,
https://doi.org/10.1007/978-3-031-07121-8_25

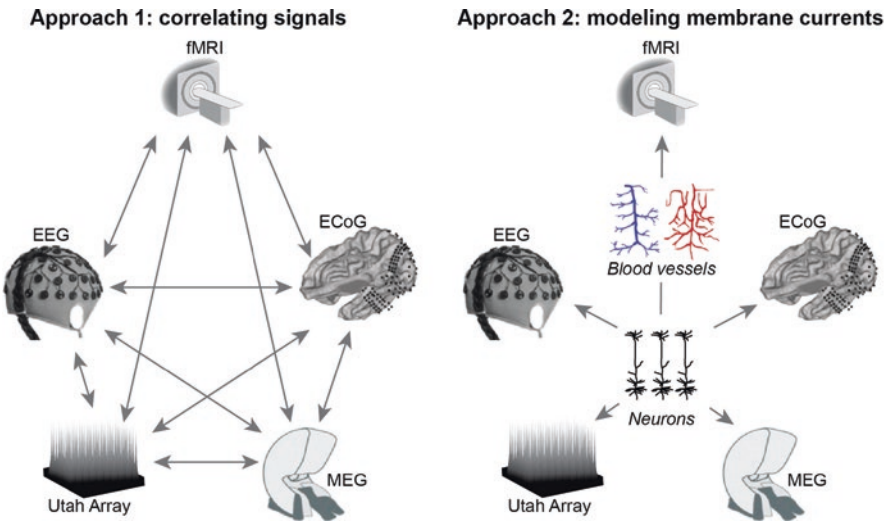

Fig. 25.1 From correlating signals to modeling underlying neuronal activity. Many methods can be used to measure brain signals, such as fMRI, ECoG, MEG, Utah Array, and EEG. Approach 1: these signals can be correlated. Approach 2: each of these signals is generated, either directly or indirectly, by a neuronal (or vascular) population

BOLD response, on the other hand, is most commonly measured in humans with functional MRI (fMRI). The BOLD response is driven by blood flow, blood volume, and oxygen metabolism and evolves over seconds. EEG and fMRI thus measure brain function in fundamentally different ways: EEG measuring the potentials generated by millions of neurons with millisecond accuracy and fMRI measuring slow hemodynamic changes with precision of a few millimeters.

To better understand these techniques, many studies have directly correlated the measured signals (Fig. 25.1, left). These direct comparisons have established important common patterns of how signals correlate but have also revealed many discrepancies. To better understand these various findings, this chapter considers the fact that these signals are population signals that integrate activity of thousands of neurons (Fig. 25.1, right). An empirically driven modeling framework is provided and discussed, with simplified abstractions that establish an understanding of how signals pool over large neuronal populations in different measurements and spatiotemporal scales.

25.2 Direct Correlations Between Field Potentials and BOLD

Many studies have correlated the fMRI signal with neurophysiology measurements, including firing rates and field potentials. Firing rates sometimes correlate well with the BOLD signal (Murphy et al. 2018), and measurements in visual cortex have shown that BOLD and firing rates have a similar contrast response function (Heeger

et al. 2000; Lima et al. 2014). However, firing is unlikely to be the main drive of the BOLD signal: simultaneous measurements of cerebral blood flow and firing rates in the cerebellum of the rat have shown that BOLD signals continue even when neuronal firing is inhibited (Mathiesen et al. 1998). In addition, Logothetis et al., simultaneously measured fMRI, firing rates, and LFPs in macaque visual cortex using an in-house build MRI scanner (Logothetis et al. 2001). They found that during visual stimulation of different durations only the high-frequency power changes in the LFP (ranging from 40 to 130 Hz) correlated with the BOLD signal, whereas firing rates did not. Since the LFP is largely driven by synaptic inputs, this study concluded that synaptic inputs are the main neurophysiological basis driving the BOLD response and firing rates (neuronal output) are not.

Many studies have since replicated the finding that high-frequency power changes correlate positively with the BOLD signal. Correlations between BOLD and high-frequency power changes have been found in visual cortex, motor cortex, language areas, or auditory cortex in both humans and nonhuman primates (Hermes et al. 2011, 2014, 2017; Mukamel et al. 2005; Ojemann et al. 2013; Siero et al. 2014). However, these studies have also noted exceptions. First, power changes from 40 to 130 Hz do not always correlate with BOLD; the BOLD signal can increase without concurrent field potential changes (Sirotin and Das 2009) or MEG–measured gamma band signals can increase in power without matching BOLD changes (Muthukumaraswamy and Singh 2008). Second, power changes from 40 to 130 Hz are not the only correlate of the BOLD signal; low-frequency power changes (<24 Hz) also correlate with BOLD and explain variance in addition to high frequencies (Hermes et al. 2011; Magri et al. 2012; Scheeringa et al. 2011; Murta et al. 2017). Thirdly, to make things more complicated, high-frequency power changes from 40 to 130 Hz include different signals, such as broadband power changes and narrowband (oscillatory gamma) power changes (Hermes et al. 2015; Ray and Maunsell 2011). Therefore, even though high-frequency power changes often correlate with BOLD, it is too simple to consider the BOLD signal simply as the low-pass filtered signal of one signal measured in the field potential.

25.3 Neuronal Population Activity and the BOLD Signal

The BOLD signal is driven by changes in the amount of deoxyhemoglobin in the blood (Ogawa et al. 1990). This amount is influenced by changes in blood flow and blood volume but also by changes in the metabolic rate of oxygen. A widely used framework that combines the aforementioned hemodynamics and oxygen metabolism into a predicted BOLD response is the "balloon" model (Buxton and Frank 1997; Buxton et al. 2004; Mandeville et al. 1999). The complex cascade of how neuronal activity results in these hemodynamic changes is the realm of neurovascular coupling, which is an area of ongoing investigation and has been described elsewhere (Attwell et al. 2010; Hillman 2014; Iadecola 2017). It should be noted that not only neurovascular coupling mechanisms drive the BOLD response; the physiological baseline state (such as resting blood flow) and the

organization of the cerebral vasculature also modulate the BOLD response. These "passive" modulators will likely impact the BOLD response more dominantly with increased spatiotemporal fMRI resolution. Rather than going into these details, this chapter is meant to provide a simplified modeling framework that provides intuition into how the EEG and BOLD signals integrate neuronal population activity.

As stated above, the BOLD response correlates better with synaptic activity compared to firing rates and several models have therefore modeled the BOLD response as a function of synaptic activity. Some of these previous models have captured nonlinear components in terms of scaling and amplitude to relate synaptic activity and the BOLD response (Friston et al. 2000). However, a simple rescaling of positive inputs to capture BOLD changes is not sufficient because both depolarization and hyperpolarization of cells can result in increases in the BOLD signal (Mathiesen et al. 1998; Caesar et al. 2003; Uhlirova et al. 2016). Adding a nonlinearity that captures this aspect, such as the power of the membrane fluctuations (with zero indicating rest), is therefore necessary. Therefore, we have made the assumption that the power is (linearly) summed across a neuronal population of n neurons (Hermes et al. 2017), which responds to a stimulus or task during a brief epoch (time 0 to T):

$$\mathrm{BOLD} \propto \beta \cdot \sum_{i}^{n} \left(\int_{0}^{T} \left(I_i(t)^2 \right) \mathrm{d}t \right) \tag{25.1}$$

Each neuron produces a time-varying transmembrane current, denoted as $I_i(t)$ for the ith neuron, resulting from the transmembrane potential.

Assuming this, relation between transmembrane currents and the BOLD signal has two consequences. Firstly, subthreshold membrane fluctuations can have a large effect on the BOLD signal while not resulting in changes in neuronal firing (Saalmann and Kastner 2009). Secondly, inhibitory inputs that reduce the membrane potential either can increase the BOLD signal, if they hyperpolarize the membrane potential, or they can decrease the BOLD signal in case they decrease the depolarization of the membrane potential, bringing it closer to the resting potential.

25.4 Neuronal Population Activity and Field Potential Measurements

Field potentials can be measured at different scales with penetrating electrodes measuring the LFP, to sEEG, ECoG, MEG, or EEG. The electrical fields generated by groups of neurons influence these signals: LFPs measured with penetrating electrodes integrate within ~250 μM of the electrode (Katzner et al. 2009) while ECoG electrodes typically have a size of ~2.4 mm in diameter, and EEG/MEG integrates even larger areas of cortex (Dale and Halgren 2001). While the number of neurons

measured with each and the sources of noise thus differ, these measures have in common that they arise largely from the electrical fields generated by synaptic transmembrane currents (Buzsáki et al. 2012).

If we assume that transmembrane currents form the most important contribution to field potential measurements, the contribution for each neuron to the field potential can be approximated by $\alpha_i \times I_i(t)$, with $I(t)$ the transmembrane current as in Eq. (25.1) (Hermes et al. 2017). The term α_i depends on the distance and orientation of the neuron with respect to the electrode as well as an electrode's impedance. If we then assume, for simplicity, that each neuron is equidistant from the electrode and has the same orientation, like pyramidal neurons perpendicular to the cortical surface; therefore, its contribution to the electrode measurement is scaled by the same constant, α, and these neurons act together like a single, equivalent circuit; hence the LFP time series will sum the contribution from each neuron.

$$\mathrm{LFP}(t) = \alpha \cdot \sum_{i}^{n} I_i(t) \tag{25.2}$$

Field potential recordings are often summarized in the power spectrum. When the power spectrum is summarized over a small time window T, it can be summarized as:

$$\text{LFP power} = \alpha \cdot \int_0^T \left(\left[\sum_{i}^{n} I_i(t) \right]^2 \right) \mathrm{d}t \tag{25.3}$$

With T a time segment and n the number of neurons and α a constant (a factor $1/T$ could be added to get the average power). Interestingly, the power of the sum is mathematically equivalent to the sum of the power, plus the cross power:

$$\int_0^T \left(\left[\sum_{i}^{n} X_i(t) \right]^2 \right) \mathrm{d}t = \sum_{i}^{n} \left(\int_0^T \left(X_i(t)^2 \right) \mathrm{d}t \right) + \sum_{i \neq j}^{n} \left(\int_0^T \left(X_i(t) \cdot X_j(t) \right) \mathrm{d}t \right) \tag{25.4}$$

Therefore, if we approximate the LFP power by the power of the sum of the membrane currents, the LFP is highly sensitive to both the absolute power (any changes from baseline) and the coherence (cross power) between neuronal membrane fluctuations. Any inputs that are synchronous across neurons will thus have a large influence on the LFP.

25.5 Theoretical Predictions for BOLD and Field Potential Measurements

The described modeling framework makes several predictions. Let's consider LFP and fMRI signals from one neuronal population and look back at Eqs. (25.1) and (25.3). In Eq. (25.1), the BOLD signal was proportional to the sum of the power,

whereas in Eq. (25.3) the field potential power is proportional to the power of the sum of the membrane currents. There is a specific mathematical relation between the power of the sum and the sum of the power: the power of the sum is equal to the sum of the power plus the cross power. Applying this theorem to our models of the LFP and BOLD signal gives:

$$\text{LFP power} = {}^{\alpha}\!/_{\beta} \cdot \text{BOLD} + \alpha \cdot \sum_{i \neq j}^{n} \left(\int_{0}^{T} \left(I_i(t) \cdot I_j(t) \right) \mathrm{d}t \right) \tag{25.5}$$

which predicts that if the cross power is large, BOLD and LFPs will not be tightly correlated (Hermes et al. 2017; Butler et al. 2017; Murta et al. 2016).

To be able to make predictions using this framework, we have to consider the membrane currents to simulate. Previous studies correlating BOLD and field potential measurement have reported that high-frequency broadband signals often correlate with BOLD, narrowband gamma oscillations sometimes correlate with BOLD and sometimes do not, and that alpha power decreases are often negatively correlated with BOLD. In order to test what kind of predictions Eqs. (25.1), (25.3), and (25.5) make for the BOLD signal and LFP, we thus need to simulate membrane currents that generate high-frequency broadband signals, narrowband gamma oscillations, and low-frequency alpha power changes. We thus consider the theory behind these particular spectral components.

25.6 Theories About Field Potential Components

25.6.1 Broadband Power Changes

A neuronal population receives many inputs: each neuron has about 4×10^3 synapses, and neurons in 1 mm (Lima et al. 2014) have about 5×10^8 synapses. The temporal properties of the excitatory and inhibitory inputs to a neuronal population will influence the properties of the measured field potential. The incoming presynaptic action potentials occur most randomly with arrival times that follow a Poisson distribution. These arriving spikes are filtered with a postsynaptic potential with exponential decay (Fig. 25.2), followed by integration across 6000 synapses. Charge accumulates over time and is lost, ohmically, across the dendritic membrane (Fig. 25.2) and is integrated across neurons. This will result in a random walk process with a power spectrum that has a shape of $1/f^n$ (Fig. 25.2) (Miller et al. 2009, 2010). In this model, increases in the arriving spiking rate will then result in broadband increases across all frequencies, as has been observed with intracranial measurements.

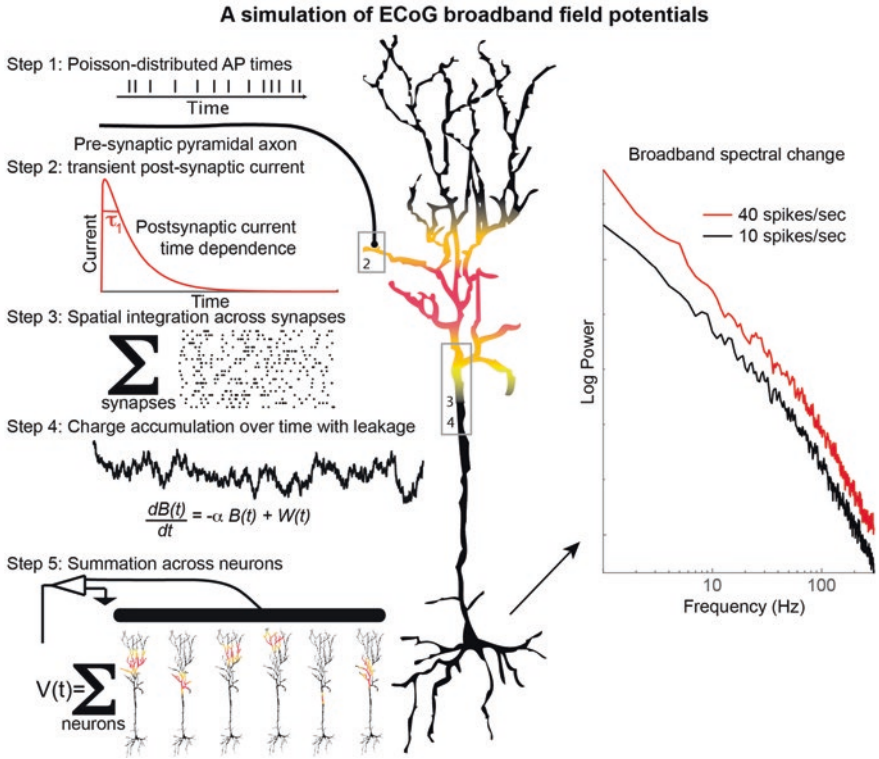

Fig. 25.2 A simulation of ECoG broadband field potentials. Left: Step 1: The model of the ECoG signal adapted from (Miller et al. 2009, 2010) uses Poisson-distributed action potential (AP) times drawn from a random distribution, we model 6000 of these. Step 2: We model the postsynaptic current with a time dependence of $\tau_2 = 40$ ms with a shape of $t^{13} \times e^{1-t/\tau_s}$ as in (Miller et al. 2009, 2010). Step 3: Inputs from the synapses are summed at each point in time, resulting in time course $W(t)$. Step 4: The time course of the broadband potential $B(t)$ of a single neuron is generated by temporal integration with ohmic leakage according to $\frac{dB(t)}{dt} = -\alpha B(t) + W(t)$, with timescale $\alpha^{-1} = 200$ ms. Step 5: The modeling was performed for the summation of six model neurons. Right: The PSD from this simulation in a double logarithmic plot. The black line indicates the simulation using an input rate of 10 spikes/s, and the red line indicates the simulation using an input rate of 40 spikes/s. Evident in this simulation is that LFP broadband power increases when the input spike rate increases. (Adapted from Miller et al. 2009; Miller et al. 2010)

25.6.2 Peaks in the Field Potential Power Spectrum in the Range from 30 to 80 Hz

Field potentials sometimes show a peak in the power spectrum at frequencies between 30 and 80 Hz. Peaks in the power spectrum can be evoked by regular perceptual inputs, such as light flashing at 30 Hz resulting in regular synaptic inputs in

visual cortex, which evoke a peak in the power spectrum at the stimulation frequency. Even when cortex is not stimulated in rhythmic fashion, peaks in the power spectrum between 30 and 80 Hz are commonly observed. Gamma oscillations were first observed in hippocampus (Buzsáki et al. 1983), and when high-contrast grating patterns are presented, visual cortex typically shows large narrowband gamma oscillations at frequencies ranging from 30 to 80 Hz (Hermes et al. 2015; Ray and Maunsell 2011; Jia et al. 2013; Bartoli et al. 2019).

Gamma oscillations are thought to be generated by loops between excitatory and inhibitory neurons (Buzsáki et al. 2012; Buzsáki and Wang 2012). Recordings from mouse visual cortex have shown that membrane potentials of pyramidal and parvalbumin-positive interneurons can oscillate in these ranges (Perrenoud et al. 2016), and models of such an *E*/*I* circuit can generate gamma oscillations that match those observed in macaque visual cortex (Jia et al. 2013; Kang et al. 2010). These gamma oscillations are often coherent between neurons and indicate a level of neuronal synchrony at the population level. Note that following Eq. (25.4), synchronous activity will have a large contribution to the LFP, as it contributed to the cross power between neurons. However, Eq. (25.1) predicts that it will have little effect on the BOLD signal.

25.6.3 Low Frequency Alpha Oscillations

Peaks in the power spectrum of field potentials can also occur at lower frequencies, around 5, 10, or 20 Hz. Oscillations around 10 Hz measured with EEG on occipital areas were already observed in the 1930s by Berger when subjects closed their eyes (Berger 1931). While frequency ranges are typically characterized with theta (3–8 Hz), alpha (9–12 Hz), and beta (12–24 Hz) ranges, it is important to consider that a peak at 10 Hz in one brain area, such as visual cortex, probably has different underlying mechanism as a 10-Hz peak in motor cortex, and even alpha oscillations in visual cortex can already have various underlying sources (Bollimunta et al. 2008). While such variability makes it extremely difficult to make general observations about the roles and neuronal substrates of these oscillations, we consider one recent idea that can be used to explain why low frequencies often correlate negatively with the BOLD signal: oscillations may show asymmetry (Cole and Voytek 2017; Jensen and Mazaheri 2010; Schalk 2015; Schalk et al. 2017).

Asymmetric oscillations do not oscillate around zero but push the signal up or down. Several previous studies have proposed that asymmetric low-frequency oscillations may be related to rhythmic, inhibitory inputs (Jensen and Mazaheri 2010; Schalk 2015). In this case, inhibitory synaptic inputs arrive at regular intervals, for example, around 10 Hz, at pyramidal neurons. This pulsed inhibition can push the membrane potential down in a rhythmic fashion (Fig. 25.3), making it more difficult to generate action potentials. This may explain why at the same time cortex is more inhibited (at certain phases of the oscillation) when oscillatory power is increased.

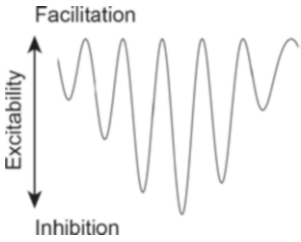

Fig. 25.3 Asymmetric oscillations are hypothesized to change excitability. A schematic of an oscillation in the membrane potential of a neuron that is asymmetric. Because the oscillation is asymmetric, an increase in power results in either repolarization or hyperpolarization of the membrane potential, decreasing excitability. Conversely, decreases in power result in a more depolarized membrane potential, increasing excitability. (Figure adapted from Schalk 2015)

25.6.4 Measured Field Potential Data Will Be a Summation Across All Underlying Processes

Field potential data reflect the activity of large populations of neurons that receive hundreds and thousands of inputs. As a result, different processes will be reflected in the observed power spectrum. It is thus possible to simultaneously observe broadband, narrowband gamma and low-frequency power changes (Hermes et al. 2017). Interpreting each frequency band individually becomes a problem in this case (Cole and Voytek 2017) as different processes can overlap in the power spectrum. When relating the different frequency bands of field potential data to the evoked BOLD responses, it is thus necessary to find a paradigm in which frequency band-specific processes are independently driven, as different predictive variables cannot be distinguished when they are correlated.

25.7 Predicting Empirical Data with This Modeling Framework

In previous work testing this modeling framework, we measured ECoG data in which visual stimuli drove broadband, gamma and alpha power changes in different manner (Hermes et al. 2017, 2015). The underlying activity driving broadband, gamma and alpha power changes were modeled according to the theories: broadband signals were driven by random membrane currents, uncorrelated across neurons, gamma oscillations were driven by changes in synchrony across neurons and alpha power changes were driven by asymmetric oscillations with fixed coherence across neurons and varying amplitude pushing the membrane potential from a small offset to zero (with zero indicating the resting potential; Fig. 25.4). These random broadband, gamma and alpha inputs were summed in each neuron followed by a leaky integration. Then, a summation across neurons resulted in a simulated field potential with a certain amplitude of broadband, gamma and alpha.

It is impossible to know whether the measured field potentials were driven exactly by these inputs. Infinite source resolutions are possible, but intracellular and laminar recordings can provide valuable insight into neurophysiology driving the measured field potential signals at the mesoscale.

Simulated field potentials can be fit to ECoG data, for example, to recordings in human visual cortex (Hermes et al. 2017). The simulated ECoG and BOLD outputs explained why the data show strong correlations between broadband and BOLD, no

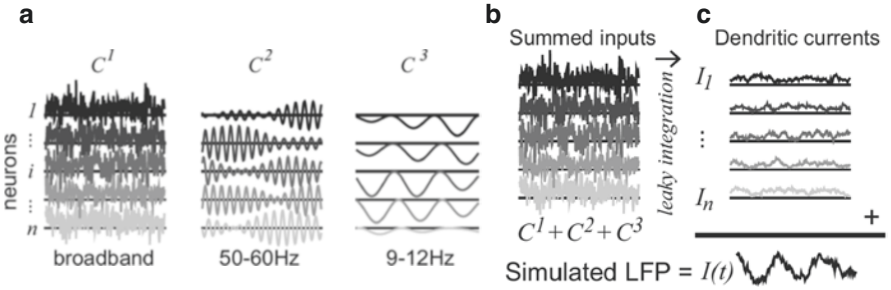

Fig. 25.4 Simulated local field potential (LFP). (**a**) Three different inputs to each neuron were simulated: a broadband, random input with a small positive offset (C1), an oscillatory input with a timescale of 40–60 Hz (C2), and a negative input with a timescale of 10 Hz (C3). (**b**) The three inputs (C1, C2, C3) were summed in each neuron to produce the total input to the neuron. (**c**) The total input was passed through a leaky integrator to produce the dendritic dipole current (I_i). The LFP was simulated by summing the dendritic currents. (Adapted from Hermes et al. 2017)

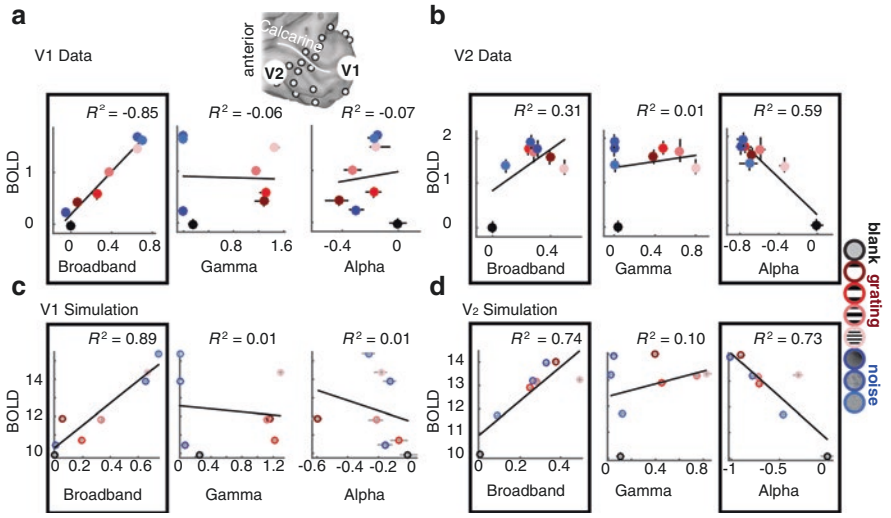

Fig. 25.5 The correlation between ECoG and BOLD signals for measured and simulated V1 and V2 sites. The locations of a sample electrode in V1 and V2 are indicated by the enlarged white discs on the cortical surface. (**a**) In a foveal V1 site, the broadband ECoG amplitude accurately predicts the BOLD signal across several stimuli (left). Error bars show 68% confidence intervals across bootstraps. Narrowband gamma power (center) and alpha power (right) were uncorrelated with BOLD. (**b**) In a V2 site, the broadband ECoG was weakly correlated with BOLD (left). Narrowband gamma did not predict BOLD (middle). Alpha was negatively correlated with BOLD (right). (**c**, **d**) The same as (**a**) and (**b**) but for simulated neuronal population data fit to the V1 and V2 ECoG data. The trend lines are least square fits to the eight stimulus conditions plotted. The R^2 values are the coefficients of determination computed by cross-validation. The black outlines indicate the reliable predictors of the BOLD signal: broadband in V1, broadband and alpha in V2/V3. (Adapted from Hermes et al. 2017)

correlation between gamma and BOLD, and negative correlation between alpha and BOLD in some of the electrodes located on V2 and V3, but generally not on V1 (Fig. 25.5). These findings match previous observations that broadband and BOLD

are generally correlated, BOLD and gamma sometimes correlate, and low-frequency alpha decreases explain additional variance in BOLD increase.

25.8 Discussion

In order to integrate field potential and fMRI data, it is necessary to make assumptions about the neuronal activity driving the field potential signals. Understanding whether mesoscale signals are paired with neuronal synchrony or hyperpolarization or depolarization of the membrane has a large effect on the field potential or on the energy demand.

In the example in visual cortex, we made assumptions about broadband, gamma and alpha signals in visual cortex. The level of broadband was driven entirely by activity and not by synchrony, whereas the opposite was true for gamma. When we changed these assumptions, for example, broadband being entirely driven by synchrony rather than amplitude, the model predictions did not explain the data as well (Hermes et al. 2017). These assumptions were based on previous studies measuring at smaller scales, and understanding the sources of population (mesoscale) signals throughout the human brain is a large challenge.

The modeling framework of how BOLD and field potential signals integrate across neuronal populations provides an intuition for why certain correlations and differences can be observed. Modeling neuronal synchrony is important to explain why some studies have reported strong correlations between gamma oscillations and BOLD and while others have not: BOLD will only correlate with a synchronous signal when synchrony is also paired with the level of activity. Other studies have similarly shown that synchrony differently drives BOLD and EEG signals (Butler et al. 2017). This is an important consideration in applications for epilepsy, where synchrony can have large effects on the measured field potential (Murta et al. 2016).

Modeling asymmetric oscillations and assuming a nonlinearity in which positive and negative deflections from the resting potential result in BOLD increases could explain negative correlations between BOLD and alpha oscillations. Many previous studies have found negative correlations between BOLD and various low-frequency power (Hermes et al. 2011, 2014; Scheeringa et al. 2011; Murta et al. 2017; Maier et al. 2008; Conner et al. 2011). Whether the asymmetries assumed in the current simulation extend to other brain regions and task conditions is an open question.

Model predictions can be empirically tested and further modified. For example, can this modeling framework explain measured relations between slow cortical potentials and BOLD (He and Raichle 2009)? Extending this framework and testing its limitations can help better understand the signals measured in the human brain.

25.9 Conclusion

Measuring a machine with many tools can help assess its function (or dysfunction). Each measurement of human brain function similarly reflects a different aspect of a system, and fMRI, EEG, MEG, ECoG, LFPs will all inform in a different way about

the underlying system. For example, field potentials are highly sensitive to neuronal synchrony, while the fMRI signal is not. When combining measurements, and making models to integrate EEG and fMRI, it is necessary to take a step back to take into account how each measurement pools neuronal population activity.

Acknowledgments The authors thank Jonathan Winawer for many discussions about the modeling framework described in this chapter.

References

Attwell D et al (2010) Glial and neuronal control of brain blood flow. Nature 468:232–243
Bartoli E et al (2019) Functionally distinct gamma range activity revealed by stimulus tuning in human visual cortex. Curr Biol 29:3345–3358.e7
Berger H (1931) Über das Elektrenkephalogramm des Menschen. Arch Für Psychiatr Nervenkrankh 94:16–60
Bollimunta A, Chen Y, Schroeder CE, Ding M (2008) Neuronal mechanisms of cortical alpha oscillations in awake-behaving macaques. J Neurosci 28:9976–9988
Butler R, Bernier PM, Lefebvre J, Gilbert G, Whittingstall K (2017) Decorrelated input dissociates narrow band gamma power and BOLD in human visual cortex. J Neurosci 37:5408–5418. https://doi.org/10.1523/JNEUROSCI.3938-16.2017
Buxton RB, Frank LR (1997) A Model for the coupling between cerebral blood flow and oxygen metabolism during neural stimulation. J Cereb Blood Flow Metab 17:64–72
Buxton RB, Uludağ K, Dubowitz DJ, Liu TT (2004) Modeling the hemodynamic response to brain activation. NeuroImage 23:S220–S233
Buzsáki G, Wang X-J (2012) Mechanisms of gamma oscillations. Annu Rev Neurosci 35:203–225
Buzsáki G, Lai-Wo SL, Vanderwolf CH (1983) Cellular bases of hippocampal EEG in the behaving rat. Brain Res Rev 6:139–171
Buzsáki G, Anastassiou CA, Koch C (2012) The origin of extracellular fields and currents — EEG, ECoG, LFP and spikes. Nat Rev Neurosci 13:407–420
Caesar K, Gold L, Lauritzen M (2003) Context sensitivity of activity-dependent increases in cerebral blood flow. Proc Natl Acad Sci 100:4239–4244
Cole SR, Voytek B (2017) Brain oscillations and the importance of waveform shape. Trends Cogn Sci 21:137–149
Conner CR, Ellmore TM, Pieters TA, DiSano MA, Tandon N (2011) Variability of the relationship between electrophysiology and BOLD-fMRI across cortical regions in humans. J Neurosci 31:12855–12865
Dale AM, Halgren E (2001) Spatiotemporal mapping of brain activity by integration of multiple imaging modalities. Curr Opin Neurobiol 11:202–208
Friston KJ, Mechelli A, Turner R, Price CJ (2000) Nonlinear responses in fMRI: the balloon model, volterra kernels, and other hemodynamics. NeuroImage 12:466–477
He BJ, Raichle ME (2009) The fMRI signal, slow cortical potential and consciousness. Trends Cogn Sci 13:302–309
Heeger DJ, Huk AC, Geisler WS, Albrecht DG (2000) Spikes versus BOLD: what does neuroimaging tell us about neuronal activity? Nat Neurosci 3:631–633
Hermes D et al (2011) Neurophysiologic correlates of fMRI in human motor cortex. Hum Brain Mapp 33:1689–1699
Hermes D et al (2014) Cortical theta wanes for language. NeuroImage 85:738–748
Hermes D, Miller KJ, Wandell BA, Winawer J (2015) Stimulus dependence of gamma oscillations in human visual cortex. Cereb Cortex 25:2951–2959
Hermes D, Nguyen M, Winawer J (2017) Neuronal synchrony and the relation between the blood-oxygen-level dependent response and the local field potential. PLoS Biol 15:e2001461

Hillman EMC (2014) Coupling mechanism and significance of the BOLD signal: a status report. Annu Rev Neurosci 37:161–181
Iadecola C (2017) The neurovascular unit coming of age: a journey through neurovascular coupling in health and disease. Neuron 96:17–42
Jensen O, Mazaheri A (2010) Shaping functional architecture by oscillatory alpha activity: gating by inhibition. Front Hum Neurosci 4:186
Jia X, Xing D, Kohn A (2013) No consistent relationship between gamma power and peak frequency in macaque primary visual cortex. J Neurosci 33:17–25
Kang K, Shelley M, Henrie JA, Shapley R (2010) LFP spectral peaks in V1 cortex: network resonance and cortico-cortical feedback. J Comput Neurosci 29:495–507
Katzner S et al (2009) Local origin of field potentials in visual cortex. Neuron 61:35–41
Lima B, Cardoso MMB, Sirotin YB, Das A (2014) Stimulus-related neuroimaging in task-engaged subjects is best predicted by concurrent spiking. J Neurosci 34:13878–13891
Logothetis NK, Pauls J, Augath M, Trinath T, Oeltermann A (2001) Neurophysiological investigation of the basis of the fMRI signal. Nature 412:150–157
Magri C, Schridde U, Murayama Y, Panzeri S, Logothetis NK (2012) The Amplitude and timing of the BOLD signal reflects the relationship between local field potential power at different frequencies. J Neurosci 32:1395–1407
Maier A et al (2008) Divergence of fMRI and neural signals in V1 during perceptual suppression in the awake monkey. Nat Neurosci 11:1193–1200
Mandeville JB et al (1999) Evidence of a cerebrovascular postarteriole windkessel with delayed compliance. J Cereb Blood Flow Metab 19:679–689
Mathiesen C, Caesar K, Akgören N, Lauritzen M (1998) Modification of activity-dependent increases of cerebral blood flow by excitatory synaptic activity and spikes in rat cerebellar cortex. J Physiol 512:555–566
Miller KJ, Sorensen LB, Ojemann JG, den Nijs M (2009) Power-law scaling in the brain surface electric potential. PLoS Comput Biol 5:e1000609
Miller KJ et al (2010) Dynamic modulation of local population activity by rhythm phase in human occipital cortex during a visual search task. Front Hum Neurosci 4:197
Mukamel R et al (2005) Coupling between neuronal firing, field potentials, and fMRI in human auditory cortex. Science 309:951–954
Murphy MC, Chan KC, Kim S-G, Vazquez AL (2018) Macroscale variation in resting-state neuronal activity and connectivity assessed by simultaneous calcium imaging, hemodynamic imaging and electrophysiology. NeuroImage 169:352–362
Murta T et al (2016) A study of the electro-haemodynamic coupling using simultaneously acquired intracranial EEG and fMRI data in humans. NeuroImage 142:371–380
Murta T et al (2017) Phase–amplitude coupling and the BOLD signal: a simultaneous intracranial EEG (icEEG) - fMRI study in humans performing a finger-tapping task. NeuroImage 146:438–451
Muthukumaraswamy SD, Singh KD (2008) Functional decoupling of BOLD and gamma-band amplitudes in human primary visual cortex. Hum Brain Mapp 30:2000–2007
Ogawa S, Lee TM, Kay AR, Tank DW (1990) Brain magnetic resonance imaging with contrast dependent on blood oxygenation. Proc Natl Acad Sci 87:9868–9872
Ojemann GAM, Ramsey NFP, Ojemann JMD (2013) Relation between functional magnetic resonance imaging (fMRI) and single neuron, local field potential (LFP) and electrocorticography (ECoG) activity in human cortex. Front Hum Neurosci 7:34
Perrenoud Q, Pennartz CMA, Gentet LJ (2016) Membrane potential dynamics of spontaneous and visually evoked gamma activity in V1 of awake mice. PLoS Biol 14:e1002383
Ray S, Maunsell JHR (2011) Different origins of gamma rhythm and high-gamma activity in macaque visual cortex. PLoS Biol 9:e1000610
Saalmann YB, Kastner S (2009) Gain control in the visual thalamus during perception and cognition. Curr Opin Neurobiol 19:408–414
Schalk G (2015) A general framework for dynamic cortical function: the function-through-biased-oscillations (FBO) hypothesis. Front Hum Neurosci 9:352

Schalk G, Marple J, Knight RT, Coon WG (2017) Instantaneous voltage as an alternative to power- and phase-based interpretation of oscillatory brain activity. NeuroImage 157:545–554
Scheeringa R et al (2011) Neuronal dynamics underlying high- and low-frequency EEG oscillations contribute independently to the human BOLD signal. Neuron 69:572–583
Siero JCW et al (2014) BOLD matches neuronal activity at the mm scale: a combined 7T fMRI and ECoG study in human sensorimotor cortex. NeuroImage 101:177–184
Sirotin YB, Das A (2009) Anticipatory haemodynamic signals in sensory cortex not predicted by local neuronal activity. Nature 457:475–479
Uhlirova H et al (2016) Cell type specificity of neurovascular coupling in cerebral cortex. elife 5:e14315

Part IV

Modelling

BOLD-Response and EEG Gamma Oscillations

26

Gregor Leicht, Christoph S. Herrmann, and Christoph Mulert

26.1 Introduction

While techniques like Positron Emission Tomography (PET) or functional Magnetic Resonance Imaging (fMRI) allowing us to investigate brain activity with high spatial resolution are indirect measurements of brain activity, loosing most or all of the temporal resolution of neuronal activity, some conclusions are possible about how brain regions interact (Friston 2002). However, detailed questions about how information is processed by the brain and how brain regions cooperate can only be answered sufficiently if the real temporal dynamics of brain activity is considered (Engel and Singer 2001). In this context, much effort has been made to explore the role of high-frequency oscillations in the gamma band.

The integration of the high temporal resolution of EEG with the high spatial resolution of fMRI provides the possibility to look for correlations between human EEG gamma band responses and BOLD response in combined experiments. In this chapter, we discuss recent developments and findings in this field and present some data from EEG and fMRI recordings.

G. Leicht (✉)
Psychiatry Neuroimaging Branch, Department of Psychiatry and Psychotherapy, University Medical Center Hamburg-Eppendorf, Hamburg, Germany
e-mail: g.leicht@uke.de

C. S. Herrmann
Department of Psychology, European Medical School, Carl von Ossietzky University, Oldenburg, Germany
e-mail: christoph.herrmann@uni-oldenburg.de

C. Mulert
Centre of Psychiatry, Justus Liebig University, Giessen, Germany
e-mail: Christoph.Mulert@psychiat.med.uni-giessen.de

C. Mulert, L. Lemieux (eds.), *EEG - fMRI*,
https://doi.org/10.1007/978-3-031-07121-8_26

The rhythmic activities in the resting or "spontaneous" EEG are usually divided into several frequency bands (delta: <4 Hz; theta: 4–8 Hz; alpha: 8–12 Hz; beta: 12–30 Hz; and gamma: 30–70 Hz or higher, centered at 40 Hz) which are associated with different behavioral states, ranging from sleep to relaxation, heightened alertness, and mental concentration (Lindsley 1952; Niedermeyer and Lopes Da Silva 2004; Nunez 1995). High-frequency EEG oscillations such as gamma oscillations can be measured on the scalp with relatively small amplitudes due to the fact that scalp EEG recording sensors are physically separated from intracranial activities by the resistive skull tissue acting as a low-pass filter. Since the amplitudes of the EEG oscillations decrease with increasing frequencies, the importance of high-frequency EEG oscillations like gamma oscillations with respect to cognitive functions and disorders is often underestimated, compared to slower oscillations. However, in recent years, special interest for oscillations in the gamma frequency range has emerged in neuroscience because there is a lot of evidence for a close correlation of gamma activity and cognitive functions (Engel and Singer 2001).

Evidence from neuropsychological and physiological studies suggests that consciousness and its different aspects, like sensory awareness for example, has to be understood as a cooperating system of several different brain regions, such as structures responsible for sensory perception, memory functions, executive control, or manipulation of emotion and motivation (Delacour 1997; Young and Pigott 1999). Theories about the neural correlates of consciousness must explain how multiple component processes can be integrated and which mechanisms underlie the dynamic selection of specific components of neuronal responses gaining access to consciousness from all available information. For both aspects, so called "neuronal binding" seems to play an important role (Crick and Koch 1990; Engel and Singer 2001). The concept of dynamic binding by synchronization of neuronal discharges has been developed mainly in the context of perceptual processing and was first introduced in the context of feature integration (Gray et al. 1989; Treisman 1996) and perceptual segmentation (von der Malsburg 1994). The synchronization of activity in neuronal assemblies appears to support specific processes during neural communication, whereas the behavioral specificity of synchronization phenomena suggests a functional role of synchronized activity for neural information processing (Fries 2005). Meanwhile, the concept of binding has been applied to many different domains and is now employed in theories on object recognition (Hummel and Biederman 1992), arousal (Struber et al. 2000), attention (Fell et al. 2003; Niebur et al. 1993; Pantev et al. 1991; Tiitinen et al. 1993), memory formation and recall (Damasio 1990; Herrmann et al. 2004), motor control (Murthy and Fetz 1992), sensorimotor integration (Roelfsema et al. 1997), and language processing (Eulitz et al. 1996; Pulvermuller 1999; Pulvermuller et al. 1995).

In the context of the theory of neuronal binding, the synchronous firing of neurons in the gamma band was proposed to represent an important integration

mechanism of the brain (Gray et al. 1989). The gamma frequency range is defined substantially different across various studies. Whereas some human studies have mostly focused on activity around 40 Hz (Eckhorn et al. 1988; Tallon-Baudry et al. 1996), others explicitly investigated activity in higher frequency ranges (Crone et al. 2001; Lachaux et al. 2005; Muller and Keil 2004). Animal data have even considered gamma activity in still higher frequency ranges above 100 Hz (Bragin et al. 1995; Neuenschwander and Singer 1996).

26.2 Methodical Issues

Different methods have been suggested in order to investigate the relationship between fMRI and special oscillatory EEG components. Compared to the analysis of EEG components with slower frequencies, the investigation of high-frequency oscillations such as gamma oscillations produces additional difficulties. Since the skull tissue acts as a low-pass filter, high-frequency EEG oscillations can be measured on the scalp with relatively small amplitudes. Therefore, signal-to-noise ratio for these subtle EEG rhythms is usually low, especially in the MRI environment with high artifact contamination. Moreover, the clear separation of high-frequency activity from other frequency components is difficult, as it is often masked by more prominent, slower oscillatory EEG components. Statistical methods like principal component analysis (PCA) or independent component analysis (ICA) seem to present possible solutions for this problem. Additionally, functional modulation of individual rhythm strength, for example, by experimental tasks, should facilitate the identification of subtle EEG rhythms as an individual component (Ritter and Villringer 2006).

Concerning technical problems, a sufficient analysis of EEG gamma activity recorded during simultaneous EEG/fMRI measurement is hampered by EEG artifacts caused by the MRI environment. Namely, high frequency ranges of the EEG data are corrupted by the gradient artifact produced by the magnetic field gradient switching needed for imaging.

In order to improve the quality of EEG data in simultaneous EEG–MRI experiments, especially regarding high-frequency EEG components, Anami et al. introduced the so called “stepping stone sampling” method (Anami et al. 2003). By modifying a blip-type echo planar sequence, EEG sampling at a digitization rate of 1000 Hz is exclusively done in a period in which the gradient artifact resides around the baseline level. This method was able to substantially attenuate the amplitude of the imaging artifact. Here, periodically artifact-free interspaces emerged (“sparse fMRI sequence”) that allowed EEG sampling with a high signal-to-artifact ratio. Analyses with Fast Fourier transform showed, apart from successful retrieval of physiological α-activity, that the high-frequency EEG during scanning had very similar power distributions compared to data recorded outside the MRI scanner (Anami et al. 2003).

Sparse fMRI sequences result in some limitations in the temporal sampling or spatial coverage of the fMRI data acquired, which are due to long TRs and/or a small number of slices in sparse sequences. In order to overcome these limitations, multiband fMRI can be used in order to shorten TRs and acquisition time and increase brain coverage for a given TR, which would lengthen the gradient-free time window in which EEG data can be collected (Uji et al. 2018). Using this approach, Uji et al. demonstrated a positive correlation between gamma and BOLD responses in motor regions in response to index finger abduction (Uji et al. 2018).

Mandelkow et al. reported an improved EEG quality increasing the usable bandwidth of the EEG signal to higher frequencies after synchronization of the MRI sequence with the sampling pattern of the EEG (Mandelkow et al. 2006). This was done by synchronizing the internal clocks of both the MRI and the EEG acquisition system and setting the TR of the MRI sequence a multiple of the EEG sampling interval. This way, the variability of the notorious MRI artifact was reduced and its removal by means of the established method of averaged artifact subtraction was facilitated. A direct comparison of EEG spectra from recordings done with and without synchronization showed that the usable bandwidth of the EEG signal was increased to about 150 Hz, thus covering the full gamma frequency range (Mandelkow et al. 2006).

Freyer et al. demonstrated, that even ultrafast EEG oscillations above 100 Hz can be continuously monitored during fMRI, if the acquisition of EEG–fMRI data is optimized regarding the invariantly sampling of gradient artifacts (necessary for optimal averaged artifact subtraction), and the artifact correction is extended by methods coping with sources of gradient artifact variations such as subject movements and by an elimination of residual artifacts by means of principal component analysis (Freyer et al. 2009). Moreover, EEG source reconstruction methods have been shown to be helpful regarding the management of the gradient artifact, which even more applies to high channel density EEG setups. The use of a source reconstruction approach using the beamforming method was reported to facilitate the recording of effects in the gamma frequency range even at magnetic field strength of 7 T (Brookes et al. 2009).

Another example of EEG artifacts in the gamma frequency range originating from the MRI environment is artifact in the range between 30 and 60 Hz generated by the helium pump of the MRI scanner. Switching this pump off for some time during the simultaneous EEG/fMRI recording can solve this problem (Mulert et al. 2007) (see Fig. 26.1). A recursive approach for removing the helium-pump artifact by means of EEG-segment-based principal component analysis has been proposed by Kim et al. (2015). Another systematic artifact in the gamma frequency range of the EEG signal may be induced by vibrations due to the internal ventilation system of certain MR scanners (Nierhaus et al. 2013).

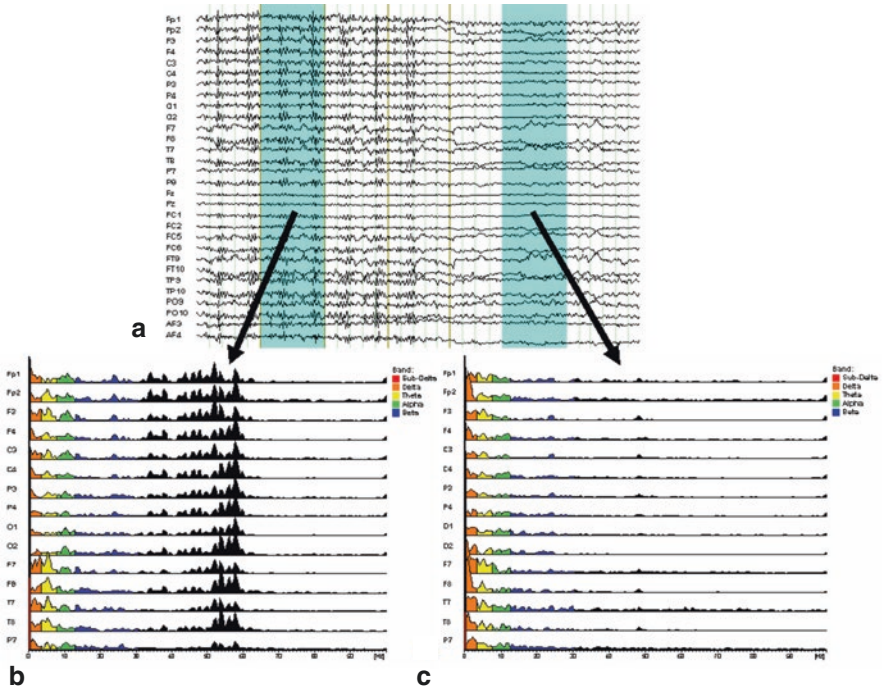

Fig. 26.1 EEG in the MRI environment. Effects of artifacts caused by the fMRI scanners helium pump to the EEG frequency spectrum shown in a FFT analysis. (**a**) Left side: Helium pump switched ON, right side: Helium pump switched OFF. (**b**) FFT analysis with pump artifacts which can clearly be recognized in the frequency range between 40 and 60 Hz. (**c**) FFT analysis without pump artifacts. Data were recorded on a Siemens Sonata 1.5 T MRI scanner (Mulert et al. 2007)

26.3 Gamma activity and BOLD Response

26.3.1 Covariation of High Frequency Oscillations and BOLD Signal

In a seminal study, Logothetis et al. simultaneously recorded the BOLD signal and intracranial recordings of single-unit activity, multiunit activity, and local field potentials (LFPs) in monkeys (Logothetis 2002; Logothetis et al. 2001). They reported that the time course of LFPs correlated best with that of the BOLD signal for rotating checkerboard stimuli of variable durations. Such LFPs typically show discharges at frequencies in the gamma frequency range (approx. 30–80 Hz). Subsequently, recordings in cats and monkeys revealed that correlations between LFPs and BOLD signal are especially high in the gamma band frequency range (Niessing et al. 2005; Hutchison et al. 2015).

Similar results were found in studies combining fMRI and intracranial EEG recordings in human epilepsy patients, for example, by correlating intra-cortical

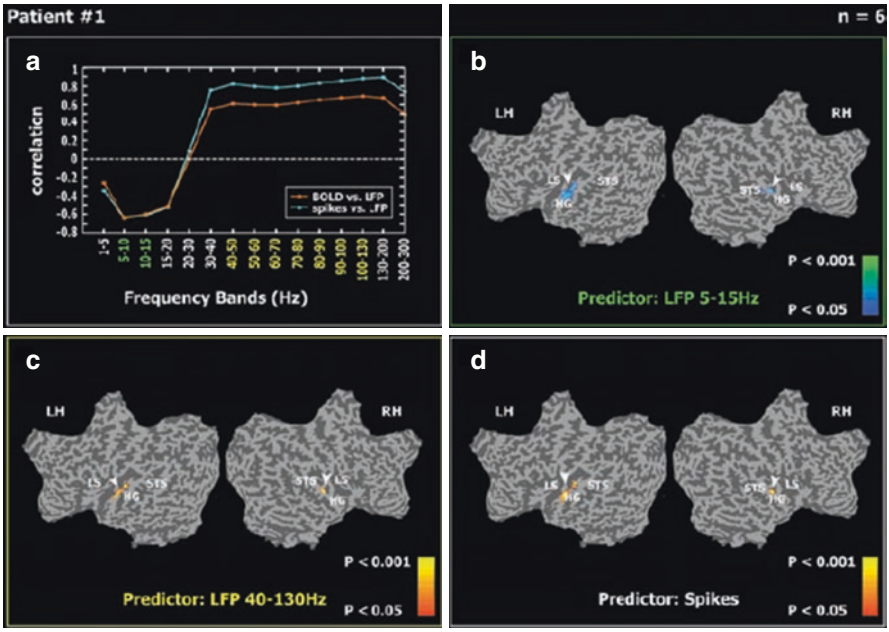

Fig. 26.2 Correlation maps between the fMRI BOLD signal and different EEG frequency components. (**a**) The correlation of the different local field potential (LFP) predictors of one patient with the average fMRI BOLD signal in Heschl's gyrus (orange trace) and with the spike predictor calculated from the sum of auditory responses of 20 single neurons convolved with a standard hemodynamic response function (cyan trace) as a function of frequency bands. Note the strong negative correlations between the BOLD activation and the low-frequency LFPs (5–15 Hz) and the strong positive correlation with the high-frequency LFPs (40–130 Hz). (**b**–**d**) Multisubject random effect GLM map correlating the BOLD signal of six participants with the low-frequency (5–15 Hz) LFP predictor (**b**), the high-frequency (40–130 Hz) LFP predictor (**c**), and the spike predictor (**d**). LS, lateral sulcus; STS, superior temporal sulcus; HG, Heschl's gyrus; RH and LH, right and left hemisphere, respectively. Arrowheads point to regions of highly significant correlation in Heschl's gyrus. (From: Mukamel, R., Gelbard, H., Arieli, A., Hasson, U., Fried, I., and Malach, R. Coupling between neuronal firing, field potentials, and FMRI in human auditory cortex. Science (2005) 309(5736):951–4. Reprinted with permission from AAAS)

electrophysiological recordings in the auditory cortex of two neurosurgical patients and BOLD responses from 11 healthy subjects during presentation of an identical movie segment (Mukamel et al. 2005). A predicted fMRI signal derived from the spiking activity of single neurons of the patients and the measured fMRI signal from the auditory cortex of the healthy subjects showed a highly significant correlation, especially for high-frequency local field potentials (see Fig. 26.2).

By investigating three patients with epilepsy in separate measurements of intracranial EEG recordings and fMRI, Lachaux et al. found spatially congruent patterns of BOLD responses and gamma activations in a visual cognitive task trying to answer the question whether fMRI has any predictive value about the anatomical location of cross-condition gamma band modulations (Lachaux et al. 2007) (see Fig. 26.3).

In intracranial EEG recordings of a single patient with epilepsy, Brovelli et al. found that it was possible to differentiate ERPs as well as beta frequency (15–30 Hz)

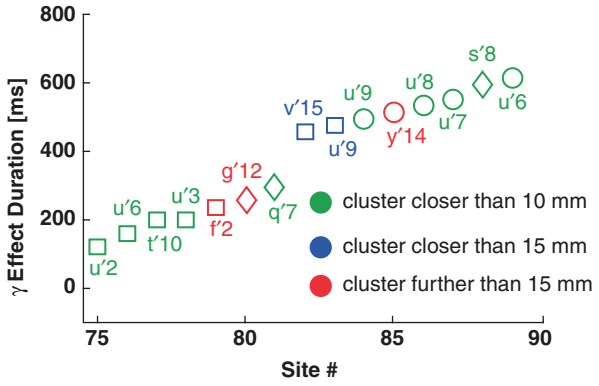

Fig. 26.3 Intracranial EEG sites with a stronger gamma energy increase in a contrast between two experimental conditions were significantly closer than the other sites to fMRI activation clusters revealed in the same contrast. 15 intracranial EEG sites for which the maximal duration of significant gamma (40–150 Hz) energy difference between the two experimental conditions is longer than 100 ms (= strong gamma energy increase). For each site, this value corresponds to the duration of the longest time window, across all frequencies in the gamma band, during which the *p*-value for the Mann–Whitney comparison between the two conditions stays lower than 1×10^4. The markers' shapes indicate which of the three patients was recorded. Sites closer than 10 mm (resp. 15 mm) away from the fMRI activation cluster (i.e., sets of contiguous voxels above the significance threshold) in the same contrast between the two conditions are shown in green (resp. blue). By contrast, the three "distant" EEG sites (shown in red, >15 mm away from an fMRI activation cluster) showed a later inversion of the earlier gamma energy increase causing the total gamma energy during the whole response window to be equivalent in the two conditions. This analysis revealed that 12 of these 15 (80%) sites with significant gamma energy increase were located <15 mm away from an fMRI activation cluster documenting an increase of BOLD-response. In comparison, only 35 of the 74 (47%) non-gamma sites (not displayed here) were <15 mm away from the fMRI activation cluster. (From: Hum Brain Mapp Vol. 28, No. 12, 2007, 1368–75. Copyright 2007 Wiley-Liss, Inc. Reprinted with permission of Wiley-Liss, Inc., a subsidiary of John Wiley & Sons, Inc.)

and gamma frequency (60–200 Hz) activity during processes of spatial attention and memory in contrast to motor intention processes. However, concerning the localization of intracranial electrodes, ERPs and beta frequency activity showed weak or no spatial relation with the BOLD response measured in a fMRI study in the same conditional visuomotor task, whereas the high gamma frequency activity did co-localize with fMRI regions of interest (Brovelli et al. 2005).

Foucher et al. tried to find an answer to the question why the auditory evoked P300 and fMRI activations differ in response to the presentation of two kinds of rare events (i.e., Target and Novel stimulus in an oddball task). It was reported that the auditory evoked P300 is of lower amplitude when a Target has to be detected than when a Novel is presented, which is unrelated to the task. On the other hand, there are fMRI studies in which no Novel-related activation was reported although there were activations elicited by Targets (Clark et al. 2001; Kirino et al. 2000). These findings of differential reactivity of event-related potentials (ERPs) and BOLD signal were replicated by Foucher et al. using combined measurement of EEG and fMRI. Additionally, in accordance with fMRI results, Target-related gamma oscillations were more intense than their Novel-related counterparts (Foucher et al. 2003) (see Fig. 26.4). The authors

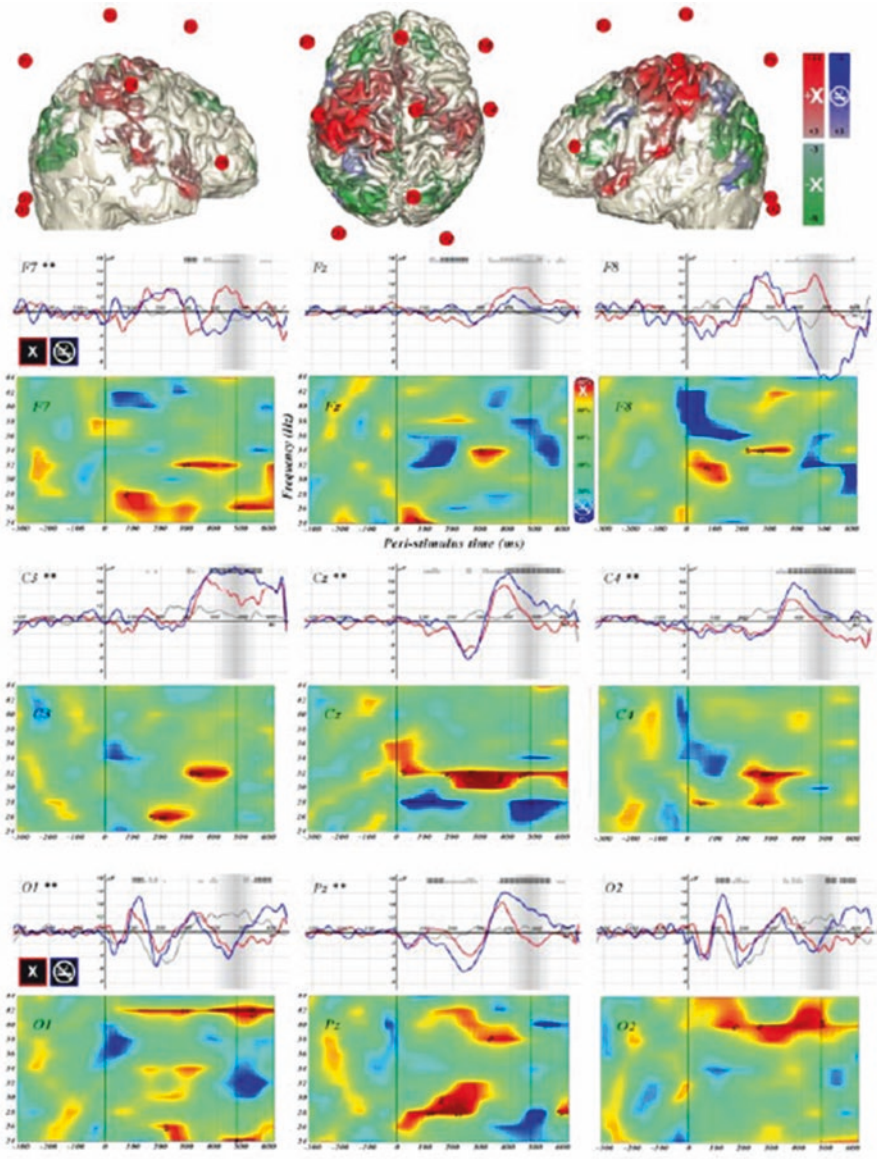

Fig. 26.4 FMRI results, evoked potentials (ERPs, P300) and event-related oscillations (EROs, gamma activity) calculated over all subjects ($n = 5$). The upper part presents three different views of the average electrode position relative to the areas with BOLD activation (threshold $p \leq 0.001$, 100 voxels; Target-related activation—red; Target-related deactivation—green; Novel-related (rare distractor) activation—blue). The lower part displays ERPs and EROs for each electrode (Targets—red and "X" marks; Novels—blue and "no-smoking" symbol; frequent distractor—gray). On the one hand, for C3, Cz, C4 and Pz Novels (blue) yielded larger ERPs than Targets (red). On the other hand, for all the electrodes the EROs showed significantly more oscillations in the gamma frequency range around 300–400 ms for Targets (red) in comparison to Novels (blue) which was in line with stronger fMRI BOLD response in the Target condition. (Reprinted from: Foucher, J. R., Otzenberger, H., and Gounot, D. The BOLD response and the gamma oscillations respond differently than evoked potentials: an interleaved EEG-fMRI study. BMC Neurosci (2003) 4:22)

propounded a physiological hypothesis suggesting that the discrepancy shown between ERPs on the one hand and fMRI signal and gamma oscillation on the other hand support evidence demonstrating that the BOLD signal is better correlated with high- than with low-frequency oscillations. In search of reasons for this observation, the authors discuss the fact that, as opposed to ERPs reflecting synchronous activity of synapses within milliseconds (Baillet et al. 2001; Speckmann and Elger 1999), event related gamma oscillations do not require to be time-locked to the stimulus that precisely and, therefore, are less dependent on the small jitter of the neuronal response relative to a stimulus (Tallon-Baudry and Bertrand 1999), like BOLD signal is. Furthermore, the authors mention the fact that ERPs reflect the synaptic input function of pyramidal cells only (Baillet et al. 2001; Speckmann and Elger 1999), whereas fMRI reflects the synaptic activity of all neural cells including inhibitory interneurons (Logothetis et al. 2001; Mathiesen et al. 2000; Matsuura and Kanno 2001) which are involved in the synchronization of gamma oscillations (Traub et al. 1996) too. A third possible reason could be related to the assumption that ERPs might correspond to the simple phase resetting of ongoing cerebral activity (Makeig et al. 2002) which should not consume much energy (Foucher et al. 2003).

Beyond the power of high frequency EEG bands the strength of the coupling between the phase of low-frequency and the amplitude of high-frequency EEG activity seems to play a crucial role in brain function. Simultaneously recorded intracranial EEG and fMRI in seven patients with epilepsy undergoing invasive EEG monitoring revealed, that the beta-gamma-phase-amplitude coupling explained variance of the amplitude of the BOLD signal, which was not explained by a combination of single EEG band powers. Thus, including the strength of the phase–amplitude coupling in the BOLD signal model in addition to the power of EEG frequency bands may increase the sensitivity of EEG-informed fMRI studies (Murta et al. 2017).

26.3.2 Gamma Activity and BOLD Response: Variation Across Subjects

In a combined experiment, Herrmann et al. set out to test the hypothesis that human EEG gamma band responses correlate with the BOLD responses. Since oscillatory activity in the gamma band range is of very low amplitude (a fraction of a microvolt) and within the frequency range of the MR gradient switching which results in EEG artifacts, it was chosen to carry out EEG and fMRI measurements separately.

Both gamma band responses as well as BOLD responses have been repeatedly shown to vary across subjects. For example, oscillatory gamma responses show interindividual variations both in frequency and amplitude (Busch et al. 2004). One source for this variation lies in the different polymorphisms of the subjects. Demiralp et al. demonstrated that the more effective variant of the DRD4 receptor results in enhanced gamma responses (Demiralp et al. 2007). At the same time, such variations correlate with differences in cognitive processes. Strüber et al. showed that subjects with high-amplitude gamma oscillations switch more often between two

alternative percepts of an ambiguous figure (Struber et al. 2000). Also, the BOLD response shows variance across subjects. For example, spatial variations of BOLD activity can stem from anatomical variations since even monozygotic twins have a slightly different brain anatomy (Lohmann et al. 1999). Recent findings have shown that already early sensory cortices underlie inter-individual variations (Amunts et al. 2000). For these reasons, atlases of the human brain are no longer based on a single brain such as the one by Talairach and Tournoux (1988). Instead, anatomical variations are taken into regard in newer atlases (Rademacher et al. 2001).

Herrmann et al. separately recorded EEG and fMRI in 18 subjects (mean age 23.9 years, 8 male). They had to view circular moving gratings that either moved outward ($p = 0.75$) or inward ($p = 0.25$). Gratings had a spatial frequency of 0.67 cycles per degree visual angle and were presented for 600 ms. During these 600 ms, one full cycle of movement occurred. The direction of movement had to be indicated by a button press (inward = right). In run1, a static grating remained visible during the inter-stimulus-interval (ISI). Thus, at the onset of a stimulus, only a motion onset was visible. In run2, a gray screen was presented during the ISI. Thus, at stimulus onset, both the stimulus and the motion set on. The fMRI recording was carried out as rapid event-related fMRI design. The identical timing was used for EEG recording. Based on the amplitude of their evoked gamma band response, subjects were assigned to either a low- or a high-gamma group.

Comparing run1 and run2 revealed that gamma responses were significantly stronger in run2 where motion onset was preceded by a blank screen ($t = 5.042$, $p < 0.001$). This contrast also yielded more activated voxels in posterior brain regions ($t = 6.668$, $p < 0.001$) and a higher percent signal change ($t = 4.744$, $p < 0.001$) (see Fig. 26.5).

Comparing the groups of the low-gamma and the high-gamma subjects for run2 yielded no differences in BOLD response, neither for the number of activated voxels ($t < 1$, $p > 0.3$) nor for percent signal change ($t < 1$, $p > 0.6$). Of course, the gamma responses were significantly stronger in the high-gamma group ($t = 5.190$, $p < 0.001$), since this was the criterion for assigning subjects to the groups (see Fig. 26.6).

The results from comparing different runs, are in line with the notion that BOLD and gamma band responses covary (Logothetis et al. 2001; Mukamel et al. 2005; Niessing et al. 2005). However, comparing subjects either showing high or low gamma responses in their EEG yielded no differences in their BOLD responses. The latter result was unexpected and one can only offer a speculative explanation. It was demonstrated that the BOLD response shows interindividual variations (Aguirre et al. 1998). Sources of variation have been identified in genetic polymorphisms (Goldberg and Weinberger 2004). At the same time, gamma band responses are influenced by a number of parameters that vary interindividually, such as age (Bottger et al. 2002), dopamine polymorphisms (Demiralp et al. 2007), and the individual rate at which the two percepts of bistable figures switch (Struber et al. 2000). Interestingly, dopamine polymorphisms modulate gamma and BOLD responses. However, while the VNTR polymorphisms of DRD4 modulates gamma band responses, the Val158Met polymorphism of COMT does not (Demiralp et al.

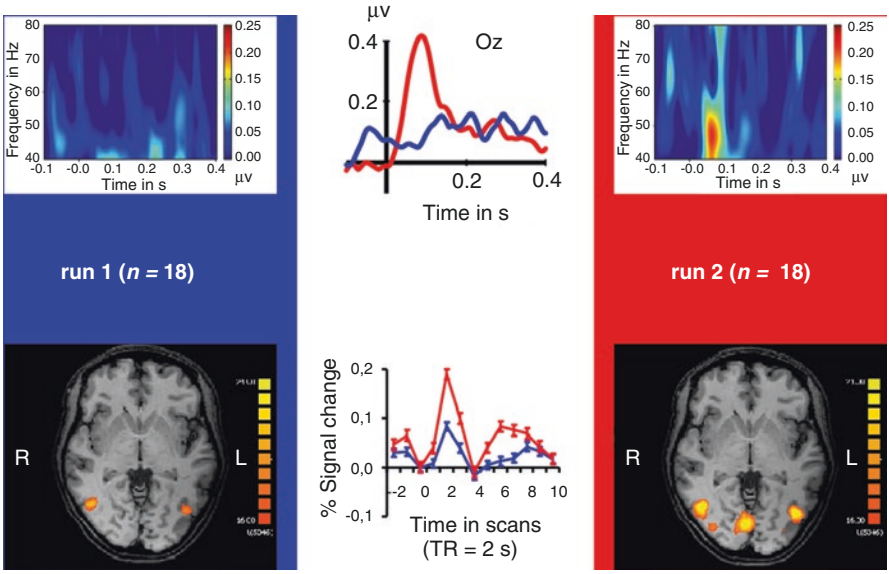

Fig. 26.5 Gamma band responses and BOLD responses from the comparison of the two runs. Both response types were significantly stronger in run2 where motion onset was preceded by a blank screen. Top row: Time frequency representations (left and right) show the gamma band responses. A prominent response is visible for run2 between 40 and 50 Hz shortly before 100 ms after stimulus onset (right). The difference between the two runs is most prominent in the time courses of the gamma band response (middle) which were computed from individual best response frequencies (roughly 45 Hz). Bottom row: The BOLD response is also stronger for run2 (right) than for run1 (left). The time course (middle) averaged across five regions of interest again shows this difference most prominently

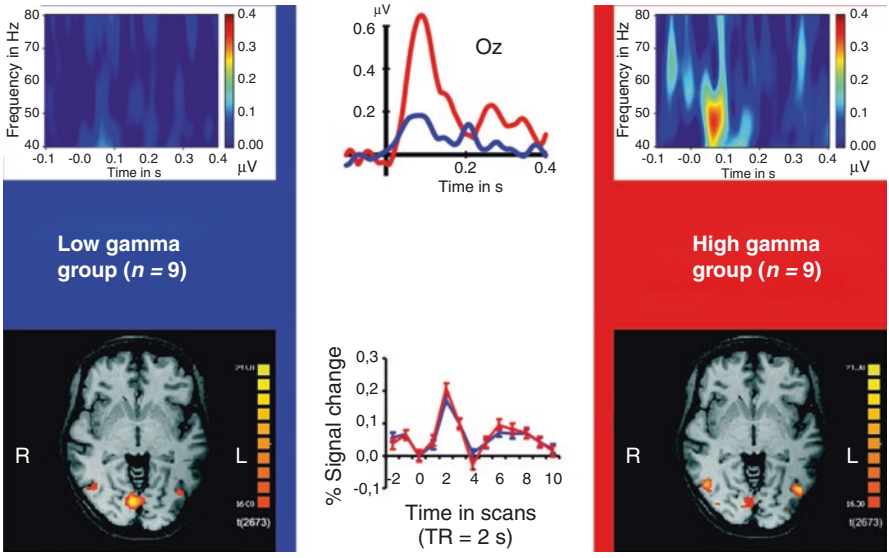

Fig. 26.6 Gamma band responses and BOLD responses comparing the low (left) versus the high gamma group (right). While the gamma band responses were, of course, significantly different between groups (top row), no differences could be found for the BOLD responses (bottom row)

2007). By contrast, the COMT polymorphism does modulate the BOLD response (Winterer et al. 2006). One difference between the two is the locus of effect. While the COMT polymorphism influences the amount of dopamine in the synaptic cleft, the DRD4 polymorphism affects the dopamine receptor but not the amount of dopamine. Thus, it seems plausible to assume that the amount of extra-cellular dopamine affects the BOLD but not the gamma band response but the dopaminergic activation of neurons affects the gamma band response but not the BOLD response.

26.3.3 Gamma Activity and BOLD Response: Further Reports

Performing simultaneous measurement of EEG and fMRI, Giraud et al. showed functional brain asymmetries in speech processing to be at the bottom of different intrinsic sampling properties in each auditory cortex. Time courses of power from certain EEG bands calculated with short-time Fourier transform were convolved with hemodynamic response function and used as regressors in a general linear model. As a result of this investigation, the authors report that, in line with the Asymmetric Sampling in Time theory (Poeppel 2003), spontaneous power fluctuations of 3–6 and 28–40 Hz intrinsic oscillations (which are tuned to major acoustic temporal characteristics of speech) are paralleled by specific modulations of neural activity in auditory/temporal cortices. The auditory activity in regions overlapping Heschl's gyrus is more prominently associated with the 3- to 6-Hz band in the right hemisphere and the 28- to 40-Hz band in the left hemisphere. Moreover, ventral premotor cortex activity is correlated with spontaneous neural oscillations at the syllabic rate of natural speech (Giraud et al. 2007).

Research in the field of resting state networks raised the question if the analysis of the modulation of the whole EEG frequency spectrum could help to find electrophysiological signatures of such networks. In the EEG of the resting human brain, spontaneous rhythms are detectable showing different oscillatory signatures and being unrelated to any external or internal event. For the investigation of hemodynamic correlates of these phenomena, simultaneous measurement of EEG and fMRI is necessary because fusing the data after separate recordings of electrical and hemodynamic measures is not possible (Ritter and Villringer 2006). Mantini et al. used a data-driven approach to investigate the relationship between neuronal oscillatory processes in different EEG frequency bands and coherent fMRI fluctuations. BOLD signal time course corresponding to each of the independent components, identified by using independent component analysis (ICA), was correlated with the EEG reference waveforms of power time series of the various frequency bands. In general, more than one rhythm was associated with the same network, whereas, resting-state networks could be separated on the basis of their specific EEG power profile. Regarding observations about gamma activity, the authors report a strong weighting of EEG power spectra associated with the ventromedial prefrontal cortex (resting state network 6) toward gamma power (see Fig. 26.7), whereas the rest of the default network (resting state network 1) was more strongly associated with alpha and beta power (Mantini et al. 2007).

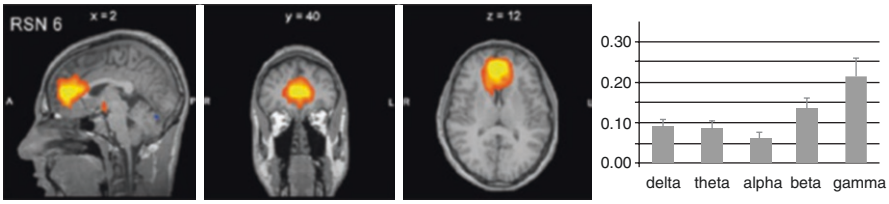

Fig. 26.7 Association between EEG rhythms and fMRI resting state network (RSN) 6. Left: sagittal, coronal, and axial spatial map of the RSN 6. Right: bar plots of the average correlations between the brain oscillatory activity in the delta, theta, alpha, beta, and gamma band, and the RSN 6 time course. In general, more than one rhythm was associated with the same network, confirming that neurons oscillating at different frequencies may contribute to the same functional system. RSNs 1 (default) and 2 (dorsal attention) had stronger relationships with alpha and beta rhythms, RSN 3 (visual) with all rhythms except gamma rhythm, RSN 4 (auditory) with delta, theta, and beta rhythms and RSN 5 (somato-motor) with beta rhythm. The RSN 6 shown here [including the medial-ventral prefrontal cortex, the pregenual anterior cingulate, the hypothalamus and the cerebellum, putatively related to self-referential mental activity (D'Argembeau et al. 2005)] was mainly associated with gamma rhythm. (From Mantini, D., Perrucci, M. G., Del Gratta, C., Romani, G. L., and Corbetta, M. Electrophysiological sig-natures of resting state networks in the human brain. Proc Natl Acad Sci U S A (2007) 104(32):13170–5. Copyright (2007) National Academy of Sciences, USA)

Recently, Huang et al. introduced a new method of obtaining the EEG global signal and investigated the relationship between resting-state EEG and fMRI global signal by means of simultaneously recorded EEG and fMRI. The authors report a positive correlation between the global signal of resting state fMRI and power fluctuations of the EEG global signal in the gamma band (Huang et al. 2019). High-frequency electrical substrates of fMRI-based resting state networks have been observed using simultaneously recorded multiband fMRI and EEG and parallel independent component analysis, which does not require the down sampling of EEG to fMRI temporal resolution (Kyathanahally et al. 2017). The examination of five healthy subjects with MEG and fMRI using a simple visual task, supplied evidence of event-related synchronization in the gamma band which covaried spatio-temporally with the BOLD effect in the occipital cortex (Brookes et al. 2005) (see Fig. 26.8). Castelhano et al. reported a functional topography for distinct gamma sub-bands. In a simultaneous EEG–fMRI study, a low gamma sub-band activity (near 40 Hz) was tightly related to the decision-making network, whereas a high gamma sub-band was found to be linked to early visual processing regions (Castelhano et al. 2014). In a cued visual spatial attention task, the fMRI activity in visual cortical regions representing attended locations in space covaried positively with gamma-band activity recorded from occipital EEG electrodes (Green et al. 2017). Moreover, in this study, the pulvinar nucleus of the thalamus covaried with this spatially specific, attention-related oscillatory phenomenon. These results illuminate dynamical interactions of cortical and subcortical processes underlying spatial visual attention and highlight the potential of simultaneous recordings of EEG and fMRI in uncovering dynamical interactions between brain regions including subcortical regions, which are unlikely to be direct generators of scalp-recorded EEG.

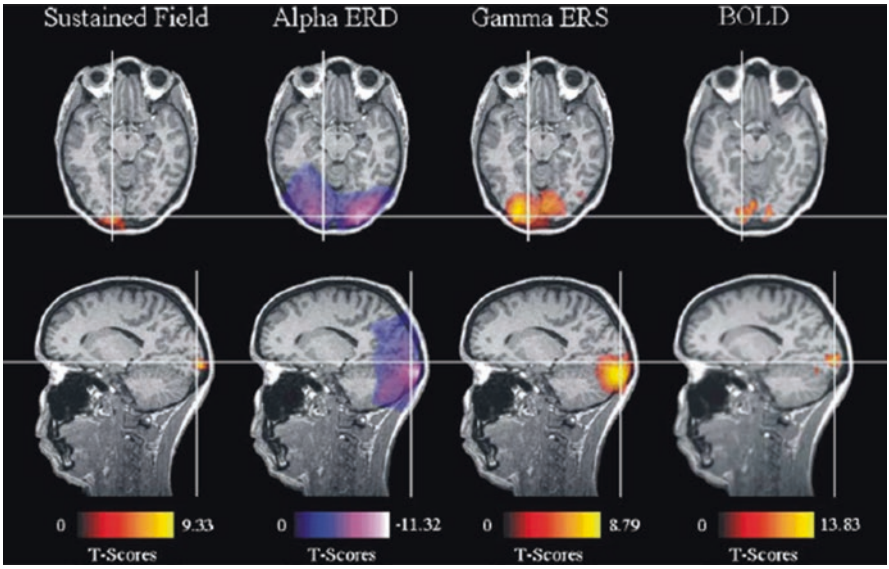

Fig. 26.8 Spatial distribution of the MEG sustained field, alpha-band power change, gamma-band power change, and BOLD signals for a single subject. Left: MEG-sustained field. Inside left: event-related desynchronization (ERD) in the alpha band (8–13 Hz). Inside right: event-related synchronization (ERS) in the gamma band (55–70 Hz). Right: fMRI BOLD signal ($p < 0.05$, corrected for multiple testing). Functional images are overlaid onto axial and sagittal slices of a high-resolution anatomical MRI. For the alpha and gamma-band images (probability maps, $p < 0.001$, uncorrected), the red overlay represents an increase in power, whereas the blue overlay represents a decrease. The sustained field image represents the spatial distribution of a significant sustained response. (Reprinted from Neuroimage, 26(1), Brookes, M. J., Gibson, A. M., Hall, S. D., Furlong, P. L., Barnes, G. R., Hillebrand, A., Singh, K. D., Holliday, I. E., Francis, S. T., and Morris, P. G., GLM-beamformer method demonstrates stationary field, alpha ERD and gamma ERS co-localisation with fMRI BOLD response in visual cortex, p. 302–8 (2005), with permission from Elsevier)

A possible link between induced gamma activity and hemodynamic response was found in a work investigating spatiotemporal correlates of repetition priming in cortical word recognition networks and their modulation by stimulus familiarity. The repetition of familiar stimuli (real words) led to reduced activation for repeated words in occipitotemporal cortical regions and significant reduction of induced gamma band responses and phase synchrony between electrode positions. By contrast, the repetition of unfamiliar stimuli (pseudowords) results in activation increase for repeated pseudowords in the same areas, to increased GBRs, and to an increased phase coupling (Fiebach et al. 2005).

Load-dependent modulations in the EEG gamma frequency band during processes of working memory have been described in EEG studies (e.g., Haenschel et al. 2009). Moreover, positive correlations between gamma activity and BOLD signal within dorsolateral and medial prefrontal cortex as well as temporal and parietal brain regions during the retention period of working memory tasks have been

described (Michels et al. 2010; Zhao et al. 2017). A simultaneous EEG–fMRI visual working memory study revealed an association of the modulation of fast EEG oscillatory power with cortical activity within the visual cortex, while these fast oscillations showed a phase–amplitude coupling to slow oscillations associated with activity within mnemonic circuit brain regions. Thus, EEG–fMRI might help uncovering the processes of communication between mnemonic and sensory circuits (Mizuhara et al. 2015).

26.3.4 Single-Trial Coupling of Auditory Evoked Gamma Band Response and BOLD Signal

With regard to the findings that BOLD and gamma band responses covary (Logothetis et al. 2001; Niessing et al. 2005; Mukamel et al. 2005), the direct fusion of information about the power of gamma activity and BOLD response following external stimulation in simultaneous measurements by single-trial coupling seems to be promising. Regarding evoked gamma activity, both in terms of phase and latency strictly triggered to stimulus onset, several authors have described its role in the context of attentional processes (Fell et al. 2003; Gurtubay et al. 2004; Senkowski et al. 2007). One example of early evoked gamma activity is the "transient" gamma-band response (GBR) to auditory stimulation (between 25 and 100 ms after stimulus presentation) which is known to be closely related to selective attention (Debener et al. 2003; Tiitinen et al. 1993). In preparation for a study simultaneously measuring EEG gamma activity and BOLD response investigating a possible ACC generator of the early auditory evoked GBR (aeGBR) and its functional role in auditory information processing, Mulert et al. showed a significant influence of the task difficulty on the aeGBR and the auditory-evoked N1-component (Mulert et al. 2007) (see Fig. 26.9a–e). Generators of the aeGBR were found in the auditory cortex (primary and secondary auditory cortex) and in the dorsal anterior cingulate cortex (ACC) as well as medial frontal gyrus in the whole-head LORETA analysis (Mulert et al. 2007; Polomac et al. 2015). Mulert et al. suggested that the aeGBR might represent an early synchronization of sensory and supervisory or monitoring brain areas in terms of a process of early top-down influence on information processing in the sensory area (Busch et al. 2006; Herrmann et al. 2004).

In order to gain more precision concerning localization and the possibility of investigating subcortical structures (e.g., the thalamus), these findings were transferred to a study simultaneously measuring EEG and fMRI. Mulert et al. explored the specific BOLD-response corresponding to the aeGBR using single-trial coupling of EEG and fMRI after matrix decomposition of the specific GBR information using Schmidt-Gram orthogonalization. Distinct "aeGBR-specific" activations were found within the auditory cortex, the ACC, and the thalamus (Mulert et al. 2010) (see Fig. 26.9f). Patients with schizophrenia show a reduction of the aeGBR and a reduced activity of its generators within auditory cortex and ACC across all stages of the disease accompanied by cognitive symptoms, for which reason it has been interpreted as an intermediate phenotype of the disease (Leicht et al. 2010,

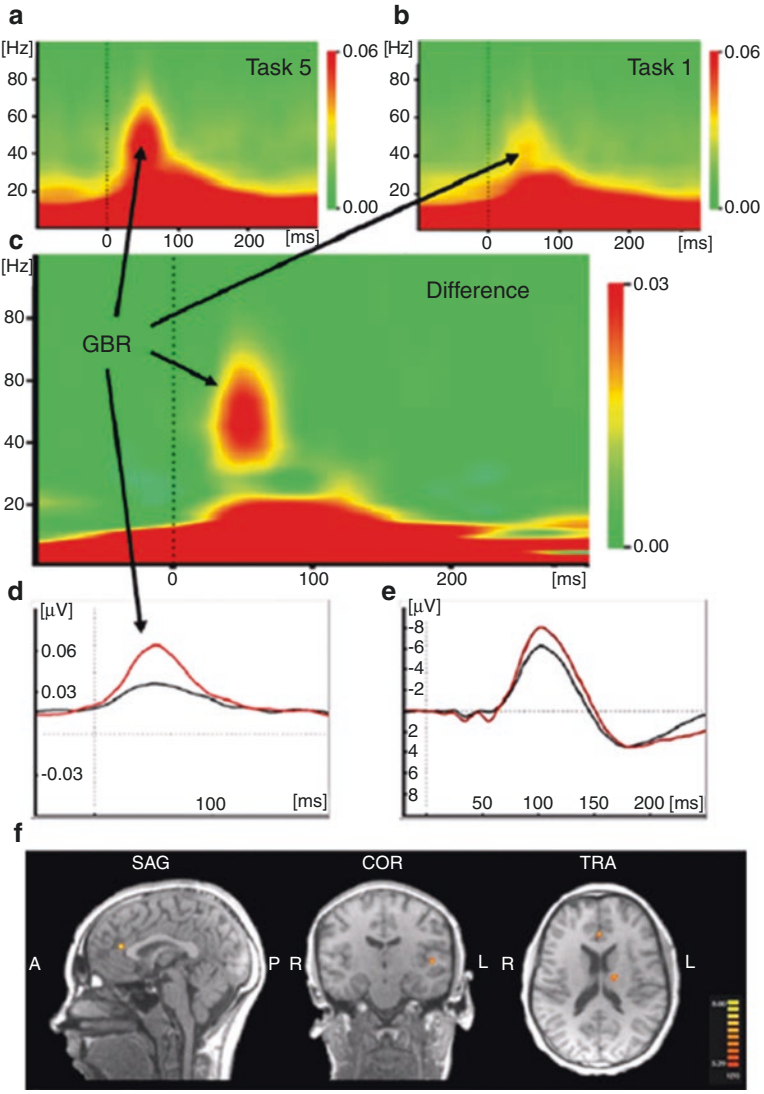

Fig. 26.9 Dependency on cognitive demands and generators of the auditory-evoked gamma band response as shown by means of EEG and simultaneous EEG and fMRI. Time frequency analyses for the timeframe 0–200 ms after stimulus presentation averaged over all subjects in task 1 (**a**, control condition, lowest difficulty comparing the 6 presented auditory choice reaction tasks of different difficulty) and 5 (**b**, highest difficulty comparing the 6 presented auditory choice reaction tasks of different difficulty) and the difference between task 5 and task 1 (**c**). Scaling was uniform for (**a**–**c**). As indicated (black arrows) the evoked GBR can be seen as an increased activity at about 50 ms in the frequency range around 40 Hz. (**d**) GBR displayed as the result of the wavelet analysis (complex Morlet wavelet) focused on 40 Hz for task 1 (black) and task 5 (red). (**e**) N1 amplitude for task 1 (black) and task 5 (red). (**f**) Single-trial coupling of the GBR-amplitude and the corresponding BOLD signal (random effects analysis, $n = 10$, $p < 0.0005$): GBR-related activations can be seen in the ACC, left auditory cortex and thalamus. (**a**–**e**: Reprinted from Neuropsychologia 45(10), Mulert, C., Leicht, G., Pogarell, O., Mergl, R., Karch, S., Juckel, G., Moller, H. J., and Hegerl, U., Auditory cortex and anterior cingulate cortex sources of the early evoked gamma band response: relationship to task difficulty and mental effort, p. 2294–306 (2007), with permission from Elsevier)

2011, 2015, 2016). Simultaneous recordings of EEG and fMRI revealed a reduced activation of an aeGBR-specific network in subjects at high risk of developing schizophrenia, which might be applicable as a marker for the prediction of transition of subjects at risk into full-blown schizophrenia (Leicht et al. 2016).

26.4 Conclusions

We discussed problems, recent developments, and research findings regarding the relation of EEG gamma activity and fMRI BOLD signal and possible applications of the integration of EEG and fMRI in this field. According to several investigations, there seems to be a stronger correlation between the high-frequency components of the EEG signal, for example, the gamma band, and the BOLD response compared to lower frequency bands (Brovelli et al. 2005; Foucher et al. 2003; Hutchison et al. 2015; Lachaux et al. 2007; Logothetis et al. 2001; Logothetis 2002; Mukamel et al. 2005; Murta et al. 2017; Niessing et al. 2005). Some problems emerge in the simultaneous recordings of fMRI and gamma activity since the amplitudes of high frequency EEG fractions are small and the artifact handicap carries more weight. Statistical methods like principal component analysis (PCA) or independent component analysis (ICA), as well as various innovations in EEG- and fMRI-recording techniques may be possible solutions for some of these technical challenges. The information of fMRI analyses with time courses of EEG gamma activity has been applied for uncovering processes of communication in the brain, for example, during the resting state, processes of visual spatial attention or working memory and cognitively demanding auditory information processing.

References

Aguirre GK, Zarahn E, D'Esposito M (1998) The variability of human, BOLD hemodynamic responses. NeuroImage 8(4):360–369

Amunts K, Malikovic A, Mohlberg H, Schormann T, Zilles K (2000) Brodmann's areas 17 and 18 brought into stereotaxic space-where and how variable? NeuroImage 11(1):66–84

Anami K, Mori T, Tanaka F, Kawagoe Y, Okamoto J, Yarita M, Ohnishi T, Yumoto M, Matsuda H, Saitoh O (2003) Stepping stone sampling for retrieving artifact-free electroencephalogram during functional magnetic resonance imaging. NeuroImage 19(2 Pt 1):281–295

Baillet S, Mosher JC, Leahy RM (2001) Electromagnetic brain mapping. IEEE Signal Proc Mag 18:14–30

Bottger D, Herrmann CS, von Cramon DY (2002) Amplitude differences of evoked alpha and gamma oscillations in two different age groups. Int J Psychophysiol 45(3):245–251

Bragin A, Jando G, Nadasdy Z, Hetke J, Wise K, Buzsaki G (1995) Gamma (40-100 Hz) oscillation in the hippocampus of the behaving rat. J Neurosci 15(1 Pt 1):47–60

Brookes MJ, Gibson AM, Hall SD, Furlong PL, Barnes GR, Hillebrand A, Singh KD, Holliday IE, Francis ST, Morris PG (2005) GLM-beamformer method demonstrates stationary field, alpha ERD and gamma ERS co-localisation with fMRI BOLD response in visual cortex. NeuroImage 26(1):302–308

Brookes MJ, Vrba J, Mullinger KJ, Geirsdóttir GB, Yan WX, Stevenson CM, Bowtell R, Morris PG (2009) Source localisation in concurrent EEG/fMRI: applications at 7T. NeuroImage 45(2):440–452

Brovelli A, Lachaux JP, Kahane P, Boussaoud D (2005) High gamma frequency oscillatory activity dissociates attention from intention in the human premotor cortex. NeuroImage 28(1):154–164
Busch NA, Debener S, Kranczioch C, Engel AK, Herrmann CS (2004) Size matters: effects of stimulus size, duration and eccentricity on the visual gamma-band response. Clin Neurophysiol 115(8):1810–1820
Busch NA, Schadow J, Frund I, Herrmann CS (2006) Time-frequency analysis of target detection reveals an early interface between bottom-up and top-down processes in the gamma-band. NeuroImage 29(4):1106–1116
Castelhano J, Duarte IC, Wibral M, Rodriguez E, Castelo-Branco M (2014) The dual facet of gamma oscillations: separate visual and decision making circuits as revealed by simultaneous EEG/fMRI. Hum Brain Mapp 35(10):5219–5235
Clark VP, Fannon S, Lai S, Benson R (2001) Paradigm-dependent modulation of event-related fMRI activity evoked by the oddball task. Hum Brain Mapp 14(2):116–127
Crick F, Koch C (1990) Towards a neurobiological theory of consciousness. Semin Neurosci 2:263–275
Crone NE, Hao L, Hart J Jr, Boatman D, Lesser RP, Irizarry R, Gordon B (2001) Electrocorticographic gamma activity during word production in spoken and sign language. Neurology 57(11):2045–2053
D'Argembeau A, Collette F, Van der Linden M, Laureys S, Del Fiore G, Degueldre C, Luxen A, Salmon E (2005) Self-referential reflective activity and its relationship with rest: a PET study. NeuroImage 25(2):616–624
Damasio AR (1990) Synchronous activation in multiple cortical regions: a mechanism for recall. Semin Neurosci 2:287–296
Debener S, Herrmann CS, Kranczioch C, Gembris D, Engel AK (2003) Top-down attentional processing enhances auditory evoked gamma band activity. Neuroreport 14(5):683–686
Delacour J (1997) Neurobiology of consciousness: an overview. Behav Brain Res 85(2):127–141
Demiralp T, Herrmann CS, Erdal ME, Ergenoglu T, Keskin YH, Ergen M, Beydagi H (2007) DRD4 and DAT1 polymorphisms modulate human gamma band responses. Cereb Cortex 17(5):1007–1019
Eckhorn R, Bauer R, Jordan W, Brosch M, Kruse W, Munk M, Reitboeck HJ (1988) Coherent oscillations: a mechanism of feature linking in the visual cortex? Multiple electrode and correlation analyses in the cat. Biol Cybern 60(2):121–130
Engel AK, Singer W (2001) Temporal binding and the neural correlates of sensory awareness. Trends Cogn Sci 5(1):16–25
Eulitz C, Maess B, Pantev C, Friederici AD, Feige B, Elbert T (1996) Oscillatory neuromagnetic activity induced by language and non-language stimuli. Brain Res Cogn Brain Res 4(2):121–132
Fell J, Fernandez G, Klaver P, Elger CE, Fries P (2003) Is synchronized neuronal gamma activity relevant for selective attention? Brain Res Brain Res Rev 42(3):265–272
Fiebach CJ, Gruber T, Supp GG (2005) Neuronal mechanisms of repetition priming in occipitotemporal cortex: spatiotemporal evidence from functional magnetic resonance imaging and electroencephalography. J Neurosci 25(13):3414–3422
Foucher JR, Otzenberger H, Gounot D (2003) The BOLD response and the gamma oscillations respond differently than evoked potentials: an interleaved EEG-fMRI study. BMC Neurosci 4:22
Freyer F, Becker R, Anami K, Curio G, Villringer A, Ritter P (2009) Ultrahigh-frequency EEG during fMRI: pushing the limits of imaging-artifact correction. NeuroImage 48(1):94–108
Fries P (2005) A mechanism for cognitive dynamics: neuronal communication through neuronal coherence. Trends Cogn Sci 9(10):474–480
Friston K (2002) Beyond phrenology: what can neuroimaging tell us about distributed circuitry? Annu Rev Neurosci 25:221–250
Giraud AL, Kleinschmidt A, Poeppel D, Lund TE, Frackowiak RS, Laufs H (2007) Endogenous cortical rhythms determine cerebral specialization for speech perception and production. Neuron 56(6):1127–1134

Goldberg TE, Weinberger DR (2004) Genes and the parsing of cognitive processes. Trends Cogn Sci 8(7):325–335

Gray CM, Konig P, Engel AK, Singer W (1989) Oscillatory responses in cat visual cortex exhibit inter-columnar synchronization which reflects global stimulus properties. Nature 338(6213):334–337

Green JJ, Boehler CN, Roberts KC, Chen LC, Krebs RM, Song AW, Woldorff MG (2017) Cortical and subcortical coordination of visual spatial attention revealed by simultaneous EEG-fMRI recording. J Neurosci 37(33):7803–7810

Gurtubay IG, Alegre M, Labarga A, Malanda A, Artieda J (2004) Gamma band responses to target and non-target auditory stimuli in humans. Neurosci Lett 367(1):6–9

Haenschel C, Bittner RA, Waltz J, Haertling F, Wibral M, Singer W, Linden DE, Rodriguez E (2009) Cortical oscillatory activity is critical for working memory as revealed by deficits in early-onset schizophrenia. J Neurosci 29(30):9481–9489

Herrmann CS, Munk MH, Engel AK (2004) Cognitive functions of gamma-band activity: memory match and utilization. Trends Cogn Sci 8(8):347–355

Huang X, Long Z, Lei X (2019) Electrophysiological signatures of the resting-state fMRI global signal: a simultaneous EEG-fMRI study. J Neurosci Methods 311:351–359

Hummel JE, Biederman I (1992) Dynamic binding in a neural network for shape recognition. Psychol Rev 99(3):480–517

Hutchison RM, Hashemi N, Gati JS, Menon RS, Everling S (2015) Electrophysiological signatures of spontaneous BOLD fluctuations in macaque prefrontal cortex. NeuroImage 113:257–267

Kim HC, Yoo SS, Lee JH (2015) Recursive approach of EEG-segment-based principal component analysis substantially reduces cryogenic pump artifacts in simultaneous EEG-fMRI data. NeuroImage 104:437–451

Kirino E, Belger A, Goldman-Rakic P, McCarthy G (2000) Prefrontal activation evoked by infrequent target and novel stimuli in a visual target detection task: an event-related functional magnetic resonance imaging study. J Neurosci 20(17):6612–6618

Kyathanahally SP, Wang Y, Calhoun VD, Deshpande G (2017) Investigation of true high frequency electrical substrates of fMRI-based resting state networks using parallel independent component analysis of simultaneous EEG/fMRI data. Front Neuroinform 11:74

Lachaux JP, George N, Tallon-Baudry C, Martinerie J, Hugueville L, Minotti L, Kahane P, Renault B (2005) The many faces of the gamma band response to complex visual stimuli. NeuroImage 25(2):491–501

Lachaux JP, Fonlupt P, Kahane P, Minotti L, Hoffmann D, Bertrand O, Baciu M (2007) Relationship between task-related gamma oscillations and BOLD signal: new insights from combined fMRI and intracranial EEG. Hum Brain Mapp 28(12):1368–1375

Leicht G, Kirsch V, Giegling I, Karch S, Hantschk I, Möller HJ, Pogarell O, Hegerl U, Rujescu D, Mulert C (2010) Reduced early auditory evoked gamma-band response in patients with schizophrenia. Biol Psychiatry 67(3):224–231

Leicht G, Karch S, Karamatskos E, Giegling I, Möller HJ, Hegerl U, Pogarell O, Rujescu D, Mulert C (2011) Alterations of the early auditory evoked gamma-band response in first-degree relatives of patients with schizophrenia: hints to a new intermediate phenotype. J Psychiatr Res 45(5):699–705

Leicht G, Andreou C, Polomac N, Lanig C, Schöttle D, Lambert M, Mulert C (2015) Reduced auditory evoked gamma band response and cognitive processing deficits in first episode schizophrenia. World J Biol Psychiatry 16(6):387–397

Leicht G, Vauth S, Polomac N, Andreou C, Rauh J, Mußmann M, Karow A, Mulert C (2016) EEG-informed fMRI reveals a disturbed gamma-band-specific network in subjects at high risk for psychosis. Schizophr Bull 42(1):239–249

Lindsley DB (1952) Psychological phenomena and the electroencephalogram. Electroencephalogr Clin Neurophysiol 4(4):443–456

Logothetis NK (2002) The neural basis of the blood-oxygen-level-dependent functional magnetic resonance imaging signal. Phil Trans R Soc Lond Ser B Biol Sci 357(1424):1003–1037

Logothetis NK, Pauls J, Augath M, Trinath T, Oeltermann A (2001) Neurophysiological investigation of the basis of the fMRI signal. Nature 412(6843):150–157
Lohmann G, von Cramon DY, Steinmetz H (1999) Sulcal variability of twins. Cereb Cortex 9(7):754–763
Makeig S, Westerfield M, Jung TP, Enghoff S, Townsend J, Courchesne E, Sejnowski TJ (2002) Dynamic brain sources of visual evoked responses. Science 295(5555):690–694
von der Malsburg C (1994) The correlation theory of brain function. In: Domany E et al (eds) Models of neural networks, vol II. Springer, New York, NY, pp 95–119
Mandelkow H, Halder P, Boesiger P, Brandeis D (2006) Synchronization facilitates removal of MRI artefacts from concurrent EEG recordings and increases usable bandwidth. NeuroImage 32(3):1120–1126
Mantini D, Perrucci MG, Del Gratta C, Romani GL, Corbetta M (2007) Electrophysiological signatures of resting state networks in the human brain. Proc Natl Acad Sci U S A 104(32):13170–13175
Mathiesen C, Caesar K, Lauritzen M (2000) Temporal coupling between neuronal activity and blood flow in rat cerebellar cortex as indicated by field potential analysis. J Physiol 523(Pt 1):235–246
Matsuura T, Kanno I (2001) Quantitative and temporal relationship between local cerebral blood flow and neuronal activation induced by somatosensory stimulation in rats. Neurosci Res 40(3):281–290
Michels L, Bucher K, Lüchinger R, Klaver P, Martin E, Jeanmonod D, Brandeis D (2010) Simultaneous EEG-fMRI during a working memory task: modulations in low and high frequency bands. PLoS One 5(4):e10298
Mizuhara H, Sato N, Yamaguchi Y (2015) Cortical networks dynamically emerge with the interplay of slow and fast oscillations for memory of a natural scene. NeuroImage 111:76–84
Mukamel R, Gelbard H, Arieli A, Hasson U, Fried I, Malach R (2005) Coupling between neuronal firing, field potentials, and FMRI in human auditory cortex. Science 309(5736):951–954
Mulert C, Leicht G, Pogarell O, Mergl R, Karch S, Juckel G, Moller HJ, Hegerl U (2007) Auditory cortex and anterior cingulate cortex sources of the early evoked gamma-band response: relationship to task difficulty and mental effort. Neuropsychologia 45(10):2294–2306
Mulert C, Hepp P, Leicht G, Karch S, Lutz J, Moosmann M, Reiser M, Hegerl U, Pogarell O, Möller HJ, Jäger L (2010) High frequency oscillations in the gamma-band and the corresponding BOLD signal: trial-by-trial coupling of EEG and fMRI reveals the involvement of the thalamic reticular nucleus (TRN). NeuroImage 49(3):2238–2247
Muller MM, Keil A (2004) Neuronal synchronization and selective color processing in the human brain. J Cogn Neurosci 16(3):503–522
Murta T, Chaudhary UJ, Tierney TM, Dias A, Leite M, Carmichael DW, Figueiredo P, Lemieux L (2017) Phase-amplitude coupling and the BOLD signal: a simultaneous intracranial EEG (icEEG) - fMRI study in humans performing a finger-tapping task. NeuroImage 146:438–451
Murthy VN, Fetz EE (1992) Coherent 25- to 35-Hz oscillations in the sensorimotor cortex of awake behaving monkeys. Proc Natl Acad Sci U S A 89(12):5670–5674
Neuenschwander S, Singer W (1996) Long-range synchronization of oscillatory light responses in the cat retina and lateral geniculate nucleus. Nature 379(6567):728–732
Niebur E et al (1993) An oscillation-based model for the neuronal basis of attention. Vis Res 33:2789–2802
Niedermeyer E, Lopes Da Silva F (2004) Electroencephalography: basic principles, clinical applications and related fields, 5th edn. Lippincott Williams and Wilkins, Philadelphia, PA
Nierhaus T, Gundlach C, Goltz D, Thiel SD, Pleger B, Villringer A (2013) Internal ventilation system of MR scanners induces specific EEG artifact during simultaneous EEG-fMRI. NeuroImage 74:70–76
Niessing J, Ebisch B, Schmidt KE, Niessing M, Singer W, Galuske RA (2005) Hemodynamic signals correlate tightly with synchronized gamma oscillations. Science 309(5736):948–951
Nunez PL (1995) Neocortical dynamics and human EEG rhythms. Oxford University Press, New York, NY

Pantev C, Makeig S, Hoke M, Galambos R, Hampson S, Gallen C (1991) Human auditory evoked gamma-band magnetic fields. Proc Natl Acad Sci U S A 88(20):8996–9000
Poeppel D (2003) The analysis of speech in different temporal integration windows: cerebral lateralization as 'asymmetric sampling in time'. Speech Comm 41:245–255
Polomac N, Leicht G, Nolte G, Andreou C, Schneider TR, Steinmann S, Engel AK, Mulert C (2015) Generators and connectivity of the early auditory evoked gamma band response. Brain Topogr 28(6):865–878
Pulvermuller F (1999) Words in the brain's language. Behav Brain Sci 22(2):253–279. discussion 280–336
Pulvermuller F, Lutzenberger W, Preissl H, Birbaumer N (1995) Spectral responses in the gamma-band: physiological signs of higher cognitive processes? Neuroreport 6(15):2059–2064
Rademacher J, Morosan P, Schormann T, Schleicher A, Werner C, Freund HJ, Zilles K (2001) Probabilistic mapping and volume measurement of human primary auditory cortex. NeuroImage 13(4):669–683
Ritter P, Villringer A (2006) Simultaneous EEG-fMRI. Neurosci Biobehav Rev 30(6):823–838
Roelfsema PR, Engel AK, Konig P, Singer W (1997) Visuomotor integration is associated with zero time-lag synchronization among cortical areas. Nature 385(6612):157–161
Senkowski D, Talsma D, Grigutsch M, Herrmann CS, Woldorff MG (2007) Good times for multisensory integration: effects of the precision of temporal synchrony as revealed by gamma-band oscillations. Neuropsychologia 45(3):561–571
Speckmann EJ, Elger CE (1999) Introduction to the neurophysiological basis of the EEG and DC potentials. In: Niedermeyer E, Lopes da Silva F (eds) Electroencephalography, basic principles, clinical applications and related fields. Lippincott Williams and Wilkins, Philadelphia, PA, pp 15–27
Struber D, Basar-Eroglu C, Hoff E, Stadler M (2000) Reversal-rate dependent differences in the EEG gamma-band during multistable visual perception. Int J Psychophysiol 38(3):243–252
Talairach J, Tournoux P (1988) Co-planar stereotaxic atlas of the human brain. Thieme Medical Publishers, New York, NY
Tallon-Baudry C, Bertrand O (1999) Oscillatory gamma activity in humans and its role in object representation. Trends Cogn Sci 3(4):151–162
Tallon-Baudry C, Bertrand O, Delpuech C, Pernier J (1996) Stimulus specificity of phase-locked and non-phase-locked 40 Hz visual responses in human. J Neurosci 16(13):4240–4249
Tiitinen H, Sinkkonen J, Reinikainen K, Alho K, Lavikainen J, Naatanen R (1993) Selective attention enhances the auditory 40-Hz transient response in humans. Nature 364(6432):59–60
Traub RD, Whittington MA, Colling SB, Buzsaki G, Jefferys JG (1996) Analysis of gamma rhythms in the rat hippocampus in vitro and in vivo. J Physiol 493(Pt 2):471–484
Treisman A (1996) The binding problem. Curr Opin Neurobiol 6(2):171–178
Uji M, Wilson R, Francis ST, Mullinger KJ, Mayhew SD (2018) Exploring the advantages of multiband fMRI with simultaneous EEG to investigate coupling between gamma frequency neural activity and the BOLD response in humans. Hum Brain Mapp 39(4):1673–1687
Winterer G, Musso F, Vucurevic G, Stoeter P, Konrad A, Seker B, Gallinat J, Dahmen N, Weinberger DR (2006) COMT genotype predicts BOLD signal and noise characteristics in prefrontal circuits. NeuroImage 32(4):1722–1732
Young GB, Pigott SE (1999) Neurobiological basis of consciousness. Arch Neurol 56(2):153–157
Zhao X, Li X, Yao L (2017) Localized fluctuant oscillatory activity by working memory load: a simultaneous EEG-fMRI study. Front Behav Neurosci 11:215

EEG–fMRI in Animal Models

27

Abhijeet Gummadavelli, Basavaraju G. Sanganahalli, Peter Herman, Famheed Hyder, and Hal Blumenfeld

27.1 Introduction

Neuroscientists have long sought techniques for investigating the neuronal mechanisms of normal behavior and disease. The uniquely enigmatic nature of the brain and the difficulties inherent to its study limited early physiological investigations of brain

A. Gummadavelli
Department of Neurosurgery, Yale University School of Medicine, New Haven, CT, USA
e-mail: abhijeet.gummadavelli@yale.edu

B. G. Sanganahalli · P. Herman
Department of Radiology and Biomedical Imaging, Yale University School of Medicine, New Haven, CT, USA

Department of Biomedical Engineering, Yale University School of Medicine, New Haven, CT, USA
e-mail: basavaraju.ganganna@yale.edu; peter.herman@yale.edu

F. Hyder
Department of Radiology and Biomedical Imaging, Yale University School of Medicine, New Haven, CT, USA

Department of Biomedical Engineering, Yale University School of Medicine, New Haven, CT, USA

Magnetic Resonance Research Center, Yale University School of Medicine, New Haven, CT, USA
e-mail: fahmeed.hyder@yale.edu

H. Blumenfeld (✉)
Department of Neurosurgery, Yale University School of Medicine, New Haven, CT, USA

Magnetic Resonance Research Center, Yale University School of Medicine, New Haven, CT, USA

Department of Neurology, Yale University School of Medicine, New Haven, CT, USA

Department of Neuroscience, Yale University School of Medicine, New Haven, CT, USA
e-mail: hal.blumenfeld@yale.edu

C. Mulert, L. Lemieux (eds.), *EEG - fMRI*,
https://doi.org/10.1007/978-3-031-07121-8_27

function. For example, although able to provide great insight into the localization of brain function, lesion studies are inherently destructive, and thus reveal limited information about brain functioning in situ. Techniques for the noninvasive monitoring of brain function were needed. The advent of recording electrical brain activity via electroencephalography (EEG) opened new avenues for the noninvasive study of brain activity (Berger 1929). For many decades, neuroimaging lagged behind electrophysiological techniques; the MR revolution began in the 1970s (Lauterbur 1973) and soon applied to human pathology (Damadian 1971). Early studies of cerebral hemodynamic responses showed that brain function could be related to measurements of blood flow. Seizures occurring during neurosurgery have long been known to produce a focal blood flow increase in the cerebral cortex (Horsley 1892; Penfield 1933), and early measurements using intracarotid sensors likewise demonstrated increased cerebral blood flow during seizures (Gibbs et al. 1934). Advancements in electrical recording and functional imaging technology in recent decades have now made it possible to noninvasively study the brain at sufficiently high temporal and spatial resolutions to reveal fundamental neuronal processes in detail.

EEG measures extracellular electrical field potentials generated by populations of cortical neurons and can capture brain electrical activity with millisecond temporal resolution. Although EEG provides high temporal resolution, it is limited in its spatial sampling and cannot completely characterize neuronal activity throughout the entire brain. High-density electrode placement can improve spatial resolution, however remain limited to measuring electrical fields from a portion of the cortex. The electrical signal recorded in the EEG reflects a spatial summation of the underlying cortical electrical activity and does not sample subcortical areas; thus EEG with scalp electrodes may not detect deeply originating discharges (Gloor 1985).

Neuroimaging techniques offer a noninvasive comprehensive spatial sampling of the brain and can look deep into subcortical structures. Functional magnetic resonance imaging (fMRI) with blood oxygenation level-dependent (BOLD) contrast is an important tool for mapping brain activity. Because fMRI has good spatiotemporal resolution and allows noninvasive imaging of almost the entire brain, it has great translational possibilities (Matthews et al. 2006). The BOLD signal, however, reports indirectly on neural activity because it measures the hyperemic response (Menon et al. 1993). BOLD–fMRI signals depend on blood oxygenation and cerebral blood flow and oxidative metabolism, the specific implications of which we will discuss, and can therefore provide useful surrogate information about neuronal activity (Ogawa et al. 1990, 1993, 1998).

There has been enormous interest in utilizing fMRI to study normal and abnormal brain function in humans. Simultaneous EEG–fMRI is an ideal method to study the interdependent neuronal, neuroenergetic, and hemodynamic changes that occur during brain activity. However, human fMRI studies of pathological brain processes have been limited. As fMRI techniques are highly sensitive to motion, many human studies are limited to the study of neuronal processes with limited movement, such as the spike-wave seizures associated with absence epilepsy, the interictal (between seizures) period of other epilepsy syndromes, the intrinsic mental state (resting state), or purely cognitive tasks. Secondly, human studies are inherently less well

controlled than animal models due to intersubject variability, while in animal models consistent experimental methods and invasive techniques can be used.

Animal models offer the opportunity to fully utilize the power of EEG–fMRI methods to noninvasively record normal and abnormal activity across brain networks. The ictal (during seizure) activity of multiple seizure types can be investigated using animal models, and these studies are not limited by movement as animals can be studied under anesthetized, paralyzed, and ventilated conditions. Variables affecting brain activity can be better controlled in animals, such as the onset and type of seizure, and the induction and type of anesthesia. Furthermore, invasive studies of electrical, hemodynamic, and histological properties can be performed in animals to relate fMRI signals to underlying neuronal activity. Thus, simultaneous EEG–fMRI studies of animal models can provide an important contribution to the understanding of many types of neuronal activity, including epilepsy, sleep, and sensory–motor processing. Additionally, studies of animal models can contribute to our knowledge of fMRI interpretation, thereby informing our understanding of neuroimaging studies in humans and the neuronal basis of human pathology. Human studies of simultaneous EEG–fMRI including those of epilepsy, sleep, evoked activity, behavior, and cognition have recently been reviewed elsewhere (Salek-Haddadi et al. 2002; Ritter and Villringer 2006).

Many animal MRI studies are highly relevant for investigating changes in functional and structural anatomy and exploring physiology (Blumenfeld 2007; Grohn and Pitkanen 2007; Hiremath and Najm 2007). In this chapter we will focus on studies that employed *simultaneous* EEG–fMRI methods in the same preparation.

27.2 Advantages of EEG–fMRI in Animal Models

Animal models offer a number of distinct advantages, compared to human subjects, in utilizing simultaneous EEG–fMRI to study neuronal function. Animal models allow the investigator to exert greater control over the timing and conditions of neurological events, including seizures, sleep, and sensory–motor processing. Animal models also allow for the invasive monitoring and control of anesthesia and physiological parameters that may influence neuronal activity and fMRI signal changes. Small animal models allow for the use of higher magnetic field strengths up to 16.4 T, where the hemodynamic response to neural activity is more sensitive to BOLD contrast mechanisms (Menon et al. 1993; Turner et al. 1993; Yang et al. 1999). Additionally, the use of paralyzed animals allows for the near elimination of movement artifact, important for all fMRI studies and particularly so for studying events associated with excessive muscle activity, such as partial or generalized motor seizures. Finally, balistocardiogram artifact (i.e., strong electrical signals from the heart), a common problem in human fMRI, is comparatively minimal in small animals (Sijbers et al. 2000).

Animals also provide an excellent model for studying the relationship between neuronal activity and cerebral hemodynamic and metabolic responses. These fundamental relationships can be studied with invasive electrophysiological

measurements and multiple imaging techniques (Logothetis et al. 2001; Schwartz and Bonhoeffer 2001; Smith et al. 2002; Hyder and Blumenfeld 2004; Nersesyan et al. 2004a, b; Shmuel et al. 2006; Maandag et al. 2007; Schridde et al. 2007; Sanganahalli et al. 2016). Simultaneous EEG–fMRI investigations can guide in vivo bench studies to specific brain regions of interest and contribute to elucidating molecular/cellular mechanisms related to seizure susceptibility or other disorders. Finally, animal models with genetic variants can be studied with simultaneous EEG–fMRI to examine the neurophysiological changes associated with these genes.

27.3 Limitations and Technical Challenges of EEG–fMRI in Animal Models

Animal models are only an approximation of human disease and need to be interpreted with appropriate caution. There are also several technical challenges to simultaneous EEG–fMRI studies of animals related to their size and the spatial constraints due to using relatively high magnetic fields (Blumenfeld 2007; Mirsattari et al. 2007).

Although desirable for many investigations, recording simultaneous EEG–fMRI in animals presents a number of challenges. Anesthesia must be carefully considered; as we will discuss, many anesthetic agents can alter the cerebral hemodynamic response and may alter the neurophysiological behavior under investigation. Guaranteeing the quality of the MR image can be a formidable challenge, as the imaging signals are sensitive to small degrees of movement, and to magnetic susceptibility differences, especially at air–tissue interfaces, that can introduce unwanted image distortions. Animal movement in the scanner must be restricted, either by chemical muscular blockade (curarization) or through habituation to a restraining device in awake experiments. Electrodes must be carefully chosen to avoid unwanted interactions with magnetic fields and with the tissue (e.g., scalp, subdermal, brain) they contact. Lastly, animal physiology must be carefully monitored during experiments utilizing anesthesia (Mirsattari et al. 2005a, b).

Investigations of particular brain processes will present their own unique challenges. For example, animal studies of epilepsy often encounter additional complications as seizure activity is prone to alteration by commonly used anesthetic agents, seizures may be difficult to induce in anesthetized animals, and motion artifact can occur during seizures (Blumenfeld 2007).

27.4 Anesthesia

Choosing an appropriate anesthetic agent is crucial in simultaneous EEG–fMRI studies; considerations of the agent's effects on the EEG data, fMRI signal intensity, long-term physiology, and on the neurological event being studied must all be carefully considered. Furthermore, anesthetic agents are known to induce changes in the EEG data (Winters 1976; Sloan 1998; Hudetz 2002), and different experimental designs are best served by different combination of anesthetic agents.

Anesthetic agents that are inhaled may be ideal for some designs because of the swiftness with which the depth of anesthesia can be adjusted (Makiranta et al. 2005; Mirsattari et al. 2005a, b). However, these agents can alter the hemodynamic response. Isoflurane has been found to greatly diminish the BOLD signal changes seen in the gamma-butyrolactone (GBL)-induced spike-and-wave discharge (SWD) rat model (Tenney et al. 2003). Conversely, the use of both fentanyl and haloperidol does not block the occurrence of SWDs in two rat genetic models of absence epilepsy (Pinault et al. 1998; Nersesyan et al. 2004a, b). Furthermore, haloperidol can actually increase the frequency of SWDs (Coenen and Van Luijtelaar 1987; Midzianovskaia et al. 2001). Fentanyl in combination with haloperidol has also been used successfully to produce anesthesia without blocking tonic-clonic seizures in a rat model (Nersesyan et al. 2004a, b; Schridde et al. 2007).

A change in the strength of the BOLD–fMRI signal compared to the awake state can be seen with anesthetic agents such as alpha-chloralose (Shulman et al. 1999; Peeters et al. 2001; Hyder et al. 2002a, b; Smith et al. 2002) propofol (Lahti et al. 1999) and halothane (Maandag et al. 2007). In a porcine model, sudden deepening of thiopental anesthesia in nonepileptic animals produced significant signal changes in the fMRI response (Makiranta et al. 2002). High-dose morphine and the sedating antihistamine acepromazine was found to provide adequate anesthesia in a sheep model of penicillin-induced focal epilepsy with minimal EEG suppression (Opdam et al. 2002). Alpha-chloralose with urethane has been successfully used in a rat model of pentylenetetrazol-induced seizures (Keogh et al. 2005). Ketamine and xylazine produce adequate anesthesia without blocking limbic seizures studied by fMRI (Englot et al. 2008).

In a rat model, halothane was found to have no effect on the BOLD response at doses that showed a clear reduction in the baseline neuronal activity on EEG, while a transition from halothane to alpha-chloralose showed an immediate reduction in the spatial extent of the BOLD response without a change in the peak signal change, which evolved over several hours to an increase in both the spatial extent and peak signal change of the BOLD signal (Austin et al. 2005; Maandag et al. 2007). Halothane has been successfully used to induce temporary anesthesia in rodent models during subject preparation, with data acquired from paralyzed non-anesthetized animals treated with mivacurium (Van Camp et al. 2003), however, special training is needed for non-anesthetized preparations as discussed shortly. Halothane is commonly used as an induction agent to allow rapid anesthesia of an animal for placement of intravascular lines, tracheostomy, electrodes, and placement in a holding apparatus for positioning of the surface coil (Nersesyan et al. 2004a, b, Schridde et al. 2007). A 1-h period has been used to allow complete washout of the halothane (Keogh et al. 2005).

Limiting the use of general anesthesia to the period of preparing the animal with reversal of the anesthesia during simultaneous EEG–fMRI acquisition has also been accomplished with the combination of the anesthetic medetomidine (alpha 2-adrenoreceptor agonist) and the reversal agent atipamezole (alpha 2-adrenergic antagonist) in rats (Tenney et al. 2003), or with ketamine and medetomidine reversed with atipamezole in rats (Tenney et al. 2004a, b; Brevard et al. 2006), or with the

combination of medetomidine, ketamine, and isoflurane reversed with atipamezole in marmoset monkeys (Tenney et al. 2004a, b).

In situations where significant movement does not occur, such as during spike-wave seizures or during the resting state, the study of unanesthetized animals may be feasible (Tenney et al. 2003; Van Camp et al. 2003; Scholvinck et al. 2010). This raises additional technical challenges, as lengthy training of animals is necessary to habituate them to the recording procedures (Khubchandani et al. 2003; Sachdev et al. 2003). Recording from awake animals can further be facilitated by the use of a topical anesthetic (e.g., lidocaine gel) at any pressure points from restraint devices or needle electrodes (Tenney et al. 2004a, b). Performing simultaneous EEG–fMRI studies in awake animals is an important technical challenge to overcome as these studies more closely resemble human studies of conscious subjects.

The anesthetic approaches discussed show great promise in expanding the utility of EEG–fMRI studies in animal models and in contributing to our understanding of human studies. The wide variety of successful protocols illustrates the importance of tailoring the experimental design to the specific animal model and research question being investigated.

27.5 Movement: Curarization and Habituation

As in human studies, subject movement must be addressed in studies with animal models to limit the creation of artifact in the MR images. As previously discussed, anesthetic agents must be carefully considered for possible interference with the neurological event being studied and for possibly altering the hemodynamic response. Lightly anesthetized preparations or unanesthetized preparations are advantageous for preserving the normal electrophysiology and neurovascular response but will increase the likelihood of movement by the subject. This has been overcome by curarization with non-depolarizing neuromuscular blockers, such as mivacurium (Van Camp et al. 2003), pancuronium (Opdam et al. 2002; Makiranta et al. 2005), D-tubocurarine (Nersesyan et al. 2004a, b; Schridde et al. 2007; Englot et al. 2008), or vacuronium (Mirsattari et al. 2006). Curarization requires the animal be ventilated (e.g., tracheotomy or tracheal intubation) and their physiology monitored throughout the experiment.

Habituation to the restraint device and noise of the MRI scanner is required for the study of awake and conscious animals. This has been accomplished through the use of habituation to a custom designed restraint devices in rats (Khubchandani et al. 2003; Sachdev et al. 2003) and monkeys (Scholvinck et al. 2010). Habituation to a restraint device may be facilitated by positive reinforcement (e.g., chocolate milk) combined with diazepam administrated 1 h prior to data acquisition to minimize stress (Sachdev et al. 2003).

An important problem can arise in high-field magnet even with well-habituated and carefully head-fixed animals, especially with rodents. The shimming (homogenizing the B_0 field in the studied volume) is important in MRI experiments because it is the base of identification of voxel location, that is, the three dimensional

position of every independently measured data point is coded by frequency shift regarding the B_0 field. Since a small movement (e.g., licking, chewing, whisking) of the animal inside or outside just below the shimmed brain volume can change the B_0 field, the voxel locations apparently change in the recording since the reference point of the frequency code changed. Moreover, the signal origin of the voxels can be very distant from the location of the voxel.

It is critical to review data carefully after acquisition for movement artifact using methods such as cine review, center of mass analysis (Nersesyan et al. 2004a, b) and to reject data in which significant movement or B_0 field-related apparent movement occurs, since even miniscule movements can produce large false fMRI signal changes on difference calculations. Movement artifact can further be corrected with multichannel post-processing algorithms, such as reference layer artifact subtraction, Moiré phase tracking, and wire loop motion sensors.

27.6 Physiology

Physiological stability is crucial in the study of animals during simultaneous EEG–fMRI. Animal models are commonly studied using inhaled anesthetic agents, which require that the animals undergo a tracheostomy and be ventilated. Animals require physiological stabilization for the duration of the experiment (Wood et al. 2001). Monitoring of heart rate, blood pressure, temperature, and ventilation rate can be done continuously (Nersesyan et al. 2004a, b; Schridde et al. 2007). Arterial blood gas measurements of pH, pCO2, and pO2 can be performed to monitor the physiological state of the animal, as these parameters will affect the hemodynamic response and may affect neuronal function (Jones et al. 2005; Mirsattari et al. 2005a, b). Mechanical ventilation may be required for some anesthesia regiments or when muscle paralysis is used (Nersesyan et al. 2004a, b; Tenney et al. 2004a, b; Schridde et al. 2007). Mechanical ventilation, blood pressure monitoring, and anesthesia delivery machinery should be kept far from the imaging field to avoid disturbances in the images.

Hypercapnia can alter the cerebral hemodynamic response, causing vasodilatation of veins and microcapillaries in rat cortex at even mild levels (Nakahata et al. 2003). Hypercapnia has also been shown to reduce blood flow and volume changes during whisker stimulation and may also affect changes in the BOLD–fMRI signal (Jones et al. 2005). Furthermore, hypercapnia can alter neuronal activity in rats (Kida et al. 2007) possibly by inducing periods of cortical desynchronization that may be associated with changes in oxidative metabolism (Martin et al. 2006).

27.7 MRI Compatible Electrodes

MRI-compatible electrodes and EEG recording equipment has been developed and utilized in multiple studies using simultaneous EEG–fMRI (Mirsattari et al. 2007). EEG electrodes commonly contain metals that are affected by an external magnetic

field; silver–silver chloride (Ag/AgCl), gold-plated silver, platinum, stainless steel, and tin. Silver and copper electrodes are theoretically compatible with MRI but are not appropriate for invasive recording that may involve direct contact of the electrode to brain tissue due to possible toxicity (Babb and Kupfer 1984). Gold and platinum electrodes have been found to be nontoxic to living tissue (Tallgren et al. 2005). Custom-made gold electrodes were found to be superior compared to both custom-made carbon and commercial platinum–iridium alloy electrodes in size and effect on image quality (Jupp et al. 2006). However, gold and platinum may cause artifacts in MR images due to differences between their magnetic susceptibly and that of brain tissue (Mirsattari et al. 2007). Choosing appropriate MRI compatible EEG recording equipment will depend on whether the goal is for scalp, subdermal, or intracranial recordings.

Scalp and subdermal electrodes have the advantage of leaving the brain intact and theoretically will introduce the least amount of artifact in the MR images. Carbon fiber electrodes are the most widely used material for EEG with simultaneous MRI, for scalp (Van Audekerkea et al. 2000) and subdermal recordings (Nersesyan et al. 2004a, b; Makiranta et al. 2005; Schridde et al. 2007), and directly overlying the cortex via insertion through burr holes (Mirsattari et al. 2006). Carbon fiber electrodes can also be used for intracranial recordings (Opdam et al. 2002; Mirsattari et al. 2005a, b; Motelow et al. 2015). Teflon-coated silver–silver chloride (Ag/AgCl) electrodes can be used alone or in combination with carbon fiber electrodes (Mirsattari et al. 2005a, b; Young et al. 2006). fMRI-compatible electrodes designed for human use, such as conductive plastic cups and gold-plated silver disc electrodes attached to copper wires can be used in larger animal studies (Mirsattari et al. 2007).

Intracranial EEG recordings with simultaneous fMRI has the advantage of recording neuronal activity from specific areas of the brain, such as the occipital cortex (Logothetis et al. 2001; Shmuel et al. 2006), or from the site of seizure induction in animal models of focal epilepsy (Opdam et al. 2002; Englot et al. 2008). However, intracranial electrode placement increases the risk of damaging the cerebral cortex and may cause artifact in the MR images if there is bleeding under the burr holes or at the craniotomy site (Mirsattari et al. 2007). Burr holes should be made with a drill that is compatible with MRI, for example, one coated by titanium or made of diamond to avoid artifacts from any metallic particles the drill may leave (Mirsattari et al. 2007).

Intracranial electrodes may also be used for stimulating brain regions during fMRI experiments. Electrical stimulation has been accomplished in the rat; including in the motor cortex with carbon fiber electrodes (Austin et al. 2003), in the amygdale kindling model with custom-made carbon and gold electrodes, and commercial platinum–iridium electrodes (Jupp et al. 2006), in rat medial thalamus with glass-coated carbon fiber microelectrode (Shyu et al. 2004), and in perforant pathway (Angenstein et al. 2007) and dorsal hippocampus using bipolar tungsten electrodes (Englot et al. 2008). Precise electrical stimulation of the Macaque monkey visual cortex using custom glass-coated iridium microelectrodes during fMRI signal acquisition has also been done (Tolias et al. 2005). Recently, optogenetic

stimulation (using specifically emitted wavelengths to activate genetically inserted light-sensitive channels) with simultaneous fMRI has been achieved with carbon fiber optrodes (Duffy et al. 2015; Chuapoco et al. 2019).

27.8 fMRI Signal Generation

The BOLD–fMRI signal (S) is indirectly related to neuronal activity. Animal models provide an excellent opportunity to more precisely investigate this relationship. Neuronal activity consumes energy, which is repleted through increased delivery of oxygen and nutrients via neurovascular and neurometabolic coupling. Measurement of S depends on levels of oxygenated versus deoxygenated hemoglobin (Ogawa et al. 1998), and therefore on the balance between oxygen delivery and consumption. During neuronal activity, there is an increase in cerebral blood flow (CBF) and oxygen delivery through neurovascular coupling, but there is also an increase in the cerebral metabolic rate of oxygen consumption ($CMRO_2$) (Ogawa et al. 1998; Hyder et al. 2001). Increased oxygen delivery normally exceeds oxygen consumption, so that S usually increases in response to increased neuronal activity. However, as we will discuss below, exceptions can occur, especially during the intense neuronal activity accompanying tonic-clonic seizures. The complex relationship between changes in BOLD signal compared to baseline ($\Delta S/S$) and physiology is given in Eq. (27.1) (Kennan et al. 1994; Weisskoff et al. 1994; Ogawa et al. 1998).

$$\Delta S / S = M\left[1-\left(\mathrm{CMR_{O2}} / \mathrm{CMR_{O2,0}}\right)^{\beta}\left(\mathrm{CBF} / \mathrm{CBF_0}\right)^{-\beta}\left(\mathrm{CBV} / \mathrm{CBV_0}\right)\right] \quad (27.1)$$

where α links CBV to CBF by a power law relationship ($0 < \alpha < 0.4$) originally described by PET scans in primates (Grubb et al. 1974), β links CMR_{O2} to CBF by a power law relationship ($1 < \beta < 2$) measured both in human and rat brain (Hyder et al. 2000), M is an echo time-dependent constant that incorporates the resting hemodynamic and metabolic values (Hoge et al. 1999; Hyder et al. 2001), and the parameters with and without subscripted "0" represent the basal and activated values, respectively. To quantify CMR_{O2} with Eq. (27.1), parameters like M, α, and β are needed in conjunction with independent measurements of BOLD, CBV, and CBF (Hoge et al. 1999; Hyder et al. 2001). All of these parameters can be measured in animals (Kida et al. 2007; Shu et al. 2016a, b) and in principle they can be measured in humans as well. Although CBV is not directly measured in human studies, it can be measured in animal studies with exogenous superparamagnetic MRI contrast agents that primarily reside in the intravascular space (for recent reviews, see Hoge 2012; Hyder and Rothman 2012). Because the majority of neuronal energy is ultimately produced through oxidative metabolism (Shulman et al. 2004) measuring changes in the $CMRO_2$ offers the most direct neuroimaging measure of neuronal activity. We will discuss further the complex relationship between various cerebral blood flow parameters, neuronal activity, and the BOLD signal, as exemplified with somatosensory cortical (Sanganahalli et al. 2009; Herman et al. 2013) and

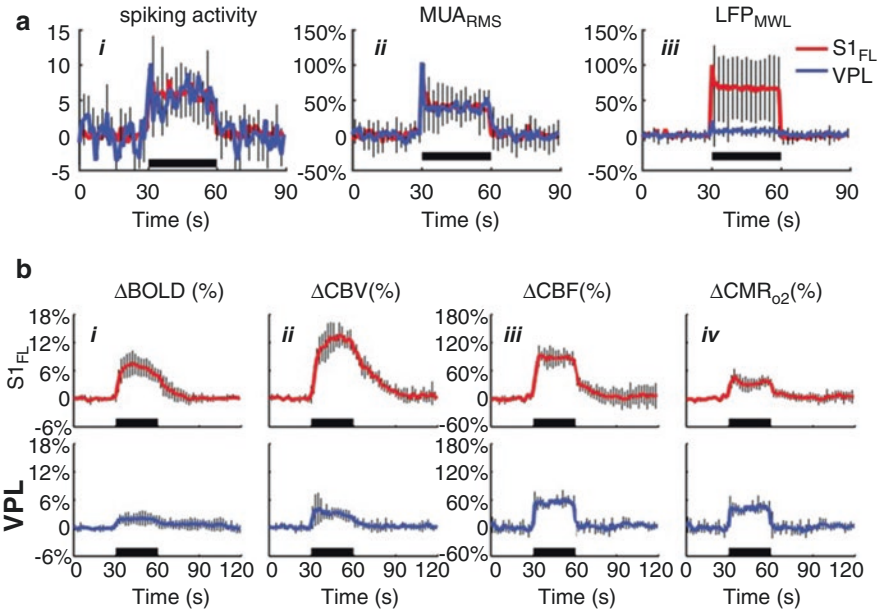

Fig. 27.1 Multimodal sensory-induced responses. (**a**) Sensory-induced dynamics of spike rate and relative MUA changes in S1FL (red) and VPL (blue) during forepaw stimulation (i.e., 30 s black horizontal lines). The data represent mean ± SD of many trials from six rats (each trial: 30 s rest, 30 s stimulation, 30 s rest). The spike rate change is shown from the basal firing in each region. The MUA data are shown as 1-Hz root mean square (RMS) time courses, with a binned RMS approach. The MUA responses (both spike rate change and MUARMS) were not significantly different between S1FL and VPL. The mean wavelet response of LFPs (LFPMWL) were calculated. LFPMWL responses between S1FL and VPL are significantly different. The evoked LFP at VPL are significantly smaller than S1FL. The LFP data are shown as maximum wavelet coefficient responses (see Methods). (**b**) Sensory-induced dynamics of hemodynamic (ΔBOLD, ΔCBV, and ΔCBF) and metabolic (ΔCMRO2) responses from the contralateral S1FL (red) and VPL (blue) during forepaw stimulation (i.e., 30 s black horizontal lines). All signals were represented as the fractional change from the pre-stimulus baseline. These data represent the mean ± SD of many trials in each case across different subjects. The measured time courses of BOLD, CBV, and CBF were localized to the middle layers of S1FL and VPL, and they were used to calculate the respective CMRO2 responses by calibrated fMRI. The stimulus presentation is indicated by horizontal black bar. (Reproduced with permission from Sanganahalli et al. 2016)

subcortical (Sanganahalli et al. 2016) activation with forepaw stimulation in a rodent (Fig. 27.1) (Sanganahalli et al. 2016).

27.8.1 Measurement of $CMRO_2$ by MR Spectroscopy

fMRI signals originate with changes in energy consumption and blood flow. Neuronal activity is dependent on neurotransmission, the stoichiometry of glutamate and GABA neurotransmission, and the energy consumption supplied by

glucose oxidation, as has been established in vivo by ^{13}C magnetic resonance spectroscopy (MRS) (Rothman et al. 1999). The relationship between neuronal activity and energy consumption provides insight into brain function and the interpretation of the neuroimaging signal obtained in fMRI experiments (Shulman et al. 2001, 2002). Early ^{13}C MRS experiments in animals and humans used glucose labeled at the C1 carbon atom (Behar et al. 1986; Gruetter et al. 1994). Infused glucose-C1 enters the TCA cycle via pyruvate dehydrogenase activity and labels glutamate-C4 in the first turn of the neuronal TCA cycle. The C3 and C2 carbon atoms are labeled in the following turn of the cycle. Thus, the time course of ^{13}C turnover of glutamate-C4 can be converted into a measure of the neuronal TCA cycle flux (Mason et al. 1992, 1995; Gruetter et al. 1998).

27.8.2 Estimation of $CMRO_2$ by Calibrated BOLD

Equation (27.1) can be rearranged and approximate $CMRO_2$ maps can be obtained where $\Delta CMRO_2/CMRO_2$ can be calculated by using the data from separate measurements of $\Delta CBF/CBF$, $\Delta S/S$, and $\Delta CBV/CBV$ in the same experiment (Kida et al. 2000; Hyder 2004). This technique is referred to as "calibrated BOLD" and has been validated by showing agreement with $CMRO_2$ measurements made using MRS during somatosensory stimulation over a wide range of conditions (Hyder et al. 2002a, b, 2010; Sanganahalli et al. 2009, 2016; Herman et al. 2013). Changes in spiking frequency have been directly linked to calibrated fMRI measurements of energetics in rat somatosensory cortex (Smith et al. 2002; Maandag et al. 2007). Calibrated BOLD allows $CMRO_2$ maps to be obtained at the same spatial and temporal resolution as fMRI, which is much higher than in MRS experiments. Although $CMRO_2$ can be measured by neuroimaging methods, the BOLD–fMRI signal is a more convenient, although indirect, method of mapping neuronal activity.

27.8.3 CBV

CBV-weighted fMRI, using long half-life and plasma-borne intravascular contrast agents, has become an attractive alternative to BOLD-weighted fMRI in animal models. As the earliest fMRI maps of human brain function with CBV contrast using repeated bolus injections of a paramagnetic contrast agent that has a relatively short half-life in blood circulation (Belliveau et al. 1991), intravascular paramagnetic contrast agents that maintain a steady blood concentration over several hours have allowed CBV measurements in animals with much better spatiotemporal resolution (Kennan et al. 1998). Because these MRI contrast agents are solely plasma borne (Mandeville et al. 1998), concerns remain about whether these signals reflect changes in total CBV.

The relative changes in CBV from baseline can be measured by the administration of a high susceptibility MRI contrast agent to enhance the blood volume-induced changes (Hyder et al. 2002a, b). An ultrasmall iron oxide nano-colloid

particles (AMI-227, Combidex; 15 mg/kg; AMAG) agent can be used to measure CBV contrast, and the agent remains in the intravascular space for several hours (Kennan et al. 1994).

27.8.4 CBF

Absolute CBF maps can be obtained by using spin echo slice selective and non-slice selective inversion recovery-weighted EPI data (Hyder et al. 2001). Arterial spin labeling (ASL) MRI utilizes endogenous water as a magnetic contrast agent. Arterial blood water flowing into the brain is saturated in the neck region with a slice-selective saturation imaging sequence, creating an endogenous tracer in the form of saturated or inverted spins. As this RF-labeled arterial water enters the brain, it mixes with unlabeled tissue water in the brain. The perfusion level is commensurate with level of signal change in brain. This technique allows regional perfusion maps to be measured noninvasively (Detre et al. 1992; Detre and Wang 2002). Optical imaging techniques like laser Doppler flowmetry (LDF) can measure CBF, although these methods differ in the underlying physical mechanisms from ASL-MRI (He et al. 2007). LDF values for CBF have proven useful in calculating $CMRO_2$ and are comparable to CBF measurements acquired using ASL-MRI (Mandeville et al. 1999; He et al. 2007; Schridde et al. 2007; Herman et al. 2009).

27.9 Signal Artifact and Artifact Removal

Signal artifact presents an additional problem as fMRI equipment can cause artifact in the EEG recording in general, and particularly during image acquisition (Ives et al. 1993), EEG equipment can cause significant artifact in the fMRI images (Krakow et al. 2000). Gradient coil-induced magnetic field variations and radiofrequency pulses associated with image acquisition can cause high voltages in the EEG recording electrodes that obscure EEG signals. Revealing the full EEG signal may require removal of the MRI artifact through offline digital filtering, including simple low-pass frequency filtering (Fig. 27.2) (Nersesyan et al. 2004a, b), or using methods such as temporal principle component analysis (Negishi et al. 2004). Care must be taken in placing the EEG electrodes and stabilizing screws on the animal skull in such a way as to minimize unwanted magnetic field inhomogeneity and image distortion (Nersesyan et al. 2004a, b).

Movement-related artifact has already been discussed, and any runs containing significant movement should be rejected from the analysis. Low frequency drift can also occur, especially during prolonged fMRI acquisitions, which may be related to a number of physiological or technical factors. It is important to be aware of these slow signals, and to take them into consideration when planning data analysis, or to prevent them at the source when appropriate. Although low frequency drift in some situations can be related to physiology, in other cases it can be shown to occur due

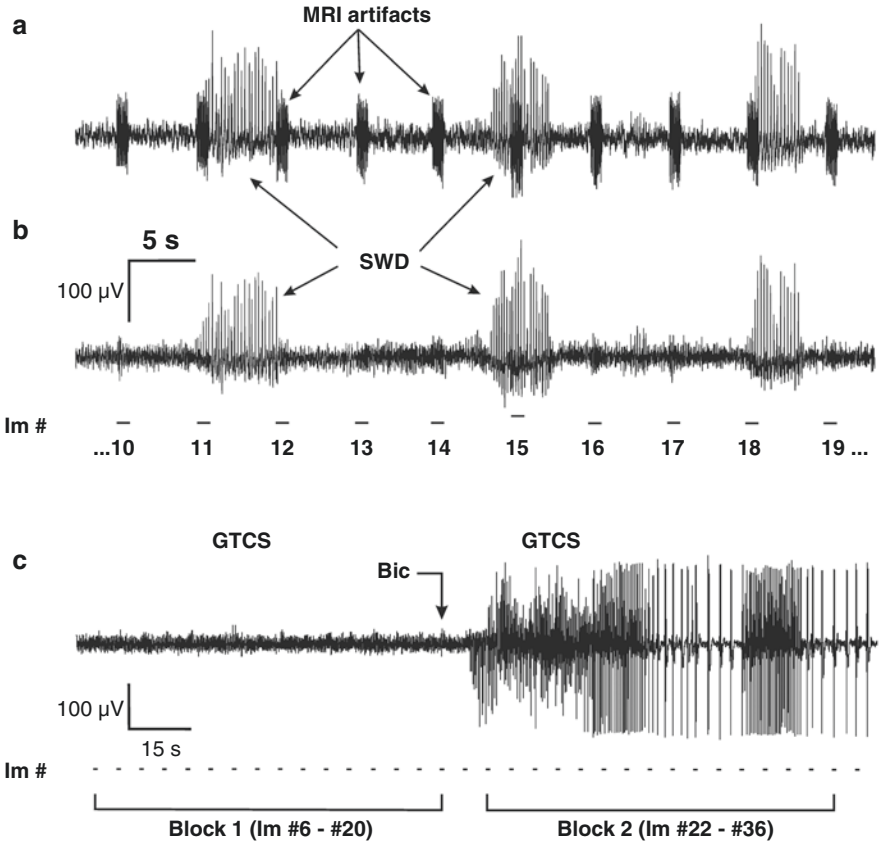

Fig. 27.2 EEG recordings from simultaneous EEG–fMRI experiment of spike-wave discharges (SWD) and generalized tonic clonic seizures (GTCS) in the rat. (**a**) EEG acquired from WAG/Rij rat showing intermittent episodes of SWD. Large high-frequency artifacts produced by the MRI gradient coils appear every 5 s during the MRI data acquisitions, partially obscuring the EEG. (**b**) Digital low-pass filter with 30-Hz cutoff eliminates most of the MRI-related artifacts. Image acquisition numbers (Im #) for this data run are seen below the EEG tracing. To analyze SWD images versus baseline, *t*-maps were constructed comparing pairs of consecutive images, each consisting of a quiet baseline image just before a given SWD, followed immediately by an image acquired during or within 2 s after the same SWD. In the example shown here, pairs of consecutive baseline and SWD images, respectively, would include images, #11 and 12; 14 and 15; 18 and 19; and other similar pairs from this data run. Baseline images Bi (images 11, 14, 18, etc.) were then contrasted with SWD images Ai (images 12, 15, 19, etc.) to construct *t*-maps. Scale bar in (**b**) applies to EEG traces in both (**a**) and (**b**). (**c**) EEG acquired during a bicuculline-induced GTCS. The seizure onset is predictable and occurred approximately 5 s after the bolus injection of 0.2 mg intravenous bicuculline (Bic, arrow). Average BOLD signal changes can be calculated by comparing two blocks of images ($n = 15$ per block) corresponding to baseline (Block 1) and the initial portion of the seizure (Block 2) on the EEG. Baseline images Bi (images 6–20 in the example) were contrasted with seizure images Ai (images 22–36 in the example) to construct the *t*-map. (Reproduced with permission from Nersesyan et al. 2004a, b)

to purely technical factors and not physiology (e.g., by demonstrating similar drift when scanning a phantom or a nonliving perfused brain).

27.10 Data Analysis

Data analysis of simultaneous EEG–fMRI experiments allows for pairing of fMRI acquisitions with neuronal signal. Prior knowledge of the time course of CBF changes during the neuronal function being studied will direct the analysis of the fMRI signal. For example, in analyzing fMRI signals during rodent spike-wave discharges (SWD), prior measurements using LDF showed that CBF peaked 3–4 s after SWD onset began on EEG, and then decreased back to baseline after 3–4 s (Nersesyan et al. 2004a, b). Pixel-based measurements of the BOLD signal response showed a similar time course (Nersesyan et al. 2004a, b). Therefore, in constructing functional maps of BOLD signal changes during SWD compared to baseline, it was first assumed that each BOLD image acquisition should be related mainly to SWD occurring in the preceding 5-s EEG interval. Pairs of consecutive images and associated pairs of consecutive EEG intervals were selected where the first EEG interval contained quiet EEG baseline, and the second contained SWD (Fig. 27.2a, b) (Nersesyan et al. 2004a, b). Statistical *t*-maps can also be constructed by be combined with region of interest (ROI) analysis to evaluate differences in BOLD signal change and time course limited to specific brain regions (Fig. 27.3) (Tenney et al. 2003, 2004a, b; Schridde et al. 2007; Mishra et al. 2011).

Alternatively, the time course of generalized tonic-clonic seizures (GTCS) begins with an abrupt onset of sustained, high-frequency neuronal firing during the tonic phase, followed by rhythmic high-frequency firing in the clonic phase with a total duration of several minutes (Matsumoto and Marsan 1964; Avoli et al. 1990). Therefore, analysis of more prolonged events such as tonic-clonic seizures requires a different approach to analysis. Comparison of bicuculline induced tonic-clonic seizures to baseline activity has been done by comparing a set of baseline images before bicuculline injection to a set of images after seizure onset (Fig. 27.2c) (Nersesyan et al. 2004a, b; Schridde et al. 2007). *t*-maps can then be constructed by comparing the set of baseline images to the set of images during the beginning of seizure activity (Fig. 27.4) (Nersesyan et al. 2004a, b, Schridde et al. 2007).

Hierarchical clustering algorithms can also be used to identify voxels of interest in the fMRI data (Keogh et al. 2005). The clustering analysis utilizes a *t* test applied independently to each voxel, comparing a chosen baseline period to a period of signal activity; voxels without significant changes are discarded. Voxels that are acting similarly to another portion of brain can be chosen by applying a further test requiring that each voxel have a correlation with two other voxels.

Changes in $CMRO_2$ can be estimated for individual brain regions using the known general relationship between oxygen consumption and BOLD, CBV, and CBF data at steady state (Eq. 27.1) (Kida et al. 2007; Schridde et al. 2007). This can be done using CBF values obtained from ASL-MRI or from LDF, together with separate measurements of BOLD and CBV (Fig. 27.5) (Schridde et al. 2007).

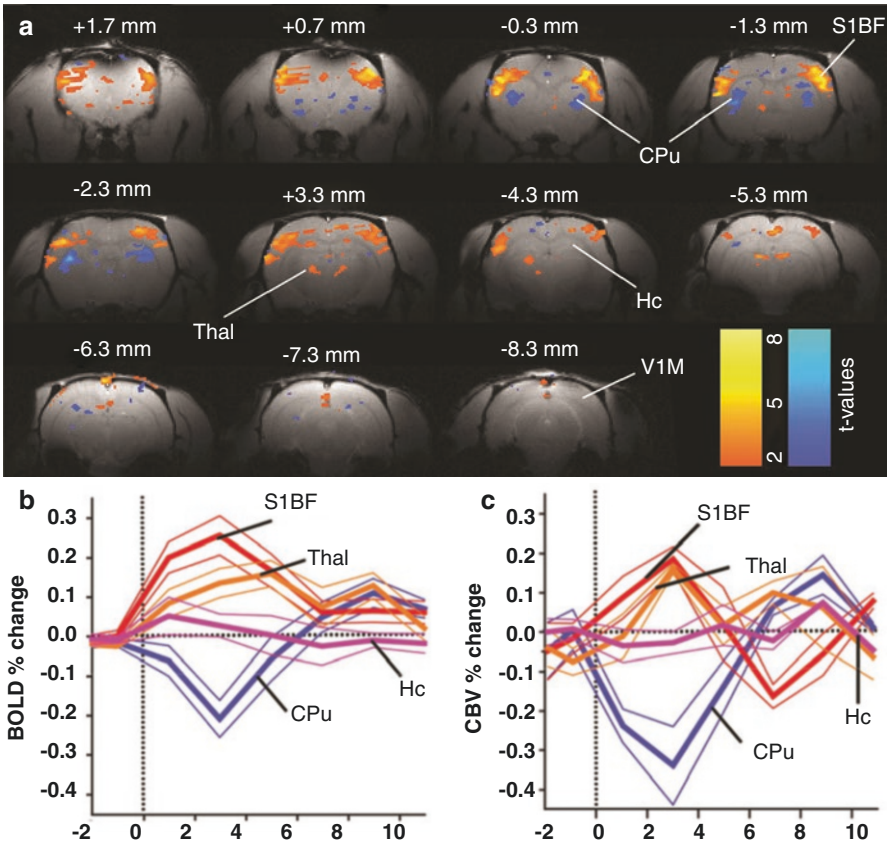

Fig. 27.3 BOLD fMRI and CBV increase in S1BF and thalamus (Thal) but decrease in CPu during SWDs. Time course of signals is displayed as percentage change relative to pre-seizure baseline data. (**a**) Example of BOLD fMRI changes 2–4 s after SWD onset in a WAG/Rij rat at 9.4 T. S1BF and thalamus (Thal) show prominent increases in BOLD signal during SWDs. Prominent BOLD decreases are present in the CPu. No changes are seen in V1M or hippocampus (Hc). Smaller changes are seen in other areas. Simultaneous EEG acquired during fMRI was used to identify images obtained 2–4 s after SWD onset for comparison with baseline images obtained immediately before start of SWDs. Results are displayed as *t* maps of BOLD–fMRI signal superimposed on high-resolution anatomical images. *t* values were generated using a paired *t* test in which pairs consisted of one seizure acquisition taken 2–4 s after seizure onset and the baseline images acquired just preceding SWD onset ($n = 26$ SWD episodes). Slices are shown from anterior to posterior, with approximate coordinates relative to bregma (Paxinos and Watson 1998). Color bars indicate *t* values for increases (warm colors) and decreases (cold colors). Threshold value $t > 2$. (**b**) BOLD signals changes ($n = 22$ animals; data are from 1856 SWDs total). (**c**) CBV signal changes ($n = 5$ animals; data are from 418 SWD total). Time courses are displayed as mean ± SEM, with 2-s time bins. Vertical line at time = 0 marks SWD onset. Hc, Hippocampus. (Reproduced with permission from Mishra et al. 2011)

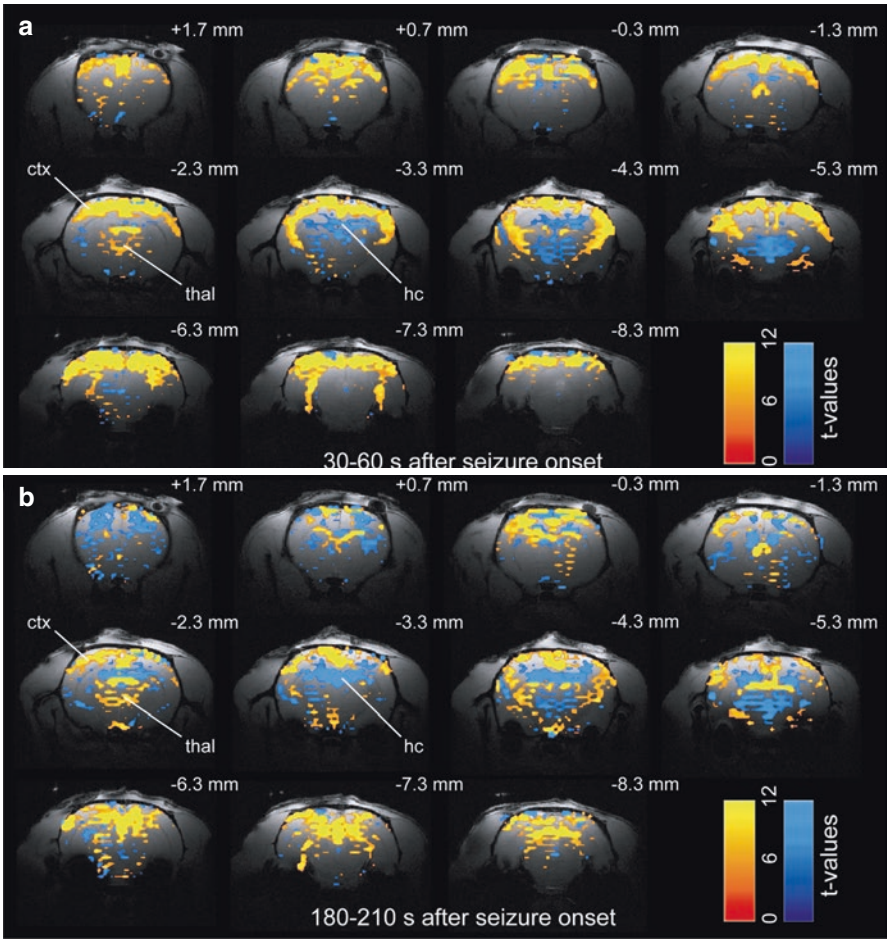

Fig. 27.4 BOLD–fMRI increases and decreases at 9.4 T during bicuculline-induced generalized tonic clonic seizure (GTCS) in Wistar rats. (**a**) BOLD–fMRI signals during the beginning of the seizure show not only a mixed pattern of widespread increases across the whole brain, including cortex (ctx) and thalamus (thal) but also prominent focal decreases, especially in hippocampus (hc). (**b**) Toward the end of the seizure, BOLD increases became less prevalent, though still prominent, whereas decreases became more widespread throughout the brain. In (**a**) and (**b**), *t*-maps are shown for 30 s of data (ten consecutive fMRI images acquired every 3 s) during seizure compared with 30 s baseline. Maps are superimposed on high-resolution anatomical images. Slices are shown from anterior to posterior, with approximate coordinates relative to bregma (Paxinos and Watson 1998). Color bars indicate *t* values for increases (warm colors) and decreases (cool colors). (Reproduced with permission Schridde et al. 2007)

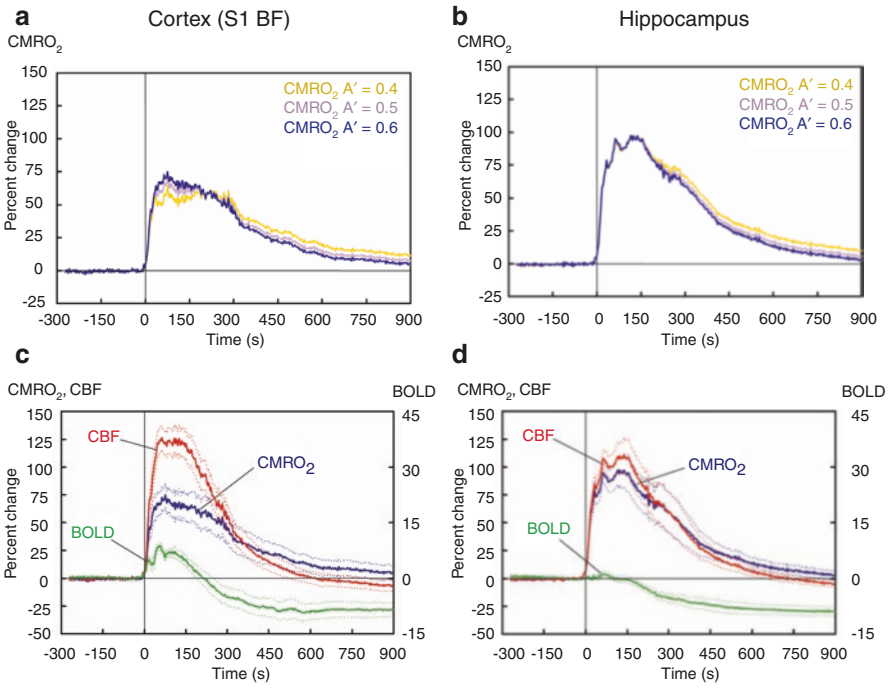

Fig. 27.5 Average time courses of percent signal change of the BOLD–fMRI response, cerebral blood flow (CBF), and cerebral metabolic rate of oxygen consumption ($CMRO_2$) over time during bicuculline-induced tonic-clonic seizures. The changes show that blood supply exceeds oxygen consumption in the barrel field cortex but not the hippocampus. In all graphs, the straight vertical line at time = 0 marks seizure onset. (**a**, **b**) Time courses of mean signal change in $CMRO_2$ over time, calculated for three different values of the BOLD calibration parameter A' (0.4, 0.5, and 0.6) (see Eq. 27.1), for the barrel field cortex (S1BF) (**a**) and hippocampus (**b**). In all cases $CMRO_2$ showed a pronounced increase in both structures during seizures but was higher in hippocampus compared with cortex, independent of (**a**). (**c**, **d**) Relationship between the mean percent signal changes for BOLD, CBF, and estimated $CMRO_2$ ($A' = 0.6$) for cortex (SIBF) (**c**) and hippocampus (**d**). In the cortex, the increase in CBF during seizures was nearly double compared with the increase in $CMRO_2$, accompanied by an increase in the BOLD signal. In the hippocampus, however, increases of CBF and $CMRO_2$ during seizures nearly matched, and no signal changes were observed in the BOLD signal on average, despite strong neuronal activity in both structures. (Reproduced with permission from Schridde et al. 2007)

27.11 Sequential EEG–fMRI Studies in Animals

Experimental designs where the timing of the hemodynamic response is relatively controlled may circumvent the technical challenges inherent to simultaneous EEG–fMRI studies by using *sequential* EEG–fMRI. These studies record the EEG–fMRI under the same conditions and where the time course is relatively consistent allowing for investigation of both neuronal electrical data and cerebral hemodynamic

responses. Sequential EEG–fMRI has been employed to study epilepsy in the rat model of pentylenetetrazol-induced seizures (Keogh et al. 2005; Brevard et al. 2006). Sequential electrical recording and BOLD–fMRI has also been used to investigate visual processing in the cat (Kayser et al. 2004).

Sequential investigations are limited in the accuracy with which fMRI signals can be correlated to EEG activity. Therefore, sequential measurements are not ideal for the study of animal models where the neuronal function under investigation is variable, and where the variability is an important aspect of the phenomenon being studied.

27.12 Applications of Simultaneous EEG–fMRI in Animals

Simultaneous EEG–fMRI investigations of animal models have distinct advantages, as previously mentioned, in the correlating of brain electrical, hemodynamic, and neurometabolic responses. Simultaneous EEG recording with MRI was first performed in a rat cortical spreading depression model in 1995 (Busch et al. 1995). Subsequent EEG–fMRI studies in animal models have mainly focused on epilepsy. Here, we will review EEG–fMRI animal studies of epilepsy, including generalized and partial seizures, sleep, and studies where electrical stimulation was applied during signal acquisition. We will also discuss animal studies where the primary aim was to investigate the relationship between neuronal activity and the BOLD signal response.

27.13 Epilepsy

The first animal model studies of epilepsy with simultaneous EEG–fMRI were performed in the 2000s (Van Audekerkea et al. 2000). As we have mentioned, animal models allow the full power of fMRI methods to be employed to noninvasively map epileptic networks throughout the brain. Animal models provide a means to study the ictal activity of all seizure types and are not limited by movement artifact as animals can be studied under anesthetized, paralyzed, and ventilated conditions. The onset and type of seizure can be controlled in animal models, and invasive studies can be done to relate fMRI signals to underlying neuronal activity (Blumenfeld 2007).

Simultaneous EEG–fMRI in epilepsy can be used to accomplish several goals, including the accurate localization of seizure onset, the evolving physiology of seizures in focal regions or distributed networks, and to relate fMRI signals to underlying physiology. Interpretation of human studies will be improved by a better understanding of the relationship between neuronal activity and the fMRI signal in animal models. A better understanding of the local and remote networks and brain regions involved in specific seizure disorders may help design improved focal resective surgery and could provide targets for deep brain stimulation, medication, or even gene therapy. Animal studies may also improve our understanding of functional brain impairment and cognitive dysfunction (Blumenfeld and Taylor 2003; Blumenfeld 2005a, b, 2012).

27.14 Absence Seizure Models

Human studies of spike-wave discharges (SWD) in absence epilepsy patients (Archer et al. 2003; Salek-Haddadi et al. 2003; Aghakhani et al. 2004) have revealed a great deal regarding the neural networks involved in SWD formation and propagation. However, additional information is needed to correctly interpret fMRI signal increases and decreases in this disorder. Animal models can be used to study in depth the relationship of fMRI signal changes to underlying neuronal activity, and molecular mechanisms during SWDs (Blumenfeld 2005a, b). The Wistar Albino Glaxo rats of Rijswijk (WAG/Rij) have spontaneous spike-and-wave discharges and are an established model of human absence epilepsy (Coenen and Van Luijtelaar 2003). fMRI studies in this model have shown BOLD signal increases in focal bilateral regions of the cortex and thalamus (Nersesyan et al. 2004a, b). Interestingly, although considered a generalized seizure disorder, focal anterior regions of the brain are most intensely involved both in fMRI and electrical recordings of SWD, while other brain regions are relatively spared (Meeren et al. 2002; Nersesyan et al. 2004a, b). Although human fMRI studies of SWD have shown both increase and decreases in the cortex (Archer et al. 2003; Salek-Haddadi et al. 2003; Gotman et al. 2005; Labate et al. 2005; Aghakhani et al. 2006; Hamandi et al. 2006; Laufs et al. 2006), studies in WAG/Rij rats have so far shown mainly increases in the cortex (Nersesyan et al. 2004a, b; Tenney et al. 2004a, b). However, studies have shown that the basal ganglia show prominent fMRI signal decreases during SWD in rodent models (Fig. 27.3) (Guillemain et al. 2007; Mishra et al. 2007, 2011).

Gamma-butyrolactone (GBL) is a precursor of gamma-hydroxybutyrate and produces robust SWD in rats, resembling petit mal status epilepticus (Snead et al. 1999; Tenney et al. 2003). A simultaneous EEG–fMRI study, using epidural electrodes, of SWD in rats treated with GBL showed thalamic increases and mixed cortical increases and decreases in fMRI signals (Tenney et al. 2003). However, a similar study in marmoset monkeys given GBL showed only fMRI increases during SWD (Tenney et al. 2004a, b). Simultaneous fMRI–EEG in an anesthetized ferret model of 3- to 4-Hz SWD with bicuculline administration also demonstrated cortical increases in BOLD signal associated with various forms of SWDs (Youngblood et al. 2015). Recent investigations in a sequential fMRI and EEG rat model of genetic absence epilepsy suggest that the fMRI cortical BOLD increases may have been anesthesia related; future experiments should carefully examine the neurovascular and metabolic effects of anesthetics as separate from pathophysiology.

27.15 Generalized Tonic-Clonic Seizure Models

Generalized tonic-clonic seizures (GTCS) in animal models can be induced by pharmacologic means, allowing the investigator control over the timing of seizures and thereby allowing for study with advanced imaging techniques. The first investigation of GTCS using fMRI was performed early in the development of fMRI as a method (Ogawa and Lee 1992). Simultaneous EEG–fMRI studies of GTCS in

animals face the challenge of constraining movement in the scanner (Van Camp et al. 2003; Nersesyan et al. 2004a, b; Schridde et al. 2007).

The primary agents to chemically induce GTCS include kainic acid, pentylenetetrazol, and bicuculline. Kainic acid, a potent central nervous system stimulant, has been used to induce GTCS in animals (Ben-Ari et al. 1979). A distinct change in the BOLD–fMRI signal has been seen following injection of kainic acid (Ogawa and Lee 1992). Another pro-convulsive agent is pentylenetetrazol (PTZ) and acts as a GABA antagonist. PTZ has also been used to induce GTCS in rats (Van Camp et al. 2003; Keogh et al. 2005; Brevard et al. 2006). Finally, bicuculline, another GABA receptor antagonist, has also been used to induce rat GTCSs, showing widespread cortical BOLD–fMRI increases (Fig. 27.4) (Nersesyan et al. 2004a, b, Schridde et al. 2007).

Studies of bicuculline-induced GTCS using multiple techniques to investigate neuronal activity, CBF, CBV, $CMRO_2$, and BOLD signal changes indicate that these parameters all increase in parallel in the cortex during bicuculline-induced GTCS. In contrast, some regions such as the hippocampus may show variable BOLD signal changes or even BOLD decreases even though direct recordings of neuronal activity from the hippocampus showed consistent large increases in neuronal activity during GTCS (Fig. 27.4) (Schridde et al. 2007; DeSalvo et al. 2010). Interestingly, the CBF increase exceeded the $CMRO_2$ increase in the cortex, producing the expected consistent increase in BOLD. However, in the hippocampus, CBF increases did not on average exceed $CMRO_2$ so that mismatch between metabolism and CBF can lead to paradoxical BOLD decreases in some cases (Fig. 27.5) (Schridde et al. 2007).

27.16 Partial Seizure Models

Simultaneous EEG–fMRI in animal models of focal epilepsy necessitates additional operative techniques to induce localized seizure activity. Where genetic and systemic pharmacologic models allow the study of generalized seizure disorders, direct focal introduction of seizure-inducing drugs, commonly penicillin, or electrical stimulation is required to cause focal seizures. One such early study used focal penicillin infusion into the prefrontal cortex of sheep (Opdam et al. 2002). Localized increases in the fMRI signal were identified in the sheep cortex during seizures (Opdam et al. 2002). Penicillin has also been applied to the somatosensory cortex in a porcine model, showing regional signal increases during interictal spikes (Makiranta et al. 2005), and to the occipital cortex in rats, showing regional signal increases during seizures (Mirsattari et al. 2006).

Electrical stimulation of the dorsal hippocampus has been performed during simultaneous depth electrode and fMRI studies in a rodent model that recapitulate clinically observed electrophysiological cortical slow waves (low-frequency high-amplitude) during temporal lobe focal seizures with impaired awareness (Blumenfeld et al. 2004a, b). Following electrical stimulation, neuronal electrical activity and fMRI–BOLD increased intensely in the hippocampus, as expected during induced seizures, while electrophysiological cortical slow waves and BOLD decreases were

observed in cortical association cortices such as the lateral orbitofrontal cortex with a gradual return to baseline (Fig. 27.6) (Englot et al. 2008; Motelow et al. 2015). Similarly, BOLD signal increases were also observed in anterior hypothalamus and septal nuclei during induced focal seizures; interestingly, the intralaminar thalamus and brainstem arousal structures showed BOLD decreases (Fig. 27.6) (Motelow

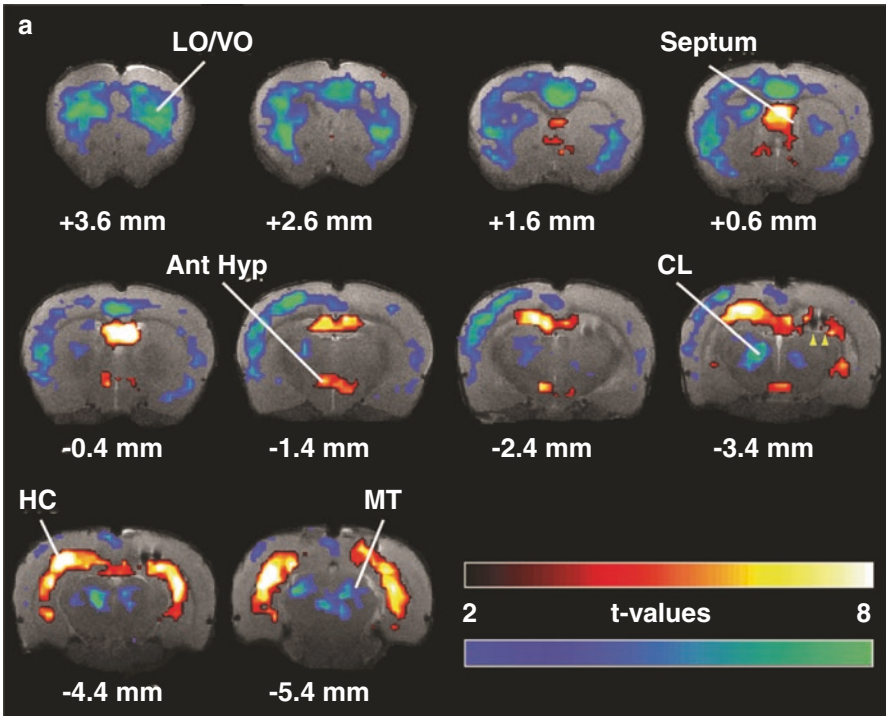

Fig. 27.6 BOLD region of interest (ROI) time courses reveal increases and decreases during focal temporal lobe seizures and eventual return to baseline. (**a**) *T*-map of ictal changes during partial seizures (from 30-s pre-seizure baseline) reveals complicated network of changes. Widespread cortical decreases are accompanied by mixed subcortical increases and decreases. Increases are seen in known areas of seizure propagation such as the hippocampus (HC) and lateral septum as well as in sleep-promoting regions such as the anterior hypothalamus (Ant Hyp). Decreases are seen in the cortex, most prominently in lateral and ventral orbital frontal cortex (LO/VO) and in medial regions including cingulate and retrosplenial cortex. Decreases are also seen in arousal promoting regions such as the thalamic intralaminar nuclei including centrolateral nucleus (CL), as well as in the midbrain tegmentum (MT). The arrowheads at AP −3.4 mm signify the hippocampal electrode artifact. Warm colors represent fMRI increases, and cool colors decreases, superimposed on coronal anatomical images from the template animal. AP coordinates in millimeters relative to bregma (Paxinos and Watson 1998). Ten animals, with FDR-corrected threshold $p < 0.05$. (**b**) Mean ROI time courses (±SEM) for data 30 s prior to seizure onset, seizure time course scaled to mean seizure duration, and unscaled postictal time course aligned to seizure end. Ant Hyp, anterior hypothalamus; HC, hippocampus; LO, lateral orbital frontal cortex; CL, central lateral (intralaminar) thalamus; MT, midbrain tegmentum; Septum, lateral septal nuclei. (Reproduced with permission from Motelow et al. 2015)

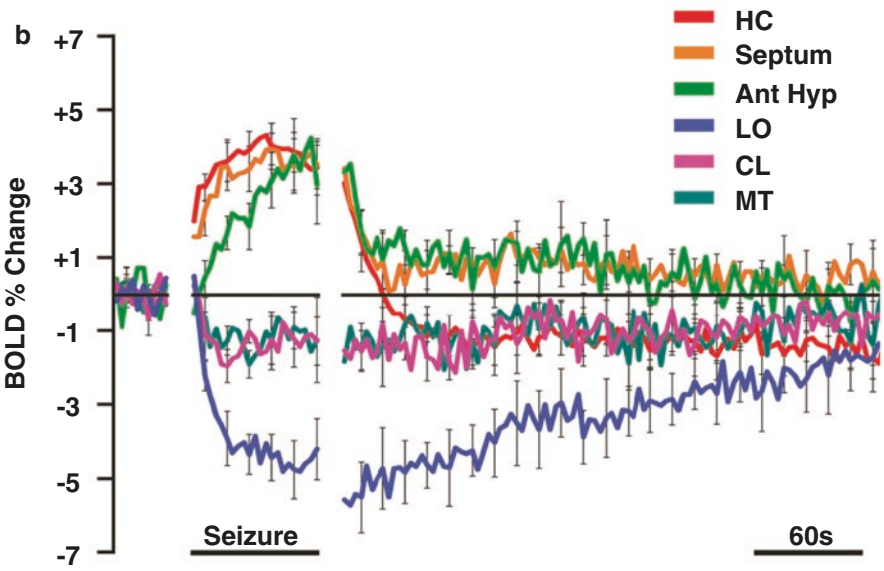

Fig. 27.6 (continued)

et al. 2015). These later two regions were confirmed to have decreased multiunit and single-unit firing rates with subsequent electrophysiological investigations (Motelow et al. 2015; Feng et al. 2017). Separate experiments also showed neuronal electrical activity increase in the GABAergic lateral septal nuclei, that were essential in the generation of cortical slow waves and in the reduction of cortical cholinergic transmission (Li et al. 2015). In concert, simultaneous fMRI–EEG studies demonstrated the network by which focally induced temporal lobe seizures propagate to inhibitory structures such as the lateral septum to inhibit subcortical arousal structures. This leads to decreased neuromodulatory input to the intralaminar thalamus and basal forebrain. Consequently, widespread decreased cortical arousal manifests electrophysiologically in cortical slow waves, hemodynamically with cortical BOLD decreases, and behaviorally with automatisms or behavioral arrest (Blumenfeld 2012).

27.17 Sleep

Simultaneous EEG–fMRI has also been used to investigate sleep in rodent models (Khubchandani et al. 2005). Simultaneous EEG allows for the determination of sleep and wake cycles in the animal while scanning. fMRI signal increases were shown in the medial preoptic area during sleep, corroborating other work indicating the importance of this area in maintaining slow wave sleep (Khubchandani et al. 2005). Simultaneous EEG–fMRI has been used primarily in epilepsy research, but potential exists for much additional work in other fields, including sleep.

27.18 Sensory–Motor Stimulation Models

Simultaneous EEG–fMRI can be used to study the activation of specific brain regions during sensory–motor stimulation. Electrical forepaw stimulation has been used to compare cortex activation during fully conscious curarization compared to during alpha-chloralose anesthesia (Peeters et al. 2001). Simultaneous acquired EEG data were used to identify the awake and anesthetized states, showing that the BOLD signal was smaller under alpha-chloralose anesthesia, compared to the awake state (Peeters et al. 2001). Simultaneous EEG–fMRI has also been used to study the interaction between simultaneous and sequential electrical forepaw stimulations in the rat and the effects on the associated stimulation-evoked potentials and BOLD signal responses (Ogawa et al. 2000) showing fMRI signal modification in response to two stimuli directly following another, although on EEG the changes associate with the second stimulation was extinguished. Studies investigating fMRI changes during anesthesia with parallel electrophysiology recordings during forepaw stimulation have shown differences in the strength of fMRI changes under different types of anesthesia (Hyder et al. 2002a, b; Smith et al. 2002; Maandag et al. 2007). These sensory studies have often been a model system under which to study the neural underpinnings of the BOLD signal.

27.19 Relating fMRI Signals to Electrophysiological Recordings

One of the major goals of animal studies in this field is to relate neuroimaging signals to underlying electrical neuronal activity. Direct measurement of neuronal activity in these models is therefore essential. Simultaneous recordings of single neurons, local field potential (LFP), and BOLD–fMRI signals have been accomplished in anesthetized monkeys (Logothetis et al. 2001; Tolias et al. 2005; Shmuel et al. 2006), but this method remains a significant challenge technically.

The relationship between fMRI signals and electrophysiology can be successfully investigated by parallel benchtop electrophysiology and fMRI experiments performed under identical conditions (Hyder et al. 2002a, b; Smith et al. 2002). Studies designed to investigate both modalities in the same animal model have shown good correspondence between fMRI increases and physiological measurements (Nersesyan et al. 2004a, b; Schridde et al. 2007; Sanganahalli et al. 2013). Specifically, anterior brain regions such as the somatosensory cortex where fMRI signals are increased during SWD show increased neuronal firing and CBF, while posterior areas such as visual cortex spared by fMRI signal changes show few changes in physiological measurements (Nersesyan et al. 2004a, b). Similarly, in the WAG/Rij model of SWD absence seizures, the caudate–putamen showed inverse hemodynamic measure (fMRI BOLD, CBV, and CBF) as compared to electrophysiological measures (Fig. 27.1) (Mishra et al. 2011). Direct physiologic measurements during generalized tonic-clonic seizures, on the other hand, show increases in both anterior and posterior brain regions, in agreement with fMRI measurements in

the same areas (Nersesyan et al. 2004a, b). Interestingly, in the somatosensory cortex, the magnitude of BOLD fMRI, neuronal firing, and CBF changes were greatest for generalized tonic-clonic seizures, less for normal whisker stimulation, and even less for SWD (Nersesyan et al. 2004a, b). The degree to which fMRI–BOLD is coupled to neural metabolic activity is variable and brain region-dependent (Sloan et al. 2010; Devonshire et al. 2012). Recent studies assessing fMRI–BOLD and electrophysiology in deep (thalamus) and cortical structures during sensory-evoked responses with rat forepaw stimulation showed the effects of measured neural–hemodynamic coupling of metabolic demand (Fig. 27.1) (Sanganahalli et al. 2016). Understanding the relationship between fMRI signal increases and decreases in other regions will be the subject of future investigations, as will understanding the neuroenergetic mechanisms of fMRI signal changes. The complexity of animal model-, brain region- (Shu et al. 2016a, b), and anesthesia-dependence (Maandag et al. 2007) makes one approach the interpretation of the BOLD signal with caution.

27.20 Future Directions

The use of fMRI as a research tool in animal models of epilepsy is still nascent in its development, and there is tremendous potential for additional future work in this field. Simultaneous EEG–fMRI is now a reality and has contributed greatly to our understanding of hemodynamic responses that precede, accompany, and follow epileptiform discharges and to our understanding of hemodynamic and metabolic responses to neuronal activity. Additionally, the use of simultaneous EEG–fMRI will open many lines of investigation and will continuously refine our understanding of the temporal and spatial characteristics of neuronal activity. BOLD signal acquisition is only one of many promising MRI modalities, and it will become increasingly feasible to fully investigate the neuroenergetic basis of activity changes in the brain using multimodal techniques. The integration of measurements of BOLD–fMRI, CBV, and CBF can be used to obtain estimates of the $CMRO_2$, thereby allowing a full investigation into neuronal energetics (Davis et al. 1998; Hyder et al. 2002a, b; Smith et al. 2002; Hyder and Blumenfeld 2004; Shulman and Rothman 2004; Stefanovic et al. 2004; Maandag et al. 2007).

Further technical advances in fMRI acquisition and analysis, combined with advances in combining the EEG data, will allow for a better signal-to-noise ratio, and improved spatial and temporal resolution. Future studies will be able to perform detailed investigations of the time course of the hemodynamic response to varying neuronal events and across brain networks. Intracranial electrical recording during fMRI is magnifying the resolution with which we can measure the activity of individual brain regions. The increased cell-type specificity with insertion of light-sensitive channels in animal models and optode placement allow technically challenging but immensely controlled stimulation experiments (Bernal-Casas et al. 2017; Lee et al. 2017). Additionally, intracranial electrical stimulation is opening new avenues of investigation with the development of models of partial seizures and into the fundamental relationship between neuronal activity and the cerebral

hemodynamic and metabolic response. Crucial questions regarding the fMRI changes during epileptiform events, and other neuronal processes, remain unanswered. Which region(s) are involved in seizure-generating network? Which regions of the brain are involved in sensory–motor processing? How do different regions of the brain vary in their hemodynamic and metabolic response regarding temporal and amplitude characteristics from varying stimuli or processes? How do these hemodynamic and metabolic responses relate to electrical activity before, during and after neuronal events? Answering these questions will contribute to our understanding of neuronal function and to the development of targeted investigations of molecular and genetic changes associated with abnormal brain function.

27.21 Conclusions

Simultaneous EEG–fMRI in animals is now a fully developed investigational tool. We have reviewed the technical challenges related to animal preparation, data analysis, signal acquisition, and study design, and the innovative solutions to these problems have been highlighted. EEG–fMRI studies in animals can contribute to our understanding of epilepsy, sensory–motor processing, and other neuronal events, and the relationship between fMRI signals their underlying neural underpinnings.

The animal model studies discussed here have yielded important data, elucidating specific cortical and subcortical network changes during epileptiform events and will guide future studies of this disorder. More work is needed to map the anatomic distribution of the changes, and to fully investigate the physiology of brain responses using modalities that measure changes in CBV, CBF, and $CMRO_2$, and electrical neuronal activity throughout the brain. These studies will enhance our ability to interpret human studies and will guide the design of new therapeutic targets for surgical treatment, neurostimulation, and other innovative therapies.

Acknowledgments We thank Ms. Katherine Steadman for administrative support. This chapter is dedicated in memory of Dr. Damien Ellens, a beloved member of the Blumenfeld Lab.

References

Aghakhani Y, Bagshaw AP, Benar CG, Hawco C, Andermann F, Dubeau F, Gotman J (2004) fMRI activation during spike and wave discharges in idiopathic generalized epilepsy. Brain 127(Pt 5):1127–1144

Aghakhani Y, Kobayashi E, Bagshaw AP, Hawco C, Benar CG, Dubeau F, Gotman J (2006) Cortical and thalamic fMRI responses in partial epilepsy with focal and bilateral synchronous spikes. Clin Neurophysiol 117(1):177–191

Angenstein F, Kammerer E, Niessen HG, Frey JU, Scheich H, Frey S (2007) Frequency-dependent activation pattern in the rat hippocampus, a simultaneous electrophysiological and fMRI study. NeuroImage 38(1):150–163

Archer JS, Abbott DF, Waites AB, Jackson GD (2003) fMRI "deactivation" of the posterior cingulate during generalized spike and wave. NeuroImage 20(4):1915–1922

Austin VC et al (2003) Differences in the BOLD fMRI response to direct and indirect cortical stimulation in the rat. Magn Reson Med 49(5):838–847
Austin VC, Blamire AM, Allers KA, Sharp T, Styles P, Matthews PM, Sibson NR (2005) Confounding effects of anesthesia on functional activation in rodent brain: a study of halothane and alpha-chloralose anesthesia. NeuroImage 24(1):92–100
Avoli M, Gloor P, Kostopoulos G, Naquet T (eds) (1990) Generalized epilepsy. Birkhauser, Boston, MA
Babb TL, Kupfer W (1984) Phagocytic and metabolic reactions to chronically implanted metal brain electrodes. Exp Neurol 86(2):171–182
Behar KL, Petroff OA, Prichard JW, Alger JR, Shulman RG (1986) Detection of metabolites in rabbit brain by 13C NMR spectroscopy following administration of [1-13C]glucose. Magn Reson Med 3(6):911–920
Belliveau JW, Kennedy DN Jr, McKinstry RC, Buchbinder BR, Weisskoff RM, Cohen MS, Vevea JM, Brady TJ, Rosen BR (1991) Functional mapping of the human visual cortex by magnetic resonance imaging. Science 254(5032):716–719
Ben-Ari Y, Lagowska J, Tremblay E, Le Gal La Salle G (1979) A new model of focal status epilepticus: intra-amygdaloid application of kainic acid elicits repetitive secondarily generalized convulsive seizures. Brain Res 163(1):176–179
Berger H (1929) Ueber das Elektrenkephalogramm des Menschen. Arch Psychiatry 87:527
Bernal-Casas D, Lee HJ, Weitz AJ, Lee JH (2017) Studying brain circuit function with dynamic causal modeling for optogenetic fMRI. Neuron 93(3):522–532.e525
Blumenfeld H (2005a) Cellular and network mechanisms of spike-wave seizures. Epilepsia 46(Suppl 9):21–33
Blumenfeld H (2005b) Consciousness and epilepsy: why are patients with absence seizures absent? Prog Brain Res 150:271–286
Blumenfeld H (2007) Functional MRI studies of animal models in epilepsy. Epilepsia 48(Suppl. 4):18–26
Blumenfeld H (2012) Impaired consciousness in epilepsy. Lancet Neurol 11(9):814–826
Blumenfeld H, Taylor J (2003) Why do seizures cause loss of consciousness? Neuroscientist 9(5):301–310
Blumenfeld H, McNally KA, Vanderhill SD, Paige AL, Chung R, Davis K, Norden AD, Stokking R, Studholme C, Novotny EJ, Zubal IG, Spencer SS (2004a) Positive and negative network correlations in temporal lobe epilepsy. Cereb Cortex 14(8):892–902
Blumenfeld H, Rivera M, McNally KA, Davis K, Spencer DD, Spencer SS (2004b) Ictal neocortical slowing in temporal lobe epilepsy. Neurology 63:1015–1021
Brevard ME, Kulkarni P, King JA, Ferris CF (2006) Imaging the neural substrates involved in the genesis of pentylenetetrazol-induced seizures. Epilepsia 47(4):745–754
Busch E, Hoehn-Berlage M, Eis M, Gyngell ML, Hossmann KA (1995) Simultaneous recording of EEG, DC potential and diffusion-weighted NMR imaging during potassium induced cortical spreading depression in rats. NMR Biomed 8(2):59–64
Chuapoco MR, Choy M, Schmid F, Duffy BA, Lee HJ, Lee JH (2019) Carbon monofilament electrodes for unit recording and functional MRI in same subjects. NeuroImage 186:806–816
Coenen AM, Van Luijtelaar EL (1987) The WAG/Rij rat model for absence epilepsy: age and sex factors. Epilepsy Res 1(5):297–301
Coenen AM, Van Luijtelaar EL (2003) Genetic animal models for absence epilepsy: a review of the WAG/Rij strain of rats. Behav Genet 33:635–655
Damadian R (1971) Tumor detection by nuclear magnetic resonance. Science 171(3976):1151–1153
Davis TL, Kwong KK, Weisskoff RM, Rosen BR (1998) Calibrated functional MRI: mapping the dynamics of oxidative metabolism. Proc Natl Acad Sci U S A 95(4):1834–1839
DeSalvo MN, Schridde U, Mishra AM, Motelow JE, Purcaro MJ, Danielson N, Bai X, Hyder F, Blumenfeld H (2010) Focal BOLD fMRI changes in bicuculline-induced tonic-clonic seizures in the rat. NeuroImage 50(3):902–909
Detre JA, Wang J (2002) Technical aspects and utility of fMRI using BOLD and ASL. Clin Neurophysiol 113(5):621–634

Detre JA, Leigh JS, Williams DS, Koretsky AP (1992) Perfusion imaging. Magn Reson Med 23(1):37–45
Devonshire IM, Papadakis NG, Port M, Berwick J, Kennerley AJ, Mayhew JE, Overton PG (2012) Neurovascular coupling is brain region-dependent. NeuroImage 59(3):1997–2006
Duffy BA, Choy M, Chuapoco MR, Madsen M, Lee JH (2015) MRI compatible optrodes for simultaneous LFP and optogenetic fMRI investigation of seizure-like after discharges. NeuroImage 123:173–184
Englot DJ, Mishra AM, Purcaro MJ, Herman P, Hyder F, Blumenfeld H (2008) Simultaneous fMRI and electrophysiology during intracerebral stimulation of partial seizures in rats. ISMRM:Abs
Feng L, Motelow JE, Ma C, Biche W, McCafferty C, Smith N, Liu M, Zhan Q, Jia R, Xiao B, Duque A, Blumenfeld H (2017) Seizures and sleep in the thalamus: focal limbic seizures show divergent activity patterns in different thalamic nuclei. J Neurosci 37(47):11441–11454
Gibbs FA, Lennox WG, Gibbs EL (1934) Cerebral blood flow preceding and accompanying epileptic seizures in man. Arch Neruol Psychiatry 32:257–272
Gloor P (1985) Neuronal generators and the problem of localization in electroencephalography: application of volume conductor theory to electroencephalography. J Clin Neurophysiol 2(4):327–354
Gotman J, Grova C, Bagshaw A, Kobayashi E, Aghakhani Y, Dubeau F (2005) Generalized epileptic discharges show thalamocortical activation and suspension of the default state of the brain. Proc Natl Acad Sci U S A 102(42):15236–15240
Grohn O, Pitkanen A (2007) Magnetic resonance imaging in animal models of epilepsy-noninvasive detection of structural alterations. Epilepsia 48(Suppl 4):3–10
Grubb RL Jr, Raichle ME, Eichling JO, Ter-Pogossian MM (1974) The effects of changes in PaCO2 on cerebral blood volume, blood flow, and vascular mean transit time. Stroke 5(5):630–639
Gruetter R, Novotny EJ, Boulware SD, Mason GF, Rothman DL, Shulman GI, Prichard JW, Shulman RG (1994) Localized 13C NMR spectroscopy in the human brain of amino acid labeling from D-[1-13C]glucose. J Neurochem 63(4):1377–1385
Gruetter R, Seaquist ER, Kim S, Ugurbil K (1998) Localized in vivo 13C-NMR of glutamate metabolism in the human brain: initial results at 4 tesla. Dev Neurosci 20(4–5):380–388
Guillemain I, David O, Depaulis A (2007) EEG and fMRI evidence for a cortical focus of absence seizures in the genetic absence rats from strasbourg (gaers)
Hamandi K, Salek-Haddadi A, Laufs H, Liston A, Friston K, Fish DR, Duncan JS, Lemieux L (2006) EEG-fMRI of idiopathic and secondarily generalized epilepsies. NeuroImage 31(4):1700–1710
He J, Devonshire IM, Mayhew JE, Papadakis NG (2007) Simultaneous laser Doppler flowmetry and arterial spin labeling MRI for measurement of functional perfusion changes in the cortex. NeuroImage 34(4):1391–1404
Herman P, Sanganahalli BG, Blumenfeld H, Hyder F (2009) Cerebral oxygen demand for short-lived and steady-state events. J Neurochem 109(Suppl 1):73–79
Herman P, Sanganahalli BG, Blumenfeld H, Rothman DL, Hyder F (2013) Quantitative basis for neuroimaging of cortical laminae with calibrated functional MRI. Proc Natl Acad Sci U S A 110(37):15115–15120
Hiremath GK, Najm IM (2007) Magnetic resonance spectroscopy in animal models of epilepsy. Epilepsia 48(Suppl 4):47–55
Hoge RD (2012) Calibrated FMRI. NeuroImage 62(2):930–937
Hoge RD, Atkinson J, Gill B, Crelier GR, Marrett S, Pike GB (1999) Linear coupling between cerebral blood flow and oxygen consumption in activated human cortex. Proc Natl Acad Sci U S A 96(16):9403–9408
Horsley V (1892) An address on the origin and seat of epileptic disturbance. Br Med J 1:693–696
Hudetz AG (2002) Effect of volatile anesthetics on interhemispheric EEG cross-approximate entropy in the rat. Brain Res 954(1):123–131
Hyder F (2004) Neuroimaging with calibrated FMRI. Stroke 35(11 Suppl 1):2635–2641

Hyder F, Blumenfeld H (2004) Relationship between CMRO2 and neuronal activity. In: Shulman RG, Rothman DL (eds) Brain energetics and neuronal activity: applications to fMRI and medicine. John Wiley & Sons, Inc., New York, NY, pp 173–194

Hyder F, Rothman DL (2012) Quantitative fMRI and oxidative neuroenergetics. NeuroImage 62(2):985–994

Hyder F, Kennan RP, Kida I, Mason GF, Behar KL, Rothman D (2000) Dependence of oxygen delivery on blood flow in rat brain: a 7 tesla nuclear magnetic resonance study. J Cereb Blood Flow Metab 20(3):485–498

Hyder F, Kida I, Behar KL, Kennan RP, Maciejewski PK, Rothman DL (2001) Quantitative functional imaging of the brain: towards mapping neuronal activity by BOLD fMRI. NMR Biomed 14(7–8):413–431

Hyder F, Kida I, Smith AJ, Blumenfeld H, Shulman RG, Rothman DL (2002a) Quantitative fMRI of rat brain by multi-modal MRI and MRS measurements. In: International Symposium on Brain Activation and CBF Control, International Congress Series

Hyder F, Rothman DL, Shulman RG (2002b) Total neuroenergetics support localized brain activity: implications for the interpretation of fMRI. Proc Natl Acad Sci U S A 99(16):10771–10776

Hyder F, Sanganahalli BG, Herman P, Coman D, Maandag NJ, Behar KL, Blumenfeld H, Rothman DL (2010) Neurovascular and neurometabolic couplings in dynamic calibrated fMRI: transient oxidative neuroenergetics for block-design and event-related paradigms. Front Neuroenerg 2:18

Ives JR, Warach S, Schmitt F, Edelman RR, Schomer DL (1993) Monitoring the patient's EEG during echo planar MRI. Clin Neurol 87:417–420

Jones M, Berwick J, Hewson-Stoate N, Gias C, Mayhew J (2005) The effect of hypercapnia on the neural and hemodynamic responses to somatosensory stimulation. NeuroImage 27(3):609–623

Jupp B, Williams JP, Tesiram YA, Vosmansky M, O'Brien TJ (2006) MRI compatible electrodes for the induction of amygdala kindling in rats. J Neurosci Methods 155(1):72–76

Kayser C, Kim M, Ugurbil K, Kim DS, Konig P (2004) A comparison of hemodynamic and neural responses in cat visual cortex using complex stimuli. Cereb Cortex 14(8):881–891

Kennan RP, Zhong J, Gore JC (1994) Intravascular susceptibility contrast mechanisms in tissue. Magn Reson Med 31:9–21

Kennan RP, Scanley BE, Innis RB, Gore JC (1998) Physiological basis for BOLD MR signal changes due to neuronal stimulation: separation of blood volume and magnetic susceptibility effects. Magn Reson Med 40(6):840–846

Keogh BP, Cordes D, Stanberry L, Figler BD, Robbins CA, Tempel BL, Green CG, Emmi A, Maravilla KM, Schwartzkroin PA (2005) BOLD-fMRI of PTZ-induced seizures in rats. Epilepsy Res 66(1–3):75–90

Khubchandani M, Mallick HN, Jagannathan NR, Mohan Kumar V (2003) Stereotaxic assembly and procedures for simultaneous electrophysiological and MRI study of conscious rat. Magn Reson Med 49:962–967

Khubchandani M, Jagannathan NR, Mallick HN, Mohan Kumar V (2005) Functional MRI shows activation of the medial preoptic area during sleep. NeuroImage 26(1):29–35

Kida I, Kennan RP, Rothman DL, Behar KL, Hyder F (2000) High-resolution CMR(O2) mapping in rat cortex: a multiparametric approach to calibration of BOLD image contrast at 7 Tesla. J Cereb Blood Flow Metab 20(5):847–860

Kida I, Rothman DL, Hyder F (2007) Dynamics of changes in blood flow, volume, and oxygenation: implications for dynamic functional magnetic resonance imaging calibration. J Cereb Blood Flow Metab 27(4):690–696

Krakow K, Allen PJ, Symms MR, Lemieux L, Josephs O, Fish DR (2000) EEG recording during fMRI experiments: image quality. Hum Brain Mapp 10(1):10–15

Labate A, Briellmann RS, Abbott DF, Waites AB, Jackson GD (2005) Typical childhood absence seizures are associated with thalamic activation. Epileptic Disord 7(4):373–377

Lahti KM et al (1999) Comparison of evoked cortical activity in conscious and propofol-anesthetized rats using functional MRI. Magn Reson Med 41(2):412–416

Laufs H, Lengler U, Hamandi K, Kleinschmidt A, Krakow K (2006) Linking generalized spike-and-wave discharges and resting state brain activity by using EEG/fMRI in a patient with absence seizures. Epilepsia 47(2):444–448

Lauterbur PC (1973) Image formation by induced local interactions: examples employing nuclear magnetic resonance. Nature 242(5394):190–191

Lee JH, Kreitzer AC, Singer AC, Schiff ND (2017) Illuminating neural circuits: from molecules to MRI. J Neurosci 37(45):10817–10825

Li W, Motelow JE, Zhan Q, Hu YC, Kim R, Chen WC, Blumenfeld H (2015) Cortical network switching: possible role of the lateral septum and cholinergic arousal. Brain Stimul 8(1):36–41

Logothetis NK, Pauls J, Augath M, Trinath T, Oeltermann A (2001) Neurophysiological investigation of the basis of the fMRI signal. Nature 412(6843):150–157

Maandag NJ, Coman D, Sanganahalli BG, Herman P, Smith AJ, Blumenfeld H, Shulman RG, Hyder F (2007) Energetics of neuronal signaling and fMRI activity. Proc Natl Acad Sci U S A 104(51):20546–20551

Makiranta MJ, Jauhiainen JP, Oikarinen JT, Suominen K, Tervonen O, Alahuhta S, Jantti V (2002) Functional magnetic resonance imaging of swine brain during change in thiopental anesthesia into EEG burst-suppression level--a preliminary study. MAGMA 15(1–3):27–35

Makiranta M, Ruohonen J, Suominen K, Niinimaki J, Sonkajarvi E, Kiviniemi V, Seppanen T, Alahuhta S, Jantti V, Tervonen O (2005) BOLD signal increase preceeds EEG spike activity--a dynamic penicillin induced focal epilepsy in deep anesthesia. NeuroImage 27(4):715–724

Mandeville JB, Marota JJ, Kosofsky BE, Keltner JR, Weissleder R, Rosen BR, Weisskoff RM (1998) Dynamic functional imaging of relative cerebral blood volume during rat forepaw stimulation. Magn Reson Med 39(4):615–624

Mandeville JB, Marota JJ, Ayata C, Moskowitz MA, Weisskoff RM, Rosen BR (1999) MRI measurement of the temporal evolution of relative CMRO(2) during rat forepaw stimulation. Magn Reson Med 42(5):944–951

Martin C, Jones M, Martindale J, Mayhew J (2006) Haemodynamic and neural responses to hypercapnia in the awake rat. Eur J Neurosci 24(9):2601–2610

Mason GF, Behar KL, Rothman DL, Shulman RG (1992) NMR determination of intracerebral glucose concentration and transport kinetics in rat brain. J Cereb Blood Flow Metab 12(3):448–455

Mason GF, Gruetter R, Rothman DL, Behar KL, Shulman RG, Novotny EJ (1995) Simultaneous determination of the rates of the TCA cycle, glucose utilization, alpha-ketoglutarate/glutamate exchange, and glutamine synthesis in human brain by NMR. J Cereb Blood Flow Metab 15(1):12–25

Matsumoto H, Marsan CA (1964) Cortical cellular phenomena in experimental epilepsy: ictal manifestations. Exp Neurol 9:305–326

Matthews PM, Honey GD, Bullmore ET (2006) Applications of fMRI in translational medicine and clinical practice. Nat Rev Neurosci 7(9):732–744

Meeren HK, Pijn JP, Van Luijtelaar EL, Coenen AM, Lopes da Silva FH (2002) Cortical focus drives widespread corticothalamic networks during spontaneous absence seizures in rats. J Neurosci 22(4):1480–1495

Menon RS, Ogawa S, Tank DW, Ugurbil K (1993) Tesla gradient recalled echo characteristics of photic stimulation-induced signal changes in the human primary visual cortex. Magn Reson Med 30(3):380–386

Midzianovskaia IS, Kuznetsova GD, Coenen AML, Spiridonov AM, van Luijtelaar ELJM (2001) Electrophysiological and pharmacological characteristics of two types of spike-wave discharges in WAG/Rij rats. Brain Res 911:62–70

Mirsattari SM, Bihari F, Leung LS, Menon RS, Wang Z, Ives JR, Bartha R (2005a) Physiological monitoring of small animals during magnetic resonance imaging. J Neurosci Methods 144(2):207–213

Mirsattari SM, Ives JR, Bihari F, Leung LS, Menon RS, Bartha R (2005b) Real-time display of artifact-free electroencephalography during functional magnetic resonance imaging and magnetic resonance spectroscopy in an animal model of epilepsy. Magn Reson Med 53(2):456–464

Mirsattari SM, Wang Z, Ives JR, Bihari F, Leung LS, Bartha R, Menon RS (2006) Linear aspects of transformation from interictal epileptic discharges to BOLD fMRI signals in an animal model of occipital epilepsy. NeuroImage 30(4):1133–1148

Mirsattari SM, Ives JR, Leung LS, Menon RS (2007) EEG monitoring during functional MRI in animal models. Epilepsia 48(Suppl 4):37–46

Mishra AM, Schridde U, Motelow JE, Hyder F Blumenfeld H (2007) Physiology and imaging of increases and decreases in BOLD signals during spike-wave seizures in WAG/Rij rats. http://web.sfn.org/

Mishra AM, Ellens DJ, Schridde U, Motelow JE, Purcaro MJ, DeSalvo MN, Enev M, Sanganahalli BG, Hyder F, Blumenfeld H (2011) Where fMRI and electrophysiology agree to disagree: corticothalamic and striatal activity patterns in the WAG/Rij rat. J Neurosci 31(42):15053–15064

Motelow JE, Li W, Zhan Q, Mishra AM, Sachdev RN, Liu G, Gummadavelli A, Zayyad Z, Lee HS, Chu V, Andrews JP, Englot DJ, Herman P, Sanganahalli BG, Hyder F, Blumenfeld H (2015) Decreased subcortical cholinergic arousal in focal seizures. Neuron 85(3):561–572

Nakahata K, Kinoshita H, Hirano Y, Kimoto Y, Iranami H, Hatano Y (2003) Mild hypercapnia induces vasodilation via adenosine triphosphate-sensitive K+ channels in parenchymal microvessels of the rat cerebral cortex. Anesthesiology 99(6):1333–1339

Negishi M, Abildgaard M, Nixon T, Constable RT (2004) Removal of time-varying gradient artifacts from EEG data acquired during continuous fMRI. Clin Neurophysiol 115(9):2181–2192

Nersesyan H, Herman P, Erdogan E, Hyder F, Blumenfeld H (2004a) Relative changes in cerebral blood flow and neuronal activity in local microdomains during generalized seizures. J Cereb Blood Flow Metab 24(9):1057–1068

Nersesyan H, Hyder F, Rothman D, Blumenfeld H (2004b) Dynamic fMRI and EEG recordings during spike-wave seizures and generalized tonic-clonic seizures in WAG/Rij rats. J Cereb Blood Flow Metab 24(6):589–599

Ogawa S, Lee T (1992) Blood oxygen level dependent MRI of the brain: effects of seizure induced by kainic acid in the rat. Proc Soc Magn Reson Med 1:501

Ogawa S, Lee TM, Kay AR, Tank DW (1990) Brain magnetic resonance imaging with contrast dependent on blood oxygenation. Proc Natl Acad Sci U S A 87(24):9868–9872

Ogawa S, Menon RS, Tank DW, Kim SG, Merkle H, Ellermann JM, Ugurbil K (1993) Functional Brain mapping by blood oxygenation level-dependent contrast magnetic resonance imaging. Biophys J 64:803–812

Ogawa S, Menon RS, Kim SG, Ugurbil K (1998) On the characteristics of functional magnetic resonance imaging of the brain. Annu Rev Biophys Biomol Struct 27:447–474

Ogawa S, Lee TM, Stepnoski R, Chen W, Zhu XH, Ugurbil K (2000) An approach to probe some neural systems interaction by functional MRI at neural time scale down to milliseconds. Proc Natl Acad Sci U S A 97(20):11026–11031

Opdam HI, Federico P, Jackson GD, Buchanan J, Abbott DF, Fabinyi GC, Syngeniotis A, Vosmansky M, Archer JS, Wellard RM, Bellomo R (2002) A sheep model for the study of focal epilepsy with concurrent intracranial EEG and functional MRI. Epilepsia 43(8):779–787

Paxinos G, Watson C (1998) The rat brain in stereotaxic coordinates. Academic Press, San Diego, CA

Peeters RR, Tindemans I, De Schutter E, Van der Linden A (2001) Comparing BOLD fMRI signal changes in the awake and anesthetized rat during electrical forepaw stimulation. Magn Reson Imaging 19(6):821–826

Penfield W (1933) The evidence for a cerebral vascular mechanism in epilepsy. Ann Intern Med 7:303–310

Pinault D, Leresche N, Charpier S, Deniau JM, Marescaux C, Vergnes M, Crunelli V (1998) Intracellular recordings in thalamic neurones during spontaneous spike and wave discharges in rats with absence epilepsy. J Physiol 509(Pt 2):449–456

Ritter P, Villringer A (2006) Simultaneous EEG-fMRI. Neurosci Biobehav Rev 30(6):823–838

Rothman DL, Sibson NR, Hyder F, Shen J, Behar KL, Shulman RG (1999) In vivo nuclear magnetic resonance spectroscopy studies of the relationship between the glutamate-glutamine

neurotransmitter cycle and functional neuroenergetics. Phil Trans R Soc Lond B Biol Sci 354(1387):1165–1177
Sachdev RN, Champney GC, Lee H, Price RR, Pickens DR III, Morgan VL, Stefansic JD, Melzer P, Ebner FF (2003) Experimental model for functional magnetic resonance imaging of somatic sensory cortex in the unanesthetized rat. NeuroImage 19(3):742–750
Salek-Haddadi A, Merschhemke M, Lemieux L, Fish DR (2002) Simultaneous EEG-correlated ictal fMRI. NeuroImage 16(1):32–40
Salek-Haddadi A, Lemieux L, Merschhemke M, Friston KJ, Duncan JS, Fish DR (2003) Functional magnetic resonance imaging of human absence seizures. Ann Neurol 53(5):663–667
Sanganahalli BG, Herman P, Blumenfeld H, Hyder F (2009) Oxidative neuroenergetics in event-related paradigms. J Neurosci 29(6):1707–1718
Sanganahalli BG, Herman P, Behar KL, Blumenfeld H, Rothman DL, Hyder F (2013) Functional MRI and neural responses in a rat model of Alzheimer's disease. NeuroImage 79:404–411
Sanganahalli BG, Herman P, Rothman DL, Blumenfeld H, Hyder F (2016) Metabolic demands of neural-hemodynamic associated and disassociated areas in brain. J Cereb Blood Flow Metab 36:1695
Scholvinck ML, Maier A, Ye FQ, Duyn JH, Leopold DA (2010) Neural basis of global resting-state fMRI activity. Proc Natl Acad Sci U S A 107(22):10238–10243
Schridde U, Khubchandani M, Motelow J, Sanganahalli BG, Hyder F, Blumenfeld H (2007) Negative BOLD with large increases in neuronal activity. Cereb Cortex 18:1814
Schwartz TH, Bonhoeffer T (2001) In vivo optical mapping of epileptic foci and surround inhibition in ferret cerebral cortex. Nat Med 7(9):1063–1067
Shmuel A, Augath M, Oeltermann A, Logothetis NK (2006) Negative functional MRI response correlates with decreases in neuronal activity in monkey visual area V1. Nat Neurosci 9(4):569–577
Shu CY, Herman P, Coman D, Sanganahalli BG, Wang H, Juchem C, Rothman DL, de Graaf RA, Hyder F (2016a) Brain region and activity-dependent properties of M for calibrated fMRI. NeuroImage 125:848–856
Shu CY, Sanganahalli BG, Coman D, Herman P, Rothman DL, Hyder F (2016b) Quantitative beta mapping for calibrated fMRI. NeuroImage 126:219–228
Shulman RG, Rothman DLE (2004) Brain energetics and neuronal activity: applications to fMRI and medicine. John Wiley & Sons, Inc, New York, NY
Shulman RG, Rothman DL, Hyder F (1999) Stimulated changes in localized cerebral energy consumption under anesthesia. Proc Natl Acad Sci U S A 96(6):3245–3250
Shulman RG, Hyder F, Rothman DL (2001) Cerebral energetics and the glycogen shunt: neurochemical basis of functional imaging. Proc Natl Acad Sci U S A 98(11):6417–6422
Shulman RG, Hyder F, Rothman DL (2002) Biophysical basis of brain activity: implications for neuroimaging. Q Rev Biophys 35(3):287–325
Shulman RG, Rothman DL, Behar KL, Hyder F (2004) Energetic basis of brain activity: implications for neuroimaging. Trends Neurosci 27(8):489–495
Shyu BC, Lin CY, Sun JJ, Sylantyev S, Chang C (2004) A method for direct thalamic stimulation in fMRI studies using a glass-coated carbon fiber electrode. J Neurosci Methods 137(1):123–131
Sijbers J, Vanrumste B, Van Hoey G, Boon P, Verhoye M, Van der Linden A, Van Dyck D (2000) Automatic localization of EEG electrode markers within 3D MR data. Magn Reson Imaging 18(4):485–488
Sloan TB (1998) Anesthetic effects on electrophysiologic recordings. J Clin Neurophysiol 15(3):217–226
Sloan HL, Austin VC, Blamire AM, Schnupp JW, Lowe AS, Allers KA, Matthews PM, Sibson NR (2010) Regional differences in neurovascular coupling in rat brain as determined by fMRI and electrophysiology. NeuroImage 53(2):399–411
Smith AJ, Blumenfeld H, Behar KL, Rothman DL, Shulman RG, Hyder F (2002) Cerebral energetics and spiking frequency: the neurophysiological basis of fMRI. Proc Natl Acad Sci U S A 99(16):10765–10770

Snead OC III, Depaulis A, Vergnes M, Marescaux C (1999) Absence epilepsy: advances in experimental animal models. Adv Neurol 79:253–278

Stefanovic B, Warnking JM, Pike GB (2004) Hemodynamic and metabolic responses to neuronal inhibition. NeuroImage 22(2):771–778

Tallgren P, Vanhatalo S, Kaila K, Voipio J (2005) Evaluation of commercially available electrodes and gels for recording of slow EEG potentials. Clin Neurophysiol 116(4):799–806

Tenney JR, Duong TQ, King JA, Ludwig R, Ferris CF (2003) Corticothalamlic modulation during absence seizures in rats: a functional MRI assessment. Epilepsia 44(9):1133–1140

Tenney JR, Duong TQ, King JA, Ferris CF (2004a) FMRI of brain activation in a genetic rat model of absence seizures. Epilepsia 45(6):576–582

Tenney JR, Marshall PC, King JA, Ferris CF (2004b) fMRI of generalized absence status epilepticus in conscious marmoset monkeys reveals corticothalamic activation. Epilepsia 45(10):1240–1247

Tolias AS, Sultan F, Augath M, Oeltermann A, Tehovnik EJ, Schiller PH, Logothetis NK (2005) Mapping cortical activity elicited with electrical microstimulation using FMRI in the macaque. Neuron 48(6):901–911

Turner R, Jezzard P, Wen H, Kwong KK, Le Bihan D, Zeffiro T, Balaban RS (1993) Functional mapping of the human visual cortex at 4 and 1.5 tesla using deoxygenation contrast EPI. Magn Reson Med 29(2):277–279

Van Audekerkea J, Peeters R, Verhoye M, Sijbers J, Van der Linden A (2000) Special designed RF-antenna with integrated non-invasive carbon electrodes for simultaneous magnetic resonance imaging and electroencephalography acquisition at 7T. Magn Reson Imaging 18(7):887–891

Van Camp N, D'Hooge R, Verhoye M, Peeters RR, De Deyn PP, Van der Linden A (2003) Simultaneous electroencephalographic recording and functional magnetic resonance imaging during pentylenetetrazol-induced seizures in rat. NeuroImage 19:627–636

Weisskoff RM, Zuo CS, Boxerman JL, Rosen BR (1994) Microscopic susceptibility variation and transverse relaxation: theory and experiment. Magn Reson Med 31:601–610

Winters WD (1976) Effects of drugs on the electrical activity of the brain: anesthetics. Annu Rev Pharmacol Toxicol 16:413–426

Wood AK, Klide AM, Pickup S, Kundel HL (2001) Prolonged general anesthesia in MR studies of rats. Acad Radiol 8(11):1136–1140

Yang Y, Wen H, Mattay VS, Balaban RS, Frank JA, Duyn JH (1999) Comparison of 3D BOLD functional MRI with spiral acquisition at 1.5 and 4.0 T. NeuroImage 9(4):446–451

Young GB, Ives JR, Chapman MG, Mirsattari SM (2006) A comparison of subdermal wire electrodes with collodion-applied disk electrodes in long-term EEG recordings in ICU. Clin Neurophysiol 117(6):1376–1379

Youngblood MW, Chen WC, Mishra AM, Enamandram S, Sanganahalli BG, Motelow JE, Bai HX, Frohlich F, Gribizis A, Lighten A, Hyder F, Blumenfeld H (2015) Rhythmic 3-4Hz discharge is insufficient to produce cortical BOLD fMRI decreases in generalized seizures. NeuroImage 109:368–377

EEG–fMRI Information Fusion: Biophysics and Data Analysis

28

Nelson J. Trujillo-Barreto, Jean Daunizeau, Helmut Laufs, and Karl J. Friston

28.1 Introduction

Cerebral activity has many attributes: bioelectrical, metabolic, hemodynamic, hormonal, endogenous, exogenous, specialized, integrated, pathological, stable, dynamic, to mention but a few. It then seems obvious that moving from unimodal recordings to multimodal measurements will allow neuroscientists to better capture and understand the nature and structure of cerebral activity. However, the complex and diverse nature of the biological processes underlying the data recorded noninvasively outside the brain means that fusing electrophysiological data and BOLD-related measurements is a challenging endeavor.

The realization of any cognitive, motor, or sensory process rests on cerebral dynamics and creates order in the bioelectric and hemodynamic signals measured with Electroencephalography (EEG) and functional Magnetic Resonance Imaging (fMRI), respectively. To detect and interpret the relevant features of these signals, one typically describes processes at their own temporal and spatial scales. The main sources of scalp EEG signals are postsynaptic cortical currents associated with large pyramidal neurons, which are oriented perpendicular to the cortical surface (Nunez

N. J. Trujillo-Barreto (✉)
Division of Neuroscience and Experimental Psychology, University of Manchester, Manchester, UK
e-mail: nelson.trujillo-barreto@manchester.ac.uk

J. Daunizeau
Motivation, Brain and Behavior Group Brain and Spine Institute, Paris, France

H. Laufs
Department of Neurology, Christian-Albrechts-University Kiel, Kiel, Germany
e-mail: h.laufs@neurologie.uni-kiel.de

K. J. Friston
Wellcome Centre for Human Neuroimaging, Institute of Neurology, UCL, London, UK
e-mail: k.friston@ucl.ac.uk

C. Mulert, L. Lemieux (eds.), *EEG - fMRI*,
https://doi.org/10.1007/978-3-031-07121-8_28

1981). However, the scalp topology of measured electrical potentials does not, without additional (prior) information, uniquely specify the location of underlying bioelectric activity. This issue is referred to as the ill-posed nature of the EEG inverse problem. Conversely, even though fMRI discloses complementary features of neuronal activity (Mukamel 2005; Nunez and Silberstein 2000), it is only an indirect measure, through metabolism, oxygenation and blood flow, where these slow mechanisms provide temporally smoothed correlates of neuronal activity.

Standard unimodal EEG (fMRI) data analysis relies on the specificity of a given bioelectric (hemodynamic) feature of neuronal activity. The vast majority of existing EEG–fMRI integration strategies attempt to enhance the spatial or temporal resolution of the combined EEG–fMRI dataset. But can we exploit their complementary nature to infer the underlying neuronal activity and its dynamics? What specific aspects of the underlying neuronal dynamics can really benefit from such data integration and what aspects can't? This chapter focuses on the alternative approaches to integrating EEG and fMRI information, from a biophysical modeling and signal analysis perspective. We have tried to represent state-of-the-art knowledge and know-how in this important neuroimaging challenge. We will identify promising research directions in EEG–fMRI fusion and the sorts of scientific questions that this approach can address.

28.2 EEG–fMRI Information Fusion: Limitations

Observed mismatches between EEG and fMRI can be interpreted as: (a) a *decoupling* between the electrophysiological and the hemodynamic activity or (b) a signal detection failure (i.e., false-positive/negative results). This distinction is important, because decoupling itself might be very informative. For example, in clinical applications (neuroimaging investigations of epilepsy), evidence for a decoupling between electrophysiological and metabolic activity might be a feature of the pathology itself. Furthermore, factors such as age or medication may also alter both the vascular and the neural function (Tsvetanov et al. 2015), which adds to the confounding effects of changes in neurovascular coupling (NVC) when investigating neurocognitive functioning with EEG–fMRI. The question is whether one can reliably distinguish between a neurovascular decoupling and a signal detection failure. In the following, we will try to list the potential physiological and experimental confounds that constitute the main limitations of any EEG–fMRI information fusion procedure.

28.2.1 Coupling of Electrophysiological and Hemodynamic Responses

The nature of the NVC is at the heart of any possible association between electrophysiological and hemodynamic markers of neuronal activity. Despite the increasing amount of literature in the field of NVC (Riera et al. 2006; Riera and Sumiyoshi

2010), none of the existing biophysical models specify precisely what is meant by "neural activity" that drives hemodynamic responses. Therefore, these models cannot tell us what aspect of neural information processing is reflected in the BOLD signal. Neural information processing within a cortical unit can be described in many different ways, and its relationship to neurophysiological processes can be characterized on different scales; for example, local field potentials versus spiking activity, excitatory versus inhibitory postsynaptic potentials, or different types of receptor activation (Stephan et al. 2004).

Sophisticated animal studies that combine invasive multielectrode recordings with fMRI (Jones et al. 2004; Logothetis et al. 2001; Logothetis and Wandell 2004; Patel et al. 2005, 2004; Puce et al. 1997; Shmuel et al. 2006; Ureshi et al. 2004) or with optical imaging techniques (Martindale et al. 2003; Mathiesen et al. 1998) have started to address these issues. These studies have shown a significant correlation between the time courses of hemodynamic and electrophysiological signals. These encouraging results, at the mesoscopic scale, have supported the assumption that hemodynamic signals underlying fMRI reflect metabolic demand generated by local neuronal activity, with equal increases in hemodynamic signal implying equal increases in the underlying neuronal activity (Heeger et al. 2000; Shulman et al. 2004). The later has also been suggested by noninvasive studies at the macroscopic scale mainly comparing locations of EEG and fMRI sources for a given subject and task. For example, these studies have shown a good concordance for primary sensorimotor (Korvenoja et al. 1999) and visual (Mangun et al. 1998) sources. Similar conclusions emerge when using more complex cognitive tasks; for example, the motor response to visual stimulation (Kawakami et al. 2002), decision-making tasks (Thees et al. 2003), and face perception (Horovitz et al. 2004).

However, a similar number of studies at both the mesoscopic and the macroscopic level have challenged the 1:1 match between imaging signals and local neuronal activity. For example, Sirotin and Das (2009) used optical imaging and intracranial recordings to jointly measure cerebral blood volume, oxygenation, multiunitary activity (MUA), and Local Field Potentials (LFP) from V1, continuously, in alert behaving monkeys. The authors demonstrated a component of the hemodynamic signal that was locked to trial onsets but was independent of visual stimulation and could not be predicted from concurrent spiking or LFP. The authors concluded that therefore, is that "hemodynamic signals in alert individuals engaged in a task are a complicated resultant of multiple neuronal processes that are likely not equivalent to each other on any common measure measured (e.g., energy consumption)" (Das and Sirotin 2011). This conclusion has also been supported by noninvasive macroscopic recordings showing significant differences between the regions implicated by EEG and in fMRI. Gonzalez-Andino et al. (2001) list many of these case reports (mostly involving sensorimotor and auditory cortices) as well as ambiguous multimodal identifications of epileptogenic foci (see also Laufs et al. 2008). Using a bilateral auditory stimulation with ten subjects, Stippich et al. (1998) found an average distance of 14 mm between the MEG dipole and the centre of the fMRI activation.

Additionally, although standard fMRI analysis is usually based on the modulation of the main positive peak of the BOLD response, several studies have suggested that other transients of the signal might be better correlated to the underlying neuronal activity and/or the associated EEG signals. For example, using simultaneous fMRI and electrophysiological recording, Shmuel et al. (2006) demonstrated a negative BOLD response associated with local decreases in neuronal activity (LFP and MUA) below spontaneous activity, detected 7.15 ± 3.14 mm away from the closest positively responding region in V1. At the macroscopic level, Whittingstall et al. (2007) found that the source of the N75 component of the visual evoked potential (checkerboard stimulus) co-localized with a region of positive BOLD activation, while the P100 co-localized with a region of negative BOLD activation. These findings highlight the importance of considering both neuronal and vascular transients for an accurate integration of EEG and fMRI.

In brief, the principal limitations on multimodal EEG–fMRI integration are imposed by physiology. One reason why EEG and fMRI sources may be dislocated is the distance between the neuronal population whose electrical activity is generating the EEG signal and the vascular tree, which provides the blood supply to these neurons, since BOLD signal changes are essentially hemodynamic (Beisteiner et al. 1997). Similarly, in addition to pre- and postsynaptic electrochemical dynamics, a number of physiological processes require energetic support; for example, neurotransmitter synthesis (Patel et al. 2004), glial cell metabolism (Lauritzen 2005), maintenance of the steady-state transmembrane potential (Kida et al. 2001), and so on. These phenomena may cause hemodynamic BOLD changes without EEG correlates (Arthurs and Boniface 2003). This differential sensitivity to neuronal activity and energetics can also arise whenever hemodynamic activity is caused by unsynchronised electrophysiological activity, or if the latter has a closed source configuration that is invisible to EEG. Conversely, if the electrophysiological activity is transient, it might not induce any significant (i.e., detectable) metabolic activity changes (Nunez and Silberstein 2000).

28.2.2 Experimental Limitations

Another important potential source of bias in EEG–fMRI fusion is experimental variability. In some situations, it might be necessary to acquire the EEG and fMRI data in separate sessions. In this case, habituation effects, variations in the stimulation paradigm, or any other difference between sessions may lead to differential activity of neural networks (Gonzalez-Andino et al. 2001; Rosen et al. 1998; Wagner and Fuchs 2001).

Simultaneous EEG–fMRI acquisition techniques have been developed specifically to address these issues. This technical challenge was largely pioneered by neuroimaging groups focusing on pharmacoresistant epilepsy (Ives et al. 1993; Lemieux et al. 2001; Warach et al. 1996) and later on used for the identification of intrinsic brain states reflecting cognitive default modes by assessing associations between spontaneous EEG oscillations and fluctuations of the fMRI resting-state

signal (see Tagliazucchi and Laufs 2015 for a review) as well as for answering basic research questions in the context of classical cognitive experiments (Ullsperger and Debener 2010). Nevertheless, and despite advances in simultaneous EEG–fMRI hardware and software, the signal-to-noise ratio (SNR) of these signals is still significantly lower than the corresponding unimodal paradigms (but see Liston et al. 2006). As MRI moves toward using ultrahigh magnetic fields in the quest for increased signal-to-noise, the question arises whether combined EEG–fMRI measurements are feasible at magnetic fields of 7 T and higher (see Neuner et al. 2014 for a recent review). This is mainly due to reciprocal electromagnetic perturbations (Krakow et al. 2000; Kruggel et al. 2000). For the EEG signal, this SNR degradation can be catastrophic: the most important artifacts in the raw data can completely mask the signal of interest. These are due to a complex combination of factors, including the MR field strength (and thus frequency) and the orientation/positioning of the EEG recording equipment relative to the RF coil and the MR gradients. All of these unavoidable artifacts manifest themselves as induced voltages that add linearly to the EEG signal and obscure the biological signal of interest; see the chapters "EEG Instrumentation and Safety," "EEG Quality: Origin and Reduction of the EEG Cardiac-Related Artefact," and "EEG Quality: The Image Acquisition Artefact." Although denoising algorithms have been reasonably successful in gradient artifact correction (Allen et al. 2000; Garreffa et al. 2003), the pulse-related artifact remains a challenge (Ellingson et al. 2004; Nakamura et al. 2006), as described in the chapter "EEG Quality: Origin and Reduction of the EEG Cardiac-Related Artefact."

28.3 EEG–fMRI Information Fusion: Solutions

Despite its great promising potential, simultaneous EEG–fMRI does not necessarily yield both the spatial and the temporal resolution that might be desirable given the properties of each recording modality alone. Since the main limitations of EEG–fMRI information fusion are well established, many data analysts have argued that dedicated modeling and signal processing tools should be used to combine the advantages of EEG and fMRI (Dale and Halgren 2001; Hallett 2002; Liu et al. 2006; Mulert et al. 2004; Trujillo-Barreto et al. 2001). Nevertheless, because the intrinsic features of the chosen analysis method strongly influence the putative outcome, the choice of the method used for data integration is of crucial importance.

28.3.1 Information Fusion: Definition

Reconstructing the spatial deployment of current density from EEG measurements is an intrinsically ill-posed problem. On the other hand, estimating neuronal activity from the hemodynamic response is a difficult temporal deconvolution problem. Critically, the dual fitting of the bioelectric and hemodynamic responses does not necessarily circumvent the difficulties of the inverse problems that attend each

modality. So what exactly do we expect to gain from EEG–fMRI information fusion? What does "information fusion" mean? The *Collins Concise Dictionary* gives the following definitions: "information: knowledge acquired through experience or study" and "fusion: the act or process of fusion or melting together." Although we may be able to reconcile these two notions, intuitions about information fusion can be finessed using psychoacoustics and the link between "consonance" and "auditory sensation of fusion."

In music, a consonance (Latin *consonare*, "sounding together") is a harmony, chord, or interval that is considered stable, as opposed to a dissonance, which is considered unstable. The strict definition of consonance may relate to sounds that are pleasant, while the more general definition includes any sounds that are used freely. An example of perfect consonance is the octave interval. The correlation between consonance and fusion has been known since the mid-nineteenth century: the more the interval is consonant, the more we tend to perceive only one sound; the more the interval is dissonant, the more we can tease apart the different sounds that comprise the chord.

This characteristic is an essential aspect of information fusion procedures, which rely on the coherence of information, in the context of uncertainty. In other words, optimal information fusion should be framed in information theoretic terms. Bayesian inference furnishes a probabilistic framework that allows one to formalize the propagation of both information and uncertainty from observations (the data) to unknown causes. This framework requires a so-called *generative model* (or forward model) that specifies the (possibly uncertain) relationships between the data and what caused them. In this context, data analysis entails specifying an appropriate model, with a set of unknown parameters, and then looking for parameter distributions that explain the data. This is called *model inversion* and involves extracting information from data by quantifying the uncertainty associated with a model of the system generating data. If the model can generate multimodal data, its inversion corresponds to a *model-driven* approach to data fusion.

However, the underlying generative model of the multimodal data may be too complicated or simply unknown. In the case of joint EEG and fMRI, generative models are rather complex, including nonlinear dependencies between the variables of the model and a high number of parameters. More importantly, these generative models critically rely on assumptions about the nature of the NVC, which, as we will discuss later, is still not sufficiently understood. Therefore, not all approaches to EEG–fMRI fusion rely on a multimodal generative model, but a good part of the literature has focused on the development of *data-driven* approaches. These approaches make the fewest assumptions and use the simplest models, both within and across modalities. Typical assumptions can include linear relationships between variables (avoiding model-dependent parameters) and/or use of model-independent priors such as sparsity, non-negativity, statistical independence, low rank, and smoothness, among others. A data-driven approach is therefore self-contained in the sense that it relies only on the observations and the assumed relationships in the data: it avoids external input. For this reason, data-driven methods are sometimes called "blind." Because data fusion depends bilaterally on multimodal data, it is

inherently symmetric. However, there are other (asymmetric) approaches, where one modality is treated as a cause or predictor of the other. Given the wide variety of existent approaches, here we use an all-embracing definition of data fusion: *it is the analysis of multiple datasets such that the different datasets can interact and inform each other*. We now consider the distinction between symmetrical and asymmetrical procedures.

28.3.2 Asymmetrical vs. Symmetrical Approaches

As noted above, the quantitative contribution of neurophysiological processes in "active" areas to electromagnetic and hemodynamic signals is largely unknown (Daunizeau et al. 2005; Gonzalez-Andino et al. 2001; Stephan et al. 2004). Nevertheless, one can define "neuronal activity" operationally as the state of nodes in a network responding to specific events (e.g. cognitive, sensorimotor, or spontaneous changes in brain activity) (Friston 2005a). This allows one to consider event-related (ER) EEG and fMRI data as measures of "neuronal activity," since the ER response is a reproducible EEG or fMRI signature that can be elicited systematically (Friston 2005b). However, electromagnetic and metabolic responses, as detected by EEG and fMRI, are not necessarily caused by the same underlying neuronal processes.

"Neuronal activity" Ω can be decomposed into two overlapping subspaces, Ω_{EEG} and Ω_{fMRI}, which correspond to the parts of Ω that contribute to EEG and fMRI signals, respectively (Pflieger and Greenblatt 2001). The intersection Ω_1 (see Fig. 28.1a) defines a "common substrate" of neuronal activity. Conversely, Ω_2 (Ω_3) denotes the subspace of neuronal activity detected by EEG (fMRI) that does not contribute to fMRI (EEG) measurements. This decomposition formalizes the apparent coupling–uncoupling between bioelectrical and hemodynamic responses.

What should we expect to learn about neuronal activity by combining EEG and fMRI? Since no information about Ω_2 (Ω_3) is available from the fMRI (EEG), no multimodal procedure will provide a better characterization of this activity subspace than a unimodal EEG (fMRI) analysis. However, a multimodal approach should benefit from the complementary nature of EEG and fMRI by providing different perspectives on the common subspace, Ω_1.

During the past two decades, many reports have focused on analytical techniques devoted to EEG–fMRI integration. These techniques can be broadly divided into asymmetrical or symmetrical approaches (see Fig. 28.1). Asymmetrical approaches use information from one modality in order to predict or constrain the other modality and therefore can be further subdivided into (Fig. 28.1b (i)) asymmetrical EEG to fMRI approaches and (Fig. 28.1b (ii)) asymmetrical fMRI to EEG approaches. In general, these approaches only consider certain features of the recorded data and hence, important spatial information or temporal information measured from fMRI and EEG respectively may be overlooked. Additionally, prior knowledge of one modality is used to guide and improved the results in the other modality, which stablishes a degree bias (asymmetry) in favor of the guiding modality.

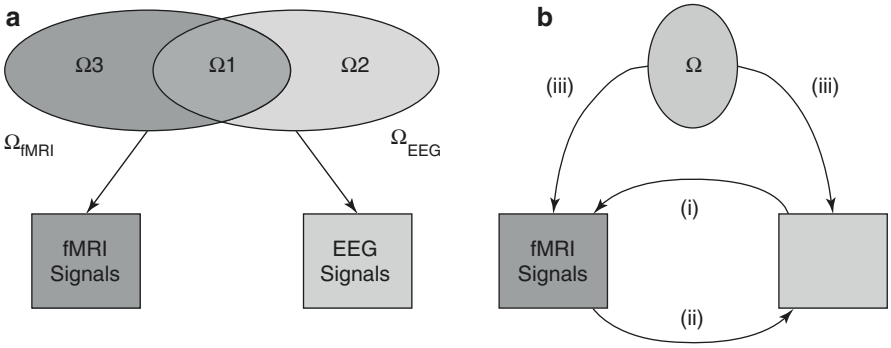

Fig. 28.1 Formalization of the EEG–fMRI coupling–uncoupling (**a**) and EEG–fMRI fusion approaches (**b**). Any multimodal information fusion approach will be beneficial for inferring common neuronal states, Ω_1. This means that asymmetrical EEG–fMRI approaches systematically bias their estimate of Ω_1 by introducing information from Ω_{EEG} ((i): EEG to fMRI approaches, i.e., integration through prediction) or Ω_{fMRI} ((ii): fMRI to EEG approaches, i.e., integration through constraints). In contrast, symmetrical EEG–fMRI fusion approaches rely on a joint EEG–fMRI generative model, which allows the estimation of Ω_1 to be derived from an optimal balance between EEG- and fMRI-derived information ((iii): integration through forward models). (Adapted from Daunizeau et al. 2007 and Kilner et al. 2005)

Symmetrical fusion approaches (Fig. 28.1b (iii)), on the other hand, incorporate both modalities into a joint analysis where they can mutually inform each other, allowing full spectrum exploration between the different data types. Importantly, symmetric approaches rely on a common generative model, offering a multimodal fusion where the two data sources are given the same weight. In the following we will review each of these techniques to EEG–fMRI integration.

28.3.3 EEG to fMRI Approaches

This type of EEG–fMRI integration is necessarily implemented within a simultaneous EEG–fMRI acquisition paradigm. These techniques consider covariations of changes over time between a given EEG-defined event or feature and region-specific fMRI signals at a within-subject level. The goal is to localize brain regions whose fMRI response is temporally correlated with a given EEG-defined event or feature. That is, temporal information from the EEG signal is used as a constraint or predictor variable in the fMRI time series model. Here, EEG is typically preprocessed to a point where a specific EEG feature of interest over the time course of the recording can be extracted. fMRI data then follow standard procedures up to the point of formulating the General Linear Model (GLM) for first-level statistics. At this point, hemodynamic responses are parameterized using the trial-wise extracted EEG feature. Typically, the regressors in the GLM are defined by convolving the EEG feature with a hemodynamic response function (HRF). The idea is that an enhanced amplitude in the EEG feature leads to an upscaling of the hemodynamic response function for a given event.

The different methods used to implement this approach can be largely subdivided into univariate and multivariate methods (see Abreu et al. 2018a for a recent review), depending on the number of EEG channels used to extract the feature of interest. In univariate methods, a limited number of EEG time courses (often a single time course) representative of the phenomena of interest are selected, and temporal or spectral features are then extracted and used to predict BOLD changes. Multivariate methods, in contrast, consider multiple EEG channels in the feature extraction step. The choice of method ultimately depends on the type of activity of interest.

The pioneering work in this direction has been pursued largely by functional imaging groups focusing on presurgical planning for pharmacoresistant epilepsy (Aghakhani et al. 2004; Al-Asmi et al. 2003; Archer et al. 2003; Boor et al. 2003; Grova et al. 2008; Krakow et al. 2000; Lemieux et al. 2001; Salek-Haddadi et al. 2003; Warach et al. 1996); see the chapter "EEG–fMRI in Adults with Focal Epilepsy" for an overview. In the simplest approach, after artifact correction, the epileptiform activity is identified by an expert on the EEG. These events are then convolved with a HRF and used as a regressor in standard GLM analysis (Bagshaw et al. 2005; Leal et al. 2016; Lemieux et al. 2001; LeVan and Gotman 2009); as described in the chapter "Experimental Design and Data Analysis Strategies." The epileptic events can be further subdivided into a succession of stages (e.g., early ictal, clinical seizure onset, and late ictal) and model each stage separately (Thornton et al. 2010). Other features of the interictal epileptiform discharges (IED) as possible predictors of the epilepsy-related BOLD changes. These include the amplitude, energy, width, slope of the rising phase, and spatial extent of the IED to modulate the amplitude of the stick function modeling of the IED events in the GLM (Bénar et al. 2002; LeVan et al. 2010; Murta et al. 2016). In the context of task-related EEG–fMRI studies, temporal EEG features are typically extracted from the associated single trial ERPs and used to predict the trial-specific amplitude and response latency of the BOLD fluctuations (Bénar et al. 2007; Debener 2005; Debener et al. 2006; Nguyen and Cunnington 2014; Wirsich et al. 2014).

The rich temporal and spectral information contained in the EEG has also motivated using spectral features extracted from the time–frequency decomposition of the EEG signal, as predictors of the fMRI signal (Laufs et al. 2006; Moosmann et al. 2003; Scheeringa et al. 2008). This method has been used to investigate the neuronal correlates of spontaneous cerebral activity occurring when the subject is not exposed to any extrinsic stimulation or pathological activity. After simultaneous EEG–fMRI acquisition, spontaneous fluctuations of power in specific frequency bands are quantified in the EEG traces. Time-dependent power in each of these frequency bands is used to form a regressor in the GLM of fMRI (Goldman et al. 2002). This can also be extended to include EEG power over multiple frequency bands as simultaneous repressors in a GLM analysis of the fMRI data, so that their individual contributions to the BOLD signal, as well as their interactions, can be investigated (de Munck et al. 2009; Mantini et al. 2007). Other spectral features used include (but are not restricted to) the total power (Wan et al. 2006), linear combination of band-specific power values (Goense and Logothetis 2008), mean

frequency (Rosa et al. 2010a, b), and root mean square frequency (Kilner et al. 2005; Rosa et al. 2010a, b). In the context of invasive recordings, the phase to amplitude coupling of intracranial EEG recorded simultaneously with fMRI during a motor task has also been reported to be a good predictor of the BOLD response (Murta et al. 2017).

Other authors have proposed multivariate EEG to fMRI methods, which use multiple EEG channels for the feature extraction in order to capture spatial information, which cannot be assessed by the univariate methods. The extraction of the features in this case can be based on: (1) the spatial correlation of EEG maps with reference spatial maps, such as spatial templates from separate EEG recordings (Grouiller et al. 2011) or EEG microstates' maps (Britz et al. 2010; Schwab et al. 2015; Yuan et al. 2012); (2) |functional connectivity measures across different EEG channels such as partial directed coherence (Biazoli et al. 2013) or phase synchronization index (Abreu et al. 2018b; Mizuhara et al. 2005); and (3) multiway decomposition methods (Marecek et al. 2016; Schwab et al. 2015), among others. After the feature extraction, the multivariate methods for asymmetrical integration approach follows more or less the same steps as in univariate methods by including the extracted feature or combination of features as predictors of the fMRI signal in a standard GLM analysis.

Until very recently, most EEG–fMRI approaches focused on predicting the BOLD signal at each voxel based on the EEG extracted feature. However, there is increasing effort in the development of similar approaches for the study of the temporal fluctuations of BOLD signal correlations across the brain, the so-called dynamic functional connectivity (see (Tagliazucchi and Laufs 2015) for a recent review). Although this area of research is relatively recent, and the neurophysiological meaning of these connectivity fluctuations is still not clear, including EEG information in this type of analysis seems like a promising way forward, opening new opportunities for the development of novel EEG–fMRI methods.

There are several points that one has to bear in mind when interpreting the results obtained using EEG to fMRI approaches. These approaches assume that the neural properties contributing to the signals captured by both modalities partly overlap and exhibit a linear association. However, no specific assumption is made about the spatial organization of activation patterns. Therefore, effects can be obtained in brain structures or networks that are not necessarily the biophysical generators of, say, the ERP recorded at the scalp (Debener 2005; Minati et al. 2008). Additionally, single-trial EEG analyses have to rely on techniques that increase the signal-to-noise ratio of individual trials. When dealing with spectral signatures, considering narrow frequency bands of the EEG can be thought of as a filtering mechanism. Another commonly used method is to apply algorithms that allow unmixing of spatiotemporally overlapping EEG signals before feature extraction, such as Independent Component Analysis (ICA) (James and Hesse 2005; Onton et al. 2006). But invariably, only a fraction of the ongoing brain activity can be used for an EEG to fMRI analysis. Critically, the selection of the feature of interest is usually determined by the research question addressed, and the obtained results should be interpreted with caution. For example, although both ERP amplitudes and latencies

have been shown to be correlated with hemodynamic responses, latencies are less likely to directly reflect activations of potential generators (Bénar et al. 2007).

28.3.4 fMRI to EEG Approaches

The aim of these techniques is to finesse the study of fast dynamics of neuronal activity as measured by EEG by using fMRI-derived spatial priors in the EEG source reconstruction problem. Again, this has been the subject of many reports in the past two decades. The conceptual framework that dominates in this field rests on functional integration or coupling among sources (Lin et al. 2004; Liu et al. 2006). Going beyond functional specialization (Friston et al. 1996), evoked responses are understood as arising in an interacting network of connected "nodes" (the localized regions); these interactions are referred to as "arcs" or "edges" in graph theory. Interactions are expressed in the temporal dynamics of neuronal activity, since they shape the influence of one neuronal population on another. It is thought that characterizing these connections requires the use of EEG, since this is the only neuroimaging modality whose temporal resolution is similar to that of the underlying neuronal processes (but see Friston et al. 2019 for a discussion about the possibility of using fMRI to estimate conduction delays in the millisecond range). However, the EEG spatial inverse problem induces uncertainty about the number and deployment of nodes in the network, which is why fMRI constraints are potentially useful.

This approach can be divided into two classes, associated with the EEG source model employed: (a) the equivalent current dipole (ECD) model (Kiebel et al. 2008) and (b) the distributed source model (Friston et al. 2008). Dipolar fMRI to EEG approaches simply associate each fMRI focus with an ECD, whose position lies a priori at the centre of the activation (Wagner and Fuchs 2001). This type of a priori constraint is hard, in the sense that the results of the fMRI analysis are not questioned (e.g., the number of active regions). In addition, since the ECD model does not accommodate the spatial extent of underlying active regions, it is difficult to assess the relevance of the fMRI constraint (Liu et al. 2006). For example, it has been shown that many ECDs are required to model spatially extended regions correctly (Shiraishi et al. 2005).

Distributed fMRI to EEG approaches rely on "weighted regularization techniques" for source reconstruction, which can be reformulated in a Bayesian framework where regularization terms or soft constraints are included in the form of prior distributions on the sources (Trujillo-Barreto et al. 2004). In this approach, fMRI data are used to bias the EEG inverse solution toward those locations deemed as statistically significant in the view of fMRI. In brief, fMRI activations are treated as empirical priors on the spatial profile of cortically distributed sources, such that their influence depends on the EEG data (Daunizeau et al. 2005). As a consequence, the Bayesian posterior estimates penalize sources whose fMRI-derived activation probability is low. Importantly, these estimates represent our updated posterior beliefs (with respect to the fMRI prior) about the spatial deployment of the sources, after having observed the EEG data. In doing so, potential biases due to spatial

decoupling between the two modalities can be alleviated. In practice, initial applications of this approach showed robust estimation of the position and extent of underlying sources whenever the fMRI-derived constraints were valid (Ahlfors and Simpson 2004). However, when some sort of decoupling occurred, the EEG source reconstruction incurred significant bias (Liu et al. 2006), which is why many variants of the fMRI penalty term have been proposed (Babiloni et al. 2003; Halchenko et al. 2005; Liu et al. 1998; Rosa et al. 2010a, b).

There are two possible reasons for the observed biases. First, in initial fMRI to EEG approaches, an fMRI-derived BOLD activation map was used to compute a single global spatial prior in the form of a fix form (usually diagonal) source covariance matrix scaled by a single hyperparameter that controlled the balance between the effect of the prior and the information in the EEG data (Daunizeau et al. 2005; Liu et al. 2006). As a result, all fMRI-activated areas either valid or not are given the same importance in the source estimation. Therefore, depending on the reliability (level of noise) of EEG data, sources corresponding to invalid fMRI activations can be artificially boosted if the majority of fMRI activations are supported by the EEG data. In other words, supporting fMRI activations in one area will affect the inference in another area. Second, in standard approaches, the same static global spatial prior is usually applied simultaneously to all time points in the EEG data (Nguyen et al. 2016). The later means that biases can occur even if all the fMRI activations correspond to true EEG source activations, because they are not necessarily coupled in time (Whittingstall et al. 2007).

To overcome these problems, several developments of the Bayesian framework for fMRI to EEG integration have been proposed during the last two decades (Daunizeau et al. 2005; Henson et al. 2010; Nguyen et al. 2018, 2016). For example, Henson et al. (2010) capitalized on the use of multiple sparse priors (MSP) for EEG source reconstruction (Friston et al. 2008) and proposed to construct fMRI-derived priors where each suprathreshold fMRI cluster is treated as a separate covariance component, each weighted by its own scale hyperparameter (MSP-fMRI). This allowed for imposing multiple local spatial fMRI priors so that the individual effect of each fMRI cluster on the estimation of the sources can be assessed by estimating the corresponding hyperparameters from the data. In this way, fMRI clusters that do not receive support from the EEG data are automatically penalized in favor of those which do contribute. The authors compared using (1) multiple versus single, (2) valid versus invalid, (3) binary versus continuous, and (4) variance versus covariance fMRI priors. Interestingly, they found that the MSP method benefited little from additional fMRI information and suggested that using MSP already provides a sufficiently flexible generative model.

However, in the above study, the MSP-fMRI was applied to the full time window of analysis, which did not allow for assessing the effect of the temporal uncoupling. In a related approach, Nguyen et al. (2018, 2016) proposed segmenting the EEG data first into nonoverlapping time windows and then applying the same MSP-fMRI on each window separately. The authors reported significant improvement of the results in an ERP study, when compared to the standard method of using a single fMRI global prior. Unfortunately, the difference between the proposed windowed

MSP-fMRI analysis and a common MSP-fMRI for the whole time window was not analyzed. Finally, given solutions constrained or unconstrained by fMRI, which should be chosen? In Daunizeau et al. (2005), a Bayesian model comparison method was proposed to decide whether one should use the fMRI constraint or not. This approach has been applied successfully to clinical epilepsy data (Grova et al. 2008).

One obvious advantage of the fMRI to EEG approach is that it can be applied to EEG and fMRI data acquired under comparable, but not necessarily identical experimental conditions, as information derived from single trials is not taken into account. This allows for an individual optimization of experimental conditions for each modality, by avoiding the complications of joint EEG–fMRI recordings. One interesting possibility would be to apply the MSP-fMRI windowed approach described above at the single trial level. However, even with the most advanced methods, the optimality and validity of the fMRI to EEG approach strongly relies on the assumption of a tight coupling between electrophysiological and fMRI markers of neuronal activity.

28.3.5 Symmetrical EEG–fMRI Approaches

As noted above, divergences between the anatomical localization obtained by functional techniques and those obtained from electrocortical stimulations are not infrequent. This has insidious consequences for asymmetrical EEG–fMRI approaches, since the relative importance of EEG and fMRI is not evaluated. For instance, in Dale et al. (2000), the authors recognized that when fMRI was considered the "truth" for spatial information, serious biases could occur in fMRI-regularized EEG source reconstruction when the actual electrophysiological activity did not induce significant variations in the BOLD signal. Therefore, it has been observed that the "integration of functional modalities into the solution of the neuroelectromagnetic inverse problem should be cautiously considered until a tighter coupling between BOLD effects and electrophysiological measurements could be established" (Gonzalez-Andino et al. 2001). However, even if there is no one-to-one relationship between EEG and BOLD measurements, both modalities can still inform each other, if they provide complementary constraints on model parameters.

28.3.5.1 Model-Driven Approaches

It has been argued that "the search for the spectral (electrophysiological) correlates of hemodynamic responses is doomed to failure because electrophysiological responses do not cause hemodynamic responses and hemodynamic responses do not cause induced responses. Instead, both are caused by underlying neuronal activity"; and that "instead of trying to understand the relationship between EEG and BOLD measurements, it is more tenable to treat both as the observable consequences of hidden neuronal activity, and try to understand how neuronal activity causes these (multimodal) measurements" (Friston et al. 2019).

As noted earlier, any generative model would have to rely on an accurate NVC model to effectively disentangle the neuronal and vascular parameters. Therefore,

an outstanding modeling effort has focused on designing forward models of NVC that are neurophysiologically grounded. This has been done for the healthy brain (Attwell and Iadecola 2002; Aubert and Costalat 2005; Babajani-Feremi and Soltanian-Zadeh 2010, 2006; Lauritzen 2005; Riera et al. 2007, 2006; Shulman et al. 2001; Sotero and Trujillo-Barreto 2008, 2007) and in the context of neurological pathology (see e.g., Iadecola 2004; Lu et al. 2004).

These advances have been limited due to the lack of a full understanding of the biophysical mechanisms underlying NVC. In a recent systematic review (Hosford and Gourine 2019) carried out a meta-analysis of published data reporting the effects of pharmacological or genetic blockade of all hypothesized signalling pathways of NVC (Fig. 28.2a). The outcome measure was the percent reduction of the NVC response assessed using in vivo animal models. The authors found that blockade of neuronal Nitric Oxide Synthase (nNOS) had the largest effect of inhibiting any individual target, reducing the neurovascular response by 64% (average of 11 studies). Moreover, inhibition of multiple targets in combination with nNOS blockade had no further effect (Fig. 28.2b). This study suggests the existence of an unknown signalling mechanism accounting for about one third of the NVC response.

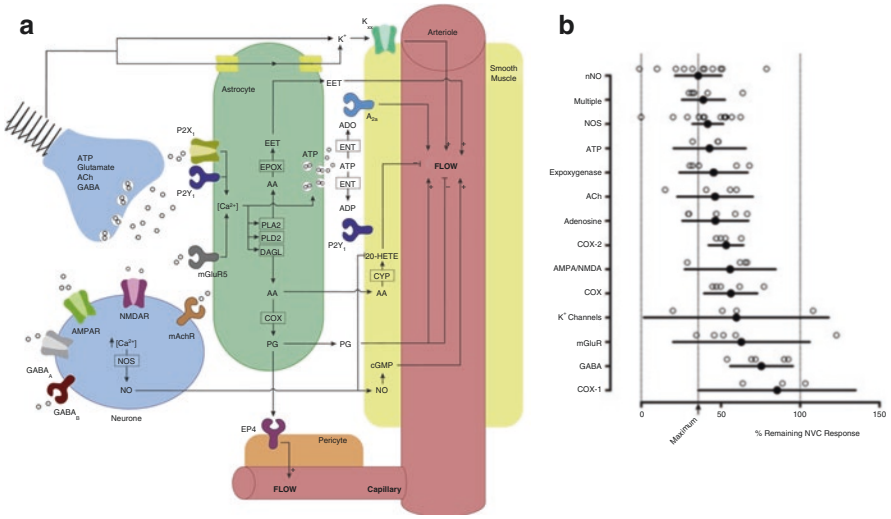

Fig. 28.2 Hypothesized signalling mechanisms of the NVC. (**a**) Schematic illustration of all hypothesized pathways mediating the NVC response, included in the meta-analysis of Hosford and Gourine (2019). (**b**) Summary plot illustrating the percentage means (with 95% confidence intervals) of coupling (NVC) responses that remain in conditions of pharmacological or genetic blockade of hypothesized signalling pathways in vivo. Individual data points illustrate the magnitude of the effects of the 79 experimental treatments. "Multiple" category includes the results of combined neuronal Nitric Oxide Synthase (nNOS) inhibition with blockade of at least one other target. See the original publication for a detailed description of all the acronyms in the figure and references to all the studies included in the meta-analysis. (Reprinted from Figures 1 and 2 of Hosford and Gourine 2019)

Despite the lack of established NVC models, the main link between electrophysiological activity and energy consumption has been invariably modeled through glucose metabolism. This assumes a monotonic mapping between excitatory activity and energy budget, and thus the BOLD signal (through blood flow). The last part of this metabolic–hemodynamic cascade (i.e., the mesoscopic relationship between blood flow and measured BOLD signal) is relatively well established and forms the basis of the "balloon model" (Buxton et al. 1998) and its extensions (Buxton et al. 2004; Friston et al. 2000; Havlicek et al. 2015; Sotero and Trujillo-Barreto 2007; Stephan et al. 2007, 2004) (see Buxton et al. 1998 for seminal work, and Friston et al. 2000 for its extension).

Despite these advances, four major issues regarding the NVC at the level of the mapping between energy budget and blood flow changes remain unresolved: (a) some authors emphasize the potentially important role of interplay between neuronal and glial metabolisms in the NVC (Aubert and Costalat 2005; Pellerin and Magistretti 1994); (b) whether or not the energy consumption drives cerebral blood flow directly or is flow modulated by independent fast neurotransmitters (Attwell and Iadecola 2002; Riera et al. 2006); (c) so far, the quantitative contribution of inhibitory neuronal activity to energy consumption remains unclear (Chatton et al. 2003; Kida et al. 2001; Sotero and Trujillo-Barreto 2007); (d) the contribution of physiological noise to the variability of induced electroencephalographic and hemodynamic responses may have been overlooked (Buckner and Vincent 2007; Fukunaga et al. 2008; Krüger and Glover 2001).

Figure 28.3 summarises the key components of a neurophysiologically and biophysically grounded generative model of both EEG and fMRI data, considering modeling on both the anatomofunctional and the NVC. This model would ideally involve many levels of description, including (a) the macroscale, that is, the relationship among active brain regions, shaping the dynamics of local (mesoscale) neuronal populations (Friston et al. 2019, 2003); (b) the mesoscale, that is, the interplay of local excitatory and inhibitory neuronal populations (Kiebel et al. 2007); and (c) the microscale, where NVC is mediated through cellular mechanisms (Riera et al. 2006; Riera and Sumiyoshi 2010). The availability and reliable inversion of this kind of generative models would provide principled framework within which to combine different modalities. A first step toward such an integrated EEG–fMRI generative model was proposed by Sotero et al. (2007) and Sotero and Trujillo-Barreto (2008). This biophysically informed model couples neuronal activity, cerebral metabolic rates of glucose and oxygen consumption, and finally cerebral blood flow in order to predict both electroencephalographic and BOLD responses. More recently, the Dynamical Causal Model (DCM) framework (Friston et al. 2003) was extended to include a common four population canonical microcircuit model underlying the generation of both the EEG and the fMRI responses (Friston et al. 2019). This extended DCM has the potential to reveal laminar specific contributions to the BOLD signal measured with high-resolution fMRI.

Inversion of these integrative DCMs for EEG and fMRI may provide us with the key insights into the genesis of neuronal activity and how it is mediated by intrinsic–extrinsic connections. Moreover, having a physiologically informed neuronal

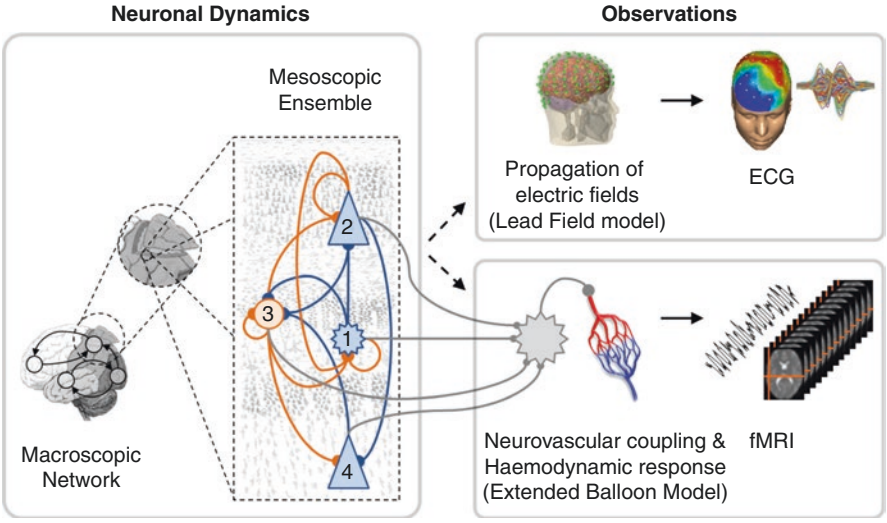

Fig. 28.3 Components of a generative model for EEG–fMRI symmetrical fusion. In this sort of model, the EEG scalp data are assumed to be an instantaneous measure of the electrical potential generated by the activity of a subpopulation or neural mass (e.g., pyramidal cells), which has been propagated through the head tissues (Baillet et al. 2001). On the other hand, the fMRI data are modeled as a temporally smoothed response to mostly presynaptic neuronal activity (Logothetis et al. 2001) that results from a slow cascade of metabolic–hemodynamic events (Aubert and Costalat 2005; Friston et al. 2000; Riera et al. 2006). Left: laminar specific canonical microcircuit (CMC) comprising four populations per brain region: (1) spiny stellate cells, (2) superficial pyramidal cells, (3) inhibitory interneurons and (4) deep pyramidal cells. Each CMC is linked through extrinsic (between region) forward and backward connections (extrinsic connections from other areas are omitted in the CMC for simplicity). Right: observed signals. Pre- or postsynaptic neuronal signals are combined (at the level of the putative astrocytes), and this drives the hemodynamic part of the model. Blood flow is increased to the venous compartment (pictured), which is accompanied by changes of blood volume and the level of deoxyhemoglobin. Electrophysiological and fMRI measurements arise from the neuronal and hemodynamic parts of the model respectively, mediated by a spatial lead field model for EEG and a BOLD signal model for fMRI

and hemodynamic model would also allow, in principle, resolving outstanding questions about the nature of the BOLD response (Friston et al. 2019). Let's take the above two model development as examples. Using simulations, Sotero and Trujillo-Barreto (2007) were able to reproduce experimental results confirming a tight link between negative BOLD responses and inhibitory activity (Shmuel et al. 2006). The model assumed that cerebral blood flow (CBF) is not directly controlled by energy usage, but it is only related to excitatory activity. In a further study the same authors used fMRI data recording during a motor task to test this hypothesis (Sotero et al. 2009). The authors used a Bayesian model Comparison approach to adjudicate between three different models in which CBF was related to (1) inhibition only, (2) excitation only, and (3) both inhibition and excitation. The authors found significant evidence in favor of model (2) which supported their previous hypothesis. When extended to explain EEG–fMRI data fusion (Sotero and Trujillo-Barreto 2008), this

model could also reproduce phenomenological predictions such as a linear relationship between the increase in BOLD signal and a shift in the EEG spectral profile to higher frequencies (Kilner et al. 2005). Moreover, the model was also able to reproduce the experimentally observed pattern of positive BOLD–EEG correlations in thalamus and negative BOLD–EEG correlations in the occipital cortex (Goldman et al. 2002; Laufs et al. 2003; Moosmann et al. 2003).

In another simulation results, using the four populations, extension of the DCM approach (Friston et al. 2019) was also able to demonstrate decoupling between fMRI and EEG/LFP data features, despite having the same underlying neuronal sources. More recently, using realistic simulations, the same integrative DCM was used to evaluate whether integrating EEG and fMRI data offered a better characterization of functional brain architectures than either modality alone (Wei et al. 2020). In brief, the authors used a Bayesian fusion approach for inversion of the model, where empirical neuronal priors derived from DCM of the EEG data were used to inform subsequent DCM of the fMRI data. The authors found that multimodal data fusion provided a substantial improvement in model evidence, indicating a more efficient estimation of model parameters, compared to inverting fMRI data alone. Importantly, the results suggested that using information from EEG data can improve (due to increased information gain) estimates of hemodynamic parameters; providing a proof of principle that Bayesian fusion is necessary to resolve conditional dependencies between neuronal and hemodynamic estimators.

The above results suggest that, even in the absence of a one-to-one relationship between EEG and BOLD measurements, both modalities can still inform each other, if they provide complementary constraints on model parameters (Friston et al. 2019). Until a multimodal generative model based on a more realistic NVC and its associated inversion is available, the objectives of any symmetric fusion of multimodal EEG–fMRI information should be twofold. First, the approach should be able to identify the parts of EEG and fMRI signals that convey complementary information about the common substrate underlying these signals (i.e., Ω_1 in Fig. 28.1). Second, it should exploit such information to decrease uncertainty when inferring on this common subspace. As a consequence, a symmetrical fusion approach requires the explicit definition of the common neuronal states that engenders both EEG and fMRI measurements. This entails building a model that encompasses our knowledge about the link between bioelectrical and hemodynamic activities and being able to invert that model, given the joint EEG–fMRI data. In practice, very few fusion approaches (i.e., data analysis techniques) have relied on realistic neurophysiological models (Riera et al. 2006). This is because the complexity of real metabolic–hemodynamic cascades renders the estimation of their parameters an intractable problem (see discussion in Sotero and Trujillo-Barreto 2008; Sotero and Trujillo-Barreto 2007).

Other researchers have relied on simplified variants of the NVC model by restricting its parameters to model some common properties exhibited by "active" areas contributing to both event-related EEG and fMRI measurements. For example, Kilner et al. (2005) applied dimensional analysis to relate hemodynamic changes (as monotonically mapped from rates of energy dissipation) to the spectral

profile of EEG activity. The analysis suggested that increases in BOLD signal should be associated with a shift in the EEG spectral profile to higher frequencies. The predictions of this phenomenological model have been partially experimentally verified in a single-subject case study (Laufs et al. 2006) and have also been reproduced by biophysically informed neurogenerative models of EEG–fMRI (Sotero and Trujillo-Barreto 2008) but have not been included in any symmetrical EEG–fMRI fusion approach so far.

As another example, in Daunizeau et al. (2007), a symmetrical multimodal EEG–fMRI information fusion was applied to the analysis of recordings from a patient with epilepsy in order to identify areas involved in the generation of epileptic spikes formulated in a Bayesian framework, the authors restricted common parameters to the spatial profile (i.e., the position and extent) of the EEG and fMRI sources, which was introduced in the form of an unknown hierarchical prior on cerebral activity. In other words, the only parameters affecting both bioelectrical and hemodynamic responses were those defining the spatial support of the signal generators. The inversion of this model yields an estimate of the common spatial profile, which embodies a trade-off between information harvested from the EEG and fMRI data. The estimated cortical sources exhibited a similar temporal response to concurrently measured intracranial EEG. In contrast, the estimated hemodynamic responses did not conform to the same chronology. Since hemodynamic responses are driven partly by biophysical processes that are independent of the underlying neuronal activity (e.g., glial cell processes), one might be inclined to favor EEG-related analysis in any inference regarding causal relations within the active network.

Despite its somewhat heuristic aspect, this Bayesian fusion approach is not confounded by the lack of detailed information about NVC, since the spatial structure of the EEG–fMRI coupling–uncoupling is elucidated from the data. Other approaches have included the balloon model itself as a surrogate for the NVC (Deneux and Faugeras 2010, 2006; Trujillo-Barreto et al. 2001), but have not, so far, included any estimation of the hemodynamic parameters. In this sense, the recent extension of DCM (Friston et al. 2019) may be an appropriate framework for models of bioelectric and metabolic activity in neural populations, allowing for the estimation of both neuronal and hemodynamic parameters. These techniques, any of which can be framed in Bayesian terms, represent the state-of-the-art in the attempts to bridge the gap between EEG and fMRI signals in a symmetrical, physiologically rigorous, and optimum way. No doubt, research efforts during the next decade will bring increasingly sophisticated models and inversion methods that will extend the validity and accuracy of EEG–fMRI information fusion.

However, any EEG–fMRI fusion procedure that is necessarily "model-based" will suffer from the usual limitation of modeling: refutability. Whether the assumptions of the model are satisfied or not in a given experimental context will remain a question in itself (Calhoun and Sui 2016). There is a subtle balance between the plausibility of the assumptions and the efficiency of any model to make precise inferences. The tighter the prior belief regarding the underlying causes of our observations, the more precise our interpretations of the data. However, these inferences become increasingly constrained by our priors and indeed the space of models

examined. Therefore, theoretical neurobiology, experimental evidence, and dedicated statistical data analysis may have to make significant progress before any robust information fusion technique is adopted by the neuroimaging community (see (Hosford and Gourine 2019; Riera et al. 2006; Riera and Sumiyoshi 2010; Wan et al. 2006) for recent insights from complementary invasive recordings and sophisticated metabolic modeling).

28.3.5.2 Data-Driven Approaches

Over the last few years, there has been an explosion in the application of machine learning algorithms to the analysis of joint EEG–fMRI data. These algorithms use the full spectrum of available information from the two modalities to jointly decompose the two datasets into latent variables reflecting common patterns between the two modalities. Since they are not based on a generative model, these methods are considered to be data-driven and descriptive or exploratory (for a recent review see Sui et al. 2012). However, in the broader sense, data-driven methods can be classified as symmetric EEG–fMRI approaches since they capitalize on the strength of each modality in a joint analysis, rather than a separate analysis of each. Therefore, we have decided to review them here.

Relevant methods for EEG–fMRI data fusion are mainly based on algorithms such as ICA, Canonical Correlation Analysis (CCA) and Partial Least Squares (PLS) adapted to the analysis of multimodal data (Calhoun and Sui 2016; Sui et al. 2012). Joint ICA (jICA) (Calhoun et al. 2010, 2006; Moosmann et al. 2008) is a second-level analysis method that maximizes the spatial and temporal independence of the fMRI and EEG components, respectively. This is done under the assumption that EEG and fMRI are generated by similar neuronal processes and therefore, the EEG and fMRI features can share the same mixing matrix (Mijović et al. 2012a, b). In brief, jICA performs ICA on the horizontally concatenated EEG and fMRI features (along time points and voxels, respectively). It is a straightforward and effective method suitable for examining a common modulation across subjects among the two modalities. However, as we have discussed in this chapter, the underlying assumption about the strong link between the two modalities, is sometimes unrealistic and represents an important limitation of jICA. Additionally, jICA requires the two modalities to have similar sample size in order to avoid providing priority to the modality with the most samples (Correa et al. 2010b; Dahne et al. 2015).

Parallel ICA (pICA) (Liu et al. 2009; Liu and Calhoun 2007) relaxes the assumption of jICA of a common mixing matrix for the two modalities, by assuming that the two datasets are mixed in a similar but not identical way. This is done by performing a spatial ICA of fMRI data and a temporal ICA of EEG data. The two datasets are integrated by assuming that unmixing matrices are maximally correlated (Eichele et al. 2008). Compared to jICA, pICA has been demonstrated to be more consistent and flexible, allowing the datasets to have different dimensions (Correa et al. 2010a). However, rigorously speaking, pICA does not provide a full data fusion because the two modalities do not share information during the decomposition step (Mijović et al. 2012a, b). A related method called linked ICA (lICA)

aims at discovering common latent factors among the two datasets. This method is implemented based on a Bayesian framework that optimizes the weighting of each modality (Lei et al. 2012). Similar to pICA, lICA applies ICA separately to the two modalities but allows results from one modality to be used as priors for the other modality. Being Bayesian, lICA can handle datasets with different scaling and noise levels (Dahne et al. 2015).

Multimodal CCA (mCCA) (Correa et al. 2009, 2008) is a method rather complementary to jICA in that it assumes that each modality has a different mixing matrix and aims to identify a transformed coordinate system that maximises the intersubject covariations between the two datasets (Michalopoulos et al. 2013; Sui et al. 2012). mCCA provides a more flexible framework than ICA-based methods for the exploration of the relationship between the two datasets (Correa et al. 2010b). However, mCCA produces component maps that may not be sparse enough, making the interpretation of the results difficult (Michalopoulos et al. 2013).

The complementary nature of mCCA and jICA has also been exploited by combining them into a common framework (mCCA + jICA) in order to take advantage of the benefits of each individual method. mCCA + jICA assumes that the components decomposed from each modality have some degree of correlation between their mixing profiles among subjects. mCCA makes the jICA job more reliable by providing a closer initial match via correlation; while jICA further decomposes the remaining mixtures in the associated maps and relaxes the requirement of sufficiently distinct canonical correlation coefficients. By allowing both highly and weakly connected modulations as well as joint independent components, mCCA + jICA can achieve both flexible modal association and source separation. Although to our knowledge it hasn't been applied to EEG–fMRI data fusion, (mCCA + jICA) has been used for fusion of other combination of modalities such as fMRI and DTI (Sui et al. 2011), providing superior performance without increasing the computational cost.

The data-driven methods reported so far ignore the underlying multidimensional structure of the data in at least one of the modalities; and/or assume hard coupling (equality constraints) between the different modalities (e.g., sharing mixing matrices in jICA). fMRI and EEG datasets are inherently multidimensional, including information in time, space (voxels or channels), subjects, trials and so on. The multiscale nature of EEG signals can also be represented by further expending in additional dimensions, for example, by including spectral features. This multidimensional structure suggests adopting a tensor (multiway) representation of the EEG and fMRI datasets and using tensor decomposition methods for data fusion. These methods assume that the process underlying the data can be decomposed into a relatively small number of components or "atoms," which are extracted while respecting the multidimensional nature of datasets (Lahat et al. 2015). Most importantly, the factorization of tensors can be unique under mild conditions, as opposed to matrix factorizations such as ICA-based ones. During optimization, the "shared" factors are appropriately "coupled," and thus a link between the two modalities is established. Various types of coupling have been proposed depending on the coupled factors: (a) spatial factor coupling via the lead field, which summarizes the

volume conduction effects in the head (Karahan et al. 2015); (b) temporal factor coupling via convolution with an HRF (Martínez-Montes et al. 2004; Van Eyndhoven et al. 2017); and (c) subjects factor coupling, assuming that the same neural processes are reflected in both modalities with the same covariation (Acar et al. 2017a, b; Hunyadi et al. 2016).

Most tensor-based methods so far have focused on Coupled Matrix and Tensor Factorizations (CMTF), where one of the datasets (usually fMRI) is assumed to be bidimensional (a matrix), rather than multidimensional. Additionally, in most of cases, the coupling is "hard," meaning that the shared factors are equal in the two datasets. The hard coupling arises from the assumption that the neural sources affect both modalities identically, which as we have discussed is not realistic. A pioneering application of these techniques used multiway partial least square (N-PLS) for EEG and fMRI fusion (Martínez-Montes et al. 2004). N-PLS is a multiway generalization of partial least square regression that aims to find a linear decomposition of fMRI data that maximally covaries with a time–frequency decomposition of the EEG. The downside of this method is that the data are first decomposed separately, and then the decompositions are correlated, so the optimal association between EEG and fMRI data may not be detected (Sui et al. 2012). Additionally, as in any regression model, there is an implicit asymmetry associated with fusion analysis, since one of the modalities is assumed to predict (EEG) the other one (fMRI). More recently, a tensor-based EEG and fMRI fusion method that allows both full tensor decomposition of the two datasets as well as soft coupling (assuming similarity rather than equality) between any of the factors was proposed (Chatzichristos et al. 2018). Although more empirical studies are required in order to fully assess the advantages and limitations of this method, the authors reported performance gains compared to ICA methods as well as to the separate analyses of the datasets.

The data-driven methods reviewed here may also differ in the type of data used to feed the analysis. For example, while some methods (e.g., jICA) are typically applied to subject-level summary statistics such as fMRI statistical maps and ERP data, other methods (e.g., N-PLS and other tensor-based methods) extend the amount of data processed by additionally considering variations at the level of single trials, thereby not relying on prior information from within-subject statistics or extraction of data features prior to the fusion analysis (Chatzichristos et al. 2018; Goldman et al. 2009; Martínez-Montes et al. 2004).

Although these data-driven methods lack the explanatory power of model-driven approaches, data-driven methods are easier to implement, and they are not based on assumptions about the complicated physiological relationship between the EEG and fMRI signals. Therefore, in the absence of a complete understanding of the neurophysiological processes linking EEG and fMRI, data-driven methods can be of high utility by providing unbiased and multivariate analysis schemes for simultaneous EEG–fMRI analysis. On the other hand, due to the variety of data-driven methods already available for EEG–fMRI fusion, the selection of a particular one for a specific research question might sometimes be difficult. Moreover, some of the current methods still rely on physiological presumptions, thereby not yet taking full advantage of the full power of these algorithms.

28.4 Conclusion

We have reviewed the advances and issues relating to EEG–fMRI information fusion. We have emphasized the importance of NVC for generative models, which are the key to any balanced fusion procedure. This issue underlies many of the challenges to fusion and has been a source of much debate: "it is far from trivial to suppose, for instance, that a statistically significant *Z*-score in the left inferior frontal gyrus and a large left anterior negativity at 200 ms after stimulus presentation correspond to the same thing" (Horwitz and Poeppel 2002). In this chapter, we tried to identify those features of cerebral activity that could form the basis of models of electromagnetic and hemodynamic markers of neuronal activity and are required for EEG–fMRI multimodal fusion. We have emphasized the importance of developing statistical methods for model inversion, given EEG and fMRI signals.

Finally, gathering the knowledge and know-how necessary for EEG–fMRI fusion has proven to be a challenging exercise for the neuroimaging community. However, very few rational criticisms have questioned the intrinsic motivation of EEG–fMRI fusion. In short: what is the type of scientific question (apart from established diagnostic applications, e.g., epilepsy) that really requires EEG–fMRI fusion? This potentially controversial question must be addressed before we can finesse our scientific strategy in this challenging area.

Acknowledgments An EPSRC Fellowship (EP/N006771/1) to Dr. Trujillo-Barreto funded this work.

References

Abreu R, Leal A, Figueiredo P (2018a) EEG-informed fMRI: a review of data analysis methods. Front Hum Neurosci 12:29. https://doi.org/10.3389/fnhum.2018.00029

Abreu R, Leal A, Lopes da Silva F, Figueiredo P (2018b) EEG synchronization measures predict epilepsy-related BOLD-fMRI fluctuations better than commonly used univariate metrics. Clin Neurophysiol 129:618–635. https://doi.org/10.1016/j.clinph.2017.12.038

Acar E, Levin-Schwartz Y, Calhoun VD, Adali T (2017a) Tensor-based fusion of EEG and FMRI to understand neurological changes in schizophrenia. In: 2017 IEEE International Symposium on Circuits and Systems (ISCAS). IEEE, Washington, DC, pp 1–4. https://doi.org/10.1109/ISCAS.2017.8050303

Acar E, Levin-Schwartz Y, Calhoun VD, Adali T (2017b) ACMTF for fusion of multi-modal neuroimaging data and identification of biomarkers. In: 2017 25th European Signal Processing Conference (EUSIPCO). IEEE, Washington, DC, pp 643–647. https://doi.org/10.23919/EUSIPCO.2017.8081286

Aghakhani Y, Bagshaw AP, Bénar CG, Hawco C, Andermann F, Dubeau F, Gotman J (2004) fMRI activation during spike and wave discharges in idiopathic generalized epilepsy. Brain 127:1127. https://doi.org/10.1093/brain/awh136

Ahlfors SP, Simpson GV (2004) Geometrical interpretation of fMRI-guided MEG/EEG inverse estimates. NeuroImage 22:323–332. https://doi.org/10.1016/j.neuroimage.2003.12.044

Al-Asmi A, Bénar C-G, Gross DW, Khani YA, Andermann F, Pike B, Dubeau F, Gotman J (2003) fMRI Activation in Continuous and Spike-triggered EEG-fMRI Studies of Epileptic Spikes. Epilepsia 44:1328–1339. https://doi.org/10.1046/j.1528-1157.2003.01003.x

Allen PJ, Josephs O, Turner R (2000) A method for removing imaging artifact from continuous EEG recorded during functional MRI. NeuroImage 12:230–239. https://doi.org/10.1006/nimg.2000.0599

Archer JS, Briellmann RS, Syngeniotis A, Abbott DF, Jackson GD (2003) Spike-triggered fMRI in reading epilepsy: involvement of left frontal cortex working memory area. Neurology 60:415–421. https://doi.org/10.1212/WNL.60.3.415

Arthurs O, Boniface S (2003) What aspect of the fMRI BOLD signal best reflects the underlying electrophysiology in human somatosensory cortex? Clin Neurophysiol 114:1203–1209. https://doi.org/10.1016/S1388-2457(03)00080-4

Attwell D, Iadecola C (2002) The neural basis of functional brain imaging signals. Trends Neurosci 25:621–625

Aubert A, Costalat R (2005) Interaction between astrocytes and neurons studied using a mathematical model of compartmentalized energy metabolism. J Cereb Blood Flow Metab 25:1476–1490. https://doi.org/10.1038/sj.jcbfm.9600144

Babajani-Feremi A, Soltanian-Zadeh H (2006) Integrated MEG/EEG and fMRI model based on neural masses. IEEE Trans Biomed Eng 53:1794–1801. https://doi.org/10.1109/TBME.2006.873748

Babajani-Feremi A, Soltanian-Zadeh H (2010) Multi-area neural mass modeling of EEG and MEG signals. NeuroImage 52:793–811. https://doi.org/10.1016/j.neuroimage.2010.01.034

Babiloni F, Babiloni C, Carducci F, Romani GL, Rossini PM, Angelone LM, Cincotti F (2003) Multimodal integration of high-resolution EEG and functional magnetic resonance imaging data: a simulation study. NeuroImage 19:1–15. https://doi.org/10.1016/S1053-8119(03)00052-1

Bagshaw AP, Kobayashi E, Dubeau F, Pike GB, Gotman J (2005) Correspondence between EEG-fMRI and EEG dipole localisation of interictal discharges in focal epilepsy. NeuroImage 30:417. https://doi.org/10.1016/j.neuroimage.2005.09.033

Baillet S, Mosher JC, Leahy RM (2001) Electromagnetic brain mapping. IEEE Signal Process Mag 18:14–30

Beisteiner R, Erdler M, Teichtmeister C, Diemling M, Moser E, Edward V, Deecke L (1997) Magnetoencephalography may help to improve functional MRI brain mapping. Eur J Neurosci 9:1072–1077. https://doi.org/10.1111/j.1460-9568.1997.tb01457.x

Bénar C-G, Gross DW, Wang Y, Petre V, Pike B, Dubeau F, Gotman J (2002) The BOLD response to interictal epileptiform discharges. NeuroImage 17:1182–1192. https://doi.org/10.1006/nimg.2002.1164

Bénar C-G, Schön D, Grimault S, Nazarian B, Burle B, Roth M, Badier J-M, Marquis P, Liegeois-Chauvel C, Anton J-L (2007) Single-trial analysis of oddball event-related potentials in simultaneous EEG-fMRI. Hum Brain Mapp 28:602–613. https://doi.org/10.1002/hbm.20289

Biazoli CE, Sturzbecher M, White TP, dos Santos Onias HH, Andrade KC, de Araujo DB, Sato JR (2013) Application of partial directed coherence to the analysis of resting-state EEG-fMRI data. Brain Connect 3:563–568. https://doi.org/10.1089/brain.2012.0135

Boor S, Vucurevic G, Pfleiderer C, Stoeter P, Kutschke G, Boor R (2003) EEG-related functional MRI in benign childhood epilepsy with centrotemporal spikes. Epilepsia 44:688–692. https://doi.org/10.1046/j.1528-1157.2003.27802.x

Britz J, Van De Ville D, Michel CM (2010) BOLD correlates of EEG topography reveal rapid resting-state network dynamics. NeuroImage 52:1162–1170. https://doi.org/10.1016/j.neuroimage.2010.02.052

Buckner RL, Vincent JL (2007) Unrest at rest: default activity and spontaneous network correlations. NeuroImage 37:1091–1096. https://doi.org/10.1016/j.neuroimage.2007.01.010

Buxton RB, Wong EC, Frank LR (1998) Dynamics of blood flow and oxygenation changes during brain activation: the balloon model. Magn Reson Med 39:855–864. https://doi.org/10.1002/mrm.1910390602

Buxton RB, Uludağ K, Dubowitz DJ, Liu TT (2004) Modeling the hemodynamic response to brain activation. NeuroImage 23(Suppl 1):S220–S233. https://doi.org/10.1016/j.neuroimage.2004.07.013

Calhoun VD, Sui J (2016) Multimodal fusion of brain imaging data: a key to finding the missing link(s) in complex mental illness. Biol Psychiatry Cogn Neurosci Neuroimag 1:230–244. https://doi.org/10.1016/j.bpsc.2015.12.005

Calhoun VD, Adali T, Giuliani NR, Pekar JJ, Kiehl KA, Pearlson GD (2006) Method for multimodal analysis of independent source differences in schizophrenia: combining gray matter structural and auditory oddball functional data. Hum Brain Mapp 27:47–62. https://doi.org/10.1002/hbm.20166

Calhoun VD, Wu L, Kiehl KA, Eichele T, Pearlson GD (2010) Aberrant processing of deviant stimuli in schizophrenia revealed by fusion of fMRI and EEG data. Acta Neuropsychiatr 22:127–138. https://doi.org/10.1111/j.1601-5215.2010.00467.x

Chatton J-Y, Pellerin L, Magistretti PJ (2003) GABA uptake into astrocytes is not associated with significant metabolic cost: implications for brain imaging of inhibitory transmission. Proc Natl Acad Sci 100:12456–12461. https://doi.org/10.1073/pnas.2132096100

Chatzichristos C, Davies M, Escudero J, Kofidis E, Theodoridis S (2018) Fusion of EEG and fMRI via soft coupled tensor decompositions. In: 2018 26th European Signal Processing Conference (EUSIPCO). IEEE, Washington, DC, pp 56–60. https://doi.org/10.23919/EUSIPCO.2018.8553077

Correa NM, Li Y-O, Adali T, Calhoun VD (2008) Canonical correlation analysis for feature-based fusion of biomedical imaging modalities and its application to detection of associative networks in schizophrenia. IEEE J Select Top Signal Process 2:998–1007. https://doi.org/10.1109/JSTSP.2008.2008265

Correa NM, Li Y-O, Adali T, Calhoun VD (2009) Fusion of fMRI, sMRI, and EEG data using canonical correlation analysis. In: 2009 IEEE International Conference on Acoustics, Speech and Signal Processing. IEEE, Washington, DC, pp 385–388. https://doi.org/10.1109/ICASSP.2009.4959601

Correa NM, Adali T, Li Y-O, Calhoun V (2010a) Canonical correlation analysis for data fusion and group inferences. IEEE Signal Process Mag 27:39–50. https://doi.org/10.1109/MSP.2010.936725

Correa NM, Eichele T, Adalı T, Li Y-O, Calhoun VD (2010b) Multi-set canonical correlation analysis for the fusion of concurrent single trial ERP and functional MRI. NeuroImage 50:1438–1445. https://doi.org/10.1016/j.neuroimage.2010.01.062

Dahne S, Bieszmann F, Samek W, Haufe S, Goltz D, Gundlach C, Villringer A, Fazli S, Muller K-R (2015) Multivariate machine learning methods for fusing multimodal functional neuroimaging data. Proc IEEE 103:1507–1530. https://doi.org/10.1109/JPROC.2015.2425807

Dale AM, Halgren E (2001) Spatiotemporal mapping of brain activity by integration of multiple imaging modalities. Curr Opin Neurobiol 11:202–208. https://doi.org/10.1016/S0959-4388(00)00197-5

Dale AM, Liu AK, Fischl BR, Buckner RL, Belliveau JW, Lewine JD, Halgren E (2000) Dynamic statistical parametric mapping: combining fMRI and MEG for high-resolution imaging of cortical activity. Neuron 26:55–67

Das A, Sirotin YB (2011) What could underlie the trial-related signal? A response to the commentaries by Drs. Kleinschmidt and Muller, and Drs. Handwerker and Bandettini. Neuroimage 55:1413–1418. https://doi.org/10.1016/j.neuroimage.2010.07.005

Daunizeau J, Grova C, Mattout J, Marrelec G, Clonda D, Goulard B, Pelegrini-Issac M, Lina J-M, Benali H (2005) Assessing the relevance of fMRI-based prior in the EEG inverse problem: a bayesian model comparison approach. IEEE Trans Signal Process 53:3461–3472. https://doi.org/10.1109/TSP.2005.853220

Daunizeau J, Grova C, Marrelec G, Mattout J, Jbabdi S, Pélégrini-Issac M, Lina J-M, Benali H (2007) Symmetrical event-related EEG/fMRI information fusion in a variational Bayesian framework. NeuroImage 36:69–87. https://doi.org/10.1016/j.neuroimage.2007.01.044

Debener S (2005) Trial-by-trial coupling of concurrent electroencephalogram and functional magnetic resonance imaging identifies the dynamics of performance monitoring. J Neurosci 25:11730–11737. https://doi.org/10.1523/JNEUROSCI.3286-05.2005

Debener S, Ullsperger M, Siegel M, Engel AK (2006) Single-trial EEG – fMRI reveals the dynamics of cognitive function. Trends Cogn Sci 10:558–563. https://doi.org/10.1016/j.tics.2006.09.010

Deneux T, Faugeras O (2006) EEG-fMRI fusion of non-triggered data using kalman filtering. In: 3rd IEEE International Symposium on Biomedical Imaging: Macro to Nano, 2006. IEEE, Washington, DC, pp 1068–1071. https://doi.org/10.1109/ISBI.2006.1625106

Deneux T, Faugeras O (2010) EEG-fMRI fusion of paradigm-free activity using kalman filtering. Neural Comput 22:906–948

Eichele T, Calhoun VD, Moosmann M, Specht K, Jongsma MLA, Quiroga RQ, Nordby H, Hugdahl K (2008) Unmixing concurrent EEG-fMRI with parallel independent component analysis. Int J Psychophysiol 67:222–234. https://doi.org/10.1016/j.ijpsycho.2007.04.010

Ellingson M, Liebenthal E, Spanaki M, Prieto T, Binder J, Ropella K (2004) Ballistocardiogram artifact reduction in the simultaneous acquisition of auditory ERPS and fMRI. NeuroImage 22:1534–1542. https://doi.org/10.1016/j.neuroimage.2004.03.033

Friston KJ (2005a) A theory of cortical responses. Phil Trans R Soc B Biol Sci 360:815–836. https://doi.org/10.1098/rstb.2005.1622

Friston KJ (2005b) Models of brain function in neuroimaging. Annu Rev Psychol 56:57–87. https://doi.org/10.1146/annurev.psych.56.091103.070311

Friston KJ, Price CJ, Fletcher P, Moore C, Frackowiak RSJ, Dolan RJ (1996) The trouble with cognitive subtraction. NeuroImage 4:97–104. https://doi.org/10.1006/nimg.1996.0033

Friston KJ, Mechelli A, Turner R, Price CJ (2000) Nonlinear responses in fMRI: the Balloon model, Volterra kernels, and other hemodynamics. NeuroImage 12:466–477. https://doi.org/10.1006/nimg.2000.0630

Friston KJ, Harrison L, Penny W (2003) Dynamic causal modelling. NeuroImage 19:1273–1302. https://doi.org/10.1016/S1053-8119(03)00202-7

Friston K, Harrison L, Daunizeau J, Kiebel S, Phillips C, Trujillo-Barreto NJ, Henson R, Flandin G, Mattout J (2008) Multiple sparse priors for the M/EEG inverse problem. NeuroImage 39:1104–1120. https://doi.org/10.1016/j.neuroimage.2007.09.048

Friston KJ, Preller KH, Mathys C, Cagnan H, Heinzle J, Razi A, Zeidman P (2019) Dynamic causal modelling revisited. NeuroImage 199:730–744. https://doi.org/10.1016/j.neuroimage.2017.02.045

Fukunaga M, Horovitz SG, de Zwart JA, van Gelderen P, Balkin TJ, Braun AR, Duyn JH (2008) Metabolic origin of bold signal fluctuations in the absence of stimuli. J Cereb Blood Flow Metab 28:1377–1387. https://doi.org/10.1038/jcbfm.2008.25

Garreffa G, Carnì M, Gualniera G, Ricci GB, Bozzao L, De Carli D, Morasso P, Pantano P, Colonnese C, Roma V, Maraviglia B (2003) Real-time MR artifacts filtering during continuous EEG/fMRI acquisition. Magn Reson Imaging 21:1175–1189. https://doi.org/10.1016/j.mri.2003.08.019

Goense JBM, Logothetis NK (2008) Neurophysiology of the BOLD fMRI signal in awake monkeys. Curr Biol 18:631–640. https://doi.org/10.1016/j.cub.2008.03.054

Goldman RI, Stern JM, Engel J, Cohen MS (2002) Simultaneous EEG and fMRI of the alpha rhythm. Neuroreport 13:2487–2492. https://doi.org/10.1097/00001756-200212200-00022

Goldman RI, Wei C-Y, Philiastides MG, Gerson AD, Friedman D, Brown TR, Sajda P (2009) Single-trial discrimination for integrating simultaneous EEG and fMRI: identifying cortical areas contributing to trial-to-trial variability in the auditory oddball task. NeuroImage 47:136–147. https://doi.org/10.1016/j.neuroimage.2009.03.062

Gonzalez-Andino S, Blanke O, Lantz G, Thut G, Grave de Peralta R (2001) The use of functional constraints for the neuroelectromagnetic inverse problem: alternatives and caveats. Int J Bioelectromagn 3:53–62

Grouiller F, Thornton RC, Groening K, Spinelli L, Duncan JS, Schaller K, Siniatchkin M, Lemieux L, Seeck M, Michel CM, Vulliemoz S (2011) With or without spikes: localization of focal epileptic activity by simultaneous electroencephalography and functional magnetic resonance imaging. Brain 134:2867–2886. https://doi.org/10.1093/brain/awr156

Grova C, Daunizeau J, Kobayashi E, Bagshaw AP, Lina J-M, Dubeau F, Gotman J (2008) Concordance between distributed EEG source localization and simultaneous EEG-fMRI

studies of epileptic spikes. NeuroImage 39:755–774. https://doi.org/10.1016/j.neuroimage.2007.08.020
Halchenko YO, Hanson SJ, Pearlmutter BA (2005) Multimodal integration: fMRI, MRI, EEG, MEG. In: Landini L, Positano V, Santarelli MF (eds) Advanced image processing in magnetic resonance imaging. Taylor & Francis, Boca Raton, FL, pp 223–265
Hallett M (2002) Multimodality brain imaging. Int Congr Ser 1226:17–26. https://doi.org/10.1016/S0531-5131(01)00493-9
Havlicek M, Roebroeck A, Friston K, Gardumi A, Ivanov D, Uludag K (2015) Physiologically informed dynamic causal modeling of fMRI data. NeuroImage 122:355–372. https://doi.org/10.1016/j.neuroimage.2015.07.078
Heeger DJ, Huk AC, Geisler WS, Albrecht DG (2000) Spikes versus BOLD: what does neuroimaging tell us about neuronal activity? Nat Neurosci 3:631–633. https://doi.org/10.1038/76572
Henson RN, Flandin G, Friston KJ, Mattout J (2010) A parametric empirical bayesian framework for fMRI-constrained MEG/EEG source reconstruction. Hum Brain Mapp 1531:1512–1531. https://doi.org/10.1002/hbm.20956
Horovitz SG, Rossion B, Skudlarski P, Gore JC (2004) Parametric design and correlational analyses help integrating fMRI and electrophysiological data during face processing. NeuroImage 22:1587–1595. https://doi.org/10.1016/j.neuroimage.2004.04.018
Horwitz B, Poeppel D (2002) How can EEG/MEG and fMRI/PET data be combined? Hum Brain Mapp 17:1–3. https://doi.org/10.1002/hbm.10057
Hosford PS, Gourine AV (2019) What is the key mediator of the neurovascular coupling response? Neurosci Biobehav Rev 96:174–181. https://doi.org/10.1016/j.neubiorev.2018.11.011
Hunyadi B, Van Paesschen W, De Vos M, Van Huffel S (2016) Fusion of electroencephalography and functional magnetic resonance imaging to explore epileptic network activity. In: 2016 24th European Signal Processing Conference (EUSIPCO). IEEE, Washington, DC, pp 240–244. https://doi.org/10.1109/EUSIPCO.2016.7760246
Iadecola C (2004) Neurovascular regulation in the normal brain and in Alzheimer's disease. Nat Rev Neurosci 5:347–360. https://doi.org/10.1038/nrn1387
Ives JR, Warach S, Schmitt F, Edelman RR, Schomer DL (1993) Monitoring the patient's EEG during echo planar MRI. Electroencephalogr Clin Neurophysiol 87:417–420. https://doi.org/10.1016/0013-4694(93)90156-P
James CJ, Hesse CW (2005) Independent component analysis for biomedical signals. Physiol Meas 26:R15–R39. https://doi.org/10.1088/0967-3334/26/1/R02
Jones M, Hewson-Stoate N, Martindale J, Redgrave P, Mayhew J (2004) Nonlinear coupling of neural activity and CBF in rodent barrel cortex. NeuroImage 22:956–965. https://doi.org/10.1016/j.neuroimage.2004.02.007
Karahan E, Rojas-Lopez PA, Bringas-Vega ML, Valdes-Hernandez PA, Valdes-Sosa PA (2015) Tensor analysis and fusion of multimodal brain images. Proc IEEE 103:1531–1559. https://doi.org/10.1109/JPROC.2015.2455028
Kawakami O, Kaneoke Y, Maruyama K, Kakigi R, Okada T, Sadato N, Yonekura Y (2002) Visual detection of motion speed in humans: spatiotemporal analysis by fMRI and MEG. Hum Brain Mapp 16:104–118. https://doi.org/10.1002/hbm.10033
Kida I, Hyder F, Behar KL (2001) Inhibition of voltage-dependent sodium channels suppresses the functional magnetic resonance imaging response to forepaw somatosensory activation in the rodent. J Cereb Blood Flow Metab 21:585–591. https://doi.org/10.1097/00004647-200105000-00013
Kiebel SJ, Garrido MI, Friston KJ (2007) Dynamic causal modelling of evoked responses: the role of intrinsic connections. NeuroImage 36:332–345. https://doi.org/10.1016/j.neuroimage.2007.02.046
Kiebel SJ, Daunizeau J, Phillips C, Friston KJ (2008) Variational Bayesian inversion of the equivalent current dipole model in EEG/MEG. NeuroImage 39:728–741. https://doi.org/10.1016/j.neuroimage.2007.09.005
Kilner JM, Mattout J, Henson R, Friston KJ (2005) Hemodynamic correlates of EEG: a heuristic. NeuroImage 28:280–286. https://doi.org/10.1016/j.neuroimage.2005.06.008

Korvenoja A, Huttunen J, Salli E, Pohjonen H, Martinkauppi S, Palva JM, Lauronen L, Virtanen J, Ilmoniemi RJ, Aronen HJ (1999) Activation of multiple cortical areas in response to somatosensory stimulation: combined magnetoencephalographic and functional magnetic resonance imaging. Hum Brain Mapp 8:13–27

Krakow K, Allen PJ, Symms MR, Lemieux L, Josephs O, Fish DR (2000) EEG recordings during fMRI experiments: image quality. Hum Brain Mapp 10:10–15

Krüger G, Glover GH (2001) Physiological noise in oxygenation-sensitive magnetic resonance imaging. Magn Reson Med 46:631–637. https://doi.org/10.1002/mrm.1240

Kruggel F, Wiggins CJ, Herrmann CS, von Cramon DY (2000) Recording of the event-related potentials during functional MRI at 3.0 Tesla field strength. Magn Reson Med 44:277–282. https://doi.org/10.1002/1522-2594(200008)44:2<277::AID-MRM15>3.0.CO;2-X

Lahat D, Adali T, Jutten C (2015) Multimodal data fusion: an overview of methods, challenges, and prospects. Proc IEEE 103:1449–1477. https://doi.org/10.1109/JPROC.2015.2460697

Laufs H, Krakow K, Sterzer P, Eger E, Beyerle A, Salek-Haddadi A, Kleinschmidt A (2003) Electroencephalographic signatures of attentional and cognitive default modes in spontaneous brain activity fluctuations at rest. Proc Natl Acad Sci 100:11053–11058. https://doi.org/10.1073/pnas.1831638100

Laufs H, Holt JL, Elfont R, Krams M, Paul JS, Krakow K, Kleinschmidt A (2006) Where the BOLD signal goes when alpha EEG leaves. NeuroImage 31:1408–1418. https://doi.org/10.1016/j.neuroimage.2006.02.002

Laufs H, Daunizeau J, Carmichael DW, Kleinschmidt A (2008) Recent advances in recording electrophysiological data simultaneously with magnetic resonance imaging. NeuroImage 40:515–528. https://doi.org/10.1016/j.neuroimage.2007.11.039

Lauritzen M (2005) Reading vascular changes in brain imaging: is dendritic calcium the key? Nat Rev Neurosci 6:77–85. https://doi.org/10.1038/nrn1589

Leal A, Vieira JP, Lopes R, Nunes RG, Gonçalves SI, Lopes da Silva F, Figueiredo P (2016) Dynamics of epileptic activity in a peculiar case of childhood absence epilepsy and correlation with thalamic levels of GABA. Epilepsy Behav Case Rep 5:57–65. https://doi.org/10.1016/j.ebcr.2016.03.004

Lei X, Valdes-Sosa PA, Yao D (2012) EEG/fMRI fusion based on independent component analysis: integration of data-driven and model-driven methods. J Integr Neurosci 11:313–337. https://doi.org/10.1142/S0219635212500203

Lemieux L, Krakow K, Fish DR (2001) Comparison of spike-triggered functional MRI BOLD activation and EEG dipole model localization. NeuroImage 14:1097–1104. https://doi.org/10.1006/nimg.2001.0896

LeVan P, Gotman J (2009) Independent component analysis as a model-free approach for the detection of BOLD changes related to epileptic spikes: a simulation study. Hum Brain Mapp 30:2021–2031. https://doi.org/10.1002/hbm.20647

LeVan P, Tyvaert L, Gotman J (2010) Modulation by EEG features of BOLD responses to interictal epileptiform discharges. NeuroImage 50:15–26. https://doi.org/10.1016/j.neuroimage.2009.12.044

Lin F-H, Witzel T, Hämäläinen MS, Dale AM, Belliveau JW, Stufflebeam SM (2004) Spectral spatiotemporal imaging of cortical oscillations and interactions in the human brain. NeuroImage 23:582–595. https://doi.org/10.1016/j.neuroimage.2004.04.027

Liston AD, Lund TE, Salek-Haddadi A, Hamandi K, Friston KJ, Lemieux L (2006) Modelling cardiac signal as a confound in EEG-fMRI and its application in focal epilepsy studies. NeuroImage 30:827–834. https://doi.org/10.1016/j.neuroimage.2005.10.025

Liu J, Calhoun V (2007) Parallel independent component analysis for multimodal analysis: application to fMRI and EEG data. In: 2007 4th IEEE International Symposium on Biomedical Imaging: From Nano to Macro. IEEE, Washington, DC, pp 1028–1031. https://doi.org/10.1109/ISBI.2007.357030

Liu AK, Belliveau JW, Dale AM (1998) Spatiotemporal imaging of human brain activity using functional MRI constrained magnetoencephalography data: Monte Carlo simulations. Proc Natl Acad Sci 95:8945–8950. https://doi.org/10.1073/pnas.95.15.8945

Liu Z, Ding L, He B (2006) Integration of EEG/MEG with MRI and fMRI. IEEE Eng Med Biol Mag 25:46–53. https://doi.org/10.1109/MEMB.2006.1657787

Liu J, Pearlson G, Windemuth A, Ruano G, Perrone-Bizzozero NI, Calhoun V (2009) Combining fMRI and SNP data to investigate connections between brain function and genetics using parallel ICA. Hum Brain Mapp 30:241–255. https://doi.org/10.1002/hbm.20508

Logothetis NK, Wandell BA (2004) Interpreting the BOLD signal. Annu Rev Physiol 66:735–769. https://doi.org/10.1146/annurev.physiol.66.082602.092845

Logothetis NK, Pauls J, Augath M, Trinath T, Oeltermann A (2001) Neurophysiological investigation of the basis of the fMRI signal. Nature 412:150–157

Lu H, Golay X, Pekar JJ, van Zijl PCM (2004) Sustained poststimulus elevation in cerebral oxygen utilization after vascular recovery. J Cereb Blood Flow Metab 24:764–770. https://doi.org/10.1097/01.WCB.0000124322.60992.5C

Mangun GR, Buonocore MH, Girelli M, Jha AP (1998) ERP and fMRI measures of visual spatial selective attention. Hum Brain Mapp 6:383–389

Mantini D, Perrucci MG, Del Gratta C, Romani GL, Corbetta M (2007) Electrophysiological signatures of resting state networks in the human brain. Proc Natl Acad Sci 104:13170–13175. https://doi.org/10.1073/pnas.0700668104

Marecek R, Lamos M, Mikl M, Barton M, Fajkus J, Rektor, Brazdil M (2016) What can be found in scalp EEG spectrum beyond common frequency bands. EEG–fMRI study. J Neural Eng 13:046026. https://doi.org/10.1088/1741-2560/13/4/046026

Martindale J, Mayhew J, Berwick J, Jones M, Martin C, Johnston D, Redgrave P, Zheng Y (2003) The hemodynamic impulse response to a single neural event. J Cereb Blood Flow Metab 23:546–555. https://doi.org/10.1097/01.WCB.0000058871.46954.2B

Martínez-Montes E, Valdés-Sosa PA, Miwakeichi F, Goldman RI, Cohen MS (2004) Concurrent EEG/fMRI analysis by multiway partial least squares. NeuroImage 22:1023–1034. https://doi.org/10.1016/j.neuroimage.2004.03.038

Mathiesen C, Caesar K, Akgören N, Lauritzen M (1998) Modification of activity-dependent increases of cerebral blood flow by excitatory synaptic activity and spikes in rat cerebellar cortex. J Physiol 512:555–566. https://doi.org/10.1111/j.1469-7793.1998.555be.x

Michalopoulos K, Zervakis M, Bourbakis N (2013) Current trends in ERP analysis using EEG and EEG/fMRI synergistic methods. In: Modern electroencephalographic assessment techniques: theory and applications, pp 323–350. https://doi.org/10.1007/7657_2013_67

Mijović B, Vanderperren K, Novitskiy N, Vanrumste B, Stiers P, Van den Bergh B, Lagae L, Sunaert S, Wagemans J, Van Huffel S, De Vos M (2012a) The "why" and "how" of Joint ICA: results from a visual detection task. NeuroImage 60:1171–1185. https://doi.org/10.1016/j.neuroimage.2012.01.063

Mijović B, Vanderperren K, Van Huffel S, De Vos M (2012b) Improving spatiotemporal characterization of cognitive processes with data-driven EEG-fMRI analysis. Prilozi 33:373–390

Minati L, Rosazza C, Zucca I, D'Incerti L, Scaioli V, Bruzzone MG (2008) Spatial correspondence between functional MRI (fMRI) activations and cortical current density maps of event-related potentials (ERP): a study with four tasks. Brain Topogr 21:112–127. https://doi.org/10.1007/s10548-008-0064-3

Mizuhara H, Wang L-Q, Kobayashi K, Yamaguchi Y (2005) Long-range EEG phase synchronization during an arithmetic task indexes a coherent cortical network simultaneously measured by fMRI. NeuroImage 27:553–563. https://doi.org/10.1016/j.neuroimage.2005.04.030

Moosmann M, Ritter P, Krastel I, Brink A, Thees S, Blankenburg F, Taskin B, Obrig H, Villringer A (2003) Correlates of alpha rhythm in functional magnetic resonance imaging and near infrared spectroscopy. NeuroImage 20:145–158. https://doi.org/10.1016/S1053-8119(03)00344-6

Moosmann M, Eichele T, Nordby H, Hugdahl K, Calhoun VD (2008) Joint independent component analysis for simultaneous EEG–fMRI: principle and simulation. Int J Psychophysiol 67:212–221. https://doi.org/10.1016/j.ijpsycho.2007.05.016

Mukamel R (2005) Coupling between neuronal firing, field potentials, and fMRI in human auditory cortex. Science 309:951–954. https://doi.org/10.1126/science.1110913

Mulert C, Jäger L, Schmitt R, Bussfeld P, Pogarell O, Möller H-J, Juckel G, Hegerl U (2004) Integration of fMRI and simultaneous EEG: towards a comprehensive understanding of localization and time-course of brain activity in target detection. NeuroImage 22:83–94. https://doi.org/10.1016/j.neuroimage.2003.10.051

de Munck JC, Gonçalves SI, Mammoliti R, Heethaar RM, Lopes da Silva FH (2009) Interactions between different EEG frequency bands and their effect on alpha–fMRI correlations. NeuroImage 47:69–76. https://doi.org/10.1016/j.neuroimage.2009.04.029

Murta T, Hu L, Tierney TM, Chaudhary UJ, Walker MC, Carmichael DW, Figueiredo P, Lemieux L (2016) A study of the electro-haemodynamic coupling using simultaneously acquired intracranial EEG and fMRI data in humans. NeuroImage 142:371–380. https://doi.org/10.1016/j.neuroimage.2016.08.001

Murta T, Chaudhary UJ, Tierney TM, Dias A, Leite M, Carmichael DW, Figueiredo P, Lemieux L (2017) Phase–amplitude coupling and the BOLD signal: a simultaneous intracranial EEG (icEEG) - fMRI study in humans performing a finger-tapping task. NeuroImage 146:438–451. https://doi.org/10.1016/j.neuroimage.2016.08.036

Nakamura W, Anami K, Mori T, Saitoh O, Cichocki A, Amari S (2006) Removal of ballistocardiogram artifacts from simultaneously recorded EEG and fMRI data using independent component analysis. IEEE Trans Biomed Eng 53:1294–1308. https://doi.org/10.1109/TBME.2006.875718

Neuner I, Arrubla J, Felder J, Shah NJ (2014) Simultaneous EEG–fMRI acquisition at low, high and ultra-high magnetic fields up to 9.4T: perspectives and challenges. NeuroImage 102:71–79. https://doi.org/10.1016/j.neuroimage.2013.06.048

Nguyen VT, Cunnington R (2014) The superior temporal sulcus and the N170 during face processing: single trial analysis of concurrent EEG–fMRI. NeuroImage 86:492–502. https://doi.org/10.1016/j.neuroimage.2013.10.047

Nguyen T, Potter T, Nguyen T, Karmonik C, Grossman R, Zhang Y (2016) EEG source imaging guided by spatiotemporal specific fMRI: toward an understanding of dynamic cognitive processes. Neural Plast 2016:1–10. https://doi.org/10.1155/2016/4182483

Nguyen T, Potter T, Karmonik C, Grossman R, Zhang Y (2018) Concurrent EEG and functional MRI recording and integration analysis for dynamic cortical activity imaging. J Vis Exp (36):56417. https://doi.org/10.3791/56417

Nunez PL (ed) (1981) Electric fields of the brain. Oxford University Press, New York, NY

Nunez PL, Silberstein RB (2000) On the relationship of synaptic activity to macroscopic measurements: does co-registration of EEG with fMRI make sense? Brain Topogr 13:79–96

Onton J, Westerfield M, Townsend J, Makeig S (2006) Imaging human EEG dynamics using independent component analysis. Neurosci Biobehav Rev 30:808–822. https://doi.org/10.1016/j.neubiorev.2006.06.007

Patel AB, de Graaf RA, Mason GF, Kanamatsu T, Rothman DL, Shulman RG, Behar KL (2004) Glutamatergic Neurotransmission and Neuronal Glucose Oxidation are Coupled during Intense Neuronal Activation. J Cereb Blood Flow Metab 24:972–985. https://doi.org/10.1097/01.WCB.0000126234.16188.71

Patel AB, de Graaf RA, Mason GF, Rothman DL, Shulman RG, Behar KL (2005) The contribution of GABA to glutamate/glutamine cycling and energy metabolism in the rat cortex in vivo. Proc Natl Acad Sci 102:5588–5593. https://doi.org/10.1073/pnas.0501703102

Pellerin L, Magistretti PJ (1994) Glutamate uptake into astrocytes stimulates aerobic glycolysis: a mechanism coupling neuronal activity to glucose utilization. Proc Natl Acad Sci 91:10625–10629. https://doi.org/10.1073/pnas.91.22.10625

Pflieger ME, Greenblatt RE (2001) Nonlinear analysis of multimodal dynamic brain imaging data. Int J Bioelectromagn 3:63–82

Puce A, Allison T, Spencer SS, Spencer DD, McCarthy G (1997) Comparison of cortical activation evoked by faces measured by intracranial field potentials and functional MRI: two case studies. Hum Brain Mapp 5:298–305. https://doi.org/10.1002/(SICI)1097-0193(1997)5:4<298::AID-HBM16>3.0.CO;2-A

Riera JJ, Sumiyoshi A (2010) Brain oscillations: ideal scenery to understand the neurovascular coupling. Curr Opin Neurol 23:374. https://doi.org/10.1097/WCO.0b013e32833b769f

Riera JJ, Wan X, Jiménez JC, Kawashima R (2006) Nonlinear local electro-vascular coupling. Part I: A theoretical model. Hum Brain Mapp 27:896–914

Riera JJ, Jimenez JC, Wan X, Kawashima R, Ozaki T (2007) Nonlinear local electrovascular coupling. II: from data to neuronal masses. Hum Brain Mapp 28:335–354. https://doi.org/10.1002/hbm.20278

Rosa MJ, Daunizeau J, Friston KJ (2010a) EEG-fMRI integration: a critical review of biophysical modeling and data analysis approaches. J Integr Neurosci 9:453–476. https://doi.org/10.1142/S0219635210002512

Rosa MJ, Kilner J, Blankenburg F, Josephs O, Penny W (2010b) Estimating the transfer function from neuronal activity to BOLD using simultaneous EEG-fMRI. NeuroImage 49:1496–1509. https://doi.org/10.1016/j.neuroimage.2009.09.011

Rosen BR, Buckner RL, Dale AM (1998) Event-related functional MRI: past, present, and future. Proc Natl Acad Sci 95:773–780

Salek-Haddadi A, Lemieux L, Merschhemke M, Friston KJ, Duncan JS, Fish DR (2003) Functional magnetic resonance imaging of human absence seizures. Ann Neurol 53:663–667. https://doi.org/10.1002/ana.10586

Scheeringa R, Bastiaansen MCM, Petersson KM, Oostenveld R, Norris DG, Hagoort P (2008) Frontal theta EEG activity correlates negatively with the default mode network in resting state. Int J Psychophysiol 67:242–251. https://doi.org/10.1016/j.ijpsycho.2007.05.017

Schwab S, Koenig T, Morishima Y, Dierks T, Federspiel A, Jann K (2015) Discovering frequency sensitive thalamic nuclei from EEG microstate informed resting state fMRI. NeuroImage 118:368–375. https://doi.org/10.1016/j.neuroimage.2015.06.001

Shiraishi H, Ahlfors SP, Stufflebeam SM, Takano K, Okajima M, Knake S, Hatanaka K, Kohsaka S, Saitoh S, Dale AM, Halgren E (2005) Application of magnetoencephalography in epilepsy patients with widespread spike or slow-wave activity. Epilepsia 46:1264–1272. https://doi.org/10.1111/j.1528-1167.2005.65504.x

Shmuel A, Augath M, Oeltermann A, Logothetis NK (2006) Negative functional MRI response correlates with decreases in neuronal activity in monkey visual area V1. Nat Neurosci 9:569–577. https://doi.org/10.1038/nn1675

Shulman RG, Hyder F, Rothman DL (2001) Cerebral energetics and the glycogen shunt: neurochemical basis of functional imaging. Proc Natl Acad Sci 98:6417–6422

Shulman RG, Rothman DL, Behar KL, Hyder F (2004) Energetic basis of brain activity: implications for neuroimaging. Trends Neurosci 27:489–495. https://doi.org/10.1016/j.tins.2004.06.005

Sirotin YB, Das A (2009) Anticipatory haemodynamic signals in sensory cortex not predicted by local neuronal activity. Nature 457:475–479. https://doi.org/10.1038/nature07664

Sotero RC, Trujillo-Barreto NJ (2007) Modelling the role of excitatory and inhibitory neuronal activity in the generation of the BOLD signal. NeuroImage 35:149–165. https://doi.org/10.1016/j.neuroimage.2006.10.027

Sotero RC, Trujillo-Barreto NJ (2008) Biophysical model for integrating neuronal activity, EEG, fMRI and metabolism. NeuroImage 39:290–309. https://doi.org/10.1016/j.neuroimage.2007.08.001

Sotero RC, Trujillo-Barreto NJ, Iturria-Medina Y, Carbonell F, Jimenez JC (2007) Realistically coupled neural mass models can generate EEG rhythms. Neural Comput 19:478–512. https://doi.org/10.1162/neco.2007.19.2.478

Sotero RC, Trujillo-Barreto NJ, Jiménez JC, Carbonell F, Rodríguez-Rojas R (2009) Identification and comparison of stochastic metabolic/hemodynamic models (sMHM) for the generation of the BOLD signal. J Comput Neurosci 26:251–269. https://doi.org/10.1007/s10827-008-0109-3

Stephan KE, Harrison LM, Penny WD, Friston KJ (2004) Biophysical models of fMRI responses. Curr Opin Neurobiol 14:629–635. https://doi.org/10.1016/j.conb.2004.08.006

Stephan KE, Weiskopf N, Drysdale PM, Robinson PA, Friston KJ (2007) Comparing hemodynamic models with DCM. NeuroImage 38:387–401. https://doi.org/10.1016/j.neuroimage.2007.07.040

Stippich C, Freitag P, Kassubek J, Sörös P, Kamada K, Kober H, Scheffler K, Hopfengärtner R, Bilecen D, Radü E-W, Vieth J-B (1998) Motor, somatosensory and audi-

tory cortex localization by fMRI and MEG. Neuroreport 9:1953–1957. https://doi.org/10.1097/00001756-199806220-00007

Sui J, Pearlson G, Caprihan A, Adali T, Kiehl KA, Liu J, Yamamoto J, Calhoun VD (2011) Discriminating schizophrenia and bipolar disorder by fusing fMRI and DTI in a multimodal CCA+ joint ICA model. NeuroImage 57:839–855. https://doi.org/10.1016/j.neuroimage.2011.05.055

Sui J, Adali T, Yu Q, Chen J, Calhoun VD (2012) A review of multivariate methods for multimodal fusion of brain imaging data. J Neurosci Methods 204:68–81. https://doi.org/10.1016/j.jneumeth.2011.10.031

Tagliazucchi E, Laufs H (2015) Multimodal imaging of dynamic functional connectivity. Front Neurol 6:1–9. https://doi.org/10.3389/fneur.2015.00010

Thees S, Blankenburg F, Taskin B, Curio G, Villringer A (2003) Dipole source localization and fMRI of simultaneously recorded data applied to somatosensory categorization. NeuroImage 18:707–719

Thornton RC, Rodionov R, Laufs H, Vulliemoz S, Vaudano A, Carmichael D, Cannadathu S, Guye M, McEvoy A, Lhatoo S, Bartolomei F, Chauvel P, Diehl B, De Martino F, Elwes RDC, Walker MC, Duncan JS, Lemieux L (2010) Imaging haemodynamic changes related to seizures: comparison of EEG-based general linear model, independent component analysis of fMRI and intracranial EEG. NeuroImage 53:196–205. https://doi.org/10.1016/j.neuroimage.2010.05.064

Trujillo-Barreto N, Martínez-Montes E, Melie-García L, Valdés-Sosa PA (2001) A symmetrical Bayesian model for fMRI and EEG/MEG neuroimage fusion. Int J Bioelectromagn 3:89–100

Trujillo-Barreto NJ, Aubert-Vázquez E, Valdés-Sosa PA (2004) Bayesian model averaging in EEG/MEG imaging. NeuroImage 21:1300–1319. https://doi.org/10.1016/j.neuroimage.2003.11.008

Tsvetanov KA, Henson RNA, Tyler LK, Davis SW, Shafto MA, Taylor JR, Williams N, Cam CAN, Rowe JB (2015) The effect of ageing on fMRI: correction for the confounding effects of vascular reactivity evaluated by joint fMRI and MEG in 335 adults. Hum Brain Mapp 36:2248–2269. https://doi.org/10.1002/hbm.22768

Ullsperger M, Debener S (2010) Simultaneous EEG and fMRI: recording, analysis, and application, simultaneous EEG and fMRI: recording, analysis, and application. Academic Press, London. https://doi.org/10.1093/acprof:oso/9780195372731.001.0001

Ureshi M, Matsuura T, Kanno I (2004) Stimulus frequency dependence of the linear relationship between local cerebral blood flow and field potential evoked by activation of rat somatosensory cortex. Neurosci Res 48:147–153. https://doi.org/10.1016/j.neures.2003.10.014

Van Eyndhoven S, Hunyadi B, De Lathauwer L, Van Huffel S (2017) Flexible fusion of electroencephalography and functional magnetic resonance imaging: revealing neural-hemodynamic coupling through structured matrix-tensor factorization. In: 2017 25th European Signal Processing Conference (EUSIPCO). IEEE, Washington, DC, pp 26–30. https://doi.org/10.23919/EUSIPCO.2017.8081162

Wagner M, Fuchs M (2001) Integration of functional MRI, structural MRI, EEG, and MEG. Int J Bioelectromagn 3:101–116

Wan X, Riera J, Iwata K, Takahashi M, Wakabayashi T, Kawashima R (2006) The neural basis of the hemodynamic response nonlinearity in human primary visual cortex: implications for neurovascular coupling mechanism. NeuroImage 32:616–625. https://doi.org/10.1016/j.neuroimage.2006.03.040

Warach S, Ives JR, Schlaug G, Patel MR, Darby DG, Thangaraj V, Edelman RR, Schomer DL (1996) EEG-triggered echo-planar functional MRI in epilepsy. Neurology 47:89–93. https://doi.org/10.1212/WNL.47.1.89

Wei H, Jafarian A, Zeidman P, Litvak V, Razi A, Hu D, Friston KJ (2020) Bayesian fusion and multimodal DCM for EEG and fMRI. NeuroImage 211:116595. https://doi.org/10.1016/j.neuroimage.2020.116595

Whittingstall K, Stroink G, Schmidt M (2007) Evaluating the spatial relationship of event-related potential and functional MRI sources in the primary visual cortex. Hum Brain Mapp 28:134–142. https://doi.org/10.1002/hbm.20265

Wirsich J, Bénar C, Ranjeva J-P, Descoins M, Soulier E, Le Troter A, Confort-Gouny S, Liégeois-Chauvel C, Guye M (2014) Single-trial EEG-informed fMRI reveals spatial dependency of BOLD signal on early and late IC-ERP amplitudes during face recognition. NeuroImage 100:325–336. https://doi.org/10.1016/j.neuroimage.2014.05.075

Yuan H, Zotev V, Phillips R, Drevets WC, Bodurka J (2012) Spatiotemporal dynamics of the brain at rest — exploring EEG microstates as electrophysiological signatures of BOLD resting state networks. NeuroImage 60:2062–2072. https://doi.org/10.1016/j.neuroimage.2012.02.031

Sparse and Data-Driven Methods for Concurrent EEG–fMRI

29

Pamela K. Douglas, Farzad V. Farahani, Ariana Anderson, and Jerome Gilles

29.1 Introduction

The extent to which bioelectric and hemodynamic phenomena are coupled has been studied extensively yet remains at least partially unknown, and likely varies across brain region and subject, and furthermore there are effects related to task (Daunizeau et al. 2009) and certain pathologic conditions such as epilepsy (Grova et al. 2008) and stroke (Bonakdarpour et al. 2007). Developing a principled method for EEG–fMRI fusion is challenging for a number of reasons beyond overcoming the temporal and spatial signal detection limitations of fMRI and EEG, respectively. EEG is thought to arise primarily from synchronous neuronal spikes and other voltage potential fluctuations in the extracellular medium associated with neuronal computation (Buzsáki et al. 2012). The BOLD signal measures physiologically delayed and temporally smoothed changes in oxygenation level within the vasculature (Mark and Cohen 1997). Given that EEG and fMRI measure different variables, which are themselves in different dimensional spaces, determining information described mutually by each of these imaging modalities is nontrivial (Valdes-Sosa et al. 2009).

P. K. Douglas (✉)
SMST, Computer Science, UCF, Orlando, FL, USA

Psychiatry & Biobehavioral Medicine, UCLA, Los Angeles, CA, USA

F. V. Farahani
Department of Biostatistics, Johns Hopkins University, Baltimore, MD, USA

A. Anderson
Psychiatry & Biobehavioral Medicine, UCLA, Los Angeles, CA, USA
e-mail: ariana82@ucla.edu

J. Gilles
Department of Mathematics, San Diego State University, San Diego, CA, USA

C. Mulert, L. Lemieux (eds.), *EEG - fMRI*,
https://doi.org/10.1007/978-3-031-07121-8_29

Perhaps the most challenging aspect of quantifying EEG–fMRI couplings is the temporal variability of these measurements—even in response to the same stimuli. Habituation and repetition suppression are clear examples of varied response to repeated stimuli (Auksztulewicz et al. 2016). However, even with jittered experimental paradigms, responses can vary considerably across time within an individual (Müller et al. 2008; Blankertz et al. 2006). Quantifying and predicting these nonstationarities is one of the most difficult problems that has impeded widespread adoption of single-trial EEG decoding for the purpose of brain–computer interfaces (Wojcikiewicz et al. 2011; Douglas and Douglas 2019).

The nonstationary nature of EEG–fMRI data has motivated concurrent data collection for reasons beyond localization of the generators of epileptic seizures and interictal events. Representational drift and subject habituation to stimuli may alter responses even in serially collected multimodal data. When the data are collected simultaneously, the temporal (and potentially spatial) response variability no longer contributes added complexity to disentangling mutual and distinct information in these measurements. However, analysis of EEG data collected in the MRI environment has proven quite challenging, given a number of artifacts introduced during concurrent recordings.

A number of recent studies suggest that neural systems use parsimonious functional representations for information processing (Eavani et al. 2015), and that low-dimensional global brain signatures are evident across multiple tasks (Anderson et al. 2012; Shine et al. 2019). Sparse decomposition methods (e.g, ICA) have also been used effectively for encoding and decoding fMRI (Xie et al. 2016; Douglas et al. 2011; Colby et al. 2012; Anderson et al. 2014) and EEG (Douglas et al. 2013), as well as group membership classification (Colby et al. 2012; Rosa et al. 2015). In this chapter we review empirical techniques that leverage sparse representations for the following purposes:

- Determining optimal sampling times for fMRI;
- Artifact removal from EEG data collected in the MRI scanning environment;
- Data-driven techniques for EEG–fMRI fusion.

29.2 Sparse Sampling of the Hemodynamic Response Function

Even in the early days of fMRI, a number of investigators noted considerable variability in the hemodynamic response function (HRF), a mathematical function estimated by fitting selected empirical data to a chosen basis set. For example, in 1995, Lee and colleagues reported HRF delay latencies ranging from 4 to 14 s (Lee et al. 1995). The HRF varies both in its magnitude and response latency even within functionally specialized regions in the healthy brain (e.g, visual cortex, for a review, see Handwerker et al. 2012), as well as in the aging brain (e.g, Anderson et al. 2020). Taking this variability into account also boosts fMRI decoding accuracy (Choupan et al. 2020). Despite this knowledge, many studies continue to convolve event time series with a single, the "canonical," HRF kernel. This convenient simplification

allows one to answer questions "assuming that the HRF is canonical, what is the location?"

Analyses of large publicly available fMRI datasets including the Human Connectome data collected with rapid sampling rates, or repetition times (TRs), of 600 ms have again called into question the appropriateness of using a canonical HRF function to analyze fMRI data (Wu et al. 2013). Using the Human Connectome data, Webb et al. (2013) noted that voxels that were spatially adjacent to arteries were found to be Granger Causal sources, and their downstream venous drainage counterparts were conversely found to be Granger sinks, effectively recapitulating the early HRF delay maps of Lee et al. (1995), demonstrating that there are characteristic delays between the HRF peak in a voxel proximal to an artery verses the venous bed. Studies carried out at 7 T have only further complicated the issue. For example, HRF peak activation magnitude and time appear to vary across laminar layers in the brain (Harel et al. 2006; Koopmans et al. 2011).

Understanding HRF variability and effectively sampling, the subtle variations and nonlinearities in the HRF may prove to be an essential component of determining EEG–fMRI couplings. However, the sampling of fMRI is periodic and fixed at the repetition time (TR). Therefore, altering the timing of stimulus presentation is one method that enables varied sampling of the HRF. Effectively jittering the stimulus timing in this manner in turn changes the relative point at which the response signal is measured.

Although varying the interstimulus interval (ISI) is a standard practice in psychometric research, this is generally applied using simple randomization to reduce adaptation to repeated stimuli, or to improve subtraction results within a GLM framework (Glover 1999). Theoretically, randomized sampling over an infinite amount of time should enable reconstruction of any unknown signal (Donoho 2006). However, within a given fMRI experiment, we are limited practically by the total number of observations that are feasible within a data collection session. Furthermore, we have a reasonable a priori estimate of the expected HRF signature itself.

Previous work has shown that the HRF can be modeled using a Volterra series formulation using only a few state variables (Friston et al. 2000). In sparse optimal sampling schedule (SOSS) designs, we seek to determine n time points at which measurements should be taken to achieve maximal accuracy in recovering parameter estimates, p, with the minimum number of observations, $y(t)$. The theoretical basis for many SOSS techniques make use of the Cramer-Rao inequality (DiStefano 1982; Kalicka & Bochen 2005), which states that the covariance matrix Cov(p) of parameter estimates is bounded below by the inverse of the Fisher information matrix, M:

$$m_{ij}\left(t_1 \ldots t_n\right) = \sum_{k=1}^{n} \frac{1}{\sigma^2} \frac{\partial y\left(t_k\right)}{\partial p_i} \frac{\partial y\left(t_k\right)}{\partial p_j}$$

The goal then is to find estimates of minimal covariance, which can be achieved by minimizing M^{-1}, or equivalently by maximizing the det(M), since:

$$M^{-1} = \frac{adj\, M}{\det M}$$

After decomposing the double-gamma HRF signal into Jordan canonical form, and applying the Akaike information criterion, Douglas (2017) found that a 12-parameter model, or equivalently that the sum of six exponentials, adequately described the HRF signal without extraneous parameters (Fig. 29.1, Table 29.1).

The results of applying this sparse optimal sampling schedule (SOSS) to detect HRF variability were demonstrated on simulated data (Fig. 29.2). The SOSS was found to be more effective at recovering the HRF parameter estimates after 10, 50, and 100 events. Interestingly, a fixed or periodic stimulus presentation yielded more robust estimates than a randomly jittered stimulus presentation after 50 and 100 events (Fig. 29.2, lower left). However, presenting stimuli according to the SOSS design yielded more robust estimates of the HRF when the amount of added Gaussian noise varied (Fig. 29.2, lower right).

The SOSS schedule was then implemented into an fMRI data collection session whereby subjects viewed photic stimuli. A total of ten healthy individuals (aged 23–30, 12 males) without history of neurological disease were recruited to participate in this study, which was approved by the UCLA Institutional Review Board.

Each individual provided written informed consent at the Staglin Center for Cognitive Neuroscience prior to participation in the study. The experiment consisted of concurrent EEG–fMRI data collection, in a dimly lit MR scanner room while a subject passively viewed visual stimuli, presented via an MR projector screen. Stimuli consisted of Gabor element "flashes" presented radially against a black background. The general linear model (GLM) results at the group level are shown in Fig. 29.3, left. The mean recovered HRF time course with the standard

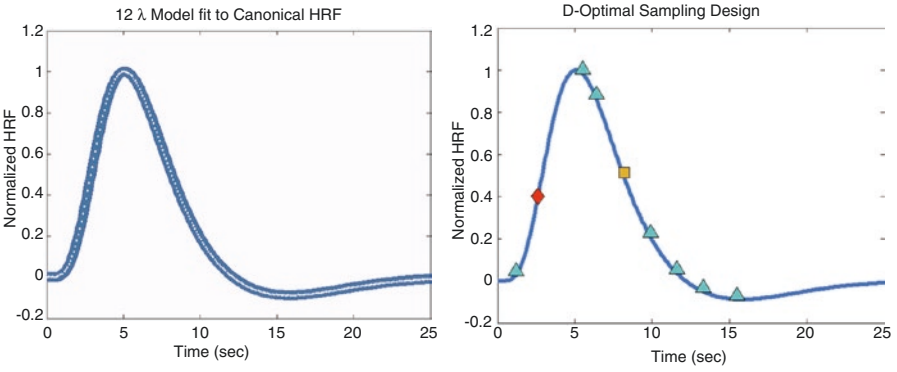

Fig. 29.1 (Left) The standard double gamma HRF kernel is shown in blue. Overlaid (in white) is the winning 12-parameter model fit to the HRF. The sum of squared error for this fit was less than 0.001% of the variance. (Right) The sampling points along the HRF determined by the D-Optimal sparse sampling schedule design are overlaid onto the HRF. Green triangles indicate sampling points half as many times as those with yellow squares, and one third as many times as points indicated with a red diamond

Table 29.1 Sparse optimal sampling schedule parameter estimates

Parameter	Value	Parameter	Value
A_1	0.3172	λ_1	5.0537
A_2	6.8339	λ_2	0.0296
A_3	−4.578	λ_3	4.2034
A_4	−1.1125	λ_4	0.0112
A_5	2.4824	λ_5	0.1342
A_6	−7.7615	λ_6	0.0657

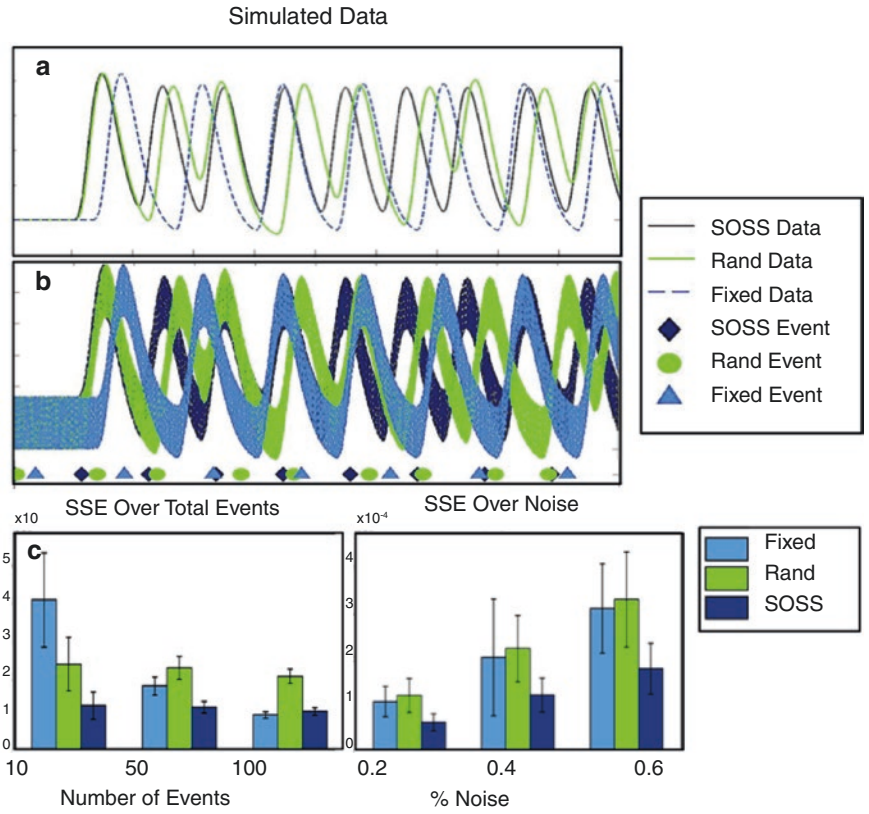

Fig. 29.2 (**a**–**c**) Comparison of fixed, random, and sparse optimal sampling schedule (SOSS) on simulated Data. (Top) Simulated fMRI Data was constructed using the SPM software and the classic double gamma hemodynamic response function (HRF). Data were simulated using either a fixed inter-stimulus interval (ISI) (light blue) a stimulus design jittered randomly with mean inter-stimulus interval (ISI) of 10 ± 3 s (green) or a D-Optimal SOSS also constructed with a mean ISI of 10 ± 3 s (dark blue). (Middle) Simulated data shown with added Gaussian Noise, with stimulus events that generated the response shown below with event markers. (Lower Left) Sum of Squared Error ± SEM for recovering HRF estimates for each sampling schedule after 10, 50, or 100 stimulus presentation events, with 0.4% added noise. (Lower Right) Error of estimates at varying noise levels as a percentage of the maximum HRF magnitude after 10 stimulus events

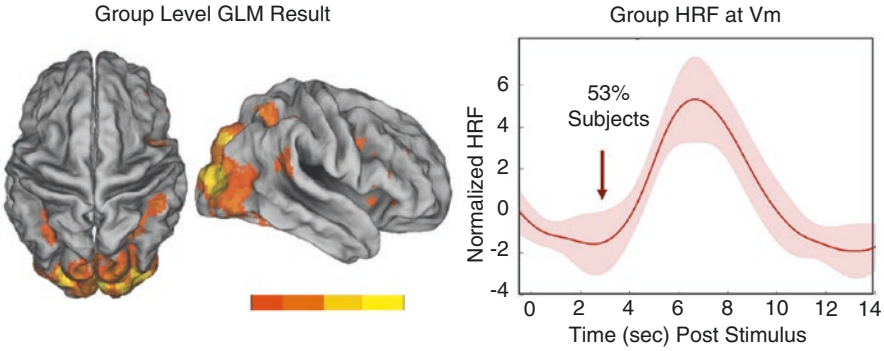

Fig. 29.3 Empirical results using a SOSS stimulus presentation schedule. Group Level Results. (Left) General Linear Model Contrast results z-thresholded from 2.3 to 10 for the photic stimulation task. (Right) Average and standard deviation of the recovered hemodynamic response function, where the initial dip was observed in 53% of subjects

deviation across the group is shown in Fig. 29.3, right. After only 50 stimuli presentations, the initial dip was recovered in 53% of subjects (Fig. 29.3).

29.3 Leveraging Sparsity for Artifact Removal

As discussed in Chap. 8, a number of artifacts are introduced into the EEG signal during simultaneous acquisition including the MR gradient-switching artifact, cardiac pulsatile motion effects (Srivastava et al. 2005), and noise due to the magnetic cryo-pump in some MR systems. For a discussion of these artifacts at higher field, see Chap. 11. The issue of MR gradient artifact removal appears to be mostly solved via subtraction of an exponentially weighted moving average template (Goldman et al. 2002). However, the presence of the remaining artifacts can dramatically change the spectral properties of the signal and obscure the ability to perform trial-by-trial analyses.

Many artifact removal techniques have been developed to address these issues including template-based methods (Allen 1998), adaptive noise cancelation (Allen 2000), adaptive filtering methods (Masterton et al. 2007; Correa et al. 2008), maximum noise fraction (Sun et al. 2009), principal components (Niazy et al. 2010), independent component-based methods (Jung et al. 2000; Zou et al. 2012), and combined methods (Mantini et al. 2007; Debener et al. 2007; Calhoun & Adali 2012).

One method that appears to be highly effective at cardiac pulse artifact removal on both simulated and empirical data is low rank + sparse decomposition (LR + SD) (Gilles et al. 2014). Importantly, this method obviates the need for any reference or template artifact signal. As such, the combined effects of many types of artifacts can be removed in a single decomposition without the need for manual identification of artifact components in the data.

In brief, the LR + SD method assumes that each recorded EEG channel $\overset{\ddot{\cup}}{f}_i(k)$ is a linear combination of its cleaned version $f_i(k)$, and j different artifacts $f_j^{\mathrm{A}}(k)$, within unknown mixing coefficients a_{ij}.

$$\overset{\ddot{\cup}}{f}_i(k) = f_i(k) + \sum_{j=1}^{J} a_{ij} f_j^{\mathrm{A}}(k)$$

The key to this method is to assume that true EEG events occur at specific times and only effect a limited number of electrodes. In this case, the matrix F is sparse, and thus the artifact removal problem is equivalent to performing a low-rank + sparse decomposition on the measurement matrix (see Gilles et al. 2014). Figure 29.4 shows group-level results of classic ICA-based removal and the LR + SD method on the data described above while subjects viewed Gabor flashes using the SOSS stimulus presentation. These data are compared to EEG results obtained outside of the scanning environment on these subjects. The LR + SD method resulted in an improved signal-to-noise ratio. Results from a single subject are shown in Fig. 29.5.

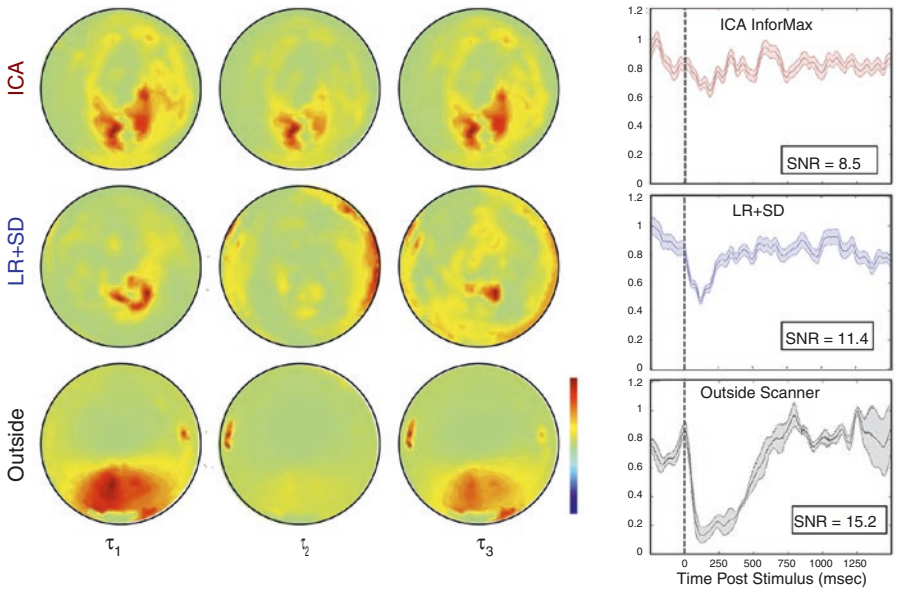

Fig. 29.4 Group Level Results comparing independent component analysis (ICA) and LR + SD based cleaning to EEG data collected outside of the MR scanner environment. (TOP PANEL) Normalized Alpha Power time courses derived from the ocular EEG channel averaged across all subjects plotted with mean ± SEM for ICA, LR + SD and Outside Scanner Results. Signal-to-Noise ratios are shown in the lower left corner for each result with the stimulus occurring at time equal to zero. (LOWER PANEL) Group level alpha power results projected topographically for 500 ms prior to stimulus onset (t1), 50 ms following stimulus onset (t2), and 500 ms following stimulus onset (t3)

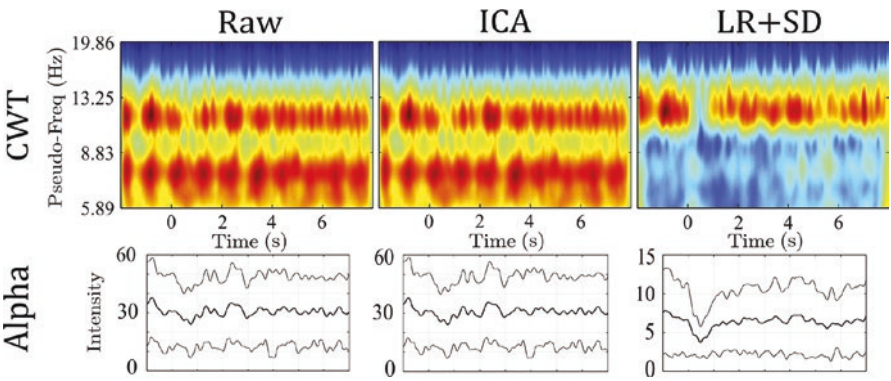

Fig. 29.5 Single-subject alpha band continuous wavelet transform (CWT) averaged over photic stimuli. Columns denote the raw MRI signal (top left), the ICA-cleaned signal (top centre), and LR + SD cleaned CWT (top right). The corresponding time series filtered in the alpha range of 8–12 Hz is shown in the lower panel

29.4 Data Driven Methods for EEG–fMRI Integration

A variety of data-driven methods have been developed to study EEG–fMRI couplings. As discussed in previous chapters, the most common approach is the asymmetric approach, whereby information from one modality is used to inform analysis of the other (Valdes-Sosa et al. 2009). In EEG constrained fMRI analysis, temporal information from EEG recordings can be convolved with a classic HRF kernel to analyze fMRI data (e.g, Goldman et al. 2002; Campanella et al. 2013). However, given the time scale of EEG fluctuations and the blurred and variable latency of the HRF (e.g, Wu et al. 2013; Handwerker et al. 2012; Webb et al. 2013), it is unclear if these methods are advantageous over simply convolving the HRF with externally (i.e, experimentally) determined task timestamps. The exception to this is when the events occur at a priori unknown times, as is the case with epileptiform discharges on EEG (Thornton et al. 2011).

Asymmetric fMRI to EEG methods typically use fMRI spatial information in the form of a prior (Wagner et al. 2000; Lin et al. 2006) to help solve the unidentifiable problem of reconstructing EEG sources from voltage potentials measured at the scalp. The extent to EEG and fMRI measure activity from the same brain loci requires thoughtful consideration (Daunizeau et al. 2005; Douglas and Douglas 2019). However, EEG and fMRI data are both nonstationary. Therefore, the couplings themselves can also vary in time. For this reason, a data-driven symmetric approach may be desirable. A variety of data-driven methods for blind source separation (BSS) have been discussed in previous chapters. Here, we discuss tensor-based methods and methods that consider nonstationarities between instantaneous bioelectric–hemodynamic couplings.

29.4.1 Tensor Factorization

Tensor decompositions are a generalization of matrix decompositions (e.g, singular value decomposition) to higher dimensions. Some work (e.g, Chatzichristos et al. 2018) suggests that these decompositions may outperform ICA methods (e.g, Anderson et al. 2011) for EEG–fMRI fusion on both simulated and empirical data. Here, we discuss two common approaches to tensor factorization: *canonical polyadic decomposition* (CPD) and the *Tucker decomposition*. CPD is best used for the estimation of latent parameters, but Tucker decomposition applied for cases of subspace estimation, compression, and dimensionality reduction (Rabanser et al. 2017). Remarkably, a unique solution under mild conditions is achieved in tensor decomposition techniques, making them well suited for blind source separation (BSS) problems.

29.4.2 Canonical Polyadic Decomposition (CPD)

Canonical polyadic decomposition (CPD) represents a tensor as the sum of a finite number of rank-one components (Kolda and Bader 2009). Given a tensor $\chi \in \mathrm{R}^{I_1 \times I_1 \times \cdots I_n}$, the n-way CPD case is formulated as follows:

$$\chi = \sum_{r=1}^{R} \lambda_r a_r^{(1)} \circ a_r^{(2)} \circ \cdots \circ a_r^{(n)} = \left[\left[\lambda; A^{(1)}; A^{(2)}; \cdots; A^{(n)} \right]\right]$$

where $\circ$ is the outer product, and $A^{(1)} = \left[a_1^{(1)}, a_2^{(1)}, \cdots, a_R^{(1)} \right]$, $A^{(2)}$ and $A^{(n)}$ are similarly defined as *factor matrices* and hold the combination of the vectors from the rank-one components as columns. The smallest R for which equality holds is known as the *tensor rank*. In this setting, λ_r acts as a weighting factor during normalization of the factor matrices' columns. Different algorithms for CPD include alternating least squares (ALS), Jennrich's algorithm, and tensor power (Rabanser et al. 2017). Unlike more conventional BSS techniques, CPD provides a unique solution without the need to impose constraints such as orthogonality (e.g, principal component analysis) and statistical independence (e.g, independent component analysis). For example, the CPD of a three-way tensor is unique if two factor matrices have linearly independent columns and the third factor matrix has no collinear columns. However, one can impose these additional constraints if desired (Fig. 29.6).

One implementation of CPD is through the Parafac algorithm. In fMRI, the linear decomposition methods of group-ICA and Linear Tensor ICA have successfully established that, across scan sessions and subjects, consistent functional networks exist (8). Tensor Algebra can represent an observation, such as an image or an fMRI brain scan, by employing a linear decomposition, rank-R, or a multilinear decomposition, rank-(R_1, R_2, …, R_N). An optimal linear decomposition of an n-way array ("data tensor") is computed via Parafac/CANDECOMP. Tensor ICA (as implemented in FSL) is a linear Parafac variant subject to statistical independence constraints.

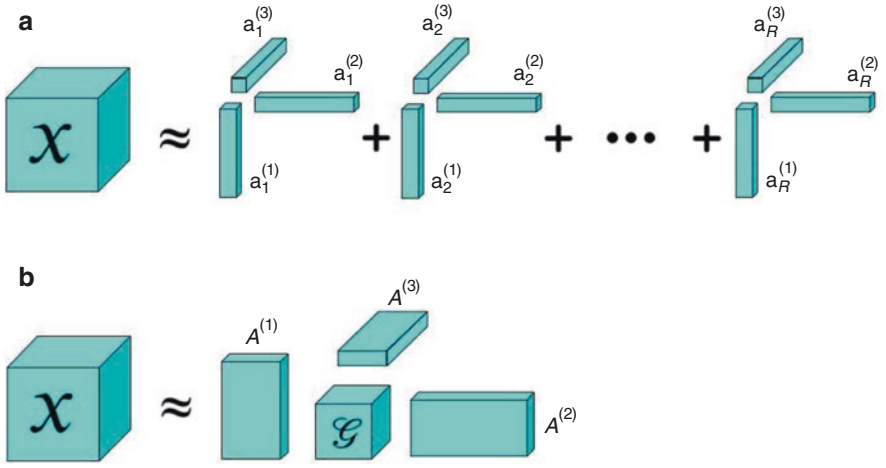

Fig. 29.6 Illustration of two common tensor decomposition techniques. (**a**) Canonical polyadic decomposition, and (**b**) Tucker decomposition

29.4.3 Tucker Decomposition

In the Tucker model (Kolda and Bader 2009), a tensor $\mathcal{X} \in \mathrm{R}^{I_1 \times I_1 \times \cdots I_n}$ is decomposed into a core tensor along with multiple factor matrices (similar to a higher order PCA):

$$\mathcal{X} = \sum_{r_1=1}^{R_1} \sum_{r_2=1}^{R_2} \cdots \sum_{r_n=1}^{R_n} g_{r_1 r_2 \cdots r_n} a_{i_1 r_1}^{(1)} \circ \cdots \circ a_{i_n r_n}^{(n)} = \mathcal{G} \times_1 A^{(1)} \times_2 \cdots \times_n A^{(n)} = \left[\left[\mathcal{G}; A^{(1)}; \cdots; A^{(n)} \right]\right]$$

where $R_1 \leq I_1$, $R_2 \leq I_2$, $R_n \leq I_n$, and the factor matrices $A^{(1)}$, $A^{(2)}$, and $A^{(n)}$ are generally referred to as the principal component along the respective tensor mode. The tensor $\mathcal{G} = g_{r_1 r_2 \cdots r_n}$ is the *core tensor*, which adjusts the magnitude of interactions between the different components. Note that there is no requirement for the core tensor to have the same dimensions as $\mathcal{X}$. CPD is considered a special case of constrained Tucker decomposition. Although the Tucker decomposition provides a good model fit due to the high degrees of freedom, its factors are typically not unique, unlike the CPD and matrix SVD (Kolda and Bader 2009; Zhou and Cichocki 2012). The nonuniqueness occurs because the core tensor $\mathcal{G}$ can be arbitrarily configured, permitting multiple solutions to the same problem. Each component is allowed to interact with other components. Uniqueness can be enforced by introducing constraints. For example, the CPD can be expressed as a special case of the Tucker model with a superdiagonal core tensor. Finally, the *higher order singular value decomposition* (HOSVD) results in an all-orthogonal core and thus relies on yet another type of special core structure.

29.4.4 Coupled Matrix–Tensor Factorization (CMTF)

Tensor-based approaches are useful for joint factorization of multiple tensors, which leverage higher order signal structures (Cong et al. 2015; Ferdowsi et al. 2015). They can also circumvent the strong independence constraint in joint BSS through very mild uniqueness conditions. Similarly to the joint ICA, it is assumed that one mode of variability is shared among the tensors, for instance, time (Martínez-Montes et al. 2004) or participant (Acar et al. 2014; Hunyadi et al. 2017, 2016). Consider a set of m tensors $\mathcal{X}^m \in \mathrm{R}^{I_1 \times I_{2,m} \times \cdots I_{K_m,m}}$, $m \in \{1, \cdots, M\}$, with different orders K_m and different sizes $I_{K_m,m}$, except for the first mode I_1, which is common among all tensors. Then, we can formalize the coupled CPD of this set of tensors as follows:

$$\mathcal{X}^m = \sum_{r=1}^{R} a_r^{(1)} \circ a_r^{(2,m)} \circ \cdots \circ a_r^{(K_m,m)}$$

Notably, the uniqueness conditions in this case are even more relaxed than single tensor decomposition (Sørensen and De Lathauwer 2015). One particular case, namely coupled matrix–tensor factorization (CMTF) has been studied considerably in EEG–fMRI analysis and beyond (Acar et al. 2014). Reconsider the previous example of patients with epilepsy. Suppose we have a matrix $X^{\mathrm{fMRI}} \in \mathrm{R}^{M \times L}$ and a third-order tensor $\mathcal{X}^{EEG} \in \mathbb{R}^{M \times J \times K}$, sharing the same patient-by-patient variability (M, L, J, and K denote the number of patients, voxels, channels, and time samples, respectively). Their coupled decomposition is formulated as the minimization of the following objective function:

$$\begin{aligned} f\left(A^{(1)}, A^{(2,\mathrm{fMRI})}, A^{(2,EEG)}, A^{(3,EEG)}\right) &= X^{\mathrm{fMRI}} - \sum_{r=1}^{R} a_r^{(1)} \circ a_r^{(2,\mathrm{fMRI})2} \\ &+ \mathcal{X}^{EEG} - \sum_{r=1}^{R} a_r^{(1)} \circ a_r^{(2,EEG)} \circ a_r^{(3,EEG)2} \end{aligned}$$

where $a_r^{(1)}$, $a_r^{(2,\mathrm{fMRI})}$, $a_r^{(2,EEG)}$, and $a_r^{(3,EEG)}$ denote the rth column of the matrices $A^{(1)}$, $A^{(2,\,\mathrm{fMRI})}$, $A^{(2,\,\mathrm{EEG})}$, and $A^{(3,\,\mathrm{EEG})}$. The same mild conditions hold for the uniqueness of the factors $A^{(1)}$, $A^{(2,\,\mathrm{EEG})}$ and $A^{(3,\,\mathrm{EEG})}$, similar to the CPD. The uniqueness of $A^{(2,\,\mathrm{fMRI})}$ is also guaranteed in case the common factor $A^{(1)}$ has full column rank (Fig. 29.7) (Sørensen and De Lathauwer 2015).

However, this model rests on the assumption that the factors in the shared dimension are the same, which may limit its applications to the extent that the neural substrates drive each measurement are distinct. To address this limitation, Acar et al. (2014) developed a more relaxed version of CMTF, named advanced CMTF, that permits the existence of both shared and non-shared factors. Common factors may instead be constrained to be similar as opposed to equivalent, as done in relaxed ACMTF (Rivet et al. 2015), soft coupling (Seichepine et al. 2014), approximate coupling (Cabral Farias et al. 2016), and multiway partial least squares (Martínez-Montes et al. 2004). Finally, Jonmohamadi et al. (2019) proposed a soft approach based on the use of coupled tensor–tensor decomposition (CTTD) of a fourth-order EEG tensor and third-order fMRI tensor, coupled partially in time and participant.

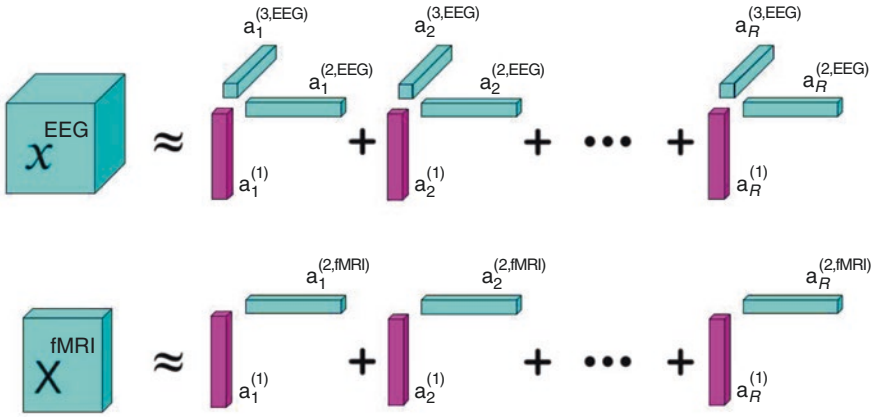

Fig. 29.7 Coupled matrix-tensor factorization (CMTF) for EEG-fMRI recordings, shown with a matrix of fMRI and a third order EEG tensor for a particular participant (magenta)

29.5 Canonical Correlation Analysis

Traditionalcanonical correlation analysis (CCA) is a statistical tool that finds an instantaneous linear relationship between variables by maximizing the correlation between projected variates that have undergone a linear transformation (Hotelling 1936). CCA, and variations on it, have been used to discover multimodal relationships between fMRI and EEG data (Correa et al. 2010, 2008). The resulting filters effectively reveal which features maximally give rise to data couplings. When the number of dimensions exceeds the number of data samples, as is the case for fMRI, performing these operations on covariance matrices is likely to become both numerically unstable and computationally intractable. Kernel CCA (kCCA) is well suited for this task, since a "kernel trick" can be applied to make computations more tractable (Akaho 2001; Bach and Jordan 2003). A linear kernel is commonly used in practice.

When the coupling between two signals is delayed, the temporal dynamics may be best revealed when correlations are computed on time shifted versions. Temporal kernel CCA recursively computes maximally correlated projections over time revealing non-instantaneous dynamic couplings (Bießmann et al. 2009). By comparison to time-shifted kCCA, and to multiway kCCA, tkCCA was found to be both faster and more accurate when operating on simulated data, and has been applied successfully to calculate couplings between nonhuman primate depth electrode recordings and fMRI data (Logothetis et al. 1999, 2002; Bießmann et al. 2009; Biessmann et al. 2011).

In considering the dynamic coupling between EEG and fMRI, nonstationarity or signal temporal dependency must be also considered. Temporal kernel CCA (tkCCA) recursively computes maximally correlated projections over time revealing non-instantaneous dynamic couplings (Bießmann et al. 2009). tkCCA, in effect, calculates a temporal filter that describes the relationship between variables. Similar to convolution methods, only one signal is shifted with respect to the other. In many

applications, it is useful to compute the maximal correlation between two variates $x \in R^{M}$ and $y \in R^{N}$, which is defined typically as:

$$\rho(x,y) = \max \operatorname{corr}(x,y) = \frac{C_{xy}}{(\operatorname{var} x)^{1/2}(\operatorname{var} y)^{1/2}}$$

where C_{xy} is the covariance between two variables. It may be useful to discuss CCA in relation to principal component analysis (PCA), which has been applied widely to neuroimaging data. Whereas PCA maximizes variance projections of a single variable, CCA works by maximizing correlations between sets of variable projections. PCA diagonalizes the covariance matrix with the goal of finding a linear transformation of components that are uncorrelated. By contrast, CCA is concerned with finding maximal correlations between components, where each dataset nominates a component for a given pairwise comparison. Traditional CCA calculates two normalized linear filters, $w_x \in R^{M}$ and $w_y \in R^{N}$ called *canonical variates* that maximize the correlation between projected variables, $U_a = w_x^{T} x$ and $U_b = w_y^{T} y$, as follows:

$$\rho(x,y) = \max \operatorname{corr}\left(w_x^{T} x, w_y^{T} y\right) = \frac{w_x^{T} C_{xy} w_y}{\left(w_x^{T} C_{xx} w_x\right)^{1/2}\left(w_y^{T} \operatorname{var} w_y\right)^{1/2}}$$

$$(\alpha,\beta) = \arg\max \operatorname{corr}\left(w_x^{T} x, w_y^{T} y\right)$$

$$\text{s.t.}: \operatorname{var}(U_a) = \operatorname{var}(U_b) = 1$$

In this case, a canonical correlogram is used to reflect couplings between signals. Figure 29.8 shows an example of these extracted filters and couplings while subjects viewed Gabor flashes in the data described above. In some sense, this suggests that

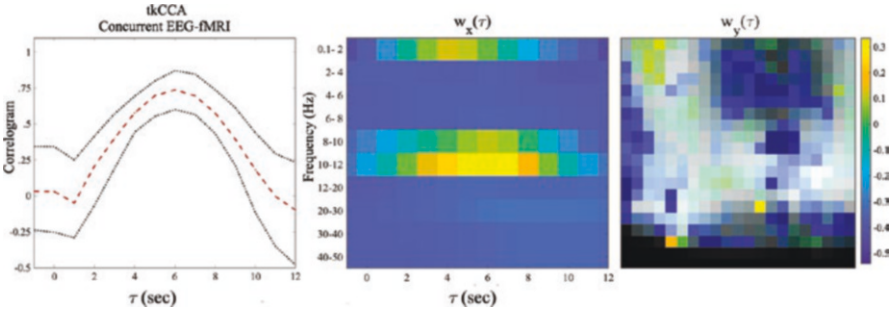

Fig. 29.8 Temporal kernel canonical correlation (tkCCA) applied to concurrently collected EEG-fMRI data while subjects viewed Gabor light "flashes". The correlogram combined with the variates reveal bioelectric-hemodynamic couplings. The correlogram (left) computed across 100 trials, reaches its peak at a time-lag of approximately 6 seconds, similar to the canonical hemodynamic response function. The variate w¬¬x shows the EEG-fMRI couplings across frequency bands, while the w¬¬y variate shows the spatial couplings mapped onto a region of interest in the visual cortex which was selected for tkCCA analysis. Couplings appeared most prominently between fMRI and the alpha and delta EEG frequency bands (Douglas, unpublished data)

convolving EEG temporal events with a canonical HRF function to perform asymmetric EEG-fMRI fusion may be a reasonable approx-imation. However, the majority of evoked and induced EEG signatures that have been mapped to cognitive tasks take place during the first few hundred milliseconds following a stimulus. Thus, convolving the HRF with temporal signatures that vary on the order of milliseconds is unlikely to produce significantly different results in a classic univariate fMRI analysis, given that the HRF is delayed and temporally smoothed. Other algorithms such as multimodal source power correlation analysis (mSPoC) are also well suited for examining nonstationary and multimodal data to include simultaneous EEG-fMRI data.

29.6 Conclusion

EEG signals evolve rapidly on the millisecond scale, and EEG sources resolve to relatively course spatial regions. It is generally thought that scalp EEG reflects neural activity in superficial regions of cortical gray matter. However, recent evidence suggests that neural activity in white matter, and the gray-white matter boundary may also contribute to scalp EEG measurements. In contrast, the fMRI BOLD signals can be resolved to more precise spatial loci and can be used as a proxy for neural activity in deep brain regions, yet the signal evolves slowly due to the physiologic time scale of the hemodynamic response. Here, we discussed a number of data-driven approaches to remove artifact from EEG signals collected concurrently in the MRI scanning environment. Improving artifact removal and data analysis techniques for multimodal EEG-fMRI remains an active area of research. Concurrent EEG-fMRI maybe of vital importance for patients with epilepsy by providing a "where" and a "when" for seizure activity. Sparse and data-driven approaches to studying these data may help improve our understanding of the non-linear and non-stationary couplings between EEG and fMRI recordings.

References

Acar E, Papalexakis EE, Gürdeniz G, Rasmussen MA, Lawaetz AJ, Nilsson M, Bro R (2014) Structure-revealing data fusion. BMC Bioinform 15:1–17. https://doi.org/10.1186/1471-2105-15-239

Akaho S (2001) A Kernel method for canonical correlation analysis. In: Proceedings of the International Meeting of the Psychometric Society

Allen PJ, Josephs O, Turner R (2000) A Method for Removing Imaging Artifact from Continuous EEG Recorded during Functional MRI. NeuroImage 12(2):230–239. S1053811900905998. https://doi.org/10.1006/nimg.2000.0599

Allen PJ, Polizzi G, Krakow K, Fish DR, Lemieux L (1998) Identification of EEG Events in the MR Scanner: The Problem of Pulse Artifact and a Method for Its Subtraction. NeuroImage 8(3):229–239. S1053811998903615. https://doi.org/10.1006/nimg.1998.0361

Anderson A et al (2011) Large sample group independent component analysis of functional magnetic resonance imaging using anatomical atlas-based reduction and bootstrapped clustering. Int J Imaging Syst Technol 21(2):223–231

Anderson A et al (2012) Real-time functional MRI classification of brain states using Markov-SVM hybrid models: peering inside the rt-fMRI black box. In: Machine learning and interpretation in neuroimaging. Lecture notes in computer science, vol 7263. Springer, Berlin

Anderson A et al (2020) Hemodynamic latency is associated with reduced intelligence across the lifespan: an fMRI DCM study of aging, cerebrovascular integrity, and cognitive ability. Brain Struct Funct 225(6):1705–1717

Anderson A, Douglas PK, Kerr WT, Haynes VS, Yuille AL, Xie J, Wu YN, Brown JA, Cohen MS (2014) Non-negative matrix factorization of multimodal MRI fMRI and phenotypic data reveals differential changes in default mode subnetworks in ADHD. NeuroImage 102:207–219. S1053811913012196. https://doi.org/10.1016/j.neuroimage.2013.12.015

Auksztulewicz R, Friston K (2016) Repetition suppression and its contextual determinants in predictive coding. Cortex 80:125–140. S0010945216000101. https://doi.org/10.1016/j.cortex.2015.11.024

Bach FR, Jordan MI (2003) Kernel independent component analysis, vol 4. IEEE, Washington, DC, 876–9, p IV. https://doi.org/10.1109/ICASSP.2003.1202783

Bießmann F, Meinecke FC, Gretton A, Rauch A, Rainer G, Logothetis NK, Müller K-R (2009) Temporal kernel CCA and its application in multimodal neuronal data analysis. Mach Learn 79:5–27. https://doi.org/10.1007/s10994-009-5153-3

Biessmann F, Plis S, Meinecke FC, Eichele T, Muller K-R (2011) Analysis of multimodal neuroimaging data. IEEE Rev Biomed Eng 4:26–58. https://doi.org/10.1109/RBME.2011.2170675

Buzsáki G, Anastassiou CA, Koch C (2012) The origin of extracellular fields and currents — EEG, ECoG, LFP and spikes. Nat Rev Neurosci 13(6):407–420. https://doi.org/10.1038/nrn3241

Bonakdarpour B, Parrish TB, Thompson CK (2007) Hemodynamic response function in patients with stroke-induced aphasia: Implications for fMRI data analysis. NeuroImage 36(2):322–331. S1053811907001371. https://doi.org/10.1016/j.neuroimage.2007.02.035

Blankertz B, Dornhege G, Krauledat M, Muller K.-R, Kunzmann V, Losch F, Curio G (2006). The Berlin brain-computer interface: EEG-based communication without subject training. IEEE Transactions on Neural Systems and Rehabilitation Engineering 14(2):147–152. 1642756. https://doi.org/10.1109/TNSRE.2006.875557

Cabral Farias R, Cohen JE, Comon P (2016) Exploring multimodal data fusion through joint decompositions with flexible couplings. IEEE Trans Signal Process 64:4830–4844. https://doi.org/10.1109/TSP.2016.2576425

Calhoun VD, Adali T (2012) Multisubject independent component analysis of fMRI: a decade of intrinsic networks, default mode, and neurodiagnostic discovery. IEEE Rev Biomed Eng 5:60–73. https://doi.org/10.1109/RBME.2012.2211076

Campanella S, Bourguignon M, Peigneux P, Metens T, Nouali M, Goldman S, Verbanck P, De Tiège X (2013) BOLD response to deviant face detection informed by P300 event-related potential parameters: a simultaneous ERP–fMRI study. NeuroImage 71:92. https://doi.org/10.1016/j.neuroimage.2012.12.077

Chatzichristos C, Davies M, Escudero J, Kofidis E, Theodoridis S (2018) Fusion of EEG and fMRI via soft coupled tensor decompositions. In: 2018 26th European Signal Processing Conference (EUSIPCO), Rome, pp 56–60. https://doi.org/10.23919/EUSIPCO.2018.8553077

Choupan J et al (2020) Temporal embedding and spatiotemporal feature selection boost multi-voxel pattern analysis decoding accuracy. J Neurosci Methods 345:108836. https://doi.org/10.1016/j.jneumeth.2020.108836

Colby JB et al (2012) Insights into multimodal imaging classification of ADHD. Front Syst Neurosci 6:59. https://doi.org/10.3389/fnsys.2012.00059

Cong F, Lin QH, Kuang LD, Gong XF, Astikainen P, Ristaniemi T (2015) Tensor decomposition of EEG signals: a brief review. J Neurosci Methods 248:59–69. https://doi.org/10.1016/j.jneumeth.2015.03.018

Correa NM, Li Y-O, Adali T, Calhoun VD (2008) Canonical correlation analysis for feature-based fusion of biomedical imaging modalities and its application to detection of associative networks in schizophrenia. IEEE J Select Top Signal Process 2(6):998–1007. https://doi.org/10.1109/JSTSP.2008.2008265

Correa N, Adali T, Li Y-O, Calhoun V (2010) Canonical correlation analysis for data fusion and group inferences. IEEE Signal Process Mag 27(4):39–50. https://doi.org/10.1109/MSP.2010.936725

Correa AG, Laciar E, Patiño HD, Valentinuzzi ME (2007) Artifact removal from EEG signals using adaptive filters in cascade. Journal of Physics: Conference Series 90012081. https://doi.org/10.1088/1742-6596/90/1/012081

Cohen MS (1997) Parametric analysis of fMRI data using linear systems methods. NeuroImage 6(2):93–103. S1053811997902780. https://doi.org/10.1006/nimg.1997.0278

Daunizeau J, Laufs H, Friston KJ (2009) EEG–fMRI information fusion: biophysics and data analysis. In: Mulert C, Lemieux L (eds) EEG - fMRI. Springer, Berlin, pp 511–526. http://www.springerlink.com/index/10.1007/978-3-540-87919-0_25

Daunizeau J, Grova C, Mattout J, Marrelec G, Clonda D, Goulard B, Pelegrini-Issac M, Lina J-M, Benali H. Assessing the relevance of fMRI-based prior in the EEG inverse problem: a bayesian model comparison approach. IEEE Transactions on Signal Processing 53(9):3461–3472. 1495883. https://doi.org/10.1109/TSP.2005.853220

Debener S et al (2007) Improved quality of auditory event-related potentials recorded simultaneously with 3-T fMRI: removal of the ballistocardiogram artefact. NeuroImage 34(2):587–597

DiStefano JJ (1982) Algorithms, software and sequential optimal sampling schedule designs for pharmacokinetic and physiologic experiments. Math Comput Simul 24(6):531–534. https://doi.org/10.1016/0378-4754(82)90654-1

Donoho DL (2006) Compressed sensing. IEEE Transactions on Information Theory 52(4):1289–1306. 1614066. https://doi.org/10.1109/TIT.2006.871582

Douglas PK (2017) Leveraging sparsity to detect HRF variability in fMRI. Proc SPIE 10160:2256943. https://doi.org/10.1117/12.2256943

Douglas PK, Douglas DB (2019) Reconsidering spatial priors in EEG source estimation. In: 7th International Winter Conference on Brain-Computer Interfaces (BCI)

Douglas PK, Harris S, Yuille A, Cohen MS (2011) Performance comparison of machine learning algorithms and number of independent components used in fMRI decoding of belief vs. disbelief. NeuroImage 56:544–553

Douglas PK et al (2013) Single trial decoding of belief decision making from EEG and fMRI data using independent components features. Front Hum Neurosci 7:392

Eavani H et al (2015) Identifying sparse connectivity patterns in the brain using resting-state fMRI. NeuroImage 105:286–299

Ferdowsi S, Abolghasemi V, Sanei S (2015) A new informed tensor factorization approach to EEG-fMRI fusion. J Neurosci Methods 254:27–35. https://doi.org/10.1016/j.jneumeth.2015.07.018

Friston KJ et al (2000) Nonlinear responses in fMRI: the balloon model, volterra kernels, and other hemodynamics. NeuroImage 12:466–477

Gilles J, Meyer T, Douglas PK (2014) Leveraging Sparsity: A Low-Rank + Sparse Decomposition (LR+SD) Method for Automatic EEG Artifact Removal. STMI Proceedings.

Glover GH (1999) Deconvolution of impulse response in event-related BOLD fMRI. NeuroImage 9(4):416429

Goldman RI, Stern JM, Engel J Jr, Cohen MS (2002) Simultaneous EEG and fMRI of the alpha rhythm. Neuroreport 13(18):2487–2492. https://doi.org/10.1097/01.wnr.0000047685.08940.d0

Grova C, Daunizeau J, Kobayashi E, Bagshaw AP, Lina J-M, Dubeau F, Gotman J (2008) Concordance between distributed EEG source localization and simultaneous EEG-fMRI studies of epileptic spikes. NeuroImage 39(2):755–774. https://doi.org/10.1016/j.neuroimage.2007.08.020

Handwerker D et al (2012) The continuing challenge of understanding and modeling hemodynamic variation in fMRI. NeuroImage 62(5):1017–1023

Harel N et al (2006) Combined imaging-histological study of cortical laminar specificity of fMRI signals. NeuroImage 29:879–887

Hotelling H (1936) Relations between two sets of variates. Biometrica 28(3/4):321–377

Hunyadi B, Van Paesschen W, De Vos M, Van Huffel S (2016) Fusion of electroencephalography and functional magnetic resonance imaging to explore epileptic network activity. In: Eur Signal Process Conf 2016–November, pp 240–244. https://doi.org/10.1109/EUSIPCO.2016.7760246

Hunyadi B, Dupont P, Van Paesschen W, Van Huffel S (2017) Tensor decompositions and data fusion in epileptic electroencephalography and functional magnetic resonance imaging data. Wiley Interdiscip Rev Data Min Knowl Discov 7:1–15. https://doi.org/10.1002/widm.1197

Jonmohamadi Y, Muthukumaraswamy S, Chen J, Roberts J, Crawford R, Pandey A (2019) Extraction of common task features in EEG-fMRI data using coupled tensor-tensor decomposition. Brain Topogr 33:636

Jung T et al (2000) Removing electroencephalographic artifacts by blind source separation. Psychophysiology 37:163–178

Kalicka R, Bochen D (2005) Properties of D-optimal sampling schedule for compartmental models. Biocybernet Biomed Eng 25(1):23–36

Kolda TG, Bader BW (2009) Tensor decompositions and applications. SIAM Rev 51:455–500. https://doi.org/10.1137/07070111x

Koopmans P et al (2011) Multi-echo fMRI of the cortical laminae in humans at 7T. NeuroImage 56(3):1276–1285

Lee AT, Glover GH et al (1995) Discrimination of large venous vessels in time- course spiral blood-oxygen-level-dependent magnetic-resonance functional neuroimaging. Magn Reson Med 33(6):745754

Lin F-H, Belliveau JW, Dale AM, Hämäläinen MS (2006) Distributed current estimates using cortical orientation constraints. Hum Brain Mapp 27(1):1–13. https://doi.org/10.1002/hbm.20155

Logothetis NK, Guggenberger H, Peled S, Pauls J (1999) Functional imaging of the monkey brain. Nat Neurosci 2(6):555–562. https://doi.org/10.1038/9210

Logothetis N, Merkle H, Augath M, Trinath T, Ugurbil K (2002) Ultra high-resolution fMRI in monkeys with implanted RF coils. Neuron 35(2):227–242

Mantini D, Perrucci MG, Cugini S, Ferretti A, Romani GL, Del Gratta C (2007) Complete artifact removal for EEG recorded during continuous fMRI using independent component analysis. NeuroImage 34(2):598–607. S1053811906009761. https://doi.org/10.1016/j.neuroimage.2006.09.037

Martínez-Montes E, Valdés-Sosa PA, Miwakeichi F, Goldman RI, Cohen MS (2004) Concurrent EEG/fMRI analysis by multiway partial least squares. NeuroImage 22:1023–1034. https://doi.org/10.1016/j.neuroimage.2004.03.038

Masterton AJ et al (2007) Measurement and reduction of motion and BCG from simultaneous EEG and fMRI recordings. NeuroImage 37:202–211

Müller K-R, Tangermann M, Dornhege G, Krauledat M, Curio G, Blankertz B (2008) Machine learning for real-time single-trial EEG-analysis: From brain–computer interfacing to mental state monitoring. Journal of Neuroscience Methods 167(1):82–90. S0165027007004657. https://doi.org/10.1016/j.jneumeth.2007.09.022

Niazy RK et al (2010) Removal of fMRI environment artifacts from EEG data using optimal basis sets. NeuroImage 28(3):720–737

Rabanser S, Shchur O, Günnemann S (2017) Introduction to tensor decompositions and their applications in machine learning. arXiv:1–13

Rivet B, Duda M, Guérin-Dugué A, Jutten C, Comon P (2015) Multimodal approach to estimate the ocular movements during EEG recordings: a coupled tensor factorization method. In: Proc. Annu. Int. Conf. IEEE Eng. Med. Biol. Soc. EMBS 2015–November, pp 6983–6986

Rosa MJ et al (2015) Sparse network-based models for patient classification using fMRI. NeuroImage 105:493–506

Seichepine N, Essid S, Fevotte C, Cappe O (2014) Soft nonnegative matrix Co-factorization. IEEE Trans Signal Process 62:5940–5949. https://doi.org/10.1109/TSP.2014.2360141

Shine JM et al (2019) Human cognition involves the dynamic integration of neural activity and neuromodulatory systems. Nat Neurosci 22:289–296

Sørensen M, De Lathauwer LD (2015) Coupled canonical polyadic decompositions and (coupled) decompositions in multilinear rank-terms---Part I: Uniqueness. SIAM J Matrix Anal Appl 36:496–522

Srivastava G, Crottaz-Herbette S, Lau KM, Glover GH, Menon V (2005) ICA-based procedures for removing ballistocardiogram artifacts from EEG data acquired in the MRI scanner. NeuroImage 24(1):50–60. S1053811904005683. https://doi.org/10.1016/j.neuroimage.2004.09.041

Sun L, Rieger J, Hinrichs H (2009) Maximum noise fraction (MNF) transformation to remove ballistocardiographic artifacts in EEG signals recorded during fMRI scanning. NeuroImage 46(1):144–153. S1053811909000937. https://doi.org/10.1016/j.neuroimage.2009.01.059

Thornton R et al (2011) Epileptic networks in focal cortical dysplasia revealed using electroencephalography-functional magnetic resonance imaging. NeuroImage 70(5):822–837

Valdes-Sosa PA, Sanchez-Bornot JM, Sotero RC, Iturria-Medina Y, Aleman-Gomez Y, Bosch-Bayard J, Carbonell F, Ozaki T (2009) Model driven EEG/fMRI fusion of brain oscillations. Hum Brain Mapp 30(9):2701–2721. https://doi.org/10.1002/hbm.20704

Wagner M, Fuchs M, Kastner J (2000) fMRI-constrained dipole fits and current density reconstructions. In: 2th Intl Conf Biomag, pp 785–788

Webb JT et al (2013) BOLD granger causality reflects vascular anatomy. PLoS One 8(12):1–19

Wojcikiewicz W, Vidaurre C, Kawanabe W (2011) Stationary common spatial patterns: towards robust classification of non-stationary EEG signals. In: IEEE International Conference on Acoustics, Speech and Signal Processing (ICASSP)

Wu G-R et al (2013) A blind deconvolution approach to recover effective connectivity brain networks from resting state fMRI data. Med Image Anal 17:365–374

Xie J, Douglas PK, Wu Y, Anderson A (2016) Decoding the encoding of functional brain networks: an fMRI classification comparison of non-negative matrix factorization (NMF), independent component analysis (ICA), and sparse coding algorithms. Int J Imaging Syst Technol 21:223–231

Zhou G, Cichocki A (2012) Fast and unique Tucker decompositions via multiway blind source separation. Bull Pol Acad Sci Tech Sci 60:389–405. https://doi.org/10.2478/v10175-012-0051-4

Zou Y et al (2012) Automatic EEG artifact removal based on ICA and hierarchical clustering. In: IEEE ICASSP, pp 649–652

Integrating EEG–fMRI Through Brain Simulation

30

Michael Schirner and Petra Ritter

30.1 Introduction

Several approaches for multimodal information fusion have been proposed and categorized (see Valdes-Sosa et al. 2009; Rosa et al. 2010; Huster et al. 2012; Jorge et al. 2014 for reviews). Brain simulation can be called, as the name suggests, a *model-based* integration approach. Model-based approaches rely on increasingly realistic, biophysically oriented, neuronal models. In contrast, *data-driven* approaches rely on signal processing, thereby avoiding the need for computationally expensive simulation of neuronal and neurovascular coupling dynamics. Model-based approaches are typically recognized as *symmetrical*, meaning that the underlying assumption is that EEG and fMRI measure distinct, only partially overlapping aspects of neuronal activity. *Asymmetrical* approaches, on the other hand, use information from one modality to guide the analysis of the other, for example, fMRI-informed EEG analysis and EEG-informed fMRI analysis. For example, fMRI was used to guide EEG source imaging by using statistical maps of the fMRI result to confine the putative source space (Dale et al. 2000; Ou et al. 2010). The basic idea underlying such methods is to use fMRI to estimate the location of a neural event, while EEG is used to retrieve the time course of that event.

M. Schirner · P. Ritter (✉)
Berlin Institute of Health at Charité—Universitätsmedizin Berlin, Charitéplatz, Berlin, Germany

Department of Neurology with Experimental Neurology, Charité—Universitätsmedizin Berlin, Corporate member of Freie Universität Berlin and Humboldt Universität zu Berlin, Charitéplatz, Berlin, Germany

Bernstein Focus State Dependencies of Learning and Bernstein Center for Computational Neuroscience, Berlin, Germany

Einstein Center for Neuroscience Berlin, Charitéplatz, Berlin, Germany

Einstein Center Digital Future, Wilhelmstraße, Berlin, Germany
e-mail: michael.schirner@bih-charite.de; petra.ritter@charite.de

C. Mulert, L. Lemieux (eds.), *EEG - fMRI*,
https://doi.org/10.1007/978-3-031-07121-8_30

The opposite direction is also possible—using EEG to inform fMRI analyses. For example, BOLD responses were predicted by convolving EEG measures—like the amplitude of an ERP component or the power of a frequency band—with a hemodynamic response function, yielding so-called EEG regressors (e.g., Debener et al. 2006). Asymmetrical approaches are often criticized for relying on the assumption that the fMRI signal at a certain location contains information about electric activity at that location. Or, vice versa, that the neural generators of scalp potentials generate a hemodynamic response that can be detected in the fMRI signal. While there is clearly a biological motivation for these assumptions, one can also easily construct scenarios where they might not hold true, for example, by considering regions that do not contribute to scalp EEG due to their geometry and orientation; or neural processes that come at no additional metabolic cost, which might be the case when the mean firing rate of the population does not change, but still important computations are performed by means of other neural codes. Summarizing, multimodal data fusion is a considerable challenge that has been the source of much debate, but also of promising avenues to better understand brain function than with each method alone. Clearly, the spatiotemporal co-occurrence of, say, a statistically significant activation in fMRI, and an EEG ERP after stimulus presentation, is not sufficient for concluding that they both are different manifestations of the same neural event. Or, more generally, correlations in EEG and fMRI data that occur time locked at the same location are not necessarily caused by the same neural event. We simply do not know enough about the underlying neurophysiological processes to arrive at far-reaching conclusions from the mere observation of correlated signal patterns.

Brain simulation-based approaches for the integration of multimodal data are based on a *generative* computational model of the underlying physiological activity that is thought to give rise to observed signals in the measured modalities. In the case of EEG–fMRI, such brain models can be divided into two parts. The first part simulates the activity and interaction of neurons or neural populations, like the fluctuation of firing rates, neurotransmitter concentrations, or postsynaptic potentials. The second part provides a mapping between neural activity (e.g., fluctuating postsynaptic potentials) and the representation of this activity as a signal in a given modality (e.g., fluctuating voltage in an EEG channel). Here, we call this second part of the model *forward model* to designate its direction *from source to data*, in contrast to *inverse models*, which seek a mapping *from data to source* (note that often the entirety of the two parts is called "forward model"). For model-based EEG–fMRI integration we need two forward models, one for EEG, to describe the propagation of electrical activity from neural sources to EEG sensors, and one for fMRI, to describe the coupling between neural activity, changes in cerebral blood flow and blood oxygenation. As generative models specify a forward relationship, from model to data, multimodal data integration often seeks *model inversion*, that is, finding a model that adequately explains the multimodal dataset, which for an existing model corresponds to finding parameter distributions that lead to optimal predictions of the data. In practice, model inversion is rendered difficult due to the complexity of realistic neuronal-metabolic-hemodynamic cascades (Rosa et al.

2010). Clearly, the performance of brain simulation-based approaches depends not only on assumptions about the neuronal model, but also about the mapping between the simulated neural state variables and measured electrophysiological or hemodynamic signals, which is far from being established (e.g., neurovascular coupling; Logothetis et al. 2001; Raichle and Mintun 2006).

In this chapter we discuss EEG–fMRI integration work that is based on the simulation of the evolution of neuronal states in the entire brain, or at least the entire neocortex. That is, we consider it a brain simulation if there exists an anatomical interpretation, or one-to-one mapping, between the nodes of a brain network model and a regional brain parcellation that covers large parts of the brain. Furthermore, we require the state variables of the model to have a biophysical interpretation (like firing rates, electric potentials, neurotransmitter concentrations) and that the state variables are part of a dynamical system, that is, coupled differential equations, that model their biophysical interaction. Importantly, with BNMs we require the system to explicitly simulate the coupling and interaction between different neural state variables, like the effects that excitatory and inhibitory current flows, or the average rate of spikes emitted by a population of neurons, have on other populations. This approach is motivated by the idea to use such models to learn something about unobservable (hidden) neural activity and information processing that underlies observable signals. Because full-brain simulation on a microscopic scale is infeasible for practical simulations (meaning: it is possible (Izhikevich and Edelman 2008), but impractical as it consumes many resources and is weakly constrained by empirical data), it involves abstracting from detailed simulations of neurons on a microscopic (e.g., multicompartment neuron) level, or from a mesoscopic scale (local connectivity), to a macroscopic scale, in which the average ensemble activity is simulated on the basis of a *mean-field theory*, the basic idea of which is that individual neuron models can be lumped together and represented by an approximation of their mean activity.

30.2 Brain Network Models

Brain network models rest on the basic assumption that for understanding brain activity, it is crucial to take the dynamic interaction of neurons, or neural populations, along their anatomical connectivity into account (Fig. 30.1). To generate a mathematical model, this involves the application of dynamical systems theory in order to describe coupled neural activity using coupled differential equations (see Breakspear 2017 for a current review). For example, a system of first-order ordinary differential equations has the form

$$\frac{\mathrm{d}x}{\mathrm{d}t} = f\left(x\right)$$

where $x(t) \in \mathrm{R}^{\mathrm{d}}$ is a vector of dependent variables, $f: \mathrm{R}^{\mathrm{d}} \rightarrow \mathrm{R}^{\mathrm{d}}$ is a vector field, and $\mathrm{d}x/\mathrm{d}t$ is the time derivative, which we may regard as describing the evolution of the d-dimensional state variable $x(t)$.

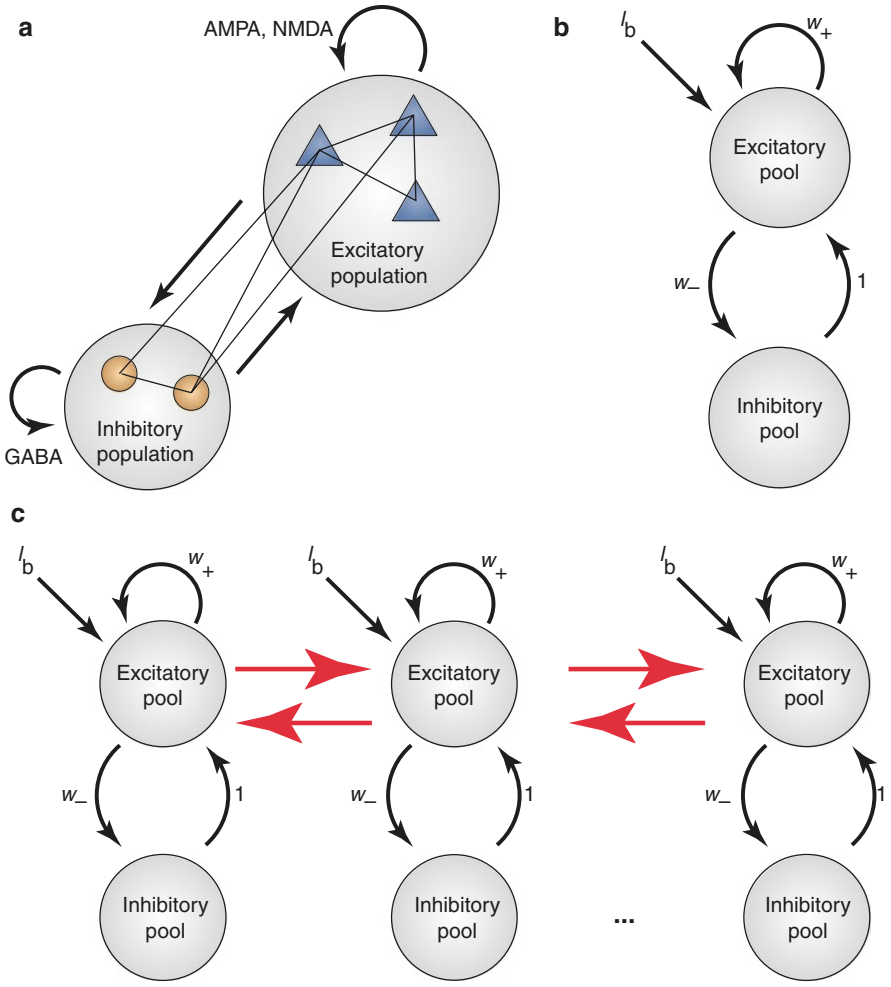

Fig. 30.1 From spiking networks to neural mass models to brain network models. (**a**) Brain network model construction starts by considering networks of spiking neurons that interact via recurrent and feedforward excitatory (AMPA, NMDA) and inhibitory (GABA) connections. (**b**) Neurons can be organized into populations defined by shared characteristics like similar inputs, outputs, and connectivity. To form neural mass models, average population dynamics, like the evolution of the population's mean membrane potential or mean firing rate, are described by simplified models that only capture the main modes of these dynamics, while ignoring the details of individual neuron dynamics. (**c**) Brain network models are constructed by coupling several neural mass models to form a global network (red arrows) of local networks (black arrows). The global network is structured by structural connectivity that specifies the coupling of large-scale brain areas by white-matter fiber bundles; for human BNMs, it is often obtained by diffusion-weighted MRI tractography. (Adapted with permission from Deco et al. 2011)

The underlying idea is to use such a mathematical system of interacting (coupled) differential equations in order to express the temporal dynamics and interaction of interesting quantities of the physical system (state variables). In the brain, quantities of interest are usually the dynamics of physiological processes or entities like membrane potentials, firing rates, sequences of spike times, or synaptic currents. The goal of such modeling approaches is often to express the way these quantities are connected in the real system in terms of physical laws. However, attempts to fully reduce neural activity to more fundamental physical laws within a single model would lead to impractical complexity of the model and might miss the level of emergence at which the relevant explanatory mechanisms actually take place. Therefore, one often seeks a parsimonious model that accomplishes a desired level of explanation or prediction with as few predictor variables as possible.

In order to determine the future state of the system at time t, the system needs to be solved analytically or numerically. Solving the system leads to a *trajectory* or *orbit* in the *phase space* of the system that starts from the used *initial conditions*. The phase space can be interpreted as a geometric equivalent of the algebraic form of the system, as its differential equations describe a *flow* in this space, that is, the temporal change of the system for each possible point in its phase space. Nonlinear evolution equations are, except for rare special cases, not explicitly solvable, and even apparently simple equations can produce complicated behavior such as chaos, which is why the focus is often set on understanding the qualitative behavior of the solutions. Trajectories in the phase space often converge toward so-called attractors, which include *fixed-points* (the system's state does not change at this point) or *limit cycles* (a closed trajectory). For example, the regular, periodic spiking of a single neuron, or the oscillation of brain rhythms, like the alpha rhythm (8–12 Hz), can be described by limit cycle attractors.

Often, terms of the ordinary differential equations that make up the model are replaced by stochastic processes, which corresponds to adding small random perturbations to the orbits at each time step. Noise lends interesting properties to such *stochastic differential equations,* like the ability to spontaneously switch between different attractors (e.g., see the study by Freyer et al. 2011, discussed below), which may be identified as a principle underlying neuronal computation. Representing parts of the system by stochastic processes can be used to simplify the model. With these *neural ensembl*e approaches, we assume that for a description of the collective behavior of a large number of neurons, the state of individual neurons is irrelevant, and, furthermore, that the evolution of neuronal states is uncorrelated. Using the central limit theorem, this allows us to express the state of a large number of neurons by a Gaussian probability distribution, regardless of the individual distributions of states. Hence, the uncorrelated spiking of a large number of neurons can be reduced to the mean and variance of the average population firing rate, which reflects the response of a population to its total synaptic input. The dynamics of our assumed ensemble can then be described by a so-called Fokker–Planck equation that can be analytically derived from dynamic neuron models and captures the ensemble's *drift* of the mean and its *diffusion*—its change in variance. In summary, such diffusion approximation provides a parsimonious way to reduce the enormous

degrees of freedom of direct simulation, by capturing mean and variance of ensemble activity, based on the assumption that the statistics of local ensembles are Gaussian and uncorrelated. Assuming strong coherence between neurons, we can further drop the diffusion of the variance term from the model and describe collective neural behavior by its mean only. The resulting models are called *neural mass models* (NMMs), and they build the basis for many brain simulation endeavors (Breakspear 2017; Deco et al. 2011, 2008). Problematically, converging evidence from neuronal recordings suggests that neural population activity is heavy-tailed (the tail corresponding to bursts of activity) and not Gaussian (Roberts et al. 2015), and that synaptic currents have nonzero time-lagged autocorrelation (Haider et al. 2016; Okun et al. 2010). The accommodation of non-Gaussian distributions with FPEs is an active area of research that can be expected to further drive development of improved ensemble models.

NMMs are used to simulate the mean activity of local groups of neurons that show coherent behavior, such as pyramidal neurons or inhibitory interneurons. That is, with NMMs, cortical areas are understood as ensembles of strongly interacting excitatory and inhibitory neurons that are clustered into the respective subpopulations. Examples of popular neural mass models are the model developed by Jansen and Rit (1995) and the model developed by Wong and Wang (2006). The evolution of population dynamics is then often decomposed into two parts. One part simulates the steady-state response of a neural population to an input in terms of average postsynaptic membrane potential or firing rates. A second part then transforms the model state into an output, like an ongoing firing rate, which is often assumed to be instantaneous and following a sigmoid function. While biological neurons interact via many individual synapses, in the neural ensemble approach synaptic interaction is, similarly to population activity, understood as the combined effect of many individual synaptic connections. To bridge the scale from a small patch of cortex to the entire brain, ensembles of NMMs are coupled to form mesoscopic circuits (e.g., cortical columns), or macroscopic large-scale brain networks, or both. One node of a large-scale brain network is often formed by one excitatory NMM and one inhibitory NMM that are mutually and recurrently coupled. In addition, these nodes are then globally coupled to form *brain network models* consisting of one global network that connects several local excitatory/inhibitory networks. In contrast to NMMs, which treat the cortex as a discrete network of nodes coupled by the connectome, *neural field models* treat the cortex as a continuous sheet, which additionally involves modeling the change of neural activity along space.

Problematically, even small network models involve a large number of free parameters to specify their *long-range connectivity*, that is, the mutual coupling strengths between each pair of nodes. As direct measurements of the so-called *effective connectivity*, the causal influence between ensembles, is scarce for humans, these parameters are often informed by either generic considerations about the potential distribution of such connections, or estimations that are based on analyses of diffusion-weighted magnetic resonance (dwMRI) imaging data. dwMRI *tractography* is a model-based technique to reconstruct the trajectories of

white-matter long-range axon bundles connecting brain regions, which is called *structural connectivity*. Metrics like the relative volume or the relative diameter of such structural connections are then used as a proxy for *effective connectivity*. While tractography is widely used, one can show that tractography-based connectivity strength estimation gives higher weights to short and straight connections, while underestimating the impact of long-range and especially interhemispheric connections (Maier-Hein et al. 2017). Apart from that, other problems are associated with this technique; for example, it does not allow determining the direction of the reconstructed axon bundles and the relative proportion of excitatory and inhibitory neurons that are targeted by long-range axons. As a remedy, structural connectivity obtained from dwMRI is often further constrained by aggregated results from invasive animal tract tracing studies, like the CoCoMac database (Stephan et al. 2001) for monkey data or the Allen Mouse Brain Connectivity Atlas (Oh et al. 2014) for rodents. Having constrained connectivity with relative weights obtained from tractography, these relative weights are normalized by a free parameter that is often obtained by fitting the model to empirical data. Likewise, a second conduction velocity parameter is often used to compute conduction delays from connection lengths.

Applying BNMs to the analysis of brain data is an active area of research that yielded important insights into the neurophysiological mechanisms underlying healthy and pathological brain signals (Bansal et al. 2018; Breakspear 2017). The basic brain simulation approach is didactically illustrated in Bojak et al. (2011) and Ritter et al. (2013). Open source, freely available software packages like the Python neuroinformatics platform the Virtual Brain (Sanz-Leon et al. 2013) and the MATLAB/C++ software package NFTsim (Sanz-Leon et al. 2018) enable simulation, post-processing, and analysis of BNMs. (Semi-)automatic preprocessing pipelines allow convenient construction of individualized BNMs on the basis of multimodal data like dwMRI, structural MRI, fMRI, MEG, and EEG (Proix et al. 2016; Schirner et al. 2015). Given empirical multimodal data, a brain network model, and EEG/fMRI forward models, underlying neural activity is then estimated by so-called inverse modeling, which means that the parameters of the involved models are optimized until a good fit between simulated and empirical activity is found (Triebkorn et al. 2018). Straightforwardly, this can be realized by brute-force simulation, that is, testing parameter combinations and estimating the fit. While model inversion is an appealing concept, its application involves considerable difficulties in practice, because the inverse problem is *ill-posed* for complex models like brain models, which involve cascades of dynamical systems with large numbers of free parameters. First, there may be no unique solution, as can be seen from the underdetermination of the source reconstruction problem, which involves a large number of unknowns (current sources), but only a small number of observations (EEG channels). Second, the solution may be unstable with respect to small perturbations in the data, which can be expected from the convoluted and highly nonstationary nature of brain dynamics. This means, in practice, we often have heuristic approaches as our only option for full-brain simulation.

Despite the involved challenges, brain simulation found broad success in modeling epilepsy (Proix et al. 2018; Taylor et al. 2013), Alzheimer's (Stefanovski et al. 2018; Zimmermann et al. 2018), brain tumor patients (Aerts et al. 2018), stroke (Adhikari et al. 2015; Falcon et al. 2016), structural disconnection (Cabral et al. 2012), lesions (Alstott et al. 2009), and plasticity effects (Roy et al. 2014), to cite some examples. Examples of brain simulation to model evoked potentials, resting-state activity, and the alpha rhythm in the context of EEG–fMRI integration are discussed in more detail below.

30.3 EEG and fMRI Forward Models

EEG-forward models simulate the propagation of electromagnetic waves from sources to EEG sensors (Hallez et al. 2007). To estimate electromagnetic propagation, usually a multicompartment volume conductor head model is constructed using tessellations of cortical, skull, and scalp surfaces from structural MRI data; T1-weighted MRI protocols provide adequate contrast to differentiate between the involved tissue types. After specifying a forward model on the basis of a realistic model of head geometry and the spatial arrangement of neural populations, an aggregated mapping can be computed that provides a linear transformation from source to sensor space called *lead field*. Source activity is assumed to be well approximated by the fluctuation of equivalent current dipoles generated by excitatory neurons located in the cortical sheet, which in turn is assumed to be proportional to membrane potential or input current fluctuation. For further simplification, one often constrains the dipolar orientation of electric sources at each location to be normal to the cortical surface, reasoning that pyramidal neurons in cortex are mainly organized in columns that are roughly perpendicular to the cortical surface, which consequently represents source activity as a dipole layer parallel to the cortical surface. Inhibitory neurons are sparse (~15%), and their dendrites fan out spherically; hence, their contributions to the EEG signal are thought to be negligible. As the main contributor to the EEG signal, the ensemble of postsynaptic potentials of a neural population at a given location is then used as input to the lead field mapping.

BOLD–fMRI forward models simulate neurovascular coupling, that is, the relationship between neural activity and associated changes in cerebral blood flow, blood volume, and deoxyhemoglobin content. The mechanistic details of this relationship remain unclear (Iadecola 2017). Empirical data related to neurovascular coupling come from invasive animal studies that combine metabolic/vascular measurements (e.g., using fMRI or optical imaging) with multiunit recordings; such studies revealed significant correlations between hemodynamic and electrophysiological signals, identifying input or sub-threshold synaptic activity, rather than output spiking or energy demand, as the primary driver for the local vascular response (see Rosa et al. 2010 for an overview and discussion). Neurovascular coupling is

conceptualized by the idea of a "neurovascular unit": a tightly interacting compound of neurons, astrocytes, and several other cells and also chemicals, that detect and respond to the needs of neuronal supply (see Iadecola (2017) for a recent and comprehensive review). This conceptual understanding is currently undergoing a shift from a unidimensional process, that only involves neuronal-astrocytic signaling, to a multidimensional one in which chemical signals engage in multiple pathways and effector systems in a highly orchestrated manner. The basic principle underlying neurovascular coupling in this model is that increasing neuronal activity uses increasing amounts of energy, in the form of oxygen and glucose, and that cerebral blood flow varies in proportion to the amount of utilized energy in a given brain region. These considerations indicate a feedback model, where already existing metabolic needs increase blood flow post hoc. Measurements, however, show that the increase in CBF is larger than the need for oxygen, resulting in excess delivery of O_2 (Raichle and Mintun 2006), and that increases in CBF even occur under conditions of excess oxygen and glucose (Attwell and Iadecola 2002). In light of this evidence, a *feedforward* model was proposed, which suggests that CBF delivery is regulated by signaling pathways that are initiated by the activation of postsynaptic glutamate receptors that drive the release of vasoactive by-products like K^+, nitric oxide, and prostanoids. Both views may be reconciled by a model that proposes that an initial (potentially) exaggerated feedforward flow response to neural activity is accompanied by a secondary feedback component, driven by reduced tissue O_2, to adjust CBF to better match the actual metabolic needs of the tissue (Iadecola 2017). Another far-reaching assumption underlying functional brain imaging is that the spatiotemporal correspondence between neural activity and hemodynamic response is sufficiently precise. However, in some regions, CBF exceeds the area of activation (e.g., auditory, visual, and cerebellar cortices), which is likely due to nonoverlapping neural and vascular topologies and retrograde vasodilation (see Iadecola 2017 for an overview of related studies), and therefore, such effects become increasingly relevant as fMRI resolution increases. Mirroring our lack of understanding of the exact nature of neurovascular coupling, different studies often use different forward models; different inputs to BOLD forward models, typically involving state variables as diverse as the number of incoming spikes to a neuronal population, the postsynaptic membrane potential or the synaptic gating amplitude; and different considerations regarding the exclusive inclusion of input signals in contrast to using a combination of input and output signals—output is often not taken into account following empirical observations (Logothetis et al. 2001).

A straightforward approach to simulate local BOLD signals often used in literature is based on the (linear) convolution of cortical current density with a kernel function that approximates the canonical shape of a hemodynamic response: a brief, time-delayed, and intense positive signal change that peaks approximately after 4–6 s, followed by an undershoot that peaks after 6–10 s, and slow recovery to baseline. More elaborate approaches, like the Balloon-Windkessel model (Buxton et al. 1998; Friston et al. 2000), explicitly simulate the relationship between blood flow

and measured BOLD signal using a dynamical system description that couples blood flow and blood volume dynamics and relates them to BOLD contrast:

$$
\begin{aligned}
\dot{s}_i &= z_i - \kappa_i s_i - \gamma_i \left(f_i - 1 \right) \\
\dot{f}_i &= s_i \\
\tau_i \dot{v}_i &= f_i - v_i^{1/\alpha} \\
\tau_i \dot{q}_i &= \frac{f_i}{\rho} \left[1 - \left(1 - \rho \right)^{1/f_i} \right] - q_i v_i^{1/\alpha - 1} \\
B_i &= V_0 \left[k_1 \left(1 - q_i \right) + k_2 \left(1 - q_i / v_i \right) + k_3 \left(1 - v_i \right) \right] \\
k_1 &= 7 \rho_i \\
k_2 &= 2 \\
k_3 &= 2 \rho_i - 0.2
\end{aligned}
$$

This part of the metabolic–hemodynamic cascade is based on the long-lasting idea that an increase in neuronal activity z_i causes an increase in a vasodilatory signal s_i, which increases inflow of blood f_i and concomitant changes in blood volume v_i and, accompanied by that, changes in deoxyhemoglobin content q_i and ultimately the BOLD signal B_i. A list of parameters is provided in Table 30.1. A consequence of this forward model is that its parameters can be varied without affecting the temporal dynamics of electric scalp potentials, which means that the fusion of fMRI with EEG for model inversion cannot inform parameters better than fMRI alone. The reverse is, however, not true: changing the parameters of the neural mass model will affect EEG and fMRI predictions. Sotero and Trujillo-Barreto (2008) propose a variation of the model from Friston et al. (2000) that postulates, in addition to the direct effect that excitatory activity has on CBF (and consequently CBV), a second effect, namely, that excitatory, as well as inhibitory, neuronal activity modulate glucose and oxygen consumption, which is supposed to have further (in addition to the glutamate–CBF cascade) downstream effects on CBV. The authors note in their article that this model has the interesting property to reconcile observations on the effect of insulin: while BOLD responses were significantly lower, insulin had no effect on visual evoked potentials (Seaquist et al. 2007), which could be explained

Table 30.1 Balloon-Windkessel model parameters

Parameter	Physiological interpretation
ρ	Resting oxygen extraction fraction
V_0	Baseline blood volume
k_1	Weight for deoxyhemoglobin change
k_2	Weight for the relative change of deoxyhemoglobin to volume
k_3	Weight for blood volume change
τ_i	Balloon transit time
γ_i	Rate of flow-dependent elimination
κ_i	Rate of signal decay

by considering an effect of insulin on glucose and CBF-related parameters, which can, under this model, be achieved without affecting the EEG signal (Sotero and Trujillo-Barreto 2008).

It should be stressed, again, that many aspects of the coupling between neurophysiology and EEG, respectively fMRI, are not yet fully understood, and forward models are based on simplifying assumptions, for example, regarding equivalent current dipoles, the exact nature of neurovascular coupling or the dependence of the hemodynamic response on brain state and anatomical location. Improving forward models is an active area of research. For example, recent approaches aim to retrieve the onset and shape of hemodynamic responses by fitting models to voxel-wise fMRI time series and then use shape parameters as pathophysiological indicator (Wu and Marinazzo 2016). To summarize, the combination of BNMs with forward models attempt to provide mechanistic interpretations of large-scale neural dynamics over a wide range of temporal scales and for different modalities on the basis of neural dynamics models that can be derived from simplifying spiking-network models. In the following we review some work that applied brain simulation to analyze EEG–fMRI data.

30.4 Evoked Potentials

Sotero and Trujillo-Barreto (2008) were among the first to perform full-brain simulations for integrating EEG–fMRI and also positron emission tomography. Their model is based on an extension of the neural mass model developed by Jansen and Rit (1995) and Zetterberg et al. (1978), which includes recurrent excitatory connections, to better simulate pyramidal-to-pyramidal connections within a cortical column. The NMM was coupled with a metabolic–hemodynamic forward model that relates excitatory/inhibitory neuronal activity with glucose consumption, subsequent oxygen consumption, and cerebral blood flow (CBF); output is fed into a Balloon model (Buxton et al. 2004, 1998) to simulate a BOLD signal. In addition, a lead field matrix was used to project the average membrane potentials of pyramidal cells into EEG channel space. This *local* model, intended to characterize the dynamics in one cortical voxel, was then coupled with other local models, belonging to the same cortical area, via excitatory and inhibitory short-range connections, in order to simulate one cortical region. Short-range connectivity was modeled by exponential functions that reduce coupling weight with coupling distance. Thalamus was simulated by two populations, one to model excitatory thalamocortical relay neurons and one to model thalamic inhibitory reticular neurons. Furthermore, excitatory long-range connectivity, constrained by dwMRI tractography results, was implemented to *globally* connect regions to form a large-scale brain network. In total, the model consisted of 12 random differential equations (RDE) for the thalamus and a system of 16 RDE for each simulated cortical voxel. Sotero and Trujillo-Barreto (2008) compared their model with empirical activity in several ways. First, they showed that their model had reproduced realistic visual evoked potentials (VEP) in O1 and O2 electrodes and corresponding BOLD signal changes. Visual stimulation was

simulated by adding a brief transient on top of the Gaussian random input to drive thalamocortical excitatory relay neurons in ten VEP-related regions. Interestingly, the authors observed that the excitation–inhibition ratio of a local population has a modulating effect on the initial dip, the peak of the BOLD signal, and its undershoot. This is important as it indicates that the shape of the hemodynamic response can be determined by factors that are independent of metabolic–hemodynamic coupling, but can be explained by neuronal activity alone, and should therefore be considered in studies that aim to infer the shape of local hemodynamic response, in addition to purported changes of glucose and CBF-related parameter in the current models. In addition to VEPs, Sotero and Trujillo-Barreto (2008) reproduced resting-state alpha activity with the model, which is further described below.

30.5 Resting-State

Resting-state is characterized by the absence of a task. In fMRI, resting-state typically goes along with strong, coherent fluctuations of BOLD in a frequency range below 0.1 Hz. When brain activity at different locations shows correlated activity, the regions are said to form *resting-state networks* (RSNs), with the *default mode network* as, arguably, the most prominent example (Raichle et al. 2001). The brain regions partaking in a given network are said to entertain *functional connectivity*, which involves coherent activity in wide-spread cortical and subcortical areas covering the entire brain. When it comes to electric activity, like EEG, resting-state networks are often linked with a specific composition of oscillatory band powers, most prominently, the alpha rhythm. For example, the default-mode network is characterized by increased alpha and beta activity, while prefrontal networks can be associated with high gamma (~30 to 80 Hz) power (Mantini et al. 2007). Importantly, RSNs strongly overlap with sensory–motor, visual, auditory, attention, language, and default networks that appear during active behavioral tasks; atypical resting state activity was linked with atypical brain function (e.g., Rombouts et al. 2005; Seeley et al. 2009).

To better understand the functional role of resting-state activity, it would be helpful to characterize the underlying neurophysiological processes. It therefore may come as a surprise that even after almost a century since its discovery, and a considerable amount of findings on its behavioral correlates, the origin of alpha rhythms is still incompletely understood. Different hypotheses have been proposed that typically fall into two categories: (1) rhythms are endogenously produced by thalamic or cortical "pacemaker" cells, that function like clocks that entrain other cells; and (2) rhythms arise as an emergent property from the interaction of networks of cells, where not a single neuron or population is responsible for the rhythm; for example, by means of limit cycle attractors in the networks state space, or through filtering properties of the network that filter white noise network input (Buzsaki 2006).

The works of Robinson et al. (2002), Honey et al. (2007), Ghosh et al. (2008), Deco et al. (2009), Valdes-Sosa et al. (2009), and Freyer et al. (2011) are examples of the pioneering application of BNMs to study the network mechanisms that give

rise to the emergence of resting-state-like activity in fMRI, electric activity, or both (see Deco et al. 2011 for a review). The general takeaway from such studies is that coupling parameters that replicate realistic conductance enable neural masses to spontaneously engage into complex activity patterns, characteristic of neural time series, which includes intermittency, phase synchrony, multistability, and spontaneous switching between synchronized cell assembly formation and desynchronizing bursts. The notion of multistability refers to a property of many dynamical systems to have multiple stable attractors in its phase space that are surrounded by basins of attraction and separated by unstable equilibria, which, in neural models, often separate a high-activity from a low-activity state. BNM dynamics suggest a resting-state mechanism where noise or bifurcation enables the system to switch between multiple stable states that are spawned by the basins of attraction of fixed point or limit-cycle attractors. In such a multistable phase space, the state of the system can show different kinds of behavior, like steady-state equilibrium or chaotic oscillations, depending on the initial state and the geometry of the phase space. States can switch between different attractors driven by perturbations that move the state over the boundaries of different basins of attraction. That is, noise or stimuli enable the exploration of the state space in the vicinity of multiple stable equilibria, which offers a geometric explanation for seemingly chaotic time series behavior. In addition to the intrinsic dynamics of NMMs, structural coupling may give rise to the oscillatory entrainment of the populations' state variables, which can lead to the emergence of coherent oscillations over a wide range of frequencies, from <0.1 Hz up to 100 Hz, that in turn shape functional network topology. The aforementioned modeling studies show that, with BNMs, realistic functional connectivity in the slow band of resting-state activity can be easily produced on the basis of coupled oscillating population models. Importantly, it was shown that the electric population activity, which serves as input for the BOLD and EEG forward models, likewise resembles empirical data. For example, Valdes-Sosa et al. (2009) simulated a 16,138-regions large-scale model for a full-cortex and thalamus parcellation to produce resting-state EEG–fMRI. Nodes were simulated by the classical Jansen and Rit neural mass model (Jansen and Rit 1995) and coupled by structural connectivity estimates computed by dwMRI tractography. Gaussian white noise with mean 20 and variance 2 pulses/s was used to drive excitatory relay populations of the posterior right thalamus. Changing levels of thalamic stimulation were simulated by increasing the input to a mean of 100 pulses/s for a duration of 2 s. In addition to fMRI time series, ongoing alpha band power fluctuation of simulated local field potentials was computed and convolved with a hemodynamic response function to yield an alpha-regressor for BOLD, that is, a prediction of BOLD based on alpha-band power fluctuation, which is a common technique in empirical EEG–fMRI. For each node of the network, its alpha-regressor was correlated with its fMRI prediction, which was also done in initial EEG–fMRI analytic studies (Goldman et al. 2002; Laufs et al. 2003a, b; Moosmann et al. 2003). The resulting correlation coefficients were spatially mapped to cortex and thalamus surfaces and the resulting pattern was compared with the pattern obtained by performing the same analysis with empirical EEG–fMRI data. Strikingly, Valdes-Sosa and colleagues found the

same general pattern of electric–hemodynamic correlation—positive correlations in frontal cortices and thalamus and negative correlations in occipital regions—for simulated data as for their empirical data.

To fit BNMs to empirical data one often varies free parameters that, that is, represent global transmission speed, global scaling of connection weights, or the level of noise at each region. Such global parameters control the qualitative behavior of the system, that is, the geometry of its phase space, and determine the relative location and stability of equilibria and their attraction domains. Global parameter exploration elucidated that the optimal fit between empirical and simulated data is near the brink of a bifurcation, where the system's behavior undergoes a qualitative change (Ghosh et al. 2008). At the edge of such a critical instability, the spatial correlations of the noisy excursions are mainly shaped by SC, while the system retains maximal sensitivity to external stimulation and is able to efficiently and quickly respond even to weak inputs that push the system into a different state (Deco et al. 2013). In addition to global parameters, the specific topology of the models' structural connectivity, that is, the heterogeneous region-to-region coupling weights and time delays, have an effect on the specific network dynamics and the topology of emerging functional connectivity. Important in this regard is that empirical functional connectivity is not static, but network connections gain and loose functional connections in an ongoing manner, which is called functional connectivity dynamics (FCD) or "switching" between functional networks (Allen et al. 2014). Honey et al. (2007) showed with BNM simulations that in the electrical activity underlying simulated BOLD, network switching was reflected by alternating periods of elevated or decreased information flow (as measured by transfer entropy) on multiple time scales. At the slowest time scale (several minutes), functional coupling was relatively static and a good indicator of the presence of a structural link, while at intermediate time scales (~0.1 Hz), functional couplings fluctuated and gave rise to different functional networks. At the fast time scale of alpha oscillations (~10 Hz), this network switching was then linked to intermittent synchronization and desynchronization between brain regions. That is, resting-state fMRI oscillations and FCD were reflected by the time-varying fast synchronization and desynchronization of population dynamics, which emerged despite the absence of time-varying inputs or variation of connection strengths. Importantly, SC topology had a decisive effect on the emergence of FCD: corrupting SC topology by degree-preserving randomization considerably reduced the fluctuation of inter-regional information flow and consequently FCD. This simulation outcome thereby addresses important open questions regarding the relationships between resting-state activity on different time scales, because not only slow BOLD fluctuations but also fast electric rhythms, as well as their ongoing power modulation, can be explained by noise-driven multistable switching between different attractors.

The ongoing, seemingly chaotic, "waxing and waning" of the alpha rhythm power attracted the curiosity of researchers for many decades, but a biophysical explanation, that is, a theory based on the activity of neurons or neuronal populations, has not been established until recently. In contrast to earlier accounts that interpreted neural activity as chaotic, robust analysis of resting-state EEG suggests

that cortical activity operates in a multistable regime that can be described as jumping between a high-amplitude 10-Hz oscillation and low-amplitude filtered "noise." Hence, the histogram of empirical alpha's power fluctuations is not unimodal but composed of two distinct modes (Freyer et al. 2009). Here, again, dynamical systems theory gave rise to novel impulses for the interpretation of the alpha rhythm's "erratic" switching between different states. Using a corticothalamic neural field model with realistic parameters, Freyer et al. (2011) were able to reproduce the bimodal distribution of alpha rhythm power fluctuation with a strikingly close match. Specifically, variation of the excitatory corticothalamic coupling parameter controlled a subcritical Hopf bifurcation, that enables the coexistence of damped equilibrium behavior with unstable periodic oscillations over a range of physiologically plausible values. In the vicinity of this bifurcation, spontaneous switching between low- and high-amplitude activity was triggered by noise that drove the specific thalamic nucleus.

30.6 EEG–fMRI (Anti)Correlation

Depending on the settings of excitatory and inhibitory kinetic parameters and the strength of input currents, the Jansen–Rit neural mass model is able to produce 10-Hz oscillations that resemble cortical alpha rhythms. Underlying is a Hopf bifurcation that renders the system's stable equilibrium point unstable and gives rise to a stable limit cycle with a frequency close to 10 Hz, when input exceeds a certain threshold.

With other settings also oscillatory activity in delta, theta, beta, and gamma bands can be produced (Fig. 30.2). Sotero and Trujillo-Barreto (2008) simulated alpha activity, computed ongoing alpha band power fluctuation time courses, and

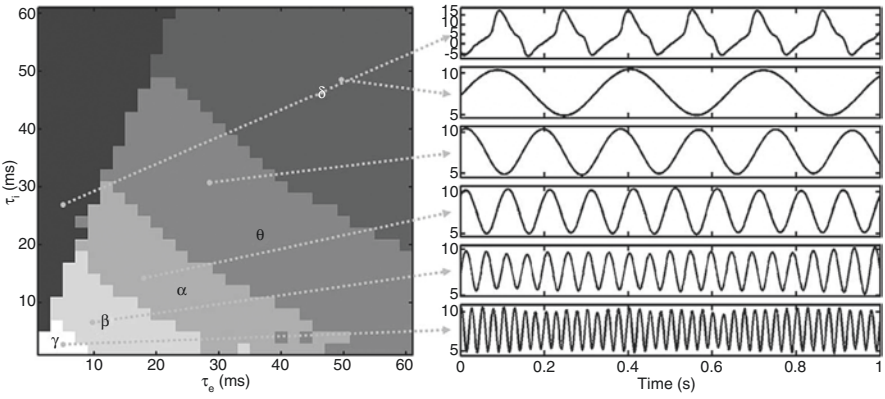

Fig. 30.2 Depending on its excitatory and inhibitory synaptic kinetics parameters τ_e, respectively τ_i, the Jansen–Rit model produces delta (1–4 Hz), theta (4–8 Hz), alpha (8–12 Hz), beta (12–30 Hz), or gamma (>30 Hz) oscillations (left). Examples of simulated signals are shown on the right-hand side. (Reproduced with permission from David and Friston 2003)

convolved them with a hemodynamic response function. In line with similar work, the resulting negative and positive correlation patterns were in agreement with experimental results (Goldman et al. 2002; Laufs et al. 2003a, b; Moosmann et al. 2003) in occipital, temporal, and frontal regions; interestingly, the simulation result additionally predicted positive EEG–fMRI correlations in several cortical areas that have not been found by earlier experimental work but were only discovered later (Gonçalves et al. 2006). Sotero and Trujillo-Barreto (2008) studied EEG–fMRI correlations for power-modulated alpha, by stimulating thalamus with 2-s pulse trains consisting of 10^4 action potentials per second and 20-s intervals between pulse trains. This time, positive BOLD–alpha correlations were found in the thalamus and the cuneus, whereas negative correlations have been obtained for all the other areas. Next, the authors studied alpha desynchronization by delivering an excitatory 2-s pulse of 10^6 action potentials to the thalamus to represent visual stimulation. The effect of this stimulation was a shift in the EEG power spectrum from alpha band toward higher frequencies, accompanied by an increase of CBF and BOLD amplitudes, which the authors interpret as consistent with the finding that eye-opening increases CBF in the visual cortex (Raichle et al. 2001). To summarize, stimulation with a lower frequency (10^4 AP/s) caused a mere shift of the alpha peak, while stimulation with a higher frequency (10^6 AP/s) lead to alpha desynchronization, indicating that increased neural activity is associated with decreased alpha power. The idea that neural activation causes a shift in the EEG spectrum toward higher frequencies accompanied by an increased BOLD amplitude is consistent with a hypothesis formulated by Kilner et al. (2005) that is based on a simple heuristic starting from dimensional analysis of electric and hemodynamic data. To test this hypothesis with explicit simulation, Sotero and Trujillo-Barreto (2008) increased input frequencies in steps from 10^5 to 10^6 AP/s and found an almost linear relationship between EEG spectral mass and the maximum BOLD amplitude. Finding that increased neural activity increased BOLD, but decreased alpha, the authors went on to study two scenarios for creating a dip in the BOLD signal. In their first experiment they delivered a 2-s pulse to thalamocortical excitatory relay neurons and doubled the value of the connection strength from these neurons onto cortical inhibitory neurons. As may be expected, high levels of inhibitory activity resulted from this coupling parameter change, while excitatory activity was consequently reduced, which caused a decrease in the BOLD signal. While a changing level of excitation versus inhibition surely is a candidate explanation for BOLD signal fluctuation, synaptic scaling by 100% over a short-time scale of a few seconds seems unlikely (Zenke et al. 2017). In their second experiment, thalamocortical excitatory relay cells were inhibited and cortical inhibitory interneurons were excited and the result was studied at the left and right occipital poles. As a result of this stimulation, inhibitory activity increased and excitatory activity decreased below baseline levels, accompanied by a decrease of BOLD amplitude. While these results are in agreement with experimental data, indicating that a substantial component of the negative BOLD response originates from decreased neuronal activity, it remains unclear what exactly causes this increase in inhibition relative to excitation (apart from implausible connection weight changes or selective stimulation) and how it is

related to the alpha rhythm. That is, how can the decrease of fMRI signals be reconciled with increased alpha rhythm power? Or more precisely: how would a large alpha rhythm inhibit cortical activity?

30.7 From EEG–fMRI to Neural Activity

The observation that increasing EEG alpha power is often spatially co-localized with decreasing fMRI amplitudes (Goldman et al. 2002; Laufs et al. 2003a, b; Moosmann et al. 2003) seems counterintuitive. Why should stronger or more synchronous fluctuation of input currents and postsynaptic potentials be less metabolically demanding? Adding to the puzzle are multiunit recordings in monkeys that show that not only alpha power *but also alpha phase* was negatively correlated with neural firing and task performance (Haegens et al. 2011). That is, firing of neurons was at its maximum despite input currents and membrane potentials in their vicinity were at their minimum. Of course, these findings are not entirely surprising when looked at from the "historical" perspective of alpha as an "idling rhythm" or from the perspective of more recent hypotheses termed "gating by inhibition" and "pulsed inhibition" (Jensen and Mazaheri 2010; Klimesch et al. 2007). These theories ascribe to alpha important functional roles related to information processing, attention, perceptual awareness, and cognitive performance, because all of these cognitive phenomena appear to be rhythmically modulated by it (Busch et al. 2009; Klimesch 1999; Mathewson et al. 2009).

Two findings seem to prevail: First, alpha power decreases or shifts to higher frequencies, during task performance in regions related to task–execution; second, stronger alpha decreases at the moment of task–execution correlate with better task performance. In other words, alpha desynchronization correlates with brain activation, while alpha synchronization correlates with inhibition of brain areas that are not relevant for the task at hand at that particular time (Jensen and Mazaheri 2010; Klimesch 1999). Regardless of its functional interpretation, the anticorrelation between neural firing and alpha, as well as the anticorrelation between BOLD and alpha, trigger the conclusion that alpha rhythms have the ability to decrease neural activity. The question is: how would this process be neurophysiologically implemented? To better understand the involved neurophysiological processes, Becker et al. (2015) used a BNM consisting of Stefanescu-Jirsa 3D NMM populations (Stefanescu and Jirsa 2008) to simulate neural firing, LFP and BOLD of cortex, reticular nucleus, and thalamus. Tuning global coupling strength yielded band-limited oscillations in the alpha range and its band-power time course showed alpha-typical fluctuations ("waxing-and-waning"). Comparisons showed that both, neural firing and fMRI had an inverse relationship with the alpha power time course, reproducing aforementioned empirical observations. Furthermore, and in line with invasive recordings (Haegens et al. 2011), firing was inversely related to alpha *phase*. Importantly, this result from Becker et al. (2015) shows that firing and fMRI are negatively correlated with alpha *even without any change of coupling strengths*, which was the proposed mechanism in Sotero and Trujillo-Barreto (2008).

Nevertheless, variation of network coupling strengths clearly shows an effect on alpha: the negative correlation between firing, fMRI, and alpha *vanished* for uncoupled neural masses, which indicates that the presumed inhibitory effect of alpha is brought about as a network effect by several connected populations. Also in line with the previously mentioned work, an increase of excitatory long-range coupling strengths led to decreased alpha power, accompanied by a shift of oscillatory power toward higher frequencies, which is compatible with the idea that neural activation is indexed by a loss of power in lower frequencies in favor of higher frequencies (Kilner et al. 2005).

In summary, the reviewed studies support the ideas that (1) the inverse relationship between alpha and firing may be *caused* by alpha; (2) alpha's inhibitory effect on neural activity depends on network interaction; and (3) a change of coupling strengths is not required to bring about the inhibitory effect. Firing inhibition without the necessity of changing connection strengths allows for a functional interpretation of alpha as a mechanism for temporally inhibiting or dynamically uncoupling regions from neural processing as formulated in "gating by inhibition" hypotheses. It is, however, still unclear how such an inhibitory effect can be brought about.

30.8 From EEG–fMRI to Neural Mechanisms

A possible explanation for the mutual (anti)correlations between neural firing, fMRI, and the alpha rhythm was recently proposed in a study that uses a novel form of brain simulation based on injecting BNMs with empirical EEG source activity to predict simultaneously measured fMRI (Schirner et al. 2018). The advantage of this "hybrid" modeling approach is that not only model structure but also model dynamics are constrained by empirical data.

Upon injecting the BNMs of 15 subjects with their resting-state EEG source activity, the hybrid model was able to predict each subject's individual whole-brain, large-scale fMRI time series (Fig. 30.3). By fitting BNMs to fMRI *time series*, that is, to *dynamical*, instead of static features of neural activity (like FC or power spectra), this approach allows the study of neural population dynamics, like firing rate or synaptic activity, that are usually hidden from direct observation. That is, because the forward modeling of BNM activity produced signals that closely correlate with the subjects' moment-to-moment EEG–fMRI activity, model activity may enable the study of the neurocomputational processes underlying the measured EEG–fMRI signals. The approach therefore provides a natural way for the integration of EEG–fMRI with the benefit of *providing an explanation of the observed EEG–fMRI dynamics in terms of neurophysiological activity*.

In contrast to "regular" BNMs, which are typically driven by noise, in hybrid models noise terms are replaced by EEG source activity. While this additional component corrupts the autonomy of the model—it is no longer an independent description of brain activity, but requires supply of empirical data—hybrid modeling has important advantages. Specifically, the approach maintains a low model complexity,

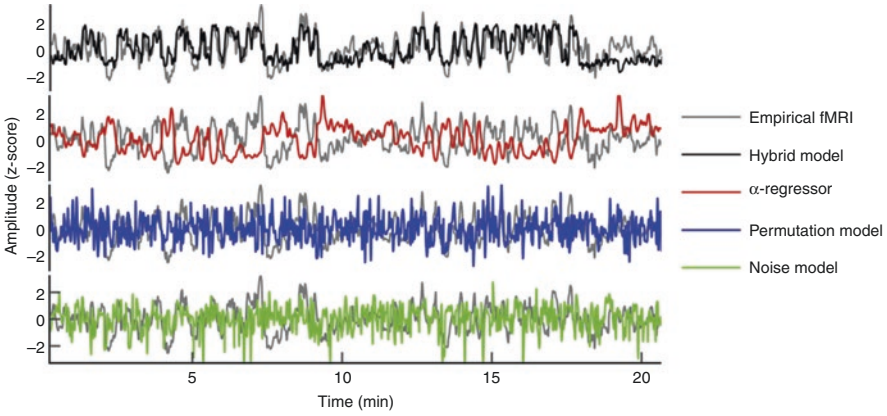

Fig. 30.3 Example time series of hybrid BNM simulation results. Upper trace: Hybrid BNMs predict resting-state fMRI time series on the basis of injected EEG source activity. The fMRI prediction is related to the anticorrelation of ongoing alpha power fluctuation of the injected EEG with fMRI (second trace from above), but hybrid model simulation yielded significantly better fits with observed fMRI than alpha-based regressors alone. Importantly, the intrinsic activity of fitted models, like firing rates or synaptic gating variables, may reveal neurodynamic processes that are hidden from direct observation with noninvasive techniques like EEG and fMRI. Models that are injected with randomly permuted activity (third trace from above) or regular, noise-driven BNMs (lowest trace) cannot recapture the specific ongoing dynamics of fMRI activity. (Reproduced from Schirner et al. 2018)

while enabling to simulate realistic dynamics with exceptional temporal detail. Injected currents are intended to serve as an approximation of those aspects of the brain that are not captured by the model, for example, due to the simplification inherent in mean field techniques. Thereby, the approach allows the systematic testing of neural theory as captured by BNMs in light of biologically plausible network activity. In the following we will review the findings obtained from the very first application of this novel approach.

Using resting-state EEG–fMRI data, the model predicted several independent empirical phenomena from different modalities and temporal scales (Fig. 30.4): (1) the spatial topologies and temporal dynamics of fMRI RSNs, (2) excitation–inhibition balance of synaptic input currents, (3) the inverse relationship between alpha-oscillation phase and spike-firing on short time scales, (4) the inverse relationship between alpha-band power and fMRI, respectively firing, on long time scales, (5) and fMRI power-law scaling. Importantly, subsequent analyses of the produced activity revealed neurophysiological mechanisms that could explain how brain networks produce all of these signal patterns and how they are interrelated in terms of neural population activity.

Upon finding that the hybrid BNMs predict subject-specific ongoing fMRI time series, Schirner et al. (2018) analyzed population activity and found that the ongoing alpha power fluctuation of the injected EEG was the main driver behind the emergence of the predicted fMRI oscillations. As may be expected from the work

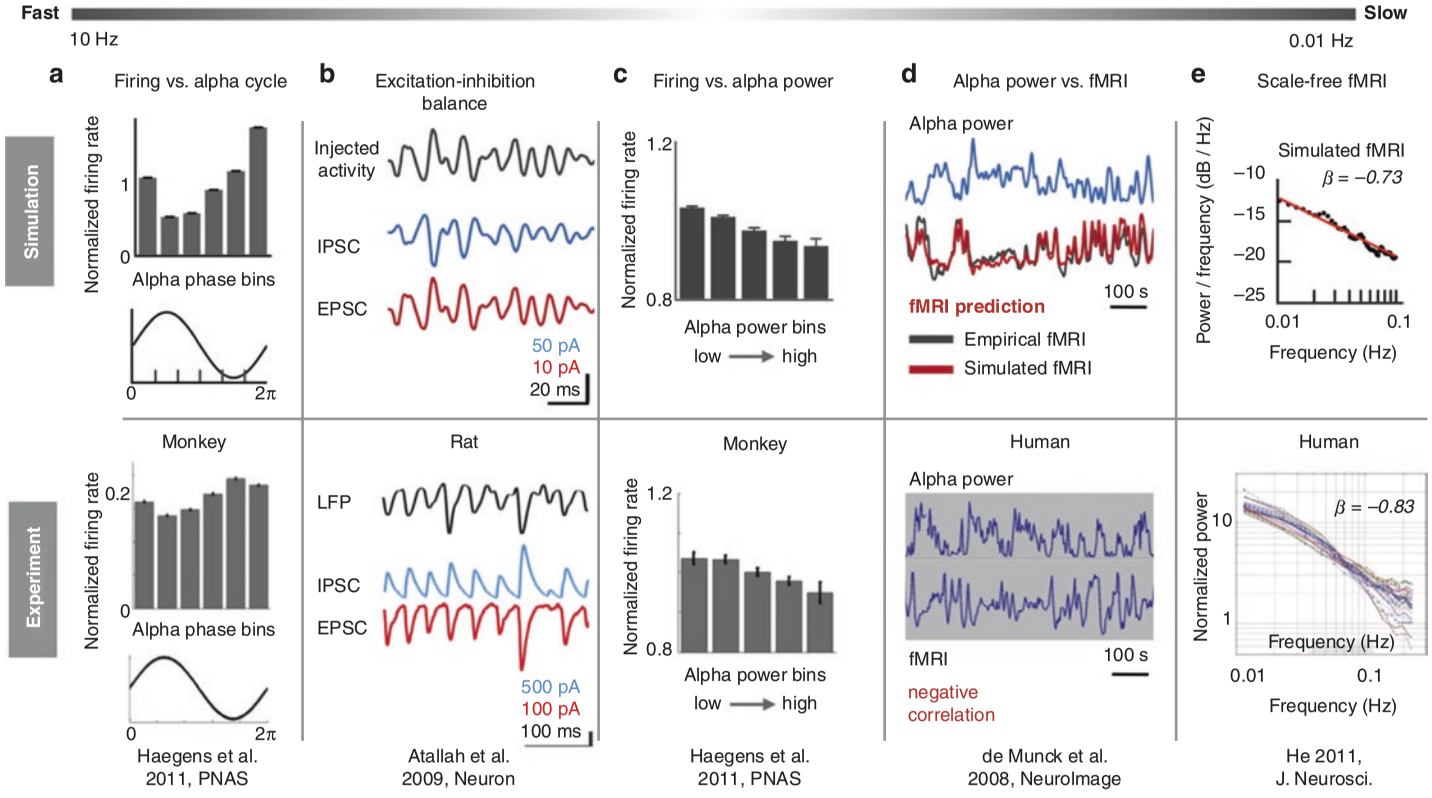

Fig. 30.4 Hybrid model simulations reproduced several empirical phenomena measured by different modalities and on different time scales. From fast to slow time scale: the inverse relationship between neural firing and alpha cycle (**a**), the ongoing balancing of excitatory and inhibitory postsynaptic currents (EPSC and IPSC, respectively) and their relation to local field potentials (LFP), respectively injected EEG (**b**), the inverse relationship between alpha band-power fluctuation and firing rates (**c**), the inverse relationship between alpha band-power fluctuation and fMRI (**d**), scale-free fMRI power spectra (**e**). (Reproduced from Schirner et al. 2018)

reviewed in this chapter, excitatory population firing rates and synaptic gating decreased, when alpha power increased, and vice versa. Strikingly, the underlying mechanism seemed to be related to the activity of the inhibitory populations, because these showed the exact *opposite* effect: when alpha power increased, their activity likewise increased, leading to increased inhibition, and vice versa. Indeed, when looking at the excitatory and inhibitory postsynaptic currents (EPSCs and IPSCs, respectively), the authors found that the modulation of the input currents relevant for producing slow fMRI oscillations was largely due to the effect of inhibitory populations and long-range network input (Fig. 30.5). Due to the interaction of excitatory and inhibitory populations, the power modulation of injected alpha activity was transformed into an amplitude fluctuation of firing rates, synaptic activity, and consequently fMRI activity on the slow time scale of fMRI resting-state oscillations. To identify how alpha increased inhibition on slow time scales (<0.1 Hz), the authors looked at the activity at the fast time scale of individual alpha cycles (Fig. 30.6). Therein, it was found that for increasing alpha power the positive half-cycle of an alpha wave led to increasingly higher levels of inhibitory population firing rates, which dampened excitatory population activity, while the negative deflections of the alpha cycle simply silenced the inhibitory population. As alpha power was increasing, the increasingly large positive half-cycles of the alpha wave led to an increasingly large inhibitory effect. By contrast, the increasingly large negative half-cycles of the alpha wave had no compensatory effect for larger amplitudes, because firing rates cannot be smaller than 0 Hz. As a consequence of the declining capability of inhibitory populations to balance oscillatory input current peaks, and resulting inhibition bursts, excitatory populations' firing rates became increasingly lower for increasing alpha power (see Fig. 30.6 for a visual explanation).

Upon identifying a mechanism that explains the inhibitory effect of alpha activity, the study took a closer look at the role of the long-range network, because parameter space exploration showed that when global coupling was turned off, the prediction of fMRI was considerably decreased. Interestingly, along with the decreased predictability of empirical fMRI, analyses showed a strong reduction of the "scale-freeness" of the time series produced by simulations with disabled long-range coupling. Compared to empirical fMRI, disabled long-range coupling led to a decreased power-law exponent. That is, the power spectrum of fMRI was less steep. Power-law scaling means that the decrease of power of frequencies in a signal's power spectrum follows a power-law $P \propto f^{\beta}$, with power P, frequency f, and power-law exponent β. Power-law scaling was found to be ubiquitous in nature, for example, occurring in sandpiles, earthquakes, foraging patterns of various species, frequencies of family names, sizes of craters on the moon, and neural activity, to name a few. Importantly, power-laws were found to emerge near the critical point of phase transitions and can be associated with the spontaneous acquisition of structure and complex behavior, and is therefore an appealing concept as it could point toward a general theory of self-organization in biological systems. Schirner et al. (2018) therefore asked how the previous findings on the emergence of fMRI oscillations from alpha

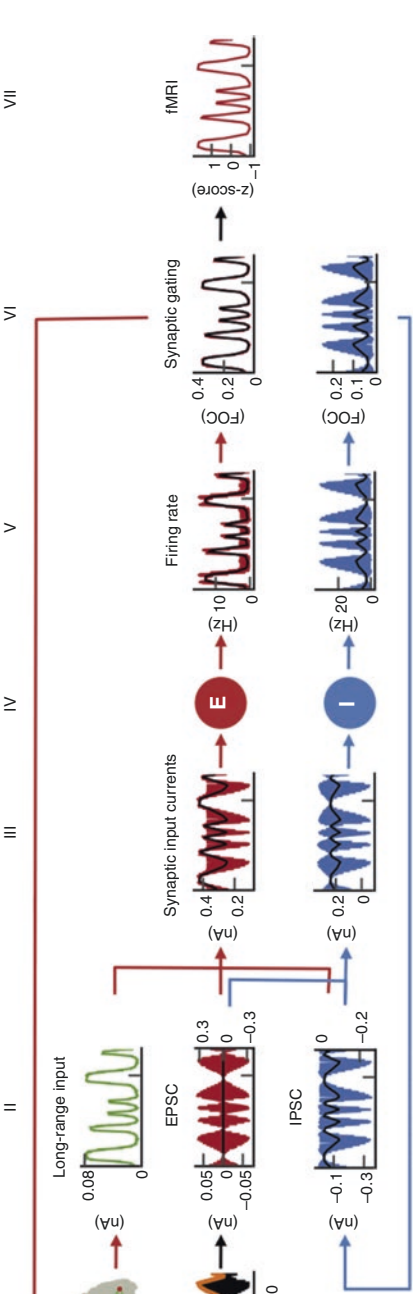

Fig. 30.5 Alpha activity (I, black trace: alpha amplitude) with ongoing power fluctuation (I, orange trace: power envelope) is injected into BNM nodes, which leads to the emergence of anticorrelated fMRI amplitude fluctuations (VII, red trace). Alpha activity enters the model as an excitatory postsynaptic current (EPSC, II, red trace) and is added to the sum of all input currents (III, red and blue trace) that enter the excitatory, respectively inhibitory, populations (IV) at each node. Note that the alpha-modulated EPSCs are centered at zero (II, EPSC, black trace); that is, injected alpha on average neither increases nor decreases the constant overall effective EPSC of the model (0.382 nA; not shown). The modulation of total synaptic input (III, black trace), which gives rise to fMRI oscillations, is due to inhibitory postsynaptic currents (II, blue trace) and long-range network input (II, green trace). (Reproduced from Schirner et al. 2018)

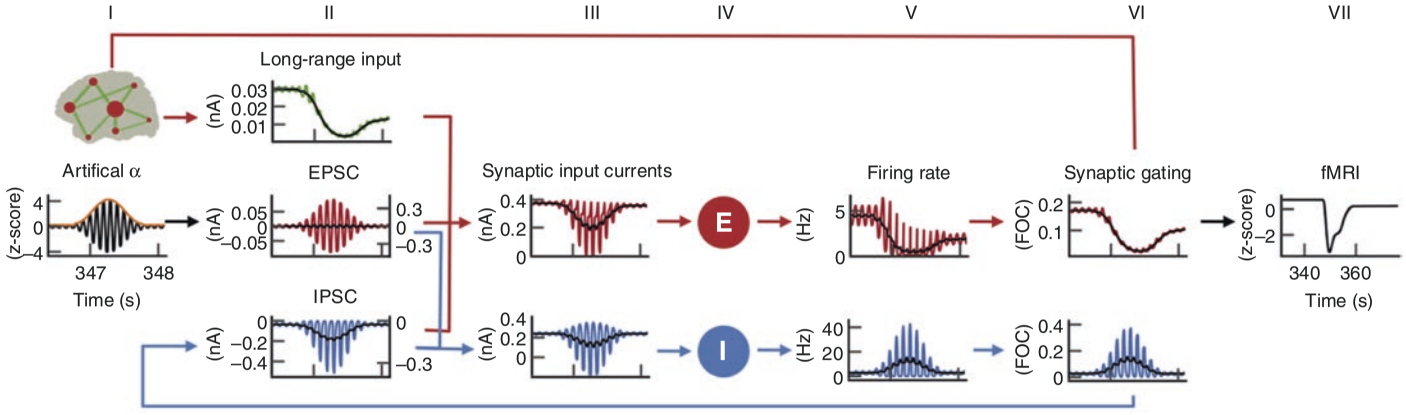

Fig. 30.6 On the fast time scale of individual alpha cycles, the inhibitory effect of increasing alpha power (II, black trace: alpha amplitude; orange trace: power envelope) can be visually inferred. By modulating the synaptic input of inhibitory populations (III, blue trace), alpha modulated the firing rates of inhibitory populations (IV, blue trace). Importantly, for increasing alpha power, inhibitory firing became increasingly stronger during positive deflections of the alpha wave. This is because increasingly positive amplitude peaks of alpha progressively increased firing of inhibitory populations, while the balancing effect of troughs of alpha was bounded by zero firing, as there are no "negative" firing rates in nature (V, blue trace). Consequently, due to the decreasing capability to balance inhibitory populations' excitation, net firing of excitatory populations decreased for increased alpha power. (Reproduced from Schirner et al. 2018)

power fluctuation could be integrated with long-range network interaction and the emergence of power-law scaling.

To explain the underlying cause, it helps to express power-law scaling with the formula "slower oscillations go along with stronger signal modulation than faster oscillations." This effect can be nicely observed when comparing Figs. 30.5 and 30.7. When alpha power oscillation was very slow, the resulting fMRI amplitude peaks were large, while fast alpha power oscillations produced smaller fMRI amplitude peaks (Fig. 30.5). Intriguingly, this effect vanished when long-range coupling was turned off: then all amplitude peaks had roughly the same height (Fig. 30.7). In other words, network coupling translated the duration of an alpha power oscillation into the height of the fMRI amplitude's peak during that oscillation. This effect can be explained (1) by recurrent excitation through the large-scale network, which further amplified the effect of alpha-band power oscillations on neural firing, and (2) the relatively slow time scale of NMDA excitatory synaptic gating (100 ms), which enabled recurrent long-range excitation to accumulate for the time duration during which high alpha power inhibited neural firing. During the troughs of slow alpha power oscillations, recurrent excitation had more time to build up, which resulted in larger amplitudes compared to slower alpha oscillations. Accordingly, the power of slower oscillations increased in fMRI relative to faster oscillations, leading to steeper power-law slopes. This observation, therefore, addresses open questions in neuroscience on the origin of power-law behavior, and whether power-laws in neural networks originate from cellular-level or global network-level processes (Beggs and Timme 2012). Furthermore, these results explicitly account for structured input activity, while in vitro and in silico studies have so far focused on systems without or considerably decreased input (Hesse and Gross 2014). Lastly, the co-emergence of spatial long-range correlations and power-law scaling may point to a unifying explanation of resting-state activity within the framework of self-organized criticality, which offers a general mechanism for the emergence of correlations and complex dynamics in stochastic multiunit systems (Linkenkaer-Hansen et al. 2001).

A recent study challenged the widely held view that alpha–BOLD anticorrelation originates from alpha power fluctuation, instead proposing that both originate from high- and low-frequency components of the same underlying cortical activity, and that the inverse correlation arises from variations in the strengths of corticothalamic and intrathalamic feedback (Pang and Robinson 2018). The arguing is that the high-pass filtering of EEG, commonly done in empirical studies to improve signal quality, discards slow-frequency fluctuations that may drive BOLD. The study used a corticothalamic neural field model that was successively fitted to power spectra of 4-s epochs of EEG data using 1-s steps with the goal to track assumed temporal changes in gain parameters. The resulting model activity then reproduced the evolution of empirical EEG power spectra on the basis of second-by-second fluctuations of six fitted corticothalamic gain parameters that correspond to the responses of the simulated populations to input. This theory should be easily testable by empirical EEG–fMRI data. Instead, the authors analyzed EEG-only data, using the low-frequency component of EEG as a proxy for BOLD data, arguing that both are slow signals and correlations between them

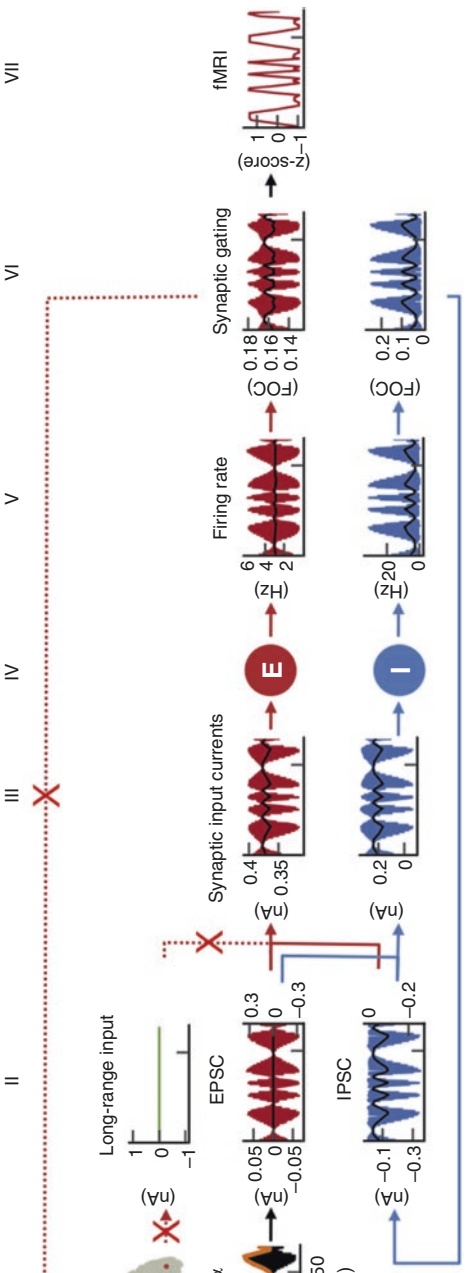

Fig. 30.7 When long-range coupling is turned off, power-law scaling of fMRI decreased. In Fig. 30.5, one can see that slow alpha power oscillations produce large peaks of fMRI amplitude, while faster oscillations produce smaller peaks. Intriguingly, when long-range coupling was turned off, all amplitude peaks were equally high, regardless of alpha power frequency. Long-range coupling seemed to "translate" the power oscillation of alpha into the height of amplitude peaks in fMRI. (Reproduced from Schirner et al. 2018)

have been reported in literature. Upon finding negative correlations between low-frequency EEG power and alpha EEG power, the authors conclude that this analysis reproduced the BOLD–alpha anticorrelation widely reported in literature. Problematically, using slow EEG as a proxy for BOLD in order to show that slow EEG and BOLD are correlated (respectively, the implied idea that BOLD originates from slow electric fluctuations) is circular reasoning. To restate, the result from Pang and Robinson (2018) indicates that slow EEG oscillations, slow power modulation of alpha activity as well as fMRI oscillations all originate from moment-to-moment oscillatory gain modulation of corticothalamic interaction. The results from Schirner et al. (2018), on the other hand, indicate that the low-frequency oscillation assumed to underlie BOLD oscillations emerges from local and global interaction of excitatory and inhibitory neural populations, which transforms slow alpha-power oscillation into a low-frequency amplitude oscillation of neural activity. Importantly, the latter mechanism does not require any change of parameters like the former, but explains the emergence of slow frequency oscillations just by means of a neurophysiological mechanism that is captured by the model itself. That is, even if the reasoning in Pang and Robinson (2018) was not circular, the theory does not explain the data in terms of a neurophysiological mechanism that emerges from model dynamics, but merely shifts the correlational reasoning from EEG–fMRI data comparison to a proposed ongoing fluctuation of cortical gains that was obtained from moment-to-moment fits of the model to the data, which is in itself problematic as by the very same approach presumably every kind of moment-to-moment signal change can be explained. In any case, the two theoretical results are nice examples how brain simulation-based integration helps formulating novel theories and testable predictions that may help explain the underlying processes that lead to the observation of EEG–fMRI signals.

Summarizing, the reviewed results may help explaining several observations from EEG–fMRI research in terms of neurophysiological mechanisms. Because respiration, cardiac pulsation, subject movement and other processes are correlated with resting-state fMRI oscillations, it is hard to differentiate which part of the signal is of neural origin and which part of the signal is noise. Importantly, it is unclear how exactly hemodynamic oscillations and networks relate to neural activity (e.g., Murphy et al. 2013; Yuan et al. 2013). Problematically, fluctuations of cardiac and respiratory rates are often used to form regressors that are then used to "clean" the fMRI data, although it is known that neural activity may well be temporally correlated with these physiological signals (de Munck et al. 2008; Yuan et al. 2013) and therefore erroneously removed (Birn 2012). Brain simulation-based EEG–fMRI integration may therefore be an approach to differentiate between neural and nonneural origins of fMRI variance. For example, the prediction of fMRI from EEG via hybrid BNMs suggests an explicit mechanism that relates fMRI to electric activity via a chain of neural-metabolic-hemodynamic interactions, which can then be used to distinguish neural and nonneural signal components. It is important to note that although most of the reviewed results revolved around the alpha rhythm, the alpha rhythm, though prominent, is

certainly not superior to other rhythms with respect to neural computation and can, at best, be thought of as one of several modes of brain operation. None of the mentioned simulation approaches are confined to the alpha rhythm—conventional as well as hybrid BNMs accommodate other rhythms as well.

30.9 Outlook: Diagnosis and Therapy

Brain simulation was able to reproduce and explain a variety of phenomena observed with EEG–fMRI. Models that make conflicting predictions directly point to the limits of our current understanding and help us design new experiments that may test the theories associated with the models. Despite their success, models are, per definition, abstractions from reality and trying to make them more detailed, or realistic, often makes them overly complex, which then may interfere with their ability to provide concise explanations of phenomena. Increasing model complexity may come with an increased ability to explain a specific observation, but also a potentially decreased ability to generalize to a class of observations (e.g., due to overfitting). For example, the so-called "vascular steal" phenomenon describes an effect where an increase of local CBF leads to a decrease in neighboring regions, due to the need to divert blood flow toward the active tissue (Raichle 1998). In many of the reviewed models, negative BOLD signals were obtained by increasing inhibition, be it due to fluctuations in coupling or due to an emerging network mechanism, but "vascular steal" again provides a viable alternative explanation. Does this mean we need to resign in front of the possibility that there always might be an alternative explanation? We would argue, no: To decide between alternative explanations, their consequences and predictions must be developed and compared, and this is exactly what brain simulation is supposed to do. Future brain models will simultaneously incorporate multiple scales—where necessary individual neurons and synaptic connections will be simulated with high precision, while other locations are described by simplifying NMMs. This will enable us to study single-neuron and neuron-population activity in light of realistic full-brain network activity, which will lead to better understanding of the whole and its parts. Brain simulation-based EEG–fMRI integration provides promising avenues for the better understanding of pathologies. For example, Sotero and Trujillo-Barreto (2008) related the EEG–fMRI simulations with Alzheimer's disease (AD). Based on the observation of AD patients showing a progressive cortical disconnection syndrome due to the loss of large pyramidal neurons in cortical layers III and V, the authors simulated AD by reducing all long-range connection weights by 50% and recurrent excitation by 67%. Resulting EEG showed a marked reduction of alpha activity accompanied by an increase in delta and theta bands; resulting BOLD showed reduced amplitudes. In a second experiment, the effect of external stimulation was studied by delivering a 2-s pulse of 106 action potentials to excitatory thalamocortical relay neurons, which was

also done previously to simulate alpha rhythm desynchronization (but there without reducing connectivity parameters). Compared to their simulation with standard parameter values, BOLD signal fluctuation decreased, which the authors found in agreement with empirical studies, concluding that cortical disconnection may contribute to the shift of the EEG spectrum toward lower frequencies and decreased BOLD amplitudes. In another study, Stefanovski et al. (2019) used PET data to heterogeneously set the excitation–inhibition ratios of NMM parameters to simulate individual amyloid beta burdens in Alzheimer's patients' models, which yielded insights that may lead to an explanation for the slowing of EEG in Alzheimer's and points to its potential reversibility mediated by NMDA receptor antagonists.

An emerging picture in clinically relevant FC literature is that it is often not the whole-brain network pattern that differentiates patients and healthy controls, but rather the form and frequency of dynamical transitions between brain states (Cohen 2017). For example, Schizophrenia patients spent significantly more time in a disconnected brain state and transitioned less often to integrated brain states than controls (Damaraju et al. 2014). Similar examples of atypical temporal FC dynamics from attention deficit hyperactivity disorder (Tomasi and Volkow 2012) and autism (Falahpour et al. 2016; Rashid et al. 2018). To exploit such observations and bring it to use in clinics, a critical next step would be to investigate the neural mechanisms underlying the formation and dissolution of functional connections to move beyond mere descriptive measures. So far, however, experimental approaches to probe how topological features of brain networks relate to pathophysiological processing had limited success. By contrast, brain simulation-based EEG–fMRI integration showed its potential to uncover the dynamic principles underlying observable signals. Not much work has been devoted so far to relate FCD signatures in EEG and fMRI with brain network model dynamics, but precisely this avenue may help us gain understanding in the processes that lead to aberrant network dynamics by enabling the direct probing of the effect of structural and dynamic perturbations in silico; for example, atypical FCD might be reproduced and the underlying mechanisms studied by using EEG data of patients as a constraint for electric activity in a hybrid brain simulation approach to simulate fMRI (Schirner et al. 2018). We do not know what the future of brain simulation-based EEG–fMRI integration holds, but given the recent advances in brain simulation and brain *stimulation* (Berényi et al. 2012; Ngo et al. 2013), it seems likely that joining forces between the two separate research streams (e.g., model-based closed loop stimulation) will improve the quality of life of many patients suffering from various disorders.

Acknowledgements

Funding

Funder	Grant reference number	Author
Horizon 2020	683049 ERC Consolidator	Petra Ritter
	650003 Human Brain Project	
	826421 VirtualBrainCloud	
	Research and Innovation Action Grant Human Brain Project SGA2 785907 Research and Innovation Action Grant Human Brain Project SGA3 945539 Research and Innovation Action Grant Interactive Computing E-Infrastructure for the Human Brain Project ICEI 800858 Research and Innovation Action Grant EOSC VirtualBrainCloud 826421 Research and Innovation Action Grant AISN 101057655 Research Infrastructures Grant EBRAINS-PREP 101079717 European Innovation Council PHRASE 101058240 Research Infrastructures Grant EBRAIN-Health 101058516 European Research Council Grant ERC BrainModes 683049	
Stiftung Charité/Private Exzel-lenzinitiative Johanna Quandt and Berlin Institute of Health	RI 2073/6-1	Petra Ritter
German Research Foundation	SFB 1315/1	Petra Ritter
	SFB 1436 (project ID 425899996) SFB 1315 (project ID 327654276) SFB 936 (project ID 178316478) SFB-TRR 295 (project ID 424778381) SPP Computational Connectomics RI 2073/6-1 SPP Computational Connectomics RI 2073/10-2 SPP Computational Connectomics RI 2073/9-1	
	JPND ERA PerMed PatternCog 2522FSB904	

References

Adhikari MH, Beharelle AR, Griffa A, Hagmann P, Solodkin A, McIntosh AR, Small SL, Deco G (2015) Computational modeling of resting-state activity demonstrates markers of normalcy in children with prenatal or perinatal stroke. J Neurosci 35(23):8914–8924

Aerts H, Schirner M, Jeurissen B, Van Roost D, Achten E, Ritter P, Marinazzo D (2018) Modeling brain dynamics in brain tumor patients using the virtual brain. eNeuro 5:ENEURO.0083-18.2018

Allen EA, Damaraju E, Plis SM, Erhardt EB, Eichele T, Calhoun VD (2014) Tracking whole-brain connectivity dynamics in the resting state. Cereb Cortex 24(3):663–676

Alstott J, Breakspear M, Hagmann P, Cammoun L, Sporns O (2009) Modeling the impact of lesions in the human brain. PLoS Comput Biol 5(6):e1000408

Attwell D, Iadecola C (2002) The neural basis of functional brain imaging signals. Trends Neurosci 25(12):621–625

Bansal K, Nakuci J, Muldoon SF (2018) Personalized brain network models for assessing structure–function relationships. Curr Opin Neurobiol 52:42–47
Becker R, Knock S, Ritter P, Jirsa V (2015) Relating alpha power and phase to population firing and hemodynamic activity using a thalamo-cortical neural mass model. PLoS Comput Biol 11(9):e1004352
Beggs JM, Timme N (2012) Being critical of criticality in the brain. Front Physiol 3:163
Berényi A, Belluscio M, Mao D, Buzsáki G (2012) Closed-loop control of epilepsy by transcranial electrical stimulation. Science 337(6095):735–737
Birn RM (2012) The role of physiological noise in resting-state functional connectivity. NeuroImage 62(2):864–870
Bojak I, Oostendorp TF, Reid AT, Kötter R (2011) Towards a model-based integration of co-registered electroencephalography/functional magnetic resonance imaging data with realistic neural population meshes. Phil Trans R Soc Lond A Math Phys Eng Sci 369(1952):3785–3801
Breakspear M (2017) Dynamic models of large-scale brain activity. Nat Neurosci 20(3):340
Busch NA, Dubois J, VanRullen R (2009) The phase of ongoing EEG oscillations predicts visual perception. J Neurosci 29(24):7869–7876
Buxton RB, Wong EC, Frank LR (1998) Dynamics of blood flow and oxygenation changes during brain activation: the balloon model. Magn Reson Med 39(6):855–864
Buxton RB, Uludağ K, Dubowitz DJ, Liu TT (2004) Modeling the hemodynamic response to brain activation. NeuroImage 23:S220–S233
Buzsaki G (2006) Rhythms of the brain. Oxford University Press, Oxford
Cabral J, Hugues E, Kringelbach ML, Deco G (2012) Modeling the outcome of structural disconnection on resting-state functional connectivity. NeuroImage 62(3):1342–1353
Cohen JR (2017) The behavioral and cognitive relevance of time-varying, dynamic changes in functional connectivity. NeuroImage 180:515
Dale AM, Liu AK, Fischl BR, Buckner RL, Belliveau JW, Lewine JD, Halgren E (2000) Dynamic statistical parametric mapping: combining fMRI and MEG for high-resolution imaging of cortical activity. Neuron 26(1):55–67
Damaraju E, Allen EA, Belger A, Ford J, McEwen S, Mathalon D, Mueller B, Pearlson G, Potkin S, Preda A (2014) Dynamic functional connectivity analysis reveals transient states of dysconnectivity in schizophrenia. NeuroImage Clin 5:298–308
David O, Friston KJ (2003) A neural mass model for MEG/EEG:: coupling and neuronal dynamics. NeuroImage 20(3):1743–1755
Debener S, Ullsperger M, Siegel M, Engel AK (2006) Single-trial EEG–fMRI reveals the dynamics of cognitive function. Trends Cogn Sci 10(12):558–563
Deco G, Jirsa VK, Robinson PA, Breakspear M, Friston K (2008) The dynamic brain: from spiking neurons to neural masses and cortical fields. PLoS Comput Biol 4(8):e1000092
Deco G, Jirsa V, McIntosh AR, Sporns O, Kötter R (2009) Key role of coupling, delay, and noise in resting brain fluctuations. Proc Natl Acad Sci U S A 106:10302
Deco G, Jirsa VK, McIntosh AR (2011) Emerging concepts for the dynamical organization of resting-state activity in the brain. Nat Rev Neurosci 12(1):43
Deco G, Ponce-Alvarez A, Mantini D, Romani GL, Hagmann P, Corbetta M (2013) Resting-state functional connectivity emerges from structurally and dynamically shaped slow linear fluctuations. J Neurosci 33(27):11239–11252
Falahpour M, Thompson WK, Abbott AE, Jahedi A, Mulvey ME, Datko M, Liu TT, Müller R-A (2016) Underconnected, but not broken? Dynamic functional connectivity MRI shows underconnectivity in autism is linked to increased intra-individual variability across time. Brain Connect 6(5):403–414
Falcon MI, Riley JD, Jirsa V, McIntosh AR, Chen EE, Solodkin A (2016) Functional mechanisms of recovery after chronic stroke: modeling with the virtual brain. eNeuro 3(2):ENEURO. 0158-0115.2016
Freyer F, Aquino K, Robinson PA, Ritter P, Breakspear M (2009) Bistability and non-Gaussian fluctuations in spontaneous cortical activity. J Neurosci 29(26):8512–8524
Freyer F, Roberts JA, Becker R, Robinson PA, Ritter P, Breakspear M (2011) Biophysical mechanisms of multistability in resting-state cortical rhythms. J Neurosci 31(17):6353–6361

Friston KJ, Mechelli A, Turner R, Price CJ (2000) Nonlinear responses in fMRI: the Balloon model, Volterra kernels, and other hemodynamics. NeuroImage 12(4):466–477
Ghosh A, Rho Y, McIntosh AR, Kötter R, Jirsa VK (2008) Noise during rest enables the exploration of the brain's dynamic repertoire. PLoS Comput Biol 4(10):e1000196
Goldman RI, Stern JM, Engel J Jr, Cohen MS (2002) Simultaneous EEG and fMRI of the alpha rhythm. Neuroreport 13(18):2487
Gonçalves SI, De Munck JC, Pouwels P, Schoonhoven R, Kuijer J, Maurits N, Hoogduin J, Van Someren E, Heethaar R, Da Silva FL (2006) Correlating the alpha rhythm to BOLD using simultaneous EEG/fMRI: inter-subject variability. NeuroImage 30(1):203–213
Haegens S, Nácher V, Luna R, Romo R, Jensen O (2011) α-Oscillations in the monkey sensorimotor network influence discrimination performance by rhythmical inhibition of neuronal spiking. Proc Natl Acad Sci 108(48):19377–19382
Haider B, Schulz DP, Häusser M, Carandini M (2016) Millisecond coupling of local field potentials to synaptic currents in the awake visual cortex. Neuron 90(1):35–42
Hallez H, Vanrumste B, Grech R, Muscat J, De Clercq W, Vergult A, D'Asseler Y, Camilleri KP, Fabri SG, Van Huffel S (2007) Review on solving the forward problem in EEG source analysis. J Neuroeng Rehabil 4(1):46
Hesse J, Gross T (2014) Self-organized criticality as a fundamental property of neural systems. Front Syst Neurosci 8:166
Honey CJ, Kötter R, Breakspear M, Sporns O (2007) Network structure of cerebral cortex shapes functional connectivity on multiple time scales. Proc Natl Acad Sci 104(24):10240–10245
Huster RJ, Debener S, Eichele T, Herrmann CS (2012) Methods for simultaneous EEG-fMRI: an introductory review. J Neurosci 32(18):6053–6060
Iadecola C (2017) The neurovascular unit coming of age: a journey through neurovascular coupling in health and disease. Neuron 96(1):17–42
Izhikevich EM, Edelman GM (2008) Large-scale model of mammalian thalamocortical systems. Proc Natl Acad Sci 105(9):3593–3598
Jansen BH, Rit VG (1995) Electroencephalogram and visual evoked potential generation in a mathematical model of coupled cortical columns. Biol Cybern 73(4):357–366
Jensen O, Mazaheri A (2010) Shaping functional architecture by oscillatory alpha activity: gating by inhibition. Front Hum Neurosci 4:185
Jorge J, Van der Zwaag W, Figueiredo P (2014) EEG–fMRI integration for the study of human brain function. NeuroImage 102:24–34
Kilner JM, Mattout J, Henson R, Friston K (2005) Hemodynamic correlates of EEG: a heuristic. NeuroImage 28(1):280–286
Klimesch W (1999) EEG alpha and theta oscillations reflect cognitive and memory performance: a review and analysis. Brain Res Rev 29(2):169–195
Klimesch W, Sauseng P, Hanslmayr S (2007) EEG alpha oscillations: the inhibition–timing hypothesis. Brain Res Rev 53(1):63–88
Laufs H, Kleinschmidt A, Beyerle A, Eger E, Salek-Haddadi A, Preibisch C, Krakow K (2003a) EEG-correlated fMRI of human alpha activity. NeuroImage 19(4):1463–1476
Laufs H, Krakow K, Sterzer P, Eger E, Beyerle A, Salek-Haddadi A, Kleinschmidt A (2003b) Electroencephalographic signatures of attentional and cognitive default modes in spontaneous brain activity fluctuations at rest. Proc Natl Acad Sci 100(19):11053–11058
Linkenkaer-Hansen K, Nikouline VV, Palva JM, Ilmoniemi RJ (2001) Long-range temporal correlations and scaling behavior in human brain oscillations. J Neurosci 21(4):1370–1377
Logothetis NK, Pauls J, Augath M, Trinath T, Oeltermann A (2001) Neurophysiological investigation of the basis of the fMRI signal. Nature 412(6843):150
Maier-Hein KH, Neher PF, Houde J-C, Côté M-A, Garyfallidis E, Zhong J, Chamberland M, Yeh F-C, Lin Y-C, Ji Q (2017) The challenge of mapping the human connectome based on diffusion tractography. Nat Commun 8(1):1349
Mantini D, Perrucci MG, Del Gratta C, Romani GL, Corbetta M (2007) Electrophysiological signatures of resting state networks in the human brain. Proc Natl Acad Sci 104(32):13170–13175
Mathewson KE, Gratton G, Fabiani M, Beck DM, Ro T (2009) To see or not to see: prestimulus α phase predicts visual awareness. J Neurosci 29(9):2725–2732

Moosmann M, Ritter P, Krastel I, Brink A, Thees S, Blankenburg F, Taskin B, Obrig H, Villringer A (2003) Correlates of alpha rhythm in functional magnetic resonance imaging and near infrared spectroscopy. NeuroImage 20(1):145–158

de Munck JC, Gonçalves SI, Faes TJ, Kuijer JP, Pouwels PJ, Heethaar RM, da Silva FL (2008) A study of the brain's resting state based on alpha band power, heart rate and fMRI. NeuroImage 42(1):112–121

Murphy K, Birn RM, Bandettini PA (2013) Resting-state fMRI confounds and cleanup. NeuroImage 80:349–359

Ngo H-VV, Martinetz T, Born J, Mölle M (2013) Auditory closed-loop stimulation of the sleep slow oscillation enhances memory. Neuron 78(3):545–553

Oh SW, Harris JA, Ng L, Winslow B, Cain N, Mihalas S, Wang Q, Lau C, Kuan L, Henry AM (2014) A mesoscale connectome of the mouse brain. Nature 508(7495):207

Okun M, Naim A, Lampl I (2010) The subthreshold relation between cortical local field potential and neuronal firing unveiled by intracellular recordings in awake rats. J Neurosci 30(12):4440–4448

Ou W, Nummenmaa A, Ahveninen J, Belliveau JW, Hämäläinen MS, Golland P (2010) Multimodal functional imaging using fMRI-informed regional EEG/MEG source estimation. NeuroImage 52(1):97–108

Pang J, Robinson P (2018) Neural mechanisms of the EEG alpha-BOLD anticorrelation. NeuroImage 181:461–470

Proix T, Spiegler A, Schirner M, Rothmeier S, Ritter P, Jirsa VK (2016) How do parcellation size and short-range connectivity affect dynamics in large-scale brain network models? NeuroImage 142:135

Proix T, Jirsa VK, Bartolomei F, Guye M, Truccolo W (2018) Predicting the spatiotemporal diversity of seizure propagation and termination in human focal epilepsy. Nat Commun 9(1):1088

Raichle ME (1998) Behind the scenes of functional brain imaging: a historical and physiological perspective. Proc Natl Acad Sci 95(3):765–772

Raichle ME, Mintun MA (2006) Brain work and brain imaging. Annu Rev Neurosci 29:449–476

Raichle ME, MacLeod AM, Snyder AZ, Powers WJ, Gusnard DA, Shulman GL (2001) A default mode of brain function. Proc Natl Acad Sci 98(2):676–682

Rashid B, Blanken LM, Muetzel RL, Miller R, Damaraju E, Arbabshirani MR, Erhardt EB, Verhulst FC, van der Lugt A, Jaddoe VW (2018) Connectivity dynamics in typical development and its relationship to autistic traits and autism spectrum disorder. Hum Brain Mapp 39:3127

Ritter P, Schirner M, McIntosh AR, Jirsa VK (2013) The virtual brain integrates computational modeling and multimodal neuroimaging. Brain Connect 3(2):121–145

Roberts JA, Boonstra TW, Breakspear M (2015) The heavy tail of the human brain. Curr Opin Neurobiol 31:164–172

Robinson P, Rennie C, Rowe D (2002) Dynamics of large-scale brain activity in normal arousal states and epileptic seizures. Phys Rev E 65(4):041924

Rombouts SA, Barkhof F, Goekoop R, Stam CJ, Scheltens P (2005) Altered resting state networks in mild cognitive impairment and mild Alzheimer's disease: an fMRI study. Hum Brain Mapp 26(4):231–239

Rosa M, Daunizeau J, Friston KJ (2010) EEG-fMRI integration: a critical review of biophysical modeling and data analysis approaches. J Integr Neurosci 9(4):453–476

Roy D, Sigala R, Breakspear M, McIntosh AR, Jirsa VK, Deco G, Ritter P (2014) Using the virtual brain to reveal the role of oscillations and plasticity in shaping brain's dynamical landscape. Brain Connect 4(10):791–811

Sanz-Leon P, Knock SA, Woodman MM, Domide L, Mersmann J, McIntosh AR, Jirsa V (2013) The Virtual Brain: a simulator of primate brain network dynamics. Front Neuroinform 7:10

Sanz-Leon P, Robinson PA, Knock SA, Drysdale PM, Abeysuriya RG, Fung FK, Rennie CJ, Zhao X (2018) NFTsim: theory and simulation of multiscale neural field dynamics. PLoS Comput Biol 14(8):e1006387

Schirner M, Rothmeier S, Jirsa VK, McIntosh AR, Ritter P (2015) An automated pipeline for constructing personalized virtual brains from multimodal neuroimaging data. NeuroImage 117:343–357

Schirner M, McIntosh AR, Jirsa V, Deco G, Ritter P (2018) Inferring multi-scale neural mechanisms with brain network modelling. elife 7:e28927

Seaquist ER, Chen W, Benedict LE, Ugurbil K, Kwag J-H, Zhu X-H, Nelson CA (2007) Insulin reduces the BOLD response but is without effect on the VEP during presentation of a visual task in humans. J Cereb Blood Flow Metab 27(1):154–160

Seeley WW, Crawford RK, Zhou J, Miller BL, Greicius MD (2009) Neurodegenerative diseases target large-scale human brain networks. Neuron 62(1):42–52

Sotero RC, Trujillo-Barreto NJ (2008) Biophysical model for integrating neuronal activity, EEG, fMRI and metabolism. NeuroImage 39(1):290–309

Stefanescu RA, Jirsa VK (2008) A low dimensional description of globally coupled heterogeneous neural networks of excitatory and inhibitory neurons. PLoS Comput Biol 4(11):e1000219

Stefanovski L, Triebkorn P, Spiegler A, Mohajerani M, Solodkin A, Jirsa V, McIntosh A, Ritter P (2018) The neurodegenerative virtual brain. SfN

Stefanovski L, Triebkorn P, Spiegler A, Diaz-Cortes MA, Solodkin A, Jirsa VK, McIntosh AR, Ritter P (2019) Linking molecular pathways and large-scale computational modeling to assess candidate disease mechanisms and pharmacodynamics in Alzheimer's disease. Front Comput Neurosci 13:54

Stephan KE, Kamper L, Bozkurt A, Burns GA, Young MP, Kötter R (2001) Advanced database methodology for the Collation of Connectivity data on the Macaque brain (CoCoMac). Phil Trans R Soc Lond B Biol Sci 356(1412):1159–1186

Taylor PN, Goodfellow M, Wang Y, Baier G (2013) Towards a large-scale model of patient-specific epileptic spike-wave discharges. Biol Cybern 107(1):83–94

Tomasi D, Volkow ND (2012) Abnormal functional connectivity in children with attention-deficit/hyperactivity disorder. Biol Psychiatry 71(5):443–450

Triebkorn P, Zimmermann J, Stefanovski L, Dipanjan R, Solodkin A, Jirsa V, Deco G, Breakspear M, McIntosh A, Ritter P (2018) Identifying optimal working points of individual virtual brains: a large-scale brain network modelling study. SfN

Valdes-Sosa PA, Sanchez-Bornot JM, Sotero RC, Iturria-Medina Y, Aleman-Gomez Y, Bosch-Bayard J, Carbonell F, Ozaki T (2009) Model driven EEG/fMRI fusion of brain oscillations. Hum Brain Mapp 30(9):2701–2721

Wong K-F, Wang X-J (2006) A recurrent network mechanism of time integration in perceptual decisions. J Neurosci 26(4):1314–1328

Wu G-R, Marinazzo D (2016) Sensitivity of the resting-state haemodynamic response function estimation to autonomic nervous system fluctuations. Phil Trans R Soc A 374(2067):20150190

Yuan H, Zotev V, Phillips R, Bodurka J (2013) Correlated slow fluctuations in respiration, EEG, and BOLD fMRI. NeuroImage 79:81–93

Zenke F, Gerstner W, Ganguli S (2017) The temporal paradox of Hebbian learning and homeostatic plasticity. Curr Opin Neurobiol 43:166–176

Zetterberg L, Kristiansson L, Mossberg K (1978) Performance of a model for a local neuron population. Biol Cybern 31(1):15–26

Zimmermann J, Perry A, Breakspear M, Schirner M, Sachdev P, Wen W, Kochan NA, Mapstone M, Ritter P, McIntosh AR (2018) Differentiation of Alzheimer's disease based on local and global parameters in personalized Virtual Brain models. NeuroImage Clin 19:240–251

Index

C. Mulert, L. Lemieux (eds.), *EEG - fMRI*,
https://doi.org/10.1007/978-3-031-07121-8